JOURNAL OF THE MYANMAR ACADEMY OF ARTS AND SCIENCE

Chemistry

Vol. XVIII, No.1A, July, 2020

Myanmar Academy of Arts and Science

Journal of the Myanmar Academy of Arts and Science

Vol. XVIII, No.1A

Contents

Chemistry

Edition

2020, July, 1000 Copies

Published by

Dr Aung Min (00322) Chairman, Journal Publication Committee,
Myanmar Academy of Arts and Science

ISSN 2520-0186
LCCN 2003-323143

Printed by

U Win Aung (00171), Manager,
Universities Press, Yangon, Myanmar

CARDENOLIDE GLYCOSIDES FROM *Streptocaulon tomentosum* WIGHT & ARNOTT (မြင်းစုံနီ) (ASCLEPIADACEAE) in MYANMAR

Myint Myint Khine[1], Norbert Arnold[2], Katrin Franke[2], Ludger A. Wessjohann[2]

Abstract

This paper describes the isolation and comparative studies on NMR spectra of cardenolide glycosides from *Streptocaulon tomentosum* Wight & Arnott (Asclepiadaceae). Nine cardenolides were isolated from the roots of *Streptocaulon tomentosum*. by column chromatography and identified by NMR spectroscopy. They are 17α-H-periplogenin, 17α-H-periplogenin-β-*D* digitoxose,17α-H-periplogenin-β-*D* cymarose, 17α-H-periplogenin-β-glucosyl-(1-4)-2-*O*-acetyl-digitalose, 17β-H-periplogenin, 17β-H-periplogenin-β-*D* digitoxose, 17β-H-periplogenin-β-*D* cymarose, 17α -H-digitoxigenin, and 17 α-H-digitoxigenin-β-*D*-digitoxoside. Comparative studies on NMR spectra of cardenolide glycosides were carried out. Six cardenolides isolated from *Streptocaulon tomentosum* were tested for their antiproliferative activity *in vitro* against MCF-7 (human breast cancer cell line) and L 929 (mouse fibroblast cell line). Among these six cardenolides, 17α-H-periplogenin-3-*O*-β-*D*-digitoxoside and 17α-H-periplogenin-3-*O*-β-*D*-cymaroside exhibit significant antiproliferative activity (IC_{50} values, < 1μM) against MCF-7. Four cardenolides were examined for their cellular viability in the tumor cell and U 937 (human leukemic cell line) at concentrations 100 μM, 10 μM, and 1 μM. All these four cardenolides show the induction of apoptosis at 100 μM and 10 μM in both cell lines.

Keywords: *Streptocaulon tomentosum*, Asclepiadaceae, cardenolides, antiproliferative activity, cellular viability

Introduction

The genus *Streptocaulon* belongs to the family Asclepiadaceae and includes five species. Two species, *S. tomentosum* and *S. griffithii* J. D. Hooker grow in Myanmar. The roots of *Streptocaulon tomentosum* are used in Myanmar in traditional medicine for the treatment of anticancer, dysentery and stomachache, and the leaves are used externally for the treatment of snake poisoning and abscesses. In previous studies, nobody reported about the isolation of bioactive substances from S.*tomentosum*. However the isolation of cardenolides from the root of *S. juventas* (Lour.) Merr. and antiproliferative activity of cardenolides isolated from *S. juventas* have been reported (Ueda *et al*., 2003a; 2003b). Cardenolides occur in several plant families including the Asclepiadaceae, the Apocynaceae, the Scrophulariaceae, the Celastraceae, and the Tiliaceae. The cardiac glycosides, digitoxin and digoxin, have been used for the treatment of heart failure for hundreds of years. In 2005, digitoxin, digoxin, gitoxin and their corresponding aglycones were evaluated for growth inhibition activity in three human cancer cell lines TK-10 (renal), MCF-7 (breast), and UACC-62 (melanoma) at concentrations commonly found in cardiac patients. Digitoxin (IC_{50} 3.2-33.5 nM) and digoxin (IC_{50}14.6-29.5 nM) showed the highest level of growth inhibition in the three cell lines investigated (Lázaro *et al*., 2005). The above-mentioned reports suggest that digitalis may have an anticancer utilization.

[1] Dr, Professor, Department of Chemistry, University of Yangon
[2.] Dr, Professor, Department of Bioorganic Chemistry, Leibniz Institute of Plant Biochemistry
[*] Best Paper Award Winning Paper in Chemistry (2019)

Materials and Methods

Sample Collection and Identification of Plant Samples

Streptocaulon tomentosum Wight and Arn. (Asclepiadaceae), roots collected in May 2002 from Mawlamyine Township, Myanmar by Dr Daw Hla Ngwe. The species was identified by Prof. Dr Aung Aung Min, Department of Botany, University of Yangon.

A voucher specimen of the clamberer (No. Y.H.V. 1004) is deposited in University of Yangon.

Spectral Studies

1D NMR spectra (^{1}H, ^{13}C) were recorded on a Varian Mercury 300 at 300.94 MHz for 1H, and at 100.57 MHz for ^{13}C NMR. 2DNMR spectra (HSQC, HMBC, COSY, ROESY) were recorded on a Varian Inova 500 at 499.81 MHz for ^{1}H. Chemical shifts in ppm were referenced to internal TMS (δ =0) for 1H and C_5D_5N (δ 149.81, 135.48, 123.50 ppm) for ^{13}C, respectively.

Isolation and Identification of Cardenolides from the Roots of *Streptocaulon tomentosum*

Dried powdered root of *S. tomentosum* (1000 g) was extracted with 80% aqueous EtOH. After evaporation of the solvent, the resulting crude extract was successively partitioned between organic solvents (*n*-hexane, ethylacetate, *n*-butanol) and water. The ethyl acetate crude extract (12 g) was chromatographically separated on silica gel 60 (70-230 mesh, Merck) with *n*-hexane, ethyl acetate, and methanol (increasing polarity) to afford 23 fractions. Fraction 12 and 15 were rechromatographed on silica gel 60 (230-400 mesh, Merck) using $CHCl_3$:MeOH (9.5:0.5, v/v) and silica RP18 using MeOH:H_2O (9:1, v/v) to give compound **1**. Compound **2** and **3** were obtained from fraction 14 (Kawaguchi *et al*., 1988). The subfractions 14 and 15 of the ethyl acetate extract provided, after silica gel and RP-18 column chromatography, the known compound **5** and the unknown compound **6**. Fraction 13 was rechromatographed on sephadex LH-20 eluting with MeOH to afford compound **4**. Fractions 5 to 11 were repurified on silica gel 60 (230-400 mesh, Merck) using $CHCl_3$:MeOH (9.5:0.5, v/v) to give compounds **8** and **9**.

The *n*-butanol fraction (18 g) was separated on silicagel 60 (230-400 mesh, Merck) using $CHCl_3$:MeOH (9.5:0.5, v/v) to give 28 subfractions. The subfraction 7 was purified by silica RP-18 using MeOH:H_2O (8:2, v/v) to give compound **7.**

Antiproliferative Activity of Cardenolides

Acid phosphatase assay: Cells were grown in 96-well plates at densities upto 100,000 cells per well. The culture medium was removed from these cells with a multichannel pipettor (Wheaton), and each well was washed once with 200 μl phosphate-buffered saline (PBS, pH 7.2). For nonadherent cells, to remove solution from plates, the 96-well plates were centrifuges at 2500 rpm for 10 min (Beckman GS-15R centrifuge). To each well, 100 μl of buffer containing 0.1 M sodium acetate (pH 5.0), 0.1 % Triton X-100, and 5 mM *p*-nitrophenyl phosphate was added. The plates were placed in a 37 °C incubator for 2 h. The reaction was stopped with the addition of 10 μl of 1 N NaOH, and colour development was assayed at 405 nm using a microplate reader (THERMOmax plate reader, Molecular Devices, Inc.). The nonenzymatic

hydrolysis of the pNPP substrate was determined for each assay by including wells that did not contain cells. This background value was typically 0.07-0.2 absorbance units.

Cellular Viability of Cardenolides

Cell culture and stimulation

Human U 937 myeloid leukemia cells were grown in RPMI 1640 medium supplemented with 10% heat-inactivated fetal calf serum (FCS), 100 µg/ml penicillin, 100 µg/ml streptomycin, 2 mM L-glutamine (Gibco, Grand Island, N.V., USA). Human TUR myeloid leukemic cells (ATCC #2367) were grown in a similar medium supplemented with 400 µg/ml G418 (Sigma Chemical Co., St. Louis, MO/USA). The maintenance of the TUR cells in the presence of G418 was terminated one week before the appropriate experiments. U 937 and TUR cells were treated with the appropriate substances at a density of 2 x 10^5cells/ml for up to 72h, respectively. The cell number and viability of each culture was assessed by a Vi-Cell cell viability analyzer (Beckman Coulter) using an assay kit and the quantification software Vi-Cell version 1.01 according to the manufacturers protocol (Beckman Coulter).

Cell cycle analysis

Following an appropriate incubation the cells were fixed in 70% (v/v) ice-cold ethanol at 4 °C for 24 h. The fixed cells were stained with CyStain DNA 2 step kit (Partec GmbH, Münster, Germany) and filtered through a 50 µm filter. The samples were then analyzed in a Galaxy flow cytometer (Dako-Cytomation GmbH, Hamburg, Germany) using FloMax analysis software (Partec) and the MultiCycle cell cycle software (Phoenix Flow Systems Inc., San Diego, CA.

Results and Discussion

Structure Elucidation of Cardenolides

(a) 17α-H-Periplogenin (1), 17α-H-periplogenin-β-*D* digitoxose (2), 17α-H-periplogenin-β-*D* cymarose (3)

Fraction 12 of the ethyl acetate extract gave compound **1**. Compound **2** and **3** were obtained from fraction 14 (Kawaguchi *et al*., 1988). The ^{1}H NMR (C_5D_5N) data of compound **1** (HR-ESI-MS: 413.23098 $[M+Na]^+$, calc. for $C_{23}H_{34}O_5Na$ 413.22984) agreed with the characteristic peaks of cardenolides. The signal of H-21 a and b in the butenolide ring showed at δ5.36 and 5.08 ppm (*dd*, *J* 18.1/1.4 Hz).

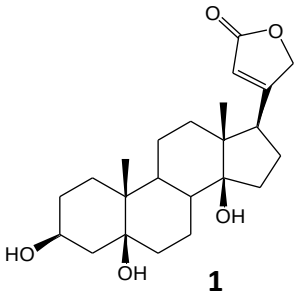

1

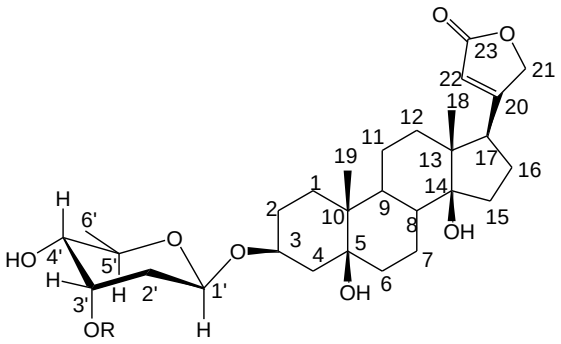

2 R = H

3 R = CH_3

The H-22 was observed as a singlet at δ 6.17 ppm. The H-3 signal appeared as a broad singlet at δ 4.46 ppm. The H-17 signal appeared at δ 2.84 as *dd* (*J* 9/3 Hz) and the H_3-18 and H_3-19 signals at 0.88 and 0.94 as singlet. According to EI-MS, the fragments at *m/z* 391 and 373 indicated the presence of a cardenolide aglycone.

Compound **2** (HR-ESI-MS: 543.2924 $[M+Na]^+$, calc. for $C_{29}H_{44}O_8Na$ 543.2928) and compound **3** (557.3088 $[M+Na]^+$, calc. for $C_{30}H_{46}O_8Na$ 557.3084) exhibited a mass difference of 131 and 145 in comparison to compound **1**. Because this difference was derived from the sugar moiety, the molecular formula of these sugars was deduced to be $C_6H_{11}O_3$ and $C_7H_{13}O_3$, identified a digitoxose and cymarose by acid hydrolysis and GC-MS analysis required derivatization MSTFA (*N*-methyl-*N*-trimethylsilyltrifluoroacetamide) with authentic sugars sample. The data agree with 17α-H-periplogenin-β-*D*-digitoxose (**2**), and 17α-H-periplogenin-β-*D*-cymarose (**3**) (Ueda *et al*., 2003a).

(b) 17α-H-Periplogenin-β-glucosyl-(1-4)-2-*O*-acetyl-digitalose (4)

Fraction 13 of the ethyl acetate extract afforded the new compound **4** after column chromatography on sephadex LH 20 with MeOH.

The ESI-MS spectrum exhibited a $[M+Na]^+$ ion at *m/z* 777. Its molecular formula, $C_{38}H_{58}O_{15}$, (calcd. for $C_{38}H_{58}O_{15}Na$ 777.36679) was obtained through a combined application of ESI-MS, EI-MS, FT-ICR, ^{1}H NMR, and ^{13}C NMR. The ^{1}H NMR spectrum (in CD_3OD) of the aglycone was similar to compound **1**. The signal of H-21a and b also showed a pair of double doublets at δ 5.09 ppm and δ 4.91 ppm. The H-22 was observed as a singlet at δ 5.89 ppm. The H-3 signal appeared as a broad singlet at δ 4.12 ppm, revealing its α-configuration. The ^{1}H NMR and ^{13}C NMR data (in CD_3OD) demonstrated two molecules of sugar by two anomeric protons at δ 4.44 ppm for H 1′ (*dd*, *J* = 8, 3.8 Hz) and δ 4.57 ppm for H 1″ (*dd*, *J* = 8, 3.5 Hz). They were connected to the anomeric carbons at δ 102.1 and 104.6 ppm in the HSQC spectrum respectively. Their chemical shifts and coupling constants suggested β-linkage of the sugars.

The structural assignment was confirmed by carrying out 2D NMR techniques such as HSQC and H-H COSY. The HMBC spectral analysis displayed correlation peaks between H-3 and C-1′of the digitalosyl (3-*O*-methyl-β-fucopyranosyl) unit, the anomeric proton of the glucosyl residue and C-4′ of the digitalosyl unit, H-2′ of digitalosyl and OAc. The connectivity between H-H and H-C in the NOESY and HMBC were also presented in Table 1. According to these spectral data, the structure of compound **4** was assigned as 17α-H-periplogenin-3-*O*-β-glucopyranosyl-(1-4)-2-*O*-acetyl-3-*O*-methyl-β-fucopyranoside. It is a new combination of the known aglycone and sugar moieties.

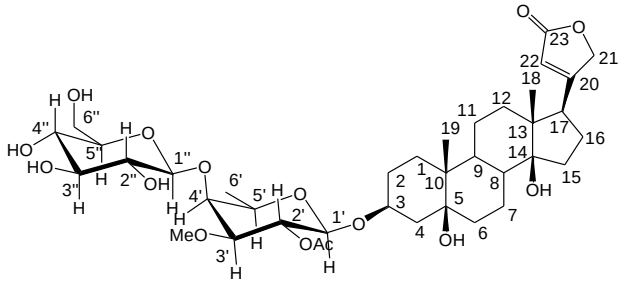

Compound 4

(c) 17*β*-H-Periplogenin (5), 17*β*-H-periplogenin-*β*-*D*-digitoxose (6), 17*β*-H-periplogenin-*β*-*D*-cymarose (7)

The subfractions 14 and 15 of the ethyl acetate extract provided, after silica gel and RP-18 column chromatography, the known compound **5** and the unknown compound **6**. Compound **7** was isolated from the *n*-butanol fraction. The compound **5** and **7** were identified as 17*β*-H-periplogenin **(5)** and 17*β*-H-periplogenin-*β*-*D*-cymarose **(7)** by different MS and 2D NMR experiments and by comparison with the spectral data from literature (Furuya *et al*., 1988).

Compound **5** had the composition $C_{23}H_{34}O_5$ on the basis of HR-MS. In the ^1H NMR (C_5D_5N) spectrum of **5**, the methyl proton signals H_3-18 and H_3-19 were shifted downfield to δ 1.227 and 1.186 ppm (each 3H, *s*) by comparison with that of compound **1**. The methine proton signal of H-17, coupling with the methylene protons of C-16, was also shifted downfield to δ 3.463 (1H, *t*, *J* 9.5 Hz). In the ROESY spectrum, a correlation peak between H-17 and H_3-18 was found. In the ^{13}C NMR spectrum (Table 3), the carbon C-12 and C-17 signals were shifted upfield to δ 31.1 and 48.8 ppm. Thereby the configuration of H-17 was revealed to be β (Furuya *et al*., 1988).

Compound **6** was isolated as a white powder. The molecular formula $C_{29}H_{44}O_8$ was deduced from positive ion ESI-FT-ICR-MS (*m/z* 543.29240 $[M+Na]^+$, calcd. for $C_{29}H_{44}O_8Na$ 543.29283). The ^1H and ^{13}C NMR data of the aglycone agree with the characteristic peaks of 17*β*-H-periplogenin (Furuya *et al*., 1988). The HMBC correlation between C-3 and the anomeric proton H-1′ proved the presence of the sugar moiety at C-3. This is further supported by the NOE of H-3 with H-1′. According to the EI-MS data, the fragments at *m/z* 391 and 373 indicated a aglycone moiety and *m/z* 131 and 113 fragments of a 2,6-deoxy sugar moiety. The 2D NMR correlation peaks of the sugar moiety and the vicinal ^1H, ^1H coupling constants confirmed the presence of digitoxose. After hydrolyses with HCl, the hydrolysed sugar moiety could be also identified as digitoxose by GC analysis as its trimethylsilylether.

According to the spectral data, compound **6** was identified as a new combination of the known aglycone and known sugar 17*β*-H-periplogenin-*β*-*D*-digitoxoside.

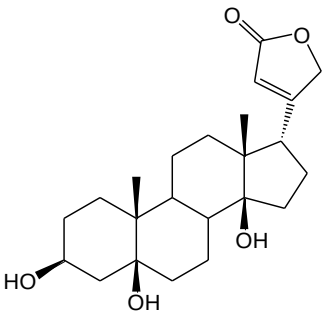

5

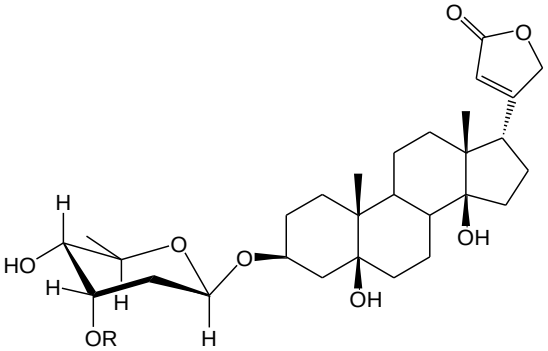

6 R = H
7 R = Me

(d) 17α-H-Digitoxigenin (8), 17α-H-digitoxigenin-β-*D*-digitoxoside (9)

Compounds **8** and **9** were isolated from fractions 10 and 11 of the ethyl acetate extract after silica gel chromatography. Their structures were confirmed by 2D NMR and comparison to reported data (Danieli *et al*., 1966).

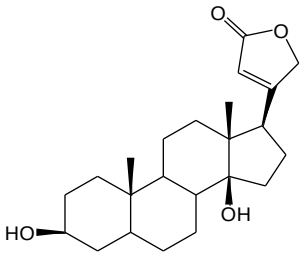

8

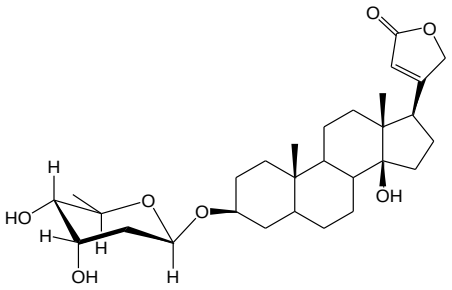

9

Table 1 NMR Data of Compound 4 (500 MHz, CD_3OD)

Atom	δ_H [ppm]	δ_C [ppm]	$^nJ_{CH}$ coupling. δ_H [ppm], HMBC
1	1.36, 1.70 (*m*)	26.5	1.02 (19)
2	1.75, 1.64 (*m*)	26.9	
3	4.37 (*br s*)	78.7	4.84 (1′)
4	2.20, 1.65 (*m*)	36.1	1.70 (6A)
5		75.1	1.65 (4B), 1.70 (6A)
6	1.70, 1.50 (*m*)	35.6	1.02 (19)
7	2.30, 1.35 (*m*)	24.9	1.70 (6A), 1.85 (8)
8	1.85 (*m*)	41.6	2.30 (7A)
9	1.60 (*m*)	40.1	1.85 (8), 1.02 (19)
10		41.8	1.02 (19)
11	1.35, 1.25 (*m*)	22.7	1.60 (9)
12	1.36 (*m*)	40.9	1.00 (18), 2.81 (17)
13		50.9	1.00 (18), 2.81 (17)
14		86.3	1.00 (18), 2.81 (17), 2.10, 1.85 (15)
15	2.10, 1.85 (*m*)	33.3	
16	2.10, 2.00 (*m*)	28.0	2.81 (17)
17	2.818 (*m*)	51.9	2.00 (16B), 1.00(18)
18	1.001 (*s*)	16.3	1.36 (12)
19	1.029 (*s*)	17.3	
20		178.3	5.10 (21B), 6.16 (22), 2.81 (17)
21	5.10, 5.34 (*dd*, 8.4/1.7)	75.3	2.81 (17)
22	6.161 (*br s*)	117.9	2.81 (17)
23		177.2	6.16 (22)
1′	4.841 (*d*, 8.0)	102.1	3.73 (5′), 5.82 (2′)
2′	5.828 (*dd*, 10.2/8.0)	72.7	3.60 (3′), 4.44 (4′)
3′	3.608 (*dd*, 10.1/3.0)	83.5	5.82 (2′), 4.44 (4′), 3.45 (OMe)
4′	4.448 (*br d*, 3.0)	75.2	3.73 (5′)
5′	3.738 (*m*)	71.8	1.55 (6′)
6′	1.557 (*d*, 6.4)	17.3	3.73 (5′)
3′-OMe	3.457 (*s*)	58.5	3.60 (3′)
2′-OAc	2.225 (*s*)	21.1	
2′-OCOMe		172.2	5.82 (2′), 2.22 (COMe)
1″	5.149 (*d*, 7.7)	104.6	4.44 (4′), 3.99 (2″)
2″	3.99	75.9	5.14 (1″)
3″	4.248 (*dd*, 8.8/8.8)	77.9	4.19 (4″)
4″	4.190 (*dd*, 9.4/8.8)	71.8	3.96 (5″)
5″	3.96	78.2	4.36 (6″B), 4.19 (4″)
6″	4.36, 4.60 (*br d*, 11.5)	63.0	3.96 (5″)

Table 2 ^{1}H NMR Spectral Data of Cardenolides 1-3, 5-9 (300, 500 MHz, C_5D_5N)

H-Atom	δ_H [ppm]							
	1	**2**	**3**	**5**	**6**	**7**	**8**	**9**
1		1.44, 2.08 (*m*)	1.42, 2.04 (*m*)	1.50, 2.28 (*m*)	1.48, 2.12 (*m*)	1.48, 2.08 (*m*)		1.56, 1.76 (*m*)
2		1.72, 2.08 (*m*)	1.72, 2.04 (*m*)	1.84 (*m*)	1.76, 2.12 (*m*)	1.78, 2.08 (*m*)		1.22, 1.82 (*m*)
3	4.46 (*br s*)	4.397 (*br s*)	4.373 (*br s*)	4.483 (*br s*)	4.426 (*br s*)	4.424 (*br s*)	4.42 (*br s*)	4.335 (*br s*)
4		1.72, 2.18 (*m*)	1.74, 2.22 (*m*)	1.82, 2.34 (*m*)	1.76, 2.24 (*m*)	1.76, 2.24 (*m*)		1.60, 1.87 (*m*)
5								1.86 (*m*)
6		1.52, 1.90 (*m*)	1.52, 2.22 (*m*)	1.64, 1.98 (*m*)	1.56, 1.94 (*m*)	1.56, 1.96 (*m*)		1.82 (*m*)
7		1.30, 2.28 (*m*)	1.30, 2.28 (*m*)	1.34, 2.34 (*m*)	1.32, 2.34 (*m*)	1.34, 2.31 (*m*)		2.12 (*m*)
8		1.84 (*m*)	1.84 (*m*)	1.96 (*m*)	1.94 (*m*)	1.94 (*m*)		1.78 (*m*)
9		1.64(*m*)	1.64 (*m*)	1.66 (*m*)	1.62 (*m*)	1.62 (*m*)		1.76 (*m*)
11		1.24, 1.38 (*m*)	1.26, 1.40 (*m*)	1.24, 1.50 (*m*)	1.42 (*m*)	1.24, 1.48 (*m*)		1.38 (*m*)
12		1.40 (*m*)	1.40 (*m*)	1.12, 1.18 (*m*)	1.12, 1.18 (*m*)	1.12, 1.18 (*m*)		1.40 (*m*)
15		1.86, 2.08 (*m*)	1.86, 2.08 (*m*)	1.88, 2.18 (*m*)	1.86, 2.12 (*m*)	1.86, 2.10 (*m*)		1.90, 2.12 (*m*)
16		1.96, 2.10 (*m*)	1.96, 2.10 (*m*)	1.84, 2.13 (*m*)	1.78, 2.06 (*m*)	1.78, 2.08 (*m*)		1.98, 2.12 (*m*)
17	2.84 (*dd*, 9/3)	2.817 (*m*)	2.818 (*d*, 8.0)	3.463 (*t*, 9.5)	3.438 (*br dd*, 9.6/9.6)	3.447 (*br dd*, 9.6/9.6)	2.84 (*m*)	2.805 (*m*)
18	0.88 (*s*)	1.036 (*s*)	1.038 (*s*)	1.227 (*s*)	1.198 (*s*)	1.201 (*s*)	1.05 (*s*)	1.021 (*s*)
19	0.94 (*s*)	1.087 (*s*)	1.093 (*s*)	1.186 (*s*)	1.127 (*s*)	1.133 (*s*)	0.99 (*s*)	0.899 (*s*)
21	5.08, 5.36 (*dd*, 18.1/1.4)	5.06, 5.34 (*dd*, 18.1/1.4)	5.06, 5.34 (*dd*, 18.1/1.4)	4.85, 4.99 (*dd*, 17.5/1.4)	4.83, 4.99 (*dd*, 17.6/1.8)	4.83, 4.99 (*dd*, 17.6/1.8)	5.06, 5.36 (*dd*, 18.1/1.4)	5.06, 5.34 (*dd*, 18.1/1.4)
22	6.17 (*br s*)	6.158 (*br s*)	6.159 (*br s*)	6.162 (*br s*)	6.133 (*br s*)	6.131 (*br s*)	6.15 (*br s*)	6.156 (*br s*)
1′		5.465 (*dd*, 9.7/1.4)	5.177 (*dd*, 9.7/1.8)		5.489 (*dd*, 9.6/1.9)	5.186 (*dd*, 9.6/1.9)		5.494 (*dd*, 9.7/1.7)
2′		1.96 (*m*), 2.391 (*br d*, 13.2)	1.74, 2.30 (*m*)		1.99 (*ddd*, 3.2 /9.6/2.6) 2.41 (13.6 /3.6/1.9)	1.92-2.00 2.26-2.34 (*m*)		2.472
3′		4.426 (*d*, 2.7)	3.554 (*d*, 2.9)		4.439 (*d*, 2.6)	3.734 (*d*, 2.9)		4.498 (*d*, 2.9)
4′		3.623 (*dd*, .4/9.3)	3.536 (*dd*, .4/9.3)		3.633 (*m*)	3.562 (*m*)		3.669 (*dd*, 2.4/9.3)
5′		4.305 (*m*)	4.233 (*m*)		4.319 (*dq*, 9.4/6.2)	4.135 (*dq*, 9.4/6.2)		4.368 (*m*)
6′		1.597 (*d*, 6.1)	1.540 (*d*, 6.1)		1.602 (*d*, 6.2)	1.544 (*d*, 6.2)		1.634 (*d*, 6.3)
3′-OMe			3.417 (*s*)			3.417 (*s*)		

Table 3 ^{13}C NMR Spectral Data of Cardenolides 1-3, 5-9 (300, 500 MHz, C_5D_5N)

C-Atom	δ_C [ppm]							
	1	2	3	5	6	7	8	9
1	25.95	26.3	26.2	25.7	26.2	26.0	27.5	30.8
2	28.7	26.6	26.6	28.6	26.6	26.4	28.9	27.1
3	67.9	75.9	75.9	67.8	75.9	75.9	66.1	73.1
4	36.1	35.6	35.6	37.9	35.5	35.4	34.5	30.4
5	74.5	73.8	73.8	74.5	73.9	73.8	36.9	37.0
6	37.9	35.6	35.6	35.9	35.5	35.4	27.5	27.1
7	24.6	24.5	24.5	24.0	24.1	24.0	22.3	21.9
8	41.5	41.1	41.1	40.8	40.9	40.7	42.1	41.8
9	40.1	39.4	39.4	39.3	39.5	39.4	36.0	35.8
10	41.1	41.3	41.3	41.3	41.3	41.1	35.9	35.5
11	22.3	22.2	22.2	21.2	21.3	21.1	21.8	21.5
12	39.3	40.1	40.0	31.1	31.1	31.0	33.4	39.8
13	50.1	50.1	50.1	49.3	49.4	49.2	50.3	50.1
14	84.7	84.7	84.7	85.3	85.3	85.2	84.8	84.6
15	33.3	33.3	33.3	31.6	31.7	31.6	30.6	33.1
16	27.4	27.4	27.4	24.9	25.0	24.9	27.5	27.3
17	51.4	51.4	51.4	48.8	48.9	48.8	51.6	51.4
18	16.4	16.4	16.4	18.6	18.7	18.5	16.4	16.2
19	17.6	17.4	17.4	17.4	17.5	17.3	24.3	23.9
20	175.9	175.9	175.8	172.9	172.8	172.9	174.5	174.6
21	73.8	73.8	73.8	74.2	74.2	73.8	73.8	73.7
22	117.7	117.7	117.7	116.7	116.6	116.6	117.7	117.6
23	174.5	174.5	174.4	174.3	174.2	174.3	175.9	176.1
1′		97.6	97.4		97.5	97.4		96.7
2′		39.9	35.9		39.8	35.8		40.1
3′		68.6	78.8		68.6	78.7		68.7
4′		74.1	74.1		74.1	74.0		74.2
5′		70.7	71.2		70.6	71.1		70.3
6′		19.2	19.2		19.2	19.0		19.1
3′-OMe			58.1			58.0		

Antiproliferative Activity of Cardenolides

Six cardenolides isolated from *Streptocaulon tomentosum* were tested for their antiproliferative activity *in vitro* against MCF-7 (human breast cancer cell line) and L 929 (mouse fibroblast cell line) by acid phosphatase method (Yang *et al*., 1996). The antiproliferative activity of compounds **1, 2, 3, 4, 6** and **8** are summarized in Table 4. Cardenolides **1, 2, 3, 4, 6** and **8** show significant antiproliferative activity against MCF 7 cells (IC_{50} < 1 μM - 15,3 μM after 2 days; IC_{50} < 1 μM - 4,31 μM after 5 days incubation). However, cardenolides **2** and **3** possess considerable activity against L 929 (IC_{50} 24.2 and 32.1 μM after 5 days), while other cardenolides show no activity (IC_{50} > 100 μM). The antiproliferative activities of monoglycosidic cardenolides **2, 3** attached to digitoxose are stronger, while those of **4** attached to a disaccharide is weaker than the activity of the aglycone **1**. In addition, the antiproliferative activities of **2** and **3**

are also stronger than that of **5**. Therefore, the configuration of the γ-lactone ring is also significant. The 17α-configuration of the lactone ring correlates with a weaker effect than the 17β-configuration. Similarly, the induction of apoptosis by compounds **2** and **3** in tumor and U 937 cell lines is stronger in comparison to the other compounds.

Cellular Viability and Cell Cycle Analysis of Cardenolides

Four cardenolides (**2, 3, 6,** and **8**) were examined for cellular viability in the tumor cell line and U 937 (human leukemic cell line) at concentrations 100 μM, 10 μM, and 1 μM. All these four cardenolides show toxicity induction of apoptosis at high concentration (> 10 μM) (Table 5) in both cell lines. Compound **2** is the most detrimental at higher concentration in both of cell lines whereas compounds **6** and **8** show less activity. The most interesting observation is the higher activity of compound **2** against tumor cells vs U 937-cells at low concentration (1 μM). The same cardenolides (**2, 3, 6,** and **8**) were also analysed for the percentage of cells in G0, S, G2, G1 phases of the cell life cycle using flow cytometry. 2 cell lines were used, these are human U 937 myeloid leukemia cell line and tur cell line. Compounds **2** and **3** cause a block at the G_2/M-phase at 100 μM and 10 μM in both of cell lines whereas compounds **6** and **8** block at the G_2/M-phase at 100 μM.

Table 4 Antiproliferative Activities of Constituents Isolated from *S. tomentosum* in MCF-7 (Human Breast Cancer Cell Line) and L 929 (Mouse Fibroblast Cell Line)

No		IC_{50} (μM) (2 days incubation)		IC_{50} (μM) (5 days incubation)	
		MCF-7	**L 929**	**MCF-7**	**L 929**
1	17α-H-periplogenin	5.29	> 100	2.57	> 100
2	17α-H-periplogenin-3-*O*-β-*D*-digitoxoside	< 1	51.5	< 1	24.2
3	17α-H-periplogenin-3-*O*-β-*D*-cymaroside	< 1	64.0	< 1	32.1
4	17α-H-periplogenin-β-glucopyranosyl-(1→4)-2-*O*-acetyl-β-digitalopyranoside	15.3	> 100	4.31	> 100
6	17β-H-periplogenin-*3-O*-β-*D*-digitoxoside	7.19	> 100	3.73	> 100
8	17α-H-digitoxigenin	4.16	> 100	< 1	> 100
control	camptothecin	0,0804	0,179	0,0122	0,0285
control	doxorubicin	0,207	0,359	0,0049	0,0168

Table 5 Cell Viability of Constituents Isolated from *S. tomentosum* in U 937 (Human Leukemic Cell Line) and Tumor Cell in %.

compound	Cell Viability (%)					
	U 937			Tumor		
	100 μM	10 μM	1 μM	100 μM	10 μM	1 μM
2	14,60	26,10	82,80	21,50	11,10	69,50
3	26,90	28,90	68,10	42,30	11,50	27,60
6	28,60	93,90	97,10	28,00	70,20	91,20
8	26,70	77,50	97,30	28,90	32,10	89,80
control (1% DMSO)	98,20	98,40	98,70	94,30	94,30	96,10

Conclusion

Some cardenolides isolated from the roots of *Streptocaulon tomentosum* Wight show strong antiproliferative activity. Among six cardenolides, 17α-H-periplogenin-3-*O*-β-*D*-digitoxoside, and 17α-H-periplogenin-3-*O*-β-*D*-cymaroside exhibit significant antiproliferative activity (IC_{50} values, < 1μM) against MCF-7. Four cardenolides were examined for their cellular viability in the tumor cell and U 937 (human leukemic cell line) at concentrations 100 μM, 10 μM, and 1 μM. All these four cardenolides show the induction of apoptosis at 100 μM and 10 μM in both cell lines. So the roots of *Streptocaulon tomentosum* Wight may be useful for the treatment of anticancer.

Acknowledgements

The authors acknowledge Dr Pho Kaung, Rector, University of Yangon for his kind permission to carry out this research and also thank to Dr Ni Ni Than (Professor

and Head), Department of Chemistry, University of Yangon.

References

Danieli, N., Mazur, Y., and Sondheimer, F. (1966). "The Synthesis of Digitoxigenin". *Tetrahedron*, vol. 22, pp.3189-3193.

Furuya, T., Kawaguchi, K., and Hirotani, M. (1988). "Studies on Plant-tissue Cultures. 55. Biotransformation of Digitoxigenin by Cell-suspension Cultures of *Strophanthus gratus*". *Phytochemistry*, vol.27, pp.2129-2133.

Kawaguchi, K., Hirotani, M., and Furuya, T. (1988). "Biotransformation of Digitoxigenin by Cell Suspension Cultures of *Strophanthus amboensis*". *Phytochemistry*, vol.27, pp.3475-3479.

López-Lázaro, M., Pastor, N., Azrak, S.S., Ayuso, M.J., Austin, C.A., and Cortés, F. (2005). "Digitoxin Inhibits the Growth of Cancer Cell Lines at Concentrations Commonly Found in Cardiac Patients". *Journal of Natural Products*, vol. 68, pp. 1642–1645.

Ueda, J.Y., Tezuka, Y., Banskota, A.H., Tran, Q.L., Tran, Q.K., Saiki, I., and Kadota, S. (2003a). "Constituents of the Vietnamese Medicinal Plant *Streptocaulon juventas* and their Antiproliferative Activity against the Human HT-1080 Fibrosarcoma Cell". *J. Nat. Pro,*.vol. 66, pp.1427-1433.

Ueda, J.Y., Tezuka, Y., Banskota, A.H., Tran, Q.L., Tran, Q.K., Saiki, I., and Kadota, S. (2003b). "Antiproliferative Activity of Cardenolides Isolated from *Streptocaulon juventas*". *Biol. Pharm. Bull*, vol.26, pp.1431-1435.

Yang , T.T., Sinai, P., and Kain, S.R. (1996). "An Acid Phosphatase Assay for Quantifying the Growth of Adherent and Nonadherent cells". *Anal Biochem*, vol. 241(1), pp. 103-8.

DEGRADATION OF METHYLENE BLUE DYE IN AQUEOUS SOLUTION USING GREEN SYNTHESIZED NANO-SIZED ZnO PARTICLES

Khin Mar Cho[1], Aye Thet Khine[2]

Abstract

This research deals with degradation of methylene blue (MB) dye in aqueous solution using green synthesized nano-sized ZnO particles. The aim of this research is to prepare, characterize and study the degradation efficacy of green synthesized nano-sized ZnO particles. Leaves of Ma-yo-gyi (*Calotropis gigantea* L.) were collected from Kathitkan village in Aung Lan Township, Magway Region, Myanmar. Nano-sized ZnO particles were synthesized from zinc nitrate and zinc acetate sources using aqueous leaves extract of Ma-yo-gyi as a reducing agent via green synthesis. The green synthesized nano-sized ZnO particles were characterized by TG-DTA, XRD, SEM and TEM techniques. The effects of calcination temperature on the preparation and average crystallite size of particles were also studied. The green synthesized nano-sized ZnO particles have hexagonal phase with average crystallite size of (24-34) nm. Supported SEM and TEM images by the degradation efficacy of green synthesized nano-sized ZnO particles on MB nethylene blue(MB) dye were studied via various parameters such as effect of pH (3, 4, 5, 6, 7 and 8), effect of contact time (0, 30, 60, 90, 120, 150 and 180 min) and effect of dosage of nano-sized ZnO particles (0.02, 0.03, 0.04 and 0.05 g). Dye removal activity was highest at pH 7 using both of green synthesized nano-sized ZnO particles. From the contact time experiment, at the end of the reaction (after 180 min), MB dye removal efficacy was upto 80-85 % of its initial value. Degradation percent of MB dye solution increased gradually with an increase in dosage of nano-sized ZnO particles.

Keywords : Nano-sized ZnO, Ma-yo-gyi, methylene bue dye, degradation

Introduction

The green synthesis of metal oxide nanoparticles using biological material as the reducing and stabilizing agents has attracted a lot of attention and consideration in the field of pharmaceuticals and biomedical sectors as compared to the toxic chemical and physical methods due to the usage of ecofriendly, non-toxic and safe reagents during the green synthesis process (Tamanna *et al*., 2015). Furthermore, synthesis in plants tends to be faster than microorganisms, is more cost-effective and is relatively easy to scale up for the production of large quantities of nanoparticles (Shah *et al*., 2015). Zinc oxide nanoparticles have received considerable attention due to their unique antibacterial, antifungal, and UV filtering properties, high catalytic and photochemical activity (Shabnan *et al*., 2019). Photocatalytic activity of nanoparticles offers a promising method for wastewater treatment and ZnO nanoparticles behave as wastewater purifiers (Jawad *et al*., 2018). Methylene blue is one of the most common organic pollutants discharged from the industries directly or indirectly into water sources causing water pollution. ZnO exhibits very good photochemical reactivity and efficiently degrades toxic water pollutants released from textile and dying industries by utilizing natural source of energy, sunlight. This is due to the presence of many active sites and fabrication of hydroxyl radicals on ZnO surface (Tamanna *et al*., 2015). When the ZnO nanoparticles are irradiated with UV light, valence band electrons are excited to the conduction band, which leaves holes behind. Then the generated holes create hydroxyl radicals by oxidizing H_2O and OH^- and the excited electrons are captured by oxygen in the air. The resulting anionic radicals are highly reactive and degrade the organic dyes into carbon dioxide and water (Isik *et al.*, 2019). The objective of this study was to study the synthesis, characterization and the effectiveness of green synthesized zinc oxide

[1] Dr, Associate Professor, Department of Chemistry, University of Yangon
2. MRes Candidate, Department of Chemistry, Pyay University

nanoparticles as catalyst for the removal of Methylene Blue (MB), a cationic dye from aqueous solutions. Laboratory batch studies were conducted to estimate the dye degradation efficacy using the nano-sized ZnO particles via the effect of dosage, effect of pH and effect of contact time on the degradation of MB dye.

Materials and Methods

Sample Collection and Scientific Classification of Ma-yo-gyi

The leaves of Ma-yo-gyi were collected from Kathitkan village, Aunglan Township in Magway Region, Myanmar. The botanical name was identified in Department of Botany, Pyay University. *Calotrophis gigantea* L. is also known as Crown flower plant, Maddar, Rui. It is a large shrub growing to 4 m tall. Largely found in Cambodia, Indonesia, Malaysia, Philippines, Thailand, Sri Lanka, India, China and Pakistan. Botanical name of Ma-yo-gyi is *Calotropis gigantea* L(Chandrabhan *et al.*, 2011). Figure 1 shows the plant of Ma-yo-gyi.

Figure 1 *Plant of Ma-yo-gyi*

Preparation of Nano-sized ZnO Particles by Green Synthesis

(a) Preparation from zinc nitrate as precursor

Ma-yo-gyi leaves extract was prepared by placing 10 g of cleaned and dried crushed leaves in 250 mL glass beaker along with 100 mL of distilled water. The mixture was then boiled for 20 min until the color of aqueous solution changed from watery to brown-yellow. Then, the mixture was cooled to room temperature and filtered with Whatman No. 1 filter paper.

For the synthesis of nano-sized ZnO particles, 50 mL of aqueous leaves extract of Ma-yo-gyi was taken and boiled to 60-80 ºC using a magnetic stirrer heater. Zinc nitrate (5 g) was added to the boiled solution and maintained the temperature about 80 ºC. This mixture was continued boiling until it reduced to a deep yellow coloured paste. This paste was then collected in a ceramic crucible and calcined in muffle furnace at 200, 300, 400, 500 and 600 ºC for 2 h. A white coloured powder was obtained and this was carefully collected and stored in air-tight container.

(b) Preparation from zinc acetate as precursor

The nano-sized ZnO particles were also green synthesized from zinc acetate. Briefly, zinc acetate (2 M) was prepared in 50 mL of deionized water under constant stirring conditions. After complete dissolution of the mixture, 1 mL of 25 % aqueous leaves extract of Ma-yo-gyi and 50 mL of 2 M NaOH were added to the prepared solution of zinc acetate. The mixture was stirred continuously for 2 h on magnetic stirrer resulting in white precipitate. The precipitate was filtered and washed repeatedly with distilled water and then, followed by ethanol in order to remove the impurities. Finally, a white-grey powder ZnO was obtained after overnight drying of the purified precipitate at 60º C in oven. It was calcined in muffle furnace at 500 ºC for 2 h and white powder ZnO was obtained.

Characterization of the Green Synthesized Nano-sized ZnO Particles

The green synthesized nano-sized ZnO particles from two metal sources were characterized by TG-DTA, XRD, SEM and TEM techniques.

Investigation on Degradation of Methylene Blue Dye by using the Green Synthesized Nano-sized ZnO Particles

The wavelength of maximum absorption (λ_{max}) should be necessarily determined prior to the quantization of a substance by UV-visible spectrophotometry (Dod, 1967). UV-vis spectrophotometer (UV-vis 240, Shimadzu) was used throughout the degradation experiments. The wavelength of maximum absorption (λ_{max}) of MB solutions was recorded at wavelength range of 500-700 nm and standard calibration curve was constructed at λ_{max} 664 nm using 0.2-1.0 $\times$ 10^{-5} M MB solution at pH 5. Degradation experiments were conducted via effect of dosage, effect of pH, effect of contact time. A 0.04 g of prepared nano-sized ZnO particles was separately added into 250 mL capacity of six clean and dry beakers each containing 50 mL of 2.97 x 10^{-5} M methylene blue solution at pH of 3, 4, 5, 6, 7 and 8 by adjusting with 0.01 M HCl and NaOH solutions. The mixtures were stirred for 120 min and sampling out 10 mL and centrifuged immediately the sampling mixture at 100 rpm for 20 min to obtain the clear blue solution. The absorbance of each solution was measured at wavelength 664 nm using UV-Vis spectrophotometer. In the effect of contact time experiment, after the pH was adjusted at 7 and the solution was taken out 10 mL in every 15 min interval. In effect of dosage experiment, 0.02, 0.03, 0.04 and 0.05 g of prepared nano-sized ZnO particles was separately added into beakers each containing 50 mL of 2.97 x 10^{-5} M methylene blue solution at pH 7. The absorbance of each solution was recorded according to above procedure.

Results and Discussion

Characterization of the Green Synthesized Nano-sized ZnO Particles by TG-DTA Analysis

Thermal stability of green synthesized nano-sized ZnO particles from nitrate salt was investigated by TG-DTA technique (Figure 2). TGA data of the prepared nano-sized ZnO particles before calcination showed the total weight loss 52.98 % in the temperature range of 38.59-601.76 °C. This is attributed to the evaporation of trapped water in the crystal, decomposition of organic residue and zinc nitrate to zinc oxide in the preparation of green synthesized zinc oxide. The DTA curve indicated the two endothermic peaks at 139.56 °C and 198.98 °C corresponding to the loss of trapped water, decomposition of organic matter in sample. The small exothermic peak at 369.97 °C was related with decomposition of organic residue. TG-DTA data indicated that the green synthesized nano-sized ZnO particles were found to be thermally stable in the temperature range of 460-500 °C.

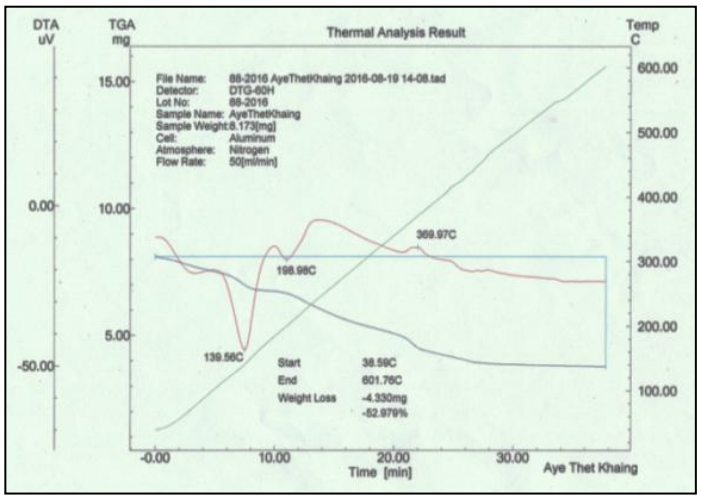

Figure 2 TG-DTA thermogram of the green synthesized ZnO from zinc nitrate

Characterization of the Green Synthesized Nano-sized ZnO Particles by XRD

Figures 3 (a) - (e) show the XRD diffractograms of the calcined ZnO nanoparticles synthesized from nitrate source at different calcination temperatures of 200, 300, 400, 500 and 600 °C respectively. **Figure. 3** (a) shows the XRD diffractogram of the green synthesized ZnO nanoparticles obtained at calcination temperature of 200 °C which is matched with the PDF file of 80-0074 of ZnO. It can be seen not only ZnO peak but also other phases were present due to incomplete formation of ZnO. Figure 3 (b) shows the XRD diffractogram of the calcined ZnO nanoparticles at calcination temperature of 300 °C. There are nine typical diffraction peaks, (100), (002), (101), (102), (110), (103), (200), (112) and (201) which may be assigned to the characteristic peaks of hexagonal ZnO crystal and are matched with library card number 80-0074 of ZnO. Some of the $Zn(NO_3)_2$ were transformed to ZnO, but other phases still exist. Figure 3 (c) shows the XRD diffractogram of the calcined ZnO nanoparticles at calcination temperature of 400°C. There are nine typical diffraction peaks, (100), (002), (101), (102), (110), (103), (200), (112) and (201) which may be assigned to the characteristic peaks of hexagonal ZnO crystal and are matched with PDF library card number 80-0074 of ZnO. Most of the $Zn(NO_3)_2$ are transformed to ZnO, but a few other phases still exist. This may be due to the presence of some impurities in the sample preparation.

The XRD diffractogram of the calcined ZnO nanoparticles at 500 °C is shown in Figure 3 (d). There are nine typical diffraction peaks, which may be assigned to the characteristic peaks of hexagonal ZnO crystal and are matched with the PDF library card number 89-1397 of ZnO. The ZnO crystals were developed at this temperature, it can be said that $Zn(NO_3)_2$ were completely transformed to ZnO. So that, transformation of $Zn(NO_3)_2$ to ZnO between temperature 400-500 °C and it is also consistent with TG-DTA data. At calcination temperature of 600°C, the XRD diffractogram of the calcined ZnO nanoparticles is shown in **Figure 3** (e) with nine typical diffraction peaks, which may be assigned to the characteristic peaks of hexagonal ZnO crystal and are matched with the PDF library card number 89-1397 of ZnO. From the study on effect of calcination on preparation of green synthesized ZnO nanoparticles, diffraction angles (2θ) of hkl planes were increased with increased in calcination temperature from 200 to 500 °C and slightly decreased at the calcination temperature 600°C. As the diffraction angle (2θ) increase, crystallite sizes of ZnO nanoparticles also increased with increased in calcination temperature. When calcination temperature reached 600 °C, the diffraction angle slightly decreased and average crystallite size also decreased. This may be due to agglomeration slightly occurring due to the presence of phytochemicals that can stabilize the nanoparticles formed.

The XRD diffractogram of nano-sized ZnO particles from zinc acetate source after calcined at 500 °C is shown in **Figure 4**. There are nine typical diffraction peaks, (100), (002), (101), (102), (110), (103), (200), (112) and (201) which may be assigned to the characteristic peaks of hexagonal ZnO crystal and are matched with library card number 89-1397 of ZnO. High purity and crystallinity of nano-sized ZnO particles was obtained at this temperature.

Characterization of Green Synthesized Nano-sized ZnO Particles by SEM and TEM

The morphologies of green synthesized nano-sized ZnO particles from zinc nitrate source, ZnO (I) and zinc acetate source, ZnO (II) after calcined at 500 ºC for 2 h were investigated by SEM and TEM techniques. **Figures 5**(a and b) show the SEM images of green synthesized nano-sized ZnO particles from zinc nitrate and zinc acetate sources, ZnO (I) and ZnO (II), after calcined at 500 ºC for 2 h, respectively. According to SEM micrographs of green synthesized nano-sized ZnO particles, the green synthesized nano-sized ZnO (I) have porous nature where those of ZnO (II) have aggregate and dense particles.

Figures 6 (a) and (b) show the TEM images of green synthesized ZnO particles from zinc nitrate source, ZnO (I) and zinc acetate source, ZnO (I) and ZnO (II) after calcined at 500 ºC for 2 h. According to TEM images, the green synthesized nano-sized ZnO (I) has within the nano scale 21.70-37.29 nm and ZnO (II) has 31.25-35.71 nm. The size distribution of green synthesized of ZnO particles from TEM images were closed to XRD data.

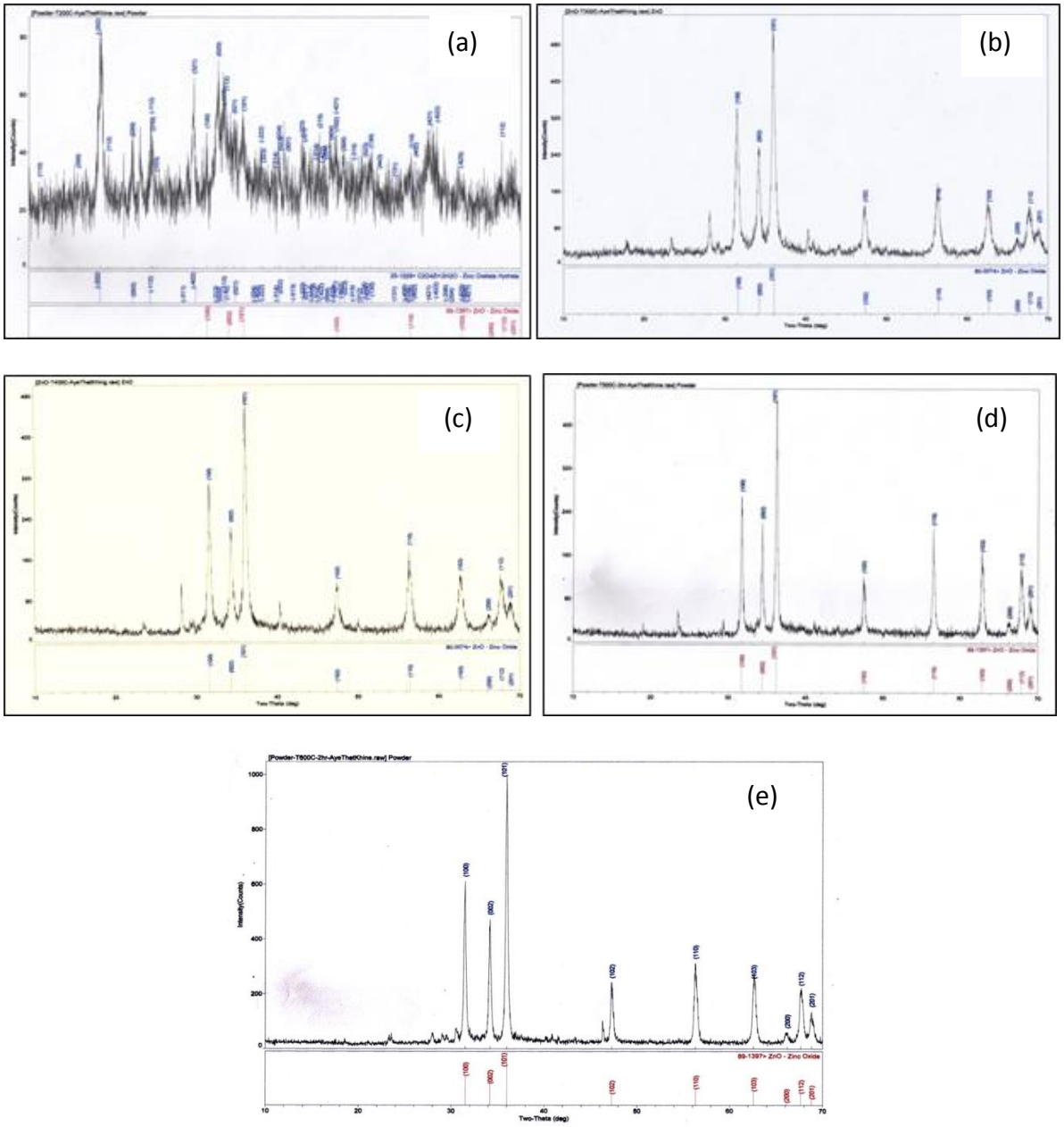

Figure 3 X-ray diffractograms of the green synthesized nano-sized ZnO particles from zinc nitrate source after calcination at (a) 200 ºC (b) 300 ºC (c) 400 ºC (d) 500 ºC (e) 600 ºC

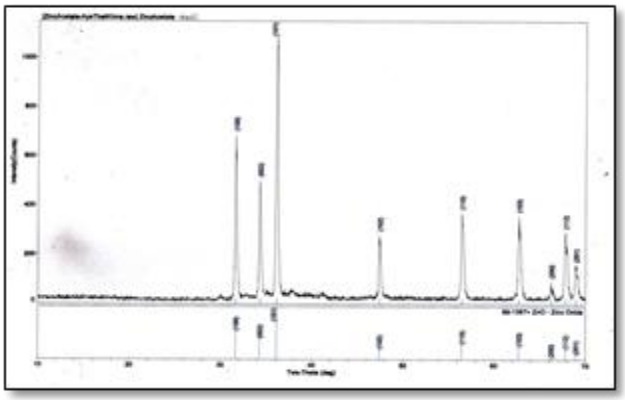

Figure 4 X-ray diffractogram of the green synthesized nano-sized ZnO particles from zinc acetate source after calcination at 500 ºC

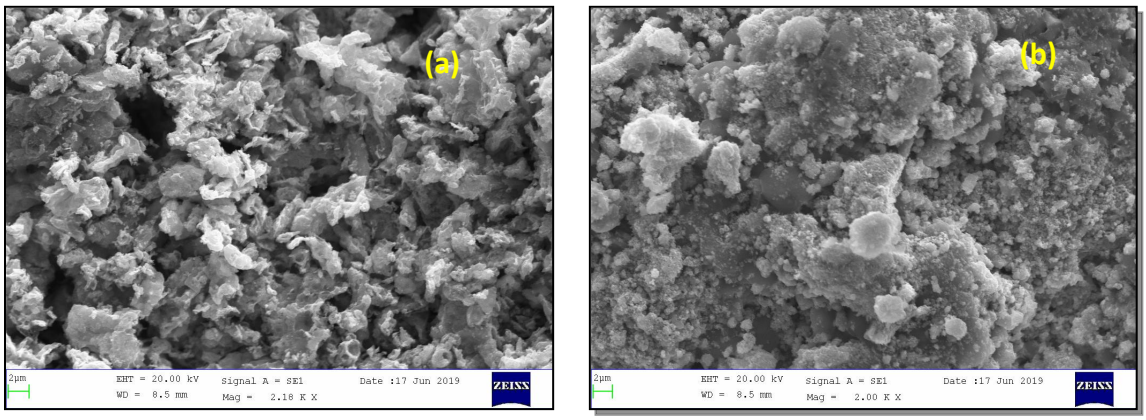

Figure 5 SEM images of the green synthesized nano-sized ZnO particles (a) ZnO (I) (b) ZnO (II) after calcined at 500 ºC

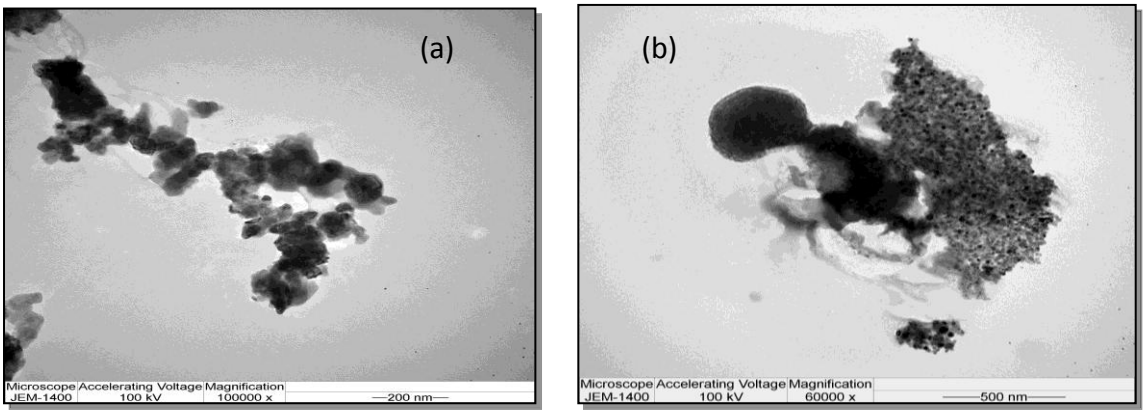

Figure 6 TEM images of the green synthesized nano-sized ZnO particles after calcined at 500 ºC (a) ZnO (I) and (b) ZnO (II)

Average crystallite sizes of the green synthesized nano-sized ZnO particles

The average crystallite sizes of green synthesized nano-sized ZnO particles were calculated from XRD data by using Debye-Scherrer equation. After calcined at 400 °C, amorphous nature disappeared and crystalline nature of ZnO appeared but its crystal structure has some impurities peaks. When the calcination temperature was higher than 500 °C, the XRD patterns showed the strong diffraction peaks of ZnO. Moreover, the characteristic peaks of ZnO become sharper and stronger when the calcination temperatures changed from 300 to 400, 500 and 600 °C, indicating that ZnO were getting better nanocrystalline size. The size data revealed

that the crystallite size increased with the increase in the final calcination temperature. Their difference in crystallization and crystallite size could be mainly attributed to the relative calcination temperature. The average crystallite sizes of green synthesized nano-sized ZnO particles from nitrate source at different calcinations temperature were calculated to be 24.82 nm at 300 °C, 25.99 nm at 400 °C, 31.26 nm at 500 °C and 30.31 nm at 600 °C, respectively. It was found that average crystallite size increase with increase in calcination temperature up to 500 °C but decreased in calcination temperature of 600 °C. It may be due to agglomeration in the calcination process. However, the average crystallite sizes of green synthesized nano-sized ZnO particles from acetate source after calcinations at 500 °C the average crystallite sizes were found to be 34.21 nm. The data are shown in Table 1. In order to obtain smaller ZnO particles with well-developed crystal structures, calcination temperature of 500 °C was chosen for the study the application of nano-sized ZnO particles.

Table 1 Average Crystallite Size of the Green Synthesized Nano-sized ZnO Particles at Different Calcination Temperatures

Metal Source	Calcination Temp. (ºC)	Average Crystallite Size (nm)
Zinc nitrate	300	24.82 (17.30-33.33)
	400	25.99 (22.10-30.37)
	500	31.26 (24.65-37.81)
	600	30.31 (24.79-35.13)
Zinc acetate	500	34.21 (30.47-38.96)

Degradation Efficacy of Green Synthesized Nano-sized ZnO (I) and ZnO (II) on Methylene Blue Dye

In this work, the absorption spectra of MB dye (0.2-1.0 × 10^{-5} M at pH 5) were recorded in the wavelength range of 500-700 nm. It was observed that the wavelength of maximum absorption was 664 nm. Standard calibration curve for methylene blue dye at various concentrations (1.0 ×10^{-5}, 0.8 × 10^{-5}, 0.6 × 10^{-5}, 0.4 × 10^{-5} and 0.2 × 10^{-5} M) was constructed. Removal efficacy was calculated by the equation, A_0-A/A_0 x 100, where A_0 is the absorbance of MB solution without nano-sized ZnO particles and A is the absorbance of the MB solution in reaction mixture with nano-sized ZnO particles after irradiation for time t. The degradation efficacy of green synthesized nano-sized ZnO particles was performed and assessed by evaluating the degradation of MB dye as model contaminant under daylight. The degradation efficacy was studied by employing the green synthesized nano-sized ZnO (I) and ZnO (II) in order to study the degradation of aqueous solution of methylene blue dye via effect of contact time, effect of pH and effect of dosages. Figure 7 shows UV-visible absorption spectra of MB dye showing degradation efficacy at different time intervals (0, 30, 60, 90, 120, 150, 180 min up to overnight) using green synthesized nano-sized ZnO particles from nitrate salt, ZnO (I) under day light without controlling any parameters. It has been observed that the characteristic absorption peak of MB at 664 nm diminishes sharply indicated that green synthesized nano-sized ZnO particles act as photocatalyst for degradation of MB dye.

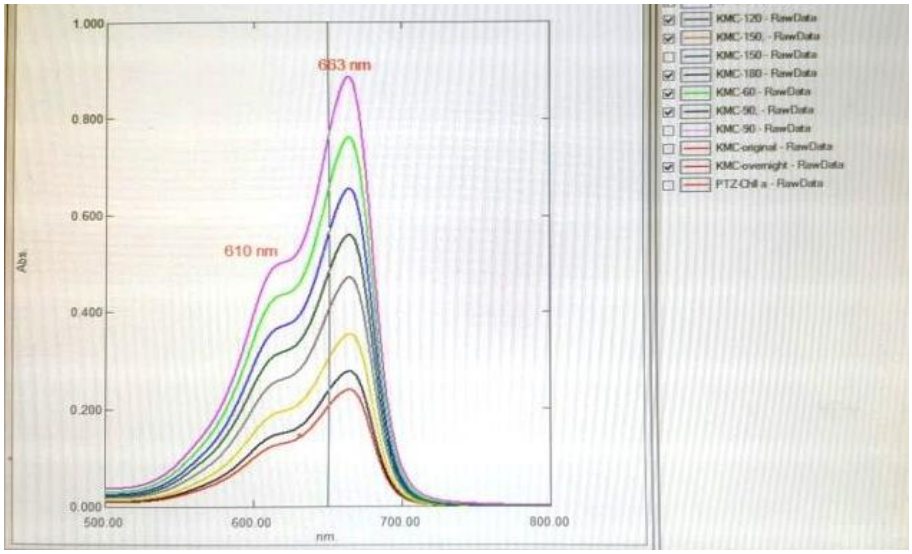

Figure 7 UV-visible absorption spectra of methylene blue dye showing removal efficacy of green synthesized nano-sized ZnO particles from nitrate source, ZnO (I) at different time intervals

Effect of pH

Effect of pH on removal of MB dye under daylight was studied via 50 mL of 2.97×10^{-5} M MB dye solution using of 0.04 g green synthesized nano-sized ZnO particles at various pH after 2 h contact time. Removal efficacy was found to be 21.08 %, 21.31 %, 25.25 %, 31.79 %, 80.38 % and 73.73 % of MB dye by using green synthesized nano-sized ZnO particles synthesized from nitrate source, ZnO (I) and 35.12 %, 40.30 %, 43.40 %, 65.78 %, 68.21 % and 32.98 % of MB dye by using nano-sized ZnO particles synthesized from acetate source, ZnO (II) at various pH of 3, 4, 5, 6, 7 and 8, respectively shown in Table 2 and Figure 8(a). Dye removal activity was highest at pH 7 using both of nanoparticles.

Effect of contact time

Effect of contact time on degradation of 2.97×10^{-5} M/100 mL MB dye solutions was studied at different time interval (0, 30, 60, 90, 120, 150, 180 min) using 0.1 g of green synthesized nano-sized ZnO particles at pH 7. The degradation efficiency of nano-sized ZnO particles as percent degradation was plotted as a function of time shown in Table 3 and Figure 8(b). The percent degradation of MB under daylight were 60.32 %, 72.77 %, 74.86 %, 84.49 %, 84.67 % and 84.89 % using green synthesized nano-sized ZnO particles synthesized from nitrate source, ZnO (I) and 70.07 %, 71.48 %, 73.90 %, 79.48 %, 79.93 % and 80.44 % using green synthesized nano-sized ZnO particles synthesized from acetate source, ZnO (II) at 0, 30, 60, 90, 120, 150 and 180 min contact time, respectively. Interestingly, methylene blue was degraded to 60 % of its initial value within first 30 min of exposure and degradation was increased up to 120 min, after that few degradation of dye was observed (Table 3). At the end of the reaction after 180 min, MB dye removal efficacy was up to 85 % of its initial value. This is in good match with the observed decolourization of MB in first 30 min (Tamanna *et al.,* 2015).

Effect of dosage of nano-sized ZnO particles

Effect of dosage on removal of MB dye under daylight was studied via 2.97 $x10^{-5}$ M/50 mL MB dye solution using various dosage of green synthesized nano-sized ZnO particles at contact time 2 h. Different amounts of nano-sized ZnO particles were used (0.02 to 0.05 g) and the results are given in Table 4 and Figure 8(c). Removal percent of methylene blue dye solution increased gradually with an increase in dosage of nano-sized ZnO particles. The removal percent of methylene blue dye using green synthesized nano-sized ZnO particles at dosages of 0.02, 0.03, 0.04 and 0.05 g were found to be (50.78 %, 59.47 %, 70.41 %, 79.65 %) using nano-sized ZnO (I) and (53.95 %, 66.85 %, 71.53 %, 82.13 %) using nano-sized ZnO (II), respectively. This study provides proof of concept for nano-sized ZnO particles, ZnO (I) and ZnO (II) to be used as efficient degrading agent in environmental remediation applications.

Table 2 Percent Removal of MB Dye at Various pH using Nano-sized ZnO particles

No.	pH	Absorbance at 664 nm		Percent Removal (%)	
		ZnO (I)	ZnO (II)	ZnO (I)	ZnO (II)
1	3	1.400	1.151	21.08	35.12
2	4	1.396	1.059	21.31	40.30
3	5	1.326	1.004	25.25	43.40
4	6	1.210	0.607	31.79	65.78
5	7	0.348	0.564	80.38	68.21
6	8	0.466	1.189	73.73	32.98

Table.3 Percent Removal of MB Dye at Various Contact Time

No.	Contact time (min)	Absorbance at 664 nm		Percent Removal (%)	
		ZnO (I)	ZnO (II)	ZnO (I)	ZnO (II)
1	0	1.774	1.774	-	-
2	30	0.704	0.531	60.32	70.07
3	60	0.483	0.506	72.77	71.48
4	90	0.446	0.463	74.86	73.90
5	120	0.275	0.364	84.49	79.48
6	150	0.272	0.356	84.67	79.93
7	180	0.268	0.347	84.89	80.44

Table.4 Percent Removal of MB Dye with Various Dosages of Nano-sized ZnO particles

No.	Dosage (g)	Absorbance at 664 nm		Percent Removal (%)	
		ZnO NPs (I)	ZnO NPs (II)	ZnO NPs (I)	ZnO NPs (II)
1	0.02	0.873	0.817	50.78	53.95
2	0.03	0.719	0.588	59.47	66.85
3	0.04	0.525	0.505	70.41	71.53
4	0.05	0.361	0.317	79.65	82.13

Where, ZnO NPs (I) and ZnO NPs (II) are nano-sized ZnO particles green synthesized from zinc nitrate source and zinc acetate source after calcined at 500 ºC for 2 h

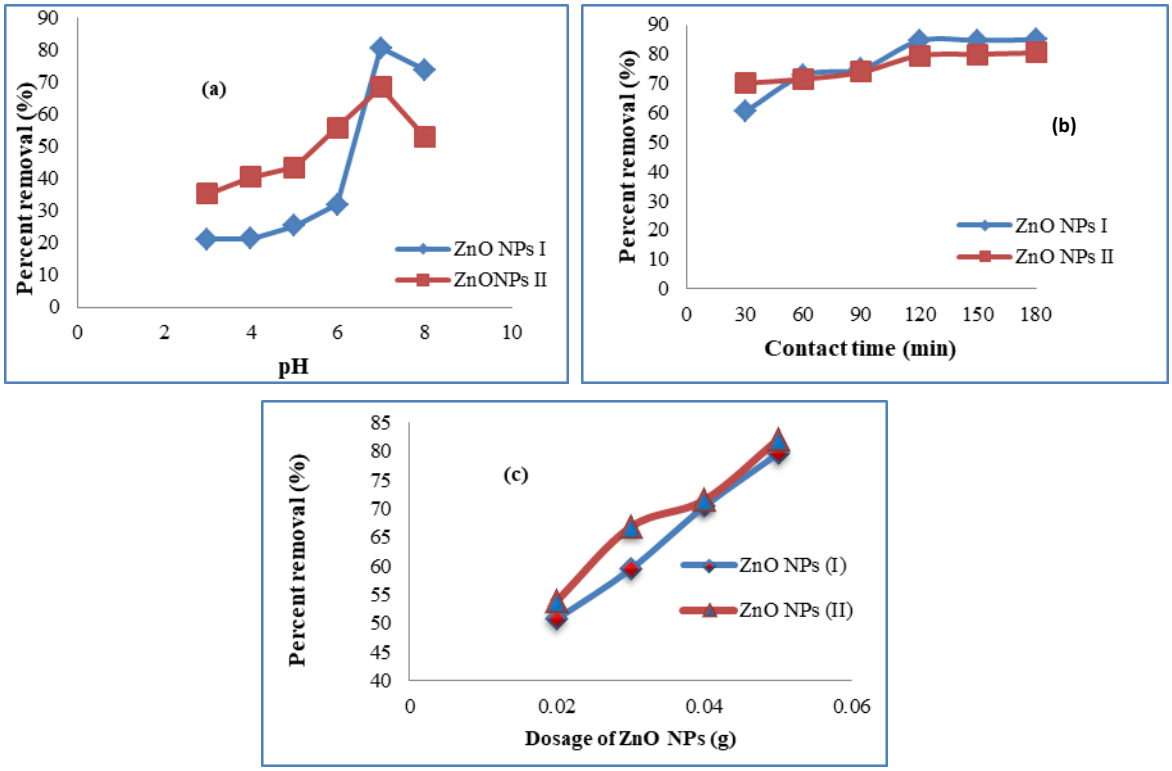

Figure 8 Changes of percent removal of MB dye (a) at various pH using nano-sized ZnO particles (b) at various contact time (c) with various dosage of nano-sized ZnO particles

Conclusion

The present research reported eco-friendly and inexpensive approach for the green synthesis of nano-sized ZnO particles from zinc nitrate and zinc acetate sources using aqueous leaves extracts of Ma-yo-gyi, which act as an effective reducing and stabilizing agent. TG-DTA data of green synthesized zinc oxide from zinc nitrate source revealed the decomposition of $Zn(NO_3)_2$ to ZnO start at 369.9 ºC and completely formed zinc oxide between 400-500 ºC. XRD data confirmed complete formation of pure zinc oxide at 500 ºC with hexagonal phase. The green synthesized nano-sized ZnO particles from two sources have average crystallite size in the range of 24-34 nm with hexagonal structure. SEM and TEM images of the green synthesized zinc oxide from zinc nitrate source and zinc acetate source confirmed the XRD data. It was found that the green synthesized nano-sized ZnO particles form zinc nitrate source have nanoporous and those from zinc acetate source have aggregate particles. From the study on the effect of calcination temperature on average crystallite size of green synthesized nano-sized ZnO particles from zinc nitrate source, average crystallite size increased with increased in calcination temperature up to 500 ºC and at 600 ºC, small decreased in size due to agglomeration of particles in the preparation step. From this finding, calcination temperature was chosen at 500 ºC for green synthesized nano-sized ZnO particles from zinc acetate source. The degradation efficacy of green synthesized nano-sized ZnO particles prepared from two metal sources on degradation of methylene blue dye provided proof of concept for green synthesized nano-sized ZnO particles to be used as efficient degrading agent for environmental remediation application.

Acknowledgements

The authors would like to mention their sincere thanks to Dr Tun Cho, Professor of Head of Department of Chemistry from Pyay University for providing research facilities and Myanmar Academy of Arts and Science Association for submission of this research paper.

References

Chandrabhan, S., Sumint, S., T. and Santosh, K.V. (2011). "Antibacterial Efficacy and Phytochemical Analysis of Organic Solvent Extracts of *Calotropis gigantea*". *J. Chem. Pharm. Res*., vol. 3 (6), pp. 330-336

Dod, R. E. (1967). *Chemical Spectroscopy*. New York: Elsevier Pub. Co., pp. 292-300

Jawad, A., Rabia, I., Baoshan, L., Kamran, T., Aftab, A., Muhammad, S., Naeem, U., K. and Zia, U. H. K. (2018). "Synthesis and Characterization of Phytochemical Fabricated Zinc Oxide Nanoparticles with Enhanced Antibacterial and Catalytic Applications". *Journal of Photochemistry and Photobiology, B : Biology*. vol.183, pp.349-356

Shabnan, F., Mina, J. and Hassan K. F., (2019). "Green Synthesis of Zinc Oxide Nanoparticles: A Comparison, *Green Chemistry Letters and Review*, vol. 12 (1), pp. 19-24

Shah, M., Fawcett, D., Sharma, S., Tripathy, S. K. and Poinern, G. E. J. (2015). "Green Synthesis of Metallic Nanoparticles via Biological Entities". *Materials*, vol.8, pp. 7278-7308

Tamanna, B., Mishra, K, Khanuja, M., and Prasad, R. (2015). "Biosynthesis of Zinc Oxide Nanoparticles from *Azadirachta Indica* for Antibacterial and Photocatalytic Applications". *Material Science in Semiconductor Processing*, vol. 32, pp. 55-61

Isik, T., Hilal, M. E. and Horzum, N. (2019). "*Green Synthesis of Zinc Oxide Nanostructures: Zinc Oxide Based Nanomaterials and Devices*". pp.1-29

http://dx.doi.org/10.5772/intechopen.83338 (accessed 7June 2019)

EFFECT OF *TRICHODERMA* INOCULATED COMPOST IOFERTILIZER ON THE GROWTH AND YIELD OF BRINJAL

Thet Su Min[1], Nyo Nyo Win[2]

Abstract

The present work deals with the study on the effect of *Trichoderma* inoculatedcompost biofertilizer on growth and yield of Brinjal (*Solanum melongena*). Tthe processing of compost biofertilizer was carried out by utilization of *Trichoderma* substrate (Yezin Isolate)based on farm waste bedding materials namely rice straw, cow dung and rice bran. Physicochemical properties of cow dung, rice straw and prepared compost biofertilizer were determined by conventional method and modern technique. Field experiment was conducted at Water Utilization Research Section, Department of Agricultural Research, Yezin and laid out in Randomized Complete Block (RCB) design with four treatments and five replications. Four treatments were T1 (chemical fertilizer), T2 (30% biofertilizer), T3 (chemical fertilizer with 30% biofertilizer), T4 (control without fertilizer). Analytical assays of the untreated soil and the prepared fertilizer treated soil were also carried out before sowing and after harvesting. The effect of prepared fertilizers on the growth of brinjal plant was studied on the basis of growth parameters and total yield were estimated. Among these treatments, T3(chemical fertilizer with 30% biofertilizer) was able to produce the highest yield of 8995.58 kg/ha compared with other treatments including control without fertilizer, the lowest yield of 6290.38 kg/ha. According to this study, 30% compost biofertilizer treatment produced the second highest yield of brinjal (7458.13 kg/ha).This study indicated that a combination treatment of biofertilizer and chemical fertilizer had significant effect on the yield and growth of brinjal. Therefore, *Trichoderma* inoculated compost can also be used as biofertilizer to reduce on chemical inputs in the perspective of sustainable agriculture and conservation of natural resources.

Keywords: *Trichoderma* inoculated compost biofertilizer, brinjal, growth and yield

Introduction

Plant nutrients are essential for the production of crops and healthy food for the world's expanding population. Plant nutrients are therefore a vital component of sustainable agriculture. Increased crop production largely relies on the type of fertilizers used to supplement essential nutrients for plants. The nature and the characteristics of nutrient release of chemical, organic and biofertilizers are different, and each type of fertilizer has its advantages and disadvantages with regard to crop growth and soil fertility. For optimum plant growth, nutrients must be available in sufficient and balanced quantities.

Soils contain natural reserves of plant nutrients, but these reserves are largely in forms unavailable to plants, and only a minor portion is released each year through biological activity or chemical processes. This release is too slow to compensate for the removal of nutrients by agricultural production and to meet crop requirements. Therefore, fertilizers are designed to supplement the nutrients already present in the soil. The use of chemical fertilizer, organic fertilizer or biofertilizer has its advantages and disadvantages in the context of nutrient supply, crop growth and environmental quality. The advantages need to be integrated in order to make optimum use of each type of fertilizer and achieve balanced nutrient management for crop growth (Chen, 2007).

[1] Dr, Associate Professor, Department of Chemistry, Myitkyina University
[2] Dr, Associate Professor, Department of Chemistry, Myitkyina University

Chemical fertilizer also reduces the protein content of crops, and the carbohydrate quality of such corps also gets degraded. Excess potassium content on chemically overfertilized soil decreases vitamin C, carotene content and antioxidant compounds in vegetables. Vegetables and fruits grown on chemically overfertilized soil also more prone to attacks by insects and disease. Although chemical fertilizers have been claimed as the most important contributor to the increase in world agricultural productivity over the past decades, the negative effects of chemical fertilizer on soil and environment limit its usage in sustainable agricultural systems. Weakening soil quality requires increasing inputs to maintain high yields. This in turn, threatens future food security and raises production costs for often already poor farmers (Kochakinezhad *et al.,* 2012)

Composting is the transformation of organic material through decomposition into a soil-like material called compost. Invertebrates (insects and earthworms) and microorganisms (bacteria and fungi) help in the transformation. *Trichoderma* spp. is a fungal genus found in many regions of the world and widely used because of the multiple beneficial effects on plant growth and disease resistance, in other words it is widely used as biofertilizers and biopesticides (Alkadious and Abbas, 2012). In recent years, biofertilizers, the products containing living cells of different types of microorganisms, are also used in the integrated nutrient supply system. Biofertilizers can convert nutrionally important elements from unavailable to available form through biological processes leading to crop yields (Hedge *et al*., 1999). The present work deals with the study on the effect of *Trichoderma* inoculated compost biofertilizer on the growth and yield of eggplant.

Materials and Methods

Sample Collection and Preparation

Farm waste materials such as cow dung, rice straw and rice bran were collected from Sein Sar Pin Village, Maeutaw village group, Zaeyarthiri Township, Nay Pyi Taw. Cow dung, rice straw, rice bran, bioinoculant *Trichoderma* substrate (10^7 cfu/g) (200:40:4:1) and water (18 L) were to be used in composting process for preparation of biofertilizer by open heap layering method. Size of box used in composting was 8ft x 4 ft x 2.5 ft. After about 75 days, germination percent is 82% and then the inoculated compost biofertilizer were ready to be used. By using inoculated compost fertilizer, the brinjal (*Solanum melogena* L.) were grown in a research field at Water Utilization Research Section, Department of Agricultural Research, Yezin, Nay Pyi Taw. The experiment was arranged in a randomized complete block design and comprised four different fertilizers, namely chemical fertilizer (83N- 37P- 64K kg/ha), 30 % (w/w) *Trichoderma* inoculated compost biofertilizer, chemical fertilizer with 30 % (w/w) *Trichoderma* inoculated compost biofertilizer and unfertilized plots as control. The size of each experimental plot was (6x3) square feet. Each treatment had five replications with 6 plants in each replicate. There were 3 rows in each plot. Weeding, irrigation and other intercultural operation were done when necessary.

Weekly plant height measurements were taken from two weeks after transplanting and the shoot fresh and dry weight, root fresh and dry weight and fruity-yield per plant were recorded after the harvest. Land preparation was done by cutting the vegetation of scraping the soil surface.

Methods

All samples were subjected to physical and chemical analyses using conventional and modern techniques. And also four treatments were analysed before sowing and after harvesting. Standard methods of analyses were followed. Some part of this research work was done in Water Utilization Research Section, Department of Agricultural Research, Yezin, Nay Pyi Taw. Soil texture was determined by international pipette method. Measurement of moisture content was determined by oven drying method and soil pH was measured with a glass electrode using a 1:2.5 soil to water ratio. Organic carbon was determined Tyurin's method, electrical conductivity was determined by conductivity meter, available nitrogen content was determined by alkaline permanganate method and available phosphorous content by Olsen's method. Available potassium, exchangeable calcium, magnesium and potassium were determined by AAS. In the analytical procedures of the experiments, recommended methods and techniques were applied (FAO, 2008; AOAC, 2009). Statistical analysis was carried out using International Rice Research Institute (IRRISTAT version 5.0) in this study.

Results and Discussion

Some Physicochemical Properties and Nutrients of Raw Materials

Table.1 represents the moisture, bulk density, pH and organic carbon of raw materials. Some physicochemical properties of cow dung, rice straw and rice bran were moisture content (15.64 %, 10.37 %, 12.29 %), bulk density (0.43 g/mL, 0.18 g/mL, 0.47 g/mL), pH value (7.63, 7.27, 5.51) and organic carbon (12.42 %, 46.82 %, 53.05 %). Rice bran has higher bulk density and organic carbon than that of cow dung and rice straw. It indicated that the pH values of cow dung and rice straw are suitable to prepare natural fertilizer.

The nutrient contents of the raw materials (cow dung, rice straw and rice bran) are presented in Table 2. Cow dung contains 1.79 % of N, 1.43 % of P, 0.26 % of K, rice straw contains 1.02 % of N, 0.33 % of P, 0.13 % of K and rice bran contains 2.03 % of N, 3.43 % of P, 1.58 % of K. The most common element contents in cow dung, rice straw and rice bran were iron (967.50 ppm, 133.40 ppm and 152.30 ppm), manganese (798.40 ppm, 914.00 ppm and 117.00 ppm), copper (20.02 ppm, 16.38 ppm and 14.46 ppm) and zinc (68.23 ppm, 28.33 ppm and 73.32 ppm) respectively. The sufficient amount of N, P, K and micronutrients were found to be present in raw materials.

Physicochemical Properties and Nutrients of Compost Biofertilizer

The physicochemical characteristics such as moisture content (4.28%), bulk density (0.45 g/mL), water holding capacity (57.00%), pH value (7.20), organic carbon (18.17%), organic matter (31.33), C/N ratio (17.47) and electrical conductivity (3.88 dS/m) were found in prepared biofertilizer (Table 3). Organic carbon plays a very important and sometimes spectacular role in the maintenance and improvement of soil properties.

The prepared biofertilizer was found to contain 1.04 % of N, 0.20% of P, 0.86 % of K, 0.69 % of Ca, 0.15 % of Mg and 0.05 % of S. The most common trace elements in biofertilizer were iron, manganese and zinc. The contents of NPK are essential to maintain and sustain the soil fertility. In the present work, the calcium contents were higher than that of magnesium and

sulphur in raw materials. Iron is necessary for chlorophyll formation. Manganese has several functions in the plant. Copper is probably associated with some of the plant enzyme systems and zinc is one of the most widely used micronutrient. So, the sufficient amount of N, P, K and macro and micronutrients were present in compost biofertilizer (Table 4). Toxic metals of the biofertilizer were described in Table 5. No toxic metals analysed by AAS were found in prepared biofertilizer.

Table 1 Some Physicochemical Properties of Raw Materials

Properties	Cow Dung	Rice Straw	Rice Bran
Moisture (%)	15.64	10.37	12.29
Bulk Density (g/mL)	0.43	0.18	0.47
pH	7.63	7.27	5.51
Organic Carbon (%)	12.42	46.82	53.05

Table 2 Nutrients of Raw Materials

Macro and Micronutrients	Cow Dung	Rice Straw	Rice Bran
Total N (%)	1.79	1.02	2.03
Total P_2O_5 (%)	1.43	0.33	3.43
Total K_2O (%)	0.26	0.13	1.58
Total Ca (%)	1.32	0.48	1.20
Total Mg (%)	0.71	0.03	0.68
Total S (%)	0.03	0.04	0.04
Fe (ppm)	967.50	133.40	152.30
Mn (ppm)	798.40	914.00	117.00
Cu (ppm)	20.02	16.38	14.46
Zn (ppm)	68.23	28.33	73.32

Table 3 Physicochemical Properties of Compost Biofertilizer

Properties	Content
Moisture (%)	4.28
Bulk Density (g mL^{-1})	0.45
Water Holding Capacity (%)	57.00
pH	7.20
Organic Carbon (%)	18.17
Organic Matter (%)	31.33
C/N ratio	17.47
Electrical Conductivity (dS/m)	3.88

Table 4 Macro and Micronutrients in Prepared Biofertilizer

Macro and Micronutrients	Composition (%)
Total N	1.04
Total P_2O_5	0.20
Total K_2O	0.86
Total Ca	0.69
Total Mg	0.15
Total S	0.05
Fe	0.0908
Mn	0.0074
Zn	0.0098
Cu	ND

ND = Not Detected

Table 5 Toxic Metal Contents in Compost Biofertilizer by AAS

Toxic Metals	Content (ppm)	Concentration limits (ppm)*	German Standard (ppm)**
Lead	ND	300	150
Nickel	ND	420	50
Cadmium	ND	35	3
Chromium	ND	-	150
Arsenic	ND	41	-
Mercury	ND	7.8	3

* (Ohio Enviromental Protection Agency, 2012) ND-Not Detected

** (European Commission Orbit Association, 2008)

Analysis of the Soil Treated with Chemical Fertilizer and Biofertilizer before Sowing

Table.6 shows the physical parameters and chemical compositions in terms of N, P, K, Ca and Mg of farm soil media before sowing of the Brinjal. These soils were subjected to different treatments by using prepared chemical fertilizer, biofertilizer and chemical fertilizer with biofertilizer and also the soil, without any fertilizer treatment, which was kept as a control.

The farm soil T4 as control (before sowing) shows sand 70.92 %, silt 16.04 %, and clay 13.00 %. The category of this type of soil falls in the sandy loam. The sand and silt in the soil take only a small active part in the plant growth. Soil pH may influence nutrient absorption and plant growth. The pH values of treated soils (T1 to T4) were found to be in the range of 6.34 and 6.44 and thus, it can be considered as a slightly acidic type of soil. A degree of salinity can be measured by determining the electrical conductivity (EC) of soil (FAO, 2008). It has been found that the electrical conductivity of control soil was 0.59 dS/m. By treating the soil with fertilizers the value of EC of soil was higher (0.64 -1.07) than that of the original free soil. The EC values of all treated soils were ranged from 0 to 2, and thus all soil samples were salt free (salinity effect negligible). Chemical compositions of the prepared soil were organic carbon, humus, total nitrogen, available phosphorous and available potassium together with exchangeable calcium and magnesium. These elements are the macronutrients for plant growth.

Humus is a potential soil food for plant growth and yield. The microbes become a part of the soil humus along with materials that have partially or entirely resisted the process of decomposition. The continuous slow release of plant nutrients from decomposing humus is a very important part of the ability of the soil to supply the needs to plant. If there is plentiful supply of humus or organic carbon, the decay of these by microorganisms liberates carbon dioxide, which may be converted to increase the biomass (Teakle and Boyle, 1958).The humus content of treated soil were higher than that of original control soil.

The content of available nitrogen in the farm soil was 42.00 ppm. The available phosphorous and potassium in the farm soil were 43.70 meq/100g and 150.93 meq/100g, respectively. The amounts of exchangeable Ca, Mg and K were about 7.50 me/100 g, 1.38 meq/100 g and 0.29 meq/100 g respectively. On the context of what has been described above, low N, P and K contents were found in the farm soil. Hence, the fertilizer treated soils would have more pronounced effect on the plant growth.

Table 6 Analysis Data of the Soil before Sowing Brinjal

Analytical Item	**T1**	**T2**	**T3**	**T4**
Texture-Sand (%)	69.40	69.64	70.28	70.92
Silt (%)	16.92	16.44	17.32	16.04
Clay **(%)**	13.68	13.92	12.36	13.00
Moisture (%)	1.52	0.58	0.40	1.01
pH	6.40	6.34	6.39	6.44
Electrical Conductivity (dS/m)	0.78	0.64	1.07	0.59
Organic Carbon (%)	1.08	1.15	1.14	1.06
Humus (%)	1.86	1.98	1.96	1.83
Total N (%)	0.25	0.19	0.21	0.17
C/N ratio	4.32	6.05	5.43	6.24
Available N (ppm)	45.78	44.03	52.30	42.00
Available P (ppm)	48.23	34.90	34.92	43.70
Available K (ppm)	228.25	225.28	230.43	150.93
Exchangeable Ca (meq/100g)	8.97	8.23	9.95	7.50
Exchangeable Mg (meq/100g)	0.67	1.25	0.93	1.38
Exchangeable K (meq/100g)	0.24	0.32	0.39	0.29

T1 = Chemical fertilizer, T2 = 30% compost (biofertilizer),
T3 = Chemical fertilizer + 30% compost (biofertilizer), T4 = Control

(a) Brinjal (two months after sowing) (b) Brinjal (three months after sowing)

Figure 1 View of field experiment for brinjal

Analysis of the Soil after Harvesting Brinjal

View of field experiment and vegetative growth stage of brinjal are shown in Figures 1 and 2. The analysis data of soil after harvesting brinjal are described in Table 6. All types of soil are sandy loam and it cannot be any changed before and after harvesting. pH value of treated and untreated soils were 7.01 to 7.11. In addition, in the field work study, the pH of the soil (after harvesting) was found to increase than before the transplanting stage. The effect of organic materials on the increase of pH of the soil has been reported (IRRI, 1979). It is normally due to the reduction of soil materials, but may also be caused by mineralization of organic materials to ammonia. Soil organic carbon and nitrogen are used as indexes of soil quality assessment and sustainable land use management. Soil C/N ratio is often considered as a sign of soil nitrogen mineralization capacity. High soil C/N ratio can slow down the decomposition rate of organic matter and organic nitrogen by limiting the soil microbial activity ability, whereas low soil C/N ratio could accelerate the process of microbial decomposition of organic matter and nitrogen (Wu *et al*., 2001). After harvesting stage, it was found that lowest value of C/N ratio in 30% biofertilizer treated soil (T2) and the highest value of C/N ratio in chemical fertilizer treated soil (T2). After harvesting stage, as for total N, available N, P, K and exchangeable Ca , Mg and K in all treatments, showed the reduced amounts as compared to the treated soils before sowing. It can be ascertained that the plants have taken up N, P, K, Ca and Mg on an enhance way.

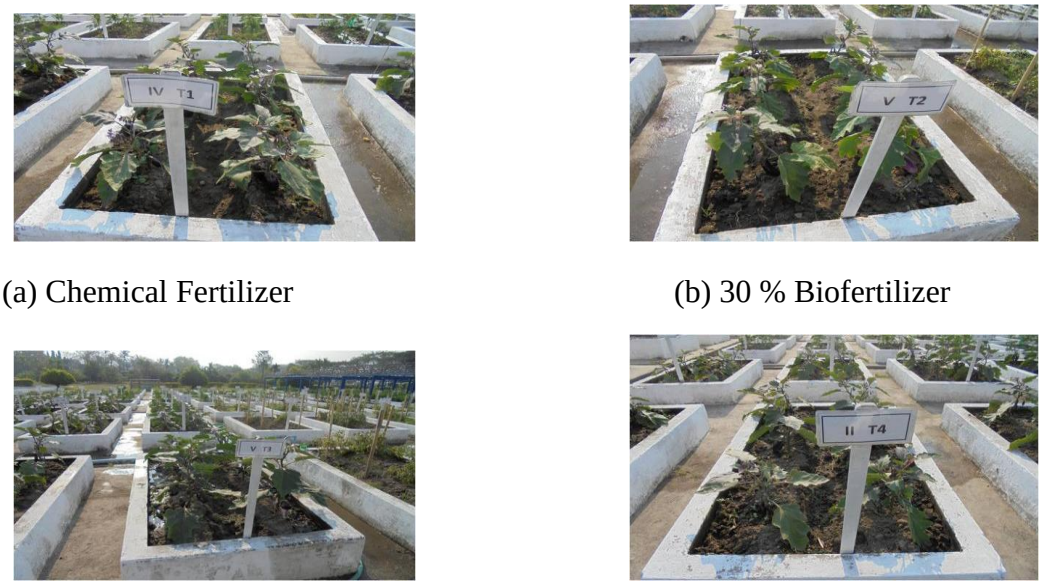

(a) Chemical Fertilizer (b) 30 % Biofertilizer

(c) Chemical fertilizer with (d) Control 30% Biofertilizer

Figure 2 Vegetative growth stage of brinjal

Table 7 Analysis Data of the Soil after Harvesting Brinjal

Analytical Item	**T1**	**T2**	**T3**	**T4**
Texture-Sand (%)	65.92	72.28	70.88	69.18
Silt (%)	16.68	13.60	14.40	15.86
Clay **(%)**	17.40	14.12	14.76	14.96
Moisture (%)	0.11	1.52	0.12	0.23
pH	7.09	7.01	7.03	7.11
Electrical Conductivity (dS/m)	0.64	0.48	0.82	0.58
Organic Carbon (%)	1.30	1.40	1.50	1.38
Humus (%)	2.24	2.41	2.59	2.38
Total N (%)	0.14	0.18	0.19	0.16
C/N ratio	9.28	7.78	7.89	8.63
Available N (ppm)	22.78	42.42	48.52	39.11
Available P (ppm)	26.21	33.69	32.91	39.32
Available K (ppm)	97.75	109.68	152.55	102.70
Exchangeable Mg (meq/100g)	0.59	1.13	0.70	1.08

T1 = Chemical fertilizer, T2 = 30% compost (biofertilizer),
T3 = Chemical fertilizer + 30% compost (biofertilizer),
T4 = Control

Effect of Chemical Fertilizer and Biofertilizer on the Growth and Yield of Brinjal

Factors affecting plant growth are air, heat (temperature), light, mechanical supports, nutrients and water. In the field experiment, these external factors except nutrients supplying to soil were same condition for all treated soils and control plot. Growth, yield, and quality of brinjal depend on nutrients availability in soil, which is related to the judicious application of manures and fertilizers. The results are shown in Table 8.

Plants get their nutrients from three sources; air, whereas hydrogen, some oxygen, and possibly some carbon are taken from the air, whereas hydrogen, some oxygen, and possibly some carbon are taken from the soil solution. If a soil is to produce crops successfully, it must have, among other things, an adequate supply of all the necessary nutrients which plants take from the soil. The effect of inoculated compost (biofertilizer) on plant growth was studied in this work. Vegetative growth stages of brinjal in field experiment are shown in Figure 2.

During cultivation, daily determinations of plant height were recorded. The results are shown in Table 8. In this work, plant height was highly significant for brinjal ($p < 0.01$). There was highly significant in root fresh weight, root dry weight, shoot fresh weight and shoot dry weight for brinjal ($p < 0.01$). Number of total fruits of T3 was significantly higher than those of T1, T2 and T4 for brinjal ($p < 0.01$). After harvesting, the yield components such as the shoot fresh weight(g), root fresh weight(g), shoot dry weight(g), root dry weight(g), number of total fruit per plant and fruit weight per plant (g plant^{-1}) were measured and total yield (kg/ha) were calculated. *Trichoderma* inoculated biofertilizer (T3) the highest yield, which was significantly higher than the other treatments T1(chemical fertilizer), T2 (30 % Biofertilizer) and T4 (control).

The maximum total yield of about 8995.58 kg/ha for eggplant was obtained by using chemical fertilizer with biofertilizer (T3) (Figure 3). These results implied that yield of brinjal

was significantly increased when *Trichoderma* inoculated biofertilizer were combined with chemical fertilizer. The combined treatment gave significantly higher yield of all crops than the treatment T1. i.e., recommended rate of NPK fertilizer.

Generally, the NO_3^- form of N fertilizer could not retain long time to the rhizosphere zone of plants and therefore, split application of N fertilizer was suggested at different stages of crop growth. Conversely, the organic amendments and microbes played a role to slow by release the plant nutrients. The microbial population in soil releases some exudates (organic substances), increases nutrient uptake through enhanced root growth or promotes availability of necessary nutrients and solubilize a number of poorly soluble nutrients, such as Mn^{4+}, Fe^{3+} and Cu^{2+} etc. (Altomare *et al*., 1999). Therefore, in present study the combined treatments enhanced efficient utilization of nutrients than the others which expedited crop growth and yield.

Chemical fertilizer

30% Biofertilizer

Chemical fertilizer with 30% Biofertilizer

Control

Figure 3 Maturity stage of brinjal

Table 8 Effect of Chemical Fertilizer and Biofertilizer on Growth and Yield of Brinjal (Field Experiment)

Treatment	Plant height (cm)	Shoot fresh weight (g)	Root fresh weight (g)	Shoot dry weight (g)	Root dry weight (g)	Number of total fruits plant^{-1}	Fruit weight plant^{-1}	Total yield (kg/ha)
T1	60.07	73.24	26.40	14.84	8.96	27	1020.30	7407.38
T2	58.43	86.24	29.72	17.08	9.68	28	1027.29	7458.13
T3	62.67	121.28	35.49	23.96	11.8	35	1239.06	8995.58
T4	53.33	53.18	21.64	10.52	7.42	21	866.44	6290.38
F Test	**	**	**	**	**	**	*	*
LSD(5%) 6.64		16.49	2.45	2.23	1.81	6.02	232.43	1687.44
CV(%)	8.20	14.30	6.30	9.70	13.80	15.70	16.20	16.20

T1=Chemical fertilizer,T2=Biofertilizer,
T3=Chemical fertilizer with biofertilizer,T4=Control LSD=Least Significant Difference, CV=Coefficient of Variation
** = significant at 1% ($p<0.01$), * = significant at 5% ($p<0.05$)

Conclusion

In this research work, physicochemical properties of raw materials (cow dung, rice straw and compost biofertilizer) have been studied by conventional methods and modern instrumental techniques. In this process, *Trichoderma* (cellulolytic) was used as composting accelerator for initiation of prepared biofertilizer. Biofertilizer was prepared from the selected waste materials (cow dung, rice straw) by over heap layering method for the composting process with the aid of bioinoculant *Trichoderma*. The prepared biofertilizer was found to contain macro and micro nutrients. And also, there is no detectable values of all toxic metals (Pb, Ni, Cd, Cr, As, Hg) in prepared biofertilizer. In the present study, it was clearly observed that the *Trichoderma* inoculated biofertilizer had positive impact on growth and yield of brinjal.

Based on the field work investigation, the efficacy of *Trichoderma* inoculated biofertilizer accelerated when it was supplemented with chemical fertilizer application. Superior and significant growth and yield were increased by supplementation of chemical fertilizer with *Trichoderma* inoculated biofertilizer. The maximum 8995.58 kg/ha yield increase over control of brinjal was noticed in T3, which was 6290.38 kg/ha in T4. It may be concluded that application of *Trichoderma* inoculated biofertilizer along with chemical fertilizer could save at least 30 % biofertilizer giving higher yields in brinjal compared to T1 (chemical fertilizer).

Undoubtedly, there is a positive and potential of *Trichoderma* inoculated biofertilizer in crop cultivation to achieve attractive yield and reducing chemical fertilizer. With biofertilizer, a low input system can be carried out, and it can be supported achieving outcome for farms. Agriculture wastes recycling can bring tremendous benefits to agriculture and land management in long run. Therefore, this research may contribute to the development of the biofertilizer for agricultural sector in Myanmar.

Acknowledgements

The authors wish to thank Dr Aung Win (Rector), Dr Aye Aye Ko and Dr Soe Myint Aye Pro-Rectors of Myitkyina University for permitting the opportunity to present this paper. We wish to express our gratitude to Professor and Head Dr Ni Ni Aung and Professor Dr Nant Si Si Htay Department of Chemistry, Myitkyina University for their permission and encouragement to carry out this research. We would like to express our profound gratitude to the Department of Higher Education (Yangon Office), Ministry of Education, Yangon, Myanmar, for provision of opportunity to do this research and Myanmar Academy of Arts and Science for allowing to present this paper.

References

Akladious, S.A. and Abbas, S.M. (2012). "Application of *Trichoderma harzianum* T22 as a Biofertilizer Supporting Maize Growth". *African Journal of Biotechnology*, vol. 11(35), pp. 8672-8683

Altomare, C., Norvell, W.A., Bjorkman, T. and Harman, G.E. (1999). "Solubilization of Phosphates and Micronutrients by the Plant-Growth-Promoting and Biocontrol fungus *Trichoderma harzianum"*. *Applied and Environmental Microbiology*, vol. 65**,** pp. 2926-2933

AOAC. (2009). *Methods of Analysis*. Washington: 3rd Ed., Benijamin Franlin Station, pp. 530-543

Chen, J.H. (2007). *The Combined Use of Chemical and Organic Fertilizers and Biofertilizer for Crop Growth and Soil Fertility*. Taichung, Taiwan: National Chung Hsing University, pp. 22-25

European Commission Orbit Association. (2008). Comments Heavy Metals in Last Meeting of Fertilisers Working Group – European Commission

FAO. (2008). *Guide to Laboratory Establishment for Plant Nutrient Analysis.* Rome: FAO, pp. 30-44

Hedge, D.M., Dwive, B.S. and Sudhakara, S.N. (1999). "Plant Growth Enhancement and Disease Control by *Trichoderma harzianum* in Vegetable Seedlings Grown under Commercial Conditions". *European Journal of Plant Pathology*, vol. 100, pp. 337-346

IRRI. (1979). *Annual Report for 1978*. Los Baños, Philippines: International Rice Research Institute. pp. 478

Kochakinezhad, H., Peyvast, Gh., Kashi, A.K., Olfati, J.A and Asadii, A. (2012). "A Comparison of Organic and Chemical Fertilizers for Tomato Production". *Journal of Organic Systems*, vol. 7(2), pp. 14-25

Ohio EPA. (2012). OEPA Workgroup. Ohio Division, United State: Ohio Environmental Protection Agency

Teakle, L. J. H. and Boyle, R.A. (1958). *Fertilizers for the Farm and Garden*. London: Angus and Robertson. 1st Ed. pp. 24-26

Wu, H.B., Guo, Z.T. and Peng, C.H. (2001). "Changes in Terrestrial Carbon Storage with Global Climate Changes since the Last Interglacial". *Quaternary Sciences*, vol. 21(4), pp.366-367

SYNTHESIS, CHARACTERIZATION AND ANTIMICROBIAL ACTIVITY OF SILVER-POLYVINYL ALCOHOL NANOCOMPOSITE FILMS

Aye Mya Nwe[1], Mya Kay Thi Aung[2], Khin Than Yee[3]

Abstract

In this research work, silver nanoparticles were synthesized by using chemical synthesis. In chemical synthesis, trisodium citrate was used as reducing agent. Silver nanoparticles (SNP) were prepared by mixing different volume ratios of 1 % trisodium citrate solution and 1 mM $AgNO_3$ solution (1:10, 2:10 and 3:10 v/v). The existence of SNP in colloidal solutions was confirmed by Tyndall effect and UV-visible spectroscopy. The UV-visible spectrum was revealed the formation of silver nanoparticles by exhibiting the typical surface plasmon absorption maxima at 415 nm. The silver nanoparticles were characterized by modern techniques such as XRD, FT IR, SEM and EDXRF analyses. In XRD analysis, it was found that average crystallite size of SNP powders are in the range of 36.5 nm to 41.7 nm and all the SNP-TSC had the crystalline nature. According to the XRD spectra of all prepared SNP-TSC, there was impurity peaks in the SNP-TSC 2 and SNP-TSC 3 but no impurity peaks in the SNP-TSC 1. From the FT IR spectra of all prepared SNP-TSC, it was observed that a strong symmetrical stretch was observed in the range of 1400 cm^{-1} to 1200 cm^{-1} where major peaks at 1390-1380 cm^{-1} which showed the C-H stretching. SEM micrographs of all prepared SNP-TSC showed agglomeration and therefore larger particle size distribution. From EDXRF analyses, the main constituent element in the SNP-TSC1 is Ag (87.177 %). The different types of polyvinyl alcohol (PVA) film were prepared by using different concentrations (1 - 5 % w/v) of PVA to distilled water. The obtained PVA films were designated as PVA-1, PVA-2, PVA-3, PVA-4 and PVA-5. According to the mechanical properties, PVA-3 film was chosen as selected film. The selected PVA-3 film was characterized by SEM, FT IR and TG-DTA analyses. The PVA-SNP composite films were prepared by varying the volume ratios of 3 % (w/v) PVA solution and colloidal SNP-TSC 1 solution. According to the mechanical properties, PVA-SNP-3 was selected and characterized by SEM, FT IR, TG-DTA and EDXRF analyses. The antimicrobial activity of prepared PVA-SNP composite films were investigated using agar well diffusion method.

Keywords; trisodium citrate, silver nanoparticles, chemical synthesis, PVA- SNP compositfilms

Introduction

Nanoparticles are now being developed for various biological applications such as medicines, antimicrobial agents, wound dressing, drug targeting and deliveries, transfection vectors, bioimaging, and labeling agents etc. Colloidal particles are increasingly receiving attention as an important starting point for the generation of micro and nanostructures. Nanoparticles are under active research because they posses interesting physical properties differing considerably from that of the bulk phase. It comes from small sizes and high surface/volume ratio. The extremely small size of nanoparticles means they exhibit enhanced or different properties when compared with the bulk material. Silver nanoparticles thus allows them to easily interact with other particles and increases their antibacterial efficiency. This effect can be so great that one gram of silver nanoparticles is all that is required to give antibacterial properties to hundreds of square meters of substrate material (Basavaraj, 2012). Silver is a nontoxic, safe inorganic antibacterial agent used for centuries and is capable of killing about 650 type of diseases causing microorganisms.

[1] Assistant Lecturer, Department of Chemistry, Pyay University
PhD Candidate, Department of Chemistry, University of Yangon
[2] Associate Professor, Department of Chemistry, Technological University (Myeik)
[3] Lecturer, Department of Chemistry, Myeik University

Silver has been described as being oligodynamic because of its ability to exert a bactericidal effect at minute concentrations. It has a significant potential for a wide range of biological applications such as antifungal agent, antibacterial agents for antibiotic resistant bacteria, preventing infections, healing wounds and anti-inflammatory. Silver ions (Ag^+) and its compounds are highly toxic to microorganisms exhibiting strong biocidal effects on many species of bacteria but have a low toxicity towards animal cells. Therefore, silver ions, being antibacterial component, are employed in formulation of dental resin composites, bone cement, ion exchange fibers and coatings for medical devices (Prema, 2011).

The synthesis of silver nanoparticles by chemical methods is popular as they require little instrumental and are relatively inexpensive. The most common way to synthesize silver nanoparticles is via chemical reduction (Zaheer, 2011), where the reduction of silver ions take place in controlled conditions, which can limit the nucleation of reduced (neutral) silver atoms (Angela *etal*., 2018). The most popular preparation of SNP colloids is chemical reduction of silver salts by trisodium citrate. This preparation is simple, but the great care must be exercised to make stable and reproducible colloid (Basavaraj, 2012). Among the methods, chemical reduction was widely studied, due to its advantages of yielding nanoparticles without aggregation, high yield and low preparation cost and simplicity (Prema, 2011).

Mechanism of reaction could be expressed as follows:

$4Ag^+ + C_6H_5O_7Na_3 + 2H_2O \rightarrow 4Ag^0 + C_6H_5O_7H_3 + 3Na^+ + H^+ + O_2\uparrow$

Trisodium citrate has the chemical formula of $Na_3C_6H_5O_7.2H_2O$.Trisodium citrate anhydrous occurs as white, granular crystals or as white, crystalline powder. It is freely soluble in water and practically insoluble in ethanol (96 %). It is a non-toxic, neutral salt with low reactivity. It is chemically stable if stored at ambient temperatures. Trisodium citrate anhydrous is fully biodegradable and can be disposed of with regular waste or sewage. Trisodium citrate is a tribasic salt of citric acid. It is widely used in food, beverages and various technical applications mainly as buffering, stabiliser or emulsifying agent.

Polyvinyl alcohol (PVA) is a bio- friendly polymer as it is water soluble and has extremely low cytotoxicity. PVA belongs to the group of polymers which can be used in combination with silver nitrate. PVA is one of the synthetic, biodegradable, biocompatible polymer utilized in medical applications such as wound dressing, artificial skin, coatings, transdermal patches, cardiovascular devices and drug delivery systems (Sayed, 2014). In this research work, antimicrobial activities PVA-SNP composite films are investigated against strains of different bacteria.

Materials and Methods

Chemicals

Silver nitrate ($AgNO_3$, 99.8 %), trisodium citrate ($C_6H_5Na_3O_7.2H_2O$, 99 %) and polyvinyl alcohol (Molecular weight 14,000, degree of hydrolysis 98 %) were purchased from the British Drug House (BDH) Chemical Ltd., England.

Preparation of Silver Nanoparticles (SNPs)

Silver nanoparticles were prepared by using chemical reduction method. All solutions of reacting materials were prepared in deionized water. Firstly, 50 mL of 1mM $AgNO_3$ was heated and stirred on magnetic stirrer to boiling. To this solution 5mL of 1 % (w/v) trisodium citrate was added drop by drop. Silver nanoparticles (SNP) were prepared by mixing different volume ratios of 1 % trisodium citrate solution and 1 mM $AgNO_3$ solution (1:10, 2:10 and 3:10 v/v). During this process solution was mixed vigorously and heated until colour change was evident (yellowish brown). Then it was removed from heating element and stirred until cool to room temperature. This solution was placed on ultrasonic bath for 30 min. Sonication was

carried out to reduce size and purify the silver nanoparticles in the colloidal solution. The solution containing silver nanoparticles were centrifuged at 7000 rpm for 20 min. The purified particles were dried by using a hot air oven up to 70 ºC for one and half hours. And then solid silver nanoparticles were obtained. The prepared silver nanoparticles were denoted as SNP-TSC 1 for 1:10, SNP-TSC 2 for 2:10 and SNP-TSC 3 for 3:10 v/v ratios respectively.

Confirmation for the Existence of Silver Nanoparticles in Solution by Tyndall Effect

The laser pointer was placed to the edge of the bottle containing SNP colloidal solution and the light was passed through the solution.

Characterization of Silver Nanoparticles

UV-visible spectrophotometer (SHIMADZU UVmini-1240, JAPAN) by using UV spectra of the silver colloid in the range 330 nm - 460 nm were measured. UV absorption spectra have proved to be quite sensitive to the formation of silver colloids because silver nanoparticles exhibit an intense absorption peak due to the surface plasmon excitation. The absorption band in visible light region (350 nm- 550 nm) is typical for silver nanoparticles.

The phase identification of the silver nanoparticles was carried out by X-ray diffraction method. The solid sample was grounded using a motar and pestle into powder. X-ray powder diffraction measurement was carried out by using (Rigaku, Miniflex-600) powder diffractometer with long fine focus Cu anode.

FT IR measurements were carried out to identify the biomolecules for capping and efficient stabilization of the metal nanoparticles synthesized. The samples were measured by using Perkin Elmer GX System, FT IR spectrophotometer.

Morphology of the silver nanoparticles were observed on JSM 5610 LV Scanning Electron Microscopy, JEOL-Ltd., Japan Elemental compositions in the prepared silver nanoparticles were determined by EDXRF using EDX-8000 spectrometer (Shimadzu Co.Ltd., Japan).

Preparation of Pure Polyvinyl Alcohol Films (PVA)

Polyvinyl alcohol (PVA) films were prepared by solution casting method. Different concentrations of PVA (molecular weight 14,000, degree of hydrolysis 98 %) (1, 2, 3, 4 and 5 % w/v) solution were prepared with distilled water by stirring and heating at 50 ºC. The PVA solutions were placed in an autoclave at 0.1 MPa and 121 ºC for 20 min. Each polymer solution was casted on melamine plate and dried in air. The series of PVA films were obtained. The prepared PVA films were designated as PVA-1, PVA-2, PVA-3, PVA-4 and PVA-5 according to the percent of PVA.

Preparation of Polyvinyl Alcohol- Silver Nanoparticles Composite Films (PVA-SNP)

Polyvinyl alcohol- silver nanoparticles composite films were prepared by mixing different volume ratios of 3 % (w/v) of PVA solution and the prepared SNP-TSC1 solution (95:5, 90:10, 85:15, 80:20, 75:25, 70:30 v/v) to make up 100 mL. The mixed solutions were stirred by using a magnetic stirrer at 80 rpm for 20 min. Then polymer solutions were kept for sufficient time to remove any bubble formation. Each polymer solution was placed on melamine plate and dried in air. The melamine plates containing the composite solutions were left about 7 days to obtain PVA-SNP composite films. The composite films after drying were removed easily from the melamine plates. The obtained composite films were designated as PVA-SNP-1, PVA-SNP-2, PVA-SNP-3, PVA-SNP-4, PVA-SNP-5 and PVA-SNP-6 respectively.

Determination of the Antimicrobial Activity by Agar Well Diffusion Method

The PVA-SNP composite films were tested with (a) *Bacillus subtilis* (b) *Staphylococcus aureus* (c) *Pseudomonas aeruginosa* (d) *Bacillus pumilus* (e) *Candida albicans* (f) *Escherichia coli* species to investigate the nature of antimicrobial activity.

Results And Discussion

Synthesis of Silver Nanoparticles by using Trisodium Citrate as Reducing agent

Different volumes of 1% w/v trisodium citrate were mixed with 1mM $AgNO_3$ solution in three different ratios of 1:10, 2:10 and 3:10 v/v without varying the other conditions to obtain SNP-TSC 1, SNP-TSC 2 and SNP-TSC 3 respectively. The formation of silver nanoparticles occurs after the reduction of aqueous silver salts with trisodium citrate(1 %) within duration of 10-20 minutes, colour change appear after the completion of reaction, it is well known that, the silver nanoparticles exhibit pale yellow colour. This is due to the excitation of surface plasmon vibration in silver nanoparticles.

Tyndall Effect

Tyndall effect on silver nanoparticles (SNPs) is shown in Figure 1. It was found that the laser light passes through the solution due to the presence of nanoparticles.

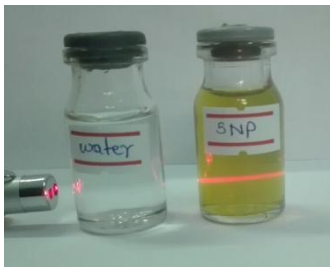

Figure 1 Tyndall effect on the prepared SNPs by chemical synthesis

Characterization of Silver Nanoparticles

UV-visible Studies

The sample when treated with complete reaction conditions, changed in colour of colloids solution from pale yellow to yellowish brown. This colour change preliminary showed the presence of silver nanoparticles or reduction of Ag^+ of $AgNO_3$ to Ag^0. The maximum absorbance was observed at 415 nm due to surface resonance of silver nanoparticles (Figure 2).

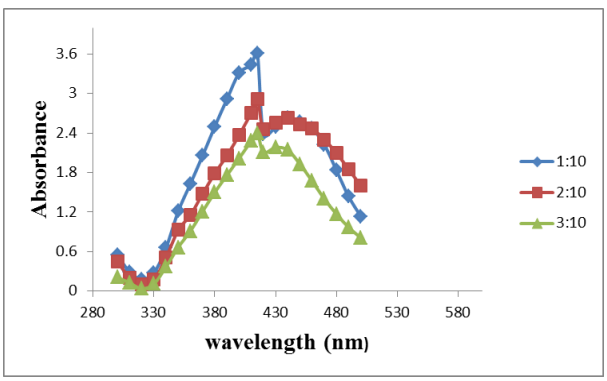

Figure 2 Wavelength of maximum absorption of the prepared silver nanoparticles (SNP-TSC) by chemical method

X Ray Diffraction Studies

The XRD data were obtained in the 2θ range from 10º to 70º in step scan mode with 2θ step of 0.02º. The diffraction pattern indicated that the sample is the silver nanoparticles. The XRD pattern of SNPs is shown in the Figure 3 (a, b, c). The intensive diffraction peak at a 2θ value of 38.08º from the (111) lattice plane of face centered cubic(fcc) silver unequivocally indicated that the particles are made of pure silver. Two additional broad bands were observed at 44.27º (2θ) and 64.41º (2θ) corresponding to the (200) and (220) planes of silver respectively. However, SNP-TSC1 samples showed only single phase of Ag and no impurity peaks. Therefore, SNP-TSC1 was chosen for the further experiment. The crystallite sizes of all of the prepared SNP powders were calculated by Debye-Scherrer equation (Table 1). According to the Table, the average crystallite size of the prepared SNP powders are SNP-TSC1 (40.6 nm), SNPTSC2 (36.5 nm) and SNP-TSC 3 (41.7 nm).

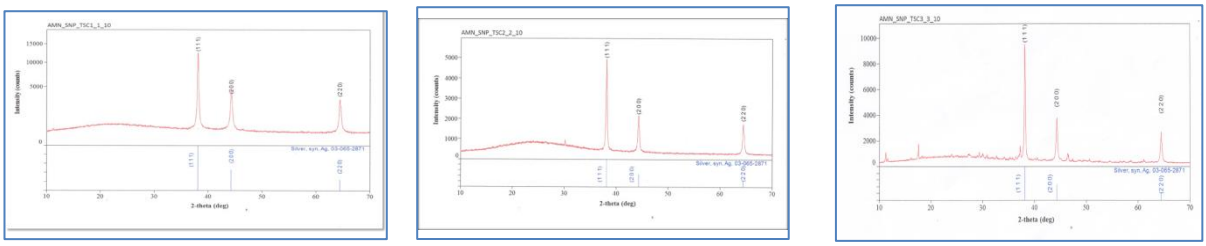

(a) (b) (c)

Figure 3 XRD diffractograms of silver nanoparticles by chemical synthesis
(a) SNP-TSC 1, (b) SNP-TSC 2 and (c) SNP-TSC 3

Table 1 Crystallite Size of Silver Nanoparticles by XRD Analysis

Sample	2θ (degree)	FWHM (degree)	(hkl)	Crystallite size(nm)	Average crystallite size(nm)
SNP-TSC 1	38.089	0.196	111	44.7	
	44.269	0.266	200	33.7	40.6
	64.409	0.226	220	43.4	
SNP-TSC 2	38.116	0.242	111	36.2	
	44.282	0.294	200	30.5	36.5
	64.421	0.229	220	42.8	
SNP-TSC 3	38.128	0.197	111	44.6	
	44.307	0.249	200	36.0	41.7
	64.438	0.219	220	44.7	

FT IR Analysis

Figure 4 shows the FT IR spectra of all of the prepared SNP-TSC samples. The characteristic absorption bands at 3441, 2874, 1583, 1386 and 576 cm^{-1} were observed. These peaks correspond to groups present in the sample and are indicated to O-H stretching, C-H stretching, C=C stretching, O-H bending and C-H out of plane bending. These bands are attributed from tri-sodium citrate a capping agent. FT IR spectral peaks of SNP-TSC1, SNP-TSC2 and SNP-TSC3 are shown in Table 2.

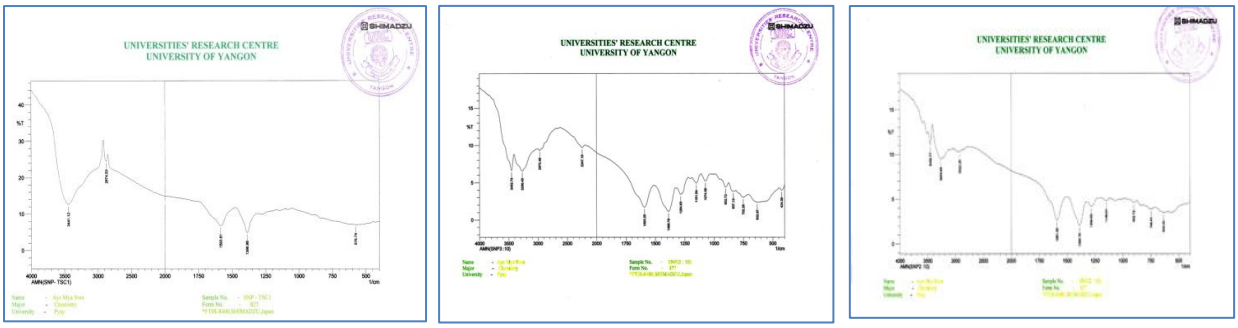

(a) (b) (c)

Figure 4 FT IR spectra of the prepared (a) SNP-TSC1, (b) SNP-TSC2 and (c) SNP-TSC3

Table 2 FT IR Spectral Assignments of the Prepared Silver Nanoparticles

Observed Frequency (cm^{-1})			*Literature Frequency (cm^{-1})	Band Assignments
SNP-TSC1	SNP-TSC2	SNP-TSC3		
3441	3450	3452	3600-3200	-OH stretching vibration
2874	2922	2970	2980-2850	C-H stretching vibration of sp^3 hydrocarbons
1583	1591	1593	1610-1560	C=C ring skeletal stretching vibration
1386	1388	1388	1425-1380	-OH bending vibration
576	748,636	837,752,632	830-500	C-H out of plane bending vibration

*Silverstein and Webster, 1998

SEM Analysis

The scanning electron micrographs of the prepared silver nanoparticles are shown in Figure 5. The present investigation of nanoparticle using SEM micrograph clearly illustrates the spherical shaped or roughly spherical shaped and some irregular shaped nanoparticles having the size range of 40 nm. It can be concluded that SNPs are initially monodispersed but drying process lead to agglomeration of many particles resulted into larger size particles.

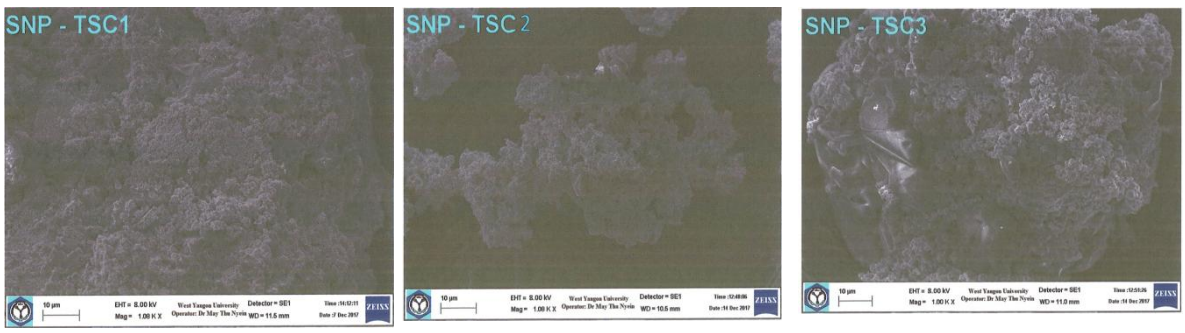

(a) (b) (c)

Figure 5 Scanning electron micrographs of the silver nanoparticles by chemical synthesis (a) SNP-TSC1, (b) SNP-TSC 2 and (c) SNP-TSC3

EDXRF Analysis

Figure 6 shows EDXRF spectrum of SNP-TSC1. According to the EDXRF spectrum of the prepared SNP-TSC1, silver was the major constituent (87.177 %) and other were trace constituents. Table 3 shows the relative abundance of elements in the prepared SNP-TSC1 by EDXRF.

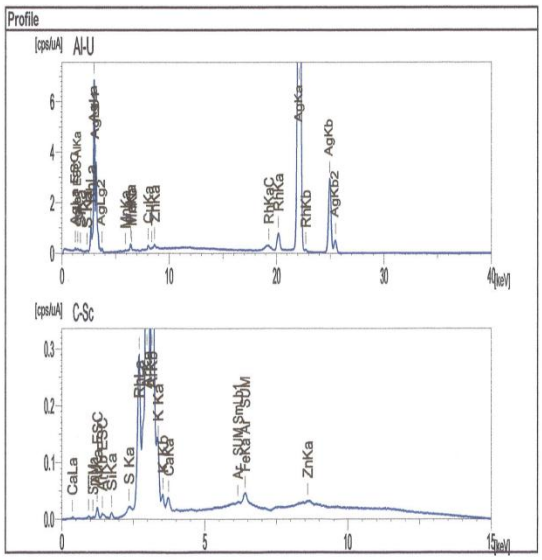

Figure 6 EDXRF spectrum of SNP-TSC1

Table 3 Relative Abundance of Elements in Prepared SNP-TSC1 by EDXRF

No.	Elements	Relative Abundance (%)
1	Silver	87.177
2	Aluminum	7.166
3	Silicon	2
4	Potassium	1.997
5	Calcium	0.465
6	Iron	0.43
7	Sulphur	0.357
8	Copper	0.15
9	Zinc	0.146
10	Manganese	0.112

Aspect of the Preparation of Pure PVA Film

Pure PVA films were prepared using various percents of PVA (1 % to 5 % w/v) in distilled water by solution casting method. The prepared pure PVA films appeared to be homogeneous, transparent and colourless. According to the mechanical properties (tensile strength, elongation at break and tear strength) of prepared PVA films, PVA-3 was chosen for the optimum films (Figure 7 and Table 4).

Figure 7 The photographs of (a) PVA-1 (b) PVA-2 (c) PVA-3 (d) PVA-4 (e) PVA-5 films

Table 4 Mechanical Properties of the Prepared Polyvinyl Alcohol Films

Prepared Films	PVA(%) w/v	Tensile Strength (MPa)	Elongation at Break (%)	Tear Strength (kNm^{-1})
PVA-1	1	26.0	128	96.3
PVA-2	2	29.7	202	114.0
PVA-3	3	31.7	241	155.8
PVA-4	4	27.1	216	87.9
PVA-5	5	33.0	282	101.0

Thickness = ~ 0.57 mm

Characterization of the Prepared PVA Film

The selected prepared PVA-3 film was characterized by modern techniques such as SEM, FT IR and TG-DTA as shown in Figure 8 (a, b, c). The SEM micrograph of the prepared PVA-3 membrane has smooth surface and homogeneous film. The FT IR spectrum of pure PVA film exhibits a major peaks associated with PVA. The major peaks were observed at 3600 cm^{-1}, 2955 cm^{-1}, 1568 cm^{-1} and 1458 cm^{-1} corresponding to O-H stretching, C-H stretching, C=C stretching and O-H bending. As seen in Figure 8(c), the thermogram of PVA-3 film possesses three stages of distinct weight loss between 38 ºC to 600 ºC. The first stage ranged between 38 ºC and 120 ºC with 11.04 % of weight loss and this was due to the evaporation of loosely bound water. The second stage ranged between 120 ºC and 350 ºC was due to the scission of functional group of polymer chain. The third stage of weight loss indicated the degradation of polymer backbone and progressive rupture of chain, combustion and formation of residue (Table 5)

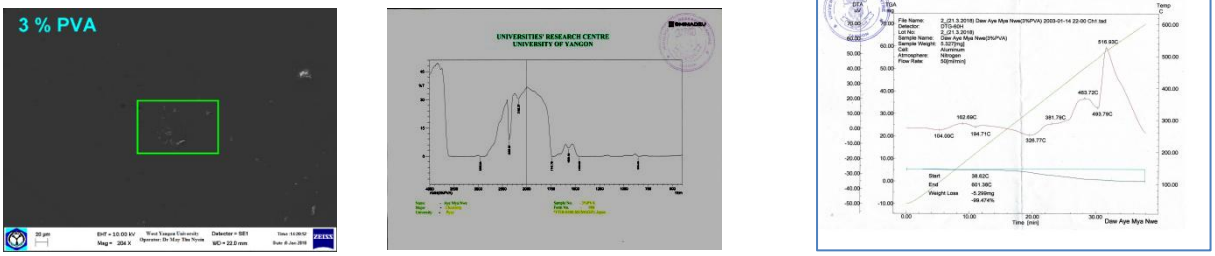

(a) (b) (c)

Figure 8 (a) SEM micrograph, (b) FT IR spectrum and (c) TG-DTA thermogram of the prepared polyvinyl alcohol PVA-3 film

Table 5 Thermal Analysis Data of the Prepared Polyvinyl Alcohol PVA-3 Film

TG Thermogram			Nature of Peak DTA	Remark
Temperature Range (°C)	**Total Weight Loss (%)**	**Break in Temperature (°C)**		
38-120	11.04	104	endothermic	-due to the evaporation of loosely bound water
120-350	33.13	326	endothermic	due to the scission of functional group of polymer chain
350-600	55.30	463 516	exothermic	Due to the degradation of polymer backbone and progressive rupture of the chain, combustion and formation of residue

Aspect of Preparation of PVA-SNP Films

The PVA-SNP composite films were prepared by solution casting method from solutions of PVA-3 and SNP–TSC1 in deionized water at various compositional ratios. The basic method for the synthesis of NPs in PVA is to disperse metal ion solution in the polymer and reduce to zero valent states. The PVA-SNP composite films were prepared by using different volume ratios of PVA-3 solution and SNP-TSC1 colloidal solutions (95:5, 90:10, 85:15, 80:20, 75:25 and 70:30). Solutions of PVA-SNP appeared to be homogeneous and transparent. The colour of the solution varied from colourless of pure PVA solution to greenish yellow colour with increasing SNP content. The distinctive colours of nanosilver are due to the phenomenon known as plasmon absorbance. With an increase in reaction time, particle size and aggregation of silver nanocrystal gradually increased together. The prepared PVA-SNP composite films are shown in Figure 9.

(a) (b) (c) (d) (e) (f)

Figure 9 The photographs of PVA-SNP composite films (a) PVA-SNP-1, (b) PVA-SNP-2, (c) PVA-SNP-3, (d) PVA-SNP-4, (e) PVA-SNP-5 and (f) PVA-SNP-6

Aspect of Mechanical Properties of Polyvinyl Alcohol- Silver Nanoparticles Composite Films

The mechanical properties of polyvinyl alcohol-silver nanoparticles composite films are shown in Table 6. From the resulting data, PVA-SNP-3 composite film was found that tensile strength of 37.7 MPa, elongation at break of 262 % and tear strength of 139 kNm^{-1}. Therefore, PVA-SNP-3 was chosen for optimum film due to its highest elongation at break.

Table 6 Mechanical Properties of Polyvinyl Alcohol- Silver Nanoparticles composite Films

No.	Parameters	PVA-SNP Composite Films					
		PVA-SNP-1	**PVA-SNP-2**	**PVA-SNP-3**	**PVA-SNP-4**	**PVA-SNP-5**	**PVA-SNP-6**
1	Tensile strength (MPa)	39.4	35.1	37.7	29.3	27.6	32.9
2	Elongation at Break (%)	256	219	262	158	235	168
3	Tear Strength (kNm^{-1})	146.7	129.2	139.0	125.5	156.0	172.7

Thickness = ~ 0.43

Characterization of the Prepared Optimum PVA-SNP-3 Film

The selected prepared PVA-SNP-3 film was characterized by modern techniques such as SEM, FT IR and TG-DTA analysis (Figures 10 and 11). The surface morphology of PVA-SNP-3 film was observed using SEM micrograph as shown in Figure 10(a). The PVA-SNP-3 film exhibits a smooth and compact surface with spherical in shape. This spherical shape is due to the distribution of silver nanoparticles through the PVA matrix. To determine the functional group on PVA-SNP-3 film, FT IR analysis was performed. The band intensities in different regions of the spectrum for PVA-SNP-3 film is shown in Figure 10(b). The band intense absorption peak around 3292 cm^{-1} was due to the O-H stretching vibration. The peak located at around 2938 cm^{-1} was attributed to the C-H stretching. The peak at 1714 cm^{-1} indicated the C=O stretching vibration. The peak at 836 cm^{-1} was due to C-H bending vibration. According to TG-DTA thermogram, the initial weight loss (around 100 ºC) observed was due to the loss of moisture present in the PVA-SNP-3 film. The subsequent steps of degradation were varied depending on the type of film. The second decomposition step of PVA-SNP-3 film was observed approximately 140-370 ºC, which was described to the decomposition of volatile materials. The main stage of weight loss or the
maximum thermal decomposition exhibited around 400 ºC (Figure 11 and Table 7).

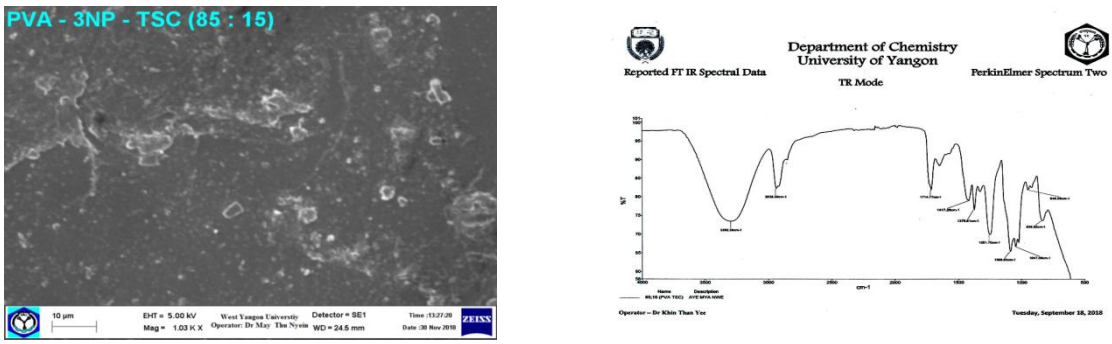

Figure 10 (a) SEM micrograph and (b) FT IR spectrum of PVA-SNP- 3 film

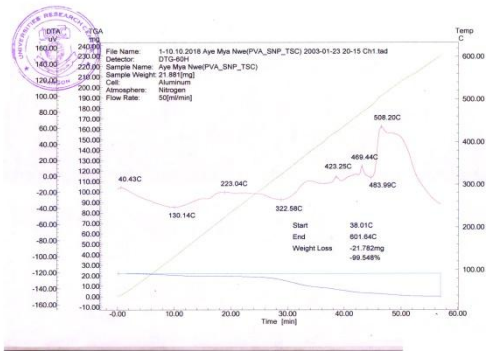

Figure 11 TG-DTA thermogram of PVA-SNP-3 film

Table 7 Thermal Stability of PVA-SNP-3 Film

Temperature Range (°C)	Weight Loss (%)	Peak's Temperature (°C)	Nature of Peak	TG and DTA Remarks
38 -140	7.03	130	endothermic	due to the removal adsorbed water and moisture due to the decomposition of volatile materials
140 -370	42.17	322	endothermic	
370 – 600	50.33	508	exothermic	due to the degradation and decomposition of polymers

EDXRF Analysis

Figure 12 shows the EDXRF spectrum of PVA-SNP-3 film. According to the EDXRF spectrum of the prepared PVA-SNP-3 film, carbon and hydrogen were major constituent (99.951 %) and silver was trace constituent (0.002 %) (Table 8).

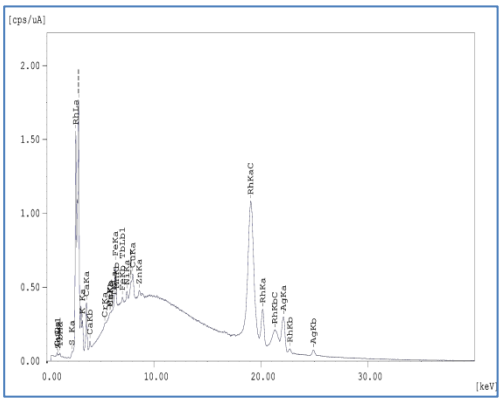

Figure 12 EDXRF spectrum of PVA-SNP-3 film

Table 8 Relative Aboundance of Element in PVA-SNP-3 Film

Elements	Relative Abundance (%)
Potassium	0.019
Calcium	0.012
Sulphur	0.011
Silver	0.002
Iron	0.001
Copper	0.001
Terbium	0.001
CH	99.951

Antimicrobial Activity of PVA-SNP Composite Films

Silver is known for its antimicrobial properties and has been used for many years in the medical field for antimicrobial applications. Additionally, silver has been used in water and air filtration to eliminate microorganisms. Inhibition zone diameters were obtained from the synthesized PVA and PVA-SNP composites tested against six microorganisms: (a) *Bacillus subtilis* (b) *Staphylococcus aureus* (c) *Pseudomonas aeruginosa* (d) *Bacillus pumilus* (e) *Candida albicans* (f) *Escherichia coli*. Antimicrobial activity of PVA-SNP composite films was investigated by agar well diffusion method as shown in Figure 13 and Table 9. It was

observed that the prepared PVA-3 film did not show antimicrobial activity, however PVA-SNP composite films showed the antimicrobial activity. According to the antimicrobial screening, PVA-SNP-3 film possesses higher antimicrobial activity than other PVA-SNP films.

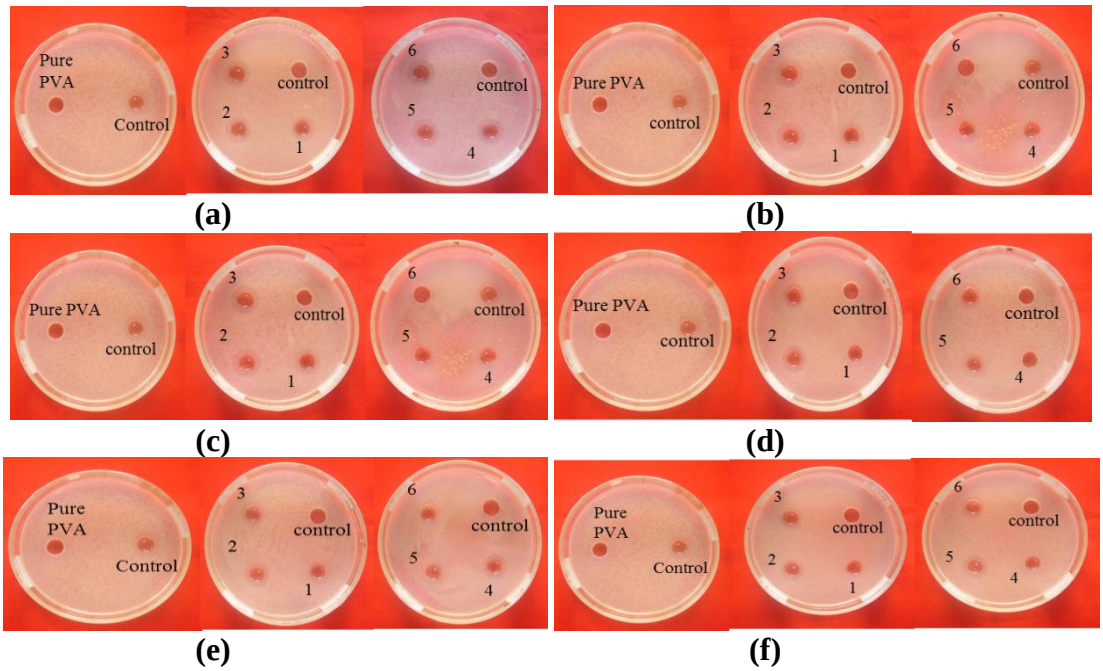

Figure 13 Antimicrobial activity of the prepared (1) PVA-SNP-1, (2) PVA-SNP-2, (3) PVA-SNP-3, (4) PVA-SNP-4, (5) PVA-SNP-5 and (6) PVA-SNP-6 composite films
(a) *Bacillus subtilis* (b) *Staphylococcus aureus*
(c) *Pseudomonas aeruginosa* (d) *Bacillus pumilus* (e) *Candida albicans*
(f) *Escherichia coli*

Table 9 Antimicrobial Activity of the Prepared Polyvinyl Alcohol-Silver Nanoparticles Composite Films by Agar Well Diffusion Method

Sample Films	Inhibition zone diameters of the samples against six microorganisms (mm)					
	Bacillus subtilis	***Staphylococus aureus***	***Pseud-omonas aeruginosa***	***Bacillus pumilus***	***Candida albicans***	***Escher-ichia coli***
Pure PVA	-	-	-	-	-	-
PVA-SNP-1	-	-	12 (+)	12 (+)	-	11 (+)
PVA-SNP-2	14 (+)	14 (+)	13 (+)	15 (++)	13 (+)	14 (+)
PVA-SNP-3	16 (++)	15 (++)	18 (++)	17 (++)	17 (++)	16(++)
PVA-SNP-4	15 (++)	13 (+)	17 (++)	16 (++)	15 (++)	14 (+)
PVA-SNP-5	13 (+)	13 (+)	12 (+)	13 (+)	13 (+)	13 (+)
PVA-SNP-6	16 (++)	16 (++)	12 (+)	17 (++)	17 (++)	16(++)

Agar Well 10 mm (-), 10 mm ~14 mm (+), 15 mm ~19 mm (++), 20 mm ~above (+++)

Conclusion

In this research work, the silver nanoparticles were synthesized by using trisodium citrate as reducing agent by chemical synthesis. In this synthesis, the volume ratio of silver nitrate (1 mM) and 1% w/v trisodium citrate solution was changed at optimum pH. The synthesized silver nanoparticles were characterized by UV-Visible spectroscopy, XRD, FT IR, SEM and EDXRF analyses. By the determination of UV-Visible spectrum, the maximum absorption peak of colloidal silver nanoparticles were appeared at 415 nm. According to the XRD spectra of all of the prepared SNP-TSC, there was no impurity peaks in the SNP-TSC1 and the crystallite size of SNP-TSC1 is 40.6 nm. In the FT IR spectrum of prepared SNP-TSC1, the characteristic absorption bands at 3441, 2874, 1583,1386 and 576 cm^{-1} were observed. From the SEM analysis, all prepared SNP-TSC illustrate the spherical shape and roughly spherical shape. According to SEM micrographs, the individual SNP were agglomerated to form either clusters or large nanoparticles. From the EDXRF spectrum of prepared SNP-TSC1, silver was major constituent (87.177 %) and other were trace constituents. The polyvinyl alcohol- silver nanoparticles (PVA-SNP) composite films were prepared using SNP and the optimum concentration of PVA solution (3 % w/v) solvent evaporating method. According to the mechanical properties of the prepared PVA-SNP composite films, PVA-SNP-3 has optimum tensile strength (37.7 MPa), elongation at break (262 %) and tear strength (139 kNm^{-1}) respectively. The characterization by modern techniques such as FT IR, SEM, TG-DTA and EDXRF analyses were able to reveal the characteristic functional group, morphological texture, thermal stability and relative abundance of the constituent elements. Antimicrobial activity of the prepared composite films (PVA-SNP) were investigated by Agar well diffusion method. According to the antimicrobial activity, pure PVA-3 film did not show antimicrobial activity but all prepared PVA-SNP composite films were observed to exhibit the antimicrobial activity against all of the tested microorganism. According to the antimicrobial screening, PVA-SNP-3 film possesses higher antimicrobial activity than other PVA-SNP films.

Acknowledgements

The authors would like to thank Professor and Head Dr Myint Myint Than, Department of Chemistry, Pyay University and Professor and Head Dr Ni Ni Than, Department of Chemistry, University of Yangon for their kind encouragement.

References

Angela, P., Bryan, A. and Juan Carlo, F. R . (2018). "Protocol for The Synthesis of Silver Nanoparticl UsingSodium Citrate and Sodium Borohydride As Reducing Agents". *White Paper in Nanomaterials*, pp. 1-7

Basavaraj, U. Praveenkumar, N. Sabiha, T. S. and Rupali, S. (2012). "Synthesis and Characterization of Silver Nanoparticles" . *International Journal of Pharmacy and Biological Sciences*, vol. 2 (3), pp. 10-14

Prema, P. (2011). "Chemical Mediated Synthesis of Silver Nanoparticles and Its Potential Antibacterial Application". *Progress in Molecular and Environmental Bioengineering*, vol. 6, pp. 151-166

Sayed, M. (2014). "Green Synthesis and Characterisations of Antibacterial Silver- Polyvinyl Alcohol Nanocomposite Films for Wound Dressing". *Journal of Applied Polymer Science*, vol. 3, pp. 229-234

Silverstein, R. M. and Webster, F. X. (1998). *Spectrometric Identification of Organic Compounds*. New York : 2nd ed., John Wiley and Sons, Inc., USA, 81-109

Zaheer, K. (2011). "Preparation and Characterization of Silver Nanoparticles by Chemical Reduction Method". *Colloids and Surfaces B : Biointerfaces*, vol. 82 (2) , pp. 513-517

STUDY ON THE SORPTION OF NATURAL DYES EXTRACTED FROM *ACACIA AURICULIFORMIS* A.CUNN. (MALAY-SHA-PADAUK) BARK ON COTTON AND ITS ANTIMICROBIAL ACTIVITIES

Zin Mar Win[1], Hmwe Nantthar[2], Nwe Nwe Aung[3]

Abstract

In this research work, the bark of *Acacia auriculiformis* A.cunn (malay-sha-padauk) was collected from Pyay Township, Bago Region. Physicochemical parameters of the raw bark powder such as moisture content, ash content, bulk density and pH content were determined. Natural dyes were extracted from the bark of malay-sha-padauk by different solvents (water, ethanol and methanol). The prepared natural dyes were characterized by FT IR, EDXRF and UV-Visible analyses. Relative abundances of elements in the extracted dye were analyzed by EDXRF which showed the chemical constituents of the element. The phytochemical tests of extracted natural dye were carried out. Furthermore, the antimicrobial activities of malay-sha-padauk dye were investigated by Agar Disc Diffusion method on six tested organisms. The maximum wavelength (λ_{max}) of dyes extracted with water, ethanol and methanol were 490 nm**,** 489 nm and 497 nm, respectively. Sorption properties of 1000 ppm natural dye solutions dyeing on cotton were studied at different temperatures (40, 50, 60, 70 and 80 °C) and contact time and pH (3, 4, 5, 6, 7 and 8) by UV-Visible spectrophotometer at different wavelengths for the various extract of malay-sha-padauk bark. From the experiment, it was revealed that the optimum temperature of dyes were at 70 °C and the optimum condition of dyeing on cotton were contact time of 50 min and pH 6. At optimum conditions, natural dye solutions with different alum dosages dyeing on cotton were studied by using UV-Visible spectrophotometer and more effective mordant (alum) dosage of 0.1 g was achieved for the dyeing process. The dye sample solutions were prepared by mixing natural dye powder with alum, onion peel, jengkol peel and tea waste to improve colour strength of dyes. Natural dye solutions dyeing on cotton were studied under optimum conditions by using three mordanting methods (pre-mordanting, simultaneously mordanting and post-mordanting).The colour intensities of these dyeing cotton was determined by Reflection Transmission Color Densitometer.

Keywords: Natural dye, *Acacia auriculiformis* A.cunn. , Malay-sha-padauk bark, antimicrobial activities, mordants

Introduction

Nature provides a wealth of plants which will yield their colour for the purpose of dyeing, many natural dyes have been used since antiquity. Natural dyes are known for their use in colouring of food substrate, leather as well as natural protein fibers like wool, silk and cotton as major areas of application since pre-historic times. Natural dyes are those obtained from plants, animals and minerals. Most of the natural dyes are found to be non-carcinogenic in nature. The use of non-allergic, non-toxic and eco-friendly natural dyes on textiles have become a matter of significant importance due to the increased environmental awareness in order to avoid some hazardous synthetic dyes (Alam, 2004).

Natural dyes produce very uncommon, soothing and soft shades as compared to synthetic dyes. On the other hand, synthetic dyes are widely available at an economical price and produce

[1] Assistant Lecturer, Department of Chemistry, Pyay University
PhD Candidate, Department of Chemistry, University of Yangon
[2] Dr, Lecturer, Department of Chemistry, Pyay University
[3] Dr, Lecturer,Department of Chemistry, University of Yangon

a wide variety of colours; these dyes, however, produce skin allergy, toxic wastes and other harmfulness to human body. For successful commercial use of natural dyes, the appropriate and standardized dyeing techniques need to be adopted without scarifying required quality of dyed textiles materials.

Aqueous extraction of natural dyes was most preferred method by textile dyers. The standardized dyeing techniques are needed for the better commercialization of natural dyes. Natural dyes have less substantivity to the fiber and have poor fastness properties, hence requires a mordant to improve their fixation in the fiber by forming a mordant- dye complex through chemical bonds. Mordants are metal salts which produce affinity between dye and the fiber. Mordants not only help in dye uptake and colour fastness, it also helps in achieving different colour shades in the textiles (Samanta and Agarwal, 2009). Biomordants are onion peel, jengkol peel and tea waste. Tannin is a widely used as biomordant. Tannin was used for dyeing and printing by people from onion peel, jengkol peel and tea waste.

The need to identify active chemical constituents in the plant extract required phytochemical and analytical techniques. Phytochemical surveys are being seen as the first step towards the discovery and structural elucidation of useful natural organic constituents for textile or medicinal applications. Many plants are chemically very variable depending on the locality where they are found with some of the constituents occurring only of certain seasons of the year (Adelani, 2007).

Moreover, natural dyes have positive effect on antifungal and antibacterial growth. Natural dyes not only release medicinal properties but also improve the aesthetic value of the product and they are unique and ecofriendly. Many of the plants used for dye extraction are classified as medicinal and some of these have recently been shown to possess remarkable antimicrobial activity (Machado *et al*., 2003). Many other common natural dyes are reported as potent antimicrobial agents owing to the presence of a large amount of tannins (Hussein *et al*.,1997).

Materials and Methods

Sample Collection

Acacia auriculiformis A.Cunn. is the plant used in this study for extraction of dye, which was collected from Pyay Township, Bago Region. The part used for the dye extraction was only bark.

Collection of Cotton

Cotton was purchased from Shwetaung Myoema Market, Bago Region.

Pretreatment of Cotton

The degummed cotton was soaked in mixture of 1 g L^{-1} of sodium carbonate and 2.5 g $L^{-1}$of detergent at 80°C for 30 min and then washed with running tap water to remove the natural impurities and improve the texture of cotton for dyeing.

Extraction of Tannin

The raw tea waste, onion peel and jengkol peel (10g each) were extracted with distilled water (1L) and the setup was kept boiling for 60 min.The extracted tannin was filtered and was used for mordanting.

Mordanting

Tannin extracted from tea waste,onion peel and jengkol peel has been used as biomordants to avoid toxicity caused by harmful chemical mordants. Extraction method has been standardized for maximum yield of tannin.

Utilization of Biomordants in Dyeing Method

Biomordants (tea waste, onion peel and jengkol peel) were utilized with different concentrations (10 %,20 %,30 %) for 1 h for mordanting with cotton cloth.The optimum concentration for each biomordant was selected and then dyeing method; pre-mordanting, simultaneous mordanting and post-mordanting were carried out.

Extraction of Dyes with different solvents

Aired dried powder of malay-sha-padauk bark (10 g) was extracted with each 100 ml of solvents (water, ethanol and methanol) in sonicator for 3 times each 30 mins and filtered. The filtrates were evaporated by distillation at various temperature (100,78,65) °C respectively. And then, they were dried in oven and were crushed in motar and pestle for semi-dried solid mass and sieved with 90 μm aperture size. Finally, dye powders of water extract, ethanol extract and methanol extract were 49.6%, 40.8%, 44.7% respectively.

Optimization of Dyeing

The pretreated cotton was dyed using dyes extracted (water,ethanol and methanol) from malay-sha padauk.Optimization of dyeing of cotton were studied at different temperature (40, 50, 60, 70 and 80 °C) and contact time (20,30,40,50,60,70 and 80)mins and pH (3, 4, 5, 6, 7 and 8) by using UV-Visible spectrophotometer.The optimum temperature, contact time and pH of water,ethanol and methanol dyes extracted were selected. And then,the most suitable conditions for dyeing on cotton was selected.

Dyeing procedure

The pretreated cotton was dyed using selected water extracted dye from malay-sha padauk bark and selected 20 % of biomordant (tea waste), 30 % of biomordants (onion peel and jengkol peel) at the optimum temperature 70°C, contact time 50min and pH 6 by using pre-mordanting, simultaneous mordanting and post- mordanting methods.

Determination of colour density

The colour density of the dyed cotton before and after lighting and washing were determined by Reflection Transmission Colour Densitometer at Universities' Research Center, Yangon.

Determination of Physicochemical Properties and Characterization of Dyes

Physicochemical Properties

Malay-sha padauk bark powder were washed with water to remove the adhering dirt and impurities. They were dried at room temperature and weighed. The physicochemical characteristics of malay-sha padauk bark powder such as moisture content, ash content, bulk density were determined by AOAC method and pH was determined by pH meter.

Phytochemical Investigation of Malay-sha padauk dye

Phytochemical investigation of malay-sha padauk dye was performed to determine the presence or absence of phytochemical compounds according to the methods and procedures expressed in the Phytochemical Bulletin of Botanical Society of America (Harborne, 1998).

UV-Visible Spectroscopy

The dye extracts were analyzed in UV-Visible spectrophotometer at the range of 400-800 nm ,to determine the wavelength of maximum absorption (λ_{max}) of the dye pigments.

FT IR Spectroscopy

FT IR measurements were carried out to determine the functional group of natural dye extracted from malay-sha-padauk. All measurements were carried out in the range of 400 -4000 cm^{-1}.The dye samples were measured by using Prekin Elmer GX system, FT IR spectrophotometer

EDXRF Spectroscopy

Elemental compositions in extracted dye from malay-sha-padauk by using solvents such as water and ethanol were determined by EDXRF spectrometer (Shimadzu Co.Ltd.,Japan).

Determination of the Antimicrobial Activities

The extracted dye solution were tested with *Aspergillus flavous, Bacillus subtilis, Candida albicans, Pseudomonas fluorescens , Xanthomonas oryzae* and *Escherichia coli* species to investigate the nature of antimicrobial activities by Agar Disc Diffusion Method.

Adsorption Capacity

The adsorption capacity of dyes was calculated using an equation on the basis of absorbance values recorded before and after dyeing with UV-Visible spectrophotometer.

$$\mathbf{q_t(mg\ g^{-1}) = \frac{C_o - C_e(mg\ L^{-1})}{Unit\ mass\ of\ adsorbent(g)} \times Volume\ of\ Solution\ (L)}$$

where,

q_t = adsorption capacity (mg g^{-1})
C_o=Initial concentration (mg L^{-1})
C_e=equilibrium concentration (mg L^{-1})
unit mass of adsorbent = 1g
Volume of solution = 0.1 L

Results and Discussion

The physicochemical characteristics of malay-sha-padauk bark powder and phytochemical investigation of water extracted dye sample were determined. Table 1 indicates that the results of 16.34 %w/w moisture content, 3.97 %w/w ash content and 0.98 gcm^{-3} bulk density in raw sample were observed. pH of the extract was 6.8. According to the results of physicochemical analysis, it was found that alkaloids, steroids, terpenoidsgly, flavonoids, cosides, phenolic compounds, tannins, α-amino acids, saponins, and cyanogenic glycosides were present in malay-sha-padauk dye sample whereas carbohydrates, starch and reducing sugar were absent in this extracted dye sample.

Table 1 Physicochemical Properties of Malay-sha-padauk Bark Powder

No	Characteristics	MLS
1	Moisture content (%)	16.34
2	Ash content (%)	3.97
3	Bulk density (g cm^{-3})	0.98
4	pH	6.8

Characterization of Malay-sha-padauk Dyes

Relative abundances of elements present in water and ethanol extracted dyes from malay-sha-padauk were determined by EDXRF analysis. According to EDXRF spectrum, water extract dye sample contained calcium 35.05 %, iron 28.74 %,potassium 26.31 %, silicon 4.97 %, sulphur 1.96 %,titanium 0.87 % and manganese 1.19 %. Ethanol extract dye sample contained calcium 66.46 %,iron 12.64 %, potassium 12.37 %,silicon 3.57 %,sulphur 2.64 %, titanium 1.48 % and copper 0.53 % (Figures 1 and 2 and Table 2).

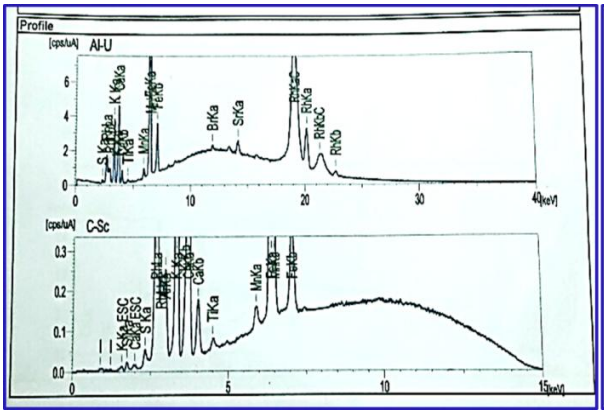

Figure 1 EDXRF spectrum of water extracted dye from bark of malay-sha-padauk

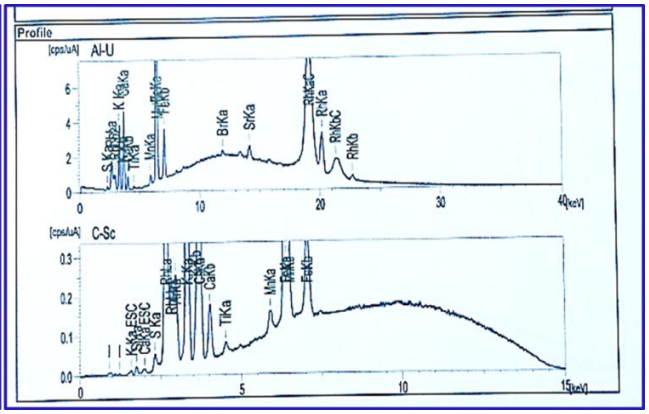

Figure 2 EDXRF spectrum of ethanol extracted dye from bark of malay-sha-padauk

Table 2 Relative Abundance of Element present in Water and Ethanol Extracted Dyes of *A.auriculiformis* (Malay-sha-padauk)

Element	Relative Abundance (%)	
	Water Extract	Ethanol Extract
Ca	35.05	66.46
Fe	28.74	12.64
K	26.31	12.37
Si	4.97	3.57
S	1.96	2.64
Ti	0.87	1.48
Mn	1.19	-
Cu	-	0.53

UV-Visible Analysis

The wavelengths of maximum absorption (λ_{max}) of extracted dyes were found to be 490 nm for water, 489 nm for ethanol and 497 nm for methanol extracts by using UV-Visible spectrophtometer.

FT IR Analysis

Figures (3)(a)(b) and (c) show that FT IR spectra of natural dye extracted from *A. auriculiformis* (malay-sha-padauk) with different solvents (water,ethanol and methanol).The characteristic absorption bands at 3221 cm^{-1},1612 cm^{-1},1523 cm^{-1} and 1033 cm^{-1} were observed.These peaks correspond to groups present in the sample and appeared due to

O-H stretching,C=O stretching,C=C aromatic stretching, and C-O-C stretching which is the good correlation with that of literature.These bands confirmed the presence of terpenoids, flavonoids and tannin in natural dyes (Table 3).

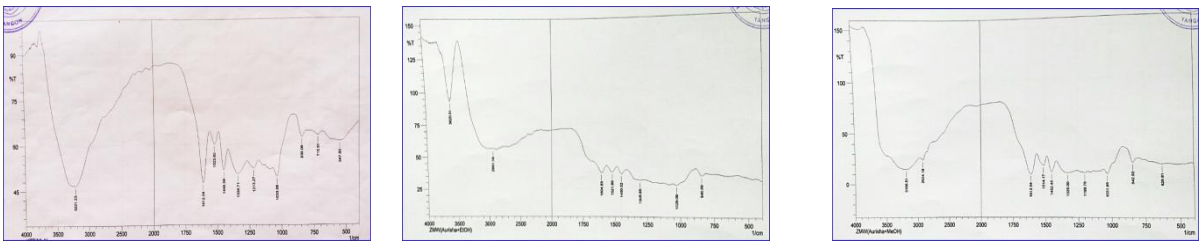

(a) (b) (c)

Figure 3 FT IR spectra of natural dyes extracted from *A.auriculiformis* (malay-sha- padauk) with different solvents

Table 3 Absorption Bands Assignments of Malay-sha-padauk Dye Extracted with Water, Ethanol and Methanol

Observed Frequency (cm^{-1})			Literature frequency* (cm^{-1})	Band assignments
MLS-W	MLS-EtOH	MLS-MeOH		
3221.23	3620.51	3210.51	3650 - 3200	O-H stretching
-	2951.19	2924.18	3000-2800	C-H stretching
1612.54	1604.83	1612.54	1700-1600	C=O stretching
1523.82	1521.89	1514.17	1550-1510	C=C aromatic stretching
1448.59	1450.52	1452.45	1465-1440	C-H bending(CH_3)
1213.27	-	1199.76	1280-1150	C-O stretching
1033.88	1028.09	1031.95	1070-1020	C-O-C stretching
839.06	840.99	842.92	900-800	=CH bending
715.61	-	-	800-700	N-H wagging

*** (**Silverstein *et al*., 2003)

Antimicrobial Activities of Malay-sha-padauk Dye

Screening of the antimicrobial activities of ethyl acetate, acetone, chloroform, ethanol, methanol, pet- ether and water extract was tested on six tested organisms such as *Aspergillus flavous, Bacillus subtilis, Candida albicans, Escherichia coli, Pseudomonas fluorescens, Xanthomonas oryzae* by Agar Disc Diffusion method. Among them, petroleum ether extract showed higher activity on five types of microorganism such as *Aspergillus flavous, Bacillus subtilis, Candida albicans, Escherichia coli* and *Pseudomonas fluorescens except Xanthomonas oryzae* and watery extracts showed no activity on all tested microorganism. In addition, malay-sha-padauk dye extract with pet-ether shows more significant zone of inhibition on five tested microorganisms when compared with other extracts. Therefore,it was found that antimicrobial activity of pet-ether extract was found to be more potent than other extracts as shown in Figure 4 and Table 4.

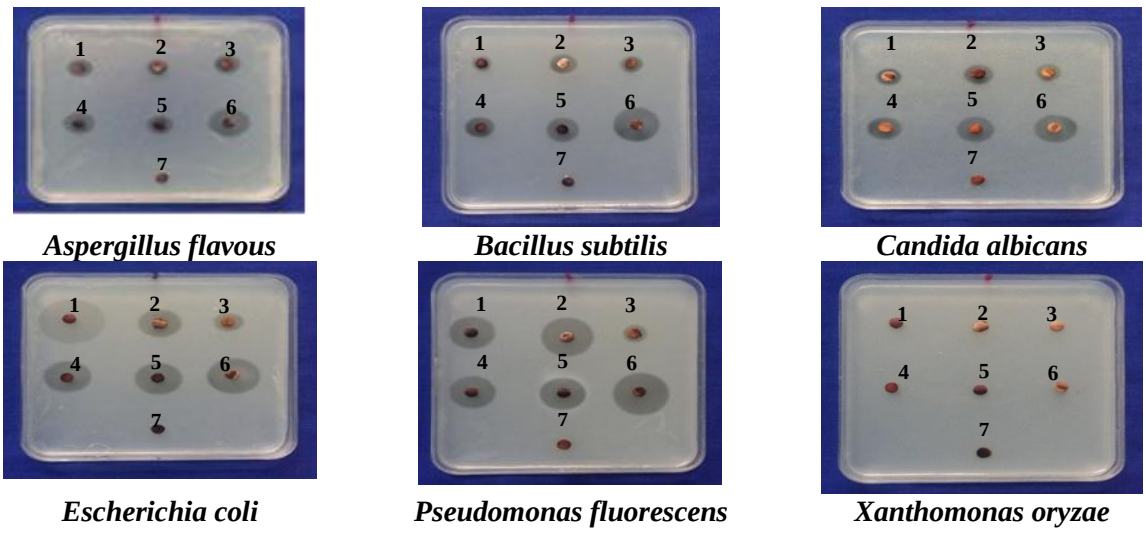

Figure 4 Antimicrobial activities of various solvent extracts of malay-sha-padauk dye

Table. 4 Antimicrobial Activities of Malay-sha-padauk Dye

No	Test Organisms	Acetone	$CHCl_3$	EtoAc	EtOH	MeOH	Pet. ether	H_2O
		Inhibition Zone Diameters (mm)						
1.	*Aspergillus flavous*	12(++)	10(+)	12(++)	15(++)	14(++)	23(+++)	-
2.	*Bacillus subtilis*	8(+)	12(++)	10(+)	14(++)	16(++)	20(+++)	-
3.	*Candida albicans*	10(+)	14(++)	8(+)	14(++)	15(++)	28(+++)	-
4.	*Escherichia coli*	23(+++)	18(+++)	12(++)	16(+++)	20(+++)	23(+++)	-
5.	*Pseudomonas fluorescens*	20(+++)	22(+++)	10(+)	18(+++)	20(+++)	23(+++)	-
6.	*Xanthomonas oryzae*	-	-	-	-	-	-	-

Agar well - 6 mm, 6 mm ~ 10mm (+), 11mm ~ 15mm (++), 16 mm above (+++), No activity (-)

Sorption of Extracted Dye from Malay-sha-padauk on CottonEffect of temperature

Batch adsorption experiments were conducted by 1 g of cotton to 100 mL of dye solutions with water in 250 mL beaker. A 100 mL dye solution contain in a 250 mL beaker was put in water bath. Natural dye solution dyeing on cotton were allowed to equilibrium for 60 minutes in a water bath at 40, 50, 60, 70 and 80°C. At 10 min intervals, the dye solution was taken from the beaker. The remaining concentration was determined by UV-Visible spectrophotometer at λ_{max} of water extract dye (490 nm). The result are shown in Table 5 and Figure 5. Similarly, sorption properties of ethanol and methanol were also determined at 40, 50, 60, 70 and 80°C by UV-Visible spectrophotometer at λ_{max} 489 nm and 497 nm, respectively. In dyeing, the optimum temperature of extracted natural dyes on cotton was 70 °C.

Table 5 Effect of Temperature on Dyeing with Extracted Malay-sha-padauk Dye on Cotton

Temperature (°C)	q_t (mg/g)		
	water	methanol	ethanol
40	55.39	36.11	59.39
50	66.18	54.17	62.09
60	74.09	60.19	63.72
70	86.39	80.09	77.61
80	64.03	75.07	71.52

q_t = amount of adsorbate per mass of adsorbent
Dose=1.0 g in 1000 mL of sample solution, time= 1 h

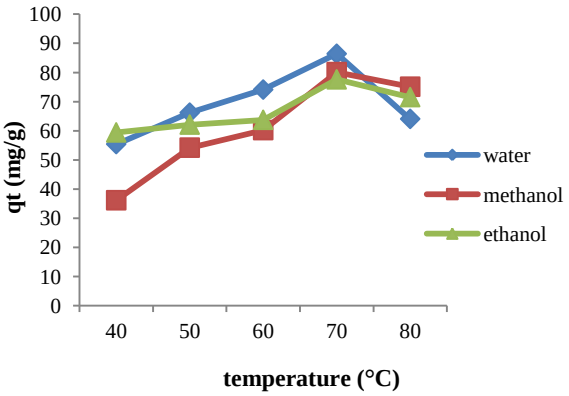

Figure 5 Effect of temperature on dyeing with the extracted malay-sha-padauk bark on cotton

Effect of contact time

Studies on the effect of contact time on dyeing of extracted dye on cotton were conducted by the same procedure for an equilibrium over a range of contact time (20, 30, 40, 50, 60 and 70) min in 250 mL beaker with a temperature control of 70°C. The results are illustrated in Table 6 and Figure 6. It was found that maximum sorption capacities were reached at contact time 50 min.

Table 6 Effect of Contact Time on Dyeing with the Extracted Malay-sha-padauk Bark Dye on Cotton

Time (min)	q_t (mg/g)		
	water	methanol	ethanol
20	48.34	26.85	39.43
30	52.66	33.79	43.16
40	63.38	35.65	54.97
50	77.69	46.77	71.09
60	73.98	42.46	69.03
70	72.45	45.64	62.76
80	69.59	41.67	58.83

q_t = amount of adsorbate per mass of adsorbent
Dose=1.0 g in 1000 mL of sample solution, 70°C

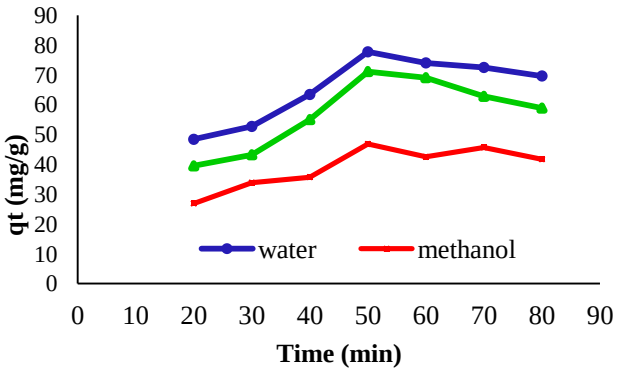

Figure 6 Effect of contact time on dyeing of extracted malay-sha-padauk bark on cotton

Effect of pH

Studies on the effect of pH on dyeing of extracted dye on cotton were conducted by the same procedure for an equilibrium over a range of pH values of 3, 4, 5, 6, 7 and 8 which pH were adjusted with 1% HCl and 1% NaOH .The extracted dyes were dyed on cotton allow to equilibrate for 50 mins in a water bath at 70 °C. The results are illustrated in Table 7 and Figure 7. In dyeing on cotton, the optimum pH of extracted natural dyes was 6.

Table 7 Effect of pH for on Dyeing with the Extracted Malay-sha-padauk Bark Dye on Cotton

pH	q_t (mg/g)		
	water	methanol	ethanol
3	72.68	59.39	66.68
4	80.18	62.09	73.22
5	85.89	66.34	78.89
6	93.76	81.41	88.75
7	89.91	77.61	82.91
8	71.33	79.87	75.34

q_t = amount of adsorbate per mass of adsorbent
Dose=1.0 g in 1000 mL of sample solution, 70 °C , 50 min

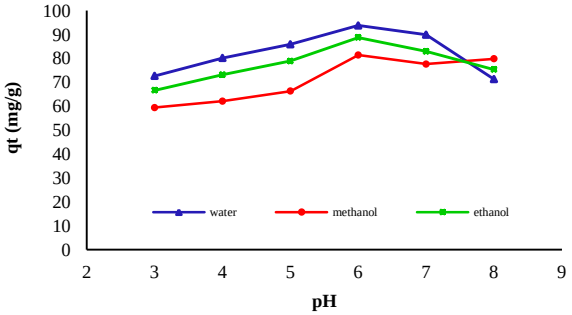

Figure7 Effect of pH on dyeing of extracted malay- sha- padauk bark on cotton

Effect of Mordant (Alum) Dosage

At the dye concentration 1000 ppm,contact time 50 min and temperature 70 °C studies on the effect of mordant (alum) dosage on dyeing of extracted dye on cotton were conducted by the same procedure for an equilibrium over a range of alum dosage (0.00625, 0.0125, 0.025, 0.05, 0.075, 0.1, 0.125 and 0,15)g by using UV-Visible spectrophotometer. Among the different alum dosage, 0.1g of alum dosage was the effective sorption capacity for dyeing process. The result was illustrated in Table 8 and Figure 8.

Table 8. Effect of Alum Dosage on Dyeing of Malay-sha-padauk bark on Cotton

Alum Dosage(g)	q_t (mg/g)		
	water	methanol	ethanol
0.00625	45.32	36.01	37.46
0.0125	54.12	41.61	55.34
0.025	70.12	60.11	65.98
0.05	79.53	72.11	74.28
0.075	81.68	72.78	76.54
0.1	93.41	82.21	86.73
0.125	80.02	79.55	65.19
0.15	74.28	73.19	56.04

q_t= amount of adsorbate per unit mass of adsorbent
Dose=1.0g in 1000 mL of sample solution, 70°C ,50 min

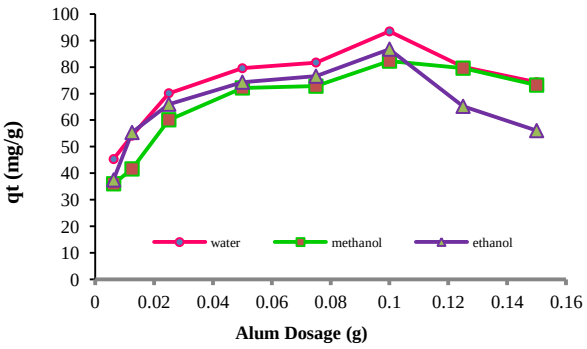

Figure 8 Effect of alum dosage on dyeing of extracted malay-sha-padauk bark on cotton

Colour Fastness Properties of five Dye Solutions Dyeing on Cotton

In this research, biomordants (onion peel, jengkol peel and tea waste) and chemical mordant (alum) were studied for dyeing process.The colour density on the cotton was increased significantly by using mordant.For dyeing process, colour fastness of cotton samples were prepared using pre-mordanting, simultaneous mordanting and post-mordanting. The colour

density for five dyeing cotton cloth before and after colour fastness testing were compared in Tables 9 (a)(b)(c)and(d) and Figures 9 (a)(b)(c)and (d). Desorption properties for post-mordanting are shown in Table 10.

In dyeing, poor substantivity and fastness properties are often found in natural dyes for cotton and can be improved if the cotton was first treated with a solution containing mordant, such as a salt of alum. Metallic mordant and biomordants improve the fixation and fastness properties of dyes lacking substantivity for cotton.

The colour fastness results of five dyeing cotton in pre-mordanting, simultaneous mordanting and post-mordanting are shown in Table 9 a. The sample S_1 (natural dye) was seen the lowest colour density.The sample S_5 (tea waste biomordant) was medium colour density and S_4 (jengkol peel biomordant) was the highest colour density. The sample S_2(alum) and S_3 (onion peel biomordant) were nearly equal colour density.Therefore, biomordant (onion peel) can be used instead of chemical mordant (alum) for malay-sha-padauk dye solution (Li *et al*., 2016).

According to the desorption properties, S_4 (jengkol peel biomordant) was good colour fastness biomordant among the five mordants such as S_1 S_2 S_3 S_4 and S_5.So,it can be applied in home-made dyeing process. The results were shown in Table (10).

Table 9(a) Colour Density of Cotton Dyed with Water Extract of Malay-sha- padauk Dye

Type of Mordants	**Colour Density /**				
mordanting	Without S_1	Alum S_2	Onion peel S_3	Jengkol Peel S_4	Tea waste S_5
Pre-mordanting	0.38	0.41	0.44	0.73	0.61
Simultaneous mordanting	0.38	0.43	0.43	0.86	0.74
Post mordanting	0.38	0.48	0.52	0.90	0.79

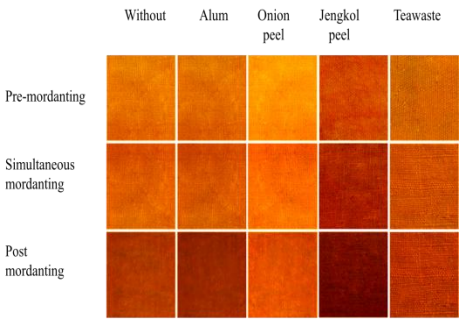

Figure 9(a) Colour density of cotton dyed with water extract of malay-sha padauk dye

Table 9 (b) Variations in Colour Density of Cotton Dyed AfteFastnesTest(Pre-modanting with water extract of Malay-sha padauk Dye)

	Colour Density / Mordants				
Mordant	**Without** S_1	**Alum** S_2	**Onion peel** S_3	**Jengkol peel** S_4	**Tea waste** S_5
Before	0.38	0.41	0.44	0.73	0.61
lighting	0.33	0.37	0.42	0.71	0.57
Washing	0.31	0.37	0.40	0.56	0.41

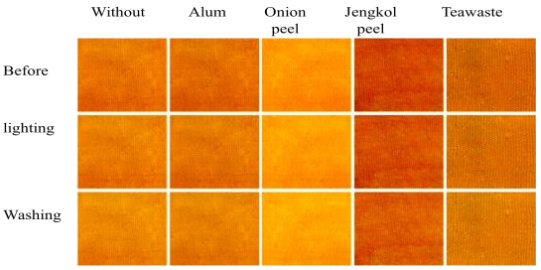

Figure 9(b) Variations in colour density of cotton dyed after fastness test (pre - modanting with water extract of malay-sha padauk dye)

Table 9 (c) Variations in Colour Density of Cotton Dyed After Fastness Test (Simultaneous modanting with water extract of Malay-sha padauk Dye)

	Colour Density / Mordants				
Mordant	**Without** S_1	**Alum** S_2	**Onion Peel** S_3	**Jengkol Peel** S_4	**Tea waste** S_5
Before	0.38	0.43	0.43	0.86	0.74
lighting	0.37	0.41	0.43	0.72	0.73
Washing	0.36	0.40	0.41	0.65	0.55

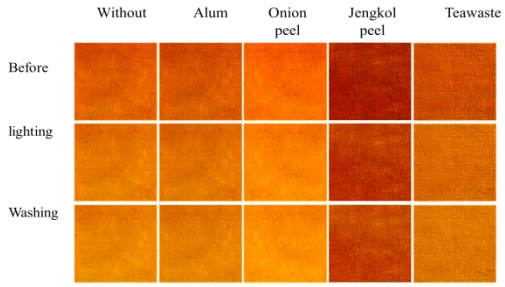

Figure 9(c) Variations in colour density of cotton dyed after fastness test (simultaneous modanting with water extract of malay-sha padauk dye)

Table 9 (d) Variations in Colour Density of Cotton Dyed After Fastness Test (Post-modanting with water extract of Malay-sha padauk Dye)

	Colour Density / Mordants				
Mordant	Without S_1	Alum S_2	Onion peel S_3	Jengkol Peel S_4	Tea waste S_5
Before	0.38	0.48	0.52	0.90	0.79
lighting	0.36	0.47	0.50	0.90	0.76
Washing	0.36	0.46	0.49	0.89	0.77

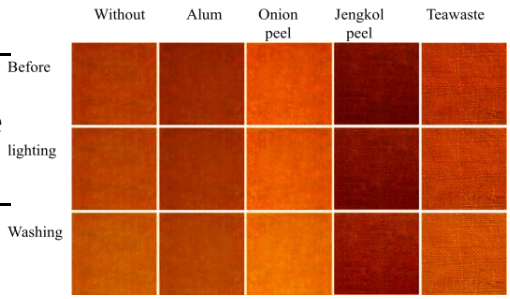

Figure9 (d) Variations in colour density of cotton dyed after fastness test (post-modanting with water extract of malay-sha padauk dye)

Table 10 Difference Before and After Wash Fastness (Post-Mordanting) Properties of Five Dye Solutions on Cotton

	Without	Alum	Onion peel	Jengkol Peel	Tea waste
	S_1	S_2	S_3	S_4	S_5
Desorption values	0.02	0.02	0.03	0.01	0.02

Conclusion

In this research work, an eco-friendly dye from natural source and dyeing on cotton with biomordants. The physicochemical parameters of bark of malay-sha-padauk such as moisture content 16.34 %, ash content 3.97 %, bulk density 0.98 gcm^{-1} and pH 6.8 were observed. The preliminary phytochemical screening tests of bark dye showed the presence of alkaloids, steroids, terpenoids, flavonoids, glycosides, phenolic compounds, tannins, α-amino acids, saponins, and cyanogenic glycosides whereas carbohydrates, starch and reducing sugar were absent in this extracted dye sample. By the determination of UV-Visible spectra, the maximum absorption peak of water, ethanol and methanol extracted natural dyes were appeared to 490 nm, 489 nm and 497 nm respectively. FT IR spectrum of extracted natural dyes indicated that the intensity band at 3221 cm^{-1} is corresponding to OH stretching,1612 cm^{-1} is C=O stretching, 1523 cm^{-1} is due to C=C aromatic stretching and 1033 is corresponding to C-O-C stretching. According to EDXRF spectra, the relative abundance of element present in water and ethanol extracted of natural dye were 35.05 % and 66.46 % of calcium respectively. From the experimental result, the best dyeing was achieved at pH 6, 70°C for 50mins with dye concentration 1000 ppm for extracted natural dyes by using UV-visible spectrophotometer. Among the various extracted natural dyes, water extracted dye was the most suitable for dyeing on cotton. Among three mordanting methods, post-mordanting method was the best for dyeing process. In this research, biomordants (onion peel, jengkol peel and tea waste) and chemical mordant (alum) were studied for dyeing process. The sample S_1 (natural dye) has the lowest colour density. The sample S_5 (tea waste) was medium colour density and S_4 (jengkol peel) was the highest colour density. The colour density sample S_2 (alum) and S_3 (onion peel) were nearly equal. Therefore, biomardant (onion peel) can be used as instead of chemical mordant (alum) for dye sample solution. According to the desorption properties, S_4 (jengkol peel) was good colour fastness biomordant among the five mordants such as S_1 S_2 S_3 S_4 and S_5. So, it can be applied in home-made dyeing process. Screening of the antimicrobial activities of ethyl acetate, acetone, chloroform, ethanol, methanol, pet- ether and water extract was tested on six tested organisms by Agar Disc Diffusion method. Among them, malay-sha-padauk dye extract with pet-ether shows more significant zone of inhibition on five tested microorganisms when compared with other extracts. Therefore, it was found that antimicrobial activity of pet-ether extract was found to be more potent than other extracts. Many natural dye possess medicinal properties. So, these textile dyed with natural dyes can be very useful in developing clothing for infants, elderly and infirm people to protect them against common infections. Nowadays, there is increasing awareness among people towards natural products.

Acknowledgements

The authors would like to thank the Department of Higher Education, Ministry of Education, Myanmar, for the permission of doing this research and Myanmar Academy of Arts and Sciences allowing the writing of this paper, Professor and Head Dr Daw Myint Myint Than, Department of Chemistry, Pyay University and Professor and Head Dr Daw Ni Ni Than, Department of Chemistry, University of Yangon, for their kind encouragement.

References

Adelani, P.O. (2007). "Synthetic Pathway of 8-Hydroxyl-9,10-Dimethoxyanthracene-2- Aldehyde (Oruwalol)". *European Journal of Scientific Research*, vol.16 (1), pp. 44-54.

Alam. (2004). "Studies of Some Natural Dyes". *Journal of the Chemical Society*, vol. 26 (3), pp. 255-263.

Harborne, J.B. (1998). *Phytochemical Methods, A Guide to Modern Technique of Plant Analysis*. New York; 3rd Ed., Chapman and Hall, pp. 120-160.

Hussein, S.A.M., Barakat, H.H., Merfort, I. and Nawwar, M.A.M.(1997). "Tannins from the Leaves of *Punica granatum". Phytochemistry*, vol.45, pp. 819-823.

Li, Y.V., Malensek, N., Sarkar, A.K. and Xiang, C.(2016). "Colorfastness Properties of Persimmon Dye on Cotton and Wool Fabrics". *Clothing and Textile Research Journal*, vol. 34(3), pp. 223-234.

Machado, T.B., Pinto, A.V., Pinto, M.C.F.R., Leal, I.C.R., Silva, M.G., Amaral, A.C.F., Kuster, R.M. and Netto-dosSantos, K.R. (2003). "In Vitro Activity of Brazilian Medicinal, Plants Naturally Occurring Naphthoquinones and their Analogues,against Methicillin Resistant S*taphylococcus aureus*". *Int. J Antimicrob Agents*, vol. 21, pp. 279-284.

Samanta, A.K. and Agarwal, P . (2009). "Application of Natural Dyes on Textiles". *Indian Journal of Fibre and Textile Research*, vol. 34, pp. 384-399.

Silverstein, R.M., Webster, F.X. and Kiemle, D.J. (2003). *Spectrometric Identification of Organic Compounds.* New York: 7th Edition., John Wiley and Sons Inc.

MACROLIDE ANTIBIOTICS AND INDOLE ALKALOID PRODUCED FROM MARINE AND TERRESTRIAL BACTERIA

Hnin Yu Win[1], Hartmut Laatsch[2]

Abstract

Chemical investigation of terrestrial bacteria *Bacillus subtilis* M 8 and marine-derived *Streptomyces* sp. B 8406 led to the identification of macrolide antibiotics, namely, macrolactin F (1) and borrelidin (3) respectively. Additionally, the strains delivered the precursor of indole alkaloid, tryptophan (2) and indole alkaloid, 6-prenyltryptophol (4) respectively. The structures of these metabolites were elucidated based on 1D and 2D NMR experiments and mass studies. Macrolactin F (1) showed weak antibacterial properties. Borrelidin (3) showed high activity against *Escherichia coli*, *Candida albicans* and *Mucor miehei* (Tü 284) by causing inhibition zones of 25, 30 and 30 mm, at 40 μg/ disk; it showed medium activity against *Staphylococcus aureus*, *Streptomyces viridochromogenes* (Tü 57) and weak activity against *Bacillus subtilis*. It was also found to have an activity against *Artemia salina* of 93 %. Moreover, biogenesis of borrelidin (3) was discussed.

Keywords: macrolide, indole, alkaloid, antibiotics

Introduction

Natural products are still an important source of new pharmaceutical compounds, and natural products are metabolites from microorganisms, plants or animals (Baker *et al*., 2000). Traditionally, the major sources of these secondary metabolites are plants and terrestrial microorganisms (Barry *et al*., 1997). Over the past decades, microorganisms and especially marine bacteria have been recognized as an important source for novel bioactive compounds that are active against antibiotic-resistant human pathogens. The study of biologically active marine natural products has greatly influenced the drug discovery from natural sources in fields ranging from pharmacology to cancer medicine.

The macrolides are a class of natural products that consist of a large macrocyclic lactone ring. A great number of new macrolides from marine organisms has been discovered. Most of them have been found to have interesting biological activity such as antibiotics and some of them play vital roles as potential molecules for drug development or as tools for basic biological research. Actinomycetes are the largest source of natural macrolides and produce more than three hundred 16-membered derivatives thereof, nearly one hundred 14-memberedmacrolides and some other compounds with various ring sizes up to a 60-membered ring, including polyene macrolides,macrodiolides, macrotetrolides, and immune-suppressive macrolide lactams (Shiomi and Ōmura, 2002). Erythromycin ([McGuire] *et al*., 1952), a representative glycosidic 14-membered ring macrolide, and its related macrolides are also produced by actinomycetes and are widely used as antibacterial antibiotics.

In the search for novel and pharmacologically active metabolites, a screening of extracts from terrestrial and marine-derived bacteria was performed. In the screening of *Bacillus subtilis* M 8, the strain delivered macrolactin F (1) and tryptophan (2). Marine *Streptomyces* sp. B 8406 delivered borrelidin (3) and 6-prenyltryptophol (4).

[1] Dr. rer. nat., Associate Professor, Department of Chemistry, University of Mandalay
[2] Professor, Institute of Organic and Biomolecular Chemistry, The University of Göttingen, Göttingen, Germany

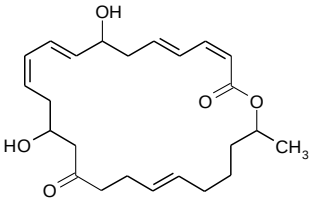

(1)

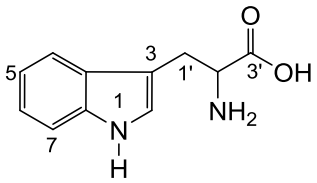

(2)

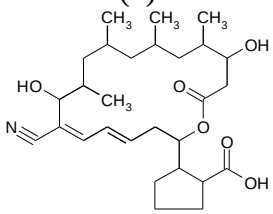

(3)

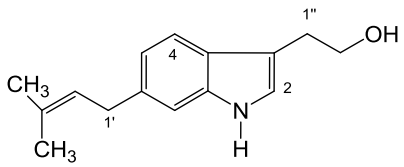

(4)

Materials and Methods

General Experimental Procedures

NMR spectra were measured on a Varian Inova 600 (599.740 MHz) and a Varian Unity 300 (300.145 MHz) spectrometer. ESIMS were measured on a Quattro Triple Quadrupol mass spectrometer with a Finnigan TSQ 7000 with nano-ESI API ion source. EIMS at 70 eV with Varian MAT 731, Varian 311A, AMD-402, high resolution with perflurokerosene as standard. HRESIMS were measured on a Micromass LCT mass spectrometer coupled with a HP 1100 HPLC and a diode array detector. Column chromatography was carried out on MN silica gel 60, 0.05-0.2 mm; TLC was performed on Polygram SIL G/UV_{254}. All silica gel materials were purchased from Macherey-Nagel, Düren, Germany. Size exclusion chromatography was done on Sephadex LH-20 (Lipophilic Sephadex; Amersham Biosciences, Freiburg, Germany, purchased from Sigma-Aldrich Chemie, Steinheim, Germany). XAD-16 adsorber resin was obtained from Rohm and Haas (Frankfurt, Germany).

Spray reagents

Anisaldehyde/sulphuric acid: 1 mL anisaldehyde was added to 100 mL of a stock solution containing 85 mL methanol, 14 mL acetic acid and 1 mL sulphuric acid. After spraying, the TLC cards were heated with hot air until colour development.

Biological screening

The crude extract was dissolved in $CHCl_3$/10% MeOH (400 μg/paper disk), in which the paper disks were dipped, dried under sterile conditions (flow box) and put on an agar plates inoculated with *Bacillus subtilis* (ATCC6051), *Staphylococcus aureus*, *Streptomyces viridochromogenes* (Tü 57), *Escherichia coli*, *Chlorella vulgaris*, *Chlorella sorokiniana*, *Scenedesmus subspicatus*, *Candida albicans* and *Mucor miehei* (Tü 284). The plates were incubated at 37 °C for bacteria (12 h), 27 °C for fungi (24 h), and 24-26 °C under day-light for micro-algae (96 h). The diameter of the inhibition zones was measured by ruler.

Brine shrimp microwell cytotoxicity assay

To a 500 mL separating funnel filled with 400 mL of artificial seawater, 0.5 g of dried eggs of *Artemia salina* was added. The suspension was aerated by bubbling air into the funnel and kept for 24 to 48 h at room temperature. After aeration had been removed, the suspension was kept for 1 h undisturbed, whereby the remaining unhatched eggs dropped. In order to get a higher density of larvae, one side of the separating funnel was covered with aluminium foil and the other illuminated with a lamp, whereby the phototropic larvae were gathering at the illuminated side and could be collected by pipette. 30 to 40 shrimp larvae were transferred to a deep-well microtiter plate (wells diameter 1.8 cm, depth 2 cm) filled with 0.2 mL of salt water and the dead larvae counted (number N). A solution of 20 µg of the crude extract in 5 to 10 µL DMSO was added and the plate kept at room temperature in the dark. After 24 h, the dead larvae were counted in each well under the microscope (number A). The still living larvae were killed by addition of ca. 0.5 mL methanol so that subsequently the total number of the animals could be determined (number G). The mortality rate M was calculated in %. Each test row was accompanied by a blind sample with pure DMSO (number B) and a control sample with 1 µg/test actinomycin D. The mortality rate M was calculated using the following formula:

$$M = \left[\frac{(A - B - N)}{(G - N)} \right] \cdot 100$$

Where

M	=	percent of the dead larvae after 24 h
A	=	number of the dead larvae after 24 h
B	=	average number of the dead larvae in the blind samples after 24 h
N	=	number of the dead larvae before starting of the test and
G	=	total number of brine shrimp

Primary screening

Antibiotic screening (disk diffusion test): The test is performed using paper discs with a diameter of 8 mm under standardized conditions. If the inhibition zone is ranging from 11 to 20 mm, the compound is considered to be weakly active (+), from 21 to 30 mm designated as active (++) and over 30 mm is highly active (+++). Chemical screening: evaluation of the separated bands by the number, intensity and colour reactions with different staining reagents on TLC. Toxicity test with brine shrimps: by counting survivors after 24 h, the mortality of the extracts was calculated (see above). The extracts, fractions or isolated compounds were considered inactive when the mortality rate was lower than 10% (-), from 10 to 59% as weakly active (+), from 60 to 95% as active (++) and over 95% as strongly active (+++).

Fermentation, Work-up and Isolation

The strain *Bacillus subtilis* M 8 was cultivated on LB-medium [tryptone (10 g), yeast extract (5 g), sodium chloride (10 g) in 1000 mL tap water] in a 25 L scale. Well-grown agar plates were used to inoculate 60 Erlenmeyer flasks (1 L flask size), each containing 250 mL LB medium at pH 7. The cultures were cultivated on the linear shaker for 72 h at 34 °C. The resulting culture broth was filtered with the aid of the filter press. The water phase was subjected

to an XAD-16 column and extracted with MeOH. The mycelium was extracted with ethyl acetate and acetone. The two combined phases was brought to dryness under reduced pressure to yield 14.2 g crude extract. The resulting crude extract was subjected to a silica gel column chromatography using a CH_2Cl_2/MeOH gradient and separated into fractions I-V. Further purification of fractions III by Sephadex LH-20 and RP-18 silica gel yielded macrolactin F (1). Tryptophan (2) was isolated as white amorphous from the very polar fraction. It exhibited UV absorption at 254 nm and gave red colour reaction with anisaldehyde/sulphuric acid.

The subculture of marine *Streptomyces* sp. B 8406 was used to inoculate a 25 L shaker culture using M_2^+ medium [malt extract (10 g), yeast extract (4 g) and glucose (4 g) were dissolved in 500 mL tap water and 500 mL sea water, pH 7.8 before sterilisation]. After 7 days, the fermentor broth was harvested and the resulting reddish brown culture broth was subjected to filtration over Celite using a filter press. The filtrate was given on XAD-16, and the adsorbed metabolites were eluted with methanol. The methanol was evaporated under reduced pressure and the resulting water residue was extracted by ethyl acetate. The biomass was extracted by ethyl acetate and acetone until the colour had disappeared. The combined organic solutions were evaporated under vacuum to yield 2.56 g of reddish brown crude extract. Separation was performed by a flash silica gel column chromatography (CH_2Cl_2/MeOH gradient, 2.5 L CH_2Cl_2, 1.0 L CH_2Cl_2/2% MeOH, 1.0 L CH_2Cl_2/4% MeOH, 1.0 L CH_2Cl_2/5% MeOH, 0.5 L CH_2Cl_2/10% MeOH, 0.5 L CH_2Cl_2/20% MeOH, 0.5 L CH_2Cl_2/50% MeOH, 0.5 L MeOH). Borrelidin (3) (10 mg) was isolated from fraction III by subjecting on a silica gel column with a CH_2Cl_2:MeOH gradient. 6-prenyltryptophol (4) was isolated from fraction II by passing it over Sephadex LH-20 (MeOH).

Results and Discussion

Macrolactin F (1)

Macrolactin F (1) was isolated as oily substance and showed a UV absorbing band at 254 nm, which stained to green with anisaldehyde-sulphuric acid. Structure assignment of macrolactin F was achieved by interpretation of spectroscopic analysis, particularly by H,H COSY NMR data. In the ^{1}H NMR spectrum (Figure 1), there were 10 olefinic proton signals, three oxygen-bound proton signals, many CH_2 signals and one methyl doublet. Analysis of the ^{13}C NMR (Figure 2) and HSQC spectra showed a ketone and an ester carbonyl signal at δ 211.8 and 167.9, ten olefinic carbon signals, three oxygenated carbon signals, 8 CH_2 and one CH_3. The (+)-ESI mass spectrum indicated an $[M + Na]^+$ ion peak at *m/z* 425. By analysis of the COSY spectrum (Figure 3), three substructures were constructed (Figure 4).

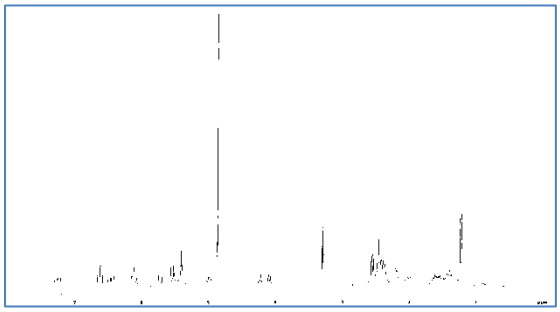

Figure 1 ^{1}H NMR spectrum (CD_3OD, 300 MHz)

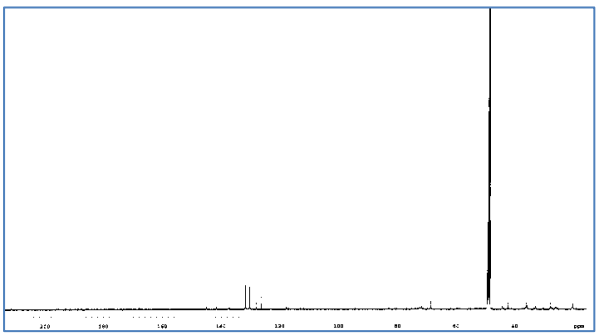

Figure 2 ^{13}C NMR spectrum (CD_3OD, 125 MHz) of macrolactin F

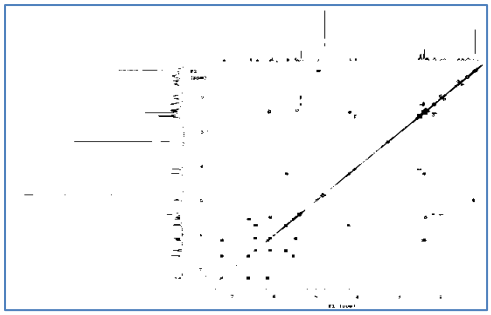

Figure 3 COSY spectrum (CD_3OD, 600 MHz) of macrolactin F

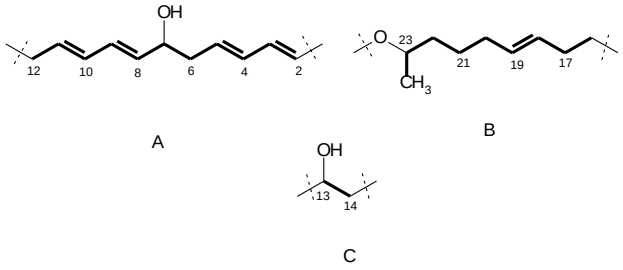

Figure 4 Fragments of macrolactin F (1) resulting from the COSY (▬) spectrum

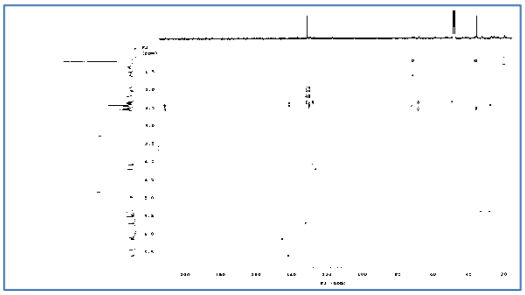

Figure 5 HMBC spectrum (CD_3OD, 600 MHz) of macrolactin F

While the methine proton at δ 5.55 (H-2) showed the HMBC correlation to the acid carbonyl at δ 167.9 (C-1), the two CH_2 groups at δ 2.56 and 2.46 (H-14 and H-16) showed HMBC interactions with the ketone carbonyl at δ 211.8 (C-15) (Figure 5). The H-14 exhibited correlation again with one oxygenated methine carbon at δ 68.7 (C-13) and methylene group at δ 35.9 (C-12) from fragment A. The HMBC correlations of a methyl doublet at δ 1.23 (H-24) with one oxygenated methine carbon at δ 71.8 (C-23) and one methylene at δ 36.2 (C-22) confirmed the COSY correlations (Figure 6).

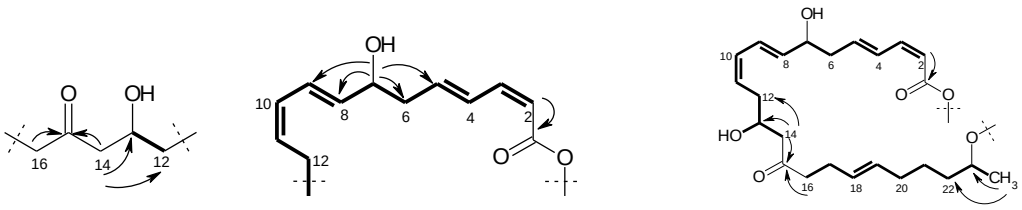

Figure 6 Selected HMBC (→) correlations in macrolactin F

By closing the two open chains as lactone, the complete structure was deduced and it was assigned as macrolactin F. It was a geometrical isomer of macrolactin K, which has a *trans* double bond between C-10 and C-11 (Figure 7). The coupling constant between H-10 and H-11 was less than 12 Hz in compound and it was interpreted as *cis* double bond.

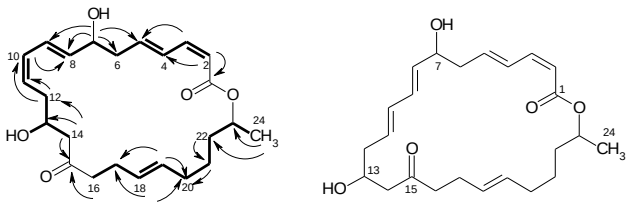

Figure 7 H,H COSY (▬)and selected HMBC (→) correlations of macrolactin F (1) and macrolactin K

Table 1 shows the NMR spectroscopic data for macrolactin F (1).

Table 1 NMR spectroscopic data for macrolactin F (1)

Position	δ_C	δ_H (mult.; *J* in Hz)
1	167.9	CO
2	117.9	5.55 (d, 11.4)
3	145.1	6.62 (t, 11.4)
4	130.4	7.26 (ddd, 1.1, 11.3, 15.3)
5	141.6	6.17 (dd, 8.1, 14.6)
6	42.4	2.46 (t, 7.4)
7	72.6	4.23 (q, 6.4)
8	137.5	5.73 (dd, 6.4, 15.3)
9	126.5	6.46 (dd, 10.9, 15.2)
10	131.8	6.11 (t, 11.0)
11	128.1	5.49 (q, 8.1)
12	35.9	2.39 (m)
13	68.7	4.09 (q, 6.3)
14	49.6	2.56 (dd, 4.5, 6.2)
15	211.8	CO
16	44.4	2.46 (t, 7.4)
17	27.9	2.21 (m)
18	130.3	5.41 (m)
19	131.9	5.41 (m)
20	32.9	2.05, 1.96 (m)
21	26.1	1.39 (m)
22	36.2	1.62, 1.53 (m)
23	71.8	4.99 (m)
24	20.3	1.23 (d, 6.3)

Tryptophan (2)

The ^{1}H NMR spectrum (Figure 8) of tryptophan (2) shows two 1H doublets and two 1H triplets of doublets at δ 7.59, 7.37, 7.06 and 6.97 for a 1,2-distubstituted benzene ring. Additionally, the spectrum shows a singlet at δ 7.29. The signal pattern in the aromatic region indicated the presence of a 3-substituted indolic moiety. In the aliphatic region, a heteroatom bearing methine signal at δ 3.61 and diastereotopic methylene signals at δ 3.36 and 3.07 indicated the neighbourhood of an sp^2 carbon or heteroatom.

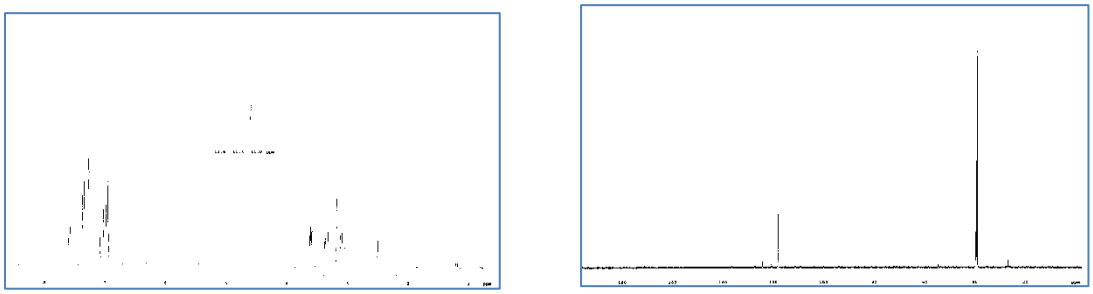

Figure 8 ^{1}H NMR spectrum (CD_3OD, 300 MHz) and ^{13}C NMR spectrum (CD_3OD, 125 MHz) of tryptophan

The ^{13}C NMR spectrum shows 11 signals, whereof those at δ 171.2 could be assigned to carbonyl of acid, ester or amide. In addition, there were eight signals sp^2 carbons, one nitrogen bearing carbon and one methylene carbon.

The (-)-ESI mass spectrum indicated a *quasi*molecular ion at *m/z* 203 $[M - H]^-$ leading to the molecular weight of 204 Dalton. Comparison with authentic spectra identified the isolated compound as tryptophan. Tryptophan is one of the 20 proteinogenic as well as an essential amino acid. In genetic code, it is encoded by the codon UGG.

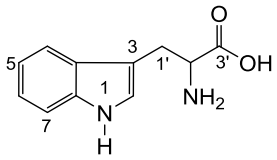

(2)

Borrelidin (3)

Borrelidin (3) was isolated as colourless oil from fraction III by passing through a silica gel column. It showed UV absorption at 254 nm and stained to green with anisaldehyde/sulphuric acid. The ESI mass spectrum indicated an $[M + Na]^+$ ion peak at *m/z* 512 for a molecular weight of 489 Dalton, and the HR ESI mass spectrum afforded the molecular formula $C_{28}H_{43}NO_6$ with 8 double bond equivalents.

The ^1H NMR spectrum displayed three olefinic protons at δ6.89, 6.59 and 6.30, three oxygenated protons at δ 4.97, 4.18 and 3.92, one methyl doublet at δ1.01, three overlapped methyl doublets at δ 0.83 and the other multiplets between δ 2.80 and 1.01, which were assigned as long chain of CH and CH_2 groups. The carbon spectrum indicated the presence of 28 carbons, which were assigned by chemical shifts and analysis of HSQC to two carbonyls of acid, ester or amide, three methine sp^2 atoms, two olefinic quaternary atoms, three oxygenated methine atoms, eight aliphatic methylenes, six aliphatic methines and four methyls. $^1H,^1H$ COSY data established the fragments **A, B, C** and **D** (Figure 9-13).

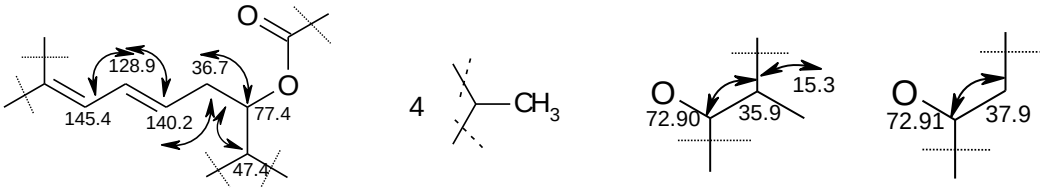

A **B** **C** **D**

Figure 9 Partial structures of borrelidin (3) from H,H COSY spectrum

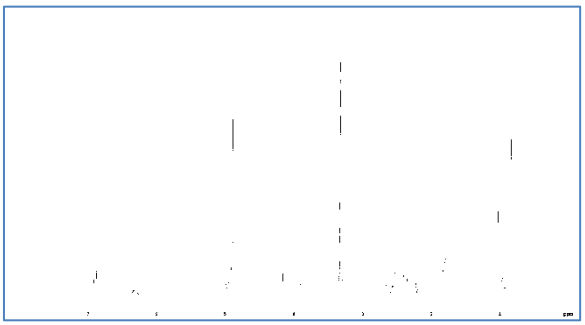

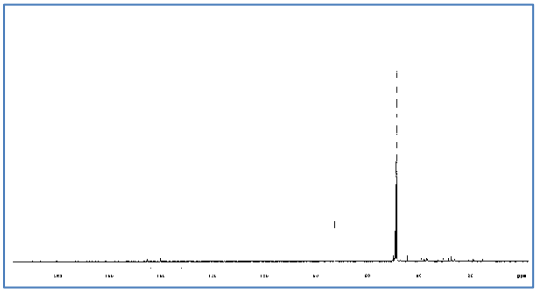

Figure 10 ^1H NMR spectrum (CD_3OD, 300 MHz) of borrelidin (3)

Figure 11 ^{13}C NMR spectrum (CD_3OD, 125 MHz) of borrelidin (3)

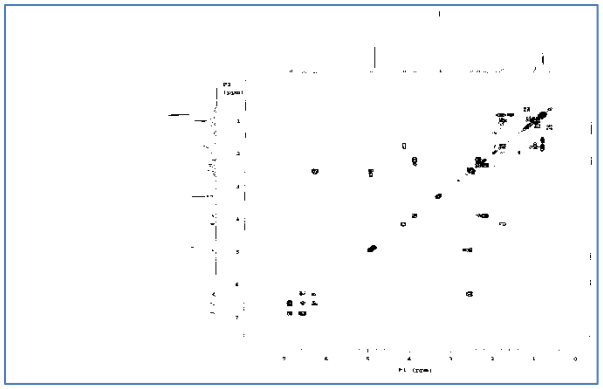

Figure 12 H, H COSY spectrum (CD_3OD, 600 MHz) of borrelidin (3)

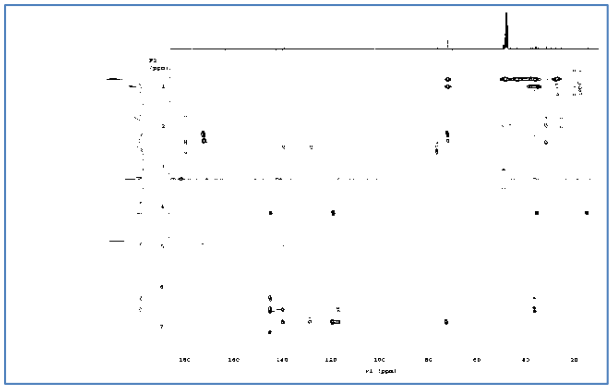

Figure 13 HMBC spectrum (CD_3OD, 600 MHz) of borrelidin (3)

The HMBC data were used to connect these partial structures and to obtain the complete structure. In the HMBC spectrum (Figure 13), from H-6 (δ□6.80, δ□145.4) correlations were observed to C-4, C-5, C-7, C-8 (fragment C) and C-24. There was only one position possible for the nitrogen, which was attached to C-24. Hence, it was assigned as nitrile group, which was confirmed by the chemical shift (Figure 14).

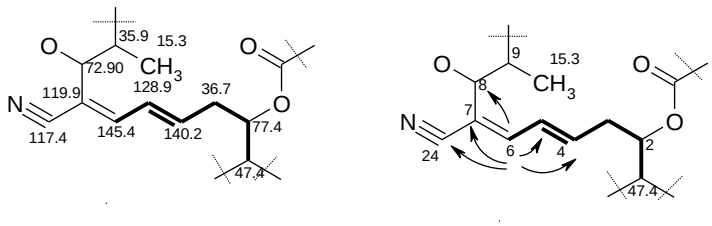

Figure 14 H,H COSY (▬) and HMBC (→) correlations of borrelidin (3)

The methyl doublet at δ1.01 (δ_C 15.3) correlated to C-8, C-9 and C-10 (CH_2, δ 39.1), while the C-10 methylene signal showed correlation to the methine carbon at δ27.6 (C-11), which was connected with the methyl group at δ20.9 (C-25). This methyl correlated with the methylene at δ 49.9 (C-12) and the methylene carbons at δ 49.9 (C-12) and 44.6 (C-14) correlated to three methyl doublets at δ0.83 (Figure 15).

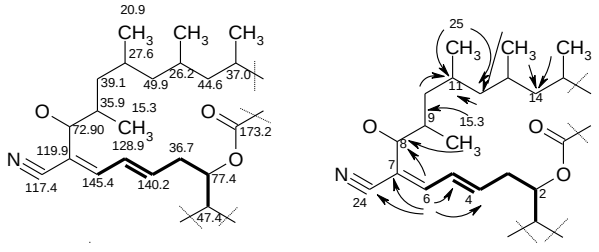

Figure 15 HMBC (→) correlations of borrelidin (3)

H-2 (δ 4.99, δ 77.4) and H-17 (δ 2.35, δ 37.9, fragment D) showed correlations to carbonyl at δ 173.2 and the methine proton at δ 3.90 (δ 72.91) correlated to the methyl at δ 18.7. According to these data, a macrolide ring system could be drawn (Figure 16).

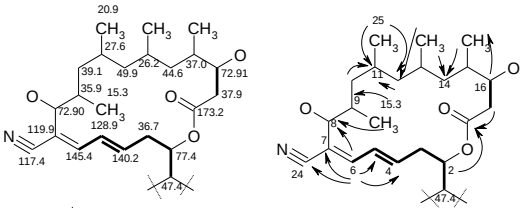

Figure 16 HMBC (→) correlations of borrelidin (3)

The methine protons at δ 2.66 (δ 47.4, C-19) and 2.40 (δ 50.2, C-20) showed cross peaks to carbonyl at δ 180.6. The three remaining CH_2 groups were assigned as a ring system, which accounted for the remaining double bond equivalents. The isolated compound was assigned as nitrile-containing macrolide antibiotic borrelidin (3) (Figure 17).

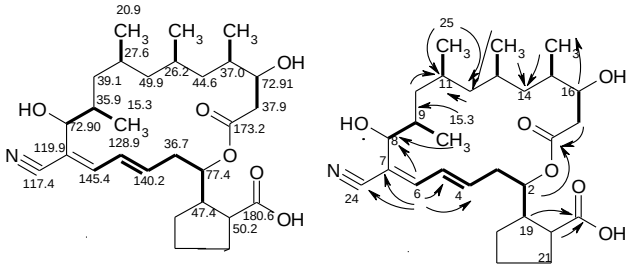

Figure 17 H,H COSY (▬)and HMBC (→) correlations of borrelidin (3)

In our agar diffusion test, borrelidin showed high activity against *Escherichia coli*, *Candida albicans* and *Mucor miehei* (Tü 284) by causing inhibition zones of 25, 30 and 30 mm at 40 µg/ disk; it showed medium activity against *Staphylococcus aureus*, *Streptomyces viridochromogenes* (Tü 57) and weak activity against *Bacillus subtilis*. It was also found to have an activity against *Artemia salina* of 93 %.

Biogenesis of Borrelidin (3)

Macrolide antibiotics are synthesized by a series of condensation reactions catalysed by polyketide synthetases (PKSs). Various post-polyketide modifications involved mainly methylations, hydroxylations, epoxidation and glycosylation. Borrelidin contains a non-glycosylated, macrocyclic polyketide lactone ring and presents a unique structural feature not frequently occurring in any other macrolide natural products; that is the presence of a nitrile moiety at C-7 and a 1,2- *trans* substituted cyclopentane carboxylic acid moiety attached to C-2. The production of nitrile-containing compounds by microorganisms is relatively rare, even though more than 120 nitrile-containing natural products from different sources have been reported. The biosynthesis of borrelidin was predicted to involve a borrelidin polyketide skeleton which must be performed by a modular polyketide synthase (PKS) incorporated with *trans* cyclopentane-1,2-dicarboxylic acid as the starter unit and eight extender units (three malonyl-CoA and five methylmalonyl-CoA units) in the pre-polyketide step (Figure 18) ([Olano] *et al*., 2004). In the post-polyketide step, the formation of the nitrile group on C-7 from methyl group, which is formed from third round chain extension of methyl malonyl CoA, it was proposed that C-7 methyl carbon was first oxidized by BorI to introduce an allylic hydroxyl group and then to formyl derivative. Conversion of the formyl group to an amino group was performed by aminotransferase BorJ and further oxidation catalysed by BorI to a gem-dihydroxyl species and then by subsequent dehydration to borrelidin (Figure 19). BorI and BorJ play a major role in the

biosynthesis of borrelidin, therefore inactivation of these genes would cause the accumulation of pre-borrelidin.

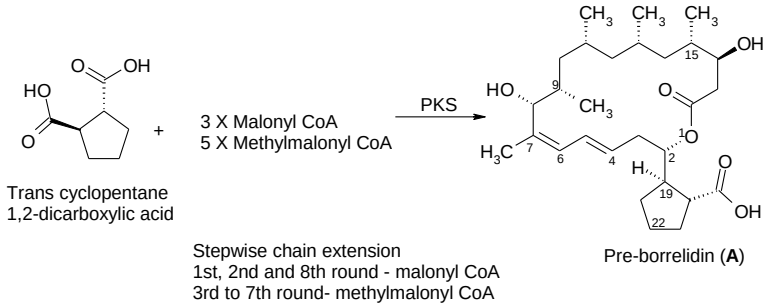

Figure 18 Proposed mechanism for pre-borrelidin (A)

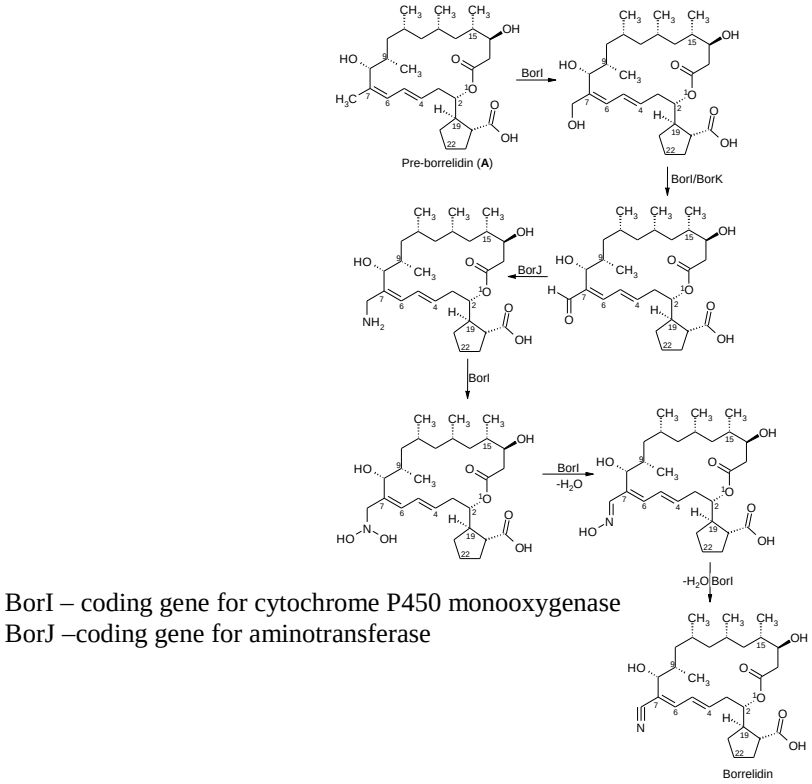

BorI – coding gene for cytochrome P450 monooxygenase
BorJ –coding gene for aminotransferase

Figure 19 Proposed mechanism for the generation of the nitrile moiety as post-polyketide step in borrelidin synthesis (Olano, et al., 2004)

6-Prenyltryptophol (4)

The ^{1}H NMR spectrum (Figure 20) of 6-prenyltryptophol (4) shows the presence of two *ortho* coupled protons at δ 7.41 and 6.82 and two singlets at δ 7.09 and 6.98. These data suggested the presence of a 3,6-disubsituted indole nucleus. In the aliphatic region, the spectrum exhibited two triplets at δ 3.78 (^{3}J = 7.2 Hz, 2H) and 2.93 (^{3}J = 7.2 Hz, 2H) for a 1, 2-disubstituted ethanediyl group connected with two electronically different groups namely an sp^2 carbon and a hetero atom (O or N). The spectrum showed additionally a singlet at δ 1.74 for two CH_3 groups attached to an sp^2 carbon. The spectrum also revealed that an sp^2 attached proton (1H triplet at δ 5.35, ^{3}J = 7.4 Hz) must be of adjacent to a methylene group. This allylic methylene group showed a doublet at δ 3.39 (2 H, ^{3}J = 6.8 Hz). These patterns are evidence of an isoprene unit attached at C-6 position of the indole ring.

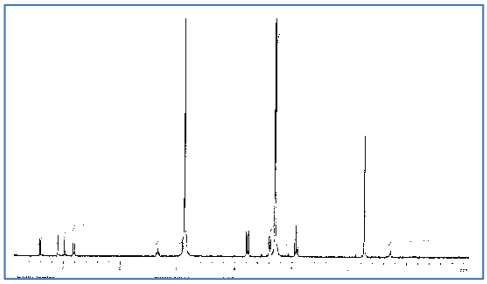

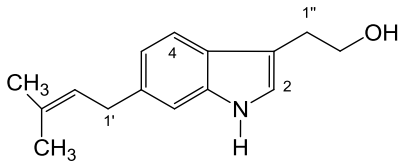

(4)

Figure 20 ^{1}H NMR spectrum (CD_3OD, 300 MHz) of 6-prenyltryptophol

The EI mass spectrum showed the molecular ion peak at *m/z* 229. It gave the base peak at *m/z* 198 by the loss of CH_2OH (MW 31) from the molecular ion. The compound was identified as 6-prenyltryptophol by searching in AntiBase with the above spectroscopic data as well as the molecular weight. It was further confirmed by comparison with an authentic spectrum and literature data. 6-Prenyltryptophol showed activities against fungi and was cytotoxic against a panel of 14 different tumor cell lines with the GI_{50} values in a micromolar range (José *et. al*., 2003)

Table 2 Antimicrobial Activity of the Crude Extract from Strain B 8406 on M_2^+ Medium [40 µL/paper disk (100 mg/mL)], Diameter of Inhibition Zones in mm.

Test microorganisms	Inhibition zone ∅ [mm]
Bacillus subtilis	30
Staphylococcus aureus	19
Streptomyces viridochromogenes (Tü 57)	12
Escherichia coli	11
Candida albicans	18
Chlorella vulgaris	11

Macrolactin F (1): oily substance, 5.1 mg, UV absorbing band at 254 nm, R_f = 0.11 (CH_2Cl_2/10% MeOH), green with anisaldehyde/sulphuric acid. – **^{1}H NMR** (CD_3OD, 300 MHz) and – **^{13}C NMR** (CD_3OD, 125 MHz), (Table 1). – **(+)-ESIMS** 425 ([M + Na]$^+$, 86), 827 ([2 M + Na]$^+$, 100).

Tryptophan (2): white amorphous, 30 mg, R_f = 0.35 ($CHCl_3$/5% MeOH), polar UV absorbing band at 254 nm, red colour with anisaldehyde/sulphuric acid. – **^{1}H NMR** (CD_3OD, 300 MHz) δ 7.59 (d, ^{3}J = 7.8 Hz, 1H, H-4), 7.37 (d, ^{3}J = 8.0 Hz, 1H, H-7), 7.29 (s, 1H, H-2), 7.06 (td, ^{3}J = 7.1 Hz, ^{4}J = 1.1 Hz, 1H, H-5), 6.97 (td, ^{3}J = 7.9 Hz, ^{4}J = 0.9 Hz, 1H, H-6), 3.61 (dd, ^{3}J = 4.3 Hz, 1H, H-2'), 3.36 (dd, ^{3}J = 15.1 Hz, ^{4}J = 4.2 Hz, 1H, H_A-1'), 3.07 (dd, ^{3}J = 8.4 Hz, 1H, H_B-1'). – **(+)-ESIMS** *m/z* 205 ([M + H]$^+$, 100). – **(-)-ESIMS** *m/z* 203 ([M - H]$^-$, 100), 407 ([2 M - H]$^-$, 60).

Borrelidin (3): colourless oil, 10 mg, R_f = 0.90 (CH_2Cl_2/10% MeOH), very strong UV absorbing band at 254 nm, green with anisaldehyde/sulphuric acid. – **^{1}H NMR** (CD_3OD, 300 MHz) δ 6.89 (d, ^{3}J = 11.3 Hz, 1H, H-6), 6.59 (t, ^{3}J = 11.4 Hz, 1H, H-5), 6.30 (m, 1H, H-4), 4.97 (dt, ^{3}J = 11.1 Hz, 3.2 Hz, 1H, H-2), 4.18 (d, ^{3}J = 9.8 Hz, 1H, H-8), 3.92 (dt, ^{3}J = 10.1 Hz, 2.9 Hz, 1H, H-16), 2.66 (quin, ^{3}J = 9.1 Hz, 1H, H-19), 2.54 (m, 2H, CH_2-3), 2.40 (m, 1H, H-20),

2.35 (d, ^3J = 2.8 Hz, 2H, CH_2-17), 1.99 (m, 2H, H_A-21, 23), 1.83 (m, 6H, H-9, 13, 15, H_B-21, CH_2-22), 1.62 (m, 1H, H-11), 1.36 (m, 1H, H_B-23), 1.20 (m, 1H, H_A-10), 1.18-0.88 (m, 4H, CH_2-12, 14), 1.01 (d, ^3J = 6.4 Hz, 3H, CH_3-9), 0.83 (d, ^3J = 6.8 Hz, 9H, CH_3-11, 13, 15), 0.68 (br t, 1H, H_B-10). – **^{13}C NMR** (CD_3OD, 125 MHz) δ 180.6 (C-28), 173.2 (C-18), 145.4 (CH-6), 140.2 (CH-4), 128.9 (CH-5), 119.9 (Cq-7), 117.4 (C_q-24), 77.4 (CH-2), 72.91 (CH-16), 72.90 (CH-8), 50.2 (CH-20), 49.9 (CH_2-14), 47.4 (CH-19), 44.6 (CH_2-12), 39.1 (CH_2-10), 37.9 (CH_2-17), 37.0 (CH-15), 36.7 (CH_2-3), 35.9 (CH-9), 32.5 (CH_2-21), 30.5 (CH_2-22), 28.5 (CH-13), 27.6 (CH-11), 26.2 (CH_2-23), 20.9 (CH_3-27), 19.1 (CH_3-26), 18.7 (CH_3-28), 15.4 (CH_3-25). – **(+)-ESIMS** *m/z* 1001 ([2 M + Na]$^+$, 100), 512 ([M + Na]$^+$, 8). – **(-)-ESIMS** *m/z* 977 ([2 M - H]$^-$, 86), 488 ([M - H]$^-$, 100). – **(+)-HRESIMS** *m/z* 512.29838 [M + Na]$^+$, (calcd. 512.29826 for $C_{28}H_{43}NO_6Na$).

6-Prenyltryptophol (4): colourless solid, 2.1 mg, R_f = 0.5 (CH_2Cl_2/ 5% MeOH), UV absorption band at 254 nm, pink by spraying with anisaldehyde/sulphuric acid. -**^{1}H NMR** (CD_3OD, 300 MHz) δ 7.41 (d, ^3J = 7.9 Hz, 1 H, H-4), 7.09 (s, 1 H, H-7), 6.98 (s, 1 H, H-2), 6.82 (dd, ^3J = 8.1 Hz, ^4J = 1.4 Hz, 1 H, H-5), 5.35 (m, 1 H, H-2'), 3.78 (t, ^3J = 7.2 Hz, 2 H, CH_2-2''), 3.39 (d, ^3J = 6.8 Hz, 2 H, CH_2-1'), 2.93 (d, ^3J = 7.5 Hz, 2 H, CH_2-1''), 1.74 (s, 6 H, CH_3-3'). - **EIMS** (70 eV) *m/z* 229 ([M]$^{+\cdot}$, 86), 198 ([M - CH_2OH]$^{+\cdot}$, 100), 182 (10).

Conclusion

In this study, macrolide antibiotics macrolactin F (1) from *Bacillus subtilis* M 8 and borrelidin (3) from marine *Streptomyces* sp. B 8406 were isolated and characterized. Macrolactin F (1) showed weak antibacterial properties. Borrelidin (3) showed high activity against *Escherichia coli*, *Candida albicans* and *Mucor miehei* (Tü 284), medium activity against *Staphylococcus aureus*, *Streptomyces viridochromogenes* (Tü 57) and weak activity against *Bacillus subtilis*. It was also found to have an activity against *Artemia salina* of 93 %.

Acknowledgements

The authors thank Dr H Frauendorf and R Machinek for the mass and NMR spectra, the German Academic Exchange Service (DAAD) for the financial support. Sincere thanks are extended to Dr Yi Yi Myint, Professor & Head, Department of Chemistry, University of Mandalay, for her permission to submit the paper.

References

Baker, D., Mocek, U. and Garr, C. (2000) "New Leads for Pharmaceutical and Agrochemical, Industries. In Biodiversity." Wrigley, S. K., Hayes, M. A., Thomas, R., Chrystal, E. J. T. and Nicholson, N. Eds Cambridge UK: The Royal Society of Chemistry, pp 66-72.

Barry, K. J. and Wainwright, N. R. (1997) "Biosynthetic Induction of a Secondary Metabolite by a Marine Bacterium under Nutritional Stress: Potential Role of the Incomplete Oxidation of an Organic Acid." *Biol. Bull*. vol. 193, pp. 274-275.

José, M., López, S., Insua, M. M., Baz, J. P., José, L., Puentes, F., Librada, M. and Hernández, C. (2003) "New Cytotoxic Indolic Metabolites from a Marine *Streptomyces." J. Nat. Prod.* vol. 66, pp. 863-864.

McGuire, J. M., Bunch, R. L., Anderson, R. C., Boaz, H. E., Flynn, E. H., Powell, H. M. and Smith, J. W. (1952) "Ilotycin, a New Antibiotic." *Antibiot. Chemother*. vol. 2, pp. 281-283.

Olano, C., Wilkinson, B., Sánchez, C., Moss, S. J., Sheridan, R., Math, V., Weston, A. J., Braña, A. F., Martin, C. J., Oliynyk, M., Méndez, C., Leadlay, P. F. and Salas, J. A. (2004) "Biosynthesis of the Angiogenesis Inhibitor Borrelidin by *Streptomyces* parvulus Tü4055: Cluster Analysis and Assignment of Functions." *Chem. Biol*. vol. 11, pp. 87–97.

Shiomi, K. and Ōmura, S. (2002) "Macrolide Antibiotics, Chemistry, Biology and Practice." Ōmura, S., Ed, California: 2nd Edition, Elsevier Science: p 8.

STUDY ON SORPTION PROPERTIES OF ACTIVATED BIOSORBENTS (FISHSCALE AND SEASHELL) FOR THE REMOVAL OF ANIONIC SURFACTANT

Myint Myint Than[1], Nwe Nwe Aung[2], Aye Thant Zin[3]

Abstract

In this study, waste fishscale and seashell were used as biosorbents for the removal of surfactants from industrial wastewater. These biosorbents were collected from fish market in Pathein Township, Ayeyarwady Region. The selected samples were washed with distilled water for three times and were soaked in 3 % nitric acid for 24 h and then were washed again with distilled water until pH 7 and dried in an oven at 105˚C and were made to powder form. The physiocochemical properties such as moisture content, bulk density and pH of raw fishscale powder (RFSP) and raw seashell powder (RSSP) were determined by conventional methods and characterized by modern techniques such as EDXRF, SEM, TG-DTA and FT IR analyses. RFSP and RSSP were calcined at various temperatures (400˚C to 1000˚C) to obtain heat activated fishscale powder 1-7 (HAFSP 1-7) and heat activated seashell powder 1-7 (HASSP 1-7). The critical micelle concentration (CMC) of sodium dodecyl sulphate (SDS) were obtained as $7x10^{-3}$ M, $7x10^{-3}$ M, $7x10^{-3}$ M, $4x10^{-3}$ M, $6x10^{-3}$ M and $5x10^{-3}$ M at pH 1, 2, 3, 4, 5 and 6 respectively. From these results, $7x10^{-3}$ M at pH 3 and $5x10^{-3}$ M at pH 6 were selected as optima CMC of SDS. The adsorption properties of different biosorbents (HAFSP-1, 2, 3, 4, 5, 6 and 7) and (HASSP-1, 2, 3, 4, 5, 6 and 7) were compared for the removal of SDS at pH 3 and 6. According to these analyses, HAFSP-5 and HASSP-7 were found to be more effective than other samples. Adsorption capacities of HAFSP-5 and HASSP-7 were determined at different contact time and pH by using UV-Vis spectrophotometer at λ_{max} 498 nm and 25˚C. The optimum contact time was 60 min and pH were 3 and 6 respectively for the removal of SDS solution from the paper industrial wastewater by HAFSP-5 and HASSP-7. The outcome of the present research is the preparation of waste biosorbents for the removal of anionic surfactants from the paper industrial wastewater.

Keywords: fishscale, seashell, sodium dodecyl sulphate, critical micelle concentration, biosorbents

Introduction

Surfactants are surface active agents with a diverse group of chemicals consisting of a polar, water-soluble head group and a nonpolar hydrocarbon tail group. They are widely used in household and industrial products (Eriksson *et al*., 2008; Reemtsma *et al*., 2006). After use, residual surfactants are discharged into sewage systems or directly into surface water and most of them end up dispersed in different environmental compartments such as soil, water or sediment. They are harmful to human beings, fishes and vegetation and are responsible to cause foams in rivers and effluent treatment plants and to reduce the quality of water. They cause short term as well as long term changes in ecosystem (Sigoillot and Nguyex, 1992; Margesin and Schinner, 1998; Eichhorn *et al*., 2001. 2002). They are classified into four main groups: anionic, nonionic, cationic and zwitterionic (amphoteric).

Surfactants can assume several supramolecular arrangements in solution, including circular aggregates called micelles. Micelles are formed when the surfactant concentration reaches a certain value, termed the critical micelle concentration (CMC). They are arranged with hydrophobic tails oriented inward and hydrophilic heads oriented toward the aqueous solution. Fishscale (FS) and seashell (SS) are waste product and abundant. The cell wall surface of biosorbents contained several of functional groups for surfactants attached onto adsorbents and the porous layer may provide a good possibility of surfactants to be adsorbed on its surface

[1] Assistant Lecturer, Department of Chemistry, Mandalar Degree College
[2] Dr, Lecturer, Department of Chemistry, Yangon University
[3] Dr, Associate Professor, Department of Chemistry, Mandalar Degree College

(Kumar *et al*., 2008; Nadeem *et al*., 2008; Vieira *et al*., 2011). Almost all the methods for spectrophotometric determination of anionic surfactants are based on the formation of ion associates and their subsequent extraction into organic solvents. In this paper, the removal of anionic surfactant from industrial wastewater was conducted by using activated biosorbents (Fishscale and Seashell).

Materials and Methods

Preparation of Biosorbents

Waste fishscale and seashell were collected from fish market in Pathein Township, Ayeyarwady Region. The fishscales were washed first with distilled water and were soaked in 3% nitric acid for 24 h and then were washed again with distilled water until pH 7. The seashell were washed with distilled water to remove any adhering impurities. They were dried in an oven at 105 °C for 2 h. The dried raw fishscale powder (RFSP) and raw seashell powder (RSSP) were obtained by grinding with motar and pestle followed by sieving (Srividya and Mohanty, 2009). RFSP and RSSP were calcined at various temperatures (400 °C to 1000 °C) to obtain heat activated fishscale powder 1-7 (HAFSP 1-7) and heat activated seashell powder 1-7 (HASSP 1-7).

Preparation of Stock Solution

Acridine orange (ACO) was used for the preparation of $5x10^{-3}$ M solution to be used as a stock. Sodium dodecyl sulphate (SDS) was purchased from BDH, Yangon Region. Toluene was used as an extractant. Glacial acetic acid was used to maintain the pH during extraction.

Determination of Physicochemical Properties of Raw Fishscale Powder (RFSP) and Raw Seashell Powder (RSSP)

Determination of bulk density

A clean dry 10 mL graduated measuring cylinder was weighed. It was filled with the dry powder sample to reach the mark and reweighed. The graduated cylinder was placed in a tapping box and the cylinder was tapped gently with several times until no more reduction in volume. The minimum volume was recorded and the bulk density was calculated.

Determination of Critical Micelle Concentration (CMC) of Sodium Dodecyl Sulphate (SDS)

The various concentration of SDS solution were prepared from $1x10^{-3}$ M to $10x10^{-3}$ M. This solution were maintained at pH 1, 2, 3, 4, 5 and 6. 0.5 mL of each concentration was placed into a beaker and 5 mL of toluene was added followed by the addition of 2 drops each of acridine orange and glacial acetic acid. The contents were shaken with separating funnel for 1 min and allowed to settle for 5 min. The toluene layer was discarded and it was measured by using UV-Vis spectrophotometer at λ_{max} 498 nm and 25°C.

Experimental Procedure

0.1 g of heat activated fishscale powder (HAFSP 1-7) was added into 100 mL of surfactant solution. It was shaken with electric shaker and filtered. This solution (10 mL) was placed into a beaker and 5 mL of toluene was added followed by the addition of 2 drops each of acridine orange and glacial acetic acid. The contents were shaken with separating funnel for 1 min and allowed to settle for 5 min. The toluene layer was discarded and it was measured by

using UV-Vis spectrophotometer at λ_{max} 498 nm and 25˚C. Similarly, heat activated seashell powder (HASSP 1-7) was operated by using the above method.

Results and Discussion

Physicochemical Properties of Raw Fishscale Powder (RFSP) and Raw Seashell Powder (RSSP) Samples

The physicochemical properties such as moisture content, bulk density and pH of raw fishscale powder (RFSP) and raw seashell powder (RSSP) samples presented in Table 1. It was found that RFSP was higher than RSSP in moisture content. However, RSSP was higher than RFSP in bulk density and pH.

Table 1 Physicochemical Properties of Raw Fishscale Powder (RFSP) and Raw Seashell Powder (RSSP) Samples

Sample	Moisture (%)	Bulk Density (gcm^{-3})	pH
RFSP	9.77	0.79	6.8
RSSP	0.64	1.76	9.3

EDXRF Analysis

In this research, according to EDXRF spectra, RFSP contained calcium oxide as the major constituent and phosphorus(V) oxide as the second major constituent and other trace constituents. RSSP contained carbon dioxide as the major constituent, calcium oxide as the second major constituent and other trace constituents (Figures 1, 2 and Table 2).

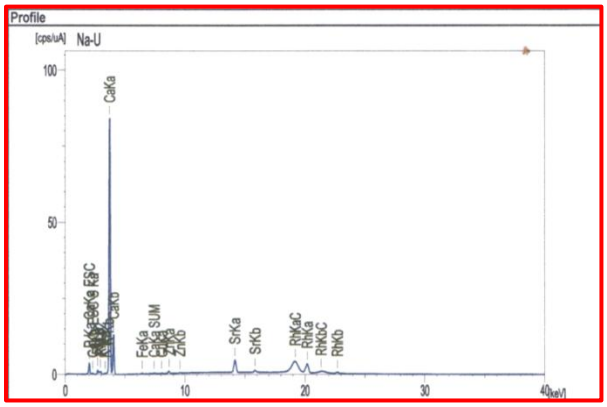

Figure 1 EDXRF spectrum of raw fishscale powder (RFSP)

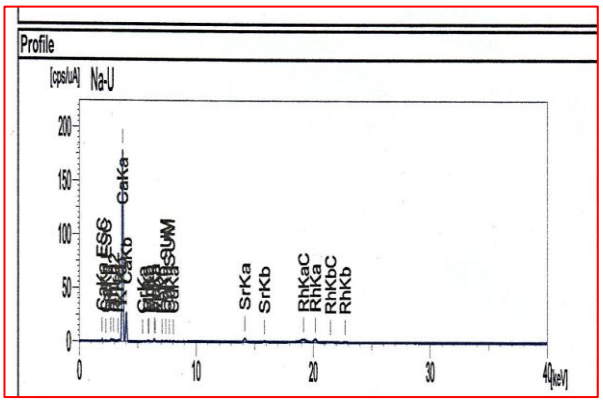

Figure 2 EDXRF spectrum of raw seashell powder (RSSP)

Table 2 Results from EDXRF Spectrum of Raw Fishscale Powder (RFSP) and Raw Seashell Powder (RSSP)

Constituents	Relative Abundance of Some metallic Oxide (%)	
	RFSP	**RSSP**
CaO	59.018	48.584
P_2O_5	39.254	-
SO_3	1.023	-
K_2O	0.391	0.287
SrO	0.180	0.075
ZnO	0.062	-
Fe_2O_3	0.057	0.201
CuO	0.014	0.010
MnO	-	0.120
Cr_2O_3	-	0.014
CO_2	-	50.710

SEM Analysis

SEM micrographs of RFSP and RSSP are indicated in Figures 3 and 4. In these SEM micrograph, RFSP was observed as non-porous structure and RSSP as rough and disordered surface with low porosity grains.

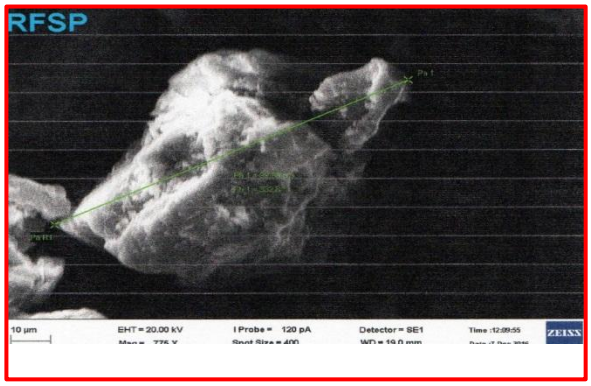

Figure 3 Scanning electron micrograph of raw fishscale powder (RFSP)

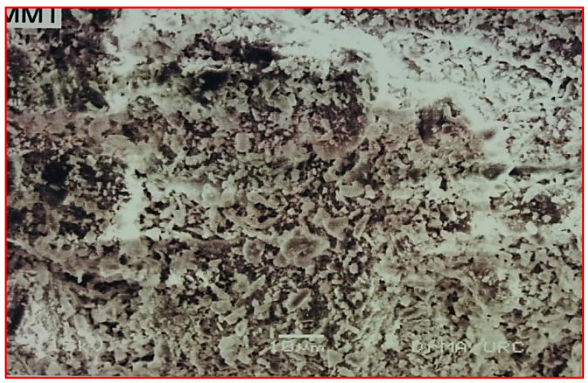

Figure 4 Scanning electron micrograph of raw seashell powder (RSSP)

FT IR Analysis

FT IR spectra of RFSP and RSSP are presented in Figures 5 and 6. The broad bands at 3460 and 3454 cm^{-1} are assigned to stretching vibration of O-H bonds. The bonds observed between 2950 and 2940 cm^{-1} are assigned to C-H stretching groups. The results are shown in Table 3.

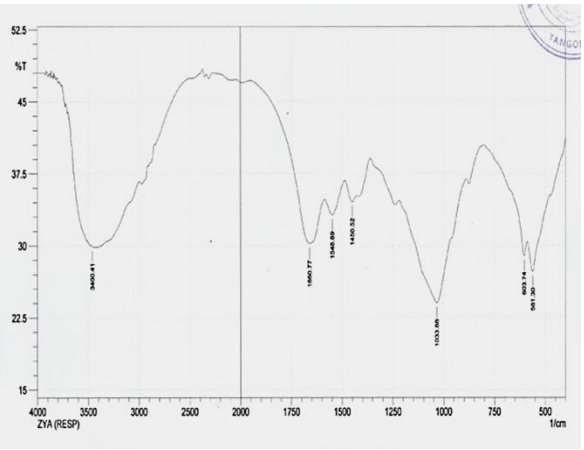

Figure 5 FT IR spectrum of raw fishscale powder (RFSP**)**

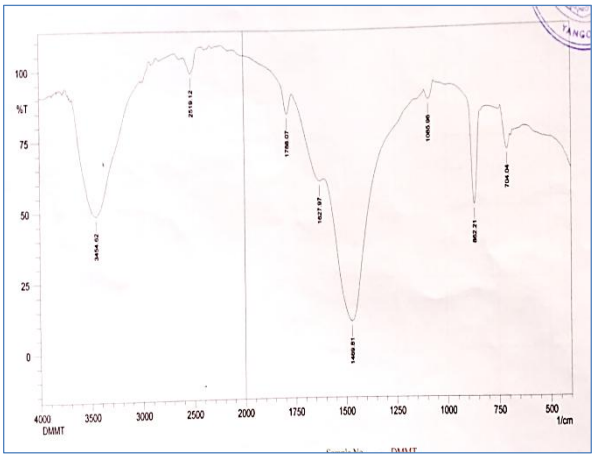

Figure 6 FT IR spectrum of raw seashell powder (RSSP**)**

Table 3 Absorption Bands and Assignment of FT IR Spectral Data of RFSP and RSSP

Observed Frequency (cm^{-1})		Reference*	Possible Assignment
RFSP	**RSSP**		
3460	3454	3700-3200	Stretching vibration of O-H bonds
2950	2940	2980-2850	C-H stretching
-	1788	1810-1790 (s)	C=O stretching
1660	1627	1670-1640	Stretching vibration of C=O bonds
1548	-	1600-1400	C=C stretching
1450	1469	1625-1430	C=C stretching of aromatic ring
1033	1085	1100-1000	P-O-C stretching vibration
-	862	890-850 (s)	C-C stretching
-	704	705-570	C-C stretching
603	-	615-535	C=O out of plane bending

*Silverstein *et al*., (2003)

TG-DTA Analysis

In this experiment, the weight loss percent of RFSP was found to be 7.87 % due to the dehydration of surface water and moisture and there was endothermic peak at 80.53 °C. The exothermic peak was observed at about 370.13 °C and weight loss was 18.55 % due to the decomposition of volatile materials. The third weight loss was 14.44 % due to the decomposition and combustion of residual organic components at the temperature range of 380 °C to 600 °C (Figure 7 and Table 4). In RSSP, no weight loss was observed due to the absence of moisture and absorbed water at the temperature range of 38-280 °C. The exothermic peak was observed at about 361-450 °C due to the removal of organic volatile materials (Figure 8 and Table 5).

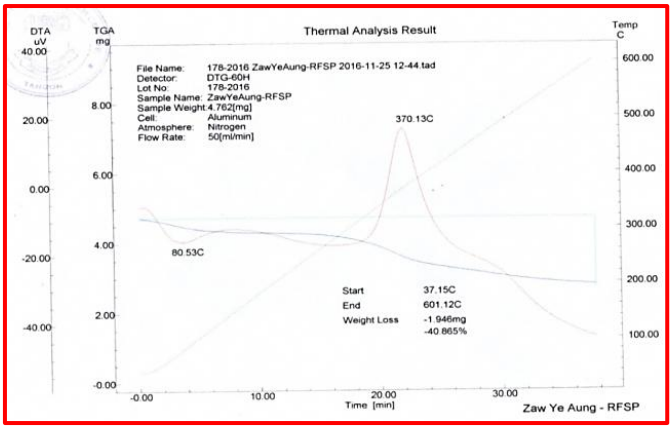

Figure 7 TG-DTA thermogram of raw fishscale powder (RFSP)

Table. 4 TG-DTA Thermal Analysis Data of Raw Fishscale Powder (RFSP)

Temp: range (℃)	Weight loss (%)	Peak's Temperature (℃)	Nature of Peak	TG Remark
37-120	7.87	80.53	endothermic	- This weight loss is due to the removal of surface water and moisture
120-380	18.55	370.13	exothermic	- The second weight loss is due to the decomposition of volatile materials
380-600	14.44	-	-	- The third weight loss is due to the decomposition and combustion of residual organic components in the fish scales sample

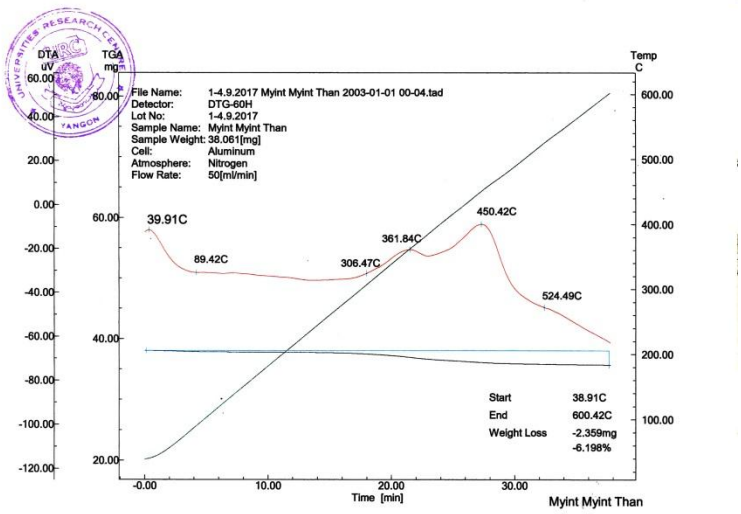

Figure 8 TG – DTA thermogram of raw seashell powder (RSSP)

Table 5 TG-DTA Thermal Analysis Data of Raw Seashell Powder (RSSP)

Temp: range (℃)	Weight loss (%)	Peak's Temperature (℃)	Nature of Peak	TG Remark
38-280	-	-	-	- No weight loss due to the absence of moisture and absorbed water.
280-600	6.19	361-450	exothermic	-This weight loss was due to the removal of organic volatile materials.

Determination of Critical Micelle Concentration (CMC) of Sodium Dodecyl Sulphate (SDS)

The literature reported value for the CMC of SDS in water is $8.1x10^{-3}$ M (Haigh *et al.*, 1996). In this experiment, CMC of SDS were obtained as $7x10^{-3}$ M, $7x10^{-3}$ M, $7x10^{-3}$ M, $4x10^{-3}$ M, $6x10^{-3}$ M and $5x10^{-3}$ M at pH 1, 2, 3, 4, 5 and 6 respectively. The optima CMC of SDS were $7x10^{-3}$ M at pH 3 and 5×10^{-3} M at pH 6. The results are shown in Tables (6–7) and Figures (9–14).

Table 6 CMC of SDS at pH 1, 2, 3, 4, 5 and 6 at 25°C

Concentration (10^{-3} M)	Absorbance					
	pH 1	pH 2	pH 3	pH 4	pH 5	pH 6
1	0.323	0.819	0.683	0.223	0.256	0.286
2	0.491	0.337	0.398	0.269	0.228	0.275
3	0.512	0.373	0.532	0.259	0.220	0.286
4	0.523	0.396	0.499	0.220	0.237	0.268
5	0.372	0.327	0.521	0.255	0.246	0.224
6	0.376	0.391	0.374	0.271	0.234	0.262
7	0.273	0.253	0.219	0.243	0.252	0.296
8	0.573	0.329	0.33	0.240	0.274	0.283
9	0.25	0.269	0.28	0.201	0.269	0.317
10	0.635	0.299	0.373	0.239	0.248	0.296

Table 7 Critical Micelle Concentration (CMC) of SDS at pH 1,2,3,4,5 and 6 at 25°C

pH	Critical Micelle Concentration (CMC) (10^{-3} M)
1	7
2	7
3	7
4	4
5	6
6	5

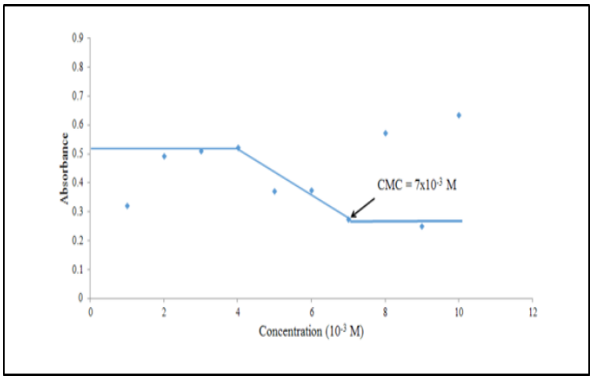

Figure 9 CMC of SDS at pH 1 and 25˚C

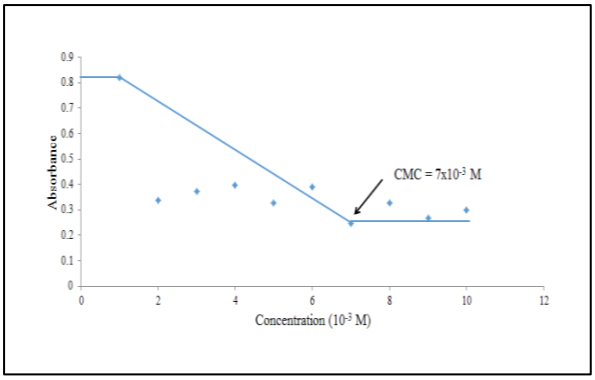

Figure 10 CMC of SDS at pH 2 and 25˚C

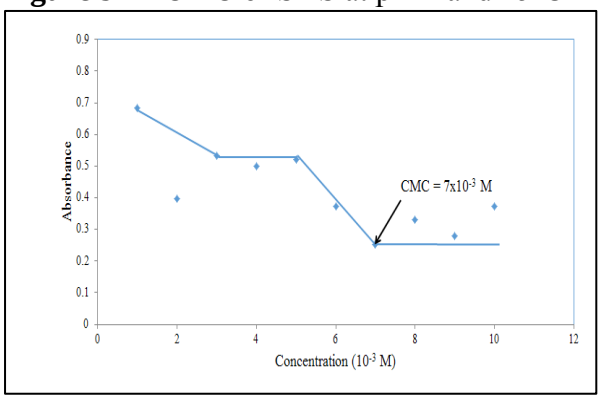

Figure 11 CMC of SDS at pH 3 and 25˚C

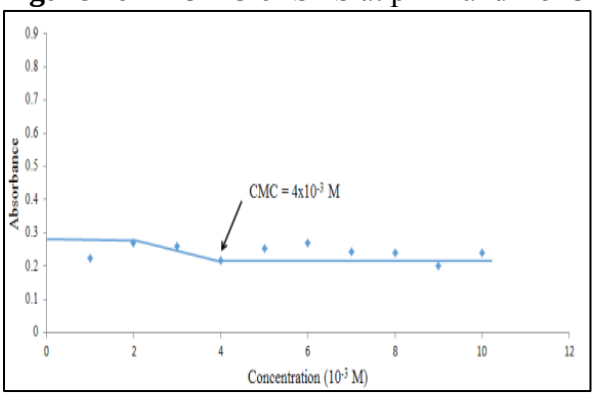

Figure 12 CMC of SDS at pH 4 and 25˚C

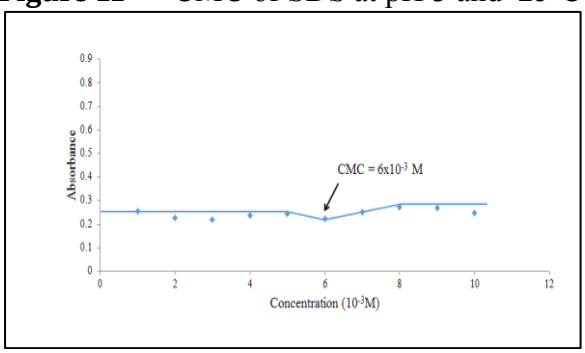

Figure 13 CMC of SDS at pH 5 and 25˚C

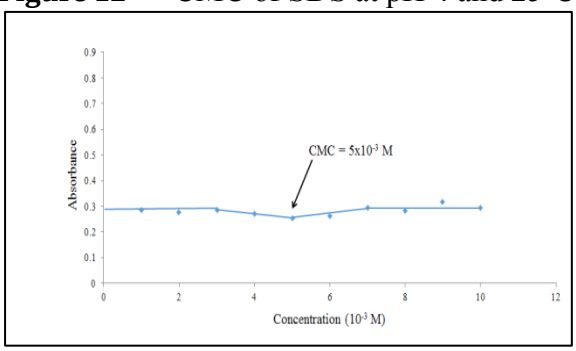

Figure 14 CMC of SDS at pH 6 and 25˚C

Comparison of the Adsorption Properties of Heat Activated Fishscale Powder 1-7 (HAFSP 1-7) and Heat Activated Seashell Powder 1-7 (HASSP 1-7)

Adsorption properties of biosorbents (HAFSP and HASSP) activated at (400 ˚C to 1000 ˚C) were compared for the removal of SDS at pH 3 and 6. It was found that, HAFSP-5 and HASSP-7 were more effective than other samples. The results are shown in Table 8 and Figure 15 for pH 3 and Table 9 and Figure 16 for pH 6.

Table 8 Comparison of the Adsorption Capacities of the Different Samples of Raw and (HAFSP 1-7) at pH 3 and 25°C

Time (min)	q_t (mg/g)							
	Raw	HAFSP 1	HAFSP 2	HAFSP 3	HAFSP 4	HAFSP 5	HAFSP 6	HAFSP 7
60	25.44	27.33	32.11	37.22	48.61	51.55	47.96	47.55
120	26.34	27.67	30.34	36.77	47.15	50.34	45.46	46.87
180	25.22	23.54	31.54	35.27	48.54	50.55	46.89	47.78

Initial concentration of SDS = 100 ppm
Dosage of HAFSP = 0.1 g
pH = 3
Stirring rate = 200 rpm

$$q_t = \frac{C_0 - C_e}{\text{mass of adsorbent}} \times \text{volume of solution}$$

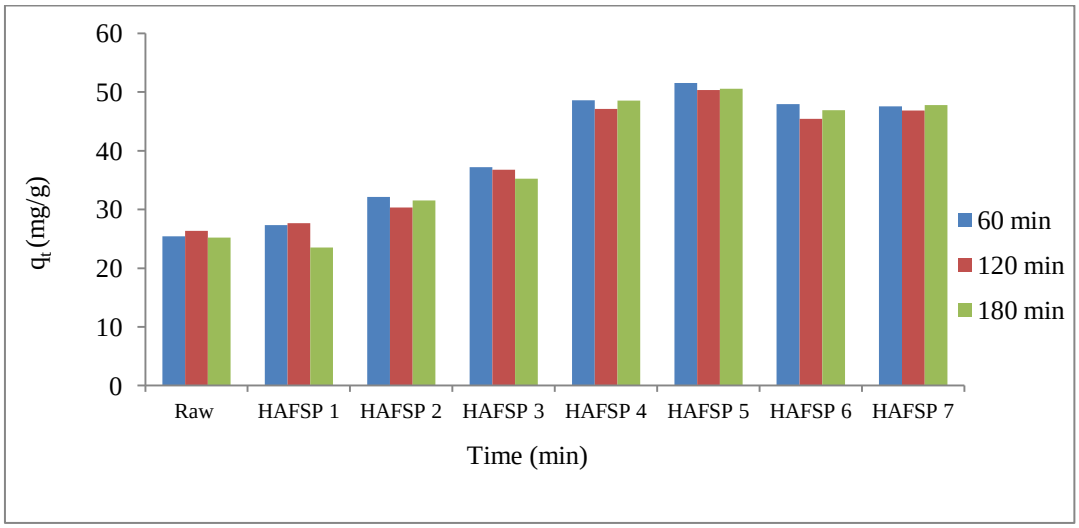

Figure 15 Comparison of the adsorption capacities of the different samples of raw and (HAFSP 1-7) at pH 3 and 25°C

Table 9 Comparison of the Adsorption Capacities of the Different Samples of Raw and (HASSP 1-7) at pH 6 and 25°C

Time (min)	q_t (mg/g)							
	Raw	HASSP 1	HASSP 2	HASSP 3	HASSP 4	HASSP 5	HASSP 6	HASSP 7
60	24.11	27.78	28.92	29.87	32.53	34.61	36.42	49.80
120	24.82	30.45	27.85	28.41	28.95	30.52	32.91	49.43
180	25.43	29.10	27.63	29.21	32.43	34.51	36.35	48.45

Initial concentration of SDS = 100 ppm
Dosage of HASSP = 0.1 g
pH = 6
Stirring rate = 200 rpm

$$q_t = \frac{C_0 - C_e}{\text{mass of adsorbent}} \times \text{volume of solution}$$

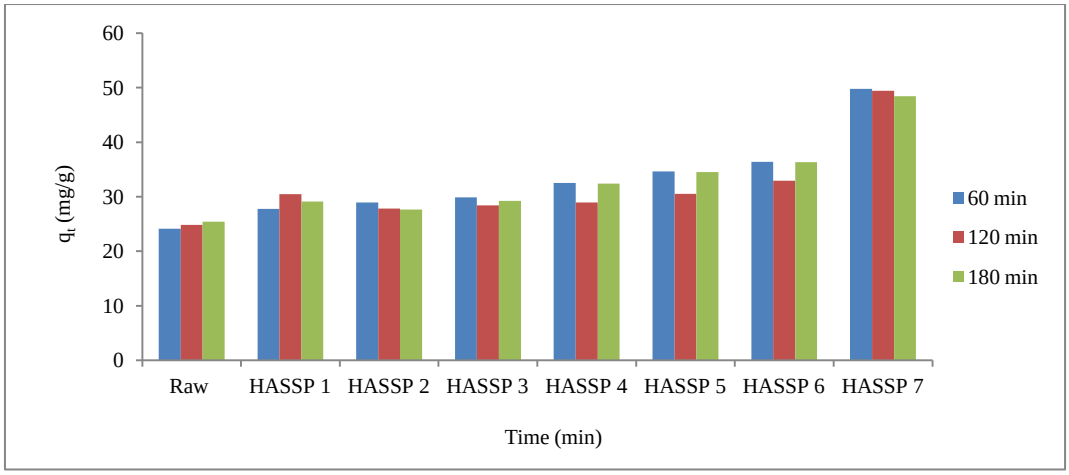

Figure 16 Comparison of the adsorption capacities of the different samples of raw and (HASSP 1-7) at pH 6 and 25°C

Effect of Different Contact Time and pH on the Removal of SDS by HAFSP-5 and HASSP-7

Adsorption capacities of HAFSP-5 and HASSP-7 were determined with different contact time and pH by using UV-Vis spectrophotometer at λ_{max} 498 nm and 25°C. It was observed that the optimum contact time for removal of SDS by HAFSP-5 and HASSP-7 was 60 min (Table 10 and Figure 17) and the pH optima were 3 and 6 by HAFSP-5 and HASSP-7, respectively (Table 11 and Figure 18).

Table 10 Effect of Contact Time on the Removal of SDS by HAFSP-5 (pH 3) and HASSP-7 (pH 6)

Time (min)	q_t (mg/g)	
	HAFSP-5 (pH 3)	HASSP-7 (pH 6)
30	34.42	30.11
60	51.61	49.89
90	50.64	48.72
120	50.46	49.50
150	50.12	48.95
180	49.63	48.57

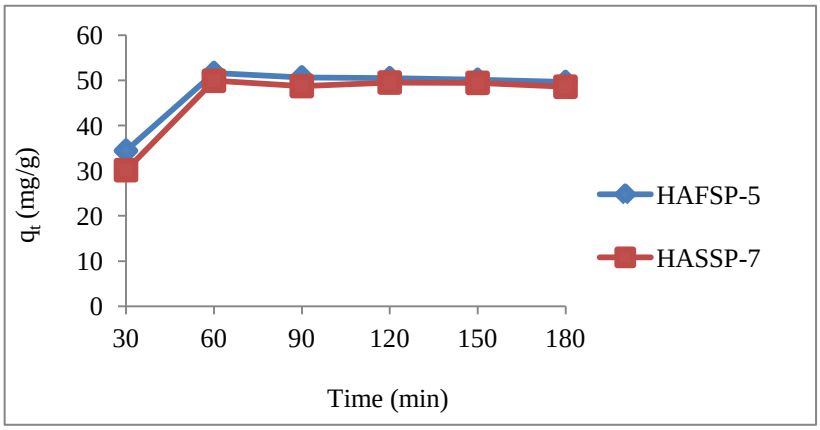

Figure 17 Effect of contact time on the removal of SDS by raw and HAFSP-5 (pH 3) and HASSP-7 (pH 6)

Table 11 Effect of pH for the Removal of SDS by HAFSP-5 and HASSP-7 at 60 min and 25°C

pH	q_t (mg/g)	
	HTFSP-5	HTSSP-7
1	25.42	48.54
2	44.38	7.29
3	68.54	51.46
4	31.04	42.71
5	59.58	39.79
6	51.67	57.92
7	53.78	55.34
8	57.5	56.87
9	59.38	57.79
10	54.17	46.88

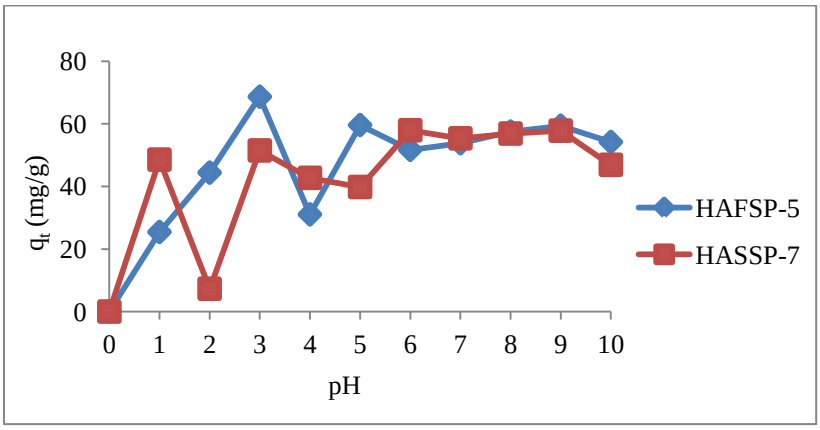

Figure 18 Effect of pH for the removal of SDS by HAFSP-5 and HASSP-7 at 60 min and 25°C

Conclusion

In this research work, the moisture percent of RFSP and RSSP was found to be 9.77% and 0.64%. From EDXRF spectrum, the preparing samples show CaO and CO_2 for major constituent and P_2O_5, SO_3, K_2O, SrO, ZnO, Fe_2O_3, CuO, MnO and Cr_2O_3 for second major constituent. From SEM results, RFSP was non-porous structure and RSSP was rough and disordered surface. In this experiment, the critical micelle concentration (CMC) of sodium dodecyl sulphate (SDS) were $7x10^{-3}$ M at pH 3 and $5x10^{-3}$ M at pH 6. HAFSP-5 and HASSP-7 were more effective among other samples. Adsorption capacities of selected samples HAFSP-5 and HASSP-7 at optima contact time and pH were 60 min and pH 3 and 6 for the removal of SDS solution at λ_{max} 498 nm and 25˚C. The contribution of this study is that fishscale and seashell samples can be utilized as biosorbents in wastewater treatment.

Acknowledgements

The authors would like to express their profound gratitude to the Myanmar Academy of Arts and Science for giving permission to submit this paper and to Professor and Head, Dr Daw Ni Ni Than, Department of Chemistry, University of Yangon, for her kind encouragement.

References

Eichhorn, P., Flavier, M.E., Paje, M.L. and Knepper, T.P. (2001). "Occurrence and Fate of Linear and Branched Alkylbenzene Sulfonates and Their Metabolites in Surface Waters in Philippines". *Journal of Science Total Environmental*, vol. 269, pp. 75-85

Eichhorn, P., Rodrigues, S.V., Baumann, W. and Knepper, T.P. (2002). "Incomplete Degradation of Linear Alkylbenzene Sulfonate Surfactants in Brazilian Surface Waters and Pursuit of Their Polar Metabolites in drinking waters". *Journal of Science Total Environmental*, vol. 284, pp. 123-134

Eriksson, E., Auffarth, K., Eilersen, A.M., Henze, M. and Ledin, A. (2003). "Household Chemicals and Personal Care Products as Sources for Xenobiotic Organic Compounds in Grey Wastewater". *Journal of Water S.A*, vol. 29, pp. 135-146

Haigh, S.D. (1996). "A Review of the Interaction of Surfactants with Organic Contaminants in Soil". *Journal of Sci*ence *Total Environment*, vol. 185, pp. 161-170

Kumar, R., Bishnoi, N.R. and Bishnoi, K. (2008). "Biosorption of Chromium(VI) from Aqueous Solution and Electroplating Wastewater using Fungal Biomass". *Journal of Chemical Engineering*, vol. 135(3), pp. 202–208

Margesin, R. and Schinner, F. (1998). "Low-Temperature Bioremediation of a Wastewater Contaminated with Anionic Surfactants and Fuel Oil". *Journal of Application Microbiology and Biotechnology*, vol. 49, pp. 482-486

Nadeem, R., Ansari, T.M. and Khalid, A.M. (2008). "Fourier Transform Infrared Spectroscopic Characterization and Optimization of Pb (II) Biosorption by Fish (Labeo Rohita) Scales". *Journal of Hazardous Materials*, vol. 156(1-3), pp. 64–73

Reemtsma, T., Weiss, S., Mueller, J., Petrovic, M., Gonzalez, S., Barcelo, D., Ventura, F. and Knepper, T.P. (2006). "Polar Pollutants Entry into the Water Cycle by Municipal Wastewater: A European Perspective". *Journal of Environmental Science Technology*, vol. 40, pp. 5451-5458

Sigoillot, J.C. and Nguyex, M.H. (1992). "Complete Oxidation of Linear Alkyl-Benzene Sulfonate by Bacterial Communities Selected from Coastal Seawater". *Journal of Application Environmental and Microbiology*, vol. 58, pp. 1308-1312

Silverstein, R.M., Webster. F.X. and Kiemle, D.J. (2003). *Spectrometric Identification of Organic Compounds*, New York: 7th Edition, John Wiley and Sons, Inc.

Srividya, K. and Mohanty, K. (2009). "Biosorption of Hexavalent Chromium from Aqueous Solution by Calta Scales: Equilibrium and Kinetics Studies". *Journal of Chemical Engineering*, vol. 155 (3), pp. 666-673

Vieira, E.F.S., Cestari, A.R., Carvalho, W.A.S., Oliveira, C. and Chagas, R. A. (2011). "The Use of Freshwater Fish Scale of the Species Leporinus Elongatus as Adsorbent for Anionic Dyes". *Journal of Thermal Analysis and Calorimetry*, vol. 109(3), pp. 1407-1412

STUDY ON THE BACTERIOLOGICAL EXAMINATIONS OF PREPARED EFFECTIVE MICROORGANISM SOLUTIONS FROM NATURAL WASTES (VEGETABLE WASTES , COW DUNG AND SESAME MEAL CAKE)

Tin Tin Sein*****

Abstract

In this research, EM (effective microorganism) solutions were prepared from waste of the vegetables by primary fermentation. The cow dung and commercial sesame meal cake were also applied. The preparation of EM solutions were carried out under two different conditions such as condition C1 (vegetable waste) and condition C2 (vegetable waste, cow dung and sesame meal cake) at different pH values. pH values of used solvent / solutions were 6.5 for purified water, 9.5 for slaked lime solution and 2.5 for lemon juice. During the fermentation, biogas was evolved. The volume of evolved gas were measured hourly till to five days. The microorganisms in EM solutions were isolated, cultured and characterized by cultural and microscopic morphology at department of biotechnology, Mandalay Technological University.

Keywords: effective microorganisms, vegetable waste, sesame meal cake, cow dung,

Introduction

Effective Microorganisms (EM) are mixed cultures of beneficial naturally-occurring organisms that can be applied as inoculants to increase the microbial diversity of soil ecosystem. They consist mainly of the photosynthesizing bacteria, lactic acid bacteria, yeasts, actinomycetes and fermenting fungi. These microorganisms are physiologically compatible with one another and can coexist in liquid culture. There is evidence that EM inoculation to the soil can improve the quality of soil, plant growth and yield (Kengo and Hui-lian, 2000).

The use of effective microorganisms in agricultural soil suppress soil-borne pathogens**.** These effective microorganism**s** also increases the decomposition of organic materials and consequently the availability of mineral nutrients and important organic compounds to plants (Singh *et al*., 2003).

In addition, EM enhances the activities of beneficial indigenous microorganisms, for example mycorrhizae which fix atmospheric nitrogen thereby supplementing the use of chemical fertilizer and pesticides. Improvement in soil fertility has significant positive effect on plant growth, flowering, fruit development and ripening in crops (Lévai *et al*., 2006). The concept of effective microorganisms (EM) was developed by Professor Teruo Higa, University of the Ryukyus, Okinawa, Japan (Higa, 1991; Higa and Wididana, 1991a). EM consists of mixed cultures of beneficial and naturally-occurring microorganisms that can be applied as inoculants to increase the microbial diversity of soils and plant. The inoculation of EM cultures to the soil/plant ecosystem can improve soil quality, soil health and the growth yield and quality of crops (Higa and James, 1994).

EM contains selected species of microorganisms including predominant populations of lactic acid bacteria and yeasts and smaller numbers of photosynthetic bacteria, actinomycetes and other types of organisms. All of these are mutually compatible with one another and can coexist in liquid culture (Higa, 1994).

EM is not a substitute for other management practices. It is, however, an added dimension for optimizing our best soil and crop management practices such as crop rotations, use of organic

amendments, conservation tillage, crop residue recycling and biocontrol of pests. If used properly, EM can significantly enhance the beneficial effects of these practices (Higa and Wididana, 1991b).

Materials and Methods

Sample Collection

The natural waste materials such as vegetable wastes, cow dung and sesame meal cake were collected for the preparation of effective microorganism solution and production of biogas. Vegetable waste was collected from local market, Chanmyatharsi Township, Mandalay Region. Cow dung was collected from Taung Pyone Village, Madaya Township, Mandalay Region. Sesame meal cake was collected from Local market, Mandalay Region.

Vegetable waste samples were cut into small pieces and washed with water. Cow dung samples were dried under the sunlight. These cow dung samples were pounded and sieved to get the size of powder. Sesame meal cake were ground to get powder sample. Three solvent solutions (purified water (pH 6.5), lemon juice (pH 2.5) and slaked lime solution (pH 9.5) were prepared to add into vegetable waste (Figure 1).

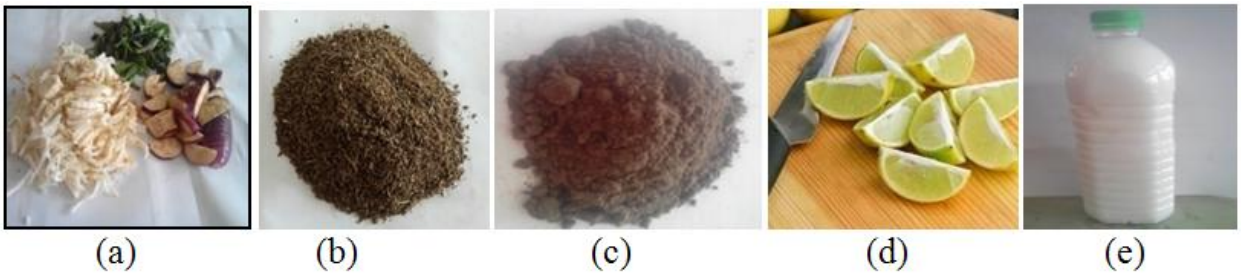

Figure 1 (a) Vegetable waste, (b) Cow dang powder, (c) Sesame meal cake, (d) Lemon and (e) Slaked lime solution

Preparation of Effective Microorganism Solution and Production of Biogas from Vegetable Waste Only (Control, C)

Effective microorganism solution was prepared by using vegetable waste only. Six kilogram of small pieces of fresh vegetable wastes were put into the anaeroboic digester. The neck of the digester was entwined with teflon. The lid was also tightly sealed with the damp wheat. The gas delivery pipe was also set up as shown in Figure 2. While the preparation of effective microorganism solution, the biogas was evolved. The liberated biogas was collected by downward displacement of water. The amount of biogas produced was recorded 1 h interval till 5 h and also determined daily till 5 days. The prepared digester is shown in Figure 2. After production of biogas for 5 days, the anaerobic digester was tightly sealed kept for one month. After one month, the mixture in the anaerobic digester can be used as EM solution.

Figure 2 The production of biogas

Preparation of Effective Microorganism Solutions and Production of Biogas from Vegetable Waste with Purified Water (C_1W)

Six kilogram of small pieces of fresh vegetable wastes and one liter of purified water were put into the anaerobic digester. The amount of biogas produced was recorded hourly and also recorded daily till 5 days. After production of biogas for 5 days anaerobic digester was tightly sealed and kept for one month. After one month, the mixture in the anaerobic digester can be used as EM solution (C_1W).

Preparation of Effective Microorganism Solutions and Production of Biogas from Vegetable Waste with Lemon Juice (C_1A)

Six kilogram of small pieces of fresh vegetable wastes and one liter of lemon juice (pH 2.5) were put into the anaerobic digester. The amount of biogas produced was recorded hourly and also recorded by daily till 5 days. After production of biogas for 5 days, the anaerobic digester was tightly sealed and kept for one month. After one month, the mixture in the anaerobic digester can be used as EM solution (C_1A).

Preparation of Effective Microorganism Solutions and Production of Biogas from Vegetable Waste with Slaked Lime Solution (C_1B)

Six kilogram of small pieces of fresh vegetable wastes and one liter of slaked lime solution (pH 9.5) were put into the anaerobic digester. The amount of biogas produced was recorded hourly and also recorded daily till 5 days. After production of biogas for 5 days, the anaerobic digester was tightly sealed kept for one month. After one month, the mixture in the anaerobic digester can be used as EM solution (C_1B).

Preparation of Effective Microorganism Solutions and Production of Biogas from Vegetable Waste, Cow Dung and Sesame Meal Cake with Purified Water (C_2W)

Two kilogram of small pieces of fresh vegetable waste, two kilogram of cow dung and two kilogram of sesame meal cake were put into the anaerobic digester by successive layers and one liter of purified water was added into the anaerobic digester. The biogas was evolved and the gas production was checked. The amount of biogas was recorded hourly and also determined daily till 5 days. After production of biogas for 5 days, the anaerobic digester was tightly sealed and kept for one month. After one month, the mixture in the anaerobic digester can be used as EM solution (C_2W).

Preparation of Effective Microorganism Solutions and Production of Biogas from Vegetable Waste, Cow Dung and Sesame Meal Cake with Lemon Juice (C_2A)

Two kilogram of small pieces of fresh vegetable waste, two kilogram of cow dung and two kilogram of sesame meal cake were put into the anaerobic digester by successive layers and one liter of lemon juice was added into the anaerobic digester. The biogas was evolved and the gas production was checked. The amount of biogas was recorded hourly and also determined daily till 5 days. After production of biogas for 5 days, the anaerobic digester was tightly sealed and kept for one month. After one month, the mixture in the anaerobic digester can be used as EM solution (C_2A).

Preparation of Effective Microorganism Solutions and Production of Biogas from Vegetable Waste, Cow Dung and Sesame Meal Cake with Slaked Lime Solution (C_2B)

Two kilogram of small pieces of fresh vegetable waste, two kilogram of cow dung and two kilogram of sesame meal cake were put into the anaerobic digester by successive layers and one liter of slaked lime solution was added into the anaerobic digester. The biogas was evolved and the gas production was checked. The amount of biogas was recorded hourly and also

determined daily till 5 days. After production of biogas for 5 days, the anaerobic digester was tightly sealed and kept for one month. After one month, the mixture in the anaerobic digester can be used as EM solution (C_2B).

Isolation and Characterization of Microorganisms

The microorganisms were isolated from the prepared EM solutions and commercial EM solutions were characterized by cultural morphology and microscopic morphology at Department of Biotechnology, Mandalay Technological University.

Results and Discussion

Production of Biogas

While the preparation of effective microorganism solution, the biogas was evolved. The amount of bio gas was determined for hour by hour till five hours. The amount of biogas was also recorded by daily till five days. The results are described in Tables 1 and 2 and Figure 3.

Table 1 Production of Biogas (Hourly)

No.	Time taken (hour)	Volume of collected biogas (mL)						
		C	**C_1W**	**C_1A**	**C_1B**	**C_2W**	**C_2A**	**C_2B**
1	1	800	1800	1600	1500	1400	1200	2500
2	2	700	400	800	100	600	800	1300
3	3	600	200	400	-	300	500	300
4	4	300	100	300	-	200	100	100
5	5	200	100	100	-		-	-
	Total	**2600**	**2600**	**3200**	**1600**	**2500**	**2600**	**4200**

Table 2 Production of Biogas (Daily)

No.	Time taken (day)	Volume of collected biogas (mL)						
		C	C_1W	C_1A	C_1B	C_2W	C_2A	C_2B
1	1	3500	5000	5200	2000	4200	3600	6200
2	2	2600	3200	3500	-	200	1200	1000
3	3	1200	1300	300	2000	-	200	-
4	4	100	700	-	-	-	-	600
5	5	100	700	-	-	-	300	-
	Total	**7500**	**10900**	**9000**	**4000**	**4400**	**5300**	**7800**

C = Control = Vegetable Wastes only
C_1W = Vegetable Wastes with Purified Water
C_1A = Vegetable Wastes with Lemon Juice
C_1B = Vegetable Wastes with Slaked Lime Solution
C_2W = Vegetable Wastes, Cow Dung and Sesame Meal Cake with Purified Water
C_2A = Vegetable Wastes, Cow Dung and Sesame Meal Cake with Lemon Juice
C_2B = Vegetable Wastes, Cow Dung and Sesame Meal Cake with Slaked Lime Solution

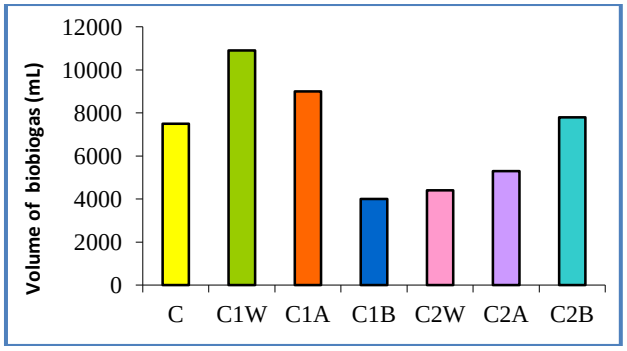

Figure 3 Total volume of biogas (daily) from various conditions

According to this table, the highest amount of biogas was evolved from vegetable waste with purified water.

Isolation and Characterization of Microorganisms in Prepared Effective Microorganism and Commercial Effective Microorganism Solutions

The microorganisms were isolated from prepared effective microorganism solution and commercial effective microorganism solutions were characterized according to cultural and microscopic morphology at Department of Biotechnology, Mandalay Technological University. The results are presented in Tables 3-17 and Figures 4-10.

Table 3 Cultural Morphology of C_1W (Vegetable Waste with Purified Water)

Sample	Cultural Morphology					
	Shape	**Color**	**Opacity**	**Elevation**	**Size (mm)**	**Family**
Condition-C_1W (Liquid)	Circle	Pale yellow	Opaque	Convex	2	Bacillaceae
	Circle	Pale yellow	Opaque	Convex	0.2	Bacillaceae
Condition-C_1W (Residue)	Irregular	Yellow	Opaque	Raised	2	Bacillaceae
	Irregular	Cream	Opaque	Flat	4	Bacillaceae
	Circle	Pale yellow	Opaque	Convex	0.5	Bacillaceae
	Circle	Pale yellow	Opaque	Convex	2	Streptomyceae

Table 4 Microscopic Morphology of C_1W(Vegetable Waste with Purified Water)

Sample	Microscopic Morphology				
	Shape	**Size (µm)**	**Gram Stain**	**Spore +/–**	**Family**
Condition-C_1W (Liquid)	Rod	2 × 4	+	+	Bacillaceae
	Rod	1× 2-4	+	-	Bacillaceae
Condition-C_1W (Residue)	Rod	1.5×2.5-2	+	-	Bacillaceae
	Rod	0.5 × 2-3	+	-	Bacillaceae
	Rod	1 × 2-4	+	-	Bacillaceae
	Rod	1.5 × 4-7	+	-	Streptomyceae

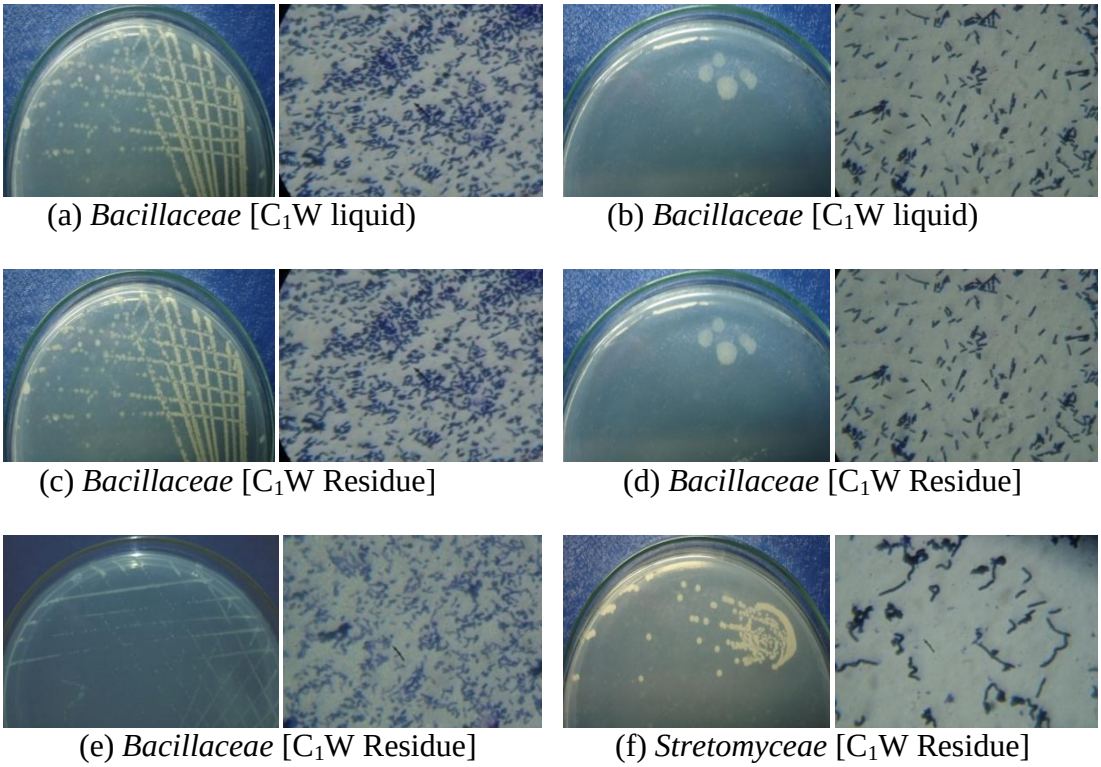

(a) *Bacillaceae* [C_1W liquid) (b) *Bacillaceae* [C_1W liquid)

(c) *Bacillaceae* [C_1W Residue] (d) *Bacillaceae* [C_1W Residue]

(e) *Bacillaceae* [C_1W Residue] (f) *Stretomyceae* [C_1W Residue]

Figure 4 Cultural and microscopic morphology of the C_1W condition (vegetable waste with purified water)

Table 5 Cultural Morphology of Condition –C_1A (Vegetable Waste with Lemon Juice)

Sample	Cultural Morphology					
	Shape	**Color**	**Opacity**	**Elevation**	**Size (mm)**	**Family**
Condition-C_1A (Liquid)	Filamentous	Creamy	Opaque	Raised	Small	Streptomyceae
Condition-C_1A (Residue)	Circle	Pale	Opaque	Putrinate	2	Streptomyceae
	Circle	Pale	Opaque	Convex	0.5	Streptomyceae
	Irregular	Pale	Opaque	Flat	3	Streptomyceae

Table 6 Microscopic Morphology of C_1A (Vegetable Waste with Lemon Juice)

Sample	Microscopic Morphology				
	Shape	**Size (µm)**	**Gram Stain**	**Spore +/–**	**Family**
Condition-C_1A Liquid	Y - Rod	1 × 1-2	+	–	Streptomyceae
Condition-C_1A Residue	Rod	1.5 × 4-7	+	–	Streptomyceae
	Rod	1 × 2-2.5	+	–	Streptomyceae
	Rod	1 × 2	+	–	Streptomyceae

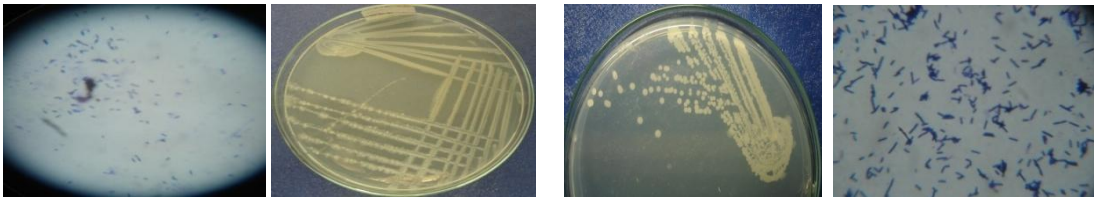

(a) *Stretomyceae* [C_1A, Liquid] (b) *Stretomyceae* [C_1A, Residue]

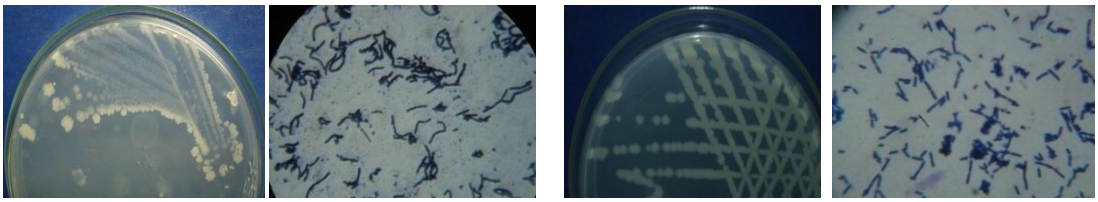

(c) *Stretomyceae* [C_1A, Residue] (d) *Stretomyceae* [C_1A, Residue]

Figure 5 Cultural and microscopic morphology of the C_1A condition (vegetable waste with lemon juice)

Table 7 Cultural Morphology of C_1B (Vegetable waste with Slaked Lime Solution)

Sample	Cultural Morphology					
	Shape	**Color**	**Opacity**	**Elevation**	**Size (mm)**	**Family**
Condition-C_1B Liquid	Irregular	Pale	Opaque	Flat	2	Streptomyceae
	Circle	Pale	Opaque	Convex	0.5-0.7	Bacillaceae
Condition-C_1B	Circle	Pale	Opaque	Convex	0.5	Streptomyceae
	Circle	Pale	Opaque	Convex	0.5	Bacillaceae
Residue	Irregular	Yellow	Opaque	Flat	2.5	Bacillaceae

Table 8 Microscopic Morphology of C_1B (Vegetable Waste with Slaked Lime Solution)

Sample	Microscopic Morphology				
	Shape	**Size (µm)**	**Gram Stain**	**Spore +/–**	**Family**
Condition-C_1B Liquid	Rod	1 × 2	+	+	Streptomyceae
	Rod	2 × 3-5	+	_	Bacillaceae
Condition-C_1B	Rod	1 × 1.5-2	+	_	Streptomyceae
	Rod	0.5 × 2-3	+	_	Bacillaceae
Residue	Rod	1.5 × 4-7	+	_	Bacillaceae

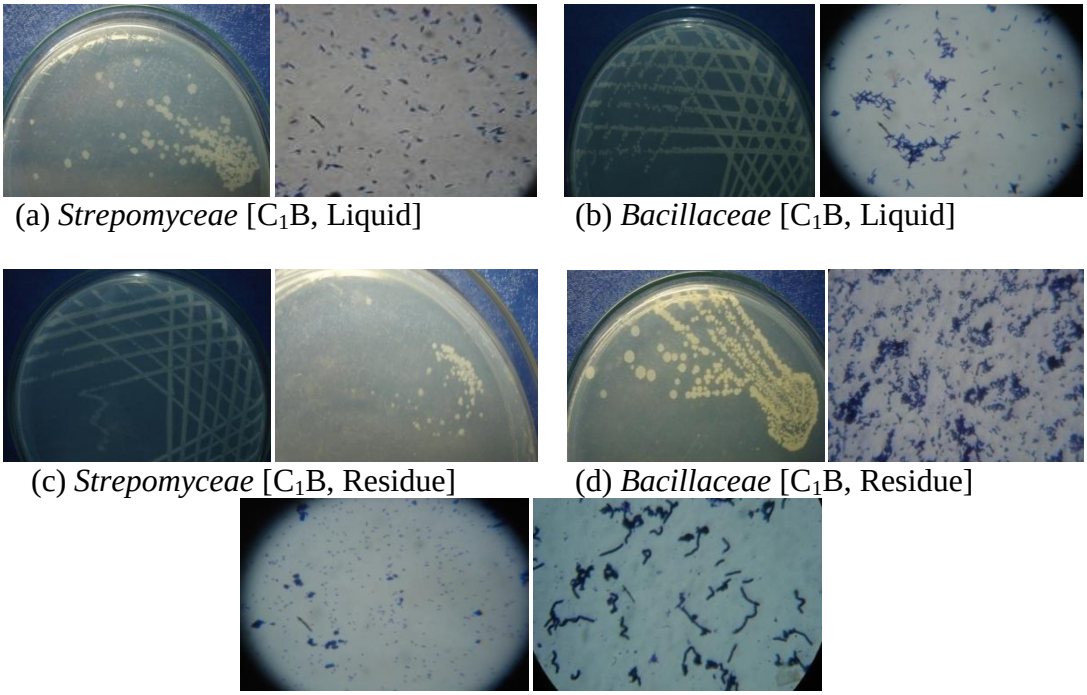

(a) *Strepomyceae* [C_1B, Liquid] (b) *Bacillaceae* [C_1B, Liquid]

(c) *Strepomyceae* [C_1B, Residue] (d) *Bacillaceae* [C_1B, Residue]

(e) *Bacillaceae* [C_1B, Residue]

Figure 6 Cultural and microscopic morphology of the C_1 B condition (vegetable waste with slaked line solution)

Table 9 Cultural Morphology of C_2W (Vegetable Waste, Cow Dung, Sesame Meal Cake with Purified Water)

Sample	Cultural Morphology					
	Shape	**Color**	**Opacity**	**Elevation**	**Size (mm)**	**Family**
Condition-C_2W Liquid	Circle	Pale	Opaque	Convex	2.5	Streptomyceae
	Circle	Pale	Opaque	Convex	1	Bacillaceae
	Spindle	Pale	Opaque	Flat	3	Bacillaceae
Condition - C_2W Residue	Irregular	Pale	Opaque	Convex	1.5-2	Streptomyceae
	Circle	Pale	Opaque	Umbonate	2	Streptomyceae

Table 10 Microscopic Morphology of C_2W (Vegetable Waste, Cow Dung, Sesame Meal Cake with Purified Water)

Sample	Microscopic Morphology				
	Shape	**Size (µm)**	**Gram Stain**	**Spore +/–**	**Family**
Condition -C_2W Liquid	Rod	2 × 4-7	+	_	Streptomyceae
	Rod	0.5 × 2-3	+	_	Bacillaceae
	Rod	1 × 2-3	+	_	Bacillaceae
Condition- C_2W Residue	Rod	1 .5× 3-5	+	_	Streptomyceae
	Rod	1.5 × 6	+	_	Streptomyceae

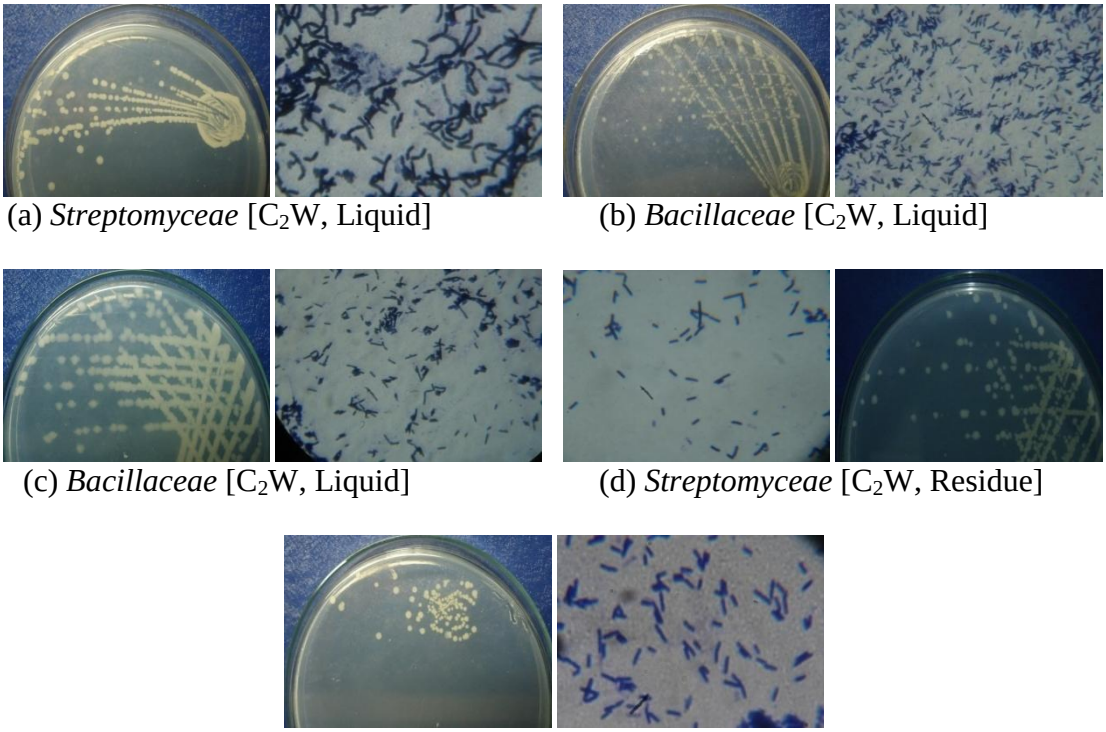

(a) *Streptomyceae* [C_2W, Liquid] (b) *Bacillaceae* [C_2W, Liquid]

(c) *Bacillaceae* [C_2W, Liquid] (d) *Streptomyceae* [C_2W, Residue]

(e) *Streptomyceae* [C_2W, Residue]

Figure 7 Cultural and microscopic morphology of the C_2W condition (vegetable waste, cow dung, sesame meal cake with purified water)

Table 11 Cultural Morphology of C_2 A (Vegetable Waste, Cow Dung, Sesame Meal Cake with Lemon Juice)

Sample	Cultural Morphology					
	Shape	**Color**	**Opacity**	**Elevation**	**Size (mm)**	**Family**
Condition-C_2 A Liquid	Circular	Creamy	Transparent	Raised	Very Small	Latobacillaceae
	Irregular	yellowish	Opaque	Flat	Normal	Bacillaceae
Condition-C_2 A Residue	Irregular	Creamy	Opaque	Flat	Irregular	Bacillaceae
	Filamentous	Creamy	Opaque	Raised	Small	Streptomyceae

Table 12 Microscopic Morphology of C_2A (Vegetable Waste, Cow Dung, Sesame Meal Cake with Lemon Juice)

Sample	Microscopic Morphology				
	Shape	**Size (µm)**	**Gram Stain**	**Spore +/–**	**Family**
Condition-C_2 A Liquid	Double Rod	1 × 1-1.5	+	–	Lactobacillaceae
	Rod Chain	1 × 2-3	+	+	Bacillaceae
Condition-C_2 A Residue	Rod Cluster	1 × 1-2	+	–	Bacillaceae
	Double Rod	0.8-1 × 1-1.5	+	–	Streptomyceae

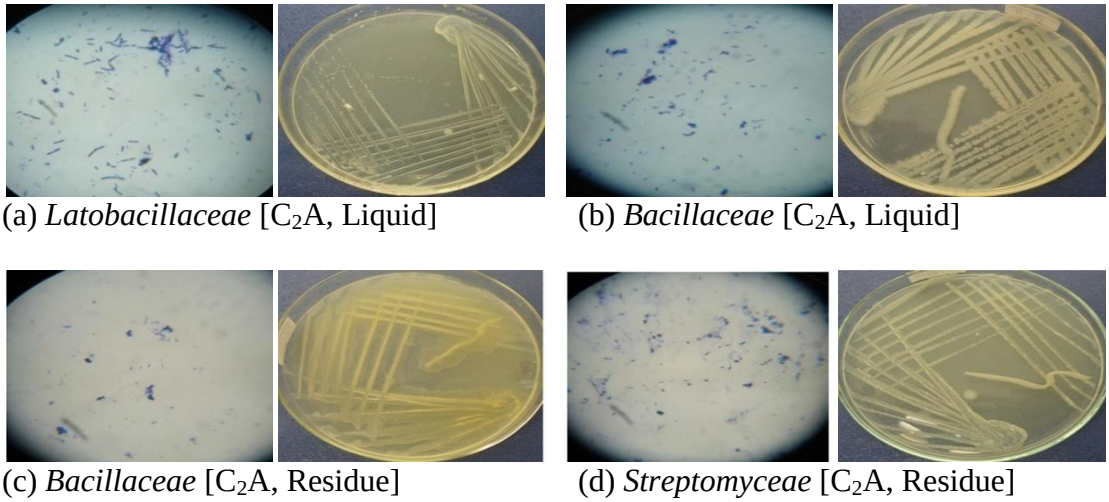

(a) *Latobacillaceae* [C_2A, Liquid] (b) *Bacillaceae* [C_2A, Liquid]

(c) *Bacillaceae* [C_2A, Residue] (d) *Streptomyceae* [C_2A, Residue]

Figure 8 Cultural and microscopic morphology of the C_2A condition (vegetable waste, cow dung, sesame meal cake with lemon juice)

Table 13 Cultural Morphology of C_2B (Vegetable Waste, Cow Dung, Sesame Meal Cake with Slaked Lime Solution)

Sample	Cultural Morphology					
	Shape	**Color**	**Opacity**	**Elevation**	**Size (mm)**	**Family**
Condition- C_2B Liquid	Circle	Yellow	Opaque	Convex	1.5	Streptomyceae
	Irregular	Cream	Opaque	Flat	2	Streptomyceae
	Irregular	Yellow	Opaque	Convex	1	Corynebacterium
Condition- C_2B Residue	Circle	Pale	Opaque	Convex	3	Streptomyceae
	Circle	Pale	Opaque	Flat	1	Streptomyceae

Table 14 Microscopic Morphology of C_2B (Vegetable Waste, Cow Dung, Sesame Meal Cake with Slaked Lime Solution)

Sample	Microscopic Morphology				
	Shape	**Size (µm)**	**Gram Stain**	**Spore +/–**	**Family**
Condition- C_2B Liquid	Rod	2 × 4-6	+	_	Streptomyceae
	Rod	2 × 3.5	+	_	Streptomyceae
	Rod	0.5-1 × 2-3	+	_	Cornyebacterium
Condition- C_2B Residue	Rod	1 × 3	+	_	Streptomyceae
	Rod	1-1.5×3-4	+	_	Streptomyceae

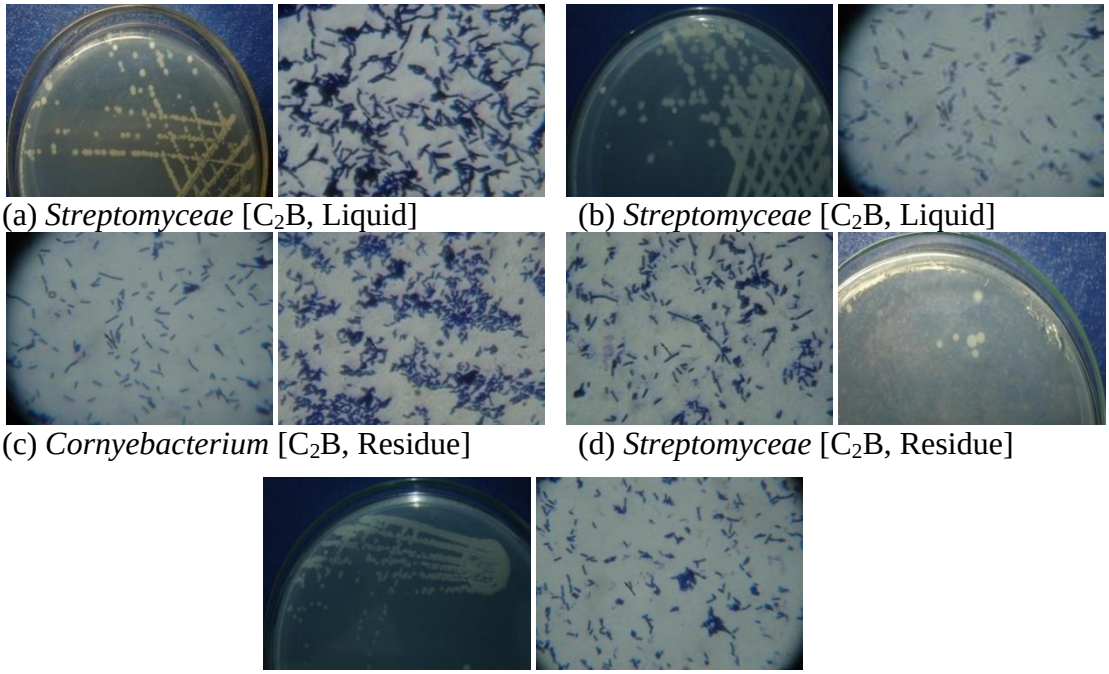

(a) *Streptomyceae* [C_2B, Liquid] (b) *Streptomyceae* [C_2B, Liquid]

(c) *Cornyebacterium* [C_2B, Residue] (d) *Streptomyceae* [C_2B, Residue]

(e) *Streptomyceae* [C_2B, Residue]

Figure 9 Cultural and microscopic morphology of the C_2 B condition (vegetable waste, cow dung, sesame meal cake with slaked lime solution**)**

Table 15 Cultural Morphology of Commercial EM

Sample	Cultural Morphology				
	Shape	**Color**	**Elevation**	**Size**	**Family**
Commercial EM	Irregular	White (Opaque)	Raised	0.5-1	Bacillaceae
	Irregular	Creamy	Flat	1-1.5	Bacillaceae
	Irregular	White	Flat	1.5	Bacillaceae

Table 16 Microscopic Morphology of Commercial EM

Sample	Microscopic Morphology			
	Shape	Size	Gram stain	Family
Commercial EM	Rod	2 × 2-3	+	Bacillaceae
	Rod	2-3 × 3-5	+	Bacillaceae
	Short rod	1-2 × 2-3.5	+	Bacillaceae

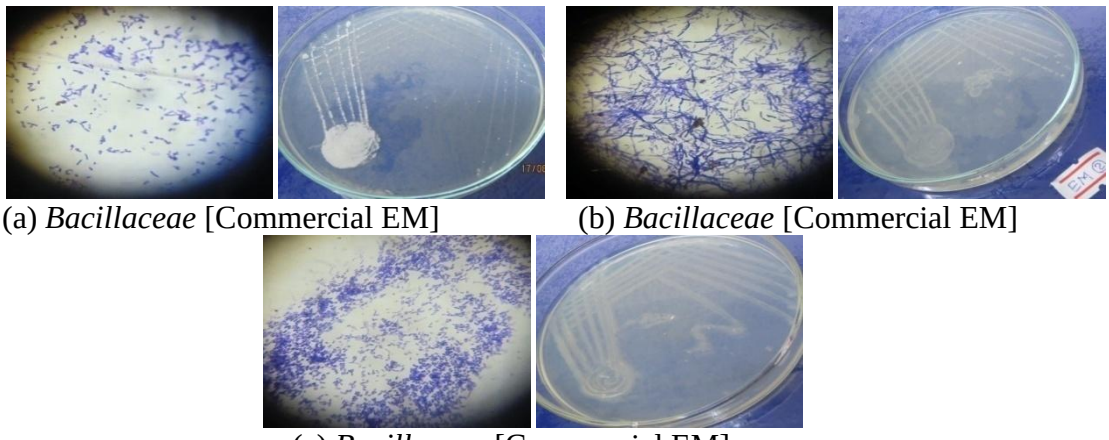

(a) *Bacillaceae* [Commercial EM] (b) *Bacillaceae* [Commercial EM]

(c) *Bacillaceae* [Commercial EM]

Figure 10 Cultural and microscopic morphology of commercial EM Solution)

Table 17 Microorganisms and their Family from the Prepared and Commercial EM Solutions

No.	Condition	No. of Isolated Microorganism	Family
1	C_1w (liquid)	2	Bacillaceae
2	C_1w (Residue)	4	Three- Bacillaceae, Streptomyceae
3	C_1B(Liquid)	2	Streptomyceae, Bacillaceae
4	C_1B (Residue)	3	Streptomyceae, two- Bacillaceae
5	C_1A(Liquid)	1	Streptomyceae
6	C_1A(Residue)	3	Three- Streptomyceae
7	C_2W (Liquid)	3	Streptomyceae, two- Bacillaceae
8	C_2W (Residue)	2	Two-Streptomyceae
9	C_2A (Liquid)	2	Lactobacillaceae, Bacillaceae
10	C_2A(Residue)	2	Bacillaceae, Streptomyceae
11	C_2B(liquid)	3	Two-Streptomyceae, Cornyebacterium
12	C_2B(Residue)	2	Two-Streptomyceae
13	Commercial EM	3	Bacillaceae

For condition C_1, prepared EM solutions contain families of Bacillaceae and Streptomyceae. For condition C_2, prepared EM solutions consist of Bacillaceae, Streptomyceae, Cornyebacterium and Lactobacillaceae. This means that adding materials such as cow dung (humic substance support) and sesame meal cake (protein support) can supply more effective microorganisms. Commercial EM solution contains families of Bacillaceae.

Conclusion

In this research, EM (effective microorganism) solutions were prepared from waste of vegetables, cow dung and sesame meal cake. While EM solution were prepared by primary fermentation, biogas was evolved. Two conditions such as C_1 (vegetable waste) and C_2 (vegetable waste, cow dung and sesame meal cake) with different pH values were performed and the amount of biogas produced were determined hourly and daily till 5 days. The highest amount of biogas was evolved from condition C_1W(vegetable waste with purified water). The microorganisms that contained in EM solutions were found to be Bacillaceae**,** Streptomyceae**,** Lactobacillaceae and Cornyebacterium. Commercial EM solution contains only Bacillaceae. Therefore using prepared EM solutions are suitable for agriculture for reducing the dependency on chemical fertilizers and pesticides, for solving all kinds of environmental problems such as water, air and soil pollution, for recycling of kitchen waste into valuable organic materials. The evolved biogas can also be used as renewable energy source.

Acknowledgements

The author wishes to thank the Myanmar Academy of Arts and Science for allowing to present this paper and Professor and Head, Dr Thidar Aung and Professor Dr Htay Htay Win, Department of Chemistry, Magway University for their provision and suggestions of the research facilities.

References

Higa, T. (1991). *Effective Microorganisms: A Biotechnology for Mankind*. In Parr, J.F., Hornick, S.B. and Whitman C.E. (ed.). Proceedings of the First International Conference on Kyusei Nature Farming. Washington, D.C., U.S. Department of Agriculture, p.8-14.

Higa, T. (1994). *Effective Microorganisms: A New Dimension for Nature Farming*. In Parr, J.F., Hornick, S.B. and Simpson M.E. (ed.). Proceedings of the Second International Conference on Kyusei Nature Farming. Washington, D.C., U.S. Department of Agriculture, P. 20-22.

Higa, T. and James, F. (1994). "Beneficial and Effective Microorganisms for a Sustainable Agriculture and Environment". *International Nature Farming Research Center*, Atami, Japan, pp 4-7

Higa, T. and Wididana, G. N. (1991a). *The Concept and Theories of Effective Microorganisms*. In Parr, J.F., Hornick, S.B. and Whitman C.E. (ed.). Proceedings of the First International Conference on Kyusei Nature Farming. Washington, D. C., U.S. Department of Agriculture, p.118-124

Higa, T. and Wididana, G. N. (199lb). *Changes In the Soil Microflora Induced by Effective Microorganisms*. In Parr, J.F., Hornick, S.B. and Whitman C.E. (ed.). Proceedings of the First International Conference on Kyusei Nature Farming. Washington, D. C., U.S. Department of Agriculture, p.153-162

Kengo, Y. and Hui-lian, X. (2000). "Properties and Applications of an Organic Fertilizer Inoculated with Effective Microorganisms". *Journal of Crop Production*, Vol **3**(1), pp 255-268.

Lévai, L., Veres, S.Z., Makleit, P., Marozsán, M. and Szabó, B. (2006). "New Trends in Plant Nutrition". *Proceedings of 41st Croatian and 1st International Symposium on Agriculture*.

Singh, D.S., Chand, S, Anvar, M. and Patra (2003). "Effect of Organic and Inorganic Amendment on Growth and Nutrient Accumulation by Isabgol (*Plantagoovata*) in Sodic Soil Under Greenhouse Conditions". *J. Med. Arom. Plant Sci*., Vol. 25, pp. 414-419

REMOVAL OF SOME HEAVY METALS FROM INDUSTRIAL WASTEWATER BY USING DRY BIOMASS OF *HYDRILLA VERTICILLITA* (L. F.) ROYLE

Thandar[1], Hnin Thanda Aung[2], Khaing Khaing Kyu[3]

Abstract

The aim of this research work is to reduce the concentration of Cd^{2+}, Cr^{3+} and Pb^{2+} ions in three industrial wastewater samples from dry cell battery factory, nickel plating factory and leather factory in industrial zones I and II, Mandalay Region, Myanmar. The aquatic plant namely *Hydrilla verticillata* (L. F.) Royle (Mhaw Gyan) was used as dry biomass for the removal of heavy metal ions from three industrial wastewater samples within the optimum experimental conditions. The sorption parameters (optimum contact time and loading weight) were determined using Langmuir isotherm. According to the results, the experimental data for sorption of Cd^{2+} and Cr^{3+} ions were fitted to the Langmuir model except Pb^{2+}. The optimum contact time and optimum loading weight were used for the removal of selected metal ions from three industrial wastewater samples. The result revealed that the removal order of metal ions from three industrial wastewater samples using dry biomass was found to be $Cd^{2+} > Cr^{3+} > Pb^{2+}$.

Keywords: dry biomass, industrial wastewaters, Langmuir isotherm, sorption, heavy metal ions

Introduction

The increasing of urbanization and industrialization has dramatically led into the production of the intensity of wastewater around the world (Asia *et al*., 2006). Heavy metal pollution comes in streams from industrial sectors. The industrial sectors produces harmful heavy metal waste, as a result contaminating water resources and ground resources (Tariq *et al*., 2018). With increasing environmental awareness and legal constraints being imposed on the discharge of effluents, a need for cost-effective alternative technologies are essential. In this endeavor plant biomass can emerged as an option for developing economic and eco-friendly wastewater treatment through a process called biosorption (Dixit *et al*., 2015). Biosorption is a physiochemical process that occurs naturally in certain biomass which allows it to passively concentrate and bind contaminants onto its cellular structure (Ramasubramaniam *et al*., 2012). It is a biological method of environmental controlled and can be an alternative to conventional contaminate wastewater treatment facilities (Dixit *et al*., 2015). Biosorbent materials are derived from raw microbial, seaweed or even some plant biomass through different kinds of simple procedures. They may be chemically pretreated for better performance and suitability for process applications. Biosorbents are capable of directly sorbing metal ionic species from aqueous solutions (Ramasubramaniam *et al*., 2012). Studies on biological methods are very important area of research with huge potential for research and applicability for removal of heavy metals (Dhokpande and Kaware., 2013). Adsorption is the adhesion of atoms, ions, biomolecular or biomolecules of gas, liquid, or dissolved solid to a surface (Itodo *et al*., 2013). Several mathematical models can be used to describe experimental data of adsorption isotherms. The Freundlich, Langmuir and Temkin models are employed to analysis of adsorption occurred in the experiment (Rahimi and Vadi., 2014). In this research work, the optimum contact time and

[1] Dr, Lecturer, Department of Chemistry, Magway University
[2] Dr, Associate Professor, Department of Chemistry,University of Mandalay
[3] Dr, Professor, Department of Chemistry, University of Mandalay

optimum loading weight were determined and the removal of selected metal ions (Cd^{2+}, Cr^{3+}, Pb^{2+}) with dry biomass *Hydrilla verticillata* (L.F.) Royle was investigated.

Materials and Methods

Samples Collection

Two selected wastewater samples from dry cell battery factory and nickel plating factory were collected from Industrial Zone I in Pyigyitagun Township, Mandalay Region (Figure 1). Another wastewater sample from leather factory was collected from Industrial Zone II in Amarapura Township, Mandalay Region (Figure 2).

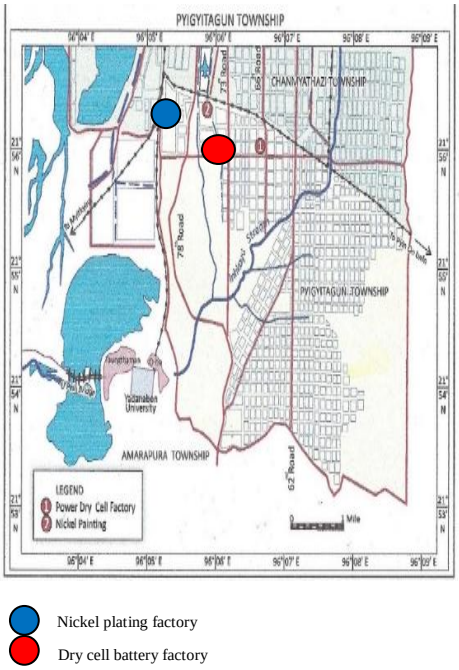

Figure 1 Location map of the study area (1)

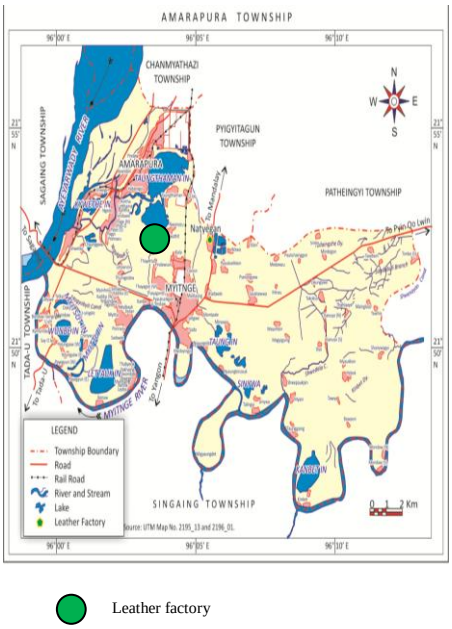

Figure 2 Location map of the study area (2)

Hydrilla verticillata (L. F.) Royle (Mhaw Gyan) was collected from Mandalay moat in Mandalay, Myanmar. It is shown in Figure 3.

Figure 3 *Hydrilla verticillata* (L. F.) Royle (Mhaw Gyan)

Wastewater Treatment by Using Dry Biomass

Adsorption method was applied for the wastewater treatment by using dry biomass (Baig*et al*., 2015).

Preparation of Dry Biomass

The collected aquatic plant was washed with pure water and dried in an oven at 60ºC for 36 h. The dried sample was ground and sieved through a 100 mesh sieve.

Effects of Adsorption Time of Dry Biomass

2.5 g of dry biomass was weighed and washed twice with 0.1 M HCl and once again with distilled water. The biomass was suspended in 500 mL of 0.01 M sodium acetate to obtain a tissue concentration of 5 mg/mL. After adjusting the pH to 5, 50 mL of the suspension was transferred to conical flask. The suspension was centrifuged and the supernatant was discarded. And then, 50 mL of wastewater samples was added to each precipitate in 100 mL conical flask with various time intervals (5, 10, 15, 30, 60, 90 and 120 min). All the conical flasks were shaken on a shaker for 90 min. After the mixtures were shaken, centrifuged and filtered, the supernatants were analyzed by atomic absorption spectrophotometer.

Effect of Loading Weight of Dry Biomass

Different weights (0.20 g, 0.25 g, 0.30 g, 0.35 g and 0.40 g) of dry biomass were weighed and washed twice with 0.1 M HCl and once again with distilled water. The biomass was suspended in 50 mL of 0.01 M sodium acetate to obtain a tissue concentration of 5 mg/mL.

After adjusting the pH to 5, 50 mL of the suspension was transferred to 100 mL conical flask and settled for 15 min. The suspensions were centrifuged and the supernatants were discarded. And then, 50 mL of wastewater sample was added to each precipitate in 100 mL conical flask. All the conical flasks were shaken on a shaker for 90 min. After the mixtures were shaken, centrifuged and filtered, the supernatants were analyzed by atomic absorption spectrophotometer.

Adsorption Study

The phenomena of adsorption is generally applied for the heavy metal (Cd^{2+}, Cr^{3+} and Pb^{2+}) ions removal from industrial wastewater. The sorption studies of the wastewater can be carried out by the sorbent-sorbate interaction with the dry biomass. In the sorption studies, the different loading weights and the different contact times were used.

Adsorption Study on Effect of Loading Weight of Dry Biomass

In the sorption studies the loading weight (mass of sorbent (dry biomass)) was varied and concentration of wastewater (5 mg/mL) was fixed. The different mass of sorbents (0.20 g, 0.25 g, 0.30 g, 0.35 g and 0.40 g) were used.

Wastewater Treatment by Using Dry Biomass

Each 0.25 g and 0.35 g of dry biomass were weighed and washed twice with 0.1 M HCl and washed again with distilled water. The biomass was suspended in 50 mL of 0.01 M sodium acetate for 15 min and 90 min to obtain a concentration of 5 mg/mL. The pH was adjusted to 5. After 15 min and 90 min later, the suspensions were transferred to conical flasks. The suspensions were centrifuged and the supernatants were discarded. And then, 50 mL of wastewater sample was added to each precipitate in 100 mL conical flask. All the conical flasks were shaken on a shaker for 90 min, centrifuged and filtered. Finally, the supernatants were analyzed by atomic absorption spectrophotometer.

Results and Discussion

Wastewater Treatment by Using Dry Biomass

The optimum experimental conditions (the contact time and loading weight) were used for the removal of selected heavy metal ions from dry cell battery factory, nickel plating factory and leather factory wastewater samples using dry biomass.

Effects of Contact Time on the Removal of Cd^{2+}, Cr^{3+}, Pb^{2+}Ion from Three Industrial Wastewater by Dry Biomass

In this study, the effects of contact time using dry biomass with initial concentration 5 mg/mL at 0.25 g adsorbent weight on the removal of Cd^{2+}, Cr^{3+} and Pb^{2+} from dry cell battery factory, nickel plating factory and leather factory wastewater samples were investigated. The resulted data is shown in Table 1 and Figure 4, the optimum time for the removal percentage of Cd^{2+} ion from wastewater samples of dry cell battery factory (52.99 %), nickel plating factory (56.68 %) and leather factory (58.33 %) were observed at 90 min using the dry biomass. Furthermore, the optimum time for the removal percentage of Cr^{3+} ion from dry cell battery factory (33.45 %), nickel plating factory (35.96 %) and leather factory (33.60 %) were also found at 90 min using the dry biomass (Table 2 and Figure 5). As shown in Table 3 and Figure 6, dry biomass could remove Pb^{2+} ion from dry cell battery factory (3.30 %), nickel plating factory (4.35 %) and leather factory (3.33 %), after 15 min.

Table 1 Effect of Contact Time on the Removal of Cd^{2+} Ion from Three Industrial Wastewater Samples by Dry Biomass

Contact time (min)	Removal percent of Cd^{2+} ion (%)								
	Dry cell battery factory			Nickel plating factory			Leather factory		
	Before treatment	After treatment	Removal (%)	Before treatment	After treatment	Removal (%)	Before treatment	After treatment	Removal (%)
5		0.270	40.13		0.271	41.59		0.029	39.58
10		0.245	43.68		0.268	42.24		0.027	43.75
15		0.235	47.89		0.261	43.75		0.025	47.91
30	0.451	0.216	52.11	0.464	0.245	47.19	0.048	0.024	50.00
60		0.214	52.54		0.227	51.08		0.022	54.16
90		0.212	52.99		0.201	56.68		0.020	58.33
120		0.217	51.88		0.215	53.66		0.203	52.08

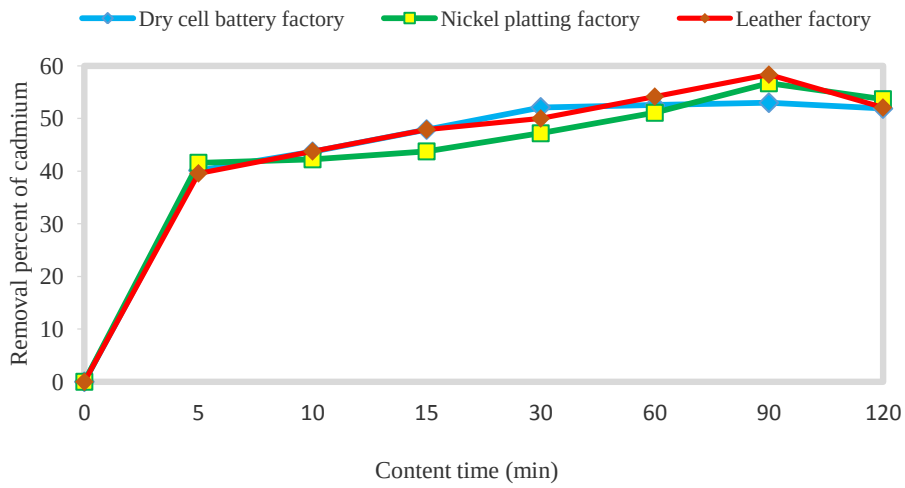

Figure 4 Effect of contact time on the removal of Cd^{2+} ion from three industrial wastewater samples by modified dry biomass

Table 2 Effect of Contact Time on the Removal of Cr^{3+} Ion from Three Industrial Wastewater Samples by Dry Biomass

Contact time (min)	Removal percent of Cr^{3+} ion (%)								
	Dry cell battery factory			Nickel plating factory			Leather factory		
	Before treatment	After treatment	Removal (%)	Before treatment	After treatment	Removal (%)	Before treatment	After treatment	Removal (%)
5		0.200	28.10		0.375	23.22		0.283	24.53
10		0.194	30.21		0.321	30.96		0.261	30.40
15		0.193	30.58		0.317	31.83		0.256	31.73
30	0.278	0.190	31.65	0.465	0.315	32.26	0.375	0.255	32.00
60		0.189	32.01		0.304	34.62		0.252	32.80
90		0.185	33.45		0.299	35.96		0.249	33.60
120		0.187	32.73		0.303	34.83		0.252	32.80

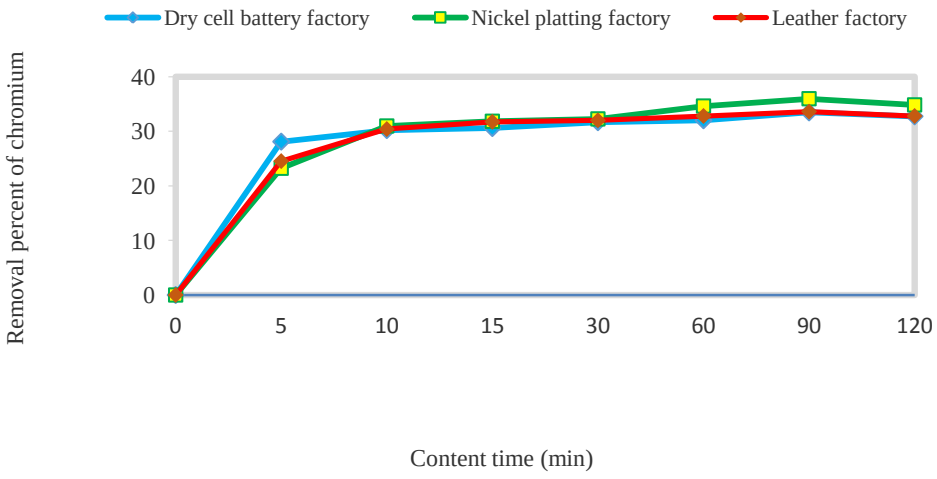

Figure 5 Effect of contact time on the removal of Cr^{3+} ion from three industrial wastewater samples by dry biomass

Table 3 Effect of Contact Time on the Removal of Pb^{2+} Ion from Three Industrial Wastewater Samples by Dry Biomass

Contact time (min)	Removal percent of Pb^{2+} ion (%)								
	Dry cell battery factory			Nickel plating factory			Leather factory		
	Before treatment	After treatment	Removal (%)	Before treatment	After treatment	Removal (%)	Before treatment	After treatment	Removal (%)
5		1.930	1.91		0.910	3.39		0.762	2.23
10		1.935	3.10		0.901	3.93		0.751	2.34
15		1.925	3.30		0.905	4.35		0.654	3.33
30	1.991	1.931	3.01	0.942	0.908	3.61	0.981	0.685	3.02
60		1.929	3.12		0.923	2.02		0.670	3.17
90		1.926	3.16		0.924	1.91		0.675	3.12
120		1.927	3.21		0.925	1.80		0.673	3.14

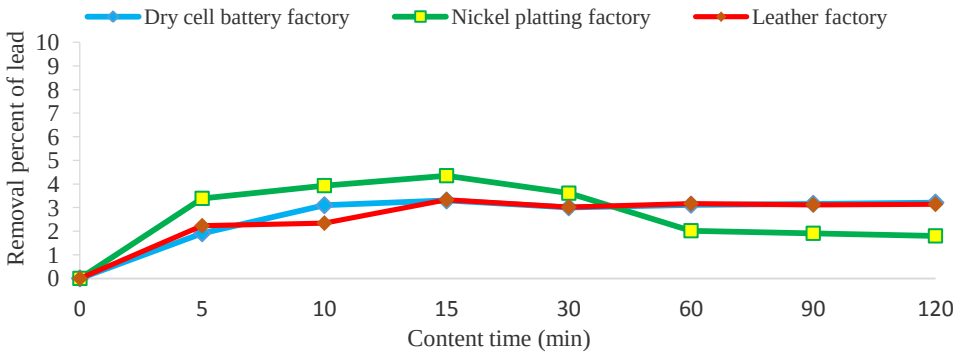

Figure 6 Effect of contact time on the removal of Pb^{2+} ion from three industrial wastewater samples by dry biomass

Effects of Loading Weight of the Removal of Cd^{2+}, Cr^{3+}, Pb^{2+} Ions from Three Industrial Wastewater by Dry Biomass

In this study, the effect of loading weight of dry biomass in initial concentration 5 mg/mL taking the range of the weight 0.20 g to 0.40 g for dry cell battery factory, nickel plating factory and leather factory were investigated at contact time 90 min.

In resulted data indicated in Table 4 and Figure 7, dry biomass at 0.35 mg showed the highest removal percent of Cd^{2+} ion (71.37 %, 70.90 % and 72.92 %) respectively. Furthermore, it was also found that the weight of biomass at 0.35 mg showed the highest removal percent Cr^{3+} ion (67.27 %, 67.52% and 66.93 %) from dry cell battery, nickel plating and leather factories wastewater samples (Table 5 and Figure 8). As shown in Table 6 and Figure 9, dry biomass at 0.25 mg could remove the highest removal percent of Pb^{2+} ion (3.10 %, 4.56 % and 4.99 %) from dry cell battery, nickel plating and leather factories wastewater samples.

Table. 4 Effect of Loading Weight of Dry Biomass on the Removal of Cd^{2+} Ion from Three Industrial Wastewater Samples

Loading weight (g)	Removal percent of Cd^{2+} ion (%)								
	Dry cell battery factory			Nickel plating factory			Leather factory		
	Before treatment	After treatment	Removal (%)	Before treatment	After treatment	Removal (%)	Before treatment	After treatment	Removal (%)
0.20	0.451	0.245	45.68	0.464	0.265	42.88	0.048	0.028	41.67
0.25		0.220	51.22		0.225	51.50		0.026	45.83
0.30		0.190	57.78		0.198	57.33		0.023	52.08
0.35		0.129	71.37		0.135	70.90		0.013	72.92
0.40		0.135	70.06		0.150	67.67		0.015	68.75

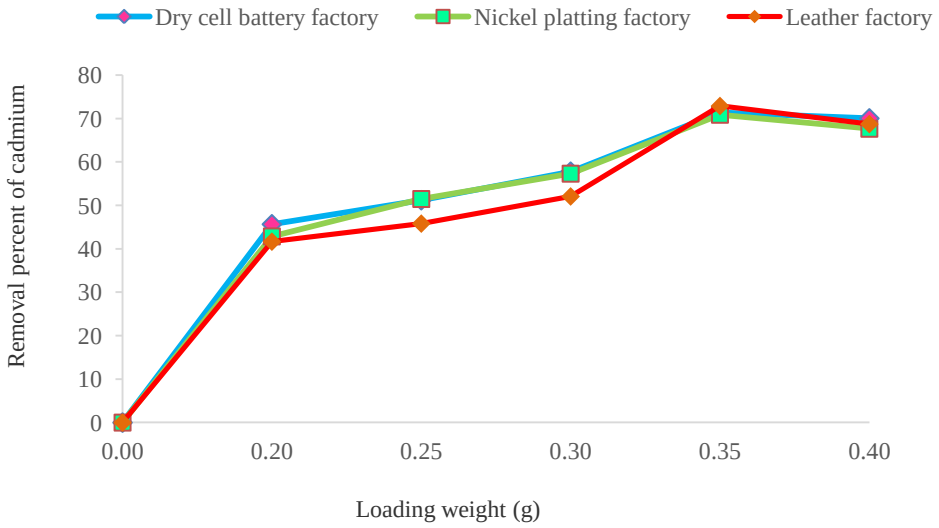

Figure 7 Effect of loading weight of dry biomass on the removal of Cd^{2+} ion from three industrial wastewater samples

Table 5 Effect of Loading Weight of Dry Biomass on the Removal of Cr^{3+} Ion from Three Industrial Wastewater Samples

Loading weight (g)	Removal percent of Cr^{3+} ion (%)								
	Dry cell battery factory			Nickel plating factory			Leather factory		
	Before treatment	After treatment	Removal (%)	Before treatment	After treatment	Removal (%)	Before treatment	After treatment	Removal (%)
0.20	0.278	0.215	22.67	0.465	0.355	23.66	0.375	0.300	20.00
0.25		0.197	29.13		0.341	26.67		0.277	26.13
0.30		0.181	34.89		0.298	35.91		0.250	33.33
0.35		0.091	67.27		0.151	67.52		0.124	66.93
0.40		0.101	63.66		0.162	65.16		0.129	65.60

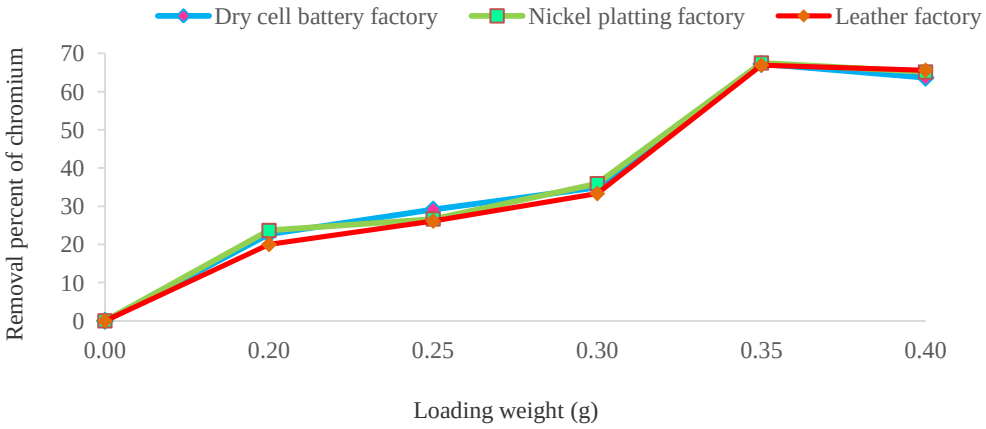

Figure 8 Effect of loading weight of dry biomass on the removal of Cr^{3+} ion from three industrial wastewater samples

Table 6 Effect of Loading Weight of Dry Biomass on the Removal of Pb^{2+} Ion from Three Industrial Wastewater Samples

Loading weight (g)	Removal percent of Pb^{2+} ion (%)								
	Dry cell battery factory			Nickel plating factory			Leather factory		
	Before treatment	After treatment	Removal (%)	Before treatment	After treatment	Removal (%)	Before treatment	After treatment	Removal (%)
0.20	1.991	1.984	2.15	0.942	0.911	3.30	0.981	0.957	2.45
0.25		1.930	3.10		0.899	4.56		0.932	4.99
0.30		1.935	2.81		0.907	3.71		0.949	3.26
0.35		1.946	2.20		0.921	2.23		0.960	2.14
0.40		1.941	2.51		0.925	1.81		0.961	2.04

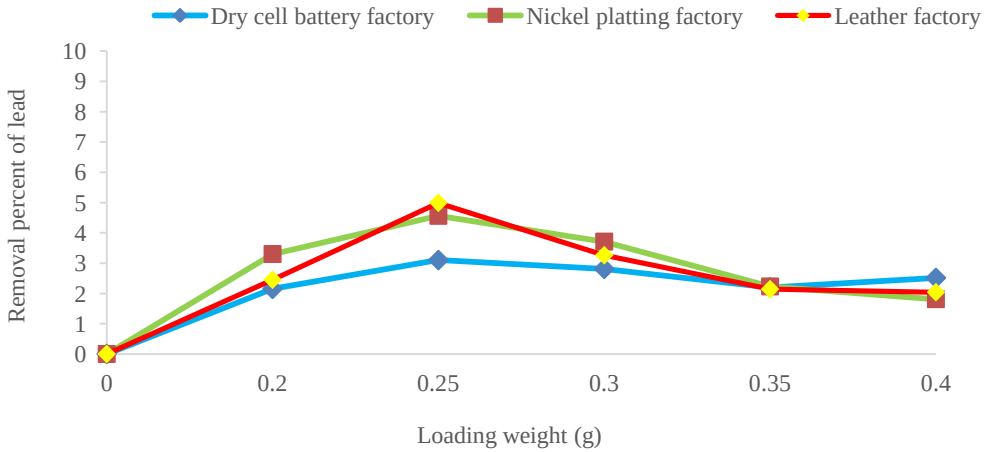

Figure 9 Effect of loading weight of dry biomass on the removal of Pb^{2+} ion from three industrial wastewater samples

Study on Adsorption Isotherm

The amount of Cd^{2+}, Cr^{3+} and Pb^{2+} adsorbed onto the dry biomass from *Hydrilla verticillata* (L. F.) Royle, q_e (mg g^{-1}) was calculated by

$$q_e = (C_0 - C_e)\ \frac{v}{w}$$

where C_o and C_e are the initial and equilibrium concentrations of wastewater (mg g^{-1}), 'v' the volume of the solution (L), and 'w' the weight of the plant biomass (g) (Nethaji*et al.*, 2013).

There are two well-known types of adsorption isotherm; the Langmuir isotherm and, Freundlich isotherm.

The Langmuir adsorption isotherm is mathematically expressed as;

$$\frac{x}{m} = \frac{X_m bC}{1+bC}$$

$$q_e = \frac{X_m bC_e}{1+bC_e}$$

$$\frac{1}{q_e} = \frac{1}{X_m} + \frac{1}{X_m bC_e}$$

$$\frac{C_e}{q_e} = \frac{C_e}{X_m} + \frac{1}{X_m b}$$

where X_m = Langmuir monolayer capacity parameter

b = constant for a given adsorbate and adsorbent at a particular temperature.

From the isotherm model plot, Langmuir and model constants are calculated to know its isotherm model fit to the adsorption of biomass on adsorbent Cd^{2+}, Cr^{3+} and Pb^{2+} ions.

Adsorption Isotherm from Three Industrial Wastewater Samples onto the Dry Biomass

The adsorption of heavy metal ions such as Cd^{2+}, Cr^{3+} and Pb^{2+} ions from three industrial wastewater onto dry biomass were determined by using Langmuir's adsorption isotherm. The optimum contact time and optimum loading weight were determined. The adsorption nature of sorbent-sorbate interaction with dry biomass was studied by using the optimum time (90 min for Cd^{2+} and Cr^{3+}) and (15 min for Pb^{2+}).

As shown in Figure 10, the linear coefficient values (R^2) from wastewater samples of dry cell battery, nickel plating and leather factories were 0.9105, 0.9211 and 0.9184 for Cd^{2+} ion. Therefore, for the adsorption of Cd^{2+} ion from three industrial wastewater samples the data fitted with the Langmuir isotherm.

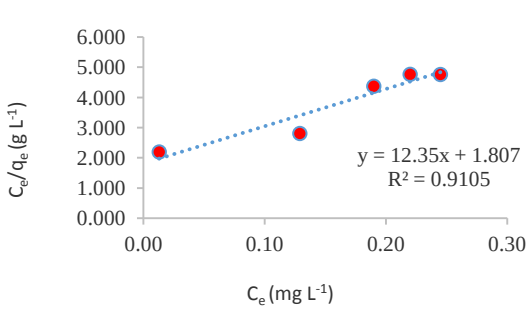

(a)

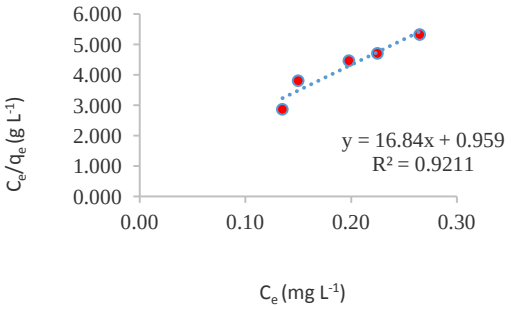

(b)

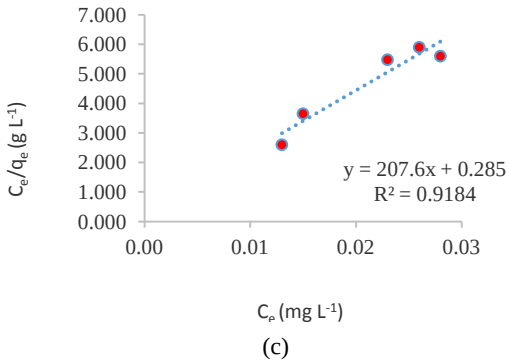

(c)

Figure 10 Langmuir isotherm for Cd^{2+} ion from three industrial wastewater samples onto the dry biomass (a) dry cell battery factory (b) nickel plating factory and (c) leather factory

According to Figure 11, the linear coefficient values (R^2) from wastewater samples of dry cell battery, nickel plating and leather factories were 0.9985, 0.9868 and 0.9985 for Cr^{3+} ion. Therefore, for the adsorption of Cr^{3+} ion from three industrial wastewater samples the data fitted with the Langmuir isotherm.

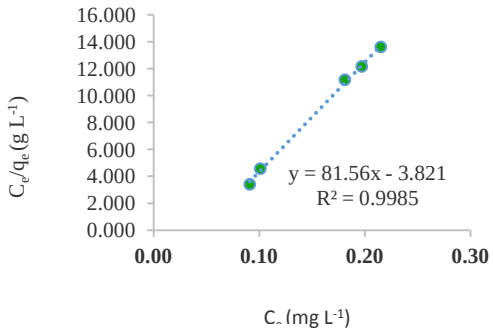

(a)

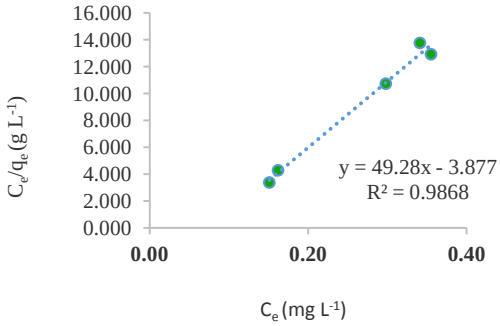

(b)

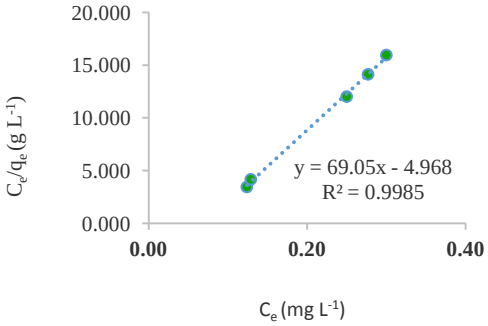

(c)

Figure 11 Langmuir isotherm for Cr^{3+} ion from three industrial wastewater samples onto the dry biomass (a) dry cell battery factory (b) nickel plating factory and (c) leather factory

The linear coefficient values (R^2) from wastewater samples of dry cell battery, nickel plating and leather factories were 0.1760, 0.5884 and 0.6354 for Pb^{2+} ion in Figure 12. Therefore, the adsorption of Pb^{2+} ion from three industrial wastewater samples were found to be deviation from the Langmuir isotherm.

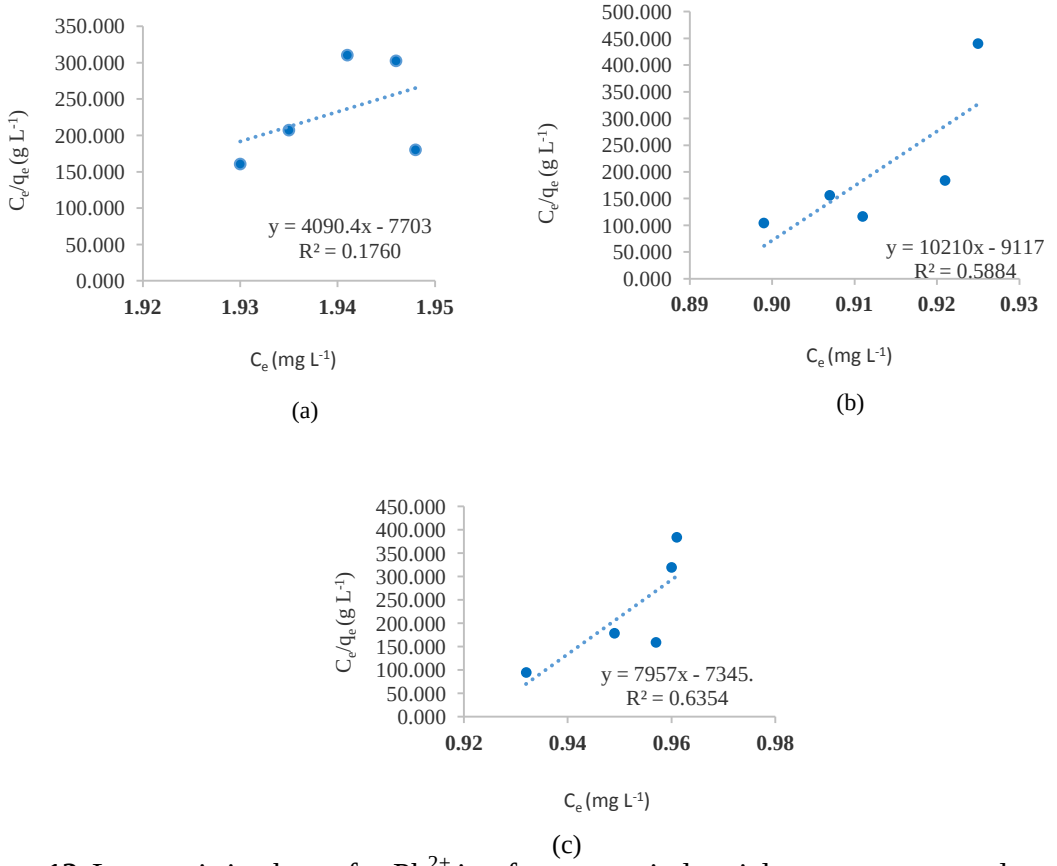

Figure 12 Langmuir isotherm for Pb^{2+} ion from three industrial wastewater samples onto the dry biomass (a) dry cell battery factory (b) nickel plating factory and (c) leather factory

Removal of Metal Ions from Three Industrial Wastewater Samples by Using Dry Biomass

In this study, the optimum time was 90 min for the removal of Cd^{2+}, Cr^{3+} ions and 15 min for the removal of Pb^{2+} ion from dry cell battery, nickel plating and leather factories wastewater samples. The optimum loading weight of dry biomass at 0.35 g was used for the removal of Cd^{2+}, Cr^{3+} ions whereas the loading weight at 0.25 g was used for the removal of Pb^{2+} ion.

As shown in Table 7 and Figure 13, dry biomass could remove metal ions, 46.87 % of Cd^{2+}, 44.03 % of Cr^{3+} and 8.45 % of Pb^{2+} ions from dry cell battery factory wastewater sample. Moreover, dry biomass could remove metal ions, 44.00 % of Cd^{2+}, 35.96 % of Cr^{3+} and 8.26 % of Pb^{2+} ions from nickel plating factory wastewater sample. This study revealed that the dry biomass could reduce 46.99 % of Cd^{2+}, 43.39 % of Cr^{3+} and 10.83 % of Pb^{2+} ions from leather factory wastewater sample.

Table 7 Comparative Data for Removal of Metal Ions from Three Industrial Wastewater Samples Using Dry Biomass

Metal ions	Dry cell battery factory			Nickel plating factory			Leather factory		
	Before treatment	After treatment	Removal (%)	Before treatment	After treatment	Removal (%)	Before treatment	After treatment	Removal (%)
Cd^{2+}	0.064	0.034	46.87	0.050	0.028	44.00	0.583	0.309	46.99
Cr^{3+}	0.604	0.338	44.03	0.570	0.365	35.96	0.053	0.030	43.39
Pb^{2+}	0.142	0.130	8.45	0.109	0.100	8.26	0.120	0.107	10.83

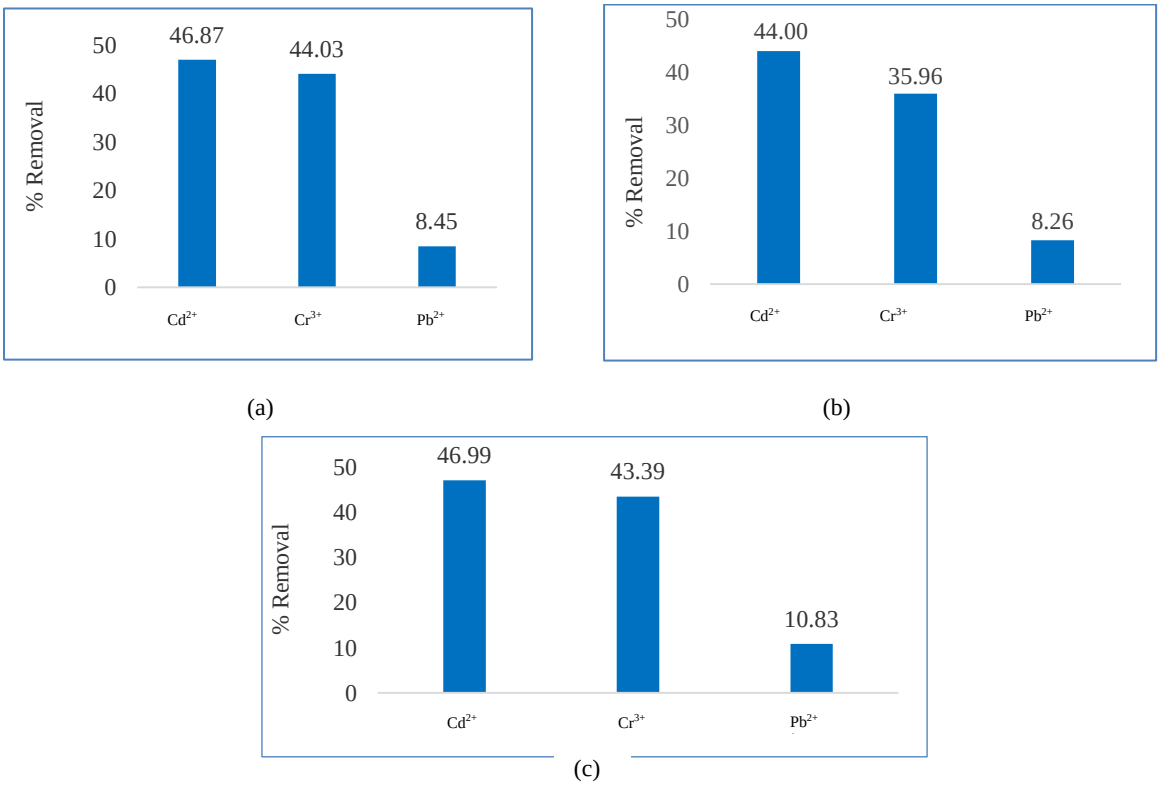

Figure 13 Removal of metal ions from three industrial wastewater samples using dry biomass (a) dry cell battery factory (b) nickel plating factory and (c) leather factory

Conclusion

In this research work, the reduction of the concentration of metal ions (Cd^{2+}, Cr^{3+} and Pb^{2+}) from three industrial wastewater samples using dry biomass was studied. Initially, aquatic plant namely *Hydrilla verticillata* (L.F.) Royle was introduced as dry biomass to study the sorption of heavy metal ions from wastewater sample under different times and different loading weights. The experimental conditions (contact times 5, 10, 15, 30, 60 and 90) min and loading weights (0.20 g, 0.25 g, 0.30 g, 0.35 g and 0.40 g) were used for the process of removal metal ions from dry cell battery, nickel plating and leather factories wastewater samples. It was found that the optimum time for removal of Cd^{2+}, Cr^{3+} and Pb^{2+} ions were 90 min, 90 min and 15 min, respectively using dry biomass. The loading weight of dry biomass at 0.35 g showed that the highest removal percent of Cd^{2+} and Cr^{3+} ions from three industrial wastewater samples. And then, the loading weight of biomass at 0.25 g showed that the highest removal percent of Pb^{2+} ion

from three industrial wastewater samples. In accordance with Langmuir isotherm, the linear coefficient values, R^2 were found to be 0.9105, 0.9211 and 0.9184 for Cd^{2+} ion, 0.9985, 0.9868 and 0.9985 for Cr^{3+} ion and 0.1760, 0.5884 and 0.6354 for Pb^{2+} ion from dry cell battery factory, nickel plating factory and leather factory wastewater samples respectively. According to the results given by Langmuir isotherm, the sorption of Cd^{2+} and Cr^{3+} ions were fitted to the Langmuir model but the experimental data for the Pb^{2+} was not fitted to the Langmuir model. Then, the dry biomass was studied for the removal of selected metal ions from three industrial wastewater samples at their optimum experimental conditions. The results revealed that the dry biomass could remove 46.87 % (Cd^{2+}), 44.03 % (Cr^{3+}) and 8.45 % (Pb^{2+}) ions of wastewater sample from dry cell battery factory. Furthermore, the percentage of metal ions removed by the dry biomass decreased up to 44 % (Cd^{2+}), 35.96 % (Cr^{3+}) and 8.26 % (Pb^{2+}) ions of wastewater sample from nickel plating factory. In addition, the dry biomass could remove 46.99 % (Cd^{2+}), 43.39 % (Cr^{3+}) and 10.83 % (Pb^{2+}) ions of wastewater sample from leather factory. The removal order of metal ions in wastewater samples from dry cell battery factory, nickel plating factory and leather factory using the dry biomass were found to be $Cd^{2+} > Cr^{3+} > Pb^{2+}$.

According to the experimental data, the dry biomass could be applied in the wastewater treatment for removal of Cd^{2+} and Cr^{3+}.

Acknowledgement

The authors would like to thank the Myanmar Academy of Arts and Science for allowing to present this paper and Professor and Head Dr Thidar Aung, Department of Chemistry, Magway University for her kind encouragement.

References

Asia, I.O., Oladoja, N.A. and Barmuza-pemu, E. E. (2006). "Treatment of Textile Sludge Using Anaerobic Technology". *African Journal of Biotechnology*, vol. 5 (18), pp.1678-1683

Baig, T.H., Garcia, A.E., Tiemann, K.J. and Torresdey, G.J.L. (2015). "Adsorption of heavy metals ions by the biomass of *Solanum elaeagniforlium* (Silver Leaf Night–shade)". *Proceeding of the Conferenceon Hazardous Waste Research*, pp. 131-142

Dhokpande, S.R. and Kaware, J.P. (2013). "Biological Methods for Heavy Metal Removal, A Review". *International Journal of Engineering Science and Innovative Technology (IJESTI)*, vol. 2 (5), pp. 304-309

Dixit, A., Dixit, S., and Goswami, C. S. (2015). "Eco-friendly Alternatives for the Removal of Heavy Metal Using Dry Biomass of Weeds and Study the Mechanism Involved". *Journal of Bioremediation & Biodegration, India*, vol. 6 (3), pp. 1-7

Itodo, A. U., Aisagbonhi, N. B., Adelagun, R.A.O. and Itodo, H. U. (2013). "Divalent Nickel (Ni^{2+}) Removal Using Thermally Derived and Regenerated Activated *Cocos uncifera* Shells". *Elixier international journal*, vol. 60, pp. 1-6

Nethaji, S., Sivasamy, A. and Mandal, A. B. (2013) "Adsorption Isotherms, Kinetics and Mechanism for the Adsorption of Cationic and Anionic Dyes onto Carbonaceous Particles Prepared from *Juglans regia* Shell Biomass." *Int. J. Environ. Sci. Technol*, vol. 10, pp. 231-242

Rahimi, M. and Vadi. M. (2004). "Langmuir, Freundlich and Temkin Adsorption Isotherms of Propanolon Multiwall Carbon Nanotube". *Journal of Modern Drug Discovery and Drug delivery Research*, vol.1(13), pp. 1-3

Ramasubramaniam, S., Govindarajan, C., Gomathi, T. and Sudha, P.N. (2012). "Removal of Chromium (VI) from Aqueous Solution Using Chitosan Starch Blend". *Scholar Research Library*, vol. 4 (1), pp. 240-248

Tariq, W., Saifullah, M., Anjum, T., Javed, M., Tayyab, N. and Shoukat, I. (2018). "Removal of Heavy Metals from Chemical Industrial Wastewater Using Agro Based Bio-sorbents". *Acta Chemica Malaysia (ACMY)*, vol. 2 (2), pp. 1-6

ACUTE TOXICITY OF THE ETHANOLIC PLANT EXTRACT AND STRUCTURE ELUCIDATION OF ISOLATED BIOACTIVE COMPOUND FROM THE STEM BARK OF *PROTIUM SERRATUM* (WALL.EX COLEBR.) ENGL.

Thin Yu Mar,[1] Arnt Win,[2] Aye Mon Thida Nyo[3]

Abstract

In this research work, one of Myanmar traditional medicinal plants, *Protium serratum* (Wall.ex Colebr.) Engl., Myanmar named Gati was selected for chemical analysis and pharmacological investigation. The stem bark of the selected plant was collected from Pyin Oo Lwin Township, Mandalay Region. Acute toxicity test of 95% ethanolic extract of the stem bark of the selected plant was examined by Organization of Economic Cooperation and Development (OECD) guideline 425. According to acute oral toxicity test of ethanolic extract of the stem bark of this plant, the test substance can be considered relatively safe to the dose level of 5000 mg/kg body weight. Furthermore, the bioactive compound was isolated from ethyl acetate portion *serratum* (Wall.ex Colebr.) Engl. by thin layer and column chromatographic method. The yield percent of this pure compound was found to be 1.21 based upon the ethyl acetate crude extract. The molecular formula of this isolated flavonoid compound was determined as $C_{15}H_{14}O_6$ by using some spectroscopic techniques, such as FT IR, ^{1}HNMR, ^{13}CNMR, DEPT, HSQC and DART-Mass spectrometry. The structure of this compound was elucidated by using DQF-COSY, ^{1}HNMR splitting patterns, coupling constant (*J* values) and HMBC spectroscopic data. IUPAC name of the isolated compound is C_2(*S*), C_3(*R*)-2-(3'-4'-dihydroxyphenyl)- 3,4,-dihydro-2*H*-chromene-3,5,7-triol.

Keywords: *Protium serratum* (Wall.ex Colebr.) Engl., acute toxicity, thin layer and column chromatography.

Introduction

Medicinal plants and plant-derived medicine are widely used in traditional cultures all over the world and there are becoming increasingly popular in modern society as natural alternatives to synthetic chemicals. Natural products and their derivatives represent more than 50% of all drugs in critical used in the world. Plant drugsare plant-derived medicines that contain a chemical compound or more usually mixtures of chemical compounds that act individually or combination on human body to prevent disorders and to restore or maintain health. Chemical entities are pure chemical compounds that are used for medicinal purposes (Van Wyk and Wink, 2004).In Myanmar, medicinal uses of *Protium serratum* (Wall.ex Colebr.) Engl. are less known. Thus, with the objectives of promotion of its medicinal uses, biologically active component from the stem bark of *serratum* is intended to be investigated.

Pure pale yellow needle-shaped compound was isolated from the stem bark of *serratum*, locally known as Gati, which is one of the indigenous medicinal plant. Local people in Pyin Oo Lwin Township use the stem bark *serratum* for the treatment of anti-inflammatory, hypertension, diabetic, dysentery and diarrhea (Figure 1). Pale yellow needle-shaped flavonoid compound was isolated from the stem bark of *serratum* by using thin-layer and column chromatographic methods. The molecular formula and the structure of this isolated compound were assigned by using advanced spectroscopic methods such as FT IR, ^{1}HNMR (500 MHz), ^{13}C NMR (125 MHz), DEPT, HSQC, DQF-COSY, HMBC and DART-MS spectral data.

[1] Dr, Lecturer, Department of Chemistry, University of Magway
[2] Dr, Associate Professor, Department of Chemistry, Kyaukse University
[3] Dr, Associate Professor, Department of Chemistry, University of Mandalay

Botanical Description


Figure 1 Leaves, Fruits and Stem Bark of *Protium serratum* (Wall.ex Colebr.) Engl**.**

Family : Burseraceae
Genus : *Protium*
Species : *P.serratum*
Botanical name : *Protium serratum* (Wall. ex Colebr.) Engl.
Myanmar name : Gati
Part used : Stem bark
Medicinal uses : Hypertension, antibacterial, antifungal, diuretic, antidiabetes, dysentery, diarrhea and mouth ulcers (Localpeople in Pyin Oo Lwin Township, Myanmar)

Materials and Methods

The advanced instruments were used in the characterization of sample and structural elucidation of organic compound. These are UV lamp (Lambda 40, Perkin Elmer Co. England), FT IR spectrometer (Shimadzu, Japan), ^{1}H NMR spectrometer (500 MHz, Japan), ^{13}C NMR spectrometer (125 MHz, Japan), and DART-MS spectrometer, Japan.

Analar grade reagents and solvents were used throughout the experiment. Analytical preparative thin-layer chromatography was performed by using aluminium coated sheets silica gel (Merck. Co. Inc. Kiesel gel 60 F_{254}) and silica gel (70 to 230 mesh ASTM) was used for column chromatography.

Plant material

The stem bark of *Protium serratum* (Wall.ex Colebr.) Engl. (Burseraceae), Myanmar name Gati was collected from Pyin Oo Lwin Township, Mandalay Region in Myanmar.

Preliminary Phytochemical Test of the Stem Bark of *Serratum*

The phyotochemical tests of the selected plant were carried out by usual method.

Determination of Acute Toxicity

Acute toxicity study was performed on the ethanolic extract of the stem bark of *serratum* using mice as the experimental model. The acute toxicity test on 95% ethanolic extract of the stem bark of selected plant could be carried out according to OECD (Organization of Economic Co-operation and Development) guidelines 425 (OECD, 2008; Dixon, 1965, 1991; Bruce, 1985; Gallagher, 2003).

Extraction and Isolation

The air-dried stem barks of *serratum* (1000 g)were extracted with ethanol at room temperature for two months. The ethanol extract was concentrated in air. The ethanol extract was then re-extracted with ethyl acetate and evaporated to dryness at room temperature. The ethyl acetate crude sample extract (2.5 g) was obtained. The ethyl acetate crude extract was fractionated by column chromatography over silica gel with various ratios of *n*-hexane and ethyl acetate from non-polar to polar. Totally 280 fractions were collected. Then each fraction was checked on TLC using iodine as visualizing agent. The fraction with same R_f values were

combined. Major combined fraction gave only one spot on TLC and it was UV active. Pale yellow needle-shaped crystal, flavonoid compound (30.2 mg) was obtained.

Flow Sheet for Isolation of Organic Compound from EtOAc Extract

Ethyl acetate extract (2.5 g)
- Separated by column chromatography
  Adsorbent = SiO_2 (70-230 mesh)
  Eluent = *n* hexane: EtOAc (various volume ratio)
  (non polar to polar)

Totally (280) fractions
- Checked by TLC, I_2vapour and UV lamp
- Combined

(15) Combined fractions
- Checked by TLC

major combined fraction — Other fractions

major combined fraction
- checked by TLC
- one spot on TLC
- UV active

pale yellow solid compound
- re-crystallized by 30% EtOAc in *n*-hexane for two times

pale yellow needle-shaped crystal (30.2 mg)
R_f = 0.32
n-hexane: EtOAc1 :1 (v/v)1.21% yield based upon EtOAc extract

Spectroscopic Studies and Structure Elucidation of the Isolated Compound

The isolated organic compound was subjected to analyze by FT IR, ^{1}H NMR (500 MHz), ^{13}C NMR (125 MHz) DEPT, HSQC, DQF-COSY, DART-MS and NOESY spectroscopic techniques (Silverstein *et al.*, 2005). FT IR spectrum of the isolated organic compound was measured at the Department of Chemistry, Monywa University. The remaining spectral data were measured at the Department of Natural Resources Chemistry, Faculty of Pharmacy, Meijo University, Nagoya, Japan.

Conformational Phytochemical Test of the Isolated Compound

Phytochemical test for the isolated compound gave positive for flavonoid and phenolic tests. Therefore, compound is a flavonoid compound.

Results and Discussion

Preliminary Phytochemical Test

Preliminary phytochemical tests were carried out by standard methods and the observed results are shown in **Table 1.**

Table. 1 Preliminary Phytochemical Test of the Stem Bark of *Protium serratum* (Wall.ex Colebr.) Engl.

No.	Test	Reagent used	Observation	Result
1.	Alkaloid	Dragendorff's reagent	Orange ppt	+
2.	Flavonoid	EtOH, Conc: HCl, Mg ribbon	Pink colour solution	+
3.	Glycoside	10 % Lead acetate	White ppt	+
4.	Phenolic	10 % $FeCl_3$	Green colour solution	+
5.	Polyphenol	1 % $K_3[Fe(CN)_6]$, 1 % $FeCl_3$	Greenish blue colour solution	+
6.	Lipophilic	0.5 N KOH solution	Deep blue colour solution	+
7.	Saponin	Shaked with H_2O	Frothing	+
8.	Sugar	Benedict's solution	Brick red ppt	+
9.	Steroid	$(CH_3CO)_2O$, Conc.H_2SO_4	Blue colour solution	+
10.	Terpene	$(CH_3CO)_2O$, $CHCl_3$, Conc.H_2SO_4	Reddish brown colour solution	+
11.	Tannin	1% $FeCl_3$	Yellowish brown ppt	+

(+) = present of constituents

Acute Toxicity of the Stem Bark of *serratum*

Different groups of mice administered with 4 different doses of ethanolic extract of the selected plant and vehicle (distilled water) 10 mL/kg body weight (control) were kept under observations for two weeks. The results based on daily body weight record are shown in Table 2.

Table 2 Acute Toxicity Study of the Stem Bark of *Protium serratum* (Wall.ex Colebr.) Engl. Based on Daily Body Weight Record (in grams)

Groups	Marking	Sex	Dose in mg/kg Body Weight	Weight of Mice/kg		
				1st day	7th day	14th day
I	Head	Female	175	23.7	24.6	29.8
	Head	Male		23.5	24.8	28.3
	Back	Male		28.0	29.2	32.4
			Mean value	25.1	26.2	30.2
II	Back	Female	550	23.3	25.4	27.7
	Tail	Male		24.4	24.9	25.9
	R.Hand	Male		26.8	27.1	27.8
			Mean value	24.8	25.8	27.1
III	Tail	Female	2000	25.6	26.5	26.8
	R.Hand	Female		22.5	22.3	23.0
	L.Hand	Male		22.5	23.5	24.6
			Mean value	23.5	24.1	24.8
IV	Head	Female	5000	23.2	24	25.2
	Back	Female		22.0	22.6	24.6
	Head-Back	Female		28.04	29.5	30.6
			Mean value	24.4	25.4	26.8
Control	R-Hand	Female	Distilled Water	24.0	24.9	24.3
	R-Leg	Male		27.4	26.9	28.0
	L-Leg	Male		26.5	26.9	30.0
			Mean value	25.9	26.2	27.4

Body weight is an important factor to monitor the health of an animal. Loss of body weight is the first indicator of an adverse effect (Gallagher, 2003). According to the daily body weights record, all the animals from treated groups increased body weight for all the 14 days as compared with the 0 day body weights values. Hence, the test substance, ethanolic extract of the stem bark of *Protium serratum* indicating no sign of toxicity and lethality.

After two weeks, all the mice were alive and did not show any toxic symptoms such as body weight loss, diarrhea, inactivity, aggressiveness, restlessness, etc. and no death when compared with that of the control group. The results of mortality records and cage side observations are described in Tables 3 and 4.

Table 3 Acute Toxicity Study on the Ethanolic Extract of the Stem Bark of *Protium serratum* (Wall.ex Colebr.) Engl. Based on Mortality Record

Extracts	Groups	Number of mice/group	Dose of extract (mg/kg)	Observed period	Ratio of dead and tested	Death %
Ethanol	I	3	175	Two weeks	0/3	0
	II	3	550	Two weeks	0/3	0
	III	3	2000	Two weeks	0/3	0
	IV	3	5000	Two weeks	0/3	0
	Control	3	D/W 10mL/kg	Two weeks	0/3	0

Table. 4 Acute Toxicity Study on Ethanolic Extract of the Stem Bark of *Protium serratum* (Wall.ex Colebr.) Engl. Based on Cage Side Observations

Parameters	Observations
Condition of the fur	Normal
skin	Normal
Subcutaneous swelling	Nil
Abdominal distention	Nil
Eyes - dullness	Nil
Eyes - opacities	Nil
Pupil diameter	Normal
ptosis	Nil
Colour and consistency of the faces	Normal
Wetness or soiling of the perineum	Nil
Condition of teeth	Normal
Breathing abnormalities	Nil
Gait	Normal

Mortality is the main criteria in assessing the acute toxicity of any drug (Lalitha, 2012). The acute toxicity (Table 3) on mortality recorded was found nil. The dose level (LD_{50} value) of the test substance was found to be more than 5000 mg/kg. From the cage-side observation, the tested animals at all dose levels showed no significant changes in behaviors after oral administration.

According to the results of daily body weight recorded and cage side observation the test substance, ethanolic extract of the stem bark of *serratum* can be considered safe. Moreover, the acute toxicity mortality is found nil, so the test substance can be considered free from toxic effect up to the dose level of 5000 mg/kg for oral administration.

Molecular Formula Determination of the Isolated Pure Compound

The isolated compound was obtained as pale yellow needle-shaped crystal. The structure of the isolated compound was elucidated by modern instrumental techniques (Figures 2 -9). The molecular formula was determined to be $C_{15}H_{14}O_6$ from the observation of DART-MS spectrometry (Figure 9). The FT IR spectrum showed absorption bands at 3330, 3020, 2921, 2851, 1619, 1520, 1464, 1289, 1145, 1095, 979 and 766 cm^{-1} ascribable to hydroxyl, sp^2 H/C, sp^3 H/C, aromatic ring and ether functional group respectively (Figure 2). The ^{1}H NMR spectrum (Figure 3 and Table 5) revealed two sp^3 methylene protons at δH (2.73, 2.88 ppm), two sp^3 methine protons δH at (4.18, 4.82 ppm) and five sp^2 methine protons at δH (5.91, 5.94, 6.78, 6.80, 6.97 ppm).

The FT IR and DEPT spectral data (Figure 2 and Figure 6) show the presence of one sp^3 methylene carbon, two sp^3 methine carbons, seven sp^2 quaternary carbons, five sp^2 methine carbons, one hydroxyl group and one ether group.

Table. 5 ^{1}H NMR Spectral Data of the Isolated Compound (500 MHz) Solvent used = Deuterated chloroform

No.	Chemical shift (δ/ppm)	No. of protons	Splitting pattern	Coupling constant (*J* values Hz)	Proton assignment
1	2.73 2.88	2H	dd dd	2.8, 16.7 4.23, 16.7	sp^3 methylene proton
2	4.18	1H	dt	4.23, 2.8	sp^3 methine proton
3	4.82	1H	-	-	sp^3 methine proton
4	5.91	1H	d	2.3	sp^2 methine proton
5	5.94	1H	d	2.3	sp^2 methine proton
6	6.78	1H	d	8.1	sp^2 methine proton
7	6.80	1H	dd	2.01, 8.1	sp^2 methine proton
8	6.97	1H	d	2.01	sp^2 methine proton
Total number of protons = 9					

Table 6 ^{1}H-^{13}C Correlation in HSQC spectrum of the Isolated Compound

No.	^{13}C NMR chemical shift (δ/ppm)	^{1}H NMR chemical shift (δ/ppm)	Carbon Assignment
1	30.74	2.73, 2.85	sp^3 methylene carbon
2	67.51	4.18	sp^3 methine carbon
3	79.90	4.82	sp^3 methine carbon
4	95.90	5.94	sp^2 methine carbon
5	96.32	5.91	sp^2 methine carbon
6	100.09	–	sp^2 quaternary carbon
7	115.34	6.97	sp^2 methine carbon
8	115.92	6.80	sp^2 methine carbon
9	115.96	6.78	sp^2 methine carbon
10	132.31	–	sp^2 quaternary carbon
11	145.80	–	sp^2 quaternary carbon
12	145.97	–	sp^2 quaternary carbon
13	157.38	–	sp^2 quaternary carbon
14	157.70	–	sp^2 quaternary carbon
15	158.01	–	sp^2 quaternary carbon
Total no. of carbons = 15			

Structure Elucidation of the Isolated Compound

The structure of pure compound could be determined by ^{1}H NMR, DQF-COSY, HSQC and HMBC spectral data, respectively (Figures 5,7 and 8).

In the structure elucidation, the tri-substituted benzene ring fragments a, b and d could be assigned by DQF-COSY, ^{1}H NMR splitting patterns, coupling constant (*J*-values), HSQC and HMBC spectra.

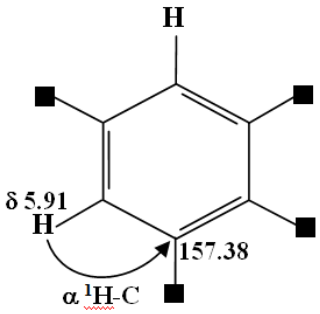

a

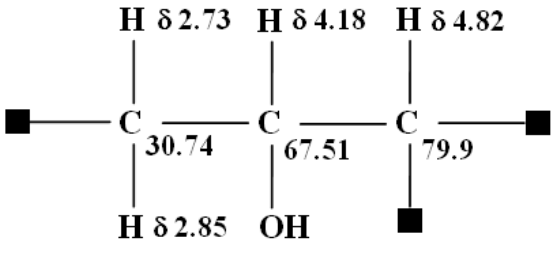

b

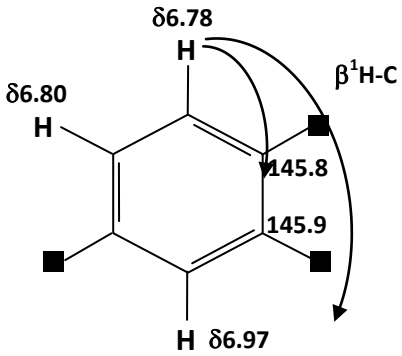

d

Fragments a and b could be connected according to the HMBC spectrum which gives rise to fragment c.

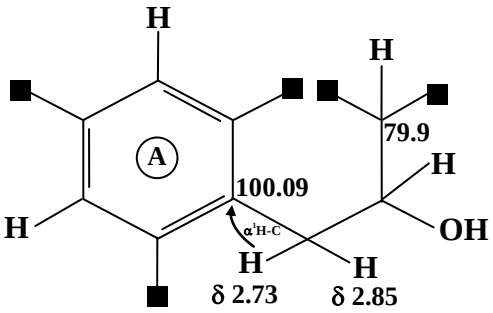

c

Fragments c and d could be connected by HMBC spectrum which leads to fragment e.

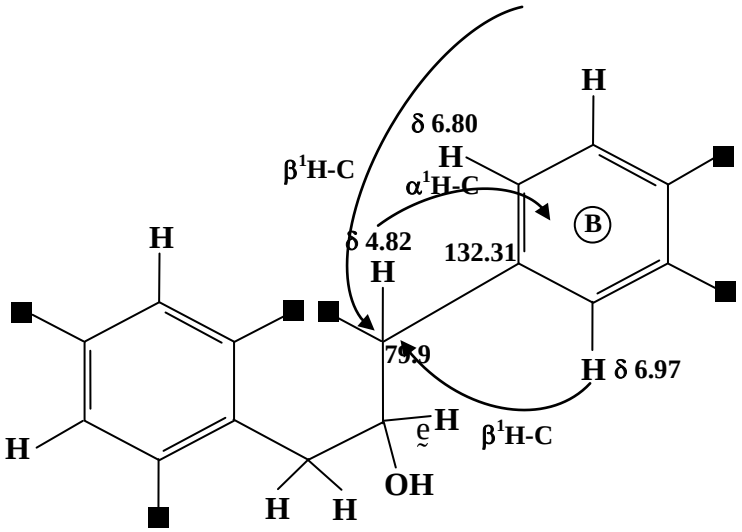

In this state, elucidated HDI is 8. Remaining HDI one must be one ring. The ether oxygen atom flanked between the reasonable down filed chemical shifts of aromatic quaternary carbon (δ 158.01 ppm) and sp^3 methine carbon (δ 79.9 ppm) which established the following fragment f .

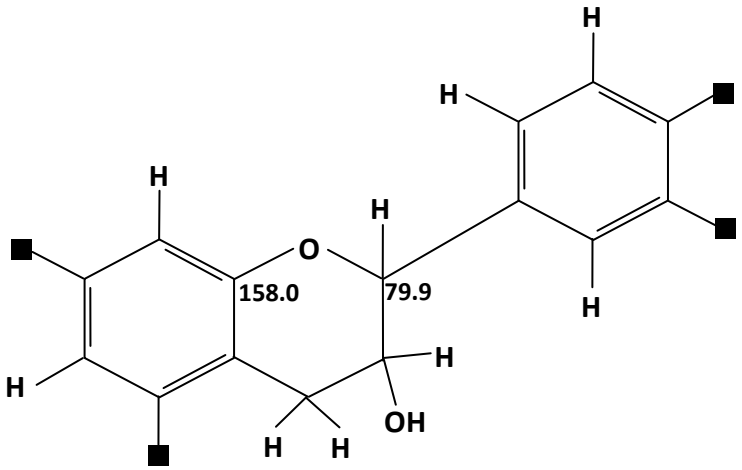

f

In the above fragment f , elucidated molecular formula is $C_{15}H_{10}O_2$.

The remaining molecular formula = $C_{15}H_{14}O_6 - C_{15}H_{10}O_2$

= H_4O_4,

∴ It must be four – OH groups:

The remaining four hydroxyl groups could be connected to the four downfield chemical shift carbons (δ 145.8 ppm, δ 145.97 ppm, δ157.38 ppm and δ157.7ppm) which accomplished the following complete structure of compound.

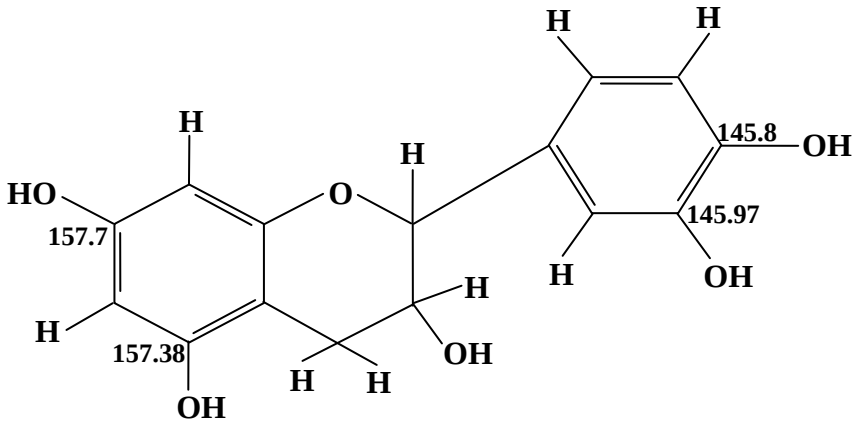

IUPAC name of the isolated compound is C_2(*S*), C_3(*R*)-2-(3',4'-dihydroxyphenyl) - 3,4-dihydro-2*H*-chromene-3,5,7-triol

Confirmation of Molecular Formula of Compound

Molecular formula of compound could be confirmed by DEPT and FT-IR spectra.
The partial molecular formula = $C_{15}H_{11}O_3$
The partial molecular mass = 239
According to DART-mass spectrum, M + H (M + 1) peak m/z = 290.0852
Therefore, molecular mass = 290
The remaining molecular mass = 290 – 239 = 51
It must be three hydroxyl groups.
Therefore, the real molecular formula of isolated compound = $C_{15}H_{14}O_6$

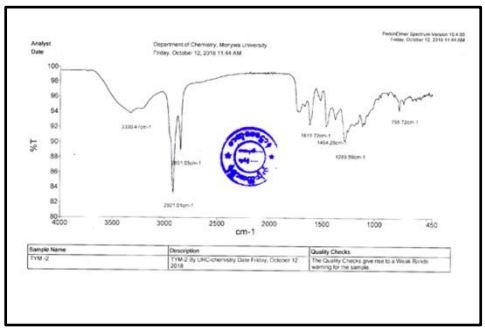

Figure 2 FT IR Spectrum of Isolated Compound

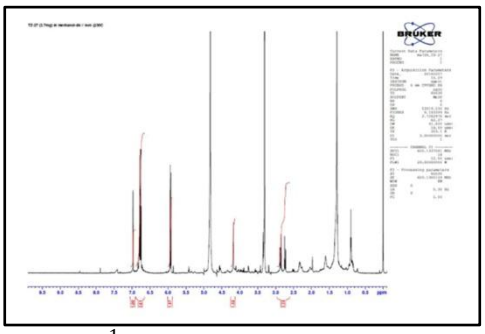

Figure 3 ^{1}H NMR Spectrum of Isolated Compound

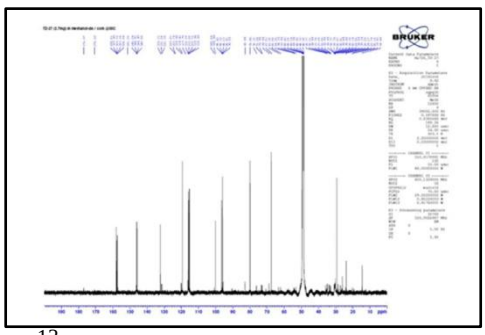

Figure 4 ^{13}C NMR Spectrum of Isolated Compound

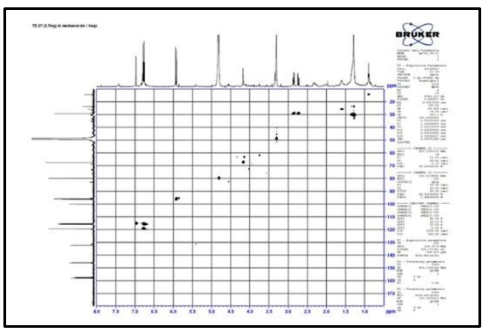

Figure 5 HSQC Spectrum of Isolated Compound

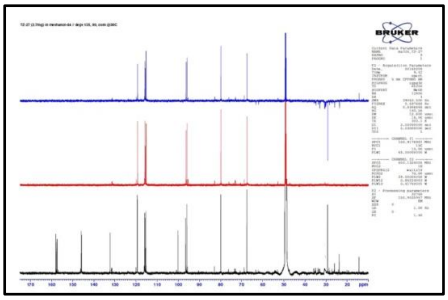

Figure 6 DEPT Spectrum of Isolated Compound

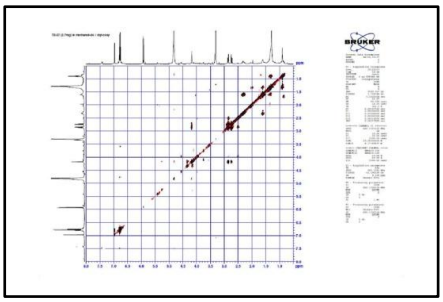

Figure 7 DQF-COSY Spectrum of Isolated Compound

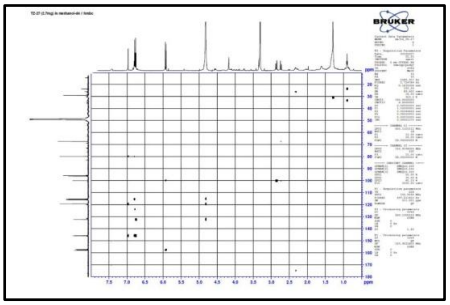

Figure 8 HMBC Spectrum of Isolated Compound

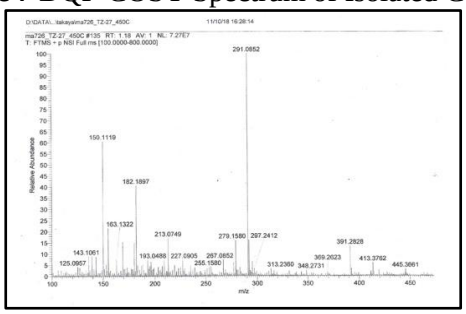

Figure 9 DART-Mass Spectrum of Isolated Compound

Conclusion

In the present investigation, acute toxicity and isolation of flavonoid compound [C_2(*S*),C_3(*R*)-(3',4'-dihydroxyphenyl)-3,4-dihydro-2*H*-chromene-3,5,7-triol] which has so many biological activities, especially anti-inflammatory and anti-diabetic activities from the stem bark of *serratum* were evaluated. From the determination acute toxicity, all the mice from treated groups increased body weight for all the 14 days as compared with 0 day body weight values. In addition the acute toxicity mortality recorded was found nil. The dose level of tested substance was found to be more than 5000 mg/kg based on body weight. After two weeks, all the mice were alive and did not show any toxic symptoms. Therefore the ethanolic extract of the stem bark of *serratum* can be considered relatively safe. Moreover, the pale yellow needle-shaped compound could be illustrated by using sophisticated spectroscopic method and confirmed by DART-MS spectroscopy. This studies support that the stem bark of *serratum* could be safely used for anti-inflammatory and anti-diabetic drug without harmful effect. Further studies are required and in progress here.

Acknowledgements

The authors would like to thank the Myanmar Academy of Art and Science for allowing to present this paper and Professor and Head Dr Thida Aung, Department of Chemistry, Magway University, for her kind encouragement.

References

Bruce, R. D. (1985). "An Up-and-Down Procedure for Acute Toxicity Testing". *Journal of Fundamental Apply Toxicity*, vol. 5, pp. 151-157

Dixon, W. J. (1965). "The Up-and-Down Method for Small Samples". *Journal of the American Statical Association*, vol. ~~60,~~ pp. 967-978

Dixon, W. J. (1991). "Staircase Bioassay: The Up-and-Down Method". *Journal of Neuroscience and Biobehavioral Review*, vol. 15, pp.47-50

Gallagher, M. E. (2003). "Toxicity Testing Requirements, Methods and Proposed Alternatives". *Environ.*, vol. 26, pp.257-258

Lalitha, P., Sripathi, S. K. and Jayanthi, P. (2012)." Acute Toxicity Study of Extracts of *Eichhorinacrassipes* (Mart.) Solms". *Asian Journal of Pharmaceutical and Clinical Research*, vol.5(4), pp.59-61

OECD. (2008).*OECD Guidelines for the Testing of Chemicals.*

Silverstein, R. M., Webster, F. X. and Kiemle, D. J. (2005), *Spectrometric Identification of Organic Compounds*, Singapore: 7thed, John Wiley & Sons, Inc.

Van Wyk, B. E. and Wink, M. (2004). *Medicinal Plants of the world*. Singapore: Selangor Darul Ehsan Alam, Times edition, pp.1-22

PREPARATION OF FLUORINE DOPED NANOCRYSTALLINE TIN OXIDE THIN FILM

Khin Moh Moh Hlaing[1], Khin Than Yee[2], Hlaing Hlaing Oo[3]

Abstract

The increasing demand for energy that human beings are faced with the photovoltaic (PV) technology which converts solar radiation into electricity has undergone increasable development. Fluorine doped Tin oxide (FTO) thin film is widely used in various fields of electronic devices such as window layer in solar cell, substrates for electrode deposition and transparent contact in optoelectronic and so on. In this work, nanocomposites of FTO thin film was fabricated by sol-gel dip coating method and then it was applied as dye sensitized solar cell (DSSC) component. The effect of concentration of precursor solution, annealed temperature and heating time in the growth of FTO on glass substrates were studied and discussed. The prepared FTO thin film was analyst by FT IR. The surface morphology of FTO thin films was studied using Scanning Electron Microscope (SEM) to identify the distribution of grain and the growths of nanostructure with prefer orientation. The electrical properties of sample were analyzed by using four-point probe methods. The optical property was studied using UV-Vis spectrophotometer. The structural investigation of as-prepared film was performed using X-ray diffraction (XRD). The minimum value of sheet resistance was found to be 1.02 Ω sp^{-1} for the prepared SnO_2:F film at annealed temperature 400°C. The X-ray analysis confirmed the polycrystalline nature of FTO film with preferential orientation along 110 plane. The method was found to be economic and suitable for research and development. The prepared FTO was applied as an electrode in the dye sensitized solar cell (DSSC) electrode application and the photovoltaic effect was observed.

Keywords: SnO_2:F thin film, optoelectronic, nanocomposites, polycrystalline, solar cell

Introduction

Nowadays, the study and application of thin film technology is entirely entered into almost all the branches of science and technology due to brisk development of Nanotechnology. Fluorine doped tin oxide thin films belong to a special class of metal oxide thin films *i.e* transparent conducting oxide thin films which are a special part of nanostructure thin film solar cells. As it permits the transmission of solar radiation directly to the active region with little or no attenuation, these solar cells have improved sensitivity in the high-photon-energy portion of the solar spectrum and make thin film solar cells suitable for large scale application with high efficiency (Abdullahi *et al.,* 2014).

Many techniques have been employed to deposit SnO_2:F such as sputtering (Kang *et al.,* 2011; Singh *et al.,* 2013), inkjet printing technique (Samad *et al.,* 2011), aerosol assisted chemical vapour deposition (AACVD) (Jafar *et al.,* 2013), sol gel (Wu *et al.,* 2010), atmospheric-pressure plasma deposition system (Tsai and Huang, 2010), spray pyrolysis (Russo and Cao, 2007). Out of all the above methods sol-gel technique play an important role due to several advantages such as easy control on film thickness with a high porosity area which can improve the efficiency of the sensors, low processing cost, greater homogeneity and more purity. Generally, there are three methods used in corporate with sol-gel technique; they are spin coating, dip coating and spray coating. There are many reports regarding the preparation, characterization and application of the SnO_2:F thin films for dye sensitized solar cells (DSSC) (Alhamed *et al.,* 2012 ; Shelke *et al.,* 2013).

In the present work, an atmospheric chemical vapour deposition (APCVD) system was designed and fabricated for the deposition of fluorine doped tin oxide (SnO_2: F) thin films on glass with the aim of growing SnO_2: F thin films for fabrication of solar cells. Tin(IV) chloride

[1] Dr, Lecturer, Department of Chemistry, Meiktila University

[2] Dr, Lecturer, Department of Chemistry, University of Yangon

[3] Dr, Professor and Head, Department of Chemistry, West Yangon University

and ammonium fluoride were used as the precursor and dopant. The characteristics of prepared transparent conductive films were investigated by FT IR, XRD, SEM, UV and also studied the various electrical and optical properties of the SnO_2:F thin film with number of coating, heat treatment temperature and heating time using four point probe methods. Furthermore, the structure and morphology characteristics for the prepared transparent conductive films were investigated. Finally, the prepared SnO_2:F thin films was tested in fabrication of dye sensitized solar cells.

Materials and Methods

Transparent conducting fluorine doped tin oxide thin films were prepared by sol-gel method accompanied with deposition methods. Structural, optical and electrical properties were studied under different preparation conditions like dopant concentration of ammonium fluoride, aging time, deposition methods, number of coatings, heat treatment temperature and heating time.

Preparation of fluorine doped tin oxide (SnO_2:F) solution

Fluorine doped tin oxide sol solution was prepared from tin(IV)chloride pentahydrate and ammonium fluoride by sol-gel method. About 13 g of tin(IV)chloride pentahydrate was added to 100 mL of ethyl alcohol in a beaker and stirred for 5 h. Then 10mL of ammonium fluoride solution (1 % w/w NH_4F) was slowly added to the beaker containing tin(IV) chloride solution. Five milliliter of 1 M hydrochloric acid solution was then added into the above solution drop by drop. Then the solution was stirred for at least 5 h. Finally, the solution was stirred and refluxed for one hour at 60 °C. Then the solution was cooled under room temperature and aged in open beaker for about 9 days. The same procedure was carried out with different concentrations of ammonium fluoride solutions (2.5 %, 5 %, 7.5 % and 10 %). The same procedure was carried out to prepare pure tin oxide thin film without ammonium fluoride. The prepared SnO_2:F solutions with various weight percent of ammonium fluoride (1 %, 2.5 %, 5 %, 7.5 % and 10 %) was taken and the viscosity was measured by Oswald viscometer.

Preparation of fluorine doped SnO_2 thin films

The preparation of fluorine doped tin oxide thin films composed of two steps (Yousaf, and Ali, 2008). For thin film deposition, glass slides (75 mm × 25 mm) were used as the substrates. The substrates were washed with detergent solution and with water. These substrates were boiled in chromic acid for five minutes and cleaned with distilled water. Then they were kept in sodium hydroxide solution to remove the acidic contamination and were again washed with distilled water. Finally, the substrates were dried in alcohol (methanol) vapour. And then, the prepared sol solution was deposited on cleaned glass substrate by the layer and layer deposition cycle (dip-, spin-, spray- coating) was done by alternatively between coating a thin layer and drying in air after each new layer (Figure 1). The coated glass substrate was annealed at temperature 100 °C, 200 °C, 300 °C, 400 °C and 500 °C for about 1 h, 2 h, 3 h, 4 h and 5 h in an electric furnace. In all, more than ten samples were produced simultaneously at each substrate temperature. Process was repeated several times for each parameter.

(a) (b) (c)

Figure 1 Deposition of thin films using various methods (a) Spray coating (b) Spin coating and (c) Dip coating

Characterization of the Prepared Fluorine Doped Tin Oxide Thin Film

Physicochemical properties of these prepared thin film were characterized by using modern techniques such as FT IR, XRD, SEM and UV.

Determination of electrical properties

The electrical measurements were carried out by LCR meter at room temperature by four-point probe methods. The electrical properties of the prepared fluorine doped tin oxide films were measured by LCR meter. The techniques employed were in accordance with the recommended standard procedure as reported in the company's catalogue. The resistance values of prepared SnO_2:F thin films with different dopant concentration of ammonium fluoride were measured by four point probe method.

Results and Discussion

In the present work, SnO_2:F transparent thin films were prepared by the Atmospheric Pressure Chemical Vapour Deposition (APCVD) method. Transparent conductors are needed as the front surface electrodes in all types of solar cells. Deposition of high quality, uniform thin films, is an intensive area of research which has yielded different deposition techniques. Each technique falls into one of three broad categories: wet chemical deposition; physical vapour deposition and chemical vapour deposition. The APCVD method was chosen due to its low cost of deposition and the optical and electrical characterizations of the deposited film were examined. SnO_2:F films were produced over a range of deposition temperatures, number of coatings and various weight percent of fluorine in the precursor solution from tin IV chloride pentahydrate and ammonium fluoride in ethanol.

The effect of fluorine concentration on the structural, surface morphological and characteristic properties of the SnO_2:F films were studied. The characteristic properties of the multi-coating have been investigated, including their electrical conductivity and optical transparency. The surface morphologies of the prepared thin films were characterized by scanning electron microscopy (SEM) and the crystalline phase of SnO_2:F thin films were determined by XRD (X-ray diffraction) using a diffractometer with CuK a radiation. At present, the main method of utilization of solar energy is the converse of solar energy into other energy sources.

Effect of Aging Time of the SnO_2:F Sol Solution

The fluorine doped tin oxide (SnO_2:F) thin films are a special kind of material that exhibit electrical conductivity and transmittance in visible region making it suitable for solar all application. The specific viscosity of the prepared SnO_2:F sol solution with the various weight percent of ammonium fluoride (1 %, 2.5 %, 5 %, 7.5 %, 10 %) at ambient temperature were measured by Oswald viscometer. The rheological behaviour of the sol solution using 7.5 % w/w NH_4F is shown in Figure 2. The viscosity of SnO_2: F sol solution gradually increased first two days. After two days, the viscosity breaks off the base line termed as break off point (viscosity markedly increased) and saturated on the sixth day called as the saturation point (viscosity slightly changed). It was evident that viscosity abruptly increase between the third and sixth day of aging (*i.e.* between the break off point and saturation point) and this rise was apparently due to the occurrence of polymerization, *i.e.* condensation, among the hydroxyl ligands attached to the tin ions. The saturation behaviour indicated the colloidal nature of the gelatinous suspension, which was devoid of strong cross-linking among the clusters in the solution. The physical observation of the solution during the entire period shows increasing cloudy nature of the solution, due to depolymerization.

According to the experimental evidence in this research, if the films were developed by using the gel aged lower than its break-off point, then the spreading and thinning mechanism of the sol becomes strong and as a result the evaporation process was also rapid. Above 7 days of aging time non-uniformity in films thickness and striation, resistance cannot be measured. If the films were coated with the solution above the saturation point, most quantity of the sol gel is thrown away from the substrate due to high viscosity, leading to poor adherence and also causes comet formation on the as-coated film. Among 2 to 6 days of aging, good and uniform coating can be obtained. Therefore, it can be inferred that the optimum coating period of the sol solution, so as to obtain good quality films, a time $t_{½}$ can be adopted, at which the viscosity reaches one-half of the sum of the break off and saturation viscosities. From Figure 2, $t_{½}$ value is found to be 4 days and this is regarded as the optimum coating time for the sol solution. But experimental observation revealed that sol solution coated between the period 4 and 6 days provided good quality films. According to weight of ammonium fluoride percent 5 to 10 give $t_{½}$ values nearly the same, weight of ammonium fluoride percent above 5 should be used for SnO_2:F film preparation.

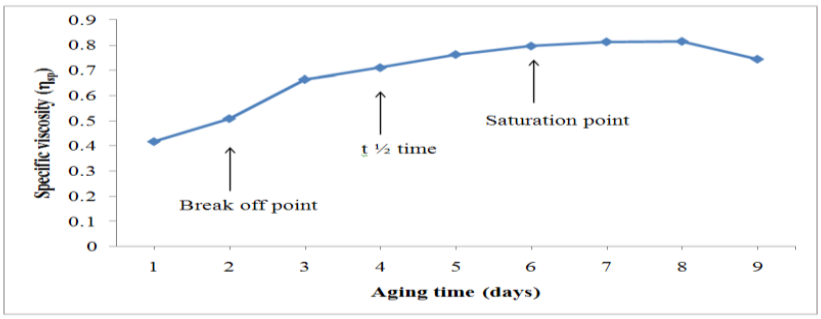

Figure 2 Variation of specific viscosity of the prepared SnO_2:F sol solution (7.5 % w/w NH_4F) with aging time

FT IR analysis for prepared fluorine doped tin oxide films

FT IR spectra of prepared SnO_2:F thin films on glass substrate at (300 °C and 500 °C) are shown in Figure 3. FT IR spectra have been assigned to the absorption peaks of Sn-O, Sn-O-Sn, Sn-OH or O-H bond vibrations. The absorption peaks between 400 cm^{-1} to 700 cm^{-1} can be assigned to Sn-O and Sn-O-Sn vibration of SnO_2. Small peaks between 1600 cm^{-1} to 1900 cm^{-1} are attributed to Sn-OH vibration mode. Since the precursor solution contains water, Sn-OH vibration mode appears in the spectrum. In the spectrum, an absorption and corresponding to the presence of adsorbed water (1630-1640 cm^{-1}) and hydroxide absorption bands in the range of 3500-3700 cm^{-1} were observed. The bonds nearly 1000 cm^{-1} was assigned to chloride contamination, which arises from chloride precursor. The peaks were assigned to O-Sn-O and Sn-OH in the range of 500 cm^{-1} to 900 cm^{-1} (Stretching vibrations and variations).

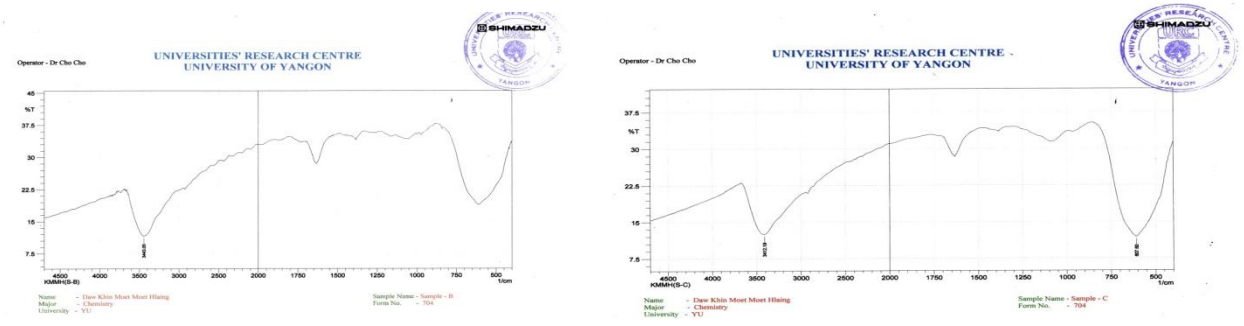

Figure 3 FT IR spectra of prepared SnO_2:F thin films at (a) 300 °C (b) 400 °C

X-ray diffraction analysis for prepared fluorine doped tin oxide films

The crystal structure of the prepared SnO_2:F thin films were identified by XRD diffractometer. The X-ray diffractogram of prepared undoped tin oxide (SnO_2) thin film and prepared 7.5% w/w NH_4F SnO_2 thin film at 400 °C and 500°C are presented in Figure 4. The crystal structure of fluorine doped thin films were studied in the 2q range of 10° to 70°. X-ray diffraction measurements were made to determine the d-values, crystallographic structure, lattice parameters and grain size. All the diffractograms contained the characteristic of SnO_2 orientations. The observed d-values are compared with the standard ones from the (JCPDS-no-70-0377) data files. The matching of the observed d-values and standard d-values confirms that the deposited films are of tin oxide with tetragonal structure.

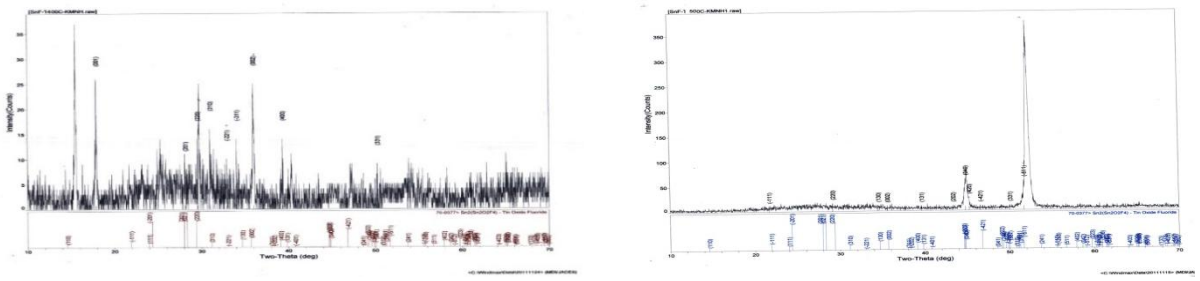

(a) (b)

Figure 4 XRD diffraction patterns of prepared SnO_2:F thin film 7.5% w/w NH_4F at (a) 400 °C and (b) 500 °C

SEM analysis

SEM micrographs showed agglomeration of the grain particles and flower like structure. The morphology of the prepared SnO_2:F thin films studied by SEM analysis indicated the films comprise of small grain size particles with less crack on the surface. SEM micrographs of prepared fluorine doped tin oxide films with different heat treatment temperature (300 °C, 400 °C and 500 °C) are shown in Figures 5. All of the images were found to be polycrystalline with various surface grain shapes and sizes. It was observed that the grain size become larger and the crystallinity was improved with the increase in the heat treatment temperature. The surface roughness was observed to be improved because the radical's mobility at the sample surface enhanced with substrate temperature. These results agree with the results of Tatar *et al.*, (2013). The fluorine doped tin oxide film characterized by uniform size grains with cubical shape at the substrate temperature 400 °C, which is on the average smaller than grains in the high temperature region. Consequently, the results were good agreement with XRD observation.

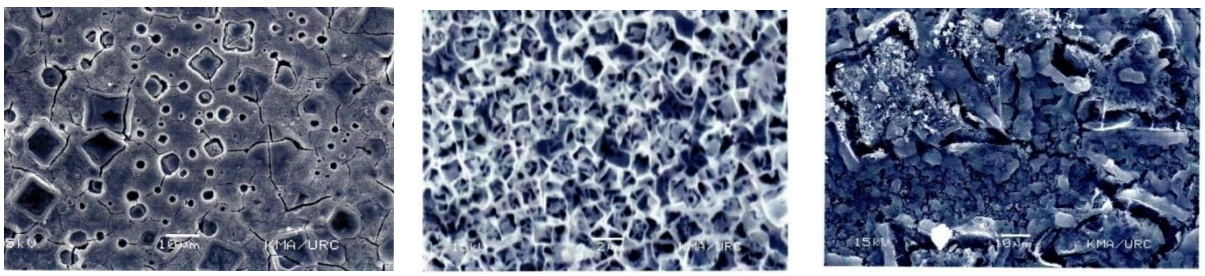

(a) (b) (c)

Figure 5 SEM micrographs of prepared SnO_2:F thin films (7.5% w/w NH_4F) at different temperature (a) 300°C (b) 400°C and (c) 500°C

Optical Properties of the Prepared Fluorine Doped Tin Oxide Thin Film

Optical analysis of fluorine doped tin oxide thin film on glass substrate at different temperatures was studied from transmission (%) vs wavelength curve in the wavelength range 400-1000 nm. The high optical transmittance for the film heat treated at the temperature 400 °C which is shown in Figure 6. Highest value of transmittance is observed to be 95.15 % for the film heat treated at 400 °C and this is attributed to the low scattering effect and uniform film thickness caused by smooth and good surface texture of the film. In the visible region of the spectra, the transmission of film was very high, due to fact that the reflectivity is low and there is less absorption due to excitation of electrons from the valence band to conduction band (Tripathy *et al.,* 2013). It may be concluded that the transmittance was more which may be due to high porosity and larger grain size and less absorption in the film. According to the transmittance data it was found that the deposition temperature was improved the optical transmittance between 85 % T and 95 % T.

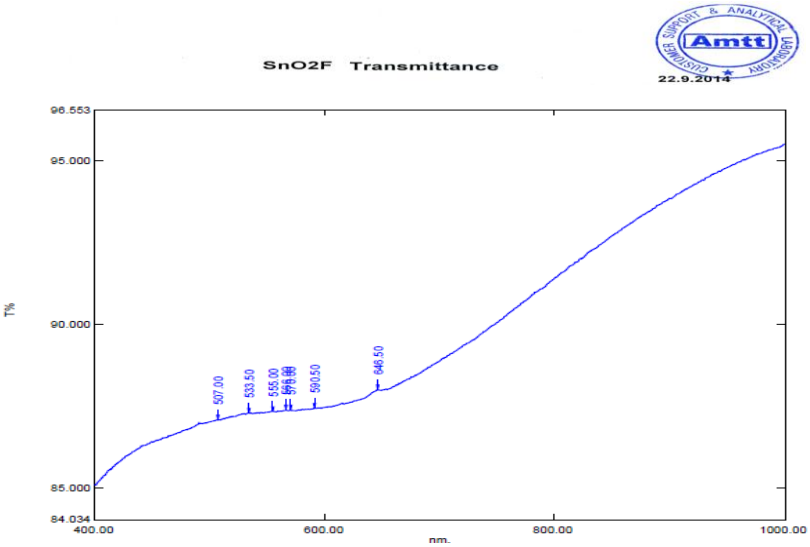

Figure 6 Transmission spectrum of SnO_2:F thin film (7.5% w/w NH_4F, 400 °C) as a function of wavelength

Electrical Properties of the Prepared Fluorine Doped Tin Oxide Thin Film

Electrical testing was done to assess the electrical performance of the best films produced from each deposition technique. Sheet resistance measurements were recorded using a linear four-point probe (Olopade *et al.,* 2012) method. Four-point probe method is an electrical resistance measuring technique that uses separate pairs of current-carrying and voltage-sensing electrodes to make more accurate measurements than traditional two-terminal (2T) sensing. Hall Effect measurements were done using the Van der Pauw technique in order to determine the dominant charge carrier type, charge carrier mobility and charge carrier concentration.

The change of sheet resistance of the SnO_2:F thin films coated on glass substrate for a substrate temperature of 200 °C and different weight percent of fluorine 1.0 % w/w to 10.0 % w/w NH_4F, the minimum sheet resistance value was obtained at 7.5 % w/w NH_4F. The increasing of sheet resistance after a specific level of fluorine content probably represents doping limit of fluorine in the tin oxide lattice. The excess fluorine atoms do not occupy the proper lattice position to contribute to the free carrier concentration and at the same time the increasing disorder leads to the increase of the sheet resistance (Miao *et al.,* 2010).

According to the literature, in sol-gel derived thin films, the highly porous with small crystal sizes is formed especially in the case of single layer coating. However, in multiple

coating, sheet resistance of SnO_2:F thin films can be increased (Gasparro *et al.*, 1998). The sheet resistance decreased gradually from 73.99 W sq^{-1} to the minimum 8.91 W sq^{-1} with the number of coating from 2 times to 10 times. Therefore, number of coating was optimized to 10 times, in order to get film of good electrical and optical properties.

Deposited films by sol-gel method, contain water and organic materials, and mechanical properties of the film are poor and must be improved. Therefore, the sample should be put in an oven for a suitable time and temperature. This improves the optical and mechanical properties of thin film and also removes water and organic materials from thin film. The sheet resistance value of SnO_2:F thin films at 250 °C was (9.85 W sq^{-1}) and its gradually decrease to 3.71 W sq^{-1} with the heat treated temperature of 400 °C. And then, the resistance value increased with the heat treated temperature of 450 °C and 500 °C. According the previous reports, the substrate temperature was over 400 °C, the amorphous structure transformed into crystal structure, and then the narrowing of grain boundaries which result in an decreased in the conductivity (Aldelkani *et al.*, 2007). The sheet resistance does not change more with the temperature increase from 400 °C to 500 °C, due to the slight change of the crystal structure. Therefore, the sheet resistance was slightly varied with the substrate temperature in the range of 400-500 °C. Therefore, the sheet resistance value and polycrystalline nature depends directly on the heat treated temperature. Thus, the sheet resistance of prepared SnO_2:F thin films at 400 °C was observed lowest value and this temperature is optimal temperature for that treatment process.

The change of sheet resistance of the SnO_2: F thin films coated on glass substrate with heat treated temperature (400 °C), number of coating (10) times, weight percent of (7.5 % w/w NH_4F) and heating time (1, 2, 3, 4 and 5) h, it was found that the sheet resistance value decreased when the annealed time was increased from 1 to 3 h and then increased when annealed time was increased from 4 to 5 h. The minimum sheet resistance value was 1.02 W sq^{-1} at the annealed time of 3 h. This is because the carrier concentration decreased with higher rate due to the loosing of fluorine atom. The optimum point was found at the annealed time of 3 h.

Table 1 shows the variation of sheet resistance value of prepared fluorine doped tin oxide thin film (7.5 % w/w NH_4F) with three deposition methods such as spray, spin and dip coating. Among them, a dip-coating deposition is one of the most promising ones, due to the simplicity of the apparatus, lost-effectiveness, good uniformity of the films and well suitability for large-scale production. It was also found that the minimum resistance value (1.7 W sq^{-1}) for dip-coating method. Therefore, based on their resistance value, dip-coating method is suitable for the preparation of fluorine doped tin oxide thin film.

Table 1 Sheet Resistance of the Prepared SnO_2:F Thin Films by Various Deposition Methods

Sr. No	Deposition Method	Sheet Resistance (Ω sq^{-1})
1	Spray	3.49
2	Spin	2.06
3	Dip	1.70

No. of coating = 10 times
Heated Temperature = 400 °C
Sample = 7.5 % w/w NH_4F

Conclusion

The present investigation revealed that transparent conducting fluorine doped tin oxide thin films (SnO_2:F) were prepared on glass substrate by atmospheric pressure chemical vapour deposition and sol gel dip-coating method. The precursor sol solution was prepared from tin(IV) chloride pentahydrate $SnCl_4.5H_2O$, ammonium fluoride and ethanol as solvent. Structural, optical and electrical properties under different preparation conditions like concentration of ammonium fluoride, viscosity of the sol solution, coating period, heat treatment temperature, heating time duration and deposition method. Then the prepared thin films were characterized by modern techniques such as FT IR, XRD, SEM and UV. Fluorine doped tin oxide thin film of excellent reproducibility, adherence and device quality was prepared by dip coating method via sol gel route under optimized conditions viz, dopant concentration 7.5 % w/w NH_4F, heat treatment temperature 400 °C, number of coating 10 times and heating time duration 3 hour. The rheological studies indicated that the optimum coating period for the sol solution lie between 4 and 6 days.

The X-ray diffraction studies confirmed the tetragonal structure with polycrystalline nature. The preferred directions of crystal growth in the diffractogram of SnO_2: F films correspond to the reflection from the (110), (200), (220) and (310) planes. The matching of the observed and standard d-values confirmed that the deposited films are of tin oxide with tetragonal structure. FT IR spectroscopy showed strong Sn-O and Sn-O-Sn bonding. The minimum value of resistance was 1.02 W for the film heat treated at 400 °C for 3 h (7.5 % w/w NH_4F). The nature of the films indicated that at lower temperature (100°C-400°C), chemi-sorptions mechanism predominates and grain boundary scattering become low, which reduced the film resistance. At higher temperature (above 400 °C) oxygen desorption phenomena become predominant with higher grain boundary scattering which causes an increased in resistance.

The SEM micrographs showed that the variation of substrate temperature results in different grain size and shapes for different orientations while the SnO_2:F film heat treated at 400 °C shows uniform surface pattern with evenly distributed fine grains. The film deposited by dip-coating showed clear flowerlike crystal shape on the surface and the presence of uniform and dense microstructure apparently devoid of any cracks and voids, although it was possible that some microscale porosity was present in the film. Besides that, there are some crystal shapes structures like as mostly tetragonal shape. This observation was approved to the XRD results as tetragonal structure of prepared SnO_2:F thin films.

The optical property of prepared SnO_2:F thin film showed that thin films are fully transparent in the visible region (400 to 1000 nm). All the SnO_2:F thin films showed good transmittance in the visible region and the fundamental absorption edge lies in the UV region. In the present work, highest value of transmittance is observed to be 95.15 % at 1000 nm for the film heat treated at 400 °C and this is attributed to the low scattering effect and uniform film thickness caused by smooth and good surface texture of the film.

Thus, this studies indicated that sol gel dip coated SnO_2:F films prepared under the optimized operating conditions could be potential for the solar cell application. Consequently, a large area of solar panel can be fabricated based on the preparation of dye sensitized solar cell using prepared SnO_2:F transparent conductive films. Further research will be much more necessary to develop these types of material in the future.

Acknowledgements

We would like to thank to the Department of Higher Education, Ministry of Education in Myanmar, for giving as the opportunity to do this research. Our deepest gratitude is expressed to Dr Ba Han, Rector, Meiktila University, his encouragement and kind help to do this research. We wish to thank Dr Kay Thi Thin, Prorector, Meiktila University, for her invaluable advice and encouragement. Thanks, are also extended to Dr Ni Ni Aung (Professor and Head, Department of Chemistry, Meiktila University) and Dr Ni Ni Sein (Professor, Department of Chemistry, Meiktila University), for their helpful advice.

References

Abdullahi, S., Moreh, A.U., Hamza, B., Sadiya, U., Abdullahi, Z., Wara, M. A., Kamaludeen, H., Kebbe, M. A. and Monsurat. U. F. (2014). "Electrical Characterization of Fluorine Doped Tin Oxide Deposited by Spray Pyrolysis Technique and Annealed under Nitrogen Atmosphere". *International Journal of Nano and Material Sciences,* vol 3 (1), pp 41-46

Aldelkani, H., Mellatnavaz, B., Roohi, H. and Noorbakhsh, M. (2007). "New Sol-Gel Solution with 45 Days Stability for Preparation Silica Thin Films". *Iran J. Chem Eng,* vol 26 (3), pp 25-29

Alhamed, M. and Issa, A. S. and Doubal, A. W. (2012). "Studying of Natural Dyes Properties as Photo-sensitizer for Dye Sensitized Solar Cells (DSSC)". *Journal of Electron Devices,* vol 16, pp 1370-1383

Gasparro, G., Putz, J., Gantz, D. and Aegerter, M. A. (1998). "Parameters Affecting the Electrical Conductivity of SnO_2: Sb Sol-Gel Coatings". *Solar Energy Materials & Solar Cells.* vol 54, pp 287-296

Jafar, A.M., Kiffah, A., Farham L. R. and Ibrahin, K.F. (2013). "Fabrication and Characterization of Fluorine Doped Tin Oxide Transparent Conductive Nano Films". *International Journal of Innovative Research in Engineering and Science,* vol 6 (2), pp 49-58

Kang, M., Inkoo, K., Minwoo, C. and Sok, W.K. (2011). "Optical Properties of Spattered Indium Tin Oxide Thin Films". *Journal of the Korean Physical Society,* vol 59(5), pp 3280-3283

Miao, D., Zhao, Q., Wu, S., Wang, Z., Zhang, X. and Zhao, X. (2010). "Effect of Substrate Temperature on the Crystal Growth Orientation of SnO_2: F Thin Films Spray-Deposited on Glass Substrates". *Journal of Non-Crystalline Solids,* vol 356, pp 2557-2561

Olopade, M. A., Awe, O. E., Awobode, A. M. and Al, N. (2012). "Characterization of SnO_2:F Films Deposited by Atmospheric Pressure Chemical Vapour Deposition for Optimum Performance Solar Cell". *The African Review of Physics,* vol 7, pp 177-181

Russo, B. and CaO, G. Z. (2007). "Fabrications and Characterization of Fluorine Doped Tin Oxide Thin Films and Nanorods Arrays Via Spray Pyrolysis". *Applied Physics,* vol 9, pp 311-315.

Samad, W. Z., Salleh, M. M., Shafiee, A. and Yarmo. M. A. (2011). "Structural, Optical and Electrical Properties of Fluorine Doped Tin Oxide Thin Films Deposited Using Inject Printing Technique". *Sains Malaysiana,* vol vol 40 (3), pp 251-257.

Shelke, R. S., Thombre, S. B. and Patrikar, S. R. (2013). "Status and Perspectives of Dye Used in Dye Sensitized Solar Cells". *International Journal of Renewable Energy Resources,* vol 3, pp 12-19

Singh, P. B., Rakash, K., Ashwani, K., Jyoshana, G., Sunder, P.S. and Tyagi, R.C. (2013). "Effect of Annealing on Properties of Transparent Conducting Tin Oxide Film Deposited by Thermal Evaporation". *Journal of Pure and Applied Physics,* vol 51, pp 558-562

Tatar, D., Guven, T. and Bahattin, D. (2013). "Effect of Substrate Temperature on the Crystal Growth Orientation and Some Physical Properties of SnO_2:F Thin Films Deposited by Spray Pyrolysis Technique". *Rom Journal of Physics,* vol 58 (1-2), pp 143-158

Tripathy, S. K., Nagarjum, B. and Siva Jahnavy,V. (2013). "Optical and Structural Characteristics of Copper Doped Tin Oxide Thin Film Prepared by Thermal Evaporation Method". *International Journal of Engineering and Innovative Technology (IJEIT),* vol 3 (1), pp 296-300

Tsai, C. and Huang, C. (2013). "Surface Treatment and Characterization of Indium Tin Oxide Thin Films Modified Using Cyclonic Atmospheric Pressure Plasma". *Japanese Journal of Applied Physics,* vol 52, pp 1-7

Wu, S., Shuai, Y., Liyi, S., Yin, Z. and Jinbui, F. (2010). "Preparation, Characterization and Electrical Properties of Fluorine-doped Tin Oxide Nanocrystals". *Journal of Colloid and Interface Science,* vol 346, pp 12-16

Yousaf, S.A. and Ali, S. (2008). "The Effect of Fluorine Doping on Optoelectronic Properties of Tin-Dioxide (F: SnO_2) Thin Films". *CODEN JNSMAC,* vol 48 (1 & 2), pp 43-50

ISOLATION AND OPTIMIZATION OF SOME FERMENTATION PARAMETERS OF THE SELECTED SOIL FUNGUS (SK-6) FROM PYAWBWE TOWNSHIP, MANDALAY REGION

Su Su Kyi[1], Ni Ni Aung[2] and Zar Zar Yin[3]

Abstract

Six different soil samples were collected from six different places in Pyawbwe Township, Mandalay Region. Thirty different soil fungi SK-1 to SK-30 were isolated from six different soil samples. Isolation of fungi SK-1 to SK-30 were undertaken by serial dilution method. The isolated fungi were cultured on Blakeslee's Malt Extract Agar (BMEA), Czapek Dox Agar (CZA), Malt Extract Agar (MEA) and Potato Glucose Agar (PGA) media. Antimicrobial activity of isolated fungal strains was evaluated by using the agar well diffusion method with seven test organisms. Among them, three fungal strains SK-1, SK-3 and SK-6 showed the antimicrobial activity against *Bacillus subtilis* and *Candida albicans* at 7 days. Especially, SK-6 gave the best antifungal activity against *Candida albicans*. Therefore, SK-6 was selected and the optimum conditions for antimicrobial metabolite production on *Candida albicans* of SK-6 were the fermentation period, suitable age and size of inoculum, different carbon and nitrogen sources.

Keywords : soil fungi, antimicrobial activity, fermentation, agar well diffusion

Introduction

Soil is the upper layer of most of the earth's surface and varies in depth from inches to over twenty feet. It is a product of weathered rock, but quite distinct in its characteristic. Soils are excellent cultural media for the growth of many types of organisms (Angelov, 2008). This includes bacteria, fungi, algae, protozoa and viruses. A spoonful of soil contains billions of microorganisms. In general the majority of microbial population is found in the upper six to twelve inches of soil and the number decreases with depth (Cattle, 2002). The number and kinds of organisms found in soil depend upon the nature of soil, depth, season of the year, state of cultivation, reaction, organic matter, temperature, moisture, aeration, etc. (Omalu, 2011).

Fungi have fundamental functions in terrestrial ecosystems, in degradation of organic matter and in nutrient uptake of plants through mycorrhizal interactions. From a human point of view, there are both good and bad fungi. There are quite some delicious edible fungi and other are used in productions of food like soysauce, tempe and bread. They are also a source of important drugs like the penicillins, the cholesterol-lowering lovastatin and cyclosporins, which counteracts the rejection of transplanted organs (Harayama and Isono, 2002).

Antimicrobial describes a substance that can either kill or hinder the growth of microbes such as bacteria, viruses, fungi and protozoa. It is a general term that includes antibiotics, antivirals, antifungals and antiprotozoals. Antibiotics treat bacterial infections while antivirals are specific for viral infections. Antifungals help treat such as thrush, candidiasis, athlete's foot or ringworm, while antiprotozoals specifically deal with microscopic parasites in body. Antimicrobials that kill microbes are called microbicidal, those that merely inhibit their growth are called microbiostatic (Trease and Evans,1980).

This research paper aims to investigate the isolation of soil microorganisms and to know the different soil microorganisms from various soil samples. Studies were carried out to investigate the effect of pH, temperature, static, and shaking culture on the fermentation.

[1] Assistant Lecturer, Department of Chemistry, Meiktila University
[2] Professor and Head, Department of Chemistry, Meiktila University
[3] Associate Professor, Department of Botany, Pathein University

Materials and Methods

Collection of Soil Samples and Isolation of Soil Fungi

The soil samples were collected from six different locations of Pyawbwe Township, Mandalay Region, during July, 2017. Sampling sites (address, latitude and longitude) and it's condition were recorded in Table 1. The fungi were isolated by using serial dilution method, and cultured on Blakeslee's Malt Extract Agar (BMEA), Czapek Dox Agar (CZA), Malt Extract Agar (MEA) and Potato Glucose Agar (PGA).

Table 1 Six Different Soil Samples Collected from Pyawbwe Township

Soil Samples	Samples Area	Location
S.I	Lat Thae` Kyoe Village	N. 20˚ 45′ 34.209″ E. 95˚ 53′ 56.545″
S.II	War Yin Toke Village	N. 20˚ 44′ 33.441″ E. 95˚ 55′ 24.573″
S.III	Yintaw Village	N. 20˚ 42′ 43.776″ E. 95˚ 56′ 28.376″
S.IV	Chaung Magyi Village	N. 20˚ 40′ 52.574″ E. 95˚ 54′ 19.548″
S.V	Phat TawVillage	N. 20˚ 34′ 57.105″ E. 96˚ 01′ 40.497″
S.VI	Pyi Thayar	N. 20˚ 36′ 26.142″ E. 96˚ 02′ 30.760″

Serial Dilution Method

One gram of soil sample was introduced into a conical flask containing 99 mL of distilled water. The flask was then shaken for about 30 min in order to make the soil particles free from each other. This solution was then serial diluted from 10^{-3} to 10^{-7} dilution and 0.5 mL each of the above dilution was separately transferred into sterile petridishes under aseptic condition (Dubey and Maheshwari, 2002). Chloramphenicol was added to the sterilized medium for preventing bacterial growth. The sterilized medium in conical flask was cooled down to about 45 ºC and separately poured into each of the petridish containing the respective soil dilutions.

The inoculated plates were shaken by clock-wise and anticlock wise direction for about 5 min so as to make uniform distribution of the fungi inoculums. When the agar was solidified , the inoculated plates were inverted and incubated at 27º -30º C for 3 -6 days.

Lacto Phenol Cotton Blue Teased Mount (LPCB.TM) Staining Technique for Fungi

The needles were flamed over the burning Bunsen burner to sterile. A drop of LPCB was placed on the slide. A tiny piece of the colony was transferred into the LPCB on the slide by using a sterile needle. After staining the slide was covered with a cover slip. The wet staining was examined under the x40 objective microscope for microscopic identification.

Agar Well Method

The antimicrobial assay was performed by agar well diffusion method (Perez *et al*., 1990). Agar well diffusion method is widely used to evaluate the antimicrobial activity of plants or microbial extract. The same procedure was used in disk diffusion method, the agar plate surface is inoculated by spreading a volume of the microbial inoculum over the entire agar

surface. Then, a hole with a diameter of 8 mm is punched aseptically with a sterile cork borer or a tip and a volume (20 µL) of the antimicrobial agent or extract solution at desired concentration is introduced into the well. Then, the plates are incubated under suitable conditions depending upon the test microorganism. The antimicrobial agent diffuses in the agar medium and inhibits the growth of the microbial strain tested.

Preliminary Study for Antimicrobial Activity

The isolated fungi were grown on BMEA medium for 5 days. These fungi were inoculated into 25 mL seed medium and incubated at room temperature for 3 days. After 3 days, 20 mL seed culture was transferred into the 80 mL of fermentation medium and incubated at room temperature. Fermentation was carried out for 3-10 days (Ando *et al*., 2004).

One day old culture test broth (0.01 mL) was added to 25 mL of agar well diffusion assay medium and thoroughly mixed and poured into plate. After solidification, cork borer was used to make the wells (dia. T

The fermented broth (20 µL) was carefully added into the wells and incubated at room temperature for 24 to 48 h. The diameter of the zone of inhibition around each well was measured and recorded after 24 to 48 h incubation.

Effect of Fermentation Period

The fermentation period of isolated fungi was studied for 3 days to 10 days and seed culture medium was added to 100 mL of fermentation medium. The flasks were incubated at room temperature and the fermentation culture was assayed for antifungal activity by using agar well diffusion method.

The Effect of Ages of Inoculum for Fermentation

In this study, different incubation times (48, 60, 72, 84, 96, 108, 120, 132, 144 h) were used for the production of antimicrobial metabolite and the procedure of seed culture medium was also used as the previous method. And then, seed culture was transferred to 100 mL conical flask containing of fermentation medium and incubated at room temperature. The inoculum age of fermentation studied were 48, 60, 72, 84, 96, 108, 120, 132 and 144 h. Fermentation culture was kept from 48 to 144 h and antifungal activity was tested by agar well diffusion method.

The Effect of Sizes of Inoculum for Fermentation

The size of inoculum (5%, 10%, 15%, 20%, 25%, 30% and 35%) were used for the production of antimicrobial metabolite. In the investigation of size of inoculum, well sporulated selected strain SK-6 were taken and added to 250 mL conical flask containing 100 mL of seed culture medium and incubated for 3 days at room temperature. After that 3 days old seed culture were (5 %, 10 %, 15 %, 20 %, 25 %, 30 %, 35 %) transferred to 100 mL conical flasks containing 25 mL of fermentation medium respectively. The flasks were incubated at room temperature and the fermentation culture was assayed for antifungal activity by using agar well diffusion method.

Carbon and Nitrogen Utilization

In this study, carbon and nitrogen sources were employed in the fermentation for the production of antimicrobial metabolites. Carbon sources such as carrot, corn powder, glycerol, glucose, lactose, maltose, mannitol, molasses, oat, potato, rice powder, sucrose, fructose and soluble starch were used. Nitrogen sources such as casein, fish cake, gelatin, malt extract, meat extract, peanut cake, peptone, poly peptone, rice bran, soy bean, urea, yeast extract, potassium nitrate, sodium nitrate, ammonium chloride, ammonium nitrate, and ammonium sulphate were also used.

The Effects of pH on Selected Fungus SK-6

Optimum pH was studied by varying the medium pH as 4, 5, 6, 7, 8, 9 and 10. The different pH of seed medium was adjusted by using 1 M HCl and 1 M NaOH. The selected fungus SK-6 was inoculated in the optimized fermentation media and kept at room temperature. The fermentation medium was assayed for antifungal activity.

The Effects of Temperature in Selected Fungus SK-6

The selected fungus SK-6 was inoculated and incubated at different temperatures 20 °C, 25 °C, 30 °C, 35 °C and 40 °C.

The Effect of Shaking and Static Condition Upon the Secondary Metabolite

100 mL conical flask containing 50 mL of the best fermentation medium was incubated on the rotary shaker (100 rpm) for 5 days. At the same time, another fermentation medium was incubated under static condition without shaking. The antifungal activities of shaking culture and static culture were compared by using agar well diffusion assay method.

The Effect of Fermentation Media

Fermentation media were undertaken with optimized conditions of 5 % sizes, 108 h old, pH-7, temperature 20 °C, shaking culture of inoculum with thirteen different media. Fermentation media was kept for 5 days and antifungal activity test was carried out 24 h interval.

Results and Discussion

Isolation of Fungi from Soil Samples

Thirty fungi were isolated from six different soil samples of Pyawbwe Township, Mandalay Region. The results of soil samples showed that soil type S-I of Lat Thae` Kyoe Village was sandy clay loam and pH value of 9.4. War Yin Toke Village and Yintaw Village (S-II & S-III) were loamy sand soil, pH values of 10.6 and 8.8 respectively. Chaung Magyi Village (S-IV) was sandy clay soil and pH value of 8.8. Phat Taw Village (S-V) and Pyi Thayar (S-VI) were sandy loam soil and pH values of 9.2 and 8.9 respectively (Table 2).

Total of 30 fungal isolates were obtained - six strains from S-I, eight fungi from S-II, five strains from S-III, each one fungi from S-IV and S-VI and nine strains from S-V (Table 3). The soil fungi were isolated by using four different media. 17 strains were isolated from BMEA medium, 5 strains from CZA medium, other 5 strains from MEA medium and 3 fungi from PGA medium. The surface colour of SK 1 to SK10 were white, pale gray, pale brown, center green edge white, center yellow edge white and their reverse colour were cream, white, yellow, brown, pale white, pale yellow, center black edge white, center black edge brown. The surface colour of SK 11 to SK 20 were white, gray, black, greenish white , center black edge white, center greenish yellow edge white, center green edge white, center green edge cream and the reverse colour were white, yellow, brown, cream, black, center black edge white, center yellow edge white (Figure 1).

The surface colour of SK 21 to SK 30 were white, pale green, greenish white, center black edge white, center green edge white, center brown edge white and the reverse colour were cream, yellow, pale brown, pale yellow, yellowish orange, pale green and pale greenish blue respectively.

Table 2 pH and Soil Type of Soil Sample

Soil Samples	pH	Soil Types
S.I	9.4	Sandy clay loam
S.II	10.6	Loamy sand
S.III	8.8	Loamy sand
S.IV	8.8	Sandy clay
S.V	9.2	Sandy loam
S.VI	8.9	Sandy loam

Table 3 Isolated Fungi from Soil Samples

Soil Samples	BMEA Medium	CZA Medium	MEA Medium	PGA medium	Total
S.I	SK-19, SK-21, SK-22, SK-27, SK-29	SK-23	-	-	6
S.II	SK-11, SK-18, SK-24	SK-17, SK-26	SK-20, SK-25, SK-28	-	8
S.III	SK-8	SK-9, SK-30	SK-12, SK-13	-	5
S.IV	SK-14	-	-	-	1
S.V	SK-1, SK-2, SK-3, SK-4, SK-5, SK-6, SK-7	-	-	SK-15, SK-16	9
S.VI	-	-	-	SK-10	1
Total	**17**	**5**	**5**	**3**	**30**

BMEA = Blakeslee's Malt Extract Agar, CZA = Czapek Dox Agar, MEA = Malt Extract Agar, PGA = Potato Glucose Agar

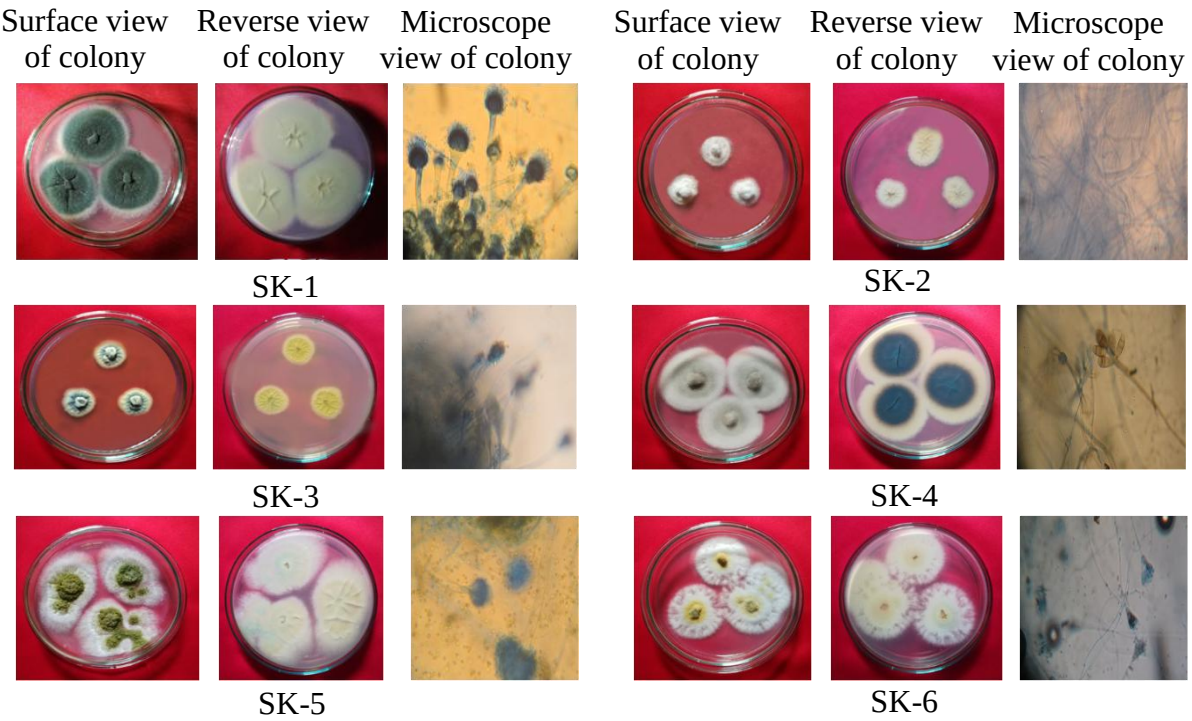

Surface view of colony	Reverse view of colony	Microscope view of colony	Surface view of colony	Reverse view of colony	Microscope view of colony
		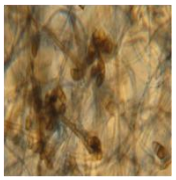			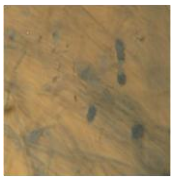
SK-7			SK-8		
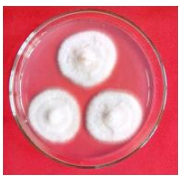		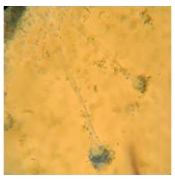	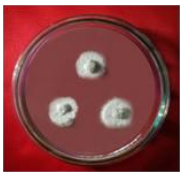		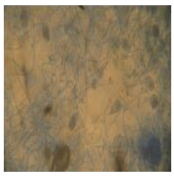
SK-9			SK-10		
	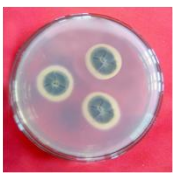				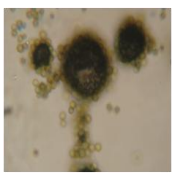
SK-11			SK-12		
			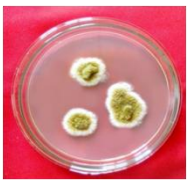		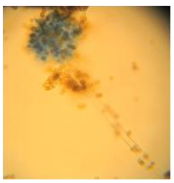
SK-13			SK-14		
		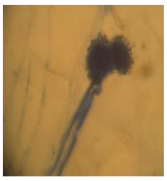			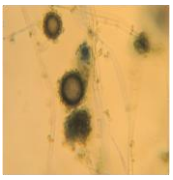
SK-15			SK-16		
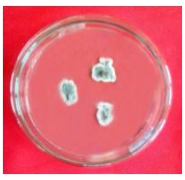			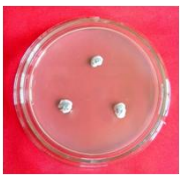	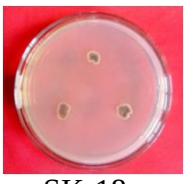	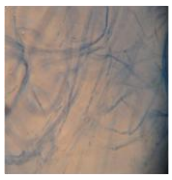
SK-17			SK-18		
		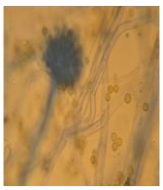			
SK-19			SK-20		
SK-21			SK-22		

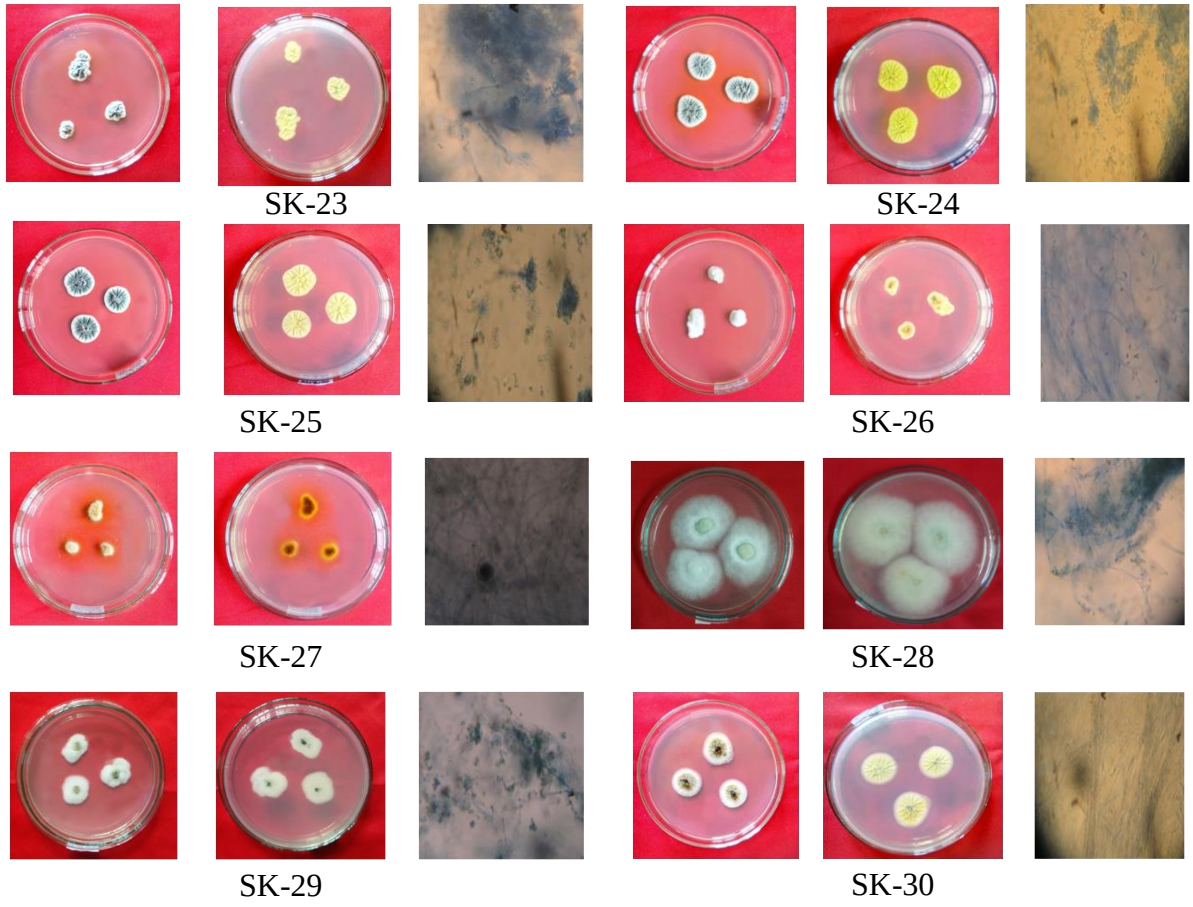

Figure 1 Morphological character of isolated fungi SK-1 to SK-30

Antimicrobial Activity of Isolated Fungi

The antimicrobial activity of all fungal strains were tested by using seven test organisms. Among them, three selected fungi- SK 1, 3 and 6 were moderate antimicrobial activity on *Bacillus subtilis* and *Candida albican*s (Table 4 and Figure 2). SK-6 showed strong antifungal activity against *Candida albicans* (28.59 mm) followed by SK-3 (28.56 mm) and SK-1 (27.78 mm). And then, SK-6 exhibited the moderate antibacterial activity against *Bacillus subtilis* (21.56 mm), SK-1 (20.28 mm) and SK-3 (18.98 mm) at 5 days fermentation period respectively. According to these results, SK-6 was selected for further investigations.

Table 4 Antimicrobial Activity of Isolated Three Fungus against *B. subtilis* and *C. albicans*

Isolated Fungi	Inhibition zone diameter	
	Bacillus subtilis	***Candida albicans***
SK-1	20.28	27.78
SK-3	18. 98	28.56
SK-6	21.56	28.59

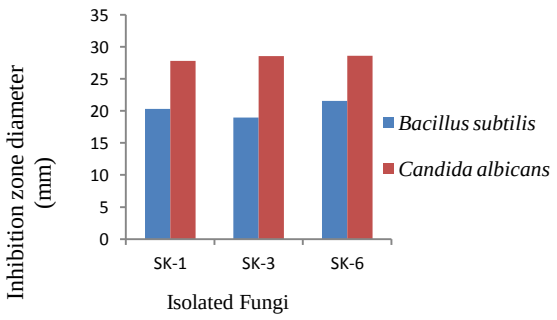

Figure 2 Antimicrobial activity of isolated fungi against *B. subtilis* and *C. albicans*

The Fermentation Period of Selected Fungus (SK-6) against *Candida albicans*

SK-6 reached the highest activities (25.77 mm) in 5 days fermentation period on *Candida albicans* (Table 5 and Figure 3).

Table 5 Antifungal Activity the Fermentation Period of Selected Fungus (SK-6) against *Candida albicans*

Fermentation period (Days)	Inhibition zone diameter (mm)
3	16.97
4	21.10
5	25.77
6	25.73
7	23.02
8	22.78
9	18.20
10	15.76

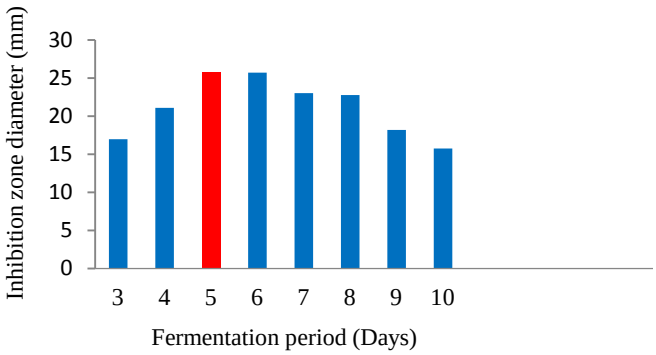

Figure 3 Antifungal activity on the fermentation period of selected fungus (SK-6) against *Candida albicans*

The Effects of Ages of Inoculums of SK-6 against *Candida albicans*

In this research work, the effect of ages of inoculum, SK-6 was examined by using 48, 60, 72, 84, 96, 108, 120, 132 and 144 h old culture age of inoculums. The results showed that 108 h age of inoculum gave the highest activities (25.02 mm), followed by (24.77 mm) at 120 h and (22.96 mm) at 132 h age of inoculum. These results are shown in Table 6 and Figure 4.

Table 6 The Effect of Ages of Inoculums of SK-6 against *Candida albicans*

Sr. No	Age of Inoculum (h)	Inhibition zone diameter (mm)
1	48	18.78
2	60	21.28
3	72	21.02
4	84	21.47
5	96	21.46
6	**108**	**25.02**
7	120	24.77
8	132	22.96
9	144	20.19

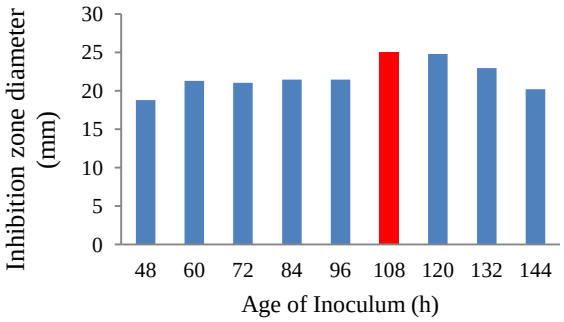

Figure 4 The effect of ages of inoculums of SK-6 against *Candida albicans*

The Effects of Sizes of Inoculums of SK-6 against *Candida albicans*

The effect of sizes of inoculums was investigated by using 5 %, 10 %, 15 %, 20 %, 25 %, 30 % and 35 % inoculums (Table 7). The use of 5 % inoculums exhibited higher activity (33.03 mm) than others, followed by 15 % and 30 % (24.22 mm and 24.16 mm) respectively in Figure 5.

Table 7 The Effects of Sizes of Inoculums of SK-6 on *Candida albicans*

Size of inoculum (%)	Inhibition zone diameter (mm)
5	**33.03**
10	24.09
15	24.22
20	21.23
25	18.92
30	24.16
35	21.11

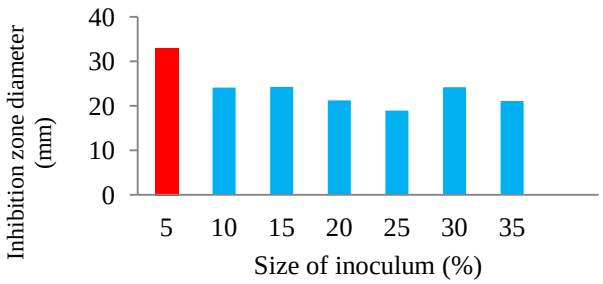

Figure 5 The effects of sizes of inoculums of SK-6 on *Candida albicans*

Antifungal activity on carbon utilization of SK-6

During these experiments, the results displayed that the different levels of antifungal activity were found when the different carbon sources were added into the fermentation medium. The inclusion of different carbon sources showed the highest antifungal activities on glucose (30.24 mm) followed by glycerol (24.15 mm), corn powder (22.89 mm), molasses (22.67 mm) and then rice powder (21.50 mm), sucrose (21.34 mm), potato (21.25 mm), carrot (21.07 mm), lactose (20.92 mm), maltose (20.48 mm), mannitol (19.89 mm) and oat (19.09 mm). These results are shown in Table 8 and Figure 6.

Table 8 Antifungal Activity on Carbon Utilization of SK-6

Sr. No	Carbon Sources	Inhibition zone diameter (mm)
1	Carrot	21.07
2	Corn Powder	22.89
3	Glycerol	24.15
4	**Glucose**	**30.24**
5	Lactose	20.92
6	Maltose	20.48
7	Mannitol	19.89
8	Molasses	22.67
9	Oat	19.09
10	Potato	21.25
11	Rice Powder	21.50
12	Sucrose	21.34
13	Fructose	15.11
14	Soluble Starch	16.18

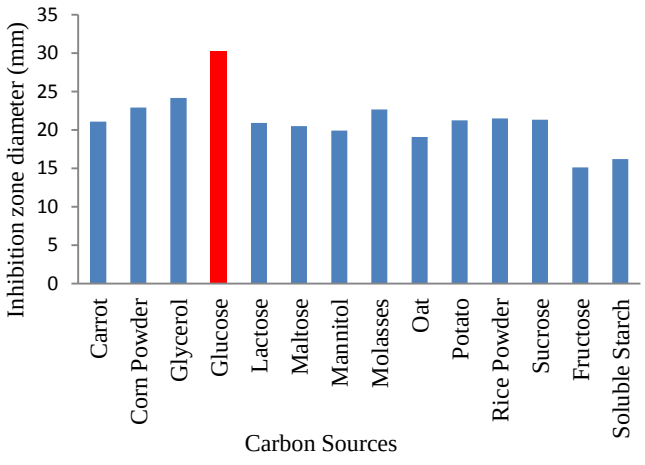

Figure 6 Antifungal activity on carbon utilization of SK-6

Antifungal Activity on Nitrogen Utilization of SK-6

There were variations in the level of antifungal activity when the different nitrogen sources were tested in the fermentation medium. When the various nitrogen sources, the significant inhibition zones were obtained in ammonium nitrate (59.21 mm), sodium nitrate (47.28 mm), potassium nitrate (43.79 mm) and malt extract (30.19 mm) respectively. Moderate inhibition zones were also found in peptone (29.77 mm), ammonium sulphate (29.19 mm), yeast extract (28.85 mm), ammonium chloride (27.95 mm), urea (26.88 mm), fish cake (26.49 mm), gelatin (26.26 mm), polypeptone (26.11 mm), meat extract (25.95 mm), casein (25.09 mm), peanut cake (24.25 mm), rice bran (23.22 mm) and soy bean (22.35 mm) (Table 9 and Figure 7).

Table 9 The Effect of Nitrogen Sources on SK-6

Sr. No	Nitrogen Sources	Inhibition zone diameter (mm)
1	Casein	25.09
2	Fish cake	26.49
3	Gelatin	26.26
	KNO_3	43.79
5	Malt extract	30.19
6	Meat extract	25.95
7	$NaNO_3$	47.28
8	NH_4Cl	27.95
9	**NH_4NO_3**	**59.21**
10	$(NH_4)_2SO_4$	29.19
11	Peanut cake	24.25
12	Peptone	29.77
13	Poly peptone	26.11
14	Rice bean	23.22
15	Soy bean	22.35
16	Urea	26.88
17	Yeast extract	28.85

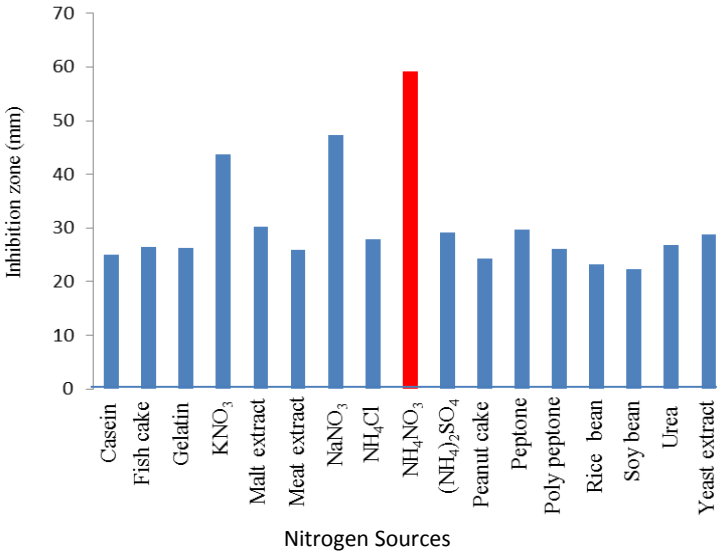

Figure 7 The effect on nitrogen sources of SK-6

The effect of pH on antifungal activity of SK-6

Effect of pH was assessed in the range of pH 4 to 10. The best antifungal activity was found at pH-7 (28.12 mm) (Table 10 and Figure 8).

Table 10 The Effect of pH on Antifungal Activity of SK-6

pH	Inhibition zone diameter (mm)
4	25.22
5	25.48
6	27.60
7	**28.12**
8	27.82
9	27.10
10	26.08

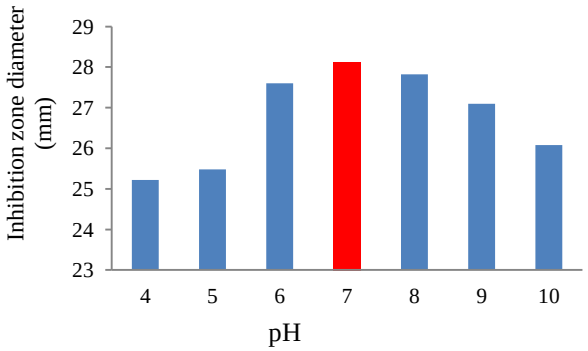

Figure 8 The Effect of pH on Antifungal Activity of SK-6

The Effect of Temperature on Antifungal Activity of SK-6

Effect of temperature was studied by changing temperature 20 °C, 25 °C, 30 °C, 35 °C and 40 °C. The maximum antifungal activity was obtained at 20 °C (27.31 mm) (Table 11 and Figure 9).

Table 11 The Effects of Temperature on Antifungal Activity of SK-6

Temperature (°C)	Inhibition zone diameter (mm)
20	**27.31**
25	27.25
30	26.76
35	25.89
40	16.17

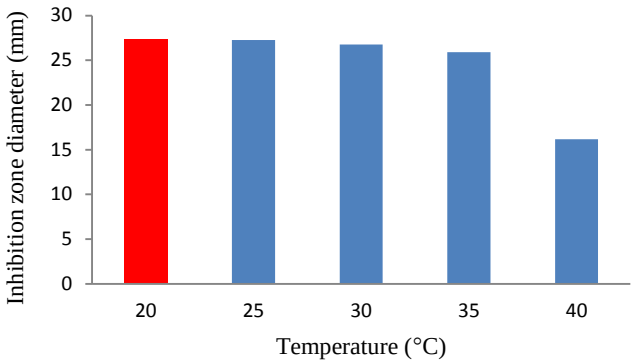

Figure 9 The effects of temperature on antifungal activity of SK-6

The Effect on Static and Shaking Culture of SK-6 against *C. albicans*.

In the comparison of shaking and static culture, the antifungal activity of shaking culture (30.60 mm) was more than that of static culture (21.90 mm) (Table 12 and Figure 10).

Table 12 Comparison on Antifungal Activity of SK-6 by using Shaking and Static Culture

Agitation and aeration condition	Inhibition zone diameter (mm)
Shaker culture	**30.60**
Static culture	21.90

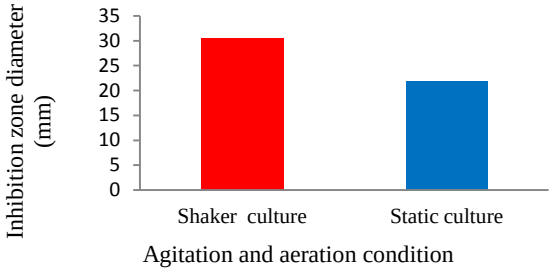

Figure 10 Comparison on antifungal activity of SK-6

Antifungal Activity of SK-6 on Various Fermentation Media

In the fermentation medium (FM), the best antifungal activity was obtained by using FM-1, (glucose and ammonium nitrate, 40.75 mm) followed by FM-2, (glucose and sodium nitrate, 40.49 mm), FM-8, (ammonium nitrate and glycerol, 32.06 mm) and FM-3, (glucose and potassium nitrate, 31.93 mm) respectively (Table 13 and Figure 11).

Table 13 The Antifungal Activity of SK-6 on Various Fermentation Media

Fermentation Media (FM)	Inhibition zone diameter (mm)
FM 1	**40.75**
FM 2	40.49
FM 3	31.93
FM 4	25.97
FM 5	25.17
FM 6	24.88
FM 7	21.80
FM 8	32.06
FM 9	29.13
FM 10	25.42
FM 11	23.83
FM 12	23.35
FM 13	21.20

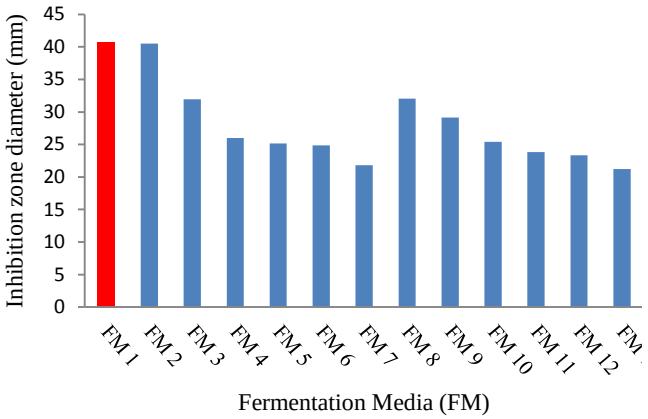

Figure 11 The antifungal activity of SK-6 on various fermentation media

Conclusion

Six different soil samples were collected from six different places at Pyawbwe Township, Mandalay Region. Soil fungi were isolated by serial dilution method.

A total of 30 strains fungal were isolated from six different soil samples of Pyawbwe Township by using four different media including BMEA, CZA, MEA and PGA medium and incubated for 3-7 days at room temperature. Pure colonies were inoculated into slant culture containing BMEA medium.

Six fungi SK-19, 21, 22, 23, 27 and 29 were isolated from soil sample S-I, SK-11, 17, 18, 20, 24, 25, 26 and 28 from sample S-II, SK-8, 9, 12, 13 and 30 from sample S-III, SK-14 from sample S-IV, SK-1, 2, 3, 4, 5, 6, 7, 15 and 16 from sample S-V and fungal strains SK 10 was isolated from sample S-VI.

A total of seventeen fungal colonies were isolated from Blakeslee's Malt Extract Agar (BMEA) medium and five fungal strains were isolated from Czapek Dox Agar (CZA) and Malt Extract Agar (MEA) respectively. Three colonies were isolated from Potato Glucose Agar (PGA) medium.

In the investigation of antimicrobial activities, ten fungi were tested by using Agar Well diffusion assay with seven test organisms. SK17 showed the highest antibacterial activities (30.28 mm) at 5 days on *Bacillus pumilus*. SK 19 exhibited the moderate antibacterial activities (24.23 mm) at 3days on *Bacillus subtilis.* Some isolated fungi did not have the antimicrobial activity on *Escherichia coli*. Mostly soil fungi were against *Bacillus pumilus*, *Bacillus subtilis* and *Candida albicans*. Especially, SK 6 showed the moderate antimicrobial activity against all test organisms.

From the research work, three fungal strains SK-1, SK-3 and SK-6 showed antimicrobial activity against on *Bacillus subtilis* and *Candida albicans* while SK-6 showed significant antimicrobial activity on *Candida albicans*. Thus, SK-6 was selected for the best fermentation conditions. The antifungal activity of SK-6 was highest against *Candida albicans* (28.59 mm) in 5 days fermentation period.

To study the optimization of inoculums age, incubation time (48, 60, 72, 84, 96, 108, 120, 132 and 144 h) were used and the maximum antifungal activity (25.02 mm) was found at 108 h.

In the appropriate size of inoculums, 5 % was the foremost suitable and the highest activities (33.03 mm) in SK-6 followed by 15 % and 30 % respectively.

In the carbon source, the colony of SK-6 was good growth on lactose, soluble starch and oat. The antifungal activity of SK-6 were affected by addition of glucose and showed the highest activity (30.24 mm), followed by glycerol and corn powder.

The nitrogen source has remarkable effect on the production of antifungal metabolite in SK-6. Especially SK-6 showed excellent growth on casein, followed by yeast extract, gelatin, ammonium chloride and peptone. Maximum antifungal metabolite of SK-6 was found in the ammonium nitrate (59.21 mm) followed by sodium nitrate, potassium nitrate respectively as nitrogen sources.

Effect of pH was investigated by varying from pH 4, 5, 6, 7, 8, 9 and 10. The highest antifungal activity was found at pH 7 (28.12 mm). Effects of temperature was observed by varying from 20 °C, 25 °C, 30°C, 35 °C and 40 °C. The best antifungal activity for temperature was found at 20 °C (27.31 mm) followed by 25 °C (27.25 mm), 30 °C (26.76 mm) respectively.

The results of static and shaking culture condition were compared, the best antifungal activity was found at shaking culture (30.60 mm).

In the fermentation medium (FM), thirteen kinds of FM were used and FM-1 gave the highest antifungal activity (40.75 mm) by using glucose and ammonium nitrate. The best production of drug by exploting sorbose in their fermentation media while others found glucose and yeast extract to be best carbon and nitrogen sources.

Thus, the results of the best fermentation conditions were investigated that antifungal metabolite of SK-6 were obtained by optimally 5 days fermentation period, 108 h age of inoculums, 5 % inoculums size, lactose and glucose in the carbon source, casein and ammonium nitrate in the nitrogen source, pH-7 and temperature 20 °C, shaking culture and fermentation medium FM-1.

It was concluded that the present research work was to study the antimicrobial properties of three isolated fungi, to investigate the fermentation conditions of selected fungus SK-6. The isolated strain will be studied for further investigation such as identification of isolated fungi and extraction of their antimicrobial compound.

Acknowledgements

We would like to thank to the Department of Higher Education, Ministry of Education in Myanmar, for giving as the opportunity to do this research. Our deepest gratitude is expressed to Dr Ba Han, Rector, Meiktila University, for his encouragement, and kind help to do this research. We wish to thank Dr Kay Thi Thin, Prorector, Meiktila University for her invaluable advices and encouragement. Thanks are also extended to Dr Ni Ni Aung (Professor and Head, Department of Chemistry, Meiktila University) and Dr Zar Zar Yin (Associate Professor, Department of Botany, Pathein University), for their helpful advice, precious suggestions and provision of research facilities at the Department of Chemistry, Meiktila University and Biological Resources and Biotechnology Development Centre, Pathein University.

References

Ando, K., Suto, M. and Inaba, S. (2004). *Sampling and Isolating Methods of Fungi*. Laboratory Workshop at University of Pathein. Biological Resource Center, National Institute of Technological and Evaluation (NITE), Japan

Angelov, G. B. (2008). "Heavy Metal Pollution in the Boatin Reserve (Bulgaria)". *Turkish J. Botany*. vol. 32, pp. 155-160

Cattle, J. A., McBratney, A. B. and Minasny, B. K. (2002). "Method Evaluation for Assessing the Spatial Distribution of Urban Soil Lead Contamination". *J. Environmental Quality*, vol.31. pp. 1576-1588

Dubey, R.C. and Maheshwari, D.K. (2002). *Practical Microbiology*. New Delhi; Chand and Company Ltd, pp. 110-155

Harayama, T. and Isono, K. (2002). "Sources of Microorganisms". *J. Microbiology*, vol. 48, pp. 46-50

Omalu, I. C. J., Ayanwale, V. A., Ajalaruru, A. B., Mohammed, A. Z., Bala, J. and Chukuuemeka V. (2011). "Isolation of Fungi and Bacteria from Housefly (*Musca Domestica* L.) Larvae". *The Internet Journal of Microbiology*, vol.9.pp.1

Perez, C., Paul M. and Bazerque, P. (1990). "An Antibiotic Assay by the Agar-Well Diffusion Method". *Acta Biol. Med. Exp*, vol. 15, pp. 113-115

Trease, G.E. and Evans, W.C. (1980). *Pharmacognosy*. London: 1st Ed., Spottiswoods Ballantyne Ltd., 108

EVALUATION OF RADICAL SCAVENGING ACTIVITY AND AFLATOXINS IN TUMERIC POWDER BY HIGH PERFORMANCE LIQUID CHROMATOGRAPHY

Hla Thidar Aung[1], Ni Ni Aung[2], Yin Yin Han[3]

Abstract

Tumeric (*Curcuma longa*) has been known to use in Myanmar traditional medicine system in connection with antioxidant, antimicrobial, anticancer and antibacterial activities and therefore locally grown tumeric (*Curcuma longa*) has been chosen for this study. It is widely used in the world for many purposes and it is also one of the exports of Myanmar. But some turmeric contains aflatoxin and it causes main barrier of earning foreign currencies. Aflatoxin-toxic carcinogenic secondary metabolities are produced *by Aspergillus flavus, Apergillus parasititicus* and *Aspergillus nomius* species of fungi. Thus the detection of aflatoxins concentration in food and feeds are very important. High Performance Liquid Chromatographic method was developed and validated according to the protocol on validation of analytical procedures. Analysis of tumeric samples was carried out for aflatoxin B1, B 2, G1 and G2 by HPLC method. Evaluation of radical scavenging activity was detected by DPPH method while contract extraction of aflatoxin was done as per AOAC method with screening by TLC and quantification by HPLC using reference standards. Thus the proposed method is simple, rapid and specific and was successfully employed for quality and quantity monitoring of aflatoxin content in tumeric.

Keywords: *Curcuma longa,* HPLC, aflatoxins, tumeric

Introduction

Natural plant products have been used throughout human history for various purposes. Many of these natural products have pharmacological or biological activity that can be exploited in pharmaceutical drug discovery and drug design. Tumeric is a product of *Curcuma longa,* a rhizomatous herbaceous perennial plant belonging to the ginger family *Zingiberaceae* , which is native to tropical South Asia. As many as 133 species of *Curcuma* have been identified worldwide (Yee Mon Than, 2006). Tumeric has been used as a food colorant, dye, cosmetic and medicine. It is widely used as a spice in Southeast Asia and Middle Eastern cooking. It is a significant ingredient in most commercial curry powders. Tumeric has been used traditionally for thousands of years as a remedy for stomach and liver ailments. A fresh juice is commonly used in many skin conditions of eczema and allergy. And it is also used for treatment of various infection and antiseptic. The most important chemical components of turmeric are a group of compounds is called curcuminoids, which include curcumin, demethoxy curcumin and bisdemethoxycurcumin. The best study compound is curcumin, which consist 0.3 to 5.4 % of raw turmeric. Cyrcumin has been a centre of attraction for potential treatment of an array of disesses, including cancer, Alzheimer's disease, diabetes, allergies, arthritis and other chronic illnesses. In addition there are other important volatile oils such as turmerone, atlantone, and zingiberene. Tumeric oil is majorly extracted in India. Tumeric oil acts as a heating and moisturizing agent, analgesic, anti-arthritic, anti-inflammatory, antioxidant, bactericidal, and a repellent against day and night bitting mosquitoes. In this research, the dried rhizomes of Tumeric were collected from Hanmyintmo village, Kyaukse Township, Mandalay Region (Figure 1). The present study is aimed to extract curcumin and determine the antioxidant activities of extracts from Tumeric (Burkill, 1996). Curcumin was extracted from turmeric oleoresin of turmeric by selected solubility method. The radical scavenging activity was done by

[1] Lecturer, Department of Chemistry, Meiktila University
[2] Professor and Head, Department of Chemistry, Meiktila University
[3] Lecturer, Department of Chemistry, Meiktila University

DPPH assay method and the presence of aflatoxin was detected by HPLC Aflatoxin test (Charopra, 1958).

Botanical Description of *Curcuma longa* L. (Tumeric)

Family	Zingiberaceae
Genus	*Curcuma*
Species	*longa*
Botanical name	*Curcuma longa* L.
Myanmar name	Na-Nwin Tumeric
Parts used	rhizome (root)

Figure 1 Plant of *Curcuma longa* L.

Curcumin

Figure 2 Dried rhizome of Turmeric

The pure orange-yellow, crystalline powder, curcumin is the main component of curcuminoid (Figure 2). There are two kinds of acidic hydrogen in curcumin. One is phenolic hydrogen; the other is active methylene hydrogen of β-diketones. Curcumin ($C_{21}H_{20}O_6$) forms a melting point 176-180 °C and is insoluble in water and ether, but soluble in ethanol, dimethyl sulphoxide and other organic solvents (Burzarbarua, 2000).

Aflatoxins

Aflatoxins are poisonous carcinogens that are produced by certain molds (*Aspergillus flavus* and *Aspergillus parasiticus*) which grow in soil, decaying vegetation, hay, and grains. They are regularly found in improperly stored staple commodities such as cassava, chili peppers, corn, cotton seed, millet, peanuts, rice, sesame seeds, sorghum, sunflower seeds, tree nuts, wheat, and a variety of spices. When contaminated food is processed, aflatoxins enter the general food supply where they have been found in both pet and human foods, as well as in feedstocks for agricultural animals. Animals fed contaminated food can pass aflatoxin transformation products into eggs, milk products, and meat. Children are particularly affected by aflatoxin exposure, which is associated with stunted growth, delayed development, liver damage, and liver cancer.

Aflatoxins are among the most carcinogenic substances known. After entering the body, aflatoxins may be metabolized by the liver to a reactive epoxideintermediate or hydroxylated to become the less harmful aflatoxin M1. Aflatoxins are most commonly ingested. However the most toxic type of aflatoxin, B1, can permeate through the skin. The United States Food and Drug Administration (FDA) action levels for aflatoxin present in food or feed is 20 to 300 ppb (Lopez C, *et al.*, 2000).

Aspergillus parasiticus

Scientific classification

Kingdom : Fungi
Division : Ascomycota
Class : Eurotiomycetes
Order : Eurotiales
Family : Trichocomaceae
Genus : *Aspergillus*

Aspergillus parasiticus is a fungus belonging to the genus *Aspergillus.* This species is an unspecialized saprophytic mold, mostly found outdoors in areas of rich soil with decaying plant material as well as in dry grain storage facilities. Often confused with the closely related species, *A. flavus*, *A. parasiticus* has defined morphological and molecular differences. *Aspergillus parasiticus* is one of three fungi able to produce the mycotoxin, aflatoxin, one of the most carcinogenic naturally occurring substances. Environmental stress can upregulate aflatoxin production by the fungus, which can occur when the fungus is growing on plants that become are damaged due to exposure to poor weather conditions, during drought, by insects, or by birds. In humans, exposure to *A. parasiticus* toxins has potential to cause delayed development in children and produce serious liver diseases and/or hepatic carcinoma in adults. The fungus is also able to cause the infection known as aspergillosis in humans and other animals. *A. parasiticus* is of agricultural importance due to its ability to cause disease in corn, peanut, and cottonseed (Makun, Anjorin, Moronfoye, 2010).

Aspergillus flavus

Kingdom : Fungi
Division : Ascomycota
Class : Eurotiomycetes
Order : Eurotiales
Family : Trichocomaceae
Genus : *Aspergillus*

Aspergillus flavus is a saprotrophic and pathogenic fungus with a cosmopolitan distribution. It is best known for its colonization of cereal grains, legumes, and tree nuts. Postharvest rot typically develops during harvest, storage, and/or transit. *A. flavus* infections can occur while hosts are still in the field (preharvest), but often show no symptoms (dormancy) until postharvest storage and/or transport. In addition to causing preharvest and postharvest infections, many strains produce significant quantities of toxic compounds known as mycotoxins, which, when consumed, are toxic to mammals. *A. flavus* is also an opportunistic human and animal pathogen, causing aspergillosis in immunocompromised individuals.

Materials and Methods

Sample Preparation

The dried rhizomes of *Curcuma longa* L.(Tumeric) were collected from Hanmyintmo Village, Kyaukse Township, Mandalay Region. They were cut into small pieces to extract curcumin and determine the amount of aflatoxin .

Isolation of Curcumin

Procedure

Ethanol extract was dissolved in a mixture of 60 mL of methanol / hexane mixture and was stirred at ambient temperature until a homogeneous suspension was achieved and then

filtered. After filtration, the powder was recovered. Then, the powder was washed with 95 % ethanol and evaporated. After evaporation, the powder was dried at 110 °C for one hour, desiccated and finally weighed. Yellow-brown powder curcumin was obtained. Then the powder was repeated washed with mixture of methanol/ hexane, hexane and stirred until the orange-yellow colour was obtained. Finally, they are crystallized with 95 % ethanol, dried, desiccated, and weighed. Orange yellow crystalline powder was formed and melting point was measured. Pure curcumin melts at 179 to 180 °C and it was confirmed by TLC check of R_f value 0.45 by using the selectd solvent system of pet ether : ethyl acetate (1:1). It was in accordance with the literature value of curcumin (Hooker, 1978).

Determination of Radical Scavenging Activities by DPPH Test

The free radical scavenging activity of crude extract of tumeric was measured using free radical scavenging assay.

Preparation of 0.002 % (w/v) DPPH solution

0.002 % DPPH solution was prepared in the brown coloured bottle by dissolving 2 mg of DPPH powder in the 100 mL of ethanol. It must be stored in the refrigerator for no longer than 24 h.

Preparation of standard solution

The stock solution (200 µg/mL) of BHT was prepared by dissolved (20mg) of each compound in 100mL of ethanol. The stock solution was two-fold serially diluted with ethanol to get the standard solution with the concentration of 200, 100, 50, 25, 12.5, 6.25 and 3.125 µg/mL Table (1).

Preparation of test sample solution

The stock solution (200 µg/mL) of the crude extracts was prepared by dissolving (20mg) of respective crude extract in 100mL of ethanol. This stock solution was two-fold serially dilution with ethanol to get the sample solution with the concentration of 200, 100, 50, 25, 12.5, 6.25 and 3.125 µg/mL.

Preparation of blank solution

Blank solution was prepared by mixing the sample solution 1.5mL with ethanol (1.5mL).

Procedure

DPPH radical scavenging activity of ethanol extract of tumeric was determined by UV-visible spectrophotometer.

The control solution was prepared by mixing 1.5 mL of 0.002 % DPPH solution and 1.5 mL of ethanol in the brown bottle. The sample solution was also prepared by mixing 1.5 mL 0.002% DPPH solution and 1.5 mL of test sample solution. These bottles were incubated at room temperature and were taken on shaker for 30 min. After 30 min, the absorbances of these solutions were measured at 517 nm and the percentage of radical scavenging activity (% RSA) was calculated by the following equation. % RSA of crude extract of tumeric results are shown in Table 1 (Shinde, *et.al*. 2012).

$$\% \text{ Inhibition} = \frac{\text{DPPH alone - (Sample } - \text{ Blank)}}{\text{DPPH alone}}$$

Where,

% Inhibition = percent inhibition of test sample
DPPH alone = absorbance of DPPH solution
Sample = absorbance of sample solution
Blank = absorbance of blank solution

The antioxidant power (IC_{50}) is expressed as the test substances concentration (µg/mL) that in a 50% reduction of initial absorbance of DPPH solution and that allows to determine the concentration. IC_{50} (50 % inhibition concentration) values were calculated by linear regressive

excel program.The standard deviation was also calculated. IC_{50} values of crude extracts of rhizomes of tumeric results are shown in Table1 and Figure 3.

Determination of Aflatoxin B1, B2, G1 and G2 present in Tumeric Powder

25.0 ± 0.1 g of sample was added to 5 g of NaCl and placed in the blender's jar. All applicable information was recorded. It was determined by the HPLC chromatogram of AIGLENT TECHNOLOGY, Thiland.

For the spike recovery sample, added an appropriate amount of working standard to 50 g of sample to give a spike level of approximately at 3 -10 times the LOD for aflatoxin B_1. As a guide, 750 µL of a 100 mg/mL standard was used.

100 mL of methanol: DI water (80:20) was added and blended at high speed for 1 minute. The extract was poured into fluted filter paper (Whatman No. 1) and collected the filtrate in a 100-mL beaker. 4.0 mL of the filtered extract was taken into another clean vessel. 16.0 mL of DI water was added and mixed well to get dilute extract. 10 mL of the diluted extract was passed through Afla Test P column at a flow rate of approximately 1-2 drops/second. The eluent was discarded.

10 mL of purified water was passed through the column at a flow rate of approximately 2 drops/second until air comes through the column. The eluent was discarded. Column with 1.0 mL acetonitrile (HPLC grade) was eluted through the column. The solution was evaporated to just dryness using nitrogen evaporator with the water bath set at 50 ± 2ºC.

0.2 mL of trifluoroacetic acid was added to the vial, swirled to mix and let it stand for 15 min at 50 ± 2 ºC.

1.8 mL of 10 % acetonitrile/water was added to the vial and mix well. For derivatized standards, suitable volumes of aflatoxin was added to the working standard into a 4 mL vial and concentrated to dryness using nitrogen evaporator with the water bath set at 50 ± 2 ºC. Then 0.2 mL of trifluoroacetic acid was added to the vial, swirled to mix and let stand for 15 minutes at 50 ± 2 ºC. 1.8 mL of 10 % acetonitrile/water was added to the vial and mixed well. Filtered through 0.2 µm nylon filter into a HPLC vial (Sahoo *et al.,* 2001).

The aflatoxin B_1, B_2, G_1 and G_2 were determined by HPLC with a fluorescence detector and the concentration percent was calculated by the following equation

$$\text{Concentration (\%)} = \frac{\text{Extraction vol (mL)} \times \text{Final vol (mL)} \times \text{Amount}}{\text{Aliquot vol (mL)} \times \text{Sample weight (g)}}$$

$$= \frac{100 \times 20 \times 2 \times \text{Amount}}{4 \times 10 \times 25} = \text{Amount} \times 4$$

Results and Discussion

Identification of Curcumin from ethanol extract of *Curcuma longa* L. by Selective Solubility Method

Curcumin was isolated from ethanol extract of *Curcuma longa* L. by selected solubility method. The yield percent of curcumin based on raw turmeric was obtained at 0.4%. It was consistent with the literature values (Charopra, 1956). Orange yellow crystalline powder was extracted.In the solubility method, there are four steps, extraction of turmeric oleoresin, evaporation of solvents, separation, and crystallization. The solubility of curcumin in some organic solvents is; acetone> ethyl methyl ketone> ethyl acetate> ethanol> 1,2 dichloro ethane> isopropanol> benzene> hexane (Hooker, 1978). In this research work, ethanol is used in extraction and crystallization steps. In the separation of turmeric oleoresin, methanol/hexane mixture was used because it can not only well dissolve turmeric oleoresin but also essential oil

containing in turmeric oleoresin. In this step, it need time to dissolve oleoresin and adequate condition (e.g stirring). Besides, methanol/hexane mixture can be used to produce powder of high purity and maximum yield. Hexane can also be used to wash or remove the oils from the turmeric oleoresin because it is the least solubility of curcumin. Then extracted curcumin was checked in melting point by using melting point measuring apparatus. The measurement result was found to be in the range of 176-180 °C. Pure curcumin also melts in the same range. So it was consistent with the literature value. And its R_f value of 0.45 by using the selected solvent system of pet ether: ethylacetate (1:1) under the UV lamp give the only one yellow spot. It was in accordance with the literature value of curcumin (Paterson, and Lima N., 2011).

Antioxidant Activities of Curcumin and Ethanol Extract by DPPH Test

Antioxidant activities of curcumin, and ethanol extract were determined in vitro by DPPH test. The principle of this method is that, in the presence of stable free radical (DPPH), the antioxidant donates a hydrogen atom to quench the stable free radical. This method is associated with the change in the absorbance. In the presence of an antioxidant, DPPH radical obtains one more electron and the absorbance decreases. Decreases in absorbance indicate increases in antioxidant activity. Antioxidant activities of curcumin and ethanol extract were usually expressed in terms of % inhibition. Ascorbic acid was used as standard. The % inhibition values of curcumin ethanol extract and aascorbic acid were described in Table 1. From the values of % inhibition IC_{50} values were calculated by computing program called Linear Regressive Excel Program. According to the table, IC_{50} of curcumin, ethanol extract and ascorbic acid were 11.21, 28.47 and 1.85 µg/mL respectively. The DPPH test demonstrated that 50 µg/mL of curcumin has significantly increased the % radical scavenging activity. The lesser the value of IC_{50} the greater the antioxidant activity (Zain, 2011).

Table 1 % Inhibition Effect of EtOH extract and Curcumin

Sample	Concentration	3.125 µg/mL	6.25 µg/mL	12.5 µg/mL	25 µg/mL	50 µg/mL	IC_{50} µg/mL
EtOH extract	Absorbance	0.303	0.279	0.247	0.179	0.096	28.47
	% inhibition	10.30	14.03	26.57	46.72	70.45	
	Concentration	1.25 µg/mL	2.5 µg/mL	5.0 µg/mL	10 µg/mL	20 µg/mL	IC_{50} µg/mL
Curcumin	Absorbance	0.258	0.23	0.218	0.125	0.089	11.21
	% inhibition	7.65	13.33	21.85	47.04	71.48	
Ascorbic acid	Concentration	0.312 µg/mL	0.625 µg/mL	1.25 µg/mL	2.5 µg/mL	5 µg/mL	IC_{50} µg/mL
	Absorbance	27.09	27.68	32.91	68.31	70,43	1.85
	% inhibition	7.65	13.33	21.85	47.04	71.48	

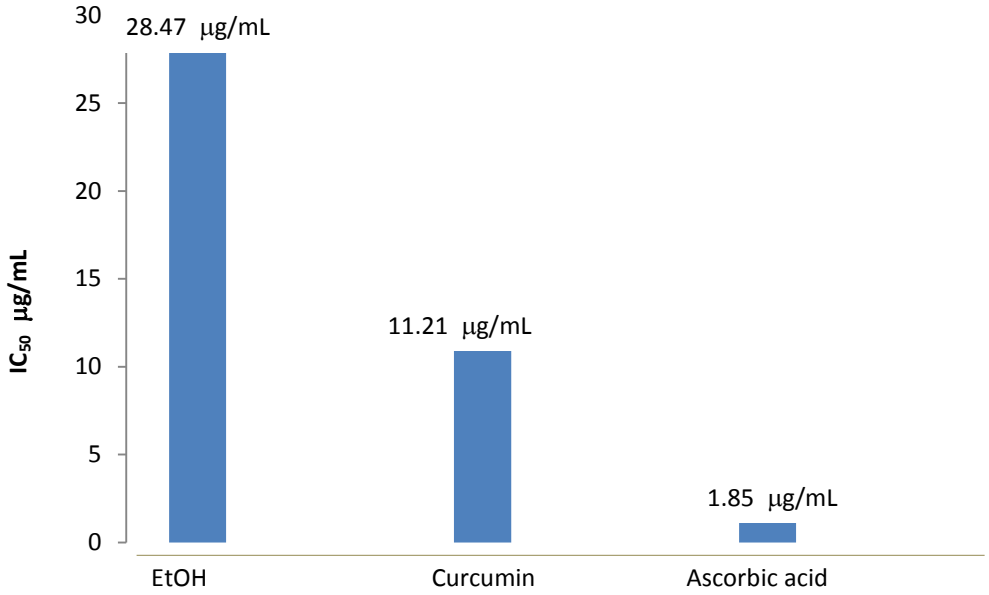

Figure 3 IC $_{50}$ values for EtOH extract of Turmeric ,Curcumin and Ascorbic acid

Aflatoxin B_1, B_2, G_1 and G_2 in Tumeric Powder by HPLC Method

High performance liquid chromatography is the single most important tool for identification of aflatoxin compounds by matching with reference spectra. The HPLC chromatogram of turmeric powder is shown in Figure 5. According to chromatogram, the first peak appears at the retention time 4.359 min with 11.833 ppb, relative abundance of G1. At the retention time of 5.721 min the HPLC spectrum (Figure 5) shows the amount of 0.259 ppb indicating the presence of aflatoxin B1. (Vial and Jardi, 2005).

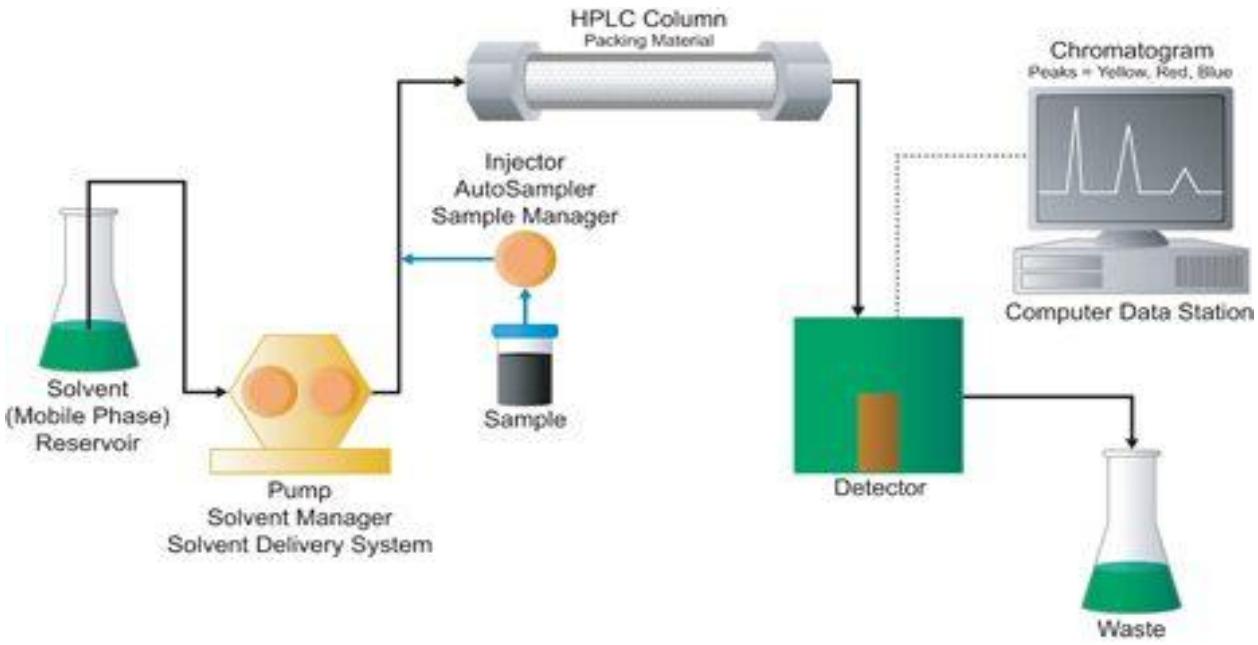

Figure 4 Schematic Diagram of HPLC chromatogram at AIGLENT TECHNOLOGY

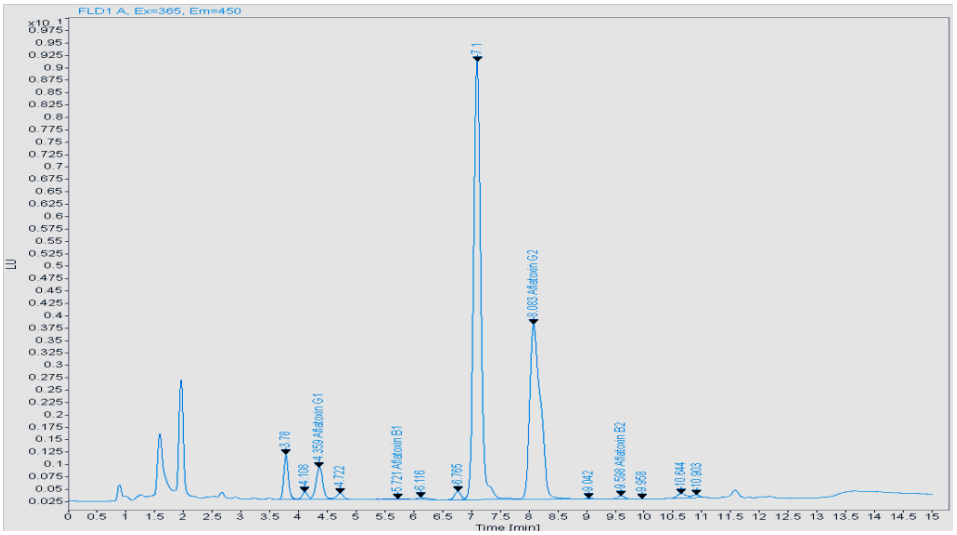

Figure 5 HPLC chromatogram of tumeric powder

At the retention time 8.083 min, the HPLC spectrum (Figure 5) shows the total amount of 55.178 ppb indicating the presence of aflatoxin G_2.At the retention time 9.598 min and total amount of 0.4 ppb, it was matching with the reference of aflatoxin G_2, it can be concluded that the present sample was mixed with aflatoxin G_2. By matching with the reference samples, turmeric powder was found that the carcinogenic aflatoxins are contained and their limits are not exceeding United States Food and Drug Administration (FDA) action levels for aflatoxin present in food or feed is 20 to 300 ppb(Park,2002). But without proper ways of maintenance, carcinogenic levels may be gradually over the range of standards.

Conclusion

The dried rhizomes of *Curcumin longa* Linn. (Tumeric) were collected from Hanmyintmo Village, Kyaukse Township, Mandalay Region .The curcumin was exploited from ethanol extract of turmeric powder by selected solubility method and the yield percent of curcumin based on raw turmeric was obtained at 0.4%. This value is consistent with the literature value and the melting point of curcumin was also obtained in the range (176-180 °C). It was also in accordance with the literature value. The radical scavenging activities of curcumin, ethanol extract and ascorbic acid were determined by in *vitro* by DPPH test. It was found that the IC_{50} values of curcumin , ethanol extract and ascorbic acid were 11.2 µg/mL 28.47µg/mL and 1.85µg/mL. According to the results, the turmeric rhizome has the moderate radical scavenging activity. Eventhough the turmeric has moderate radical scavenging activity, it also have the contamination of aflatoxin . Their level of composition is within the range of 20-300 ppb. Without proper practices and storage may lead to accumulation of mold in turmeric rhizomes. That will be the main barrier of earning foreign currencies.

In this paper, the aflatoxin's compositions of the rhizomes turmeric were identified by High Performance Liquid Chromatography (HPLC) method. The four kinds of aflatoxin, aflatoxin B_1 at the retention time 5.721 min, B_2 is at 9.598min, G_1 at 4.359min and G_2 at the retention time of 8.083min were detected. All the aflatoxins are carcinogenic to some extent to human and animals. Their abundances are 0.259ppb, 0.4ppb, 11.833ppb and 55.178ppb respectively.

The problem of contamination by aflatoxin in food products is a common problem in tropical and subtropical regions in the world. The poor practices and the humid environmental condition favor the growth of fungi. The World Health Organization WHO classifies AFB1 as a class 1 carcinogen. The highest levels of aflatoxins are usually found in warmer regions of the world where there is a great deal of climatic variation. It is important to recognize that, although

it is primary food commodities that usually become contaminated with aflatoxin by mould growth, these toxins are very stable and may pass through severe processes.

According to the results, tumeric powder can be used as spicies and good for antioxidant activity of curcumin content. But allowable dose of aflatoxin in food is not more than 20ppb. Being so, proper storage of tumeric is essential for export. Being lacking in knowledge of proper storage, harvesters are facing the problems of getting molds in their products. Sharing chemical knowledge and the harmful effect of aflatoxin in farm products, it can promote their lives and increase country's earn.

Acknowledgements

The authors would like to thank the Department of Higher Education (Lower Myanmar), Ministry of Education, Yangon, Myanmar, for allowing us to carry out this research programme. Thanks are also extended to the Myanmar Academy of Arts and Science and Professor Dr Ni Ni Aung, Head of Department of Chemistry, Meiktila University for allowing to carry out this research programme.

References

Burkill, I. H. (1966). *A Dictionary of Economic Products of Malay Peninsula.* Kualalumpur: Ministry of Agriculture and Cooperatives, vol. 1, pp. 714.

Buzarbarua, A. (2000). *A Textbook of Practical Plant Chemistry.* New Delhi: 1st ed., S. Chand & Company Ltd.

Charopra, R. N. (1958). *Indigenous Drugs of India.* New Delhi: Councils of Scientific and Industrial Research, pp. 84.

Charopra, R. N., Nayar, S. L. and Chropra, I. C. (1956). *Glossary of Indian Medicinal Plants*. New Delhi: pp. 325.

Hooker, J. D. (1978). The Flora of Birth India. India : Dehradum, vol. 6, pp. 209

Lopez C., Ramons L. and Bulacio L. (2002). "Aflatoxin B1 Content in Patients with Hepatic Diseases". *Medicina-Buenos Aries*, vol. 63, pp. 31-36.

Makun H. A., Anjorin, S. T. and Moronfoye, B. (2010). "Fungal and Aflatoxin Contamination of Some Human Food Commodities in Nigeria". *Africa J. Food Sci*., vol. 4, pp. 127-135.

Park ,D .L (2002), "Mycotoxins and food safety" *Advances in experimental medicine and biology*, vol.504, pp.173-179

Paterson R. R., and Lima, N. (2011). "Further Mycotoxin Effects from Climate Change". *Food Res int*, vol. 44, pp. 2555-2566.

Sahoo, P. K., Mukherji, S. C. and Nayak, S. K. (2001). "Acute and Subchroonic Toxicity of Aflatoxin B1 to Rahu, Labio rohita (Hamilton)". *India J Exp Biol*., vol. 39, pp. 453-458.

Shinde, A.,Ganu, J. and Naik, P. (2012). "Effect of Free Radicals & Antoixidants on Oxidative Stress". *J Dent Allied Sci*, vol. 1(2), pp. 63-66.

Vial, J. and Jardi, A. (2005). *Quantitation by Standard Addition*.: Encyclopedia of Chromatography, Florida, 2nded. Taylor and Francis Group, Boca Raton.

Yee Mon Than. (2006). *Studies on Complex Formation between Slaked Lime and Curcumin from Curcuma longa Linn. (Tumeric).* Yangon: Ph.D. Dissertation, University of Yangon, Myanmar.

Zain, M. E. (2011). "Impact of Mycotoxins on Humans and Animals". *J. Saudi. Chem. Soc.*, vol. 15, pp. 129-144.

SCREENING ON ANTIAGGREGATORY ACTIVITY OF TWO ISOLATED FLAVONOIDS FROM RHIZOMES OF *KAEMPFERIA PARVIFLORA* WALL. (BLACK GINGER)

Lett Lett Thein Tun[1]

Abstract

This paper focused on the health aspects of flavonoids for humans. Among natural compounds, present in everyday diet, flavonoids have shown beneficial effects in prevention of cardiovascular diseases which can be attributed, at least partially to the described antiaggregatory activity i.e. antiplatelet effects of flavonoids. The rhizomes of black ginger were collected from Lashio Township, Northern Shan State and identified by authorized botanist at Botany Department, University of Yangon. Preliminary phytochemical tests were carried out by test tube methods. According to the results, it was found that α-amino acids, flavonoids, glycosides, organic acids, phenolic compounds, starch and terpenoids were found to be present. However, alkaloids, carbohydrates, cyanogenic glycosides, reducing sugars and tannins were not detected. 1.78% of PE, 1.92 % EtOAc, 2.50 % EtOH, 2.87 % MeOH and 4.30 % H_2O crude extracts were prepared by successive Soxhlet extraction method. Silica gel column chromatographic separation of pet-ether extract from rhizomes of black ginger yielded 0.057% of 5-hydroxy -3,7-dimethoxy flavone (m.pt = 149-150 ºC, yellow needles) and 0.035% of 5-hydroxy-3,7,4'-trimethoxy flavone (m.pt = 144- 146 ºC, yellow needles). The isolated compounds were firstly characterized by their physicochemical properties such as R_f values, melting points, solubilities and some colour tests. The isolated compounds were also identified by using modern spectroscopic techniques such as UV-visible, FT-IR, ^{1}HNMR, ^{13}CNMR and 2DNMR spectroscopy. Black ginger contains polymethoxy flavones which are flavonoids that exhibit various bioactivities. Among these, *in vitro* aggregatory activity such as platelet-agglutination, platelet-aggregation and clot retraction were investigated by using Ackroyd's method. It was observed that the isolated compounds possessed antiaggregatory activity.

Keywords: flavonoid, Ackroyd's method, antiaggregatory, platelet-agglutination, platelet-aggregation

Introduction

Kaempferia parvilfora Wall. is with deep purple-colored rhizomes, belonging to Zingiberaceae family and it is known in common name as black ginger, black tumeric, na-nwin net and ga-mone ne (Kress, 2003). It has been mainly used as medicinal resource particularly for treating cardiovascular diseases related to oxidative stress and platelet activation. Black ginger contains abundant amounts of flavonoids and flavonoid glycosides. Especially, it was considered that black ginger is a major source of methoxy flavones with wide range of biological activities such as antiplatelet, antioxidant, anti-inflammatory, antimicrobial and gastroprotective effects (Saokaew *et al*., 2016). The photographs of black ginger are shown in Figure 1.

[1] Dr, Associate Professor, Department of Engineering Chemistry, Technological University (Banmaw)

(a) (b)

Figure 1 Photographs of *Kaempferia parviflora* Wall. (Black Ginger) (a) plant and (b) rhizome

Flavonoids are a group of polyphenolic compounds, which are classified as flavones, flavanones, catechins and anthocyanins. Many have low toxicity in mammals and some of them are widely used in medicine for maintenance of capillary integrity (Cesarone *et al.,* 1992). They have several great advantages over other therapeutic agents because many diets are rich in polyphenolic compounds and are consumed daily having a relatively long half-life with minimum side effects and is easily absorbed in the intestine after ingestion (Agrawal, 2011). In the developed countries, most of the older population is affected by cardiovascular diseases. Platelets are involved in haemostasis, thrombosis and inflammatory processes, hence as a consequence of that physiological role heart stroke and cardiovascular insult can occur. Due to the ever increasing pharmacological interest in antiplatelet agents, a systematic experimental evaluation of large flavonoid series is needed (Sweetman, 2011).

Activated platelets adhering to vascular endolhelium generate lipid peroxides and oxygen free radicals that lead to platelet adhesion and aggregation (Tzeng *et al.,* 1991). Antiaggregatory is preventing the aggregation of platelets. Platelets, the smallest of blood cells, can only be seen under a microscope. They are literally shaped like small plates in their non-active form. A blood vessel will send out a signal when it becomes damaged. When platelets receive that signal, they'll respond by travelling to the area and transforming into their "active" formation. To make contact with the broken blood vessel, platelets grow long tentacle and then resemble a spider or an octopus. A normal platelet count ranges from 150,000 to 450,000 platelets per microliter of blood. Having more than 450,000 platelets is a conduction called thrombocytosis; having less than 150,000 is known as thrombocytopenia. Once in the blood stream, platelets have a life span of 7 to 8 days. About 200 billion platelets are produced every day (Carola, 1990).

This study was undertaken to evaluate the reputation of antiaggregatory property with the isolated flavonoid compounds from the rhizomes of *Kaempferia parviflora* Wall.

Materials and Methods

Collection and Preparation of Samples

The rhizomes of black ginger were collected during the months of October to December in the year of 2002, from Lashio Township, Northern Shan State. A voucher, specimen of the

plant was identified by authorized botanists at Botany Department, Yangon University. After washing with water, the rhizomes were air-dried and ground into powder by a grinding machine. These powder samples were stored in air-tight container.

Preliminary Phytochemical Tests

The dried powdered sample (1 g) was subjected to the tests for alkaloids, α-amino acids, carbohydrates, cyanogenic glycosides, flavonoids, glycosides, organic acids, phenolic compounds, saponins, steroids, tannins and terpenoids as the preliminary phytochemical tests according to the test tube methods (M-Tin Wa, 1970).

Preparation of Various Crude Extracts

Various crude extracts (PE, EtOAc, 95 % EtOH and MeOH) were prepared by successive soxhlet extraction method and then boiled with distilled water. The extracts were concentrated by vacuum rotatory evaporator under reduced pressure to yield PE, EtOAc, 95 % EtOH, MeOH and H_2O extracts. The crude extracts were used to test bioactivities and to isolate some bioactive organic compounds.

Separation and Isolation of Phytochemical Constituents from PE Crude Extract

Compound A and compound B were isolated from column chromatographic separation and purified by washing with PE and EtOAc. After purification, these two compounds were stored for further studies.

Some Physicochemical Properties of Isolated Compounds

The isolated compounds were taken to determine the corresponding physical properties such as R_f values, melting points and solubilities in pet-ether, chloroform, ethyl acetate, ethanol and methanol. As well as some chemical properties were made on TLC chromatogram visualizing with 5 % H_2SO_4, vanillin-H_2SO_4, 1 % $FeCl_3$, Mg/HCl, Liebermann-Burchard reagent followed by heating and also treated with I_2 vapour, NH_3 vapour and NaOH.

Structural Elucidation and Identification

The structures of isolated compounds were elucidated and identified by modern spectroscopic techniques such as UV, FTIR, ^{1}H NMR and ^{13}C NMR.

***In vitro* Screening of Antiaggregatory Activity of Isolated Compounds**

To determine the effects of isolated compounds on platelet functions, *in vitro* tests such as platelet-agglutination, platelet-aggregation and clot-retraction were investigated by Ackroyd's methods at Pathology Department, Department of Medical Research, Yangon, Lower Myanmar.

(a) Blood collection

Blood was obtained from healthy volunteers who did not take any medication for 14 days and were fasting overnight prior to the study. Venous blood was collected into 1/10th volume of Acid-citrate-dectrose (ACD), in a polypropylene or siliconized glass tube. Approximately 10-20 mL of blood are needed a full aggregation study.

(b) Preparation of platelet-rich plasma (PRP)

Whole blood was collected into tubes with the anticoagulant EDTA and centrifuged for 10 min at 1500 rpm to remove the cells from plasma. The resulting supernatant is designated plasma or platelet-rich plasma (PRP). Following centrifugation, it was immediately transferred into a clean polyproplyene tube using a pipette.

(c) Preparation of serum

The whole blood was collected into a covered glass tube and allowed the blood to clot by leaving it undisturbed for 30 min at room temperature. Then remove the clot by centrifuging at 3500 rpm for 10 min. The resulting supernatant is designated as serum and it was immediately transferred into a clean polypropylene tube using a pipette.

(d) Preparation of test sample solutions

Each isolated compound (0.02 g) was dissolved in 1 mL of DMSO. These solutions were passed through a syringe filter PVDE 0.22 μm and then four-fold serial dilutions were made with normal saline to obtain solutions with the concentrations of 0.0312 μg, 0.125 μg, 0.5 μg and 2 μg/mL.

(i) Procedure for platelet-agglutination test

The same volumes of PRP, serum and serial diluted sample solutions were successively added into a respective small plastic tube and followed by incubating the mixture at 37 °C for 1 h. The mixture without serial diluted sample solutions served as a control. Then 30 μL of the mixture for each was dropped onto a slide and viewed under a microscope and the appearances on slide was recorded as well as compared with control (Dacie and Lewis, 1975).

(ii) Procedure for platelet-aggregation test

Only PRP as control and PRP with serial diluted sample solutions in each glass tube were agitated in water-bath at 37 °C and watched every 30 min followed by recording their appearances and compared with control (Dacie and Lewis, 1975).

(iii) Procedure for clot-retraction test

Only normal whole blood and whole blood with normal saline as control and whole blood with serial diluted sample solutions in each tube were warmed in water-bath at 37 °C. They were inspected after 2 h, 4 h, 6 h, 24 h and then their appearances were recorded and compared with control (Dacie and Lewis, 1975).

Results and Discussion

Preliminary Phytochemical Investigations

In order to find out the types of phytochemical constituents present in the rhizomes of black ginger, the preliminary phytochemical investigations were firstly carried out by the standard test tube methods. From these experiments, α-amino acids, flavonoids, glycosides, organic acids, phenolic compounds, saponins, starch, steroids and terpenoids were observed. However, alkaloids, carbohydrates, cyanogenic glycosides, reducing sugars and tannins were absent. These results are summarized in Table 1.

Table 1 Results of Preliminary Phytochemical Investigation on Black Ginger

No.	Types of Compounds	Extracts	Reagents	Observation	Remark
1.	Alkaloids	1% HCl	Mayer	No White ppt.	–
			Dragendorff Wagners	No Orange ppt.	–
				No Brown ppt.	–
2.	α–Amino acids	H_2O	Ninhydrin	Violet spot	+
3.	Carbohydrates	H_2O	10% α-napthol and conc. H_2SO_4	No Red ring	–
4.	Cyanogenic glycosides	H_2O	Sodium picrate	No Deep blue	–
5.	Flavonoids	EtOH	Mg and conc. HCl	Pink colour	+
6.	Glycosides	H_2O	10% lead acetate	White ppt.	+
7.	Organic acids	H_2O	Bromocresol green	Deep blue	+
8.	Phenolic compounds	H_2O	$K_3Fe(CN)_6$ and $FeCl_3$	Bluish black	+
9.	Reducing sugars	H_2O	Benedict's reagent	No brick-red ppt.	–
10.	Saponins	H_2O	Shaking	Frothing	+
11.	Starch	H_2O	Iodine	Bluish black	+
12.	Steroids	PE	H_2SO_4 and acetic anhydride	Colour change	+
13.	Tannins	H_2O	Gelatin and 1% $FeCl_3$	No ppt.	–
14.	Terpenoids	$CHCl_3$	H_2SO_4 and acetic anhydride	Colour change	+

\+ = present
– = absent

Preparation of Some Crude Extracts

After carrying out the preliminary phytochemical tests, to separate and isolate some organic constituents present in the rhizomes of black ginger, some crude extracts were successively prepared by Soxhlet extraction method. Phytochemical content in the rhizomes of black ginger is various so that different solvents were successively used by their polarity order. Data showed that watery extract had the highest yield (4.30 %) and then methanolic, ethanolic, ethyl acetate and petroleum ether extracts had yielded 2.87 %, 2.50 %, 1.92 % and 1.78 % respectively. These results informed that polar compounds can be easier to be extracted compared to non-polar compounds.

Separation, Isolation and Purification of Isolated Compounds

Compounds A and B were isolated from column chromatographic separation of 2.5 g of PE crude extract using silica gel GF_{254} as adsorbent and eluting with PE : EtOAc (20 : 1) as solvent system. Purification of these two compounds was done by washing with PE and EtOAc.

Some Physicochemical Properties of the Isolated Compounds

To identify the structures of isolated compounds, they were firstly characterized by determination of their physical properties such as R_f values, melting points and solubilities, and some chemical properties especially colour tests. To distinguish the steroid and terpenoid compounds, Liebermann-Burchard reagent was used. Steroidal compound gave blue green colour with the Liebermann-Burchard reagent in PE solvent and terpenoids provided pink colour in $CHCl_3$ solvent. Flavonoids were generally identified by treating with Mg in conc. HCl to give pink colour. 1% $FeCl_3$ was used for determining the phenolic compounds, giving deep blue/

green / brown colour. The isolated compounds were also characterized by colour tests with 5 % H_2SO_4, anisaldehyde-H_2SO_4, vanillin-H_2SO_4, Liebermann-Burchard on TLC chromatograms followed by heating, and also treated with I_2 vapour, NH_3 vapour, NaOH etc. The results of some physicochemical properties of the isolated compounds are illustrated in Tables 2 and 3.

Table 2 Some Physical Properties of the Isolated Compounds

No.	Isolated Compound	Physical State	Colour	Melting Point (°C)	R_f Value	Solvent system (PE : EtOAc)	Solubilities				
							PE	$CHCl_3$	EtOAc	EtOH	MeOH
1	A	solid	yellow	149–150	0.55	9 : 1 v/v	–	+,Δ	+, Δ	+, Δ	+, Δ
2	B	solid	yellow	144–146	0.31	9 : 1 v/v	–	+, Δ	+, Δ	+, Δ	+, Δ

\+ = soluble
– = insoluble

Table 3 Some Chemical Properties of the Isolated Compounds

No.	Isolated Compound	Spraying agents									Remark
		5 % H_2SO_4	vanillin - H_2SO_4	anisaldehyde- H_2SO_4	Liebermann-Burchard, Δ	1% $FeCl_3$	Con. HCl & Mg*	I_2 vapour	1% NaOH	NH_3 vapour	
1	A	yellow	yellow	yellow	yellow	black	yellow	yellow	yellow	yellow	Flavonoid
2	B	yellow	yellow	yellow	yellow	black	yellow	yellow	yellow	yellow	Flavonoid

Identification and Structural Elucidation of the Isolated Compounds

Compound **A** : 5-hydroxy-3,7-dimethoxy flavone (Sutthanut, 2007)

yellow needle

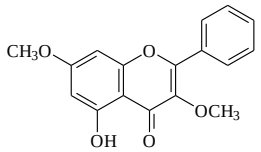

yield 0.057 %

m.pt 149 – 150 °C

TLC R_f = 0.55; PE : EtOAc = 9 : 1 v/v, yellow with 5%H_2SO_4, yellow with vanillin-H_2SO_4, yellow with anisaldehyde– H_2SO_4, Liebermann-Burchard, black with 1% $FeCl_3$, yellow with I_2 vapour, yellow with 1% NaOH, yellow with NH_3 vapour, active under UV

UV(MeOH), λ_{max} (nm) = 268, 346

MeOH / NaOH = 283, 360

MeOH / NaOAc = 267, 340

MeOH / NaOAc / H_3BO_3 = 267, 342

	MeOH / $AlCl_3$	= 276, 381
	MeOH / $AlCl_3$ / HCl	= 276, 381
IR	(KBr), ν_{max} = 3473, 3414, 2846, 1657, 1602, 1497, 1380, 1343, 1258, 1218, 1176, 1093, 1029, 1000, 815, 604 cm^{-1}	
^{1}HNMR	(400 MHz, $CDCl_3$), δ 12.58 (1H, s), 8.06 (2H, m), 7.54 (2H, m), 6.45 (1H, d), 6.35 (1H, d), 3.86 (6H, s) ppm	
^{13}CNMR	(400 MHz, $CDCl_3$), δ 55.87, 60.31, 92.26, 97.92, 106.16, 128.6, 130.49, 130.91, 139,72, 155.8, 156.90, 161.91, 165.53, 176.87 ppm	

Compound **B** : 5-hydroxy-3,7,4′-trimethoxy flavone (Sutthanut, 2007)

yellow needle

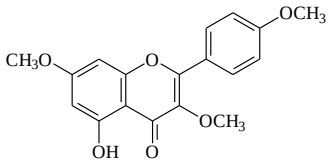

yield	0.035 %	
m.pt	144-146 °C	
TLC	R_f = 0.31; PE : EtOAc = 9 : 1 v/v, yellow spots with 5% H_2SO_4, vanillin-H_2SO_4, anisaldehyde–H_2SO_4, Liebermann- Burchard, I_2 vapour, 1%NaOH and NH_3 vapour, black with 1% $FeCl_3$, active under UV.	
UV, λ_{max} (nm)	MeOH	= 267, 339
	MeOH / NaOH	= 280, 364
	MeOH / NAoaC	= 269, 336
	MeOH / NaOAc / H_3BO_3	= 269, 336
	MeOH / $AlCl_3$	= 268, 342
	MeOH / $AlCl_3$ / HCl	= 274, 338
IR	(KBr), ν_{max} = 3451, 3076,2939,1657, 1603, 1503, 1455, 1433, 1376,1343, 1311,1253, 1226, 1166, 1199,1097, 1073, 999, 942, 895 cm^{-1}	
^{1}HNMR	(400 MHz, $CDCl_3$), δ 3.86 (3H, s), 3.87 (3H, s), 3.89 (3H, s), 6.36 (1H, d, J = 2.2 Hz), 6.44 (1H, d, J = 2.2 Hz), 7.02 (2H, d, J = 9.3 Hz), 8.07 (2H, d, J = 9.3Hz), 12.67 (1H, s, OH) ppm	
^{13}CNMR	(400 MHz, $CDCl_3$), δ 55.4, 55.8, 60.1, 92.2, 97.8, 106.0, 114.0, 122.8, 130.1, 138.8, 155.9, 156.7,161.6, 162.6,165.4, 178.7 ppm	

In vitro Antiaggregatory Activity of the Isolated Compounds

In vitro antiplatelet activity of the isolated compounds were investigated by screening on agglutination, aggregation and clot-retraction tests according to Ackroyd's method.

In agglutination test, only PRP in serum was used as control and the mixture was incubated at 37 °C for 1 h. When 30 μL of the mixture was dropped onto slide and viewed under

microscope, platelet-agglutination was found. This is due to the antibody in the serum activated the platelets to occur agglutination. However, platelets did not agglutinate by the antibody in the serum with serially diluted sample solutions. Therefore the isolated compounds can inhibit the action of agglutinant substances. These appearances are shown in Figure 2.

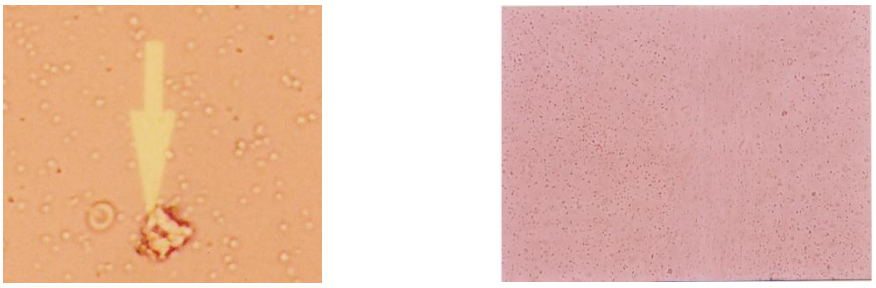

(a) (b)

Figure 2 Photographs of (a) platelet agglutination and (b) no agglutination under microscope

In aggregation test, only PRP was added into the polypropylene tube and used as control. When it was agitated in water-bath at 37 °C, platelets began suspension and their size increased as granule and then platelets aggregated as now flakes. However, PRP with serially diluted sample solutions in each tube did not show successive steps of aggregation. Therefore, the isolated compounds can prevent the activation process of platelets. This mechanism is illustrated in Figure 3.

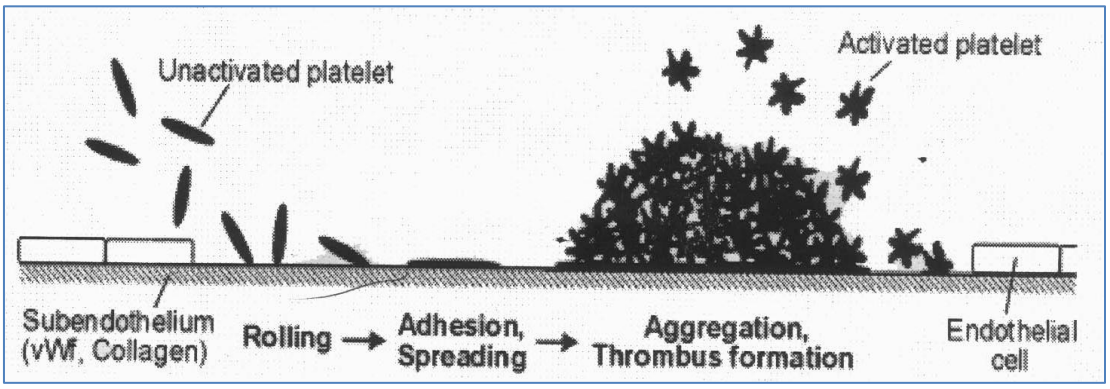

Figure 3 Mechanism of platelet aggregation (Fressinaud *et al*., 1994)

In clot-retraction test, only whole blood and whole blood with normal saline were used as controls. When they were allowed to clot at 37 °C, clotting was formed within a few minutes. Then, the blood clot began to contract and a straw colored fluid called serum was extruded out of the clot. This phenomena is called clot-retraction and it is caused by releasing of multiple coagulation factors from platelets trapped in the fibrin mesh of clot. In the case containing the serial diluted sample solutions, the prolong clot-retraction time was observed by extruding a little serum from the clot. Although normal clot-retraction time is 0-2 h, in this case prolonged nearly 6 h. This highlighted that isolated compounds can produce an inhibitory effect on the platelet functions. This appearance is shown in Figure 4.

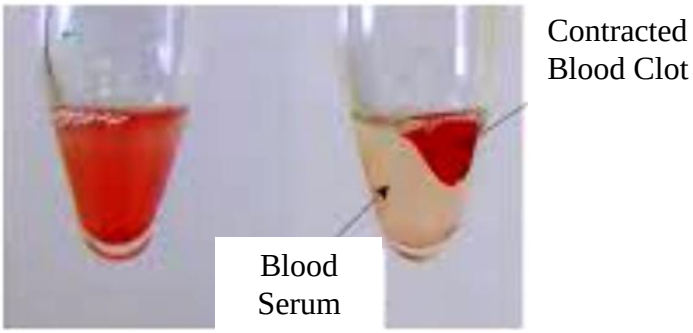

Figure 4 Photograph of clot-retraction (John, 2016)

According to the structure activity relationship (SAR), monohydroxylated flavones are most potent if substituted at position-6- of the A-ring (6-hydroxy flavone). However, most naturally occurring flavonoids are hdyroxylated at position 7, thus having lower antiaggregatory effect. Although increase in number of hydroxyl groups does not influence on antiaggregatory effect, o-methylation increases the activity (Bozina *et al*., 2009). This is probably due to greater volume and higher lipophilicity of the methyl group compared to hydroxyl group. Higher lipophilicity can lead to significant interactions with the platelet's membrane by increasing rigidity and can prevent the aggregation. Based on these observations, structure activity relationship between flavonoids and antiaggregatory activity revealed that two isolated compounds can inhibit the activation of platelet functions. Out of these, 5-hydroxy-3,7,4' -trimethoxy flavone (A) may be more potent than 5-hydroxy-3,7-dimethoxy flavone (B).

Conclusion

From the present investigations on the rhizomes of *Kaempferia parviflora* Wall. (Black Ginger), it could be deduced that the isolated flavonoids possess inhibitory effects on platelet activation and they may be used as platelet activation reducer and they can serve as source of information for further assessment of food or medicine influence on antiaggregation and anticoagulation treatment. Therefore, this structure activity relationship of flavonoids with the modulation of platelet function may guide the design, optimization and development of flavonoid scaffolds as antiplatelet agents.

Acknowledgements

I would like to express my profound gratitude to the Department of Higher Education (Yangon Office), Ministry of Education, Yangon, Myanmar, for provision of opportunity to do this research and Myanmar Academy of Arts and Science for allowing to present this paper.

References

Agrawal, A. D. (2011). "Pharmacological Activities of Flavonoids: A Review". *International Journal of Pharmaceutical Sciences and Nanotehcnology*, vol.4 (24), pp. 4

Bozina, N., Bradamanti, V. and Lovric, M. (2009). "Genetic Polymorphism of Metabolic Enzymes P450 (CYP) as a Susreptibility Factor for Drug Response, Toxicity and Cancer Risk". *Arh.Hig.Rada.Toksikol*, vol.60, pp. 217-242

Carola, R., Harley, J.P. and Nobock, C.R. (1990). *Human Anatomy and Physiology*. U.S.A: Mc Graw - Hill, Inc.,

Cesarone, M. R., Laurora, G., Ricci, A., Belcaco, G. and Pomante, P. (1992). "Acute Effects of Hydroxyethylrutosides on Capillary Filtration in Normal Volunteers, Patients with Various Hypotension and in Patients with Diabetic Micro Angiopathy". *J. Vas. Disease*, vol.21, pp. 76-80

Dacie, J.V. and Lewis, S.M. (1975). *Practical Haematology*. London: 5th Edition, Churchill Livingstone

Fressinaud, E., Federici, A.B., Gastaman, G., Rothschild, C., Rodeghiero, F., Baumgartner, H. R., Mannucci, P. M. and Meyer, D. (1994). "The Role of Platelet von Willebrand Factor in Platelet Adhesion and Thrombus Formation; A Study of 34 Patients with Various Subtypes of Type I von Willebrand Disease", *Br. J. Haematol*, vol.86, pp. 327-332

John, W. W. (2016). *Coagulation Changes Related to RBC Tranfusion*. FDA Workshop, pp. 8

Kress, W. J., Defilipps, R. A., Farr, E. and Daw Yin Yin Kyi. (2003). *A Checklist of the Trees, Shrubs, Herbs and Climbers of Myanmar*. Washington, DC: United States National Herbarium, Smithsonian Institution, vol.45, pp. 120, 123

M-Tin Wa. (1970). "Phytochemical Screening, Methods and Procedures". *Phytochemical Bulletin of Botanical Society of America*. vol.5(3), pp. 4-10

Saokaew, S., Wilairat, P., Paktanyakan, P., Dilokthornsakul, P., Dippayom, T., Kongkaew, C., Sruamsiri, R., Chuthaputti, A. and Chaiyakunapruk, N. (2016). "Clinical Effects of Krachaidum (*Kaempferia parviflora*): A Systematic Review". *Journal of Evidence-Based Complementary & Alternative Medicine*, vol.22(3), pp.413-428

Sutthanut, K., Sripanidkulchai, B., Yenjai, C. and Jay, M. (2007). "Simultaneous Identification and Quantitation of 11 Flavonoid Constituents in *Kaempferia parviflora* by Gas Chromatography". *Journal of Chromatography A*, vol.11(43), pp. 227–233

Sweetman, C. M. (2004). *The Complete Drug Reference*. London: Pharmaceutical Press

Tzeng, S.H., Ko, W.C., Ko F. N. and Teng, C. M. (1991). "Inhibition of Platelet Aggregation by Some Flavonoids". *Thromb. Res.* vol.64, pp. 91-100

BIOSYNTHESIS OF ZINC OXIDE NANOPARTICLES USING FRUITS AND LEAVES EXTRACTS OF *TERMINALIA CHEBULA* RETZ.

Sandar Myint[1], Ni Ni Sein[2], Thida Win[3]

Abstract

Green synthesis of metal oxide nanoparticles using plant extract is a promising alternative to traditional method of chemical synthesis. The biosynthesis of zinc oxide nanoparticles using fruits and leaves extracts of *Terminalia chebula* Retz. has been reported in this study. It is simple, cost-effective, rapid and eco-friendly way to synthesize zinc oxide nanoparticles. The ZnO nanoparticles were characterized by X-ray diffraction (XRD), scanning electron microscopy (SEM), ultraviolet-visible (UV-Vis) and Fourier transform infra-red (FT IR). The structure of ZnO nanoparticles was indexed as hexagonal structure. The crystallite sizes of ZnO nanoparticles from fruits and leaves extracts of *T. chebula* were calculated by Scherrer formula as 17.0 nm and 23.4 nm, respectively. Morphology of nanocrystals was observed to be aggregated spherical particles. UV absorption spectra of ZnO nanoparticles using fruits and leaves extracts of *T. chebula* indicated the absorption maxima at 376 and 375 nm, respectively. This new eco-friendly approach of synthesis is a novel, cheap, and convenient technique suitable for large scale commercial production.

Keywords: *Terminalia chebula* Retz., green synthesis, ZnO nanoparticles, *T. chebula* , hexagonal structure

Introduction

Nanoparticles are particulate materials with at least one dimension of less than 100 nanometers (nm). Metal nanoparticles have been of great interest due to their distinctive features such as catalytic, optical, magnetic and electrical properties (Garima *et al*., 2011). These nanoscale sized particles possess a larger surface area as compared to microsized particles leading to enhanced properties (Tripathi *et al*., 2014). Nanoparticles present a higher surface area to volume ratio with decrease in the size, distribution and morphology of the particles (Awwad *et al*., 2012).

Researchers are using green methods for the synthesis of various metal oxide nanoparticles because these methods are considered safe and ecologically sound the nanomaterials fabrication as an alternative to conventional methods (Liu and Lin, 2004; Yu, 2007). Chemicals used for nanoparticles synthesis and stabilization are toxic and lead to non-ecofriendly byproducts. Biological approaches using microorganisms and plant or plant extracts for nanoparticles have been suggested as valuable alternatives to chemical methods. Several biological systems including bacteria, fungi, and yeast have been used in synthesis of nanoparticles (Alagummuthu and Kirubha, 2012). Using microorganisms for the synthesis of nanoparticles were found to be more tedious and required more steps in maintaining cell culture, intracellular synthesis with more purification steps. The use of plants known as 'Green synthesis' or 'Biogenic synthesis' shows better advancement over chemical and physical methods as it is lesser toxic, cost effective, environmental friendly (Vidya *et al*., 2013) and also involves proteins as capping agents (Sangeetha *et al*., 2011).

The biosynthesis of Zinc oxide (ZnO) nanoparticles gains significant credit with reference to their cost-effective, nontoxic, self-aggregation, antibacterial and gas sensing properties. ZnO nanoparticles play vital role in the synthesis of biological pigments, photocatalytic issues, production of piezoelectric devices, chemical sensors, drug carriers in targeted drug delivery

[1] Lecturer, Department of Chemistry, Nationalities Youth Resources Development Degree College, Sagaing
[2] Dr, Professor (Retd.), Department of Chemistry, University of Yangon
[3] Rector, Dr, University of Mandalay

mechanisms, and the production of cosmetics such as sunscreen lotions etc. Zinc oxide efficiently protects broader UV range than other molecular UV-absorbers. Zinc oxide nanoparticles are employed in various biological and pharmacological applications due to its non-toxic nature.

Recently various parts of plants proved to be the potential reducing agents for production of nanoparticles. Leaves, stem, fruits, flowers, seeds, barks and gums were employed for the synthesis of eco-friendly nontoxic nanoparticles with valuable biomedical properties. Plant based zinc oxide nanoparticles are widely accepted in cosmetic industry and agriculture (Manokari *et al*., 2016). So, this study is aimed to synthesize ZnO nanoparticles with a simple, rapid, cost-effective and environmentally synthesis method of using fruits and leaves extracts of *Terminalia chebula* .

Materials and Methods

Sample Collection

Fruits and leaves of *Terminalia chebula* (Phanga) were collected from Phayapyo village, Magway Township in Magway Region, Myanmar. The botanical name was identified at Department of Botany, Magway University.

Preparation of Aqueous Extract of *Terminalia chebula*

Fresh fruits and leaves of *T. chebula* were washed several times with deionized water to remove dust particles and then air dried to remove the residual moisture for 1 day. The seed from the *T. chebula* fruit were removed and the remaining part was crushed by using an electronic blender. The leaves of *T. chebula* were cut into small pieces and then crushed by using an electronic blender. Fruits extract and leaves extract of *T. chebula* were prepared by mixing 50 g of plant sample with 500 mL of deionized water in a 1000 mL glass beaker. The mixture was heated for 2 h at 80 °C by using a magnetic stirrer. Then, the extract was cooled to room temperature and filtered with Whatman No. 1. filter paper and used for further experiments.

Synthesis of ZnO NPs

Zinc nitrate ($Zn(NO_3)_2.6H_2O$) (29.739 g) was accurately weighed and it was dissolved in deionized water and the volume was made up to 100 mL with deionized water to obtain 1 M solution. For the volume ratio of 1:2 of $Zn(NO_3)_2$ and plant extracts, 100 mL of $Zn(NO_3)_2$ solution was transferred to a 1000 mL beaker and heated for 15 min at 70 °C by using a magnetic stirrer. Then, 200 mL of plant extracts was added drop-wise and the resulting mixture was heated for 2 h at 70 °C using a stirrer-heater. The mixture was then dried in oven at temperature 100 ± 5 °C for 1 h and pale brown powder was obtained. It was washed several times with deionized water followed by washed with EtOH in 3 times. Then, pale yellow powder was calcined in a muffle furnace for 2 h at 400 °C and finally white powder ZnO was obtained. This powder was carefully collected and packed for characterization purposes. Similarly 300 mL and 400 mL of plant extracts were used to get volume ratios of 1:3 and 1:4, respectively and the experiment was carried out according to above procedure.

Characterization ZnO Nanoparticles

X-ray diffraction analysis

ZnO nanoparticles were examined by X-ray diffractometer (Rigaku Co., Tokyo, Japan) equipped with Cu K_α radiation of 1.54056 Å wavelength at Universities' Research Center, Yangon. All XRD data were collected under the same experimental conditions, in the angular range of 2θ 10° to 70° at an accelerating voltage of 40 kV.

Scanning Electron Microscopy and Transmission Electron Microscopy

A scanning electron microscope (ZEISS) operating at an accelerating voltage of 10 kV was used to observe the morphology of zinc oxide sample at West Yangon University and transmission electron microscope (TEM, JEOL TEM-3010) with an accelerating voltage of 100 kV (State Key Laboratory, College of Science , Beijing University of Chemical Technology, China) was used to investigate the size and morphology. The crystallite sizes of ZnO NPs were calculated by using Image J software programme.

Fourier transform infrared spectroscopy (FT IR)

FT IR for ZnO nanoparticles was obtained in the range 4000–400 cm^{-1} with FT IR spectrometer (FT IR-8400 SHIMADZU, Japan).

UV-vis Spectroscopy

The optical property of biosynthesized ZnO nanoparticles samples were measured at room temperature by UV-vis spectrophotometer (Shimadzu UV-1800)operated at a resolution of 1 nm between 200 and 400 nm. The ZnO nanoparticles were separately dispersed in distilled water and ethanol with concentration of 0.1 % each and then the solution were subjected for UV–visible measurements.

Results and Discussion

Effect of Volume Ratio of $Zn(NO_3)_2$ and Fruits and Leaves Extracts of *T. chebula*

In the biosynthesis of ZnO nanoparticles, three different volume ratios of $Zn(NO_3)_2.6H_2O$ and fruits and leaves extracts of *T. chebula* (1:2, 1:3 and 1:4) were investigated. After heating at 400 ^oC, white precipitate of ZnO samples were obtained. As the volume of the extract of fruits and leaves of *T. chebula* increased from 200 mL to 400 mL, the amount of ZnO increased. Higher amounts of ZnO were obtained using 400 mL of fruits and leaves extracts of *T. chebula* i.e. (7.1037 g) and (7.0943 g) respectively (Table 1). However, the amount of ZnO obtained using 400 mL of the extracts was not much different from that using 300 mL of the extracts. Yield percent of ZnO were 87.2798 % and 87.1643 % prepared by using 1:4 volume ratio of $Zn(NO_3)_2$ and fruits and leaves extracts of *T. chebula.*

Table 1 Amount of ZnO and Yield % of ZnO Prepared by Using Fruits and Leaves Extracts of *T. chebula*

No.	Volume of 1M $Zn(NO_3)_2$ (mL)	Volume of extract (mL)	Amount of ZnO (g)		Yield of ZnO(%)	
			Fruits extract	Leaves extract	Fruits extract	Leaves extract
1	100	200	6.0276	5.7112	74.0582	70.1708
2	100	300	6.9298	6.7592	85.1431	83.0471
3	100	400	7.1037	7.0943	87.2798	87.1643

Characterization by X-ray Diffraction Method

X-ray Powder Diffraction (XRD) studies were carried out to confirm the phase purity. Figures 1 and 2 show the XRD patterns of ZnO nanoparticles synthesized using leaves and fruits extracts of *T. chebula*. All the peaks of (100), (002), (101), (102),(110), (103) and (112) in both XRD patterns were found to be well-resolved. The presence of (100),(002) and(101) planes in XRD patterns indicates the formation of high purity of the ZnO nanoparticles. All peaks are in good agreement with standard diffraction data (80-0075 > ZnO). This clearly confirms that ZnO nanoparticles has been successfully synthesized by green

synthesis route. Furthermore, no impurity peaks were observed. Strong intensity and narrow width of ZnO diffraction peaks indicated that the resulting product was highly crystalline in nature.

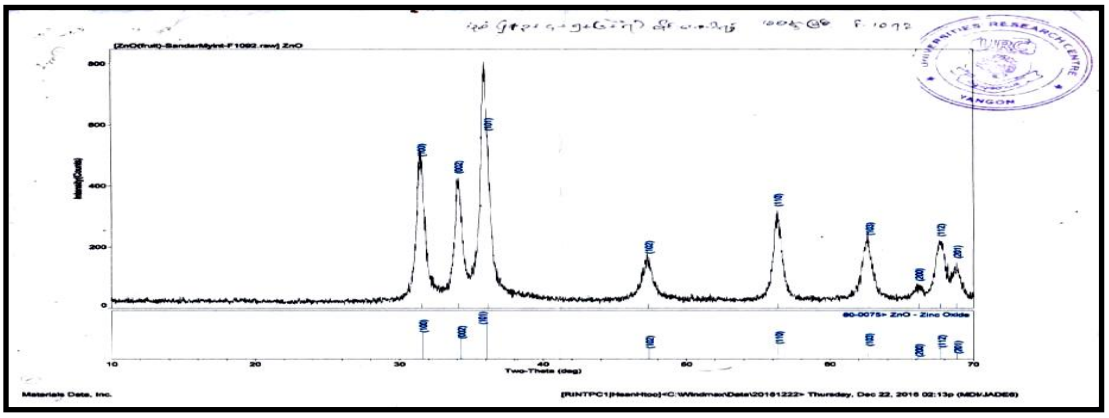

Figure 1 XRD pattern of ZnO prepared by using *T. chebula* fruits extract

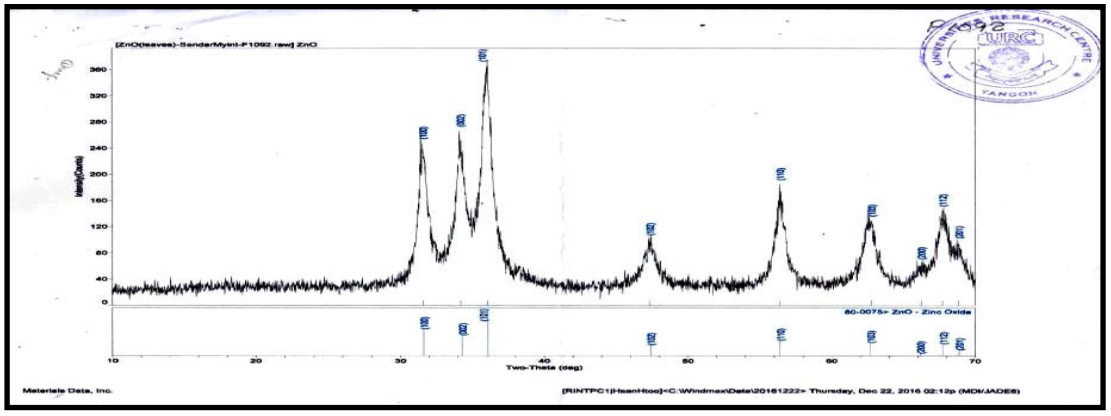

Figure 2 XRD pattern of ZnO prepared by using *T. chebula* leaves extract

The average crystallite sizes of green synthesized zinc oxide particles were calculated by using Debye Scherrer equation, $\tau = \frac{0.9\lambda}{\beta \cos\theta}$, where τ is the crystallite size, λ is the wavelength of the X-ray used, β is the full width at half maximum (FWHM) of the peak in radians and θ is the diffraction angle or the Bragg angle of the peak (Jenkins and Snyder, 1996).

Tables 2 and 3 show the calculated crystallite sizes of ZnO prepared from fruits and leaves extracts of *T. chebula* and those obtained by peak search report. Average crystallite sizes of ZnO nanoparticles prepared using fruits and leaves extracts were 17.0 nm and 23.4 nm respectively. Calculated values were not much different from those given by peak search report from XRD data. Crystallite size of ZnO from fruits extract was found to be smaller than that from leaves extract. ZnO obtained from both extracts were in the nano range.

Table 2 Crystallite Size of ZnO Prepared by Using *T.chebula* Fruits Extract

No.	Diffraction Angle '2θ' (°)	Full Width at Half Maximum 'β' (°)	Full Width at Half Maximum 'β' (radian)	Calculated Crystallite Size (nm)	Crystallite Size from XRD Data (nm)
1	31.499	0.515	0.0090	16.0	16.3
2	34.137	0.481	0.0084	17.3	17.7
3	35.975	0.555	0.0097	15.1	15.3
4	47.274	0.602	0.0105	14.4	14.6
5	56.358	0.553	0.0097	16.3	16.6
6	62.516	0.650	0.0113	14.3	14.5
7	66.080	0.350	0.0061	27.1	28.3
8	67.691	0.684	0.0119	14.0	14.1
9	68.853	0.520	0.0091	18.5	18.9
Average crystallize size				17.0	17.4

Table 3 Crystallite Size of ZnO Prepared by Using *T.chebula* Leaves Extract

No.	Diffraction Angle '2θ' (°)	Full Width at Half Maximum 'β' (°)	Full Width at Half Maximum 'β' (radian)	Calculated Crystallite Size (nm)	Crystallite Size from XRD Data (nm)
1	31.577	0.618	0.0108	13.4	13.5
2	34.190	0.537	0.0094	15.5	15.8
3	36.084	0.621	0.0108	13.4	13.6
4	47.318	0.657	0.0115	13.2	13.4
5	56.400	0.551	0.0096	16.4	16.7
6	62.540	0.566	0.0099	16.4	16.7
7	65.948	0.147	0.0026	64.4	87.7
8	67.704	0.490	0.0086	19.5	20.0
9	68.828	0.252	0.0044	38.2	41.7
Average crystallize size				23.4	26.6

Tables 4 and 5 show phase identification by X-ray diffraction analysis. It was observed that only single phase of ZnO with no other phase was found. It indicates the purity of the ZnO sample.

Table 4 Phase Identification of ZnO Prepared by Using Fruits Extract of *T.chebula*

No.	Diffraction Angle '2θ' (°)	Interplanar Spacing 'd' (Å)	Miller Indices (hkl)	Phase ID
1	31.499	2.8378	100	ZnO
2	34.137	2.6243	002	ZnO
3	35.975	2.4944	101	ZnO
4	47.274	1.9212	102	ZnO
5	56.358	1.6311	110	ZnO
6	62.516	1.4845	103	ZnO
7	66.080	1.4128	200	ZnO
8	67.691	1.3830	112	ZnO
9	68.853	1.3625	201	ZnO

Table 5 Phase Identification of ZnO Prepared by Using Leaves Extract of *T.chebula*

No.	Diffraction Angle '2θ' (°)	Interplanar Spacing 'd' (Å)	Miller Indices (hkl)	Phase ID
1	31.577	2.8310	100	ZnO
2	34.190	2.6204	002	ZnO
3	36.084	2.4871	101	ZnO
4	47.318	1.9195	102	ZnO
5	56.400	1.6300	110	ZnO
6	62.540	1.4840	103	ZnO
7	65.948	1.4153	200	ZnO
8	67.704	1.3828	112	ZnO
9	68.828	1.3629	201	ZnO

Lattice constants and crystal structure of ZnO nanoparticles obtained by using fruits and leaves extracts of *T.chebula* are shown in Table 6. By XRD analysis ZnO obtained from fruits and leaves extracts were indexed to the hexagonal wurtzite structure with equal length of ´a´ and ´b´ (3.2739 Å and 3.2672 Å respectively) and longer ´c´ (5.2313 Å and 5.2243 Å respectively).

Table 6 Lattice Constants and Crystal Structure for ZnO Prepared by Using Fruits and Leaves Extracts of *T.chebula*

No.	Sample	Lattice Constant (Å)			Crystal structure
		a-Axis	b-Axis	c-Axis	
1	ZnO (fruits extract)	3.2739	3.2739	5.2313	Hexagonal
2	ZnO (leaves extract)	3.2672	3.2672	5.2243	Hexagonal

Surface Morphology of Zinc Oxide Nanoparticles Prepared by Using Fruits and Leaves Extracts of *T.chebula* Retz.

The scanning electron microscopy was used for the morphological study of zinc oxide nanoparticles from fruits and leaves of *T.chebula*. Agglomeration of ZnO nanoparticles were observed in ZnO nanoparticles prepared by using fruits and leaves extracts of *T.chebula* (Figure 3). SEM image of ZnO nanoparticles prepared by using *Trifolium pratense* flower extract also showed agglomerated particles of ZnO (Dobrucka and Dugaszewska, 2016; Suresh, *et al*., 2015).

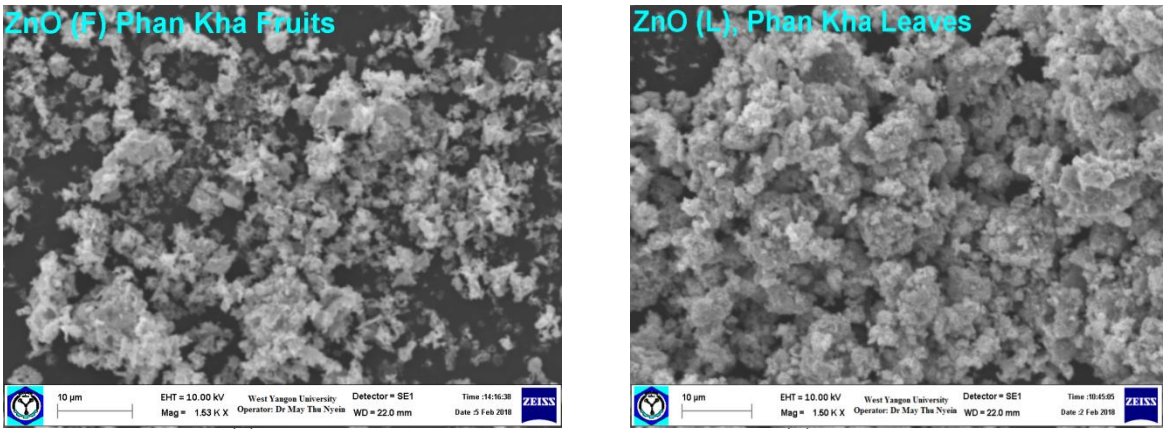

Figure 3 SEM images of ZnO nanoparticles prepared by using *T. chebula* (a) fruits extract and (b) leaves extract

Figure 4 shows the TEM images of ZnO nanoparticles prepared by using *T. chebula* leaves and fruits extracts. Crystallite sizes of ZnO nanoparticles obtained by using fruits and leaves extracts were 20.5 nm and 25.1 nm by TEM analysis which were not much different from those obtained by XRD analysis, 17.0 nm and 23.4 nm, respectively.

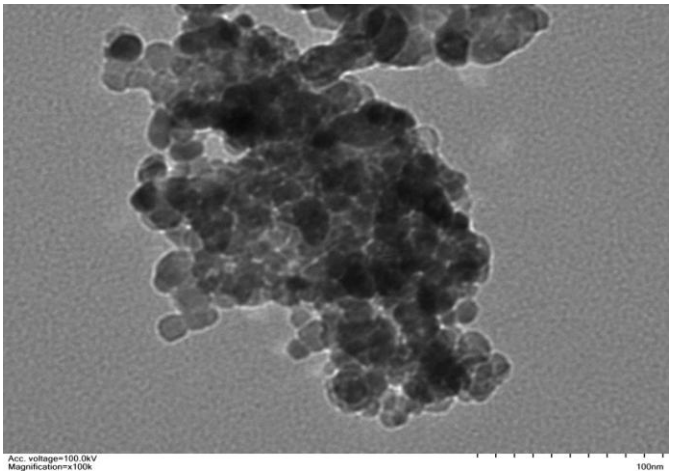

(a)

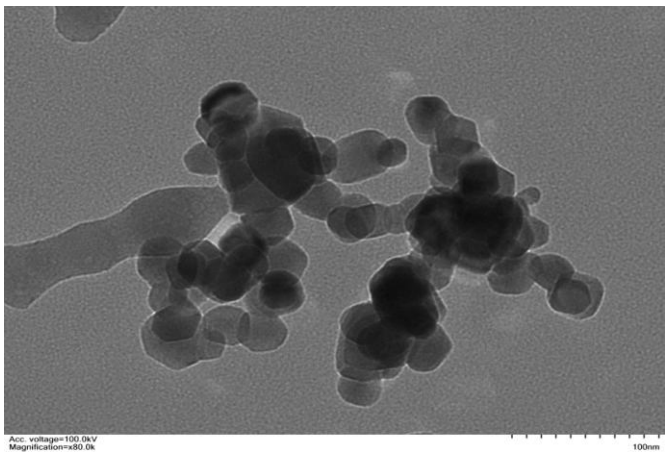

(b)

Figure 4 TEM images of ZnO nanoparticles of (a) fruits and (b) leaves extracts of *T. Chebula* (magnification X 80.0 K)

Characterization by FT IR Spectroscopy

Green synthesized zinc oxide nanoparticles by using fruits and leaves extracts of *T. chebula* were characterized by FT IR technique. Figures 5 and 6 show the FT IR spectra of green synthesized zinc oxide nanoparticles of fruits and leaves extracts of *T. chebula*. FT IR analysis showed the characteristic absorption bands of ZnO from fruits extract of *T. chebula* at 437 cm^{-1} and ZnO from leaves extract at 439 cm^{-1} (Table 7) . The peak in the region between 400 and 600 cm^{-1} was assigned to ZnO region (Yuvakkumar *et al*., 2015).The absorption band at 3435 cm^{-1} was assigned to stretching vibration of O-H stretching vibration of physically absorbed water molecules (Karthikeyan *et al*., 2016).

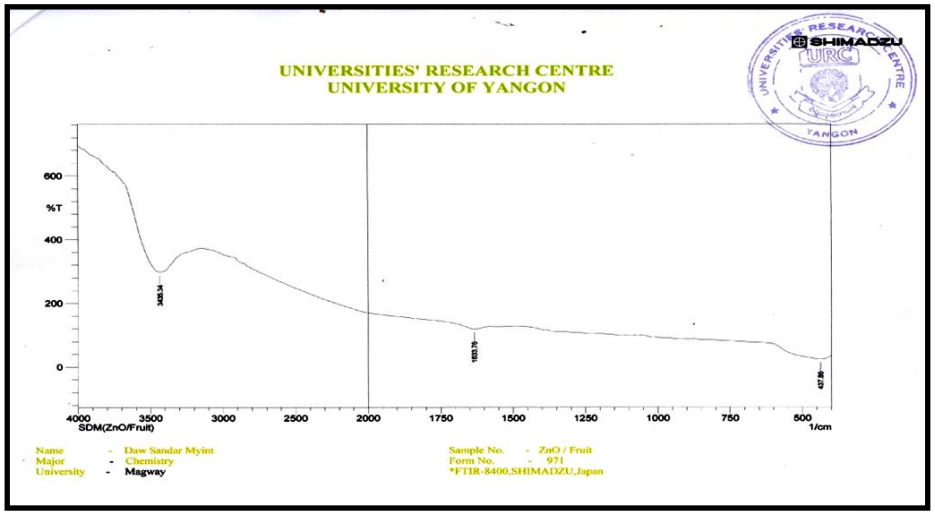

Figure 5 FT IR spectrum of ZnO prepared by using fruits extract of *T. chebula*

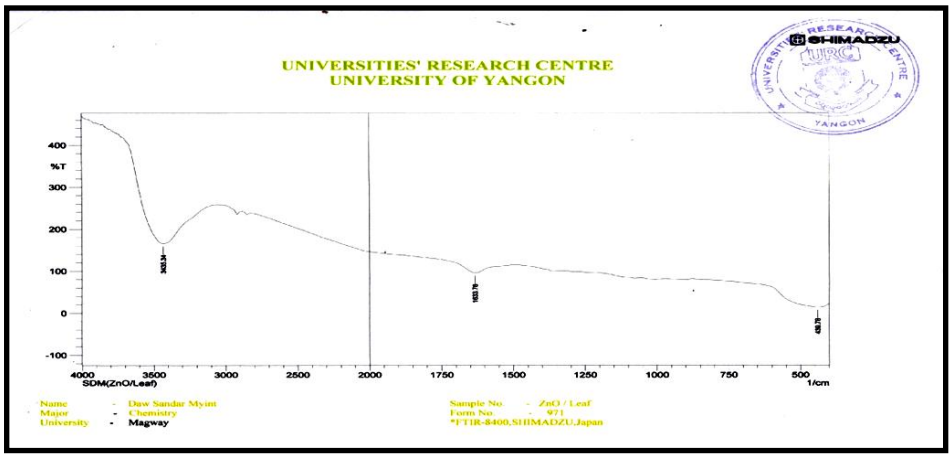

Figure 6 FT IR spectrum of ZnO prepared by using leaves extract of *T. chebula*

Table. 7 FT IR Spectral Data for ZnO Nanoparticles Prepared by Using Fruits and Leaves Extracts of *T.chebula*

No.	Wavenumber (cm^{-1})		Assignment*
	Fruits	Leaves	
1	3435	3435	O – H stretching vibration
2	437	439	Zn – O stretching vibration

* Karthikeyan *et al*., 2016; Yuvakkumar *et al*., 2015

UV Spectrum of ZnO Nanoparticles

Green synthesized zinc oxide nanoparticles of fruits and leaves of *T. chebula* were characterized by UV-visible spectroscopy. Figures 7 and 8 show the absorption spectra of ZnO nanoparticles synthesized using leaves and fruits extracts of *T.chebula*. The spectra revealed characteristic absorption peaks of ZnO prepared using leaves extract and fruits extract at wavelength of 375 nm and 376 nm, respectively. The absorption of ZnO was due to the excitation of valence electrons from the valence band to the conduction band (O2p–Zn3d) (Azarang *et al*., 2015). This implies that the ZnO nanoparticles absorb light in the ultra-violet region (Huang *et al*., 2006). The good absorption of the ZnO-NPs in the UV region proves the applicability of this product in such medical application such as sunscreen protectors or as

antiseptic ointments (Gupta, 2014). ZnO nanoparticles using aqueous *Cassia fistula* plant extract showed the absorption band at 370 nm (Suresh *et al*., 2015). Ramasami *et al*. (2017) also reported the ZnO absorption peak at 373 nm. Lakshmi *et al*. (2017) reported the absorption maximum of ZnO synthesized from spinach leaves extract at 375.4 nm and Awwad *et al.* (2012) with 374 nm. Thus, prepared ZnO nanoparticles were also confirmed by UV-visible absorption spectroscopy.

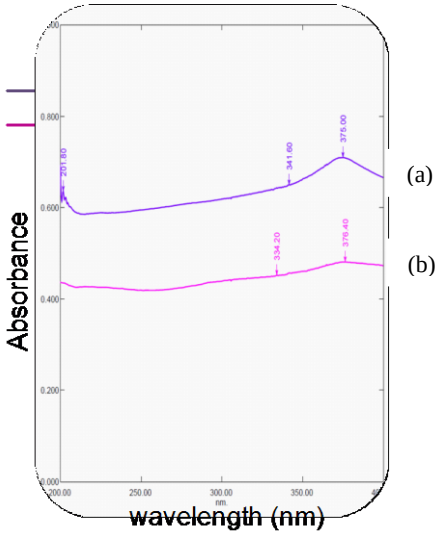

Figure 7 UV absorption spectra of ZnO prepared by using *T. chebula* (a) leaves and (b) fruits extracts (in distilled water)

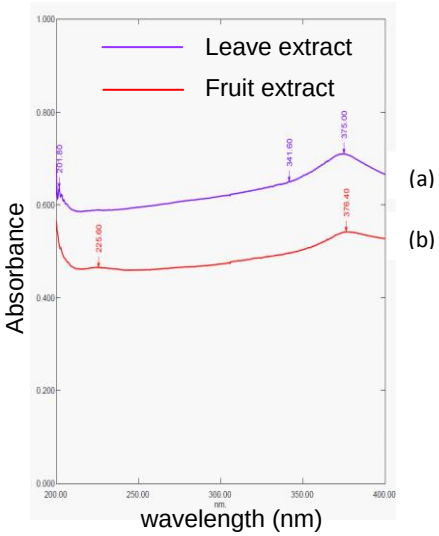

Figure 8 UV absorption spectra of ZnO prepared by using *T. chebula* (a) leaves and (b) fruits extracts (in ethanol)

.

Conclusion

ZnO nanoparticles were successfully prepared by using fruits and leaves extracts of *Terminalia chebula* Retz.via green route. It is simple, cost-effective, rapid and eco-friendly way to synthesize zinc oxide nanoparticles. The structure of nanoparticles was indexed as hexagonal using XRD analysis. The crystallite sizes of ZnO nanoparticles from fruits and leaves extracts of *T. chebula* were 17.0 nm and 23.4 nm, respectively. Morphology of ZnO nanoparticles was investigated using the SEM and observed as spherically aggregates particles. The crystallite size by TEM analysis was 20.5 nm for ZnO nanoparticles using fruits extract and 25.1 nm for leaves extract. FT IR absorption spectra showed the characteristic absorption bands of ZnO at 437 and 439 cm^{-1}, respectively, for ZnO nanoparticles using fruits and leaves extracts of *T. chebula*. The optical properties of particles were studied with UV-Vis spectroscopy and both ZnO nanoparticles showed almost the same absorption maxima. Thus, from this present study it was concluded that fruits and leaves extracts of *T. chebula* can be effectively used for synthesizing the zinc oxide nanoparticles. This approach offers environmentally advantageous alternatives to more hazardous chemicals and processes and promotes pollution prevention by the production of nanoparticles in their natural surroundings.

Acknowledgement

The authors would like to thank the Myanmar Academy of Art and Science for allowing to present this paper.

References

Alagummuthu, G. and Kirubha, R. (2012). "Green Synthesis of Silver Nanoparticles using *Cissus quadrangularis* Plant Extract and their Antibacterial Activity". *Int. J.Nano Mat Bio.*, vol.2 (3), pp. 30-33

Awwad, A.M, Albiss, B. and Ahmad, A.L. (2014). "Green synthesis,Characterization and Optical Properties of Zinc Oxide Nanosheets using *Olea europea* Leaf Extract". *Adv Mat Lett*., vol.5, pp. 520-524

Awwad, A.M., Salem, N.M. and Abdeen, A.O. (2012). "Biosynthesis of Silver Nanoparticles using *Olea europaea* Leaves Extract and its Antibacterial Activity". *Nanoscience and Nanotechnology*, vol.2(6), pp. 164-170

Azarang, M., Shuhaimi, A., Yousefic, R. and Jahromia, S.P. (2015). "One-pot Sol–gel Synthesis of Reduced Graphene Oxide Uniformly Decorated Zinc Oxide Nanoparticles in Starch Environment for Highly Efficient Photodegradation of Methylene Blue". *RSC Adv*., vol.5, pp. 21888–21896

Dobrucka, R. and Dugaszewska, J. (2016). **"**Biosynthesis and Antibacterial Activity of ZnO Nanoparticles using *Trifolium pretense* Flower Extract**".** *Saudi Journal of Biological Sciences*, vol.23, pp. 517–523

Garima, S., Bhavesh, R., Kasariya, K.R., Sharma, A.R. and Singh, R.P. (2011)."Biosynthesis of Silver Nanoparticles using *Ocimum sanctum* (Tulsi) Leaf Extract and Screening its Antimicrobia Activity". *J. Nanoparticle Res.*, vol.13, pp. 2981-2988

Gupta, M., Mahajan, V.K., Mehta, K.S. and Chauhan, P.S. (2014). "Zinc Therapy in Dermatology: A Review". *Dermatology Research and Practice*, vol. 2014(9), pp. 1-11

Huang, G.G., Wang, C.T., Tang, H.T., Huang, Y.S. and Yang, J. (2006). "ZnO Nanoparticle Modified Infrared Internal Reflection Elements for Selective Detection of Volatile Organic Compounds". *Analytical Chemistry,* vol.78, pp. 2397–2404

Jenkins, R. and Snyder, R. (1996). *Introduction to X-ray Powder Diffractometry*. New York : John Wiley & Sons, Inc.

Karthikeyan, V., Dhanapandian, S. and Manoharan, C. (2016). "Characterization and Antibacterial Behavior of MgO Nanoparticles Synthesized via Co-precipitation Method". *International Journal for Scientific Research and Development,* vol.10 (1), pp. 2321-2323

Lakshmi, S.J., Bai, R.S.R., Sharanagouda, H., Ramachandra, C.T., Nadagouda, S. and Doddagoudar, S.R. (2017). **"**Biosynthesis and Characterization of ZnO Nanoparticles from Spinach (*Spinacia oleracea*) Leaves and Its Effect on Seed Quality Parameters of Greengram (*Vigna radiata*) ". *Int.J.Curr.Microbiol. App.Sci* ., vol.6(9), pp. 3376-3384

Liu, Y.C. and Lin, L.H. (2004). **"**New Pathway for the Synthesis of Ultrafine Silver Nanoparticles from Bulk Silver Substrates in Aqueous Solutions by Sonoelectrochemical Methods". *Electrochem. Commun.,* vol.6, pp.1163-1168

Manokari, M., Ravindran, C.P. and Shekhawat, M.S. (2016). **"**Biosynthesis and Characterization of Zinc Oxide Nanoparticles using Plant Extracts of *Peperomia pellucida* L. and *Celosia argentea* L." *International Journal of Botany Studies*, vol.1(2), pp.32-37

Ramasami, A.K., Ravishankar, T.N., Nagaraju, G., Ramakrishnappa, T., Teixeira, S.R. and Balakrishna, R.G. (2017). "Gel–Combustion–Synthesized ZnO Nanoparticles for Visible Light–Assisted Photocatalytic Hydrogen Generation". *Bulletin of Material Science*, vol. 40 (2), pp. 345-354

Sangeetha, G., Rajeshwari, S. and Venkatesh, R. (2011). **"**Green Synthesis of Zinc Oxide Nanoparticles by Aloe Barbadensis Miller Leaf Extract: Structure and Optical Properties". *Mater. Res. Bull*., vol.46, pp. 2560–2566

Suresh, D., Nethravathi, P.C., Udayabhanu, C.G., Rajanaika, H., Nagabhushana, H. and Sharma, S.C. (2015). "Green Synthesis of Multifunctional Zinc Oxide (ZnO) Nanoparticles using *Cassia fistula* Plant Extract and their Photodegradative, Antioxidant and Antibacterial Activities". *Materials Science in Semiconductor Processing,* vol.31, pp. 446–454

Tripathi, P.K., Gan, L.H., Liu, M.X. and Rao, N.N. (2014). "Mesoporous Carbon Nanomaterials as Environmental Adsorbents ". *J. Nanosci. Nanotechnol*., vol.14 , pp. 1823–1837

Yu,D.G.(2007). **"**Formation of Colloidal Silver Nanoparticles Stabilized by Na+-Poly(-Glutamic Acid) Silver Nitrate Complex via Chemical Reduction Process". *Colloids and Surfaces B: Biointerfaces* , vol. 59, pp. 171-178

Yuvakkumar, R., Suresh, J., Saravanakumar, B., Nathanael, A.J., Hong, A.S. and Rajendran, V. (2015). "Rambutan Peels Promoted Biomimetic Synthesis of Bioinspired Zinc Oxide Nanochains for Biomedical Applications". *Spectrochimica Acta Part A: Molecular and Biomolecular Spectroscopy*, vol.137, pp. 250-258

Vidya, C., Hiremath, S., Chandraprabha, M.N., Antonyraj, L.M.A., Gopal, I.V., Jain, A. and Bansal, K. (2013). **"**Green Synthesis of ZnO Nanoparticles by *Calotropis gigantea*". *International Journal of Current Engineering and Technology Special Issue,* vol.1, pp. 118-120

STUDY ON THE ADSORPTION OF CARBON DIOXIDE USING CARBON- ZEOLITE COMPOSITE

Nwe Ni Win[1], May Nwe Win[2], Kyaw Myo Naing[3]

Abstract

Nowadays, carbon dioxide is produced extensively by using many industrial processes and domestic processes. The greatest physiological effect of carbon dioxide is to stimulate the respiratory center, able to cause dilation and constriction of blood vessels and formed the environmental impact. In this paper, composite carbon-zeolite sorbent was prepared and utilized to study the adsorption of carbon dioxide. The adsorption of carbon dioxide on carbon-zeolite composite was measured by using volumetric method. The adsorption capacity was studied by using Langmuir equation, Freundlich equation and Temkin equation. The comparison of these results with that of zeolite molecular sieve was also presented. It was observed that very high carbon dioxide uptake was observed with composite during gas adsorption studies.

Keywords: carbon-zeolite composite, zeolite molecular sieve, adsorption of CO_2

Introduction

Zeolites are microporous crystalline solids with well-defined structures. Generally, they contain silicon, aluminium and oxygen in their framework and cations, water and other molecules within their pores. Many occur naturally as minerals, and are extensively mined in many parts of the world. Others are synthetic, and are made commercially for specific uses, or produced by research scientists.

Zeolites have an open structure that can accommodate a wide variety of cations, such as Na^+, K^+, Ca^{2+}, Mg^{2+} and others. Zeolites have an unusual crystalline structure and a unique ability to exchange ions. Zeolites are an aluminosilicate whose major ion exchangers are potassium and calcium plus other trace minerals. One gram of zeolite provides up to several hundred square meters of surface area for chemical reactions to take place. This characteristic of zeolites gives them great absorbing power (Bekkum, 2001).

Zeolites can remove atmospheric pollutants, such as engine exahaust gases and ozone-depleting CFCs. Natural zeolites are uniquely effective in adsorbing ammonia and also adsorb hydrogen sulphide. These properties make natural zeolites ideal for use in pet litter to prevent emanation of irritating odors. For similar reasons, natural zeolites can be used for effective control of irritating gases in horse stalls, barns, kennels, etc. (Breck, 1975).

When two or more materials are mixed together, the resulting composite material very often has physical properties that are very different than the properties of the used composites.

Two types of adsorption process can be distinguished depending on which of these two force types plays the higher role in the process. Adsorption processes can be classified as either physical adsorption (Vander Waals adsorption) or chemisorption (activated adsorption) depending on the type of forces between the adsorbate and the adsorbent (Hadjar, 2004).

Materials and Methods

In this experiments, all chemicals used in this work were produced from British Drug House Chemical Ltd. (BDH). All standard solutions and all other diluted solutions through the experimental runs were prepared by using distilled water.

Commercial zeolite was used for this experiment. Commercial zeolite sample, Zibo Julong chemical Co. Ltd., were used.

[1] Dr, Assistant Lecturer, Department of Chemistry, Yangon University of Distance Education
[2] Dr, Lecturer, (Retired), Department of Chemistry, Taungoo University
[3] Dr, Professor and Head (Retired), Department of Chemistry, Kyaingtong University

Preparation of Carbon–Zeolite Composites

Zeolite molecular sieve, triethanolamine TEA (5%, 10% and 15%) solution and distilled water were mixed into a conical flask. The mixture was stirred on magnetic stirrer for 2h at ambient temperature and filtered with Buchner funnel. The filtrate was dried at 105 °C for 8h in an oven. The sample was calcined at 400 °C, 500 °C and 600 °C for 2h. Then, it was cooled to room temperature and stored in a desiccator for the removal of CO_2.

Characterization of the Carbon-Zeolite Composites

The physicochemical properties (bulk density, pH, moisture, and porosity) of carbon-zeolite composites were determined by conventional methods. Specific surface area was determined using the methylene blue absorption test (MBT) method.

X-ray diffraction (XRD) analysis was carried out using Rigaku X-ray Diffractometer, RINI 2000/PC software, Cat. No 9240 J 101, Japan.

The scanning electron microscopy (SEM) images were obtained using JSM-5610 Model SEM, JEOL-Ltd., Japan.

FT IR spectrum was recorded in the range of 4000-400 cm^{-1} by using 8400 SHIMADZU, Japan FT IR spectrophotometer.

Sorption of Carbon Dioxide by Carbon-Zeolite Composites

The different amount of prepared carbon-zeolite composites (0.5, 1.0, 1.5, 2.0 and 2.5 $\pm$ 0.0002 g) were packed tightly into the two way glass sample tube carefully. First way was for inlet of CO_2 and the other for the collection of remaining CO_2 by KOH solution. 2 g of calcium carbonate was placed in a flat bottom flask. 2 M hydrochloric acid was slowly added to the flat bottom flask. Vigorous effervescence occurs and carbon dioxide molecules were evolved. The carbon dioxide molecules were passed over the sample tube containing carbon-zeolite composite. The remaining carbon dioxide molecules passed over the carbon-zeolite composite were collected by the potassium hydroxide solution. Then the solution was titrated with 0.1 M hydrochloric acid solution using methyl orange indicator.

Results and Discussion

Characterization of the Prepared Carbon-Zeolite Composites

In this experimental work, effect of TEA concentrations, amount of zeolite and temperature on the preparation of carbon-zeolite composites (S_1-S_{10}) are presented in Table 1. Table 1 shows that the sample S_2 gives the highest yield % of carbon-zeolite composites. Therefore, the optimum ratio of the zeolite and TEA was equal part (10:10 v/v) and pyrolysis temperature was obtained at 500ºC.

The physicochemical properties of zeolite and carbon-zeolite composites are presented in Table 2. The bulk density of sample S_2 was lower than the other samples. A low bulk density means the sponge like character of zeolites. The sorptive character of sample S_2 gave better results than the others. The pH values of prepared samples were found to be in the range of 7.86 to 8.63. It can be observed that the prepared samples possessed basic character. Moisture contents of prepared samples were found to be 1.73 to 2.92% out of nine samples S_2 has the highest value indicating more porous nature of zeolites. Table 2 shows that the surface area of S_2 was obtained as 807 m^2g^{-1} while zeolite has 770 m^2g^{-1}. The sample S_2 has the highest porosity (48%) whereas zeolite has (26%) respectively.

Table 1 Effect of TEA Concentrations, Amount of Zeolite Molecular Sieve and Pyrolysis Temperature on the Preparation of Carbon-Zeolite Composite (CZC)

Samples	Zeolite (g)	TEA (%v/v)	Pyrolysis temperature (°C)	Yield (%)
ZMS	10	0	500	67.74
S_1	10	5	500	73.18
S_2	**10**	**10**	**500**	**76.99**
S_3	10	15	500	72.72
S_4	10	20	500	70.66
S_5	5	10	500	68.69
S_2	**10**	**10**	**500**	**76.99**
S_6	15	10	500	71.47
S_7	20	10	500	66.92
S_8	10	10	300	70.91
S_9	10	10	400	72.22
S_2	**10**	**10**	**500**	**76.99**
S_{10}	10	10	600	69.81

ZMS = Zeolite Molecular Sieve
TEA = Triethanolamine
CZC = Carbon-Zeolite Composite
$S_1 – S_4$ = 10 g of zeolite molecular sieve with different TEA concentrations
$S_5 – S_7$ = 10 % v/v TEA concentrations with different amount of zeolite
$S_8 – S_{10}$ = 10 g of zeolite molecular sieve and 10 % v/v TEA concentrations with different pyrolysis temperatures

Table 2 Physicochemical Properties of Zeolite Molecular Sieve and Carbon-Zeolite Composites

Sample	Bulk density (gcm^{-3})	pH	Moisture content (%)	Surface area (m^2g^{-1})	Porosity (%)
ZMS	1.51	8.82	4.21	770	26
S_1	0.90	8.39	2.25	800	43
S_2	**0.81**	**8.24**	**2.92**	**807**	**48**
S_3	0.88	8.36	2.73	803	46
S_4	0.97	8.41	2.06	801	37
S_5	1.15	7.91	1.96	790	30
S_6	0.98	7.89	2.35	795	38
S_7	1.07	8.63	1.80	797	40
S_8	1.23	7.86	2.02	782	36
S_9	1.06	8.03	2.12	793	39
S_{10}	1.08	8.60	1.73	799	32

XRD Analysis

Figures 1 (a) and (b) show the XRD spetctra of zeolite and carbon-zeolite composite S_2. XRD diffractogram of zeolite molecular sieve was found to posses the composition of zeolite A. XRD diffractogram of carbon-zeolite composite shows that the zeolite structure was not destroyed during the heat treatment and embedded in the carbon matrix. The crystallite size of carbon-zeolite composite S_2 was obtained as 36.47nm.

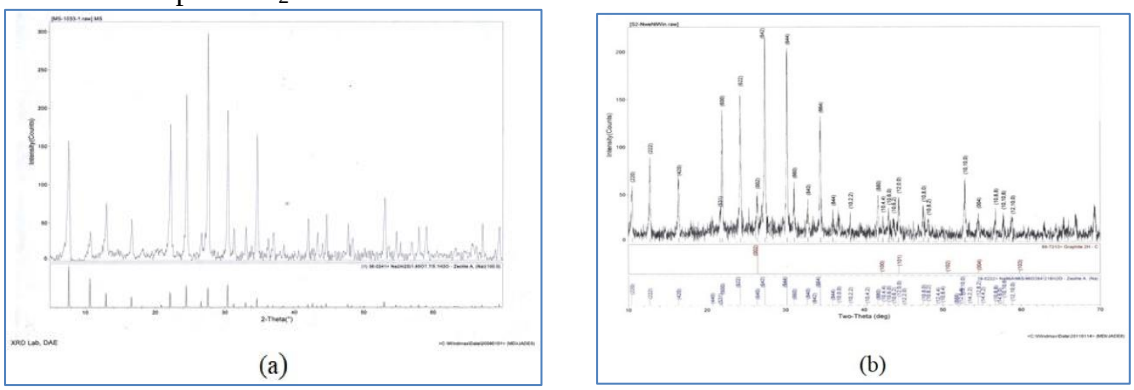

Figure 1 X-ray diffractograms of (a) spectrum of zeolite molecular sieve and (b) spectrum of carbon-zeolite composite S_2

SEM Analysis

SEM images in Figures 2(a) and 2(b) show the surface morphology of the carbon-zeolite composites and zeolite structure. White crystal indicates the zeolite molecular sieve crystals and the black spots indicate the carbon domains. The zeolite crystals are well dispersed in carbon matrix.

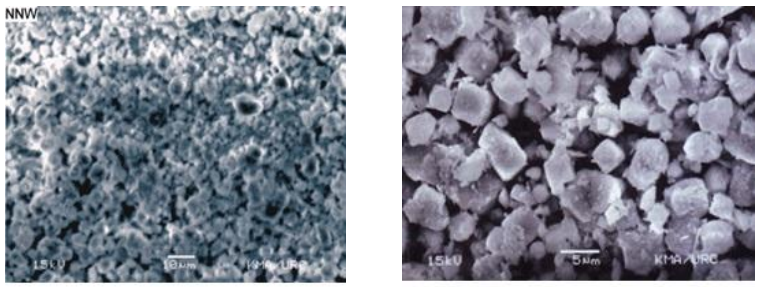

Figure 2 Scanning electron micrographs of (a) zeolite molecular sieve and (b) carbon-zeolite composite S_2

FTIR Analysis

The FT-IR spectrum of carbon-zeolite composite S_2 is shown in Figure 3. In the spectrum: the band at 3410 cm^{-1} indicate the O-H and N-H stretching, the organic compounds such as C = C stretching bands at 1666 cm^{-1} and C- H bending of CH_3, CH_2 at 1489 cm^{-1} and Si – O (or) Al-O tetrahedral stretching bands at 1018 cm^{-1} were found (Table 3).

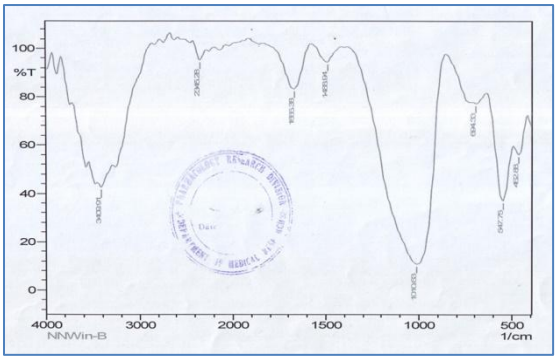

Figure 3 FTIR spectrum of carbon-zeolite composite (S_2)

Table 3 Structural Assignment for FTIR Data of Carbon-Zeolite Composite (S_2)

Observed Frequency (cm^{-1})	Reference Frequency* (cm^{-1})	Assignment
3410	3600-3200	O-H stretching, N-H stretching
1666	1680-1600	C=C stretching
1489	1400-1300	C-H bending of CH_3, CH_2
710	820-750	Si-O-Al stretching

*Nyquist and Kagel,1991; Silverstein and Terence,1991

Preliminary Sorption Study of Carbon Dioxide on Carbon-Zeolite Composites (S_1 to S_{10})

Table 4 shows the removal of carbon dioxide by carbon-zeolite composites (S_1 to S_{10}). It was found that sample (S_2) was found to have higher percent adsorption than others by using volumetric method.

Table 4 Percent Adsorption of Carbon Dioxide on Carbon-Zeolite Composites by Volumetric Method (Dosage of sample = 1g)

Sample	Amount of carbon dioxide in KOH solution (mmol)	Adsorbed amount of carbon dioxide (mmol)	Percent adsorption of carbon dioxide (%)
Without sample	13.761	-	-
S_1	8.214	5.547	40.31
S_2	**7.670**	**6.091**	**44.26**
S_3	8.152	5.609	40.76
S_4	8.199	5.562	40.42
S_5	8.800	4.961	36.05
S_6	8.694	5.067	36.82
S_7	8.163	5.598	40.68
S_8	8.932	4.829	35.09
S_9	8.225	5.536	40.23
S_{10}	8.650	5.111	37.14

Sorption Isotherms

In this research work, adsorption capacity was studied by using Langmuir, Freundlich and Temkin equation. The nature of the adsorption reaction could be described by relating the adsorption capacity (mass of solute adsorbed per unit mass of adsorbent) to the equilibrium concentration of the solute remaining in the solution such a relation is known as an adsorption isotherm.

Table 5 and Figure 4 show Langmuir model of carbon dioxide adsorption onto CZC. Estimated adsorption parameters by the Langmuir model are shown in Table 8. The Langmuir constant b (5.855) for CZC the square of regression coefficient (R^2 = 0.9792) for CZC suggesting that the adsorption of carbon dioxide on CZC can be modeled well by Langmuir equation while adsorption of carbon dioxide. It is well documented that the essential characteristic of the Langmuir isotherm may be expressed in terms of the dimensionless parameter (R_L). R_L has been defined as the isotherm shape that predicts if an adsorption system is favourable or unfavourable (Saswati and Ghosh 2005). R_L indicates the isotherm shape according to the following characteristics.

$R_L > 1$ (is unfavourable), $R_L = 1$ (linear adsorption), $R_L = 0$ (is irreversible) and $0 < R_L < 1$ is favourable. It has been expressed as, $R_L = \frac{1}{1+bC_i}$

For individual component system the R_L were found to be $0 < R_L < 1$ indicating that adsorption of carbon dioxide on CZC is favourable. The values of R^2 show that Langmuir equation can be used to describe removal of carbon dioxide by CZC very well and averagely for carbon dioxide adsorption. Based on the Langmuir parameters, that is, X_m (mg g^{-1}) for monolayer formation of sorption follows this order of: CZC 0.267 mgg^{-1}**.** It means to point out the attachment of carbon dioxide on CZC was of stronger binding nature.

It have been reported that Freundlich isotherm is an empirical relationship, which often gives a more satisfaction experimental data. It can be expressed as

$$\text{Log } q_e = \log K + \frac{1}{n} \log C_e$$

Table 6 and Figure 5 show Freundlich model of carbon dioxide adsorption on CZC. The values of K and n were obtained by ploting logarithms of adsorption capacity against logarithms of equilibrium concentration. Estimated adsorption parameters by the Freundlich model are shown in Table 6.

High levels of K and n values greater than 1 from the Freundlich isotherm suggests that the adsorption capacity of carbon dioxide on CZC. Also high values of n show that forces which are exerted on the surface of CZC during carbon dioxide adsorption are weak forces, which are in order of CZC. The square of correlation coefficients (R^2) for Freundlich isotherm are 0.966 representing a good fit ($R^2 \geq 0.95$) of the observed data. The values of R^2 also indicated that Freundlich isotherm describes adsorption of carbon dioxide on the adsorption capacities are in order of CZC.

The Temkin isotherm is an empirical relationship which often gives a more satisfactory model of experimental data (Saswati and Ghosh, 2005). It can be expressed as;

$$q_e = B \ln A + B \ln C_e$$

The values of A and B were obtained by plotting of adsorption capacity against equilibrium concentration. Estimated adsorption parameters by the Temkin model are shown in Table 7. The values of A and B from the Temkin isotherm (Table 8) suggests that the adsorption capacity of CZC was high and that any large change in the equilibrium concentration of carbon dioxide. The correlation coefficients R^2 is 0.9133 representing an average fit ($0.5 < R^2 < 0.75$ and $0.75 < R^2 < 0.95$) of the observed data. From the resulting data, CO_2 adsorption by carbon-zeolite

composite capacity was found to be in order with three isotherms, Langmuir, Freundlich and Temkin isotherms.

Table 5 Langmuir Isotherm for Carbon Dioxide by Carbon Zeolite Composite

Dosage (g)	C_i (mg)	C_e (mg)	X (mg)	q_e (mg g^{-1})	$\frac{1}{C_e}$	$\frac{1}{q_e}$
0.5	0.313	0.237	0.076	0.152	4.219	6.579
1.0	0.313	0.174	0.139	0.139	5.747	7.194
1.5	0.313	0.118	0.195	0.130	8.474	7.692
2.0	0.313	0.102	0.211	0.105	9.804	9.524
2.5	0.313	0.099	0.214	0.086	10.101	11.628

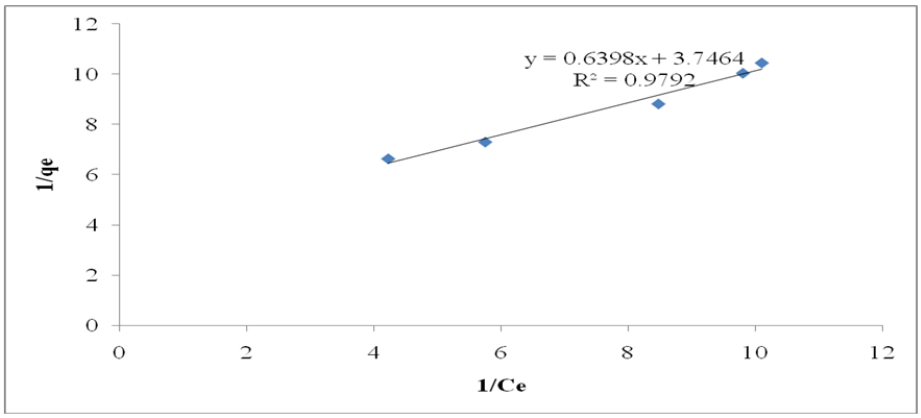

Figure 4 Langmuir adsorption isotherm for carbon-zeolite composite

Table 6 Freundlich Isotherm for Carbon Dioxide by Carbon- Zeolite Composite

Dosage (g)	C_i (mg)	C_e (mg)	X (mg)	q_e (mg g^{-1})	Log C_e	Log q_e
0.5	0.313	0.237	0.076	0.152	-0.625	-0.818
1.0	0.313	0.174	0.139	0.139	-0.759	-0.857
1.5	0.313	0.118	0.195	0.130	-0.928	-0.886
2.0	0.313	0.102	0.211	0.105	-0.991	-0.979
2.5	0.313	0.099	0.214	0.086	-1.004	-1.065

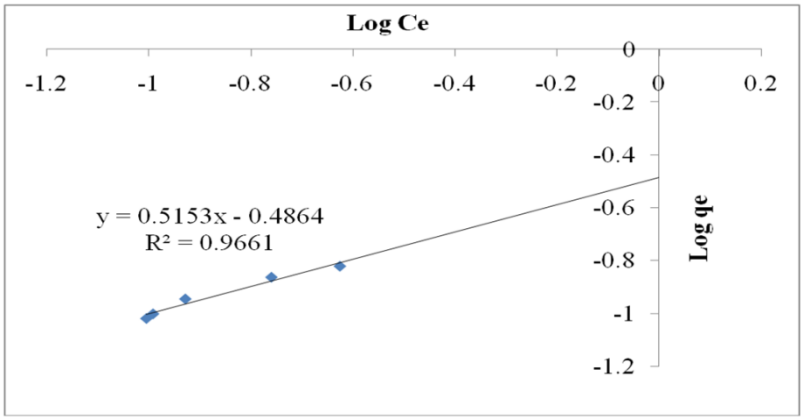

Figure 5 Freundlich adsorption isotherm for carbon- zeolite composite

Table 7 Temkin Isotherm for Carbon Dioxide by Carbon-Zeolite Composite

Dosage (g)	C_i (mg)	C_e (mg)	x (mg)	q_e (mg g^{-1})	ln C_e
0.5	0.313	0.237	0.076	0.152	-1.439
1.0	0.313	0.174	0.139	0.139	-1.749
1.5	0.313	0.118	0.195	0.130	-2.137
2.0	0.313	0.102	0.211	0.105	-2.283
2.5	0.313	0.099	0.214	0.086	-2.313

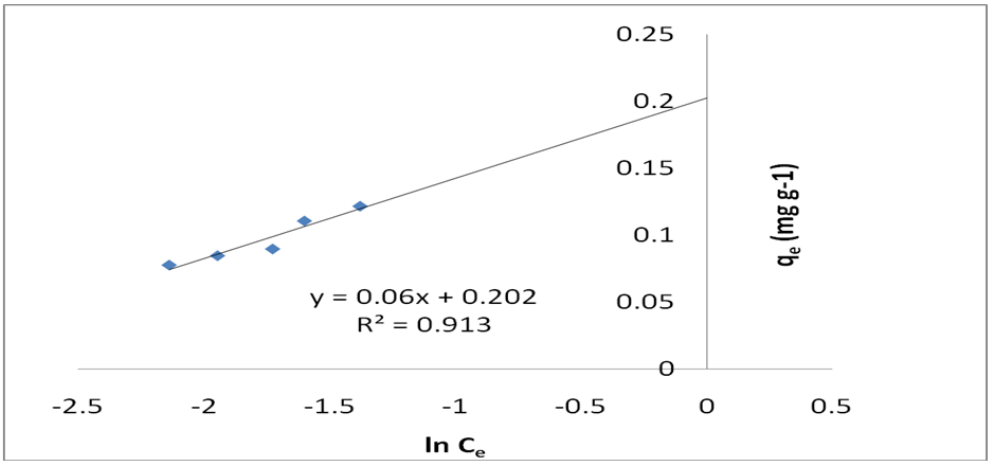

Figure 6 Temkin adsorption isotherm for carbon-zeolite composite

Table 8 Adsorption Parameters for Monolayer System by Carbon-Zeolite Composite

Sample	Langmuir Model				Freundlich Model			Temkin Model		
	X_m (mg g^{-1})	b	R^2	R_L	K (mg g^{-1})	n	R^2	A (mg g^{-1})	B	R^2
CZC	0.267	5.855	0.9792	0.353	0.721	1.941	0.9661	28.982	0.060	0.913

Conclusion

From the overall results and data, it may be deduced that; carbon-zeolite composites were prepared by incorporating zeolite into a TEA solution. Preparations were carried out by various concentration of TEA solution and various pyrolysis temperatures. Among these results, equal amount of zeolite and TEA at 500ºC. S_2 showed the highest surface area (807 m^2/g), highest moisture content (2.92%), highest porosity (48%) and the lowest bulk density (0.81 gcm^{-3}).

The characterization of carbon-zeolite composites were carried out by XRD, SEM and FTIR. From the X-ray diffractograms of zeolite and carbon-zeolite composite, the crystal structure zeolite was observed as zeolite A. In composite, it was observed that the zeolite structure was not destroyed during the heat treatment and embedded in the carbon matrix.

SEM images show the surface morphology of the carbon-zeolite composite and zeolite structure. White crystal indicates the zeolite molecular sieve crystals and black spots indicate the carbon domains. The zeolite crystals are well dispersed in carbon matrix.

From the FTIR spectrum of composite, Si-O-Al stretching was found at 710 cm^{-1} and then the organic compounds such as C = C stretching (1666 cm^{-1}) and C–H bending (1489 cm^{-1}) were observed.

The Langmuir isotherm shows that the attachment of carbon dioxide on carbon-zeolite composite was monolayer formation and stronger binding nature. The Freundlich isotherm also describe that the adsorption capacity of carbon dioxide on carbon-zeolite composite was observed and good fit attachment was formed. The Temkin isotherm suggests that the adsorption capacity was high and any large change in the equilibrium concentration of carbon dioxide.

Therefore, the carbon-zeolite composite parameters presented in this experiment have great potential for application in gas adsorption.

Acknowledgement

The authors would like to express deepest gratitude to the Department of Higher Education of the Myanmar, Ministry of Education, Yangon, Myanmar, for provision of opportunity to do this research and Myanmar Academy of Arts and Science for allowing to present this paper.

References

Bekkum, H.V., Flanigen, E.M., Jacobs, P.A. and Jansen, J.C. (2001). *Introduction of Zeolite Science and Practice, Techniques of Zeolite Characterization*, Amsterdam: 2nd Ed., Elsevier, pp. 345-353

Breck, D.W. (1975). "Synthetic Zeolites: Properties and Application". *Journal. Chem. Edu*., vol.**7**. pp. 23-39

Hadjar, H., Hamdi, B. and Kessaisia. Z. (2004). *Adsorption of Heavy Metal Ions on Composite Materials Prepared by Modification for Natural Silica*. London: pp. 132-136

Nyquist, R.A. and Kagel, R.O. (1991). *Infrared Spectra of Inorganic Compound*. New York: Academic Press, Inc., New York, pp. 7-11

Saswati, G. and Ghosh, U.C. (2005). "Studies on Adsorption Behaviour of Cr(VI) onto Synthetic Hydrox Stannic Oxide. *American International Journal of Contemporary Research*, vol-**31**. pp.597-602

Silverstein, R.M., and Terence, C.M., (1991). *Spectrometric Identification of Organic Compound*. New York: John Willey and Son, Inc., pp. 99-164

A STUDY ON THE YIELD AND SOME AGRONOMICAL CHARACTERISTICS OF THE GAMMA INDUCED OYSTER MUSHROOM (*PLEUROTUS OSTERATUS*)

Thiri San[1], Khin Cho Thant[2], Hnin Hnin Than[3]

Abstract

This research deals with the study on the effect of gamma irradiation on yield and quality of oyster mushroom in each generation. The spawn of mushrooms sample (Ngwe-Hnin-Mho) was collected from Kaung-Ei Mushroom Nursery, South-Okkalapa Township,Yangon Region. The sample of mushrooms was treated with different doses (0.25, 0.5, 0.75 and 1 kGy) of gamma radiation. After irradiation, these spawn were successively cultivated to third generation. The yield and some agronomical characteristics of different generations were determined. To be safe for consumption, the induced activity of each mutant sample (OMG 0.25, OMG 0.5, OMG 0.75, OMG 1) was monitored by using NaI(Tl) Scintillation Gamma Counter at Nuclear Laboratory, Department of Chemistry. It was found that there were no induced activity in these samples. Thus, they are safe for human consumption. Agronomical characteristics such as average diameter of mushroom, yields, fruiting period, shelf-life of mutants oyster mushrooms were determined. And then, study of SEM and FT IR measurement was done. All doses of irradiation provide the higher yield of mushroom than those of control for every generation. The shelf-life of each mutant oyster mushroom increase than that of control. It was found that the fruiting periods of OMG 0.75 and OMG 1 always provided 1 day to 5 day shorter fruiting period than that of others. Thus, it is to reduce the time of producing oyster mushroom. The study of SEM was done for morphology of irradiated oyster mushroom. From this study, one evident fact is that there is no similar pattern between non-irradiated and irradiated oyster mushroom in all generation. From the FT IR spectra, it was found that effect of gamma irradiation did not vary the functional groups in the oyster mushroom up to third generation.

Keywords *:* oyster mushroom, gamma , induced activity, nutritional value, OMG

Introduction

In general, edible mushrooms are low in fat and calories, rich in vitamins B, D, K and sometimes vitamins A and C. They contain more protein than any other food of plant origin and are also a good source of mineral nutrients. Malnutrition is a problem in developing third world countries. Mushrooms with their flavor, texture, nutritional values and high productivity per unit area have been identified as an excellent food source to alleviate malnutrition in developing countries. In a world of rising food prices, cultivation of mushrooms is a very reliable and profitable option. Oyster mushroom cultivation can play an important role in managing organic wastes whose disposal has become a problem (Chang and Hayes, 2011). These wastes can be recycled into food and environment may be less endangered by pollution. Furthermore, the use of these residues in bioprocesses may be one of the solutions to bioconversion of inedible biomass residues into nutritious protein rich food in the form of edible mushrooms. Apart from food value, its medicinal value for diabetics and in cancer therapy has been emphasized. Many of mushrooms pose a range of metabolites of intense interest to pharmaceutical e.g., antitumour, antigenotoxic, antioxidant, anti-inflammatory, anti-hypertensive and food industries (Chikelu Mba, 2013).

[1] Dr, Assistant Lecturer, Department of Chemistry, East Yangon University
[2] Dr, Associate Professor, Department of Chemistry, Maubin University
[3] Dr, Professor, Department of Chemistry, Dagon University

Gamma rays are emitted in the process of the decay of the radioisotopes cobalt-60 (^{60}Co), cesium-137 (^{137}Cs) and to a less extent, plutonium-239 (^{239}Pu). Gamma sources containing one of these radio isotopes are typically installed as gamma cell irradiators. A gamma cell is used mostly for acute irradiation (i.e., for short periods) (Dung *et al.*, 2012).The exposure of plants to irradiation for extended periods of times, irradiators are installed in specially designed gamma rooms (or chambers), greenhouses or fields. Gamma radiation has been used to useful mutations in rice, wheat, cotton, sweet paper, tomato and sesame and in maize. Induced mutations, exploitable in crop breeding, have been achieved by transporting plant propagules, mostly botanical seeds, in recoverable space orbiting satellites (Longvah and Deosthale, 1998). In this research work, the applying gamma irradiated oyster mushroom showed that a good benefit for their improve of yield percent and agronomical characteristics of oyster mushroom.

Materials and Methods

The spawn of mushrooms sample was collected from Kaung-Ei Mushroom Nursery, South Okkalapa Township, Yangon Region. The spawn of mushrooms was transported to the Department of Atomic Energy, Ministry of Science and Technology for irradiation. The spawn of oyster mushroom was cultivated as shown in Figure 1 in different doses of radiation (0.25, 0.5, 0.75, 1 kGy) up to third generation. Oyster mushrooms were firstly cultivated on rubber tree logs and were commonly grown on sawdust. Cultivation merely involved placing the sterilized and inoculated substrate in plastic bags, keeping them in the cool and dark. The mycelium has grown throughout the substrate, openings are cut through the bag to allow fruiting bodies (fruiting mushroom) to develop.

For study on safety consumption of mutant of first generation (0.25, 0.5, 0.75,1 kGy), the induced activity was monitored by NaI (Tl) Scintillation Gamma Counter at Nuclear Chemistry Laboratory, Yangon.

The study on investigation of agronomical characteristics of mutant oyster mushroom from first generation to third generation was done. The cultivated non-irradiated and mutant oyster mushrooms were characterized by using SEM and FT IR analyses.

Spawn of oyster mushroom | Substrate Preparation | Bagging | Pasteurization

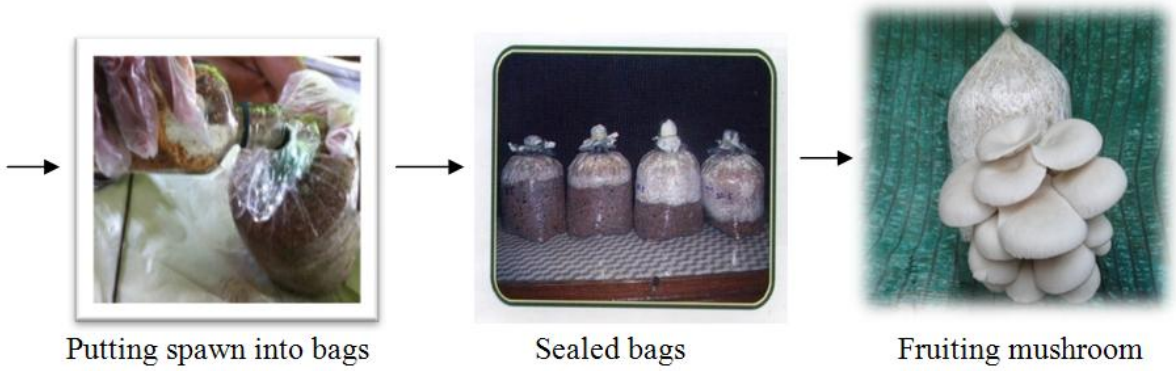

Figure 1 Cultivation procedure of oyster mushroom

Results and Discussion

Measurement of Induced Radioactivity of Mutants Oyster Mushroom

The induced activity of each mutant oyster mushroom sample (OMG 0.25, OMG 0.5, OMG 0.75, OMG 1) was monitored by using NaI(Tl) Scintillation Gamma Counter at Nuclear Laboratory, Department of Chemistry. The results are reported in Table 1. Since the induced radioactivity of each irradiated sample was monitored for safety consumption. It can be observed that there is no activity on the background for both before and after cultivation of M_1first generations. It is clear that counts for these sample were not exceed to that of background activity. Therefore, there was no induced activity in these samples. Hence, gamma irradiation mutant samples of oyster mushroom in each generation can be handled and stored, and they are safe for consumption.

Table 1 Monitoring of Induced Radioactivity in Mutant of Oyster Mushroom in First and Second Generation (after harvested)

No.	Samples	Induced activity relative to background (±%) (cp 300s)	
		M_1 generation	M_2 generation
1	OMG 0.25	1.50	1.20
2	OMG 0.5	0.55	0.25
3	OMG 0.75	0.97	0.41
4	OMG 1	1.11	0.64

± = due to fluctuation Note: activity no distinct above background

M_1 = First Generation, M_2 = Second Generation

OMG 0.25 = Gamma 0.25 kGy irradiated Oyster Mushroom

OMG 0.5 = Gamma 0.5 kGy irradiated Oyster Mushroom

OMG 0.75 = Gamma 0.75kGy irradiated Oyster Mushroom

OMG 1 = Gamma 1 kGy irradiated Oyster Mushroom

Study on Agronomical Characteristics of Mutants Oyster Mushroom Samples

The agronomical characteristics of each mutant oyster mushroom were studied to investigate some important characters (average diameter of mushroom, actual yield, yield increase, fruiting period and shelf-life of mushroom).The results of each mutant in different generations are reported in Tables 2, 3, 4, 5 and Figure 2. From basic on actual yield, percentage of yield increase were calculated. In first generation, percentage yield improvement of OMG 0.25, OMG 0.5, OMG 0.75 and OMG 1 were found to be 7.60 %, 11.50 %, 29.20 %, 17.60 % . In second generation, percentage yield improvement of OMG 0.25, OMG 0.5, OMG 0.75, OMG 1 and control were found to be 5.71 %, 9.28 %, 11.42 % and 10.00 % respectively. In third generation, percentage yield improvement of OMG 0.25, OMG 0.5, OMG 0.75 and OMG 1 were found to be 6.90 %, 30.00 %, 46.32 % and 21.64 % respectively.

The mutants 0.25 kGy, 0.5 kGy, 0.7 kGy and 1 kGy doses of gamma radiation on oyster mushroom were found to be effective in morphology, yield, fruiting period and shelf-life. Among them, OMG 0.75 sample provide the highest yield with shorter fruiting period in every generation. Therefore, the effect of gamma irradiation was found on the shelf-life, yield and fruiting period of oyster mushroom.

Table 2 Agronomical Characteristics of Mutant Oyster Mushroom Samples in First Generation (M_1)

No.	Characteristics of Oyster Mushroom	Samples				
		OMC	OMG 0.25	OMG0.5	OMG 0.75	OMG 1
1	Average diameter of mushroom (cm)	9.20	10.23	10.41	10.06	9.20
2	Actual Yield (g/ bag)	223.33 ± 20.67	233.33 ± 8.17	241.67 ± 9.57	291.67 ± 20.34	251.67 ± 24.83
3	Relative Yield	100	107.60	111.50	129.20	117.60
4	Yield Increase (%)	-	7.60	11.50	29.20	17.60
5	Fruiting Period (days)	34	34	34	31	33
6	Shelf-life (h)	18	23	24	24	24

Table 3 Agronomical Characteristics of Mutant Oyster Mushroom Samples in Second Generation (M_2)

No.	Characteristics of Oyster Mushroom	Samples				
		OMC	**OMG 0.25**	**OMG 0.5**	**OMG 0.75**	**OMG 1**
1	Average diameter of mushroom (cm)	9.00	9.50	9.70	9.40	10.40
2	Actual Yield (g/ bag)	233.00 ± 17.28	247.00 ± 11.78	255.00 ± 13.78	260.00 ± 12.64	257.00 ± 12.12
3	Relative Yield	100	105.71	109.28	111.42	110.00
4	Yield Increase (%)	-	5.71	9.28	11.42	10.00
5	Fruiting Period (days)	33	33	33	32	32
6	Shelf-life (h)	17	20	21	21	20

Table 4 Agronomical Characteristics of Different Mutants Oyster Mushroom in Third Generation (M_3)

No	Characteristics of Oyster Mushroom	Samples				
		OMC	**OMG 0.25**	**0MG0.5**	**OMG 0.75**	**OMG1**
1	Average diameter of mushroom (cm)	6.03	8.33	8.32	7.09	8.29
2	Actual Yield (g/ bag)	385.00 ± 25.88	411.66 ± 28.58	501.66 ± 22.29	563.33 ± 24.20	468.33 ± 27.21
3	Relative Yield	100	106.90	130.30	146.32	121.64
4	Yield Increase (%)	-	6.90	30.30	46.32	21.64
5	Fruiting Period (days)	33	32	29	28	28
6	Shelf-life (h)	19	24	27	27	24

Table 5 The Yield Comparison of Different Mutant Oyster Mushrooms from First to Third Generation

Generation	Samples	Actual Yield (g/bag)	Relative Yield	Yield Increase (%)
M_1	OMC	223.33	100	-
	OMG 0.25	233.33	107.60	7.60
	OMG 0.5	241.67	111.50	11.50
	OMG 0.75	291.67	129.20	29.20
	OMG 1	251.67	117.30	17.60
M_2	OMC	233.00	100	-
	OMG 0.25	247.00	105.71	5.71
	OMG 0.5	255.00	109.28	9.28
	OMG 0.75	260.00	111.42	11.42
	OMG 1	257.00	110.00	10.00
M_3	OMC	385.00	100	-
	OMG 0.25	411.66	106.90	6.90
	OMG 0.5	501.66	130.30	30.30
	OMG 0.75	563.33	146.32	46.32
	OMG 1	486.33	121.64	21.64

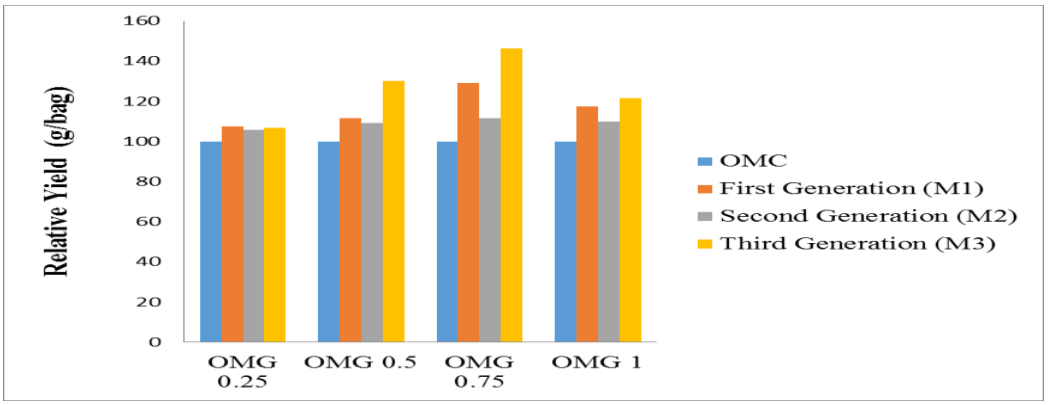

Figure 2 Bar graph of relative yield of different mutants oyster mushroom for three generations

OMC = Oyster Mushroom Control
OMG 0.25 = Gamma 0.25 kGy irradiated Oyster Mushroom
OMG 0.5 = Gamma 0.5 kGy irradiated Oyster Mushroom
OMG 0.75 = Gamma 0.75 kGy irradiated Oyster Mushroom
OMG 1 = Gamma 1 kGy irradiated Oyster Mushroom

Studies on Surface Morphology of Mutant Oyster Mushrooms up to Third Generation

In this work, the irradiated mutant oyster mushrooms had been studied by SEM. The obtained SEM photomicrographs for non-irradiated and irradiated oyster mushroom are shown in Figure 3. It can be seen that the surface morphology of before and after irradiated oyster mushroom was different. The more fine state particles are observed in irradiated spawn of mushroom. It can be said that gamma irradiation can affect surface texture of oyster mushroom. From these figures, one evident fact is that there is no similar pattern was observed. Moreover, it

was found that all of surface morphology of these gamma exposed mutant oyster mushrooms were different from non-irradiated and irradiated oyster mushroom.

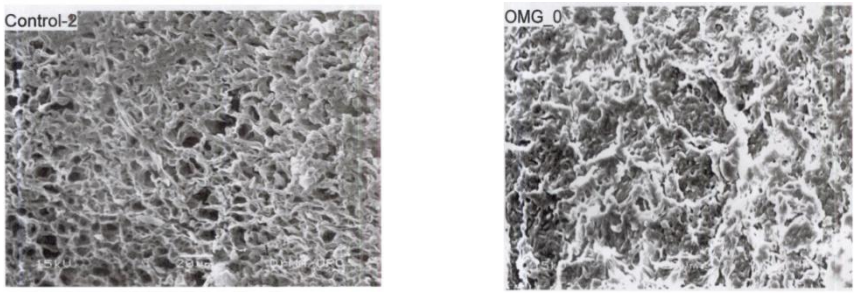

(a) (b)

Figure 3 SEM photomicrographs of (a) cultivated non-irradiated oyster mushroom (OMC) (b) cultivated mutant oyster mushroom (OMG 0.75)

FT IR Analysis of Non-irradiated and Irradiated Oyster Mushroom

From this study, the functional group of compounds present in non-irradiated and irradiated oyster mushroom (OMG 0.75) were studied by FT TR spectrometer. The FT IR spectra of cultivated non-irradiated and irradiated oyster mushroom are shown in Figure 4. The position of absorption bands of non-irradiated and irradiated are shown in Table 6. It was found that, there is no change in functional group for both samples. Hence, it can be said that there were no effect of gamma irradiation on the functional groups of control.

Table 6 FT IR Spectra Data of the Non-Irradiated and Irradiated Oyster Mushroom

Wavenumber (cm^{-1})		Band Assignment*
Non irradiated	**Irradiated**	
3327	3392	OH and NH stretching vibration
2931	2928,2924	C-H asymmetric and symmetric stretching vibration
1658	1658	C=O stretching vibration
1546, 1408	1548,1408	C=C stretching vibration
1147	1147,1149	Symmetric stretching for C-O-C
1080, 1043	1080,1043	C-O band in –C-O-H

* Silverstein *et al*., 2005

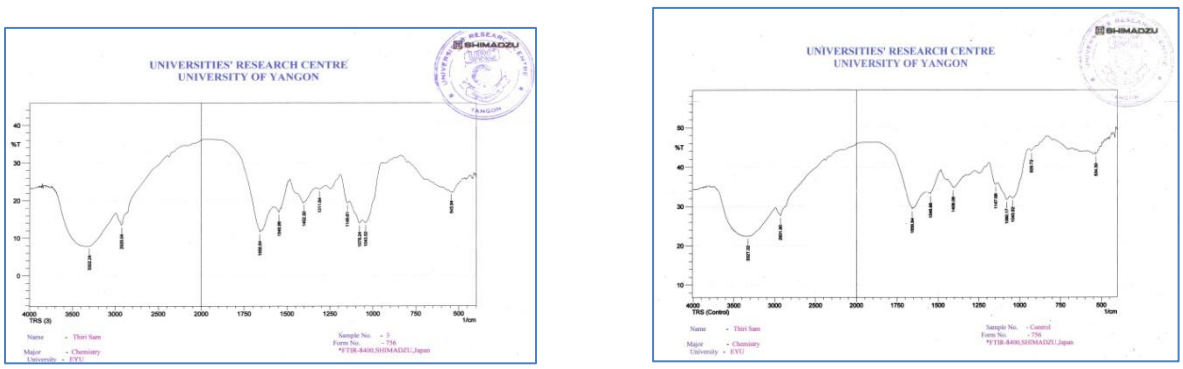

(a) (b)

Figure 4 FT IR spectra of the (a) cultivated non-irradiated oyster mushroom (OMC) (b) cultivated of mutant oyster mushroom (OMG 0.75)

Conclusion

From results, all irradiated oyster mushroom have no induced activity. Therefore, it is safe for consumption, handle and storage. Oyster mushrooms were irradiated with different doses (0.25 kGy, 0.5 kGy, 0.75 kGy and 1 kGy) of gamma irradiation and cultivated from first and third generation. The quality, yields and agronomical characteristics of mutants oyster mushroom up to third generation were studied. All dose of irradiation provide the highest yield of mushroom than those of control for every generation. From study on the long term, 0.75 kGy of gamma radiation gives the highest yield in first to third generation (29.20 %, 11.42 % and 46.32 %) respectively. The gamma irradiation has the effect on the fruiting period of oyster mushroom from first to third generation. 0.75 kGy and 1 kGy provide one day to 5 days shorter fruiting period than other irradiation doses. The shelf-life of each mutant oyster mushroom from first to third generation was increased from 4 to 6 than the control. It can be concluded that all doses of gamma radiation were found to be effective on the morphology, yield, fruiting period and shelf-life of oyster mushroom.

Acknowledgements

The authors would like to thank the Department of Higher Education (Yangon office), Ministry of Education, Yangon, Myanmar, for the permission of doing this research. Thanks are also due to Department of Atomic Energy (DAE), Ministry of Science and Technology for providing to use the nuclear facilities corporation and kind help in this work.

References

Chang, S. T. and Hayes, S. T. (2011). *The Biology and Cultivation of Edible Mushrooms*. NewYork:

http://www.cultivationofoystermushrooms.com

Chikelu Mba, M. C. (2013). "Induced Mutations Unleash the Potentials of Plant Genetic Resources for Food and Agriculture". *Agronomy 2013*, vol. 3, pp. 200-231.

Dung, N. T., Tuyen, D. B. and Quang, P. H. (2012). *Morphological, Nutritional and Genetic Characteristics of Oyster Mushrooms and Conditions Effecting on its Spawn Growing*. London: *Elsevier*, pp. 67-85.

Longvah, T. and Deosthale, Y. G. (1998). "Composition and Nutritive Studies on Edible Mushroom from Northeast India". *Journal of Food Chemistry*, vol. 63 (3), pp. 331-334.

Silverstein, R. M., Webster, F. X. and Kiemle, D. J. (2005). *Spectrometric Identification of Organic Compounds*. Singapore: 7th ed., John Wiley and Sons, Inc.

SCREENING OF NATURAL LARVICIDES FROM *SPILANTHES ACMELLA* L. (PÈ-LAYNYIN) AND *MELIA AZEDARACH* L. (PAN-TAMAR)

Khin Su Latt[1]

Abstract

Two plant materials, aerial part of *Spilanthes acmella* L. (Pè-Laynyin) and bark of *Melia azedarach* L. (Pan-Tamar) were selected for the screening of mosquito larvicidal activity against third and fourth instar larvae (*Aedes aegypti* mosquito). Petroleum ether extract from aerial part of Pè-laynyin (LC_{50} = 0.0065 %, LC_{90} = 0.0146 %) and ethanol extract from Pan-tamar bark (LC_{50} = 1.008 %, LC_{90} = 3.693 %) showed potent larvicidal activities. The larvicidal activity of commercially available synthetic larvicide, Temephos, (Abate) was LC_{50} = 0.0034 ppm and LC_{90} = 0.0075 ppm. Ethanolic extract of *S. acmella* was not observed sign to be toxic in mice at 10 g/kg that is maximum permissible dose. Therefore, *S. acmella* extract did not show harmful effect to mammalian. The maximum giving dose for ethanolic extract of *M. azedarach* in mice was 8 g/kg within survival period for 7 days to be looked forward. At a dose of 10 g/kg, one out of three mice was found to be dead. Therefore, care must be taken if bark of *M. azedarach* is used as larvicide. Petroleum ether extract of *S. acmella* was not observed lethality on fish *Clarias batrachus* (Nga-khu) at 0.025 % concentration level. Therefore, petroleum ether extract was not found harmful effect on aquatic vertebrates and can safely be used as natural larvicide in fresh water.

Keywords: *Spilanthes acmella* L., *Melia azedarach* L., *Aedes aegypti* mosquito, larvicidal activities, synthetic larvicide (Abate), *Clarias batrachus*

Introduction

Among insects, mosquitoes are the most important group in the transmissions of several human diseases, including malaria, yellow fever, dengue, encephalitis and filariasis. Mosquitoes are widely distributed throughout the world. The number of mosquito species exceeds 2500. They are separated into two medically important sub-families – the Anophelinae and Culicinae – the former is smaller but includes the vectors of human malaria and filariasis (Genus Anopheles); the Culicinae includes vectors of viral and filarial disease of man including species which are vicious biters (Genera *Aedes, Culex, Mansonia)* (WHO, 1997).

In tropical countries, *Aedes aegypti* is an important vector of dengue, dengue haemorrhagic fever, yellow fever and other viral diseases. A closely related species, *A. albopichus*, can also transmit dengue. In some areas, *Aedes* species transmit filariasis.

Aedes mosquitos bite mainly in the morning or evening. Most species bite and rest outdoors but in tropical towns, *Aedes aegypti* breeds, feeds and rests in and around houses (Rozendaal, 1997).

Dengue haemorrhagic fever (DHF) is the most common in children less than 15 years of age, but it also occurs in adult. DHF commonly begins with a sudden rise in temperature which is accompanied by facial flush and other non-specific constitutional symptoms, resembling dengue fever such as anorexia, vomiting, headache and muscle or joint pains.

[1] Lecturer, Department of Chemistry, West Yangon University

Insecticides may cause discomfort, sickness and occasionally death to human beings and other living organisms when they are carelessly or incorrectly used. To avoid this effect, research on plant extracts should be carried out to replace synthetic insecticides. The present work investigates the larvicidal ativity of two plant species of *S. acmella* and *M. azedarach* against on *A. aegypti* mosquito larvae.

Selected Myanmar Indigenous Insecticidal Plants

***Spilanthes acemella* L.**

Family	:	Compositae (Asteraceae)
Botanical name	:	*Spilanthes aecmella* L.
Myanmar name	:	Pè-laynyin
English name	:	pelitory (toothache plant)
Part used	:	Aerial part

The genus *Spilanthe*s (Asteraceae) is herb to 50 cm tall, leaves opposite, broadly ovate, 3-6 cm long, flower head terminal, solitary, avoid, about 1 cm cross, long-stalked (12 to 15 cm long) marginal ray-flowers yellow, achenes black. It is native to the tropics of Brazil, through it is grown as an ornamental (and occasionally as a medical) in various parts of the world. The flowering and fruits is November to December (Mohammad *et al*., 2017).

S. acmella (Figure 1) is also known as "toothache plant" or "paracress". *S.acmella* (Asteraceae) has 476 genera and three species in *Spilanthes* : *S. acmella*, *S. oleracea* Jacq. and *S. radicans* Schard.

Figure 1 Photograph of *Spilanthes acmella* L.

Biological Activities of *Spilanthes acmella* L.

S. acmella is sometimes called the toothache plant because chewing on one of the flower buds will numb the mouth and make salivate. The leaves and flower-heads contain

analgesic, antifungal, anthelmintic and antibacterial agents. The leaves may be used topically to treat bacterial and fungal skin diseases such as ringworm (Verma *et al*., 1993).

***Melia azedarach* L.**

Family	:	Meliaceae
Botanical name	:	*Melia azedarach* L.
Myanmar name	:	Pan-Tamar, Thinbaw-Tamar
English name	:	Indian Bead tree, Perisian Lilae
Part used	:	Bark

The genus *Melia* (Meliaceae) is commonly called Perisian Lilae, white cedar, chinaberry or bead. Tree, *M. azedarach* is a deciduous tree, native to India, Southern China and Australia. They are all deciduous or semi-evergreen small trees. The leaves are up to 50 cm long, alternate, long-petiole, 2 or 3 times compound (old-pinnate); the leaflets are dark green above and lighter green below, with serrate margins.

Figure 2 Photograph of *Melia azedarach* L.

Biological Activities of *Melia azedarach* L.

M. azedarach has insecticidal, anti-viral and possible anticancer properties. The flowers and leaves are applied as a poultice to relieve nervous headaches. The oil possess similar properties to that neem oil. The leaves and bark are used internally and externally in leprosy and scrofula. The leaves, bark and fruits are accredited with insect-repellent properties. Leaves are placed inside books and between folds of woolen garments to protect them against insect attack (Adnan, 2009).

Materials and Methods

Mosquito larvicidal activity tests were carried out by the methods described by Swaroop, 1963.

Preparation of Pet Ether Extract from Aerial Part of *S. acmella*

Dried powdered from aerial parts of *S. acmella* (200 g) was macerated in petroleum ether (1000 mL) at room temperature. Petroleum ether was removed by using rotatory evaporator at 50 ºC to obtain petroleum ether crude extract (3.0 g, 1.5 % yield).

Preparation of EtOH Extract from *M. azedarach*

Dried powdered from bark of *M. azedarach* (100 g) was extracted with EtOH (500 mL). This ethanol extract was filtered and then concentrated under reduced pressure at 45 ºC using rotary evaporator to obtain EtOH extract (3.0 g, 3.0 % yield).

Larvae and Bioassays

Laboratory reared 8-10 days old, 3rd and 4th instar *A. aegypti* mosquito larvae were used for larvicidal tests. The mosquito larvae were obtained from Medical Entomology Research Division, Department of Medical Research, Lower Myanmar. For each test 200 larvae were used. Larvae were starved for 24 h before testing. Five replications were carried out for each run.

Test Samples and Doses

(i) 0.025, 0.0125, 0.00625, and 0.003125 % (w/v) solution of petroleum ether extract from aerial part of *S. acmella* in acetone-water

(ii) 3.0, 1.5, 0.75, and 0.375 % (w/v) solution of ethanol extract from *M. azedarach* bark in distilled water

(iii) 0.0125, 0.00625, 0.003125, and 0.0015625 ppm (w/v) solution of commercially available larvicides, Abate in distilled water

Procedure

Late 3rd and 4th instar larvae were exposed to a series of four concentrations of test samples. Larvae were also exposed to either water or acetone-water (solvent used to dissolve the test sample) for control purpose. Mortalities were recorded after 24 h period. In the larvicidal test, the relative humidity (RH) was 75-80 % and temperature was 27 ± 1 ºC. The lethal concentrations (LC_{50} and LC_{90}) were investigated by using dose-effect probit analysis, and commercially available larvicide, Abate, was used for a positive control.

Acute Toxicity Study of *S. acmella* and *M. azedarach*

The purpose of acute toxicity is to identify and categorize those chemical substance that pose a potential hazard to human and other species. The acute toxicity was investigated by the up-and-down method in mice (Bruce, 1985). This method permits a major reduction in the number of animal used. In the up-and-down procedure, the animals were dosed one at a time. If an animal survives, the dose for the next animal is increased; if it dies, the dose is decreased.

Doses are usually adjusted by a constant multiplicative factor, i.e., by dose amounts of 10, 8, 6, 4, 2 and 1 g/kg. The dose for each successive animal is adjusted up or down depending upon the outcome for previous animal. For a limit test, the dosing of three mice of each sex at 5 g/kg was used for substance with low toxicity.

Animals and apparatus

Albino mice of both-sexes (weighing 30-35 g), mouse cages, animal balance, intragastric needles and 2 mL syringe

Procedure

Albino mice (12) were used in this study. The dose was calculated according to the body weight. In the acute toxicity test, EtOH extracts of *S. acmella* and *M. azedarach* were dissolved in distilled water by using intragastric needles, the EtOH extract solutions were offered to a group of those three mice by 10 g/kg per mice and another group of three mice by 8 g/kg per mice. Each group of those mice was housed separately in mice cage. Food and water were allowed to freely assess. They were observed carefully for 24 h. Survivability was observed within a period of 7 days and the lethal dose of the extract was estimated.

Toxicity of Insecticide to Aquatic Vertebrate *Clarias batrachus* (Nga-khu)

Test fish (50) of fresh water organism, *C.batrachus* (Nga-khu) with a length of 5-6 cm, up to 20 days maturity were obtained from Fresh Water Fish Hatchery, Department of Fisheries, Lay-Dauk-Kan, East Dagon Township, Yangon Region.

Apparatus

Container (capacity 1 L), beaker (500 mL), glass rods, micropipette

Procedure

Petroleum ether extract of *S. acmella* was dissolved in a mixture of acetone and distilled water. The required dose (0.025 %) was added into the test fish container filling with the fresh water (pH 7-7.5) at 27-30 ºC. In toxicity testing, 10 fish were used for each test. Five replications were made and observed carefully within 24 h period. Any abnormal behaviour symptoms of tested samples were regularly observed. Acute effects were measured after exposure to insecticide and dead or mortality was measured as acute after 24 h.

Results and Discussion

Mosquito Larvicidal Effect of Crude Extracts and Synthetic Larvicide (Abate)

Mosquito larvicidal activity of crude extracts was tested by Force feeding method. Percent mortality (LC_{50} and LC_{90} values) of test samples were evaluated by statistical analysis of the data of susceptibility of larvae, because this theory can be estimated with greater precision than lethal concentration at either end of the range. Mortality rate in distilled water (or distilled water-acetone) was investigated for untreated control. The number of dead mosquito larvae in each concentration was corrected by using Abott's formula.

$$\text{Corrected Mortality (\%)} = \frac{\text{Observed mortality (\%)} - \text{Control mortality (\%)}}{100 - \text{Control mortality (\%)}} \times 100$$

The median lethal concentration LC_{50} (the concentration needed to kill 50 % of larvae) and LC_{90} (the concentration needed to kill 90 % of larvae) were investigated from log concentration, probit mortality and linear regression.

A high mortality rate in untreated control (water or acetone-water in this experiment) may indicate that the larvae have been handled carelessly. During 24 h holding period subsequent to the exposure to insecticide, control mortality rates of less than 5 % may be disregarded but rates of 20 % or higher mean that the tests should be repeated. Between these two limit controls mortality rate is used to correct mortality rates in the exposed batches by the application of the formula.

Effect of Crude Extracts

LC_{50} and LC_{90} of *S. acmella* extracts on *A. aegypti* larvae were respectively found to be 0.0065 %, 0.0146 %. In addition, LC_{50} and LC_{90} of *M. azedarach* extract were 1.008 % and 3.693 % respectively. PE extract of *S. acemella* has more potent larvicidal activity than ethanol extract of *M. azedarach*.

The larvicidal activities of different concentrations of two plant extracts were presented in Table 1, 2 & Figure 3, 4. Table 3 and Figure 5 showed the larvicidal activity of synthetic larvicide (Abate). Table 4 represents the comparison of larvicidal activity of crude extracts and Abate (synthetic larvicide) after 24 h exposing period. The activities of two extracts were much more lower than that of Abate. However, natural insecticides are more safe and eco-friendly when compared to synthetic insecticides. All regression lines were found to be good fit that the data were not significantly heterogeneous. These test samples were fitted in regression line and showing the testing goodness of fit.

Table 1 Larvicidal Effect of PE Extract of *S. acmella* Aerial Parts on Immature Stages of *A. aegypti* Larvae

Concentration (%)	Dead/ Tested	Observed mortality (%)	Expected mortality (%)	(Observed - Expected) mortality	Contribution to χ^2 *
0.025	198/200	99	98.6	0.4	0.0010
0.0125	169/200	85	84	1	0.0007
0.00625	87/200	44	48	- 4	0.0060
0.003125	22/200	11	9	2	0.0040
				Total	**0.0117**

(* χ^2 = Chi square)

LC_{50} = 0.0065 % = 95 % Upper confidence limit of LC_{50} = 0.007
95 % Lower confidence limit of LC_{50} = 0.006

LC_{90} = 0.0146 % = 95 % Upper confidence limit of

LC_{90} = 0.0164 95 % Lower confidence limit of LC_{90} = 0.0128

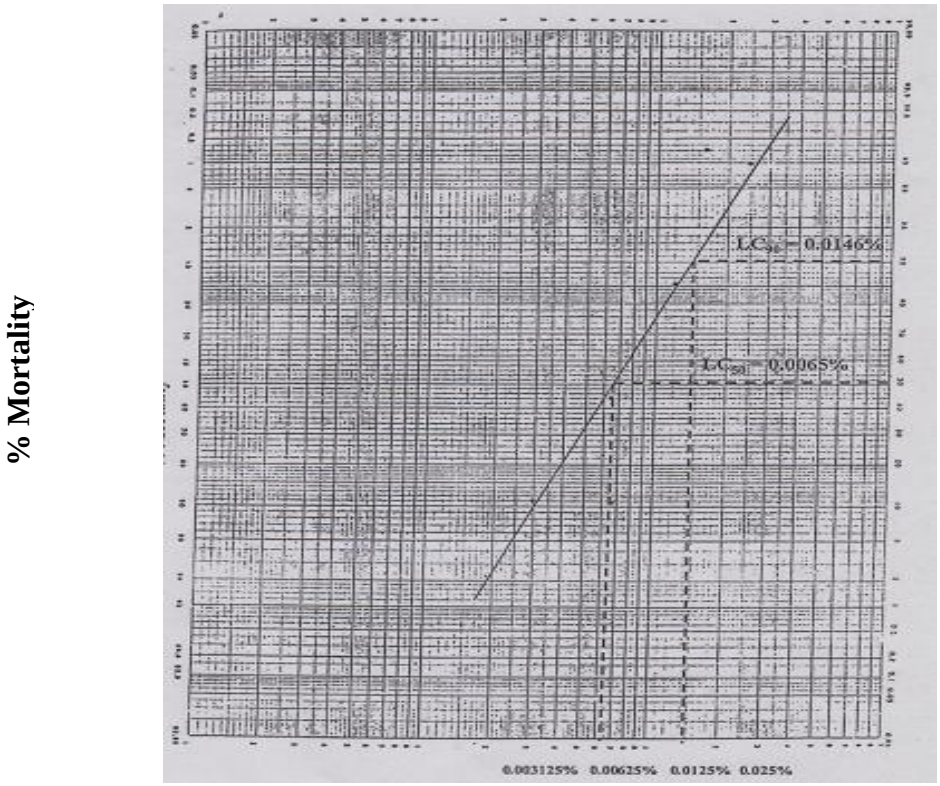

Figure 3 Testing the goodness of fit for dose effect analysis of PE Extract from *S.acmella* aerial parts (% concentration and *A.aegypti* larval mortality)

Table 2 Larvicidal Effect of EtOH Extract of *M. Azedarach* Bark on Immature Stages of *A. aegypti* Larvae

Concentration (%)	Dead/ Tested	Observed mortality (%)	Expected mortality (%)	(Observed - Expected) mortality	Contribution to χ^2
3.0	177/200	88.5	86.5	2	0.0034
1.5	128/200	64	66	-2	0.0017
0.75	68/200	34	38	-4	0.0067
0.375	29/200	14.5	16	-1.5	0.0016
				Total	0.0134

(* χ^2 = Chi square)

LC_{50} =1.008 % = 95 % Upper confidence limit of LC_{50} = 1.146

95 % Lower confidence limit of LC_{50} = 0.87

LC_{90} = 3.693 % = 95 % Upper confidence limit of LC_{90} = 4.518

95 % Lower confidence limit of LC_{90} = 2.868

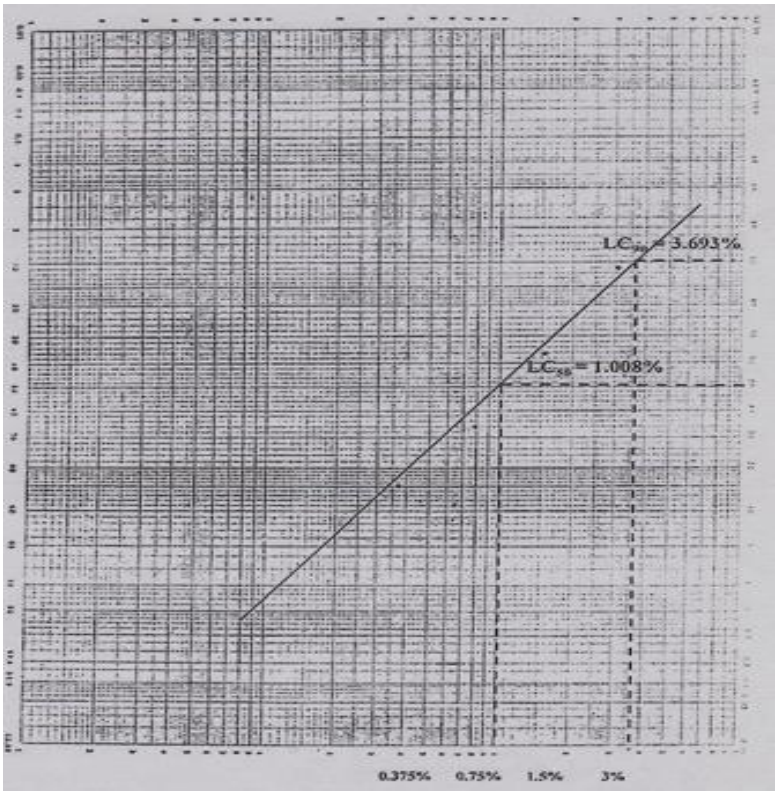

Figure 4 Testing the goodness of fit for dose effect analysis of EtOH extract of *M. azedarach* bark (%concentration and *A. aegypti* larval motality)

Table 3 Larvicidal Effect of Temephos (Abate) on Immature Stages of *A. aegypti* Larvae

Concentration (ppm)	Dead/ Tested	Observed mortality (%)	Expected mortality (%)	(Observed - Expected) mortality	Contribution to χ^2
0.0125	197/200	98.5	99	- 0.5	0.0025
0.00625	174/200	87	86	1	0.0008
0.003125	108/200	54	52	2	0.00163
0.0015625	15/200	7.5	9	-1.5	0.0027
				Total	0.0219

(* χ^2 = Chi square)

LC_{50} = 0.0034 ppm = 95 % Upper confidence limit of LC_{50} = 0.0034

95 % Lower confidence limit of LC_{50} = 0.0033

LC_{90} = 0.0075 ppm = 95 % Upper confidence limit of LC_{90} = 0.0082

95 % Lower confidence limit of LC_{90} = 0.0067

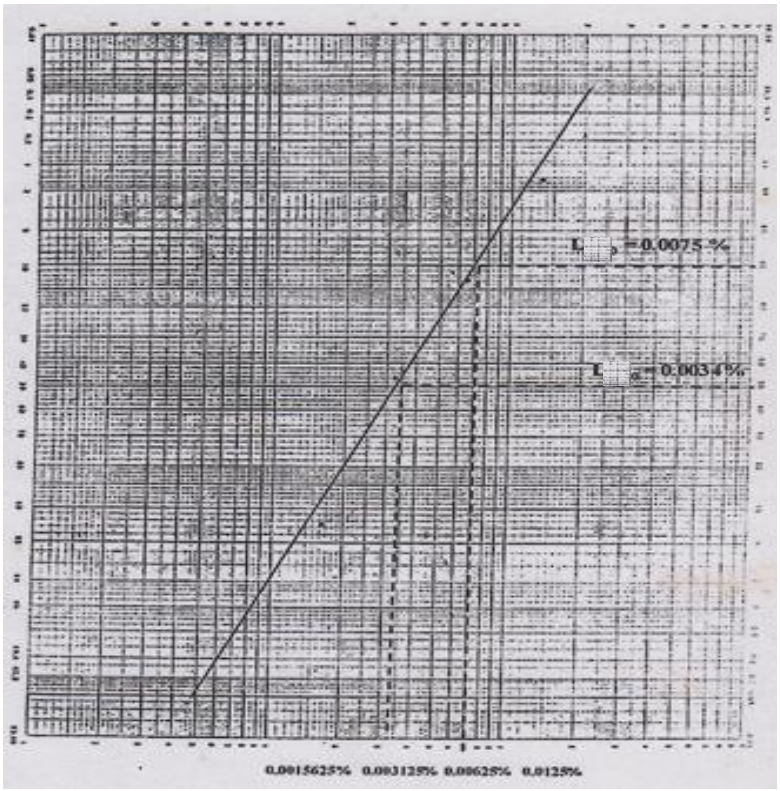

Figure 5 Testing the goodness of fit for dose effect analysis of temephos (Abate) on *A.aegypti* larvae; (% concentration and *A.aegypti* larval mortality)

Table 4 Comparison on LC_{50} and LC_{90} for tested samples

Tested samples	LC_{50} (%)	LC_{90} (%)
PE extract from aerial parts of *S.aemella*	0.0065	0.0146
EtOH extract from bark of *M. azedarach*	1.008	3.693
Temephos (Abate)	0.34×10^{-8}	0.75×10^{-8}

The Effective Persistency of Petroleum Ether Extract from *S. acmella* on *A. aegypti* Mosquito Larvae

Petroleum ether extract from aerial parts of *S. acmella* provided as a promise natural larvicides, the persistent effect of it was investigated on the immature 3rd and 4th instar stage, *A. aegypti* larvae and the results are shown in Table 5. The extract at 0.025 % concentration was found to be persisting up to 4 days (60 % in mortality rate).

Table 5 The Effective persistency of PE extract of *S. acmella* on immature stages of *A. aegypti* mosquito larvae

Concentration (%)	Effective persistency								Remark
	Day-1		Day-2		Day-4		Day-6		
	T	C	T	C	T	C	T	C	
0.025	87	2.5	76.5	1	60.5	0.5	12.5	0	*S. acmella* extract at 0.025 % persists up to 4 days and percent mortality was still 60 % on Day 4.
0.0125	38	2.5	34	1	41.5	0.5	12.5	0	
0.00625	22	2.5	12	1	9.0	0.5	1.0	0	
0.003125	1.5	2.5	4.5	1	8.5	0.5	0.5	0	

T = Test C = Control

Acute Toxicity Study of Ethanol Extracts from *S. acmella* Aerial Parts and *M. azedarach* Bark

The acute toxicity test was done according to the up-and-down procedure and the lethal dose of the ethanolic extracts of *S. acmella* and *M. azedarach* were estimated in mice. The animals are observed periodically during the first 24 h with special attention was given during the first four hours, then at least once a day after 14 days or until they recover. Clinical signs, including time of onset, duration, severity, and reversibility of toxic manifestations, were recorded at each observation period. Body weights were determined pre-treatment, weekly thereafter, and at the death of the animals or termination of the study.

In the acute toxicity test, signs of toxicity include muscle weakness, lethargy, loss of righting reflex and death.

It was observed that ethanolic extract of *S. acmella* in mice was no sign to toxic at 10 g/kg that is maximum permissible dose. Therefore, *S. acmella* extract can be safely used as larvicide and has no harmful effect to mammalian.

On the other hand, it was found that the maximum giving dose for ethanolic extract of *M. azedarach* in mice was 8 g/kg within survival period for 7 days to be looked forward. At dose 10 g/kg, one out of three mice was found to dead. *M. azedarach* showed slight toxicity. Therefore, care must be taken if bark of *M. azedarach* is used as larvicide.

Toxicity of Insecticide to Aquatic Vertebrate *Clarias batrachus* (Nga-khu)

The toxic effect of insecticide (Petroleum ether extract from aerial part of *S. acemella*) on *C. batrachus* (Nga-khu) was investigated for this study. The maximum giving dose was 0.025 % concentration level. The mortality of dead fishes was investigated after 24 h period. PE extract of *S. acemella* showed no toxic effect and no lethality was observed for 0.025 % dose. Therefore, *S. acmella* extract was not observed harmful effect on fishes *C. batrachus*.

Conclusion

PE extract from aerial part of *S. acemella* (LC_{50} = 0.0065 %, LC_{90} = 0.0146 %) and EtOH extract from bark of *M. azedarach* (LC_{50} = 1.008 %, LC_{90} = 3.693 %) showed potent larvicidal activities against the late third and fourth instar larvae (*A. aegypti* mosquito). The larvicidal

activity of synthetic larvicide, Temephos (Abate) was LC_{50}= 0.0034 ppm and LC_{90} = 0.0075 ppm. Ethanolic extract of *S. acmella* in mice was not shown sign to toxic at 10 g/kg that is maximum permissible dose. Therefore, *S. acmella* extract did not show harmful effect to mammalian.

In acute toxicity test, the maximum giving dose for ethanolic extract of *M. azedarach* in mice was 8 g/kg within survival period for 7 days to be looked forward. At dose 10 g/kg, bark of *M. azedarach* showed lethality (1 per 3 mice). Therefore, care must be taken if bark of *M. azedarach* is used as larvicide.

Petroleum ether extract of *S. acmella* was not observed lethality on fishes *C. batrachus* (Nga-khu) at 0.025 % concentration level. Therefore, PE extract of *S. acmella* was not found toxic effect to aquatic vertebrates and can be used safely as natural larvicide in fresh water.

Acknowledgement

The author would like to express profound gratitude to Myanmar Academy of Arts and Science for allowing to present this paper. Grateful thanks are also to Dr Hlaing Hlaing Oo, Professor and Head and Dr Sanda Khar, Professor, Department of Chemistry, West Yangon University, for their kind encouragement.

References

Adnan Y. A. (2009). "The Potential Uses of *Melia Azedarach* L. as Pesticidal and Medicinal Plant" *Am-Eurasian J. Sustain. Agric.*, vol. 3, pp. 185-194

Bruce, R. D. (1985). "An Up-and-Down Procedure for Acute Toxicity Testing". *Funda. Appl. Toxicol*., vol. 5, pp.151-157

Mohammad, A., Divya, J. and Amit, J. (2017). "A Review on Pharmacognostic and Phytochemical Study of a Plant *Spilanthes Acmella*". *The Pharma Innovation Journal*, vol.6, pp. 172-177

Rozendaal, J. A. (1997). Vector Control: Methods for Use by Individuals and Communities. World Health Organization, Geneva, pp.15-17

Swaroop, S. (1963). *Statistical Method in Malaria Eradication*. WHO Mono Graph Series, vol. 51, pp. 119

Verma, D. M., Balakrishnan, N. P. and Dixit, R. D. (1993). *Flora of Madhya Pradesh*. Kolkata,India: Botanical Survey of India, vol.1, pp. 612-613

WHO. (1997). *Operational Manual on the Application of Insecticides for Control of the Mosquito Vector of Malaria and other Diseases*. Division of Control of Tropical Diseases, Geneva, pp. 13

EXTRACTION, ISOLATION, ANTIMICROBIAL STUDY AND STRUCTURAL ELUCIDATION OF A PURE COMPOUND ISOLATED FROM THE TUBER OF *STEPHANIA GLABRA* (ROXB.) MIERS

Khup Lam Tuang[1], Hla Myoe Min[2], Myint Myint Sein[3]

Abstract

The tuber of *Stephania glabra* (Roxb.) Miers, one of Myanmar indigenous medicinal plants was selected for this research work. The sample was chopped in to small pieces and dried in air. The air dried tuber sample was extracted with 95% of ethanol for about one month. Moreover, it was further extracted with ethyl acetate and ran by different solvents polarities using thin layer and column chromatography. A biologically active pure compound (KLT-1) could be isolated from n-hexane and ethyl acetate solvent ratio (n-hex 19:1EtOAc, 40 mg, and R_f value 0.9). The antimicrobial activity of this pure compound was examined by agar well diffusion method on six selected organisms. It was highly responded on three microorganisms such as *Bacillus subtilis, Bacillus pumilus and E. coli*. The molecular formula of pure compound (KLT-1) was assigned as $C_{18}H_{30}O_2$ (ester compound) by FT IR (Fourier Transform Infrared), ^{1}H NMR (Proton Nuclear Magnetic Resonance), ^{13}C NMR (Carbon Nuclear Magnetic Resonance), DEPT (Distortion Enhancement by Polarization Transfer), HSQC (Heteronuclear Single Quantum Coherence) and DART (Direct Analysis of Real Time Mass Spectroscopy) mass spectral data. Moreover, the complete structure of pure compound could be elucidated by using advanced spectroscopic methods such as DQF-COSY (Double Quantum Filtered Correlation Spectroscopy) and HMBC (Heteronuclear Multiple Bond Coherence) spectral evidences. The prominent functional groups containing in this compound was assigned and its complete structure was described as follows.

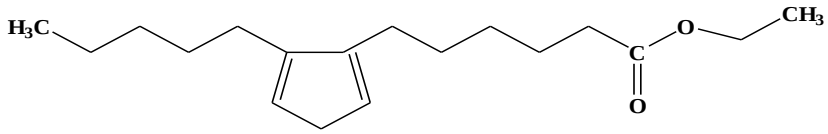

Ethyl-6-(5-pentyl) cyclopentadienyl hexanoate

Keywords: extraction, isolation, thin layer and column chromatography, antimicrobial activities, isolated compound, spectral evidences

Introduction

Medicinal plants serve as important therapeutic agents as well as valuable raw materials for manufacturing numerous traditional and modern medicines (Motaleb *et al.*, 2011). Extraction is the crucial first step in the analysis of medicinal plants, because it is necessary to extract the desired chemical components from the plant materials for further separation and characterization (Sasidharan *et al*., 2011). Successful determination of biologically active compounds from plants material is largely dependent on the type of solvent used in the extracting procedure (Tiwari, 2011). Column chromatography is generally used as a purification technique to isolate desired compounds from a mixture (Kenkel, 2003). Thin layer chromatography (TLC) is a simple, quick and a support material which is used to identify of a compound in a mixture. Additional tests involve the detection of I_2 vapour and UV lamp which cause color spots on TLC sheet (Sasidharan *et al*., 2011).

The tuber of *Stephania glabra* (Roxb.) Miers, Myanmar name is *Taung-kya* having high medicinal value was selected for this research paper. It has long been used in traditional practices

[1] Dr, Assistant Lecturer, Department of Chemistry, Mandalar Degree College
[2] Dr, Professor, Department of Chemistry, University of Mandalay
[3] Dr, Professor and Head (Retd.), Department of Chemistry, University of Mandalay

such as for treatment of asthma, tuberculosis, dysentery, hyperglycemia, cancer, fever, intestinal complaints, sleep disturbances and inflammation (Semwal and Semwal, 2015). The antimicrobial activity on six microbial strains using agar well diffusion method was prepared by its procedure. The structural elucidation of this pure compound (KLT-1) was assigned by using FT IR, NMR spectroscopic and DART MS techniques.

Morphology and Distribution of *Stephania glabra* (Roxb.) Miers

Stephania glabra (Roxb.) Miers (Figure 1) a species under the genus of climbers belonging to family menispermaceae (Semwal and Semwal, 2015). It has greenish yellowish flowers and large tubers weighing as much as 30 kg (Vashist *et al.*, 2012). It is mainly observed the flowering within April to May (Rai, 2018). Roots are tubers with fibrous roots below, round or oval also with irregular shapes (Thakur, 2016). This plant mainly grows in the tropical regions of India, Myanmar and China (Titova *et al*., 2012). It is herbaceous vines. Stems striate, glabrous, hollow. (Xianrui *et al*., 1996).

Figure 1 *Stephania glabra* (Roxb.) Miers (Source by Researcher)

Materials and Methods

Plant Material and Preparation

The tuber of *S. glabra* to be analyzed was collected from Kalay Township, Myanmar on September, 2015. This plant specimen was identified with the help of an expert, Pro-rector. Dr Soe Myint Aye, Myitkyina University. After washing and cleaning, the tuber was chopped in to small pieces and dried in air for 25 days. The dried sample was weighed and stored in a well stopper bottle and made to be ready for experiment.

Preparation of Extract

The plant sample (650 g) of *S. glabra* was occasionally percolated with 95% ethanol (6000 mL) for one month. After that, the ethanol extract was filtered by using Whatman No.1 filter paper and the filtrate was evaporated to obtain the viscous mass. The prepared extract 10.75 g (1.65 %) was obtained and stored at 4°C for further analysis. The extract yield percent (Adhikari *et al.*, 2015) was expressed as follows.

$$\text{Extraction yield (\%)} = \frac{\text{Weight of the dry extract (g)}}{\text{Weight of the sample used for the extraction (g)}} \times 100$$

Isolation

A few spots of ethyl acetate crude extract were checked on TLC plate by using n-hexane : EtOAc - 9:1, 1:1, 3:7 ratios for further separation. Common laboratory tools and commercially grade solvents were used for isolation of pure compound (KLT-1). The ethyl acetate extract sample (8.5 g) was fractioned by column chromatography over SiO_2 (70-230 mesh) eluting with n-hexane : ethyl acetate in various ratios from non-polar to polar (Figure 2). Totally (458) fractions were obtained and the resulted fractions were frequently checked by TLC with each relative solvent ratio system. Moreover, UV lamp and I_2 vapour were used as color visualizing materials for identification of the constituent compounds. The fractions of the same R_f values were combined and obtained (11) combine fractions. Among them, pure compound (KLT-1)

(40 mg and R_f = 0.9) was isolated from fraction 1 and it showed UV active as well as I_2 vapour on TLC plate (only one black spot) from the fraction of n-hexane : ethyl acetate (19:1) solvent ratio.

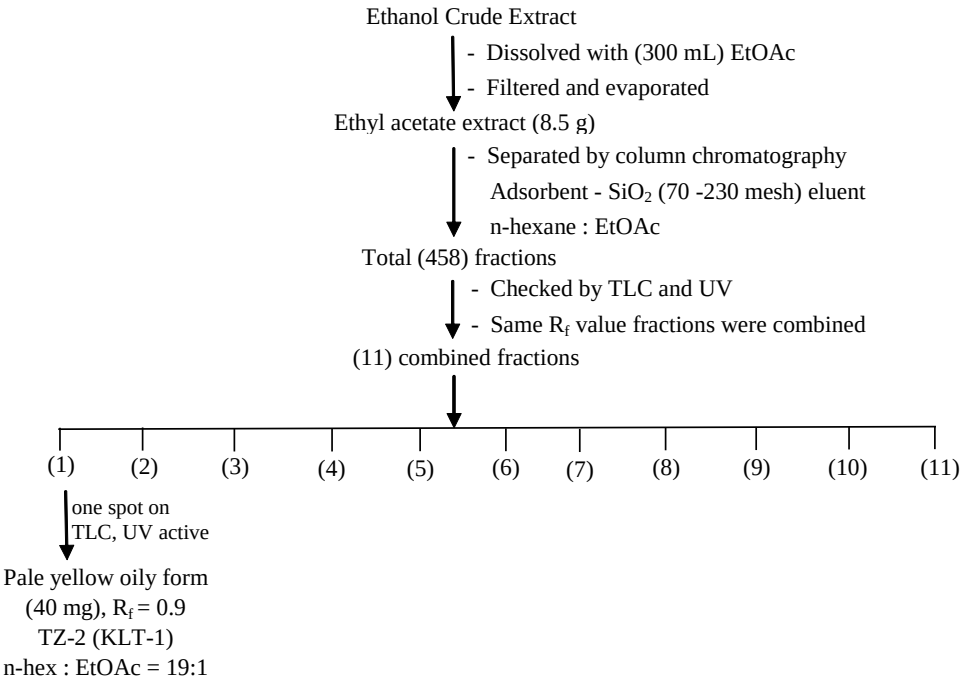

Figure 2 Isolation of pure compound (KLT-1) from the tuber of *S. glabra*

Test of The Pure Compound (KLT-1) for Antimicrobial Activity

The screening of antimicrobial activity of pure compound (KLT-1) was evaluated by Agar well diffusion method at Myanmar Pharmaceutical Industrial Enterprise, Ministry of Industry, Insein Township, Yangon. Totally, six microorganisms: *Bacillus subtilis, Staphylococcus aureus, Pseudomonas aeruginosa*, *Bacillus pumilus*, *Candida albicans* and *Escherichia coli* were used to assess their susceptibility to this compound (KLT-1)

Results and Discussion

Antimicrobial Activity of Pure Compound (KLT-1)

The antimicrobial activity of pure compound (KLT-1) was investigated against on six microorganisms; *Bacillus subtilis*(A), *Staphylococcus aureus*(B), *Pseudomonas aeruginosa* (C), *Bacillus pumilus* (D), *Candida albicans* (E), *Escherichia coli* (F). The results are shown in Table 1 and Figure 3.

Table 1 Antimicrobial Activity of Pure Compound (KLT-1) in Ethyl acetate

Compound	Inhibition zone diameter (mm)					
	A	**B**	**C**	**D**	**E**	**F**
KLT-1	20 **(+++)**	19 **(++)**	16 **(++)**	20 **(+++)**	17 **(++)**	20 **(+++)**

(+) Low = 10 ~14 mm (++) Medium = 15mm ~ 19 mm (+++) High = 20 mm above

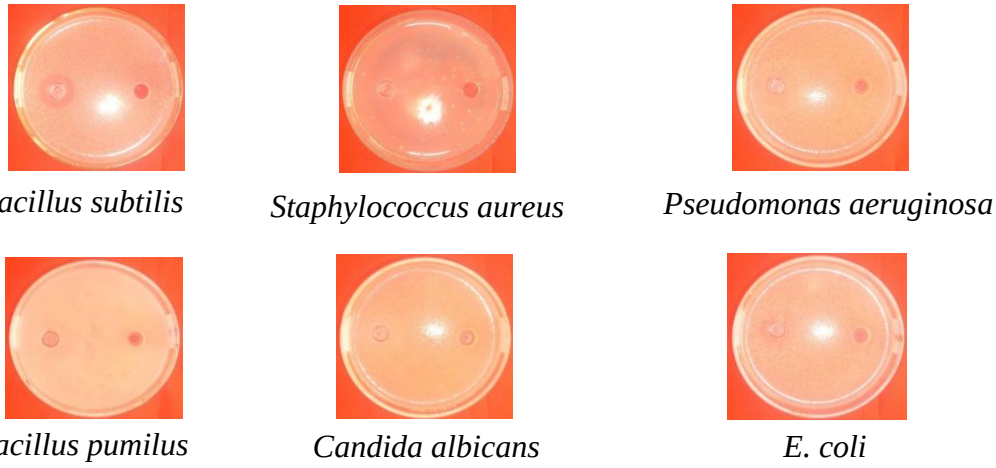

Figure 3 Antimicrobial activity of pure compound (KLT-1)

According to above table, the pure compound (KLT-1) was observed to have good antimicrobial activities on testing all organisms which especially showed high activity on three organisms such as *Bacillus subtilis*, *Bacillus pumilus* and *E.coli*. From these high microbial inhibitions, pure compound (KLT-1) could be considered as a biologically active compound for some medicinal effects on stomach disorders, skin, eye, respiratory tract and urinary tract diseases.

Determination of Molecular Formula of Pure Compound (KLT-1)

The molecular formula of isolated pure compound (KLT-1) was could be assigned by some spectroscopic methods such as FT IR, ^{1}H NMR (600MHz), ^{13}C NMR (150MHz), DEPT, HSQC and DART MS spectrometry.

Functional Groups Determination of Pure Compound (KLT-1)

FT IR spectrum of pure compound (KLT-1) is described in Figure 4 and their assignments are shown in Table 2. The peak 3072 cm^{-1} indicates C=C-H stretching vibration of sp^2 hydrocarbons. The bands at 2928 and 2854 cm^{-1} which should be asymmetric and symmetric C-H stretching vibration of sp^3 hydrocarbons. In addition, the band at 1735 cm^{-1} indicates C=O stretching vibration of carbonyl group. The C=C skeletal stretching vibration of aromatic ring could be observed at 1514 cm^{-1}. Moreover, the bands at 1458 cm^{-1} could be presented C-H in plane bending vibration of allylic hydrocarbons. The observed bands at 1273, 1230 and 1091 cm^{-1} which are due to the presence of C-C-O stretching vibration of alcohol and ether groups. The C=C-H out of plane bending vibration was presented in 864 cm^{-1}.

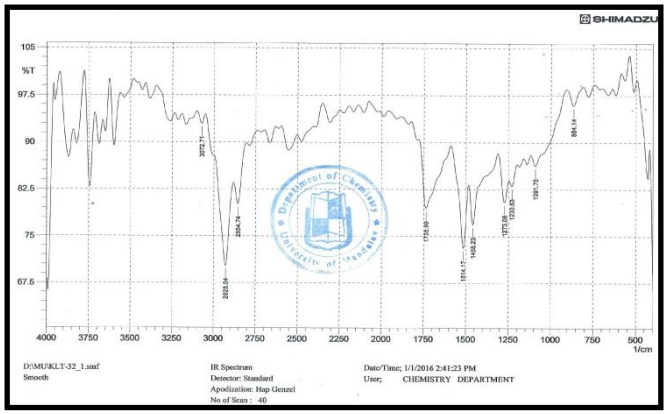

Figure 4 FT IR spectrum of pure compound (KLT-1)

Table 2 Characteristic Absorption Bands and their Assignments of Pure Compound (KLT-1)

No.	Wave number (cm^{-1})	Assignments
1	3072	C=C-H stretching vibration of sp^2 hydrocarbons
2	2928, 2854	Asymmetric or symmetric C-H stretching vibration of sp^3 hydrocarbons
3	1735	C=O stretching vibration of carbonyl group
4	1514	C=C stretching vibration of alkene
5	1458	C-H in plane bending vibration of allylic hydrocarbons
6	1273, 1230, 1091	-C-C-O stretching vibration of ester group
7	864	C=C-H out-of-plane bending vibration

^{1}H NMR Spectrum of Pure Compound (KLT-1)

According to ^{1}H NMR spectrum (Figure 5), this compound contains (30) protons and their assignments are shown in Table 3.

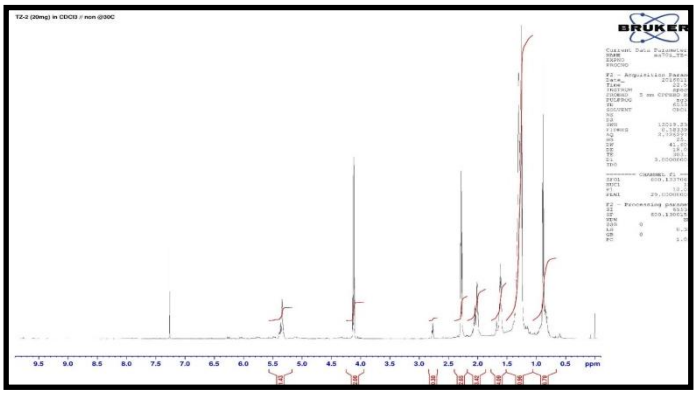

Figure 5 ^{1}H NMR spectrum of pure compound (KLT-1)

Table 3 ^{1}H NMR Spectral Data of Pure Compound (KLT-1)

Proton Assignment	^{1}H (δ/ppm)	J values (Hz)	Splitting Pattern	No. of Proton
sp^3 methyl proton	0.88	6.66, 7.14	t	3H
sp^3 methyl proton	1.25	7.14	t	3H
sp^3 methylene proton	1.2-1.3	-	overlap	12H
sp^3 methylene proton	1.62	6.84, 7.14	t	2H
sp^3 methylene proton	2.03, 2.04	-	m	2H
sp^3 methylene proton	2.28	7.50, 7.62	t	2H
sp^3 methylene proton	2.77	6.78, 6.79	t	2H
sp^3 methylene proton	4.12	7.14	q	2H
sp^2 methine proton	5.33, 5.34	-	m	2H
		Total number of protons		**30**

In this spectrum, there is overlap peaks between δ value 1.2 and 1.3 ppm protons. Thus, this compound should contain at least 30 protons (Figure 5).

^{13}C NMR Spectrum of Pure Compound (KLT-1)

The ^{13}C NMR spectrum (Figure 6), represents the total number of (18) carbons containing in this compound. The chemical shift values and their assignments are described in Table 4.

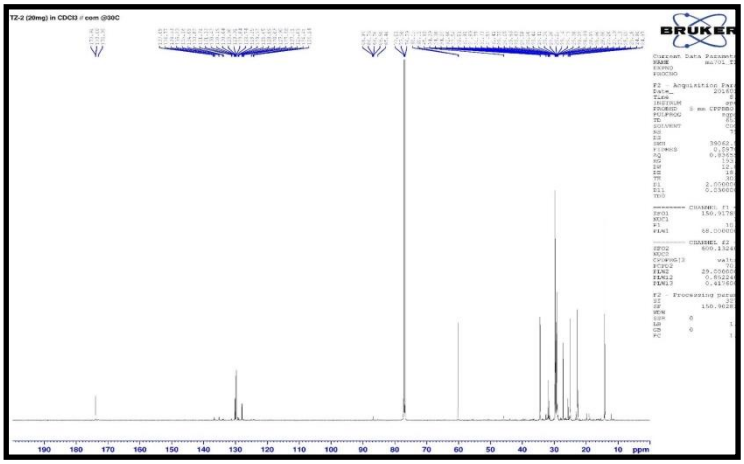

Figure 6 ^{13}C NMR spectrum of pure compound (KLT-1)

Table 4 ^{13}C NMR Spectral Data of Pure Compound (KLT-1)

No	^{1}H (δ/ppm)	Types of Carbon	Remarks
1	14.08	sp^3 methyl carbon	1
2	14.23	sp^3 methyl carbon	1
3	22.67	sp^3 methylene carbon	1
4	24.98	sp^3 methylene carbon	1
5	25.62	sp^3 methylene carbon	1
6	27.15	sp^3 methylene carbon	1
7	27.20	sp^3 methylene carbon	1
8	29.14	sp^3 methylene carbon	1
9	29.34	sp^3 methylene carbon	1
10	29.67	sp^3 methylene carbon	1
11	31.91	sp^3 methylene carbon	1
12	34.39	sp^3 methylene carbon	1
13	60.12	sp^3 methylene carbon	1
14	128.03	sp^2 methine carbon	1
15	129.89	sp^2 methine carbon	1
16	130.03	sp^2 quaternary carbon	1
17	130.19	sp^2 quaternary carbon	1
18	173.19	quaternary carbon	1
Total number of carbons			**18**

According to ^{13}C NMR spectrum (Figure 6), there is overlap proton region between δ 28-30 ppm. Number of carbon was accounted as (18) carbons. Therefore, this compound should contain at least (18) carbons.

HSQC Spectrum of Pure Compound (KLT-1)

HSQC spectrum of pure compound (Figure 7) which gives the proton-carbon direct correlation. The chemical shift values of protons and carbons are shown in Table 5.

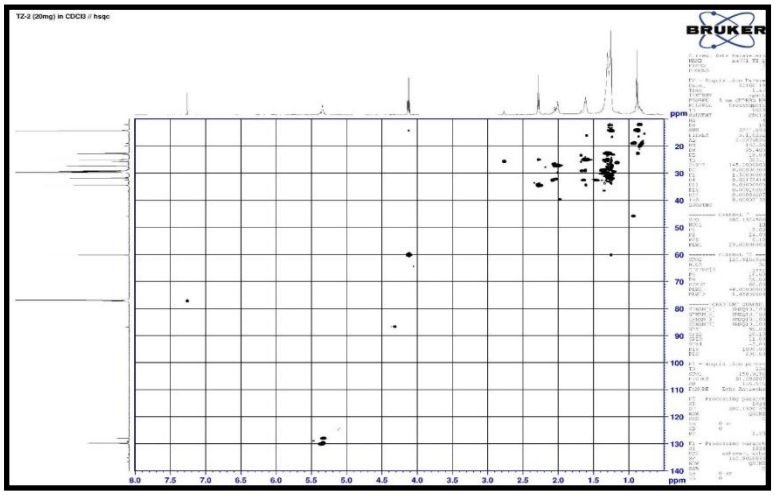

Figure 7 HSQC Spectrum of Pure Compound (KLT-1)

Table 5 ^{1}H-^{13}C Correlation Spectrum of Pure Compound (KLT-1)

No	^{13}C (δ/ppm)	^{1}H (δ/ppm)	Assignments	
1	14.08	0.88	sp^3 methyl carbon	CH_3
2	14.23	1.25	sp^3 methyl carbon	CH_3
3	22.67	1.25	sp^3 methylene carbon	CH_2
4	24.98	1.62	sp^3 methylene carbon	CH_2
5	25.62	2.77	sp^3 methylene carbon	CH_2
6	27.15	2.03	sp^3 methylene carbon	CH_2
7	27.20	2.04	sp^3 methylene carbon	CH_2
8	29.14	1.25	sp^3 methylene carbon	CH_2
9	29.34	1.25	sp^3 methylene carbon	CH_2
10	29.67	1.25	sp^3 methylene carbon	CH_2
11	31.91	1.25	sp^3 methylene carbon	CH_2
12	34.39	2.28	sp^3 methylene carbon	CH_2
13	60.12	4.12	sp^3 methylene carbon	CH_2
14	128.03	5.33	sp^2 methine carbon	=CH
15	129.89	5.34	sp^2 methine carbon	=CH
16	130.03	-	sp^2 quaternary carbon	=C
17	130.19	-	sp^2 quaternary carbon	=C
18	173.19	-	quaternary carbon	$\diagdown\!\!\diagup$C=O

Number of methylene groups that account carbon chemical shift value at about 29 ppm and proton chemical shift value at about 1.25 ppm may be at least 18 carbons and 30 protons as mentioned in the table.

DEPT Spectrum of Pure Compound (KLT-1)

DEPT spectrum (Figure 8) which classify the types of carbon and the number of carbons as well as protons containing in this pure compound (KLT-1). The respective data assignments are tabulated in Table 6.

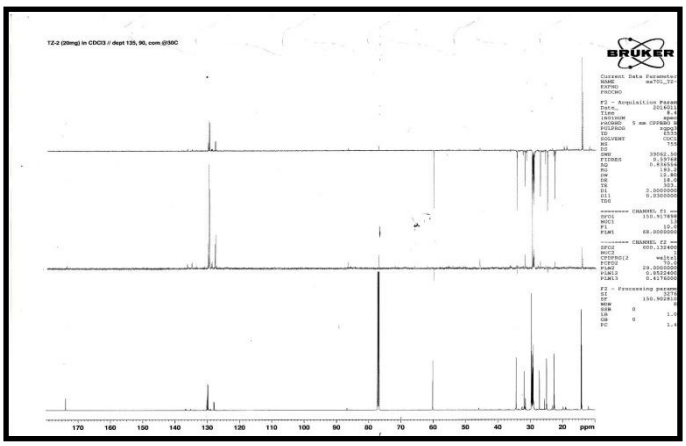

Figure 8 DEPT Spectrum of Pure Compound (KLT-1)

Table 6 DEPT Spectral Data of Pure Compound (KLT-1)

No	^{13}C (δ/ppm)	Assignments	No. of Carbons	No. of Protons
1	14.08	sp^3 methyl carbon	1	3
2	14.23	sp^3 methyl carbon	1	3
3	22.67	sp^3 methylene carbon	1	2
4	24.98	sp^3 methylene carbon	1	2
5	25.62	sp^3 methylene carbon	1	2
6	27.15	sp^3 methylene carbon	1	2
7	27.20	sp^3 methylene carbon	1	2
8	29.14	sp^3 methylene carbon	1	2
9	29.34	sp^3 methylene carbon	1	2
10	29.67	sp^3 methylene carbon	1	2
11	31.91	sp^3 methylene carbon	1	2
12	34.39	sp^3 methylene carbon	1	2
13	60.12	sp^3 methylene carbon	1	2
14	128.03	sp^2 methine carbon	1	1
15	129.89	sp^2 methine carbon	1	1
16	130.3	sp^2quaternary carbon	1	-
17	130.19	sp^2 quaternary carbon	1	-
18	173.91	quaternary carbon	1	-
Total number of protons and carbons			18	30

Confirmation of Molecular Formula of Pure Compound (KLT-1)

The elucidated partial molecular formula could be confirmed by DEPT (Figure 8) and FT IR (Figure 4) spectral evidences. The actual formula mass of this compound could be confirmed by DART MS spectrum (Figure 9). The assignments are represented in Table 7.

Table 7 Results Given by DEPT and FT IR Spectra

Assignment	Carbon	Proton	Oxygen
DEPT Spectral Data			
- Two sp^3 methyl carbon	2	6	-
- Eleven sp^3 methylene carbon	11	22	-
- Two sp^2 methine carbons	2	2	-
- Two sp^2 quaternary carbons	2	-	-
- One quaternary carbon	1	-	-
FT IR spectral data			
- One carbonyl group		-	1
- One ester group	-	-	1
Molecular Formula	C_{18}	H_{30}	O_2

The molecular formula of compound (KLT-1) could be assigned as $C_{18}H_{30}O_2$. The mass spectrum shows the molecular ion peaks either 391.2827 or 279.1580 Da. Among these two possibilities the mass at m/z 279.1580 is assigned as molecular ion peak of this compound. Hence molecular mass of pure compound (KLT-1) is now assigned as 278 by subtracting one unit of proton from the mass at m/z 279.1580 Da.

From the index of hydrogen deficiency index (HDI)

$$= C - \frac{H}{2} + \frac{N}{2} + 1$$

$$= IV - \frac{I}{2} + \frac{III}{2} + 1$$

$$= 18 - \frac{30}{2} + 0 + 1$$

$$= 4$$

According to formula index of hydrogen deficiency, the number of (HDI) is 4. This index number should be, in accordance with FT IR and NMR spectra, one $>C=O$ group, two $>C=C<$ groups and the last one should one cyclic (ring) system. Therefore, it must contain one $-C(=O)-$ group, two $C=C$ group and one ring system.

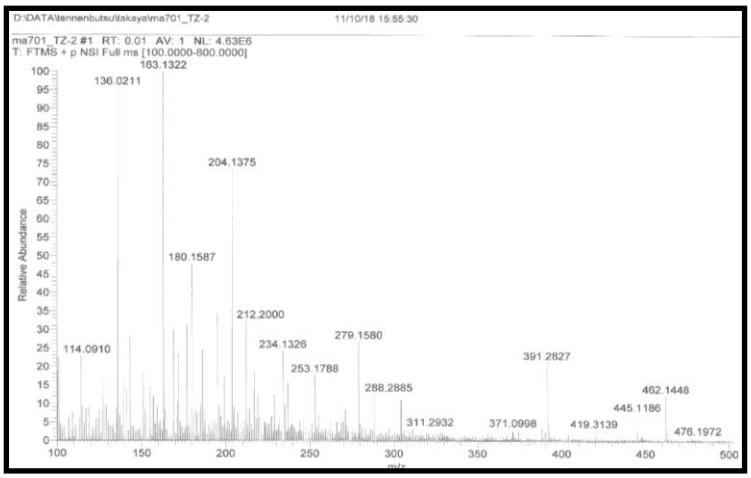

Figure 9 DART MS spectrum of pure compound (KLT-1)

Structural Elucidation of Pure Compound (KLT-1)

DQF COSY spectrum (Figure 10) shows the large square peaks that account the proton signal quartet at δ 4.12 ppm is coupling with protons at 1.25 ppm. From HSQC spectrum (Figure 7) direct attachment of these protons to carbons can be assigned as follows. In the ^{1}HNMR spectrum (Figure 5), first order coupling of signal, J = 7.14 Hz, quartet pattern clearly informs that the neighbouring carbon atom must bear three protons, that is methyl group.

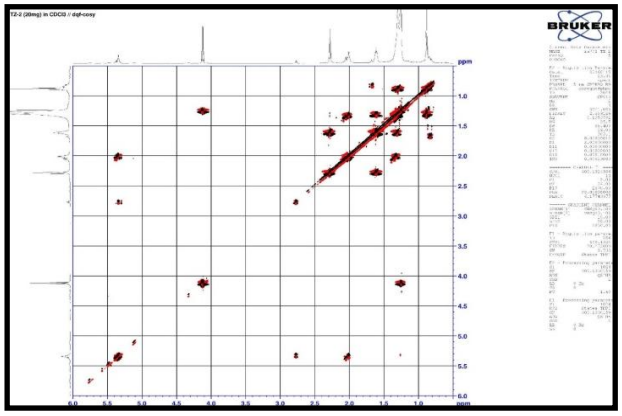

Figure 10 DQF COSY spectrum of pure compound (KLT-1)

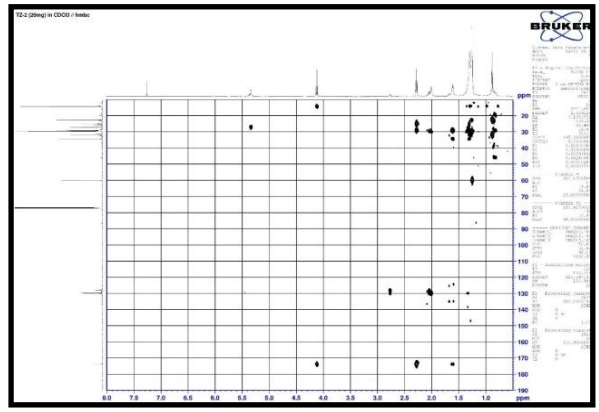

Figure 11 HMBC spectrum of pure compound (KLT-1)

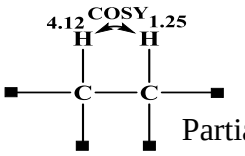

Partial (2)

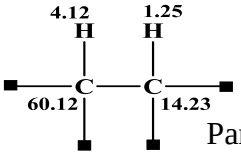

Partial (2)

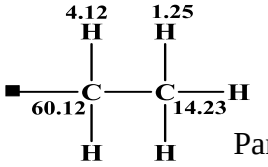

Partial (3)

In accordance with DEPT spectrum (Figure 8), above two carbons are assigned as methylene (60.12 ppm) and methyl (14.23 ppm) respectively. Again, based on lower field chemical shift values of both protons and carbon, sp^3 methylene carbon is considered to attach directly with oxygen atom. Thus following partial structure (A), ethoxy group is assigned. Presence of partial structure (A) can be confirmed by occurrence of proton-carbon correlation cross peak corresponding to δ 4.12 to 14.23 ppm and δ 1.25 to 60.12 ppm in HMBC spectrum (Figure 11).

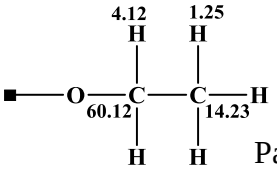

Partial structure (A)

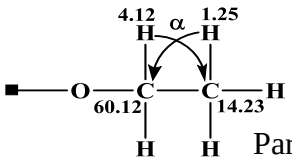

Partial structure (A)

Next, there are square cross peaks in DQF-COSY spectrum (Figure 10), that correspond to the two methylene groups at δ 2.28 ppm and 1.62 ppm respectively. This is an indication for vicinal arrangement of these two groups. Again δ 1.62 methylene protons show further vicinal coupling with respect to methylene protons appeared at δ 1.25 ppm. Therefore, following extended partial (4) can be deduced.

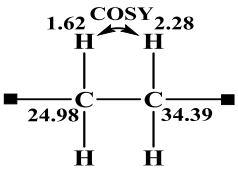

Partial (4)

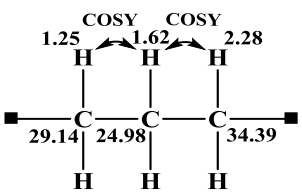

Partial (4)

Existence of partial (4) can be confirmed by HMBC spectrum (Figure 11). There are correlation cross peaks in HMBC spectrum that correspond to (i) δ1.25 ppm protons with 24.98 ppm carbon and 34.39 ppm carbon, (ii) δ 1.62 ppm protons with 29.14 ppm carbon and 34.39 ppm carbon and (iii) δ 2.28 ppm protons with 24.98 ppm carbon and 29.14 ppm carbon respectively. Moreover, there is an important long range coupling cross peak between δ 2.28 methylene protons as well as δ 1.62 ppm proton and carbonyl carbon at 173.19 ppm. This observation provides a good clue to connect carbonyl group with δ 2.28 methylene group. Thus, following partial structure (B) can be assigned. The partial structures (A) and (B) can be connected in accordance with HMBC (Figure 11).

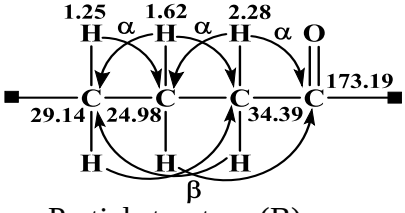

Partial structure (B)

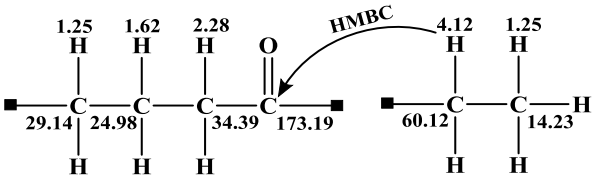

Partial structure (B) Partial structure (A)

In HMBC spectrum (Figure 11), there is a correlation cross peak between the methylene protons at δ 4.12 ppm from partial structure (A) and carbonyl carbon at δ 173.19 ppm from the partial structure (B). This cross peak shows connection sites between the two partial structures (A) and (B). Thus, the following partial structure (C) can be written.

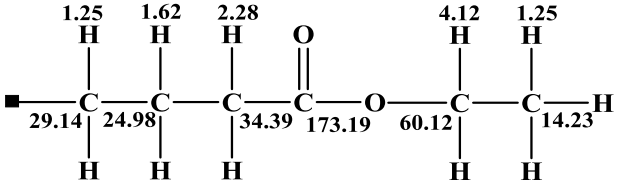

Partial structure (C)

On the other hand, the methyl signal (0.88, triplets) is assigned to coupling with its adjacent methylene protons at 1.25 ppm. This assignment is due to the clear triplet pattern appearance of methyl signals. On the basis of ^{1}H NMR (Figure 5) and DQF-COSY (Figure 10) spectral evidence, following propyl group is deduced. The presence of propyl group is confirmed by proton-carbon long range coupling cross peaks observed in HMBC spectrum (Figure 11). This propyl terminal group is assigned as partial structure (D).

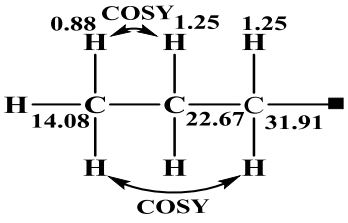

Partial structure (D)

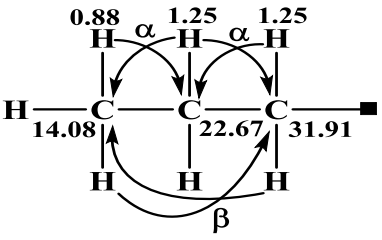

Partial structure (D)

In the ^{1}H NMR spectrum (Figure 5), the triplet proton signal at δ 2.77 ppm is assigned double allylic methylene protons. Proton-carbon assignment is taken by appearance of cross peak in HSQC spectrum (Figure 7). Downward signal in DEPT spectrum (Figure 8) supports the presence of methylene group. Proton chemical shift value δ 2.77 ppm gives a good evidence for the existence of double allylic one. In the DQF-COSY spectrum (Figure 10), these methylene protons reveal the vicinal coupling with two alkenic protons at δ 5.33 ppm and 5.34 ppm respectively. Thus, the following partial (5) can be deduced. Proton-carbon direct attachment of

alkenic protons is assigned by the correlation cross peaks observed in HSQC spectrum (Figure 8).

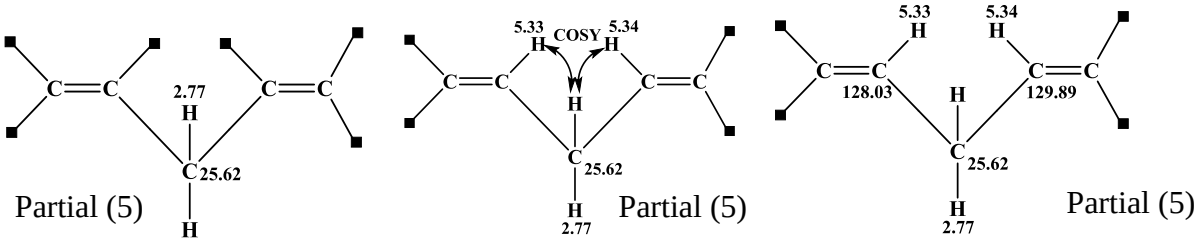

Partial (5) Partial (5) Partial (5)

Again in DQF-COSY spectrum (Figure 10), there are square peaks related to these two alkenic protons and two allylic methylene protons appeared at δ 2.03 ppm and 2.04 ppm. In accordance with this spectral evidence partial (5) is extended to following partial (6). Carbon assignment for the two allylic methylene groups is accomplished by correlation cross peak observed in HSQC spectrum (Figure 8), as well as the downward appearance in DEPT spectrum (Figure 8). In addition, DQF-COSY (Figure 10) represents that these two allylic methylene protons are further coupling with methylene groups appeared at δ 1.25 ppm. The partial (6) that has seen now assigned as partial structure (E).

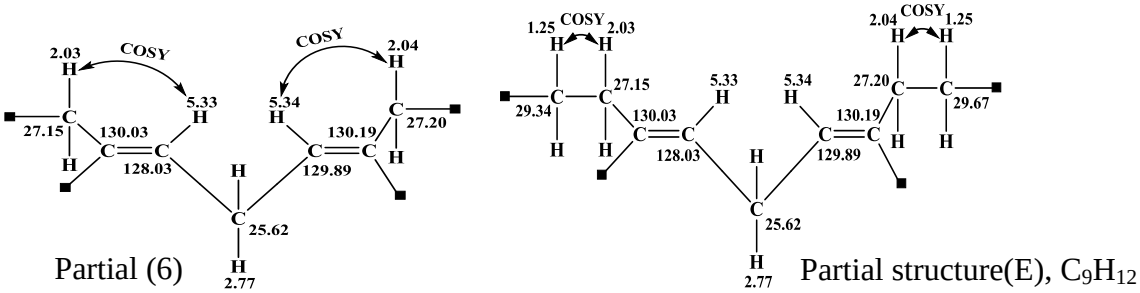

Partial (6) Partial structure(E), C_9H_{12}

Since, the compound showed UV absorption on TLC (black spot). This supported a good information that there should be conjugated system within the compound. This spectrum can have only two missing parts of alkenic quaternary carbons in the partial structure combine to form conjugated five membered cyclic ring. On the basis of UV-absorption phenomenon, partial structure (E) has changed in to following partial structure containing conjugated cyclic ring.

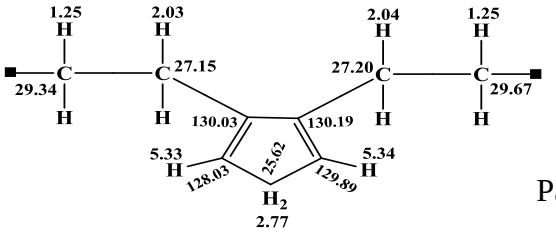

Partial structure (E), $[C_9H_{12}]$

The presence of cyclopentadienyl ring system could be further confirmed by proton-carbon correlation cross peaks found in HMBC spectrum (Figure 11). Double allylic methylene protons δ 2.77 ppm show α- and β- correlation with respect to all of alkenic carbons at δ 130.03ppm, 130.19 ppm, 128.03 ppm and 129.89 ppm. Again methylene protons at δ 2.03 ppm and 2.04 ppm also showed α- and β- correlation to these four alkenic carbons. These correlations can show only if all of alkenic carbons are the part of cyclic ring.

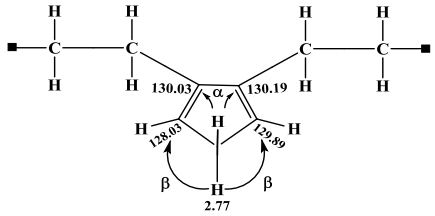

Partial structure (E), [C_9H_{12}]

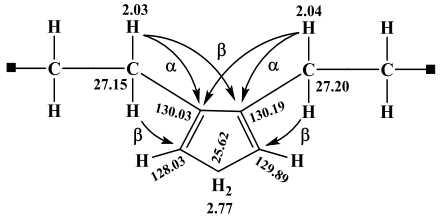

Partial structure (E), [C_9H_{12}]

Now, three partial structures could have been elucidated on the basis of spectral evidences.

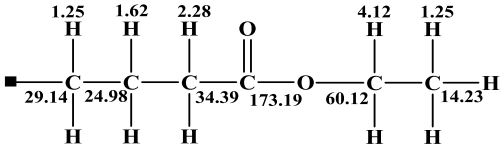

Partial structure (C), [$C_6H_{11}O_2$]

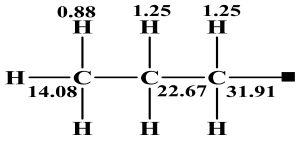

Partial structure (D), [C_3H_7]

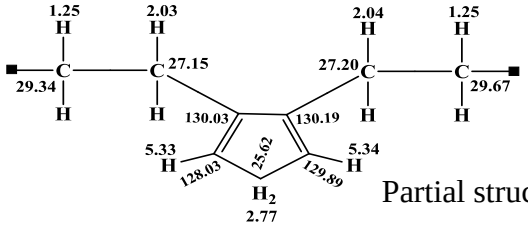

Partial structure (E), [C_9H_{12}]

Among three structures, partial structure (E) is common for linear combination of them this means that the partial structure (C) and partial structure (D) must connect with partial structure (E). But the connection sites on all partial structures show methylene groups at about δ 1.25 ppm. This gives ambiguous combination for following combine structure.

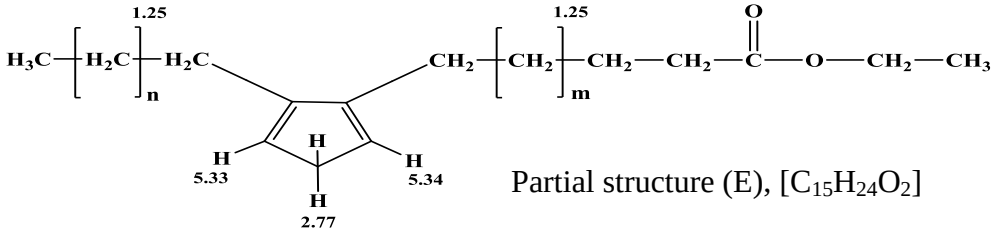

Partial structure (E), [$C_{15}H_{24}O_2$]

Mass spectrum (Figure 9) of compound (KLT-1) showed the molecular ion peak at m/z 279.1580 Da. Actual mass is therefore obtained by subtracting one unit from the molecular ion peak. Thus, molecular mass is assigned as m/z 278.1501 Da. When 'n' is taken as 3 and 'm' is 2, the resulting structure is in agreement with observed molecular mass m/z 278. The IUPAC name of pure compound (KLT-1) is assigned as ethyl-6-(5-pentyl) cyclopentadienyl hexanoate.

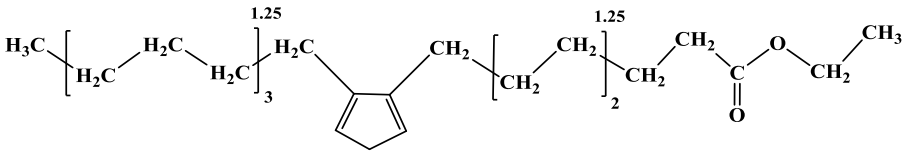

Molecular Formula = $C_{18}H_{30}O_2$ Molecular mass = 278 Da

Assignments of Some Prominent Peaks of Pure Compound (KLT-1)

In DART (Direct Analysis of Real Time) mass spectrum (Figure 9), generally the more stable and the higher the intensity (relative abundance) of the peaks are observed due to the fragmentation behavior. Some prominent peaks m/z 234, 163,136 and m/z 204 can be interpreted by following mechanistic fragmentation pathway.

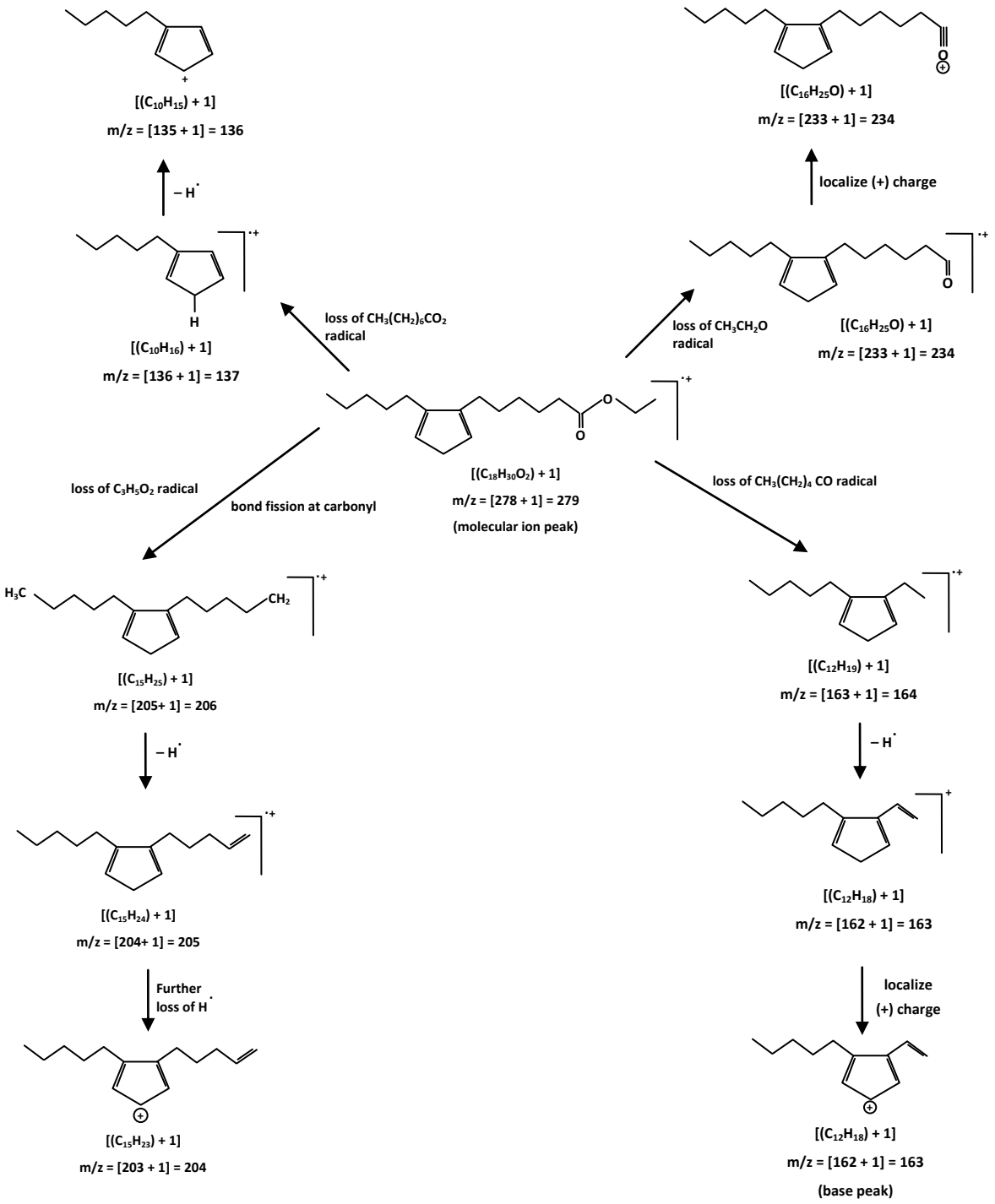

Conclusion

A biologically active wild plant, *Stephania glabra* (Roxb.) Miers (*S. glabra*), Myanmar named as *Taung-kya* was selected for this research. The tuber part (16 kg) of this plant was selected and done extraction, isolation, antimicrobial activity and structural elucidation. The crude extract from the tuber of *Stephania glabra* was performed by solvent extraction method. Furthermore, the pure compound (KLT-1), ethyl-6-(5-pentyl) cyclopentadienyl hexanoate could has been isolated by using Thin Layer and Column Chromatographic separations.

Antimicrobial activities of this isolated ester compound (KLT-1), was tested on six selected organisms by agar well diffusion method. As the results, It was observed to have good

antimicrobial activities against on testing all organisms. In addition, it showed excellent activity on three bacteria such as *Bacillus subtilis* (which causes food poison, skin and respiratory tract infection), *Bacillus pumilus* (which causes eye and food poisoning) and *E. coli* (which causes diarrhea, dysentery and urinary tract infection). According to these high activities, isolated pure compound (KLT-1) was found to have medicinal effects on stomach disorders, skin, eye, respiratory tract and urinary tract diseases, etc. Finally, the molecular formula and its structure of pure compound (KLT-1), ethyl-6-(5-pentyl) cyclopentadienyl hexanoate from the tuber extract of *S. glabra* was assigned as $C_{18}H_{30}O_2$ by applying advance spectroscopic techniques such as FT IR, ^{1}H NMR (600MHz), ^{13}C NMR (150 MHz), DEPT, HSQC, DQF COSY, HMBC, and DART MS spectral evidences.

Acknowledgements

First and foremost, the authors acknowledge the Myanmar Academy of Arts and Science (Department of Higher Education), Ministry of Education, Yangon, Myanmar, for allowing us to participate, and to present this paper. Authors would like to express special thanks to Associate Professor, Dr Yoshio Takaya, Faculty of Pharmacy, Meijo University, Nayoga, Japan, for supporting spectral data. One of the authors (Khup Lam Tuang) wish to thank Professor and Head, Dr Yi Yi Myint, Department of Chemistry, University of Mandalay, for her careful assessments and valuable suggestions.

References

Adhikari, A.V., Poojary, M.M. and Vishnumurthy, K.A. (2015). "Extraction, Characterization, and Biological Studies of Phytochemicals from *Mammea suriga*". *Journal of Pharmceutical Analysis,* vol. 5, pp. 182-183

Kenkel, J. V. (2003). *Analytical Chemistry for Technicians*. Florida: Third Edition, Boca Raton, Corporate Ltd, pp 310-367

Motaleb, M.A. (2011). *Selected Medicinal Plants of Chittagong Hill Tracts*. Dhaka: IUCN (International Union for Conservative of Nature), Bangalesh

Rai, P. (2018). *Common Flora of South Sikkim: A Glance to Ethnicity and Diversity of Common Flora of South Sikkim*.

Sasidharan, S., Chen, Y., Saravanan, D., Sundram, K.M. and Latha, L.Y. (2011). "Extraction, Isolation and Characterization of Bioactive Compounds from Plant's Extracts". *African Journal of Traditional Complement Alternative Medicine*, vol. 8, pp. 1-10

Semwal, D.K. and Semwal, R.B. (2015). "Efficacy and Safety of *Stephania glabra*: An Alkaloid-rich Traditional Medicinal Plant". *Natural Product Research: Formerly Natural Product letters*, vol. 29, pp. 396-410

Silverstein, R.M., Webster, F.X. and Kiemle, D.J. (2005). *Spectrometric Identification of Organic Compounds*. New York: 7th edition

Thakur, A. (2016). Flowers of India: *Stephania glabra*–Hairless Tape Vine, Home page. (https://www.flowersofindia.net)

Titova. M.V., Reshetnyak, O.V., Osipova, E.A., Osip'yants, A.I., Shumilo, N.A., Oreshnikov, A.V. and Nosvo, A.M. (2012). "Submerged cultivation of *Stephania glabra* (Roxb.) Miers Cells in Different Systems: Specific Feature of Growth and Accumulation of Alkaloids Stepharine". *Applied Biochemical of Microbiology,* vol. 48, pp. 645-649

Tiwari, P., Bimlesh, Kaur, B., kuar, M., kuar, G. and kuar, H. (2011). "Phytochemical Screening and Extraction: A Review". *Internationale Pharmaceutica Sciencia; An international Pharmaceutica Sciencia*, vol. 1, pp. 98-105

Vashist, H., Upmanyu, N., Gupta, A., Jindal, A., Jalhan, S. (2012). "Pharmacological Activities of *Stephania glabra*, *Woodfordia Fruticosa* and *Cissampelos pareira*-A Review". *International Journal of Pharmacy and Pharmceutical Science*, vol. 4, pp. 16-23

Xianrui, L., Tao, C. and Gilbert, M.G. (1996). *Menispermaceae*. Chinese Academic of Science: South China Botanical Garden, pp. 21-22

ISOLATION OF MICROZELANICUM FROM THE PLANT OF *CLAUSENA HEPTAPHYLLA* (ROXB.) WIGHT & ARN

Zar Chi Myint[1], Ko Ko Myo[2], Hnin Yu Win[3], Myint Myint Sein[4]

Abstract

The present research paper describes the first isolation of 7-methoxy-6-(1'-methyl-4'-oxo-3', 6'-dioxabicyclo[3.1.0]hexan-2'-yl)-2H-chromen-2-one (Microzelanicum, $C_{15}H_{12}O_6$) from the plant of *Clausena heptaphylla* (Roxb.) Wight & Arn which belongs to the family Rutaceae. The structure of isolated pure compound was confirmed by spectroscopic data measurements (^{1}H- and ^{13}C-NMR, 2D NMR, and MS). The structure of isolated pure compound, Microzelanicum ($C_{15}H_{12}O_6$), is shown below.

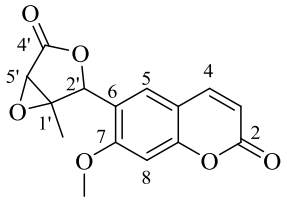

1

7-methoxy-6-(1'-methyl-4'-oxo-3',6'-dioxabicyclo[3.1.0]hexan-2'-yl)
-2*H*-chromen-2-one

Microzelanicum

Keywords: Isolation, *Clausena heptaphylla*, Rutaceae, Microzelanicum

Introduction

Clausena heptaphylla (Roxb.) Wight and Arn. (Bengali name: Panbilash, Karanphul, Pomkaphur and Myanmar name is Taw-Pyin-Taw-Thein) is a small bushy shrub and widely distributed throughout Bangladesh, India and other parts of south East Asia. *Clausena* species are known to be useful in the treatment of paralysis, ulcerated nose, headache, muscular pain and malarial fever (Begum *et al*., 2011) and are also reputed as diuretic, astringent, insecticide, tonic and vermifuge. The leaves of the plants possess antimicrobial properties (Fakruddin *et al*., 2011). Previous phytochemical investigations of *Clausena* species have been reported that led to the isolation of 7-Demethylmurralonginol isovalerate and Murralonginol (Lekphrom *et al*., 2011), Micromelin (Cassady *et al*., 1979), Clausenolide-1-methyl ether (Begum *et al*., 2011), Lunamarins A and B (Sohrab *et al*., 1999), Lunamarin C (Sohrab *et al*., 2000), Carbazole Alkaloid (Chakraborty *et al*., 1995), Clausenalene (Bhattacharyya *et al*., 1993), Clausmarin-A (Sohrab *et al*., 2000), and **Microzelanicum** (1) which is the first report of its occurrence from this plant.

[1] Assistant Lecturer, Department of Chemistry, Meiktila University
[2] Assistant Lecturer, Department of Chemistry, University of Mandalay
[3] Associate Professor, Department of Chemistry, University of Mandalay
[4] Professor and Head (Rtd.), Department of Chemistry, University of Mandalay

Materials and Methods

General Experimental Procedures

NMR spectra were measured on a Bruker Ascend TM (400 MHz) spectrometer. Mass spectra were measured on an Agilent liquid chromatography/mass spectrometry (LC/MS, Triple Quadrupol mass spectrometer). Column chromatography was carried out on silica gel (70-230) mesh. Analytical preparative thin layer chromatography was conducted on Kiesel gel 60 (F254, Merck). In thin layer chromatography, visualization was taken via UV lamp (Lambada-40, Perkin-Elmer Co, Japan) and iodine developing vapour. Crude and purified extracts were measured in Electric Balance. Common laboratory apparatus and column and thin layer chromatographic method were used for the isolation and purification of pure compounds. Commercial grade reagents and solvents were purchased from Chemico Co. Ltd., Yangon.

Sample Collection

The specimen of *Clausena heptaphylla* (Roxb.) Wight & Arn. was collected from Kalay Township, Sagaing Region, Myanmar and identified by Dr Thet Naing Oo, Pro-rector of Monywa University. The fresh stem barks of *C. heptaphylla* were chopped into small pieces and allowed to air dried at room temperature for about two weeks.

Extraction and Isolation

The air-dried sample of *C. heptaphylla* (1 kg) was percolated with methanol (2.5 L) for about one month. Then, the methanol crude extract was filtered and evaporated to concentrate at room temperature. The residue was extracted with ethyl acetate to get (13.2 g) of ethyl acetate crude extracts. Among them, the crude extract (4 g) was dissolved in ethyl acetate and 12 g of silica gel were added. The mixture was allowed to dryness under reduced pressure. The resulting crude powder extracts were subjected to silica gel column chromatographic separation by using stepwise gradient of n-hexane and ethyl acetate to give a pure compound ZCM-3 (Microzelanicum, 20.7 mg), which was isolated as pale-yellow crystals.

Results and Discussion

Structure Elucidation of Microzelanicum (ZCM-3)

Microzelanicum was isolated as pale-yellow crystals. The IR absorption band of the compound at 1727, 1562 and 1500 cm^{-1} showed common features of a coumarin framework. Another IR absorption at 3061 cm^{-1} was due to the presence of sp^2 hydrocarbons and 2972 and 2931 cm^{-1} were due to the presence of sp^3 hydrocarbons (methoxy and C-H stretching of methyl groups respectively).

Furthermore, the structural elucidation of pure compound ZCM-3 was done by applying ^{1}H NMR (400MHz), splitting patterns and coupling constant (*J* values) of some prominent protons, ^{13}C NMR (100 MHz), DEPT, DQF-COSY, HMQC, HMBC and NOESY spectral data.

In DQF-COSY spectrum (Figure 1) shows two doublets at δ_H 6.32 ppm and δ_H 7.65 ppm, integrating 1 H of each and could be confirmed by splitting pattern and coupling constant of these alkenic protons (δ_H 6.32 ppm, doublet, J = 9.5 Hz, H-3 and δ_H 7.65 ppm, doublet, J = 9.5 Hz, H-4) which indicates that the two protons are oriented as *cis* position. Moreover, HMQC spectrum (Figure 2) shows ^{1}H-^{13}C direct correlation of the two protons (δ_H 6.32 ppm, H-3) and (δ_H 7.65 ppm, H-4) with their respective carbons (δ_C 114.27 ppm, C-3

and δ_C 142.86 ppm, C-4). The observation of α ^{1}H-^{13}C long range coupling of alkenic proton (δ_H 6.32 ppm, H-3) in the HMQC spectrum, with the sp^2 methine carbon (δ 142.86 ppm, C-4) and carbonyl carbon (δ 160.39 ppm, C-2), also shows β ^{1}H-^{13}C correlation of alkenic proton (δ 7.65 ppm, H-4) with carbonyl carbon (δ 160.39 ppm, C-2) which leads to the following fragment~A.

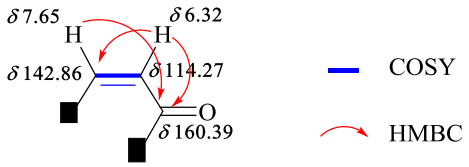

Fragment ≈ A

In ^{1}H NMR spectrum (Figure 3), the occurrence of two singlet aromatic protons at (δ_H 7.37 ppm, H-5 and δ_H 6.87ppm, H-8) are positioned as para position, which produces the following tetra-substituted benzene ring. In HMQC spectrum (Figure 2) displays ^{1}H-^{13}C direct correlation of the two aromatic protons (δ_H 7.37 ppm, H-5 and δ_H 6.87 ppm, H-8) with their respective carbons as shown below. In the HMBC spectrum, there was observed β ^{1}H-^{13}C long range coupling of aromatic proton (δ_H 6.87 ppm, H-8) with the aromatic quaternary carbons (δ_C 112.38 ppm, C-10 and δ_C 120.22 ppm, C-6). Furthermore, in HMBC spectrum (Figure 4), the observation of β ^{1}H-^{13}C long range coupling of aromatic sp^2 methine proton (δ_H 7.37 ppm, H-5) with the two aromatic quaternary carbons (δ 156.56 ppm, C-9 and δ 159.87 ppm, C-7) produces the following fragment ~ **B**.

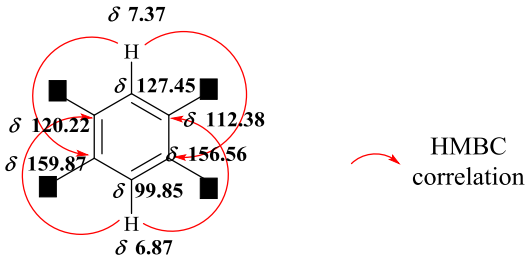

Fragment ~ B

The connection between fragment ~ **A** and **B** could be done by α ^{1}H-^{13}C long range coupling of sp^2 methine proton (δ_H 7.65 ppm, C-4) with sp^2 quaternary carbon (δ_C 112.38 ppm, C-10). Moreover, the observation of β ^{1}H-^{13}C long range coupling of sp^2 methine proton (δ_H 7.65 ppm, C-4) with carbonyl carbon, sp^2 methine carbon and sp^2 quaternary carbon (δ_C 160.39 ppm (C-2), δ_C 127.45 ppm, C-5 and δ_C 156.56 ppm, C-9) in HMBC spectrum. The presence of aromatic methoxy at C-7 (δ_C 159.87 ppm) was confirmed by ^{1}H NMR singlet single peak occurs at δ_C 3.95 ppm (OCH_3), ^{13}C NMR signal at δ_C 56.46 ppm and supported by 3*J* correlation to C-7 (δ_C 159.87 ppm) which produced the following extended fragment ~ **C**.

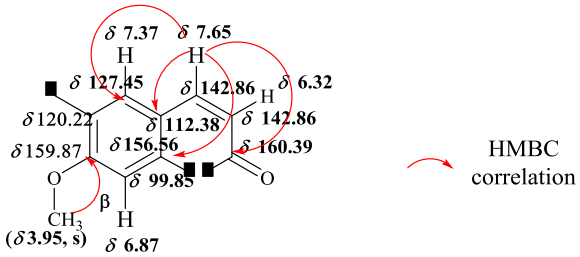

Fragment ~ C

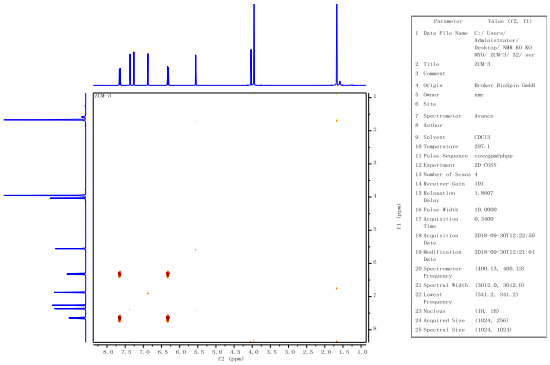

Figure. 1 DQF-COSY Spectrum ($CDCl_3$, 300 MHz)

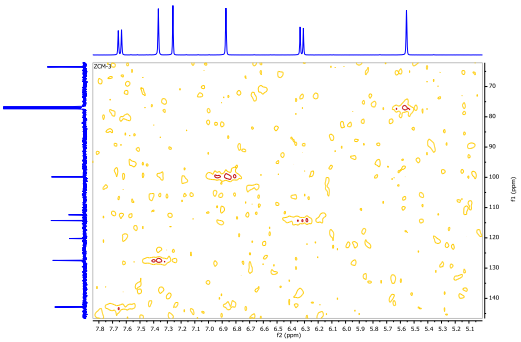

Figure 2 HMQC Spectrum ($CDCl_3$, 300 MHz))

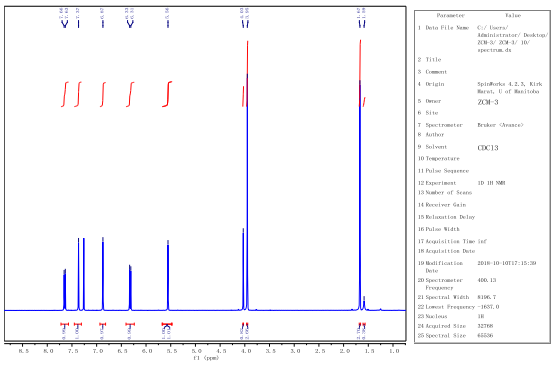

Figure 3 ^{1}H NMR Spectrum (400 MHz) ($CDCl_3$)

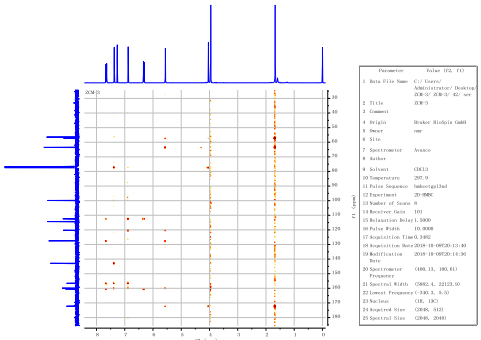

Figure 4 HMBC Spectrum ($CDCl_3$, 300 MHz)

In the ^{1}HNMR spectrum(Figure 3), the down field chemical shift of sp^3 methine proton (δ_H 5.56 ppm, singlet, 1 H, H-2′) must be connected to oxygen and also shows ^{1}H-^{13}C direct correlation with sp^3 methine carbon (δ_C 77.20 ppm, C-2′) in HMQC spectrum (Figure 2). Moreover, in HMQC spectrum, ^{1}H-^{13}C direct correlation of down field chemical shift of sp^3 methine proton (δ_H 4.03 ppm, singlet, 1 H, C-5′) and sp^3 methyl proton (δ_H 1.67 ppm, singlet, 3 H, H-1′) are connected with their respective carbons (δ_C 63.52 ppm, C-5′ and δ_C 11.26 ppm, H-7′) generates the following fragments.

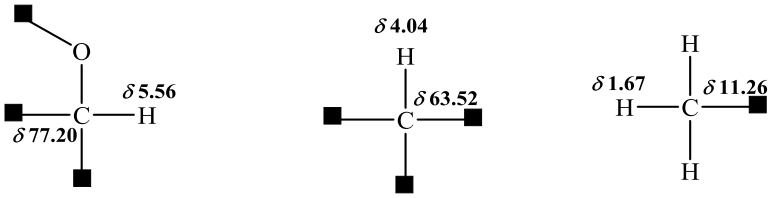

In the HMBC spectrum, the occurrence of α and β ^{1}H-^{13}C long range coupling of sp^3 methyl proton (δ_H 1.67 ppm, H-1′) with sp^3 quaternary carbon (δ_C 57.23 ppm, H-1′) and sp^3 methine carbon (δ_C 63.52 ppm, C-5′). Furthermore, in HMBC spectrum, sp^3 methine proton (δ_H 4.03 ppm, H-5′) has α and β ^{1}H-^{13}C long range coupling of carbonyl carbon (δ_C 172.23 ppm, C-4′) and sp^3 methine carbon (δ_C 77.20 ppm, C-2′). The other substituent on aromatic ring at C-6 (δ_C 120.22 ppm) is made up of prenyl unit which cyclized to form γ-lactone moiety. Moreover, the attachment of these protons in the lactone ring is further supported by 2*J* and 3*J* cross peak correlation which reveals the following fragment ~ **D**.

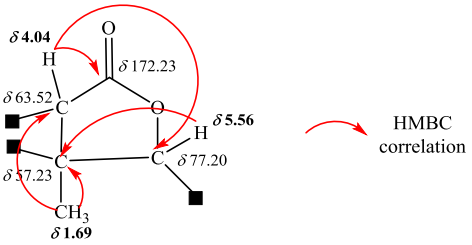

Fragment ~ D

The connection between fragment ~ **C** and **D** could be done by α ^{1}H-^{13}C long range coupling of sp^3 methine proton (δ_H 5.56 ppm, H-2′) with sp^2 quaternary carbon (δ_C 120.22 ppm, C-6) and sp^3 quaternary carbon (δ_C 57.23 ppm, C-1′). In addition, β ^{1}H-^{13}C long range coupling of sp^3 methine proton (δ_H 5.56 ppm, H-2′) with sp^3 methine carbon (δ_C 63.53 ppm, C-5′), sp^2 methine carbon (δ_C 127.45 ppm, C-5), sp^2 quaternary carbon (δ_C 159.87 ppm, C-7) and carbonyl carbon (δ_C 172.23 ppm, C-4′) in HMBC spectrum produces the following partial fragment ~ **E**.

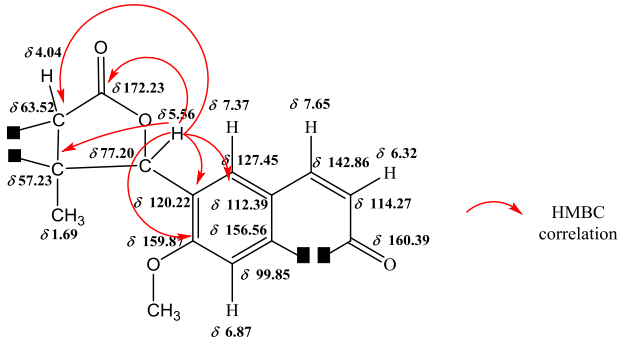

Fragment ~ E

In this stage, the partial molecular formula of the fragment ~ **E** could be calculated as $C_{15}H_{12}O_4$. In EI-MS spectrum showed the molecular ion peak and m/z is 289.0[M + H]$^{+\bullet}$, 311.1 [M + Na]$^{+\bullet}$, and 599.1 [2M + Na]$^{+\bullet}$(which represents its molecular mass of this compound). Thus, the remaining molecular mass of this compound is 288-256 = 32. It must be two 'O' atoms. The remaining two 'O' atoms must be connected to downfield chemical shift of aromatic carbon (δ_C 156.56 ppm and δ_C 160.39 ppm) and sp^3 carbons (δ_C 63.52 ppm and δ_C 57.23 ppm). Therefore, the molecular formula of this compound was determined as $C_{15}H_{12}O_6$ on the basis of EI-MS spectrum.

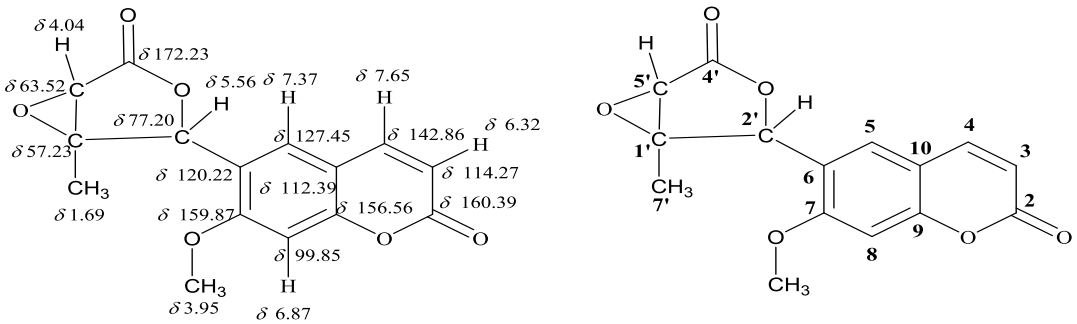

7-methoxy-6-(1'-methyl-4'-oxo-3',6'-dioxabicyclo[3.1.0]hexan-2'-yl)-2*H*-chromen-2-one

Chemical Formula: $C_{15}H_{12}O_6$

Table 1 ^{1}H NMR (400 MHz), ^{13}C NMR (100 MHz) and DEPT Spectral Data of Microzelanicum (ZCM-3) in $CDCl_3$

No.	^{13}C NMR δ (ppm)	^{1}H NMR (J in Hz)	DEPT
Carbon			
4′	172.23	-	C
2	160.39	-	C
7	159.87	-	C
9	156.56	-	C
4	142.86	7.65 (d, J = 9.5 Hz, 1H)	CH
5	127.45	7.37 (s, 1H)	CH
6	120.22	-	C
9	114.27	6.32 (d, J = 9.5 Hz, 1H)	CH
10	112.38	-	C
8	99.85	6.87 (s, 1H)	CH
2′	77.20	5.56 (s, 1H)	CH
5′	63.52	4.04 (s, 1H)	CH
1′	57.23	-	C
OCH_3	56.46	3.95 (s, 3H)	CH_3
7′	11.26	1.67(s, 3H)	CH_3

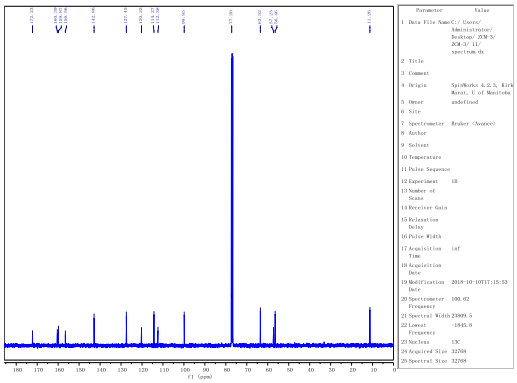

Figure 5 ^{13}C NMR Spectrum (100 MHz, $CDCl_3$)

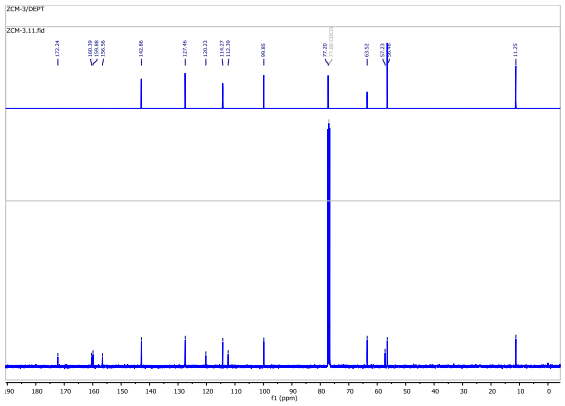

Figure 6 DEPT Spectrum

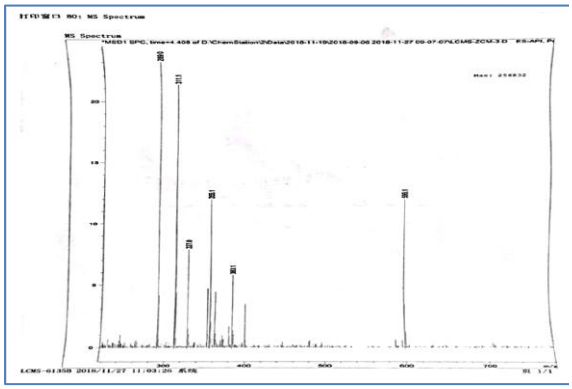

Figure 7 Mass Spectrum

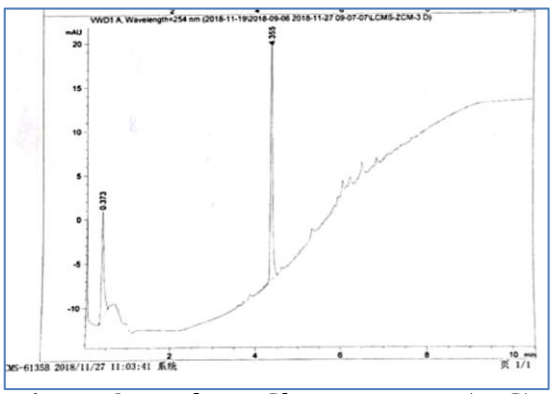

Figure 8 Total Ion Chromatogram (TIC)

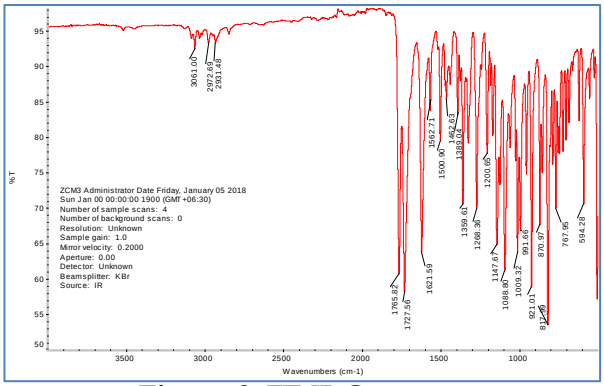

Figure 9 FT-IR Spectrum

Conclusion

In this study, the first isolation of 7-methoxy-6-(1'-methyl-4'-oxo-3', 6'-dioxabicyclo [3.1.0] hexan-2'-yl)-*2H*-chromen-2-one (Microzelanicum,$C_{15}H_{12}O_6$) from the plant of *Clausena heptaphylla* (Roxb.) Wight & Arn was presented. Although the compound was identified as a known compound, no literature data had been reported for this compound. Therefore, further investigations such as antimicrobial, anti-inflammatory and cytotoxic properties on this compound will also be studied.

Acknowledgements

The authors thank Professor Dr Yang Zhixiang, Center of Ningxia Organic Synthesis and Engineering Technology, Ningxia Academy of Agriculture and Forestry Sciences, Yinchuan, China for NMR spectra and mass measurements. The authors thank Dr Ba Han, Rector of Meiktila University and Dr Ni Ni Aung, Head of Department of Chemistry, Meiktila University for their kind permission to submit this paper.

References

Begum, R.M.A., Kaisar, M.S., Rahman, A.M., Chowdhury, S., Rahman. M.M., Hasan, C.M. and Rashid, M.A. (2011). ‘‘Clausenolide-1-methyl ether from *Clausena heptaphylla* W&A’’. *Boletín Latinoamericano y del Caribe de Plantas Medicinales y Aromáticas*, vol.10 (2), pp.136 – 138

Bhattacharyya, P., Biswas, G.K., Barua, A.K., Saha, C., Rovt, I.B. and Chowdhury, B.K. (1993). ‘‘Clausenalene, A Carbazole Alkaloid from *Clausena heptaphylla’’. Phytochemistry*, vol.33 (1), pp.248-250

Cassady, J.M., Ojima, N., Chang, C. and Mclaughlin, J.L. (1979). “An Investigation of the Antitumor Activity of *Micromelum integerrimum* (Rutaceae)”. *Journal of Natural Products*, vol.42 (3), pp.274-278

Chakraborty, A., Saha, C., Podder, G., Chowdhury, B.K. and Bhattacharyya, P. (1995). ‘‘Carbazole Alkaloid with Antimicrobial Activity from *Clausena heptaphylla*’’. *Phytochemistry*, vol.38 (3), pp.787-789

Fakruddin, M., Mannan, K.S.B., Mazumdar, R.M. and Afroz, H. (2012). ‘‘Antibacterial, Antifungal and Antioxidant Activities of the Ethanol Extract of the Stem Bark of *Clausena heptaphylla”. BMC Complementary and Alternative Medicine*, vol. 1, pp.232

Lekphrom, R., Kanokmedhakul, S., Kukongviriyapan, V. and Kanokmedhakul, K. (2011). ‘‘C-7 Oxygenated Coumarins from the Fruits of *Micromelum minutum*’’. *Arch Pharm Res*, vol.34 (4), pp.527-531

Sohrab, M.H., Hasan, C.M. and Rashid, M.A. (1999). “Lunamarins A And B: Two Novel Terpenoid Coumarins from *Clausena heptaphylla”. Natural Product Letters*, vol.14 (1), pp.47-53

Sohrab, M. H., Hasan, C.M. and Rashid, M.A. (2000).‘‘Clausmarin-A from the Leaves of *Clausena heptaphylla*’’. *Biochemical Systematics and Ecology*, vol.28, pp.91-93

STUDY ON CHANGES IN MORPHOLOGY AND PHYSICOHEMICAL PROPERTIES OF ARECA NUT FIBRE BY DIFFERENT SURFACE TREATMENT METHODS

Thwe Thwe Soe[1,2], Htin Zaw Myint[3], Saw Hla Myint[4]

Abstract

Areca nut husk is abundantly available in Mone, Kyauk-kyi Township, Bago Region as byproduct from the areca nut farm, and finding a way to convert it into a value added material to produce a useful material could be of national interest. The fibre was extracted from the areca nut husk, washed and treated with 5 % NaOH, some of the product was further treated separately with permanganate and benzoyl chloride to modify the fibre surface. As a result, considerable change in surface morphology of fibres was observed by SEM using an Evol 18 Zeiss scanning electron microscope (SEM). Lignin and hemicellulose contents were reduced by the alkali treatment as shown by the FT IR spectra recorded on a Tracer 100 Shimadzu spectrophometer. The thermal characteristics of the untreated and treated natural fibre was studied by TG TDA. The surface tension of the untreated and treated fibre (in the order given above) were found to be, 24.86, 25.86, 26.95 and 26.10 mN m^{-1}. Thus by the surface treatment, the fibre surface tension, was found to increase, which is favorable for a better fibre – matrix binding in a composite. Fibre diameter (by micrometer), fibre length (by vernier calliper) and aspect ratio of the untreated and treated fibre were found to be, respectively, 0.36, 0.38, 0.35 and 0.38 mm; 53.34, 56.61, 52.19 and 54.86 mm; 148.16, 148.97, 149.11 and 144.37. Water absorption property by soaking-squeezing method showed the water absorption % of the untreated and treated fibres at 6, 12 and 24 h, respectively, to be 277.64 , 292.17, 219.39 and 288.05 %; 268.45, 290.70 , 205.70 and 251.50 %; 250.95, 254.19 , 204.66 and 222.23 %, showing increase in water absorption of the fibre after alkaline treatment, but significant decrease by the permanganate treatment, which is good for resistance of the composite to moisture. The present study suggests improvement of fibre morphology and composition for the preparation of a useful composite material.

Keywords: Areca nut fibre, surface modification, alkali treatment, permanganate treatment, benzoyl chloride treatment, cellulose, lignin

Introduction

Nowadays natural fibres have become superior alternatives to synthetic fibres for polymeric composites due to their advantages *i.e*. cheap, lightweight, renewable, biodegradable, flexible in usage and naturally recyclable. Moreover the application of natural fibre reinforced polymeric composites are found in house construction materials, aerospace, panels, and automobile parts.

Many attempts were made by scientists to utilize the natural fibres in the fabrication of composites. Their efforts to introduce the natural fibre composites are because of the following reasons;

1. These fibres, despite their low strength can lead to composite with specific strengths because of their low density;
2. Dried natural fibres are nontoxic and eco-friendly and biodegradable and are cheap;
3. Natural fibres are abundantly available renewable resources.

[1] Assistant Lecturer, Department of Chemistry, Yangon University of Education
[2] PhD Student, Department of Chemistry, University of Yangon
[3] Dr, Associate Professor, Department of Chemistry, Taungoo University
[4] Dr, Part-Time Professor, Department of Chemistry, University of Yangon

With growing environmental awareness, new rules and legislations, scientists and engineers are forced to seek new materials which are more eco-friendly in nature.

Hence, the attention of the research community is focused toward finding an eco-friendly material which can give high performance at affordable costs.

Natural Fibre Surface Modification

Natural fibres are amenable to modification as they bear hydroxyl groups from cellulose and lignin. The hydroxyl groups may be involved in the hydrogen bonding within the cellulose molecules thereby reducing the activity towards the matrix. Chemical modifications may activate these groups or can introduce new moieties that can effectively interlock with the matrix. Interfaces play an important role in the physical and mechanical properties of composite. Simple chemical treatments can be applied to the fibres with the aim of changing surface tension and polarity of fibre surface.

Natural fibres have a good potential for chemical treatment due to presence of hydroxyl groups in lignin and cellulose. Reaction of hydroxyl groups can change the surface energy and the polarity of the natural fibres. Many studies have been undertaken to modify the performance of natural fibres.

The different surface chemical modifications of natural fibres have achieved various levels of success in improving fibre strength, fibre fitness and fibre-matrix adhesion in natural fibre composites.

Different surface treatment methods such as alkali treatment, isocyanate treatment , acrylation, benzoylation, latex coating, permanganate treatment, acetylation, silane and peroxide treatment (Baiardo *et al*., 2002) have been applied on the fibre to improve its strength, size and its shape and the fibre-matrix adhesion. Generally, mechanism of the performance of these methods is different and is depended on the chemical structure of the reagent.

Consequently, the aim of the present work is surface modification of areca nut fibres, which is abundantly available as waste material, by different chemical treatments with alkali treatment, permanganate and benzoyl chloride, and to study the changes in morphology, chemical constitution and physiochemical properties, with the final aim to prepare useful composite materials with natural rubber.

Botanical Description of *Areca catechu* L.

Botanical name : *Areca catechu* L.
Family name : Arecaceae
Order : Arecales
Genus : *Areca*
Species : *catechu*
Common name : Areca nut, Betel nut
Myanmar name : Kun-thee
Part used : Fruits

Materials And Methods

This research consists of two main parts. The first part deals with the raw material collection, isolation of areca nut fibre and its surface modification. The second part is the determination of morphology, chemical constitution and physiochemical properties, the areca nut fibre.

Preparation of Areca Nut Fibre

Sample collection

The areca nut husks were collected from the local area, Mone, Kyauk-kyi Township, Bago Region (Figure 1).

Extraction of areca nut fibre

The areca nut husks were taken directly from the areca nut fields containing a lot of dirt and dust. The dirt, dust, individual fibre and coarse fibre were removed by washing with distilled water. The selected areca fruit husks were soaked in deionized water for about five days. This process is called retting; allowing the fibre to be removed from the husk easily. Then areca nut fibre was removed from the husk and separated into different grades of purity. The selected grade of fibre was dried under direct sunlight (temperature 30 °C) for five days before the alkali treatment. The dried fibre was designated as untreated fibre.

Figure 1 Areca nut husk

Alkali treatment or mercerization

The clean and dried areca nut fibre was soaked in a stainless steel vessel containing 5 % NaOH solution. The alkali treated fibre was immersed in the distilled water for 24 hours in order to remove the residual NaOH. Final washing was done with distilled water containing a small amount of acetic acid for neutralization. Subsequently, the fibre was dewatered and dried under sun light for five days (Figure 2).

Potassium permanganate treatment

Some of the fiber, pre-treated with 5 % alkali were immersed in a 0.5 % $KMnO_4$ solution in acetone for 30 min. The permanganate treated fibers were then decanted and dried in air.

Benzoyl chloride treatment

Some of the fiber, pre-treated with 5 % alkali was immersed in acetone solution and added sodium chloride, same ratio of benzoyl chloride with acetone (0.1: 0.1), and then agitated with sodium bicarbonate solution for 15 min. This solution was filtered. Then the treated areca fiber was

soaked in ethanol solution for 1 h to remove benzoyl chloride that adhered to the fiber surface, washed thoroughly using distilled water and dried in air.

Comparative Study on the Surface Morphology of the Untreated and Treated Areca Nut Fibres

The morphological changes by the fibre surface modification was studied by Evol 18 Zeiss scanning electron microscope (SEM) at West Yangon University (Figures 3 (a), (b), (c) and (d)).

Comparative Study on the Infrared Absorption Spectra of the Untreated and Treated Areca Nut Fibres

The changes of chemical constitution of the fibre by surface chemical treatment was studied by infrared absorption spectra recorded on a Tracer 100 Shimadza, Japan spectrometer at West Yangon University (Figures 4 (a), (b), (c) and (d)).

Comparative Study on the Thermal Properties of the Untreated and Treated Areca Nut Fibres

The effect of the untreated and treated fibre thermal properties was studied using a TG DTA instrument (Hi-TGA 2950 model). The temperature range between 0 ºC and 600 ºC under nitrogen (at a rate of 50 mL/min) at Universities' Research Center, Yangon University (Figures 5 (a), (b), (c), (d) and Table 2).

Comparative Study on the Surface Tension of the Untreated and Chemically Treated Areca Nut Fibres

Approximately 20 mL each of ten aqueous solutions of methanol (various mole ratios from 1.000, 0.910, 0.840, 0.775, 0.675, 0.600, 0.530, 0.480, 0.435 and 0.395 corresponding to surface tension at 25 ºC respectively, 22.33, 23.00, 23.50, 24.00, 25.00, 26.00, 27.00, 28.00, 29.00 and 30.00 (Ghahremani et al., 2011)) was poured into a clean

50 mL beaker and the temperature adjusted at 25 ºC. Twenty pieces of each type of fibre were carefully placed on top of the liquid surface in each beaker and within for 20 s, and the number of fibres that remained floating on the liquid was counted and the percent floating fibres calculated. The surface tension of the liquid in which 50 % of the fibres floated was taken as approximate surface tension of the fibres tested (Hazendonk *et al.*, 1993) at Taungoo University (Table 3).

Determination of Water Absorption Property of Fibre

Water absorption was determined after immersion of the samples in water at room temperature for 6, 12 and 24 h (Table 5). Each sample (3 g) was weighed before and after immersion of fibre. Water absorption was determined by using the following equation.

$$\text{Water absorption}(\%) = \frac{m_2 - m_1}{m_1} \times 100$$

Where, m_1 = mass of fibre before immersion

m_2 = mass of fibre after immersion

Results and Discussion

Extraction of Areca Nut Fibre

After soaking and drying, 1.4 viss of fibre was extracted from 5 viss of raw areca husk. This is the mixture of coarse and fine fibres (Figure 2).

Figure 2 Extracted areca nut fibre

Surface Modification of the Areca Nut Fibre

Alkali treatment

$$\text{Fiber-OH} + \text{NaOH} \rightarrow \text{Fiber-ONa} + H_2O$$

Alkali treatment of areca fibers result in the formation of Fiber–cell–O–Na groups between the cellulose molecular chains. Alkali treatment leads to the increase in the amount of amorphous cellulose at the expense of crystalline cellulose and there is a change in the surface topography of the areca fibers (Dhanalakshmi *et al*., 2015). During alkali treatment the removal of hydrogen bonding takes place in the fibre network structure. Due to this, hydrophilic hydroxyl groups are reduced and the fibres moisture resistance property is increased. It also takes out certain portion of hemicelluloses, lignin, pectin, wax and oil covering materials. As a result, the fiber surface becomes cleaner. In addition to this it increases the fibre aspect ratio (Table 4). This could result in better fiber-matrix interfacial adhesion. Mechanical and thermal behaviors of the composites are improved significantly by this treatment. Alkali treated fibre have lower lignin content than untreated fibres.

In the present work, the extracted areca nut fibre was treated with 5% NaOH solution. The resulting fibre have yellowish brown colour. The untreated fibre was paler than alkali treated one.

Potassium permanganate treatment

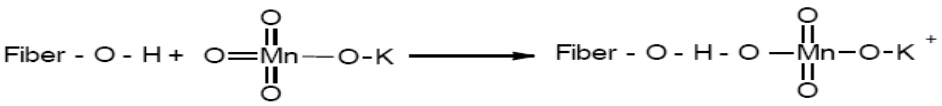

Highly reactive permanganate ions react with cellulose hydroxyl groups and form cellulose manganate. Permanganate ions also react with the lignin constituents and carve the areca fiber surface. As a result, areca fiber surface becomes darker, physically rough, bristly and this reduces hydrophilic nature of the areca fibers (Table 5). This could improve chemical interlocking at the interface and provides better adhesion with the polymeric matrix

Benzoyl chloride treatment

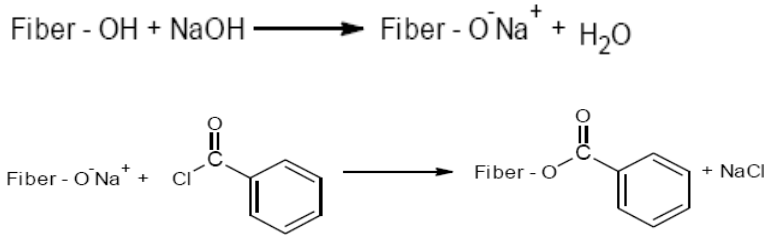

When benzoyl chloride reacts with areca fibers, an ester linkage is formed. This benzoyl chloride treatment results in the reduction of hydrophilicity of areca fibers and hence made the areca fibers to become more compatible with polymer matrix. Benzoylation treatment also enhances thermal stability of the fibers. These could improve chemical interlocking at the interface and provides effective fiber surface area for good adhesion with the matrix (Dhanalakshmi *et al*., 2015).

Morphological Study of the Areca Nut Fibres

Different chemical treatments for the fibre surface modification have effects on the fibre surface morphology (Figures 3 (a), (b), (c) and (d)).

,

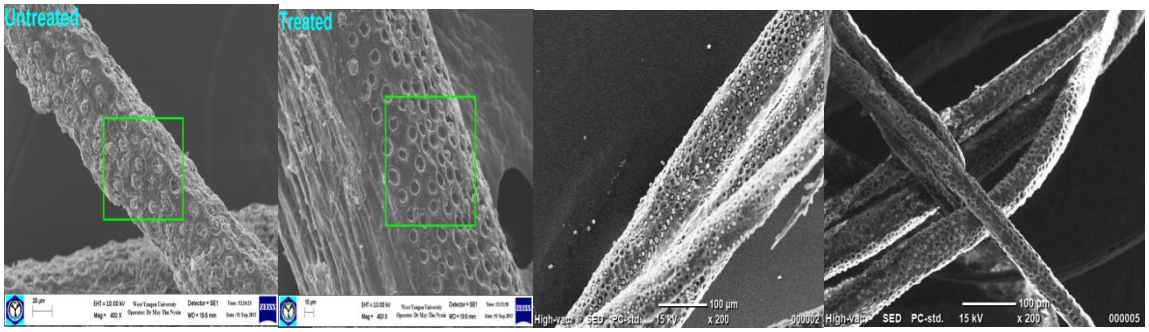

(a) **(b)** **(c)** **(d)**

Figure 3 SEM micrographs of the areca nut fibre (a) untreated (b) alkali treated (c) permanganate treated and (d) benzoyl chloride treated

The untreated fibre presents a network structure in which the fibrils are bound together by hemicelluloses and lignin. Longitudinally oriented unit cells with almost parallel orientations are present (Dhanalakshmi *et al*., 2015).

The alkali treated fibre clearly shows large number of pinholes or pits on the surface, which are due to the removal of fatty deposits from the fibre. Alkali treatment removes waxy epidermal tissue, adhesive pectin and hemicelluloses. Topographical changes because of the removal of low molecular weight compounds result in the formation of a rough surface.

The permanganate treatment (Binoj *et al*., 2016), highly reactive permanganate ions react with the cellulose hydroxyl groups and forms cellulose–manganate. This ion reacts with the lignin and carve the fiber surface and thus reduces moisture absorption. Areca fiber surface becomes physically rougher on permanganate treatment which can be evidenced from the SEM micrograph (Figure 3 (c)) and enhances effective fiber surface area for good adhesion with the matrix.

The SEM image of benzoyl chloride treated areca nut fibre clearly shows a large number of pinholes and rough surface (Figure 3 (d)). It forms an ester linkage to the areca fibers and thus

reducing hydrophilicity making it more compatible with polymer matrix. Hence, this benzoyl chloride treatment provides effective fiber surface area for good adhesion with the matrix.

Chemical Composition of the Untreated and Treated Areca Nut Fibre

In the FT IR spectra, the peak at 1737 cm^{-1} is referred to ester and ether crosslinks between cellulose and lignin or cellulose and hemicellulose (Table 1). The peaks observed between 1100-1600 cm^{-1} shows the presence of hemicellulose in the fibre (Dhanalakshmi *et al*., 2015).

Table 1 FT IR Spectral Assignment of Areca Nut Fibre

Wave number (cm^{-1})	Band Assignments
1000- 1300	Alcohols, Ether, C-O stretching vibrations
1100- 1600	Hemicellulose (ester, benzene ring, alcohol, ether)
1377	Alcohol group of cellulose
1400- 1600	Aromatic rings (C=C stretching)
1737	Ester and ether crosslinks between cellulose and lignin or cellulose and hemicellulose

(Dhanalakshmi *et al*., 2015)

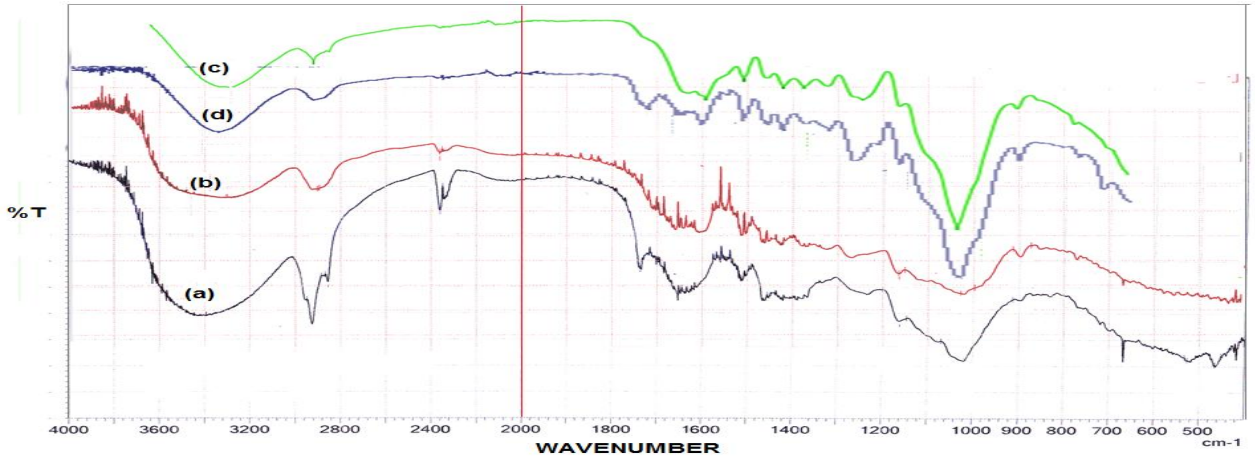

Figure 4 FT IR spectra of areca nut fibre (a) untreated (b) alkali treated (c) permanganate treated and (d) benzoyl chloride treated

After the alkali treatments, hydrolysis occurs which breaks down the ester bond or ether bond, resulting in the absence of 1737 cm^{-1} peak in alkali treated areca fibres (Figure 4 (b)). The peaks observed between 1100-1600 cm^{-1} shows the presence of hemicelluloses in untreated areca fibre and the reduced intensity of these peaks in alkali treated areca fiber indicates the slight removal of hemicelluloses from the fibre surface.

After the potassium permanganate treatments, hydrolysis occurs which breaks down the ester bond or ether bond, resulting in the further reduction of the band at 1737 cm^{-1} in potassium permanganate treated areca nut fibre (Figure 4 (c)). Further reduction of band intensity between 1100-1600 cm^{-1} shows further removal of hemicelluloses from the fiber surface in a permanganate treated areca.

The IR spectrum of benzoyl chloride treated areca nut fiber indicates a carbonyl stretching band at 1718 cm^{-1} and the C=C stretching bands of aromatic ring between 1400-1600 cm^{-1}, indicating benzoylation at the fibre surface. Further reduction of band intensity between 1100

-1600 cm^{-1} showing further removal of hemicelluloses from the fiber surface is also observed (Figure 4 (d)) (Silverstein *et al*., 2003).

Thermal Properties of the Untreated and Treated Areca Nut Fibres

In general, natural fibers have different chemical compositions of cellulose, hemicelluloses, lignin and pectin and so their flammability varies from fiber to fiber. Higher cellulose content results in higher flammability while higher lignin content results in greater char formation with lower degradation temperature (Dhanalakshmi *et al*., 2015). Hence, the cellulose and lignin content present in these natural fibers decides the thermal stability of natural fibers reinforced polymer composites. So, it is very important to promote surface modification of natural fibers with various chemical treatments to decrease hydrophilicity (Table 5) and to improve the thermal stability of natural fibers (Table 2).

Table 2 Thermal Decomposition of the Untreated and Treated Areca Nut Fibres

Fibre	Temperature (°C)	Temperature during mass loss (°C)	Weight loss (%)	Nature of peak	TG/DTA Remark
Untrated Fibre	67.04	38.56-100	6.70	Endothermic	Loss of moisture and highly volatile extractives
	349.06	100-350	65.08	Exothermic	Decomposition of cellulose and hemicelluloses
	466.58	350-470	89.62	Exothermic	Degradation of the lignin
Alkali Treated fibre	80.50	38.94-100	4.82	Endothermic	Loss of moisture and highly volatile extractives
	351.92	100-360	64.90	Exothermic	Decomposition of cellulose and hemicelluloses
	450.62	360-600	87.98	Exothermic	Degradation of the lignin
$KMnO_4$ treated fibre	57.52	38.70-100	6.08	Endothermic	Loss of moisture and highly volatile extractives
	360.05	100-370	43.76	Endothermic	Decomposition of cellulose and hemicelluloses
	423.85	370-600	76.05	Exothermic	Degradation of the lignin
C_6H_5COCl treated fibre	65.04	38.59-100	6.95	Endothermic	Loss of moisture and highly volatile extractives
	381.98	100-390	73.5	Endothermic	Decomposition of cellulose and hemicelluloses
	428.60	390-600	87.56	Exothermic	Degradation of the lignin

The TG DTA curves show the three main degradation phases (Figure 5). The initial degradation phase was due the loss of moisture and highly volatile extractives. In this degradation phase, the volatile hydrocarbons were released from the natural fibre as a result of thermal decomposition of cellulose and hemicellulose.

The second phase of degradation is due to the decomposition of cellulose and hemicellulose.

The third degradation points in the TG DTA curves represent heavy fractions mainly from lignin degradation.

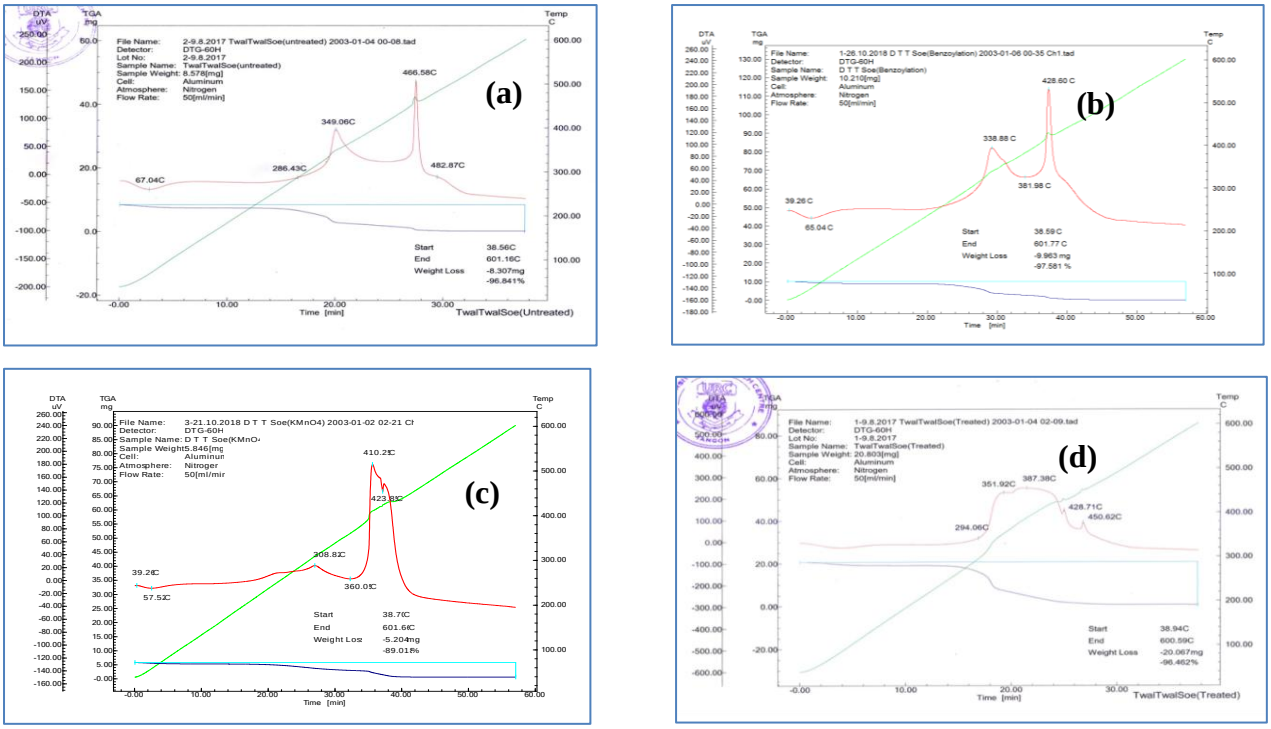

Figure 5 TG TDA thermograms of (a) untreated (b) alkali treated (c) permanganate treated and (d) benzoyl chloride treated areca nut fibres

The TG DTA results of untreated and treated areca fibres from (Table 2) revealed that the maximum decomposition for the untreated, alkali treated, permanganate treated and benzoyl chloride treated fibres were 349.06, 351.92, 360.05 and 381.98 ºC, respectively. According to the data, the main second peak decomposition temperature of benzoyl chloride treated, permanganate treated and alkali treated areca fibers in DTG curve were higher than that of untreated areca fibers. These results confirmed the improved thermal stability for treated areca nut fibers.

Surface Tension of the Untreated and Treated Areca Nut Fibre

The determination of the Surface tension at which all fibres just float proved to be difficult, because fibre heterogeneity there is a range of γ_L values in which some fibres float and other sink. So, γ_F was chosen as the surface tension where 50 % of the fibres float on the liquid surface (Ghahremani *et al.*, 2011). This surface tension was determined graphically (Figure 6). According to the data, the standard deviation is below 1 mN m^{-1}. It can be concluded that permanganate treated fibre were more hydrophobic than other untreated and treated fibres (Table 3).

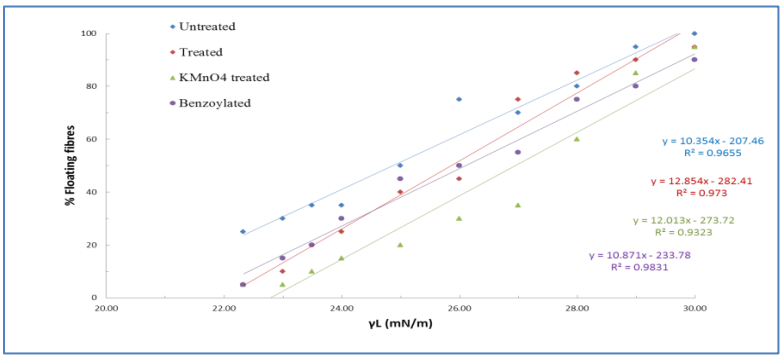

Figure 6 Plot of percent of floating fibres as a function of surface tension of water-methanol mixtures

Table 3 Surface Tensions of Water-methanol Mixtures Giving Zero Contact Angles (γ_F) for Different Fibres

Surface Tension (mN m^{-1})			
Untreated fibre	**Alkali treated fibre**	**Permanganate treated fibre**	**Benzoyl chloride treated fibre**
24.86	25.86	26.95	26.10

Comparative Study on the Physicochemical Properties of the Untreated and Treated Areca Nut Fibres

The size of lumen in natural fibre is proportional to the diameter of the untreated and treated fibre, where the lumen size increases with the increase in fibre diameter. Alkali treated fibre were observed with bigger lumen size, whereas the untreated fibre exhibits a slightly smaller and elongated lumen. By relating the lumen size of areca nut fibre in (Figure 3) with the results of areca nut fibre length shown (Table 5). Moreover, the good aspect ratio and lightweight characteristic of (permanganate treated fibre, alkali treated fibre and untreated fibre) well-suits the fabrication of lightweight composite than other treated fibre.

Table 5 Dimensional Characteristics of the Untreated and Treated Areca Nut Fibres

Measurement	Untreated Fibre	Alkali treated Fibre	Permanganate treated Fibre	Benzoyl chloride treated Fibre
Fibre diameter (mm)	0.36	0.38	0.35	0.38
Fibre length (mm)	53.34	56.61	52. 19	54.86
Aspect ratio	148.61	148.97	149. 11	144.37

Water Absorption Property of the Untreated and Treated Fibre

Alkaline treatment fibre more water absorption properties than other treated fibre, but significant decrease by the permanganate treatment, which is good for resistance of the composite to moisture (Table 6).

Table 6 Variation of Water Absorption with Soaking Time for Untreated and Treated Areca Nut Fibres

	Water absorption (%)			
Time (h)	**Untreated Fibre**	**Alkali treated Fibre**	**Permanganate treated Fibre**	**Benzoyl chloride treated Fibre**
6	277.64	292.17	219.39	288.05
12	268.45	290.70	205.70	251.50
24	250.95	254.19	204.66	222.23

Conclusion

The unmanaged disposal areca husk was collected from the local area, Mone, Kyauk-kyi Township, Bago Region. The collected husk were cleaned and soaked in distilled water for 5 days to extract the fibre. The extracted fibre was treated with 5 % of sodium hydroxide solution, and the alkali treated fibre was surface modified by 0.5 % potassium permanganate solution and benzoyl chloride solution. From SEM study, the surface morphology of the areca nut fibre was observed to change favorably for the preparation of composite materials with a matrix material by the treatment with 5 % NaOH solution, 0.5 % potassium permanganate solution and benzoyl chloride. Alkali treatment removes waxy epidermal tissue, adhesive pectin and hemicelluloses. Topographical changes because of the removal of low molecular weight compounds result in the formation of a rough surface. FT IR spectra showed that the alkali treatment, potassium permanganate treatment and benzoyl chloride treatment were also found to reduce unwanted lignins and hemicelluloses. The thermal stability of benzoyl chloride, potassium permanganate and alkali treated areca nut fibres were higher than the untreated fibre as characterized by

TG TDA method. The results from TG TDA data have also showed that the concentration of cellulose is higher in benzoyl chloride treated fibre than in potassium permanganate treated fibre. The surface treated fibres were found to possess higher fibre surface tensions than the untreated fibre. Alkali treated fibre has the highest water absorption property, followed by untreated fibre; potassium permanganate treated fibre has the lowest water absorption property. However, benzoylation shows irregular pattern of water absorption. In addition, the aspect ratio of the treated fibres, except the benzoyl chloride treated fibre, is higher than the untreated fibre. From the results of the present study, the treated fibres from the unmanaged disposal areca nut fibre has good potential for the fabrication of a useful value added composite material product. Hence, the areca fiber reinforced natural rubber composites can be considered as a very promising material for fabrication of lightweight materials and can be effectively used in industrial sectors like automobile body building, office furniture, packaging industry, partition panels.

Acknowledgements

The authors would like to express their gratitude to the Department of Higher Education (Lower Myanmar), Ministry of Education, Myanmar, for the permission to do this research and also to the Myanmar Academy of Arts and Science for giving the opportunity to read this paper.

References

Baiardo, M., Frisoni, G., Scandola, M. and Licciardello, A. (2002)."Surface Chemical Modification of Natural Cellulose Fibers". *Journal of Applied Polymer Science*, vol. 83(1), pp. 38-45.

Binoj, J. S., Raj, R. E., Sreenivasan, V. S. and Thusnavis, G. R. (2016). "Morphological, Physical, Mechanical, Chemical and Thermal Characterization of sustainable Indian Areca Fruit Husk Fibers (*areca catechu* l.) as Potential Alternate for Hazardous Synthetic Fibers". *Journal of Bionic Engineering*, vol. 13(1), pp. 156-165.

Dhanalakshmi, S., Ramadevi , P., Basavaraju, B. and Raghu, R. P. (2015) "Natural Areca Fibre: Surface Modification and Spectral Studies", *Journal of Advances in Chemistry*, vol. 10 (10).

Ghahremani, H., Moradi, A ., Abedini-Torghabeh, J. and Hassani, S. M. (2011)."Measuring Surface Tension of Binary Mixtures of Water+ Alcohols from the Diffraction Pattern of Surface Ripples". *Der Chemica Sinica*, vol. 2(6), pp. 212-221**.**

Van Hazendonka, J.M., Van der Putten, J.C., Keurentjesb, J.T.F. and Prins, A. (1993). "A Simple Experimental Method for the Measurement of the Surface Tension of Cellulosic Fibres and its Relation with Chemical Composition", *Colloids and Surfaces A: Physicochemical and Engineering Aspects*, 81, pp. 251-261.

Silverstein, R.M., Webster, F.X. and Kiemle, D.J. (2003). "Spectrometric Identification of Organic Compounds". New York: 7th Edition, John Wiley and Sons, Inc.

PREPARATIONS AND CHARACTERIZATIONS OF CHITOSAN, ZnO NANOPARTICLE AND CHITOSAN-ZnO NANOCOMPOSITE

Kyu Kyu Aung[1], Khin Thida Htun[2]

Abstract

In this research, chitosan was prepared from *Metapenaeus dobosoni* species (Pezun-phyu) shrimp shell wastes by using a chemical method. The preparation of chitosan process consists of four steps such as deproteinization, demineralization, decolouration and deacetylation, respectively. The prepared chitosan (CS) was matched with FT IR and XRD reports of the standard chitosan. The prepared CS was also characterized by SEM. The yield percent of CS and the degree of acetylation were observed as 27.82 % and 72 %, respectively. The moisture and ash percentage of CS were observed to be 8.6 % and 0.2 %, respectively. The average crystallite size of the CS was 12.20 nm. The micrographs of CS showed the layers of flakes, porous and cage like morphology. The ZnO nanoparticle was prepared by co-precipitation method. It was characterized by TG-DTA, XRD, FT IR and SEM. The average crystallite size of the prepared ZnO nanoparticle was 20.99 nm. According to the SEM, the prepared ZnO nanoparticle showed spherical shape, porous structure and irregular surface morphology. And then chitosan-ZnO (CS-ZnO) nanocomposite was also prepared by using co-precipitation method. The prepared CS-ZnO nanocomposite was characterized by XRD, FT IR and SEM techniques. The average crystallite size of prepared CS-ZnO nanocomposite was 13.78 nm. In the present study, antimicrobial activities on chitosan (CS), ZnO nanoparticles and prepared chitosan-ZnO (CS-ZnO) nanocomposite were compared.

Keyword: Shrimp shell wastes, chitosan, ZnO nanoparticle, chitosan-ZnO nanocomposite, antimicrobial activities

Introduction

Shrimp is one of the important fisheries products worldwide including Myanmar. After the process of separation of the head and shells, this product is mostly exported in frozen condition. Head and shell materials of shrimp have only a low economic value and are treated as bio-waste or sold to animal feed manufactures. About 50 % of shrimp total body weight is waste. Shrimp wastes are environmental contaminants. Therefore, utilization of these wastes can prevent environmental contamination. This bio-waste can be used to produce valuable products such as chitin. Chitin is the second most abundant biopolymers found in nature after cellulose. Chitin $(C_6H_{11}O_4N)_n$ is a liner polysaccharide consisting of β(1-4)-linked 2-acetamido- 2-deoxy-D-glucopyranose. Chitosan is the most important derivative of chitin after deacetylation (Pokhrel *et al*., 2015). Chitosan is a linear polysaccharide consisting of β (1-4)-linked 2-amino-2-deoxy-D--glucopyranose. It is insoluble in water but soluble inorganic acids and organic acid. It is the universally accepted non-toxic chitosan. Chitosan is very reactive because of its free amino groups (Younes and Rinaudo, 2015). The difference between chitosan and cellulose is the amine ($-NH_2$) group in the position C-2 of chitosan instead of the hydroxyl (-OH) group found in cellulose. However, unlike plant fiber, chitosan possesses positive ionic charges (amino group), which give it the ability to chemically bind with negatively charged fats, lipids, cholesterol, metal ions, proteins and macromolecules (Bui *et al*., 2017).

The ZnO nanoparticles can be prepared by many synthetic methods such as co-precipitation, sol-gel, hydrothermal method etc. This nanoparticles can potentially be applied to gas sensors, photocatalyst for degradation of waste water pollutants, catalysts,

[1] Dr, Associate Professor, Department of Engineering Chemistry, Technological University (Pathein)
[2] Dr, Associate Professor, Department of Chemistry, Myeik University

semiconductors, piezoelectric devices, field-emission displays, ultraviolet photodiodes, surface accoustic wave devices, UV-shielding materials, rubber, medical and dental materials, pigments and coatings, ceramic, concrete, antibacterial and bactericide, and composites (Salahuddin *et al*., 2015). The antimicrobial activity of the ZnO nanoparticles is known to be a function of the surface area in contact with the microorganisms. Large surface area of the nanoparticles enhances their interaction with the microbes to carry out a broad range of probable antimicrobial activities (Espitia *et al*., 2012).

Chitosan (CS) along with metal oxide nanoparticles has been utilized as a stability agent due to its excellent film-forming ability, mechanical strength, biocompatibility, non-toxicity, high permeability towards water, susceptibility to chemical modifications and antibacterial (Kavitha and Subashini, 2015). Chitosan also acts as a chelating agent that selectively binds trace metals and metal oxide, thereby inhibit the production of toxins and microbial growth.

Materials and Methods

Preparation of Chitosan (CS)

In the present work, preparation of chitin from *Metapenaeus dobosoni* species shrimp shell wastes were collected from Myoma market at Thanlyin in yangon Division. These wastes were washed several times with water and then dried at room temperature. Chitin was prepared by three steps such as demineralization with 4% HCl, deproteinization with 3% NaOH and decolouration with acetone by using chemical method. And then the chitosan was obtained by deacetylation of chitin by 50% NaOH (Bui *et al*., 2017). The prepared CS was characterized by FT IR, XRD and SEM.

Preparation of ZnO Nanoparticle

In the present work, ZnO nanoparticle was prepared. 150 mL of 0.05 M zinc nitrate solution was added in 1L beaker. Then, 0.1M NaOH solution was slowly added with continuous stirring using magnetic stirrer, until pH of the mixture solution is 9 by using co-precipitation method. And then, the $Zn(OH)_2$ precipitate was filtered and washed with distilled water until neutral pH. The precipitate was dried at 70^{o}C at 24 h and then calcined at 400 ^{o}C in furnace. The ZnO nanoparticle was obtained. The ZnO nanoparticle was characterized by TG-DTA, XRD, FT IR and SEM.

Preparation of Chitosan-Zinc Oxide Nanocomposite

The Chitosan-Zinc Oxide (CS-ZnO) nanocomposite was prepared by co-precipitation method. Firstly, 3 g of ZnO nanoparticle was dissolved in 2% acetic acid and 1 g of CS was dissolved in 2% acetic acid by stirring using magnetic stirrer at pH is 4. These solutions were mixed with continuous stirring until it becomes clear solution. While stirring, 0.05 M NaOH solution was added drop wise until pH of solution is to be 9. The white precipitate of Chitosan-Zinc Oxide (CS-ZnO) was obtained. It was filtered and dried at 60^{o}C for 1 h. The prepared CS-ZnO nanocomposite was characterized by FT IR, XRD and SEM.

Determination of Antimicrobial Activities on Chitosan (CS), ZnO Nanoparticle and Chitosan-Zinc Oxide Nanocomposite

The chitosan, ZnO nanoparticle and Chitosan-Zinc Oxide (CS-ZnO) nanocomposite were tested against four pathogenic bacteria: two gram-positive (*Staphylococcus aureus* and *Bacillus*

subtilis), two gram-negative (*Pseudomonas aeruginosa* and *Escherichia coli*), one pathogenic yeast (*Candida albicans*) and one fungi (*Aspergillus niger*) by agar well diffusion method**.**

Results and Discussion

Characterization of the Prepared Chitosan

In this research, the photograph of prepared CS from shrimp shell wastes is shown in Figure 1. The prepared CS was characterized by FT IR, XRD and SEM measurements.

Figure 1 Photograph of the prepared CS from shrimp shell wastes

FTIR analysis of the prepared chitosan

The FT IR spectrum of prepared CS is presented in Figures 2. The strong absorption bands around at 3460, 3360 and 3105 cm^{-1} are due to OH and amine N-H symmetrical stretching vibrations. The small peak around 2870 cm^{-1} was appeared due to CH stretching of $–CH_2–$ and $–CH_3$ groups. The peaks around at 1622 and 1552 cm^{-1} were indicated the C=O stretching of amide I and amide II. The major absorption band was observed at1151, 1077 and 1020 cm^{-1} which represents the free amino group $-NH_2$ at C-2 position of glucosamine, a major group present in CS. The peak around at 1375 and 1304 cm^{-1} represent the C-H bending vibrations of $–CH_2$ and amide III (Arafat *et al*, 2015; Knidri *et al.*, 2017). The degree of acetylation is calculated by using peaks at 3460 and 1655 in the FT IR data. The degree of acetylation of chitosan is 72%.

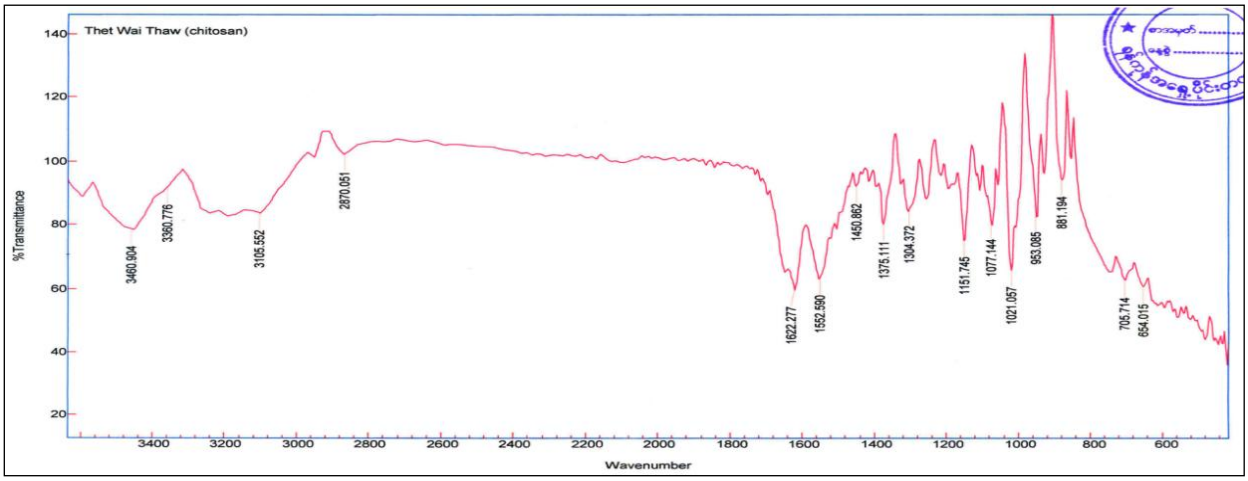

Figure 2 FTIR spectrum of the prepared CS from shrimp shell wastes

XRD analysis of the prepared chitosan

In this studies, the two peaks at 2 θ value around at 10.5º and 20º correspond to the (102) and (110) crystal planes indicating crystalline structure of chitosan (Knidri *et al.*, 2017). In the XRD data, Miller indices of chitosan were matched with JCPDS standard library data 03-0226.

Figure 3 shows the XRD diffractogram of prepared chitosan. Table 1 reveals the XRD data of chitosan. According to XRD data, the peaks at 2θ around 11º, 17º, 22º, 23º, 26º, 27º, 28º, 30º, 31º, 32º, 33º, 35º, 36º and 40º corresponding to (¯101), (¯102), (012), (¯202), (030), (031), (210), (003), (¯132), (013), (131), (¯232), (¯313) and (103) planes, respectively. The average crystallite size of chitosan was calculated by Debye-Scherrer equation. The average crystallite size of chitosan is 12.20 nm.

Table 1 The XRD Data of the prepared Chitosan from shrimp shell wastes

[chitosan-No3-MaThetWaiThaw-F296.raw] chitosan — Peak Search Report

SCAN: 10.0/70.0/0.02/0.12(sec), Cu(40kV,40mA), I(max)=160, 02/28/18 15:06

PEAK: 7-pts/Parabolic Filter, Threshold=1.0, Cutoff=0.1%, BG=1/1.0, Peak-Top=Parabolic Fit

NOTE: Intensity = Counts, 2T(0)=0.0(deg), Wavelength to Compute d-Spacing = 1.54056Å (Cu/K-alpha1)

#	2-Theta	d(Å)	(h k l)	BG	Height	Height%	Area	Area%	FWHM	XS(Å)	P/N
1	11.720	7.5445	(-1 0 1)	20	12	30.8	124	11.1	0.176	553	1.1
2	17.233	5.1415	(-1 0 2)	29	12	30.8	42	3.8	0.060	>1000	0.9
3	20.536	4.3213	(0 0 2)	69	24	61.5	861	76.9	0.610	134	1.2
4	20.707	4.2861	(1 0 1)	66	39	100.0	857	76.5	0.374	224	1.9
5	22.237	3.9945	(0 1 2)	51	11	28.2	144	12.9	0.223	407	0.7
6	23.356	3.8056	(-2 0 2)	50	23	59.0	642	57.3	0.475	175	1.3
7	26.075	3.4145	(0 3 0)	45	22	56.4	158	14.1	0.122	>1000	1.3
8	26.709	3.3349	(2 0 0)	43	10	25.6	109	9.7	0.185	523	0.7
9	27.741	3.2132	(0 3 1)	43	18	46.2	457	40.8	0.432	195	1.2
10	28.162	3.1661	(2 1 0)	47	13	33.3	199	17.8	0.260	341	0.8
11	30.985	2.8838	(0 0 3)	43	9	23.1	163	14.6	0.308	283	0.6
12	31.328	2.8529	(-1 3 2)	38	28	71.8	1120	100.0	0.680	123	1.7
13	32.734	2.7335	(0 1 3)	42	13	33.3	110	9.8	0.144	801	0.9
14	33.342	2.6850	(1 3 1)	39	12	30.8	399	35.6	0.565	149	0.8
15	35.242	2.5446	(-2 3 2)	32	15	38.5	285	25.4	0.323	271	1.1
16	35.999	2.4927	(0 4 1)	31	13	33.3	107	9.6	0.140	853	1.0
17	36.552	2.4563	(-3 1 3)	25	24	61.5	233	20.8	0.165	637	1.7
18	36.916	2.4329	(-3 1 1)	28	18	46.2	230	20.5	0.217	434	1.3
19	40.190	2.2419	(1 0 3)	32	15	38.5	330	29.5	0.374	235	1.1
20	40.921	2.2036	(0 4 2)	28	16	41.0	329	29.4	0.350	253	1.2

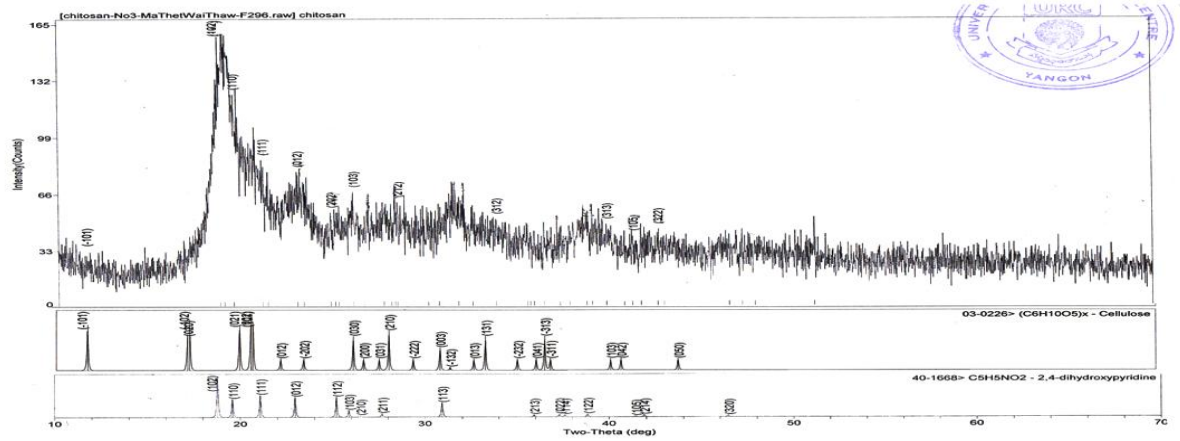

Figure 3 XRD diffractogram of the prepared CS from shrimp shell wastes

Morphological analysis of the prepared chitosan by SEM

The SEM micrograph of the prepared CS is presented in Figure 4. The prepared micrograph of CS shows the layers of flakes, porous and cage like morphology appeared on some areas.

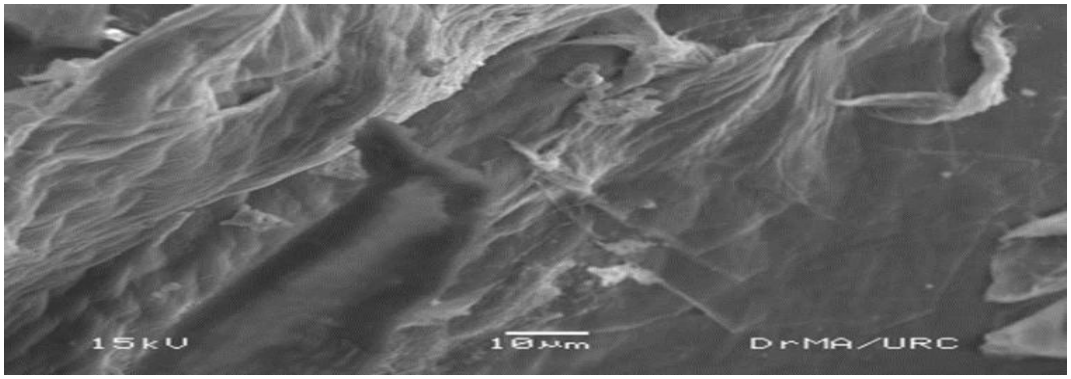

Figure 4 SEM micrograph of the prepared CS from shrimp shell wastes

Characterization of the Prepared ZnO nanoparticle

TG-DTA data of the prepared ZnO nanoparticle

The thermogravimetric curves demonstrated completely decomposition of sample at 30 to 600°C. The TG-DTA curves of prepared ZnO nanoparticle (zinc hydroxide) are illustrated in Figure 5(a). At low temperature, two endothermic peaks around 144.79 and 262.42 °C were due to loss of volatile surfactant molecules absorbed on the $Zn(OH)_2$ during synthesis conditions. At high, temperature, two peaks around 371 °C and 449 °C were assigned due to the decomposition of $Zn(OH)_2$ to ZnO. The percent of total weight loss was 11.021 %.

XRD analysis of the prepared ZnO nanoparticle

The X-ray powder Diffraction (XRD) measurement was carried out to confirm the crystallinity using Regaku X-ray diffractometer with Cu/Kα radiation (λ=1.54056 Å) in the range of 2 θ between 10º-70º. In XRD data, Miller indices of ZnO NP's were matched with ZnO from JCPDS standard library data 80-0075. Figure 5(b) showes the XRD diffractograms of ZnO nanoparticle. Table 2 reveales (a) the XRD data and (b) peaks ID Data of ZnO nanoparticle. According to the XRD data, the sharp peaks at 2 θ value around 31º; 34º, 36º, 47º, 56º, 62º, 67º and 69º are corresponding to (100), (002), (101), (102), (110), (103), (112) and (201) planes, respectively. All diffraction peaks of ZnO nanoparticle have hexagonal wurtzite structure. The average crystallite size was calculated by Debye-Scherrer equation. The average crystallite size of ZnO nanoparticle is 20.99 nm.

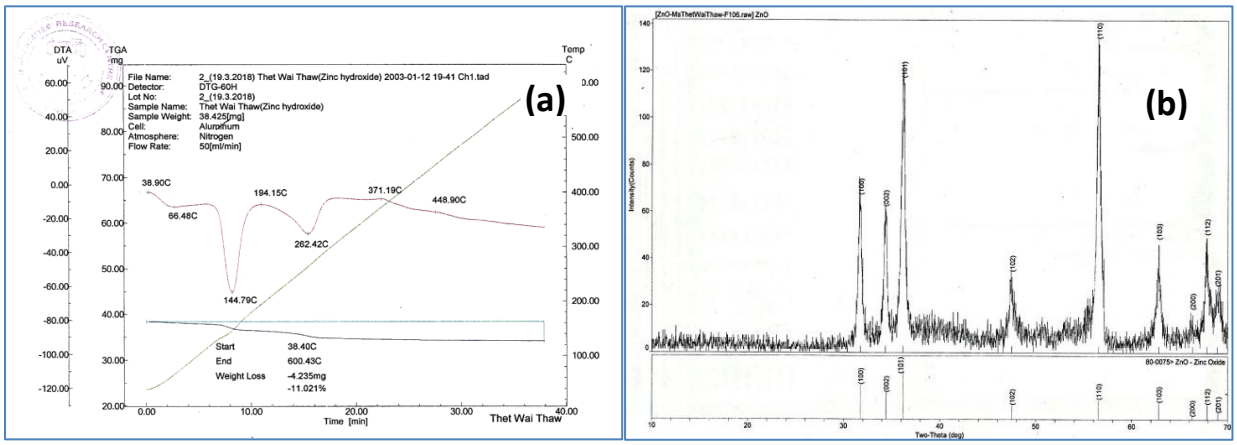

Figure 5 (a) TG-DTA thermogram of the prepared ZnO nanoparticle
(b) XRD diffractogram of the prepared ZnO nanoparticle

Table 2(a) XRD Data of the prepared ZnO nanoparticle

[ZnO-MaThetWaiThaw-F106.raw] ZnO — Peak Search Report

SCAN: 10.0/70.0/0.02/0.24(sec), Cu(40kV,40mA), I(max)=135, 01/25/18 23:32

PEAK: 9-pts/Parabolic Filter, Threshold=1.0, Cutoff=0.1%, BG=1/1.0, Peak-Top=Parabolic Fit

NOTE: Intensity = Counts, 2T(0)=0.0(deg), Wavelength to Compute d-Spacing = 1.54056Å (Cu/K-alpha1)

#	2-Theta	d(Å)	(h k l)	BG	Height	Height%	Area	Area%	FWHM	XS(Å)	P/N
1	31.712	2.8193	(1 0 0)	5	60	48.8	1492	47.7	0.423	201	3.7
2	34.321	2.6107	(0 0 2)	6	54	43.9	1230	39.4	0.387	222	3.5
3	36.157	2.4822	(1 0 1)	10	105	85.4	2765	88.5	0.448	192	4.9
4	47.480	1.9133	(1 0 2)	8	24	19.5	594	19.0	0.421	212	2.1
5	56.525	1.6267	(1 1 0)	9	123	100.0	3125	100.0	0.432	215	5.4
6	62.791	1.4786	(1 0 3)	6	40	32.5	840	26.9	0.357	272	2.9
7	66.318	1.4083	(2 0 0)	5	11	8.9	214	6.8	0.331	301	1.4
8	67.831	1.3805	(1 1 2)	10	38	30.9	850	27.2	0.380	261	2.7
9	68.933	1.3611	(2 0 1)	12	14	11.4	378	12.1	0.459	215	1.4

Table 2(b) Peaks ID Data of the prepared ZnO nanoparticle

[ZnO-MaThetWaiThaw-F106.raw] ZnO — Peak ID Report

SCAN: 10.0/70.0/0.02/0.24(sec), Cu(40kV,40mA), I(max)=135, 01/25/18 23:32

PEAK: 9-pts/Parabolic Filter, Threshold=1.0, Cutoff=0.1%, BG=1/1.0, Peak-Top=Parabolic Fit

NOTE: Intensity = Counts, 2T(0)=0.0(deg), Wavelength to Compute d-Spacing = 1.54056Å (Cu/K-alpha1)

#	2-Theta	d(Å)	Height	Height%	Phase ID	d(Å)	I%	(h k l)	2-Theta	Delta
1	31.712	2.8193	60	48.8	ZnO	2.8180	57.9	(1 0 0)	31.727	0.015
2	34.321	2.6107	54	43.9	ZnO	2.6049	44.2	(0 0 2)	34.400	0.079
3	36.157	2.4822	105	85.4	ZnO	2.4786	100.0	(1 0 1)	36.211	0.055
4	47.480	1.9133	24	19.5	ZnO	1.9128	22.9	(1 0 2)	47.493	0.013
5	56.525	1.6267	123	100.0	ZnO	1.6270	32.4	(1 1 0)	56.517	-0.008
6	62.791	1.4786	40	32.5	ZnO	1.4784	27.6	(1 0 3)	62.801	0.010
7	66.318	1.4083	11	8.9	ZnO	1.4090	4.4	(2 0 0)	66.281	-0.037
8	67.831	1.3805	38	30.9	ZnO	1.3799	24.3	(1 1 2)	67.864	0.033
9	68.933	1.3611	14	11.4	ZnO	1.3601	11.4	(2 0 1)	68.990	0.057

Line Shifts of Individual Phases:
PDF#80-0075 - Zinc Oxide <2T(0) = 0.0, d/d(0) = 1.0>

FT IR analysis of the prepared ZnO nanoparticle

In this research, FT IR analysis of prepared ZnO nanoparticle is presented in Figure 6(a). The peaks around 3400 cm^{-1} indicated the stretching vibration of hydroxyl groups on ZnO surface absorbed water vapour. The broad bands around 1600 cm^{-1} due to bending vibration of hydroxyl groups on ZnO surface absorbed water vapour. The metal oxides generally give absorption bands below 1000 cm^{-1} arising from interatomic vibrations. The bands around 860 and 450 cm^{-1} corresponded to O-Zn-O and Zn-O-Zn stretching and bending vibrations (Kumar and Rani, 2013).

SEM measurement of the prepared ZnO nanoparticle

In this study, the SEM micrograph of the prepared ZnO nanoparticle is presented in Figure 6(b). In the micrograph of the ZnO nanoparticle showed spherical shape, porous structure and irregular surface morphology.

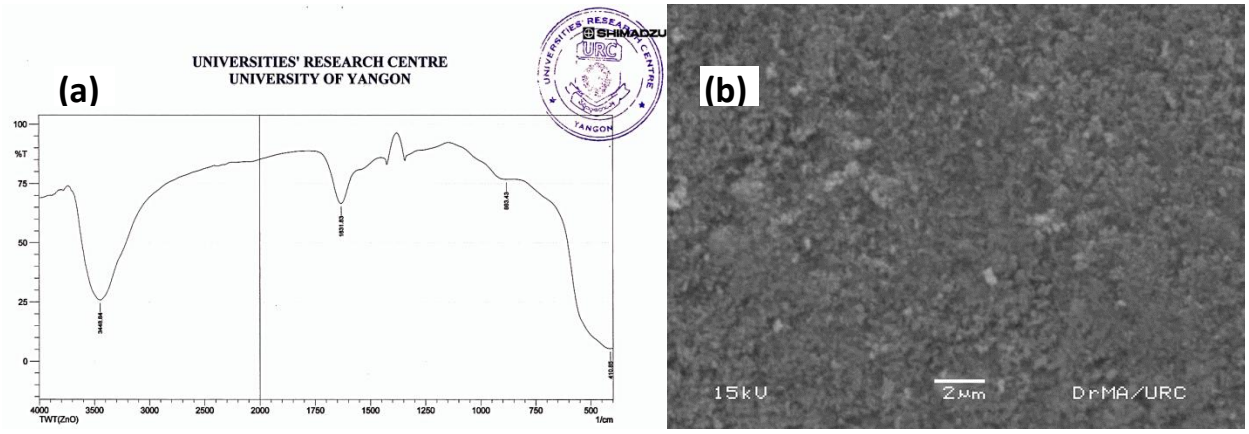

Figure 6 (a) FT IR spectrum of the prepared ZnO nanoparticle
(b) SEM micrograph of ZnO nanoparticle

Characterization of the Prepared Chitosan-Zinc Oxide (CS-ZnO) Nanocomposite

In this research, the prepared CS-ZnO nanocomposite is characterized by FT IR, XRD and SEM measurements.

FT IR analysis of the prepared CS-ZnO nanocomposite

In this research, FT IR analysis of the prepared CS-ZnO nanocomposite was carried out to characterize [Figure 7(a)]. The peak observed at 3425 cm^{-1} to the stretching vibration of $–NH_2$ group and –OH group. The C-H stretching vibration was observed at 2878 cm^{-1}. The peak 1628 cm^{-1} indicated the amine I group (C-O stretching along the N-H deformation mode). The peak 1589 cm^{-1} was assigned to the –NH deformation mode. The band around 1383 and 1332 cm^{-1} were showed C-H in plane bending vibrational group. The peak around 1157 cm^{1} showed a small shoulder peak of ß (1-4) glycosidic band in polysaccharide unit and around 1065 cm^{-1} indicated the stretching vibration of C-O-C in glucose circle. The band observed in the range of 575-532 cm^{-1} corresponds to the stretching vibration of N-Zn-O group (Dhanavel *et al.*, 2014 and Demir *et al*., 2016).

XRD analysis of the prepared CS-ZnO nanocomposite

In this studies, X-ray Powder Diffraction (XRD) measurement was carried out to confirm the crystallinity using Rigaku X-ray diffractometer with Cu/Ka radiation (λ= 1.54056 Å) in the range of 2 θ between 10º-70º. The two peaks at 2θ values around at 10.5° and 20° correspond to the crystal panes indicating crystalline structure of CS (Dhannavel *et al.*, 2014). According to the XRD data, the sharp peaks at 2θ value around 31°, 34°, 36°, 47°, 56°, 62°, 66°, 67° and 69° are corresponding to (1 0 0), (0 0 2), (1 0 1), (1 0 2), (1 1 0), (1 0 3), (2 0 0), (1 1 2) and (2 0 1) planes, respectively. Figure 7(b) shows the XRD diffractograms of prepared CS-ZnO nanocomposites. Table 3 shows the XRD data of prepared CS-ZnO nanocomposites. The average crystallite size of prepared CS-ZnO nanocomposites is 13.78 nm.

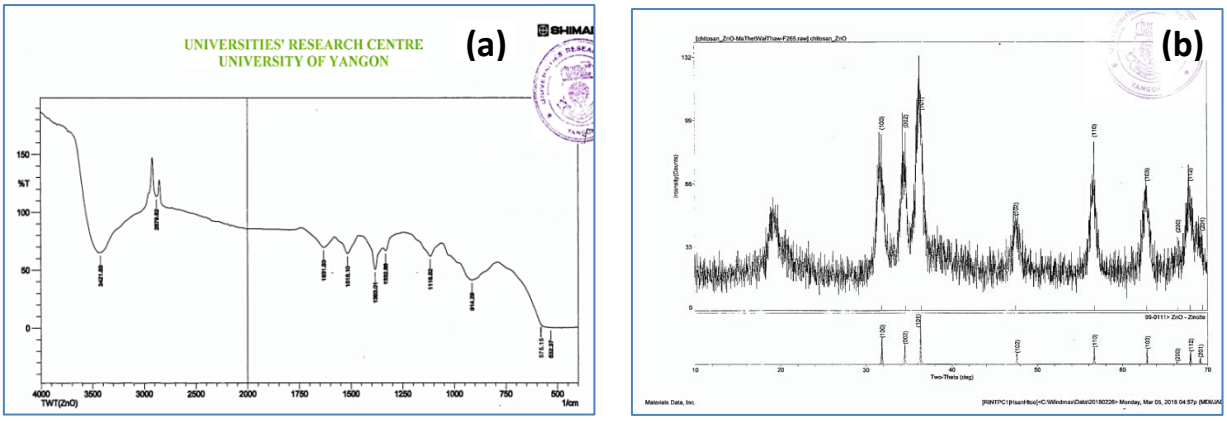

Figure 7 (a) FT IR spectrum of the prepared CS-ZnO nanocomposite
(b) XRD diffractogram of the prepared CS-ZnO nanocomposite

SEM measurement of the prepared CS-ZnO nanocomposite

The SEM micrograph of the prepared CS-ZnO nanocomposite is presented in Figure 8. In the micrograph of the prepared CS-ZnO nanocomposite showed cage like morphology indicating uniformly dispersion of ZnO nanoparticles into CS.

Table 3 XRD Data of the prepared CS-ZnO nanocomposite

[chitosan_ZnO-MaThetWaiThaw-F265.raw] chitosan_ZnO											Peak Search Report
SCAN: 10.0/70.0/0.02/0.12(sec), Cu(40kV,40mA), I(max)=133, 02/26/18 14:07											
PEAK: 9-pts/Parabolic Filter, Threshold=1.0, Cutoff=0.1%, BG=1/1.0, Peak-Top=Parabolic Fit											
NOTE: Intensity = Counts, 2T(0)=0.0(deg), Wavelength to Compute d-Spacing = 1.54056Å (Cu/K-alpha1)											
#	2-Theta	d(Å)	(h k l)	BG	Height	Height%	Area	Area%	FWHM	XS(Å)	P/N
1	31.781	2.8133	(1 0 0)	24	68	100.0	2413	83.4	0.603	139	3.5
2	34.564	2.5929	(0 0 2)	37	56	82.4	1314	45.4	0.399	215	2.9
3	36.416	2.4651	(1 0 1)	38	64	94.1	2895	100.0	0.769	110	3.2
4	47.467	1.9138	(1 0 2)	21	26	38.2	1144	39.5	0.748	117	1.9
5	56.674	1.6228	(1 1 0)	23	65	95.6	1749	60.4	0.457	202	3.5
6	62.896	1.4764	(1 0 3)	20	45	66.2	1795	62.0	0.678	139	2.8
7	66.536	1.4042	(2 0 0)	22	16	23.5	264	9.1	0.280	363	1.3
8	67.986	1.3777	(1 1 2)	28	37	54.4	1177	40.7	0.541	180	2.3
9	69.408	1.3530	(2 0 1)	24	15	22.1	408	14.1	0.462	214	1.2

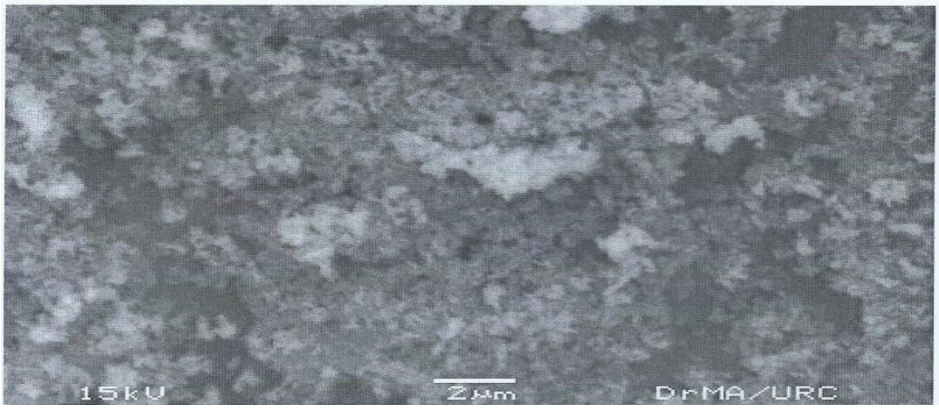

Figure 8 SEM micrograph of the prepared CS-ZnO nanocomposite

Antimicrobial Activities of Chitosan, ZnO Nanoparticle and the Prepared Chitosan-ZnO Nanocomposite

The antimicrobial activity of CS, ZnO NP's and the prepared CS-ZnO nanocomposite were tested against four pathogenic bacteria, two gram negative (*Pseudomonas aeruginos* and *Esherichia coli*), two gram positive (*Staphylococcus aureus* and *Bacillus subtilis*), one pathogenic yeast (*Candida albican*) and one fungi (*Asperigillus niger*) in Figure 9 and Table 4.

The CS against different groups of microorganisms such as bacteria, yeast and fungi are shown at below pH 6 because of the positive charge on the C-2 of the glucosamine monomer.

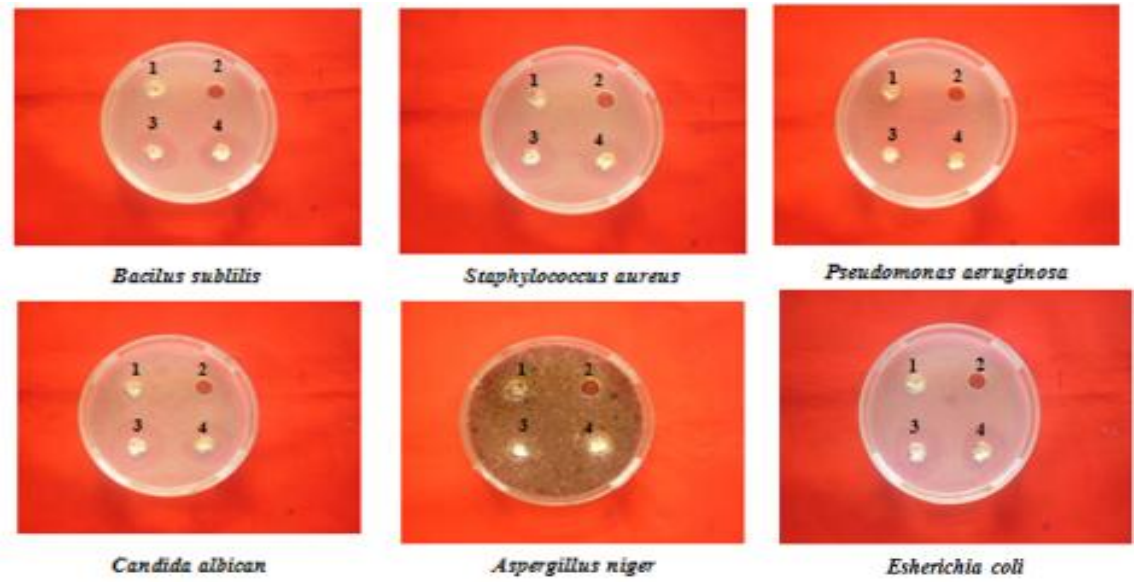

Figure 9 Antimicrobial activities of chitosan, ZnO nanoparticle and the prepared chitosan-ZnO nanocomposite

Table 4 Antimicrobial Activities of CS, ZnO NP's and Obtained CS-ZnO Nanocomposit against Pathogenic Bacteria and Fungi Strains

No.	Samples	Diameter of Inhibition Zone (nm)					
		Bacterial strains				Fungi strains	
		I	II	III	IV	V	VI
1	CS (pH = 7)	-	-	-	-	-	-
2	CS (pH = 9)	12 mm (+)	12 mm (+)	13 mm (+)	13 mm (+)	12 mm (+)	11 mm (+)
3	ZnO NP's	15 mm (++)	25 mm (+++)	26 mm (+++)	24 mm (+++)	13 mm (+)	28 mm (+++)
4	CS-ZnO nanocomposite	15 mm (++)	25 mm (+++)	25 mm (+++)	22 mm (+++)	12 mm (+)	30 mm (+++)

Organisms

I = *Pseudomonas aeruginos* (N. C. T. C-6749)
II = *Esherichia coli* (N. C. I. B-8134)
III = *Staphylococcus aureus* (N. C. P. C-6371)
IV = *Bacillus subtillis* (N. C. I. B-8982)
V = *Aspergillus niger*
VI = *Candida albicans*

Agar well – 10 mm
10 mm ~ 14 mm (+) - lower activity
15 mm ~ 19 mm (++) - higher activity
20 mm ~ above (++) - higher activity

In this research, the prepared chitosan do not show antimicrobial activities at pH 7. The chitosan was also used in the food industry as a food quality enhancer in certain countries. Dietary cookies, potato chip and noodles were produced with chitosan because of its hypocholesterolemic effect. Furthermore, vinegar products containing chitosan are manufactured and sold in Japan again because of their cholesterol lowing ability (Hirano, 1989). The prepared chitosan at pH 9 shows lowest antimicrobial activities were observed against pathogenic bacterial and pathogenic yeast and fungi.

The ZnO nanoparticle showed at highest antimicrobial activity is observed against *Esherichia coli, Staphylococcus aureus, Bacillus subtilis* and *Candida albicans.* The ZnO nanoparticle has moderated effect on *Pseudomonas aeruginosa* and lowest activity on *Aspergillus niger.*

In this research, the prepared CS-ZnO nanocomposite showed highest antimicrobial activity was observed against *Candida albicans.*

Conclusion

In this research, the chitosan was prepared from *Metapenaeus dobosoni* species shrimp shell wastes by using chemical method. The degree of acetylation and the average crystallite size of chitosan are 72% and 12.20 nm, respectively. The yield present of chitosan was 27.82 %. It was completely dissolved in 2% acetic acid. By using AOAC method, the investigation of moisture and ash presents of chitosan were observed 8.6 % and 0.2 %, respectively. The SEM micrograph of chitosan showed the layers of flakes, porous and cage like morphology. Then, the ZnO nanoparticle was prepared by co-precipitation method. In XRD data, Miller indices of the prepared ZnO nanoparticle was matched with ZnO from JCPDF standard library data 80-0075. The average crystallite size of prepared ZnO nanoparticle was 20.99 nm. And then, chitosan-ZnO nanocomposite was prepared by co-precipitation method. The prepared chitosan-ZnO nanocomposite was characterized by FT IR, XRD and SEM measurements. The average crystallite size of prepared chitosan-ZnO nanocomposite was 13.78 nm. The SEM micrograph of prepared chitosan--ZnO nanocomposite showed cage like morphology and uniforming dispersion of ZnO into chitosan. In this research, the antimicrobial activities of the prepared chitosan, prepared ZnO nanoparticle and the prepared chitosan-ZnO nanocomposite were compared. As a results, the prepared ZnO nanoparticle and the prepared chitosan-ZnO nanocomposite showed the highest antimicrobial activities were observed. But the prepared chitosan-ZnO nanocomposite was more effective than ZnO nanoparticle on yeast. Therefore, the prepared chitosan-ZnO nanocomposite can be used in sunscreens, plastic and rubber manufacturing, food, packaging, medical care as well as healthcare, etc. The progress in synthesis of nanoparticles and nanocomposites can be paved the way on the innovative approaches for development of novel antimicrobial agents.

Acknowledgements

The authors would like to express our sincere gratitude to headmaster Dr Kyaw Thu Ya (Technological University, Pathein) for his kind provision of our research Facilities. This work was financially supported by Dr Ye Myint Aung, Professors, Department of Chemistry, Pathein University. Special thanks are due to the Department of Higher Education (Yangon Office), Ministry Education, Yangon, Myanmar. Thanks are also extended to the Myanmar Academy of Arts and Science, Yangon, Myanmar, for allowing submitting this research paper.

References

Arafat, A., S. A. Samad, S. M. Masum and M. Moniruzzaman. (2015). "Preparation and Characterization of Chitosan from Shrimp Shell Waste". *Int. J. Sci & Engi. Res.*,vol. 6, pp.538

Bui, V. K. H., D. Park and Y. C. Lee. (2017). "Chitosan Combined with ZnO, TiO_2 and Ag Nanoparticles for Antimicrobial Wound Healing Applications : A Mini Review of the Research Trends". *Journal Polymer*, vol. 9 (21), pp.1-24

Chung, Y. C., C. L. KuO and C. C. Chen. (2005). "Preparation and Important Functional Properties of Water-Soluble Chitosan Produced Through Millard Reaction". *Bioresource Technology*, vol. 96, pp. 1473-1482

Demir, D., F. Ofkeli, S. Ceylan and N. B. Karagulle. (2016). "Extraction and Characterization of Chitin and Chitosan from Blue Crab and Synthesis of Chitosan Cryogel Scaffolds". *JOTCSA.*, vol,3 (3), pp. 131-144

Dhanavel, S., E.A.K. Nivethaa, V. Narayanan and A. Stephen. (2014). "Photocatalytic activity of Chitosan/ZnO Nanocompositess for Degrading Methylene Blue". *International Journal of Chem Tech Research*., vol. 6 (3), pp.1880-1882

Espitia, P. J. P., N. F. F. Soares, J. S. A. Coimbra, N. J. Andrade, R. S. Cruz and E. A. A. Medreiros. (2012). "Zinc Oxide Nanoparticles : Synthesis, Antimicrobial Activity and Food Packaging Applications". *Food Bioprocess Technol.,* vol. 5, pp.1447-1464

Hirano, S. (1989). *Production and Application of Chitin and Chitosan in Japan in Chitin and Chitosan*. London: *Elsevier Applied Science,* UK, pp. 51-69

Kavitha, A. L. and A. Subashini. (2015)."Synthesis and Characterization of Iron oxide- Chitosan for Dye Decolourization" *Int.J. Adv. Chem.Sci.Appl.,* vol. 3(1), pp. 20-23

Knidri, H. E., R. Belaabed, R. E. Khalfaouy, A. Laajeb, A. Addaou and A. Lahsini. (2017). "Physicochemical Characterization of Chitin and Chitosan Produced from *Parapenacus longirostris* Shrimp Shell Wastes". *Journal of Materials and Environmental Sciences*, vol. 8 (10), pp. 3648 – 3653

Kumar, H. and R. Rani. (2013). "Structural and Optical Characterization of ZnO Nanoparticles Synthesized by Microemulsion Route". *Int. Lett.Chem. Phys. Astronomy.*, vol. 14, pp. 26-36

Kumari, S., P. Rath and S. H. Kumar. (2016). "Chitosan from Shrimp Shell (*Crangon crangon*) and Fish Scales (*Labeorohita*) : Extraction and Characterization". *African Journal of Biotechnology*, vol. 15 (24), pp. 1258-1268

Pokhrel, S., P. N. Yadav and R. Adhikaril. (2015). "Application of Chitin and Chitosan in Industry and Medical Science : A Review". *Nepal Journal of Science and Technology*, vol. 16 (1), pp. 99-104

Salahudin, N. A., M. E. Kemary and E. M. Ibrahim, (2015). "Synthesis and Characterization of ZnO Nanoparticles via Precipitation Method: Effect of Annealing Temperature on Particle Size". *Nanoscience and Nanotechnology*, vol. **5** (4), pp. 82-88

Younes, I. and M. Rinaudo. (2015). "Chitin and Chitosan Preparation from Marine Sources Structures, Properties and Applications". *Mar. Drugs.*,vol. 13, pp.1133-1174

ANTIBACTERIAL ACTIVITY AND IDENTIFICATION OF ISOLATED ORGANIC CONSTITUENTS FROM LEAVES OF *ACACIA CONCINNA* DC. (KIN- MUN- GYIN)

Thin Thin Win[1], Myint Myint Khine[2], Saw Hla Myint[3]

Abstract

The leaves of *Acacia concinna* DC. (Kin-mun-gyin) are used as folk medicine for the treatment of jaundice, malarial fever, laxative, diarrhoea and boils. The Kin-mun-gyin leaves were chosen for determination of antibacterial activity and organic constituents. The plant sample was collected from Mingalardon Township, Yangon Region. The meso-tartaric acid and myristic acid were isolated from aqueous and ethyl acetate extracts of Kin-mun-gyin leaves by column and preparative thin layer chromatographic methods. It was identified by UV, FT IR, ^{1}H NMR, ^{13}C NMR and ESI MS spectroscopic methods. Then, *in vitro* screening of antibacterial activity was done on four crude extracts (PE, EtOAc, EtOH and H_2O) of Kin-mun-gyin leaves against 3 species of *Staphylococcus aureus* and 2 species of *Escherichia coli*, one species of *Bacillus subtilis*, one species of *Proteus morganii* and one species of *Vibrio cholerae* by employing agar disc diffusion method. Except PE extract, all of the crude extracts were found to exhibit the inhibition zones against all of the organisms tested. Minimum inhibitory concentration (MIC) values of two isolated compounds were also determined by microplate dilution method on above 8 species of bacteria. The lowest MIC values of meso-tartaric acid and myristic acid from *A. concinna* leaves were respectively found to be 0.0058 mg mL^{-1}, 0.0937 mg mL^{-1} against *S. aureus* ws. From this study, it may be concluded that meso-tartaric acid and myristic acid possess antibacterial activities useful for the medicinal purposes for the curing of diseases caused by the microorganisms tested.

Keywords: *Acacia concinna* DC. (Kin-mun-gyin), antibacterial activity, meso-tartaric acid, myristic acid, agar disc diffusion method, MIC values

Introduction

Genus *Acacia* belongs to the subfamily Mimosoideae in Leguminosae which contains 600 genera and about 12000 species. It has 750-800 species (Dastur, 1962). Among them, 34 species grow in Myanmar (Kress and Yin Yin Kyi, 2003). Most members of subfamily Mimosoideae are trees or shrubs; leaves usually bipinnate; flowers regular; calyx usually gamosepalous; stamens equal in number to the petals or twice as numerous; fruit a legume (Figure 1) (Evans, 2002).

Figure 1 Photographs of the plant and leaves of *A. concinna* DC.

[1] Dr, Associate Professor, Department of Chemistry, Kyaukse University
[2] Dr, Professor, Department of Chemistry, University of Yangon
[3] Dr, Professor and Head (Rtd.), Department of Chemistry. University of Yangon

Materials and Methods

Sample Collection

The leaves of *Acacia concinna* DC. (Kin-mun-gyin) were collected from Sein Shwe Gyone Ywar, Htauk Kyant, Mingalardon Township, Yangon Region, Myanmar during the months of September and October, in the 2006. All the fresh samples were washed with distilled water. After cleaning, the leaves were air-dired at room temperature for three weeks. The dried samples were cut into pieces and then ground in a grinding machine to powder. The dried powdered samples were stored separately in air-tight containers to prevent moisture changes and other contamination. The following instruments were used for the determination of physical data: melting point; Gallenkamp melting point apparatus, UV spectra; Shimadzu UV-240, UV-Visible spectrophotometer, IR spectra; Perkin Elmer GX FT IR spectrophotometer, ^{1}H (300 MHz), ^{13}C (300 MHz) and ^{1}H (400 MHz) NMR spectra; were measured on a Bruker 300 and JEOL JNM-GM 400 spectrometer were used to record the spectra. ESI mass spectra was recorded at the Department of Organic Chemistry, Goettingen University, Germany.

Preparation of Crude Extracts

The dried powdered sample of Kin-mun-gyin leaves (100 g) were extracted with 70 % ethanol (200 ml× 4) at room temperature for two weeks. After two weeks, the extract was filtered and concentrated by rotatory evaporator at 45 °C. The concentrated extracts were combined and then partitioned with PE (60-80 °C) to remove the fat. In this way two layers, namely PE soluble layer (upper layer) and PE insoluble layer (low layer) (or) aqueous layer were obtained. Then the aqueous layer was partitioned with ethyl acetate in a separating funnel. The aqueous layer was concentrated under vacuum rotatory evaporator to obtain the aqueous extract. The EtOAc extract was dried over anhydrous Na_2SO_4, filtered and the total filtrate was concentrated under vacuum rotatory evaporator to obtain EtOAc crude extract.

The dried powdered samples (100g) were extracted with (250 mL) of, pet-ether, ethyl acetate, 70 % ethanol and water in separate conical flask, respectively for at least 7 days and then filtered. The filtrates were evaporated by using rotatory evaporator and desiccated. Then the dried extracts were weighed. Each extract was stored in refrigerator for screening of antibacterial activity.

Isolation of Organic Compound from Aqueous Crude Extract of *A. concinna* Leaves

The aqueous crude extract was chromatographed on a silica gel column (2 cm × 55 cm) using EtOH:NH_3:H_2O (80:5:15) (v/v) solvent system. Compound A separated out as a white powder. Recrystallization thrice from EtOH gave pure compound A (0.007 %) as white crystalline powder.

Isolation of Organic Compound from EtOAc Crude Extract of *A. concinna* Leaves

The EtOAc crude extract (1 g) was subjected to silica gel chromatography by using a gradient system of $ClCH_2CH_2Cl$-MeOH. After combining together similar fractions, 4 fractions were obtained. Fraction F_3 was rechromatographed eluting with $ClCH_2CH_2Cl$-MeOH (93:7) (v/v) solvent system to yield pure compound B (0.006 %) as colourless powder.

Structural Elucidation

The structures of isolated compounds were elucidated and identified by modern spectroscopic techniques such as UV, FT IR, ^{1}H NMR, ^{13}C NMR and ESI MS spectroscopies.

***in vitro* Screening of Antibacterial Activity of Different Crude Extracts by Agar Disc Diffusion Metho**

The antibacterial activity of different crude extracts (PE, EtOAc, EtOH and H_2O) was determined by agar disc diffusion method (Mar Mar Nyein *et al.*, 1991) at Department of Medical Research (Lower Myanmar), Dagon Township, Yangon Region, Myanmar.

Procedure

The filter discs (6 mm diameter) were made by punched No.1 Whatmann filter paper. The disc were sterilized by autoclaving and following by dry heating at 60 °C for 1 hour. It was then impregnated with concentrated extracts to obtain approximately 20 µg/disc. Prior to adherence on the culture plates, the discs were allowed to dry at 42 °C in incubator. The bacterial suspension from trypticase soy broth was streak evenly onto the surface of the trypticase soy agar plate with sterile cotton swab. After the inoculums had dried (5 min), the dried discs were placed on the agar with flamed forceps and gently pressed down to ensure proper contact. One disc, impregnated individually with solvent was placed along the test disc for control and comparing purpose. The plates were incubated immediately or within 30 min after inoculation. After overnight incubation at 37 °C, the zones of inhibition diameter including 6 mm discs were measured (Finegold *et al.*,1978).

Determination of Minimum Inhibitory Concentration (MIC) of the Isolated Compounds by Microplate Dilution Method

The sample was first screened at a concentration of 100 µg mL^{-1}. For every experiment, a sterility check was done on broth medium and the extract.

For the determination of minimum inhibitory concentration (MIC) values of the tested sample. Prior to the performing of MIC, the 100 µmL of trypticase soy broth was first introduced in 96 wells. Then 100 µmL of sample was introduced into the first well to obtain 200 µg mL^{-1}. By using multi-channel pipetter (8-channels) and Titertek micro-titration equipment, 100 µmL of the mixture was used for downstream serial dilutions up to 12 consecutive wells, each already containing 100 µmL of media. The last 100 µmL was discarded.

While transferring the content of each well, the mixture was mixed thoroughly with a multi-channel pipetter. Then 20 µmL of the already prepared inoculum was introduced to its respective wells and the microplates were incubated at 37 °C for overnight. The last well with no growth of the microorganism was taken to represent the MIC of the isolated compounds.

The MIC values of the two isolated compounds were tested with 3 species of *S. aureus*, 2 species of *E. coli*, one strain *P. morganii*, one strain *B. subtilis* and one strain *V. cholerae* by using microplate dilution method.

Results and Discussion

Identification of Isolated Compound A from Aqueous Extract of *A. concinna* Leaves

The compound A was isolated from the 70 % EtOH extract of the leaves of *A. concinna*, after successively removing the petroleum ether and ethyl acetate soluble parts of the extract, that is, it comes from the remaining very polar part of the extract; in fact, compound A was eluted from the silica gel column with the polar solvent system of EtOH-ammonia-water (80:5:15), indicating that it must be a very polar compound. On TLC plate, it is invisible under UV 254 or 365 nm lights, but it is detectable as a brown spot by heating after dipping the plate in Schwepps reagent; these observations suggests an organic acid containing no system of conjugated double bonds.

The UV spectrum (Figure 2) of compound A also shows no absorptions between 200 and 400 nm range given by conjugated systems, in agreement with the above observation on TLC plate. In the FT IR spectrum (Figure 3) of compound A, the strong broad O-H stretching band at 3600-2700 cm^{-1}, which is characteristic of a carboxylic acid, and the strong C=O stretching band at 1732 cm^{-1} can be observed.

Concerning the ^{1}H NMR (Figure 4, Table 1) and ^{13}C NMR (Figure 5, Table 2) spectra of compound A, one is inclined at first sight to dismiss it as nothing significant, since the spectra were so simple with only one or two signals. However, the carbon signal at δ 174.88 is in accord with the carbonyl group of a carboxylic acid, a fact already seen in FT IR spectrum above. The only other signals observed in ^{13}C NMR are the two oxygenated sp^3 carbons at δ 73.88 and δ 73.50 ppm; and the corresponding proton on such carbon appears in ^{1}H NMR spectrum at δ 4.51 ppm, the only observed proton signal for compound A.

At this point, it may thus be supposed that there are two CHO and one COOH groups in compound A, totaling to 103 mass units; there seems to be only 3 carbons. Now, the peaks at m/z 149.0 (98 %) and 299.0 (53 %) in the ESI MS (Figure 6, Table 3) of compound A suggest, respectively, M-H and 2M-H peaks, with M having 150 mass units. Thus there remains 150 - 103 = 47 mass units. From the m/z 150(4.5 %) in mass spectrum, the maximum possible number of carbons is (4.5/98)x100/1.1= 4.2, i.e., 4. Therefore the isolated compound A can be deduced as meso tartaric acid.

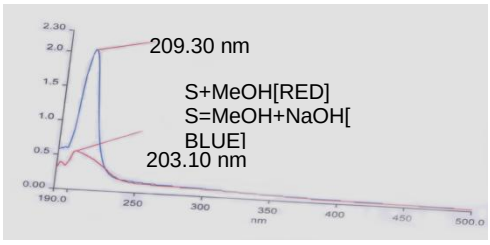

Figure 2 UV spectrum of compound A

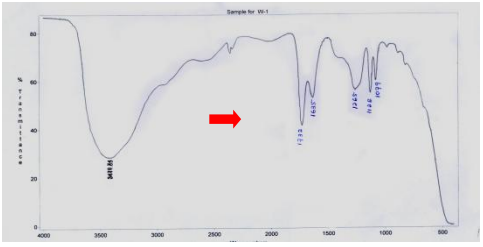

Figure 3 FT IR spectrum of compound A

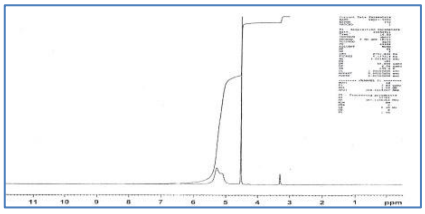

Figure 4 ^{1}H NMR spectrum of compound A

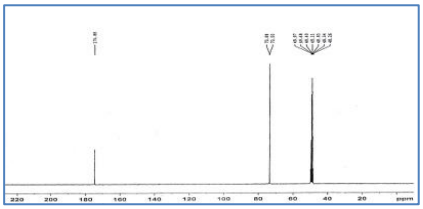

Figure 5 ^{13}C NMR spectrum of compound A

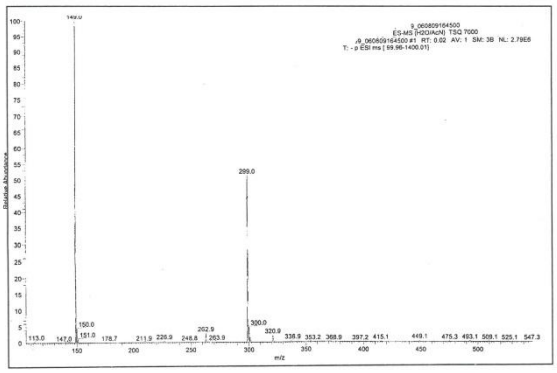

Figure 6 ESI MS spectrum of compound A

Table 1 ^{1}H NMR (300 MHz, MeOH-d_6) Spectral Data of Compound A

Chemical shift (δ)	Number of protons	Multiplicity	Structural unit
4.51	2	Singlet	HOOC(OH)C**H**-C**H**(OH)COOH

Table 2 ^{13}C NMR (150 MHz, MeOH-d_6) Spectral Data of Compound A

Chemical shift (δ)	Number of carbons	Structural unit
174.88	2	-**C**OOH, two numbers
73.88	1	-**C**H(OH)COOH, one number
73.50	1	-**C**H(OH)COOH, one number

Table 3 ESI-MS Spectral Data of Compound A

m/z	Relative abundance (%)	Remarks
149.0	98	$(M-H)^-$
150.0	4.5	$(M-H+1)^-$
299.0	53	$(2M-H)^-$

Identification of Isolated Compound B from EtOAc Extract of *A. concinna* Leaves

Compound B was isolated from the fraction 3 of ethyl acetate extract after rechromatographed on silica gel G 60 using $ClCH_2CH_2Cl$: MeOH (93:7). It gave a brown colour spot on TLC after spraying and heating with 5% H_2SO_4. Its melting point is 57 °C. The maximum absorption spectrum of UV (Figure 7) showed at 207 nm in MeOH and at 195 nm in MeOH and 2 drops 2 N NaOH.

The IR spectrum (Figure 8) showed a broad absorption band at 3500-3000 cm^{-1} due to OH- stretching vibration of carboxylic acid group. The strong absorption bands due to the CH stretching vibration of $–CH_2$ and $–CH_3$ group showed at 2919 cm^{-1} and 2852 cm^{-1}. The absorption band at 1709 cm^{-1} was assigned as carbonyl group.

The ^{1}H NMR spectrum ($CDCl_3$) (Figure 10) showed signals assignable to a saturated fatty acid at δ 2.35 (H –2), 1.64 (H –3), 1.30 (10 CH_2, H –4-13) and 0.90 (H –14)ppm (Table 4). The integration ratio of proton signals suggested the presence of 27 protons. The proton signals of compound B are also similar with that of myristic acid obtained from ACD labs (Figure 9). Therefore, according to above-stated spectral data, it was found to be myristic acid.

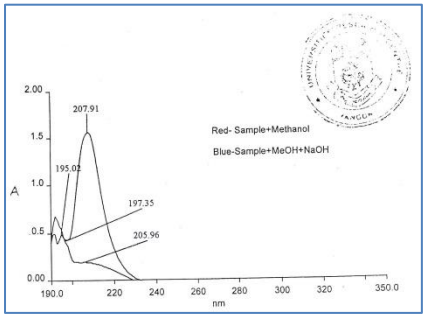

Figure 7 UV spectrum of compound B

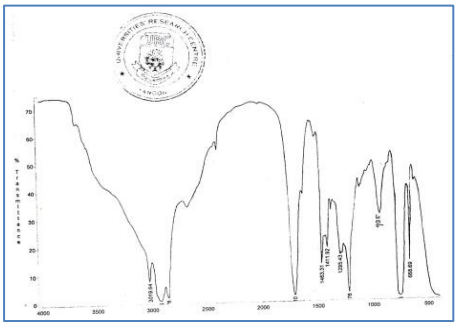

Figure 8 FT IR spectrum of compound B

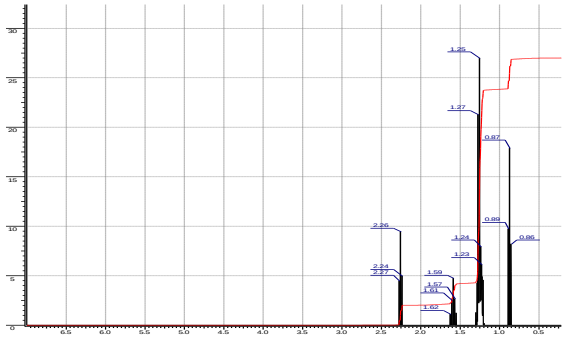

Figure 9 ^{1}H NMR spectrum of myristic acid predicted by ACD Labs software

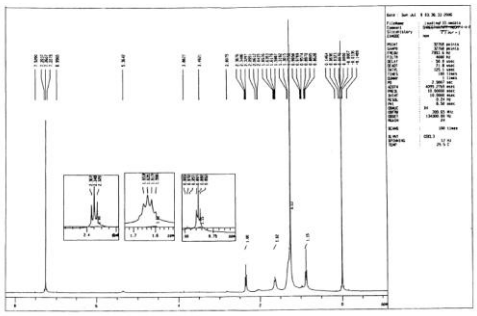

Figure 10 ^{1}H NMR spectrum of compound B

Table 4 ^{1}H NMR (300 MHz, $CDCl_3$) Spectral Data of the Isolated Compound B

Atom	δ /ppm	Integration	Assignment
H-2	2.35	2 H	- CH_2 (methylene)
H-3	1.64	2 H	- CH_2 (methylene)
H-(4-13)	1.30	20 H	- CH_2 (methylene)
H – 14	0.90	3 H	- CH_3 (methyl)

***In vitro* Screening of Antibacterial Activity of Different Crude Extracts from *A. concinna* Leaves**

The inhibition zone diameters for different crude extracts of *A. concinna* leaves are illustrated in Table 5. It can be obviously seen that PE extract (inhibition zone diameters ranged 0 mm), EtOAc extract (inhibition zone diameters ranged between14 mm - 23 mm), EtOH extract (inhibition zone diameters ranged between 15 mm - 25 mm) and H_2O crude extract (inhibition zone diameters ranged between 16 mm - 24 mm) exhibited the antibacterial activity against 3 species of *Staphylococcus aureus*, 2 species of *Escherichia coli*, one species of *Bacillus subtilis*, one species of *Proteus morganii* and one species of *Vibrio cholerae*. It was observed that pet-ether extracts of *A. concinna*

leaves did not show any antibacterial activity against all organisms tested. Therefore, EtOAc, EtOH and H_2O crude extracts of *A. concinna* leaves can be considered to be biologically active.

Table 5 Antibacterial Activities of Different Crude Extracts of *A. concinna* leaves on Different Species of Bacteria by Agar Disc Diffusion Method

No.	Type of Bacteria	Inhibition Zone Diameter (mm)			
		I	II	III	IV
1.	*Staphylococcus aureus* ws	-	23	25	24
2.	*Staphylococcus aureus* ns	-	18	18	20
3.	*Staphylococcus aureus* w sepsi	-	18	18	20
4.	*Escherichia coli* (STLT)	-	17	15	20
5.	*Escherichia coli* (ATCC)	-	17	15	16
6.	*Bacillus subtilis*	-	18	16	20
7.	*Proteus morganii*	-	14	16	18
8.	*Vibrio cholerae*	-	16	16	18

I = PE extract of *A. concinna* leaves
II = EtOAc extract of *A. concinna* leaves
III = EtOH extract of *A. concinna* leaves
IV = H_2O extract of *A. concinna* leaves

Determination of Minimum Inhibitory Concentration (MIC) of Isolated Compounds by Microplate Dilution Method

The MIC value of isolated compound A and B were determined by microplate dilution method with optical density and growth a nutrient agar (Figure 11). Three species each of *S. aureus* ws, two species each of *E. coli*, one strain *P. morganii*, one strain *B. subtilis* and one strain *V. cholerae*. The MIC values of isolated compound A and B were determined by micro plate reader at the wavelength 490 nm are shown in Table 6, Figure 12(a) and Table 7, Figure 12(b). It was found that the lowest MIC values of isolated compound A and B were respectively found to be 0.0058 mg mL^{-1} and 0.0937 mg mL^{-1} against with *S. aureus* ws.

Compound A Compound B

Figure 11 Photograph showing falcon 3072 sterile pack containing 96 wells used for the determination of MIC values of compound A and B isolated from *A. concinna* leaves by microplate dilution method

Table 6 Optical Density and Various Concentrations of Compound A from *A. concinna* (Kin-mun-gyin) on *P. morganii,* 2 species of *E.coli,* 3 species of *S. aureus, V. cholerae* and *B. subtilis* by Microplate Reader measured at the wavelength 490 nm

Concentration (mg mL^{-1})	Optical Density							
	A	B	C	D	E	F	G	H
3.0000	0.119	0.111	0.130	0.095	0.118	0.127	0.110	0.078
1.5000	0.091	0.105	0.103	0.107	0.095	0.097	0.092	0.090
0.7500	0.225	0.214	0.099	0.224	0.157	0.183	0.254	0.173
0.3750	0.235	0.220	0.090	0.220	0.169	0.263	0.159	0.198
0.1875	0.203	0.218	0.071	0.202	0.144	0.194	0.287	0.195
0.0937	0.239	0.187	0.068	0.239	0.174	0.153	0.143	0.203
0.0468	0.182	0.187	0.059	0.227	0.157	0.259	0.180	0.189
0.0234	0.222	0.186	0.102	0.204	0.120	0.133	0.261	0.185
0.0117	0.196	0.158	0.045	0.181	0.112	0.131	0.183	0.228
0.0058	0.212	0.145	0.300	0.159	0.125	0.165	0.245	0.209
0.0029	0.278	0.208	0.048	0.181	0.146	0.290	0.246	0.225
0.0014	0.031	0.043	0.027	0.018	0.039	0.060	0.101	0.061

Table 7 Optical Density and Various Concentrations of Compound B from *A. concinna* (Kin-mun-gyin) on *P. morganii,* 2 species of *E. coli,* 3 species of *S. aureus, V. cholerae* and *B. subtilis* by Microplate Reader measured at the wavelength 490 nm

concentration (mg mL^{-1})	Optical Density							
	A	B	C	D	E	F	G	H
3.0000	0.291	0.253	0.113	0.207	0.226	0.139	0.136	0.214
1.5000	0.268	0.258	0.105	0.303	0.233	0.348	0.164	0.195
0.7500	0.258	0.229	0.091	0.312	0.231	0.375	0.194	0.231
0.3750	0.291	0.260	0.089	0.271	0.212	0.206	0.189	0.202
0.1875	0.299	0.208	0.102	0.256	0.213	0.170	0.193	0.208
0.0937	0.271	0.252	0.066	0.226	0.254	0.117	0.185	0.215
0.0468	0.241	0.193	0.061	0.226	0.179	0.316	0.187	0.203
0.0234	0.235	0.178	0.059	0.208	0.186	0.295	0.181	0.187
0.0117	0.307	0.157	0.072	0.196	0.160	0.322	0.164	0.213
0.0058	0.210	0.179	0.090	0.204	0.203	0.120	0.150	0.222
0.0029	0.268	0.243	0.160	0.212	0.195	0.171	0.184	0.181
0.0014	0.025	0.030	0.008	0.029	0.060	0.039	0.021	0.025

A = *Proteus morganii*
B = *Escherichia coli* (STLT)
C = *Staphylococcus aureus* ws
D = *Escherichia coli* (ATCC)
E = *Vibrio cholerae*
F = *Staphylococcus aureus* w sepsi
G = *Staphylococcus aureus* ns
H = *Bacillus subtilis*

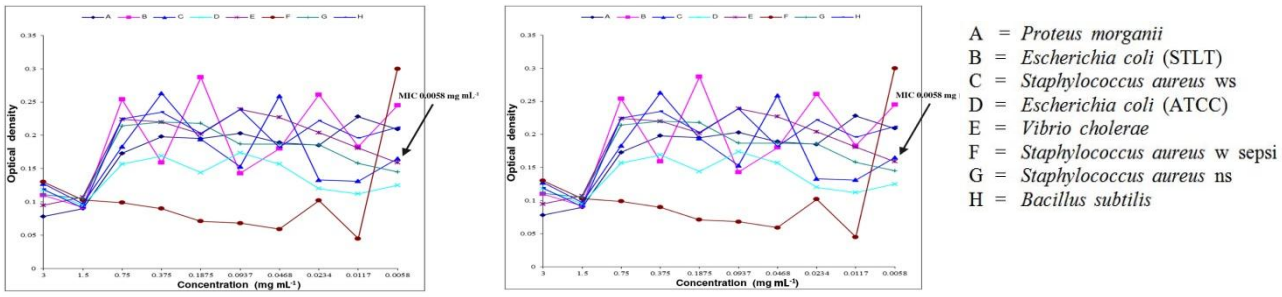

(a) (b)

Staphyloccoccus aureus ws
MIC value of compound A 0.0058 mg mL^{-1}

Staphyloccoccus aureus ws
MIC value of compound B 0.0937 mg mL^{-1}

Figure 12 Plots showing variation of optical density with concentration of (a) compound A and (b) compound B for each of the eight tested bacterial strains in the determination of the MIC values by microplate dilution method

Conclusion

The following inferences could be deduced from the overall assessment of the chemical investigation on the leaves of *A. concinna* DC .(Kin-mun-gyin). On silica gel column chromatographic separation, two compounds were isolated from aqueous and ethyl acetate crude extracts of the *A. concinna* leaves. The compounds isolated from the aqueous and ethyl acetate extracts from *A.concinna* leaves were identified to be (one dicarboxylic acid, meso-tartaric acid) (m.pt. 140 ºC, 0.007 %) and (one saturated fatty acid, myristic acid) (m.pt 57 ºC, 0.006 %). The isolated compound A and B were characterized by some physical and chemical properties and structurally identified by the combination of UV, FT IR, ^{1}H NMR , ^{13}C NMR and ESI MS spectroscopic methods and also by comparing with the reported data.

The antibacterial activity of crude extracts (PE, EtOAc, EtOH and H_2O) of *A. concinna* leaves was screened by using agar disc diffusion method on eight bacterial strains including 3 species of *S. aureus*, 2 species of *E. coli*, one *B. subtilis*, one *P. morganii* and one *V. cholerae*. Except PE extracts, all of the crude extracts were found to exhibit antibacterial activity against the organisms tested.

The lowest MIC values of isolated compound A (meso tartaric acid) and compound B (myristic acid) isolated from *A. concinna* leaves determined against *S.aureus* ws by micro plate dilution method were respectively found to be 0.0058 mg mL^{-1} and 0.0937 mg mL^{-1}.

In conclusion , it was found that crude extracts (EtOH, EtOAc and H_2O) of *A. concinna* leaves can be effective in the formulation of medicine for the treatment of diseases such as diarrhoea, fever, inflammation, laxative and boils.

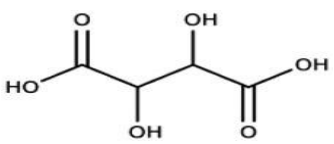

meso-tartaric acid

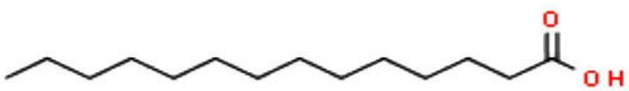

myristic acid

Acknowledgements

The authors would like to thank the Myanmar Academy of Art and Science for allowing to present this paper and Professor and Head Dr Kyae Mon Lwin, Department of Chemistry, Kyaukse University for her kind encouragement.

References

Dastur, J. F. (1962). *Useful Plants of India and Pakistan*, Bombay: D. B. Taraporevala Sons Co. Ltd., 7th Edn., p .6

Evans, W.C. (2002). *Trease and Evans Pharmacognosy*, Toronto: 15th Edn., p .26

Finegold, S.M., Martin, W.J. and Scott, E.G. (1978). *Diagnostic Microbiology*, London: The C.V. Mosby Co.Ltd., pp . 304-305

Kress, K. J., De Fillipps. R. A., Farr, E. and Daw Yin Yin Kyi. (2003). *A Checklist of the Trees, Shrubs, Herbs, and Climbers of Myanmar.* Washington D. C: Department of Systematic Biology-Botany National Museum of National History, p. 243

Mar Mar Nyein, Chit Maung, Mya Bwin and Tha, S. J. (1991). "*in vitro* Testing of Various Indigenous Plant Extracts on Human Pathogenic Bacteria." *Myanmar Health. Sci. Res. J*., vol. 3, pp. 89-99

KINETIC STUDIES OF α -AMYLASE FROM IMMATURE SEEDS OF *PHASEOLUS VULGARIS* L.

Latt Latt Chaw[1], Ni Ni Sein[2] , Thida Win[3]

Abstract

α-Amylases (1,4-α-D-glucan-glucanohydrolase EC 3.2.1.1) are found in human, several bacteria, yeast, fungi and seeds. This paper deals with the extraction of α-amylase from developing seeds of white kidney bean and studies on its kinetic properties. α-Amylase was extracted from immature white kidney bean (*Phaseolus vulgaris* L.) seeds by ammonium sulphate fractionation (20-60 %) and purified by gel filtration chromatography. The specific activity of purified α-amylase was 1.20 unit per mg of protein. The purity of enzyme was confirmed by non SDS-PAGE as a single band. The molecular weight of purified α-amylase was determined as 56.23 kDa. The optimum temperature and optimum pH for the α-amylase were 50˚C and 5.6, respectively. Kinetic parameters such as Michaelis-Menten constant K_m and maximum velocity V_{max} were 0.1267 $x10^{-2}$ g mL^{-1} and 1.64 $x10^{-5}$ M min^{-1} determined from a double reciprocal plot. K_m and V_{max}values determined by other plots were also found to be comparable.

Keywords : α-amylase, white kidney bean seed, *Phaseolus vulgaris* L.,ammonium sulphate fractionation, gel filtration chromatography

Introduction

α-Amylases (E.C.3.2.1.1.) (endo-1,4-α-D-glucanglucanohydrolase), are extracellular enzymes that randomly cleave the 1,4-α-D-glucosidic linkages between adjacent glucose units inside the linear amylose chain (Irfan, 2012). This enzyme is employed in the starch processing industries for the hydrolysis of polysaccharides such as starch into simple sugar constituents (Adu *et al*., 2005). α-Amylases are extensively used in food, textiles and pharma industries (Nerkar *et al*., 2011). α-Amylases are wide spread in nature, being found in animals, microorganisms and plants (Franco *et al.*, 2000). Commercially α-amylases are produced mostly from fungal sources, but they are also being extracted from different plant sources like barely, millets, wheat, sorghum, and maize. Immature white kidney bean seeds were chosen for the present study because of its wide distribution in Myanmar as a vegetable available throughout all the year.

The white kidney bean (*Phaseolus vulgaris* L.) is a warm season annual plant. The flowers vary in colour from white to purple. The seeds are rich in protein. White kidney beans are extensively cultivated in all parts of Myanmar.

The aim of the present study was to isolate α-amylase from immature seeds of white kidney bean and to study its kinetic properties.

Materials and Methods

Sample collection

Immature white kidney bean (*Phaseolus vulgaris* L.) seeds were collected from Sint Kaing Township, Mandalay Region.

[1] Dr, Lecturer , Department of Chemistry, Kyaukse University
[2] Dr ,Professor (Retired), Department of Chemistry, University of Yangon
[3] Dr, Rector, University of Mandalay

Extraction of α-Amylase from Immature White Kidney Bean Seeds

Immature white kidney bean seeds (200 g) were ground in a mortar to obtain a homogeneous mixture. It was then dissolved in 500 mL of 0.1 M acetate buffer (pH 5.6) and stirred for 30 min. The suspension was then centrifuged at 3000 rpm for 15 min to obtain crude enzyme extract. The crude α- amylase enzyme extract was first brought to 20 % saturation with solid ammonium sulphate (analar). After centrifugation for 15 min at 3000 rpm the supernatant was applied again with solid ammonium sulphate to achieve 60 % saturation. The resulting enzyme precipitate was collected by centrifugation at 3000 rpm for 15 min. The protein pellet dissolved in phosphate buffer (pH 5.6) and then it was then dialyzed against same buffer at 4 °C.

The partially purified α-amylase was dissolved in 0.1 M acetate buffer (pH 5.6). This solution was applied to a Sephadex G-100 gel filtration column (2.5×27 cm) previously equilibrated with the same buffer. The flow rate was adjusted to 12 mL/h by a mini pump and 1.5 mL fractions were collected per tube using a fraction collector. After collection, the protein content of each tube was checked by measuring the absorbance at 280 nm wavelength using a UV-visible spectrophotometer. Each tube was also measured from α-amylase enzyme activity by Nelson-Somogyi method (Nelson and Somogyi, 1973). The fractions that had the highest activity of α-amylase enzyme (fraction numbers 10-21, 34-38 and 41-47) were pooled and concentrated with acetone (1:9).

The protein content and α-amylase activity of enzyme solution in each purification step were analyzed by the Biuret method (Chykin, 1966) and Nelson-Somogyi method respectively.

The sample thus obtained was subjected to polyacrylamide gel electrophoresis using high molecular weight marker protein (calibration kit) from Pharmacia.

Determination of Optimum pH of α-Amylase-Catalysed Reaction

The effect of pH on activity of purified α-amylase, buffer solution from pH range of 1.0 to 10.7 were prepared by using hydrochloric acid-sodium chloride buffers (pH 1.6 and 2.2), acetate buffers (pH 3.6, 4.6, and 5.6), phosphate buffers (pH 6.2, 7.0, and 8.0) and sodium carbonate-bicarbonate buffers (pH 9.6 and 10.7). The catalytic activity of the enzymes in the above buffers was determined with starch as substrate and the assay was carried out for each buffer solution with an incubation period of 10 minutes.

A 0.1 mL of pH 1 hydrochloric acid-sodium chloride buffer solution was added into a test tube containing 0.1 mL of starch solution (2 %). Then, 0.1 mL of prepared enzyme solution was added and the contents were mixed well. After 10 min, the reaction was interrupted by adding 1 mL of alkaline copper reagent solution. The contents were then mixed thoroughly. The test tube was heated on a vigorously boiling water bath for 10 min. Next the test tube was cooled under running tap water for 1 min and 1 mL of arsenomolybdate colour reagent solution was added into the test tube. After shaking vigorouslythis solution was diluted to 10 mL with distilled water and mixed by inversion. The absorbance was measured at 750 nm. For blank solution, 0.1 mL of distilled water was used instead of 0.1 mL of prepared enzyme solution.

The whole of the above procedure was repeated with the other buffers solutions with different pH values.

Determination of Optimum Temperature of α-Amylase-Catalysed Reaction

For determination of optimum temperature for activity of the enzyme, the assay was carried out as the procedure mentioned above with the incubation temperature of 20 ^{o}C to 75 ^{o}C at pH 5.6 with an incubation period of 10 min.

Effect of Substrate Concentration on α-Amylase–Catalyzed Reaction

The enzymatic activity, was measured at different concentrations of starch (0.125 %, 0.25 %, 0.5 %, 1.0 %, 1.25 %, 1.50 %, 2.0 %, 2.5 % and 3.0 %). Then assay was carried out as mentioned earlier, with the incubation temperature of 50 ^{o}C at pH 5.6 with an incubation period of 10 min.

Results and Discussion

Purification of α-Amylase

In this study α - amylase was isolated from immature white kidney bean seeds by ammonium sulphate precipitation method followed by Sephadex G-100 gel filtration chromatography (Figure 1). α-Amylase activities, protein contents and specific activities of the enzyme solutions in each purification step are shown in

Table 1. The crude extract having specific activity of 0.10 was subjected to ammonium sulphate precipitation and resulted in specific activity of 1.20 μmol min^{-1} mL^{-1} mg^{-1} at the final purification step. So, 12.0 fold purification was achieved by purified α- amylase in this study.

Molecular Weight of α- Amylase

In this study protein from the pharmacia high molecular weight (HMW) calibration Kit: urease tetramer (480,000), urease dimer (240,000), albumin, bovine dimer (132,000) and albumin, chicken egg (45,000) were used for molecular weight determination. The homogeneity of the purified α-amylase was confirmed by a single band (Figure 2) using polyacrylamide gel electrophoresis. The molecular weight of a protein under investigation was determined by comparing its electrophoretic mobility with that of protein standards of known molecular weights (Table 2 and Figure 3). In the present study, R_f of α-amylase was found to be 0.75. Thus, the molecular weight was determined to be 56.23 kDa.

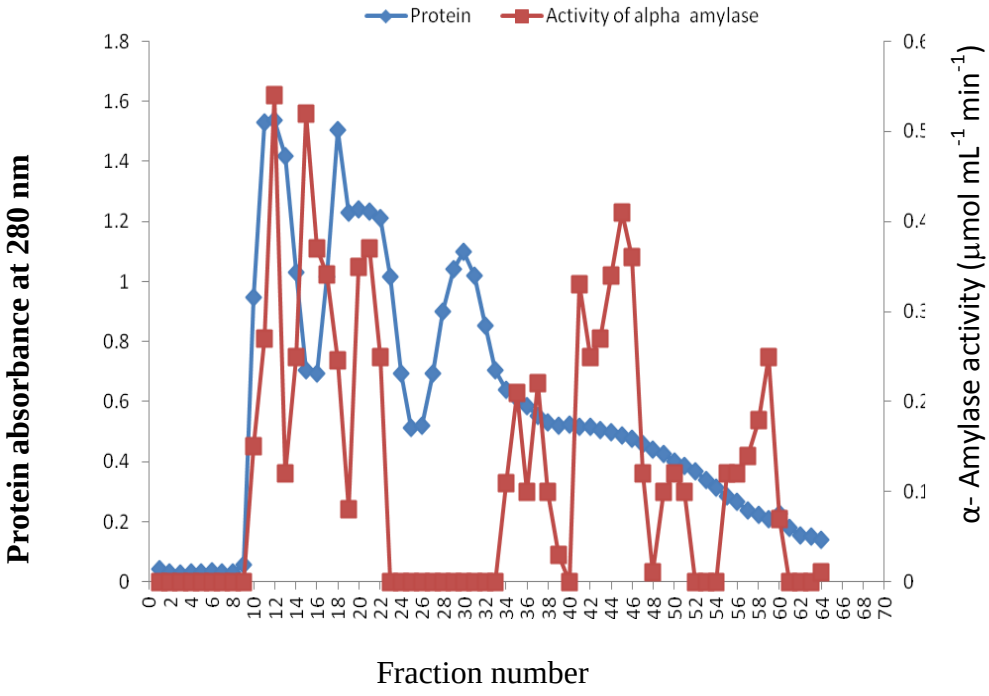

Figure 1 Chromatogram of α-amylase activity on Sephadex G-100

Table 1 Enzyme Activity and Specific Activity at Different Purification Steps

Purification steps	Total activity (µmol min^{-1})	Total protein (mg)	Specific activity (µmol min^{-1} mg^{-1})	Purification (fold)
Crude extract	781.2	7937.6	*0.10*	1
After 20 % ammonim sulphate precipitation	778.5	2412.0	0.32	3.2
After 60 % ammonium sulphate *precipitation*	149.5	243.3	0.61	6.1
Sephadex G-100	204.4	171	1.20	12.0

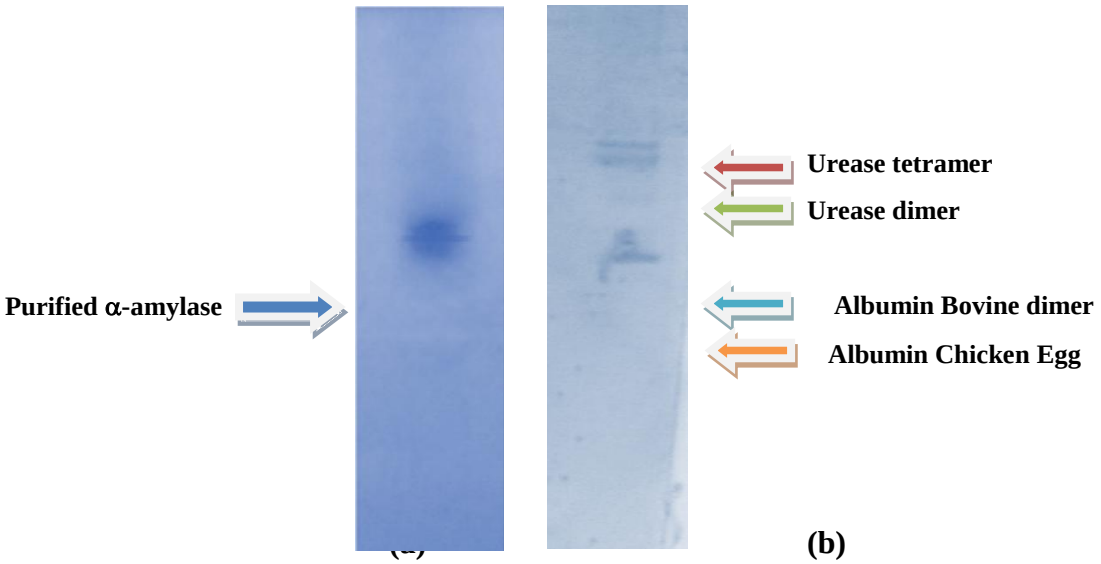

Figure 2 Photograph of polyacrylamide gel electrophoresis
Lane (a) Purified α-amylase
Lane (b) Standard marker proteins

Table 2 Relationship between Molecular Weight of Standard Protein Markers and Relative Mobility (R_f) Values

No.	Standard protein markers	Molecular weight (Dalton)	Log molecular weight	R_f
1	Urease tetramer	480,000	5.681	0.486
2	Urease dimer	240,000	5.380	0.527
3	Albumin, bovine dimer	132,000	5.121	0.625
4	Albumin, chicken egg	45,000	4.653	0.752

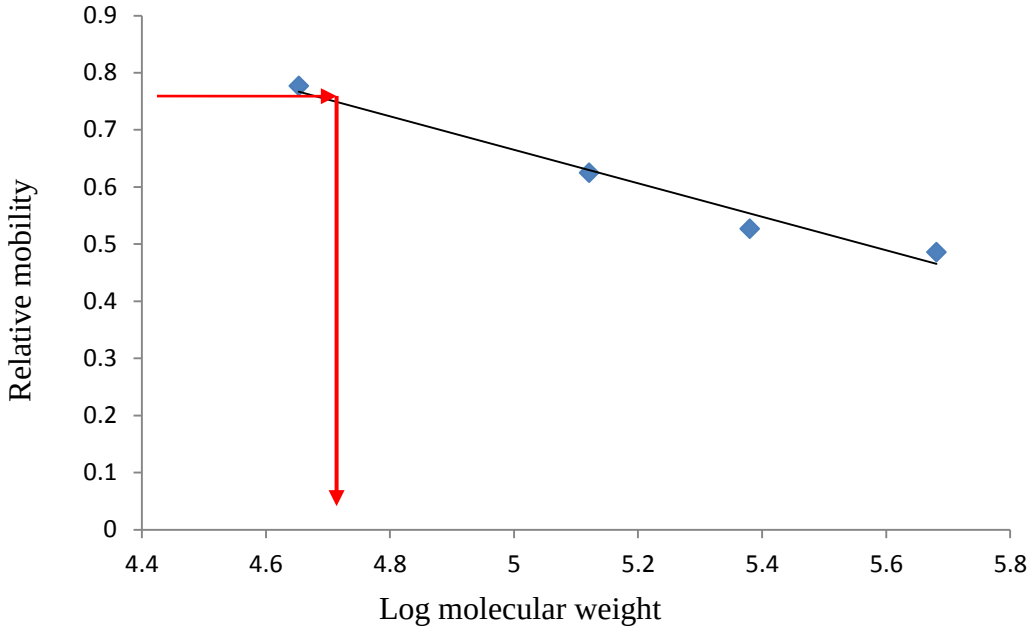

Figure 3 Log molecular weight of standard protein markers as a function of R_f values

Optimum pH of α-Amylase– Catalyzed Reaction

The effect of pH on the activity of immature white kidney bean α-amylase is shown in Figure 4. The enzyme activity increased steadily from pH 1 to 5.6 and then decreased with increasing pH. A decline in the enzyme activity was recorded on either side of pH 5.6. Enzyme showed the optimum activity at pH 5.6. It was reported that optimum pH of mango α- amylase was 5.5 (Yasin and Chaudhary, 1981). The optimum pH of α- amylase from *Phaseolus aconitifolius* was 7.0 (Chavan and Wadatkar, 2014). Khoo *et al*., (1994) reported that the α-amylase enzyme was found to have maximum activity at pH 6.0.

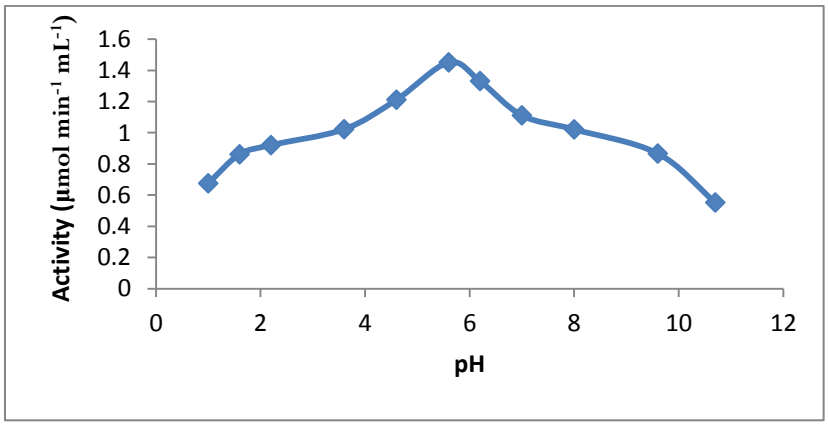

Figure 4 Plot of α–amylase activity as a function of pH of the solution

Optimum Temperature of α-Amylase– Catalyzed Reaction

Figure 5 shows the effect of temperature on the activity of immature white kidney bean α-amylase. Initially the activity increased with increase in temperature and then decreased after reaching a maximum at 50 ˚C. Mohamed *et al.*, (2009) reported that the optimum temperature for partially purified α-amylase from Wheat *Triticum aestivum* was 50 ˚C. Khoo *et al*., (1994)

reported that the optimum temperature for purified α-amylase was 55 ˚C. Plant amylases (Wheat alpha -1, Pearl millet alpha-1, and Safflower seeds) were found to have optimum temperature of 55 ^{o}C (Nerkar *et al*., 2011).

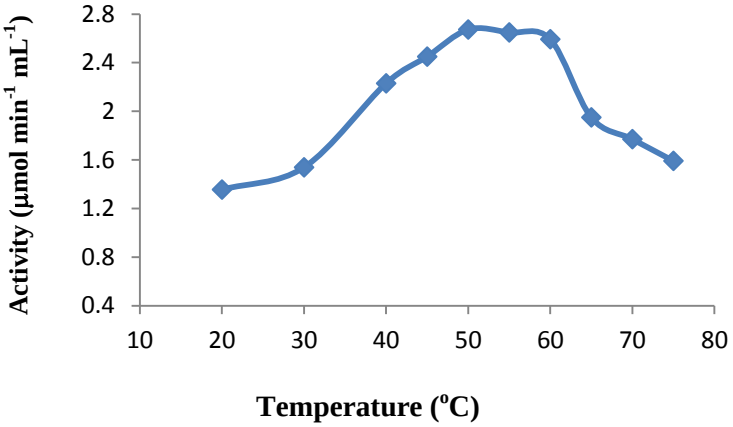

Figure 5 Plot of α–amylase activity as a function of temperature of the solution

Effect of Substrate Concentration

The effect of varying substrate on initial velocity of an enzyme catalyzed reaction is shown in Table 3 and Michaelis-Menten Plot (Figure 6). At relatively low starch concentration, initial velocity increased almost linearly with an increase in concentration of starch. In this region of the curve the reaction followed first order kinetics. At higher starch concentration, initial velocity increased by smaller and smaller extent in response to increase in concentration of starch. In this region of the curve, the reaction was mixed order type. Finally a point was reached beyond which there small was increased in the velocity with increased in the concentration of the starch. The reaction followed zero order kinetics in this region. At this stage, amylase was fully saturated with starch molecules. The immature white kidney bean α - amylase activity reached the maximum with an optimum substrate (starch) concentration of 2×10^{-2} g mL^{-1}. Kuiper *et al*. (1978) reported that the maximum activity of α-amylase enzyme was obtained at 1.67×10^{-2} g mL^{-1} of substrate (starch) concentrations.

Table 3 Relationship between Initial Starch Concentration and Velocity of α-Amylase Catalyzed Reaction

[S]×10^2 (g mL^{-1})	**-[S]×10^2 (g mL^{-1})**	**$\frac{1}{[S]}\times10^{-2}$ (g^{-1} mL)**	**v ×10^5 (M min^{-1})**	**$\frac{1}{v}\times10^{-5}$ (M^{-1}min)**	**$\frac{v}{[S]}\times10^{3}$ (M min^{-1} g^{-1} mL)**	**$\frac{[S]}{v}\times10^{-3}$ (g mL^{-1} M^{-1}min)**
0.1250	-0.1250	8.0000	0.8159	1.2256	6.5272	0.1523
0.2500	-0.2500	4.0000	1.0957	0.9127	4.3828	0.2282
0.5000	-0.5000	2.0000	1.2876	0.7766	2.5752	0.3883
1.0000	-1.0000	1.0000	1.4232	0.7026	1.4232	0.7026
1.2500	-1.2500	0.8000	1.4982	0.6675	1.1986	0.8343
1.5000	-1.5000	0.6667	1.5235	0.6564	1.0157	0.9846
2.0000	-2.0000	0.5000	1.5710	0.6365	0.7855	1.2731
2.5000	-2.5000	0.4000	1.5719	0.6362	0.6288	1.5904
3.0000	-3.0000	0.3333	1.5739	0.6354	0.5246	1.9061

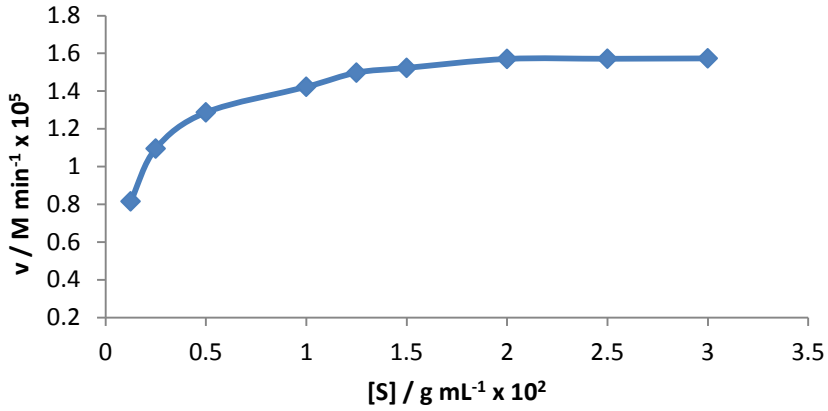

Figure 6 Michaelis-Menten plot used for graphic evaluation of V_{max} and K_m

Kinetic Parameters K_m and V_{max}

Each enzyme has a characteristic substrate concentration (K_m, the Michaelis-Menten constant) at which the reaction velocity is one-half maximal (Sawhney and Singh, 2000). Michaelis-Menten equation, $v = \frac{V_{max}[S]}{K_m} + [S]$ explains kinetics but, because it is nonlinear, is a little hard to deal with real practical data. K_m and V_{max} were found to be 0.1167×10^{-2} g $mL^{-1}$and 1.57×10^{-5} M min^{-1}, respectively, from Michaelis-Menten plot.

Most common transform is the Lineweaver-Burk plot which is also called double reciprocal plot ($\frac{1}{v}$ vs $\frac{1}{[S]}$ plot). The reciprocal transformation distorts the error in the measurements. As shown in Figure 7, the noisiest data are too heavily weighted when linear regression is used to determine the best straight line. From this Lineweaver-Burk Plot K_m and V_{max} values were found to be 0.1276×10^{-2} g mL^{-1} and 1.642×10^{-5} M min^{-1}, respectively.

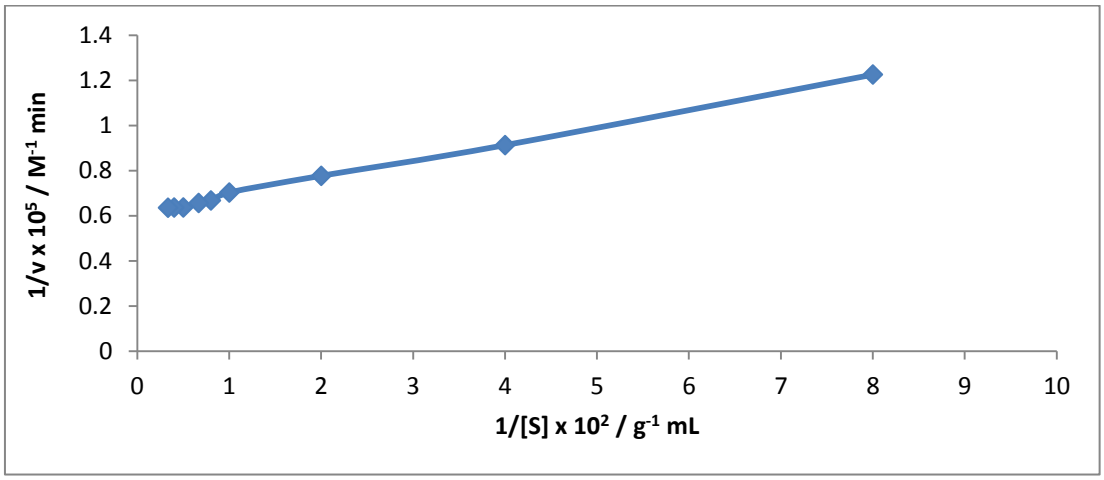

Figure7 Lineweaver-Burk plot of 1/v versus 1/[S] used for graphic evaluation of V_{max} and K_m

Figure 8 shows the Eadie-Hofstee plot of v vs $\frac{v}{[S]}$. This plot not only yields K_m and V_{max} in a very simple way but also magnifies departures from linearity which may not be apparent in a double reciprocal plot. K_m and V_{max} values obtained by this plot were 0.1276×10^{-2} g mL^{-1} and 1.643×10^{-5} M min^{-1}, respectively.

Hanes-Wilkinson plot, an alternative plot of $\frac{[S]}{v}$ vs [S] based on Hanes equation gave a straight line (Figure 9). From this plot, K_m and V_{max} values were calculated to be 0.1332×10^{-2} g mL^{-1} and 1.653×10^{-5} M min^{-1}.

Figure 10 is the direct linear plot or Eisenthal-Cornish Bowden plot. [S] values are plotted on the negative X-axis and observed v values on the Y-axis. This plot gave K_m and V_{max} values of 0.1300×10^{-2} g mL^{-1} and 1.640×10^{-5} M min^{-1}, respectively.

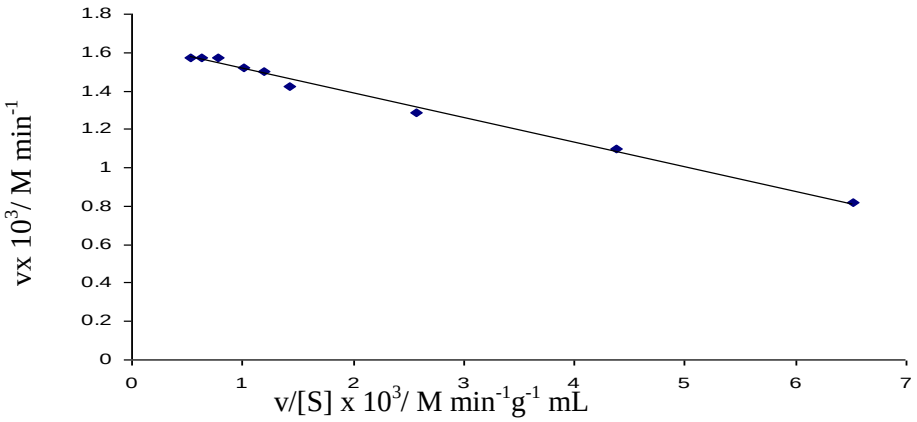

Figure 8 Eadie-Hofstee plot of v versus v/[S] used for graphic evaluation of V_{max} and K_m

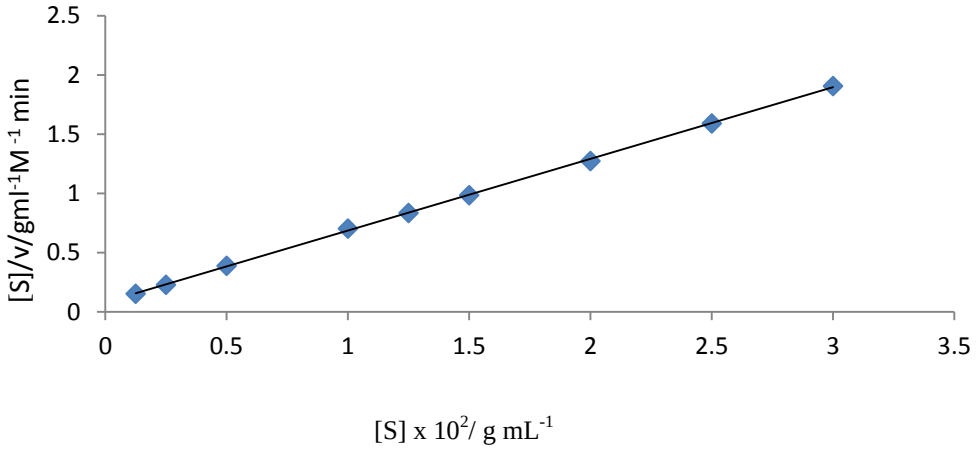

Figure 9 Hanes-Wilkinson plot of [S]/v versus [S] used for graphic evaluation of V_{max} and K_m

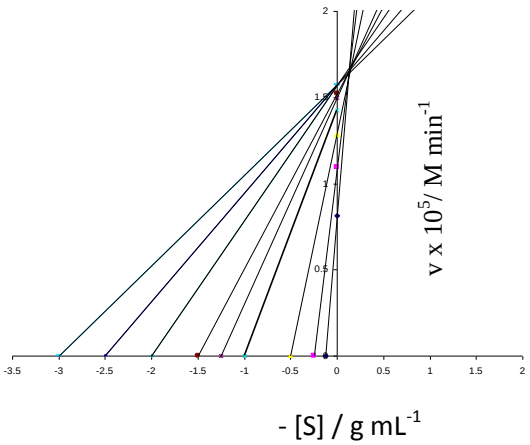

Figure 10 Eisenthal–Cornish Bowden plot of v versus –[S] used for graphic evaluation of V_{max} and K_m

K_m and V_{max} values obtained by different methods agreed with each other (Table 4). K_m value of α-amylase enzyme was reported as 2 mg mL^{-1} i.e., 0.2×10^{-2} g mL^{-1} (Kanwal *et al*., 2004). Moreover, K_m values of α - amylases from mango and *Carica papaya* were found to have same K_m value of 3.3 mg mL^{-1}, i.e., 0.33×10^{-2} g mL^{-1}(Annis, 1982).

Enzyme kinetics, K_m and V_{max} are significant coefficients in guiding scientific research and engineering design. The more firmly the enzyme binds to its substrate, the smaller will be the value of K_m. Results show good affinity of the enzyme for substrate i.e. starch. Moreover, K_m is independent of enzyme concentration and is a true characteristic of the enzyme under defined conditions of temperature, pH, etc. (Negi and Banerjee, 2009).

Table 4 Comparison of Different Methods for Reaction Kinetic Parameters of α amylase from White Kidney Bean Seeds

No.	Methods	$K_m\times10^{-2}$ (g mL^{-1})	$V_{max}\times10^{5}$ (M min^{-1})
1	Michaelis – Menten	0.1167	1.570
2	Lineweaver –Burk+	0.1276	1.642
3	Eadie – Hofstee+	0.1276	1.643
4	Hanes-Wilkinson+	0.1332	1.653
5	Eisenthal – Cornish Bowden	0.1300	1.640

+ Linear regression method

Determination of Reaction Order (n) for α- Amylase-catalyzed Reaction

The order of a chemical reaction with respect to the individual components is defined as power of the component concentration included into the rate equation. Depending on the substrate concentrations, the kinetics of an enzyme–catalyzed reaction may be described by the first–order rate equation.

The relationship between the rate of the reaction and substrate concentration has been formulated in most general terms as follows (Giese, 1973).

Rate = $K\,[S]^n$

Where, n = order of enzyme – catalyzed reaction

When the Michaelis–Menten equation is written in the form of a straight line, the Hill equation (Martin, 1993).

$\frac{\log v}{V_{max}-v} = n\log[S] - \log K_m$ is obtained. The equation states that, when [S] is low compared to K_m, the reaction velocity increases as the n^{th} power of [S].

In the present work, K_m and n values were determined from the plot of $\frac{\log v}{V_{max}-v}$ vs log [S] using the linear regression method (Table 4 and Figure 11). The reaction order (n) for α–amylase was calculated to be 1.0462 proving that the reaction order is first order.

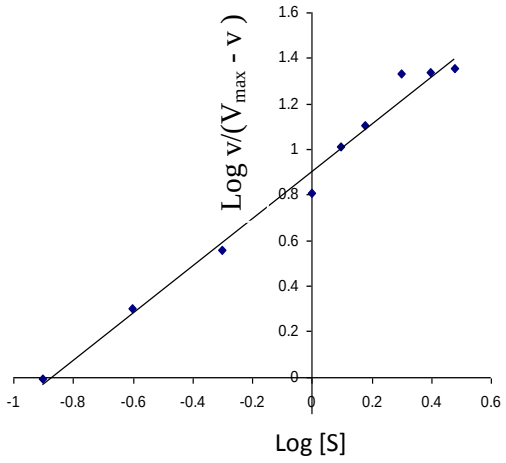

Figure 11 Plot of log $\frac{\mathbf{logv}}{\mathbf{V_{max} - v}}$ as a function of log [S] for α –amylase-catalyzed reaction

Conclusion

α-Amylase from immature white kidney bean seeds was isolated and purified by ammonium sulphate fractionation (20-60 %) followed by gel filtration chromatography and it was purified 12 fold compared to the crude extract. The molecular weight of purified α-amylase was determined as 56.23 kDa. The optimum pH of α-amylase was found to be 5.6 in acetate buffer and the optimum temperature of this enzyme was 50 ˚C. From the kinetic profile of the amylase enzyme the maximum velocity V_{max} and Michaelis-Menten constant K_m were observed to be 1.642×10^{-5} M min^{-1} and 0.1276×10^{-2} g mL^{-1} obtained by Lineweaver-Burk plot using linear regression method. For comparison purpose, K_m and V_{max} values were also evaluated from Eadie-Hofstee, Hanes-Wilkinson and Eisenthal-Cornish Bowden plots. The K_m values of α- amylase for starch by Eadie-Hofstee, Hane-Wilkinson and Eisenthal-Cornish Bowden plots were found to be comparable. The reaction order of the α- amylase catalyzed reaction was found to be 1.

Acknowledgements

The authors would like to thank the staff members of Biochemistry Research Division, Department of Medical Research (Lower Myanmar) for their provision of research facilities and invaluable cooperation.

References

Adu, E.A., Ado, S. A. and James, D. B. (2005). "Raw Starch Degrading Amylase Production by Mixed Culture of *Aspergillus niger* and *Saccharomycescerevisae* Grown on *Sorghum pomace*". *African. J. Biotechnol*., vol.4 (8), pp. 785 - 790

Annis, W., (1982). " Purification and Characterization of α – Amylase Extracted from *Carica papaya," Pakistan J. Agric. Res*.,vol. 12, pp. 34-35

Chavan,S. and Wadatkar, C.M. (2014)." Isolation, Purification and Characterisation of Alpha amylase from *Phaseolusa conitifolius*". *Journal of Advanced Drug Delivery*, vol. 1(3), pp. 114-121

Chykin, S. (1966). *Biochemistry Laboratory Techniques.* New York : John Wiley and Sons

Franco, O.L., Rigden, D.J.,Melo, F.R., Bloch , C., Silva, C. P. and Grossi de Sa, M. F. (2000). "Activity of Wheat α-Amylase Inhibitors towards Burchid α-Amylases and Structural Explanation of Observed Specificities".*Eur.J.Biochem*, vol. 267, pp. 2166-2173

Giese, A. C. (1973). *Cell Physiology*.Philadelphia: W. B. Saunders Co., pp. 378-391

Irfan,M.,Nadeem, M. and Syed, Q. (2012). "Media Optimization for Amylase Production in Solid StateFermentation of Wheat Bran by Fungal Strains".***Journal of Cell and Molecular Biology, vol.***10(1), pp. 55-64

Kanwal, B., Zia, M.A.,Yasin, M.,Rahman, K. and Sheikh, M. A. (2004). "Purification and Characterization of α–Amylase from Apple (*Maluspumila*)".*Int. J. Agri.Biol*.,vol. 6(2), pp.233-236.

Khoo,S.L., Amirul, A.A. ,Kamaruzaman, M.,Nazalan, N. and Azizan, M.N. (1994). "Purification and Characterization of α-Amylase from *Aspergillusflavus*".*Folia Microbial (Praha)*, vol. 39(5), pp. 392-398

Kuiper, J., Roels, J.A., and Zuidwedg, M.H.J. (1978). "Flow through Viscometer for Use in the Automated Determination of Hydrolytic Enzyme Activities: Applications in Protease, Amylase and Pectinase Assays", *The Netherlands Anal. Biochem.*,vol. 90, pp. 192-203

Martin, D.W. (1993). Harper's *Review of Biochemistry*. California: Lange Medical Pub, pp. 81-90

Mohamed, S. A., Al-Malki, A. L. and Kumasani, T. A. (2009). "Partial Purification and Characterization of Five α-Amylases from a Wheat Local Variety (Balady) during Germination".*Aust. J. Basic and Appl. Sci.*, vol.3 (3), pp. 1740-1748

Negi, S. and Banerjee, R. (2009). "Characterization of Amylase and Protease Produced by *Aspergillusawamori* in a Single Bioreactor".*Food Res. Intern*.,vol. 42, pp. 443-448

Nelson, N. and Somogyi, M. (1973). "A Reagent for the Copper Iodometric Determination of Very Small Amounts of Sugar".*J. Biol. Chem*., vol. 117, p. 779

Nerkar,G. S., Chaudhari, Y. A. and Khutle, N. M. (2011). "Extraction and Characterization of Alpha Amylase from *Phaseolusaconitifolius* ". *Current Pharma Research*, vol.1 (2), pp. 115-122

Sawhney, S.K. and Singh, R. (2000). *Introductory Practical Biochemistry*. New Dehli: Narosa Publishing House

Yasin, M., S. and Chaudhary, A. H. (1981). "Characterization of Amylase from Mango".*Pakistan J.Agric. Res*., vol. 2, pp. 20-23

PREPARATION OF HUMIC-CHITOSAN COMPOSITE AND ITS APPLICATION IN REMOVAL OF SULPHUR BLACK DYES FROM AQUEOUS SOLUTION

Chit Hnin Wai[1], Thè Su Nwe[2], Myint Myint Khaing[3], Min Min Yee[4]

Abstract

Humic acid(HA) is a complex molecule that exists naturally in soils, peats, oceans and fresh waters. It is an excellent natural and organic compound to provide plants and soil with a concentrated dose of essential nutrients, vitamins and trace elements. In this research, HA was extracted from the peat collected from Moeswe Village, Oattara Thiri Township, Naypyitaw, Myanmar by alkali extraction method. The yield percents of HA was found to be (6.869)%. The extracted HA was characterized by Fourier Transform Infrared Spectroscopy (FT IR). The spectroscopic analysis shows that HA contains carboxylic, phenolic and alcoholic functional groups. According to SEM image, HA possesses the voids and aggregate nature. The crystallographic information of extracted HA was investigated by XRD analysis. The nature of thermal stability of extracted HA as well as decomposition such as dehydration, liberation of volatile materials and combustion of HA were studied by Thermal Analysis. The extracted HA was composited with commercially available chitosan in three different weight ratios (1:1, 2:1 and 1:2). The composites were characterized by FT IR, XRD, SEM and TG-DTA spectroscopic methods. HA, commercially available chitosan and their composites were studied. The removal of sulphur black from aqueous solution by using humic-chitosan composite was examined. This research demonstrates that HA can be utilized as a solvent in the solving of environmental problems to some extents.

Keywords : humic acid, chitosan, composites, removal, dyes

Introduction

Humic acid is the major component of natural organic matter in soil, water and sediments, it can be obtained from any source of organic matter, among them peat and coal at different maturation degree (Skhonde, 2006; Novak, 2001). Researches involving coal for HA extraction basically aim to use this macromolecule as a soil fertilizer. However, HA has interesting surface properties, such as the presence of oxygenated functional groups, and an ability to interact with metals and metal oxides under different conditions (Skhonde, 2006). Humic molecules have great potential to be used as a dispersant in ceramic suspensions, acting similarly to the polyacrylic acids commonly used with alumina (Stevensen, 1994; Skhonde, 2006). The HA structure requires a complete characterization in order to properly evaluate its reactivity from a specific raw material, although the average properties of HA from different sources are comparable (Novak, 2001).

Peat is a light brown to black organic material, which is formed under water logged conditions from the partial decomposition of mosses and other bryophytes, sedges,

[1] Assistant Lecturer, Department of Chemistry, Kyaukse University
[2] Assistant Lecturer, Department of Chemistry, Mandalar Degree College
[3] Dr, Associate Professor, Engineering Chemistry, Technological University(Kalay)
[4] Dr, Pro-Rector, Mandalay University

grasses, shrubs, or trees (Cocozza *et al*., 2003). Significant amounts of organic carbon are stored in the form of peat.

In this research, HA was extracted from peat in Moeswe Village, Oattara Thiri Township, Naypyitaw, Myanmar by alkali extraction method. The extracted HA was used in the removal of sulphur black dye which has been widely used in textile industry, Myitnge Town, Amarapura Township, Mandalay, Myanmar.

Materials and Methods

Hydrochloric acid (HCl), sodium hydroxide (NaOH) , acetic acid (CH_3COOH), chitosan and sulphur black dyes were purchased from Able chemical company. The crude HA was extracted from the peat by alkali extraction method. All of the chemicals used were analytical reagent grade. Distilled water was used in the preparation of all experimental solution.

Extraction of Humic Acid from Peat Sample

Alkali Extraction Method

Humic acid was extracted from coal sample by using alkali extraction method (MARIA ORTIZ DE SERRA and M.SCHNITZER, 1972) extracted humic acid from dark chestnut soil by alkali extraction method. Similarly, (Saito and Seckler, 2013) extracted humic acid from an organic-mineral fertilizer. According to above alkali extraction method, humic acid was extracted from peat sample collected from the area of Moeswe Village, Oattara Thiri Township, Naypyitaw, Myanmar.

The peat sample was grounded by using mortar and pestle, and sieved to pass a 2.0 mm sieve. The sample was adjusted with 0.1 M HCl to provide a final concentration that has a ratio of 200 mL liquid /20 g dry sample. The suspension was shaken for 2 h and then supernatant was separated from the residue by decantation after allowing the solution to settle for 24 h or by low speed centrifugation. Then 0.1 M NaOH was added to give a final extractant to peat ratio of 10 : 1. The solution was shaken for 4 h. The alkaline suspension was allowed to settle overnight and the supernatant was collected by means of decantation and centrifugation. The supernatant was acidified with 6 M HCl with constant stirring to pH 1.0 for 4 h and the suspension was allowed to stand for 15 h. Humic acid was separated centrifugation as precipitate.

Characterization of the Extracted Humic Acids

FT IR analysis of the extracted humic acids

The extracted HA (0.035g) from peat was mixed with 0.346 g of potassium bromide (KBr) to give a concentration of 1% by weight. The KBr-humic acid samples were then pressed into solid disc. After the background was corrected, the pellet was measured using Perkin Elmer 1600, Fourier Transform Infrared Spectrometer (FT IR) with a scan speed of 16 scans / sec from 600-4000 cm^{-1}.

XRD analysis of the extracted humic acids

The extracted HA from peat was examined by using XRD-Diffractometer (D8 Advance, BRUKER, Germany).

SEM analysis of the extracted humic acids

The sample was examined by scanning electron microscope for a visual inspection of surface morphology at the Department of Research and Innovation (DRI), Ministry of Education, Yangon, Myanmar.

Thermal gravimetric analysis of the extracted humic acids

The extracted HA from peat was analysed by Hi-TGA 12950 Thermo Gravimetric Analyzer.

Preparation of Humic-Chitosan Composites

Chitosan (0.25 g) was dissolved in 15 mL of 10 % acetic acid solution and stirred at 80 ˚C. After dissolution of chitosan in the acetic solution, the extracted HA (0.25 g) was also added into the chitosan solution and stirred at 80 ˚C. Finally, the heterogeneous composite solution was dried at room temperature to get 1:1 humic-chitosan composite. Similarly, humic-chitosan composite (1:2) and (2:1) were prepared.

Characterization of Humic-Chitosan Composites

FT IR analysis of humic-chitosan composites

Humic-chitosan composite (0.035g) was mixed with 0.346 g of potassium bromide (KBr) to give a concentration of 1% by weight. The KBr and humic-chitosan composite samples were then pressed into solid disc. After the background was corrected, the pellet was measured using Perkin Elmer 1600, Fourier Transform Infrared Spectrometer (FT IR) with a scan speed of 16 scans/sec from 600-4000 cm^{-1}.

XRD analysis of humic-chitosan composites

Humic-chitosan composite was examined by using XRD-Diffractometer (D8 dvance, BRUKER, Germany).

SEM analysis of humic-chitosan composites

The sample was examined by scanning electron microscope for a visual inspection of surface morphology at the Department of Research and Innovation (DRI), Ministry of Education, Yangon, Myanmar.

Thermal gravimetric analysis of humic-chitosan composites

Humic-chitosan composite was analysed by Hi-TGA 12950 Thermo Gravimetric Analyzer.

Construction of Calibration of the Dye Solution

To select the maximum absorption wavelength λ_{max}, for a particular sulphur black dye (0.5625 M), a curve was plotted by determining the colour index (absorbance) of the dye solution as a function of wavelength (530 to 740 nm). The absorbance of the dye solution at different wavelengths were determined by UV spectrophotometric method. The concentration chosen was 6.2500 M. Half dilution of the stock dye solution was made by using distilled water as a diluent. In this process, the calibration curve was used to evaluate the residual colour index (absorbance).

Determination of the Removal of Dyes by Using Humic Acid and Humi-Chitosan Composites

Into a 50 mL of dye solution in 100 mL conical flask, each of the sample: humic acid (0.1 g) and humic-chitosan composite (0.1 g) was carefully added at ambient temperature (30 ± 2° C) and shaken for 15 min. Each dye solution was filtered and the clear filtrate was determined spectrophotometrically at the interval of every 15 min.

Results and Discussion

Extraction of Humic Acid from Peat

The peat sample, peat powder, the extracted HA are shown in Figures 1 (i), (ii) and (iii), respectively.

(i) Peat Sample (ii) Peat Powder (iii) Humic Acid

Figure 1 Peat sample, peat powder and humic acid

Characterization of the Extracted Humic Acids (HA)

The extracted HA was characterized by modern techniques such as FT IR, XRD, SEM and TG-DTA spectroscopic methods.

FT IR spectrum of HA from peat is shown in Figure 2. In this spectrum, the highest absorption band of the sample was at 3364 cm^{-1} due to the O-H stretching of carboxylic acids, phenols and alcohols. This broad band can also be attributed to N-H stretching of amide group. The band at 1627 cm^{-1} was due to C=O stretching of COO^{-}, ketonic C=O, aromatic C=C conjugated with COO^{-} . The peak at 1001 cm^{-1} (C–O stretching vibration of alcohols, ethers, carboxylic acids or C-N stretching vibration of amines) and 910 cm^{-1} (Out of plane bending of O–H of carboxylic acids) respectively.

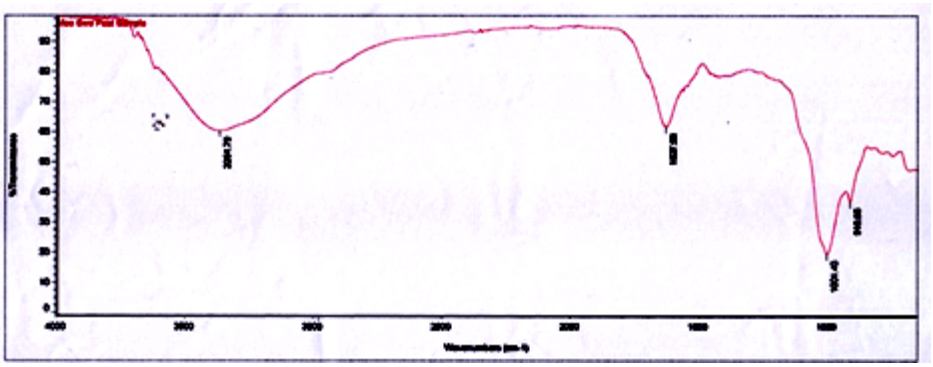

Figure 2 FT IR spectrum of the extracted humic acid from peat

The XRD diffractogram of the extracted HA was shown in Figure 3. The amorphous like nature of humic acid was found by XRD analysis.

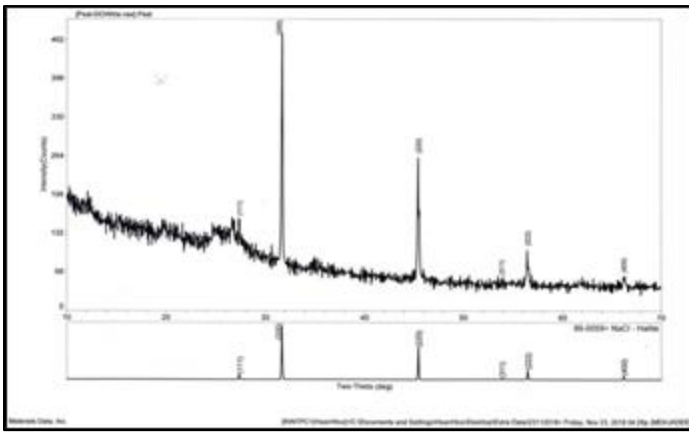

Figure 3 XRD diffractogram of the extracted humic acid from peat

The SEM micrograph of the extracted HA is shown in Figure 4. Some individual aggregates of HA particles were observed in the extracted HA. The dark shadow in SEM images was caused by thickness of HA particles.

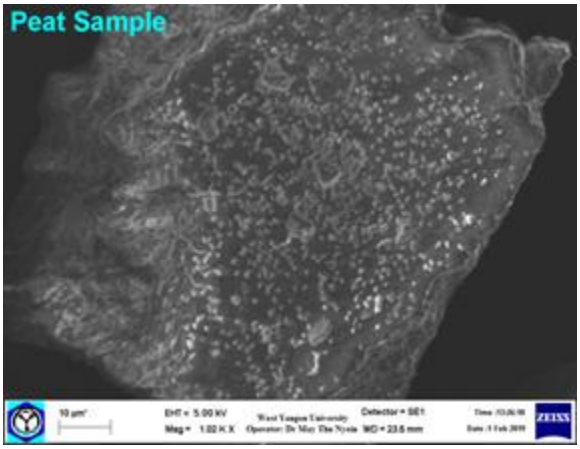

Figure 4 SEM micrograph of the extracted humic acid from peat

Thermal gravimetric analysis of the

The TG-DTA thermogram of extracted HA is shown in Figure 5. This figure depicts the onset temperature and decomposition temperature of humic acid. According to the TG-DTA analysis, the nature of decomposition such as the release of free water as well as the liberation of volatile materials and combustion were found between 40 ºC and 600 ºC. The exothermic peak was clearly observed in the TG-DTA thermogram, which may be due to decomposition of specimen.

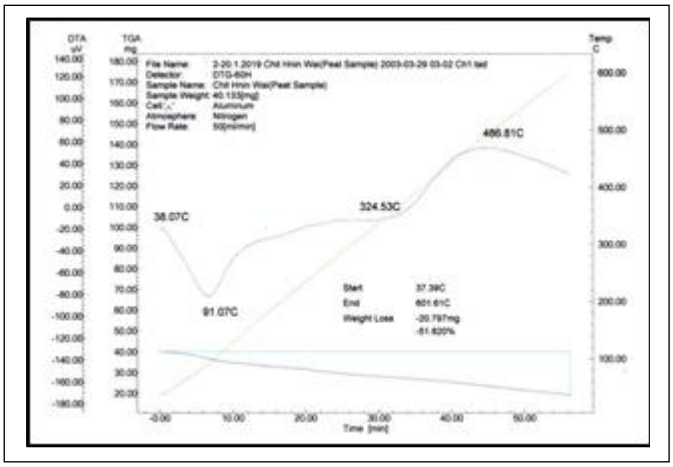

Figure 5 TG-DTA thermogram of the extracted humic acid from peat

Characterization of Humic-Chitosan Composites

Humic-chitosan composites in three different weight ratios: 1:1, 1:2 and 2:1 were characterized by modern techniques such as FT IR, XRD, SEM and TG-DTA analysis.

Comparison between FT IR spectra of three different weight ratios of humic-chitosan composite is shown in Figure 6. In this spectra, all of the humic-chitosan composite consist of broad absorption band in the range of 3000 to 3500 cm^{-1} which is attributed to O-H stretching vibrations and around 3200 cm^{-1} to vibration of N-H. The stretching vibrations of methylene C-H occur at around 2800 cm^{-1} and the absorption peak at 1550 cm^{-1} corresponds to the N-H bending vibrations. The amide II band is used as the characteristic band of N-acetylation.

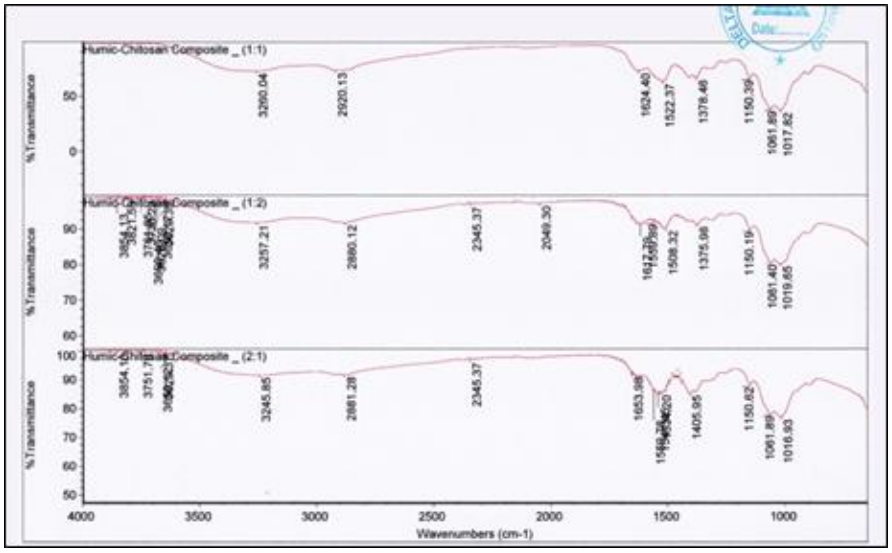

(a)

(b)

(c)

Figure 6 Comparison between FT IR spectra of three different weight ratios of humic-chitosan composites

(a) Humic-chitosan composite (1:1)

(b) Humic-chitosan composite (1:2)

(c) Humic-chitosan composite (2:1)

The XRD diffractograms of three different weight ratios of humic-chitosan composite [(1:1), (1:2) and (2:1)] are shown in Figure 7. The amorphous like nature of humic-chitosan composites were found by XRD analysis.

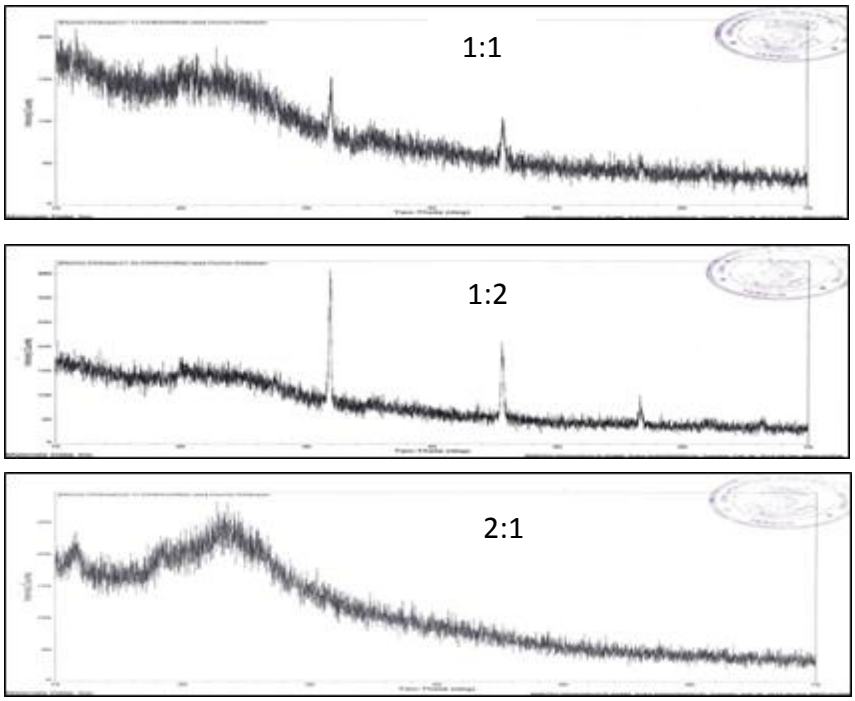

Figure 7 Comparison of XRD diffractograms of three different weight ratios of humic-chitosan composite [(1:1), (1:2) and (2:1)]

According to Figures 8, 9 and 10, the surface morphology of three different weight ratios of humic-chitosan composite can be seen. Among them, the morphology of humic-chitosan composite (1:1) has smoother surface than the other two composites. This means that the composition of HA to chitosan (1:1) is a better composition than the other ratios.

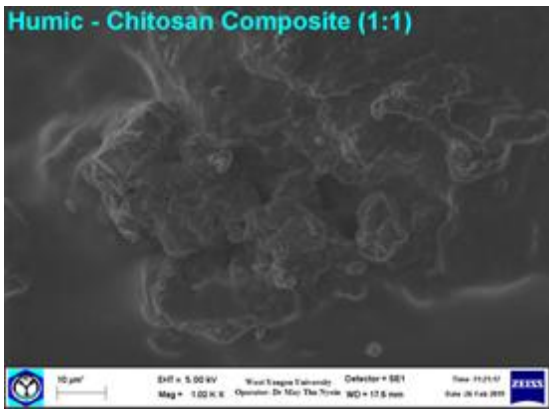

Figure 8 SEM micrograph of humic-chitosan composite (1:1)

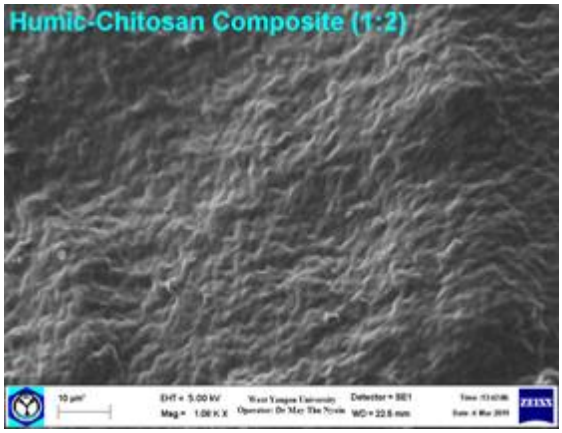

Figure 9 SEM micrograph of humic-chitosan composite (1:2)

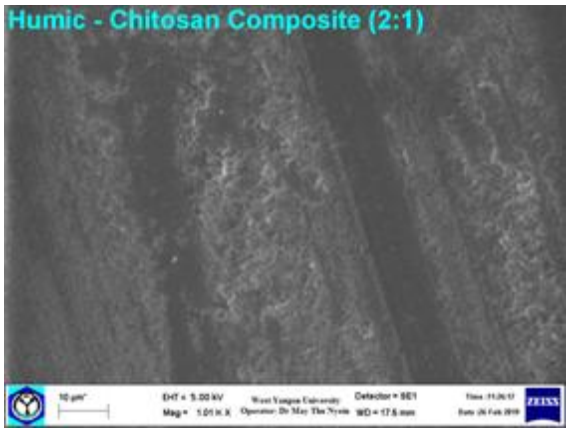

Figure 10 SEM micrograph of humic-chitosan composite (2:1)

Studying on the Figures 11, 12 and 13, the percent weight loss of three different ratios of humic-chitosan composite can be investigated. However, the percent weight loss of humic-chitosan composite (1:1) is more stable than the other composites.

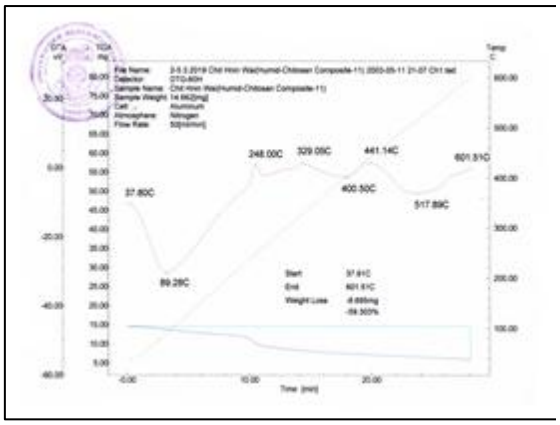

Figure 11 TG-DTA thermogram of humic-chitosan composite(1:1)

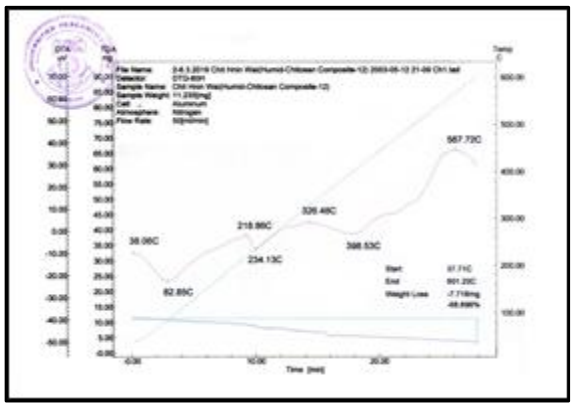

Figure 12 TG-DTA thermogram of humic-chitosan composite(1:2)

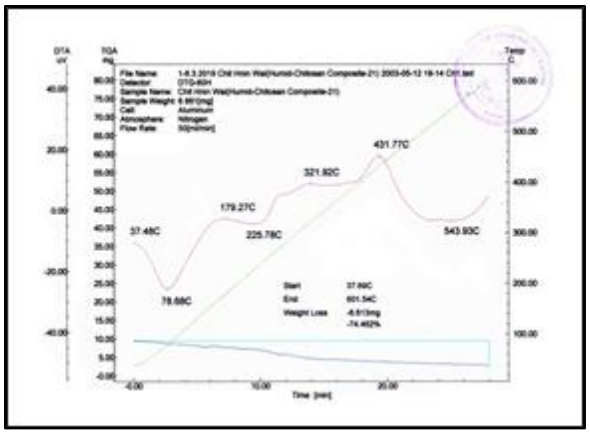

Figure 13 TG-DTA thermogram of humic-chitosan composite(2:1)

Calibration of the Dye Solution

According to Figure 14, the maximum wavelength of the dye solution is 620 nm. Figure 15 shows the standard curve of the dye solution by using maximum wavelength of 620 nm.

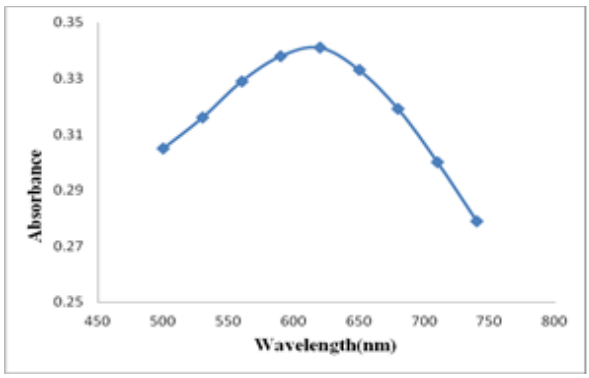

Figure 14 Maximum wavelength of the dye solution

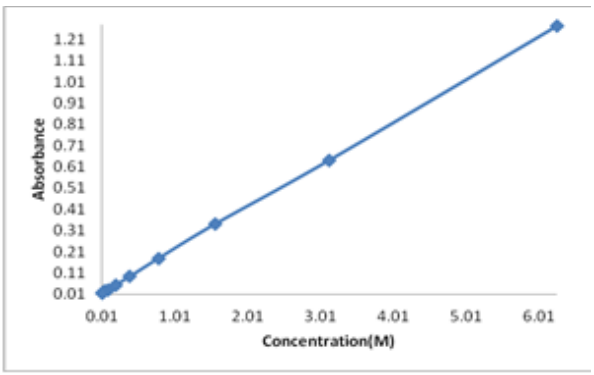

Figure 15 Calibration curve of the dye solution

Application of Humic Acid and Humic-Chitosan Composite in Removal Rates of Sulphur Black Dyes from Aqueous Solution

Before the comparison of the removal rates of sulphur black dye from aqueous solution between HA only and humic-chitosan composite, the composition ratios of three different weights of humic-chitosan composite were compared. Among them, the smoothest morphology and the highest thermal stability of humic-chitosan composite (1:1) was selected.

Figures 16 and 17 mention about the concentration vs time factor of HA only and humic-chitosan composite for the removal rate of dye solution. From these figures, the removal rate of HA only is better than the humic-chitosan composite (1:1).

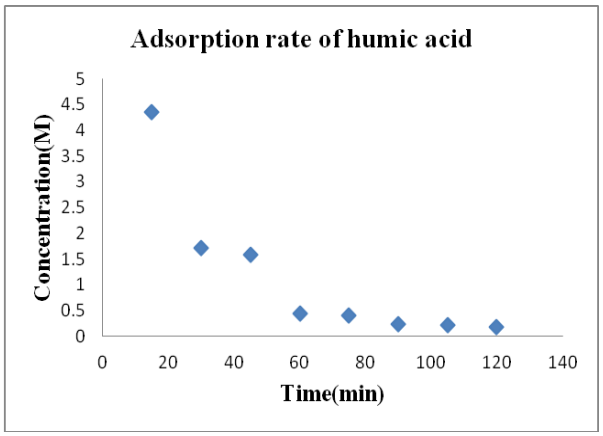

Figure 16 Adsorption rate of humic acid

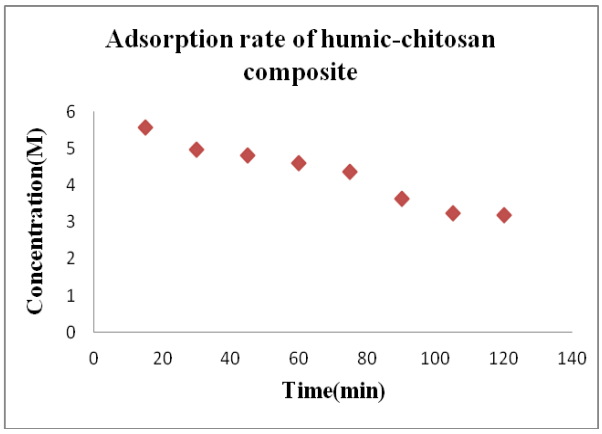

Figure 17 Adsorption rate of humic-chitosan composite

According to Table 1 and Figure 18, the sorption capacitiy for colour removal of sulphur black dye solution by HA is better than humic-chitosan composite (1:1).

Table 1 Sorption Capacities for Colour Removal of Sulphur Black Dye Solution by HA and Humic-Chitosan Composite

Time(min)	Humic acid(HA) %	Humic-Chitosan Composite %
15	30.40	10.72
30	72.48	20.64
45	74.72	23.04
60	92.96	26.4
75	93.44	30.24
90	96.16	41.76
105	96.64	48.00
120	97.12	49.12

Conditions

Initial concentration of dye solution = 6.2500 x 10^{-4}M
Dosage = 2 gL^{-1}
Temperature = ambient temperature
Stirring rate = 100 rpm
Contact time = 15 min

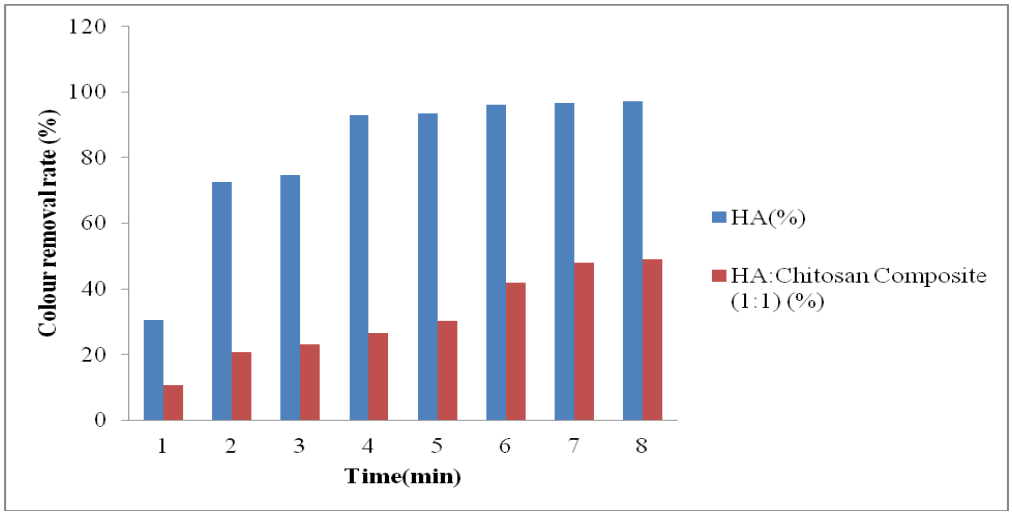

Figure 18 Sorption capacities for colour removal of sulphur black dye solution by HA and humic-chitosan composite

Conclusion

In this research work, HA was extracted from peat collected from Moeswe Village, Oattara Thiri Township, Naypyitaw, Myanmar by alkali extraction method. From the spectroscopic analysis, it was found that HA is composed of aliphatic and hydrophobic hydrocarbons. Observations from TG-DTA analysis indicated that the presence of fossilized organic carbon, HA compound was decomposed about 51.8% up to 600˚C. According to SEM analysis, the morphology of extracted HA possesses the voids and aggregate nature. The extracted HA can be effectively used in the removal of sulphur black dye which has been widely used in the aqueous solution of textile industry in Myitnge Town, Amarapura Township, Mandalay, Myanmar. Moreover, the three different weight ratios of HA-chitosan composite [(1:1), (1:2) and (2:1)] were also prepared. According to SEM and TG-DTA analysis, HA:chitosan composite (1:1) is suitable one for the application of the removal of sulphur black dye from aqueous solution. Furthermore, the comparison of dyes removal rate percent of HA only and HA:chitosan composites, HA can influence the more effective removal rate than the other composites.

Acknowledgements

We are gratefully indebted to Professor and Head, Dr Yi Yi Myint, Department of Chemistry, University of Mandalay, for her permission, supervision and providing all research facilities for our research work. Grateful thanks are also due to Dr Thida Win, Rector, University of Mandalay, for her suggestions and constant encouragement throughout this research work.

References

Cocozza, C., D'Orazio, V., Miano, T. M. And Shotyk, W. (2003). "Characterization Of Solid And Aqueous Phases Of A Peat Bog Profile Using Molecular Fluorescence Spectroscopy, ESR And FT-IR, And Comparison With Physical Properties". *Organic Geochemistry*, Vol . 34, Pp. 49-60

Maria Ortiz De Serra And Schnitzer, M. (1972). "Extraction Of Humic Acid By Alkali And Chelating Resin". Vol . 405, Pp. 365-374.

Novák, J., Kozler, J., Janos, P., Ezıkova, J., Tokarova, V., And Madronova, L. (2001). "Humic Acids From Coals Of The North-Bohemian Coal Field: I.Preparation And Characterization". *React Funct Polym*, Vol . 47 , Pp. 10–19.

Saito, B., And Seckler, M.M, (2013), "Alkaline Extraction Of Humic Substances From Peat Applied To Organic-Mineral Fertilizer Production". Vol .31, Pp. 675-682.

Skhonde, M.P, Herod, A.A, Van Der Walt, T.J, Tsatsi, W.L. And Mokoena, K. (2006). "The Effect Of Thermal Treatment On The Compositional Structure Of Humic Acids Extracted From South Africanbituminous Coal." *Int J Miner Process*; Vol . 8, Pp. 51–57.

Stevenson, F.J. (1994). *Humus Chemistry: Genesis, Composition, Reactions.* New York: 2nd Ed. John Wiley And Sons

EVALUATION OF ANTIBACTERIAL ACTIVITY AND ISOLATION OF SOME ORGANIC CONSTITUENTS FROM SEEDS OF *Myristica fragrans* Hott. (ZADEIK-PO)

Than Than Nu[1], Aye Aye Htun[2], Daw Hla Ngwe[3], Maung Maung Htay[4]

Abstract

The seeds of *Myristica fragrans* Hott. (Zadeik-po) are the chief ingredients in a variety of Myanmar Traditional Medicine Formulations (TMF). These formulations are generally used for the treatment of asthma, dysentery, diarrhoea, pneumonia, typhoid fever, hemolytic anemia and urinary tract infection. The Zadeik-po seeds were selected as plant material and collected from Mudon Township, Mon State. The research was focused on antibacterial activity of various extracts and isolation, identification of some organic constituents from Zadeik-po seeds. The polar, non-polar extracts and essential oil of Zadeik-po seeds were screened for antibacterial activity by agar disc diffusion method. The essential oil of Zadeik-po exhibited the pronounced antibacterial action against all tested 20 microorganisms. In addition, Minimum Inhibitory Concentration (MIC) values of active essential oil of Zadeik-po were also determined by microplate dilution method on five bacterial strains. The lowest MIC values of essential oil was found to be 0.0625 mg mL^{-1} with *Escherichia coli* LT. α-Pinene (0.5 %), Myristicin (0.03 %) and Eugenol (0.01 %) were isolated from essential oil of Zadeik-po by column and preparative thin layer chromatographic methods. They were identified by UV, FT IR, ^{1}HNMR and GC MS spectroscopic methods. The isolated compounds also showed antibacterial property against the *Staphylococcus aureus, Escherichia coli, Shigella boydii, Samonella typhi* and *Vibrio cholera*. From these scientifically observations, it can be inferred that Zadeik-po seeds may be used in the formulation of medicine especially for the treatment of diseases related to bacterial infections.

Keywords : *Myristica fragrans* Hott. (Zadeik-po), antibacterial activity, agar disc diffusion method, microplate dilution method, α-pinene, myristicin, eugenol

Introduction

Medicinal plants are abundant in Myanmar. Eighty five percent of the population in Myanmar lives in rural areas. Most people use the traditional medicinal plants for the treatment of diseases. There are numerous indigenous medicinal plants which are reputed to be effective against the disease of bacterial origin (Boyd and Horel, 1981). *Myristica fragrans* Hott. (Zadeik-po) commonly known as Nutmeg is one of the well-known Myanmar indigenous medicinal plant for making the traditional medicine formulations. It belongs to family Myristicaceae, spreading aromatic evergreen tree usually growing to about 5 to 13 m high, occasionally 20 m. Zadeik-po seeds are ovoid, about 20 to 35 mm long and 15 to 25 mm wide. They are grayish brown in colour with minute reddish brown spots, lines and furrowed. The odour is strong and aromatic with agreeable taste (Peter, 2001). The seeds are native of Moluccas, now cultivated in many tropical countries of both hemispheres, India, Indonesia and Srilanka. They have been introduced into Myanmar about 20 years ago presumably from Indonesia and acclimatized in Kyoneka and Mudon Agricultural farms near Mawlamyine.

[1] Dr, Associate Professor, Department of Chemistry, Kyaukse University
[2] Dr, Rector, Bago University
[3] Dr, Professor and Head (Rtd.), Department of Chemistry, University of Yangon
[4] Dr, Professor and Head (Rtd.), Department of Chemistry, University of Yangon

Zadeik-po seeds are popular as spices and also possess various therapeutic properties (Copalakrishnan, 2002). In eastern countries they are employed more as a drug than as condiment. For a long time, they have been used as a folklore medicine for treating diarrhea, mouth sores and insomnia (Assa *et al*., 2014). Oil of Zadeik-po is employed for flavouring food products. It is also used for scenting soaps, tobacco and dental creams and also in perfumery. The seeds contain volatile oil (5-10 %), fat or nutmeg butte (30-40 %), proteins, carbohydrates, starch, calcium, phosphorus, iron and colouring matter. The main chemical components of volatile oil are α -pinene, borneol, eugenol, and myristicin. α-Pinene, camphene and borneol show allergenic, antibacterial, anti-inflammatory and antiviral activities. In addition, eugenol and myristicin also have anticeptic, antiulcer, antitumor, anti-inflammatory and antibacterial properties (Asgarpanah and Kazemivash, 2012).

The present work deals with the antibacterial activity of crude extracts and essential oil of Zadeik-po seeds, isolation and identification of some organic constituents from active extract. The photograph of Zadeik-po tree, fruits and seeds are shown in Figure 1.

(a) (b) (c)

Figure 1 Photographs of (a) tree (b) fruits and (c) seeds of Zadeik-po

Materials and Methods

All chemicals were obtained from British Drug House (BDH). Trypticase soy broth from Difco, Trypticase soy agar from Becton and Triple sugar iron agar from Difco, column (3×60 cm), silica gel (40-60 μm, Wakogel), TLC precoated plates (GF_{254} aluminium plates, Merck) were employed. The following instruments were used for the determination of physical data: melting point; Gallenkamp melting point apparatus, UV spectra; Shimadzu UV-240 UV-Visible spectrophotometer, IR spectra; JEOL JNM-GX FT IR spectrophotometer, NMR spectra; ^{1}HNMR (300 MHz) and mass spectra; GC MS spectrometer at the Goettingen University in Germany and Shimadzu GC MS-QP 5050A at Myanmar Indigenous Medicine Research and Development Department, Yangon.

Zadeik-po seeds were collected from Mudon Township, Mon State. They were cut into pieces and ground in a grinding machine. The powdered sample was stored in air-tight container.

Preliminary Phytochemical Tests

A few grams of dried powdered sample was subjected to the tests of alkaloids, α-amino acids, carbohydrates, flavonoids, glycosides, phenolic compounds, saponins, steroids, cyanogenic glycosides, tannins and terpenoids as the preliminary phytochemical test according to reported methods (Robison, 1983 ; M - Tin Wa, 1972).

Preparation of Various Crude Extracts by Successive Solvent Extraction Method

The powdered sample (300 g) was first percolated with pet-ether (60-80 °C) for one week per three times. After removal of pet-ether soluble matter, the defatted marc was then extracted with ethanol. The solvent was removed under reduced pressure in a rotary evaporator. The concentrated alcohol soluble matter was partitioned between water and dichloromethane followed by ethyl acetate. The ethyl acetate and aqueous layer were separately concentrated. The condensed pet-ether, ethanol, dichloromethane, ethyl acetate and aqueous extracts were kept for screening of antibacterial activity.

Extraction of Essential Oil by Steam Distillation Method

The powdered sample (100 g) and distilled water (500 mL) were placed in the 1 L round-bottomed flask. The flask was fitted to Clevenger essential oil apparatus which was joined to water condenser. When the flask was heated, the condensed oil and water coming out from condenser were collected in the receiver flask. The oil was then extracted with pet-ether in a separating funnel. The pet-ether extract was dried over anhydrous sodium sulphate. After filtering, the pet-ether was evaporated to get the essential oil which was then weighed until to be constant weight and kept in air tight bottle.

Antibacterial Screening of Crude Extracts and Essential Oil by Agar Disc Diffusion Method

Paper discs (6 mm) were used to impregnate the extract to obtain approximately 20 μg/disc and allowed to dry at 42 °C in an incubator. The bacterial suspension from trypticase soy broth was streaked evenly onto the surface of the trypticase soy agar plates with sterile cotton swab. After the inoculum had dried for 5 min, the dried discs were placed on the agar with flamed forceps and gently pressed down to ensure proper contact. After inoculations, the plates were incubated immediately or within 30 min. After over-night incubation at 37 °C, the zone of inhibition diameter including 6 mm discs were measured (Mar Mar Nyein *et al*, 1991). In the present work, the crude extracts and essential oil were tested on 20 strains of bacteria.

Determination of Minimum Inhibitory Concentration (MIC) of Essential Oil of Zadeik-po

For the determination of MIC values of the tested sample, the positive (medium and inoculum) and negative (medium and sample) controls were always included. Prior to the performing of MIC, the 100 μ dm^3 of trypticase soy broth was first introduced in 96 wells. Then 100 μ dm^3 of sample was introduced into the first well. By using multi-channel pipette (8–channels) and Titertek micro-titration equipment, 100 μ dm^3 of the mixture was used for downstream serial dilutions up to 12 consecutive wells, each already containing 100 μ dm^3 of media. The last 100 μ dm^3 was discarded. While transferring the content of each well, the mixture was mixed thoroughly with a multi-channel pipetter. Then 20 μ dm^3 of the already prepared inoculum was introduced to its respective wells and the microplates were incubated at 37 °C for 18 h. Growth of the microorganisms was determined by absorbance at 450 nm on an automated microplate reader (Bio Rad) as well as confirming by culturing onto trypticase soy agar was subjected to incubation at 37 °C for overnight. The last well with no growth of the

microorganisms was taken to represent the MIC of the extract. The essential oil of Zadeik-po was tested with organisms: *E. coli* ETEC, *E. coli* LT, *E. coli* EHEC, *S. aureus* MLW 96, *S. aureus* KMM by microplate dilution method.

Isolation of Phytoconstituents from Essential Oil by Column and Preparative Thin Layer Chromatographic (PTLC) Methods

A chromatographic column was packed with silica gel (120 mL) using toluene as the solvent. The essential oil was carefully placed on the top of the silica gel, using a pasteur pipette by allowing it to flow down the walls of the column just above the surface of silica gel. The tap was opened just to let the sample enter into the gel. The column was then filled with solvent. Gradient elution was performed with toluene, toluene:EtOAc (49:1, 19:1 and 9:1 v/v) and 20 fractions were collected. The fractions were monitored by TLC. Finally four main fractions: FV, FVI, FVII and FVIII were obtained after combining the fractions giving similar behaviour on TLC chromatogram. From fractions FV, FVI and FVIII, compound **I** (0.5 %), compound **II** (0.03 %) after purified by PTLC with tol : EtOAc – 29:1 v/v and compound **III** (0.01 %) were isolated respectively. Fraction VII occurred as a mixture.

Identification of Isolated Compounds by Spectroscopic Techniques

By using silica gel column and PTLC techniques, three compounds were isolated from essential oil of Zadeik po. The isolated compounds were characterized by modern spectroscopic techniques such as UV, FT IR, ^{1}HNMR and GC MS spectroscopic techniques.

Determination of Antibacterial Activity of Isolated Compounds

The antibacterial activity of isolated compounds from essential oil was determined by agar disc diffusion method. The isolated compounds were screened by *S. aureus, E. coli*, *Shigella boydii*, *Samonella typhi* and *Vibrio cholera* microorganisms.

Results and Discussion

Preliminary Phytochemical Inverstigation of Zadeik-po Seeds

The phytochemical tests revealed that α-amino acids, carbohydrates, flavonoids, glycosides, phenolic compounds, saponins, steroids, tannins and terpenoids were present in Zadeik-po seeds but alkaloids and cyanogenic glycosides were not detected.

Different Crude Extracts of Zadeik-po

The powdered sample of Zadeik-po seeds was successively extracted with solvents of different polarity: pet-ether (60-80 ºC), dichloromethane, ethyl acetate ethanol and water. The soluble matter contents of pet-ether, dichloromethane, ethyl acetate, ethanol and aqueous extracts were observed to be 36.48 %, 4.07 %, 3.21 %, 10.25 % and 2.98 % respectively. However, pet-ether soluble matter content of Zadeik-po seeds was the highest, indicating that they possessed more non-polar phytoconstituents than polar constituents.

Extraction of Essential Oil by Steam Distillation Method

Essential oil of Zadeik-po seeds was extracted by using the steam distillation method. The yield percent of essential oil was found to be 3.01 % based on the powdered sample. The essential oil was kept for screening the antibacterial activity.

Antibacterial Screening of Crude Extracts and Essential Oil by Agar Disc Diffusion Method

Screening of antibacterial activity of crude extracts and essential oil has been done by agar disc diffusion method on 20 bacterial strains. According to the results presented in Table 1, it was found that pet-ether, dichloromethane, ethyl acetate and aqueous extracts of Zadeik-po did not show any antibacterial activity against all species tested. Ethanol extract of Zadeik-po showed mild antibacterial activity. However, essential oil of Zadeik-po exhibited the pronounced antibacterial action against all tested 20 bacterial strains. It was also observed that most of the active extract showed more remarkable inhibition zone. The effects of essential oil and different extracts from Zadeik-po on *Staphylococcus aureus* MLW 96 and *Escherichia coli* LT are shown in Figure 2.

Minimum Inhibitory Concentration (MIC) of Essential Oil

The MIC values of active essential oil of Zadeik-po on five bacteria strains were determined by micro plate dilution method using Falcon 3072 sterile pack containing 96 wells (Figure 3). The active essential oil was tested on 3 species of *E. coli* and 2 species of *S. aureus*. The MIC values of essential oil of Zadeik-po determined by micro plate reader at the wavelength 450 nm are shown in Table 2 and Figure 4. It was found that the lowest MIC values of essential oil of Zadeik-po were 0.0625 mg mL^{-1} obtained with *E. coli* LT and 0.125 mg mL^{-1} with *S. aureus* MLW 96. In addition, the MIC values of essential oil of Zadeik-po on five bacterial strains determined by micro plate reader at the wavelength 450 nm are shown in Table 3.

Table 1 Antibacterial Activity of Crude Extracts and Essential Oil of Zadeik-Po on Different Species of Bacteria

No.	Type of Bacteria	Diameter of inhibition zone (mm)					
		I	II	III	IV	V	VI
1	*Staphylococcus aureus* MLW 96	24	–	–	–	14	–
2	*Staphylococcus aureus*	20	–	–	–	10	–
3	*Staphylococcus aureus* D 25	24	–	–	–	12	–
4	*Staphylococcus aureus* MOE 20	18	–	–	–	12	–
5	*Escherichia coli* LT	20	–	–	–	12	–
6	*Escherichia coli* ETEC	22	–	–	–	12	–
7	*Escherichia coli* ATCC	18	–	–	–	12	–
8	*Escherichia coli* STLT	20	–	–	–	14	–
9	*Samonella typhi*	22	–	–	–	–	–
10	*Samonella stanley*	20	–	–	–	–	–
11	*Vibrio cholerae*	24	–	–	–	16	–
12	*Vibrio cholera Inaba*	20	–	–	–	14	–
13	*Vibrio cholera Ogawa*	20	–	–	–	14	–
14	*Bacillus subtilis*	22	–	–	–	12	–
15	*Bacillus pumilus*	18	–	–	–	12	–
16	*Pseudomonas aeruginosa*	18	–	–	–	–	–
17	*Proteus morganii*	20	–	–	–	–	–
18	*Shigella sonnei*	16	–	–	–	–	–
19	*Shigella boydii*	18	–	–	–	–	–
20	*Shigella flexneri*	16	–	–	–	–	–

I = Essential oil, II = Pet-ether extract, III = Dichloromethane extract, IV = Ethyl acetate extract, V = Ethanol extract, VI = Aqueous extract (Disc diameter = 6 mm)

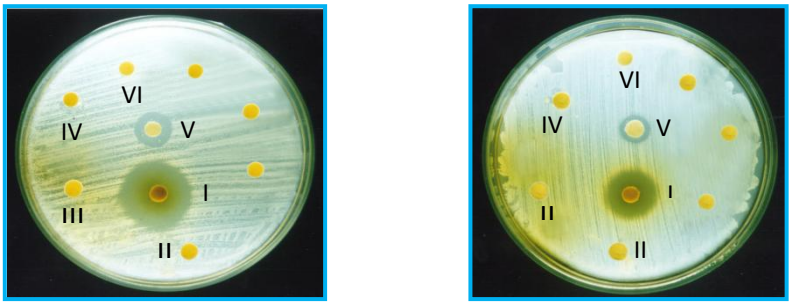

Staphylococcus aureus MLW 96 *Escherichia coli* LT

Figure 2 Effects of essential oil and different extracts from Zadeik-po on *Staphylococcus aureus* MLW 96 and *Escherichia coli* LT

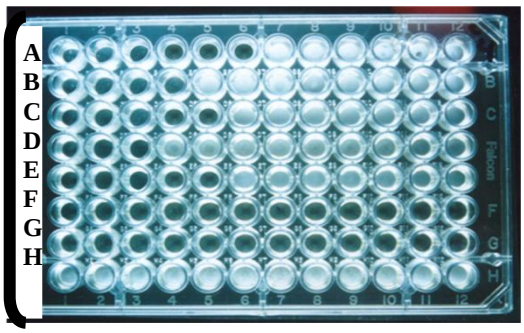

A = medium + sample + *E.coli* LT
B = medium + sample + *E.coli* EHE*C*
C = medium + sample + *E.coli* ETE*C*
D = medium + sample + *S. aureus* KMM
E = medium + sample + *S. aureus* MLW 96
F = nutrient agar
G = negative control (medium + sample)
H = positive control (medium + inoculum)

Figure 3 Falcon 3072 sterile pack containing 96 wells used for the determination of MIC values of essential oil of Zadeik-po

Table 2 Optical Density of Various Concentrations of Essential Oil from Zadeik-po on *E.coli* LT and *S. aureus* MLW 96 by Micro Plate Dilution Method at the Wavelength 450 nm

Essential Oil Conc. ($mg\ mL^{-1}$)	Optical Density			
	A	**E**	**G**	**H**
2	0.143	0.151	0.135	0.263
1	0.152	0.167	0.146	0.274
0.5	0.161	0.214	0.151	0.270
0.25	0.169	0.232	0.142	0.271
0.125	0.234	0.255	0.143	0.271
0.0625	0.251	0.310	0.144	0.275
0.0312	0.297	0.359	0.143	0.276
0.0156	0.299	0.362	0.154	0.276
0.0078	0.305	0.382	0.148	0.287
0.0039	0.313	0.399	0.146	0.275
0.0019	0.325	0.401	0.149	0.279
0.0009	0.333	0.412	0.145	0.285

A = medium + sample + *E. coil* LT E = medium + sample + *S.aureus* MLW 96
G = negative control (medium + sample) H = positive control (medium + inoculum)

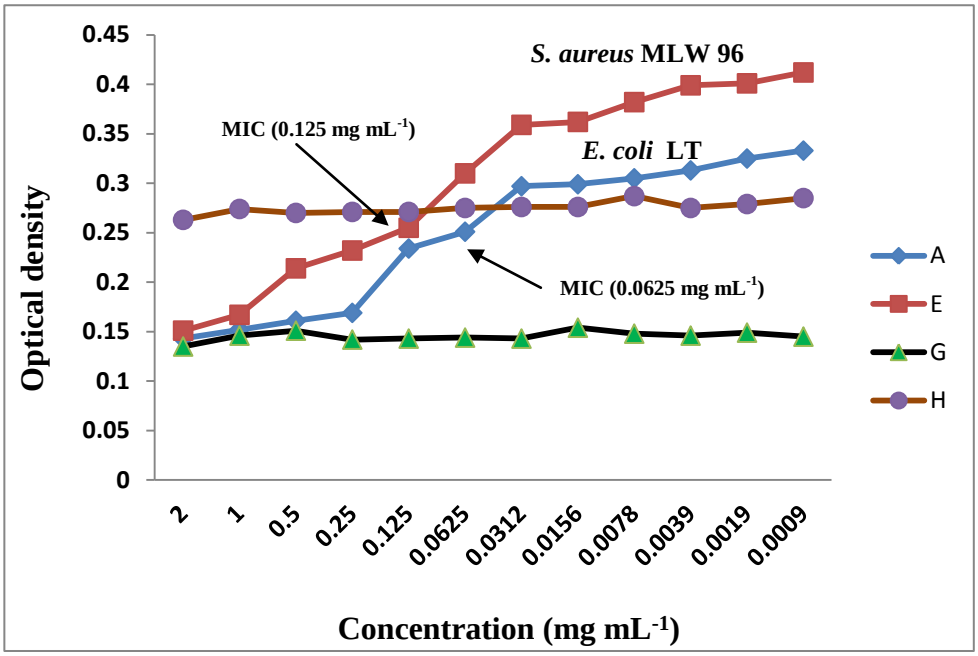

Figure 4 A plot of optical density and various concentrations of essential oil of Zadeik-po tested on *E.coli* LT and *S. aureus* MLW 96 by using micro plate dilution method

Table 3 MIC Values of Essential Oil of Zadeik-po by Micro Plate Dilution Method at the Wavelength 450 nm

No.	Bacterial strain	MIC value (mg mL^{-1})
A	*E.coli* LT	0.0625
B	*E.coli* EHE*C*	0.25
C	*E.coli* ETE*C*	0.125
D	*S. aureus* KMM	0.5
E	*S. aureus* MLW96	0.125

Isolation of Phytoconstituents from Active Essential Oil

The active essential oil of Zadeik-po was separated by column and preparative thin layer chromatographic (PTLC) methods using toluene and toluene: EtOAc with various ratios: 49:1, 19:1, 9:1 v/v as eluent. Three compounds, **I, II and III** at R_f values of 0.87 (toluene), 0.65 (toluene: EtOAc – 19:1) and 0.52 (toluene: EtOAc – 4:1) were isolated, resulting 0.5 %, 0.03 % and 0.01 % of yields respectively.

Identification of Isolated Compounds

The isolated compounds from essential oil of Zadeik-po were identified by using the modern spectroscopic methods: UV, FT IR, ^{1}HNMR and GC MS spectroscopic techniques.

α-Pinene (I): Pale yellow oil (0.5 % yield); UV-visible, λ_{max} (nm) in MeOH : 230; FT IR υ (cm^{-1}) (Neat), 2959, 2869 ($\upsilon_{asym\text{-}C\text{-}H}$ and $\upsilon_{sym\text{-}C\text{-}H}$), 1630 ($\upsilon_{C=C}$) of olefinic group, 1458, 1375 ($\delta_{C\text{-}H}$), 891, 800 (δ_{oop} of alkene); GC MS, (m/z) : 136 [M$^+$], 121, 105, 93, 79, 53, 39.

Myristicin (II): Light yellow oil (0.03 % yield);); UV-visible, λ_{max} (nm) in MeOH : 230, 240 (sh), 280; FT IR υ (cm^{-1}) (Neat), 3077, 3003 ($\upsilon_{=CH}$), 2975, 2896 ($\upsilon_{asym\text{-}C\text{-}H}$ and $\upsilon_{sym\text{-}C\text{-}H}$), 1632 ($\upsilon_{C=C}$) in vinyl compound, 1612, 1508, 1432 ($\upsilon_{C=C}$) in aromatic ring, 1357, 1317 ($\delta_{C\text{-}H}$), 1282, 1131 ($\upsilon_{asymC\text{-}O}$ of ar C–O), 1090, 1045 ($\upsilon_{C\text{-}O\text{-}C}$) in ether, 994, 966 ($\delta_{oop)}$ in vinyl compound, 827, 806 (δ_{oop} of C–H ar); ^{1}HNMR ($CDCl_3$, 300 MHz), δ_H (ppm) : 6.36 (d, *J*=8.57 Hz, 2H-1, 3), 5.81-5.98 (m,1H-8), 5.92 (s, 2H-10), 5.05-5.09 (m, 2H-9), 3.86 (s, 3H-11), 3.27 (d, *J*=5.8 Hz, 2H-7); GC MS, (m/z) : 192 [M^+], 177, 165, 161, 133, 119, 91, 71, 65.

Eugenol (III): Pale yellow oil (0.01 % yield); UV-visible, λ_{max} (nm) in MeOH : 220, 230, 280, in MeOH + NaOH : 228, 246, 296; FT IR υ (cm^{-1}) (Neat), 3513 ($\upsilon_{O\text{-}H}$ of phenolic O-H group) 3076, 3003 ($\upsilon_{=CH}$), 2975, 2896 ($\upsilon_{asym\text{-}C\text{-}H}$ and $\upsilon_{sym\text{-}C\text{-}H}$), 1637 ($\upsilon_{C=C}$) in vinyl compound, 1611, 1513, 1464, 1432 ($\upsilon_{C=C}$) in aromatic ring, 1367 (δ_{OH}), 1268, 1234 ($\upsilon_{asymC\text{-}O}$ of ar–C–O), 1149, 1034 ($\upsilon_{C\text{-}O\text{-}C}$) in ether, 995, 914 ($\delta_{oop)}$ in vinyl compound, 850, 817 (δ_{oop} of C–H ar); ^{1}HNMR ($CDCl_3$, 300 MHz), δ_H (ppm) : 6.88 (d , *J*=7.50 Hz, 1H-6), 6.69-6.72 (m,2H-3, 5), 5.91-6.02 (m, 1H-8), 5.76 (m, 1H-1 OH), 5.05-5.14 (m, 2H-9), 3.86 (s, H-10), 3.33-3.35 (d, *J*=5.8 Hz, 2H-7); GC MS, (m/z) : 164 [M^+], 149, 137, 131, 121, 91, 77.

Antibacterial Activity of Isolated Compounds

The antibacterial activity of isolated compounds was determined by agar disc diffusion method. The antibacterial activity of α-Pinene, Myristicin and Eugenol isolated from essential oil of Zadeik-po were also screened on five main bacterial strains: *S. aureus, E. coli, Shigella boydii, Samonella typhi* and *Vibrio cholera*. Myristicin and Eugenol showed antibacterial activity against all five bacterial strains. But α- Pinene is active against *S. aureus, E. coli, Shigella boydii* and *Vibrio cholera* and inactive against *Samonella typhi* (Table 4 and Figure 5).

Table 4 Antibacterial Activity of the Isolated Compounds Compared with Tetracyclin

Isolated compound	Inhibition zone diameter (mm)				
	A	**B**	**C**	**D**	**E**
α-Pinene (I)	16	16	14	18	-
Myristicin (II)	16	18	18	20	16
Eugenol (III)	24	22	24	22	20
Tetracyclin (IV)	20	24	30	24	22

A = *E.coli*, B = *S.aureus*, C = *Shigella boydii*, D = *Vibrio cholerae*, E = *Samonella typhi* (Disc diameter = 6 mm)

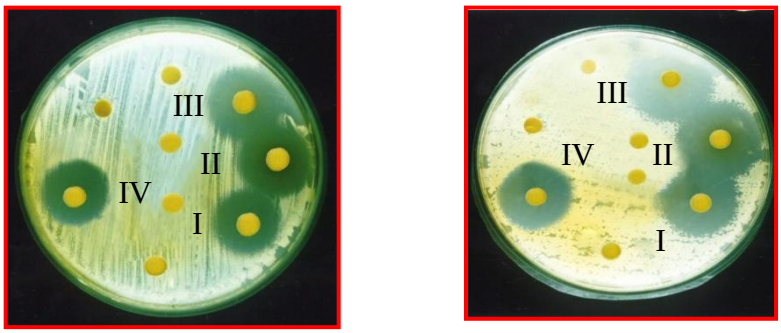

Escherichia coli *Vibrio cholerae*

Figure 5 Effects of isolated compounds from essential oil on *Escherichia coli* and *Vibrio cholerae*

Conclusion

From the research work, it could be concluded that preliminary phytochemical tests were revealed the presence of α-amino acids, carbohydrates, flavonoids, glycosides, phenolic compounds, saponins, steroids, tannins and terpenoids. Among the extracts, pet-ether soluble matter content was found to be highest. Essential oil (3 %) was also extracted from Zadeik po seeds by steam distillation method. By using agar disc diffusion method, essential oil exhibited pronounced antibacterial action against all tested 20 bacterial strains. MIC values of active essential oil of Zadeik-po were determined by microplate dilution method on five bacterial strains. The lowest MIC values of essential oil was found to be 0.0625 mg mL^{-1} with *E. coli* LT. α- Pinene (0.5%), Myristicin (0.03%) and Eugenol (0.01%) were isolated from essential oil of Zadeik-po by column chromatographic and PTLC methods. In addition, α- Pinene, Myristicin and Eugenol also showed antibacterial property. From the scientifically obervation, it can be inferred that Zadeik-po seeds have been used in the formulations of medicine for the treatment of diseases: namely pneumonia, urinary tract infection, diarrhoea, dysentery, cholera and typhoid fever.

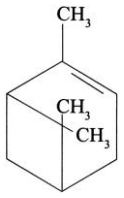

α – Pinene

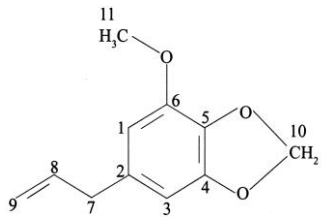

Myristicin

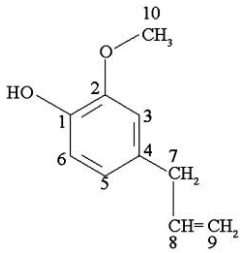

Eugenol

Acknowledgements

The authors would like to express their profound gratitude to the Ministry of Education, Department of Higher Education Office (Mandalay) for provision of opportunity to do this research and thanks are extended to the Myanmar Academy of Arts and Science, Yangon. And also thank to Dr Aung Khin Myint, Rector, Dr Su Su Win, Pro-rector and Dr Kyae Mon Lwin, Professor and Head, Department of Chemistry, Kyaukse University for their kind encouragement and allowing to submit this research paper.

References

Asgarpanah, J., and Kazemivash, N. (2012). "Phytochemistry and Pharmacologic Properties of *Myristica fragrans* Hott." *African Journal of Biotechnology*, vol. 11(65), pp. 12787-12793

Assa, J. R., Widjanarko, S. B., Kusnadi, J. and Berhimpon, S. (2014). "Antioxidant Potential of Flesh, Seed and Mace of Nutmeg (*Myristica fragrans* Hott.)." *Inter. J. Chem. Tech. Res.*, vol . 6(4), pp. 2460-2468

Boyd, R. F., and Horel, B. G. (1981). *Basic Medical Microbiology*. Boston: Little Brown Co. Ltd., pp. 395-398

Copalakrishnan, M. (2002). "Chemical Composition of Nutmeg and Mace." *Journal of Spices and Aromatic Crops*, vol. 1, pp. 49-54

M - Tin Wa. (1972). *Phytochemical Screening Method and Procedure*. Phytochemical Bulletin of Botanical Society of America Inc., vol. 5(3), pp. 4-10

Mar Mar Nyein, Chit Maung, Mya Bwin and Tha, S. J. (1991) "*In Vitro* Testing of Various Indigenous Plant Extracts on Human Pathogenic Bacteria." *Myanmar Health. Sci. Res. J.*, vol. 3, pp. 89-99

Peter, K. V. (2001). *Handbook of Herbs and Spices*. New York: CRC Press, pp. 45-62

Robison, T. (1983). *Organic Constituents of Higher Plants.* North Amherst: 5th Ed., Cordus Press, pp. 285-286

MANAGEMENT ON ENVIRONMENTAL CONTAMINATION OF WATER FROM AGRICULTURAL SITES IN PATHEINGYI TOWNSHIP, MANDALAY REGION BY USING BIOSORBENTS (CORN COB POWDER AND ACTIVATED CORN COB CHARCOAL)

Wai Hnin Phyu Phyu[1], Win Win Khaing[2], Khaing Khaing Kyu[3]

Abstract

In this research, the paddy growing surrounding area in Patheingyi Township Mandalay Region was chosen to study the environmental contamination by water from agricultural sites. Some physicochemical parameters such as pH, temperature, conductivity and turbidity were directly measured by respective apparatus. The alkalinity of each water sample was determined by acid-base titration. The total hardness of water samples was determined by EDTA titrimetric method. Nitrogen content, phosphate content, chemical oxygen demand, biochemical oxygen demand, and dissolved oxygen were also determined. The compositions of the metals such as iron, lead, cadmium and copper which can cause pollution to water were investigated by Atomic Absorption Spectroscopy. To reduce the pollutants in water samples by adsorption, corn cob powder was chosen as adsorbent. In addition, corn cob sample was activated with H_3PO_4. The elemental compositions of adsorbent samples were examined by Energy Dispersive X-ray Fluorescence (EDXRF) analysis and the surface morphology of adsorbents was characterized by Scanning Electron Microscope (SEM). The collected water samples were treated by filtration using the prepared adsorbents to reduce the extent of contamination of water from agricultural sites.

Keywords: physicochemical parameters, corn cob powder, agricultural sites, elemental compositions

Introduction

Water is the most common or major substance on earth, covering more than 70 % of the planet's surface. All living things consist mostly of water (Kumar, 2006). Its usage for many purposes such as drinking, cooking, agricultural, transport, industry and recreation immediately show the extent to which it is integral part of our life. Water is also required in industries for power generations, navigations, irrigation of crops and disposal of sewage etc. There is no doubt that fertilizers increase yields of crops around the world. Fertilizers and pesticides both have definite advantages and disadvantages associated with their use. The main problems associated with agriculture are salinization, nitrate and pesticide contamination. Irrigation has enlarged the land area available for crop production but the resulting salinization which has occurred in some areas has caused the deterioration of previously fertile soils (Bartram and Balance, 1996). Natural fertilizers are more preferable than chemical fertilizers by plants. However different kinds of chemical fertilizers are usually used to give good yield depending on growing of crops. The major or macro-nutrients in inorganic fertilizers are nitrogen, phosphorus, and potassium. Nitrogen, phosphorus, and potassium are considered macronutrients, and boron, calcium, chlorine, copper, iron, magnesium manganese among others are micronutrients (Hegde, 2009). Though the plants require three essential elements, nitrogen, potassium and phosphorus, seed bearing plants such as paddy require good amount of phosphorus and also potassium.

Contamination of soil and water through human and industrial waste and agrochemicals is a universal problem and a major issue in developing countries. Unrestrained industrial and domestic waste in urban and rural situation and pollution of reservoirs caused by agrochemical runoff are an increasing concern (Wimalawansa and Wimalawansa, 2014). The excessive use of inorganic fertilizers causes serious environmental degradation, resulting in lower crop yields. Farmers were supplied with chemical fertilizers and pesticides at a subsidized price. Farmers

[1] Dr, Assistant Lecturer, Department of Chemistry, Monywa University
[2] Dr, Associate Professor, Department of Chemistry, Bamaw University
[3] Dr, Professor, Department of Chemistry, University of Mandalay

increased the frequency of fertilizer applications to enhance yields. These practices are still used and have caused significant environmental degradation (Rahman and Zhang, 2018). The running water from agricultural sites can be rich with inorganic substances and hydrocarbons. Using chemical fertilizers can change the acidity or basicity of a soil and also can affect on the water of agricultural sites. Therefore this research was carried out to study the extent of pollution of water from agricultural sites in Patheingyi Township, Mandalay Region and to reduce the pollution by treatment with waste corn cob powder and activated waste corn cob powder.

Materials and Methods

Sample Collection

The sample was collected from agricultural sites in Gway-Gyi-Gon Village, Patheingyi Township, Mandalay Region. Seven water samples were collected once every two days within two weeks from the common drainage after using fertilizer.

Determination of Some Physicochemical Parameters of Water Samples

Some Physicochemical parameters of water samples were determined by the respective procedures. pH was determined by a pH meter (KM 200, England), conductivity by conductivity meter, turbidity by nephelometric method and total dissolved solids by gravimetric method. Alkalinity and hardness of water samples were determined by titrimetric method. Ammonia nitrogen, nitrate nitrogen and phosphate were determined by spectrophotometric method.

Determination of Organic Pollutants in Collected Water Samples

The organic pollutants of water samples such as, Dissolved Oxygen (DO), Biochemical Oxygen Demand (BOD) and Chemical Oxygen Demand (COD) were determined according to the previously described in method (APHA, 2005).

Determination of Elemental Compositions in Water Samples by Atomic Absorption Spectroscopy

The content of metals such as iron, cadmium, lead, copper, and manganese in water samples were examined by Atomic Absorption Spectrophotometric method, at Department of Chemistry, Taunggyi University.

Preparation of Biosorbents, Corn Cob Powder and Activated Corn Cob Charcoal

The biomass corn cob was collected from local market, Monywa Township, Sagaing Region. Firstly, the collected samples were washed with water and immersed in boiling water for 3 h. Then the samples were allowed to dry and crushed into small pieces and then into a powder. The dried powder was sieved with a 120-mesh sieve. The resulting samples were used through the research work.

For preparation of activated corn cob the samples were pyrolyzed in a muffle furnace in absence of air at 500 to 600°C for 2 h. After pyrolysis, the activation was carried out by impregnation of the corn cob samples with phosphoric acid in a ratio of 1:2 (w/w) for 24 h, and then washed with distilled water several times until neutral. It was dried in oven at 100°C for 2 h.

Determination of Relative Abundance of Elements in Corn Cob Powder an Corn Cob Activated Charcoal by EDXRF

The elemental compositions of sample powders were examined by using Energy Dispersive X-ray Fluorescence (EDXRF) spectrophotometer.

Characterization of Corn Cob Powder and Corn Cob Activated Charcoal by Scanning Electron Microscope (SEM)

The sample was examined by scanning electron microscope (SEM) for a visual inspection of external porosity and morphology.

Treatment of Water Samples by Adsorption Using Corn Cob Powder and Corn Cob Activated Charcoal

The water samples collected from agricultural sites on September 2018 which was polluted by cadmium and lead were treated by adsorption using corn cob powder and activated corn cob as adsorbents.

The water samples were treated by using corn cob powder by column filtration method. 500 mL of each sample was added into the 1000 mL column. Before adding the water sample, the column was filled with cleaned and dried sand at the lower part at a height of about 20 cm and then corn cob powder with the height of 20 cm was placed above the sand. The water sample which had passed the corn cob powder was treated again by column filtration already filled with corn cob powder adsorbent. The filtration process was carried out totally three times.

In addition, the water samples were also treated by activated corn cob charcoal. Treatment process was carried out as the same procedure described in corn cob powder as shown in Figure 1.

Figure 1 Treatment of water sample by column filtration process

Results and Discussion

Table 1 shows the physicochemical parameters in water samples before treatment. By studying the results, most of the measured parameters were over the limit of EPA standard. pH of the water samples were found to be alkaline. Conductivity values were in the range of 340μScm^{-1} to 501μScm^{-1} and below the permissible limit. The water samples from agriculture sites were turbid with turbidity values of 25.00 NTU to 67.40 NTU. Total dissolved solids are in the range of 460 mg/L to 720 mg/L. The palatability of drinking water has been rated, by panels of tasters, according to TDS levels as follows: excellent, less than 300 mg/L, between 600 mg/L and 900 mg/L, poor and unacceptable, greater than 1200 mg/L (Bruvold and Ongerth, 1969). The TDS value were found to be within range of 460 mg/L and 720 mg/L and poor level according to literature. In the present study, the total alkalinity values of the water samples were between 180 mg/L and 400 mg/L. Hardness values were in the range of 100 mg/L to 380 mg/L and observed to be higher than the permissible limit. If the alkalinity is less than the hardness, then salts of calcium and magnesium are present in association with sulphate, chlorides, or nitrates. In the water samples from agriculture sites PO_4^{3-} contents were higher than the permissible limits. Conductivity, turbidity, TDS, alkalinity, hardness, concentration of NO_3-N, NH_3-N and PO_4^{3-} were found to gradually decrease during the study period of seven days.

Table 1 Some Physicochemical Parameters in Water Samples before Treatment

Parameter	Unit	Samples							WHO * (2011)	EPA* * (2003)
		Day I	Day II	Day III	Day IV	Day V	Day VI	Day VII		
pH	-	7.8	7.9	8.0	7.8	7.7	7.9	7.8	8.2-8.8	6.5-8.5
Temperature	-	28.9	28.6	28.6	28.7	28.7	28.9	28.6	-	-
Conductivity	μScm^{-1}	501	447	402	380	347	340	388	600	-
Turbidity	NTU	67.40	60.00	58.00	49.01	38.11	33.00	25.00	10	-
TDS	mg/L	720	706	680	630	510	500	460	500	500
Alkalinity	mg/L	400	300	400	380	180	200	260	500	30-150
Hardness	mg/L	380	260	220	100	120	140	160	200	90-100
NO_3-N	mg/L	23.2	24.0	2.6	8.2	21.6	9.5	7.5	50	1.0
NH_3-N	mg/L	0.35	0.29	0.29	0.26	0.24	0.22	0.22	0.5	0.5
PO_4^{3-}	mg/L	0.33	0.26	0.24	0.21	0.18	0.10	0.10	0.02	0.12

* Maximum permissible limit of drinking water quality (WHO, 2011)
** United States Environmental Protection Agency for domestic water (USEPA, 2005)
Day I to Day VII = Water samples after using fertilizers

By observation of the results shown in Table 2, it can be seen that the dissolved oxygen level of water sample (Day I) was 1.7 mg/L and was the lowest among samples collected on other days. The DO levels of all water samples were lower than standard values. BOD values were 6.2 mg/L on the Day I and gradually decreased to 2.0 mg/L on Day VII. BOD values except that of Day 1 sample was lower than WHO and EPA standard values. Furthermore, chemical oxygen demand was in the range of 10.06 mg/L and 4.9 mg/L. All COD values except Day VII were higher than EPA standard.

Table 2 Results of Some Organic Pollutants in Water Samples after Using Fertilizers in September 2018

Parameter	Unit	Samples							WHO* (2011)	EPA** (2003)
		Day I	Day II	Day III	Day IV	Day V	Day VI	Day VII		
DO	mg/L	1.7	2.4	2.6	2.6	3.0	3.8	4.0	-	4-6
BOD	mg/L	6.2	4.3	2.1	2.1	2.0	1.9	2.0	6	5
COD	mg/L	10.6	9.3	7.8	7.6	7.0	6.8	4.9	10	5

* Maximum permissible limit of drinking water quality (WHO, 2011)
**United States Environmental Protection Agency for domestic water (USEPA, 2005)
Day I to Day VII = Water samples after using fertilizers

Table 3 shows the elemental compositions of water samples determined by AAS after using fertilizers. The elements determined were iron, copper, lead and cadmium. It was observed that the elements which can cause pollution to water were present in all tested water samples collected. However, these elements were below the permissible limit of EPA standard.

Table 3 Elemental Compositions of Water Samples after Using Fertilizers by Atomic Absorption Spectroscopy before Treatment

Element	Unit	Samples							WHO* (2011)	EPA** (2003)
		Day I	Day II	Day III	Day IV	Day V	Day VI	Day VII		
Fe	mg/L	0.002	0.020	0.010	0.021	0.023	0.009	0.010	2.0	0.30
Cu	mg/L	0.095	0.011	0.092	0.011	0.018	0.001	0.015	0.05	1.00
Pb	mg/L	0.003	0.015	0.010	0.001	0.002	0.010	0.011	0.01	0.05
Cd	mg/L	0.001	0.013	0.011	0.002	0.012	0.002	0.012	0.003	0.01
K	mg/L	0.003	0.001	0.002	0.002	0.003	0.001	0.092	0.05	0.05

* Maximum permissible limit of drinking water quality (WHO, 2011)
**United States Environmental Protection Agency for domestic water (USEPA, 2005)
Day I to Day VII = Water samples after using fertilizers

Relative Abundance of Elements in Corn Cob Powder and Activated Corn Cob Charcoal

Table 4 shows the relative abundance of elements in corn cob powder and activated corn cob charcoal. From the EDXRF report, it was found that corn cob powder contains chlorine in highest content of 4.325 % and vanadium the lowest, 0.004 %. Moreover, activated corn cob powder contained 0.563 % silicon followed by potassium 0.491 % and phosphorus 0.478 %. Other elements are present in small amount. It can be seen that these adsorbents are composed of significant amount of some elements.

Table 4 Elemental Compositions of Corn Cob Powder and Activated Corn Cob Charcoal

No	Element		Relative abundance (%)	
			Corn cob powder	Activated corn cob charcoal
1	Chlorine	(Cl)	4.325	-
2	Calcium	(Ca)	3.197	-
3	Silicon	(Si)	1.059	0.563
4	Potassium	(K)	0.970	0.491
5	Phosphorus	(P)	0.229	0.478
6	Aluminium	(Al)	0.052	-
7	Sulphur	(S)	0.050	0.115
8	Iron	(Fe)	0.035	0.009
9	Manganese	(Mn)	0.009	0.003
10	Titanium	(Ti)	0.009	-
11	Zinc	(Zn)	0.005	0.003
12	Barium	(Ba)	0.004	-
13	Vanadium	(V)	0.004	-
14	Copper	(Cu)	-	0.002
15	Chromium	(Cr)	-	0.001

Surface Morphology of Corn Cob Powder and Activated Corn Cob Charcoal

Figure 2 shows the SEM image of corn cob powder. Porous nature of corn cob powder was observed. It has different sizes of pores. SEM image of activated corn cob charcoal is shown in Figure 3. From the SEM images, it can be clearly seen that the corn cob charcoal particles were cluster form and have different size of holes. More pores are clearly seen in activated corn cob charcoal.

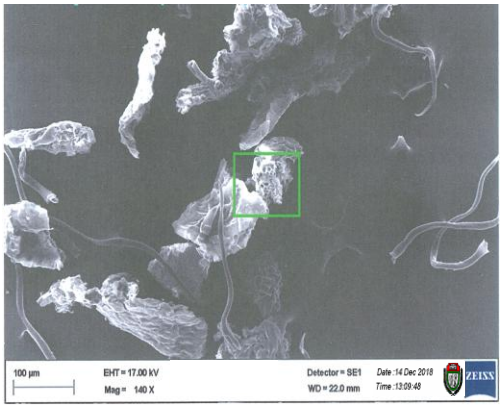

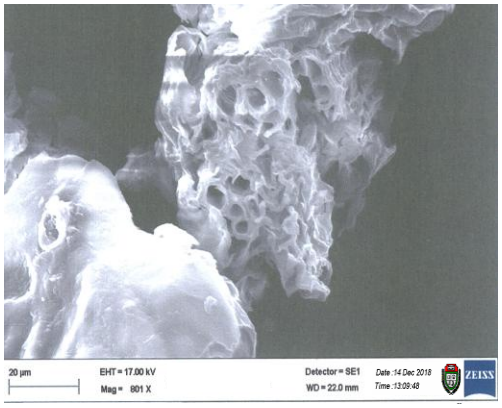

Figure 2 Scanning electron micrographic image of corn cob powder

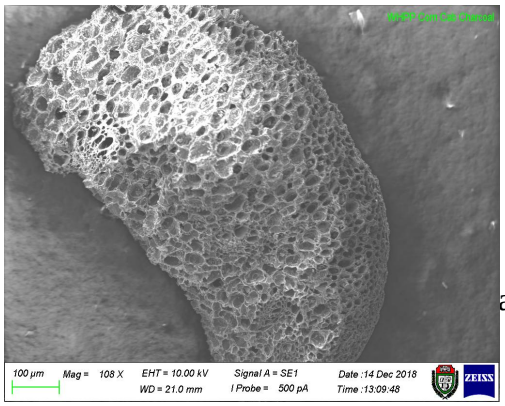

aphic

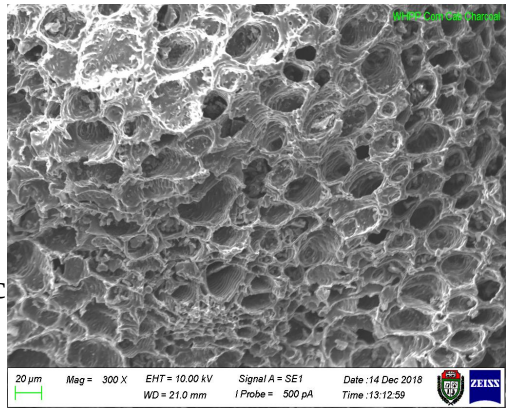

Comparison of Some Physicochemical Parameters of Water Samples after Treatment by Using Corn Cob Powder and Corn Cob Activated Charcoal

Table 8 and Figure 4 show total dissolved solids (TDS) in water samples before and after treatment by using corn cob powder and corn cob activated charcoal. Before treatment TDS values obtained on Day 1 to Day VI were higher than the permissible limit of WHO and EPA standards. After treatment with corn cob powder and corn cob activated charcoal TDS values were found to decrease and lower than the permissible limit. On Day VII, the reduction percents of TDS were 90.5 % and 93.4 %, respectively, from its original TDS value by corn cob powder and corn cob activated charcoal. It was noted that the higher amount of decrease was observed in water sample treated with corn cob activated charcoal.

Table 8 Total Dissolved Solid in Water Samples before and after Treatment by Using Corn Cob Powder and Corn Cob Activated Charcoal

Day of collection	TDS(mg/L) before treatment	TDS(mg/L) after treatment	
		Corn cob powder	Corn cob activated charcoal
Day I	720	85.6	56.2
Day II	706	60.5	50.3
Day III	680	60.5	50.0
Day IV	630	55.6	46.5
Day V	510	68.5	55.2
Day VI	500	76.5	45.1
Day VII	460	68.7	47.4

Day I to Day VII = Water samples after using fertilizers

Table 9 and Figure 5 show the total alkalinity of water samples and Table 10 and Figure 6 show hardness of water before and after treatment by using corn cob powder and corn cob activated charcoal. After treatment total alkalinity values and also the hardness were below the permissible limit. The reduction percents from its original total alkalinity value were found to be 85.0% and 90.5% for corn cob powder and activated charcoal respectively. Reduction percents of hardness from its original value were 76.1 % by corn cob powder and 79.2 % by activated charcoal. Since the many pores were present in activated charcoal the decreases by charcoal powder was more than corn cob powder.

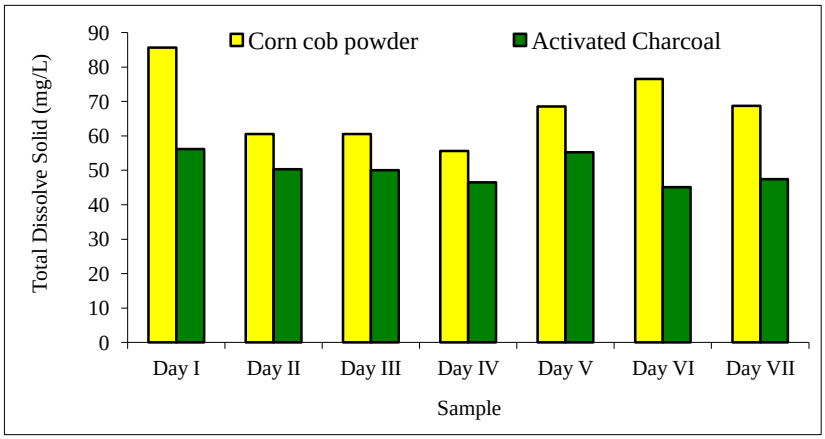

Figure 4 Total Dissolved Solids in water samples after treatment using corn cob powder and corn cob activated charcoal

Table 9 Alkalinity in Water Samples before and after Treatment by Using Corn Cob Powder and Corn Cob Activated Charcoal

Day of collection	Alkalinity(mg/L) before treatment	Alkalinity (mg/L) after treatment	
		Corn cob powder	Corn cob activated charcoal
Day I	400	140	100
Day II	300	140	110
Day III	400	80	60
Day IV	380	60	40
Day V	180	80	60
Day VI	200	60	40
Day VII	260	60	38

Day I to Day VII = Water samples after using fertilizerS

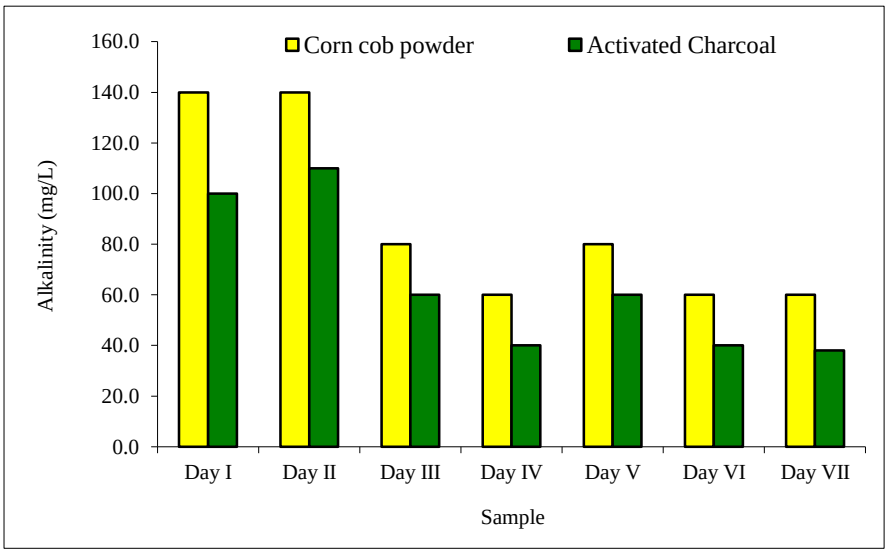

Figure 5 Alkalinity of water samples after treatment using powder and activated charcoal of corn cob

Table 10 Hardness of Water Samples before and after Treatment by Using Corn Cob Powder and Corn Cob Activated Charcoal

Day of collection	Hardness (mg/L) before treatment	Hardness (mg/L) after treatment	
		Corn cob powder	Corn cob activated charcoal
Day I	380	200	180
Day II	260	180	163
Day III	220	190	175
Day IV	100	90	83
Day V	120	80	63
Day VI	140	87	67
Day VII	160	91	79

Day I to Day VII = Water samples after using fertilizers

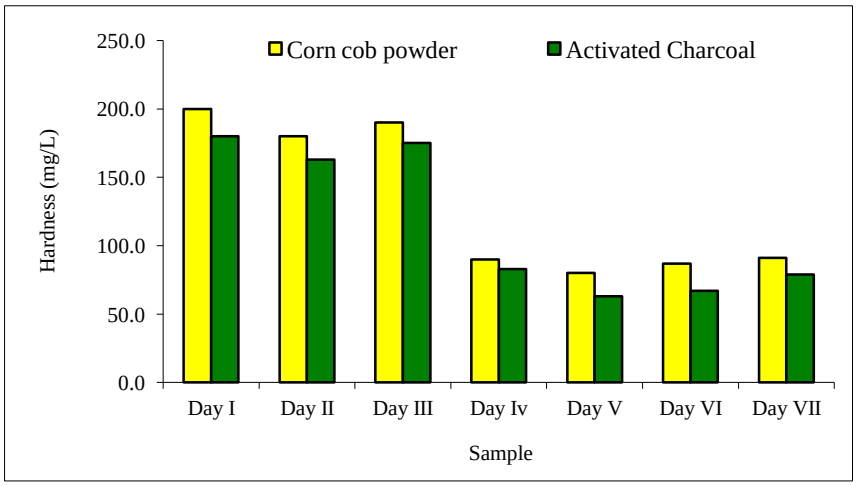

Figure 6 Hardness of water samples after treatment using powder and activated charcoal of corn cob

Table 11 and Figure 7 show nitrate nitrogen of water samples, Table 12 and Figure 8 show the ammonia nitrogen and Table 13 and Figure 9 show phosphate content in the water samples from agricultural site before and after treatment with corn cob powder and corn cob activated charcoal powder. By comparison of the results of these parameters of water samples before treatment and after treatment with corn cob powder and its charcoal, it can be clearly seen that all of the measured parameters after treatment are reduced. However, activated corn cob charcoal powder can reduce the pollutants of water more than corn cob powder due to its higher adsorptive property.

Table 11 Nitrate Nitrogen of Water Samples before and after Treatment by Using Corn Cob Powder and Corn Cob Activated Charcoal

Day of collection	NO_3-N(mg/L) before treatment	NO_3-N(mg/L) after treatment	
		Corn cob powder	Corn cob activated charcoal
Day I	23.2	5.9	ND
Day II	24.0	0.8	ND
Day III	2.6	1.0	0.4
Day IV	8.2	2.0	ND
Day V	21.6	7.0	0.6
Day VI	9.5	5.2	0.8
Day VII	7.5	3.6	ND

Day I to Day VII = Water samples after using fertilizers

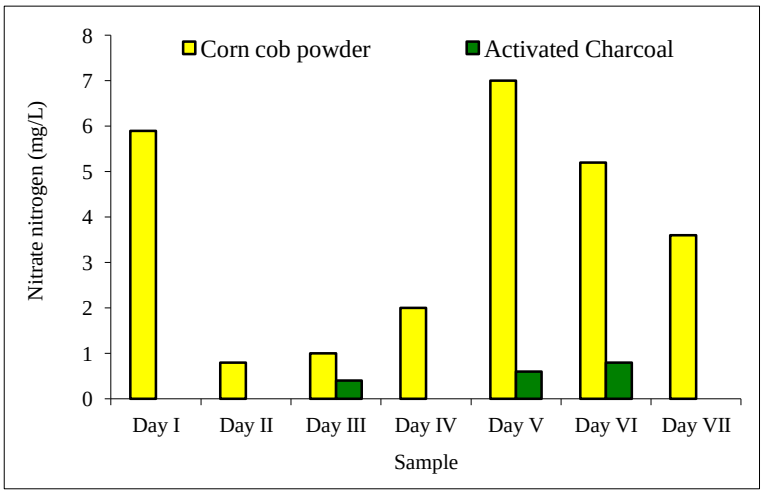

Figure 7 Nitrate nitrogen of water samples after treatment using corn cob powder and corn cob activated charcoal

Table 12 Ammonia Nitrogen of Water Samples before and after Treatment by using Corn Cob Powder and Corn Cob Activated Charcoal

Day of collection	NH_3-N(mg/L) before treatment	NH_3-N(mg/L) after treatment	
		Corn cob powder	Corn cob activated charcoal
Day I	0.35	0.13	0.12
Day II	0.29	0.11	0.09
Day III	0.29	0.14	0.12
Day IV	0.26	0.15	0.13
Day V	0.24	0.17	0.11
Day VI	0.22	0.19	0.12
Day VII	0.22	0.17	0.13

Day I to Day VII = Water samples after using fertilizers

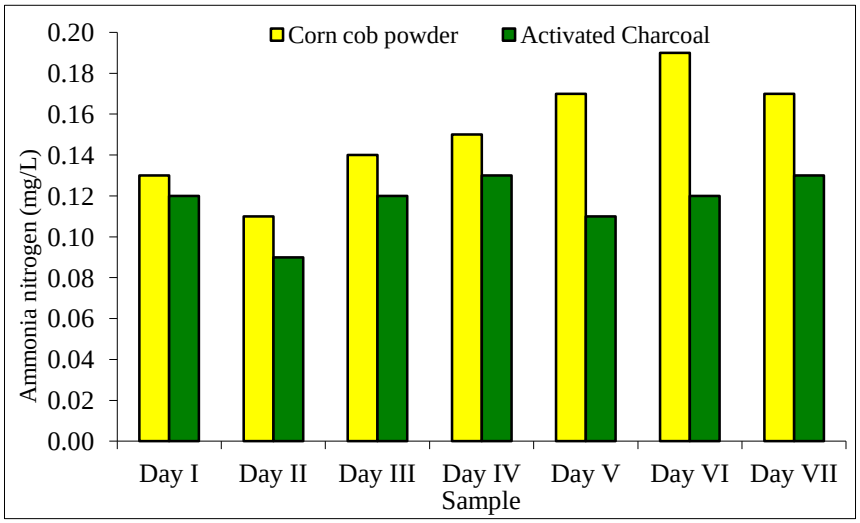

Figure 8 Ammonia Nitrogen of water samples after treatment using powder and activated charcoal of corn cob

Table 13 Phosphate of Water Samples before and after Treatment by Using Corn Cob Powder and Corn Cob Activated Charcoal

Day of collection	PO_4^{3-} (mg/L) before treatment	PO_4^{3-} (mg/L) after treatment	
		Corn cob powder	Corn cob activated charcoal
Day I	0.33	0.10	0.06
Day II	0.26	0.07	0.04
Day III	0.24	0.08	0.02
Day IV	0.21	0.08	0.01
Day V	0.18	0.05	0.02
Day VI	0.10	0.03	ND
Day VII	0.10	0.02	ND

Day I to Day VII = Water samples after using fertilizer

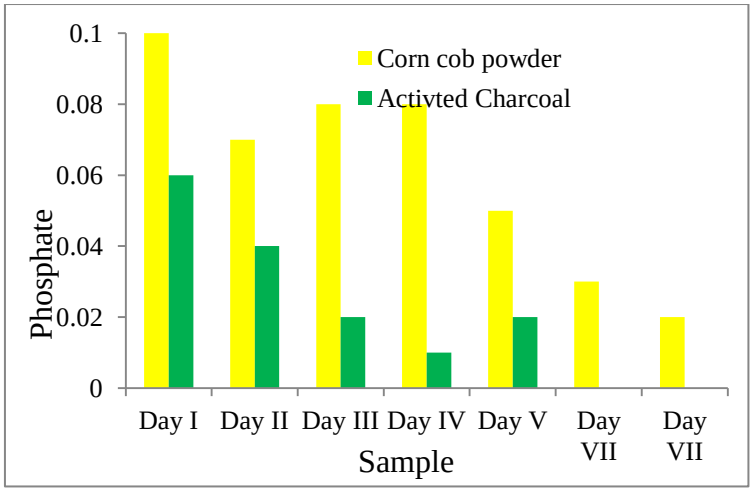

Figure 9 Phosphate in water samples after treatment using powder and activated charcoal of corn cob

Metal Composition of Water Samples after Treatment by Using Corn Cob Activated Charcoal

The metal composition of water sample was determined after treatment by using activated charcoals. The results are shown in Table 14. By observation of the results, it was found that the effective adsorbent activated corn cob charcoal reduced the trace metal contents which were non-detectable in all tested water sample.

Table 14 Elemental Compositions of Water Samples by Atomic Absorption Spectroscopy before and after Treatment using Corn Cob Activated Charcoal

Element	Elemental content (mg/L)	
	Before treatment	After treatment
Fe	0.002	ND
Cu	0.095	ND
Pb	0.003	ND
Cd	0.001	ND
K	0.003	ND

Comparison of Some Physicochemical Parameters of Water Sample after Three Column Filtration by Using Corn Cob Activated Charcoal

Water sample collected on the Day I after using fertilizer was treated continuously with three columns filtration using the more effective adsorbent, activated corn cob charcoal. Thereafter, some physicochemical properties of this sample after treatment of three times filtrations are expressed in Table 15. According to the results, it was seen that the more frequent the contact between water and adsorbent, the greater the pollution of water can be reduced.

Table 15 Comparison of Some Physicochemical Parameters in Water Sample in 2018 after Three Column Filtration by Using Corn Cob Activated Charcoal

Parameter	Unit	Before filtration	1st time filtration	2nd time filtration	3rd time filtration
TDS	mg/L	720	56.2	42	25
Alkalinity	mg/L	400	100	71	40
Hardness	mg/L	380	300	211	166
NH_3-N	mg/L	0.35	0.12	0.10	0.01
NO_3-N	mg/L	23.2	0.01	ND	ND
PO_4^{3-}	mg/L	0.33	0.10	0.06	0.01

Conclusion

In this research, sampling site (common drainage) was chosen to study the environmental contamination by water from agricultural sites in Patheingyi Township, Mandalay Region. In September 2018, from the experimental data, it was observed that first day sample after using fertilizers was more polluted than other days. Moreover, the pollution level was gradually decreased from day II to day VII. It was found that, ammonia nitrogen, phosphate, alkalinity and hardness of all water samples were over the limit of EPA standard. The dissolved oxygen level and Biochemical Oxygen Demand in all water samples were lower than EPA standard, but the Chemical oxygen demand values were over the limit of EPA standard. Thus, the water samples collected in September 2018 were chosen to treat the pollution levels due to agricultural sites. The polluted water samples in September 2018 were treated by filtration using the prepared adsorbents (corn cob powder, activated corn cob charcoal,) to reduce the extent of contamination of water from agricultural sites. All adsorbents reduced the parameters after treatment. In comparing the removal activities, activated charcoal sample can reduce the pollutants more than powder sample. The pollution level caused due to agricultural sites can be reduced by using activated charcoal obtained from food wastes such as corn cob. Corn cob charcoal was more effective adsorbent with more frequent time of filtration.

Acknowledgements

The authors would like to thank the Myanmar Academy of Arts and Science for allowing to presents this paper. The authors also like to express deepest gratitude to Professor and Head Dr Than Than Win, Department of Chemistry, Monywa University and Professor, ret., Dr Ni Ni Sein for their kind encouragement.

References

APHA. (2005). *Standard Methods for the Examination of Water and Wastewater*.Washington : 21st ed., American Public Health Association

Bartram, J. and Balance, R. (1996). *Water Quality Monitoring: A Practical Guide to the Design and Implementation of Fresh Water Quality Studies and Monitoring Programmes.* London : Chapman and Hall

Bruvold, W. H. and Ongerth, H. J. (1969). "Taste Ouality of Mineralized Water". *J. Am. Water Works Assoc.*, vol. 61, pp. 170-175

USEPA. (2005). Protecting Water Quality from Agricultural Runoff, Fat Sheet No. EPA. 841. F.05.001. March; 4-8, United States Environmental Protection Agency

Hegde, H. P. (2009). *Textbook of Agrochemistry*. New Delhi: Discovery Publishing House Pvt. Ltd., pp. 7-43

Kumar, S. (2006). *Rain Water Harvesting*. Pune: Indian Railways Institute of Civil Engineering. 1-55

Rahman, K. M. A. and Zhang, D. (2018)." Effects of Fertilizer Broadcasting on the Excessive Use of Inorganic and Environmental Sustainability". *Sustainability*, vol.10, pp. 1-15

Savci, S., (2012), "Investigation of Effect of Chemical Fertilizers on Environment". APCBEE Procedia, vol. 1, pp. 287-292

WHO. (2011). *Guidelines for Drinking-Water Quality.* 4th ed., Incorporating the first addendum World Health Organization, pp. 1-631

Wimalawansa, S. A. and Wimalawansa, S. J. (2014). "Agrochemical-Related Environment Pollution: Effect on Human Health". *Global Journal of Biology, Agriculture & Health Science*, vol. 3(3), pp. 72-83

ISOLATION AND STRUCTURAL ELUCIDATION OF PURE ORGANIC COMPOUND ISOLATED FROM THE ROOT AND STEM OF *VANDA COERULEA* GRIFF.

Nwet Nwet Win[1], Myat Lay Nwe[2],Thida Win[3]

Abstract

In this research work, *Vanda coerulea* Griff. (local name: Vanda Thit-Kwa) was selected for the chemical analysis. The root and stem of this plant contains alkaloids, glycosides, flavonoids, polyphenols, sugars, lipophilic, terpene, saponins and phenolic compounds respectively. The antimicrobial activities of the plant extracts and the pure isolated organic compound were tested by agar well diffusion method using six organisms. The pure organic compound (NNW-1) was isolated from the root and stem of Vanda Thit-Kwa by thin layer and column chromatographic separation techniques. The pure organic compound was obtained as colourless amorphous. The melting point of this compound was found to be 180-182 °C. The yields percent of pure compound is 1.408 % (35.2 mg) based upon the EtOAc crude extract. The molecular formula was done by using FT IR, ^{1}HNMR, ^{13}CNMR, DEPT, HMQC spectroscopy and Mass spectrometry and its formula is $C_{24}H_{28}O_5$ and hydrogen deficiency index is 11. In addition, the complete structure of the organic compound (NNW-1) was elucidated by applying 1D and 2D NMR spectroscopy as well as EI-Mass spectrometry. The name of the isolated compound is 3-[(5-(3-hydroxypropyl)-2–propenyl-phenyl]-2-(4-methoxy-phenoxymethyl) acrylic acid methyl ester.

Keywords: *Vanda coerulea* Griff., Vanda Thit-Kwa, chromatographic separation techniques, antimicrobial activities

Introduction

Plants have played an important role in traditional medicine in Myanmar since ancient times. Some plants are used as diet. Nowadays, plants have been used as medicines all over the world and medicinal plants are great economic importance for their medicinal values.

Orchid family is the second largest family of flowering plants with approximately 20,000 species with more than 850 genera. *Vanda coerulea* Griffis one of the important plants that can be used as antioxidant biomarker, anti-pyretic, anticonsumption and antidiarrheal effects, and for the treatment of alcoholic gastritis. A wide range of chemical compounds are presented including alkaloids, bibenzyl derivatives, flavonoid, phenanthrene and terpenoid which have been isolated recently from this species.

In this research work, the isolation of pure organic compound (NNW-1) from the root and stem of Vanda-Thit-Kwa (Figure 1) was done by using column and thin layer chromatography. The complete structure of the isolated compound (NNW-1) could be assigned by using modern sophisticated methods such as ^{1}HNMR, ^{13}CNMR, DEPT, DQF-COSY, HMQC and HMBC respectively.

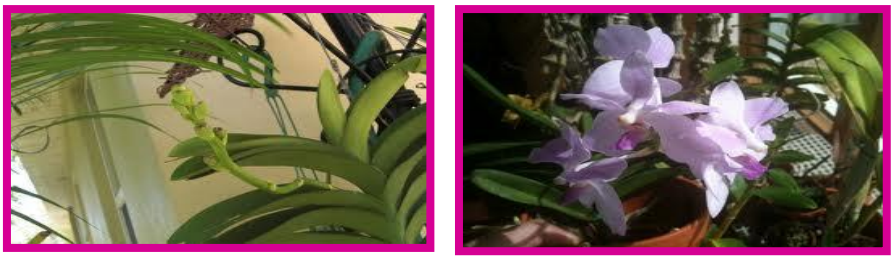

Figure 1 The Whole Plant of Vanda Thit-Kwa

[1] Dr, Lecturer, Department of Chemistry, Monywa University
[2] Dr, Associate Professor, Technological University (Keng Tung)
[3] Dr, Rector, University of Mandalay

Materials and Methods

The advanced instruments used in the characterization of samples and elucidation of pure compounds were UV lamp, Lambda - 40 Perkin-Elmer Co. England, FT IR spectrometer (Shimadsu, Japan), NMR spectrometer (500 MHz for 1H, 125 MHz for ^{13}C), EI-Mass spectrometer (JEOL, Japan), Melting Point Apparatus, SMP30 and UV spectrometer (Perkin Elmer (Lambda 25) UV/VIS spectrometer). Commercial grade reagents and solvents were used without further purification. Analytical thin layer Chromatography was performed by using precoated silica gel (Merck. Co. Inc, Kiesel gel 60 F256).

Sample Collection

In this research work, the sample, the root and stem of Vanda Thit-Kwa were collected from Loikaw Township, Kayah State. The root and stem were cut into small pieces and allowed to dry in good ventilation place. The dried sample was stored in stoppered bottle and used throughout the experiment.

Preliminary Phytochemical Test on Sample

Preliminary detection of phytochemical compounds present in plant was carried out according to the general methods mentioned in phytochemical methods (Harborne, 1993). Preliminary phytochemical analysis was performed in order to know different types of chemical constituents present in the plant sample.

Examination of Antimicrobial Activity of Plant Extracts

For the examination of antimicrobial activity of extracts from the root and stem of Vanda Thit-Kwa *in-vitro*, agar well diffusion method was used because of its simplicity, speed of performance and economy (Finegold, 1978).

Extraction and Isolation of Pure Compound (NNW-1)

450 g of air dried sample was percolated in 3 L of ethanol for two months. The ethanol extract was filtered and dried at room temperature. The ethanol crude extract was again extracted with ethyl acetate and concentrated under normal condition. The ethyl acetate crude sample (2.5 g) was obtained. It was separated by using column chromatography. Silica gel (70-230 mesh) was used as adsorbent and n-hexane: ethyl acetate mixture was used as eluent with various solvent ratios from non-polar to polar. Totally (65) fractions were obtained. Each and every fraction was checked on TLC using iodine as visualizing agent. The fractions with same R_f values were combined and nine combined fractions were obtained. Among them, fraction (IX) was rechromatographed by using same adsorbent and same eluent as mentioned in the previous column. Pure colourless amorphous was obtained and checked on TLC for purity. It gave one spot on TLC (R_f= 0.5) with n-hexane: ethyl acetate (1:1) (v/v). The weight of the isolated compound (NNW-1) was 35.2 mg and its yield percent was found to be (1.408 %) based on the ethyl acetate crude extract.

Determination of Melting Point and Phytochemical Screening of Pure Compound (NNW-1)

A few of pure organic compound (NNW-1) was inserted into the capillary tube and the melting point was determined by the aid of the electric melting point apparatus at Department of Chemistry, Monywa University. The phytochemical tests were carried out to identify the class of pure compound (NNW-1).

Examination of Antimicrobial Activity of Pure Organic Compound

Antimicrobial activity of pure compound (NNW-1) was tested by agar well diffusion method at Pharmaceutical Research Department (PRD).

Identification of the Isolated Compound (NNW-1)

Thin Layer Chromatography

Thin layer Chromatography (TLC) was conducted on 0.25 mm precoated silica gel (60 F254 Merck). It was cut into small plates (1×5 cm in size). The chromatogram was developed in the specified solvent systems for pure compound (NNW-1) (Stable, 1965).

Identification of the Pure Isolated Compound (NNW-1) by Fourier Transform Infrared (FT IR) Spectroscopic Study

The infrared spectrum of isolated compound was recorded by using Shimadzu Fourier Transform Infrared Spectrophotometer, at the Department of Chemistry, University of Mandalay. The resulted IR spectrum was applied for the identification of functional groups of the pure organic compound (NNW-1).

Identification of the Pure Isolated Compound (NNW-1) by Proton Nuclear Magnetic Resonance (^{1}H NMR) Spectroscopic Study

The ^{1}H NMR spectrum of isolated compound was recorded by means of a 500 MHz spectrometer at Meijo University, Tempaku, Nagoya, Japan. The spectrum was recorded for the DMSO-d6 solution of sample. By means of ^{1}HNMR spectrum, the number of protons of the pure compound could be estimated.

Identification of the Pure Isolated Compound (NNW-1) by Carbon Nuclear Magnetic Resonance (^{13}C NMR) Spectroscopic Study

The ^{13}C NMR spectrum of isolated compound was recorded by using a 500 MHz spectrometer (125 MHz for ^{13}C) at Meijo University, Tempaku, Nagoya, Japan. The spectrum was recorded for the DMSO-d6 solution of sample. According to ^{13}C NMR spectrum, the number of carbons present in the pure compound (NNW-1) could be determined.

Identification of the Pure Isolated Compound (NNW-1) by Distortionless Enhancement by Polarization Transfer (DEPT) Spectroscopic Study

The DEPT spectrum of isolated compound was recorded by using a 500 MHz spectrometer (125 MHz for ^{13}C) at Meijo University, Tempaku, Nagoya, Japan. The spectrum was recorded for the DMSO-d6 solution of sample. This spectrum showed the presence of quaternary carbons, methane carbons, methylene carbons and methyl carbons.

Identification of the Pure Isolated Compound (NNW-1) by Electron Impact Mass Spectrometry (EI-MS) Study

Electron impact ionization mass spectrum (EI - mass) of the isolated compound was recorded by using mass spectrometer (JEOL model, Japan) at Meijo University, Tempaku, Nagoya, Japan. The molecular mass of the pure compound (NNW-1) could be determined by using EI mass spectral data.

Results and Discussion

Preliminary Phytochemical Tests for the Root and Stem of Vanda Thit-Kwa

The results of the phytochemical tests for the root and stem of Vanda Thit-Kwa are shown in Table 1.

According to the results shown in Table 1, the root and stem of Vanda-Thit-kwa contains chemical constituents tested except steroid.

Table 1 Results of Preliminary Phytochemical Test on Vanda Thit-Kwa

No.	Tests	Reagents	Observation	Results
1.	Alkaloid	Dragendorff's reagent	Orange ppt	+
		Wagner's reagent	Reddish brown ppt	+
2.	Flavonoid	conc: HCl, Mg tunning	Red colour solution	+
3.	Terpene	Acetic anhydride , conc: H_2SO_4, $CHCl_3$	Pink colour solution	+
4.	Steroid	Acetic anhydride, conc: H_2SO_4	No reaction	-
5.	Glycoside	10 % lead acetate	Yellow ppt	+
6.	Reducing Sugar	Benedict solution	Red ppt	+
7.	Polyphenol	10 % $FeCl_3$	Green Blue colour solution	+
8.	Saponin	Distilled water	Frothing	+
9.	Lipophilic	0.5N KOH+NaOH	Deep colour solution	+

(+) = Presence of constituents (-) = Absence of constituents

Antimicrobial Activities of the Root and Stem of Vanda-Thit-kwa

From Table 2, the ethyl acetate crude extract of the root and stem of VandaThit-kwa responds highest activities on selected microorganisms such as *Staphylococcus aureus, Pseudomonas aeruginosa*, *Bacillus pumilus*, *Candida albicans* and *Escherichia coli*. The n-hexane exctract shows no activity on all selected microorganisms. Hence, the ethyl acetate crude extract was selected for the isolation of pure organic compound. The ethyl acetate extract of the pure compound responds medium activities on selected microorganisms except *Bacillus subtilis*.

Table 2 Antimicrobial Activities of the Extracts of Vanda Thit-kwa and the Pure Compound (NNW-1)

Organisms	Inhibition Zone (mm)			
	Vanda Thit-kwa			Pure Compound
	***n*-hexane**	**EtOAc**	**EtOH**	**EtOAc**
Bacillus subtilis	-	-	-	-
Staphylococcus aureus	-	23 (+++)	18 (++)	15 (++)
Pseudomonas aeruginosa	-	23 (+++)	18 (++)	15 (++)
Bacillus pumilus	-	25 (+++)	19 (++)	-
Candida albicans	-	20 (+++)	17 (++)	-
Escherichia coli	-	25 (+++)	18 (++)	-

Agar well – 10 mm

(+) = Low activity (10 mm ~ 14mm)
(++) = Medium activity (15 mm ~ 19 mm)
(+ + +) = High activity (20 mm above)

Determination of Physicochemical Properties of the Pure Organic Compound (NNW-1)

One of the physical properties, i.e melting point of compound (NNW-1), was determined. The melting point was found to be 180-182 °C.

The FT IR spectrum (Figure 2 a) of the pure organic compound (NNW-1) was measured at the Department of Chemistry, University of Mandalay. The spectral data are described in Table 3.

Table 3 FT IR Assignments of Pure Organic Compound (NNW-1)

No.	Frequency (cm^{-1})	Assignments
1	3390	OH stretching vibration band
2	3045	sp^2 CH stretching vibration band
3	2941, 2887	sp^3 CH asymmetric and symmetric stretching vibration band
4	1722	C=O stretching vibration band
5	1606,1514, 1458	C=C ring skeletal stretching vibration of aromatic hydrocarbon
6	1269, 1155	C-C-O stretching vibration band
7	1118	C-O-C stretching vibration of ether group
8	1035	C-O stretching vibration of primary alcohol
9	977	-OH out of plane bending vibration band

The isolated pure organic compound (NNW-1) contains ether, alcohol, sp^2 hydrocarbon, sp^3 hydrocarbon and carbonyl groups, respectively, by applying the FT IR spectrum.

^{1}H NMR Spectral Data of the Pure Organic Compound (NNW-1)

The ^{1}H NMR spectrum (500 MHz) was described in (Figure 2 b). In accordance with this spectrum, the number of protons could be calculated as (27) in pure organic compound and their chemical shift values were shown in Table 4.

Table 4 ^{1}H NMR Spectral Data of the Pure Compound (NNW-1)

No.	Chemical Shift (ppm)	No. of protons	Proton Assignment
1	1.81	2	sp^3 CH_2
2	2.44	2	sp^3 CH_2
3	2.52	3	sp^3 CH_3
4	3.98	2	sp^3 CH_2
5	3.72	3	sp^3 -OCH_3
6	3.73	3	sp^3 -OCH_3
7	4.98	2	sp^3 CH_2
8	6.15	1	sp^2 CH
9	6.25	1	sp^2 CH
10	6.53	1	sp^2 CH
11	6.61	1	sp^2 CH
12	6.64	1	sp^2 CH
13	6.64	1	sp^2 CH
14	6.66	1	sp^2 CH
15	6.72	1	sp^2 CH
16	6.99	1	sp^2 CH
17	6.99	1	sp^2 CH
	Total	**27**	**$C_{17}H_{27}$**

^{13}C NMR and DEPT Spectral Data of the Compound (NNW-1)

The ^{13}C NMR (125 MHz) spectrum (Figure 2 c) indicated the number of carbons to be (24) in this compound. Also DEPT spectrum (Figure 2 d) gave information of variety of hydrocarbons. In accordance with these spectral data (Table 5), six quatrenary carbons, one carbonyl carbon, ten methine carbons, four methylene carbons and three methyl carbons could be detected.

Table 5 Variety of Carbons from ^{13}CNMR and DEPT Spectrum

No.	Chemical Shift (ppm)	Variety of carbon	No. of carbons	No. of protons
1	30.71	sp^3 CH_2	1	2
2	31.23	sp^3 CH_2	1	2
3	35.45	sp^3 CH_3	1	3
4	55.22	sp^3 -OCH_3	1	3
5	55.79	sp^3 -OCH_3	1	3
6	63.11	sp^3 CH_2	1	2
7	67.4	sp^3 CH_2	1	2
8	109.72	sp^2 CH	1	1
9	113.81	sp^2 CH	1	1
10	114.13	sp^2 CH	1	1
11	114.32	sp^2 CH	1	1
12	115.01	quaternary carbon	1	-
13	115.07	sp^2 CH	1	1
14	115.28	sp^2 CH	1	1

No.	Chemical Shift (ppm)	Variety of carbon	No. of carbons	No. of protons
15	115.28	sp^2 CH	1	1
16	117.28	quaternary carbon	1	-
17	121.19	sp^2 CH	1	1
18	129.0	sp^2 CH	1	1
19	129.0	sp^2 CH	1	1
20	130.49	quaternary carbon	1	-
21	131.8	quaternary carbon	1	-
22	154.9	quaternary carbon	1	-
23	156.2	quaternary carbon	1	-
24	172.0	sp^2 carbonyl carbon	1	-
		Total	**24**	**27**

HMQC Spectrum of the Pure Organic Compound (NNW-1)

The HMQC spectrum of this compound is shown in Figure 2 e. The directly attached proton-carbon coupling could be observed in this spectrum. The chemical shift value of protons and their related carbons were shown in Table 6.

Table 6 ^{1}H-^{13}C Correlation in HMQC Spectrum of the Compound (NNW-1)

No.	Chemical Shift carbon (δppm)	Chemical Shift Proton (δppm)	Assignments
1	30.71	1.81	sp^3 methylene carbon
2	31.23	2.44	sp^3 methylene carbon
3	35.45	2.52	sp^3 methyl carbon
4	55.22	3.72	sp^3 methoxy carbon
5	55.79	3.73	sp^3 methoxy carbon
6	63.11	3.98	sp^3 methylene carbon
7	67.4	4.98	sp^3 methylene carbon
8	109.72	6.25	sp^2 methine carbon
9	113.81	6.72	sp^2 methine carbon
10	114.13	6.15	sp^2 methine carbon
11	114.32	6.53	sp^2 methine carbon
12	115.01	-	quaternary carbon
13	115.07	6.66	sp^2 methine carbon
14	115.28	6.64	sp^2 methine carbon
15	115.28	6.64	sp^2 methine carbon
16	117.28	-	quaternary carbon
17	121.19	6.61	sp^2 methine carbon
18	129.0	6.99	sp^2 methine carbon
19	129.0	6.99	sp^2 methine carbon
20	130.49	-	quaternary carbon
21	131.8	-	quaternary carbon
22	154.9	-	quaternary carbon
23	156.2	-	quaternary carbon
24	172.0	-	carbonyl carbon

According to ^{1}H NMR spectrum (Figure 2 b), there are 27 protons in this compound. There are 24 carbons in the isolated compound according to ^{13}C NMR spectrum (Figure 2 e).

From DEPT spectrum of compound (NNW-1) 6 quaternary carbons, 1 carbonyl carbon, 10 methine carbons, 4 methylene carbons and 3 methyl carbons could be observed. So the partial molecular formula of compound (NNW-1) is $C_{24}H_{27}O$ and partial mass is 331 Da according to DEPT spectrum (Figure 2 d) and HMQC spectrum (Figure 2 e).

According to EI-MS spectrum (Figure 2 f), the molecular mass of pure organic compound (NNW-1) is 396 Da. So the remaining molecular mass is 65 Da. The FT IR spectrum of the isolated compound (Figure 2 a) shows that this compound contains the hydroxyl groups 3390 cm^{-1} and the ether groups 1118 cm^{-1}. The chemical shifts of carbons in the ^{13}C NMR spectrum show that the compound should contain one hydroxyl group and three ether oxygen atoms. So, the molecular formula of the pure isolated organic compound (NNW-1) is $C_{24}H_{28}O_5$.

Its hydrogen deficiency index is 11. The calculated molecular mass of the isolated pure organic compound is in agreement with the measured molecular mass of that compound (m/z = 396 Da).

Structural Elucidation of the Compound (NNW-1)

The structure elucidation of a pure bioactive organic compound could be done by applying ^{1}HNMR, splitting patterns and coupling constant (J values) of some prominent protons, FT IR, DEPT, DQF-COSY (Figure 2 g), HMQC, and HMBC (Figure 2 h) spectral data, respectively. The complete structure of the compound NNW-1 with the value of chemical shift of carbons and protons is as follows:

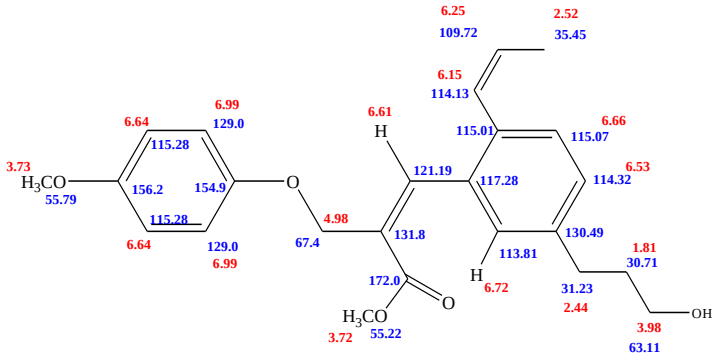

The IUPAC name of the compound NNW-1 is 3-(5- (3-hydroxypropyl)-2-propenyl-phenyl)-2-(4-methoxyphenoxy methyl)- acrylic acid methyl ester.

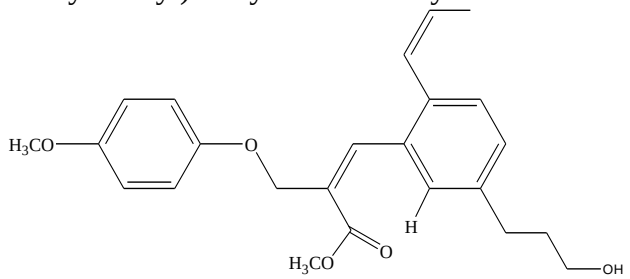

3-[5-(3-Hydroxy-propyl)-2-propenyl-phenyl]-2-(4-methoxy-phenoxymethyl)-acrylic acid methyl ester

EI -MS Fragmentation Behaviour of the Compound NNW-1

The removal of a water molecule and hydrogen radical from the pure compound NNW-1 produce the two fragment ions peaks at m/z 137 (77.87%) and at m/z 240 (90.27%) . The existence of this two fragments in EI-Mass spectrum is the good evidence for the real structure of the compound NNW-1.

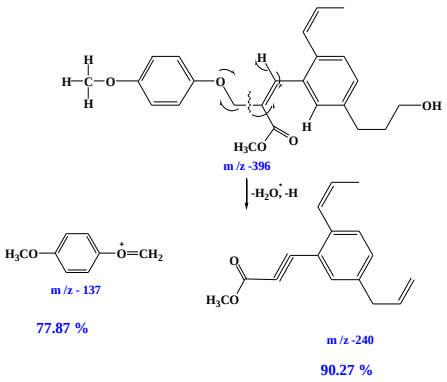

The proposed mechanisms for the formation of the base peak m/z 164 (100%) and the fragment ion peak at m/z 330 (66.37%).

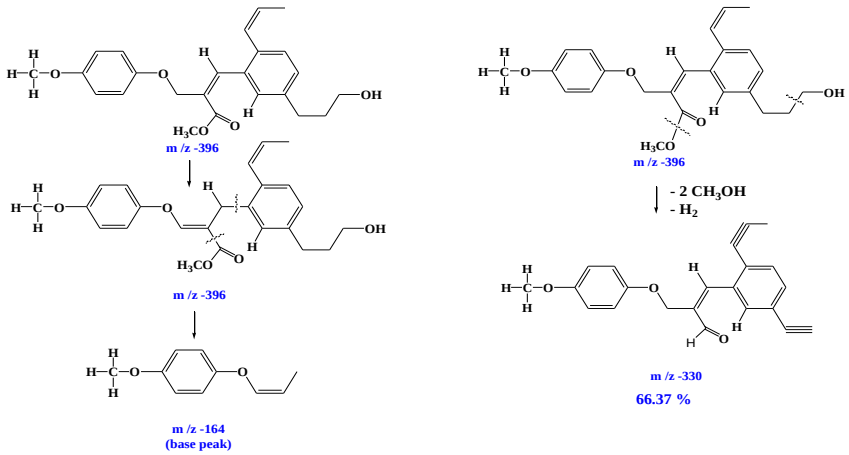

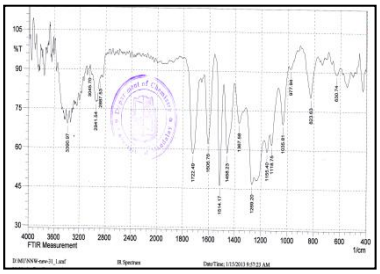

(a)

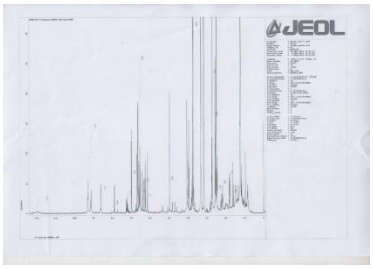

(b)

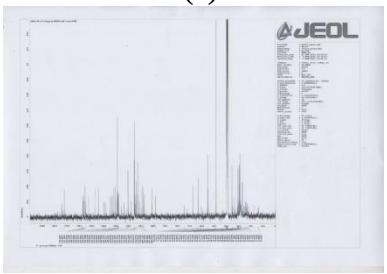

(c)

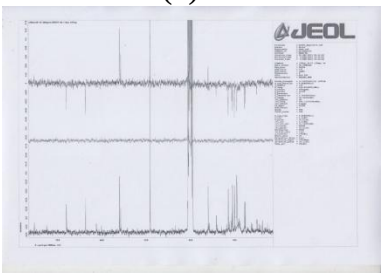

(d)

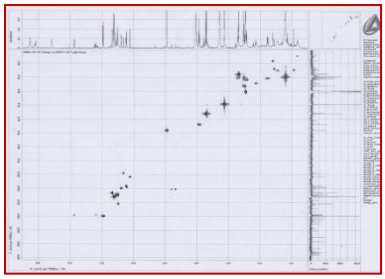

(e)

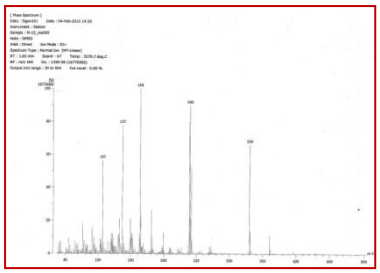

(f)

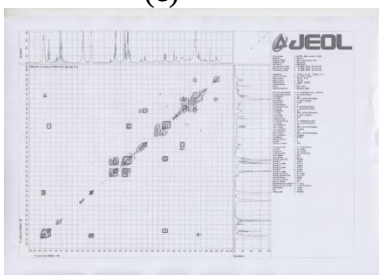

(g)

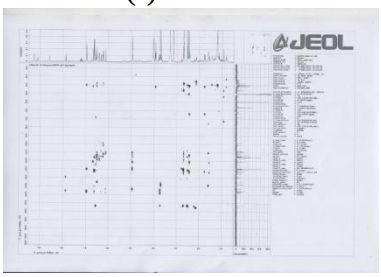

(h)

Figure 2 (a) FT IR Spectrum (b) ^{1}H NMR Spectrum (c) ^{13}C NMR Spectrum (d) DEPT Spectrum (e) HMQC Spectrum (f) EI-MS Spectrum (g) DQF-COSY Spectrum (h) HMBC Spectrum of the Pure Organic Compound (NNW-1)

Conclusion

The root and stem of *Vanda coerulea* Griff. was selected to determine the phytochemical constituents, to isolate the pure organic compound and to test the bioactivity of plant extract amd the pure organic compound. The root and stem of this plant contains alkaloids, glycosides, flavonoids, polyphenols, sugars, lipophilic,terpene, saponins and phenolic compounds respectively.

The pure organic compound (NNW-1) was isolated from the root and stem of Vanda Thit-Kwa by thin layer and column chromatographic separation techniques. The pure organic compound was obtained as amorphous. The melting point of this compound was found to be 180-182 °C. The yields percent of pure compound was 1.408 % (35.2 mg) based upon the EtOAc crude extract. The antimicrobial activities of the plant extracts and the pure isolated organic compound were tested by agar well diffusion method using six organisms. Although the EtOAc extract of plant was shown to possess high activity, the pure compound (NNW-1) was low activity on all selected organisms by agar well diffusion method.

The FT IR spectrum indicated that hydroxyl group (3390 cm^{-1}), the carbonyl group (1722 cm^{-1}), the ether group (1118 cm^{-1}) were presented in this compound. The mass spectroscopy displayed (M^{+}) at m/z 396 (corresponding to $C_{24}H_{28}O_5$) and significant peak at m/z 164 showed from the cleavage of the double bond exchange to more stable compound. The structure of compound NNW-1 could be confirmed by the combination these two fragments at m/z 137 and at m/z 240. The molecular formula determination was done by using FT IR, ^{1}HNMR, ^{13}CNMR, DEPT, HMQC spectroscopy and Mass spectrometry and its formula is $C_{24}H_{28}O_5$ and hydrogen deficiency index is 11. In addition, the complete structure of the organic compound (NNW-1) was elucidated by applying 1D and 2D NMR spectroscopy as well as EI-Mass spectrometry. The name of the isolated compoundis 3- (5- (3- hydroxypropyl)- 2- propenyl- phenyl)- 2- (4-methoxy phenoxy methyl)-acrylic acid methyl ester.

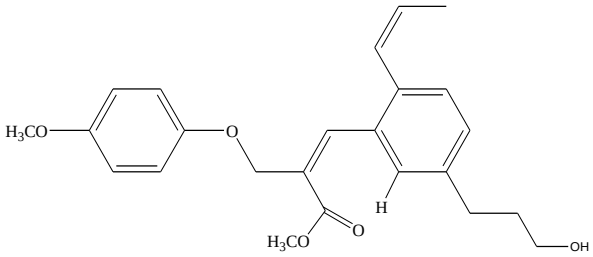

Acknowledgements

The authors wish to thank the Myanmar Academy of Arts and Science for accepting this research paper. Profound gratitude is specially expressed to Ministry of Education.

References

Finegold, S. M. and Martin, W. J. and Scolt, E .G. (1978). *Diagnostic Microbiology*. London: The C.V. Mosby Co.

Harbone, J. B. (1973). *Phytochemical Methods, a guide to modern techniques of plant analysis*. London: 4th ed, Chapman & Hall. pp. 182-192.

Kalinowski, H. O. Berger, S. and Braun, S. (1998). *Carbon 13 NMR Spectroscopy*, New York

Nichols, J. A. and Katiyar, S. K. (2010). Skin photoprotection by natural polyphenols: anti-inflammatory, antioxidant and DNA repair mechanisms. *Arch Dermatol Res*, vol. 302, pp. 71–83

Silverstein, R. M. and Webster, F. X. (1981). Spectrometric Identification of Organic Compound. New York: 4th ed, John Wiley and Sons, Inc.

Stable, E. (1965). *Thin Layer Chromatography*. New York: Academic Press, Inc.

Timothy, D. W. Claridge (1999). *High-Resolution NMR Techniques in Organic Chemistry*, New York: 1st ed, Elsevier Science

STRUCTURAL ELUCIDATION OF PURE ORGANIC COMPOUND ISOLATED FROM THE BARK OF *MYRICA NAGI* THUNB.

Tin Myo Khaing[1], Khaing Khaing Kyu[2], Thida Win[3]

Abstract

In this research work, one of the Myanmar medicinal plants, *Myrica nagi* Thunb. (Local name : Kat pha la) was selected for the chemical analysis. Preliminary detection of phytochemical compounds present in the bark of Kat pha la were carried out according to the test tube method. The percent composition of elements of the dry powder from the bark of Kat pha la was determined by using WDXRF spectrum. The antimicrobial activities of the crude extracts and the pure organic compound (TMK-1) were tested by agar well diffusion method using six organisms (*Bacillus subtilis*, *Staphylococcus aureus*, *Pseudomonas aeruginosa*, *Bacillus pumilus*, *Candida albicans* and *Escherichia coli*). The pure organic compound (TMK-1) was isolated from the bark of Kat pha la by thin layer and column chromatographic separation techniques. Melting point and phytochemical test of pure organic compound (TMK-1) were recorded. The molecular formula was determined by using FT-IR, ^{1}H NMR, ^{13}C NMR, DEPT, DQF-COSY, HMQC, HMBC spectroscopy and Mass spectrometry. In addition, the complete structure of terpene derivative compound (TMK-1) was elucidated by applying 1D and 2D NMR spectroscopic techniques as well as EI-Mass spectrometry. Moreover the conformational structure of isolated compound (TMK-1) was examined by using ^{1}H NMR spectrum, NOESY spectrum and the model study.

Keywords: *Myrica nagi* Thunb., Kat pha la, WDXRF, Chromatographic methods

Introduction

Plants, especially used in Ayurveda can provide biologically active molecules and lead structures for the development of modified derivatives with enhance activity and reduced toxicity. In some cases, the crude extract of medicinal plants may be used as medicaments. On the other hand, the isolation and identification of the active principles and elucidation of the mechanism of action of a drug is of paramount importance. Hence, works in both mixture of traditional medicine and single active compounds are very important. Where the active molecule may be obtained from the cultivation of plant material. The scientific study of the traditional medicines, derivation of drugs through bio-prospecting and systematic conservation of the concerned medicinal plants are thus of great importance (Fransworth and Soejarto, 1985).

In this research work, One Myanmar traditional indigenous plant, Kat pha la belongs to *Myrica nagi* Thunb. was chemically analyzed for new source of compound in this field (Figure 1). The bark of Kat pha la is used as an antirheumatic, an antiseptic, aromatic, an astringent, carminative, ophthalmic and a stimulant in indigenous medicine. It is used as a remedy for various body disorders such as liver diseases, fever, asthma, anaemia, chronic dysentery, ulcer and inflammation (Rastogi and Mehrotra, 1985).

Firstly, pre-phytochemical screening and antimicrobial activities of crude extract of *Myrica nagi* Thunb. were carried out. As an experimental work, a pure organic compound (TMK-1) could be isolated from the bark of Kat pha la by using thin layer and column chromatographic methods.

Its structure could be elucidated by using advanced spectroscopic methods, such as FT IR, ^{1}HNMR (500 MHz), ^{13}CNMR (125 MHz), DEPT, DQF-COSY, HMQC and HMBC spectroscopy and EI-MS spectrometry. The conformational analysis of pure organic compound

[1] Dr, Lecturer, Department of Chemistry, Monywa University.
[2] Dr, Professor, Department of Chemistry, University of Mandalay.
[3] Dr, Rector, University of Mandalay.

(TMK-1) was determined by using splitting pattern and coupling constants of proton in ^{1}H NMR spectrum, NOESY spectroscopy and modern study.

Figure 1 Tree, leaves, flowers, and bark of Kat pha la

Materials and Methods

Sample Collection

The bark of Kat pha la for experiment was collected from Pyinsa Village, Pyin Oo Lwin Township, Mandalay Region, Myanmar. The samples were cut into small pieces and allowed to air dry. Then, the dried species were stored in a well-stoppered bottle and used throughout the experiment.

Preliminary Phytochemical Test on the Sample

Preliminary detection of phytochemical compounds present in bark of *Myrica nagi* Thunb. was carried out according to the test tube methods (Harborne,1993).

Elemental content of Sample

The elements present in dried powdered sample were determined by WDXRF (Wave Dispersive X-ray Fluorescence) spectrometer (Rigaku supermini-200).

Examination of Antimicrobial Activity

The antimicrobial activity of crude extracts of sample was examined using agar well diffusion method.

Extraction and Isolation of the Pure Organic Compounds

Air dried sample (1000 g) was percolated with 2500 mL of 95 % ethanol for about one month. Percolated solution was filtered off and the filtrate was evaporated at room temperature. The ethanol crude extract was re-extracted with ethylacetate (300 mL) and the filtrate was also evaporated ethylacetate extract (2.02 g) was obtained. The crude extract was separated by column chromatography applying SiO_2 (70-230 mesh) as an adsorbent with n-hexane and ethylacetate solvent system. Totally 158 fractions were obtained. Each fraction was checked by TLC with suitable solvent system. The fractions with the same R_f value were combined to give five combined fractions. The fraction D shows nearly one spot on TLC plate and it was the major constituent. So, it was further re-chromatographed by using the same procedure as described above. All fractions were again checked by TLC and UV detector. Four combined fractions were obtained and evaporated at room temperature. The fraction IV shows only one spot on TLC plate and under UV detector. Finally, 14.02 mg of the pure organic compound (amorphous form) was obtained. This compound was sent to Japan for measurement of invaluable spectroscopic data.

Determination of Melting Point and Phytochemical Screening of the Pure Organic Compound (TMK-1)

A few white amorphous form of pure organic compound (TMK-1) were inserted into the capillary tube and the melting point was determined by using the melting point apparatus. The phytochemical test was carried out to identify the class of pure compound (TMK-1). A mixture of few drops of concentrated sulphuric acid, 1 mL of acetic anhydride and 2.5 mL of chloroform was added to ethanol extract of pure organic compound (TMK-1).

Determination of Antimicrobial Activities of the Pure Organic Compound (TMK-1)

Antimicrobial activities of pure compound (TMK-1) were tested by agar well diffusion method at Pharmaceutical Research Department (PRD).

Results and Discussion

Preliminary Phytochemical Examination of Kat pha la

The results of preliminary phytochemical test of the bark of Kat pha la are tabulated in Table 1.

Table 1 Preliminary Phytochemical Examination of Kat pha la

No	Constituent	Reagent used	Observation	Remark
1	Alkaloid	Mayer's reagent	White ppt	+
2	Flavonoid	Conc: HCl, Mg coil	Pink colour solution	+
3	Terpenoid	$CHCl_3$,Conc:H_2SO_4,$(CH_3CO)_2O$	Brown red solution	+
4	Steroid	$(CH_3CO)_2O$, Conc:H_2SO_4	Green colour solution	+
5	Glycoside	NaOH	Yellow colour solution	+
6	Reducing sugar	Benedict's solution	Brick red ppt	+
7	Tannin	1% $FeCl_3$, Dil:H_2SO_4	Yellowish brown ppt	+
8	Phenolic	10% $FeCl_3$	Green colour solution	+
9	Saponin	Distilled water	Frothing	+

(+) = presence of the constituents (-) = absence of the constituents

According to the preliminary phytochemical test, all varieties of phytochemical constituents were present in the bark of Kat pha la.

Elemental Analysis of Kat pha la by WDXRF

From the WDXRF spectrum, the percent composition of elements of the dried powder from the bark of Kat pha la could be determined. By WDXRF spectral data (Table 2), the total number of elements is 12 elements in the bark of Kat pha la. Among them, calcium, sodium and potassium were found as major elements. Iron, silicon and chlorine were also found as minor elements. Magnesium and other elements were trace elements. The order of decreasing concentration of the elements were Ca > Na > K > Fe > Si > Cl > Mg > Mn > S > Al > P> Sr.

Table 2 Relative Abundance of the Dried Powder from Bark of Kat pha la

No	Element	Relative abundance (%)
1	Na	18.3
2	Mg	1.33
3	Al	0.739
4	Si	4.71
5	P	0.45
6	S	1.25
7	Cl	2.11
8	K	9.29
9	Ca	24.6
10	Mn	1.28
11	Fe	5.53
12	Sr	0.101

Antimicrobial Activities of Bark of Kat pha la

The results of antimicrobial activity of the sample are shown in Table 3.

Table 3 Antimicrobial activities of one Myanmar indigenous Medicinal Plant (Kat pha la)

Sample	Solvents	Inhibition Zone Diameters (mm) of Various Crude Extracts Against Different Microorganisms					
		B.Subtilis	***S.aureus***	***P.aeruginosa***	***B.pumilus***	***C.albicans***	***E.coli***
Kat pha la (bark)	n-hexane	–	–	–	–	–	–
	$CHCl_3$	14 (+)	15 (+)	13 (+)	–	–	–
	Acetone	15 (++)	20 (+++)	14 (+)	19 (++)	20 (+++)	15 (++)
	EtOAc	23 (+++)	25 (+++)	25 (+++)	25 (+++)	28 (+++)	20 (+++)
	EtOH	18 (++)	19 (++)	14 (+)	20 (+++)	20 (+++)	20 (+++)

Agar well-10mm
10mm ~14mm (+)
15mm ~19mm (++)
20 mm above (+++)

I = *Bacillus subtilis*
II = *Staphylococcus aureus*
III = *Pseudomonas aeruginosa*
IV = *Bacillus pumilus*
V = *Candida albicans*
VI = *Escherichia coli*

The ethylacetate extract of bark of Kat pha la responded high activities on all tested organisms. In contrast, n-hexane extract did not show activity on all tested organisms. Ethanol extract showed high activities on *Bacillus pumilus, Candida albicans* and *Escherichia coli* and medium activities on *Bacillus subtilis* and *Staphylococcus aureus* and low activity on *Pseudomonas aeruginosa*. Acetone extract showed high activities on *Staphylococcus aureus* and *Candida albicans* and medium activities on *Bacillus subtilis, Bacillus pumilus* and *Escherichia coli* and low activity on *Pseudomonas aeruginosa*. Moreover, chloroform extract showed low activities on *Bacillus subtilis, Staphylococcus aureus* and *Pseudomonas aeruginosa* and did not show activity on *Bacillus pumilus, Candida albicans* and *Escherichia coli.* So, pure organic

compound (TMK-1) was isolated from the ethylacetate extract of bark of Kat pha la applying separation techniques.

Antimicrobial Activities of the Pure Compound (TMK-1)

The results of the antimicrobial test relevant to different types of organisms are tabulated in Table 4.

Table 4 Antimicrobial Activities of Pure Organic Compound (TMK-1)

No	Types of Organisms	Inhibition zone diameter (mm)
1.	*Bacillus subtilis*	11 (+)
2.	*Staphylococcus aureus*	12 (+)
3.	*Pseudomonas aeruginosa*	13 (+)
4.	*Bacillus pumilus*	11 (+)
5.	*Candida albicans*	13 (+)
6.	*Escherichia coli*	11 (+)

In accordance with Table 3, the pure organic compound (TMK-1) responds low activity on all tested microorganisms.

Determination of Melting Point and Phytochemical Testing for the Pure Organic Compound (TMK-1)

The melting point was found to be 239-241°C. Pure compound (TMK-1) showed positive test for terpenoid. So it may be terpenoid compound.

Molecular Formula Determination of the Pure Organic Compound (TMK-1)

Molecular formula of pure organic compound (TMK-1) could be determined by using FT-IR, ^{1}H NMR (500 MHz), ^{13}C NMR (125MHz), DEPT, DQF-COSY, HMQC, HMBC and EI-mass spectral data. (Crews *et al.,* 1998; Morrison and Boyd, 2000; Silverstein and Webster, 1998)

Infrared Spectrum of the Pure Organic Compound (TMK-1)

The FT IR spectrum of isolated pure organic compound (TMK-1) was measured at the Department of Chemistry, University of Mandalay. It is described in Figure 2 a.

According to FT IR spectral data, compound consists of –OH stretching vibration of alcohol group, –CH stretching vibration of alkenic group, unsymmetrical and symmetrical –CH stretching vibration of sp^3 hydrocarbons, –C=C stretching vibration of alkenic group,–CH in plane bending vibration of allylic hydrocarbon, -CH out of plane bending vibration of gem dimethyl group, –C-C-O stretching vibration of alcohol group and –CH out of plane bending vibration of trans or E and cis or Z alkenic groups respectively (Table 5).

Table 5 FT IR Assignments of Pure Organic Compound (TMK-1)

Absorption band (cm^{-1})	Assignments
3448	–OH stretching vibration
3066	–CH stretching vibration of alkenic group
2931, 2877	sp^3CH stretching vibration of asymmetric and symmetric hydrocarbon
1643	–C=C stretching vibration of alkenic group
1454	–CH in plane bending vibration of allylic group
1373	–CH out of plane bending vibration of gem-dimethyl group
1191, 1091	–C–C–O stretching vibration of alcohol group
929, 798	–CH out of plane bending vibration of trans or E and cis or Z alkenic group

^{1}H NMR Spectrum of Pure Organic Compound (TMK-1)

The ^{1}H NMR spectrum (500 MHz) is described in Figure 2 b. In accordance with this spectrum, the number of protons could be calculated as (50) in pure organic compound (TMK-1).

^{13}C NMR and DEPT Spectral Data of the Pure Organic Compound (TMK-1)

The ^{13}C NMR (125 MHz) spectrum (Figure 2 c) indicated the number of carbons to be (30) in the pure organic compound (TMK-1). Also DEPT spectrum (Figure 2 d) gave information of variety of hydrocarbons.

According to ^{1}H NMR (Figure 2 b), ^{13}C NMR (Figure 2 c), DEPT (Figure 2 d) and HMQC (Figure 2 e) spectral data, the partial molecular formula of pure compound (TMK-1) is $C_{30}H_{49}$ and partial molecular mass is 409 Da.

But the molecular mass of pure organic compound (TMK-1) is 426 Da according to EI-MS spectrum (Figure 2 f). So, the remaining molecular mass is 17 Da. The FT IR spectrum of the isolated compound (Figure 2 a) shows that this compound should contain one hydroxyl group. It is confirmed by FT IR spectrum in which the hydroxyl group is found to be at (3448 cm^{-1}). Due to the remaining molecular mass 17 Da and the chemical shifts of carbons and protons in their respective spectra, the pure compound should contain one hydroxyl group. So, the molecular formula of the pure isolated organic compound (TMK-1) would be $C_{30}H_{50}O$.

$$\text{Hydrogen Deficiency Index} = C - \frac{H}{2} + 1$$

$$= 30 - \frac{50}{2} + 1 = 6$$

Its hydrogen deficiency index is 6. The calculated molecular mass of the isolated pure organic compound is in agreement with the measured molecular mass of that compound (m/z = 426 Da).

Confirmation of Molecular Formula of Compound (TMK-1)

Molecular formula of compound (TMK-1) could be confirmed by DEPT spectrum (Figure 2 d) and FT IR spectrum (Figure 2 a).

Table 6 Results Given by DEPT and FT IR Spectral Data of Compound (TMK-1)

Assignments	No. of Carbon	No. of Proton	No. of Oxygen
DEPT Spectrum			
-Six sp^3 quaternary carbons	6	-	-
-Four sp^3 methine carbons	4	4	-
-Ten sp^3 methylene carbons	10	20	-
-Eight sp^3 methyl carbons	8	24	-
-One sp^2 methine carbon	1	1	-
-One sp^2 quaternary carbon	1	-	-
FT IR Spectrum			
-One –OH group	-	1	1
Complete Molecular formula	C_{30}	H_{50}	O

Structure Elucidation of Pure Organic Compound (TMK-1)

The structure of pure organic compound (TMK-1) could be elucidated by applying ^{1}HNMR, DEPT, HMQC, DQF-COSY and HMBC respectively.

In DQF-COSY spectrum (Figure 2 g), the correlation between sp^3 methylene protons (δ 1.53 and 1.59 ppm) and sp^3 methine proton (δ 3.19 ppm) gives the following fragment (1). In HMQC spectrum (Figure 2 e), the sp^3 methine proton (δ 3.19 ppm) directly attaches to the carbon (δ 79.06 ppm). The chemical shifts of these proton and carbon show that this carbon should be carbinol carbon.

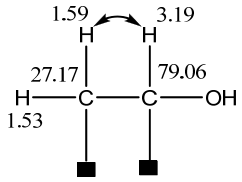

Fragment (1)

In HMBC spectrum (Figure 2 h), the β ^{1}H- ^{13}C long range signal of sp^3 methyl protons (δ 0.93 ppm) with sp^3 methine carbon (δ 55.57 ppm) gives the fragment (2) including the six- member ring (A).

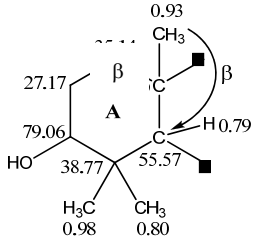

Fragment (2)

In HMBC spectrum (Figure 2 h) the β ^{1}H-^{13}C long range coupling between the sp^3 methyl protons (δ 0.93 ppm) and sp^3 quaternary carbon (δ 38.03 ppm) gives the fragment (3) including six member ring (B).

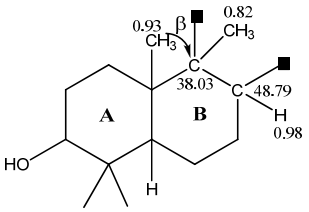

Fragment (3)

The correlations between the sp^3 methylene protons at δ (1.62 and 1.91 ppm) and sp^2 methine proton at (δ 5.52 ppm) in DQF- COSY spectrum (Figure 2 g) give rise to the fragment (4).

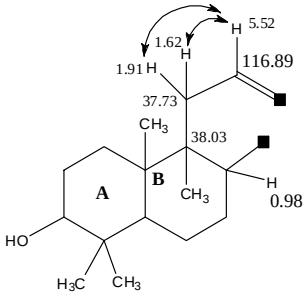

Fragment (4)

The β ^1H-^{13}C long range correlation of sp^3 methyl protons at (δ 0.90 ppm) and sp^2 quaternary carbon at (δ 158.12 ppm) in HMBC spectrum (Figure 2 h) produces the fragment (5) including six member ring (C).

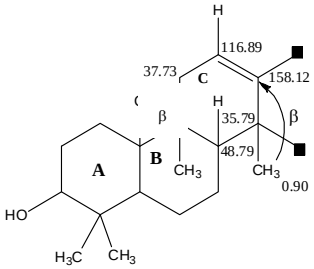

Fragment (5)

The β ^1H-^{13}C long range correlation of sp^3 methyl protons at (δ 1.08 ppm) and sp^2 quaternary carbon at (δ 158.12 ppm) in HMBC spectrum (Figure 2 h) gives the following fragment (6) including ring D.

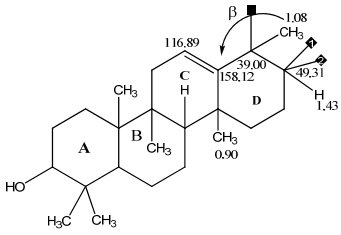

Fragment (6)

Furthermore, the β ^1H- ^{13}C long range signal of sp^3 methyl protons (δ 0.91 ppm) with this sp^3 methine carbon (δ 49.31 ppm) in HMBC spectrum (Figure 2 h) gives the fragment (7) closing the six member ring (E) as follows. It could be confirmed by the correlations between sp^3 methylene proton at (δ 1.64 ppm) with sp^3 methine carbon at (δ 49.31 ppm) in HMBC spectrum (Figure 2 h).

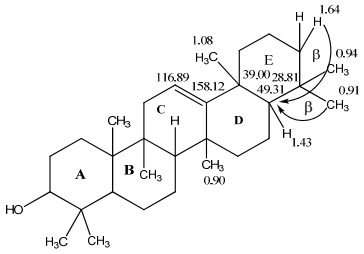

Fragment (7)

The complete planar molecular structure of the isolated pure organic compound (TMK-1) could be expressed as follows and the name of the isolated compound is (3S, 4aR, 6aR, 6bS, 8aS, 12aS, 14aS, 14bS)- 4, 4, 6b, 9, 9, 12a, 14a, 14b-octamethyl-1, 2, 3, 4, 4a, 5, 6, 6a, 6b, 7, 8, 8a, 9, 10, 11, 12, 12a, 14, 14a, 14b- icosahydropicen- 3- ol.

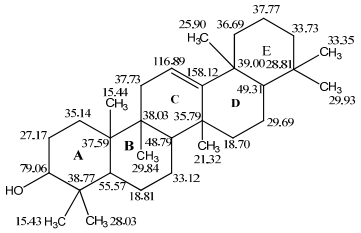

Mass Fragmentation Behaviour of the Pure Organic Compound (TMK-1) (Porter, 1971)

The structure of the compound (TMK-1) could be confirmed by EI-MS fragmentation behavior. The proposed mechanisms of the formation of fragment ion peaks formed from compound (TMK-1) (Figure 2 f) could be described as follows.

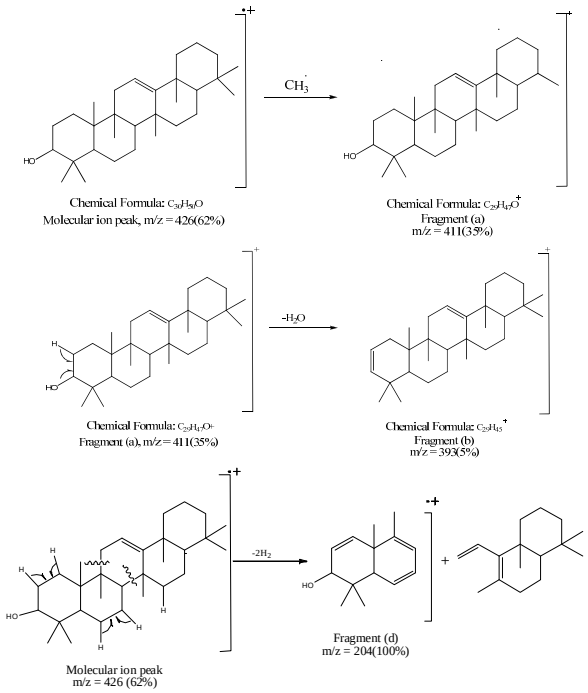

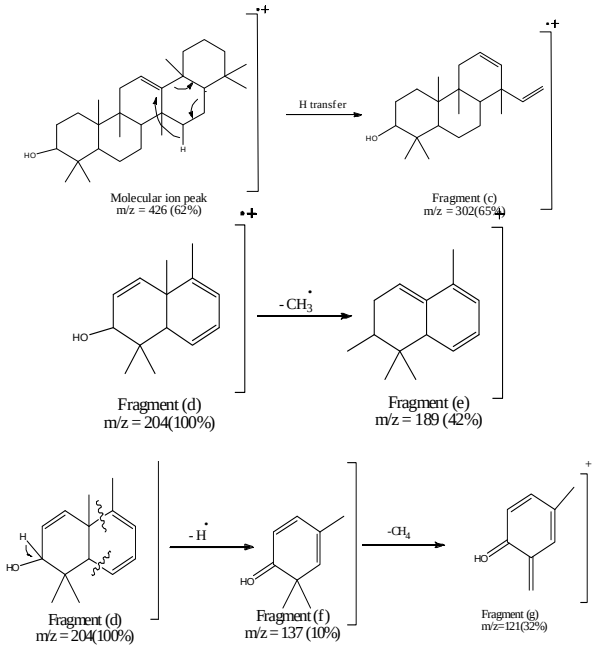

Conformational Analysis of the Pure Organic Compound (TMK-1)

The conformational analysis of pure organic compound (TMK-1) was assigned on the basis of the splitting patterns and the coupling constants of the protons in ^{1}H NMR spectrum, NOESY spectral data and the model study.

The splitting pattern of the carbinol proton at δ 3.19 ppm is double doublet and its J values are 13.5 and 5.0 Hz respectively. It is coupled with the axial proton (δ1.53 ppm) and the equatorial proton (δ 1.59 ppm). So, its coupling constant values show that this carbinol proton is at axial position (below the plane) giving the following chair like conformer of ring (A).

3.19 ppm,
dd, J = 13.5,5.0 Hz

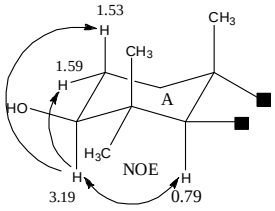

It is confirmed by the medium NOE with the axial Junction methine proton (δ 0.79 ppm) in NOESY spectrum (Figure 2 i) show that the junction methine proton is below the plane showing the chair conformer of ring (A).

The chair conformer of ring (B) was assigned by the model study. It was confirmed by the medium NOE correlation between axial junction methine proton (ring A and B) (δ 0.79 ppm) and the other junction methyl protons (ring B and **C)** (δ 0.82 ppm) in NOESY spectrum (Figure 2 i) showing the chair conformer of ring (B).

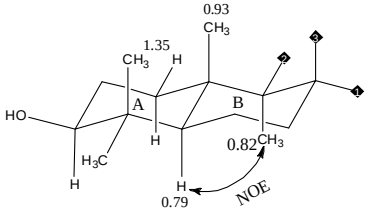

The chair conformer of ring (B) and the boat like conformer of ring (C) were assigned by the model study. The splitting pattern of the sp^2 methine proton at (δ 5.52 ppm) is double doublet and its J values are 10.0 and 5.0 Hz respectively. It is coupled with the axial proton (δ 1.62 ppm) and the equatorial proton (δ 1.91 ppm). So, its coupling constant values show that this sp^2 methine proton is at axial position (above the plane) giving the following boat conformer of ring (C).

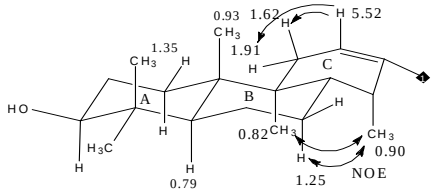

It was confirmed by the medium NOE correlation between the junction methyl protons (rings B and C) (δ 0.82 ppm) and (rings C and D) (δ 0.90 ppm) which is correlated with methylene proton (δ 1.25 ppm) (small NOE) in NOESY spectrum (Figure 2 i) showing all these protons are below the plane. The chair conformer of ring (D) was assigned by the modern study. The medium NOE between the junction methyl protons (ring C and D) (ring D and E) (δ 0.90 ppm and 1.08 ppm) and one of methylene protons (δ 0.95 ppm) in NOESY spectrum (Figure 2 i) show that all these protons are under the plane of their respective ring.

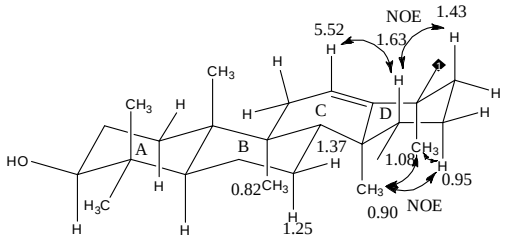

It was confirmed by the cross peak between the sp^2 methine proton in ring C (δ 5.52 ppm) and axial methylene proton (δ 1.63 ppm) which is correlated with junction methine proton (δ 1.43 ppm) (by medium NOE) in NOESY spectrum (Figure 2 i) showing all these protons are upper the plane.

The chair conformer of ring (E) was assigned by the modern study. It is confirmed by the junction methine proton (ring D and E) (δ 1.43 ppm) is medium NOE with axial methylene proton (δ 1.54 ppm) which is correlated with equatorial methyl protons (δ 0.94 ppm) showing all these protons are upper the plane in NOESY spectrum (Figure 2 i).

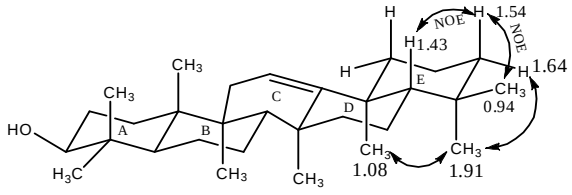

In addition, the junction methyl protons (ring D and E) (δ 1.08ppm) is medium NOE with axial methyl protons (δ 0.91 ppm) which is correlated with equatorial methylene proton (δ 1.64 ppm) (by small NOE) showing all these protons are under the plane in NOESY spectrum (Figure 2 i).

The complete conformational structure of the isolated pure organic compound (TMK-1) and its absolute configuration are shown below.

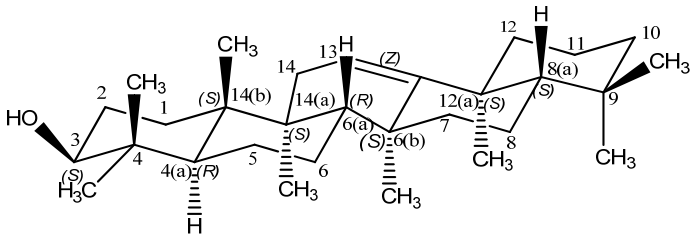

The relative conformation of eight chiral carbons could assigned as C_3 (S), $C_{4(a)}$ (R), $C_{6(a)}$(R), $C_{6(b)}$ (S), $C_{8(a)}$ (S), $C_{12(a)}$ (S), $C_{14(a)}$ (S), $C_{14(b)}$ (S) respectively.

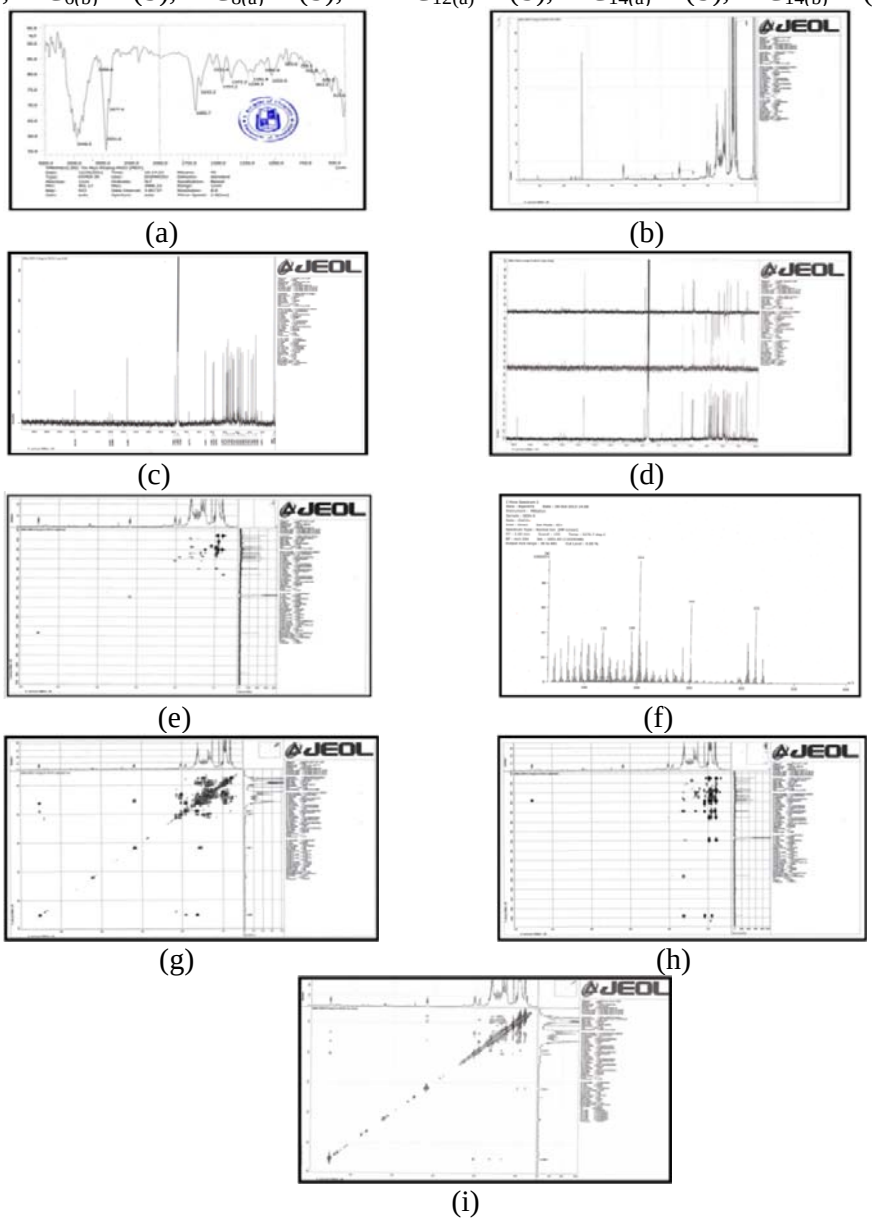

Figure 2 (a) FT IR, (b) ^{1}HNMR, (c) ^{13}C NMR, (d) DEPT, (e) HMQC,
(f) EI Mass, (g) DQF-COSY and (h) HMBC
(i) NOESY-Spectrums of the Pure Organic Compound (TMK-1)

Conclusion

In this research work the bark of *Myrica nagi* Thunb. was selected for the chemical analysis. The bark of Kat pha la contains alkaloid, flavonoid, terpenoid, reducing sugar, glycoside, tannin, phenolic and saponin compounds. The element compositions from the bark of Kat pha la were detected by using WDXRF spectrum. From the WDXRF spectral data, the total number of 12 elements was detected in the bark of Kat pha la. Among them**,** Ca, Na and K were found as major elements. Fe, Si and Cl were also found as minor elements. Mg and other elements were trace elements.

In addition, antimicrobial activities of the crude extracts and the pure organic compound (TMK-1) were tested by agar well diffusion method using six organisms (*Bacillus subtilis*, *Staphylococcus aureus*, *Pseudomonas aeruginosa*, *Bacillus pumilus*, *Candida albicans* and *Escherichia coli*). Particularly, the ethylacetate extract of bark of Kat pha la showed high activities on all tested organisms.

Moreover, the pure organic compound (TMK-1) could be isolated by thin layer and column chromatographic separation techniques. The pure organic compound (TMK-1) was obtained as pale white amorphous compound. The yield percent of the isolated compound is 0.694% based upon the EtOAc crude extract. Phytochemical test for pure compound (TMK-1) was done and it showed the positive test for terpenoid. The melting point of this compound was determined and found to be 239-241 °C. This pure compound (TMK-1) was to possess low activity on all tested organism.

Furthermore, the FT IR spectrum indicated the presence of hydroxyl group at 3448 cm^{-1}. The mass spectroscopy displayed (M^+) at m/z 426. Its formula is $C_{30}H_{50}O$ and hydrogen deficiency index is 6. The ^1H NMR spectrum reflected eight methyl groups, a hydroxyl methylene group and one olefinic proton. Finally, the complete structure analysis of the isolated pure compound (TMK-1) could be assigned by NOESY and ^1H NMR spectra. The conformational structure of pure compound (TMK-1) contains the three chair like conformer of ring A, B and D and boat conformer of ring C. The name of the pure organic compound (TMK-1) is (3S, 4aR, 6aR, 6bS, 8aS, 12aS, 14aS, 14bS)- 4, 4, 6b, 9, 9, 12a, 14a, 14b-octamethyl-1, 2, 3, 4, 4a, 5, 6, 6a, 6b, 7, 8, 8a, 9, 10, 11, 12, 12a, 14, 14a, 14b- icosahydropicen- 3- ol.

In this plant sample, valuable phytochemical compounds were found and the ethylacetate extract of this plant sample give high activity on all selected organisms. Therefore, this plant sample is suitable for medicinal purposes, further studies will be required.

CONFORMATIONNAL STRUCTURE OF PURE ORGANIC COMPOUND (TMK-1)

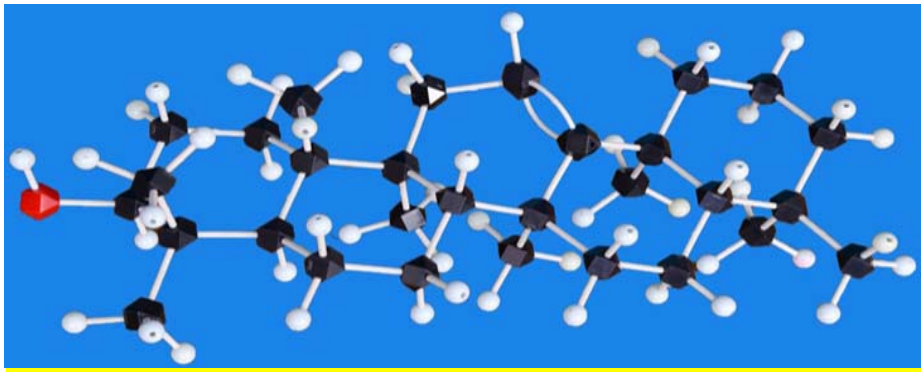

(3S, 4aR, 6aR, 6bS, 8aS, 12aS, 14aS, 14bS)- 4, 4, 6b, 9, 9, 12a, 14a, 14b-octamethyl-1, 2, 3, 4, 4a, 5, 6, 6a, 6b, 7, 8, 8a, 9, 10, 11, 12, 12a, 14, 14a, 14b- icosahydropicen- 3- ol

Acknowledgements

The authors wish to thank the Myanmar Academy of Arts and Science for accepting this research paper. Profound gratitude is specially expressed to Ministry of Myanmar.

References

Crews, P. Rodriguez, J. and Jaspars, M. (1998). *Organic Structure Analysis*, New York: Oxford University Press.

Farnsworth, N. R. and Soejarto, D.D. (1985). "Potential Consequence of Plant Extinction in the United States on the Current and Future Availability of Prescription Drugs". *Econ. Bot*. vol. 39 (3), p.231-240.

Harborne, J.B. (1993). *Phytochemical Methods, A Guide to Modern Techniques of Plant Analysis*. U.S.A: Chapman and Hall Ltd.

Morrison, R.T. and Boyd, R.N. (2000). *Organic Chemistry*, New York: 6th Edition.

Porter, Q.N. (1971). *Mass Spectrometry of Heterocyclic Compounds*, New York: John Wiley and Sons, Inc.

Rastogi, R.P. and Mehrotra, B.N. (1993). *Compendium of Indian Medicinal Plants*. New Dalhi: CDRI, Lucknow and CSIR Publication, pp. 490-492.

Silverstein, R.M. and Webster, F.X. (1998). *Spectrometric Identification of Organic Compound*, New York: 6th edition, John Wiley and Sons, Inc.

DETERMINATION ON THE OPTIMUM CONDITION FOR THE PREPARATION OF CELLULOSE ACETATES FROM MAIZE STRAW POWDER, WHEAT STRAW POWDER AND SAWDUST POWDER

Yi Yi Lwin[1], Thida Kyaw[2], Yi Yi Myint[3]

Abstract

In this research, the optimum condition for the preparation of cellulose acetate from maize straw powder, wheat straw powder and sawdust powder could be determined by four different acetylation methods. Firstly, the three sample powders were dewaxed. In the preparation of cellulose, the dewaxed sample powders were refluxed only with 15% NaOH for 9 h. Then the delignified sample masses were bleached with 5% sodium hypochloride solution for 24 h and neutralized with 5% acetic acid and water. The resultant neutral cellulosic pulps were acetylated with acetic anhydride and acetic acid in the presence of concentrated sulphuric acid as a catalyst using magnetic stirrer in method 1. In method 2, the apparatus used is ultrasonic cleaner instead of magnetic stirrer. In the third method, acetylation was carried out by using one more solvent (toluene) with ultrasonic cleaner. In the fourth method, solvents used were similar as in method 3 but with different catalyst (perchloric acid) instead of using sulphuric acid. The yield percentages of three cellulose acetates were determined and compared and then identified by FT IR spectroscopic analysis. At the same time, more reliable method that gave a good yield % and more purified product was observed.

Keywords: cellulose, cellulose acetate**,** acetylation, FT IR analysis

Introduction

Cellulose acetate is the acetate ester of cellulose. It was first prepared in 1865. Cellulose acetate was derived from cellulose by initially deconstructing wood pulp into the purified fluffy white cellulose. The cellulose is reacted with acetic acid and acetic anhydride in the presence of sulphuric acid to form cellulose acetate. The anhydroglucose unit is the fundamental repeating structure of cellulose and has three hydroxyl groups which can react to form acetate esters. The most common form is cellulose di-acetate. Cellulose triacetate is a chemical compound produced from cellulose and a source of acetate esters, typically acetic anhydride. It is commonly used for the creation of fibers and film base. It is chemically similar to cellulose acetate (diacetate). Its distinguishing characteristic is that in triacetate, at least "92 % of the hydroxyl groups are acetylated. In manufacturing process, the cellulose is completely acetylated; whereas in normal cellulose acetate or cellulose diacetate, it is only partially acetylated. Cellulose triacetate is significantly more heat resistant than cellulose diacetate. Cellulose diacetate is a synthetic polymer made by treating cellulose with acetic anhydride and acetic acid. It consists of two acetyl functional groups on each unit of D-anhydroglucopyranose of the cellulose molecule. Cellulose acetate is used as a film base in photography, as a component in some coatings, as a frame material for eyeglasses, as a synthetic fiber in the manufacture of cigarette filters and playing cards and in textiles, as a substrate for motion picture camera film, and as ingredient in sheet and molded objects etc. (Morgan E., 2013)

Cellulose is an organic compound with the formula $(C_6H_{10}O_5)_n$, a polysaccharide consisting of a linear chain of several hundred to many thousands of β (1-4) linked D-glucose units. It is a natural polymer comprising at least one third of the vegetable materials in the world and it is present in materials such as wood, seeds and agricultural wastes. Cellulose can be produced from sources of lignocellulosic materials such as corn stalks and wheat straw and rice

[1] Lecturer, Daw, Department of Chemistry, Myingyan Degree College
[2] Dr, Associate Professor, Department of Chemistry, Yadanabon University
[3] Dr, Professor and Head, Department of Chemistry, University of Mandalay

straw, agricultural byproducts such as corn fiber, rice hulls etc., and energy crops such as high fiber sugarcane. (Updegraff, D. M., 1969) Lignocellulosic materials are heterogeneous complexes composed of polymers (cellulose and hemi-cellulose) and lignin. They can be used to produce cellulose, such as wood (sawdust), cotton, sugarcane, sisal and others (Piotrowski S., Carus M., 2011) The pulping method used to isolate cellulose which consists of delignification and bleaching. Cellulose is insoluble in water and easily separated by pulping process from the other constituents of a plant (Crowford R. L., 1981**).**

In this research, the preparation of cellulosic pulp from maize straw powder, wheat straw powder and sawdust powder had been performed by pulping process and determination of the optimum condition for the preparation of cellulose acetates by acetylation with four different conditions had been carried out. Among these conditions, the optimum preparative condition could be specified. The resultant CAs from the respective samples had been identified by FT IR spectroscopy.

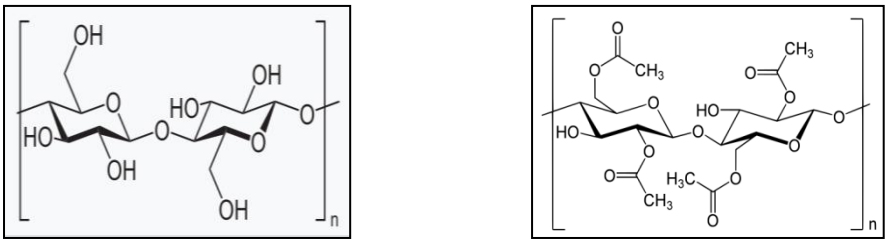

(a) (b)

Figure 1 Structural formulae of (a) Cellulose and (b) Cellulose acetate

Material and Methods

Sample Collection and Sample Preparation (Sampling)

Three types of agricultural residues such as maize straw, wheat straw and sawdust were collected from Myingyan Township, Myingyan District, Mandalay Region.

Figure 2 Raw materials of maize straw, wheat straw and sawdust

The raw materials were cut into small pieces and rinsed with water and dried. The dried pieces were blended and sieved with a 120-mesh sieve. The powder dusts under 120-mesh sieve were sieved again with 150 mesh sieve. The sample powders on the 150-mesh sieve were shown in Figure 3 and stored for cellulose isolation and acetylation.

(a) (b) (c)

Figure 3 (a) Maize straw powder (b) Sawdust powder and (c) Wheat straw powder

Methods
Preparation of Cellulose

Dewaxing process

100 g of each powdered sample was immersed in the mixture of 300 mL of toluene and 150 mL of ethanol (2:1, v/v) for 24 h to remove fats.

Pulping process

Pulping process consists of two steps: removing lignin (delignification) and removing non-cellulosic coloured materials (bleaching).

10 g of each sample powder and 100 mL of 15% NaOH were mixed in each volumetric flask and the flasks were heated to start refluxing for 3 h. Then the flasks were removed from the reflux condensers and cooled. The liquid in the flasks were decanted and 15 % NaOH was added to each flask and refluxed for another 3 h by similar performance as the previous procedure. Next, 15 % NaOH was added to each flask and refluxed similarly as the above procedures.

Bleaching

In the bleaching step, the delignified masses were suspended in 5% sodium hypochlorite solution for 24 h. Then three suspensions were filtered and the residual masses on the filter paper were washed with 5% acetic acid and then washed with water to neutral. The residues on the filter papers were dried and were allowed to stand for 24 h to obtain the constant weight. Then the yield (%) of each sample powder was calculated.

Preparation of Cellulose Acetate

Cellulose acetates from each sample were prepared by acetylation with the following four different conditions.

Acetylation with condition (1)

5 mL glacial acetic acid and 0.5 mL concentrated sulphuric acid were mixed and allowed to stand for 30 min. Then 1g of cellulose pulp was added to the flask and shaken thoroughly for 10 min. After shaking the mixture, 5 mL of acetic anhydride was added and the flask was shaken again for 30 min. After dissolving the cellulose pulp, 15 % acetic acid was added and the suspended solution was heated at 80 °C and stirred at 300 rpm with electromagnetic stirrer for 3 h. Then acetylated cellulose solution was poured into the beaker containing 150 mL distilled water. Cellulose acetate was precipitated as a suspension. The suspension was centrifuged and dried and weighed. The yield (%) of cellulose acetate in each sample powder was calculated.

Acetylation with condition (2)

In condition (2), the proportions of chemicals used were the same as in method (1), but the apparatus used is an ultrasonic cleaner under operating temperature of 80 °C for 1 h. The yield (%) of cellulose acetate in each sample powder was calculated.

Acetylation with condition (3)

In condition (3), one more solvent (toluene) was used than in method (2) and the reaction was carried out with an ultrasonic cleaner under operating temperature of 80 °C for 1 h. The yield (%) of cellulose acetate in each sample powder was calculated.

Acetylation with condition (4)

In condition (4) the solvents used were the same as in method (3), but the catalyst used was perchloric acid instead of using sulphuric acid. The yield (%) of cellulose acetate was calculated.

(a) (b) (c)

Figure 4 (a) Delignification of dewaxed samples by refluxing and acetylation of cellulose by (b) magnetic stirrer and (c) centrifuge machine

Results and Discussion

Preparation of Cellulose

Dewaxing process

The yield percentages of dewaxed sample powders were shown in Table 1.

Table 1 The Yield (%) of the Dewaxed Sample Powders

Sample powders	Yield (%)
Maize straw	96.35
Wheat straw	95.22
Wood sawdust (In)	93.46

From the above table, maize straw powder has the highest yield %. So it contains the lowest composition of pectin which is one of the main constituent of plant.

Pulping process (Preparation of Cellulose)

After pulping the three powdered samples, the yield percentages of prepared celluloses and cellulose acetates are shown by the following Tables 2 and 3.

Table 2 The Yield percentages of Celluloses

Sample powders	Yield (%) of celluloses
Maize straw	31
Wheat straw	33
Sawdust	54

According to the above table, sawdust cellulose provides the highest yield %.

Table 3 The Yield (%) of Cellulose Acetates by Acetylation with Four Different Conditions

Different Acetylation Methods	Yield (%) of Cellulose Acetates		
	Maize Straw CA	Wheat Straw CA	Sawdust CA
Condition (1)	41.89	48.61	54.21
Condition (2)	50.15	52.87	46.95
Condition (3)	58.76	60.43	57.86
Condition (4)	62.84	63.24	72.38

According to the above table, the yield (%) of cellulose acetates by condition (4) from the respective sources such as maize straw powder, wheat straw powder and sawdust powder had been found to be the highest values. So, condition (4) which was the optimum condition for the preparation of cellulose acetate had been specified.

Identification of celluloses and cellulose acetates by FT IR spectroscopic analysis

The FT IR spectra for identification of cellulose and cellulose acetates prepared from maize straw powder are shown in figure 5 (a), (b), (c) and (d) and the respective spectral assignments were shown in Table 4.

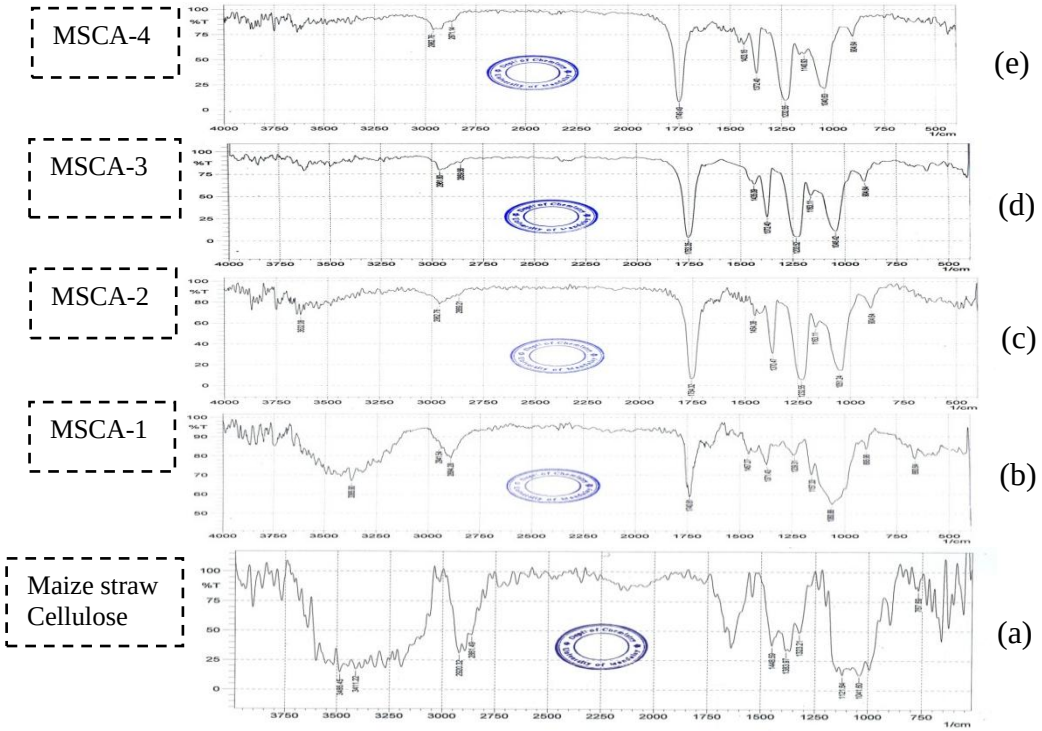

Figure 5 FT IR spectra of (a) maize straw cellulose and maize straw cellulose acetates prepared by (b) condition (1), (c) condition (2), (d) condition (3) & (e) condition (4)

Table 4 Comparison between FT IR Spectral Data of Cellulose and Cellulose Acetates Prepared from Maize Straw Powder

No.	Types of methods and compounds	υ_{O-H} (cm^{-1}) of alcohol	$\upsilon_{C=O}$ (cm^{-1}) of ester	υ_{C-O} (cm^{-1}) of ester
1.	Pulping method (Cellulose)	3486, 3411	-	-
2.	Condition-1 (Cellulose acetate)	3632	1754	1232
3.	Condition-2 (Cellulose acetate)	3365	1740	1239
4.	Condition-3 (Cellulose acetate)	-	1749	1232
5.	Condition-4 (Cellulose acetate)	-	1753	1233

From the above spectral data, the -OH stretching vibrations of alcohol groups appear at 3486 cm^{-1} and the intensity of –OH peak is distinct and there are no appearance of stretching vibrations of carbonyl (>C=O) peak and (C-O) peak of ester group. So, these spectral data assign that the compound is cellulose. In the spectra (b) and (c), there is -OH stretching vibrations appear at 3632, and 3365 cm^{-1} and the intensities of these -OH peaks gradually low. So, acetylation reactions occur but are not completely. In spectra (d) and (e), there are no -OH vibration peaks and in spectra (a), (b), (c) and (d), C=O stretching vibrations of ester groups appear at 1754, 1740, 1749, and 1753 cm^{-1} and then C-O stretching vibrations of ester group appear at 1232, 1239, 1232, and 1233 cm^{-1}, respectively. So, complete acetylations occur in condition (3) and (4). However, the yield % of condition (4) is the highest and hence the most suitable condition for preparation of maize straw cellulose acetate is condition (4).

Furthermore, FT IR spectra of wheat straw cellulose and cellulose acetates prepared from different methods are shown in Figures 6 (a), (b) (c), (c), (d) and (e). The spectral data were presented in Table 5.

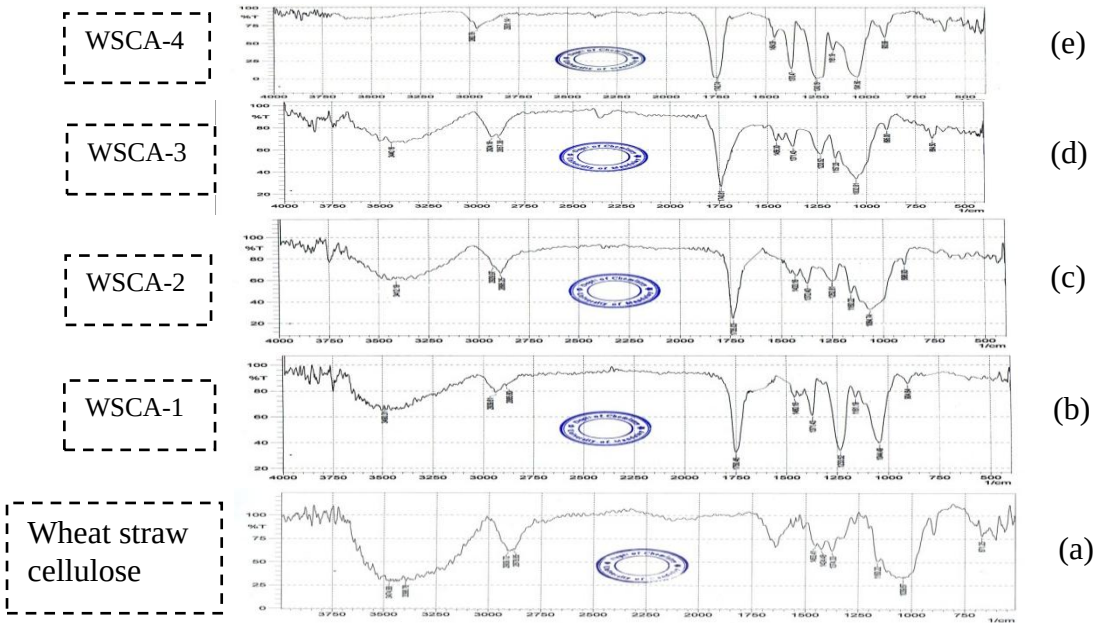

Figure 6 Comparison between FT IR spectra of (a) wheat straw cellulose and cellulose acetates by (b) condition (1),(c) condition (2), (d) condition (3) & (e) condition (4)

Table 5 Comparison between FT IR Spectral Data of Cellulose and Cellulose Acetates Prepared from Wheat Straw Powder

No.	Types of methods and compounds	υ_{O-H} (cm^{-1}) of alcohol	$\upsilon_{C=O}$ (cm^{-1}) of ester	υ_{C-O} (cm^{-1}) of ester
1.	Pulping method (Cellulose)	3474, 3396	-	-
2.	Condition-1 (Cellulose acetate)	3490	1750	1233
3.	Condition-2 (Cellulose acetate)	3412	1740	1252
4.	Condition-3 (Cellulose acetate)	3440	1749	1232
5.	Condition-4 (Cellulose acetate)	-	1742	1243

In the FT IR spectrum (a), there are two –OH stretching vibration peaks of alcohol groups of cellulose at 3474, 3396 cm^{-1}. In spectra (b), (c), (d), the intensities of OH peaks gradually low. However, C=O stretching vibrations of ester groups occur at 1750, 1740, 1749, and 1742 cm^{-1}respectively. C-O stretching vibrations of ester groups were observed at 1233, 1252, 1232, and 1243 cm^{-1} in spectra (a, b, c and d). So, complete acetylation were found to occur in condition (4).

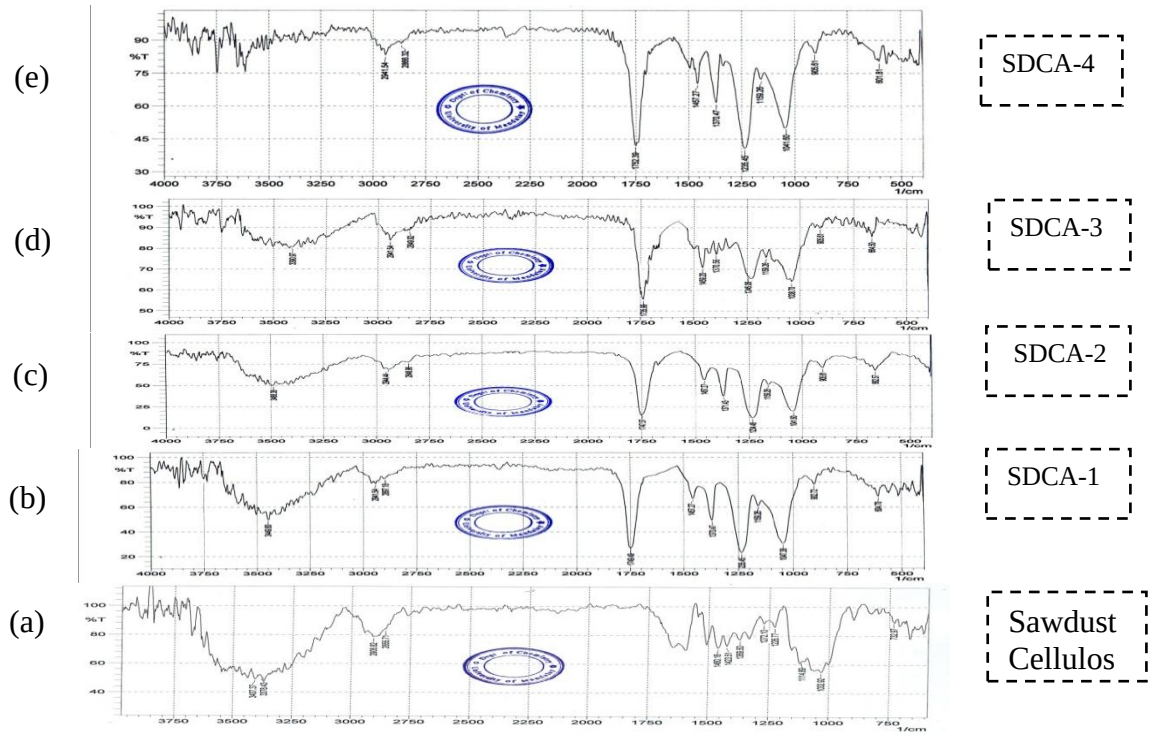

Figure 7 Comparison between FT IR spectra of (a) sawdust cellulose and prepared cellulose acetates by (b) condition (1), (c) condition (2), (b) condition (3), (e) condition (4)

Table 6 Comparison between FT IR Spectral Data of Sawdust Cellulose and Cellulose Acetates

No.	Types of method, conditions and compounds	υ_{O-H} (cm^{-1}) of alcohol	$\upsilon_{C=O}$(cm^{-1}) of ester	υ_{C-O} (cm^{-1}) of ester
1.	Pulping method (Cellulose)	3407, 3378	-	-
2.	Condition-1 (Cellulose acetate)	3449	1749	1235
3.	Condition-2 (Cellulose acetate)	3488	1747	1252
4.	Condition-3 (Cellulose acetate)	3440	1740	1233
5.	Condition-4 (Cellulose acetate)	-	1742	1243

In spectrum (a), there are two stretching vibration OH peaks of alcohol groups of cellulose at 3407, 3378 cm^{-1}. In spectra [(b), (c), (d),] the intensities of OH peaks gradually low. However, C=O stretching vibrations of ester groups occur at 1749, 1747, 1740, and 1742 cm^{-1}respectively. Furthermore, C-O stretching vibrations of ester groups were observed at 1235, 1252, 1233, and 1243 cm^{-1} in spectra [(b), (c), (d) and (e)]. So, complete acetylation also occurs in condition (4).

Conclusion

In this research, the optimum condition for the preparation of cellulose acetates from maize straw cellulose, wheat straw cellulose and sawdust cellulose had been specified. Firstly, the removal of pectin present in each sample powder was carried out by immersing into (2:1 v/v) toluene-ethanol mixture solution for 24 h. Then, in the preparation of celluloses, the pulping process had been performed by delignification and bleaching. Then, cellulose acetates were prepared by acetylation with four different conditions. From dewaxing process, the yield percentages were found to be 96.35 % for maize straw powder, 95.22 % for wheat straw powder and 93.46 % for sawdust powder. From the preparations of celluloses, the yield percentages were 31 % from maize straw powder, 33 % from wheat straw powder and 54 % from sawdust powder. After acetylation with conditions (1), (2), (3), and (4), the yield (%) of maize straw cellulose acetates were 41.89 % , 50.15 % , 58.76 % and 62.84 % .The yield (%) of the wheat straw cellulose acetates by acetylation with conditions (1), (2), (3), and (4) were 48.61 % , 52.87 % , 60.43% and 63.24 %. The yield (%) of sawdust cellulose acetates by acetylation with conditions (1), (2), (3), and (4) were 54.21 %, 46.95 %, 57.86 % and 72.38 %. The prepared cellulose acetate for each sample from different conditions had been identified by FT IR spectroscopy. From the FT IR spectral data, the optimum condition for the preparation of cellulose acetate was specified. Thus, condition (4) provides the complete acetylation and the highest yield percent.

Acknowledgements

The authors would like to express their profound gratitude to the Ministry of Education, Department of Higher Education, Yangon, for provision of opportunity to do this research and Myanmar Academy of Arts and Science for allowing to present this paper.

References

Crowford, R. L., (1981). *Lignin Biodegradation and Transformation*. New York: John Wiley and Sons.

Klemm D., Heublein B., Fink H. P., Bohn A., (2005), "*Cellulose: Fascinating Biopolymer and Sustainable Raw Material*". *Angew. Chem. Int. Ed*.44 (22), 3358-93.

Morgan, E. (2013), "*Frame Material*". All about vision. com. Retrieved 2013-08-07.

Piotrowski S., Carus M., (May 2011)."Multi-criteria evaluation of lignocellulosic niche crops for use in biorefinary processes. Nova-Institute GmbH, Hurth, Germany.

Romeo, Tony (2008). "*Bacterial Bioflims*." Berlin: Springer.pp. 258-263.

Updegraff, D. M. (1969). "*Semi-micro Determination of Cellulose in Biological Materials*". *Analytical Biochemistry*. vol. 32 (3), PP. 420-424

ANTIOXIDANT ACTIVITY AND NITRATE, FLAVONOID AND PHENOL CONTENTS OF LEAF, STALK AND ROOT OF *Apium graveolens* L. (TAYOKE NAN-NAN)

Soe Soe Tint[1,2], Saw Hla Myint[3], Ni Ni Than[4]

Abstract

Celery (*Apium graveolens* L.) is used in folk medicine as antihypertension agent and it has also been known to possess antioxidant activity. The plant is also known to be rich in nitrate which is antihypertension. Therefore the plant has been selected to study its nitrate content, antioxidant activity as well as total phenolic and flavonoid contents. It was found that crystals of potassium nitrate abundantly fell out of the ethanol extract on standing. By the first derivative UV spectrophotometric method based on nitration of salicylic acid, nitrate content in stalk of celery from Kalaw (S2) is 6,314.398 mg/kg FW (fresh weight). This is one of the highest among the different parts of celery. Total flavonoids (27.170 and 29.757 mg QE/g FW) and phenols (28.566 and 32.769 mg GAE/g FW) contents in leaf from Nyaung Hnit Pin (S1) and (S2) and antioxidant activity IC_{50} value (45.219 μg/mL) in stalk from (S2) are also high.

Keywords: Celery (*Apium graveolens* L.), potassium nitrate, flavonoids, phenols, antioxidant activity

Introduction

Most of the people use medicinal herbal plants in all over the world, including Myanmar especially in village tracts. All medicinal plants have primary and secondary metabolites which have biological activities and which are used for curing of various human diseases and also play an important role in the healing and illnesses. Among the phytochemical compounds of celery, one can mention carbohydrates, phenols such as flavonoids and alkaloids. Presence of compounds such as limonene, selinene, frocoumarin glycosides, flavonoids, and vitamins A and C are the reason that celery is the most widely used plant in traditional medicine. Celery can prevent cardiovascular diseases, jaundice, liver and lien diseases, urinary tract obstruction, gout, and rheumatic disorders (Kooti and Daraei, 2017). Tayoke Nan-nan is a plant from *Apiaceae* family which contains many phenols and antioxidant compounds which have many health benefits and that can be easily bought in the markets. *Apium graveolens* L. (celery) includes the anticancer potency of popular vegetables consumed in Indonesia (Octaviani *et al.* 2013).

Moreover, celery (*Apium graveolens* L.) is a leafy plant with significant levels of nitrites and nitrates; it is a possible natural source of these compounds for use in cured meat products. Nitrates content in celery is greater than 2500 mg/100 g fresh weight, which is very high (Santamaria, 2006).

Inorganic nitrites or nitrates therapy has potent anti-inflammatory, antioxidant properties, reduces circulating biomarker levels of oxidative stress and cardiac hypertrophy, improves rental function and lowers the blood pressure (Münzel and Daiber, 2018). Nitrates and nitrites as preservatives can be used to the cured meat flavor such as bacon, ham, sausages and hot dogs by helping to prevent the growth of microorganisms, particularly *Clostridium botulinum*, and to control rancidity by inhibiting lipid oxidation (Govari and Pexara, 2015).

An Acceptable Daily Intake (ADI) of nitrates is 0- 3.7 mg kg^{-1} of body weight (b. w) (equivalent to 222 mg nitrates per day for a 60 kg adult) (Gorenjak *et al*., 2014). The increase

[1] Lecturer, Department of Chemistry, Dagon University
[2] PhD Student, Department of Chemistry, University of Yangon
[3] Dr, Professor and Head, (Part Time Professor), Department of Chemistry, University of Yangon
[4] Dr, Professor and Head, Department of Chemistry, University of Yangon

amount of nitrates and nitrites in food can cause gastrointestinal cancer and in infants, methemoglobinema (Hord *et al.,* 2009).

Nitrates in plant tissue have been quantitatively determined by several methods. Some are potentiometric (Olmos *et al.,* 2013), chromatographic (Liu *et al.,* 2016), tirimetric (Digregorio and Moris, 1970), Cadmium reduction (Huffman and Barbarick, 1981) and spectrophotometric (Muresan *et al*., 2012) methods. The first four methods have some disadvantages, such as lower sensitivity, interferences, technician exposure to carcinogenic chemicals (Cataldo *et al.*, 1975; Vendrell and Zupancic, 1990) and time-consuming (Cataldo *et al.,* 1975), whereas the principal problem in the classical spectrophotometric method is the presence of pigments and colloidal materials (Gaya and Alimi, 2006). But nitration of salicylic acid is rapid, free of interference from other ions present in plant tissue (Cataldo *et al.,* 1975), a method was designed for nitrate–N determination in plant tissue using first-derivative spectrophotometry (Lastra, 2003). The aim of this research is to isolate some active compounds such as potassium nitrate crystals from *Apium graveolens* L. and assess some of their biological activities.

Materials and Methods

Celery samples were purchased from Kalaw in Shan State and Hmawbi Township in Yangon Region. After collection, the scientific name of the sample was verified by authorized botanist at Botany Department, Dagon University. The leaf, stalk, and root were washed with distilled water to remove dust. The samples were separately dried at 90 ˚C in Electronic Oven SEO 2260. The dried samples were cut into small pieces and then ground into powder by means of the Panasonic MX- GM 1011 (green) Blender. The dried powder samples were separately stored in the air tight containers.

Isolation of Nitrate Crystals from the Stalk Celery

Dry stalk tissue (5 g) was accurately weighed and placed in a sealed vessel, mixed with 100 mL of 95 % ethanol and then the vessel was placed in an ultrasonic cleaning bath (model number Power Sonic 410) for 90 min at 25 ˚C. After extraction, the ethanol extract was dried on a water bath. At this time, the crystals came out from the solution. The crystals were purified with methanol several times until clear crystals were obtained. The crystals, free from chlorophyll were dried on water bath.

Identification of Potassium Nitrate Crystals in the Stalk of Celery

(A) Analysis of acid radical, nitrate ions

Action of concentrated sulphuric acid and copper turnings

Concentrated sulphuric acid and copper chips were added to the crystals from stalk ethanol extract and then heated. Reddish brown fumes were observed. This observation indicated the presence of nitrate (Vogel, 1979).

By using Brown ring test

Dilute sulphuric acid was added to the crystals from the ethanol extract of stalk till the effervescence ceased. Freshly prepared ferrous sulphate solution was added to the above solution and then concentrated sulphuric acid was poured through the sides of the test-tube. Brown ring was formed at the junction of the two liquids. This observation indicated the presence of nitrate (Vogel, 1979).

(B) Analysis of the basic radical, potassium and sodium ions by AAS method

Crystals from ethanol extract of stalk were analyzed by Atomic Absorption spectroscopic method in the National Analytical Laboratory, Department of Research and Innovation.

(C) Identification of potassium nitrate

Crystals from ethanol extract of stalk were identified by FT IR spectroscopy by comparison with the spectra of $NaNO_3$ and KNO_3.

Determination of Nitrate Content from Different Parts of Celery

Nitration of salicylic acid

Apparatus

(a) Spectrophotometer- UV-1800 UV-Vis spectrophotometer (UV double beam UV-Vis with 1 cm quartz cells) from Shimadzu Company attached to a printer was used. The spectra were obtained with a spectral bandwidth of 2 nm. The derivative spectra were obtained by instrumental electronic differentiation (Lastra, 2003).

(b) Power Sonic 410- Maintain the extract of stalk tissue at 45 ˚C.

Reagents

All reagents were of analytical grade.

Nitrate-N stock standard solution

Solution of 500 mg/L was prepared from KNO_3. Working standard solutions of 10, 20, 30, 40, 50, 60, 80, and 100 mg/L were prepared by diluting the standard with distilled water and were stored at 4 ˚C.

Salicylic acid solution 5 % (m/v) in concentrated H_2SO_4

Salicylic acid (5.00 g) was dissolved in concentrated sulphuric acid and diluted to volume (100 mL) with the same acid; prepared at least once each 48 h, and stored in an amber bottle at 4 ˚C.

2 N Sodium hydroxide solution

Sodium hydroxide (40 g) was dissolved in 500 mL of distilled water and was stored at room temperature.

Calibration

Aliquots (0.1 mL) of working standard solutions (10–100 mg/L nitrate-nitrogen) in a 30 mL tube were mixed thoroughly with 0.4 mL salicylic acid solution. After 20 min at room temperature, 9.5 mL 2N NaOH solution was slowly added to obtain 0.1, 0.2, 0.3, 0.4, 0.5, 0.6, 0.8, and 1.0 mg/L nitrate-nitrogen solutions. This method is based on the formation of nitrosalicylic acid that shows, in highly basic solution, a maximum absorption at 412 nm in zero-order absorption spectrum, and 388 and 440 nm in first-order spectrum ($1D_{388–440}$). The sum of the heights of both peaks (388 and 440 nm) positive and negative (peak-to-peak) of the first derivative was used. The wavelength range selected to obtain the spectrum was 356–500 nm; data interval, 4 nm; scaling factor 18.

Extract Preparation from Plant Tissues

Portions (0.1000 g) of vegetable tissues (each celery ground sample) was suspended in 10 mL distilled water, kept at 45 ˚C for 1 h under sonication, and then filtered through filter

paper. Samples were extracted and analyzed immediately or within 24 h after extraction when stored at 4 ˚C (Catald *et al.*,1975).

Determination

A 0.1 mL volume of the preceding extract was thoroughly mixed in a 30 mL tube with 0.4 mL salicylic acid solution. After 20 min at room temperature, 9.5 mL 2 N NaOH solution was slowly added.

Calculation

Nitrate-N in plant tissue express as mg NO_3^--N per kg dry weight:

$$C_x = \frac{(1D_{388\text{-}440} - a) \times 1000}{b \times w}$$

where $1D_{388–440}$ corresponds to the spectrophotometric measurement of the sample (UD derivative unity); "b" and "a" correspond to the slope and the intercept of the calibration curve $1D_{388–440}$ (UD) vs NO_3^--N concentration (mg/L) and w = tissue weight (g) respectively.

Determination of total flavonoids and phenols Contents

Preparation of plant extract

One gram powder was accurately weighed and placed in sealed vessel by adding 70 mL of 96 % ethanol solvent, and then the vessel was placed in an ultrasonic bath (model number Power Sonic 410) for extraction for 60 min at (40 ˚C). After extraction the extract was stored in glass vials at refrigerated temperature for further analysis (Bharti and Ray, 2014). This extract was used to determine the total flavonoids and phenols contents.

Determination of total flavonoids content

Total flavonoids content (TFC) of the extract was measured by the aluminium chloride colorimetric assay. The sample (2 mL) was mixed with 0.2 mL of 5 % sodium nitrite. After 5 min, 0.2 mL of 10 % aluminum chloride was added to the mixture and mixed. After 6 min, 2 mL of 1 M sodium hydroxide was added to the mixture. The end volume of the reaction mixture was made up to 5 mL with aqueous ethanol and mixed thoroughly. Absorbance of the reaction mixture was measured at 510 nm against a blank. The flavonoid content was determined using a standard curve of Quercetin at 1.56- 100 μg/ mL and the results were expressed as μg/mL quercetin equivalents (QE) (Bharti and Ray, 2014).

Determination of total phenols content

Total phenols were determined by using Folin-Ciocalteu assay (Bharti and Ray, 2014). The extract preparation was the same as in the determination of total flavonoids content. The sample (0.2 mL) was taken in a test tube and then 0.5 mL FC reagent (1:1 diluted with distilled water) and 1 mL of saturated sodium carbonate solution were added. The final volume was made to 5 mL with water. Then the mixture was allowed to stand for 15 min. The absorbance was read at 746 nm using UV-Vis Spectrophotometer. The standard solutions of Gallic acid in water 0- 50 mg/mL were prepared to construct the calibrating curve. Total phenols content were expressed in terms of Gallic acid equivalent (GAE) (mg/g dry mass) (Bharti and Ray, 2014).

Determination of Antioxidant Activity

The ethanol extract (0.004 g) was dissolved in 10 mL to get 400 μg/mL solution. The DPPH radical scavenging activity (DPPH SA, %) is often used to evaluate the antioxidant capacity of ethanol extract (Brand-Williams *et al*., 1995). The extract solution (1.5 mL) was mixed with 1.50 mL of freshly prepared DPPH (0.05 mM) in ethanol. The mixture was shaken vigorously and kept at room temperature for 30 min. Then the absorbance was measured at 517 nm against a blank (without extract) in a UV-Vis spectrophotometer. The scavenging activity of DPPH radical (DPPH SA, %) was calculated using the following formula:

$$\text{DPPH SA (\%)} = \left[\frac{A_{control} - A_{sample}}{A_{control}}\right] \times 100$$

where $A_{control}$ and A_{sample} are the absorbance of the control (DPPH solution without sample) and the absorbance of the test sample, respectively (Dinç *et al.*, 2017).

Results and Discussion

Identification of Potassium Nitrate crystals in the Stalk of Celery (*Apium graveolens* L.)

(A) Analysis of acid radical, nitrate ions

Qualitative analysis of nitrate ions in celery (*Apium graveolens* L.) showed evolution reddish brown vapour by the action of concentrated sulphuric acid and copper; and the appearance of a brown ring by the brown ring test (Table 1). From the positive results of acid radical, the negative part of crystal is nitrate ion.

Table 1 Qualitative Analysis of Nitrate Ions in the Stalk of celery (*Apium graveolens* L.)

No.	Test	Observation
1.	Action of H_2SO_4 (conc.) acid and Cu	Reddish brown vapour was evolved.
2.	Brown ring test	Brown ring was formed at the junction of the two liquids.

(B) Analysis of basic radical, potassium and sodium ions by AAS method

The amounts of potassium and sodium ion are 27.943 % and 0.013 % respectively (Table 2). Therefore, potassium nitrate is the main component in celery.

Table 2 The Result for Crystals from Ethanol Extract of Stalk by Atomic Absorption Spectroscopy

No.	Parameters	Analysis Result (%)
1.	Sodium (Na)	0.013
2.	Potassium (K)	27.943

(C) Identification of Potassium Nitrate

Crystals from stalk ethanol extract were identified by FT IR spectroscopy (Table 3, Figure 1).

Table 3 Assignment of Bands in the FT IR Spectrum of the crystals from ethanol extract of stalk

Wavenumber (cm^{-1})		Vibrational mode	Functional group
Experimental value	**Reference Value***		
1762	1767	Stretching of N=O	NO_3^-
1366	1340- 1369	Antisymmetric stretching of NO_3^-	NO_3^-
823	830	symmetric stretching of NO_3^-	NO_3^-

* (Miller and Wilkins, 1952, Trivedi *et al.*, 2015)

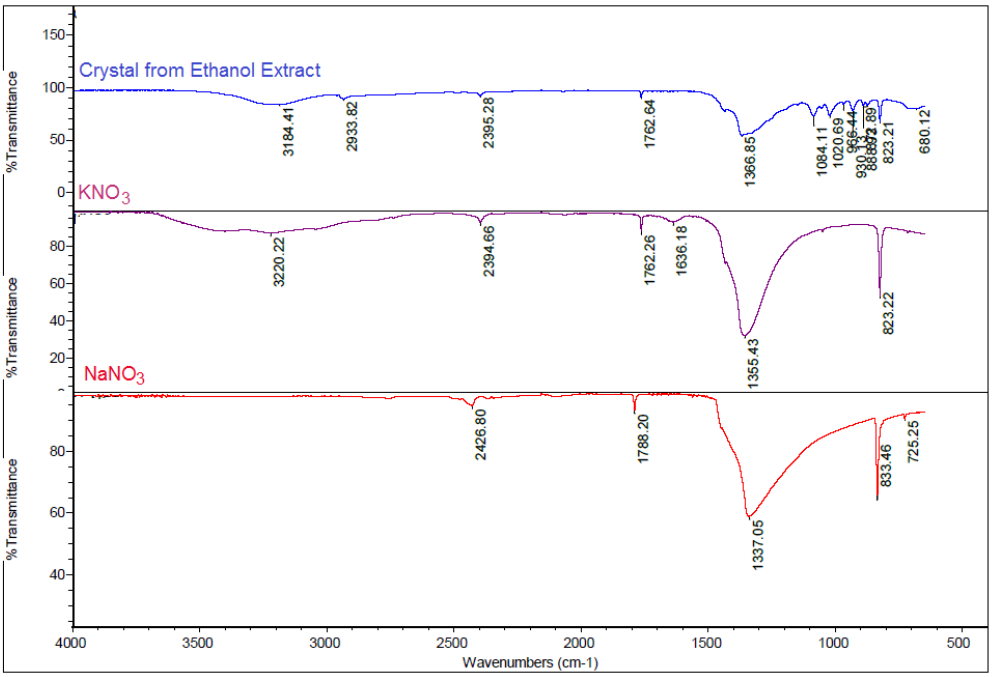

Figure 1 Comparison of The FT IR spectra of the crystals from ethanol extract of stalk, potassium nitrate and sodium nitrate

Determination of Nitrates Content from Different Parts of Celery

Construction for the calibration curve of standard potassium nitrate solution

Zero- and first-order spectra for nitro salicylic acid obtained with standard nitrate-N solutions (0.1- 1.0 mg/mL) are shown in Figures 2 and 3, respectively. The optimum conditions were first-order derivative, wavelength range of 356–500 nm, and $\Delta\lambda$ 4 nm. In this derivative method, the measurement selected to prepare the analytical calibration graphs was peak-to-peak (sum of the heights of 388 and 440 nm peaks), which exhibits good linearity to nitrate–N concentration. The intercept is near zero. The calibration graph and statistical results are given in Figure 4 and Table 4, respectively. In this experiment the highest nitrate-N and nitrate were observed in stalk from Kalaw (Table 5 and Table 6).

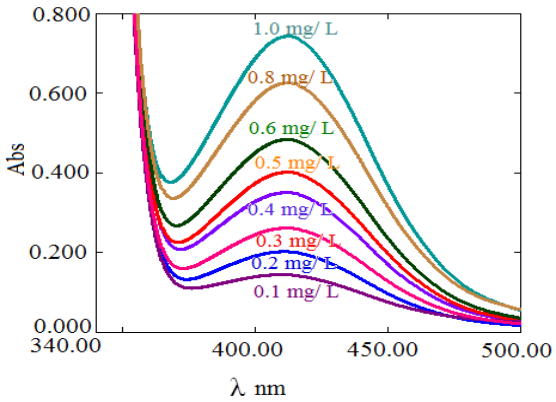

Figure 2 Zero-order overlaid spectra of nitro salicylic acid in highly basic solution obtained using standard potassium nitrate solutions

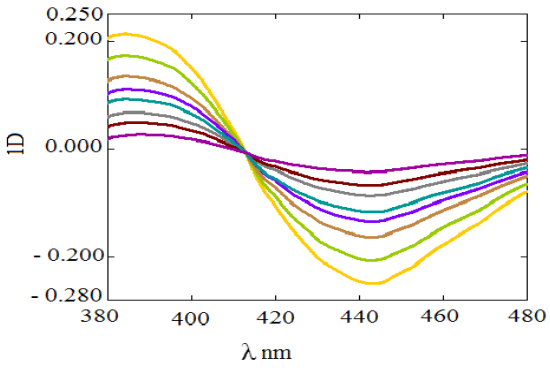

Figure 3 First-order derivative overlaid spectra of nitrosalicylic acid in highly basic solutions using standard potassium nitrate solution Δ λ 4 nm

Table 4 Concentrations of Standard Nitrate-N with their Respective Spectrophotometric Values in the First-derivative Spectrum between λ_{max} 388 - 440

Concentration (μg/ mL)	1D 388-440		mean	STDEV
	1st	2nd		
0.1	0.089	0.057	0.073	0.023
0.2	0.101	0.117	0.109	0.011
0.3	0.157	0.154	0.156	0.002
0.4	0.187	0.206	0.197	0.013
0.5	0.222	0.243	0.233	0.015
0.6	0.278	0.293	0.286	0.011
0.8	0.363	0.375	0.369	0.008
1.0	0.449	0.455	0.452	0.004

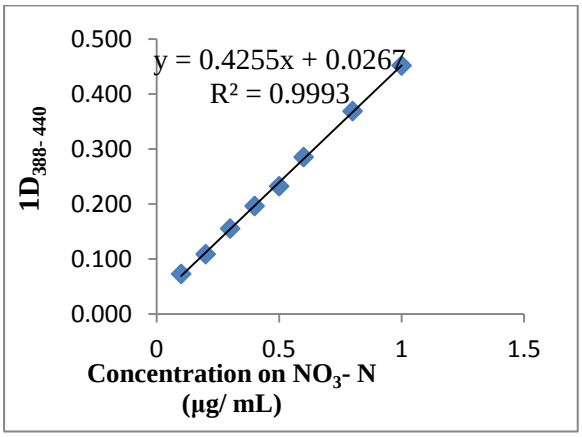

Figure 4 Calibration curve for nitrate-N determination using first-order derivative spectrophotometry

Table 5 Concentration of Nitrate-Nitrogen in Dry Leaf, Stalk, and Root

Sample	1D 388-440	Concentration mg/kg dry weight
L- S1	0.079 ±0.010	1,229.142
L- S2	0.088 ± 0.007	1,440.658
S- S1	0.068 ± 0.004	958.872
S- S2	0.154 ± 0.033	11,967.098
R- S1	0.185 ± 0.008	7,417.156
R- S2	0.199 ± 0.001	4,037.603

S1 = Nyaung Hnit Pin (Hmawbi Township)
L- S1 = Leaf from S1
S- S1 = Stalk from S1
R- S1 = Root from S1

S2 = Kalaw (Shan State)
L- S2 = Leaf from S2
S- S2 = Stalk from S2
R- S2 = Root from S2

Table 6 Concentration of Nitrate-N and Nitrate in Dry and Fresh Weight

Sample	Conc. of NO_3^- -N mg/ kg dry weight	Conc. of NO_3^- mg/ kg dry weight	Conc. of NO_3^- mg/ kg fresh weight
L- S1	1,229.142	5,443.343	680.027
L- S2	1,440.658	6,380.057	436.047
S- S1	958.872	4,246.433	513.013
S- S2	11,967.098	52,997.146	6,314.398
R- S1	7,417.156	32,847.406	3,675.234
R- S2	4,037.603	17880.812	1,896.450

Determination of Total Flavonoids Content

Flavonoids are a group of polyphenolic compounds naturally present in most yellow edible vegetables. There is evidence of a potential role for flavonoids as free radical scavenging and in lowering the risk of coronary heart disease, cardiovascular diseases, neurodegenerative diseases, osteoporosis, lung cancer and other biological disorders (Bharti and Ray, 2014). The calibration curve of the determination of flavonoids content was constructed between at 0- 100 µg /mL concentration and the results are expressed as milligram quercetin equivalent/g (Table 7 and Figure 5). The highest total flavonoids were observed in leaf from Kalaw, lowest flavonoids in root from Nyaung Hnint Pin (Table 8 and Figure 6).

Table 7 Absorbance and Concentration (µg/mL) of Total Flavonoids Content and STDEV

Concentration (µg mL^{-1})	Absorbance			Mean	STDEV
	1st	2nd	3rd		
100.000	0.355	0.350	0.352	0.352	0.003
50.000	0.170	0.166	0.170	0.169	0.002
25.000	0.084	0.085	0.085	0.085	0.001
12.500	0.045	0.042	0.042	0.043	0.002
6.250	0.023	0.025	0.023	0.024	0.001
3.125	0.017	0.018	0.019	0.018	0.001
1.560	0.008	0.009	0.008	0.008	0.001

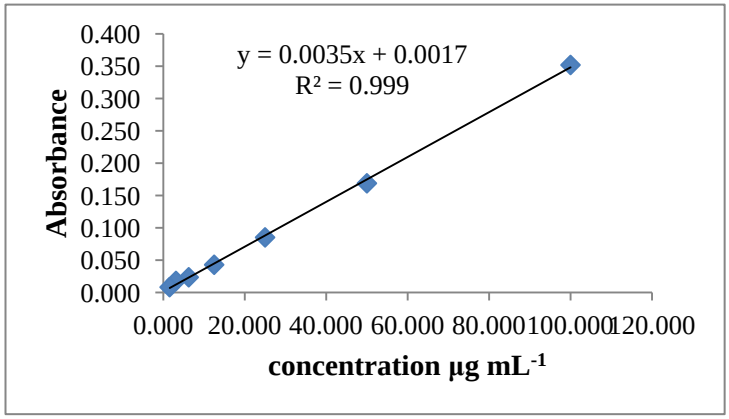

Figure 5 Calibration curve for total flavonoids content

Table 8 Total Flavonoids Content in Leaf, Stalk and Root of Celery from Two Different Sources

Sample	TFC content mg QE/g dry weight	TFC content mg QE/g fresh weight
L- S1	217.486	27.170
L- S2	263.453	29.757
S- S1	24.473	2.957
S- S2	28.743	3.425
R- S1	27.600	3.088
R- S2	37.886	4.018

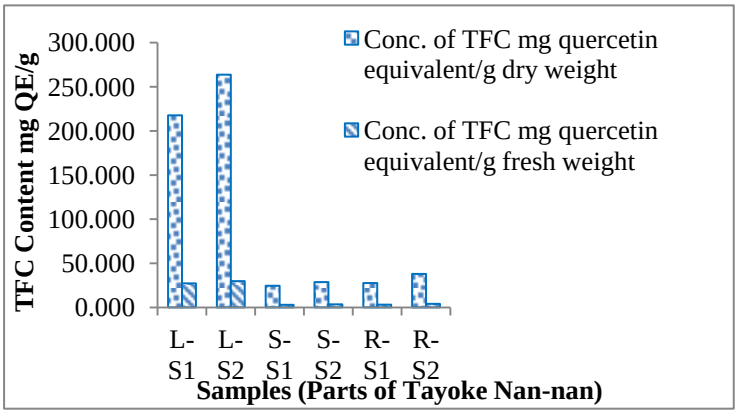

Figure 6 Total flavonoids content in dry and fresh leaf, stalk, and root of celery from S1 and S2

Total Phenols Content in Leaf, Stalk and Root of Celery

The total phenols content was determined by a modified Folin-Ciocalteu reagent method. Using the standard curve of Gallic acid (R^2 = 0.9997) (Table 9 and Figure 7), the phenols content was expressed as mg Gallic acid equivalent per g. The highest amount of total phenols content was observed in the leaf from Kalaw, the lowest in the root from Nyaung Hnint Pin (Table 10 and Figure 8).

Table 9 Absorbance Values of Standard Gallic Acid Solutions

Concentration (µg/ mL)	Absorbance
50.000	0.798 ± 0.008
25.000	0.430 ± 0.005
12.500	0.240 ± 0.006
6.250	0.135 ± 0.007
3.125	0.096 ± 0.006

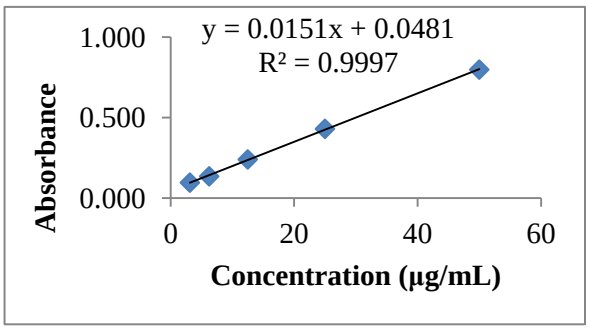

Figure 7 Calibration curve for total phenols content determination using gallic acis as standard

Table 10 Total Phenols Content in Leaf, Stalk and Root of Tayoke Nan-nan from Two Different Sources

Sample	TPC content mg GAE/g dry weight	TPC content mg GAE/g fresh weight
L- S1	228.662 ± 0.002	28.566
L- S2	290.119 ± 0.004	32.769
S- S1	42.331 ± 0.004	5.114
S- S2	51.338 ± 0.002	6.117
R- S1	41. 272 ± 0.001	4.618
R- S2	53. 987 ± 0.001	5.726

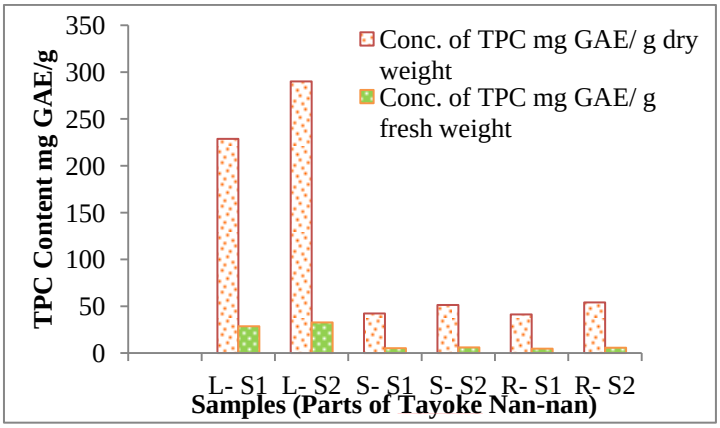

Figure 8 Bar graph showing the Total phenols content in dry and fresh leaf, stalk, and root of Tayoke Nan-nan from S1 and S2

Antioxidant Activity of Crude Extract

The radical scavenging activity of Gallic acid for 50 % scavenging (IC_{50}) of the DPPH radicals is shown in Table 11 and Figure 9. The percent inhibition and IC_{50} of DPPH by the extract of different parts of celery are recorded in Table 12 and Figures 10 and 11. In DPPH assay, the ethanol stalk extract showed most antioxidant activity when compared to ethanol leaf and root extract. DPPH scavenging activity was ranging from 2.721 ± 0.013 to 62.585 ± 0.006 % in the case of ethanol stalk extract, whereas in the case of leaf and root, they were 4.195 ± 0.004 to 56.689 ± 0.011 % and 19.728 ± 0.008 to 89.229 ± 0.010 %. In case of ethanol stalk extract, the highest scavenging activity was found at a concentration 200 μg/mL and the lowest was found at a concentration of 12.5 μg/mL .

Table 11 % Radical Scavenging Activity and IC_{50} Value of Standard Gallic acid by DPPH Assay Method

Concentration (μg/mL)	% Inhibition	IC_{50} (μg/mL)
0.3125	24.603 ± 0.004	0.492
0.625	68.481 ± 0.005	
1.250	87.642 ± 0.002	
2.500	88.776 ± 0.003	
5.000	90.249 ± 0.030	
10.000	86.508 ± 0.045	

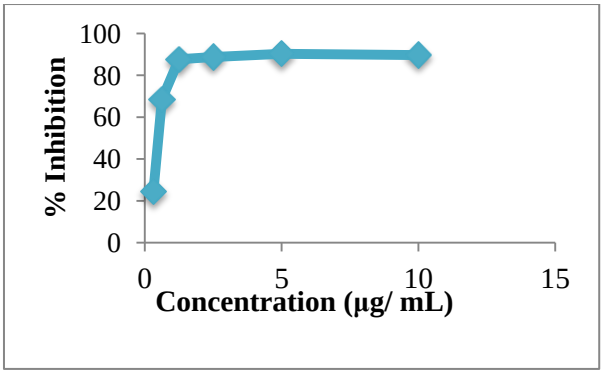

Figure 9 % Radical scavenging activity of standard gallic acid

Table 12 % Inhibition for Different Concentrations of Leaf, Stalk and Root of Celery from S2

Concentration (µg/mL)	% Inhibition Leaf	% Inhibition Stalk	% Inhibition Root
12.5	4.195 ± 0.004	2.721 ± 0.013	19.728 ± 0.008
25.0	8.617 ± 0.004	18.821 ± 0.003	23.810 ± 0.017
50.0	18.481 ± 0.004	57.37 ± 0.003	30.863 ± 0.005
100.0	50.227 ± 0.007	59.249 ± 0.001	41.950 ± 0.005
200.0	55.409 ± 0.003	62.585 ± 0.006	73.696 ± 0.055
400.0	56.689 ± 0.011	62.358 ± 0.146	89.229 ± 0.010
IC_{50}	99.646 µg/mL	45.219 µg/mL	125.342 µg/mL

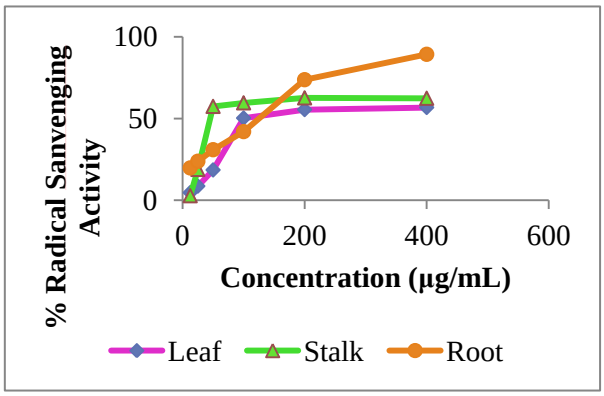

Figure 10 % Radical scavenging activity of different concentrations of ethanol crude extracts of leaf, stalk and root of celery from S2

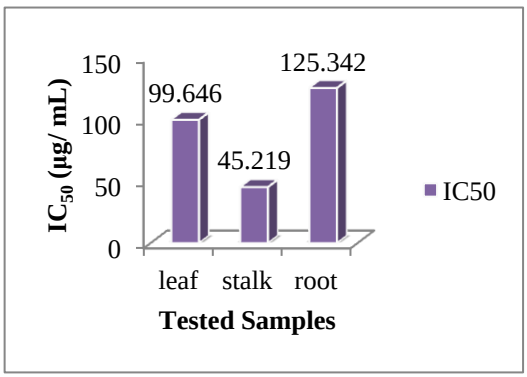

Figure 11 A bar graph of IC_{50} values of gallic acid and ethanol crude extracts of leaf, stalk and root of celery from S2

Conclusion

Nitrate contents of celery (*Apium graveolens*) (leaf, stalk and root from Kalaw and Nyaung Hint Pin) were analysed by nitration of salicylic acid using UV-1800 UV-Vis spectrophotometer. The trend of nitrate contents are stalk > root> leaf. Potassium nitrate crystals are mostly abundance in the ethanol extract of celery stalk.

Identification of acid radical on these crystals were confirmed nitrate ion, and for the basic radical, potassium ion by Atomic Absorption Spectroscopy method.

Crystals from stalk ethanol extract were identified by FT IR spectroscopy by using potassium and sodium nitrate.

In addition, the total flavonoids and phenols contents in leaf from Kalaw (S2) are the highest. Therefore the trend of total flavonoids and phenols contents are leaf > root > stalk and leaf > stalk > root.

IC_{50} values of antioxidant activities showed stalk > leaf > root (45.219 μg/mL > 99.646 μg/mL> 125.34 μg/mL). In this result, the antioxidant activity of stalk is the highest because of total phenols and nitrate contents.

Acknowledgements

The authors would like to express our gratitude to the Department of Higher Education, Ministry of Education, Myanmar, for their permission to do this research and also to the Myanmar Academy of Arts and Science for allowing to read this paper.

References

Bharti, I. and Ray, A. (20150). "Effects of Extraction Techniques on Total Flavonoids, Phenols and Antioxidant Activity of Different Plants Extract". *IJRASET*, vol. 2 (1), pp. 41- 48.

Brand-Williams, W., Cuvelier, M. E. and Berset, C. (1995). "Use of a Free Radical Method to Evaluate Antioxidant Activity". *Lebensmittel-Wissenschaft und –Technologie*, vol. 28 (1), pp. 25- 30.

Cataldo, D. A., Maroon, L. E., Schrader, L. E., and Youngs, V. L. (1975). "Rapid Colorimetric Determination of Nitrate in Plant Tissue by Nitration of Salicylic acid". *Journal of Communications in Soil Science and PlantAnalysis*, vol. 6, pp. 71- 80.

Digregrio, J. S. and Morris M. D. (1970). "Titrimetric Determination of Nitrate with Diphenylthallium(III) Sulfate". *Analytical Chemistry*, vol. 42 (1), pp. 94-97.

Dinç Zor Ş., Bat, M., Peksel, A. and Alpdoğan G. (2017). "Optimization of Ultrasound- Assisted Extraction of Antioxidants from *Apium graveolens* L. Seed using Response Surface Methodology". *JOTCSA*, vol. 4 (3), pp. 915- 930.

Gaya, U. I. and Alimi, S. (2006). "Spectrophotometric Determination of Nitrate in Vegetables Using Phenol". *J. Appl. Sci. Environ. Mgt*, vol. 10 (1), pp. 79- 82.

Gorenjak, A. H., Urih, D., Langerholc, T. and Kristl, J. (2014). "Nitrate Content in Potatoes Cultivated in Contaminated Groundwater Areas". *JFR*, vol. 3 (1), pp. 18- 27.

Govari, M. and Pexara, A. (2015). "Nitrates and Nitrites in Meat Products". *JHELLENIC VET MED SOC.*, vol. 66 (3), pp. 127-140.

Hord, N. G., Tang, Y. and Bryan, N. S. (2009). "Food Sources of Nitrates and Nitrites: the Physiologic Contex for Potential Health Benefits". *Am J Clin Nutr.*, vol. 90 (1), pp. 1- 10.

Huffman, S. A. and Barbarick, K. A. (1981). "Soil Nitrate Analysis by Cadmium Reduction". *Journal of Communications in Soil Science and Plant Analysis*, vol. 12 (1), pp. 79- 89.

Kooti, W. and Daraei, N. (2017). "A Review of the Antioxidant Activity of Celery (*Apium graveolens* L.)". *J Evid Based Complementary Altern Med.*, vol. 22 (4), pp. 1029-1034.

Lastra, O. C. (2003). "Derivative Spectrophotometric Determination of Nitrate in Plant Tissue". *JAOAC Int.*, vol. 86 (6), pp. 1101- 1105.

Liu, D., Niu, J., Kong, L. and Chen, Z. (2016). "Simultaneous Detection of Nitrite and Nitrate in Celeries and Carrots". *American Journal of Biochemistry and Biotechnology*, vol. 12(2), pp. 122-126.

Miller, **F. A. and Wilkins, C. H.** (1952). "Infrared Spectra and Characteristic Frequencies of Inorganic Ions". *Anal. Chem.*, **vol. 24** (8)**, pp. 1253-1294**

Münzel, T. and Daiber, A. (2018). "Inorganic Nitrite and Nitrate in Cardiovascular Therapy: A Better Alternative to Organic Nitrates as Nitric Oxide Donors". *Vascular Pharmacology*, vol. 102**,** pp**.** 1- 10.

Muresan, C., Tofana, M., Socaci, S. and Salanta, L. (2012). "Content Evaluation on Nitrates and Nitrites in Local and Imported Vegetables". *Bulletin UASVM Agriculture*, vol. 69 (2), pp. 510- 512.

Octaviani, C. D., Lusiana, M., Zuhrotun, A., Diantini, A., Subarnas, A. and Abdulah R. (2013). "Anticancer Properties of Daily-consumed Vegetables *Amaranthus pinosus*, *Ipomoea aquatica*, *Apium graveolens* and *Manihot utilisima* to LNCaP Prostate Cancer Cell Lines". *Journal of Natural Pharmaceuticals*, vol. 4 (1), pp. 65-70.

Olmos, R. P., Gabiola, X. and Hurtado, J.M. (2013). "Sequential Potentiometric Determination of Nitrate and Choride in Vegetables". *Chemistry Journal*, vol. 3 (3), pp. 81- 85.

Sadate, S., Farley, C., Kassu, A. and Sharma, A. (2015). "Standoff Raman Spectroscopy of Explosive Nitrates Using 785 nm Laser". *American Journal of Remote Sensing*, vol. 3 (1), pp. 1-5.

Santamaria, P. (2006). "Nitrate in Vegetables: Toxicity, Content, Intake and European Commission Regulation". *Sci Food Agric.*, vol. 86 (1), pp. 10- 17.

Trivedi M. K., Branton, A., Trivedi, D., Nayak, G., Bairwa, K. and Jana, S. (2015). "Spectroscopic Characterization of Disodium Hydrogen Orthophosphate and Sodium Nitrate after Biofield Treatment". *J Chromatogr Sep Tech*, vol. 6 (282), pp. 1- 5.

Vendrell, P. F., and Zupancic, J. (1990). "Determination of Soil Nitrate by Transnitration of Salicylic-acid". *Commun Soil Sci Plan, vol.* 21 (13), pp. 1705-1713.

Vogel, I. A. (1979). *Textbook of Marcro and Semimicro Qualitative Inorganic Analysis.*Lodon: 5th Ed., Longman.

LEAVES AND FRUITS EXTRACTS OF *TAMARIND INDICA* L (MA-GYI) MEDIATED SYNTHESIS OF COPPER(II)OXIDE NANOPARTICLES AND THEIR CHARACTERIZATIONS

Daisy[1], Ni Ni Sein[2], Daw Hla Ngwe[3]

Abstract

Leaves and fruits extracts of *Tamarindus indica* L. (Ma-Gyi) mediated synthesis of copper(II) oxide nanoparticles (CuO NPs) were conducted in this research. Formation of CuO nanoparticles was studied at four different temperatures *viz*., 200 ºC, 300 ºC, 400 ºC and 500 ºC and CuO particles formed were characterized by X-ray diffraction analysis. At the temperature of 200 ºC, formation of Cu_2O was observed. As the temperature was increased to 300 ºC most of Cu_2O particles converted to CuO and at 400 ºC Cu_2O impurities peaks were still observed. At 500 ºC, all of the Cu_2O peaks disappeared and only single phase of CuO nanoparticles was observed. Well- dissolved characteristic peaks such as (110), ($\bar{1}$11), (111), ($\bar{2}$02), (020), (202) and ($\bar{1}$13) of CuO nanoparticles were found in XRD pattern. CuO nanoparticles were indexed as monoclinic with crystallite sizes of 19.9 nm and 20.9 nm calculated by Scherrer equation. The crystallite sizes of CuO NPs obtained by using leaves and fruits extracts of *T. indica* L. were found to be 21.2 nm and 21.7 nm, respectively by TEM analysis. SEM analysis showed a large number of spherical nanoparticles with dense agglomerates. Thermal analysis of CuO nanoparticles showed that CuO was almost thermally stable beyond 400 ºC. The presence of characteristic vibration of Cu-O in the range of 430-606 cm^{-1} was confirmed by FT IR analysis.

Keywords: *Tamarindus indica* L., copper(II) oxide nanoparticles, monoclinic, Scherrer equation

Introduction

Metal oxides are the most diverse group in chemistry as their special properties covered nearly all aspects in both science and technology. Among various metal oxides, transition metal oxides are the most technologically advanced and economically attractive. Copper(II) oxides nanoparticles (CuO NPs) are of interest because it issimple, highly stable, relatively more cost effective than other metals like gold and silver, stable over a wide range of pH and high temperature resistance. CuO NPs were found to be extremely useful in wide variety of applications such as antimicrobial agent (Ren *et al*., 2009), photocatalyst (Katwal *et al*., 2015), solar cells (Kitowaki *et al.,* 2012), lithium ion battery (Thi *et al.,* 2014) and gas sensor (Zhang *et al*., 2011). Nowadays, CuO nanoparticles are utilized as heterogeneous catalysts, antioxidants, drug delivery agents, and imaging in field of biomedicine (Faheem *et al.,* 2017).

Copper(II) oxide nanoparticles can be synthesized by various chemical methods such as sol-gel method (Etefagh *et al*., 2013), precipitation (Phiwdang *et al*., 2013), hydrothermsynthesis (Outokesh *et al.*,2011), chemical reduction, thermal decomposition, electrochemical method (Ghorbani, 2014) and wet chemical method (Joshua *et al.,* 2014). However, these chemical methods have disadvantages e.g., the release of hazardous chemicals and absorption of some toxic chemicals on surface of nanoparticles. So a convenient, rapid, mild , non-toxic and natural product to produce copper oxide in aqueous environment is required. Green synthesis of metal oxide nanopatilcles involves using bacteria, fungi, algae and plants. Among them nanoparticles synthesized from plants are more stable, inexpensive, faster than in the case of microorganisms. So, this study is aimed to synthesize CuO NPs from $Cu(NO_3)_2$ by using leaves and fruits extracts of *Tamarindus indica* L. (Ma-Gyi) which is readily available in Myanmar.

[1] Lecturer, Department of Chemistry, Dagon University
[2] Dr, Professor (Retired), Department of Chemistry, University of Yangon
[3] Dr, Professor and Head (Retired), Department of Chemistry, University of Yangon

Materials and Methods

Samples Collection

The *Tamarindus indica* L. (Ma-gyi) leaves and fruits were collected from Leindaw village, Meiktila Township, Mandalay Region.

Preparation of Copper(II) Oxide Nanoparticles

Copper(II) oxide nanoparticles were prepared by dropwise addition of 50 mL 0.5 M copper(II) nitrate solution into 25 mL of extracts sample solution in a 250 mL beaker and then mixed thoroughly by a magnetic stirrer at 60 ºC. The deep blue colour of solution changed to dark green and it was heated at 80 ºC. The dried sample was then collected and calcined in a muffle furnace at 200, 300, 400 and 500 ºC for 1 h. A black coloured powder was obtained and it was carefully collected and packed for characterization purposes.

Characterization Techniques

The crystalline structure and phase purity of the synthesized CuO NPs were examined by using X-ray diffractometer (Rigaku Co., Tokyo, Japan) using Cu Kα (λ=1.54056 Å) radiation in a scattering range (2θ) of 10° to 70° at an accelerating voltage of 40 kV. The morphologies of CuO NPs were characterized by scanning electron microscopy (SEM, JEOL-JSM-5610 LV, Japan) at Universities' Research Center, Yangon and transmission electron microscopy (TEM, JEOL TEM-3010) with an accelerating voltage of 100 kV at State Key Laboratory, College of Science , Beijing University of Chemical Technology, China. The crystallite sizes of CuO NPs were calculated by using Image J software programme. TG-DTA (DTG-60H) Thermal Analyzer, SHIMADZU, Japan was employed for investigation of the thermal property of the synthesized samples. Fourier Transform (FT IR) spectra of copper(II) oxide samples were recorded on a FT IR spectrometer (FT IR-8400 SHIMADZU, Japan).

Results and Discussion

Mechanism for the Bioreduction of Cu^{2+} to CuO Nanoparticles

T. indica leaves and fruits contain polyphenolic compounds, for example gallic acid. These phenolic compounds have high reducing ability and they involve in bioreduction of Cu^{2+} to Cu_2O. Then Cu_2O was oxidized in air to produce CuO NPs. These phenolic compounds act as reducing as well as capping agents (Sharma *et al*., 2015). The proposed mechanism for the bioreduction of CuO is shown as follows:

$$Cu(NO_3)_2 \longrightarrow Cu^{2+} + 2NO_3^-$$

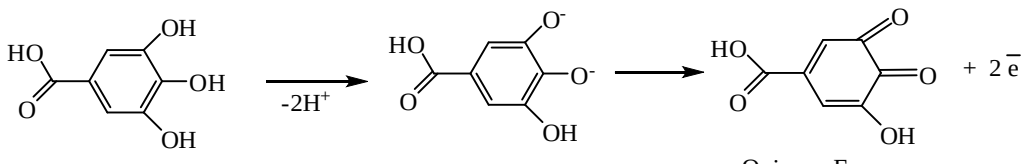

Gallic Acid (Phenolic Form) — Quinone Form

$$2\,Cu^{2+} + 4\bar{e} + \frac{1}{2}O_2 \longrightarrow Cu_2O \text{ (reduction)}$$

$$Cu_2O + \frac{1}{2}O_2 \text{ (air)} \longrightarrow 2CuO \text{ (oxidation)}$$

Characterization of the Prepared CuO NPs by XRD Analysis

Copper(II) oxide nanoparticles obtained by using leaves and fruits extracts of *T. indica* were characterized by X-ray diffraction analysis. X-ray diffraction patterns of the prepared copper(II) oxide nanoparticles at 200 ^{o}C are shown in Figure 1. Formation of Cu_2O instead of CuO was observed in the XRD pattern of copper oxide obtained by using leaves extract of *T.indica.* Phase identification of X-ray analysis shows a single phase of Cu_2O (Table 1). Furthermore, well-defined peaks were not observed in the XRD pattern of copper oxide obtained by using fruits extract of *T. indica*. Table 2 shows both CuO phase and Cu_2O phase in copper oxide obtained by using fruits extract . Increase the temperature to 300 ^{o}C and 400 ^{o}C, the diffraction peaks of CuO NPs obtained by using leaves and fruits extracts of *T. indica* were found to be well- resolved and most of Cu_2O particles were converted to CuO. However, Cu_2O peaks were still observed at these temperatures (Figures 2 and 3). At 500 ^{o}C, Cu_2O peaks disappeared in both samples obtained by using leaves and fruits extracts of *T. indica* and only single phase of CuO was observed (Figure 4). The XRD patterns show no impurity peaks. Prominent diffraction peaks of CuO were observed at 2θ values of 35.308^{o} and 38.518^{o} using leaves extract and 35.287 ^{o} and 38.473 ^{o} using fruits extract corresponding to the Miller indices of $(\bar{1}11)$ and (111) respectively. Comparison of X-ray diffractograms of copper(II) oxide nanoparticles by using leaves and fruits extracts at different temperatures are shown in the overlay of x-ray diffractograms (Figures 5 and 6). It was observed that as the temperature increased the diffraction peaks became well defined and the peaks corresponding to Cu_2O peak at 2θ of 29.444 ^{o} , 36.303 ^{o} , 42.069 ^{o} and 52.396 ^{o} disappeared.

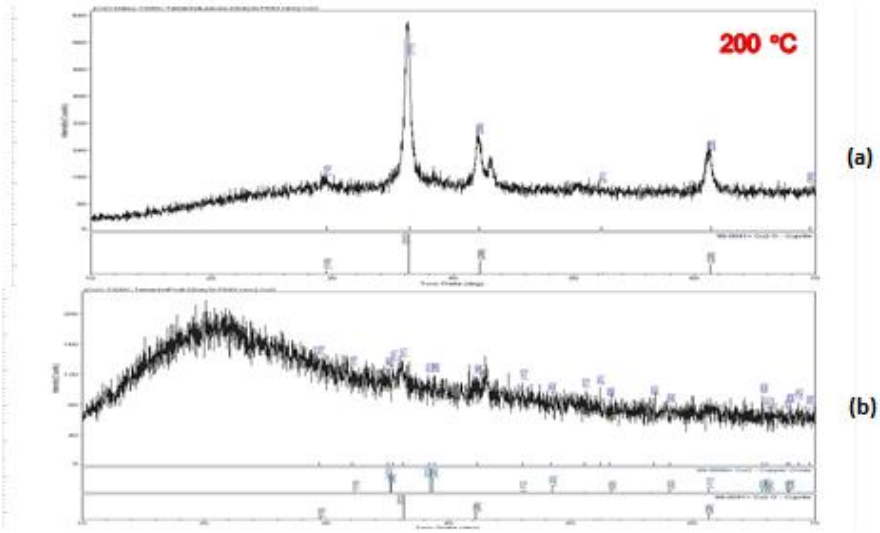

Figure 1 X ray diffractogram of the prepared CuO NPs by using (a) leaves extract and (b)fruits extract of *T. indica* at 200 °C

Table 1 Diffraction Angle, Interplanar Spacing and Miller Indices of the Prepared CuO NPs by Using Leaves Extract of *T. indica* at 200 °C

No.	Diffraction angle (2θ) (degree)	Interplanar spacing (Å)	Miller indices			Remark
			h	k	l	
1	29.119	3.0641	1	1	0	Cu_2O
2	36.243	2.4765	1	1	1	Cu_2O
3	42.121	2.1435	2	0	0	Cu_2O
4	52.050	1.7556	2	1	1	Cu_2O
5	61.258	1.5119	2	2	0	Cu_2O
6	69.546	1.3506	3	1	0	Cu_2O

Table 2 Diffraction Angle, Interplanar Spacing and Miller Indices of the Prepared CuO NPs by Using Fruits Extract of *T. indica* at 200 °C

No.	Diffraction angle 2θ (degree)	Interplanar spacing Å	Miller indices			Remark
			h	k	l	
1	29.437	3.0318	1	1	0	Cu_2O
2	32.176	2.7797	1	1	0	CuO
3	35.101	2.5544	0	0	2	CuO
4	35.400	2.5335	$\bar{1}$	1	1	CuO
5	36.211	2.4787	1	1	1	Cu_2O
6	38.453	2.3391	1	1	1	CuO
7	42.346	2.1327	2	0	0	Cu_2O
8	45.956	1.9732	$\bar{1}$	1	2	CuO
9	48.555	1.8735	$\bar{2}$	0	2	CuO
10	51.325	1.7787	1	1	2	CuO
11	52.397	1.7448	2	1	1	Cu_2O
12	53.157	1.7216	0	2	0	CuO
13	58.064	1.5872	2	0	2	CuO
14	61.149	1.5143	2	2	0	Cu_2O
15	61.262	1.5118	$\bar{1}$	1	3	CuO
16	65.713	1.4198	0	2	2	CuO
17	65.948	1.4153	$\bar{3}$	1	1	CuO
18	67.687	1.3831	1	1	3	CuO
19	67.915	1.3790	2	2	0	CuO
20	68.641	1.3662	$\bar{2}$	2	1	CuO

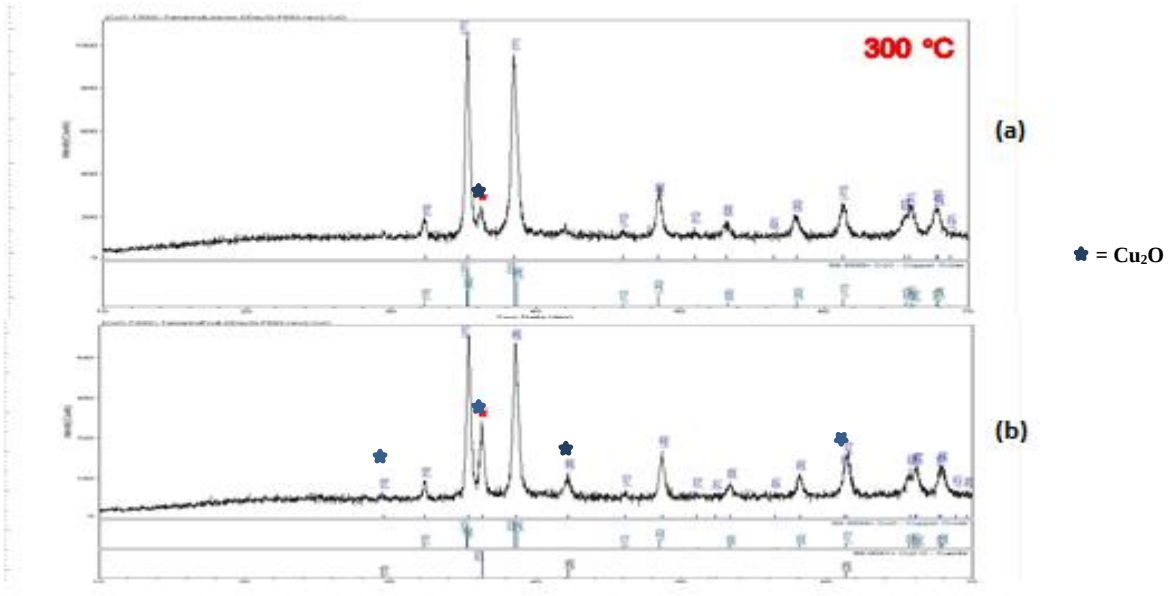

Figure 2 X ray diffractogram of the prepared CuO NPs by using (a) leaves extract and(b) fruits extract of *T. indica* at 300 °C

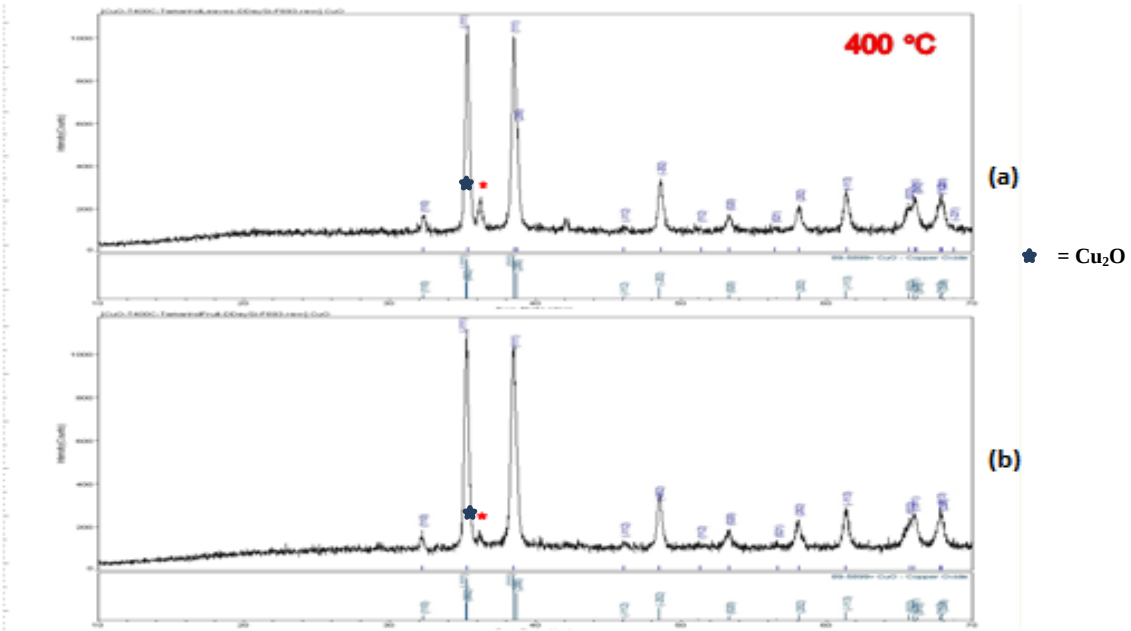

Figure 3 X ray diffractogram of the prepared CuO NPs by using (a) leaves extract and (b) fruits extract of *T. indica* at 400 °C

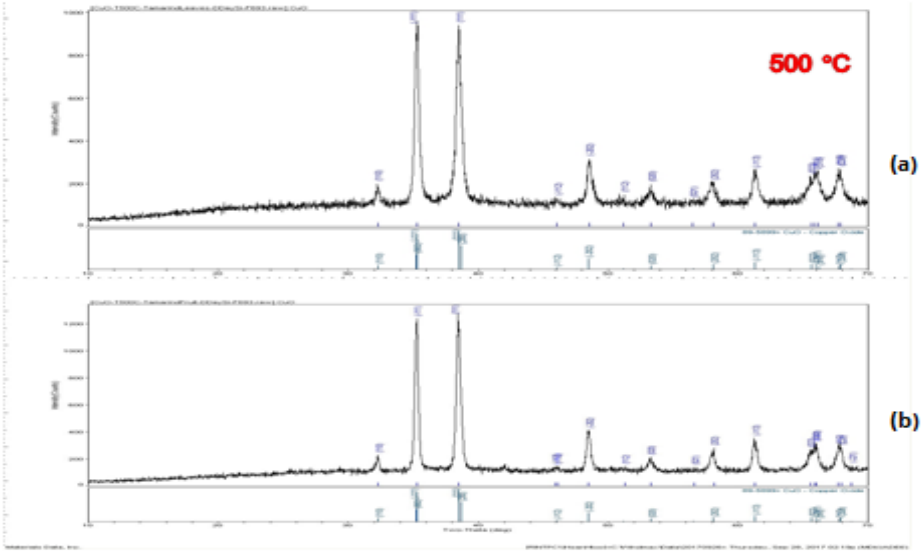

Figure 4 X ray diffractogram of the prepared CuO NPs by using (a) leaves extract and (b) fruits extract of *T. indica* at 500 °C

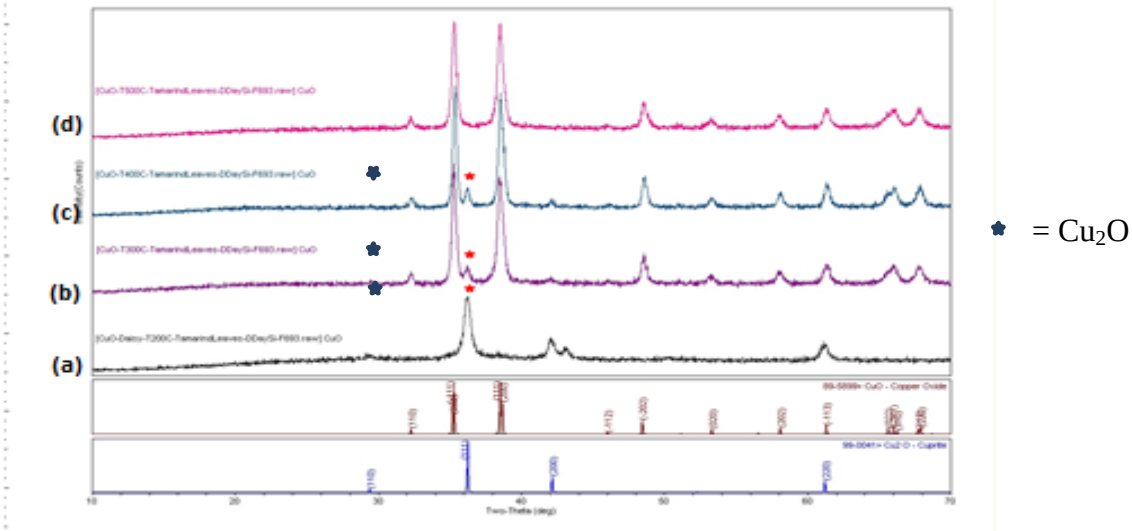

Figure 5 Comparison of X ray diffractograms of the prepared CuO NPs by using leaves extract of *T. indica* at (a) 200 °C (b) 300 °C (c) 400 °C and (d) 500 °C

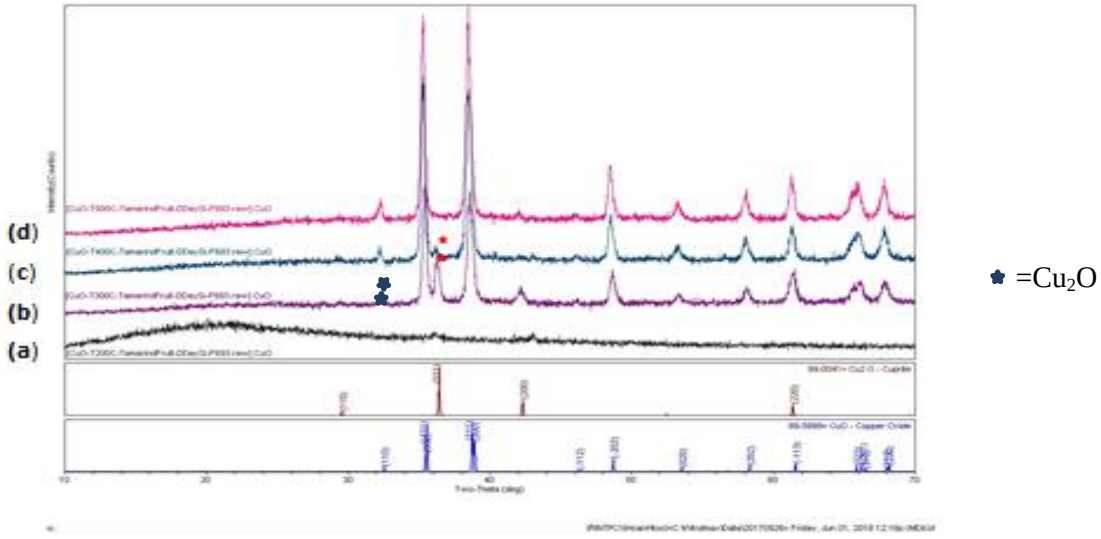

Figure 6 Comparison of the X ray diffractograms of the prepared CuO NPs by using fruits extract of *T. indica* at *(*a) 200 °C (b) 300 °C (c) 400 °C and (d) 500 °C

X –ray analysis is not only used for phase identification but also provide information on crystal structure and unit cell dimension. CuO NPs were indexed as monoclinic with a≠b≠c and $\alpha=\gamma=90^{o}$; $\beta\neq 90^{o}$ (Table 3). From X-ray diffraction analysis, the crystallite sizes of CuO NPs were calculated from full width at half maximum (FWHM) using Scherrer equation according to the following formula:

$$\tau = \frac{0.9\,\lambda}{\beta \cos\theta}$$

where τ is the crystallite size (nm), λ is the diffraction wavelength (0.154056 nm for Cu K α radiation), θ is the diffraction angle (degree) and β is the full width at half maximum (FWHM) for the diffraction peak (radian). The crystallite sizes of CuO NPs using leaves and fruits extracts are shown in Table 4 . As the temperature increased the crystallite sizes were found to decrease, however, the decrease in crystallite size was not pronounced in CuO NPs obtained by using leaves extract of *T. indica*. The crystallite sizes of CuO NPs obtained at 500 ^{o}C were 19.9 nm and 20.9 nm by using leaves extract and fruits extract respectively.

Table 3 Lattice Parameters and Crystal Structures of the Prepared CuO NPs by Using Leaves and Fruits Extracts of *T. indica* at Different Temperatures

No.	Parameter	Temperature (°C)					
		300		400		500	
		Leaves extract	Fruits extract	Leaves extract	Fruits extract	Leaves Extract	Fruits extract
1	Lattice constant Axial length (Å)	a=4.7235	a=4.6922	a=4.7007	a=4.6984	a=4.7093	a=4.6829
		b=3.4470	b=3.4443	b=3.4536	b=3.4673	b=3.4557	b=3.4614
		c=5.1666	c=5.1573	c=5.1319	c=5.1602	c=5.1307	c=5.1512
2	Interaxial angle (◦)	α,γ=90	α,γ=90	α,γ=90	α,γ=90	α,γ=90	α,γ=90
		β=99.26	β=99.60	β=99.66	β=99.91	β=99.59	β=99.87
3	Crystal structure	Monoclinic		Monoclinic		Monoclinic	

Table 4 Crystallite Sizes of the Prepared CuO NPs at Different Temperatures

No.	Temperature (^{o}C)	Average crystallite size (nm)	
		Leaves extract	Fruits extract
1	300	20.9	26.0
2	400	20.4	21.3
3	500	19.9	20.9

Characterization of the Prepared Copper(II) Oxide Nanoparticles by Scanning Electron Microscopy (SEM) and Transmission Electron Microscopy (TEM) Analysis

SEM images of prepared CuO nanoparticles by using leaves and fruits extracts are depicted in Figure 7. A large number of quasi-spherical nanoparticles were observed in CuO NPs using leaves extract of *T. indica* and particles with dense agglomerates were observed in those using fruits extract.

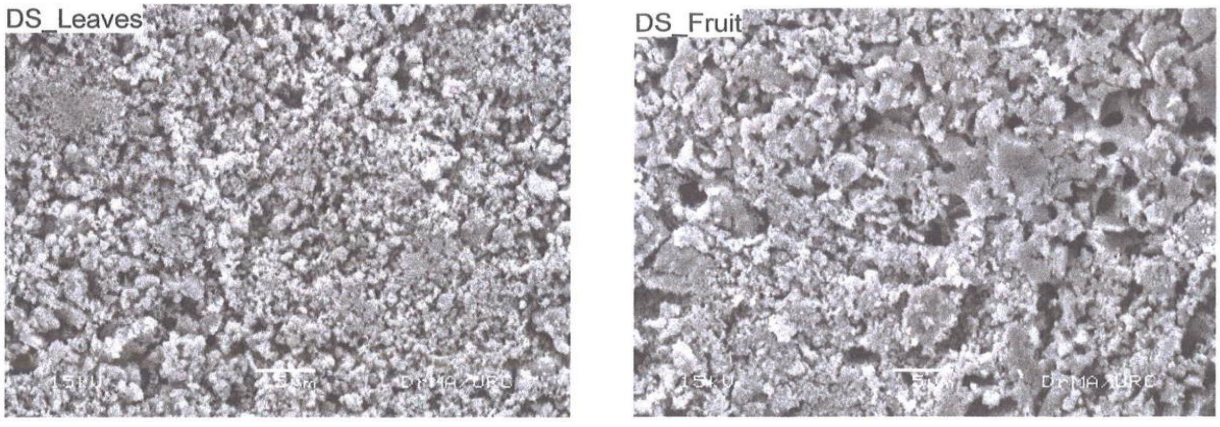

(a) (b)

Figure 7 SEM micrographs of the prepared CuO by using (a) leaves extract and (b) fruits extract of *T. indica*

Using TEM analysis, both the size and shape of the obtained nanoparticles were observed. Figure 8 shows TEM images of CuO NPs by using leaves and fruits extracts of *T. indica.* The average sizes of CuO nanoparticles by using leaves and fruits extracts of *T. indica* were found to be 21.2 nm and 21.7 nm respectively. The sizes were not much different from those obtained by X-ray diffraction analysis.

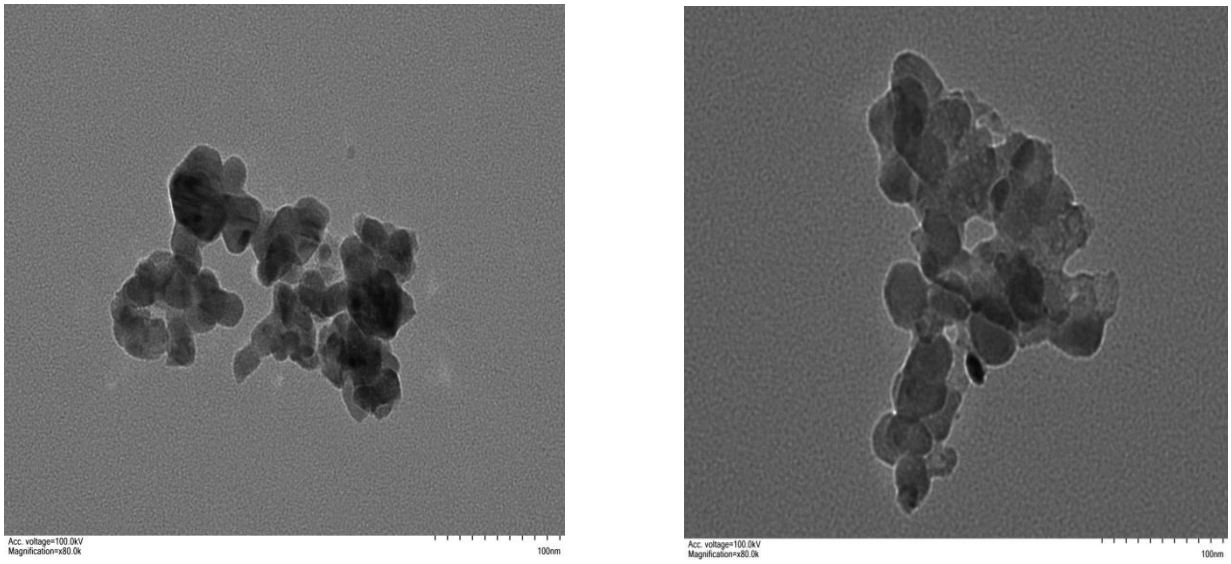

(a) (b)

Figure 8 TEM images of the prepared CuO NPs by using (a) leaves extract and (b) fruits extract of *T. indica* (Magnification=×80.0k)

Characterization of the Prepared Copper(II) Oxide Nanoparticles by Thermogravimetric-Differential Thermal Analysis

Thermal analysis of CuO NPs obtained before calcination was carried out. Figure 9 shows the TG-DTA thermogram of CuO NPs obtained by using leaves extract of *T. indica* and its thermal data are shown in Table 5. Similarly, the thermogram of CuO NPs obtained by using fruits extract and its thermal data are shown in Figure 10 and Table 6. The sfirst endothermic peak was due to the removal of physically sorbed water. The second endothermic peak was due to removal of chemisorbed water. The exothermic peak appeared at 329.43 ºC in CuO NPs by using leaves extract and that appeared at 320.29 ºC in CuO NPs by using fruits extract were due to conversion of Cu_2O to CuO (Xu *et al*., 2004). It was observed that CuO NPs were almost thermally stable beyond 400 ºC. Thus, thermal analysis data confirmed the calcination temperature of 500 ºC for synthesis of CuO.

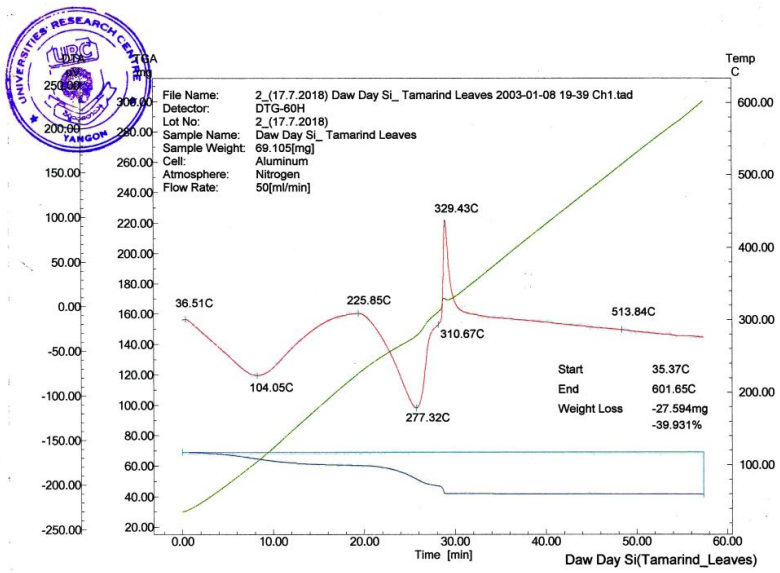

Figure 9 TG-DTA thermogram of the prepared CuO NPs by using leaves extracts of *T. indica*

Table 5 TG-DTA Data of the Prepared CuO NPs by Using Leaves of Extract *T. indica*

No.	Temperature range (°C)	Break in Temp: (°C)	Weight Loss (%)	Nature of Peak	Remark
1	36.51-230	104.05	12.886	Endothermic	Desorption of physically adsorbed water molecules
2	230-310	277.32	19.934	Endothermic	Removal of chemisorbed water
3	310-350	329.43	6.639	Exothermic	Conversion of Cu_2O to CuO
4	350-601.65	-	0.047	-	Thermally stable

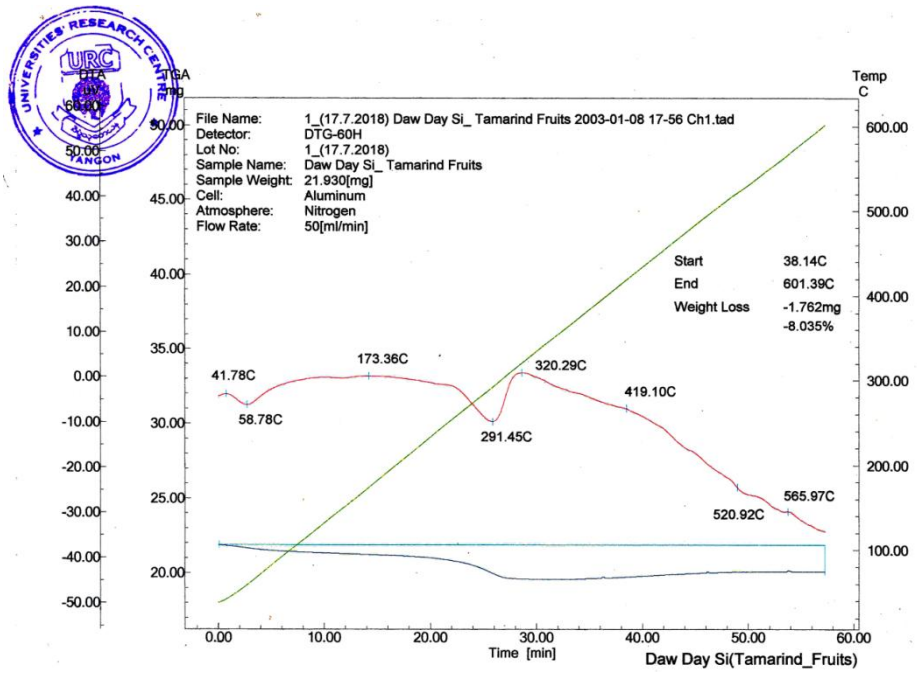

Figure 10 TG-DTA thermogram of the prepared CuO NPs by using fruits extracts of *T. indica*

Table 6 TG-DTA Data of the Prepared CuO NPs by Using Fruits of Extract *T. indica*

No.	Temperature range (ºC)	Break in Temp: (ºC)	Weight Loss (%)	Nature of Peak	Remark
1	41.78-175	58.78	3.556	Endothermic	Desorption of physically adsorbed water molecules
2	175-325	291.45	4.492	Endothermic	Removal of chemisorbed water
3	325-360	320.29	0.008	Small	Conversion of Cu_2O to CuO
4	360-601.39	-	0.002	exothermic	Thermally stable

Characterization of the Synthesized Copper(II) Oxide Nanoparticles by Fourier Transform Infrared Analysis

The synthesized CuO NPs were characterized by FT IR analysis. Figures 11 and 12 show FT IR spectra of CuO NPs. FT IR spectral data are shown in Table 7. The absorption peaks between 430-606 cm^{-1} were attributed to the vibration of Cu-O stretching and indicated the formation of CuO NPs.

Figure 11 FT IR spectrum of the prepared CuO NPs by using leaves extract

Figure 12 FT IR spectrum of the prepared CuO NPs by using fruits extract

Table 7 FT IR Spectral Data of the Prepared CuO NPs by Using Leaves and Fruits Extracts of *T. indica*

No.	Observed Wavenumber (cm^{-1})		Reported value (cm^{-1})	Assignment
	Leaves extract	Fruits extract		
1	511	530	430-606*	Characteristic Cu-O vibration
2	**434**	**461**		

* Alizadeh-Gheshlaghi *et al*., 2012

Conclusion

A simple, eco-friendly and efficient synthesis of CuO NPs by using leaves and fruits extracts of *T. indica* was reported in this study. Aqueous extracts of *T. indica* leaves and fruits have been used as reducing agent and also as a capping agent in the CuO NPs synthesis. The XRD analysis confirmed the crystalline nature of CuO NPs with monoclinic structure and the average crystallite sizes from leaves and fruits extracts were found to be 19.9 nm and 20.9 nm, respectively. Crystallite sizes of CuO nanoparticles from leaves and fruits extracts were 21.2 nm and 21.7 nm by TEM analysis. SEM images showed a large number of quasi-spherical nanoparticles with dense agglomerates. Thermal analysis of CuO nanoparticles showed that CuO was almost thermally stable beyond 400 ºC. The presence of characteristic vibration of Cu-O in the range of 430-606 cm^{-1} was confirmed by FT IR analysis. In future, this green method of synthesizing CuO nanoparticles could also be extended to the fabrication of other industrially important metal oxides.

Acknowledgement

The authors would like to express their profound gratitude to the Department of Higher Education (Yangon Office), Ministry of Education, Yangon, Myanmar, for provision of opportunity to do this research and Myanmar Academy of Arts and Science for allowing to present this paper.

References

Alizadeh-Gheshlaghi, E., Shaabani, B., Khodayari, A., Azizian-Kalandaragh , Y. and Rahimi, R. (2012). "Investigation of the Catalytic Activity of Nano-sized CuO, Co_3O_4 and $CuCo_2O_4$ Powders on Thermal Decomposition of Ammonium Perchlorate". *Powder Techno,* vol. 217, pp. 330–339

Etefagh, R., Azhir, E. and Shahtahmasebi, N. (2013). "Synthesis of CuO Nanoparticles and Fabrication of Nanostructural Layer Biosensors for Detecting Aspergillus niger Fungi". *Science Iranica*, vol. 20(3), pp.1055-1058

Faheem, I., Sammia S., Shakeel A.K. and Waqar, A. (2017). "Green Synthesis of Copper Oxide Nanoparticles using *Abutilon indicum* Leaf Extract: Antimicrobial, Antioxidant and Photocatalytic Dye Degradation Activities". *Tropical Journal of Pharmaceutical Research*, vol. 16(4), pp. 743-753

Ghorbani, H.R. (2014). "Chemical Synthesis of Copper Nanoparticles". *Oriental Journal of Chemistry*, vol. 30(2), pp. 803-806

Joshua, P. J., Krishnan, S., Raj, D.J.V., Uthrakumar, R., Laxmi, S. and Das, S.J. (2014). "Novel Synthesis of Tenorite (CuO) Nanoparticles by Wet Chemical Method". *International Journal of Chem Tech Research,* vol. 6(3), pp. 2002-2004

Katwal, R., Kaur, H., Sharma, G., Naushad, M. and Pathania, D. (2015). "Electrochemical Synthesis Copper Oxide Nanoparticles for Enhanced Photocatalytic and Antimicrobial Activity". *Journal of Industrial and Engineering Chemistry,* vol. 31, pp. 173-184

Kitowaki, H., Oku, T., Akimaya, T. and Suzuki, A. (2012). "Fabrication and Characterization of CuO-Based Solar Cells". *Journal of Materials Science Research*, vol. 1(1), pp. 138-143

Outokesh, M., Hosseinpour, M., Ahmadi, S.J., Mousavand, T., Sadjadi, S. and Soltan, I.W. (2011). "Hydrothermal Synthesis of CuO Nanoparticles: Study on Effects of Operational Conditions on Yield, Purity, and Size of the Nanoparticles". *Industrial and Engineering Chemistry Research,* vol. 50, pp. 3540-3554

Phiwdang, K., Suphankij, S., Mekprasart, W. and Pecharapa, W. (2013). "Synthesis of CuO Nanoparticles by Precipitation Method using Different Precursors". *Energy Procedia,* vol. 34, pp. 740-745

Ren, G., Hu, D., Cheng, W.C., Vargus-Reus, M.A., Reip, P. and Allaker, R.P. (2009). "Characterization of Copper Oxide Nanoparticles for Antimicrobial Applications". *International Journal of Antimicrobial Agents*, vol. 33(6), pp. 587-590

Sharma, J.K., Akhtar, M.S., Ameen, S., Srivastava, P. and Singh, G. (2015). "Green Synthesis of CuO Nanoparticles with Leaf Extract of *Calotropis gigantea* and its Dye-sensitized Solar Cells Application". *J Alloys Compd*, vol. 632, pp. 321-325

Thi, T.V., Rai, A. K., Gim, J. and Kim, J. (2014). "Potassium-Doped Copper Oxide Nanoparticles Synthesized by Solvothermal Method as an Anode Material for High-Performance Lithium Ion Secondary Battery". *Applied Surface Science*, vol. 305, pp. 617-625

Xu, C.H., Woo, C.H. and Shi, S.Q. (2004). " Formation of CuO Nanowires on Cu Foil". *Chemical Physics Letters*, vol. 399 (1), pp. 62-66

Zhang, L., Yuan, F., Zhang, X. and Yang, L. (2011). "Facile Synthesis of Flower Like Copper Oxide and their Application to Hydrogen Peroxide and Nitrite Sensing". *Chemistry Central Journal*, vol. 5 (75), pp. 220-227

ANALYSIS OF DIMETHOATE AND DIAZINON PESTICIDE RESIDUES IN SOIL BY GAS CHROMATOGRAPHY

Ohnmar Aung[1], Ohn Ohn Soe[2], Ni Ni Sein[3], Kyaw Nyaing[4], Aung Myint[5]

Abstract

Pesticides are shown to have a great effect on soil organisms, but the effect varies with pesticide group and concentration, and is modified by soil organic carbon content and soil texture. Dimethoate and diazinon pesticide residues in soil under pesticide-treated plants were detected by use of high resolution gas chromatography equipped with phosphorus flame photometric detector (GC-PFPD). The residue concentrations in the soil were related to their physicochemical properties. Diazinon exhibited the higher concentration in the soil under pesticide-treated plants areas (0.3764 ppm, 2 h after application), while dimethoate was found at lower concentration (0.3169 ppm). All two pesticides were accumulated in soil sample during the first 24 h after application but the dimethoate concentrations rapidly decreased to 97.79 % after application for 5 days, while diazinon residues decreased to 98.51 % at the end of the 7 days monitoring period. The rate constants and half-lives of double exponential decay model and pseudo-first order equations in soil under pesticide-treated plots were determined.

Keywords: pesticides, soil, dimethoate, diazinon, phosphorus flame photometric detector

Introduction

Pesticides are extensively used in agricultural production to check or control pests, diseases weeds and other plant pathogens in an effort to reduce or eliminate yield losses and preserve high product quality. Pesticides constitute a very important group of chemical compounds that have to be controlled due to their high toxicity and their widespread use in agricultural practice for field and post-harvest protection (Ortelli *et al*., 2006). Pesticides can be as liquid sprays on the soil or crop plant, may be incorporated or injected into the soil or applied as granules or as a seed treatment. Once they have reached their target area, pesticides disappears via degradation, dispersion, volatilization or leaching into surface water and groundwater, they may be taken up by plants or soil organisms or they may stay in the soil (Mahmood *et al*., 2016).

Multimedia monitoring of contaminants such as insecticides is an essential part in investigating the entire spectrum of environmental contamination. The fate of insecticides and their transformation products (TPs) in the soil depend of interaction in the soil depend on the properties of their active ingredients and degree of interaction with the soil particles (or adsorption) (Del Prodo-Lu, 2015).

The main entry ways for pesticides in the soil are either through plants pulverization or its direct application to the soil, where the persistence in this environment is influenced by several factors such as, pesticides physicochemical properties: molecular size, water solubility, volatility, molecular structure, chemical function and acid-base nature; soil properties: soil type, moisture content, organic carbon content, pH, redox potential, microbial population; environmental conditions: climate, topography, air currents, variables related to the application of pesticides:

[1] Dr, Lecturer, Department of Chemistry, Dagon University
[2] Dr, Associate Professor, Department Chemistry, Loikaw University
[3] Dr, Professor (Rtd), Department of Chemistry, University of Yangon
[4] Dr, Deputy Permanent Secretary, Ministry of Education, Nay Pyi Taw
[5] Dr, Associate Professor (Rtd), Department of Chemistry, University of Yangon

concentration, frequency and mode of application; and also used of other chemicals (Muenchen *et al*., 2016).

Soil is a complex and heterogeneous environment, composed of minerals, organisms with characteristics varying according to the climate and the source material. The soil is very important for food production and maintenance of socio-economic activities, and its prevention depends on the monitoring of contamination in order to avoid drastic impacts (Boesten, 2016). Soil is the principal reservoir of environmental pesticides, this representing a source from which residues can be released to the atmosphere, ground water and living organisms (Ghabbour *et al*., 2012).

Organophosphorus pesticides are the most widely used in agriculture, home, gardens, and veterinary practice. The implications of high pesticides residue include muscle cell degeneration, which involves the respiratory muscles. Chronic exposure to organophosphate might damage the peripheral nervous system, and patient's behavioural abilities and/or personality, chronic fatigue syndrome and effects on the heart (Akan *et al*., 2013). Most organophosphorus compounds have a short residual activity e.g., diazinon, dimethoate, malathion, chlorpyrifos, fenitrothion, etc. Dimethoate and diazinon are systemic and nonsystemic organophosphate insecticides which are widely used in vegetable farms for plant protection (Ware and Whitacre, 2004).

The main aim of this study was to investigate the gas chromatographic analysis of dimethoate and diazinon pesticide residues in soil and to compare the rate constants and half-lives of both pesticides by double exponential decay model and pseudo-first order equations.

Materials and Methods

Study Area

The experiments were conducted in the vegetable farm of Alantapo Village, Hlegu Township, in Yangon Region. The experimental farm had an area of 35 x 25 ft.

Spraying of Insecticides

The commercial plant-production products used were Danadim 40 EC (dimethoate 40 %) and Dynamite 40 EC (diazinon 40 %) pesticides, applied in the trials. These products were diluted with water to obtain recommended dose (20 mL of emulsifiable concentrate per gallon) as spray tank using manual sprayer and the application required about 20 min (Ohnmar Aung *et al*., 2007). In all the treatments the operator was the same person. The spray operator walked in and out of the rows of the benches with the plants, spraying up and down from the bottom to the top of the plants and back again (Hatzilazarou *et al*., 2005).

Sample Collection, Storage and Preparation

Soil samples under pesticide-treated plants were collected according to the sampling schedule of plant on day 0 (2 h after application), day 1, day 3, day 5, day 7 and day 9 after application of pesticides. Soil sample were taken down to a depth of 10-20 cm with a stainless steel auger of 6.5 cm diameter by turning the auger once anti-clockwise before pulling it, back to surface. The soil samples were then randomly selected and bulked together to form a composite sample before being placed in clean plastic bags. The soil portion were cut off using clean steel scissors, placed into a plastic sealed bag and transported to the laboratory where they were

analyzed immediately or stored at -4 °C until extraction and analysis. After thoroughly mixing of the collected soil samples, they were partially air dried under room temperature, then passed through sieves of 25 meshes to maintain a uniform particle size. The prepared soil samples were stored in plastic bag under room temperature, such a way of storage was considered to keep the used soil in normally physical conditions. The soil was subjected to the physical and chemical analysis (Seema, 1999).

Quality Assurance and Quality Control

Proper quality assurance procedures and precautions were taken to ensure the reliability of the results. The samples were carefully handled to avoid any external influences that could interfere with the integrity of the sample and hence contaminate it. All glassware were washed with detergent, rinsed with distilled water, thoroughly rinsed with analytical grade acetone and dried overnight in an oven at 150 ^{o}C. The glassware were then removed from the oven and allowed to cool down and stored in dust-free cabinets. Deionized water was used through out the study (Fosu-Mensah *et al*., 2016).

Extraction of Soil Samples

A standard laboratory procedure was used to analyze the material samples. A 50 g of each soil sample was obtained by using coning and quartering method (Black, 1965). Pesticides were extracted from soil samples with 150 mL of acetone: hexane (1:1) by soxhlet extraction apparatus for 3 h. Then, the volume extracted was measured and 5 mL of this extract was placed in a graduated test tube and reduced to 0.3 mL by using nitrogen gas stream. The concentrates were adjusted to 1 mL final volume with cyclohexane and made ready for silica cleanup step (Akan *et al*., 2013).

Cleanup of Soil Extract

The column contained a small piece of cotton wool, neutral alumina and a bed height of 5 mm of anhydrous sodium sulphate. A 1 mL of the extract was added onto column and eluted with cyclohexane until 5 mL of eluate was obtained. Then, it was evaporated just to the point of dryness with a slight nitrogen stream, after which internal standard solution (fenitrothion) was added prior to gas chromatography analysis. All extracts were kept frozen until quantification was achieved (Frimpong *et al*., 2013).

Gas Chromatographic Determination

The final extracts were analyzed by gas chromatography equipped with P-mode of flame photometric detector (PFPD). The GC conditions and the detector response were adjusted so as to match the relative retention times and response as spelt out by the analytical methods for agricultural chemicals (Syoku-An, 2006). The injection volume of the GC was 1.0 µL in a splitless mode. The retention time, peak area and peak height of the sample was compared with those of the standards for quantization. The flow rate of carrier gas, nitrogen, was set at 10 mL/ min and hydrogen and air were used for combustion. Dimethoate and diazinon extracts were determined on a gas chromatography-flame photometric detector equipped with a fused silica capillary (PE-1) column containing cross bond 100 % dimethylpolysiloxane as stationary phase (30 m length, 0.53 mm internal diameter (i.d), 1.5 µm film thickness). Temperature programming for the column temperature of 100 ^{o}C which was maintained for 3 min and raised to 250 ^{o}C at 30 ^{o}C /min and the temperature was maintained for 10 min. Both the injector and detector temperature were set at 250 ^{o}C.

The three different standard dimethoate solution (7.6764, 15.3528 and 30.7056 μg/mL) and those of diazinon solution (5.3525, 10.7050 and 21.4100 μg/mL) were mixed with internal standard (ISTD) fenitrothion (14.18 μg/mL) and subjected to gas chromatographic measurements. The peak areas whose retention times coincided with the standards were extrapolated on their corresponding calibration curve to obtain the concentration (Ohnmar Aung *et al*., 2008).

Fortified and blank samples were analyzed with soil samples from each sampling date. Quantification of pesticide residues in samples were performed by internal standard (fenitrothion) method. For recovery studies, 1mL of a standard dimethoate spiked solution (10.2352 μg/mL) and standard diazinon spiked solution (10.7050 μg/mL) in acetone was added to control and allowed to stand for 15 min before extraction, for three replications. Each peak was characterized by comparing relative retention time of those of standards.

Results and Discussion

Physicochemical Analysis of Soil

Table 1 summarizes the physicochemical properties of the soil samples collected from the experimental plots in relation to under pesticide-treated lettuce plants. The mean moisture content of the air-dried soli sample was found to be 0.93 ± 0.01 %. The mean pH recorded for the entire study was 5.30 ± 0.14, and thus it was slightly acidic. The low pH values recorded could be due to the amount of acidic cations present in the soil due to the leaching of basic cations or the presence of high level of organic matter within the soil zones. The mean total nitrogen content of soil samples from experimental plot was found to be 0.19 ± 0.17 %. The amount of nitrogen in surface soils generally ranges from 0.02 to 0.25 %. The mean organic carbon content was 0.76 ± 0.03 % and the mean humus content recorded in this study was 1.52 ± 0.12 %. Low organic matter content is due to high temperature in tropical soils and thus high decomposition rates.

Table 1 Physicochemical Analysis of Soil

Moisture content (%)	pH	Total nitrogen (%)	Organic carbon (%)	Humus (%)
0.93 ± 0.01	5.30 ± 0.14	0.19 ± 0.17	0.76 ± 0.03	1.52 ± 0.12

Preliminary Investigation of Soil Type of the Experimental Plot

Soil is a mixture of mineral matter, organic material, air and water. The mineral portions of soil made up of particles which vary in size from stones to powder. These particles are called soil separates. Three major groups of soil separates are sand (2.00-0.050 mm), silt (0.050-0.002 mm) and clay (<0.002 mm). The soil type of experimental plot is shown in Table 2. The soil contained 46.55 % sand, 36.64 % silt, and 14.36 % clay. The texture of soil was found to be loamy soil according to textural triangle (Gee and Bouder, 1986). It was observed that soil are said to be light soil due to low clay and high sand contents.

Table 2 Preliminary Investigation of Soil Type of the Experimental Plot

Sand (%)	Silt (%)	Clay (%)	Soil type
46.55 ± 1.35	36.64 ± 1.03	14.36 ± 2.48	Loamy soil

Relative Abundance of Elements in Soil from the Experimental Plot

Semi-quantative results of soil in experimental plots are shown in Figure 1 and Table 3. The elemental contents in decreasing order were Si> Fe> Ti> K> Ca> Zr> Cr> Cu> Zn> Ni.

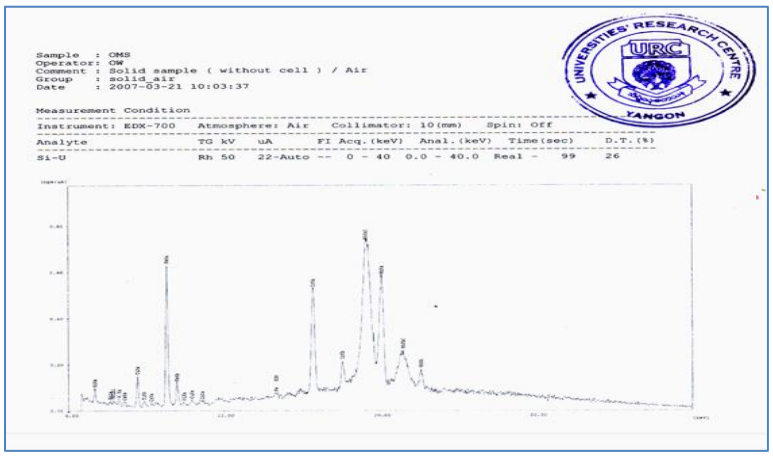

Figure 1 EDXRF spectrum of soil under study

Table 3 Relative Abundance of Elements in Soil by EDXRF

No.	Element	Relative abundance (%)	Standard deviation
1	Si	94.431	3.704
2	Fe	2.007	0.022
3	Ti	1.319	0.033
4	K	1.243	0.064
5	Ca	0.454	0.027
6	Zr	0.301	0.003
7	Cr	0.110	0.007
8	Cu	0.053	0.003
9	Zn	0.043	0.002
10	Ni	0.039	0.002

Gas Chromatograms of Standard Dimethoate and Diazinon

Figure 2 shows the gas chromatograms of standard dimethoate and diazinon. Thretention time of dimethoate and diazinon were 3.57 and 3.86 min, respectively.

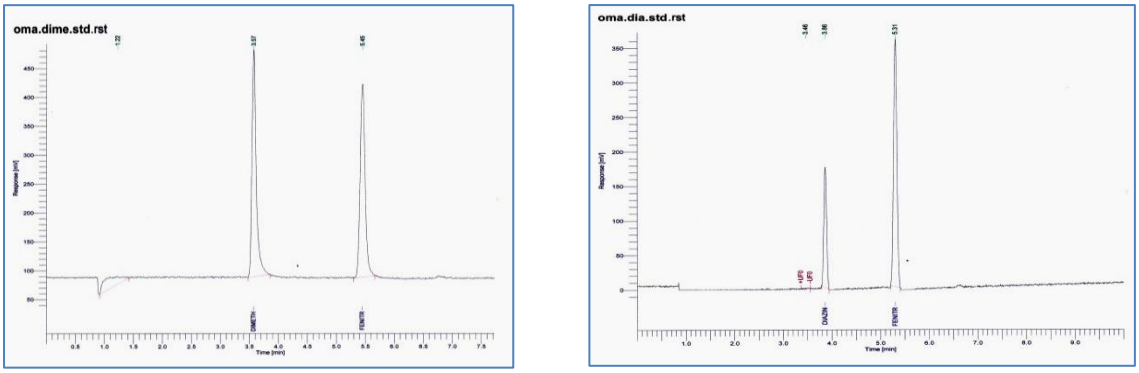

(a) (b)

Figure 2 Gas chromatograms of standard (a) dimethoate and (b) diazinon

Extraction Efficiency (Recovery Percent)

Due to the diversity and complexity of soil types and interactions of their constituents with pesticides, different physicochemical properties of pesticides and low concentrations expected for those pollutants in the soil (Singh, 2014), there is a need for efficient sample extraction techniques before their determination by chromatography (Asensio-Ramos, 2009). Extraction efficiencies of insecticidal residues were commonly measured by addition of known amounts of the chemical to an untreated sample often immediately prior to the extraction procedure followed by the determination of the recovery. The efficiency of the analytical methods (the extraction and clean-up methods) was determined by recoveries of an internal standard. The efficiencies of dimethoate and diazinon were tested by using three different standard concentration levels (Table 4). In this study, good mean recovery percentages were 91.37 ± 1.16 % for dimethoate at three different standard concentration levels (7.6764 μg/mL, 15.3528 μg/mL and 30.7056 μg/mL), and 88.95 ± 1.72 % for diazinon at three different standard concentration levels (5.3525 μg/mL, 10.7050 μg/mL and 21.4100 μg/mL) in soil at 95 % confidence level respectively. On this basis, it was concluded that the good recoveries obtained for substrates spiked in the sample indicated good analytical techniques.

Table 4 Recovery Percent of Dimethoate and Diazinon Pesticide Extracts from Soil at Three Different Standard Concentration Levels

Experimental number	Recovery (%)					
	Dimethoate			Diazinon		
	Level 1	Level 2	Level 3	Level 1	Level 2	Level 3
1	92.36	92.49	92.04	92.30	92.90	91.01
2	89.58	88.92	88.23	86.58	86.92	87.23
3	88.82	89.41	89.28	82.32	83.41	83.28
4	93.86	93.94	93.27	91.86	92.04	92.79
5	92.87	92.98	92.49	90.67	91.43	90.49
Mean	91.50	91.55	91.06	88.55	89.34	88.96
±	±	±	±	±	±	±
SD	2.18	2.24	2.18	4.05	4.04	3.76
Mean of accuracy at level 1, 2, 3	0.23 ± 0.10			0.30 ± 0.25		
Precision	0.51			0.45		
95 % confidence interval	91.37 ± 1.16			88.95 ± 1.72		

Organophosphorus Pesticide Residues in Soil under Pesticide-Treated Lettuce Plants

Table 5 presents the mean summary results of the organophosphorus pesticide residues detected in soil samples from the study area. Two organophosphorus pesticides namely; dimethoate and diazinon were detected in the soil samples under pesticide-treated plants. Dimethoate was found in the soil at lower concentrations than diazinon. The highest concentration of dimethoate was 0.3169 ± 0.0240 ppm after 2 h application but its concentration decreased steadily within the next 5 days (120 h) (Figure 3). The concentration of dimethoate was 0.0691 ± 0.0084 ppm 3 days after the insecticide application, while its concentration of 24 h after application was 0.1988 ± 0.0193 ppm. Thus, 5 days after the application its concentration was 0.0070 ± 0.0025 ppm. The concentration of dimethoate was not detected 168 h (7 days) after insecticide application. The mean concentrations of dimethoate recorded were below the maximum residue limit (MRL) of 0.02 ppm after 120 h (5 days) of its application (WHO, Codex MRL, 2002).

Diazinon, the pesticide with the higher concentration, exhibited the mean highest concentration in soil 2 h (0 day) after application (0.3764 ± 0.0321 ppm), decreasing at the end of the 7-day monitoring period to 0.0056 ± 0.0007 ppm (Figure 3). The diazinon residue levels reached below the MRL value of 0.04 ppm after (5 days) of its application (WHO, Codex MRL, 2002).

The detection of organophosphorus pesticides in the soil samples suggests that these pesticides may have found their way into the soils via spray drift during plant spraying, wash-off from treated plants and wrong disposal of left over spray solution, sprayer wash water and used pesticide containers.

Table 5 Mean Concentrations of Dimethoate and Diazinon Residues in Soil under Pesticide-Treated Plants as a Function of Sampling Interval

Sampling interval (h)	Residues (ppm)	
	Dimethoate	Diazinon
0	0.3169 ± 0.0240	0.3764 ± 0.0321
24	0.1988 ± 0.0193	0.2000 ± 0.0247
72	0.0691 ± 0.0084	0.0710 ± 0.0183
120	0.0070 ± 0.0025	0.0260 ± 0.0112
168	ND	0.0056 ± 0.0007
216	ND	ND

Figure 4 shows the results of percent degradation of two organophosphorous pesticide residues in soil under pesticide-treated plants. The results obtained show that percent degradation of dimethoate was 37.27 % after 24 h (1 day) application. Similary, percent degradationn of diazinon was in 46.87 % in soil samples analyzed after 24 h. Dimethoate and dizinon residues degraded almost completely (i.e., 100 %) 120 h (5 days) and 7 days (168 h) after application respectively. The data showed that the degradation of dimethoate proceeded at a much faster rate than that of diazinon in the soil. It is because dimethoate is rapidly broken down by soil microorganisms.

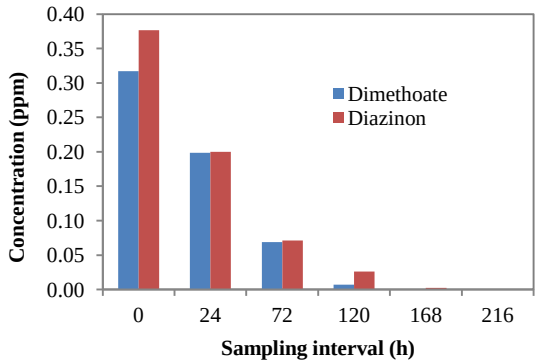

Figure 3 Concentrations of dimethoate and diazinon residues in soil as a function of sampling time interval

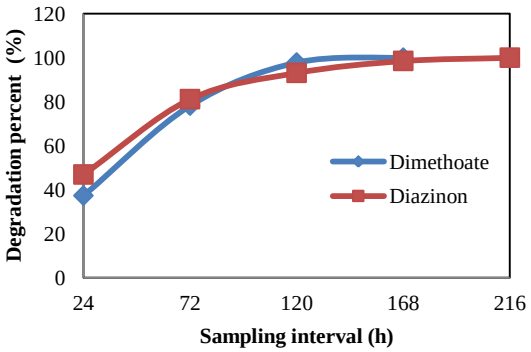

Figure 4 Percent degradation of dimethoate and diazinon residues in soil as a function of sampling time interval

Rate Constants and Half-Lives of Dimethoate and Diazinon Pesticides in Soil

In this research, the degradation of dimethoate and diazinon pesticide residues in soilwere successfully interpreted by using double exponential decay model. Non-regression model parameters of double exponential decay of dimethoate and diazinon in soil are summarized in Table 6. The dissipation curves were fitted for the individual pesticides in soil by nonlinear regression with the Sigma Plot for Windows 4.01 curve fitting package ($y = a\ e^{-bx} + c\ e^{-dx}$) with r^2= 0.9953 and 0.9998 for dimethoate and diazinon-treated soil (Laab *et al*., 2002). The data show that the calculated value from model equation (a+c) are in agreement with the measured values obtained from Gas Chromatographic analysis (GC). Rate constant and half-lives of the degradation of the pesticides were calculated by graphical method.

Table 6 Non-regression Model Parameters of Double Exponential Decay of Dimethoate and Diazinon Residues in Soil under Pesticide-Treated Lettuce Plants

$$y = a\ e^{-bx} + c\ e^{-dx}$$

Sample	Parameter						
	a (ppm)	b (h^{-1})	c (ppm)	d (h^{-1})	r^2	(a+b) (ppm)	GC (ppm)
Soil*	0.1571	0.0220	0.1644	0.0220	0.9953	0.3215	0.3169
Soil**	0.0383	1.2820	0.3381	0.0218	0.9998	0.3764	0.3764

* - under dimethoate-treated lettuce plant

** - under diazinon-treated lettuce plant

Comparison of the rate constants and half-lives of dimethoate and diazinon pesticides soil under lettuce plants were used to fit double exponential decay model and pseudo-first order equations (Table 7). Therefore, the results obtained show that the degradation rate constants and half-lives for dimethoate and diazinon pesticides in both cases were statistically not markedly different. It is because the rate constants and hence half-life do not depend on the initial concentration. The student's t test was carried out for the comparison of rate constants and half-lives between double exponential decay model and pseudo-first order equations. The calculated t-value (1.5621) is smaller than tabulated t-value (4.303) at 95 % confidence intervals (Day and Underwood, 1999). Therefore, comparison of the data obtained from double exponential decay model and pseudo-first order equations by Student's t-test indicated that no significant differences among the results.

Table 7 Comparison of the Rate Constants and Half-Lives of Dimethoate and Diazinon in Soil using Double Exponential Decay and Pseudo-First Order Equations

Pesticides	Double exponential decay		Pseudo-first order	
	k_1 (h^{-1})	$t_{1/2}$(h)	k_1 (h^{-1})	$t_{1/2}$ (h)
Dimethoate	0.0220	31.47	0.0216	32.08
Diazinon	0.0218	31.20	0.0212	32.67

Conclusion

The results of this study have provided an insight into the levels of organophoshorus pesticide residues (dimethoate and diazinon) contamination and dissipation in soils of pesticide treated lettuce plants. Dimethoate and diazinon pesticide concentrations were above their maximum residue limits (MRLs) for agricultural soils but reached under the MRLs after 5 days and 7 days respectively. Comparison of the degradation rate constants and half-lives of soil by using double exponential decay and pseudo-first order equations indicated that these were found to be not quite different. Based on the results of this study, routine monitoring of pesticide residues in the study area is necessary for the prevention, control and reduction of environmental pollution, so as to minimize health risks to humans. The farmers and inhabitants of the study areas should be educated on the danger of pesticides for pet control.

Acknowledgements

The authors would like to express their sincere thanks and deep appreciation to Rector Dr Win Naing and Pro-Rectors Dr Nay Thwe Kyi and Dr Nu Nu Yee, Professor and Head, Dr Cho Cho Win and Professor, Dr Hnin Hnin Than, Dagon University, for their kind permission to summit this paper.

References

Akan, J.C., Jafiya, L., Mohammed, Z. and Abduirahman, F. I. (2013). "Organophosphorus Pesticide Resides in Vegetables and Soil Samples from Alau Dam and Gongulong Agricultural Areas, borno State, Nigeria". *Int. J. Environ. Monitor. & Anal*., vol. 1(2), pp.58-64

Asensio-Ramos, M., Hernandez-Borges, J., Borges –Miquel, T. M. and Rodrigues-Delgado, M. A. (2009). "Evaluation of Multi-walled Carbon Nanotubes as Solid-phase Extraction Adsorbents of Pesticides from Agricultural, Ornamental and Forestall Soils". *Analytica Cmica Acta*., vol. 647 (2), pp.167-176

Black, C.A. (1965). *Methods of Soil Analysis*. New York: American Society of Agronomy, Inc., Pub., vol. 2, pp. 1149

Boesten, J.J.T.I. (2016). "Proposal for Field-Based Definition of Soil Bound Pesticide Residues". *Science of the Total Environment*, vol. 544, 114-117

Day, R.A., and Underwood, A.L. (1999). *Quantitative Analysis*. Englewood Cliffs, New Jersey: 6th Ed., Prentice-Hall Inc., p.19

Del Prodo-Lu, J. L. (2015). "Insecticide Residues in Soil, Water, and Eggplant Fruits and Farmers' Health Effects Due to Exposure of Pesticides". *Environ. Health Prev. Med*., vol. 20, pp.53-63

Fosu-Mensah, B.Y., Okoffo, E. D., Darko, G. and Gordo, C. (2016). "Organophosphorus Pesticide Residues in Soil and Drinking Water Sources from Cocoa Producing Areas in Ghana". *J. Environ. Syst. Res*., vol. 5 (10), pp.1-12

Frimpong, K. S., Gbeddy, G., Doyi, I., Arye-Quaye, F., Kokroko, W. and Asamoah, C. O. (2013). "Efficient Method Development for Atrazine Determination in Soil Samples". *An Indian J. Environ. Sci*., vol. 8 (7), pp. 264-267

Gee, G.W. and Bouder, J.W. (1986). *Particle Size Analysis*. New York: 2nd Ed. American Society of Agronomy, pp. 986-992

Ghabbour, S. I., Zidan, Z. H., Sobhy, H. M., Mikhail, W.Z.A. and Selim, M.T. (2012). "Monitoring of Pesticide Residues in Strawberry and Soil from Different Farming Systems in Egypt". *Am-Euras. J. Agric. & Environ. Sci*., vol. 12 (2), pp. 177-187

Hatzilazarou, S. P., Charizopoulos, E., Papadopoulou-Mourkidou, E. and Economou, A. S. (2005). "Persistence of Chlopyrifos, Diazinon and Dimethoate Sprayed in the Greenhouse Environment During Hydroponic Cultivation of Gerbera". *EDP Sci*., vol. 25, pp. 193-199

Laab, V., Amelung, W., Pinto, A. and Zech, W. (2002). "Fate of Pesticide in Tropical Soils of Brazil under Field Conditions". *J. Environ. Qual*., vol. 31, pp. 256-260

Mahmood, I., Imadi, S. R., Shazadi, K., Gul, A. and Hakeem, K. R. (2016). *Effects of Pesticides on Environment*. Switzerland: Plant, Soil and Microbes, Research Gate net, Springer International Publishing

Muenchen, D. K., Martinazo, J., de Cazaro, A. M., Rigo, A. A., Brezolin, A. N., Manzoil, A., de L. Leite, F., Steffens, C. and Stefffens, J. (2016). "Pesticide Detection in Soil Using Biosensors and Nonbiosensors". *Open Access Journal*, vol. 6 (6), 1659-1675

Ohnmar Aung, Ohn Ohn Soe, Ni Ni Sein, Kyaw Nyaing and Aung Myint. (2007). "Dimethoate and Diazinon Residues in Spinach". *Jour. Myan. Acad. Arts & Sc*., vol. 5, 1(B), pp. 223-240

Ohnmar Aung, Kyaw Nyaing, Ohn Ohn Soe and Aung Myint. (2008). "Degradation Study of Dimethoate and Diazinon Pesticide Residues in *Lactuca sativa* Linn (Lettuce) Plants". *Jour. Myan. Acad. Arts & Sc*., vol. 6 (1), pp. 398-417

Ortelli, D., Edder, P. and Corvi, C. (2006). "Multiresidue Analysis of 74 Pesticides in Fruit and Vegetables by Liquid Chromatography-Electrospray-Tandem-Mass Spectrometry". *Anayitica Chimica Acta*., vol. 520, pp. 33-45

Seema, T., Tahir, A., Shagufta, A., Rauf, A.W., Karam, A., Ashiq, M., Erik, K. K. and Mar, K. B. (1999). "Analysis of Pesticide Residues in Fortified Water, Soil and Vegetables Samples". *Pakistan Journal of Biological Sciences*, vol. 2 (1), pp233-235

Singh, B.S. (2014). "Nantotechnology in Agri-food Production": An Overview". *Nanotechnology, Science and Applications*, vol. **7** (2), pp. 31-53

Syoku-An. (2006). *Method as Specified by Multi-residue Method for Agricultural Chemicals by GC/MS as Released by the Department of Food Safety*. Japan: Ministry of Health, Labour and Welfare

Ware, G.W. and Whitacre, D. M. (2004). *The Pesticide Book Meister Pro Information Resources*. Ohio: 6th Ed., Meister Media Worldwide, pp. 486-496

WHO, Codex Alimentarius Commission (2002). *Food and Agriculture Organization of the United Nations*. Rome: Joint FAO/WHO, Food Standard Programme, vol. 2B, pp.351-364

PHYTOPHARMACOLOGICAL POTENTIAL OF *DREGEA VOLUBILIS* (GWE-DAUK-NWE) LEAF FOR INHIBITION OF AFLATOXIN PRODUCING FUNGUS AND HEPATOCELLULAR CARCINOMA (HepG2) CELLS

Thida Myint[1], Phyu Phyu Myint[2]

Abstract

The present work focused on the study of chemical constituents from the leaf of *Dregea volubilis* (L.f.) Benth. ex Hook.f. (Gwe-dauk-nwe) and detoxification activity to aflatoxin producing microorganisms in agricultural products and cytotoxicity to liver cancer cell line (HepG2). The leaf of the plant was collected from Kyunkalay village, Hlegu Township, Yangon Region in July 2018**.** The leaf sample was cleaned, dried and made to powder. Phytochemical investigation of *D. volubilis* leaf was performed and it was found that carbohydrates, flavonoids, glycosides, phenolic compounds, reducing sugars, saponins, steroids, tannins, terpenoids, and organic acids were present, however, cyanogenic glycosides and starch were absent. In addition, the elements such as Ca (38.32 %), K (33.72 %), Cl (12.31 %), Al (11.24 %), S (1.95 %), Zn (0.98 %) are found as major elements and small amount of other elements are found as Fe (0.77 %), Mn (0.44 %), Rb (0.11 %), Br (0.08 %), Sr (0.08 %) were also found using ED XRF method. Essential oil of *D. volubilis* leaves was extracted by steam distillation method and the organic components (7-chloro benzofuran, Phenol,2,4-bis(1,1-dimethylethyl), 6,10,14-trimethyl-2-pentadecanone, dibutyl-phthalate, 1-eicosene, phytol and uridine compounds) in it were identified by GC-MS method. The antioxidant activities of watery and ethanol extracts of the leaf sample were determined by DPPH assay method. The IC_{50} value of water and ethanol extracts were found to be 582.12 and > 1000 µg/mL, respectively. *In vitro* detoxification activity of essential oil and extracts (PE,$CHCl_3$, MeOH and H_2O extracts) of *D. volubilis* leaf was tested by aflatoxin producing fungus. Yeast, *Aspergillus flavus* and *Aspergillus niger* were cultured from corn, peanut and chilli using direct culture method. $CHCl_3$, MeOH extracts and essential oil of *D. volubilis* leaf showed detoxification activity on these yeast and fungus microorganisms (inhibition zone diameter 11 mm to 19 mm) as well as PE and H_2O extracts (inhibition zone diameter 11mm to 14 mm). Determination of minimum inhibitory concentration (MIC) of essential oil on two species of organisms, namely *A. niger* and *A. flavus* was carried by potato dextrose agar well diffusion method. The essential oil with different concentrations (1×10^5 to 0.2 µg/mL) showed inhibition zone diameter in the range of 12 to 15 mm. The MIC values for essential oil was found to be 2.5×10^4 µg/mL. (inhibition zone diameter ~ 12 mm). The cytotoxicity of MeOH extract from *D. volubilis* leaf against hepatoma liver cancer cell HepG2 was evaluated by MTT assay. The IC_{50} value of MeOH extract was found to be 168.05 µg/mL for 24 h treated time.

Keywords: *Dregea volubilis* leaf, antioxidant activity, detoxification activity, cytotoxicity, MTT assay

Introduction

Myanmar has a rich tradition of using medicinal plants to treat different diseases. Medicinal plants, also called, herbal medicine, have been discovered and used in traditional medicine practices since prehistoric time. Numerous phytochemicals potential or established biological activity have been identified. Medicinal plants are widely used in non-industrialized societies, mainly because they are readily available and cheaper than modern medicines (Ahn,

[1] Lecturer, Department of Chemistry, Dagon University
[2] Professor, Department of Chemistry, Loikaw University

2017). The world health organization estimates that the plant extracts or their active constituents are used as folk medicine in traditional therapies of 80% of the world's population (Baker, 2005).

Dregea volubilis (Gwe-dauk-nwe) is a plant in the family of Apocynaceae. It is occurring in India to Java and other tropical countries. *Dregea volublis* leaves are ovate, 7.5 to 15 centimeters long, 5 to 10 centimeters wide, rather leathery, rounded or pointed at the base, and pointed at the tip (Sudarsanma, 2015). One popular food in our society is *Drege*a *volubilis* leaves soup with chicken. This bitter taste soup is very popular soup in Myanmar and it is famous for its health benefits as detoxifying remedies especially for alcohol poisoning or alcohol overdose. This leaf soup is also believed to possess numerous medicinal values and benefits to human health and lifestyle. The leaf exhibits some anti-bacterial and antifungal properties that make it a good home remedy to several health issues such as dysentery, diarrhoea, high blood pressure and many others. Therefore, it is important to identify and evaluate the popular ingredient used in relation to efficacy and safety.

Nowadays, in our society, aflatoxins producing microorganisms are regularly found inproperly stored staple communities such as corn, peanut, chili pepper and a variety of species. Chronic exposure increases the risk of developing liver and gall bladder cancer, as aflatoxin metabolites may intercalate into DNA and alkylate the bases through epoxide moiety (Nogueira, *et. al*., 2015). For these and many other reasons, the present investigation was emphasized on the study of phytopharmacological potential from *Dregea volubilis* leaf especially enormous range of biological activities like antioxidant, cytotoxicity and detoxification to aflatoxin producing fungus.

Materials and Methods

The leaf sample of *Dregea volubilis* (Gwe-dauk-nwe) was collected from Kyunkaly Village, Hlegu Township, Yangon Region. After collection, the botanical name of the simple was identified and confirmed as *D. volubilis* leaf at Botany Department, Dagon University. The collected fresh sample was cleaned by washing thoroughly with water and air dried. After drying, the leaf sample was cut into small pieces and ground using grinding machine. And then this powdered sample was kept in the sealed air-tight container to prevent moisture changes and other contamination. It was then used without further purification or refining.

Phytochemical investigation

The dried powdered samples were used to chemical tests for the determination if the presence or absence of the major types of phytochemical constituents using standard procedure (M-Tin Wa, 1972; Marini Bettolo *et al*., 1981; Finar, 1968; Trease and Evans, 1980, Shriner *et al.*, 1980 and Robinson, 1983).

Elemental Analysis of *Dregea volubilis* by ED XRF

In order to determine the heavy toxic metals and micronutrient elements in leaf sample, elemental contents in the leaf of *D. volubilise* were determined by ED XRF method at the Universities' Research Center, Yangon. The major advantage of X-ray spectrometry is that it offers a satisfactory compromise among economy, speed and ease of operation (Ertel, 1991).

Extraction of Essential oil from *Dregea volubilies* Leaf by Steam Distillation Method

Essential oil (0.13 %) was extracted from dried powder sample by steam distillation method. Organic compounds such as 7-chloro benzofuran, Phenol,2,4-bis(1,1-dimethylethyl), 6,10,14-trimethyl-2-pentadecanone, dibutyl-phthalate, 1-eicosene, phytol and uridine compounds could be identified from this extracted essential oil by GC-MS method (James and Martin,1952) at the Department of Research and Innovation, National Analytical Laboratory, Kaba Aye Pagoda Road, Yancon

Determination of Antioxidant Activity

DPPH (1,1-diphenyl-2-picryl-hydrazyl) radical scavenging assay was chosen to assess the antioxidant activity of plant materials. This assay has been widely used of plant materials to evaluate the free radical scavenging effectiveness of various flavonoids and polyphenols in food system (Leea *et al*, 2002). In this experiment, the antioxidant activity was studied on 95 % ethanol and aqueous extract from selected leaf sample by DPPH free radical scavenging assay. DPPH (2 mg) was thoroughly dissolved in 100 mL of 95 % ethanol. This 60 µM DPPH solution was freshly prepared in the brown coloured bottle.

The control solution was prepared by mixing the 1.5 mL of 60 µM DPPH solution and 1.5 mL of 95 % ethanol in brown bottle. Blank solution was prepared by mixing the 1.5 mL of test sample solution with 1.5 mL of 95 % ethanol. Each respective H_2O and ethanol extracts (30 mg) and 30 mL of 95 % ethanol were thoroughly mixed by shaker. The mixture solution was filtered and stock solution was obtained. Desired concentration 1000 µg/mL, 800 µg/mL, 600 µg/ mL, 400 µg/mL, and 200 µg/mL of each solutions were prepared from this stock solution by dilution with appropriate amount of 95 % ethanol.

4 mg of standard Vitamin C was dissolved in 20 mL of 95 % ethanol to get the 200 µg/mL stock solution. Desired concentrations of 100 µg/mL, 50 µg/mL, 25 µg/mL, 12.5 µg/mL and 6.25 µg/mL solution were prepared by two-fold serially diluted with ethanol. These bottles were incubated at room temperature and were shaken on shaker for 30 min. After 30 min, the absorbance of these solution was measures at 517 nm by using spectrophotometer (UV-KWF, China). Absorbance measurements were done in triplicate for each solution and the mean values obtained were used to calculate % inhibition of oxidation by the following equation.

$$\% \text{ oxidative inhibition} = \frac{A-(C-B)}{A} \times 100\%$$

% oxidative inhibition = % inhibition of test sample

A= absorbance of the control solution

B= absorbance of the blank solution

C= absorbance of the test sample solution

Then IC_{50} (50 % inhibitory concentration) values were also calculated by linear regressive excel program.

Screening of Detoxification Activity by Potato Dextrose Agar Well Diffusion Method

Detoxification activity of different crude extracts ($CHCl_3$, MeOH, PE, watery extracts and essential oil) of the sample was screened in *in vitro* by Potato Dextrose Agar well Diffusion method (Dorman, 2000). Test Organisms (yeast, *Aspergillus flavus* and *Aspergillus niger*) were

obtained from agricultural products such as corn, peanut and chilli (Figures 1, 2 and 3). This experiment was carried out at Pharmaceutical Research Department (PRD), Ministry of Industry, Yangon.

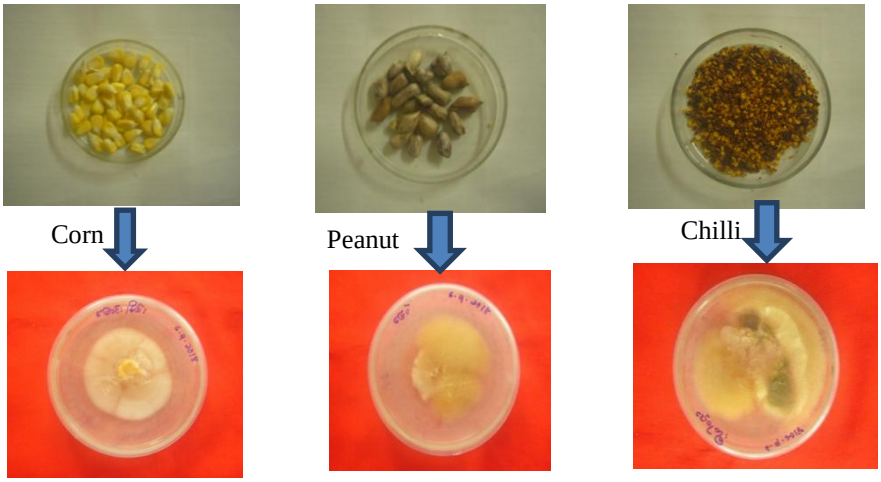

Figure 1 Culture of aflatoxin producing fungi from agricultural products

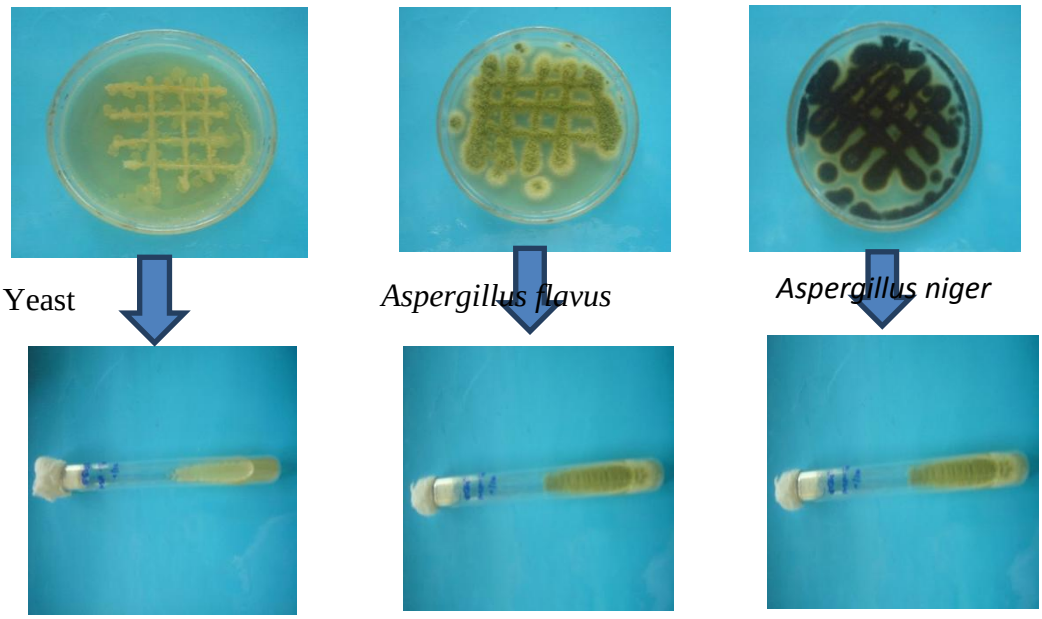

Figure 2 Growth of yeast and fungi from corn, peanut and chilli

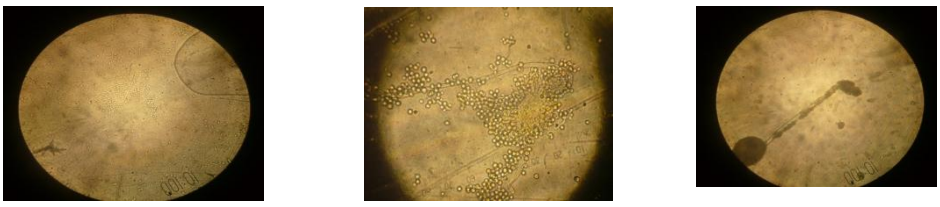

Figure 3 Morphology of Yeast, *Aspergillus flavus* and *Aspergillus niger*

Determination of Minimum Inhibitory Concentration (MIC) of Essential Oil for Detoxification Activity

In order to determine the minimum inhibitory concentration (MIC) of essential oil from leaf which inhibited the microorganisms, the specific concentration of the essential oil prepared in serial dilution in agar plates were used for testing against *A. niger* and *A. flavus* which were obtained from agricultural products such as peanut and chilli. This experiment was carried out at Pharmaceutical Research Department (PRD), Ministry of Industry, Yangon.

Minimum inhibitory concentration (MIC) values of essential oil were determined by potato dextrose agar well diffusion method. 0.2 mL from 100 mg/mL mixture (essential oil dissolved in pet-ether solution) was introduced into the agar well of first Petri dish to obtain the concentration of 1×10^5 µg/mL. By this way, 0.2 mL of each test sample solution was introduced into the agar well of different Petri dishes to obtain the concentrations of 5×10^4, 2.5×10^4, 1.25×10^4, 6.25×10^3, 3.12×10^3, 1.56×10^3, 7.81×10^2, 3.9×10^2 etc., to 0.2 µg/mL. All the Petri dish were incubated at 28 °C for one week. After incubation, the diameters of inhibition zones including 10 mm wells were measured. The amount of sample that showed in inhibition zone diameter was determined as the corresponding MIC value.

Examination of *in vitro* Cytotoxic Activity by MTT Reduction Assay method

The cytotoxicity of methanol extract of the sample was examined by using MTT reduction assay method. HepG2 cells were seeded in a 96 well flat –bottom microliter plate at a density of 1×10^4 cells/ well and allowed to adhere for 24 h at 37 °C in a CO_2 incubator. After 24h the cell were then treated with 0 to 300 µg/mL of methanol extract for 24 h at 37 °C in a CO_2 incubator. Subsequently, 10 µL of MTT solution (5 mg/mL in phosphate buffer solution) were added to each well and incubated for 4 h at 37 °C. The culture medium was discarded, and 100 µL of DMSO solution was added into each well and mixed by gently shaking for 10min. Absorbance (the interesting of the dissolved formazan crystal (purple color) was quantified using the ELISA plate (microplate reader) at 595 nm (Padhya *et al*., 2013). Cell viability was calculated from the mean values of the data from three wells using the equation below and cytotoxic activity was expressed as the IC_{50} (50 % inhibitory concentration) value.

$$(\%)\ \text{Cell viablity} = 100 \times \frac{A_{bs}\,(\text{test sample}) - A_{bs}\,(\text{blank})}{A_{bs}\,(\text{contro}) - A_{bs}\,(\text{blank})}$$

Results and Discussion

Preliminary Phytochemical Present in of *Dredge volubilis* Leaf

According to the phytochemical test results, α-amino acids, alkaloids, carbohydrates, flavonoids, glycosides, phenolic compound, reducing sugars, saponins, steroids, tannins, terpenoids and organic acids are present in the sample but cyanogenic glycosides and starch are absent (Table 1).

Table 1 Results of Phytochemical Investigation on *Dregea volubilis* Leaf

Sr. No.	Tests	Extract	Test Reagents	Observation	Remark
1.	α-amion acids	H_2O	Ninhydrin reagent	Pink colour	+
2.	Alkaloids	1 % HCl	Mayer's reagent	White ppt	+
			Dragendorff's reagent	Orange ppt	+
			Wagner's reagent	Brown ppt	+
			Sodium picrate solution	Yellow ppt	+
3.	Cyanogenic glycosides	H_2O	Conc:H_2SO_4	No brick red	-
4.	Carbohydrates	H_2O	10 % α-naphthol & H_2SO_4 (conc.)	Red ring	+
5.	Flavonoids	EtOH	Mg ribbon & HCl (conc.)	Pink colour	+
6.	Glycosides	H_2O	10 % lead acetate	White ppt	+
7.	Phenolic compounds	H_2O	1 % $FeCl_3$	Deep blue colour	+
8.	Reducing sugars	H_2SO_4 (dil)	Benedict's solution	Brick-red ppt	+
9.	Starch	H_2O	Iodine solution	No blue colour	-
10.	Saponins	H_2O	Distilled water	Frothing	+
11.	Steroids	PE	Acetic anhydride & H_2SO_4 (conc.)	Green colour	+
12.	Tannins	H_2O	1 % gelation solution	White ppt	+
13.	Terpenoids	$CHCl_3$	Acetic anhydride & H_2SO_4 (conc.)	Pink colour	+
14.	Organic acids	H_2O	Bromocresol	Green colour	+

Presnce = (+) , Absence = (-), ppt=precipitate

Elemental Analysis of *Dregea volubilis* Leaf by Energy Dispersive X-Ray Fluorescence

X-ray spectrometer permits simultaneous analysis of light element to heavy metal. Shimadzu EDX-720 spectrometer can analyze the elements from $_{11}$Na and $_{92}$U under vacuum condition. The ED XRF spectrum of the sample results was reported in Table 2. It can be seen that essential minerals for human health such as calcium and potassium in leaf were the most predominant. Ca is key for the health of bone and teeth, but it also affects muscles, hormones and nerve function. The primary functions of potassium in the body include regulating fluid balance and controlling the electrical activity of the heart and other muscle strength. According to ED XRF, no toxic element was found in leaf sample.

Table 2 Relative Abundance of Some Elements in Leaf of *Dregea volubilis* (Gwe-dauk-nwe) by ED XRF Method

No.	Elements	Relative Abundance (%)
1.	Calcium (Ca)	38.316
2.	Potassium (K)	33.721
3.	Chlorine (Cl)	12.308
4.	Aluminium (Al)	11.238
5.	Sulphur (S)	1.947
6.	Zinc (Zn)	0.980

Detection of Organic Compounds in Essential Oil of *Dregea volubilis* Laf by GC-MS Method

Gas chromatographic mass spectrometry (GC-MS) is the single most important tool for identification of unknown organic compounds by matching with reference spectra. The GC-MS chromatogram and mass spectra of essential oil from the *Dregea volubilis* leaf are shown in Table 3 and Figure 4. Identifications were made by comparison of their retention time and m/z ratio with private reference library data and from the literature.

All the compounds such as 7-chloro benzofuran, Phenol, 2, 4-bis (1, 1-dimethylethyl), 6,10,14-trimethyl-2-pentadecanone, dibutyl-phthalate,1-eicosene, phytol and uridine compounds detected in the essential oil were found to possess the pharmacological activity. Among them, benzofuran compound used as recreational drugs producing sympathetic system stimulation and euphoria. Phenol was widely used as an antiseptic. It was used as soap, known as carbolic soap. Pentadecan-2-one is flavor and fragrance agents. Phthalates are used in hundreds of products in homes, hospitals, cars and businesses, because of their strong performance, durability and stability. Eicosene are used in lubricants, lubricant additives and viscosity adjustors (eg. lubricant). Phytol is used in the fragrance industry and used in cosmetic, shampoos, toilet soap, household cleaners, and detergents. Uridine is cognitive enhancer, helps protect the brain and improve memory, and reduces pain and inflammation.

Antioxidant Activity of crude Extracts from leaf of *Dregea volubilis* (Gwe-dauk-nwe)

DPPH (1,1-diphenyl-2-picryl-hydrazyl) method is the most widely reported method for screening of antioxidant activity on many plant drugs. This method is based on the reduction of colored free radical DPPH in 95 % ethanol solution by different concentration of the samples. The antioxidant activity was expressed as 50 % oxidative inhibitory concentration (IC_{50}).

Table 3 Chemical Compositions of Essential Oil from *Dregea volubilis* Leaf

Chemical compound	MW	Retention time (min)	Formula
7-Chloro benzofuran	152	5.94	C_8H_5OCl
Phenol, 2,4-bis(1,1-dimethylethyl)	206	10.36	$C_{14}H_{22}O$
6,10,14-trimethyl-2-pentadecanone	268	13.87	$C_{18}H_{36}O$
Dibutyl-phthalate	278	14.76	$C_{16}H_{22}O_4$
1-eicosene	280	15.03	$C_{20}H_{40}$
Phytol	298	15.84	$C_{20}H_{40}O$
Uridine,2'-5'-dideoxy-5'-(3-4-dihydro-5-methyl-2,4-dioxo-1(2H)-pyrimidinyl	336	17.996	$C_{14}H_{16}O_6N_4$

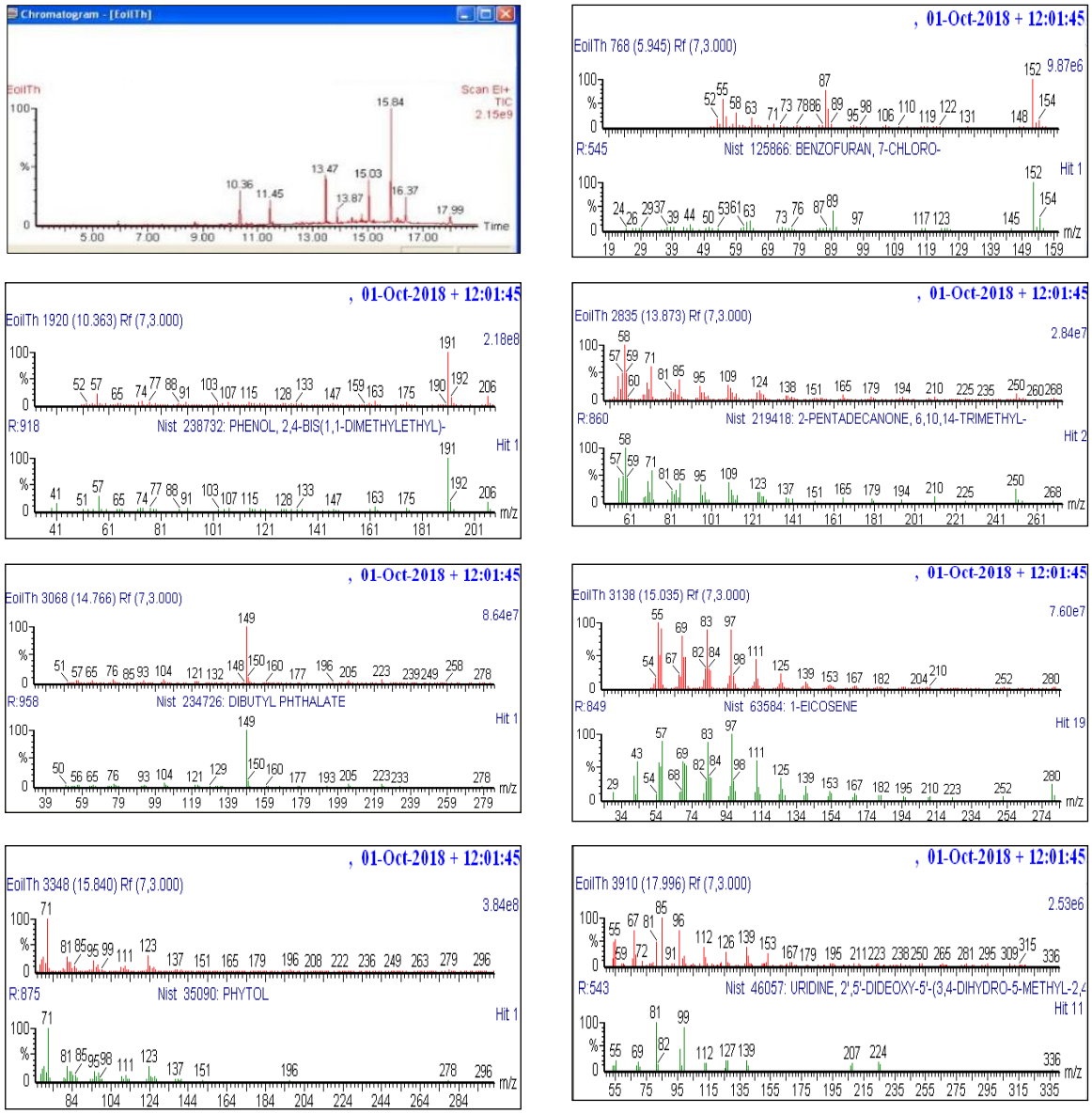

Figure 4 Gas chromatogram-Mass spectra of compounds from essential oil of *Dregea volubilis* leaf

The percent oxidative inhibition values of crude extracts measured at different concentration and the results are summarized in Table 4. From these experimental results, it was found that as the concentrations increased, the absorbance values decreased i.e. increase in radical scavenging activity of crude extracts usually expressed in term of % inhibition. From the average values of % inhibition, IC_{50} (50 % inhibition concentration) values in µg/mL were calculated by linear regressive excel program.

From these results, it can be clearly seen that IC_{50} values were found to be > 1000 µg/mL for ethanol extract and 582.12 µg/mL for water extract. The lower the IC_{50} showed the higher the free radical scavenging activity. Water extract was found to be more effective than ethanol extracts in free radical scavenging activity. However, it was observed that all of these extracts have the lower antioxidant activity than standard ascorbic acid (IC_{50}=8.99 µg/mL).

Table 4 Present Oxidative Inhibition and IC_{50} Values of 95 % Ethanol and Aqueous Extracts of *Dregea volubilis* Leaf and Standard Ascorbic Acid

Extracts	% Inhibition (mean±SD) in different concentration (μg/mL)					IC_{50} (μg/mL)
	200	400	600	800	1000	
Water	22.41 ± 4.10	26.62 ± 5.06	52.60 ± 4.45	62.86 ± 2.08	73.15 ± 4.40	582.12
EtOH	3.75 ± 1.03	4.03 ± 2.16	6.71 ± 2.86	14.84 ± 2.04	21.16 ± 0.00	> 1000
	6.25	12.50	25.0	50	100	
STD Ascorbic acid	24.50 ± 7.28	82.58 ± 4.02	94.46 ± 0.44	94.24 ± 2.68	96.16 ± 0.13	8.99

Detoxification Activity of Crude Extracts and Essential oil by Potato Dextrose Agar Well Diffusion method

Screening of detoxification activity of various crude extracts such as PE, $CHCl_3$**,** MeOH, watery extract and essential oil of *Dregea volubilis* leaf samples was done by using potato dextrose agar well diffusion method. In this study, the microorganisms were firstly cultured from agricultural products. From this process, it can be clearly seen that agricultural products are the sources of aflatoxin –producing fungi such as yeast, *Aspergillus flavus* and *Aspergillus niger*. The morphology of all cultured species could be confirmed by under the microscope (40X magnification). The samples were tested on these three species of microorganisms. The inhibition zone diameter shows the degree of detoxification activity.

The larger the inhibition zone diameter, the higher the detoxification activity. The resulting inhibition zone diameters are described in Table 5 and Figure 5.

Table 5 Inhibition Zone Diameters of Crude Extracts and Essential Oil against three Microorganisms by Potato Dextrose Agar Well Diffusion method

No.	Microorganisms	Inhibition Zone diameter (mm)				
		PE extract	$CHCl_3$ extract	MeOH extract	Water extract	Essential oil
1.	Yeast	11	15	19	14	16
2.	*Aspergillus flavus*	-	14	11	-	15
3.	*Aspergillus niger*	12	12	12	12	15

Agar well diameter – 10 mm
10mm – 14 mm (+); 15 mm – 19 mm (++); 20 mm – above (+++)

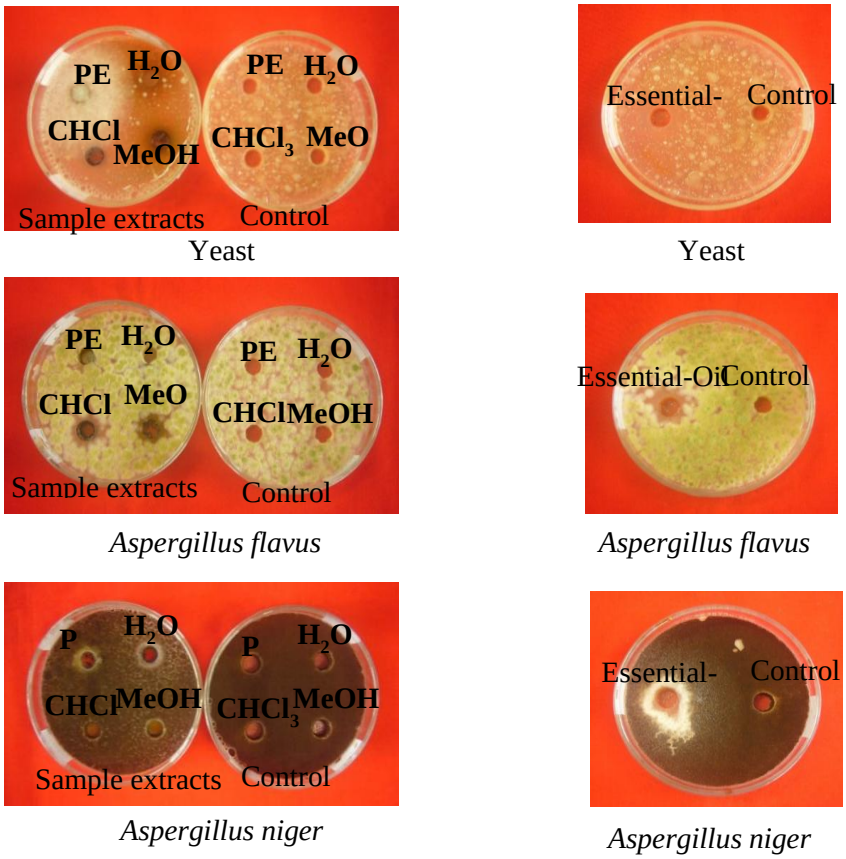

Figure 5 Screening of Detoxification activity on three microorganisms (Yeast, *Aspergillus flavus* and *Aspergillus niger*)

From these results, it was found that MeOH and essential oil are found to possess detoxification activity against three microorganisms; yeast, *Aspergillus flavus* and *Aspergillus niger* with the inhibition zone diameter range between (11 mm to 19 mm).

In addition, PE extract (inhibition zone diameter 11 mm to 12 mm), $CHCl_3$ extract (inhibition zone diameter 12 mm to 15 mm) and water extract (inhibition zone 12 mm to 14 mm). But PE and water extract were not active against *A. flavus*. According to the results the crude extracts the essential oil of *Dregea volubilis* leaf showed the detoxification properties against Yeast, *A. flavus* and *A. niger*.

Minimum Inhibitory Concentration (MIC) by Potato Dextrose Agar Well Diffusion Method

MIC values of essential oil of *Dregea volubilis* were determined by agar well diffusion method. In this study, the essential oil was tested on two species of microorganisms, *Aspergillus niger* and *Aspergillus flavus* with different concentrations. The concentrations of essential oil were range from 1×10^5 µg /mL to 0.2 µg/mL to determine the MIC value. The lowest MIC values for essential oil of *Dregea volubilis* was found to be 2.5×10^4 µg/mL against *A. niger* and *A. flavus*. These results are reported in Table 6 and Figure 6. According to literature survey, the essential oil from other plants; *Styrax tonkinensis, Lavandula angustifolia, Melaleuca alternifolia, Pelargonium graveolens* and *Rosmarinus officinalis* were also reported significantly inhibited growth of *A. niger* and to a lesser extent that of *A. flavus* with MIC (minimal inhibitory concentrations) in the range 0.078-1.25 x 10^4 µg/mL (Shine, 2003). The results showed that five

plant essential oil possess lower minimal concentrations inhibition on *A. niger* and *A. flavus* than *D. volubilis* leaf.

Table 6 Minimum Inhibitory Concentration (MIC) of Essential Oil from *Dredge volubilis* Leaf

Sample No.	Concentrations (µg/mL)	Inhibition zone diameter (mm)	
		A. niger	***A. flavous***
1	1×10^5	15 (++)	15 (++)
2	5×10^4	13 (+)	13 (+)
3	2.5×10^4	12 (+)	12 (+)
4	1.25×10^4	-	-
5	6.25×10^3	-	-
6	3.12×10^3	-	-
7	1.56×10^3	-	-
8	7.8×10^2	-	-
to	to	-	-
20	0.2	-	-

Agar well diameter – 10 mm 10 mm – 14 mm (+); 15 mm – 19 mm (++); 20 mm – above (+++)

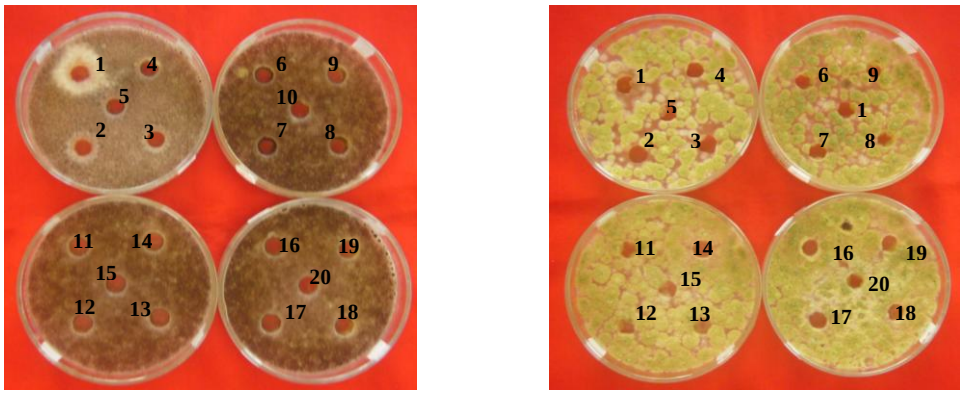

Figure 6 Minimum inhibitory concentration (MIC) of essential oil for detoxification activity on (a) *Aspergillus niger* and (b) *Aspergius flavus*

Cytotoxicity of Methanol Extract of *Dregea volubilis* leaf

The cytotoxicity of methanol extract of *Dregea volubilis* was evaluated by MTT assay. The cytotoxicity of methanol extract was expressed in terms of mean ± SDC standard deviation and IC_{50} (50 % Inhibitory Concentration) and the results are shown in Table 7 and Figure 7**.** There are many plants extracts have been used as anticancer agents even vegetables and fruits many help reduce the risk of cancer in humans. Some Thai plants namely *Glochidion daltonii, Cladogynos orientalis, Catimbium speciosum, Acorus tatarinowii, Amomum villosum and Pinus kesya* showed the highest selectivity and potent cytotoxicity in the HepG2 cell line, with an IC_{50}value of 52.0 ± 5.8 µg/mL (mean ±standard deviation) Figure 8.Extract of *Catimbium speciosum* exerted cytotoxicity with an IC_{50} value of 55.7 ± 8.1 µg/mL. Crude extracts from *Glochidion daltonii, Cladogynos orietialis, Acorus tatarinowii and Amomum villosum* exhibited cytotoxicity with IC_{50}values ranging 100 – 500 µg/mL (Machana *et al*., 2011).

In this study, the local plant extract showed moderate IC_{50} value (168.05 µg/mL) for cytotoxicity against HepG2 cell line and is recommended for medical cuisine beyond traditional cuisine.

Table 7 Viability of HepG2 Cell by MeOH Extract of *Dregea volubilis* leaf using MTT Assay

Extract	Cell Viability (mean ±SD) in different concentrations (µg/mL)						IC_{50} (µg/mL)
	0	100	150	200	250	300	
MeOH	1.0 ± 0.0	0.70 ± 0.17	0.63 ± 0.08	0.27 ± 0.10	0.19 ± 0.03	0.17 ± 0.04	168.05 ± 4.32

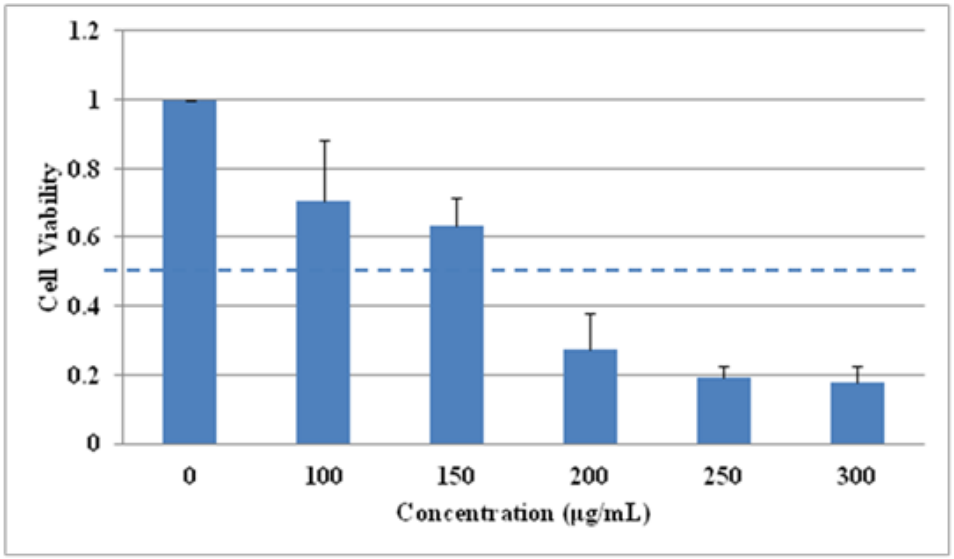

Figure 7 A bar graph of cell viability for 24 hours treated by MeOH extract

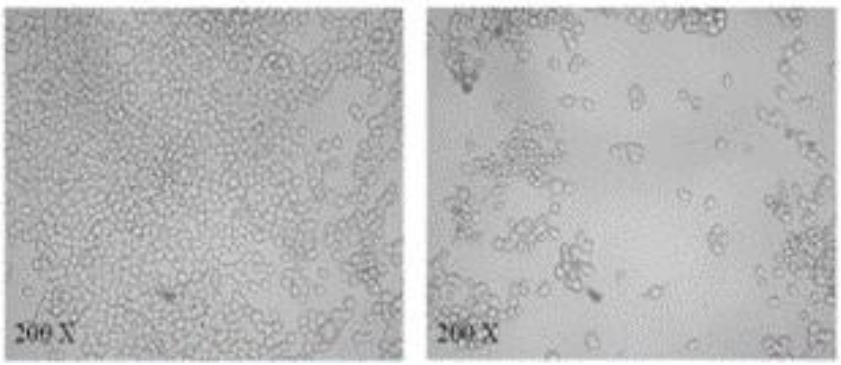

(a) (b)

Figure 8 Morphology of HepG2 cells after 24 hours treatment of **(a)** 0 µg/mL and **(b)** 250µg/mL of sample

Conclusion

From the overall assessments of the present work concerning with the phytochemical constituents, detoxification activity and cytotoxicity of *Dredge volubilis* (Gwe-dauk-nwe) leaf, the following inference could be deduced.

The GC-MS analysis results have revealed that the presence of benzofuran, phenol, pentadecan-2-one, phthalate, eicosene, phytol and uridine compounds in *D. volubilis* indicating

potential to protect the brain and improve memory, reduces pain and inflammation. Qualitative elemental analysis of plant sample by ED XRF method showed that Ca and K were the highest amount of elements in the sample. According to the elemental result, this sample was found to be effective for good help by regulating fluid balance and controlling the electrical activity of the heart and other muscles. The leaf sample also possesses antioxidant and cytotoxicity. The radical scavenging activity of water extract was found to be more effective than EtOH extract by DPPH assay. The IC_{50} value of MeOH extract against human liver cancer line (Hep G2) was observed 168.05 µg/mL. Essential oil of *D.volubilis* leaf showed detoxification activity against *A. flavus* and *A. niger* (MIC values was 2.5 x 10^4 µg/mL) whereas PE and water extracts did not show activity against *A. flavus.* According to these observations, *D. volubilis* leaf extracts could be applied not only for nutrition but also for pharmacological properties.

Acknowledgements

The authors would like to acknowledge to Dr Cho Cho Win (Professor & Head), and Professor Dr Hnin Hnin Than, Department of Chemistry, Dagon University for generously and kindly providing to do this research work. And the authors would like to express our gratitude to the Department of Higher Education, Ministry of Education, Myanmar, for their permission to do this research and also to the Myanmar Academy of Arts and Science for allowing to read this paper.

References

Ahn, K. (2017). "The Worldwide Trend of using Botanical Drugs and Strategies for Developing Global Drugs" *BMB Reports*, Vol. 50(3), pp. 111-116.

Baker, J.T., Boris, R.P. and Carte, B. (2005)."Natural Product Drug Discovery and Development". *New perceptive on international collaboration*,Vol. 58, pp. 1325-1325.

Dorman, H. J. and Deans, S. G. (2000). "Antimicrobial Agents from Plants and Antibacterial Activity of Plants Volatile Oils". *J., Applied Microbial*, Vol. 88, pp. 308-316.

Ertel, D. (1991). *X-ray Fluorescence Analysis*. Karlsruhe, Germany: Nuclear Research Centre, pp. 234-237.

Finar, I. L. (1968). *Organic Experiment*. New York: 4th Ed., D-C Health and Company, pp. 132.

James, A. T. and Martin, A. J. P. (1952). "Gas-Liquid Partition Chromatography, the Separation and Micro-Estimation of Volatile Fatty Acids from Formic Acid to Dodecanoic Acid*". Biochem, J.,*Vol. 50, pp. 679-680.

Leea, E. Vitaly, I. V. Myung, W. B. and Cherl, H. (2002). "Detection of free radicals in Gamma-irradiated Soybean Paste and Model System by Electron Spin Resonance Spectroscopy". *Radiation Physics and Chemistry*.,Vol. 64, pp. 61-64.

M-Tin Wa. (1972). "Phytochemical Screening Methods and Procedures". *Phytochemical Bulletin of Botanical Society of America Inc*., Vol. 5 (3), pp. 4-10.

Marini, G. B., Bettolo - Nicoletti, M., Patomia, M., Galeffi, C. and Messona, I. (1981). "Plant Screening by Chemical and Chromatographic Procedures Under Field Conditions". *J. Chromate.*,Vol. 46(2), pp. 359-363.

Machana, S., Weerapreeyakul, N., Barusrux, S., Nonpunya, A., Sripanidkulchai, B. and Thitimetharoch, T. (2011). "Cytotoxic and Apoptotic Effects of Six Herbal Plants against the Human Hepatocarcinoma (HepG2) cell line", *Chin Med*., Vol. 6, pp.39-46.

Nogueira, L., C. Foerster, J. Groopman, P. Egner, J. Koshiol and C. Ferreccio. (2015). "Association of aflatoxin with gallbladder cancer in Chile". JAMA. Vol.313 (20), pp.2075–2077.

Padhya. K.T., J. A. Marrero and A.G. Singal. (2013). "Recent advances in the treatment of hepatocellular carcinoma". *Curr Opin Gastroenterol*, Vol.29, pp. 285-292.

Robinson, T. (1983). *The Organic Constituents of Higher Plants.* North Amberst: 5th Ed., Cordus Press, pp.285-286 .

Shine, S., (2003). "Anti-*Aspergillus* Activities of Plant Essential Oils and their Combination Effects with Ketoconazole or Amphotericin B*" ,Arch Pharm Res*., Vol.26(5), pp.389-393.

Sudarsanam, G. and Bharathamma. G. (2015)."Phytochemical Investigation of Aqueous Fruit Extracts of *Dregea volubilis* (Linn.)Benth". Indian Journal of Plant Sciences ,Vol. 4(1) , pp.1 1-15.

Shriner, R.L., Fuson, R.C., Curtin D.Y. and Morrill, T.C. (1980). *The Systematic Identification of Organic Compounds, A Laboratory Manual* New York: 6th Ed, John Wiley and Sons, pp.34-38.

Trease, G.E. and Evans,W.C. (1980). *Pharmacognosy*. London: 1st Ed., Spottiswoode Ballantyne Ltd., pp.108, 529.

ISOLATION AND IDENTIFICATION OF SOME PHYTOCONSTITUENTS FROM LEAVES OF *MORUS ALBA* L. AND SCREENING OF ANTIOXIDANT ACTIVITY

Ei Ei Sann[1], Myint Myint Soe[2], Myint Myint Khine[3]

Abstract

This research work deals with investigation of some bioactive phytoconstituents of *Morus alba* L. (Po-sa) plant collected from Pyin-Oo Lwin Township, Mandalay Region. By silica gel column chromatographic separation technique, three compounds were isolated from selected plant. Umbelliferone (**1**,0.0045%) Scopoletin (**2**, 0.0009 %)m.pt 201ºC) and protocatechuic acid (**3,**0.0036 %) from ethyl acetate extract of Po-sa leaves. The isolated compounds were identified by physic-chemical properties and modern spectroscopic techniques such as UV, FT IR, ^{1}H NMR, ^{13}C NMR and EI MS spectrometry as well as by comparing with their reported data. Antioxidant activity of Po-sa (leaves) was also investigated by using DPPH (1, 1'-diphenyl-2-picrylhydrazyl) radical scavenging assay. The IC_{50} values of EtOAc, EtOH and watery extracts of leaves were 2.39 µg/mL, 2.11 µg/mL and 2.15 µg/ml respectively. The EtOH and watery extracts of leaves showed more radical scavenging activity than EtOAc extract. In addition, Umbelliferone, scopoletin and protocatechuic acid isolated from Po-sa (leaves) also showed radical scavenging activity determined by using semi quantitative DPPH staining method.

Keywords: Umbelliferone, Scopoletin, Protocatechuic acid, Antioxidant activity

Introduction

Morus alba is a plant species that belongs to *Moraceae* family and high economic worldwide (Donno *et al.,* 2015). Its fruits are source of alkaloids, anthocyanins, flavonoids and phenolic acids, being used as human food while its foliage contains unique nutrients for silkworm development (Butt *et al.,* 2008). This plant species is native to Asia, but due to its wide adaptation in the tropics(Europe, north and south America, Africa and India it has been considered cosmopolitan nowadays (Khan *et al*., 2013).Sericulture was the main process that drove the improvement of *Morus alba* species leading to the development of varieties that represents valuable plant genetics resources. Leaves are a good source of ascorbic acid and rich in calcium (Wealth of India, 1962). Phenolic compounds are secondary metabolites that protect plants against damage from pathogens and environmental stress. The consumption of these substances has been correlated with minimizing damaging effects of uncontrolled free radicals production, duetothei, antioxidanta ctivity (Yangthong *et al*., 2009). Mechanisms of antioxidant action are very complex, including electrons donation, which act accelerating lipids oxidation (Huang *et al*., 2005). Other mechanisms include hydrogen donation to reduce reactive oxygen species (Villaño *et al*., 2007) related to alterations in DNA and cancer. Phenolic compounds concentration and, consequently, antioxidant activity of any plant is greatly affected by environmental conditions, storage, geographicregion, varietyand the part of plant used in the biological evaluation Stem possesses antirheumatic, antispasmodic, diuretic, hypotensive and pectoral activities. They are used in the treatment of rheumatic pains and spasms, especially of the upper half of the body, high blood pressure. A tincture of the bark is used to relieve

[1] Dr, Assistant Lecturer, Department of Chemistry, University of Yangon
[2] Dr, Associate Professor, Department of Chemistry, Mandalay University of Distance Education
[3] Dr, Professor , Department of Chemistry, University of Yangon

toothache. The branches are harvested in late spring or early summer and are dried for later use (Kim *et al*., 1999).A fiber is obtained from one-year old stem, it is used in weaving clothes etc. The stem bark is fibrous and is used in China and Europe for paper making.

Materials and Methods

Plant Material

Po-sa (Leaves) was collected from Pyin Oo Lwin Township, Mandalay Region. After collection, the scientific names of *Morus alba* L. were identified by the authorized botanists at Botany Department, University of Yangon. The sample was washed with water and dried at room temperature. The dried samples were ground to get a fine powder. The dried powder were then stored in an air-tight container.

Preparation of Crude extracts

The powdered sample (700 g) of Po-sa (Leaves) was extracted with 80 % EtOH. The filtrate was evaporated to get 25 g of crude extract. And then partitioned with PE, 5 g of PE extract was obtained. After that partitioned with EtOAc , 8 g of EtOAc crude extracts was obtained.

Isolation of Compounds from Po-sa (Leaves)

The 95 % ethanol extract was extracted with pet-ether (60 °C - 80 °C), the soluble matter of pet-ether was obtained. The defatted alcohol soluble portion was then partitioned between ethyl acetate and water by using separatory funnel. After removal of the solvent from organic layer, ethyl acetate soluble extract was obtained. The ethyl acetate extract (8 g) was separated by column chromatographic separation techniques Gradient elution was performed successively using PE:EtOAc in the ratios of 5 : 1,3:1 and 1:1 v/v. From this separation, three main fractions F_1 to F_3 were collected. From the condensed fraction F_2, compound **1** (0.005 g, 0.0045 %) and **2** (0.0015 g, 0.0009 %) were collected by paper chromatography with the solvent of formic/A: H_2O (2:98).The last fraction F_3 was purified by paper chromatography with formic/A: H_2O(1:99) solvent system, compound **3** (0.003 g, 0.0036 %) were obtained. The isolated compounds were characterized by melting point determination and TLC, UV, FT IR, ^{1}H NMR and mass spectroscopic methods.

Antioxidant Activity Test

For the examination of *in vitro* antioxidant activity of Po-sa (leaves), DPPH staining method and spectrophotometric method were used. In DPPH staining method, for each diluted sample was applied as a dot on a TLC plate followed by staining solution. The appearance of white coloured spots has a potential value of antioxidant activity (Soler-Rivas *et al.*, 2000). In spectrophotometric method, the sample solutions were measured by using spectrophotometer (Marinova and Batchvarov, 2011).

Results and Discussion

Identification of the Isolated Compounds

Compounds 1 (5 mg, 0.0045 %), compound 2 (1.5 mg, 0.0009 %) and compound 3 (3 mg, 0.0036 %) were characterized by physical and chemical methods and then identified by spectroscopic techniques.

Compound 1 (Umbelliferone): UVλ_{max}^{MeOH}nm; 220, 329; UV$\lambda_{max}^{MeOH+NaOH}$nm: 221,363 (Figure 1). FT IR υ_{max}^{KBr} cm^{-1}: 3398 (υ_{O-H}), 1705 ($\upsilon_{C=O}$), 1616-1562 ($\upsilon_{C=C}$), 1234-1053 ($\upsilon_{asy-C-O}$), 840 ($\delta_{oop-C-H}$) (Figure 2). ^{1}H NMR δ (ppm) 6.2 (3H, d, J=9 Hz), 8.0 (4H, d, J=9Hz), 7.3 (5H, d, J=8Hz), 6.9 (6H, dd, J=8 Hz), 6.8 (8H, d, J=1 Hz) (Figure 3). MS m/z; 161 (M-H), 133.1, 92.9 (Figure 4). All of these chemical shifts are very similar to those in the spectrum of umbelliferone (Harborne, 1989; Mya Thandar Aung, 2007).

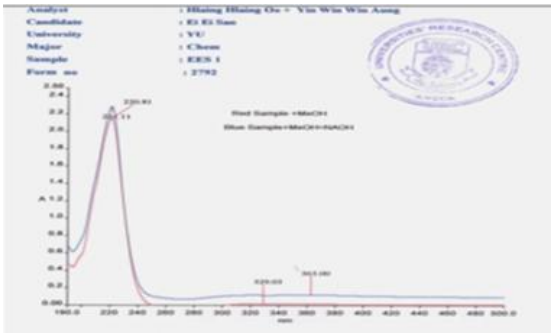

Figure 1 UV spectrum of the isolated compound1 (Solvent: MeOH and MeOH+ NaOH)

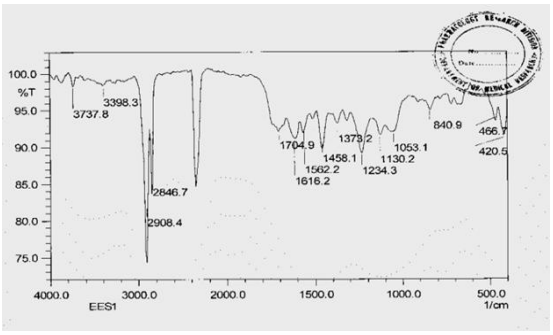

Figure 2 FTIR spectrum of isolated the compound 1(KBr)

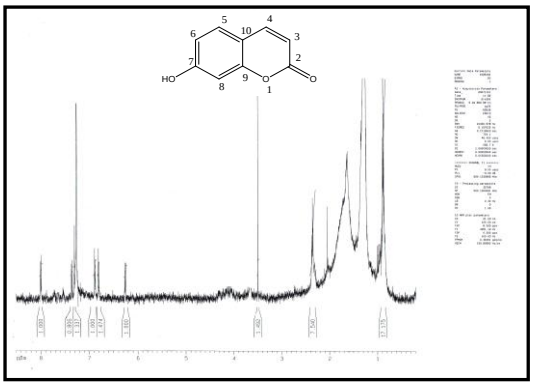

Figure 3 ^{1}H NMR spectrum of the isolated compound 1

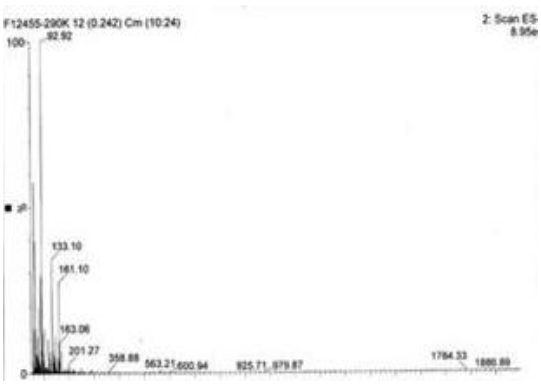

Figure 4 ESI-mass spectrum of the isolated compound 1

Compound 2 (Scopoletin): Colourless crystal, m.p. 201 °C. UV λ_{max}^{MeOH}nm: 215, 344;UV $\lambda_{max}^{MeOH+NaOH}$ nm: 218, 390 (Figure 5). FT IR $\upsilon_{max}^{KBr}$$cm^{-1}$: 3325 ($\upsilon_{O-H}$), 3055 ($\upsilon_{C-H}$ of C=CH), 2920 (υ_{C-H} of $-CH_3$, CH_2), 2850 (υ_{C-H} of $-OCH_3$), 1705 ($\upsilon_{C=O}$) of δ lactone, 1604($\upsilon_{C=C}$ of aromatic ring) (Figure 6). ^{1}H NMR δ(ppm): 6.2 (3H, d, J = 9 Hz), 7.6 (4H, d, J= 9Hz), 6.8 (5H, S), 6.9 (8H, S), 3.7 (6H-OMe, S) (Figure 7). All these spectral data of compound 2 were agree with the reported data of scopoletin(Merck Index, 2001; Harborne, 1993; Khin Tar Yar Myint, 2010)

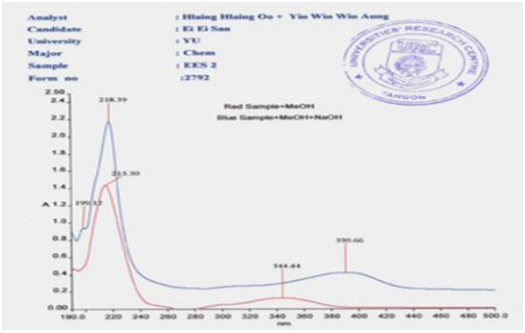

Figure 5 UV spectrum of isolated the compound 2 (Solvent MeOH and MeOH+NaOH)

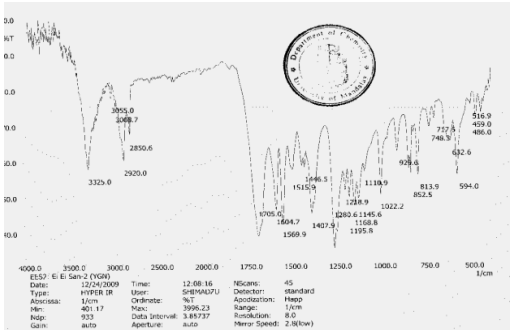

Figure 6 FTIR spectrum of the isolated compound 2 (KBr)

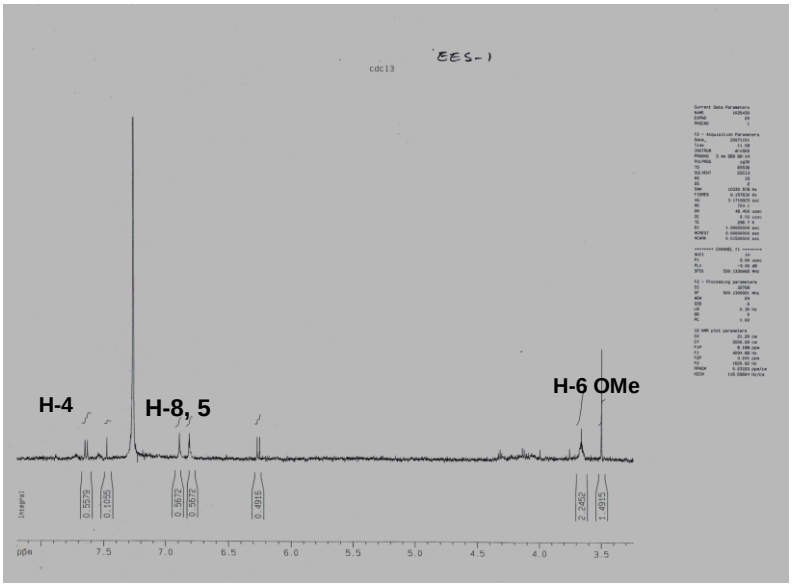

Figure 7 ^{1}H NMR spectrum of isolated compound 2

Compound 3 (Protocatechuic Acid):(UV λ_{max}^{MeOH}nm; 313, UV$\lambda_{max}^{MeOH+NaOH}$nm: 348,UV λ_{max}^{AlCl3}nm; 333, UV $\lambda_{max}^{AlCl3+HCl}$nm: 313) (Figure 8). FT IR υ_{max}^{KBr}cm^{-1}: 3028 (υ_{O-H}), 2923 (υ_{C-H} of C=CH), 1685 ($\upsilon_{C=O}$) 1596 ($\upsilon_{C=C}$ of aromatic ring) (Figure 9). ^{1}H NMRδ(ppm): 7.34 (2H, d, J = 3 Hz), 6.97 (5H, d, J= 9Hz), 7.04 (6H, dd, J= 3,9 Hz) (Figure 10).The proton signals of compound 3 was reported protocatechuic acid (Myint Myint Khine,2006).

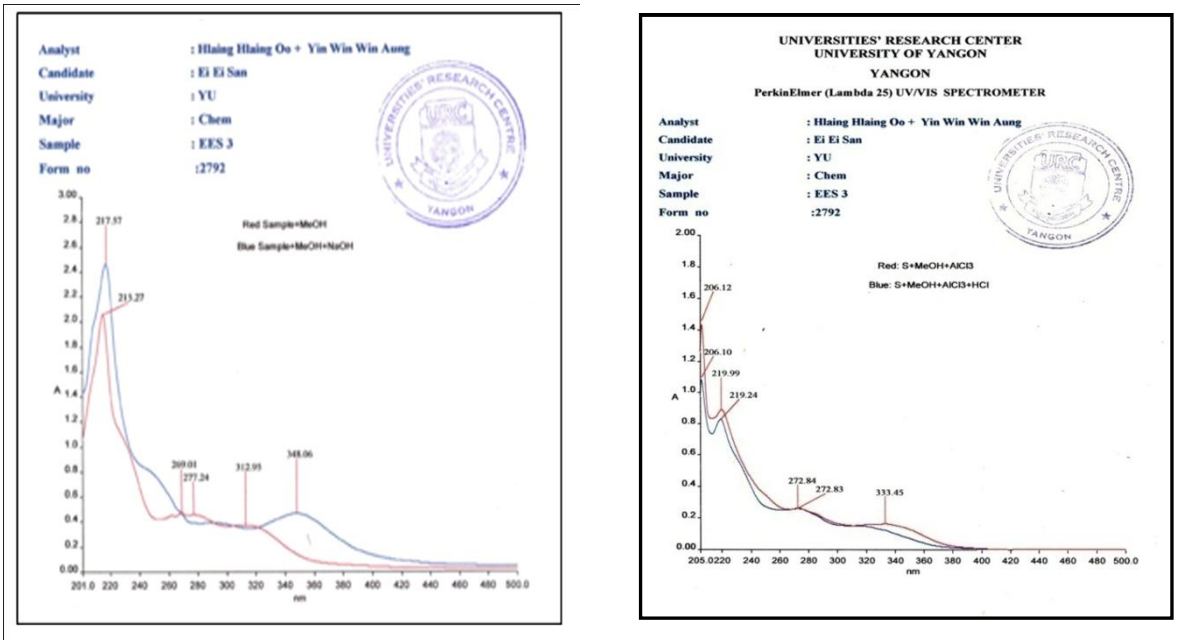

(a) MeOH (red) and MeOH/ NaOH (blue) (b) $AlCl_3$ (red) and $AlCl_3$/HCl (blue)

Figure 8 UV spectra of isolated compound 3

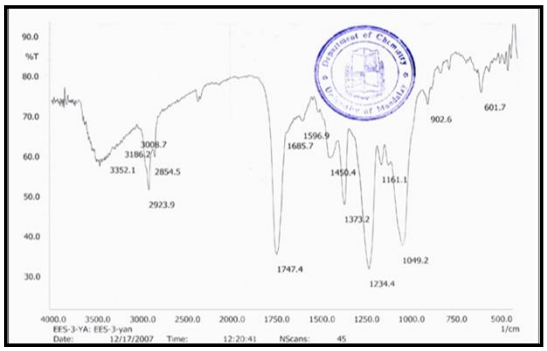

Figure 9 FT IR spectrum of isolated compound 3

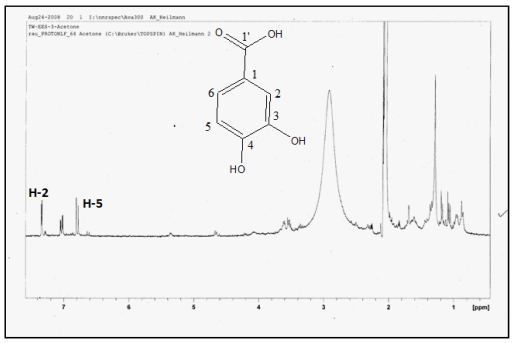

Figure 10 ^{1}H NMR spectrum of isolated compound 3

Rapid Screening of Antioxidant Activity of Two Isolated Compounds by DPPH staining method

It was observed that compounds 1, 2 and 3 from *Morus alba* L. (leaves) showed antioxidant activity on the TLC plates. After staining, white spots with strong intensity was found by staining with the amount of (6.25-200 µg) of dry matter for compounds (Figure 11). The intensity of white colour depends upon the amount and nature of radical scavenger present in the sample.

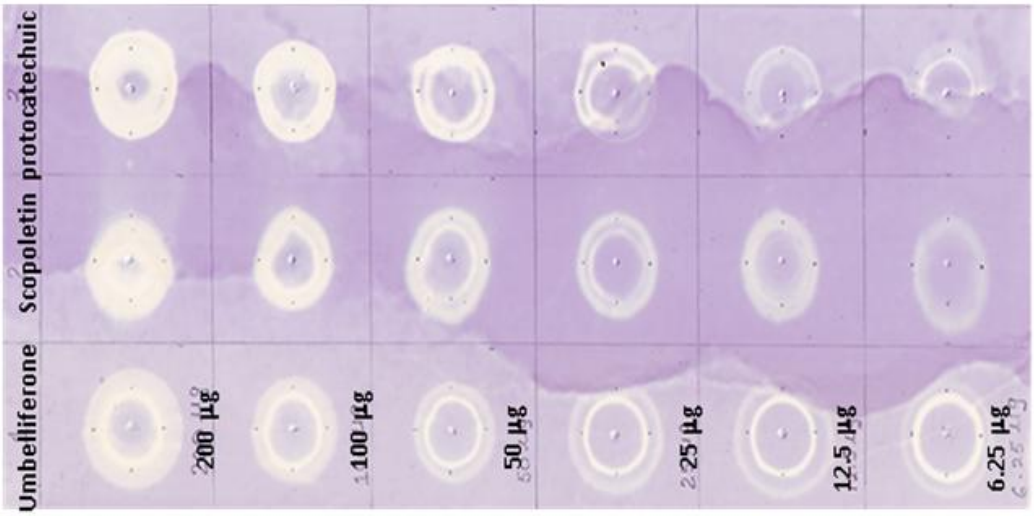

Figure 11 Screening of antioxidant activity of the isolated compounds from Po-sa (leaves) by DPPH Dot-Blot assay

DPPH Radical Scavenging Activity by Spectrophotometric Method

The antioxidant activity of EtOAc, 80%EtOH and H_2O extracts was tested according to DPPH radical scavenging activity assay by using spectrophotometric method. The H_2O extract was found to be more potent than the other extracts compared with standard BHT (Table1). From these results, increase in concentration showed increase in percent inhibition, i.e. increase free radical scavenging activity. The lower IC_{50} value indicates the greater antioxidant activity.

Table 1 Oxidative Inhibition % in Various Concentrations and IC_{50} Values of Extracts of Po-sa (Leaves)

Extracts	% Inhibition in various concentrations (µg/mL)					IC_{50} (µg/mL)
	0.625	1.25	2.5	5	10	
Po-sa -EtOH (Leaves)	21.70	40.42	50.97	57.15	69.03	2.39
Po-sa-H_2O (Leaves)	18.97	32.24	58.16	63.61	68.91	2.11
Po-sa-EtOAc (Leaves)	37.94	44.79	52.06	64.85	76.12	2.15
BHT	14.04	54.82	74.22	77.13	87.40	1.17

BHT = Butylated Hydroxy Toluene

Conclusion

On silica gel column chromatographic separation, three compounds were isolated from ethyl acetate extract of the Po-sa leaves. Umbelliferone (0.0045 %), scopoletin (0.0009 %) and protocatechuic acid (0.0036 %) were obtained from ethyl acetate extract of Po-sa (leaves) by column chromatography on silica gel using PE:EA (1:1). In antioxidant activity, ethanol extract (IC_{50}=2.11 µg/mL) and isolated compound ,protocatechuic acid (6.25-200 µg) were found to be more potent than the other extracts and other isolated compounds. The findings of the present study suggest that Po-sa leaves is a potential source of natural antioxidant that could have great importance as therapeutic agents or in slowing down of aging and its related degenerative diseases.

Acknowledgements

The authors would like to express their profound gratitude to the Department of Higher Education (Yangon Office), Ministry of Education, Yangon, Myanmar, for provision of opportunity to do this research and Myanmar Academy of Arts and Science for allowing to present this paper.

References

Butt, M. S., Nazir, A., Sultan, M. T. and Schroën, K. (2008). "*Morus alba* L.Nnature's Functional Tonic". *Trends Food Sci Technol*, vol 19, pp. 505-512.

Donno, D., Cerutti, A. K., Prgomet, I., Mellano, M. G. and Beccaro, G. L. (2015). "Foodomics for Mulberry fruit (*Morus* spp.): Analytical Fingerprint as Antioxidants' and Health Properties' Determination Tool". *Food Res Int*, vol. 69, pp. 179-188.

Harborne, J. B. (1989). *Method in Plant Biochemistry*. London: Academic Press, vol.7, pp.349-354.

Harborne, J.B. (1993). *Phytochemistry Dictionary*: *A Hand Book of Bioactive Compounds from Plants*. London: Taylor and Francis Ltd., WCIN 2ET, pp. 364-365.

Huang, D., Ou, B. and Prior, R. L. (2005). "The Chemistry behind Antioxidant Capacity Assays". *J Agric Food Chem*, vol. 53, pp. 1841-1856.

Khan, M. A., Rahman, A. A., Islam, S., Khandokhar, P., Parvin, S., Islam, M. D., Hossain, M. and Rashid, M. (2013). "A Comparative Study on the Antioxidant activity of Methanolic Extracts from Different Parts of *Morus alba* L. (Moraceae)". *BMC Res Notes*, vol 6, p. 24.

Khin Tar Yar Myint. (2010). *Isolation and Structural Identification of Some Hypoglycaemic Active Compounds from Selected Part of (Premna integrifolia L.) Taung-Tan-Gyi*. Yangon: Ph.D (Dissertation), Department of Chemistry, University of Yangon, Myanmar.

Kim, S. J., GaO, J. J., Lee, W. C., Ryu, K. S., Lee, R. R. and Kim, Y. C. (1999). "Antioxidative Flavonoids from the Leaves of *Morus alba*". *Arch Pharm*, vol. 22, pp. 81-85.

Marinova, G. and Bathvarov, V. (2011). "Evaluation of the methods for determination of the free radical scavenging activity by DPPH". *Bulgarial journal of Agricultural Science*, vol. 17, pp. 11-24.

Merck Index, (2001). *An Encyclopedia of Chemical Drugs and Biologicals.* New Jersey:13th Edition, Merck and Co., Inc. Whitehouse station.

Mya Thandar Aung. (2007). *Isolation and Identification of Some Bioactive Compounds from (Ipomoea turpethum L.) Kyar Hin and (Biophytum sensitivum L.) Shun Bwet Hti Gayon.* Yangon: Ph.D (Dissertation), Department of Chemistry, University of Yangon, Myanmar.

Myint Myint Khine. (2006). *Isolation and Characterization of Phytoconstituents from Myanmar Medicinal Plant*. PhD.(Dissertation), Instituents of Plant Biochemistry, Martin-Luhter-University, Halle-Saale, Germany.

Soler-Rivas, C., Espin, J. C. and Wichers, H. J. (2000). "An Easy and Fast Test to Compare Total Free Radical Scavenger Capacity of Foodstuffs". *Phytochem. Anal*., vol. 11, p. 330.

Villaño, D., Fernández-Pachón, M. S., Moyá, M. L., Troncoso, A. M. and García-Parrilla, M. C. (2007). "Radical Scavenging Ability of Polyphenolic Compounds towards DPPH Free Radical". *Talanta*, vol. 71(1), pp. 230-235.

Wealth of India. (1962). *Dictionary of Indian Raw Materials and Industrial Products*. New Delhi: Council of Scientific and Industrial Products, vol. 6, pp. 429-437.

Yangthong, M., Hutadilok-Towatana, N. and Phromkunthong, W. (2009). "Antioxidant Activities of Four Edible Seaweeds from the Southern Coast of Thailand". *Plant Foods Hum Nutr*, vol. 64(3), pp. 218-223.

PHYTOCHEMICAL SCREENING AND EVALUATION OF SOME BIOLOGICAL ACTIVITIES OF THE ROOTS OF *STEMONA TUBEROSA* LOUR. (THAMYA)

Yi Yi Win[1], Zin Thu Khaing[2], Yin Yin Htwe[3], Saw Hla Myint[4]

Abstract

The present study investigates some biological effects: *in vitro* antioxidant, *in vitro* α-amylase inhibitory activity, *in vivo* acute toxicity, *in vivo* anti-diabetic activity of the crude extracts and isolated compounds of *Stemona tuberosa* Lour. root. *In vitro* antioxidant activity using DPPH radical scavenging assay, with ascorbic acid as positive control, showed the ethanolic extract possessed excellent antioxidant property (IC_{50}=1.56 μg/mL). No toxic behaviour was observed up to 5000 mg/ kg oral dose of water and ethanol extracts on mice for two weeks treatment following the *in vivo* acute toxicity OECD guideline. The *in vivo* antidiabetic activity, with metformin, oral hypoglycemic agent, as a positive control, against alloxan-induced diabetic mice; and the *in vitro* antidiabetic activity, with acarbose, antihyperglycemic agent, as a positive control, for the inhibitory effect on α-amylase enzyme, was employed to determine the antidiabetic activity. The ethanolic extract of *S. tuberosa* root was found to be exhibited potent antidiabetic activity *in vitro* (IC_{50} values; 80.98 μg/mL for α-amylase activity) as well as *in vivo* (41.29±0.05 % maximum reduction (R)) in blood glucose level. By column and thin layer chromatography, tuberostemonine **J** (**1**) was isolated from active ethanol fraction and identified by modern spectroscopy. Moreover, tuberostemonine **J** (**1**) (41.62 ± 0.01 % R *in vivo*) exhibited similar antidiabetic activity ($p < 0.01$) but good proliferation of beta islet cells of Langerhans and acinar cells in pancreas of diabetic mice when compared to the positive control, metformin (41.87 ± 0.05 % R *in vivo*).

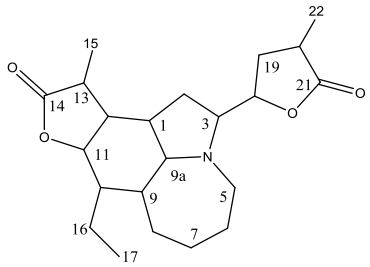

1 (tuberostemonine **J**)

Keywords: *Stemona tuberosa*, blood glucose, antidiabetic, antioxidant, tuberostemonine **J**

Introduction

The herb Radix Stemonae, known as 'Bai-Bu' in Traditional Chinese Medicine, is derived from the root of *Stemona tuberosa* Lour (Stemonaceae family). It is often used as an antitussive drug to treat respiratory disorders, e.g. bronchitis, pertussis and tuberculosis, and also as an anthelmintic agent for domestic animals (Zang Tingmo, 1977). The crude extract of this plant was found to have anti-bacterial, anti-fungal, anti-viral, antitussive, insecticidal and neuroprotective activities (Xu *et al*., 1996). The alkaloids; tuberostemonines from this species were reported to show inhibitory activity on the excitatory transmission at the crayfish

[1] Dr, Associate Professor, Department of Chemistry, Dawei University
[2] Dr, Lecturer, Department of Chemistry, University of Yangon
[3] Dr, Lecturer, Department of Chemistry, Mawlamyine University
[4] Dr, Part-time Professor, Department of Chemistry, University of Yangon

neuromuscular junction. The prominent clinical and pharmacological properties of this plant has prompted many phytochemical studies, and over a dozen stemona alkaloids isolated from this herb of different places of origin can be structurally classified into three categories: (i) stenine-type, e.g. tuberostemonine, (ii) stemoamide-type, e.g. stemoamide, and (iii) tuberostemospironine-type, e.g. tuberostemospironine (Jaing *et al*., 2002). To date, however, there have been no reports on the anti-diabetic constituents of the plant (Figure 1). Therefore, we aimed at investigating the anti-diabetic activity and some constituents possessing such activity in the present study.

(a) (b)

Figure 1 Photographs showing (a) *S. tuberosa* plant and (b) roots

Materials and Methods

Sample Collection of Preparation

Roots of *S. tuberosa* used in this study were collected from Gangaw Township, Magway Region. The collected sample was washed with water, chopped into small pieces using a stainless knife and air dried to a constant weight at room temperature for one month. The dried sample was subsequently milled into coarse powder using a grinding mill and then stored in an airtight plastic container for the experimental works.

Animal Materials

Both sexes of BALB/c mice (20-25 g) were obtained from Animal Section from Parasitology Research Division, Department of Medical Research, Yangon.

Reagents

α-amylase (Jiangsu Boli Bioproducts Co., Ltd), deionized water, disodium hydrogen phosphate, sodium dihydrogen orthophosphate, acarbose (Bayer Pharma AG, Kaiser-Whilheim-Allee, Leverkusen, Germany) and metformin (Denk Pharma Gmbtt Co., Ltd Munchen, Germany), alloxan monohydrate (Titan Biotech Ltd., India), DM sensor blood glucometer (Taiwan), sucrose (BDH), starch, iodine, ethanol, 2,2-diphenyl-1-picry-hydrazyl (DPPH) and Vitamin C were used.

Preparation of Crude Extracts

The dried powdered root (300 g) was percolated with 95% ethanol (1000 mL) for one week and filtered. This procedure was repeated for three times. The combined filtrates were evaporated under reduced pressure by means of a rotatory evaporator. Consequently, 95%

ethanol soluble extract was obtained. Water extract of three samples was prepared by boiling 300 g of sample with 1000 mL of distilled water for 6 h and filtered. It was repeated three times and the filtrates were combined followed by heating on water bath and sand bath to give water extract. Each extract was stored in refrigerator for screening of biological activities.

Screening of *In Vitro* Antioxidant Activity

(a) Preparation of DPPH solutions

DPPH (2.364 mg) was thoroughly dissolved in EtOH (100 mL). This solution was freshly prepared in the brown coloured reagent bottle and stored in the fridge for no longer than 24 h. Each tested samples (2 mg) and 10 mL of EtOH were thoroughly mixed by shaker. The mixture solution was filtered and the stock solution was obtained. By adding with EtOH, the tested sample solutions with different concentrations of 10, 5, 2.5, 1.25 and 0.625 μg/mL were prepared from the stock solution.

(b) Determination of *in vitro* antioxidant activity

The effect on DPPH radical was determined using the method by Marinova and Batchvarov (2011). The control solution was prepared by mixing 1.5 mL of 60 M DPPH solution and 1.5 mL of EtOH using shaker. The tested sample solution was also prepared by mixing thoroughly 1.5 mL of 60 M DPPH solution and 1.5 mL of each sample solution. The mixture solutions were allowed to stand at room temperature for 30 min. Then, the absorbance of these solutions was measured at 517 nm on a UV-7504 UV-visible spectrophotometer. Absorbance measurements were done in triplicate for each concentration and then mean values so obtained were used to calculate percent inhibition of oxidation by the following equation.

$$\% \text{ Inhibition} = \frac{A_{Control} - A_{Sample}}{A_{Control}} \times 100$$

where, $A_{Control}$ = absorbance of control solution

A_{Sample} = absorbance of tested sample solution.

The 50 % antioxidant inhibition concentration (IC_{50}) of tested samples and positive control were determined by linear regressive excel programme.

Screening of *In Vitro* α-Amylase Inhibition

Starch iodine assay

Alpha-amylase inhibitory activity was measured *in vitro* by hydrolysis of starch in the presence of α-amylase enzyme. This process was quantified by using iodine, which gave blue colour with starch. The reduced intensity of blue colour indicates the enzyme-induced hydrolysis of starch to monosaccharides. If the extracts possessed α-amylase inhibitory activity, the intensity of blue colour would be more. In other words, the intensity of blue colour in test sample was directly proportional to α-amylase inhibition activity (Ganapaty *et al.,* 2013). In this assay, 10 μL of α-amylase solution (0.3 U/mL where U means μmol/min, where μmol refers to the amount of substrate conversion) was mixed with 390 μL of phosphate buffer solution (40 mM containing 0.006 M NaCl, pH 7.0) containing different concentrations (100, 60, 40, 20 μg/mL) of tested samples and the positive control, acarbose. After incubation at 37 °C for 10 min, 10 μL of

starch (1 %) was added to the mixture and it was reincubated for 30 min. Then, 0.1 mL of 1 % iodine solution was added to this mixture. After adding 5 mL of distilled water, the absorbance was measured at 565 nm in the UV spectrophotometer. The absorbance of control, without test sample, and blank, without starch, were recorded under the same conditions. The inhibition of enzyme activity was calculated by using the formula,

$$\% \text{ inhibition of enzyme activity} = \frac{A_{Control} - A_{Sample}}{A_{Control}} \times 100$$

where, $A_{Control}$ = absorbance of the control (without sample)

A_{Sample} = absorbance of the tested sample

The concentration of tested samples and positive control which inhibited the hydrolysis of starch by 50 % (IC_{50}) were determined by linear regressive excel programme.

Preliminary Phytochemical Tests

A 1 g each of Thamya roots powder was subjected to the test of alkaloids, α-amino acids, carbohydrates, cyanogenic glycosides, flavonoids, glycosides, organic acids, phenolic compounds, reducing sugars, saponins, starch, steroids, tannins and terpenoids as the preliminary phytochemical test according to reported methods (CCRUM, 1977, Marini-Bettolo *et al*., 1981 and M-Tin-Wa, 1972).

Extraction and Isolation of Phytoconstituents

The air-dried roots powder (500 g) of *S. tuberosa* were extracted with 95 % ethanol (3× 1 L) at room temperature. The combined filtrates were evaporated under reduced pressure by means of a rotatory evaporator to afford an EtOH extract (18 g) which was then acidified with dilute HCl (4 %) to pH 1-2 and partitioned with CH_2Cl_2. The aqueous part was then basified with aqueous NH_3 (28 %) to pH 9-10 and extracted with CH_2Cl_2 to afford crude alkaloids. The crude alkaloids (5 g) were separated by silica gel column (ϕ 10 cm; 70-230 mesh), using gradient mixtures of n-hexane-acetone from 20:1 to 1:2 as mobile phases, affording six fractions. The fraction F3 (2.4 g) was subjected to silica gel CC (ϕ 3 cm; 230-400 mesh) and eluted with gradient solvent systems of n-hexane-CH_2Cl_2 (5:1 → 1:1) to yield compound **1** (20 mg, 0.04 % w/w). These isolated compounds were characterized by their physicochemical properties: melting point, R_f value and identified by modern spectroscopic methods: FT IR, ^{1}H NMR, ^{13}C NMR, ^{1}H ^{1}H COSY, HSQC, HMBC and ESI-MS.

Acute Toxicity Assay

The *in vivo* acute toxicity of ethanol and water extracts of *S. tuberosa* was investigated, according to the OECD Guidelines for the Testing of Chemicals 423, with two doses (5000 and 2000 mg/kg) on BALB/c mice model. A total of 50 healthy mice (both sexes, four to six weeks old, body weight 20-25 g) were grouped to five groups (Group IA for control; only distilled water, Groups IIB and IIC for 2000 mg/kg; and Groups IIIB and IIIC for 5000 mg/kg oral dose of ethanol and water extracts) of 10 mice each. The mice fasted overnight and given only water were used for the experiment. The animals were observed for the first six hours continuously for mortality and behavioral changes, if any, and then every 24 h for one month. The mice were observed from possible manifestation of physical signs of toxicity such as struggle, decreased

motor activity, decreased body/limb tones, decreased respiration and finally death. Records on the number of deaths observed were taken in each group.

Screening of *In Vivo* Antidiabetic (Hypoglycemic) Effect

Induction of diabetes

Male albino mice were made diabetic by a single dose of intraperitoneal (IP) injection of 150 mg/kg body weight of alloxan monohydrate in sterile normal saline (Yanarday and Colak, 1998). The mice were maintained on 5 % glucose solution for next 24 h to prevent hypoglycemia. Five days later, blood samples were drawn from tail vein and glucose levels were determined to confirm the development of diabetes (250 mg/dL and above). The diabetic mice were divided into six groups, each containing five animals and treated as follows:

Group I : Normal control mice

Group II : Alloxan-induced diabetic mice with 150 mg/kg body dose, Diabetic control

Group III : Alloxan-induced diabetic mice treated with 150 mg/kg body weight dose of ethanol extract

Group IV : Alloxan- induced diabetic mice treated with 150 mg/kg body weight dose of water extract

Group V : Alloxan-induced diabetic mice treated with 15 mg/kg body weight dose of compound **1**

Group VI : Alloxan-induced diabetic mice treated with 150 mg/kg body weight dose of standard drug metformin

Blood Sampling

Blood samples were collected from the tail vein just prior to and 1 h, 2 h, 3 h and 4 h after drug administration for acute study. The blood samples from each mouse was analyzed for blood glucose content at 1 h, 2 h, 3 h and 4 h subsequently using DM sensor blood glucometer and percent reduction in blood glucose level was calculated by the following equation.

$$\text{Reduction (\%)} = \frac{\text{FGBL} - \text{blood glucose level}}{\text{FGBL}} \times 100$$

where, FBGL = fasting blood glucose level at 0h

The results are expressed as mean ± standard error mean, the significance of various treatments was calculated by one-way ANOVA using SPSS software version 16 and were considered statistically significant when $p < 0.01$.

Histopathology of Pancreas

The pancreas from normal control, diabetic control and maximum drug dose treated animals were blotted free of mucus. The tissues were washed in normal saline, cut into the desired size and fixed in 10 % formalin for 24 h. After fixation, tissues were dehydrated and embedded in paraffin. Sections of tissue were cut in a microtome to 5 mm in thickness, mounted on slides, stained with Hematoxylin and Eosin for photographic observations by the pathologist from DMR, Lower Myanmar.

Results and Discussion

Preliminary phytochemical tests indicated the presence of alkaloids, α-amino acids, carbohydrates, flavonoids, glycosides, organic acids, phenolic compounds, reducing sugars, saponins, starch, steroids, tannins and terpenoids. However cyanogenic glycosides were not detected in the roots of Thamya. The presence of alkaloids, flavonoids and phenolic compounds in *S. tuberosa* indicates the antioxidant activity of that plant.

In vitro antioxidant activity by DPPH free radical scavenging assay

The presence of phenolic compounds like polyphenols, flavonoids, tannins, and terpenes in plant extracts shows significant antioxidant effect due to their free radical scavenging activity (Rahman and Moon, 2007). Free radicals such as hydrogen peroxide (H_2O_2), singlet oxygen ($^1O_2$) and superoxide anion radical are often generated by various biological oxidation reactions. These oxidative mediators can lead to the damage of important biomolecules such as proteins, nucleic acid, and lipids. The antioxidant activities of ethanolic and water extracts; and compound **1** of *S. tuberosa* roots were measured as DPPH free radical scavenging activity and exhibited significant variations (Table 1 and Figure 2). The antioxidant (radical scavenging) activity of the ethanolic extract (IC_{50} = 1.50 μg/mL) was significantly higher than that of the water extract (IC_{50} = 3.95 μg/mL) of *S. tuberosa* roots. Moreover, compound **1** (IC_{50} = 1.06 μg/mL) from ethanolic *S. tuberosa* roots extract showed a greater radical scavenging activity than the standard ascorbic acid (IC_{50} = 1.21μg/mL).

Table 1 Radical Scavenging Activity (Percent Inhibition and IC_{50} Values) of Crude Extracts of *S. tuberosa* Roots and Standard Ascorbic Acid

Samples	% Inhibition (Mean ± SD)In Different Concentration (μg/mL)						IC_{50} (μg/mL)
	0.625	**1.25**	**2.5**	**5**	**10**	**20**	
EtOH extract	32.01 ±2.58	40.80 ±0.32	51.14 ±1.29	57.53 ±1.93	62.78 ±2.26	71.68 ±1.29	1.50
H_2O extract	26.11 ±0.30	35.17 ±1.21	44.66 ±1.51	53.85 ±0.60	57.91 ±0.91	63.68 ±1.21	3.95
Compound **1**	45.05 ±0.32	52.11 ±0.11	60.23 ±0.45	70.45 ±1.32	79.17 ±1.51	85.01 ±0.98	1.06
Ascorbic acid*	47.81 ±0.88	54.18 ±1.32	61.09 ±0.22	67.5 ±0.44	71.71 ±1.54	79.21 ±2.43	1.21

Data are expressed as means of triplicate determination ± standard deviation (SD). *****- Standard

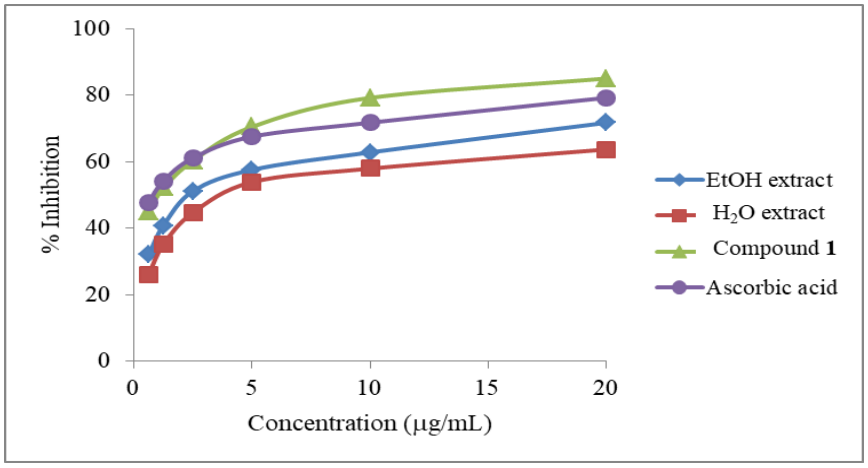

Figure 2 A plot of % radical scavenging activity versus concentration (µg/mL) of crude extracts and compound **1** from roots of *S. tuberosa* and ascorbic acid

In vitro anti-diabetic activity by α-amylase inhibition

In vitro anti-diabetic activity was carried out on the ethanol and water extracts of *S. tuberosa* roots by using alpha amylase inhibitory assays. The α-amylase is a key enzyme in our digestive system which catalyzes the degradation of dietary starch *viz*., maltose to glucose in the small intestine before absorption. Degradation of this dietary starch results in rapid increase in glucose levels, and leads to elevated post prandial hyperglycemia (Abhijit *et al*., 2014). Inhibition of alpha amylase can lead to reduction in post prandial hyperglycemia (Raman *et al*., 2012). Hence, retardation of starch digestion by inhibition of α-amylase enzyme would play a key role in the treatment of diabetes.

In this study, the alcohol and watery extracts, and compound **1** of *S. tuberosa* were evaluated for their inhibitory effect on α-amylase enzyme by *in-vitro* method. The alcohol extract, water extract, compound **1** of *S. tuberosa* (at a concentration of 100 µg/mL) and acarbose exhibited 67.26, 49.26,79.61 and 74.03 µg/mL for α-amylase inhibitory activity (Table 2 and Figure 3); respectively. Acarbose, a synthetic drug has the ability to inhibit alpha amylase was used as a standard for the assay. The α-amylase reduces the rate of starch breakdown, leading to lowered blood glucose levels and leads to minimum absorption of monosaccharides. Furthermore, it was evident that compounds like glycosides, proteins, alkaloids, flavonoids, saponins, tannins, and steroids has inhibitory action on α-amylase. The ethanolic extract and compound **1** of *S. tuberosa*, each has therefore shown best enzyme inhibitory activity with IC_{50} values, 80.98 and 59.25 µg/mL on α-amylase (Table 2 and Figure 3), which were comparable with that of acarbose (64.12 µg/mL).

Table 2 α-Amylase Inhibition % and IC_{50} Values of Crude Extracts and Isolated Compound 1 of *S. tuberosa* Root Compared with Acarbose

Sample	% Inhibition (mean ± SD) in different concentration (μg/mL)					IC_{50} (μg/mL)
	20	40	60	80	100	
EtOH extract	16.10 ± 1.38	22.71±0.89	32.59±1.95	56.11 ± 0.91	67.26 ±0.61	80.98
H_2O extract	6.75 ± 0.69	10.35±1.84	23.44±1.06	39.82 ± 1.53	49.26 ±1.76	101.48
Compound **1**	17.85 ± 0.73	30.30±1.01	50.76±1.07	70.09 ± 0.85	79.61 ±0.90	59.25
Acarbose*	18.98 ± 0.66	32.32±0.21	45.86±0.73	65.96 ± 1.11	74.12 ±0.03	64.12

Data are expressed as means of triplicate determination ± standard deviation (SD).
*= positive control

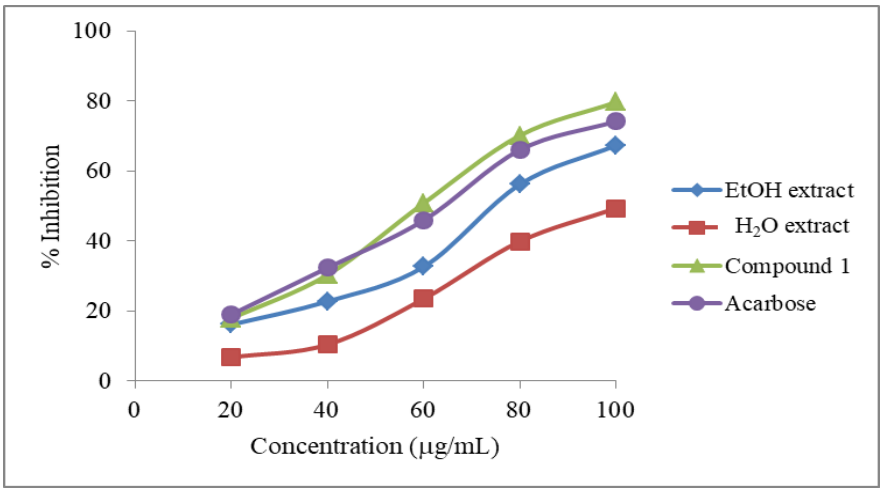

Figure 3 A plot of % inhibition of α-amylase against various concentrations of crude extracts and isolated compound **1** of *S.tuberosa* roots

In vivo acute toxicity assay

Acute toxicity screenings of ethanol and water extracts were done with two oral doses, 2000 and 5000 mg/kg body weight on each group of albino mice. The condition of mice groups were recorded after fourteen days' administration. No lethality of the mice was observed up to the day fourteen of administration. Animals of each group were also still alive and did not show any visible symptoms of toxicity like struggle, respiratory distress, decreased body/limb tone and death (Table 3). Even with up to the dose of 5000 mg/kg body weight administration, there is no lethality at the day fourteen.

Table 3 Acute Toxicity Effect of Crudes Extracts of *S. tuberosa* Roots on Albino Mice Model

No.	Group	Dosage (mg/kg)	No. of Death	% of Death at 14 Days
1	IA	-	Nil	0
2	IIB	2000	Nil	0
3	IIIB	5000	Nil	0
4	IIC	2000	Nil	0
5	IIIC	5000	Nil	0

Each group contains 10 no. of mice.
A = control, B = ethanol extract and C = water extract

In vivo hypoglycemic activity of *S.tuberosa*

Diabetes mellitus is one of the metabolic diseases characterized by hyperglycemia resulting from defects in insulin secretion. *In vivo* antidiabetic activity was determined by using alloxan-induced diabetic mice model. Alloxan caused permanent destruction of pancreatic beta cell and induced diabetes for mice. As control, determination of normal fasting blood glucose level was carried out and it was found to be 100 ± 3.39 mg/dL, showing within the normal range. In this study, mean glucose level of the mice treated with alloxan was found to be 100.00 ± 3.39 mg/dL to 253.00 ± 21.25 mg/dL. The results showed that the animals used in these experiments were in diabetic stage and hyperglycemia was developed 72 h after alloxan injection (Yanarday and Colak, 1998). In diabetes control group; without treatment, the mean blood glucose concentration was found to raise from 100.00 ± 3.39 mg/dL to 253. ± 21.25 mg/dL at 72 h, 279.00 ± 22.25 mg/dL at 73 h, 275.00 ± 29.25 mg/dL at 74 h, 275.00 ± 24.50 mg/dL at 75 h and 269.00 ± 22.50 mg/dL at 76 h. The alloxan-induced diabetic mice were treated with metformin (150 mg/kg b.wt), EtOH and H_2O extracts (150 mg/kg b.wt) and isolated compounds from EtOH extract, and compound **1** (15 mg/kg b.wt).

Table 4 Antidiabetic activity of *S. tuberosa* roots extracts and compounds during acute study

Treatment	Blood Glucose Concentration (mg/dL)				
	0 h	1 h	2 h	3 h	4 h
Normal	100.00 ±3.39	101.00 ± 7.35	100.00 ± 5.00	100.67 ± 8.37	100.67 ± 4.03
Alloxan (150 mg/kg)	253.00±21.25	279.00 ±22.25	275.00 ±29.25	275.00 ±24.50	269.00 ± 22.50
EtOH extract (150 mg/kg)	195.33±14.80	182.33 ±16.70 (6.66 % R)	161.33 ±16.10 (17.41 % R)	138.67 ±18.80 (29.01 % R)	114.67 ± 20.30 (41.29 % R)
H_2O extract (150 mg/kg)	239.00±19.20	223.00 ±12.60 (6.69 % R)	207.67 ±15.80 (13.11 % R)	185.33 ±18.00 (22.45 % R)	163.67 ± 20.80 (31.52 % R)
*Metformin (150 mg/kg)	192.67±11.61	159.67 ±11.18 (17.21 % R)	135.33 ±16.95 (29.76 % R)	123.33 ±15.67 (35.08 % R)	112.00 ± 14.14 (41.87 % R)
Compound **1** (15 mg/kg)	205.00±21.60	187.67 ±17.80 (8.45 % R)	168.00 ±26.90 (18.05 % R)	145.33 ±17.80 (29.11 % R)	119.67 ± 24.70 (41.62 % R)

R = Reduction, P < 0.05,* = Antidiabetic drug, Data are represented as mean ± SEM (n = 3).

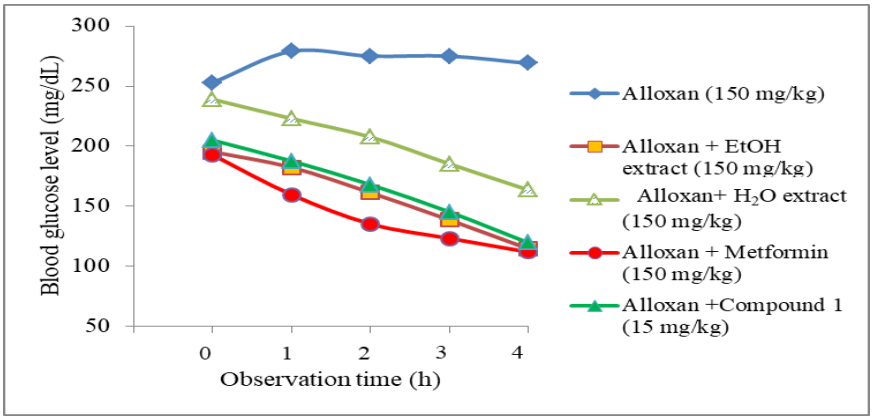

Figure 4 The effect of ethanol, water extracts and compound **1** of *S. tuberosa* roots and metformin on blood glucose levels of alloxan-induced diabetic mice

After samples injection, the blood glucose levels were dramatically reduced (Table 4 and Figure 4). Concerning with duration of action, the hypoglycemic effect of tested sample lasted for 4 h. So, all of the test samples showed significant percent reduction of blood glucose level (% R) at 4 h after treatment with samples where $p < 0.01$. The % reduction of blood glucose level in mice produced after administration at 4 h with standard metformin, EtOH and H_2O extracts; compound **1** of roots of *S. tuberosa* were compared in Figure 4. The % reduction of blood glucose levels were compound **1** (41.62%) followed by EtOH extract (41.29 %), H_2O extract (21.52 %). But that of blood glucose level of EtOH extract and compound **1** was not significantly different from standard metformin (41.87%), Therefore, EtOH extract of roots of *S. tuberosa* and compound **1** have significant hypoglycemic effect against alloxan induced diabetic albino mice.

Histopathological examination of pancreas

The histopathological examination on pancreatic islet was performed 7 days after alloxan administration by Hematoxylin and Eosin stain method and recorded by using light-microscope with specific images. The images of histopathological of pancreas obtained from mice of each group were described in Figures 5 (a-f). From the histopathological result, the pancreas of metformin treated diabetic mice (c) showed proliferation of beta islets cells and accumulation of fat globules within acinar cells in pancreas but the pancreas of diabetic untreated mice (b) showed destruction of pancreatic beta islets cell comparing with normal pancreatic tissue of normal mice (a). The pancreatic islets cell of the H_2O extracted diabetic mice (d) showed apart of regeneration of ill-defined acinar cells with absence of nucleus. The EtOH extract treated diabetic mice (e) showed regeneration of group of nucleated beta islets cells with ill-defined margin and necrosis of acinar cells in pancreas. In additions, the histological observation of pancreatic cells of mice treated with compound **1** treated diabetic mice (f) showed good proliferation of beta islets cells; two to three groups among the well-defined pyramidal shaped acinar cell and no accumulation of fat globules within acinar cells in pancreas compared with histopathological information of metformin treated diabetic mice (c). The signs of regeneration of beta cells stimulated potentiation of insulin secretion from beta cells of islets of Langerhans and so decreasing of blood glucose level. Nevertheless, the extracts of EtOH and H_2O as well as compound **1** induced regeneration of the islets responsible for the increase in the serum insulin. Therefore the ethanol extract of *S. tuberosa* root and compound **1** showed protective activity in reactive oxygen species (ROS) induce damage tissues.

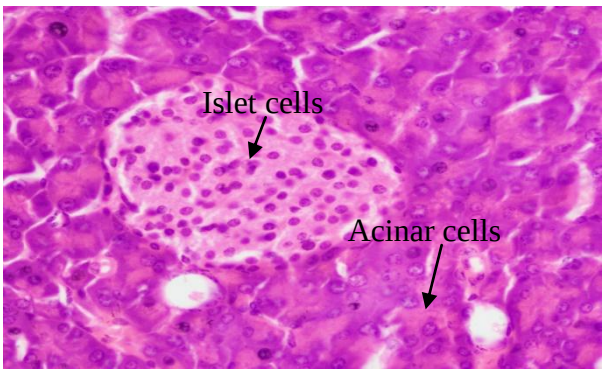

(a) Normal pancreatic tissue of normal

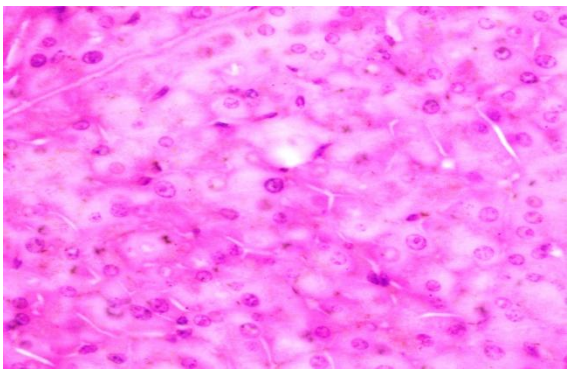

(b) Destructive pancreatic tissue of alloxan-induced diabetic mice

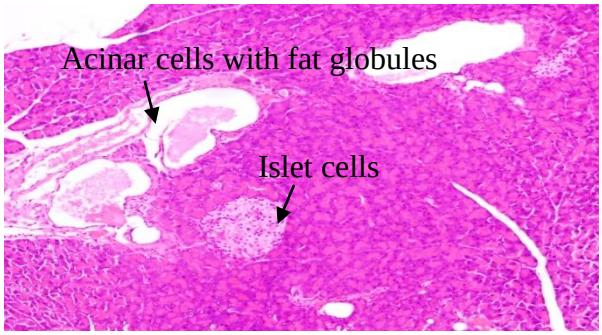

(c) Regeneration of beta islets cells among acinar cell with duct epithelial shape but accumulation of fat globules in acinar cell of pancreatic tissue of alloxan-induced diabetic mice with metformin

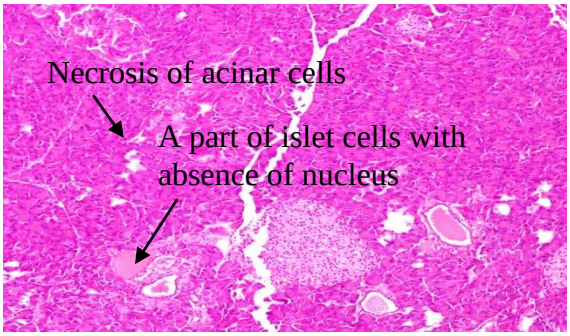

(d) A part of regeneration of beta islets cells with absence of nucleus and necrosis of some acinar cell of pancreatic tissue of alloxan-induced diabetic mice with H_2O extract

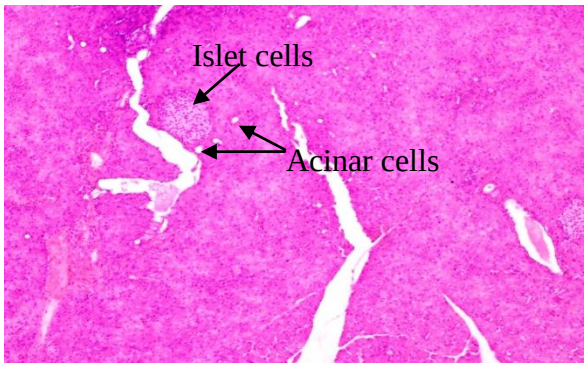

(e) Regeneration of beta islets cells among acinar cell of pancreatic tissue of alloxan-induced diabetic mice with EtOH extract

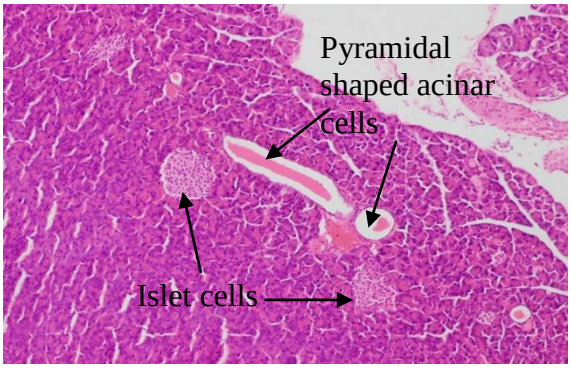

(f) Good proliferation of beta islets cells among the well-defined pyramidal shaped acinar cell of pancreatic tissue of alloxan-induced diabetic mice with compound **1**

Figure 5 (a-f) Histological examinations of pancreatic tissue of alloxan-induced diabetic mice after 7 days' treatment of antidiabetic drugs; metformin, H_2O, EtOH and compound **1** [magnification × 40]

Identification of Organic Compound 1

Compound **1** was obtained as a colorless prism. Its molecular formula was established as $C_{22}H_{33}NO_4$ by the positive molecular ion peak at m/z 376.2 $[M+H]^+$ in its ESI MS (Figure 12) with seven degrees of unsaturation. The IR band at 1762 cm^{-1} (Figure 6) and ^{13}C NMR data at δ_C 179.2 and 179.4 suggested the presence of two γ-glactone rings (Figure 8). In the ^1H NMR spectrum (Figure 7), a primary methyl group appeared at δ_H 0.96 (3H, t, J = 7.4 Hz, H-17) and the secondary methyl groups were observed at δ_H 1.61 (3H, d, J = 7.3 Hz, H-22) and 1.24 (3H, d, J = 7.3 Hz, H-15). Two low field germinal protons appeared at δ_H 2.36 and 3.30 (2H, m, H-5). Two protons at the oxygenated carbons were shown at δ_H 4.52 (1H, m, H-11) and 4.31 (1H, m, H-11). The ^{13}C NMR and ^1H-^{13}C HMQC spectra (Figures 8 and 10) showed 22 skeletal carbon signals including three methyls, seven methylenes, ten methines, and two carbonyls. The above characteristic data suggested that compound **1** is agreed structurally to tuberostemonine **J** (Chung *et al*., 2003). The ^1H-^1H COSY correlations of H-11→H-12→H-13→H15 and H-18→H-19→H-20→H3-22 with two oxomethines [δ_H 4.52 (H-11)/δ_C 80.5 (C-11) and 4.38 (H-18)/ 78.9 (C-11)] as starting points (Figure 9) and the HMBC correlations of

H13-15/C-14 and H5-20/C-21 provided evidence for two α-methyl-γ-lactone rings (Figure 11). The ^{1}H-^{1}H COSY spectrum of compound **1** exhibited the correlation of H-5→H-6→H-7→H-8→H-9→H-9a and H-9a→H-1→H2→H-3 involving typical three low field protons attached to the N-atom at [δ_H 2.36 and 3.30 (each H-5), 3.43 (H-3), and 3.05 (H-9a)], indicating the presence of the nitrogen fused perhydroazaazulene ring (Yun-Seo *et al*., 2014). Additional ^{1}H-^{1}H COSY correlations of H-11→H-10→H2-16→H3-17 and the ^{1}H-^{13}C HMBC correlations of H-3/C-1, H-3/C-9a and H-3/C-19 allowed to confirm the connectivities of the above subgroups (Figures 9 and 11). Thus, compound **1** was determined as a known stemona type alkaloid, namely, tuberostemonine **J** in Figure 13.

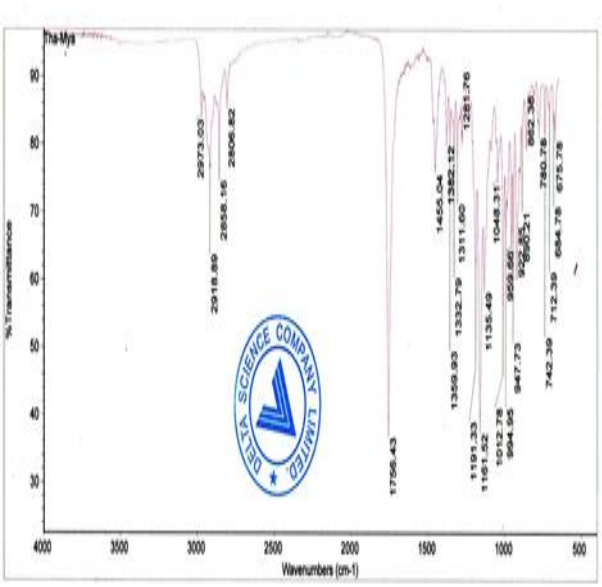

Figure 6 FT IR spectrum of compound **1**

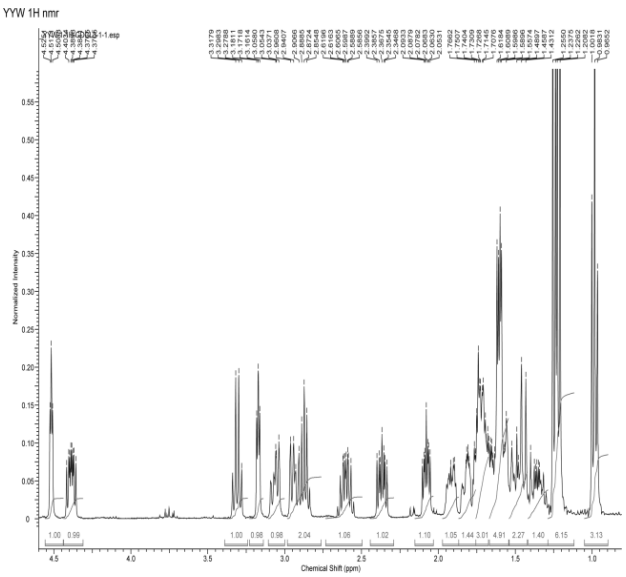

Figure 7 ^{1}H NMR (600 MHz, $CDCl_3$) spectrum of compound **1**

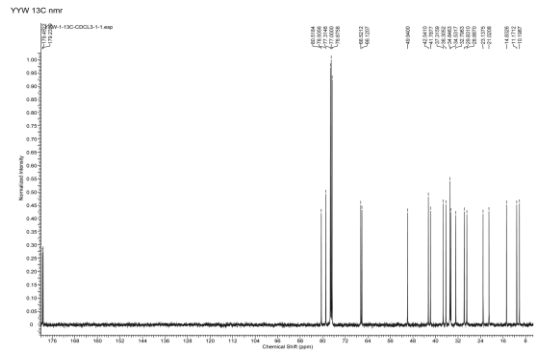

Figure 8 ^{13}C NMR (150 MHz, $CDCl_3$) spectrum of compound 1

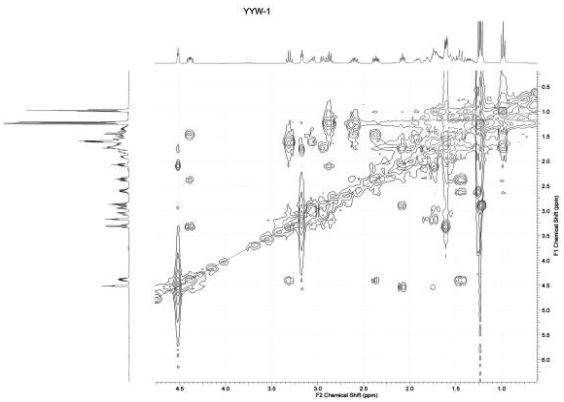

Figure 9 ^{1}H-^{1}H COSY (600 MHz, $CDCl_3$) spectrum of compound 1

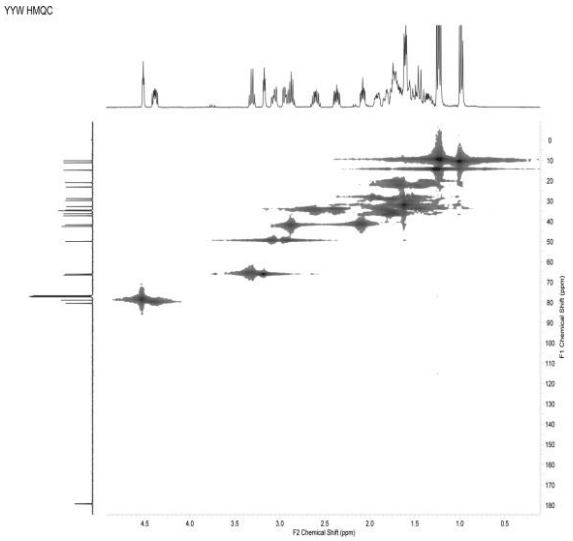

Figure 10 ^{1}H-^{13}C HMQC (600 MHz,$CDCl_3$) spectrum of compound 1

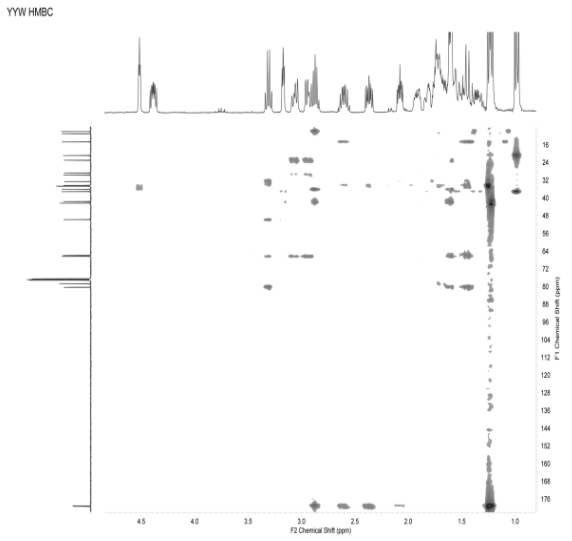

Figure 11 ^{1}H-^{13}C HMBC (600 MHz, $CDCl_3$) spectrum of compound 1

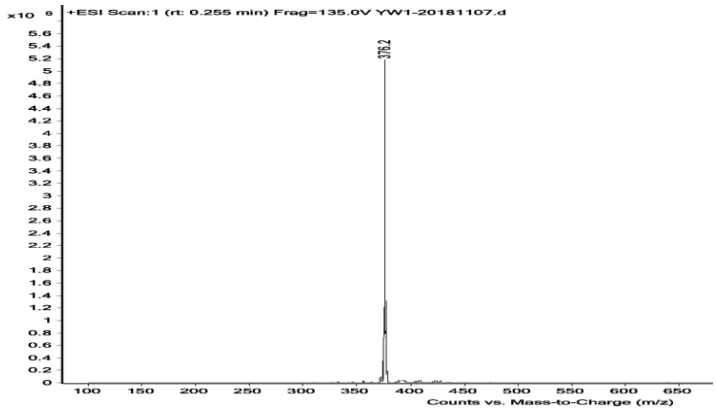

Figure 12 ESI MS spectrum of compound 1

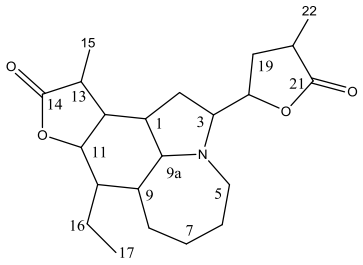

Figure 13 Chemical structure of tuberostemonine J

Compound **1** (Tuberostemonine **J**): A colorless prism crystallized from hexane/EtOAc, mp: 180-182 ^{0}C.; IR (νcm^{-1}) : 2924(ν_{C-H} asym), 1762 ($\nu_{C=O}$), 1456 (δ_{C-H}), 1167 (ν_{C-N}), 1015 (ν_{C-O}); ESI-MS m/z (% intensity): 376 $[M+H]^{+}$ (100), ^{1}H NMR (6 00 MHz, $CDC1_3$) δ_H (ppm): 1.80 (3H, t, J=7.5 Hz, H-17), 1.24 (3H, d, J=7.5 Hz, H-15), 1.61 (3H, d, J=7.5 Hz, H-22), 1.40-2.07 (15H, H-1, 2H-2, 2H-6, 2H-7, 2H-8, H-9, H-10, H-12, 2H-16, H-19), 3.17(1H, m, H-19), 2.59 (1H, m, H-20), 2.87 (1H, m, H-13), 2.36 and 3.30 (each 1H, m, 2H-5), 3.43 and 3.05 (2H, m, H-3 and H-9a), 4.38 (1H, m, H-18), 4.52 (1H, t, H-11); ^{13}C NMR (150 MHz, $CDC1_3$) δ_C (ppm): 10.2 (C-17), 11.2 (C-15), 14.8 (C-22), 21.0 (C-16), 23.1 (C-7), 28.9 (C-6), 29.8 (C-2), 32.7 (C-8), 34.4 (C-19), 34.5 (C-9), 34.8 (C-10), 36.3 (C-12), 37.3 (C-20), 41.8 (C-13), 42.5 (C-1), 49.4 (C-5), 66.1 (C-3), 66.5 (C-9a), 78.9 (C-11), 80.5 (C-18), 179.2 (C-14), 179.4 (C-21).

Conclusion

This research revealed some biological properties, antioxidant and antidiabetic effects, of the *S. tuberosa* roots extracts, and tuberostemonine **J**. In fact, the present research showed that the extracts of the roots possess not only antioxidant but also hypoglycemic effects. Moreover, tuberostemonine **J** is more potent than vitamin C in antioxidative property as well as more excellent than the antidiabetic drug metformin in proliferation of beta islets cells among the well-defined pyramidal shaped acinar cell of pancreatic tissue of alloxan-induced diabetic mice. Therefore it is hoped that the research findings will contribute to some extent to the search for the antioxidative and antihyperglycemic agent of plant origin and also to the development of the role of Myanmar traditional medicinal formulation, especially in the treatment of oxidative related diseases and diabetes.

Acknowledgements

The authors acknowledge to the Myanmar Academy of Art and Science and the Department of Higher Education (Yangon Office), Ministry of Education, Myanmar for allowing us to submit this paper. Thanks are also extended to the authorized Pathologist, Dr Moh Moh Tun (Director) from Pathology Research Division, Department of Medical Research (Lower Myanmar), Yangon, for the histological examination of pancreatic tissues from drug treated diabetic mice and the Research Scientists from Parasitology Research Division, Department of Medical Research (Lower Myanmar), Yangon, for allowing us to use research facilities regarding acute toxicity and antidiabetic activity.

References

Abhijit, S., Rashmi, S., Nikita, S., Yashwant, M. and Bhagyashri, C. (2014). "Anti-diabetic Activity of *Tridax procumbens*". *J. Sci. Innovative Res.*, vol. 3 (2), pp. 221-226.

CCRUM. (1987). *Physicochemical Standards of Unani Formulations, Part-2*, Central Council for Research in Unani Medicine, New Delhi: pp. 289-318.

Chung, H.S., Hon, P.M., Lin, G., But, P.P.H. and Dong, H. (2003). "Antitussive Activity of Stemona Alkaloids from *Stemona tuberosa* ". *Planta Medica*, vol. 69, pp. 914-920.

Ganapaty, S., Nandeesh, R., Veerapur, V.P., Thippeswamy, B.S. and Shivasharan, D. (2013). "*In Vivo* and *In Vitro* Anti-Diabetic Effects of *Madhuca indica* Roxb., in Alloxan-Induced Diabetic Rats". *IJAPBC*, vol. 2(2), pp. 282-290.

Jiang, R.W., Hon, P.M., But, P.H., Chung, H.S., Lin, G., Yed, W.C. and Maka, T.C.W. (2002). "Isolation and Stereochemistry of Two New Alkaloids from *Stemona tuberosa* ". *Tetrahedron* , vol. 58 , pp. 6705-6712.

Marini–Bettolo, G.B., Nicoletti, M., and Patamia, M. (1981), "Plant Screening by Chemical Chromatographic Procedure under Field Conditions". *J. Chromatogr*., vol. 213, pp. 113-127.

Marivona, G. and Batchvarov, V. (2011). "Evaluation of the Methods for Determination of the Free Radical Scavenging Activity by DPPH". *Bulg. J. Agric. Sci.*, vol. 17 (1), pp. 11-24.

M-Tin-Wa. (1972). "Phytochemical Screening Methods and Procedures". *Phytochemical Bulletin of Botanical Society of America*, Inc., vol. 5 (3), pp. 4-10.

OECD. (2008), *OECD Guideline for Testing of Chemical: Acute Oral Toxicity-Fixed Dose Procedure, Test Guideline 423*, pp.1-5.

Rahman, M.A. and Moon, S.S. (2007). "Antioxidant polyphenol glycosides from the Plant *Draba nemorosa*". *Bull Korean Chem. Soc*., vol. 8, pp.827-831.

Raman B.V., Naga Vamsi, A.K., Narasimha Rao, B., Pardha Saradhi, M. and Basaveswara Rao, M.V. (2012). "Plants with Antidiabetic Activities and their Medicinal Values". *Int. Res. J. Pharm*., vol. 3(3), pp.11-15.

Xu, G. J., He, H.X., Xu, L.S. and Jin, R.Y. (1996). *The Chinese Materia Medica*. Chinese Medicinal Science and Technology Publishing House, People's Republic of China: pp. 467-472.

Yanarday R. and Colac, H. (1998). "Effect Chard (*Beta vulgaris* L. *varcicla*) on Blood Glucose Level in Normal and Alloxan-Induced Diabetic Rabbit". *J. Ethnopham*., vol. 4, pp. 309-311.

Yun-Seo, K., Han, A. and Seo, E.K. (2014). "Tuberostemonine J from the Roots of *Stemona tuberosa*". *Bull. Korean Chem. Soc.*, vol. 35 (6), pp. 1891-1893.

Zang Tingmo. (1977). *Dictionary of Chinese Traditional Medicine*. Shanghai People's Publishing House, People's Republic of China: pp. 858-861.

STRUCTURAL CHARACTERISTIC, OPTICAL PROPERTIES AND AC ELECTRICAL CONDUCTIVITIES OF PEROVSKITE $LaCoO_3$ PREPARED BY DIFFERENT METHODS

Kay Thi Tun[1], Mya Theingi[2], Nwe Nwe Aung[3]

Abstract

Perovskite $LaCoO_3$ material was prepared by two different methods; citrate sol-gel and co-precipitation methods. The simple low temperature synthesis has been presented of single phased $LaCoO_3$ for cathode application in solid oxide fuel cell (SOFC). The X-ray diffraction (XRD) shows that the hexagonal $LaCoO_3$ phase was well formed at sintering temperature 900 °C in the citrate sol-gel and co-precipitation methods. Scanning electron microscopy (SEM) analysis indicates that the particle size of $LaCoO_3$ powder varies from 20 nm to 60 nm depending on the preparation method. The FT IR spectra confirm that the absorption band of La-O and Co-O bonding appeared at 665, 592 and 406 cm^{-1}. The optical properties of $LaCoO_3$ studied by UV-visible spectrophotometer in the wavelength range of 300 nm to 700 nm. The band gap values of the $LaCoO_3$ prepared by citrate sol-gel method and by co-precipitation are 2.15 eV and 2.42 eV respectively. The dielectric properties and ac electrical conductivity have been investigated by LCR meter in the frequency range of 100- 1000 kHz. The ac electrical conductivity value of $LaCoO_3$ prepared by citrate sol-gel method is 8.74 $\mu\Omega cm^{-1}$and by co-precipitation method is 4.38 $\mu\Omega cm^{-1}$ respectively. The perovskite $LaCoO_3$ prepared by citrate sol-gel method show highly dense structure, lower band gap value and high electrical conductivity than the $LaCoO_3$ obtained by co-precipitation method.

Keywords: Perovskite, $LaCoO_3$, citrate sol-gel method, co-precipitation, optical band gap, ac electrical conductivity

Introduction

Perovskite is mixed oxide of transition metals with chemical formula ABO_3 where A is transition metal or lanthanide series cation, B is transition metal cation and O is oxide anion. Many superconducting ceramic materials (the high temperature superconductors) have perovskite-like structures, often with 3 or more metals including copper, and some oxygen positions left vacant. One prime example is yttrium barium copper oxide which can be insulating or superconducting depending on the oxygen content. Important properties of perovskite for their catalytic applications include the stability of mixed and unusual valence states of the transition metal ions in their structure, the presence of defect sites, and the high mobility of oxygen ions. When compared to noble metal-based catalysts, perovskite have better thermal stability, are less sensitive towards poisoning by sulfur, phosphorus and halogens, and are less expensive (Kenta and Kumar, 2014). The La-based perovskite of $LaCoO_3$ was very interesting compounds and their application can be found in many fields The $LaCoO_3$ find application in the field of catalyst, gas sensor and cathode for fuel cell (Haron *et al*., 2016). The efficiency of these materials depends on the synthesis methods. Many methods are available for the synthesis of perovskite oxide in the group of La-based perovskite such as solid state reaction, sol-gel method, solution combustion synthesis, hydrothermal synthesis and co-precipitation method etc. (Unikoth *et al*., 2014). In this paper, $LaCoO_3$ nanocrystalline samples were synthesized by citrate sol-gel method

[1] Dr, Assistant Lecturer, Department of Chemistry, East Yangon University
[2] Dr, Lecturer, Department of Chemistry, University of Yangon
[3] Dr, Lecturer, Department of Chemistry, University of Yangon

and co-precipitation method and their structural, optical and ac electrical conductivities were investigated for further applications.

Materials and Methods

Synthesis of Perovskite $LaCoO_3$ Powders

Perovskite $LaCoO_3$ nanocrystallite powders were prepared with some based modification on the citrate sol-gel method. All chemicals were analytical grade and used without further purification. They were procured from the British Drug House Chemical Ltd., England (BDH). The deionized water was used throughout the experiment. La $(NO_3)_3$.$6H_2O$ and Co $(NO_3)_2$.$6H_2O$ were used as starting materials for preparation of $LaCoO_3$. Lanthanum nitrate (7.52 g) and Cobalt nitrate (11.6 g) were dissolved in deionized water by stirring at room temperature. The citric acid solution used as chelating agent was added to the above solution. Molar ratio between the citric acid and metal nitrate was 2:1. Then ethylene glycol (5 mL) used as gelification agent was also added to the mixture solution. The purple coloured solution was heated at 80 °C under continuous stirring. After being heated for about 6 h, the solution becomes highly viscous and the purple transparent gel was formed. The gel was dried completely at an oven at 120 °C for 4 h. The dried gels were grounded with mortar and pestle. Finally, $LaCoO_3$ particles were obtained (Khetre *et al*., 2010). The xerogel dried powder was calcined at 450 °C for 4 h. The resulting calcined powders were compacted in a mortar driven uniaxial hydraulic press, using a mold 10 mm in diameter. The pellets thus obtained were sintered at 900 °C for 4 h. The citrate sol-gel synthesis occurs according to the following overall reaction (1) which gives rise to perovskite powders and gaseous species.

$$La\ (NO_3)_3.6H_2O + Co\ (NO_3)_2.6H_2O + nC_6H_8O_7 + nC_2H_6O_2 \xrightarrow{\Delta} LaCoO_3 + nCO_2\uparrow + nN_2\uparrow + nH_2O \quad (1)$$

The second method, $LaCoO_3$ was prepared by co-precipitation in which nitrate precursors La $(NO_3)_3$.$6H_2O$ and Co $(NO_3)_2$.$9H_2O$ were mixed in the required stoichiometric ratio (i.e. La/ Co = 1/1) to make aqueous solution. Lanthanum nitrate (7.52 g) and Cobalt nitrate (5.58 g) were dissolved in deionized water by stirring at room temperature. Ammonium carbonate (5.77 g) was dissolved in deionized water. And then ammonium carbonate solution was added to the above mixture solution. Both solutions were mixed together under continuous stirring for 30 min to ensure completion of reaction and pH was maintained at 7. Then the precursor powders precipitated were filtered and dried in oven at 110 °C. The dried precipitates were grounded to getas-prepared powder andthe calcined at 500 °C for 4 h. Finally $LaCoO_3$ powders were obtained. The resulting calcined powders were compacted in a mortar driven uniaxial hydraulic press, using a mold 10 mm in diameter. The pellets thus obtained were sintered at 900 °C for 4 h (Anupama and Prasad, 2015). The precipitation and calcination reactions may be represented by equations (2), (3) and (4), respectively.

$$La\ (NO_{3)3}.6H_2O + (NH_4)_2\ CO_3 + nH_2O \longrightarrow La^{3+} + nCO_3^{2-} + nNH_4^{+} + nNO_3^{-} \quad (2)$$

$$Co\ (NO_3)_2.6H_2O + (NH_4)_2\ CO_3 + nH_2O \longrightarrow Co^{3+} + nCO_3^{2-} + nNH_4^{+} + nNO_3^{-} \quad (3)$$

$$La^{3+} + Co^{3+} + nCO_3^{2-} + nNH_4^{+} + nNO_3^{-} \longrightarrow LaCoO_3 + n\ CO_2\uparrow + nN_2\uparrow + nH_2O \quad (4)$$

Characterization of the Prepared Perovskite $LaCoO_3$

The thermal decomposition behaviours of the powders prepared by citrate sol-gel method were characterized by thermogravimetric and differential thermal analysis (TG-DTA) at a heating rate of 10 °C/min in nitrogen. The phase identification of the as-prepared powder was performed using X-ray diffractometer with CuK_α radiation (λ=1.5405Å). The lattice parameters and the average crystallite size were calculated using PDXL-software. The crystallite size was also compared with the values obtained using Debye-Scherrer formula, $D= 0.9\ \lambda/\beta \cos\theta$, where λ is X-ray wavelength and β is peak width at half maximum. The FT IR measurements have been performed in the region of 400-4000 cm^{-1} by using 8400 SHIMADZU, Japan FT IR spectrometer. The morphology of the prepared nano powders was characterized by scanning electron microscopy (SEM). The samples were characterized by UV-visible spectrophotometer (SHIMADZU UV-1800) for wavelength dependence absorption spectrum. The frequency dependence dielectric behavior was examined by LCR meter (GWInstek LCR- 8110 G).

Results and Discussion

The perovskite $LaCoO_3$ was prepared by citrate sol-gel and co-precipitation method. The precursor powders of perovskite prepared by two methods were calcined at different temperature 450 ˚C and 500 °C for 4 h. The resulting calcined powders were compacted at 5 ton pressure in a motor driven uniaxial hydraulic press, using a mold 10 mm in diameter. The pellets of perovskite $LaCoO_3$ powders obtained by the two different methods were sintered at 900 °C for 4 h. The perovskite samples obtained from two methods were characterized by TG-DTA, XRD, FT IR and SEM analysis. The crystalline pellets were characterized by XRD, FT IR and SEM analysis. The optimum sintering temperature was 900 °C and the average crystallite size was found 40.93 nm. At 900 °C, the XRD patterns of the two methods showed that the major phase of $LaCoO_3$ with hexagonal crystalline structure. The optical properties of perovskite $LaCoO_3$ obtained from two methods were studied by UV-visible absorption spectroscopy. Frequency dependence dielectric behavior of the pellet samples were determined by LCR meter.

Thermal Analysis

Thermal analysis can be utilized to identify the thermal stability and the decomposition temperature of the prepared perovskite. Figure 1 shows TG-DTA thermogram of dried $LaCoO_3$ xerogel powder prepared by citrate sol-gel. It was observed that two exothermic peaks at 170 °C and 412 °C formed in DTA thermogram. The two exothermic peaks related to the combustion and decomposition of organic residues and also metal nitrates the formation of expected perovskite $LaCoO_3$. It was also found that the losses in weight were 12.49 % and 69.10 %. Above 450 °C, there is no significant weight loss and the compound is thermally stable at that temperature. Figure 2 shows TG-DTA thermogram of dried precursor $LaCoO_3$ powder prepared by co-precipitation. The one endothermic peak observed at 82.14 °C and it was due to the dehydration of water. The other endothermic peak at 473 °C and it may be due to the combustion of volatile organic compound attached to the Co-OH group and the formation of expected perovskite phase.

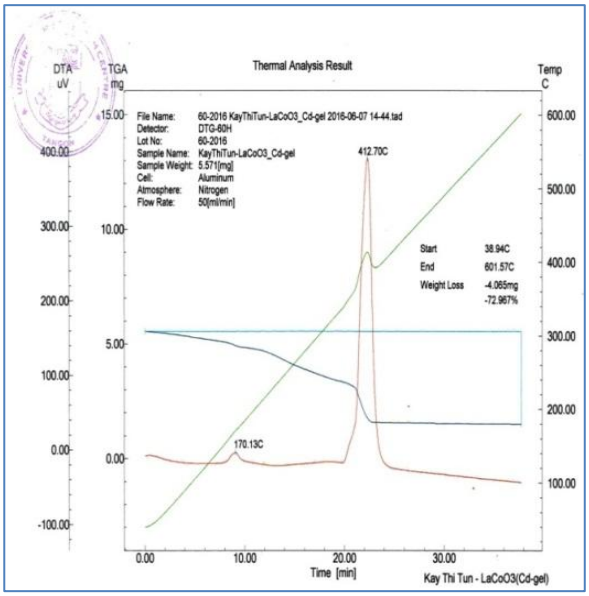

Figure 1 TG-DTA curve of the xerogel $LaCoO_3$ powder by citrate sol-gel method

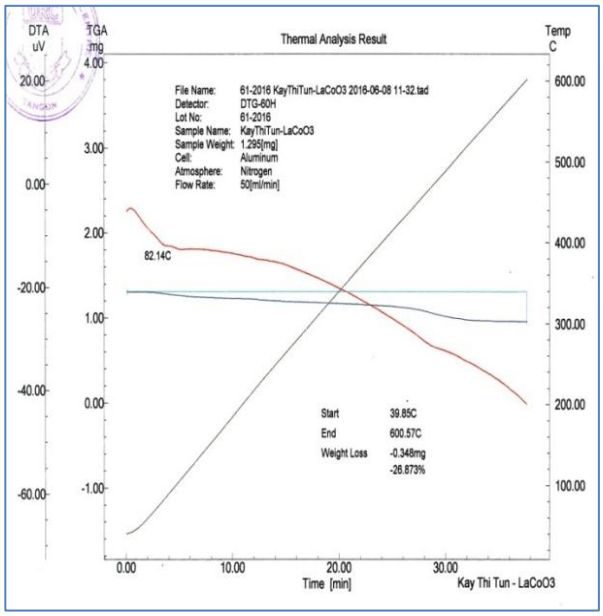

Figure 2 TG-DTA thermogram for the precursor $LaCoO_3$ powder prepared by co-precipitation method

XRD Analysis

XRD technique was used for the investigation of the crystalline or amorphous nature of the prepared compounds. Single phase perovskite structure was obtained after calcination at 450 °C as shows in Figure 3(a). The XRD patterns of the $LaCoO_3$ perovskite samples prepared by citrate sol-gel method sintered at different temperature ranging from 800 °C to 1000 °C for 4 h were shown in Figures 3(b). The XRD pattern of $LaCoO_3$ sintered at 800 °C shows that the formation of the mixture of $LaCoO_3$, La_2O_3, Co_3O_4 and some unidentified phase. The $LaCoO_3$ after sintering at 900 °C and 1000°C was found hexagonal crystallite structure but some higher angle lines and more crystalline nature appear at 1000 °C. The unit cell parameters of $LaCoO_3$ are found to be a= 5.44 Å, b= 5.37 Å, c= 13.09 Å at 800 °C, a= 5.37 Å, b= 5.37 Å, c= 12.94 Å at 900°C and a= 5.44 Å, b= 5.43 Å, c= 12.96 Å at 1000 °C respectively. The average particle sizes of $LaCoO_3$ are found in the range of 15-40 nm. According to XRD analysis, $LaCoO_3$ perovskite samples are well matched with standard library of ICDD-00-048-0123 hexagonal crystal structure with space group R3c. In the co-precipitation method, the perovskite crystallite structure of $LaCoO_3$ was obtained after calcination temperature at 500 °C. But there is more impurity phase on the XRD pattern; it may be due to the secondary phase of La-O and Co-O shows in Figure 4(a). The XRD patterns of the $LaCoO_3$ sintered at different temperature ranging from 900 °C, 1000°C and 1100 °C are shown in Figures 4(b). The XRD pattern of $LaCoO_3$ sintered at 900°C was aggrement with hexagonal crystallite structure of space group R3c with lattice parameters a= 5.36 Å, b= 5.36 Å and c= 12.89 Å. The prepared $LaCoO_3$ after sintering at 1000°C and 1100 °C was found to have the same hexagonal structure but was more crystalline in nature. Aftering sintering above 900 °C showed spilliting of some higher angle lines in XRD pattern. The crystalline perovskite type $LaCoO_3$ formed at 900°C are well matched with standard library of ICDD- 00-048-0123 (Hexagonal) and the average crystallite size are found to be 36.9 nm. It shows a trend that the average crystallite size is larger at higher calcination temperature, which is related to the grain growth (Theingi, 2013) .

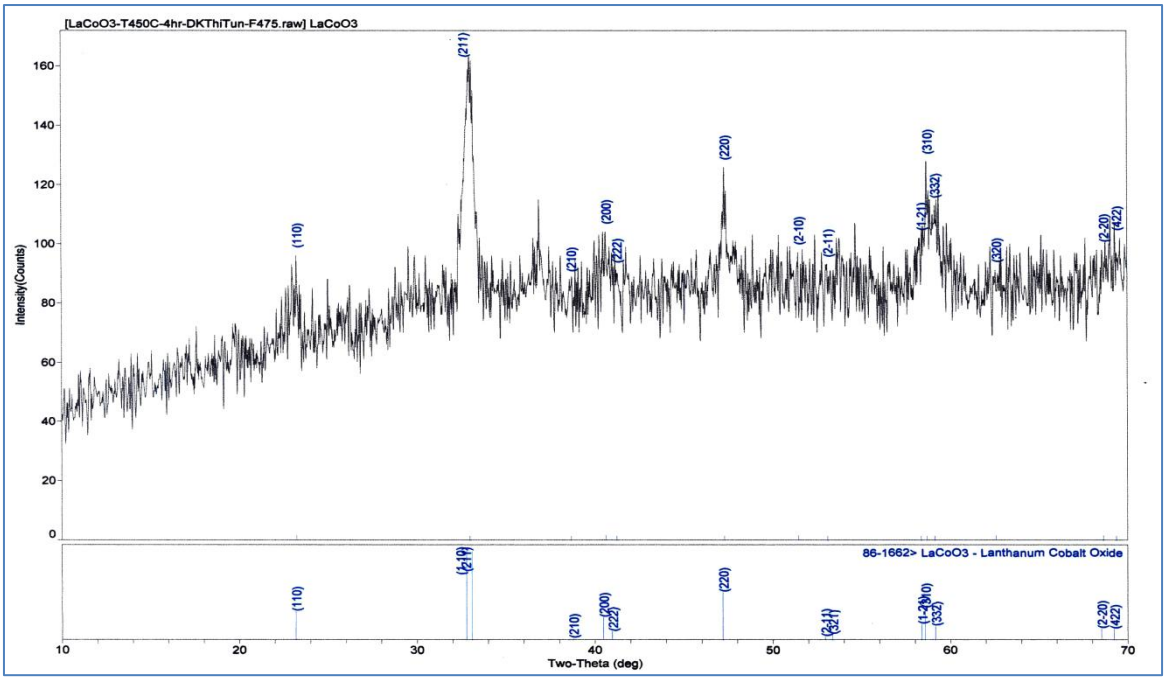

Figure 3(a) XRD diffraction pattern of $LaCoO_3$ powder prepared by citrate sol-gel method calcined at 450 °C

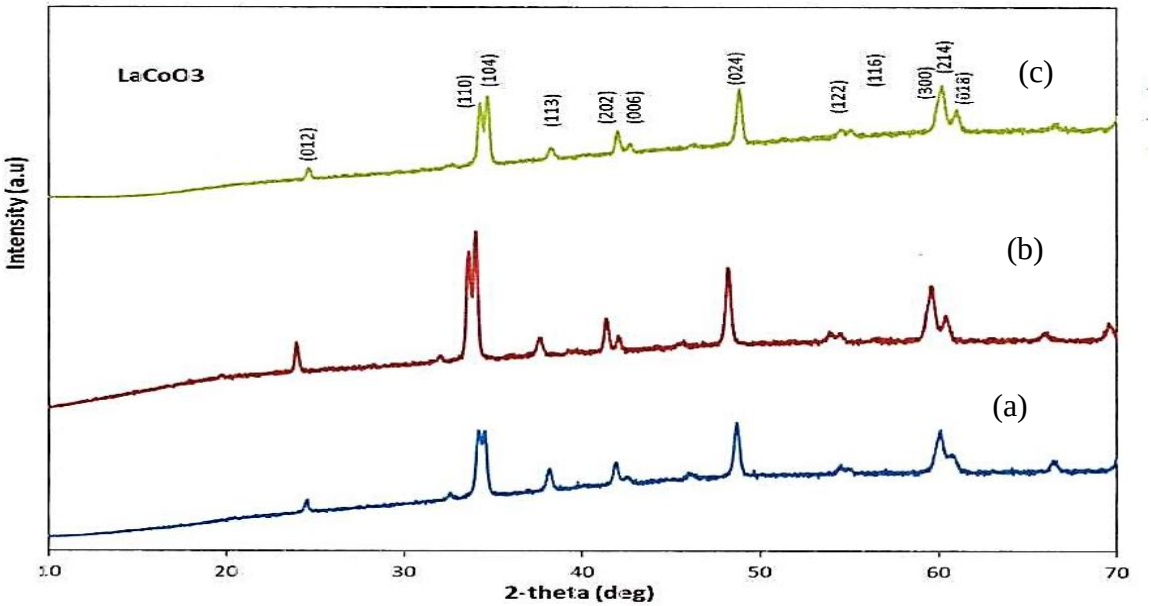

Figure 3(b) XRD diffraction pattern of $LaCoO_3$ sample prepared by citrate sol-gel method sintered at (a) 800 °C, (b) 900 °C and (c) 1000 °C

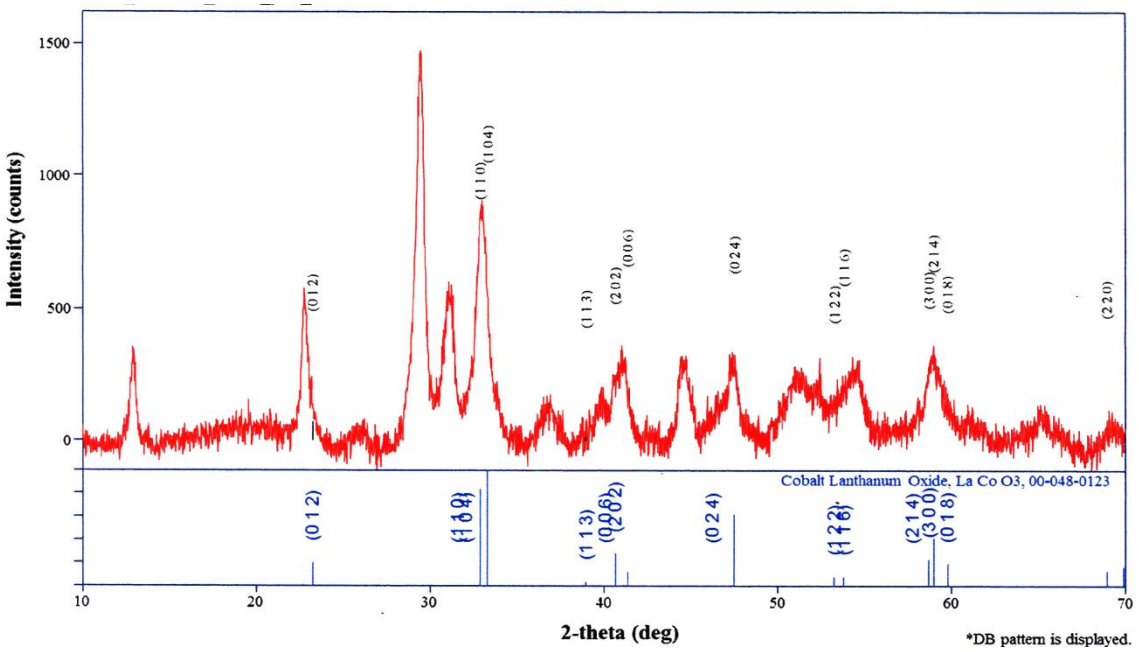

Figure 4(a) XRD diffraction patterns of $LaCoO_3$ powder prepared by co-precipitation method calcined at 500 °C

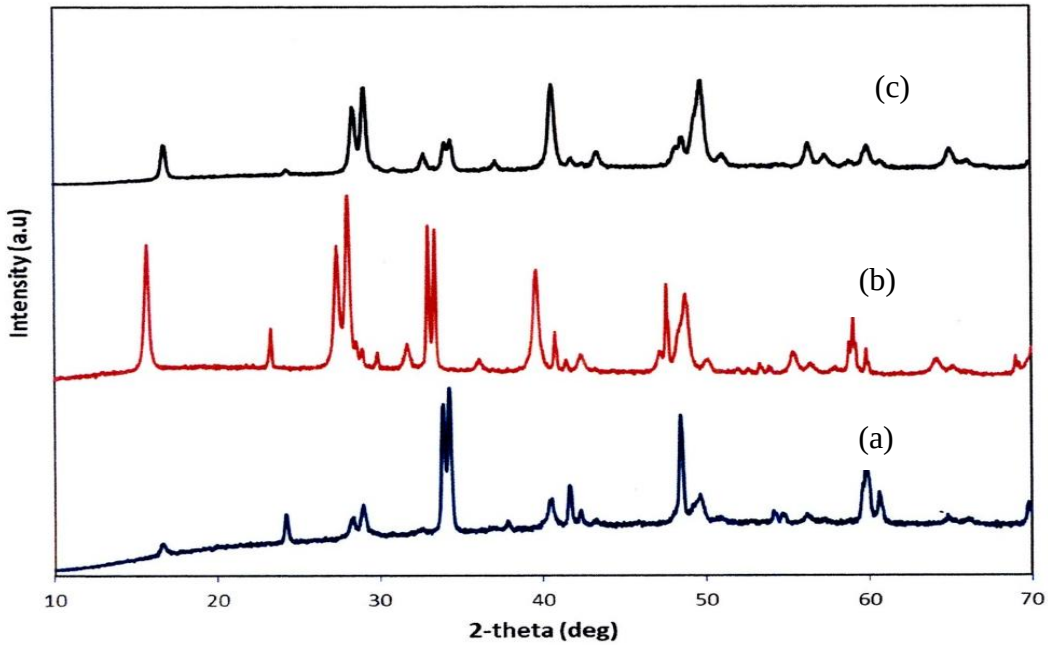

Figure 4(b) XRD diffraction patterns of $LaCoO_3$ powder prepared by co-precipitation method sintered at (a) 900 °C, (b) 1000 °C and (c) 1100 °C

FT IR Analysis

The $LaCoO_3$ nanopowders were mixed with appropiate amount of KBr salts to form pellets in order to observe FT IR spectra. FT IR spectra with wavenumber ranged from 400 – 4000 cm^{-1} are shown in Figures 5 and 6 for $LaCoO_3$ prepared by citrate sol-gel method and co-precipitation method, respectively. The characteristic absorption band of $LaCoO_3$ prepared by citrate sol- gel method at 665, 663 and 665 cm^{-1} at 800 °C, 900 °C and 1000 °C can be represented due to the stretching vibration of Co-O group which may be due the stretching modes

of metallic oxygen band. The Co-O stretching vibration and O-Co-O deformation modes of $LaCoO_3$ occurred at 584, 592 and 569 cm^{-1} and 406 and 414 cm^{-1} at 800 °C, 900 °C and 1000 °C can be assigned to the stretching vibration of La-O group (Ghosh and Dasgupta, 2010). It may be due to the formation of perovskite $LaCoO_3$. Compare to the citrate sol-gel method, the characteristic absorption band of $LaCoO_3$ prepared by co-precipitation method at 3603 cm^{-1} and 3171 cm^{-1} were observed at 1100 °C. It can be represented due to the stretchig vibration of OH group which may be due to the absorbed water molecules. The Co-O stretching vibration of $LaCoO_3$ occurred the absorption band at 597 cm^{-1}, 580 cm^{-1} and 642 cm^{-1} at all sintering temperatures. The band located at 420 cm^{-1}, 408 cm^{-1} and 412 cm^{-1} at 900 °C, 1000 °C and 1100 °C can be assigned to the stretching vibration of La-O group. It may be due to the formation of perovskite $LaCoO_3$ (Ghosh and Dasgupta, 2010)

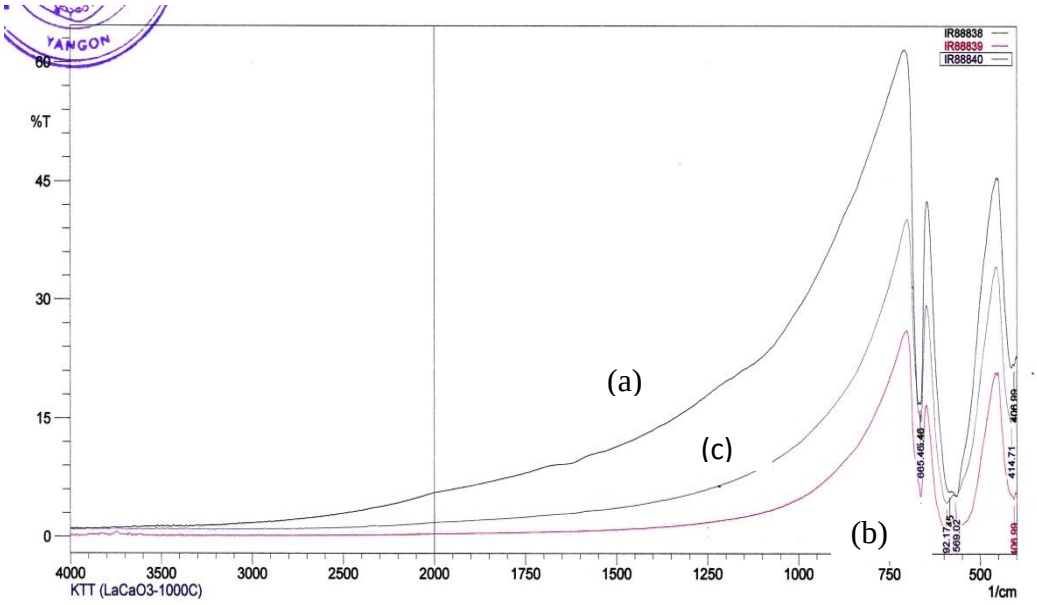

Figure 5 FT IR spectra of $LaCoO_3$ nanopowder synthesized by citrate sol-gel method sintered at (a) 800 °C, (b) 900 °C and (c) 1000 °C

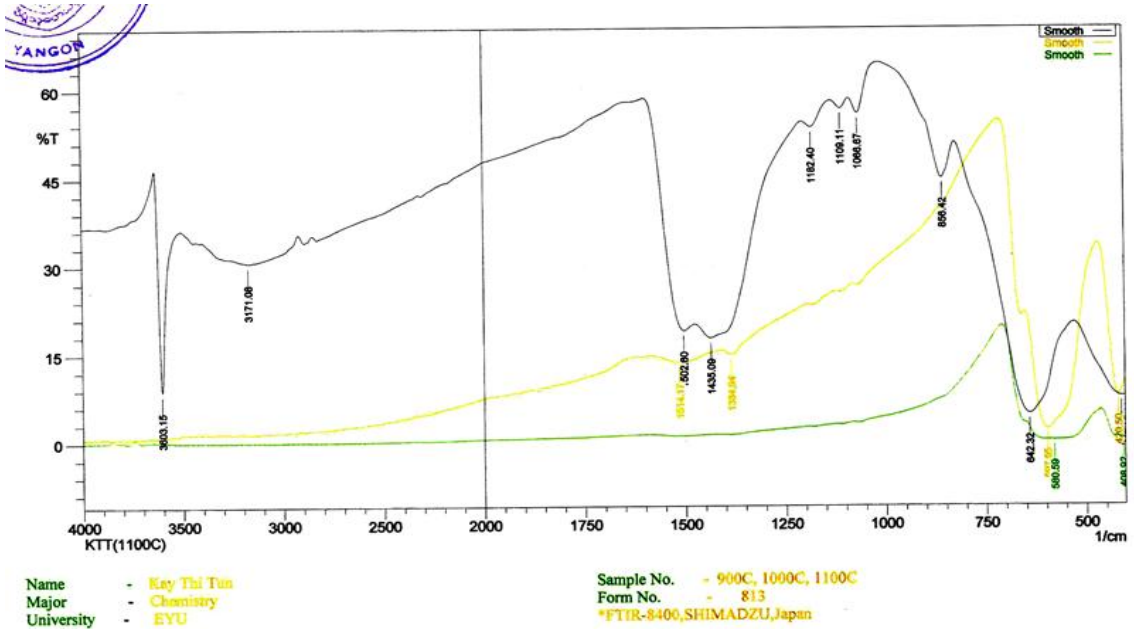

Figure 6 FT IR spectra of $LaCoO_3$ nanopowder synthesized by co-precipitation method sintered at (a) 900 °C (b) 1000 °C and (c) 1100 °C

SEM analysis

The morphology of perovskite $LaCoO_3$ sample was studied by using scanning electron microscope (SEM). The magnification of x5500 image indicates that $LaCoO_3$ prepared by citrate sol-gel method have micron size with high degree of agglomeration composed of nanocrystallite particles as shown in Figure 7. The surface morphology of perovskite $LaCoO_3$ prepared by co-precipitation method with the magnification of x30000 image indicate that $LaCoO_3$ have micron size with highly porous and uniformly distributed of nanocrystallite particles as shown in Figure8. Adjusting the sintering temperature improves the microstructure and the electronic conductivity. It can be seen that each sample has its own characteristic morphology (Haron *et al*., 2016).

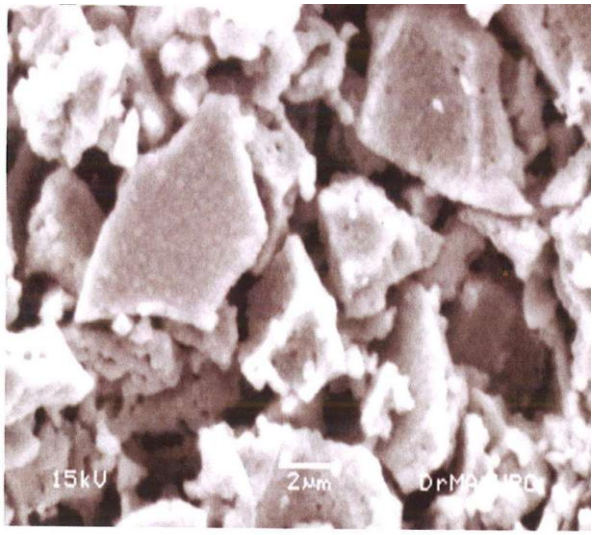

Figure 7 SEM micrograph of $LaCoO_3$ prepared by citrate sol-gel method

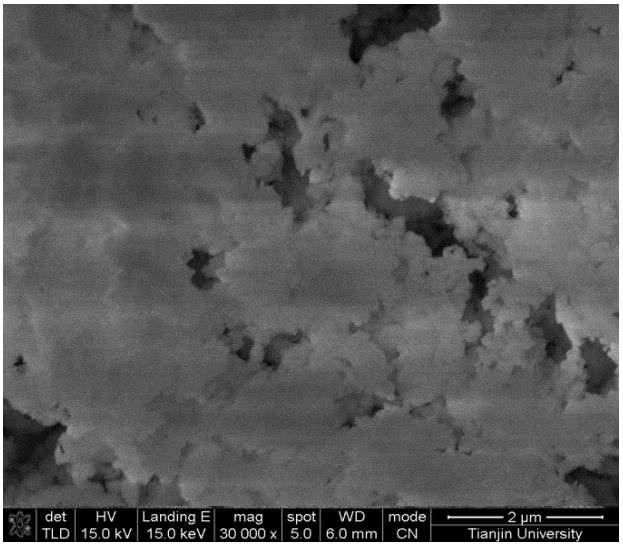

Figure 8 SEM micrograph of $LaCoO_3$ prepared by co-precipitation method

Optical Properties by UV- Vis Spectroscopy

UV-visible absorption spectroscopic method is a powerful technique to explore the optical properties of semiconducting nanoparticles. The optical properties of perovskite $LaCoO_3$ prepared by two different methods at 900 °C were studied by UV-visible absorption spectroscopy in the range of 300-700 nm. The absorption coefficient (α) was calculated from the observed absorption spectra and the optical band gap of $LaCoO_3$ samples were calculated from the Tauc's plots of $(\alpha h\nu)^2$ vs $h\nu$. Figures 9 and 10 show that the optical band gap of $LaCoO_3$ and it was found to be the band gap values of $LaCoO_3$ prepared by citrate sol-gel and co-precipitation methods are 2.15 eV and 2.42 eV, respectively. These band gap values are also reliable within the semiconductor band gap ranges. Band gap values of $LaCoO_3$ prepared by co-precipitation method are larger than that of the citrate sol-gel method. The prepared materials can be therefore used as gas sensor, cathode material for solid oxide fuel cell, solar cell and other optoelectronic devices.

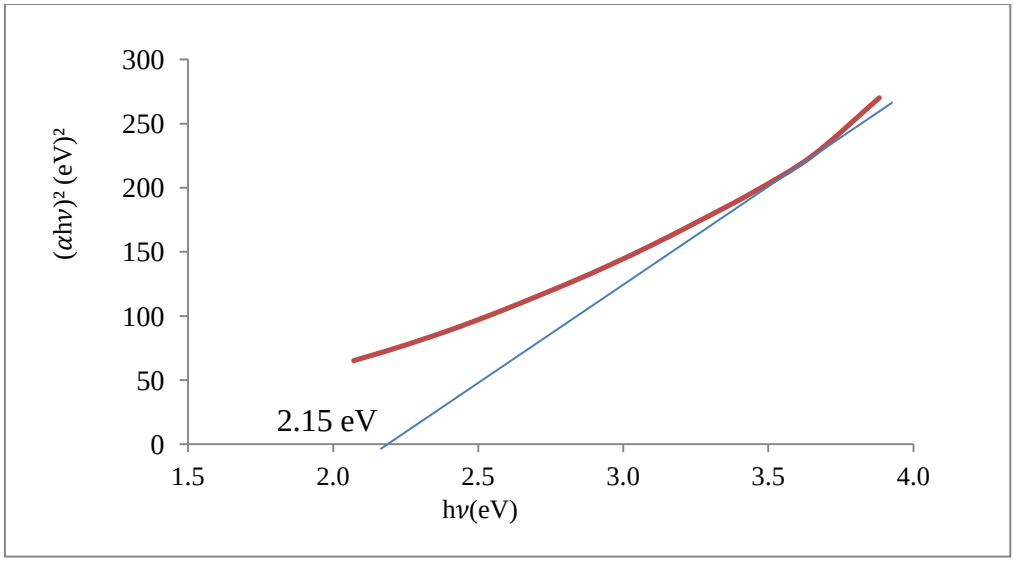

Figure 9 Plot of $(\alpha h\nu)^2$ against $h\nu$ for $LaCoO_3$ prepared by citrate sol-gel method at 900 °C

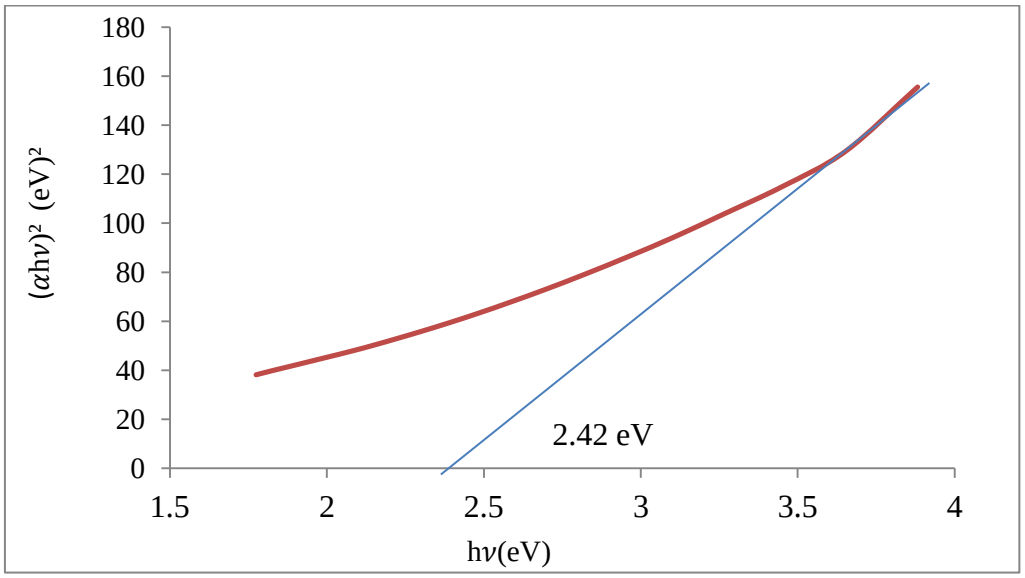

Figure 10 Plot of $(\alpha h\nu)^2$ against $h\nu$ for $LaCoO_3$ prepared by co-precipitation method at 900°C

AC Electrical Conductivities

Dielectric measurements as a function of frequency in the range of 100-1000 kHz were performed by using LCR meter. The dielectric constant was calculated by using the formula $\varepsilon = Cd/\varepsilon_0 A$ where C is the capacitance of pellet in μF, d is the thickness of the pellet; A is the cross sectional area of the flat surface of the pellet and ε_0 is the permittivity for free space. The ac conductivity (σ_{ac}) is obtained from the data of dielectric constant (ε_0) and loss tangent (tan δ) using the relation of $\sigma_{ac} = \varepsilon'\varepsilon_0\omega\tan\delta$ where ω ($2\pi f$) is the angular frequency. Thus σ_{ac} depends strongly on the frequency of the applied field (Priyanka *et al*., 2013). Dielectric analysis studied the electrical properties of a material as a function of frequency and measures the two fundamental electrical characteristic of materials. The first one is the capacitive nature, which represents its ability to store electric charge. The other is the conductive nature which represents its ability to transfer electronic charge. Through the analysis, the dielectric loss and dielectric constant of a material can be determined. The variation of dielectric loss and dielectric constant

of $LaCoO_3$ prepared by two different methods with frequency range from 100 kHz to 1000 kHz as shown in Figures 11 and 12. It was found that the dielectric loss and dielectric constant decrease with increase in frequency. When the frequency is increased, the orientation polarization decrease since it takes more time than electronic and ionic polarization. The value of dielectric loss and dielectric constant of $LaCoO_3$ have a constant value at higher frequency corresponding to interfacial polarization (EL-Mallah, 2012). The ac conductivity of $LaCoO_3$ prepared by two different methods increase linearly with increasing frequency and it is shown in Figure 13. The value of ac conductivity increase at higher frequency 1000 kHz (1MHz) is caused due to oxygen ion vacancy. The value of ac conductivity of $LaCoO_3$ prepared by citrate sol-gel is 8.74 $\mu\Omega cm^{-1}$ and co-precipitation method is 4.38 $\mu\Omega cm^{-1}$. It shows that the ac conductivity of $LaCoO_3$ prepared by citrate sol-gel method is greater than co-precipitation method.

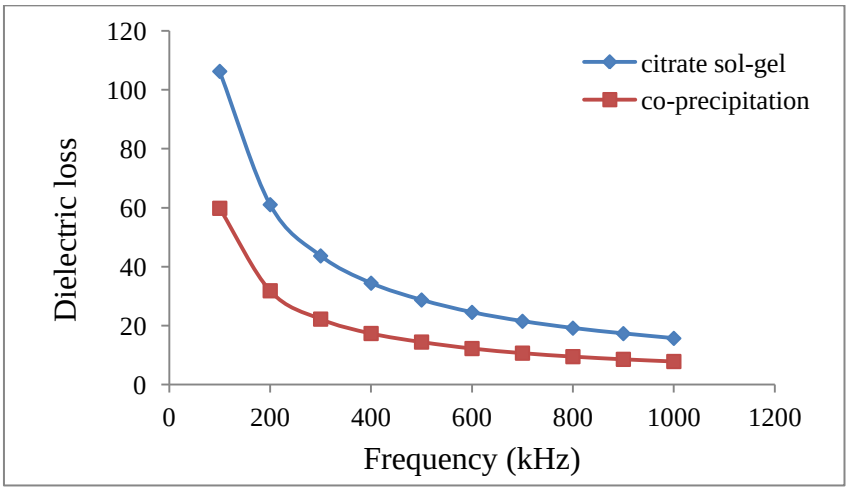

Figure 11 Variation of dielectric loss of $LaCoO_3$ prepared by citrate sol-gel method and co-precipitation method as a function of frequency

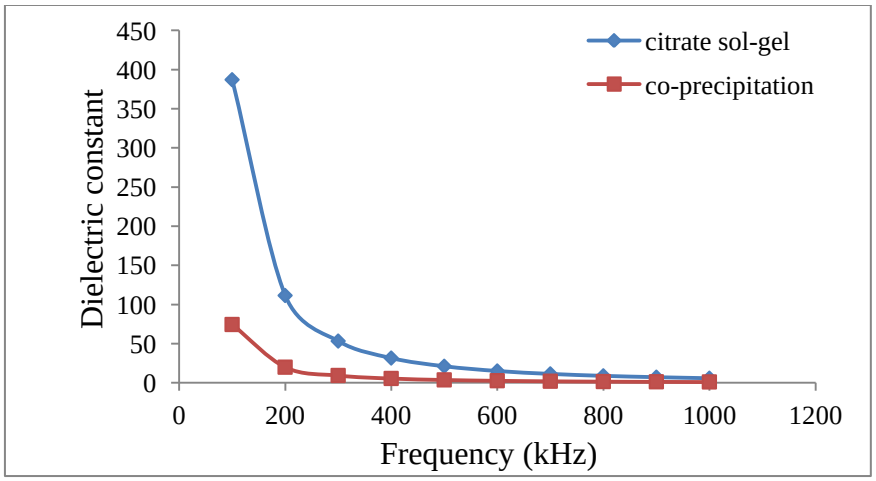

Figure 12 Variation of dielectric constant of $LaCoO_3$ prepared by citrate sol-gel method and co-precipitation method as a function of frequency

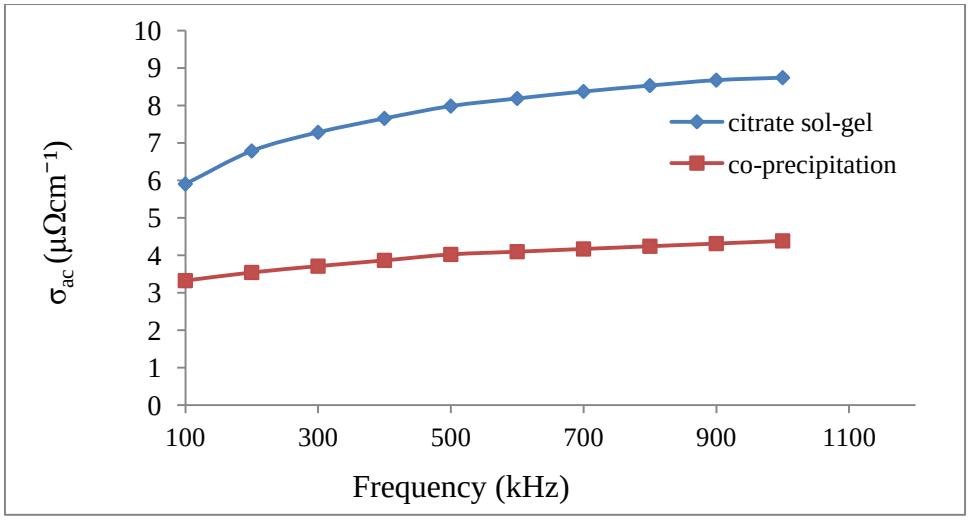

Figure 13 Variation of ac conductivity of $LaCoO_3$ prepared by citrate sol-gel method and co-precipitation method as a function of frequency

Conclusion

Perovskite $LaCoO_3$ samples have been successfully prepared by citrate sol-gel method and co-precipitation method. The different in methods lead to the difference in morphology and in electrical properties. The crystalline pellets were obtained by sintering at 900 °C and the structural, optical and ac electrical conductivities were studied. From the study of structural properties showed that the $LaCoO_3$ has hexagonal crystal symmetry with R-3c space group having crystallite size of 40.93 nm. The SEM image showed the nanostructure of the two samples. FT IR spectroscopy showed that strong absorption band appeared at 665, 592 and 406 cm^{-1} for both of citrate sol-gel and co-precipitation method and this may be due to the stretching vibration Co-O, Fe-O and La-O group. The other absorption band observed in co-precipitation method and it may be due to the presence of trace impurities. The band gap was calculated from UV-visible spectra which indicated the semiconducting nature of the materials. The optical band gap of $LaCoO_3$ prepared by citrate sol-gel and co-precipitation methods are 2.15 eV and 2.42 eV, respectively. The dielectric constant decreased in all samples with increase of frequency. The ac conductivity of $LaCoO_3$ perovskite samples were studied at the frequency range of 100-1000 kHz. The ac conductivity values of $LaCoO_3$ prepared by citrate sol-gel method are greater than the co-precipitation method. It was found that co-precipitation method required higher calcined, sintering temperatures and showed lower conductivity. These studies indicated that $LaCoO_3$ prepared by citrate sol-gel method under optimized conditions can be used as cathode material for fuel-cell technology and as touch electrode in touch sensor applications.

Acknowledgements

The authors wish to thank to Professor Dr Ni Ni Than, Head of the Department of Chemistry, University of Yangon, for her encouragement, providing necessary research facilities and good advice.

References

Anupama, M. and Prasad, R. (2015). "Effect of Preparation Method and Calcination Temperature on $LaCoO_3$ Perovskite Catalyst for Diesel Soot Oxidation". *J. Chem.,* vol. 3(1), pp. 95-107

Asad Ali, S., Naseem, S. and Khan, W. (2015). "Microstructural, Optical and Electrical Properties of $LaFe_{0.5}Cr_{0.5}O_3$ Perovskite Nanostructures". *J. Mater. Sci*., vol. 5 (16), pp. 1-3

EL-Mallah, H. M. (2012). "AC Electrical Conductivity and Dielectric Properties of Perovskite (Pb, Ca) TiO_3 Ceramic". *J. Mater. Sci*., vol. 188, pp. 174-179

Ghosh, S. and Dasgupta, S. (2010). "Synthesis, Characterization and Properties of Nano Crystalline Peroskite Cathode Materials''. *J. Mater. Sci.,* vol. 28 (2), pp. 427 -438

Haron, W., Wisitsoraat, A. and Wongnawa, S. (2016). "A Simple Synthesis and Characterization of $LaMO_3$ (M= Al, Co, Fe) Perovskite via Chemical C o-precipitation Method". *J. Sci., Tech*. vol. 437, pp. 5-20

Kenta and Kumar, D. (2014). "Study the Perovskite-Type Mixed Oxides with the General FormulaABO_3". *J. Mater. Sci.,* vol. 3(5), pp. 1-7

Khetre, S. M., Jadhav, H. V. and Bamane, S. R. (2010). "Synthesis and Characterization of Nano Crystalline $LaFeO_3$ by Combustion Route''. *J. Chem.,* vol. 3(1), pp. 82-86

Priyanka, K. P., Sunny, J. and Varghese, T. (2013). "Dielectric Properties and AC Conductivity of Nanocrystalline Titania". *Journal of Basic and Applied Physics*, vol. 2(1), pp. 4-7

Theingi, M. (2013). *Study of Electrical Properties and Laser Induced Voltage Effect in* La_{1-x} Ca_xMnO_3 *Epitaxial Thin Films*. China: PhD Dissertation, Material Science, Kunming University of Science and Technology

Unikoth, M., Shijina, K. and Varghese, G. (2014). "Nano Sized $LaCo_{0.4}$ $Fe_{0.6}O_3$ Perovskite Synthesized by Citrate Sol-Gel Auto Combustion Method''. *Processing and Application of Ceramic*s, vol. 8(2), pp. 87-92

GREEN SYNTHESIS OF GOLD NANOPARTICLES AND CHITOSAN-GOLD NANOPARTICLES COMPOSITE BEADS AND THEIR APPLICATION

Ma Ohn Kyi[1], KhinThan Yee[2], Ma Hla Ngwe[3]

Abstract

This research work concerns with the green synthesis and characterization of gold nanoparticles (GNP) and chitosan-gold nanoparticles (CS-GNP) composite beads. The gold nanoparticles (GNP) were prepared from chloroauric acid in the presence of the aqueous extract from fresh papaya leaf as well as dry papaya leaf used as reducing agents, respectively. The existence of prepared GNP in colloidal solutions was determined by using laser pointer, noted as GNP (G) and GNP (D), Tyndall effect and the synthesized gold nanoparticles (GNP) solutions were also characterized by UV-visible spectroscopy, TEM, SEM, EDXRF and XRD analyses. On the other hand, chitosan beads were produced from different concentrations of chitosan (1 % to 5 % w/v) in 1 % v/v acetic acid solution and in 2 % w/v sodium hydroxide solution. The chitosan-gold nanoparticles composites were then prepared from gold nanoparticles and 3 % w/v chitosan solutions. These composites solutions were forced through by syringe into 2 % w/v sodium hydroxide to form beads, were designed as CS-GNP (G) and CS-GNP (D).The physical properties of prepared chitosan beads and chitosan-gold nanoparticles composite beads were studied, such as water content, moisture content, pH and swelling percent in different pH of buffer solutions at different contact times, and these samples were also characterized by using FT IR, EDXRF, SEM and XRD analyses. Then these prepared composite beads were applied in drug delivery system. Aspirin (ASA) was used as a model drug. The absorption of aspirin by the composite beads was determined by using UV-visible spectrophotometer. The physical properties of drug loaded chitosan-gold nanoparticles composite beads such as ASA-CS-GNP (G) and ASA-CS-GNP (D) were studied and these drug loaded samples have been characterized by FT IR, EDXRF, SEM and XRD analyses. Then drug release behaviors of such drug loaded composite beads were investigated in simulated gastrointestinal fluid pH of buffer solutions and acute toxicity of the prepared chitosan-gold nanoparticles colloidal solutions was examined.

Keywords: Chitosan, gold nanoparticles, chitosan-gold nanoparticles composite beads,Tyndall effect, drug release behaviors, acute toxicity

Introduction

Chitosan can be obtained from deacetylation of chitin which is widely available from shrimps, crabs, and crawfish. It also exists naturally in a few species of fungi and is associated with proteins (Domard and Rinaudo, 1983). Chitosan, positive ionic charges chemically bind with negatively charged fats, lipids, cholesterol, metal ions, proteins, and macromolecules. Chitosan is readily soluble in dilute acetic acid solution below pH 6.0. The solubility is controlled by the degree of deacetylation (Mima *et al.*, 1983). Aqueous extract fresh and dry *papaya* leaves were used as reducing agents in the present study and reduced chloroauric acid solution from Au^{3+} to Au^{0} (Sumit *et al*., 2012). GNPs are nanospheres, nanorods, nanoshells, nanocages and Surface Enhance Raman Scattering properties (SERS), which depend on the size, shape and physical properties (Kirubha and Alagumuthu, 2014). GNPs have unique optical and physical properties and used as sensors in environmental science, medicine, pharmacy and

[1] Lecturer and Head, Chemistry Department, University of Medicine (Taunggyi)
[2] Dr, Lecturer, Chemistry Department, University of Myeik
[3] Dr, Professor and Head (Retired), Chemistry Department, University of Yangon

engineering due to their non-toxicity (Solomon, S. 2007). GNPs display different colours such as green, orange, dark purple and ruby red etc and are currently manufactured for targeted delivery of biomolecules and drugs to selected cells (Sharma *et al.,* 2009). Gold nanoparticles are composited with chitosan to form chitosan-gold nanoparticle composite solution followed by the composite beads which are used for biomedical purposes in the areas of tissues engineering, drug delivery and cellulose therapies (Papasani *et al.,* 2012). In this research, acute toxic effect of green synthesized chitosan-gold nanoparticles composites was studied on albino mice, and they were applied in drug delivery system.

Materials and Methods

Materials

The chemicals used in this research work were the products from British Drug House (BDH), London and Kanto Chemical Co., Inc., Japan. Fresh *papay*a leaf was collected from University of Medicine Campus, Taunggyi, Myanmar and chitosan (degree of deacetylation 81.13 %) was purchased from Golden Dragon Co., Ltd, FMI City, HlaingTharYar Township, Yangon, Myanmar.

Methods

The appropriate reported conventional and instrumental techniques were used throughout the experimental works. Some of the instruments used in the experiments were Digital pH meter, Digital Balance, Electric Furnace (100-1100ºC, Gallenkamp, West Australia), Magnetic Stirrer (Gallenkamp, England), UV spectrophotometer (UV mini 1240), XRD (Rigaku, D-max -2200, Japan).

Preparation of Fresh and Dry *Papaya* Leaves Extracts

The collected fresh *papaya* leaves were washed thoroughly three times with the distilled water and once in the deionized water. These leaves were dried for 5 days at room temperature to obtain dry leaves. The fresh and dry *papaya* leaves were used to make the respective aqueous extract which was prepared by taking 10 g of finely leaves or leaf powder in a 500 mL Erlenmeyer flask with 100 mL deionized water followed by boiling the mixture for 5 min, separately. Then the extracts were filtered through Whatman filter paper No.1 and kept in the refrigerator at 4ºC for further experiments (Farooquimaqdoom *et al.,* 2013).

Green Synthesis of Gold Nanoparticles Using 1 % w/v Chloroauric Acid with Aqueous Extracts

5 mL, 10 mL and 15 mL of each of the aqueous extract from the fresh leaves and dry leaves were taken into 20 mL test tubes separately. 1 mL of 1% w/v chloroauric acid solution added drop-wise into each of extract with the ratios of 5:1, 10:1 and 15:1, respectively. Within 10 min they changed colour from light reddish brown to deep purple and kept at room temperature for 24 h.

Characterization of the Synthesized Gold Nanoparticles Solutions

Confirmation for the existence of gold nanoparticles in solution by Tyndall effect

When the synthesized gold nanoparticles solutions (5 mL, 10 mL and 15 mL) in the test tubes were pointed out with a laser pointer, the light scattered through the solutions.

UV-visible spectroscopy, EDXRF, XRD, SEM and XRD analyses

The formation and the presence of gold nanoparticles were studied by using UV-visible spectroscopy. In this experiment, the absorbance of the synthesized gold nanoaparticles solutions (5 mL, 10 mL and 15 mL) as well as the chloroauric acid solution was measured at different wavelengths ranged from 480 to 580 nm. The gold element present in such samples was determined by EDXRF analysis and the crystallite sizes of the gold nanoparticles were investigated by XRD analysis using XRD diffractometer (Rigaku, D- max-2200, Japan).The morphology and structure of synthesized gold nanoparticles were examined by TEM (JEOL JEM, 3010) and SEM (JSM 5610, JEOL Ltd Japan).

Preparation of Chitosan Beads, Chitosan-Gold Nanoparticles Composite Beads and Determination of their Physical Properties

Chitosan flakes (1g, 2 g, 3 g, 4 g and 5 g) were placed into each of 250 mL beakers. 100 mL of 1 % v/v acetic acid solution was added into each beaker and stirred with a magnetic stirrer thoroughly until the solids were dissolved and allowed to stand overnight to become uniform solution. Then 2 % w/v sodium hydroxide solution was prepared and stirred witha magnetic stirrer for 30 min. When the prepared chitosan solutions was forced through by a syringe into the 2 % (w/v)sodium hydroxide solution separately at a constant rate of 10-12 drops per min, irregular and regular shape of chitosan beads were formed. However the regular shapes of chitosan beads were selected and allowed to stand for 12 h followed by filteration and washing three times with distilled water. The beads were dried at room temperature for 24 h and placed in an oven at 45ºC for another 24 h. Similarly chitosan-gold nanoparticles composite beads were prepared as the same procedure by using 3 g of chitosan and the synthesized gold nanoparticles colloidal solutions. These prepared chitosan beads and chitosan-gold nanoparticles composite beads were subjected to study their physical properties such as water uptake, moisture content, pH and the degree of swelling in different pH (1.4, 5.4, 6.8 and 7.4) of different buffer solutions on contact time 8 h.

Characterization of Chitosan Beads and Chitosan-Gold Nanoparticles Composite Beads

The prepared chitosan beads and chitosan-gold nanoparticles composite beads were characterized by FT IR, EDXRF, SEM and XRD analyses.

Determination of Acute Toxicity of Chitosan–Gold Nanoparticles Colloidal Solutions

Acute toxicity of different doses of chitosan-gold nanoparticles colloidal samples was evaluated by the method of OECD Guidelines for the Testing of Chemicals 423. According to the test description, 15 total number of adult female albino mice, weighing 25-30 g were selected and divided into five groups. Each group contained three animals. They were fasted for 18 h before giving the chitosan-gold nanoparticles colloidal samples. Four groups were orally administrated with 5000 mg/kg body weight dose and 2000 mg/kg body weight dose of each sample, respectively. One group performed as a control group and they were treated with clean water and normal laboratory animal food of Laboratory Animal Services Division, Department of Medical Research. All groups of mice were kept in the five mouse cages in the separated room at the room temperature of 26 ± 1º C. After administration of chitosan-gold nanoparticles colloidal samples on each group of animals, the animals were observed first 6 h continuously for mortality and behavior changes. Then the animals were checked each 24 h for fourteen days. The mortality during this period was noted (Nil or percent death).

Extraction Preparation of Aspirin solution

The aspirin crystals were extracted from aspirin tablets. Three tablets of aspirin (80 mg) were placed into 50 mL beaker and 10 mL of ethanol was added and stirred followed by filtered into a porcelain crucible and heated in an oven at 45± 5º C for 1 h. After heating the aspirin were obtained and was covered and cooled in desiccators for 30 min. When the obtained aspirin crystals crystal (0.003 g) was dissolved in 100 mL ethanol, 30 mg/L (30 ppm) of aspirin solution was obtained.

Determination of Absorbance of the Prepared Aspirin Solution by Using UV-Visible Spectrophotometer and Construction of Calibration Curve

The absorbance of prepared aspirin solution was investigated by UV visible spectroscopy. From the results it was found that the maximum absorbance was at the wavelength 276 nm which was agreed with the literature. Then a series of different concentrations of aspirin solutions (30, 15, 7.5, 3.7, 1.85, 0.925 and 0.463 mg/L) in ethanol were prepared. The absorbance of these solutions was measured by UV-visible spectrophotometer followed by plotting the calibration curve.

Preparation of Aspirin Loaded Chitosan-Gold Nanoparticles Composite Beads and Determination of their Physical Properties

Each of the wet chitosan-gold nanoparticles composite beads (about 1 g) was separately immersed in 100 mL of 30 mg/L prepared aspirin solution for 24 h, and filtered and dried at room temperature for 36 h. The amount of drug loaded on composite beads was determined by using UV-visible spectrophotometer. Some physical properties (free moisture content, pH and swelling percent) of the prepared drug loaded chitosan-gold nanoparticles composite beads were also determined.

Characterization of the Aspirin Loaded Chitosan - Gold Nanoparticles Composite Beads

The drug loaded chitosan-gold nanoparticles composite beads were characterized by EDXRF, XRD, SEM, EDXRF and FT IR analyses.

Application of the Aspirin Loaded Chitosan-Gold Nanoparticles Composite Beads in Drug Delivery System

Determination of aspirin release from aspirin loaded chitosan-gold nanoparticles composite beads using buffer solutions at different pH

0.1 g of drug loaded chitosan-gold nanoparticles composite beads were immersed in 100 mL buffer solutions at different pH (1.4, 5.4, 6.8 and 7.4) and was shaken with an orbital shaker at 75 rpm for 1 h. Then 5 mL of the above solution was withdrawn and the absorbance was measured by using a UV- visible spectrophotometer. This procedure was carried out in simulated gastric fluids at pH 1.4 for 2 h followed by carrying out in simulated intestinal fluids at pH 6.8 for 10 h. The total residence time in buffer solution was 12 h. The concentration of aspirin released was determined spectrophotometrically at 276 nm and the amount of aspirin released from such composite beads.

Results and Discussion

Green Synthesis of Gold Nanoparticles and Characterization

The gold nanoparticles solutions were synthesized from 1 % w/v chloroauricacid with 5 mL, 10 mL and 15 mL aqueous extracts of fresh *papaya* leaves as well as dry leaves, respectively. When chloroauric acid was added drop-wise into the leaves extracts used as reducing agents, the reduction of gold ions into gold particles in solution would happen and followed by colour change to deep purple colour in aqueous solution due to the surface plasmon resonance phenomenon within 10 min as the following equation (Nagajyothi *et al*., 2012).

$HAuCl_4$+ Plant extract $\longrightarrow$ Au^0 (Green synthesis)

The existence of gold nanoparticles (GNPs) in solution was investigated by Tyndall effect and was characterized by UV- visible spectroscopy, EDXRF, XRD, SEM and TEM analyses.

According to the Tyndall effect, it was observed that the light scattered by particles in a solution indicating the presence of gold nanoparticles in solution.

By UV-visible spectroscopy, the resulting GNP colloidal solutions and chloroauric acid were examined by UV- visible spectroscopy, are shown in Figure 1. From figures, it was observed that the maximum wavelength (λ_{max}) of each sample was existed at 530 nm whereas the wavelength range of the absorbance for chloroauric acid was from 480 to 580 nm. In this process, 5 mL of aqueous extract *papaya* leaves showed the λ_{max}value at 530 nm in 10 min of reaction at room temperature, which was superior other aqueous extracts (10 mL and 15 mL) under the same reaction conditions. It might be due to the rapid reduction and formation of gold nanoparticles between chloroauric acid and 5 mL of *papaya* aqueous extract while that of 10 mL as well as 15 mL aqueous extract were significantly slow and after 50 min the purple colour has appeared. The results obtained were interesting in the context of time taken for the synthesis of gold nanoparticles (Kavitha and Harini, 2013). So GNP solutions containing 5 mL of aqueous extract of fresh *papaya* or dry *papaya* leaves with chloroauric acid were chosen to use in this research.

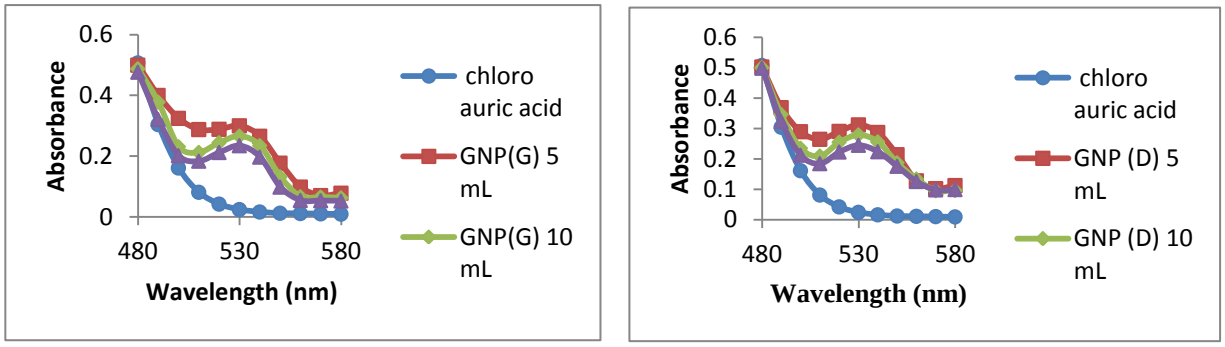

(a) (b)

Figure 1 UV- visible absorption spectra of 1 % w/v chloroauric acid solution and synthesized gold nanoparticles solutions using 5mL, 10 mL and 15 mL aqueous extracts of (a) fresh *papaya* leaves (b) dry *papaya* leaves

According to the EDXRF analysis, the presence of gold in such samples was determined by EDXRF analysis and the results are shown in Table 1. From this table, it was noted that the relative abundance of gold atom in GNP (G) was 51.5 % and 42.9 % in GNP (D).

Table 1 Relative Abundance of Gold in Prepared GNP (G) and GNP (D)

Sample	Relative abundance of gold (%)
GNP (G)	51.5
GNP (D)	42.9

* GNP (G) = Gold nanoparticles using chloroauric acid with aqueous extracts fresh *papaya* leaf
* GNP (D) = Gold nanoparticles using chloroauric acid with aqueous extracts dry *papaya* leaf

The synthesized gold nanoparticles were also examined by XRD analyses are shown in Figure 2 and Table 2. From these, it was found that the gold nanoparticles were formed andpossessed a face centered cubic (fcc) structure at 2θ value which can be indexed to the (111) orientation. Then the sizes of gold nanoparticles were calculated by using Scherer's equation (Haiss *et al*., 2007). It was observed that the size of GNP (G) was 10.75 nm and that of GNP (D) was 9.65 nm.

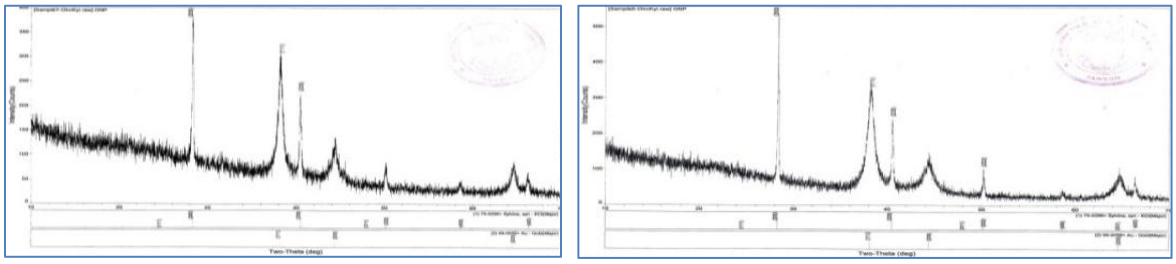

GNP (G) GNP (D)

Figure 2 XRD diffractograms of synthesized gold nanoparticles by green synthesis

Table 2 Crystallite Sizes of the Synthesized Gold-Nanoparticles Using 1 % w/v Chloroauric Acid and Aqueous Extracts of Fresh and Dry *Papaya* Leaves

Sample	2θ (deg)	d (Å)	h k l	FWHM (deg)	Size (nm)	Structure
GNP (G)	38.239	2.3517	(1 1 1)	0.542	10.75	Cubic(a=b=c)
GNP (D)	38.260	2.3505	(1 1 1)	0.606	9.65	Cubic(a=b=c)

The SEM images are shown in Figures 3 (a) and (b) for the synthesized gold nanoparticles. From images, some porous or cavities and small cracks were found on the surfaces of gold nanoparticles.

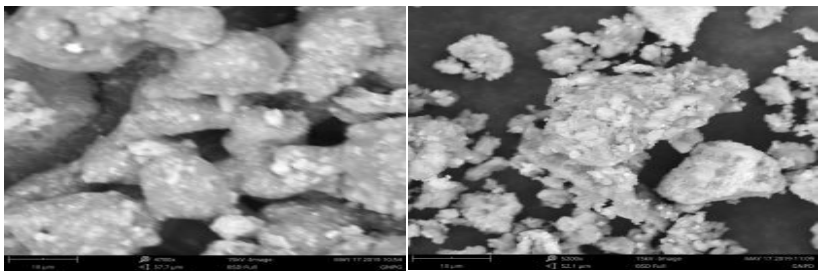

GNP (G) GNP (D)

Figure 3 SEM images of the synthesized gold nanoparticles GNP (G) and GNP (D)

The TEM images shown in Figures 4 (a) and (b) are for the synthesized gold nanoparticles. From the results, general observations indicated that the size of GNP (G) was bigger than that of GNP (D). The particles size of GNP (G) was within 100 nm while that of GNP (D) was within 50 nm.

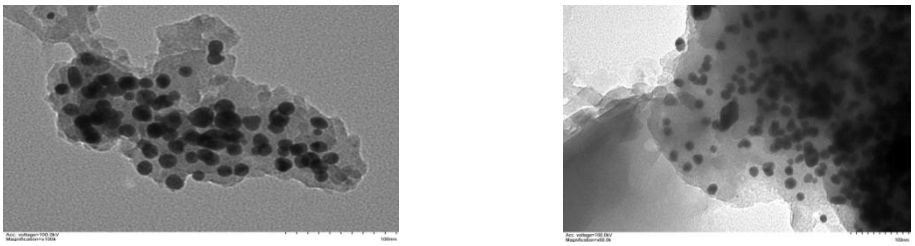

GNP (G) GNP (D)

Figure 4 TEM images of the synthesized gold nanoparticles GNP (G) and GNP (D)

Chitosan Beads and Chitosan-Gold Nanoparticles Composite beads

According to the preparation of chitosan beads, 1 % and 2 % chitosan solutions have nearly liquid so they formed irregular shape of beads with more porous structures in sodium hydroxide solution. On the other hands, a high concentration of chitosan (>3 % w/v) was not feasible because they were too viscous to extrude through the syringe. Thus 3 % w/v chitosan solution was chosen to prepare beads in this study. Similarly, chitosan-gold nanoparticles (CS-GNP) composite beads were prepared when the prepared chitosan-gold nanoparticles colloidal solutions were forced through by using a syringe into gently stirred 2 % w/v sodium hydroxide solution.

According to the determination of physical properties of such samples, water uptake percent and moisture content percent of chitosan beads were 58.82 % and 20.27 % while CS-GNP (G) composite beads showed 42.18 % of water uptake and 15.02 %of moisture and CS-GNP (D) composite beads showed 38.20 % water uptake and 12.12 % of moisture content. As a result, the water uptake percent and moisture content percent of gold nanoparticles composite beads were found to be lower than chitosan beads. From the determination of pH, all prepared beads were neutral. The swelling behaviours of all prepared beads were investigated at different pH 1.4, 5.4, 6.8 and 7.4 for 8h and are shown in Figure 5. From these investigations, it was found that the swelling percent of chitosan beads (CS) was 40.12 % in pH 1.4 whereas that of CS-GNP (G) was 39.11 %and that of CS-GNP (D) was 27.71 %. However, the swelling percent of prepared chitosan beads and chitosan-gold nanoparticles composite beads decreased significantly in increasing pH. Therefore the prepared beads had higher swelling property in acidic solution than in alkaline condition due to the protonation of amino group of chitosan in acidic solution.

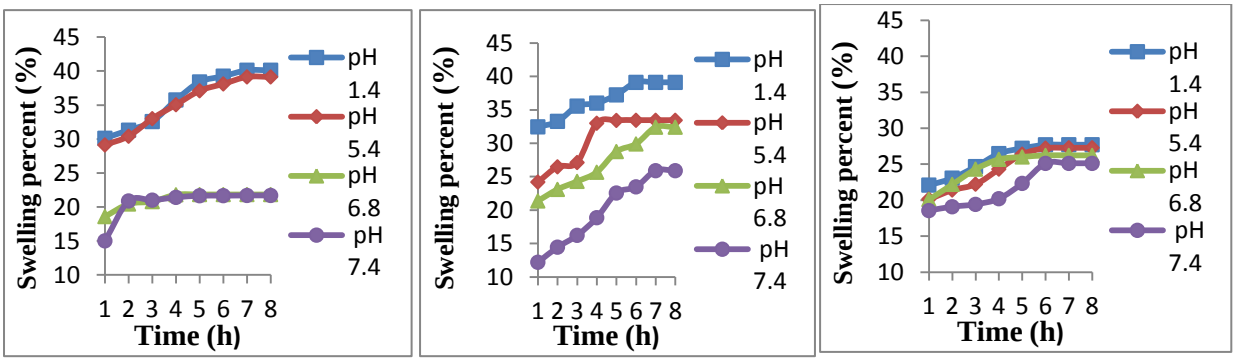

(a) (b) (c)

Figure 5 Swelling percent Vs contact time of (a) CS (b) CS-GNP (G) (c) CS-GNP (D)

Characterization of Chitosan Beads and Chitosan-Gold Nanoparticles Composite Beads

The prepared chitosan beads and chitosan-gold nanoparticles composite beads were characterized by EDXRF, XRD, SEM and FT IR analyses.

The EDXRF spectra of prepared samples are shown in Figure 6. From figures, it was noted that the relative abundance of gold percent in chitosan-gold nanoparticles composite beads was 0.102% in CS-GNP (G) and 0.144% in CS-GNP (D), however there is no gold element present in chitosan beads.

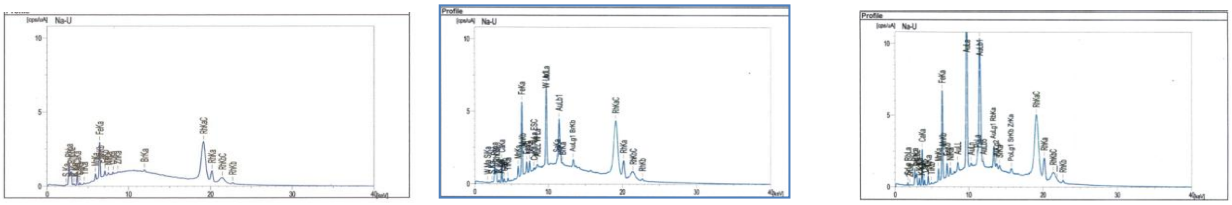

CS CS-GNP (G) CS-GNP (D)

Figure 6 EDXRF spectra of chitosan and chitosan-gold nanoparticles composite beads

Table 3 Relative Abundance of Elements Present in CS-GNP (G) and CS-GNP (D)

No	Elements	CS-GNP (G) (%)	CS-GNP (D) (%)
1	Ca	0.173	0.154
2	Au	0.102	0.144
3	Fe	0.055	0.056
4	Mn	0.014	0.015
5	K	0.013	0.019
6	Ti	0.006	0.007
7	Ag	0.004	-
8	Se	0.002	0.001
9	Br	0.002	0.001
10	Ni	0.002	0.004
11	Zr	0.001	-
12	Cu	-	0.001
13	Si	-	0.473
14	COH	99.627	99.158

The X-ray diffractogramsof prepared chitosan-gold nanoparticles composite beads are shown in Figure 7 and Table 4. The crystallite size of such chitosan-gold nanoparticles composite beads were 12.25nmfor CS-GNP (G) and 16.82 nm for CS-GNP (D), indicated that the attractive forces were formed between chitosan and gold nanoparticles.

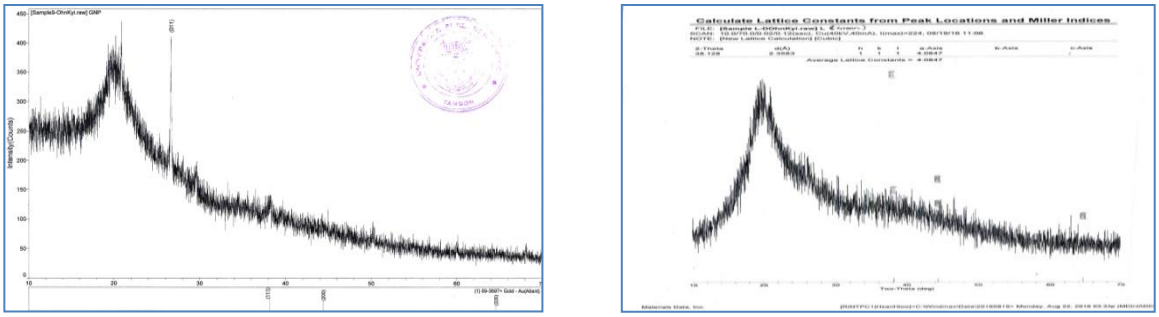

CS-GNP (G) CS-GNP (D)

Figure 7 XRD diffractograms of chitosan-gold nanoparticles composite beads

Table 4 Crystallite Sizes of Chitosan-Gold Nanoparticles Composite Beads

Sample	2θ (deg)	d (Å)	h k l	FWHM(deg)	Size (nm)
CS-GNP(G)	38.262	2.3504	(1 1 1)	0.455	12.25
CS-GNP (D)	38.128	2.3583	(1 1 1)	0.141	16.82

The SEM images of prepared beads are shown in Figure 8. From the SEM images, it was obvious that the surface of prepared samples has small pores with cracking so the surface morphology of all prepared beads was porous nature and had rough surface.

CS CS-GNP (G) CS-GNP (D)

Figure 8 SEM imagesof chitosan beads and chitosan-gold nanoparticles composite beads

The FT IR spectra of prepared chitosan beads and chitosan-gold nanoparticles composite beads are presented in Figure 9. From Figures, the -NH and -OH stretching vibrations were observed at 3358 cm^{-1}in CS, 3293 cm^{-1}in CS-GNP (D) and 3280 cm^{-1} in CS-GNP (G).The C-H symmetric and antisymmetric stretching of CH, CH_2 and CH_3 groups were appeared between 2852 cm^{-1} to 2920 cm^{-1}. Both the C=O stretching in amide bonding and -CH antisymmetric deformation were respectively observed at 1648 cm^{-1} and 1462 cm^{-1} in the spectrum of chitosan beads. However there is no peak formation in composite beads at this wave number. It can be found that the band assigned around 1576 to 1577 cm^{-1} showed new peak was appeared. The bands appeared below 700 cm^{-1} was due to metal-nitrogen stretching or metal-oxygen stretching to produce metal chelates compound (Barbara and Stuart, 2006). It showed that chitosan can bind to gold nanoparticles through free amine group in composite beads.

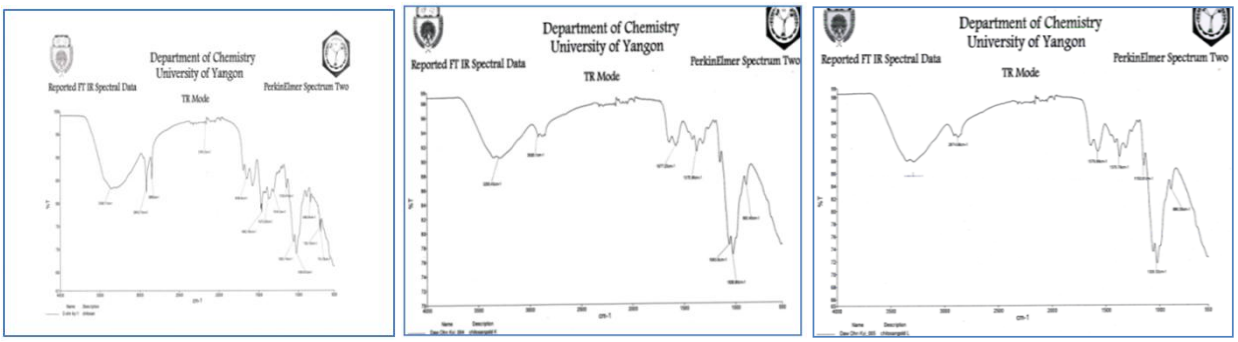

CS CS-GNP (G) CS-GNP (D)

Figure 9 FT IR spectra of chitosan and chitosan-gold nanoparticles composite beads

Acute Toxicity of Chitosan-Gold Nanoparticles Colloidal Solution

The prepared chitosan-gold nanoparticles composite samples were subjected to examine the toxicity on albino mice model in Department of Medical Research (Ygn) for 14 days. After 14 days, all albino mice were observed still alive and did not show any visible symptom of toxicity like restlessness, respiratory disorders, convulsion, aggressive activities, coma and death up to 5000 mg/ kg body weight dose. For such prepared composite beads were applied in drug delivery system.

Application of Chitosan-Gold Nanoparticles Composite in Drug Delivery System

Aspirin was used as a model drug. Firstly 0.003 g of aspirin was dissolved in 100 mL ethanol; 30 ppm of aspirin solution was obtained and determined the maximum absorptionby using UV- visible spectrophotometer (Shimazu UV-1240).The maximum absorption of aspirin solution was observed at 276 nm is agreed with the literature. The series of different concentrations of aspirin solutions (30, 15, 7.5, 3.75, 1.88, 0.94, 0.46, 0.23 and 0.115mg/L) were prepared and measured the respective absorbance by using UV-visible spectrophotometer followed by constructing the absorbance versus concentrations of aspirin calibration curve. It was used to determine the aspirin contents adsorbed and released by chitosan-gold nanoparticles composite beads.

Absorption of aspirin by chitosan-gold nanoparticles composite beads

The composite beads (CS-GNP (G) and CS-GNP (D) 1 g of each were immersed in 30 mg/L aspirin solution for 12 h to become saturated aspirin loaded composite beads and filtered followed by drying at room temperature. The obtained aspirin loaded composite beads [ASA-CS-GNP (G) and ASA-CS-GNP (D)] were found to be rigid and deep reddish brown colour due to the absorption of aspirin into composite beads matrices.

Characterization of aspirin loaded chitosan-gold nanoparticles composite beads

The aspirin loaded chitosan-gold nanoparticles composite beads [ASA-CS-GNP (G) and ASA-CS-GNP (D)]were characterized by XRD, SEM and FT IR analyses.

XRD diffractograms of aspirin loaded composite beads are shown in Figure 10. The average crystallite sizes of aspirin loaded chitosan gold nanoparticles composite beads were observed to be 29.07 nm for ASA-CS-GNP (G) and 21.12 nm for ASA-CS-GNP (D). It confirmed that the aspirin was totally covered on the surface of composite beads due to increase in size and applied in drug delivery system.

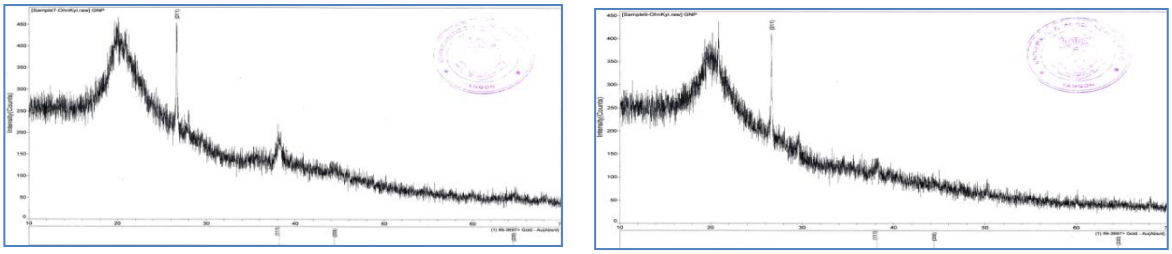

(a) (b)

Figure 10 XRD diffractogramsof (a) ASA-CS-GNP (G) (b) ASA-CS-GNP (D)

The SEM images of aspirin loaded composite beads are shown in Figure 11.The aspirin loaded composite beads were approximately spherical in shape and had a rough surface. The surface was highly wrinkled and many cavities were in the internal zones. As a result, the aspirin was found to penetrate easily into the beads and the surfaces of composite beads were almost covered with aspirin.

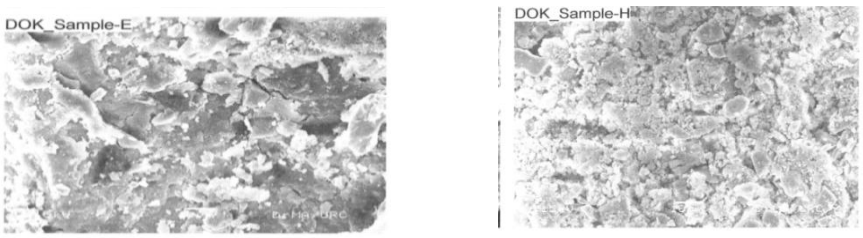

(a) (b)

Figure 11 SEM images of (a) ASA-CS-GNP (G) and (b) ASA-CS-GNP (D)

FT IR spectra of aspirin and aspirin loaded composite beads are shown in Figure 12. From figures, it was observed that the broad band appeared at 3288-3358 cm^{-1}in aspirin loaded composite beads due to -NH and -OH stretching vibration although there is no peak around this band in aspirin due to the absence of these functional groups. Then some of bands at 2918 cm^{-1}, 2849 cm^{-1}, 1681 cm^{-1} and 1604 cm^{-1}in aspirin were observed to be shifted in aspirin loaded composite beads. These stretching shifted were due to cover the most surface area with drug and also occur the intermolecular forces between aspirin and composite beads. It was found that the peak below 700 $cm^{-1}$was observed in metal oxygen or nitrogen stretching (Barbara and Stuart, 2006).

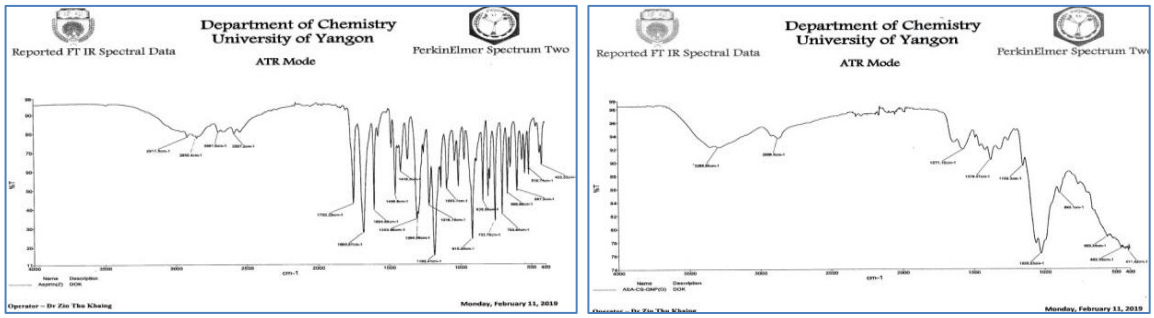

(a) (b)

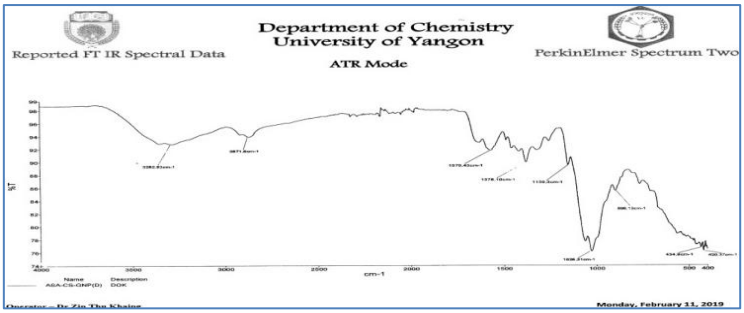

(c)

Figure 12 FT IR spectra of (a) ASA (b) ASA-CS-GNP (G) (c) ASA-CS-GNP (D)

According to the investigation of aspirin loaded composite beads in drug delivery system within 12 h, *in vitro* drug release properties of chitosan-gold nanoparticles composite beads is shown in Figure 13. It was investigated the percentage of the aspirin released from the composite beads at pH 1.4 were32.2 % in CS-GNP (G) as well as 19.9 % in CS-GNP (D) while the aspirin released at pH 6.8 were found to be increased significantly as 81.7 % in CS-GNP (G) and 92 % in CS-GNP (D). From these results, it was found that aspirin released from CS-GNP (D) composite beads was minimal at pH 1.4 while the aspirin released at pH 6.8 increased significantly. In addition, the results clearly suggested that CS-GNP (D) composite beads could hold the drug better at low pH (1.4) and released more drugs at pH 6.8 than the CS-GNP (G) composite beads so CS-GNP (D) showed excellent pH sensitivity.

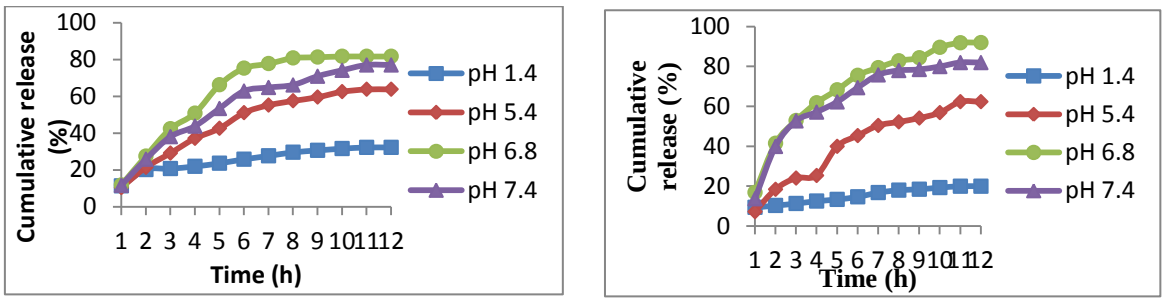

(a) (b)

Figure 13 Cumulative release curves of aspirin from (a) CS-GNP (G) composite beads and (b) CS-GNP (D) composite beads at various pH

In addition to investigate the sequential drug release circumstances, chitosan-gold nanoparticle composite beads were immersed in simulated gastric fluid for initial 2 h, and then moved to simulated intestinal fluid. Figure14 indicates that the drug release properties of chitosan-gold nanoparticles composite beads are pH dependent. The amount of aspirin released from CS-GNP (G) composite beads at pH 1.4 was very low (20 %) within 2 h while 15 % aspirin released from the CS-GNP (D) composite beads. However at pH 6.8, the amounts of aspirin release not only increased significantly to 81 % from CS-GNP (G) and 91 % from CS-GNP (D) after 10 h but also increased in release rate in the intestinal tract. This shows that it confirms the sustained drug release which is necessary to increase the drug bioavailability and prolonging therapeutic effect (Bharathi *et al.*, 2011). So the release rate of drugs from composite beads is affected by changing in pH. The increase in release rates could be due to an associated increase in the fluid filled cavities created by dissolution and diffusion of the drug particles near the surface, which in turn results in increase in the permeability of the drug (Bharathi *et al.*, 2011). In

this study, the effect of drug release was dependent upon the factors such as swelling and drug solubility that are determiner of the drug release.

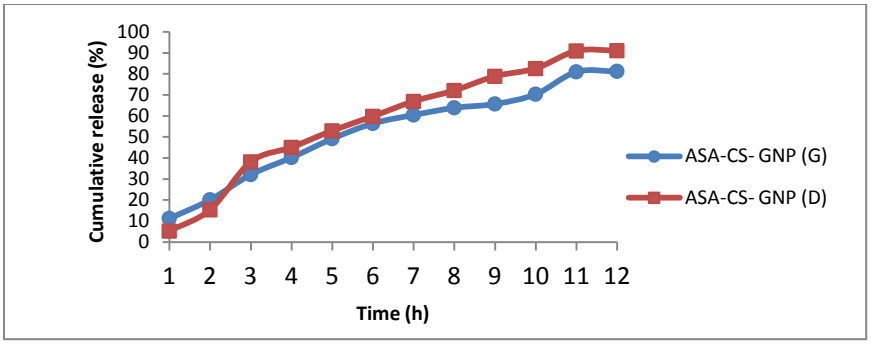

Figure 14 Sequential aspirin release from the aspirin loaded chitosan-gold nanoparticle composite beads in the simulated gastric fluid (pH 1.4) and in the intestinal fluid (pH 6.8) for 12 h

Conclusion

Present investigation deals with the synthesis of gold nanoparticles (GNP) using chloroauric acid as a metal precursor with papaya leaf extract as a reducing agent. Rapid reduction of gold ions was observed in the formation of gold nanoparticles in solution appearing the colour of deep purple under normal conditions for a long time. The dispersion of light through the solution by Tyndall effect confirmed to the existence of colloidal GNP in solution and characterized by UV, TEM, SEM and XRD analyses. From these result, it was observed that the maximum UV – visible absorption peak of colloidal GNP was appeared at 530 nm and the crystallite sizes calculated from XRD diffatograms by the Scherrer's equation were found to be 10.75 nm and 9.65 nm. Chitosan beads and chitosan-gold nanoparticles composite beads were prepared by ionotropic gelation method and studied their physical properties such as water uptake, moisture content, pH and the degree of swelling followed by characterized them by SEM, FT IR, EDXRF and XRD analyses. Aspirin was used as a model drug. The prepared composite beads were coated with aspirin and studied their characterization as well as application into drug delivery system using the different buffer solutions on contact time 12 h. From this result, it was found that aspirin loaded chitosan-gold nanoparticles composite beads using dry *papaya* leaf extract was more release drug (91 %) in alkaline solution (pH 6.8) than that of aspirin loaded chitosan-gold nanoparticles composite beads using fresh *papaya* leaf extract.

Acknowledgements

The authors hereby acknowledge their sincere thanks to chairman and all of members of Myanmar Academy of Arts and Science for celebrating the conference and allowing the writing of this paper. The authors would like to thank Rector, University of Medicine, Taunggyi for providing the research facilities and suggestion.

References

Barbara, H. and Stuart, B. (2006). "*Infrared Spectroscopy: Fundamentals and Applications"*. Sydney: John Wiley and Sons Ltd, pp.74-152.

Bharathi, A., Srinivas, N.K., Reddy, G.R and Sirisha, A. (2011). "Formulation and In-Vitro Evaluation of Diclofenac Sodium Substained Release Matrix Tablets Using Melt Granulation Technique". *Int. J. Res. in Pharm. and Bio.Sci*.vol.2(2), pp.788-808.

Domard, A. and Rinaudo, M. (1983). "Preparation and Characteristics of Fully Deacetylated Commerical Chitin and Chitosan Products". *J. Agricultural and Food Chemistry*, vol. 5(9), pp. 49-52.

Farooquimaqdoom, B., Hashmisabeen, H. and Shaikhzcarina, S. (2013). "Papaya Fruit Extract: A Potent Source for Synthesis of Bionanoparticles". *J. Environ. Res. Develop*, vol. 7, pp. 155-160.

Haiss, W., Thanh, N.T.K., Aveyard, J, and Fernig, D.G. (2007). "Determination of Size and Concentration of Gold Nanoparticles from UV-visible Spectra". *Analytical Chemistry*. 79(11), pp.4215-4221.

Kavitha, K.S., and Harini, B.P. (2013). "Plants as Green Source towards Synthesis of Nanoparticles". *Int. Res. J. Biological Sci.*, vol. 2(6), pp.66-76.

Kirubha,R. and Alagumuthu, G. (2014). "Production of Biogenic Gold Nanoparticles Using Ziziphusjujuba Fruit Extract". *World J. Pharm. Sci.*, vol. 2(11), pp. 1469-1474.

Mima, S., Mya, M., Iwamoto, K. and Yoshikawa, S. (1983). "Highly Deacetylated Chitosan and Its Properties". *J. Apply Polymer Sci*., vol. 20, pp.1909-1917.

Nagajyothi, Seong Eon Lee and KapDuk Lee, K. (2012). "Green Synthesis of Silver Gold Nanoparticles Using *Lonicera Japonica* Flower Extract". *Bull. Korean Chem. Soc*. vol. 33(8), pp. 2609-2612.

Papasani, R.,Wang, B. and Hill, R.A.(2012)."Gold Nanoparticles:the Importance of Physiological Principles to Device Strategies for Targeted Drug Delivery". *Int. Res. J.NanomedNanotechnol bio Med*. vol.8, pp. 804-814.

Sharma, V., Park, K. and Srinivasarao, M.(2009)."Colloidal Dispersion of Gold Nanorods: Historical Background, Optical Properties, Seed- Mediated Synthesis, Shape Separation and Self-Assembly". *Material Science and Engineering Reports*, vol.65, pp. 1-38.

Solomon, S. (2007). "Synthesis of Silver and Gold Nanoparticles". *J. chem. Edu*.,vol. 84, pp. 322-325.

Sumit, Lal.S and Nayak, P.L. (2012). "Green Synthesis of Gold Nanoparticles Using Various Extract of Plants and Spices". *Int. J. Science Innovations and Discoveries*, vol. 2(3), pp. 325-350.

PHOSPHATE ION REMOVAL FROM MODEL SOLUTION USING ACID TREATED COAL FLY ASH

Ohn Mar Khin[1], Hlaing Hlaing Oo[2] , Ni Ni Than[3]

Abstract

This research was aimed to examine the adsorption behaviour of phosphate ion on modified coal fly ash under different operating conditions to determine the optimum condition to remove phosphate ion. The coal fly ash was treated with hydrochloric acid and optimal conditions were found to be 2 M HCl solution, the ratio of coal fly ash and acid solution is 1:2 (w/v) and for 2 h of acid treated time at ambient temperature. Batch adsorption experiments were performed to evaluate phosphate removal efficiency of acid treated coal fly ash. The effect of various adsorption parameters, *i.e*. pH, adsorption time, adsorbent dose and initial phosphate ion concentration using the acid treated coal fly ash was studied. The maximum removal percent of phosphate ion was achieved 94.03 % at an adsorbent acid treated coal fly ash loading weight of 0.1 g/100 mL, 1 mg L^{-1} of initial concentration of phosphate solution, pH of 3 and 90 min of contact time at ambient temperature. Coal fly ash (CFA), acid treated coal fly ash (ACFA) and phosphate ion sorpted acid treated coal fly ash (PACFA) were characterized by using modern techniques such as SEM, EDXRF and XRD. According to widen applicability of the proposed method, it can be used for the removal of phosphate from eutrophicated surface water.

Keywords: Coal fly ash, acid treated coal fly ash, removal of phosphate ion

Introduction

Excess concentrations of phosphate ion in water cause eutrophication (Mikendova *et al*., 2010). In advanced stages of eutrophication, dissolved oxygen can become depleted to dangerously low levels causing fish death when algae decay. It is not only destroys the aquatic life but also disrupts the balance of the aquatic ecosystem (Mustafa *et al.,* 2008). During the past decades, various techniques, including biological treatment and chemical precipitation have been reported for phosphate removal. Adsorption is one of the techniques, which is comparatively more useful and economical for such removal (Ragheb, 2013). Fly ash is actually captured from the chimneys of coal fired power plants. It contains various trace elements in various quantities and during combustion process of coal trace elements get associated on the surface of ash particles due to evaporation and condensation (Benito *et al*., 2001). Recently, the treated coal fly ash has been used for the removal of phosphate ion.

Materials and Methods

Materials

The chemicals used were procured from British Drug House (BDH), England, Wako Co. Inc., Tokyo, Japan and Sigma Aldrich, USA. The apparatus are conventional lab ware, glassware and modern equipment**.**

Sampling and Preparation of Coal Fly Ash

Coal fly ash sample was collected from Tigyit power plant located in South-west Shan State in Myanmar (PYO, 2011). Coal fly ash sample was taken systematically from a large number of material bags. Sampling was carried out by cone and quartering method. Sample was

[1] Lecturer, Department of Chemistry, Defence Services Medical Academy
[2] Dr, Professor and Head, Department of Chemistry, West Yangon University
[3] Dr, Professor and Head, Department of Chemistry, University of Yangon

homogenized into small particles using a grinding mill and then made to obtain 250 μm mesh size. The obtained coal fly ash sample was dried at 105 °C in an oven for an hour.

Preparation of Standard Potassium Dihydrogen Phosphate Stock Solution

Standard stock solution of potassium dihydrogen phosphate 10 mg L^{-1} was firstly prepared by dissolving 0.0219 g of KH_2PO_4 in 500 mL of deionized water. In the preparation of series of phosphate solutions 2, 4, 6, 8, 10 and 12 mL of 10 mg L^{-1} stock solution were diluted to 100 mL with deionized water to give 0.2, 0.4, 0.6, 0.8, 1.0 and 1.2 mg L^{-1} solution respectively.

Preparation of Reagent Solutions

Ammonium molybdate solution

Ammonium molybdate 4 g was dissolved in 100 mL of deionized water.

2.5 M sulphuric acid

Concentrated sulphuric acid 70 mL was added to the 500 mL volumetric flask and diluted with deionized water to the mark.

Potassium antimonyl tartrate

Potassium antimonyl tartrate 1.3715 g was dissolved in 500 mL of deionized water.

Stock reagent

A stock reagent was prepared by adding 15 mL of ammonium molybdate solution, 50 mL of 2.5 M sulphuric acid, 5 mL of potassium antimonyl tartrate solution.

0.1 M ascorbic acid solution

Ascorbic acid 0.88 g was dissolved in 50 mL of deionized water.

Mixed reagent

A mixed reagent was freshly prepared on the day of each analysis by adding 30 mL of ascorbic acid solution to 70 mL of stock reagent.

Calibration curve for phosphate solution

A spectrophotometer was used to measure the residual colour, remaining after adsorption. The residual colour index is expressed as absorbance. The primary stage of the work, include the construction of calibration curve by using absorbance and concentration of the phosphate solution. The calibration carve was used to evaluate the residual colour index (*i.e.* absorbance) against a series or standard phosphate concentrations (Arnold *et al*., 1992). The stock solutions of phosphate in different concentrations range between 0.2 mg L^{-1} to 1.2 mg L^{-1} were chosen and dilution was made by using deionized water. A stock solution 50 mL was pipetted into a clean and dry beaker. Mixed reagent 8 mL was added and the solution was then allowed to stand for 10 min. A solution of the blue colour complex was formed. The absorbance of solution was measured by UV-visible spectrophotometer at 880 nm against a blank of distilled water. The data for plotting the calibration curve and plot are shown in Table 1 and Figure 1.

Table 1 Absorbance vs Concentration of Potassium Dihydrogen Phosphate Solution

Concentration (mg L^{-1})	Absorbance at 880 nm
0.2	0.11
0.4	0.24
0.6	0.37
0.8	0.50
1.0	0.62
1.2	0.75

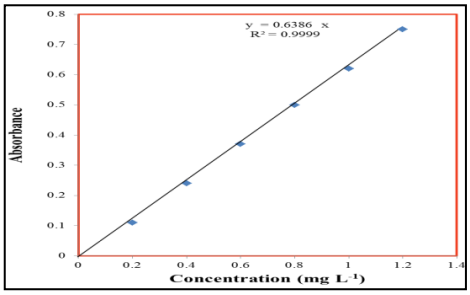

Figure 1 Calibration curve for potassium dihydrogen phosphate solution

Modification of Coal Fly Ash

The coal fly ash was subjected to the modification, because of its feasible grain composition. For the modification the solution of HCl in 1.0, 1.5, 2.0, 2.5 and 3.0 M concentrations was used. The mixture was treated at ambient temperature for 1 to 3 h. The fly ash was treated in HCl solutions in the ratio of 1:0.5, 1:1, 1:2, 1:3 and 1:4 (w/v) at ambient temperature. At the end of the treatment, the mixture was filtered and dried in the oven at 65 °C.

Phosphate Adsorption

0.08 g of each sample (acid treated coal fly ash) was added to 100 mL of KH_2PO_4 solutions in concentrations of 1 mg L^{-1} at pH 3. The samples were equilibrated by continuous shaking on a rotating shaker 150 rpm at ambient temperature. The suspensions were then filtrated. The concentrations of phosphate ion were measured by standard spectrophotometric method with a UV-Visible spectrophotometer at 880 nm.

Percent Removal of Phosphate Ion by the Acid treated Coal Fly Ash

Percent removal of phosphate ion at different pH

The model solution of potassium dihydrogen phosphate 1 mg L^{-1} was prepared and the pH was adjusted at 1, 2, 3, 4, 5, 6 and 7 by adding of 0.001 M and 1 M HCl. Each 100 mL of phosphate solution was separately mixed with 0.08 g of acid treated coal fly ash in the flasks. The flasks were shaken with electric shaker at room temperature for 1 h. At the end of the equilibrium time, each of the solution was filtered. A filtrate solution was measured by standard spectrophotometric method with a UV-Visible spectrophotometer at 880 nm.

Percent removal of phosphate ion at different contact times

The acid treated coal fly ash 0.08 g was placed into a 100 mL of phosphate solution 1 mg L^{-1} at pH 3. The solutions were shaken by an electric shaker. After the contact times 20, 40, 60, 80, 100 and 120 min each solution was filtered. A filtrate solution was measured by standard spectrophotometric method with a UV-Visible spectrophotometer at 880 nm.

Percent removal of phosphate ion at different dosages of the acid treated coal fly ash

The accurately weighed acid treated coal fly ash in 0.04, 0.08, 0.12, 0.16, 0.20 and 0.24 g was taken into a conical flask. 100 mL of constant concentration of phosphate solution 1 mg L^{-1}, pH 3 was added to each of acid treated coal fly ash in separate conical flask and shaken by electric shaker at room temperature for 1 h. After this contact time, each of the solution was

filtered. A filtrate solution was measured by standard spectrophotometric method with a UV-Visible spectrophotometer at 880 nm.

Percent removal of phosphate ion at different initial concentrations of phosphate solutions

The model solutions of potassium dihydrogen phosphate 0.5 mg L^{-1}, 1.0 mg L^{-1}, 1.5 mg L^{-1} and 2.0 mg L^{-1} were prepared and the pH of the solutions was adjusted at 3 by adding 1 M HCl solution. Each 100 mL of phosphate solution was separately with mixed 0.1 g of acid treated coal fly ash in the flasks. The flasks were shaken with electric shaker at room temperature for 90 min. At the end of the equilibrium time, each of the solution was filtered. A filtrate solution was measured by standard spectrophotometric method with a UV-Visible spectrophotometer at 880 nm.

Characterization of Coal Fly Ash, Acid Treated Coal Fly Ash and Phosphate Ion Sorpted Acid Treated Coal Fly Ash

Coal fly ash, acid treated **c**oal fly ash and phosphate ion sorpted acid treated coal fly ash were characterized by using modern instrumental techniques, such as SEM, EDXRF and XRD.

Results and Discussion

Modification of Coal Fly Ash

Effect of treated concentrations of HCl

Coal fly ash treated with a various HCl concentration showed different behaviors in the phosphate uptake. Coal fly ash treated with 1.0, 1.5, 2.5 and 3.0 M HCl showed even a lower phosphate removal percent than 2 M HCl (Figure 2). The best results were showed by the fly ash treated with 2 M HCl. The optimum condition of percent removal of phosphate ion was found to be 86.12 % by 2 M HCl treated coal fly ash while percent removal of phosphate ion by coal fly ash at pH 3 is 40.06 %.

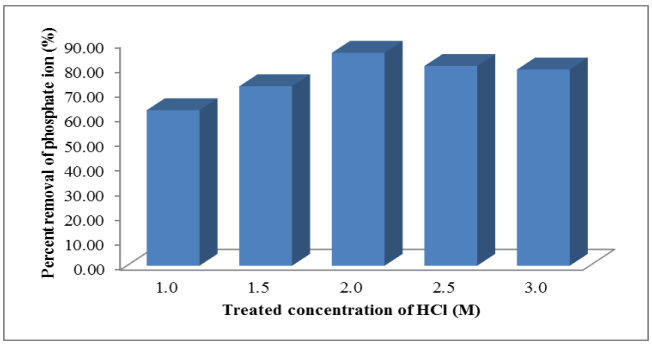

Figure 2 Effect of treated concentrations of HCl on the percent removal of phosphate ion by various HCl treated coal fly ash

Effect of treated time`

From the resulting data as treated time increases, the percent removal of phosphate ion also increases. Percent removal of phosphate ion at 2 h and 3 h treated time are nearly the same, therefore the optimum condition of treated time was 2 h. The results are shown in Figure 3.

Effect of ratio of coal fly ash and HCl concentration

The fly ash was treated in 2 M HCl solutions in the ratios of 1:0.5, 1:1, 1:2, 1:3 and 1:4 (w/v). The mixture was treated at ambient temperature for 2 h. From the resulting data,

optimum condition of ratio of coal fly ash and HCl concentration was found to be 1:2 (w/v). From the overall resulting data, optimum condition of the modification of coal fly ash was found to be 2 M HCl solution, in the ratio of 1:2 (w/v) and for 2 h of acid modification process. The results are shown in Figure 4.

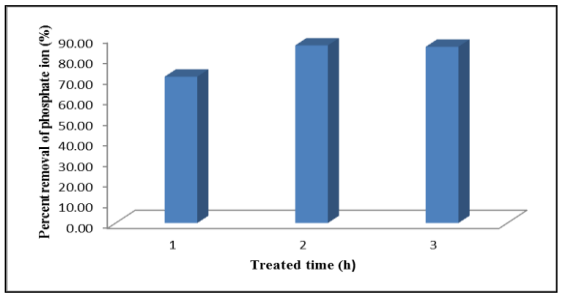

Figure 3 Effect of treated time on the percent removal of phosphate ion by 2 M HCl treated coal fly ash

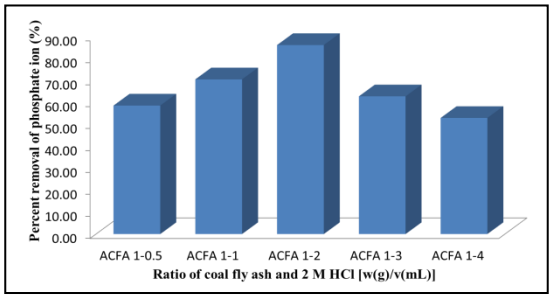

Figure 4 Effect of ratio of coal fly ash and 2 M HCl concentration on the percent removal of phosphate ion by acid treated coal fly ash

Percent Removal of Phosphate Ion by the Acid Treated Coal Fly Ash

Effect of pH

The dependence of removal of phosphate ion on pH of the aqueous dispersion for acid treated coal fly ash was studied and the results are shown in Figure 5. The percent removal of phosphate ion on acid treated coal fly ash was examined at various pH ranging from 1.0 to 7.0 with an initial phosphate ion concentration of 1 mg L^{-1} at room temperature. From the resulting data, as pH increases, the percent removal was observed to increase until it reached to the optimum condition of pH 3. The maximum percent removal of phosphate ion in 1 mg L^{-1} of initial concentration was 86.12 % by using dosage of acid treated coal fly ash 0.08 g/100 mL at pH 3 after 1 h contact time.

Effect of contact time

The effect of contact time on the percent removal of phosphate ion by using initial concentration of 1 mg L^{-1} by acid treated coal fly ash was also studied and the results were shown in Figure 6. The percent removal of phosphate ion was measured by using 0.08 g/100 mL dosage of acid treated coal fly ash under pH 3 and ambient temperature at different contact times 20, 40, 60, 80, 100 and 120 min. Results showed that the extent of adsorption was observed to increase with contact time.

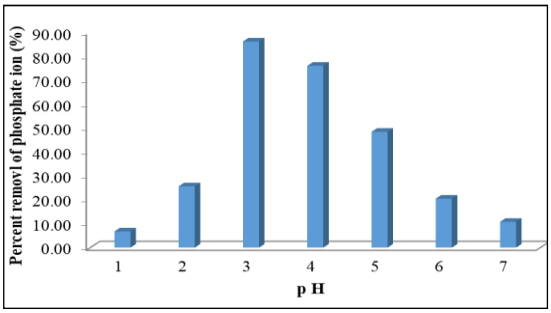

Figure 5 Effect of pH on the percent removal of phosphate ion by acid treated coal fly ash

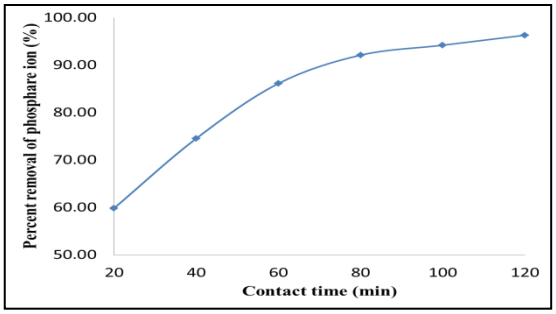

Figure 6 Effect of contact time on the percent removal of phosphate ion by acid treated coal fly ash

Effect of dosage of acid treated coal fly ash

The effect of acid treated coal fly ash dosage used for the percent removal of phosphate ion from a constant initial concentration 1 mg L^{-1} at pH 3 was also determined by using the amounts of sorbent in range from 0.04 g to 0.24 g in 100 mL potassium dihydrogen phosphate solution at contact time 1 h at ambient temperature. The corresponding resulting data in terms of percent removal with respect to sorbent dose are summarized in Figure 7. The percent removal of phosphate ion was increased by the increase of adsorbent dosage due to their increasing surface area.

Effect of initial concentration of phosphate ion

The effect of initial concentration of phosphate ion on the percent removal of phosphate ion by acid treated coal fly ash was studied at initial concentrations ranging from 0.5 mg L^{-1}, 1.0 mg L^{-1}, 1.5 mg L^{-1} and 2.0 mg L^{-1} by keeping all other parameters such as adsorbent dose 0.1 g/100 mL, pH 3 and contact time 90 min at ambient temperature. It was noticed that with increase in initial phosphate ion concentration, the percent removal of phosphate ion decreased. The maximum percent removal of phosphate ion was found to be 94.03 % by acid treated coal fly ash at 1 mg L^{-1} of initial concentration, 0.1 g/100 mL of dosage, pH 3 and 90 min of contact time at ambient temperature. The results are shown in Figure 8.

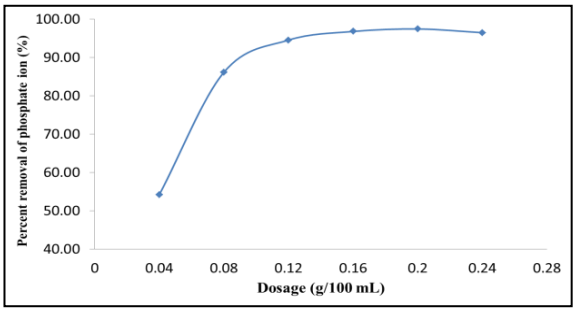

Figure 7 Effect of dosage on the percent removal of phosphate ion by acid treated coal fly ash

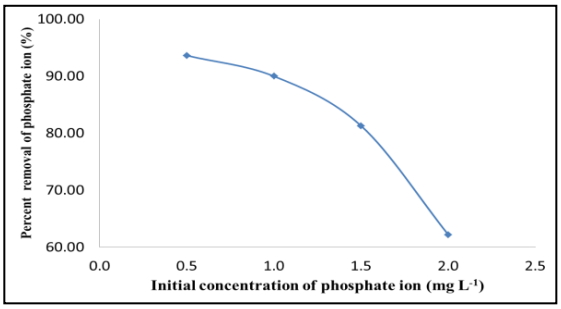

Figure 8 Effect of initial concentration of phosphate ion on the percent removal of phosphate ion by acid treated coal fly ash

Characterization of Coal Fly Ash, Acid Treated Coal Fly Ash and Phosphate Ion Sorpted Acid Treated Coal Fly Ash

SEM micrographs of the surface morphology of coal fly ash are given in Figure 9. It was found that coal fly ash showed the presence of different size of microparticles in the shape of smooth balls. SEM micrographs of the surface morphology of acid treated coal fly ash are given in Figure 10. It was found that acid treated coal fly ash showed only agglomerations of undefined shape. After acid treatment, the surface of fly ash particles is formed on the surface of a lot of grooves and holes, which can enhance the adsorption of the colloidal particles. SEM micrographs of the surface morphology of phosphate ion sorpted acid treated coal fly ash are given in Figure 11. It was found that phosphate ion sorpted acid treated coal fly ash showed that there were flocculant materials adhered to the particles or occurred separately.

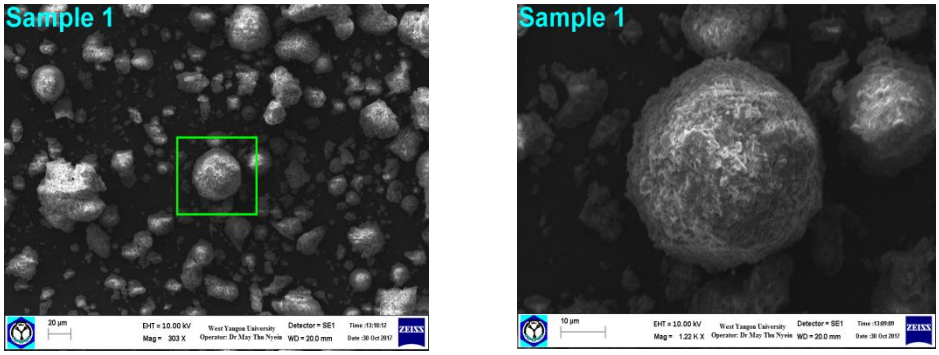

Figure 9 SEM micrographs of coal fly ash

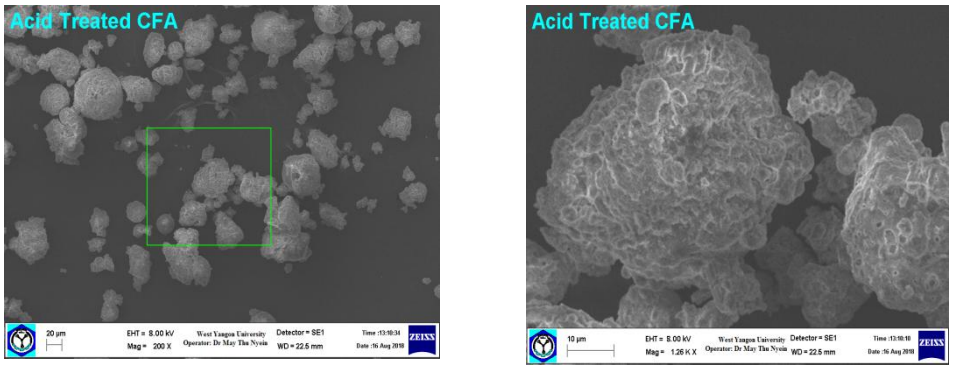

Figure 10 SEM micrographs of acid treated coal fly ash

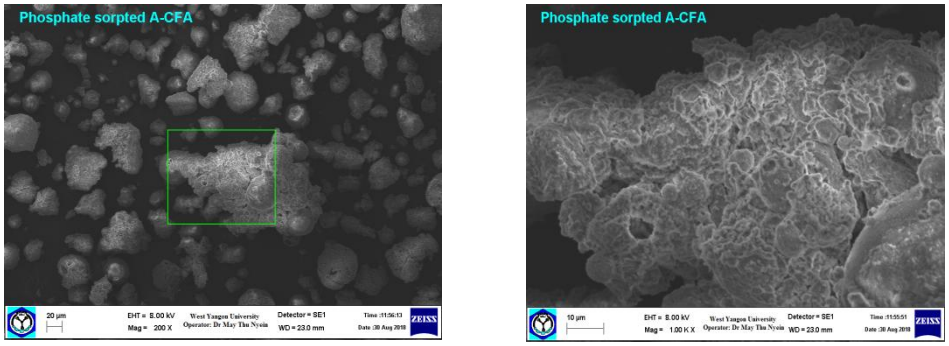

Figure 11 SEM micrographs of the phosphate ion sorpted acid treated coal fly ash

The relative abundance of metallic oxides in coal fly ash, acid treated coal fly ash and phosphate ion sorpted acid treated coal fly ash were examined by EDXRF technique. The chemical compositions of samples are shown in Table 2.

The highest amounts of SiO_2 (53.845 %), Al_2O_3 (21.330 %), CaO (17.632 %) and Fe_2O_3 (4.444 %) were found in the coal fly ash. Total relative abundance (%) of SiO_2+Al_2O_3+Fe_2O_3 is 79.619 %. Therefore this coal fly ash is class F and produced from burning of anthracite and bituminous coal.

The highest amounts of SiO_2 (47.697 %), Al_2O_3 (22.426 %), CaO (7.527 %) and Cl (10.398 %) were found in acid treated coal fly ash. After treating with HCl, it can be seen that Cl is one of the constituent in acid treated coal fly ash.

Table 2 Relative Abundance of Metallic Oxides in the Coal Fly Ash (CFA), Acid Treated Coal Fly Ash (ACFA) and Phosphate Ion Sorpted Acid Treated Coal Fly Ash (PACFA) by EDXRF

No	Metallic Oxides	Relative abundance (%)		
		CFA	ACFA	PACFA
1	SiO_2	53.845	47.697	23.545
2	Al_2O_3	21.330	22.426	5.276
3	CaO	17.623	7.527	2.525
4	Fe_2O_3	4.444	6.364	1.147
5	TiO_2	0.725	0.966	0.176
6	Cl	----	10.398	----
7	P_2O_5	----	----	35.800

The highest amounts of P_2O_5 (35.800 %), SiO_2 (23.545 %), Al_2O_3 (5.276 %) and CaO (2.525 %) were found in phosphate ion sorpted acid treated coal fly ash. After sorption with model solution, it can be seen that P_2O_5 is one of the constituent in phosphate ion sorpted acid treated coal fly ash. The oxides of Al and Fe are significantly decreased in phosphate ion sorpted acid treated coal fly ash. This is due to the binding of phosphate ion with aluminum and iron resulting in the formation of metal phosphates.

In this research, XRD measurement was carried out on coal fly ash. The resultant XRD diffractogram is shown in Figure 12. According to XRD diffractogram, presence of strong intensity peaks of quartz (SiO_2) with Miller indices (101) and (100) were observed at 2θ values of 26.433° and 20.666° respectively. And then presence of aluminum oxide (Al_2O_3) with Miller indices (201) and (400) were observed at 2θ values of 24.814° and 30.967° respectively. The phase analysis of coal fly ash indicated the presence of quartz (SiO_2), aluminum oxide (Al_2O_3), hematite (Fe_2O_3) and lime (CaO). These findings confirmed that the coal fly ash mainly consists of quartz (SiO_2) and aluminum oxide (Al_2O_3). Average crystallite size of coal fly ash was calculated and found to be 24.04 nm by Debye Scherrer equation. The crystal structure of coal fly ash was found to be hexagonal according to lattice parameters (a = b = 6.9803 Å and c = 5.4938 Å).

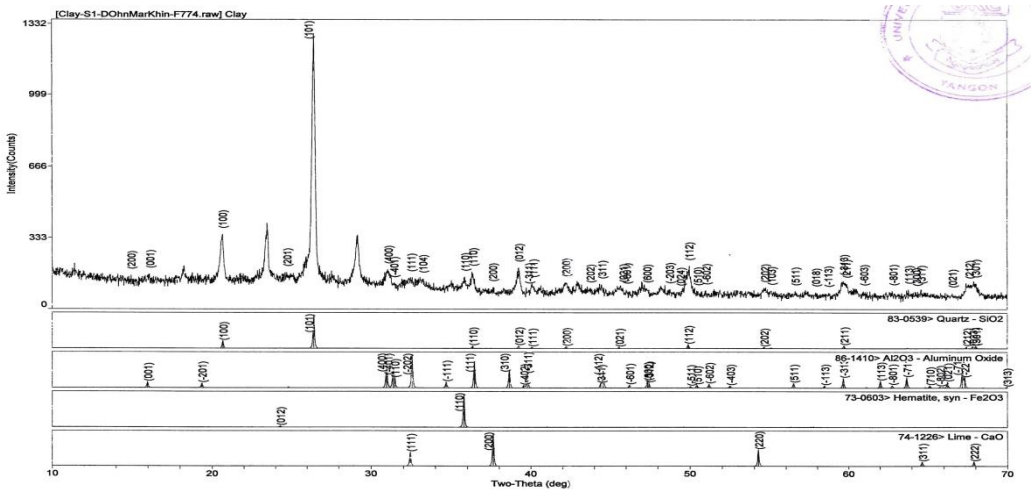

Figure 12 XRD diffractogram of coal fly ash

In this research, XRD measurement was carried out on acid treated coal fly ash. The resultant XRD diffractogram is shown in Figure 13. According to the XRD diffractogram, the presence of strong intensity peak of aluminum oxychloride (AlOCl) with Miller indices (111) was observed at 2θ values of 26.426°. The phase analysis of acid treated coal fly ash showed aluminum oxychloride (AlOCl), quartz (SiO_2), aluminum oxide (Al_2O_3), hematite (Fe_2O_3) and lime (CaO). These findings confirmed that the acid treated coal fly ash mainly consists of aluminum oxychloride (AlOCl). The presence of AlOCl was a result of the reaction of Al_2O_3 and acid soluble, aluminum containg compounds with hydrochloric acid. Average crystallite size of acid treated coal fly ash was calculated and found to be 26.51 nm by Debye Scherrer equation. The crystal structure of acid treated coal fly ash was found to be hexagonal according to lattice parameters (a = b = 8.4307 Å and c = 4.5657 Å).

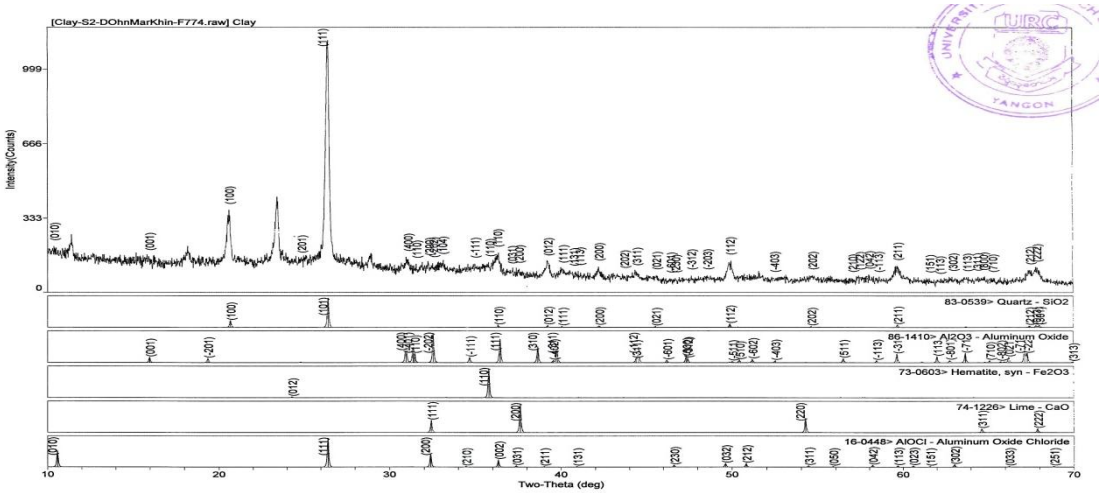

Figure 13 XRD diffractogram of acid treated coal fly ash

In this research, XRD measurement was carried out on phosphate ion sorpted acid treated coal fly ash. The resulting data are presented in Figure 14. According to XRD diffractogram, presence of strong intensity peak of aluminum phosphate ($AlPO_4$) with Miller indices (012) was observed at 2θ values of 26.414°. And then presence of iron phosphate $Fe(PO_4)$ with Miller indices (101) was observed at 2θ values of 21.873°. Average crystallite size of phosphate ion sorpted acid treated coal fly ash was calculated and found to be 31.82 nm by Debye Scherrer equation. The crystal structure of phosphate ion sorpted acid treated coal fly ash was found to be hexagonal according to lattice parameters (a = b = 8.4403 Å and c = 4.7976 Å).

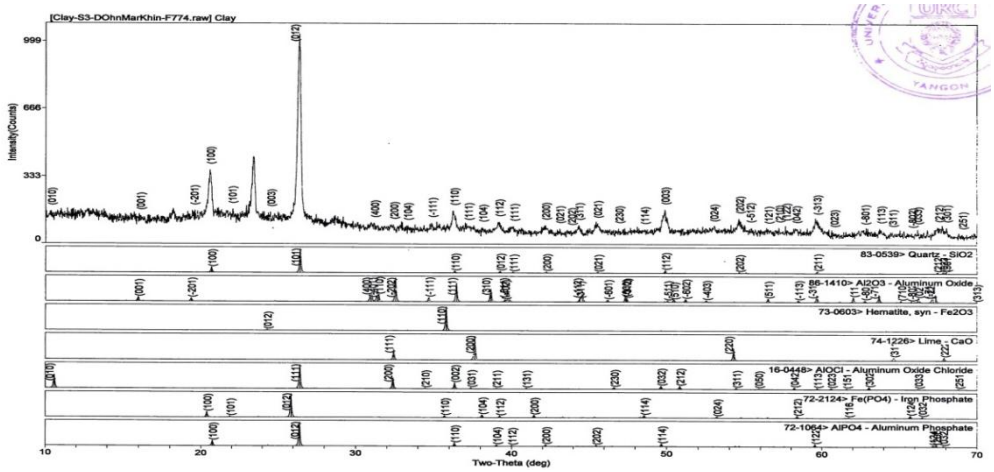

Figure 14 XRD diffractogram of the phosphate ion sorpted acid treated coal fly ash

Conclusion

In this research, adsorption method was used to remove the phosphate ion from the model solution by using acid treated coal fly ash as a sorbent. Modified acid treated coal fly ash is effective adsorbents as compared to coal fly ash collected from Tigyit power plant located in South-west Shan State in Myanmar for the removal of phosphate ion from aqueous solution. The sorption behaviors of the maximum percent removal of phosphate ion were found to be 94.03 % by acid treated coal fly ash at 1 mg L^{-1} of initial concentration, 0.1 g/100 mL of dosage, pH 3 and 90 min of contact time at ambient temperature.

Coal fly ash, acid treated coal fly ash and phosphate ion sorpted acid treated coal fly ash were characterized by using modern instrumental techniques, such as SEM, EDXRF and XRD. SEM analysis showed the presence of different size of microparticles in the shape of smooth balls found in the coal fly ash. Acid treated coal fly ash showed only agglomerations of undefined shape and flocculant materials adhered to the particles or occurred separately in phosphate ion sorpted acid treated coal fly ash. EDXRF analysis showed that total relative abundance (%) of SiO_2+Al_2O_3+Fe_2O_3 is 79.619 %. Therefore, this coal fly ash is class F and produced from burning of anthracite and bituminous coal. XRD analysis also confirmed that the coal fly ash mainly consists of quartz (SiO_2) and aluminum oxide (Al_2O_3). XRD analysis confirmed that the acid treated coal fly ash mainly consists of aluminum oxychloride (AlOCl). The presence of aluminum oxychloride was a result of the reaction of Al_2O_3 and acid soluble, aluminum containing compounds with hydrochloric acid. According to XRD diffractogram, presence of strong intensity peak of aluminum phosphate ($AlPO_4$) was observed. These findings confirmed that the phosphate ion sorpted acid treated coal fly ash mainly consists of aluminum phosphate ($AlPO_4$).

It can be inferred from this research work that acid treated coal fly ash may be used as an effective sorbent to remove phosphate ions from eutrophicated surface water. Therefore, the outcome of this research work would lead to a cleaner and healthier environment.

Acknowledgements

The authors would like to thank the Department of Higher Education (Yangon Office), Ministry of Education, Yangon, Myanmar for giving us the opportunity to do this research.

References

Arnold, E., Lenore, S. and Andrew, D. E. (1992). "*APHA Method 4500-P; Standard Methods for the Examination of Water and Waste Water".* Washington, DC : American Public Health Association, pp.108-116

Benito, Y., Ruiz, M., Cosmen, P. and Merino, L. J. (2001). "Study of Leaches Obtained from the Disposal of Fly Ash from PFBC and AFBC Processes*". Chem. Eng. J.*, vol.84, pp.167-171

Mikendova, B., Thomas, J. and Danek, T. (2010). "Phosphorus Removal from Water Using Fly Ash and Modificated Fly Ash - Comparison of X-Ray Fluorescence Spectrometry and Standard Spectrophotometric Methods". *Geosci.Eng*., vol 1(6), pp. 22-31

Mustafa, S., Zaman, M. I. and Khan, S. (2008). "Temperature Effect on the Mechanism of Phosphate Anions Sorption by β-MnO_2". *Chem. Eng. J.*, vol.141 (1-3), pp.51-57

PYO, Pa-Oh Youth Organization (2011). *Poison Clouds : Lessons from Burma's Largest Coal Project at Tigyit* http://burmacampaign.org.uk/media/PoisonClouds.pdf (Accessed 14 October 2016)

Ragheb, S. M. (2013). "Phosphate Removal from Aqueous Solution using Slag and Fly Ash". *HBRC Journal* , vol. 9, pp. 270-275

REMOVAL OF ARSENIC AND LEAD TOXIC METALS BY KYAUK PATAUNG KAOLIN AND CHARACTERIZATION OF ARSENIC AND LEAD LOADED KAOLIN

Mi Mi Lay[1], Aye Aye Lwin[2], Daw Hla Ngwe[3]

Abstract

This research work is focused on the determination of optimum conditions for the removal of arsenic and lead toxic elements in model solutions by using Kyauk Pataung (KPT) kaolin sample. In this research, removal of arsenic and lead ions from the model solutions using KPT kaolin was studied by the effect of contact time (0.5-24 h), effect of dosage (0.5- 3.5 g), effect of pH (4-9), metal concentration (50-800 ppm) at room temperature. The KPT kaolin sample was observed to remove 97.29 % of arsenic (100 ppm of initial concentration) using 2 g of KPT kaolin after 12 h contact time at pH 7, whereas 95.08 % of lead could be removed under the above conditions at pH 5. The amount of arsenic and lead remained in the solutions after treating with KPT kaolin were determined by using AAS technique. The arsenic and lead loaded kaolin sample were characterized by EDXRF, SEM and FT IR analyses.

Keywords: Removal of arsenic and lead, Kyauk Pataung Kaolin

Introduction

The problem of removing pollutants from water is an important process and is becoming more important with the increasing of industrial activities (Yakun *et al*., 2014). Therefore, removal of heavy metals such as cadmium, lead, arsenic, mercury, chromium, iron, zinc and copper from aqueous solution is necessary because of the frequent appearance of these metals in waste streams from many industries (Missana and Garcia, 2007).

The heavy metals in the waste streams can be readily adsorbed by marine animals and directly enter the human food chains, thus presenting a high health risk to consumers (Ulmanu *et al*., 2003). Different techniques for the removal of metal ions from aqueous solutions have been developed as chemical precipitation, filtration, ion-exchange, reverse osmosis, membrane systems and etc. However, all these techniques have their inherent advantages and limitations in application. In the last few years, adsorption has been shown to be an alternative technique for removing dissolved metal ions from liquid wastes (Matta, 2015).

Heavy metals is the generic term for metallic elements having an atomic weight higher than 40.04. Heavy metals enter into the environment by natural and anthropogenic means. Such sources include: natural weathering of the earth's crust, mining, soil erosion, industrial discharge, urban runoff, sewage effluents, pest or disease control agents applied to plants, air pollution fallout, and a number of others (Morais, 2012). The contamination chain of heavy metals almost always follows a cyclic order: industry, atmosphere, soil, water, foods and human (Matta, 2015). Although toxicity and the resulting threat to human health of any contaminant are, of course, a function of concentration, it is well-known that chronic exposure to heavy metals and metalloids at relatively low levels can cause adverse effects (Castro and Mendez, 2008). While focusing on

[1] Lecturer, Department of Chemistry, University of Medicine (2)
[2] Associate Professor, Department of Chemistry, Maubin University
[3] Professor and Head (Retired), Department of Chemistry, University of Yangon

developing countries the conditions is getting more disastrous due to increase in industrial complex minimal follow up of environmental and pollution control guidelines.

The most commonly found heavy metals in waste water include arsenic, cadmium, chromium, copper, lead, nickel, and zinc, all of which cause risks for human health and the environment (Alloway, 2013). Neurotoxic effects of heavy metals are also well documented, especially for mercury and lead, with numerous reports of neurobehavioral changes after occupational exposure and of developmental effects in children with pre- or early postnatal exposure. However experimental studies suggest that arsenic could also interfere with the nervous system and that all three metals may influence the dopaminergic system in different ways (Pohl, 2003). There is, a need to clear which exposure levels are likely to cause these effects, and to what extent the three metals could interfere in mixed exposures (Alloway, 2013).

In solution, heavy metals can be present either as free-ions or complexes with organic and inorganic ligands (Alleoni *et al*., 2003). In order to minimize processing costs, several investigations have focused on the use of low cost adsorbents, e.g. agricultural by-products (Samantaroy *et al*., 1997), biosorbents (Pino *et al*., 2005), slag and clay materials.

The process of adsorption has become one of the preferred methods for the removal of toxic contaminants from water as it has been found to be very effective, economical, versatile and simple. Adsorption has the additional advantages of applicability at very low concentrations, suitability for being used in batch and continuous processes. Adsorption has acquired global importance for the minimization of water and air contamination. Also, its significant addition to Green Chemistry endeavors (Irshad *et al*., 2017).

Adsorbents, mainly clay minerals, are readily available, inexpensive materials and offer a cost-effective alternative to conventional treatment. Clay porous structure and high surface area provide benefits in the absorption of liquids and the adsorption of heavy metals.

Kaolin minerals include kaolinite, dickite, nacrite, and halloysite, respectively. Kaolinite ($Al_2Si_2O_5\,(OH)_4$) is the most common kaolin mineral with the theoretical chemical composition: 46.54 % SiO_2, 39.50 % Al_2O_3, and 13.96 % H_2O. Kaolinite has 1:1 ratio of tetrahedral and octahedral layers continuous in the z- and x- axes directions, respectively, and stacked above each other in the y-direction. Kaolinite is one of the most important industrial clay minerals useful to man with a wide range of applications as raw material in ceramics, paper filling and coating, (Mefire *et al*. 2004) refractory, fiberglass, cement, rubber and plastics, cosmetics, paint, catalyst, pharmaceutic and agriculture (Ekosse, 2010) because of its relatively low cost and easy availability. Its application is a function of its physical and chemical characteristics in relation to requirements of the end user (Murray, 2007). The physical and chemical properties of kaolinite are strongly influenced by its structural order (Vaculikova *et al*. 2011).

The present study deals with the use of locally available kaolinite clay material as an adsorbent for the removal of arsenic and lead from solutions. The effect of various parameters affecting adsorption behavior as contact time, initial metal ion concentration, amount of adsorbent and pH of solution have been investigated and data on adsorption isotherms have been presented.

Materials and Methods

Collection and Preparation of Samples

The kaolinite sample was collected from Kyauk Pataung Township, Mandalay Region. After collection, the kaolinite sample was washed with tap water to remove impurities and then air-dried under shade to prevent some reaction of sunlight. Then the kaolinite was ground to fine particles and sieved into 90 μm aperture size and stored in air tight plastic bag so that the sample was free from getting molds to prevent moisture, as well as other contaminations and was ready to be used for the experimental works.

Preparation of the Adsorptive Compounds

Deionized water was used through the experiment. Stock solutions (1000 mg/L) of lead(II) nitrate solution and arsenic(III) oxide (As_2O_3) solution were prepared in deionized water. The stock solutions were diluted as required to obtain standard solutions.

Adsorption Method

Adsorption measurements were made by a batch technique at room temperature. The batch mode was selected because of its simplicity and reliability. In all experiments, the required volume (50 mL) of the adsorptive compound solution was added to kaolin absorbent at room temperature. The solutions were then shaken vigorously for a given time period to reach equilibrium. After completion of a selected shaking time, the suspensions were then filtered. The amount adsorbed was determined by analyzing the metal content before and after each experiment using Atomic Absorption Spectrometer (AAS).

Determination of Arsenic(III) Ions Sorption Capacity onto the Kyauk Pataung Kaolin

The arsenic sorption capacities of Kyauk Pataung Kaolin (KPT kaolin) sample were studied at various contact times (0.5, 1, 2, 3, 5, 7, 9, 12, 15, 18, 20, 22 and 24 h). The effect of dosage of KPT Kaolin samples (0.5 g -3.5 g) on sorption of arsenic ion was studied at initial pH. The arsenic sorption efficiencies of KPT Kaolin sample was studied at various pH (4-8). The arsenic sorption capacity of KPT Kaolin sample was studied at various concentrations of model solutions (50-500 ppm).

Determination of Lead(II) Ions Sorption Capacity onto the Kyauk Pataung Kaolin

The Pb(II) sorption capacity of KPT Kaolin sample was studied at various contact times (0.5, 1, 2, 3, 5, 7, 9, 12, 15, 18, 20, 22 and 24 h). The effect of dosage of KPT Kaolin samples (0.5 g -3.5 g) on sorption of Pb(II) ion was studied at initial pH. The Pb(II) sorption efficiencies of Kyauk Pataung Kaolin sample was studied at various pH (4-9). The Pb(II) sorption capacity of KPT Kaolin sample was studied at various concentrations of model solutions (50-900 ppm).

Elemental Analysis of the Samples by EDXRF Method

Elemental compositions in Kyauk Pataung Kaolin sample and metal loaded KPT kaolin sample were determined by EDXRF using EDX-720 spectrometer (Shimadzu Co. Ltd., Japan) at West Yangon University, Yangon.

Scanning Electron Microscopy (SEM) Analysis of the Samples

The surface morphology of the KPT Kaolin and metal loaded KPT kaolin samples were observed by using SEM technique on JSM 5610 LV scanning electron microscope, JEOL-Ltd., Japan.

FT IR Analysis of the Samples

Fourier Transform Infrared (FT IR) spectra of KPT Kaolin sample and the metal loaded KPT Kaolin sample were recorded in a range of wave number from 4300 to 400 cm^{-1} on a FT IR spectrometer (FT IR-8400 SHIMADZU, Japan) at Department of Chemistry, Yangon University.

Results and Discussion

The arsenic and lead from the respective model solution: lead(II) nitrate model solution and arsenic(III) solution were removed by using KPT kaolin sample, collected from the Kyauk Pataung Township, Mandalay Region. The removal percent of the metals (metal sorption capacities) were studied at different contact times, at different dosages of the adsorbent, at different pH of the solution and at different concentrations of the adsorptive compounds.

Effect of Contact Time on the Removal Percent of Arsenic by Kyauk Pataung Kaolin

The effect of contact time on removal percent of arsenic by Kyauk Pataung Kaolin is shown in Table 1 and Figure 1. The arsenic sorption capacity of Kyauk Pataung Kaolin sample was studied at various contact times (0.5- 24 h). Adsorption of arsenic by KPT Kaolin was very fast at the initial state and adsorbed arsenic ion is slowly released into the solution. After 24 h, the adsorption process reached equilibrium and optimum contact time was selected at 12 h with the maximum removal percent of arsenic (99.8 %).

Table 1 Effect of Contact Time on the Removal Percent of Arsenic by Kyauk Pataung Kaolin

No.	Contact time (h)	Equilibrium concentration of arsenic (ppm)	Removal % of As
1	1.0	10.1	89.9
2	2.0	9.2	90.8
3	3.0	7.1	92.9
4	5.0	5.5	94.5
5	7.0	4.7	95.3
6	9.0	2.9	97.1
7	12.0	0.2	99.8
8	15.0	0.3	99.7
9	18.0	0.3	99.7
10	20.0	0.4	99.6
11	22.0	0.6	99.4
12	24.0	0.6	99.4

Initial pH = 6.8, Dosage = 2 g, Initial concentration of Arsenic = 100 ppm

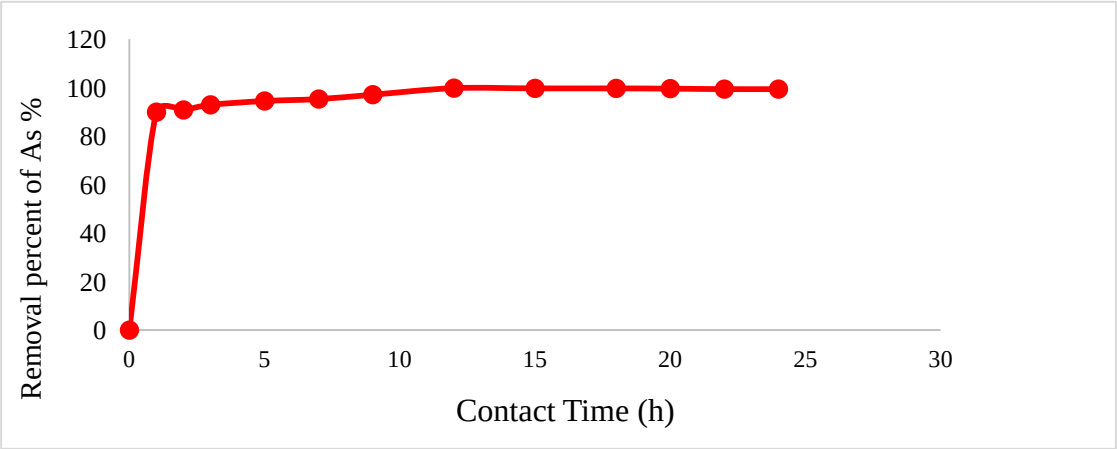

*Initial pH = 6.8, Dosage = 2 g, Initial concentration of Arsenic = 100 ppm

Figure 1 Removal percent of arsenic as a function of contact time

Effect of Dosage on the Removal Percent of Arsenic by Kyauk Pataung Kaolin

The effect of dosage on removal percent of arsenic by Kyauk Pataung kaolin was shown in Table 2 and Figure 2. The effect of dosage of KPT Kaolin samples (0.5 g -3.5 g) on sorption of arsenic ion was studied at initial pH. It was found that the percent arsenic ion adsorption efficiency increased with increasing dosage of Kaolin samples and optimum dosage of kaolin sample was 2 g with the maximum removal percent of arsenic (93.7 %).

Table 2 Effect of Dosage on the Removal Percent of Arsenic by Kyauk Pataung kaolin

No.	Dosage (g)	Equilibrium concentration of As (ppm)	Removal (%) of As
1	0.5	14.1	85.9
2	1.0	10.1	89.9
3	1.5	9.7	90.3
4	2.0	6.3	93.7
5	2.5	2.5	97.5
6	3.0	2.1	98.9
7	3.5	0.7	99.3

Initial pH = 6.8, Contact time = 12 h, Initial concentration of Arsenic = 100 ppm

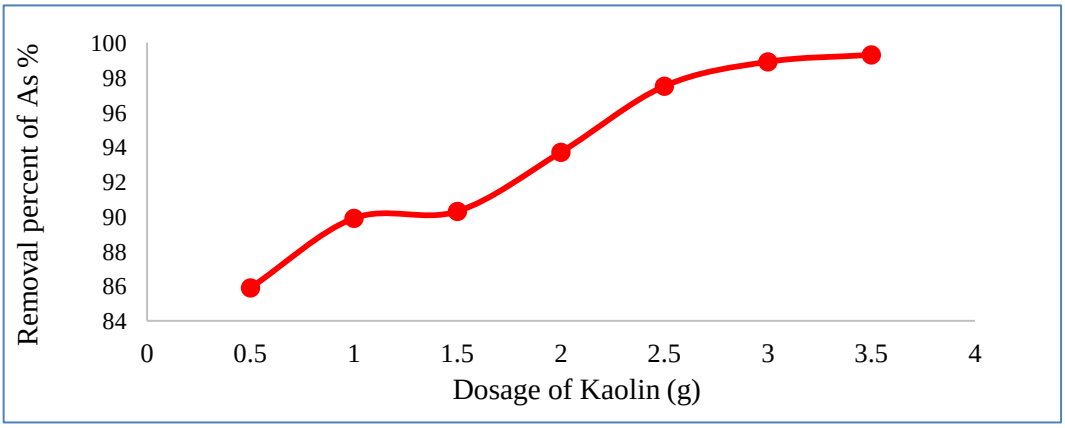

*Initial pH = 6.8, Contact time = 12 h, Initial concentration of Arsenic = 100 ppm

Figure 2 Removal percent of arsenic as a function of dosage of KPT kaolin

Effect of pH on the Removal Percent of Arsenic by Kyauk Pataung Kaolin

The effect of pH on Removal Percent of Arsenic by Kyauk Pataung Kaolin was shown in Table 3 and Figure 3. The arsenic sorption efficiencies of Kyauk Pataung Kaolin sample was studied at various pH (4-8). The pH of the solutions were adjusted by using HNO_3 solution. At pH values of greater than 7, the sorption capacity was slowly decreased and the removal percent of arsenic ion was selected at optimum pH 7 with the maximum removal percent of arsenic (98.9 %).

Table 3 Effect of pH on the Removal Percent of Arsenic by Kyauk Pataung Kaolin

No.	pH	Equilibrium Concentration of Arsenic (ppm)	Removal % of As
1	4.0	10.8	89.2
2	4.5	8.5	91.5
3	5.0	6.1	93.9
4	5.5	4.2	95.8
5	6.0	3.5	96.5
6	6.5	2.7	97.3
7	7.0	1.1	98.9
8	7.5	3.2	96.8
9	8.0	4.4	95.6

Dosage = 2 g, Contact time = 12 h, Initial concentration of Arsenic = 100 ppm

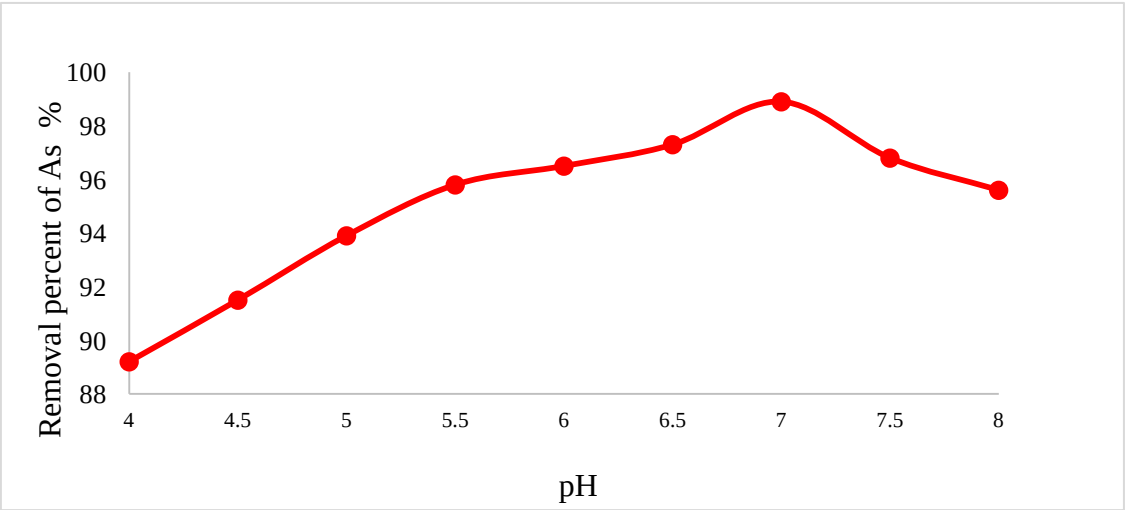

*Dosage = 2 g, Contact time = 12 h, Initial concentration of Arsenic = 100 ppm

Figure 3 Removal percent of arsenic as a function of pH

Effect of Concentration on the Removal Percent of Arsenic by Kyauk Pataung Kaolin

The effect of concentration on removal percent of arsenic by Kyauk Pataung Kaolin was shown in Table 4 and Figure 4. The arsenic ion sorption capacities of Kyauk Pataung Kaolin sample was studied at various concentrations of model solutions (50-500 ppm). The sorption efficiency become decrease as the concentration of metal ions increase and the sorption site

decrease and the optimum metal concentration was selected at 100 ppm the maximum removal percent of arsenic (96.79 %).

Table 4 Effect of Concentration on the Removal Percent of Arsenic by Kyauk Pataung K

No.	Initial Concentration of As (ppm)	Equilibrium Concentration of As (ppm)	Removal % of As
1	50	1.31	97.38
2	100	3.21	96.79
3	150	8.25	94.50
4	200	14.4	92.80
5	300	30.3	89.90
6	400	58.8	85.30
7	500	85.5	82.90

Dosage = 2 g, Contact time = 12 h, Initial pH = 6.8

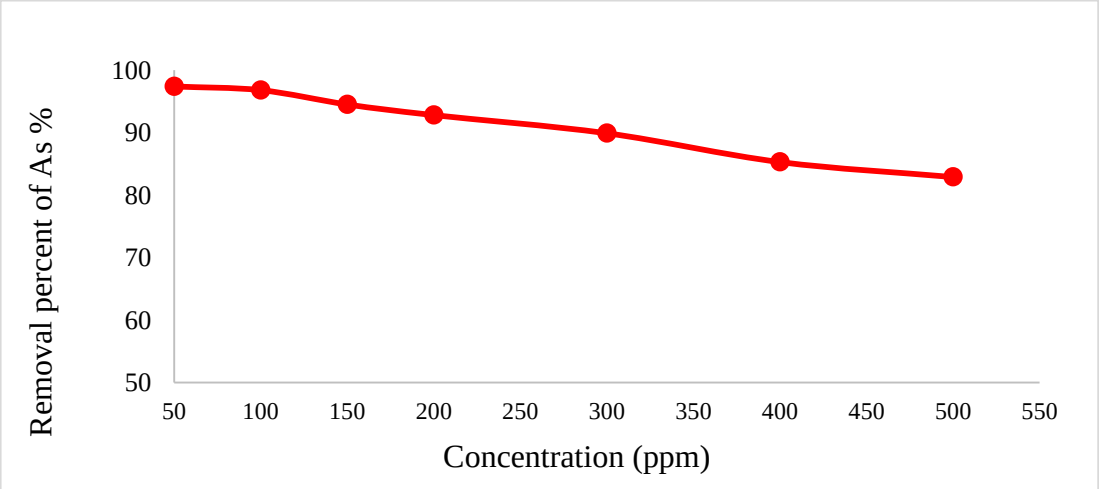

*Dosage = 2 g, Contact time = 12 h, Initial pH = 6.8

Figure 4 Removal percent of arsenic as a function of concentration

Effect of Contact Time on the Removal Percent of Lead by Kyauk Pataung Kaolin

The effect of contact time on removal percent of lead by Kyauk Pataung Kaolin was shown in Table 5 and Figure 5. The Pb(II) sorption capacities of Kyauk Pataung Kaolin sample was studied at various contact times (0.5- 24h). Adsorption of Pb(II) by KPT Kaolin was very fast at the initial state and adsorbed Pb(II) ion is slowly released into the solution. After 24 h, the adsorption process reached equilibrium and optimum contact time was selected at 12 h with the maximum removal percent of lead (92.72 %).

Table 5 Effect of Contact Time on the Removal Percent of Lead by Kyauk Pataung Kaolin

No.	Contact time (h)	Equilibrium Concentration of Pb (ppm)	Removal % of Pb
1	0.5	3.80	96.90
2	1.0	10.10	89.90
3	2.0	2.10	97.90
4	3.0	5.50	94.50
5	5.0	7.99	92.01
6	7.0	6.30	93.70
7	9.0	6.99	93.01
8	12.0	7.28	92.72
9	15.0	8.09	91.91
10	18.0	9.30	90.70
11	20.0	9.90	90.10
12	22.0	10.95	89.05
13	24.0	10.98	89.02

Initial pH = 5.9, Dosage = 2 g, Initial concentration of Pb = 100 ppm

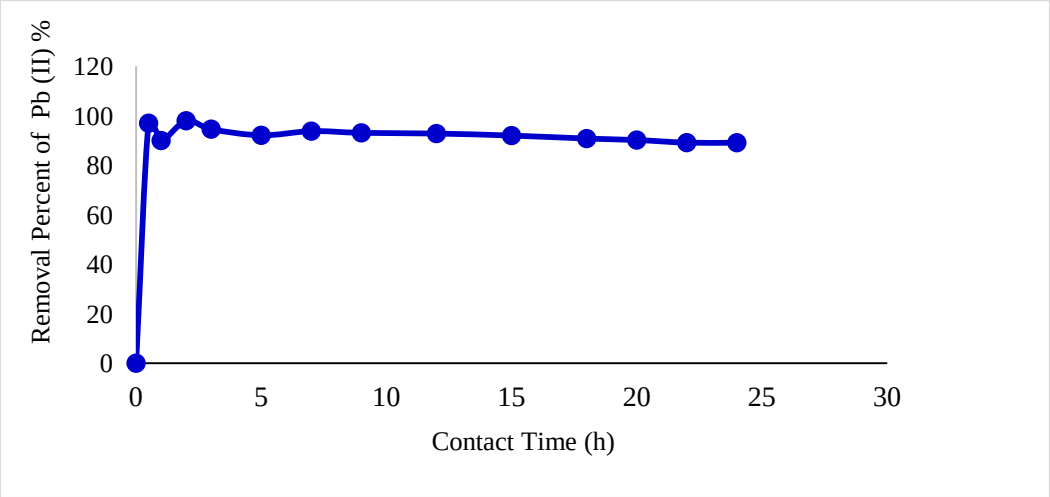

*Initial pH = 5.9, Dosage = 2 g, Initial concentration of Pb = 100 ppm

Figure 5 Removal percent of lead as a function of contact time

Effect of Dosage on the Removal Percent of Lead by Kyauk Pataung Kaolin

The effect of dosage on removal percent of lead by Kyauk Pataung Kaolin was shown in Table 6 and Figure 6.The effect of dosage of KPT Kaolin samples (0.5 g -3.5 g) on sorption of Pb(II) ion was studied at initial pH. It was found that the percent Pb(II) ion adsorption efficiency increased with increasing dosage of Kaolin samples and optimum dosage of KPT kaolin was selected was 2 g with the maximum removal percent of lead (92.5 %).

Table 6 Effect of Dosage on the Removal Percent of Lead by Kyauk Pataung Kaolin

No.	Dosage (g)	Equilibrium concentration of Pb (ppm)	Removal (%) of Pb
1	0.5	34.8	65.2
2	1.0	23.6	76.4
3	1.5	13.3	86.7
4	2.0	8.5	92.5
5	2.5	7.3	93.2
6	3.0	5.2	94.8
7	3.5	4.5	96.5

Initial pH = 5.9, Contact time = 12 h, Initial concentration of Pb = 100 ppm

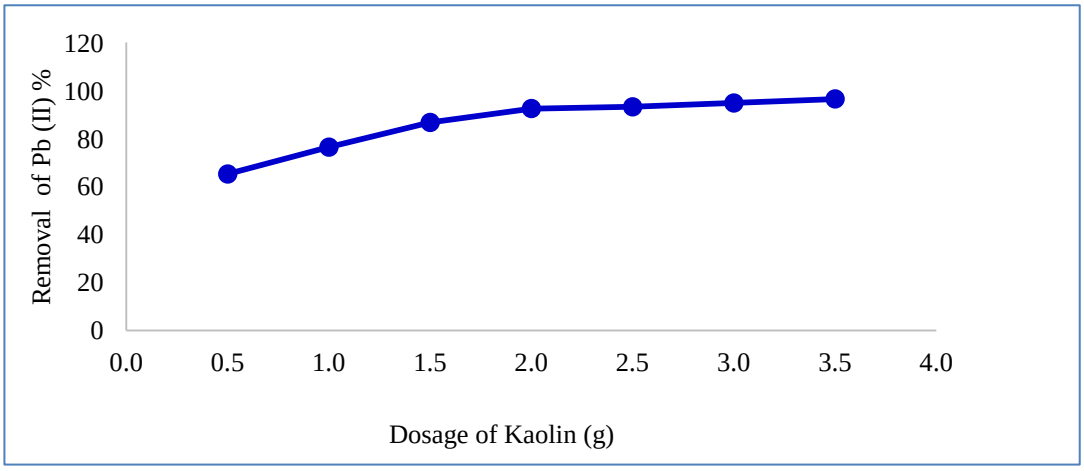

*Initial pH = 5.9, Contact time = 12 h, Initial concentration of Pb = 100 ppm

Figure 6 Removal percent of lead as a function of dosage of KPT kaolin

Effect of pH on the Removal Percent of Lead by Kyauk Pataung Kaolin

The effect of pH on removal percent of lead by Kyauk Pataung Kaolin was shown in Table 7 and Figure 7. The Pb(II) sorption efficiencies of Kyauk Pataung Kaolin sample was studied at various pH (4-9). The pH of the solutions were adjusted by addition of HNO_3 solution At pH values of greater than 5, the sorption capacity was slowly decreased and the removal the removal percent of Pb(II) was at optimum pH 5 with the maximum removal percent of lead (96.3 %).

Table 7 Effect of pH on the Removal Percent of Lead by Kyauk Pataung Kaolin

No.	pH	Equilibrium Concentration of Pb (ppm)	Removal % of Pb
1	4.0	11.6	88.4
2	4.5	5.9	94.1
3	5.0	3.7	96.3
4	5.5	6.8	93.2
5	6.0	9.9	90.1
6	6.5	10.5	89.5
7	7.0	11.5	88.5
8	7.5	10.9	89.1
9	8.0	14.6	85.4
10	8.5	17.6	82.4
11	9.0	19.4	80.6

Dosage= 2 g, Contact time = 12 h, Initial concentration of Pb = 100 ppm

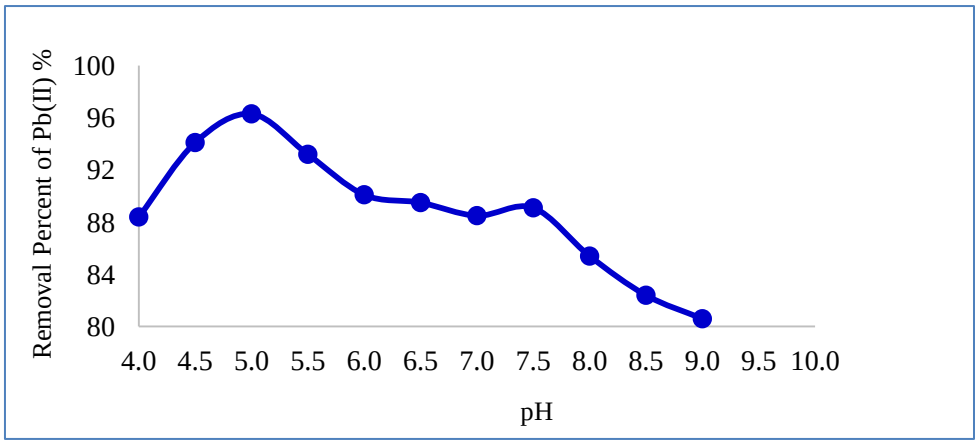

*Dosage= 2 g, Contact time = 12 h, Initial concentration of Pb = 100 ppm

Figure 7 Removal percent of lead as a function of pH

Effect of Concentration on the Removal Percent of Lead by Kyauk Pataung Kaolin

The effect of concentration on removal percent of lead by Kyauk Pataung Kaolin was shown in Table 8 and Figure 8. The Pb(II) sorption capacities of Kyauk Pataung Kaolin sample was studied at various concentrations of model solutions (50-900 ppm). The sorption efficiency become decrease as the concentration of metal ions increase and the sorption site decrease and the optimum metal concentration was selected at 100 ppm with the maximum removal percent of lead (98.0 %).

Table 8 Effect of Concentration on the Removal Percent of Lead by Kyauk Pataung Kaolin

No.	Concentration of Pb (ppm)	Equilibrium Concentration of Pb (ppm)	Removal % of Pb
1	50	2.0	98.0
2	100	2.5	97.5
3	200	29.6	85.2
4	300	78.6	73.8
5	400	128.8	67.8
6	500	205.5	58.9
7	600	291.0	51.5
8	700	386.4	44.8
9	800	477.6	40.3
10	900	539.1	40.1

Dosage= 2 g, Contact time = 12 h, Initial pH = 5.9

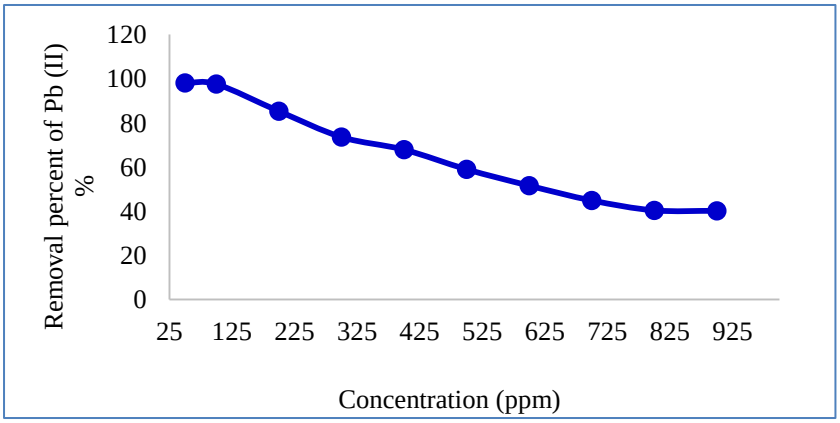

*Dosage= 2 g, Contact time = 12 h, Initial pH = 5.9

Figure 8 Removal percent of lead as a function of concentration

Adsorption of model solution of arsenic and lead by KPT Kaolin was very fast at the initial state and then adsorbed Arsenic and lead ions are slowly released into the solution. After 12 h the removal percent of arsenic and lead were nearly the same and reached the equilibrium. The contact time was selected at 12 h. The effect of dosage of KPT Kaolin samples (0.5 g -3.5 g) on sorption of arsenic and lead ions were studied at initial pH. It was found that the percent arsenic and lead adsorption efficiency increased with increasing dosage of Kaolin samples. The sorption efficiencies of arsenic was studied at various pH (4-8) and the sorption efficiencies of lead was studied at various pH (4-9). It was found that, the removal percent of arsenic at optimum pH 7 and the removal percent of lead was at optimum pH 5. The arsenic sorption capacity of Kyauk Pataung Kaolin sample was studied at various concentrations of model solutions (50-500 ppm) and the lead sorption capacity of Kyauk Pataung Kaolin sample was studied at various concentrations of model solutions (50-900 ppm). The sorption efficiency become decrease as the concentration of metal ions increase and the sorption site decrease.

EDXRF Analysis of the Kyauk Pataung Kaolin and Metal Loaded Kaolin Samples

Relative abundance of elements in kaolin samples were determined by EDXRF analysis. Figure 9 is the EDXRF spectra of KPT kaolin, lead loaded kaolin and arsenic loaded kaolin. Table 9 shows the relative abundance of elements present in kaolin samples. From EDXRF analysis, Si was observed to be present in the highest amount (32-72 %) in kaolin samples followed by Fe (17-37 %) and Ti (7-8 %). The EDXRF spectra showed the presence of As (2.33 %) in arsenic loaded KPT kaolin and Pb (7.50 %) in lead loaded KPT kaolin.

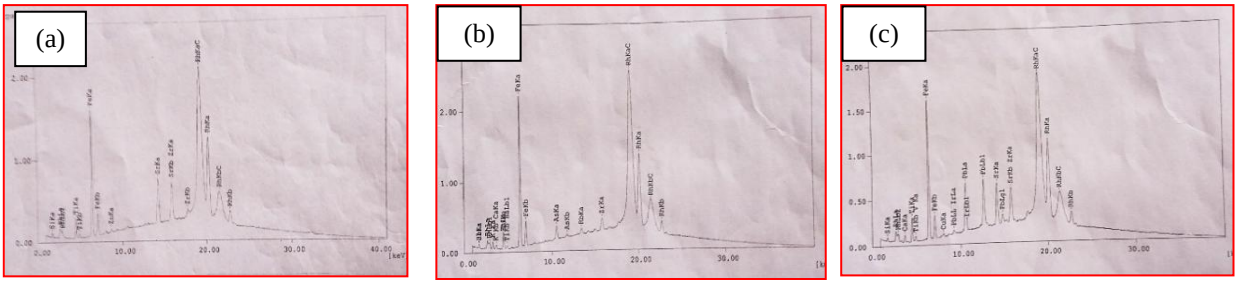

Figure 9 EDXRF spectra of (a) KPT kaolin (b) arsenic loaded kaolin (c) lead loaded kaolin

Table 9 Relative Abundance of Elements Present in KPT Kaolin, Arsenic Loaded Kaolin and Lead Loaded Kaolin

Element	Relative Abundance (%) of Elements		
	KPT Kaolin	Arsenic Loaded Kaolin	Lead Loaded Kaolin
Si	72.04	32.43	53.18
Fe	17.08	37.51	20.08
Ti	7.28	7.81	8.47
Pb	-	-	7.50
As	-	2.33	-
Sr	1.99	-	2.71
Zr	1.28	1.21	1.21

SEM Analysis of Kyauk Pataung Kaolin and Metal Loaded Kaolin Samples

Figure 10 is the SEM micrographs of Kyauk Pataung kaolin, lead loaded kaolin and arsenic loaded kaolin.The SEM micrographs of Kyauk Pataung Kaolin is formed by sheets and every sheet clinged closely to each other. Consequently, Kyauk Pataung kaolin has a large surface area and leads to adsorption of metal ions. After removal of arsenic and lead metal ions with Kayauk Pataung kaolin, arsenic and lead metal ions were adsorbed and filled onto the pores and surface of Kyauk Pataung kaolin and the surface of Kyauk Pataung kaolin was found as platelet shaped by adsorbed metal ions.

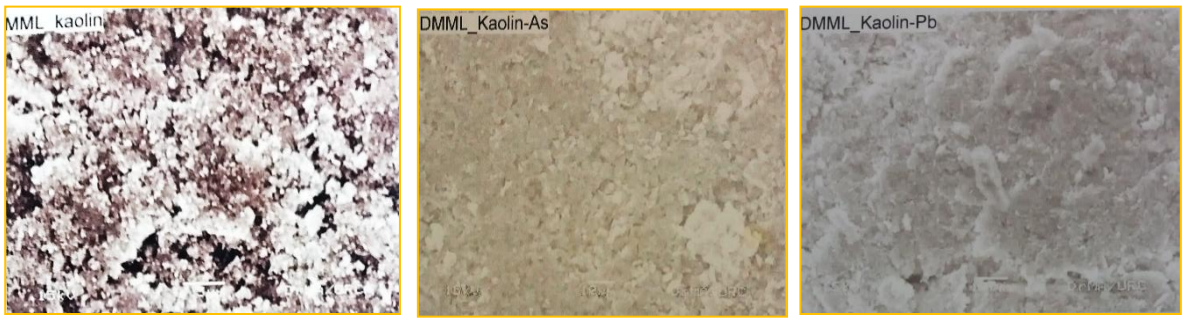

(a) (b) (c)

Figure 10 Scanning electron micrographs of (a) KPT kaolin (b) arsenic loaded kaolin (c) lead loaded kaolin

FT IR Analysis of Kyauk Pataung Kaolin and Metal Loaded Kaolin Samples

FT IR spectra of Kyauk Pataung kaolin, lead loaded kaolin and arsenic loaded kaolin are shown in Figure 11. In IR-spectra of all samples OH-stretching modes lie in the spectral region of 3619-3700 cm^{-1}. Si-O stretching modes are found in the 1004- 1028 cm^{-1} range. O-H deformation of inner hydroxyl modes occur in the 908-912 cm^{-1} region. OH deformation linked to metal modes are found in the 684-789 cm^{-1} range (Paul and Daniel, 2013).

(a) (b) (c)

Figure 11 FTIR spectra of (a) KPT kaolin (b) arsenic loaded kaolin (c) lead loaded kaolin

Conclusion

KPT Kaolin sample was found to remove 97.29 % of arsenic and 95.08 % of lead under the optimum conditions of dosage 2 g, pH 5-7, contact time 12 h and initial concentration of 100 ppm. The KPT kaolin, arsenic loaded kaolin and lead loaded kaolin were characterized by modern techniques such as EDXRF, SEM and FT IR analyses. The EDXRF spectra showed the presence of As in arsenic loaded KPT kaolin and Pb in lead loaded KPT kaolin. It confirmed that KPT kaolin could remove the arsenic and lead. The SEM micrographs of Kyauk Pataung Kaolin after removal of arsenic and lead showed that arsenic and lead were adsorbed onto the pores of Kaolin and the surface of KPT kaolin was found as platelet shaped. From the FT IR spectra of KPT kaolin, arsenic loaded KPT kaolin and lead loaded KPT kaolin were observed the corresponding functional groups. Therefore, Kyauk Pataung Kaolin can be used as effective adsorbent for the removal of heavy metals (arsenic and lead) from groundwater.

Acknowledgements

The authors are thankful to Chemistry Post-Graduate Steering Committee of Yangon University for their helpful suggestions and advices. Special thanks are extended to the Myanmar Academy of Arts and Science.

References

Alleoni, L.R.F., Silveira, M. L. A. and Guilherme, L. R. G. (2003). "Biosolids and Heavy Metals in Soil", *Scientia Agricola*, vol. 30 (4), pp. 793–806

Alloway B.J. (2013). *Heavy Metals in Soils, Trace Metals and Metalloids in Soils and their Bioavailability, Environmental Pollution*, vol. 22, pp. 3-9

Castro, G. M. I. and Mendez, A. M. (2008). *Heavy metals: Implications associated to fish consumption, Environmental Toxicology & Pharmacology*, vol. 26, pp. 263-271

Ekosse G. (2010). "Kaolin deposits and Occurrences in Africa: Geology, Mineralogy and Utilization", *Appl. Clay Sci.*, vol. 50, pp. 212-236

Irshad, A., Weqar A., Samiullah Q. and Tokeer A. (2017). "Synthesis and Characterization of Molecular Imprinted Nanomaterials for the Removal of Heavy Metals from Water", *Journal of Materials Research and Technology*, vol. 6, pp. 12-18

Matta, G., Srivastava, S., Pandey, R. R. and Saini, K. K. (2015). "Assessment of Physicochemical Characteristics of Ganga Canal water quality in Uttarakhand," *Environment development and Sustainability*, vol. 24, pp. 9-24

Mefire, A.N., Njoya A., Fouateu R. Y., Mache J. R., Tapon N.A. and Nzeugang A. N. (2015). "Occurrences of kaolin in Koutaba: Mineralogical and Physicochemical Characterization for Use in Ceramic Products", *Clay Miner*, vol. 50 (5), pp. 593 – 606

Missana T. and Garcia, M. G. (2007). "Adsorption of bivalent ions (Ca(II), Sr(II) and Co(II) onto FEBEX Bentonite", *Physics and Chemistry of the Earth*, vol. 32, pp. 559–567

Morais, S, Costa, F. G. and Pereira. M.L. (2012) "Heavy metals and Human Health, in Environmental Health – emerging Issues and Practice", *Oosthuizen J. ed*., vol. 26, pp. 227–246

Murray H. H. (2007). *Applied Clay Mineralogy. Occurrences, Processing and Application of Kaolins, Bentonites, Palygorskite–Sepiolite, and Common Clays*, 1st ed. Elsevier, Oxford, pp. 189-191

Paul, D. and Daniel, N. (2013) "FT-IR Spectroscopy Applied for Surface Clays Characterization", *Journal of Surface Engineered Materials and Advanced Technology*, vol. 3, pp. 275-282

Pino, G. H., Mesquita, L. M. S., Torem, M. L. and Pinto, G. A. S. (2005). *Proceedings of Processing and Disposal of Minerals Industry Wastes*, vol. 17, pp. 12–15

Pohl, H.R., Roney, N., Wilbur, S. and Hansen, H. (2003). *Six Interaction Profiles for Simple Mixtures, Chemosphere*, vol. 53, pp. 183–197

Samantroy, S., Mohanty, A.K. and Misra, M. (1997). "Removal of Hexavalent Chromium by Kendu Fruit Gum Dust", *Journal of Applied Polymer Science*, vol.66, pp.1485-1494

Ulmanu, M., Anger, I., Lakatos, J. and Aura, G. (2003). *The First International Conference on Environmental Research and Assessment*, vol. 5, pp. 185-192

Vaculíkova L., Plevova, E., Vallova, S. and Koutník I. (2011). "Characterization and Differentiation of Kaolinites from Selected Czech Deposits Using Infrared Spectroscopy and Differential Thermal Analysis", *Acta Geodyn. Geomater*, vol. 8 (161), pp. 59–67

Yakun, Z., Liangguo, Y., Weiying, X. and Xiaoyao, G. L. (2014). "Adsorption of Pb (II) and Hg (II) from Aqueous Solution using Magnetic $CoFe_2O_4$-Reduced Graphene Oxide", *Journal of Molecular Liquids*, vol. 25, pp.177–182

SYNTHESIS OF GOLD-SILVER BIMETALLIC NANOPARTICLES (AU-AG NPs) AND STUDY ON ITS APPLICATION

Tin Moe Swe[1], Khin Aye May[2], Khin Than Yee[3]

Abstract

In this study, gold-silver bimetallic nanoparticles (Au-Ag NPs) were synthesized by reduction of different volumes of silver nitrate ($AgNO_3$) and chloroauric acid ($HAuCl_4$) using 1 % w/v chitosan solution as reducing agent. The existence of nanoparticles in colloidal solution was confirmed by Tyndall effect. From the UV-vis spectra, the maximum absorptions of Au-Ag NPs were observed at the wavelengths of 479-562 nm which confirms the characteristic of nanoparticles. The antimicrobial activities of nanoparticles against the organisms were evaluated by agar well diffusion method. Based on the results of UV-vis spectroscopy and antimicrobial activities, sample (Au-Ag NPs 2) was chosen and characterized by XRD, FT IR and EDXRF analyses. XRD spectral data indicated that the selected sample was crystalline nature with nanosizes. The corresponding functional groups and the relative abundance of elements in nanoparticles were observed from FT IR and EDXRF analyses. The application of selected sample was also studied in biomedical field especially burn wound healing compared with standard sofratu drug. It was found that bimetallic nanoparticles (Au-Ag NPs 2) was better than sofratu for healing of burn wound with well-developed sebaceous glands, sweat glands and hair follicles in epidermis layer of skin. This research therefore contributes to academics as well as biomedical application.

Keywords : Chitosan, gold-silver bimetallic nanoparticles, antimicrobial activity, burn-wound healing

Introduction

Alloying of metals is a way of developing new materials that have better technological usefulness than their starting substances. Bimetallic nanoparticles (BMNPs) have excelled monometallic nanocrystals owing to their improved electronic, optical and catalytic performances (Ramos *et al.,* 2010). Gold-silver alloy nanoparticles might have additional biomedical applications because of their distinct optical properties ranging from visible to the near- IR wavelength region. BMNPs often improve the selectivity of metal catalyzed reactions. They show better stability, selectivity and catalytic activity over monometallic nanoparticles (Shah *et al.,* 2012). Bimetallic nanoparticles as catalysts can carry out certain chemical conversions that were unexampled with monometallic nanoparticles as catalyst. This is because bimetallic nanoparticles have a certain combination of two metals wherein each performs a particular function to carry out the overall reaction mechanism (Mandal and Sastry, 2014).

Bimetallic nanoparticles have promising usage in field of nanomedicine. Tunable chitosan-capped spiky urchin like gold-silver bimetallic nanoparticles (Au-Ag NPs) created via single reactor synthesis process, when targeted against cancer in photothermal cancer therapy gave promising results in ablating cancer cells. Bimetallic can be effectively used in drug delivery as they have high surface area to volume ratio, hence can cross blood-brain barrier and epithelial cell junction to reach target site. These bimetallic nanoparticles, due to their excellent electrical and optical properties can be used as biosensors. Bimetallic nanoparticles are of great importance in restitution of environment (Matti *et al*., 2012).

[1] Candidate, 4PhD, Department of Chemistry, University of Yangon
[2] Associate Professor, Department of Chemistry, Dagon University
3 Lecturer, Department of Chemistry, Myeik University

Bimetallic nanoparticles also serve as great antimicrobials. Bimetallic nanoparticles as antimicrobials can complement the role of antibiotics in combating with bacteria. These nanoparticles can interfere with bacterial growth either by disrupting their membrane or by producing ROS (reactive oxygen species) that cause destruction of DNA and also impede its protein functioning machinery. Au-Ag NPs show antibacterial activity against *Staphylococcus aureus* and *Klebsiella.* These bimetallic nanoparticles showing antibacterial activity can be used in the field of nanomedicine, to form nanodrugs against human pathogens in order to fill the gaps wherein antibiotics failto give positive results (Mazhar *et al*., 2017). Burns are classified as burns by flame, chemical (caused by acids or alkalis), electric high voltage (>1000 mV) and low voltage (< 200 mV), by scalding and by contact. Due to their depth they are divided in first degree that affect only epidermis (sunburn), second superficial degree that affect epidermis and papillary dermis, second deep degree that affect epidermis and reticular dermis and third degree or total thickness that affect the three layers of the skin and muscles. (Garcia-Espinoza *et al*., 2017). This study is aim to synthesize and characterize the gold-silver bimetallic nanoparticles and apply on burn wound healing.

Materials and Methods

Materials

Commercial chitosan sample from shrimp shell was purchased from Asian Technology Groups Co., Ltd., Local Industry, Yangon, Myanmar. All other chemicals used were of analytical reagent grade. In all investigations, the recommended standard methods and techniques involving both conventional and modern methods were provided.

Synthesis of Gold-Silver Bimetallic Nanoparticles (Au-Ag NPs)

Gold-silver bimetallic nanoparticles (Au-Ag NPs) were prepared using chitosan solutions (1% w/v) as reducing agents as well as stabilizing agents. 50 mL of 1% (w/v) chitosan solution was heated to 80 ± 3 ºC. Five samples of bimetallic gold-silver nanoparticles were prepared by adding equal volumes of 0.01 M silver nitrate and 0.001 M chloroauric acid (2 mL, 10 mL, 20 mL, 25 mL and 50 mL) in 50 mL of 1 % w/v chitosan solution. These samples were assigned as Au-Ag NPs 1 to 5.

Characterization of Prepared Gold-silver Bimetallic Nanoparticles

The prepared gold-silver bimetallic nanoparticles (Au-Ag NPs 1-5) were characterized by Tyndall effect, UV-vis spectroscopy, XRD analysis, FT IR, EDXRF and investigated their antimicrobial properties. Biomedical application of gold-silver bimetallic nanoparticle (Au-Ag NPs 2) was carried out.

Application of Gold-Silver Bimetallic Nanoparticles on Burn Wound Healing

A total of 3 male Wistar rats strain were used for making the burn wounds.

The wounded animals of three Wistar rats were divided into three groups. The group A used as negative control (without any treatment), group B was dressed with sofratu (standard drug) and an elastic bandage. For the group C, the burns were dressed by Au-Ag NPs 2. The progress of burn wounds of each rat were recorded by taking photographs after 3, 7, 14 and 20 days. The skins of each rat at 20 days were taken to study the histopathological finding.

Results and Discussion

Tyndall Effect

The reduction of silver nitrate and chloroauric acid to gold-silver bimetallic nanoparticles (Au-Ag NPs) were performed at 80 °C for 1 h with continuous stirring by using chitosan as reducing agent and stabilizing agent. The presence of nanoparticles in solutions was detected by using laser beam as Tyndall effect. The scattering of laser beam through solution indicated the presence of nanoparticles. Tyndall effects on gold-silver bimetallic nanoparticles are shown in Figure 1.

Au-Ag NPs 1 Au-Ag NPs 2 Au-Ag NPs 3 Au-Ag NPs 4 Au-Ag NPs 5

Figure 1 Tyndall effect on gold-silver bimetallic nanoparticles

Analysis of Gold-silver Bimetallic Nanoparticles by UV-vis Spectroscopy

The prepared Au-Ag NPs samples were subjected to UV-visible spectrophotometer and recorded the spectra. Figures 2 shows UV-visible spectra of Au-Ag NPs 1, 2, 3, 4 and 5. The maximum absorption peaks were observed at 479 nm to 562 nm for Au-Ag NPs which correspond to the wavelengths of surface plasmon resonance (SPR) of Au-Ag NPs. These results are in agreement with the various reports (Zhang *et al.,* 2007). The wavelengths of maximum absorption of prepared Au-Ag NPs are summarized in Table 1.

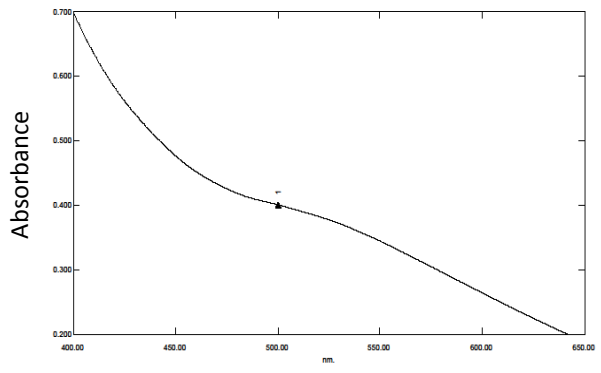

Au-Ag NPs 1

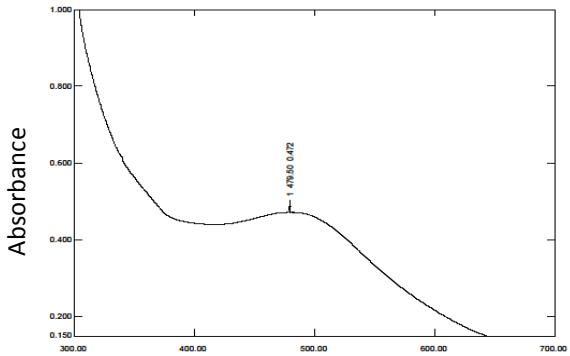

Au-Ag NPs 2

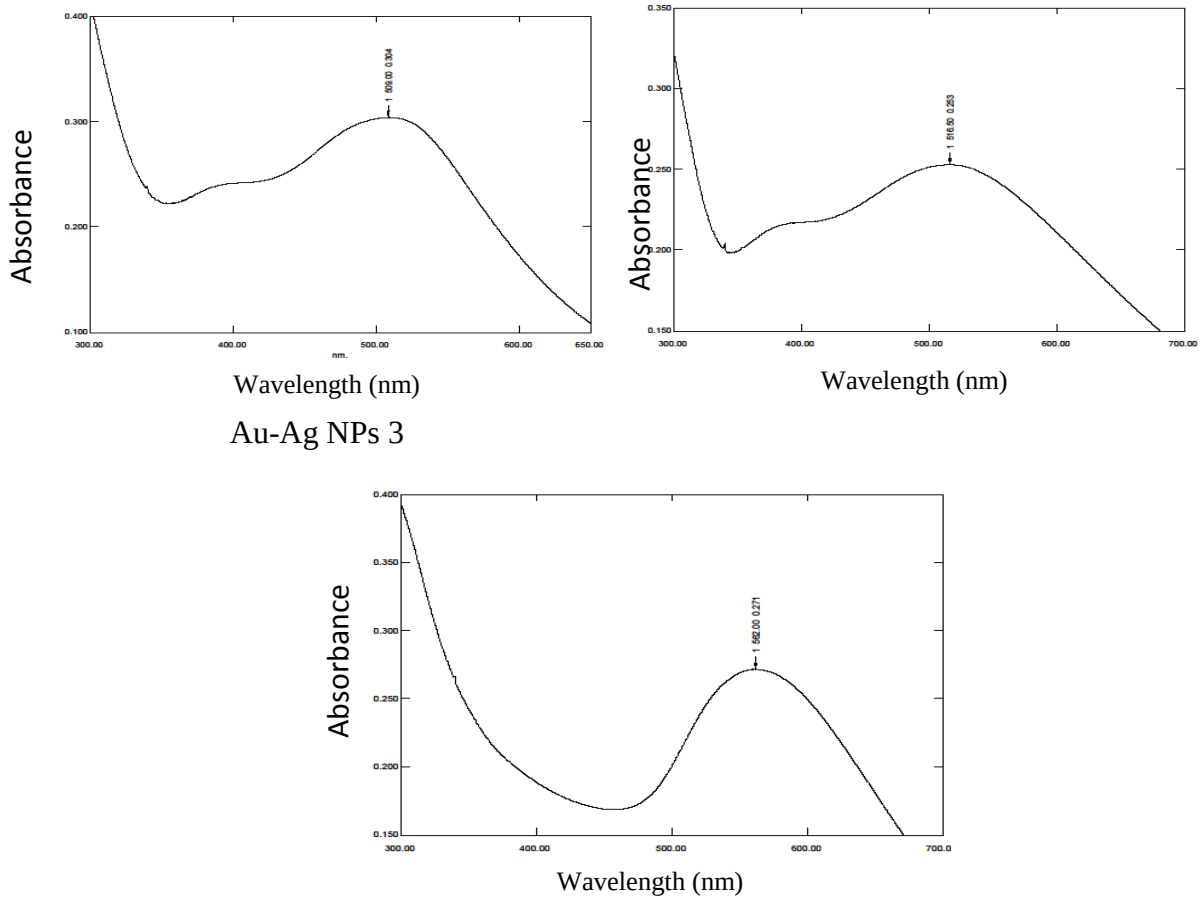

Figure 2 UV-vis spectrum of gold-silver nanoparticle in colloidal solution

Table 1 Wavelengths of Maximum Absorption of the Prepared Gold-silver Bimetallic Nanoparticles (Au-Ag NPs)

Au-Ag NPs	Observed wavelengths of maximum absorption (nm)	Literature value (nm)
1	-	
2	**479**	
3	509	*396-524
4	516	
5	562	

* Zhang *et al.*, 2007

Antimicrobial Activities of Gold-silver Bimetallic Nanoparticles (Au-Ag NPs)

Screening of antimicrobial activities of Au-Ag NPs were evaluated against with different strains of microorganisms by agar well diffusion method. The antimicrobial activities of Au-Ag NPs nanoparticles are shown in Figure 3 and the results are summarized in Tables 2. According to the results, gold-silver bimetallic nanoparticles Au-Ag NPs 1 to 5 showed active to all tested microorganisms. Based on the results of UV-visible spectroscopy and antimicrobial tests, Au-Ag NPs 2 was chosen for the treatment of burn would healing because the maximum wavelength of Au-Ag NPs 2 is more similarly with the literature values.

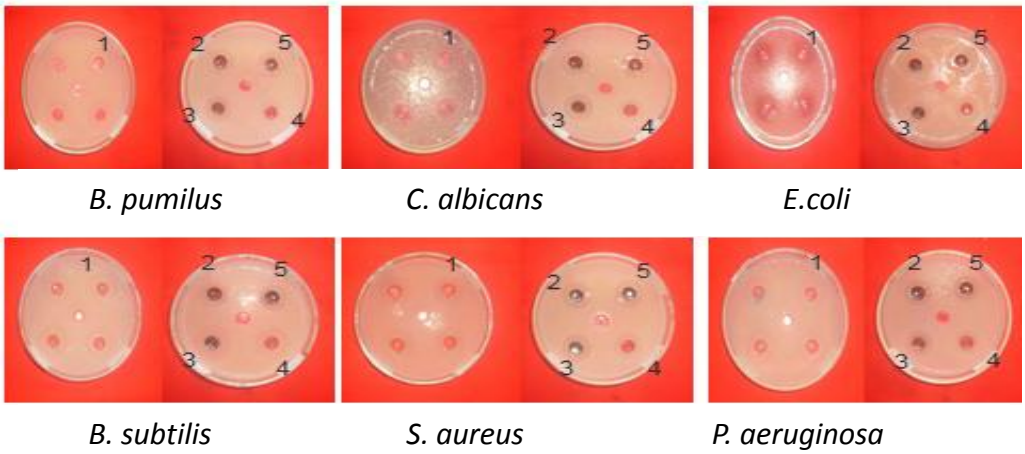

Figure 3 Antimicrobial Activities of gold-silver bimetallic nanoparticles (Au-Ag NPs 1-5)

Table 2 Antimicrobial Activities of the Prepared Gold-silver Bimetallic Nanoparticles (Au-Ag NPs 1-5) against Six Microorganisms

Au-Ag NPs	Inhibition Zone Diameters (mm)					
	B. subtilis	***S. aureus***	***P. aeruginosa***	***B.pumilus***	***C.albicans***	***E. coli***
1	13 (+)	17 (++)	20 (+++)	13 (+)	11 (+)	14 (+)
2	18 (++)	18 (++)	17 (++)	18 (++)	18 (++)	17 (++)
3	18 (++)	18 (++)	16 (++)	18 (++)	18 (++)	18 (++)
4	12 (+)	15 (++)	17 (++)	17 (++)	17 (++)	17 (++)
5	17 (++)	17 (++)	20 (+++)	19 (++)	18 (++)	17 (++)

Agar well – 10 mm, 10 mm ~ 14 mm (+), 15 mm ~ 19 mm (++), 20 mm above (+++)

X-ray Diffraction Analysis

Structural characterization had been performed using XRD analysis and the XRD diffractogram of Au-Ag NPs 2 is illustrated in Figure 4. The lattice parameters of XRD patterns and calculated average crystallite sizes using Scherrer formula are described Table 3. X-ray diffraction pattern of Au-Ag NPs 2 showed the number of Bragg's reflection angles (2θ) 36.213, 44.385 and 64.783 corresponding to planes 111, 200 and 220 respectively, peats were matched with fcc structure and showed the crystalline nature. These results were compared with the literature and found to be matched. The mean crystallite size of Au-Ag NPs 2 was12.91 nm.

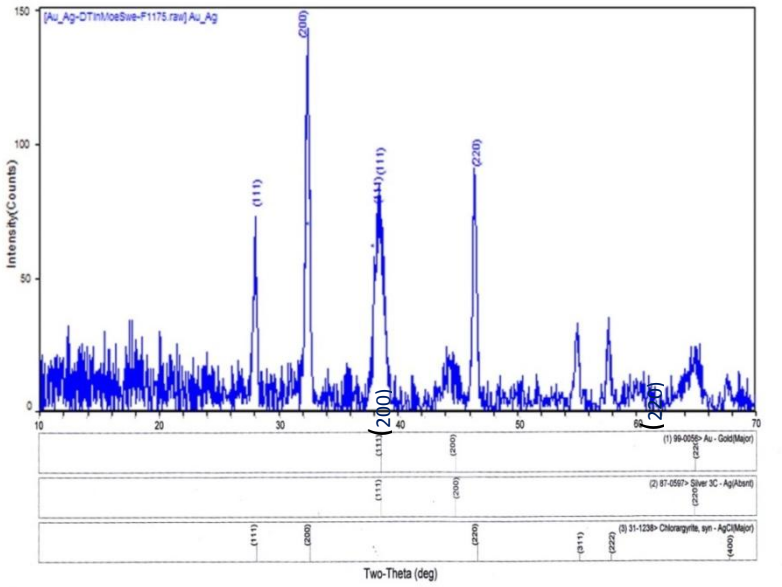

Figure 4 X-ray diffractogram of gold-silver bimetallic nanoparticles (Au-Ag NPs 2)

Table 3 Lattice Parameters of Gold-silver Bimetallic Nanoparticles (Au-Ag NPs 2)

2-Theta (°)	d (Å)	(h k l)	Peak area (%)	Phase ID	FWHM	Crystallite size (nm)
32.421	2.7592	(2 0 0)	80.2	AgCl	0.338	25.6
38.213	2.3533	(1 1 1)	90	Ag	0.775	10.9
38.409	2.3417	(1 1 1)	100	Au	0.714	11.9
44.385	2.0378	(2 0 0)	31.4	Ag	0.728	12.2
44.405	2.0384	(2 0 0)	31.5	Au	0.725	12.0
46.371	1.9565	(2 2 0)	68.5	AgCl	0.398	4.3
64.783	1.3845	(2 2 0)	29.2	Au	0.699	13.6
64.778	1.3853	(2 2 0)	29.1	Ag	0.689	12.8
Average Crystallite size						12.91

Fourier Transform Infra Red Spectrpscopy (FT IR)

Fourier transform infra-red spectroscopy of Au-Ag NPs 2 was performed to study the interaction of bimetallic gold-silver nanoparticles with that of chitosan. The respective spectrum is presented in Figure 5. The band assignments of this sample is expressed in Table 4. All spectra exhibited the functional groups of chitosan. The band appearing at 3446 cm^{-1} correspond to stretching vibration of NH. The bands nearly 1630 cm^{-1} were due to the stretching of C=O of amide group. This C=O functional group may be due to the presence of chitin left in the chitosan (incomplete the deacetylation step in synthesis of chitosan from chitin). The stretching of C-C group appears at 1540 cm^{-1}. The stretching of C-O bond observed at nearly 1400 cm^{-1}. The results indicated that chitosan may have the ability to perform reducing agent as well as capping agent.

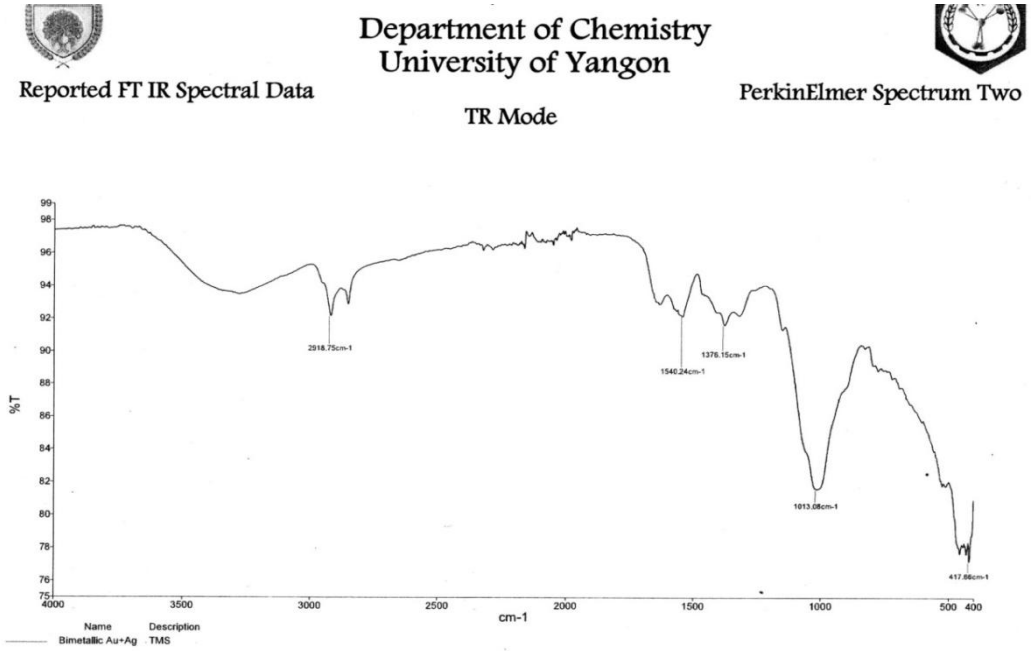

Figure 5 FT IR spectrum of gold-silver bimetallic nanoparticles (Au-Ag NPs 2)

Table 4 FT IR Spectral Assignment for Gold-silver Bimetallic Nanoparticles (Au-Ag NPs 2) using Chitosan Solution as Reducing Agent

Observed wave number (cm^{-1})	*Literature wave number (cm^{-1})	Band assignment
3446	3200-3600	-OH stretching and N-H stretching
2875	2800-2950	C-H stretching
1633	1560-1650	C=O stretching of amide
1540	1550-1600	C-C stretching
1384	1315-1441	C-O stretching

*(Silverstein and Basseler, 1967)

Energy Disperse X-ray Florescence (EDXRF)

EDXRF technique was used for the determination of relative abundance of elements present in samples. The film form of selected sample (Au-Ag NPs 2) was conducted with EDXRF analyses. Ag, Au elements (15.093 % Ag and 10.325 % Au in Au-Ag NPs 2) was detected (Figure 6). Calcium was attributed from commercial chitosan used which may be incomplete demineralization in chitosan production.

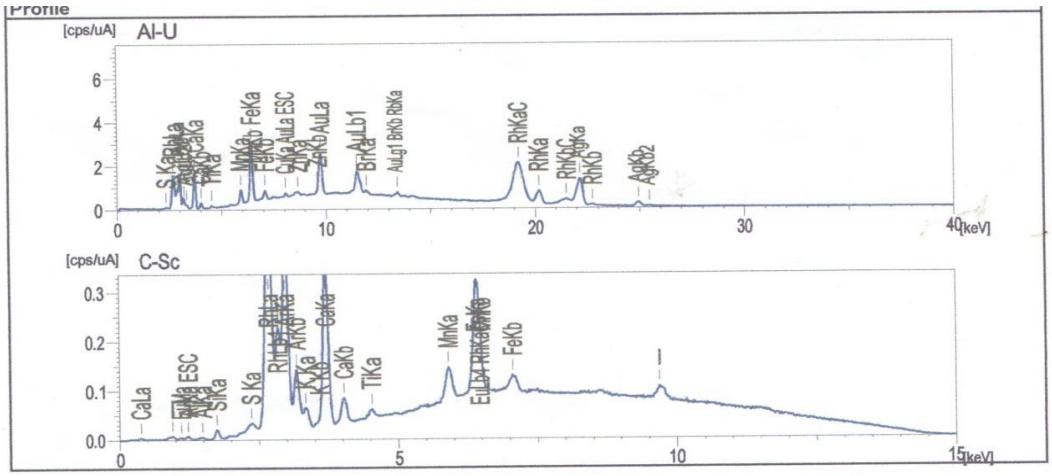

Figure 6 EDXRF spectrum of gold-silver bimetallic nanoparticles (Au-Ag NPs 2)

Biomedical Application of Gold-silver Bimetallic Nanoparticles

The biomedical application of prepared gold-silver bimetallic nanoparticles (Au-Ag NPs 2) was studied by animal experiment. The step by step making of burn wound are illustrated in Figure 7. The burn skins of rat were treated with gold-silver bimetallic nanoparticles and standard drug (Sofratu). The progress of these burned skins were recorded by photo at specific time intervals in DMR. The photograph of progression of burn skins treated with Sofratu and Au-Ag NPs 2 are shown in Figures 8 and 9.

(a) Injected the chloroform and ringer solution (b) Fleeced the blade (c) Heated the iron stick at 100˚C

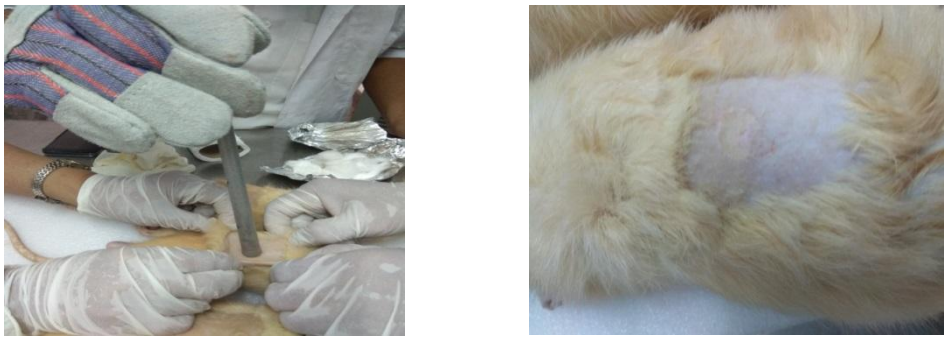

(d) The iron stick tough the skin for 20s (d) Burn-wound

Figure7 Making the burn wound on rat model

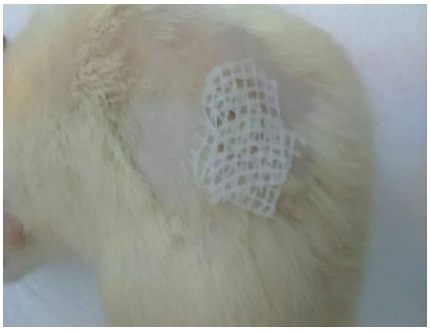

(a) Treated with standard drug (Sofratu)

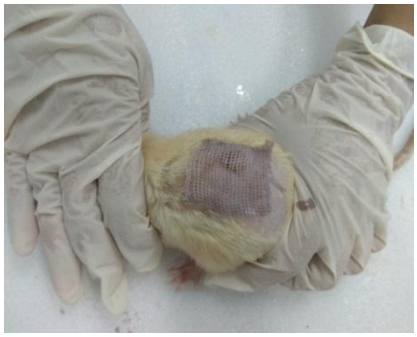

(b) Treated with Au-Ag NPs 2

Figure 8 The physical appearance of skin leaching of rats covered with standard sofratu and Au-Ag NPs 2

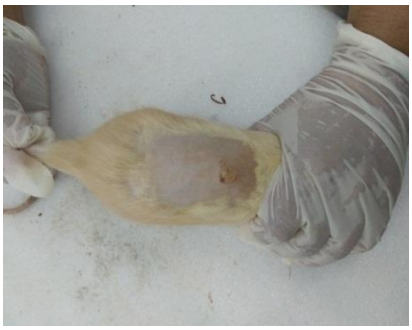

(a) Negative Control

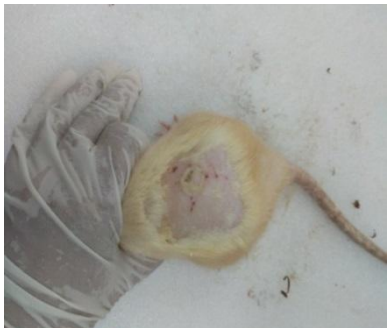

(b) Control Sofratu

(c) Au-Ag NPs 2 (3-Days)

(a) Negative Control

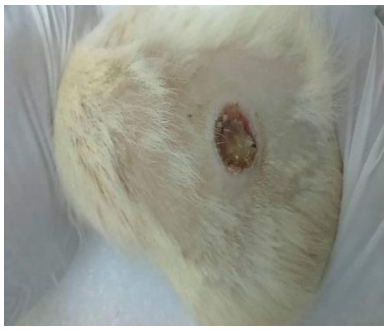

(b) Control Sofratu

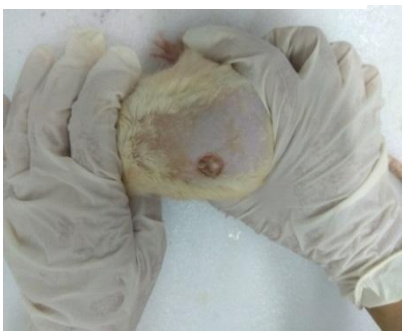

(c) Au-Ag NPs 2 (7-Days)

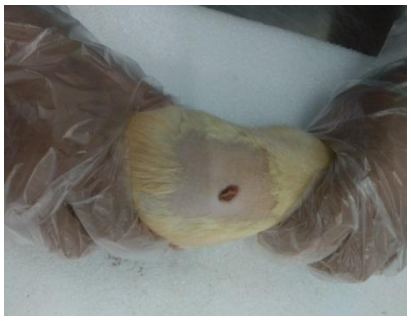

(a) Negative Control

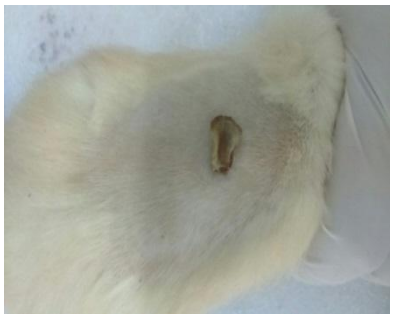

(b) Control Sofratu

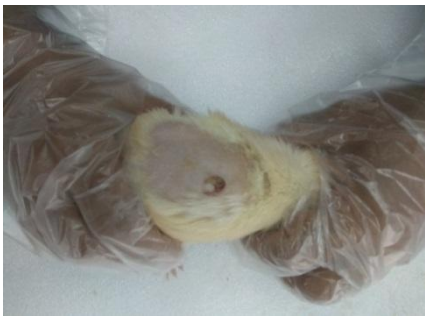

(c) Au-Ag NPs 2 (14-Days)

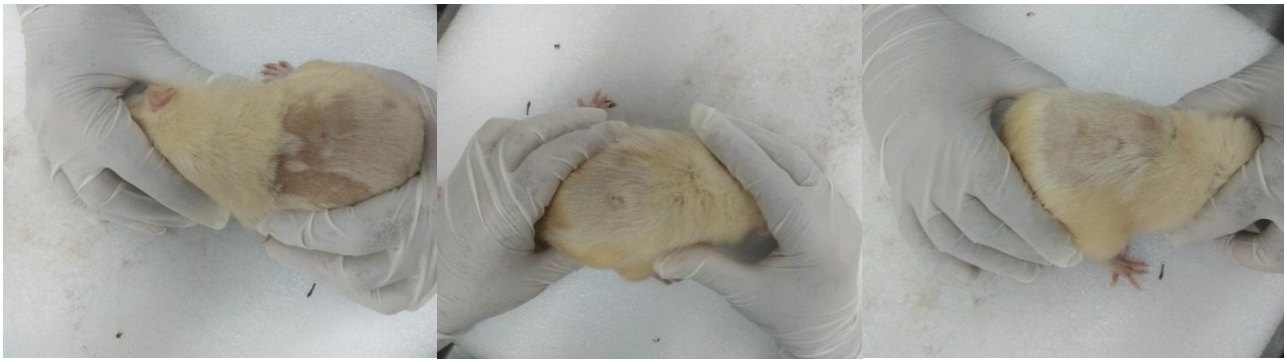

(a) Negative Control (b) Control Sofratu (c) Au-Ag NPs 2 (20-Days)

Figure 9 The physical appearences of burned skin after treatment by using standard sofratu and Au-Ag NPs 2 on 3, 7, 14 and 20 days

Histopathological finding of treated and control burned skin

Since the physical appearance changes of skin on visual is not enough to decide the efficiency of treated drugs, histopathological finding was carried out. Wound skin tissue samples treated with Sofratu and Au-Ag NPs 2 were taken on days 20 for histological observation. Histological finding of burned wound skins (epidermis and dermis) treated with Sofratu and Au-Ag NPs 2 are presented in Figure 10. This finding indicated that Au-Ag NPs 2 was better than Sofratu drug to use in burn wound healing because the skin treated with Au-Ag NPs 2 exhibited well developed granulation tissue in both epidermis and dermis layers.

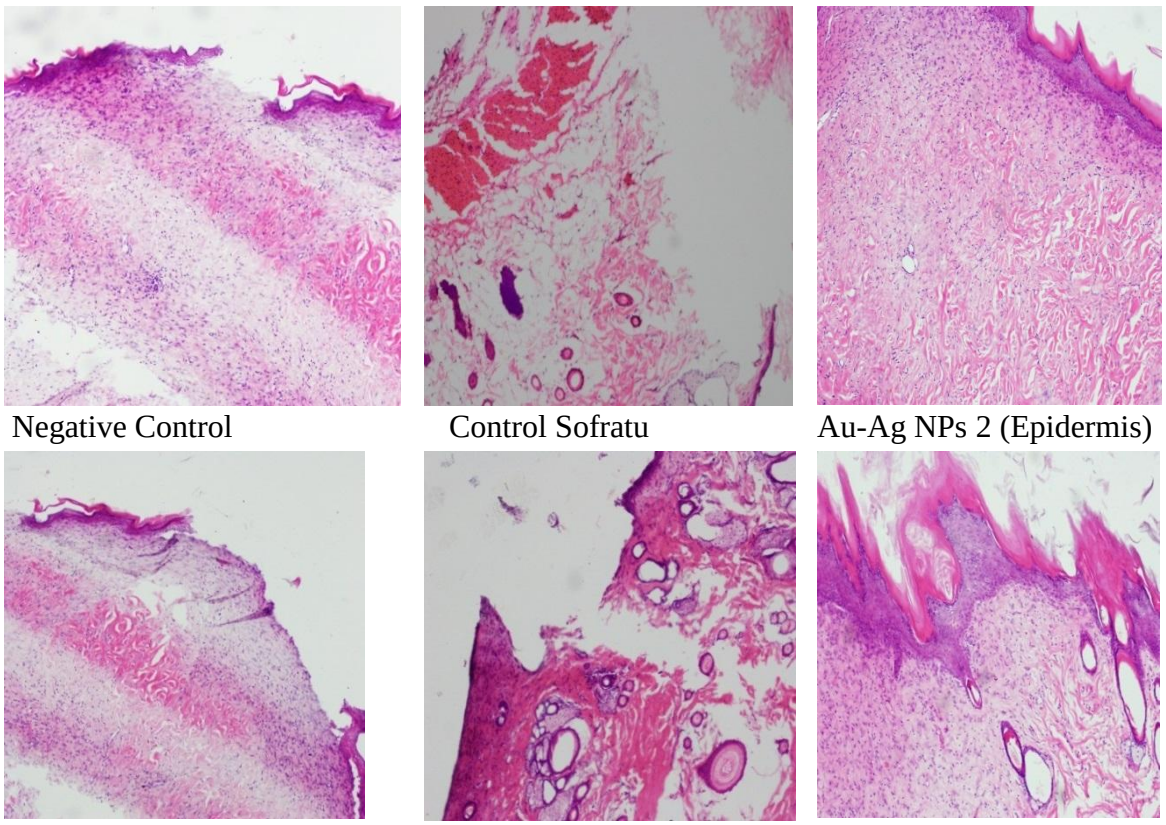

Negative Control Control Sofratu Au-Ag NPs 2 (Epidermis)

Negative Control Control Sofratu Au-Ag NPs 2 (Dermis)

Figure 10 Hematoxyline and eosin-stained section of biopsies for the morphological evaluation of skin lesions of burn skin treated with Standard Sofratu and Au-Ag NPs 2 on days 20

Conclusion

From the overall assessment of the present work, purple colour of gold-silver bimetallic nanoparticles were successfully synthesized. By the Tyndall effect, the laser light scattering indicates the presence of nanoparticles. From the UV-visible spectrum, the maximum absorption wavelengths of prepared gold-silver bimetallic nanoparticles were found to be 479-562 nm. From the results of antimicrobial investigation, all samples of Au-Ag NPs are active to all tested microorganisms. Based on UV-vis spectra and antimicrobial activities, Au-Ag NPs 2 was chosen for treatment of burn wound healing. The X-ray diffractogram of Au-Ag NPs 2 showed the crystalline nature and the average crystallite size was 12.91 nm. The FT IR spectra of selected nanoparticles showed the absorption bands of functional groups of chitosan. It also confirmed that the reducing agents have ability to perform the capping agent. From the EDXRF results, the relative abundance of Ag and Au were found to be 15.09 % Ag and 10.32 % Au in Au-Ag NPs 2. The significant improvement in burn contraction by visually was observed when using Au-Ag NPs 2 on days 20 after burning. Histopathological finding under microscope also reported that the skin treated with Au-Ag NPs 2 exhibited good wound healing and well developed granulation tissue composed of sebaceous glands, sweat gland and follicles in epidermis and dermis layers. From the results, bimetallic nanoparticle can be used effectively in treatment of burned skin.

Acknowledgement

The authors would like to thank Professor and Head, Dr Daw Ni Ni Than, Department of Chemistry, University of Yangon, for the permission of doing this research and allowing the writing of this paper. Special thanks are extended to Universities' Research Centre, University of Yangon. I would like to express my deep appreciation to Dr Aye Win Oo, Head and Research Officer, Laboratory Animal Services Division, Department of Medical Research (Lower Myanmar), providing the facilities and helpful advice through the course of burn-would healing test.

References

Garcia-Espinoza, J. A., Aguilar-Aragon, V. B., Orliz-Villalobos, E. H., Garcia-Manzano, R. A. and Antonio, B. A. (2017). "Burn: Definition, Classification, Pathophysiology and Initial Approach". *General Medicine: an open access Journal,* vol. 5(5), pp. 1-5

Mandal, A. and Sastry, T.P. (2014). "Fabrication of Gelatin Based Composites Containing Bimetallic Ag-Au Nanoparticles for Biomedical Applications". *IJRSET*, vol. 3(5), pp. 12463-12472

Matti, M., Schooneveld, C. V., Carlos, C., Pet, J., Meeldijk, D., Rijissel, J. V., Meijerink, A., Erne, B. H. and Groot, F. M. F. (2012). "Composition Tunable Cobalt-Nickel and Cobalt-Iron Alloy Nanoparticles Below 10 nm Synthesized Using Acetonated Cobalt Carbonyl". *J Nanopart Res.*, vol. 14 (991), pp.1-13

Mazhar, T., Shrivastava, V. and Tomar, R. S. (2017). "Green Synthesis of Bimetallic Nanoparticles and its Applications: A Review". *Journal of Pharmaceutical Sciences and Researh,* vol. 9 (2), pp. 101-110

Ramos, M., Ferrer, D.A., Chianelli, R.R., Correa, V., Matos, J.S. and Flores, S. (2010). "Synthesis of Ag-Au Nanoparticles by Galvanic Replacement and Their Morphological Studies by HRTEM and Computational Modeling". *Journal of Nanomaterials*, vol. 20(11), pp. 1-5

Silverstein, R. M. and Basseler, G. C. (1967). "Spectrometric Identification of Organic Compounds; Ch-4". New York: Willey and Sons

Shah, A., Rahman, L., Qureshi, R. and Rehman, Z. (2012). "Synthesis, Characterization and Applications of Bimetallic (Au-Ag, Au-Pt, Au-Ru) Alloy Nanoparticles". *Rev. Adv. Mater. Sci*., vol. 30, pp. 133-149

Zhang, Q., Lee, J.Y., Yang, J., Boothroyd, C. and Zhang, J. (2007). "Size and Composition Tunable Ag-Au Alloy Nanoparticles by Replacement Reaction". *Nanotechnology*, vol. 18, pp. 1-8

PREPARATION AND CHARACTERIZATION OF JUTE FIBER REINFORCED COMPOSITE

Kyi Win Mon[1], Thinzar Nu[2], Hnin Yu Wai[3]

Abstract

This research work is mainly concerned with the preparation of composite from 5 % NaOH modified waste jute fiber with epoxy resin as binder and the study of their characteristics. Jute fiber (JF) and epoxy resin (E) were collected from Yangon Region and this research was done at Polymer Research Department, Department of Research & Innovation (DRI), Yangon. Composites were prepared by mixing 5 % NaOH modified waste jute fiber (120 g) with various amounts (5 %, 10 %, 15 %, 20 %, 25 % and 30 %) of epoxy resin (E) using cold compressing method at 2300 psi. The prepared composites were characterized by physicochemical and physicomechanical parameters such as modulus of rupture (MOR), thickness, density, water absorption, swelling thickness as well as hardness. From the results obtained, it was found that 5 % NaOH modified waste jute fiber (120 g) with 20 % epoxy resin (E), namely (JFE 4) composite was the best quality grade composite. It possesses 1248.20 psi modulus of rupture, 0.60 cm thickness, 1.2320 g cm^{-3} density, 14.18 % water absorption, 23.35 % swelling thickness, and 68 D hardness. JFE 4 composite based on physicomechanical properties, the composite showed to possess the highest modulus of rupture value indicating that this composite was the most significant and the best among all the composites. The FT IR study confirmed the presence of cellulose, hemicellulose and lignin. In addition, Simultaneous Thermal Analyzer (STA) confirmed that the sample was thermally stable till 200 ˚C on account of the high complex structure of lignin. The melting point of composite was round about 400 ˚C studied by Simultaneous Thermal Analyzer. The surface roughness value of JFE 4 composite was 900 nm studied by Atomic Force Microscopy. The present research on making composite from waste materials can contribute to the solution of the earth's escalating environmental problems.

Keywords: Jute composite, jute fiber, epoxy resin, modulus of rupture

Introduction

The production of lignocellulose fibers-based polymer composites has become in recent years an important application for recovering, reuse and recycling a variety of by-products related to industrial exploitation of natural resources. Lignocellulose materials (wood fibers, wood flour, and agro-residues) are attractive fillers for thermoplastic polymers mainly because of their low cost and large availability. According to their botanical source, these renewable materials present large variations in their composition. Main elements are cellulose, hemicelluloses and lignin which are known to present a very complex structure (Ruxanda *et al*., 2009).

The use of natural fiber from both resources, renewable and non-renewable such as oil palm, sisal, flax, and jute to produce composite materials, gained considerable attention in the last decades, so far. The plants, which produce cellulose fibers can be classified into bast fibers (jute, flax, ramie, hemp, and kenaf), seed fibers (cotton, coir, and kapok), leaf fibers (sisal, pineapple, and abaca), grass and reed fibers (rice, corn, and wheat), and core fibers (hemp, kenaf, and jute) as well as all other kinds (wood and roots) (Faruk *et al*., 2012).

[1] 2 PhD Candidate, Department of Chemistry, University of Yangon
[2] Dr, Associate Professor, Department of Chemistry, University of Yangon
[3] Dr, Lecturer, Department of Chemistry, University of Yangon

Jute fiber is a promising reinforcement for use in composites on account of its low cost, low density, high specific strength and modulus, no health risk, easy availability, renewability and much lower energy requirement for processing. The jute fiber is an important bast fiber and comprises bundled ultimate cells, each containing spiral oriented micro- fibrils bound together (Debiprasad *et al*., 2012).

Wood fibers offer a number of advantages over the currently used reinforcing inorganic materials (e.g., glass fibers) in terms of cost on a unit volume basis, as well as flexibility during processing. Wood modification can change important properties of the wood, including biological durability, dimensional stability, hardness and Ultraviolet stability by converting hydrophilic OH-groups into larger, more hydrophobic groups. Specific wood modification processes designed for the production of wood-plastic composites may be developed having in view the properties of the wood component in the composites, but also the improved, e.g., by means of grafting processes (Ruxanda *et al*., 2009).

Composites are produced from non-chemical processed using fiber particles mixed with binder. The main objective of composite materials is their high strength and stiffness, combined with low density, when compared with bulk materials, allowing for a weight reduction in the finished part. The availability of natural fiber jutes is much abundant in Asian continent and it provides and advantages over reinforcement materials in terms of cost, density recyclability and biodegradability .Meanwhile Fiber-Reinforced Polymers (FRP) have until now been largely applied to the area of aerospace technology, these construction materials have also been used in many technical applications for achieve required strength (Abilash and Sivapragash, 2013).

In Myanmar, study on preparation and characterization of composite boards derived from natural fibers (sisal fiber) (Na-Nat-Shaw)(Zin Mar Aung, 2008), preparation and characterization of composite (plaster) board derived from renewable resource, non-wood plant fiber (Bagasse) (Myat Myat Nwe, 2008) and Particleboards Derived from Rattan Fiber Waste (Hnin Yu Wai, 2011) in Yangon University was reported. In the preparation of composites, the two main components involved are binder and the other is a fibrous material. The binder plays an important role to obtain good strength of the board and also for low cost products. This research work intends to use the epoxy resin in making composite with an agricultural waste fiber, the jute fiber. The prepared composites were characterized according to the physicochemical and physicomechanical properties as well as Simultaneous Thermal Analyzer and Atomic Force Microscopy analysis.

Materials and Methods

Composites were produced by using 120 g each of waste jute fiber with various concentrations of epoxy resin. This research work intends to use the epoxy resin in making composite with an agricultural waste fibers, more precisely using the jute fiber. The prepared composites were characterized according to the physicochemical and physicomechanical properties as well as Simultaneous Thermal Analyzer and Atomic Force Microscopy analyses. All the experimental procedures involved in this research. All necessary research facilities were provided by the Polymer Research Department, Department of Research and Innovation. All specific chemicals used were described detail in each experimental section. In all the investigations, the recommended and standard procedures of both conventional and modern

techniques were employed. The experiment was carried out in the National Analytical Laboratory, Department of Research and Innovation, Yangon Region.

Collection of Samples

In the experiments, the waste jute fibers collected from (Kyaw Htet Kyaw) company limited and epoxy resin from shine company limited, Yangon Region, Myanmar.

Preparation of Waste Jute Fiber

Raw samples were cut by cutting machine. After cutting, the fiber obtained in size as about 0.5-2.0 cm. The fibers were taken and dried in an oven at 70 ºC.

Preparation of Modification of Waste Jute Fiber

The fibers (*ca*. 400 g) were immersed in 6 L solution of (5 % w/v) NaOH (pH~ 13) for 24 h at room temperature, after which the fibers were washed thoroughly with plenty of water until drained water became neutral. After treatment, they were dried in the sunlight and then in an oven at 70 °C for 3 h.

Physicochemical Properties of Modified Waste Jute Fiber

The physicochemical properties (moisture content, ash content, solubility in hot water, solubility in 1% NaOH) of modified waste jute fiber were determined by conventional methods.

Physicochemical Properties of Epoxy Resin

The physicochemical properties (moisture content, ash content, viscosity, pH, gelation time) of epoxy resin were determined by conventional methods.

Characterization of Waste Jute Fiber and the Modified Waste Jute Fiber

FT IR Analysis

The sample was directly placed on the Spectrum 400 FT IR and FT NIR Spectrometer, diamond plate of Universal Attenuated Total Reflectance (UATR) detector over a 400-4000 cm^{-1}, scanning 5 min and wave number range at a resolution of 4 cm^{-1}.

STA Analysis

Thermal properties were monitored by simultaneous thermal analyzer. The sample (*ca*. 7 mg) was cut and placed in a ceramic crucible. The lid was placed over the sample. The system should be built with SaTurnA™ sensor and measured the temperature range of the system must be 50 °C to 950 °C or better. Temperature accuracy should be ±0.8 °C. The system must cool down less than 15 min. The flow rate of nitrogen gas wast 20.00 mL/min. The prepared modified waste jute fiber was performed by simultaneous thermal analyzer with nitrogen atmosphere.

AFM Analysis

Topography of the surfaces on the molecular scale was investigated by N 8, Rados Atomic Force Microscopy, Bruker, Germany. As the AFM probes the atomic interaction between surfaces, it can also be used to map the adhesion, friction, stiffness or other kinds of interaction such as magnetic or electric forces. In each AFM experiment, several scans were made to check the reproducibility of images and the absence of surface damage. Surface roughness and morphology can be seen and analyzed.

Characterization of Epoxy Resin

FT IR Analysis

FT IR analysis was performed in order to characterize the functional groups of the epoxy resin Perkin-Elmer Spectrum, Thailand was used for FT IR analysis.

STA Analysis

The prepared epoxy resin was performed by Simultaneous thermal analyzer with nitrogen atmosphere.

Preparation of Composites

The composites were fabricated by hand lay-up technique. The inner cavity dimension of the mould is 15.4 cm x 15.4 cm. First of all, a release gel is wiped on the mould surface to avoid the sticking of epoxy resin to the surface. Thin plastic sheets are used at the top and bottom of the mould plate to get a good surface finish of the product. The 5 % sodium hydroxide modified fiber was further with epoxy resin in liquid form was mixed thoroughly in suitable proportion with a prescribed hardener (curing agent) and poured onto the surface of mat already placed in the mould. The epoxy resin was uniformly spread with the help of the brush. Composites of different compositions with constant fiber loading are made. The composites from the cold press were kept at room temperature for 24 h. The prepared composites were cut for testing conforms to the dimensions of the specimen.

Physicochemical and Physicomechanical Properties of Composites

Modulus of Rupture

The composites were cut into pieces (14 cm × 2.54 cm), and modulus of rupture of individual composites was measured by Electro-hydraulic tensile tester according to the procedure. All of the samples were measured at least five references. Two references were taken from one and three references were taken from another of the same ingredient of composites.

Thickness

The composites were cut into pieces (14 cm × 2.54 cm), and thickness of individual composites were measured by veneer clipper at least four points of each bundle.

Water Absorption

The composites to be tested were cut into 2.54 cm × 2.54 cm in size, weighed and placed in a desiccator. Then, the test specimens were immersed in fresh clean water for 24 h. After soaking in water, each test piece was withdrawn from the water, wiped with absorbent paper to remove water on the surface and reweighed to the same degree of accuracy as before. Five replicated specimens of individual composites were tested and the results were presented as average of the tested specimens.

Swelling Thickness

The composites to be tested were cut into 2.54 cm × 2.54 cm in size, the thickness of test pieces were measured and placed in a desiccator. These pieces were immersed in clean water at room temperature. They were covered by approximately 1 inch of water. After 24 h of water soaking, these pieces were removed from water and wiped with absorbent paper to remove water

on the surface and allowed to stand under normal room condition for 2 h. The thickness of each test piece was premeasured with screw gauge and increase was recorded.

Density

The composites to be tested were cut into 2.54 cm × 2.54 cm in size. The length, width and thickness of each test piece were measured to an accuracy of ±0.01 cm. The weight in grams of each test piece was determined to an accuracy of ± 0.01 g.

Hardness

Durometer hardness readings were performed according to ASTM D 2240. The test was carried out by first placing a specimen on a hard, flat surface. The pressure foot of the instrument was pressed on to the specimen, making sure that it was parallel to the surface of the specimen. The durometer hardness was read within one second after the pressure foot was in form contact with specimen. Each specimen was subjected to durometer hardness readings, at designated positions on the sample bases.

Characterization of JFE 4 Composite

STA Analysis

The thermogram of JFE composite was analyzed by simultaneous thermal analyzer.

AFM Analysis

Topography of JFE 4 composite surface and roughness was obtained with the help of Atomic Force Microscope.

Results and Discussion

Table 1 shows that the physicochemical parameters of modified waste jute fiber. It was found that moisture content is 7.83 % , ash content is 3.34 %, solubility in hot water 4.32 % solubility in 1 % NaOH is 26.38 %.

Table 1 Physicochemical Properties of Modified Waste Jute Fiber

Characteristics	Observed Values (%)
Moisture content	7.83
Ash content	3.34
Solubility in hot water	4.32
Solubility in 1 % NaOH	26.38

Physicochemical Properties of Epoxy Resin

Table 2 shows that the physicochemical properties of epoxy. It was found that moisture content is 0.58 %, ash content is 0.88 %, viscosity is 4319 cp, pH is 6.8 and gelation time is 20 min.

Table 2 Physicochemical Properties of Epoxy Resin

Characteristics	Observed Values
Moisture content (%)	0.58
Ash content (%)	0.88
Viscosity (cp)	4319
pH	6.8
Gelation Time (min)	20

Characterization of the Modified Waste Jute Fiber

FT IR Analysis

The FT IR spectrum of modified waste jute fiber shows has especially hydroxyl and carbonyl stretching because of the presence of cellulose shown in Figure1and the description data in Table 3 are given.

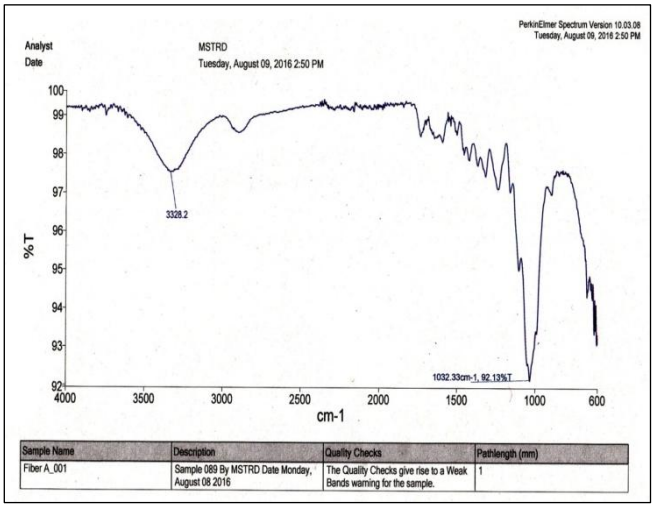

Figure 1 FT IR spectrum of the modified waste jute fiber

Table 3 FT IR Spectral Data of the Modified Waste Jute Fiber

Frequency (cm^{-1})	Band Assignments	Band Assignments
Modified Waste Jute fiber	**Literature ***	
3328	3330-3270	O-H stretching
1032	1320-1000	C=O stretching

* as Win Lab software of FT IR machine

STA Analysis

Simultaneous Thermal Analyzer (STA 6000) is a thermal method that measured the weight loss as a function of temperature or time. The STA scan of waste jute fiber is shown in Figure 2 and the description data in Table 4 are given. In the case of waste jute fiber, 8.03 % of weight loss indicated the evaporation of moisture content evinced by the presence of hydroxyl content in the fibers and other volatile matter. The major weight loss 62.22 % occurs at

365.28 °C. Endothermic peak was observed in the temperature range 200 ºC and 500 ºC that is attributed to the thermo oxidative degradation of cellulose and hemicellulose that takes place by the degradation of its lignin. The weight loss 27.29 % was gradually degraded of lignin by the breakage of its subunits.

The STA scan of the modified waste jute fiber is shown in Figure 3 and the description data in Table 5 are given.The first stage was from about 50 °C to 200 °C. In this stage of temperature, a loss in weight about 4.61 % indicated dehydration due to surface water and moisture. After that the second stage, the loss in weight about 64.61 % was observed at the temperatures range from 200 °C to 500 °C. The thermograph of individually modified waste jute fibers peak was 362.59 °C was degradation of cellulose and hemicellulose. The third stage, loss in weight about 27.69 % at temperature range of 500 °C to 800 °C was decomposition of lignin. Modified waste jute fibers were completely burnt around 462.34 °C.

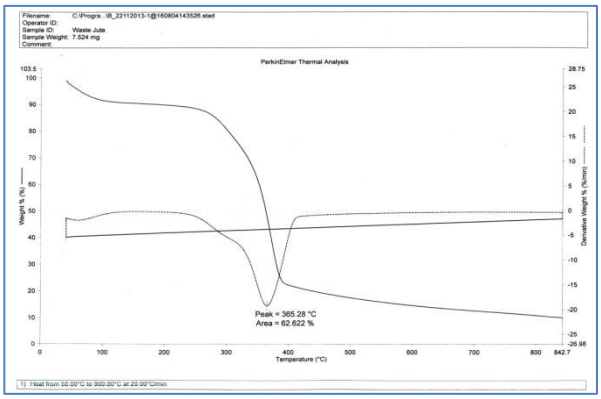

Figure 2 STA thermogram of waste jute fiber

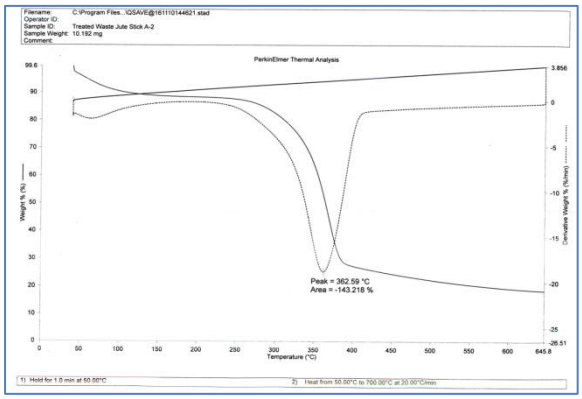

Figure 3 STA thermogram of modified waste jute fiber

Table 4 Thermal Analysis Data of Waste Jute Fiber

Sample	Melting point value (°C)	Temperature range (°C)	Weight loss (%)	Nature of peak	Remarks
Waste Jute fiber	-	50-200	8.03	-	Dehydration due to surface water and moisture content
	365.28	200-500	62.22	endo	Degradation of cellulose and hemicellulose
	-	500-800	27.29	-	Decomposition of lignin of the jute fiber

Table 5 Thermal Analysis Data of the Modified Waste Jute Fiber

Sample	Melting point value (°C)	Temperature range (°C)	Weight loss (%)	Nature of peak	Remarks
Modified waste jute fiber	-	50-200	4.61	-	Dehydration due to surface water and moisture
	362.59	200-500	64.61	endo	Degradation of cellulose and hemicellulose
	-	500-800	27.69	-	Decomposition of lignin of the jute fiber

AFM Analysis

The surface roughness of the waste jute fiber and modified waste jute fiber were also studied using Atomic Force Microscopy. AFM microphotographs of waste jute fiber and the modified waste fiber are shown in Figures 4 and 5 and the description data in Table 6 are given. It was obvious from the image that significant smoothing occur in jute fiber surface. AFM was employed to monitor the topological changes of the heterogeneous surface morphologies and the roughness of waste jute fiber. A cantilever with a sharp force sensing tip interacted with the surface. The vertical position of the scanner at each (x,y) data point in order to maintain a constant "set point" amplitude was stored by the computer to form the topographic image of the sample surface. The surface roughness values were observed as 1.425 µm and 1.500 µm because of a layer of pectin and waxy materials which covered the surface of fiber.

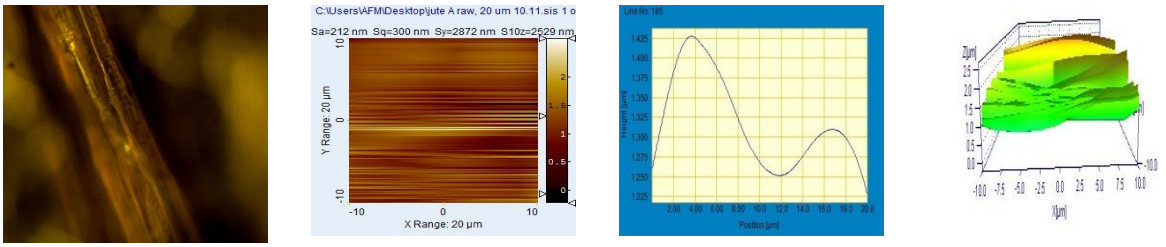

(a) **(b)** **(c)** **(d)**

Figure 4 AFM microphotographs of waste jute fiber (a) morphology (b) topography (c) line profile (d) 3 Dimension

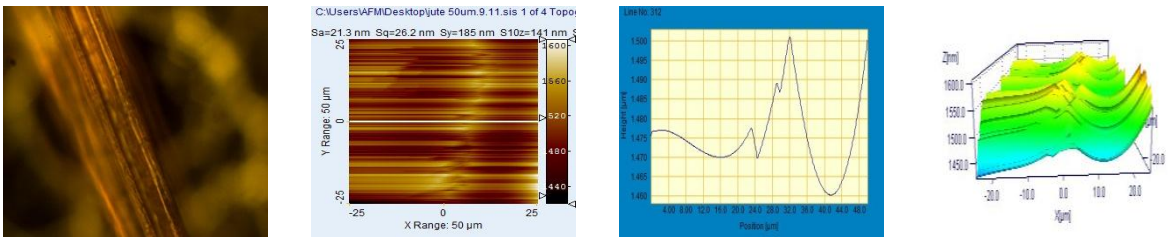

(a) **(b)** **(c)** **(d)**

Figure 5 AFM microphotographs of modified waste jute fiber (a) morphology (b) topography (c) line profile (d) 3Dimension

Table 6 Microscopic Analysis Data of Waste Jute Fiber and Modified Waste Jute Fiber

Sample	Surface roughness (µm)	Remarks
Waste jute fiber	1.425	The outer layer of pectin and waxy materials which covered the surface of fiber
Modified waste jute fiber	1.500	The outer layer of lignin was removed during alkali treatment

Characterization of Epoxy Resin

FT IR Analysis

The FT IR spectrum of epoxy resin is shown in Figure 6 and the description data in Table 7 are given.

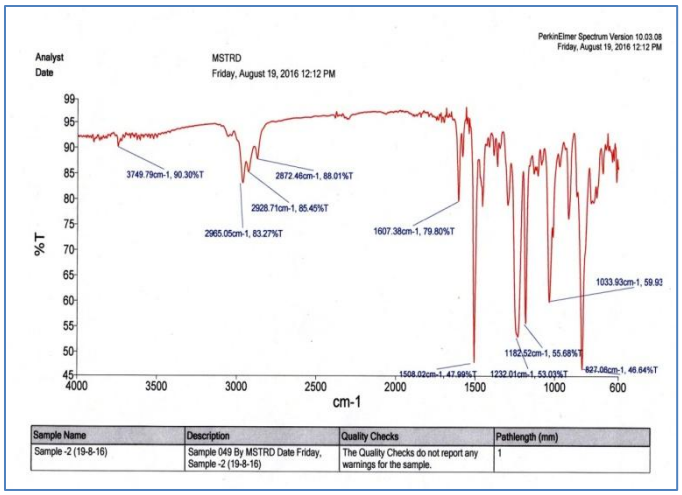

Figure 6 FT IR spectrum of epoxy resin

Table 7 FT IR Spectral Data of Epoxy Resin

Frequency (cm^{-1})		Band Assignments
Epoxy Resin	**Literature ***	
2965	3100-3000	C-H stretching
1607	1600-1585	C-C stretching(ring aromatics)
1508	1500-1400	C-C stretching(ring aromatics)
1232	1335-1250	C-H in plane bending
1033	1250-1020	C-H bending

* as Win Lab software of FT IR machine

STA Analysis

Thermal stability of epoxy resin sample was investigated by STA analyzer. The thermograph of individually epoxy resin is presented in Figure 7 and Table 8. Temperature range was occurring from 50 to 800 °C. The initial region (onset) of the STA profile at about 373.79 °C and the major endothermic peak was observed around 394.34 °C. It was completely burnt around 460.68 °C and about 93.50 % was weight loss.

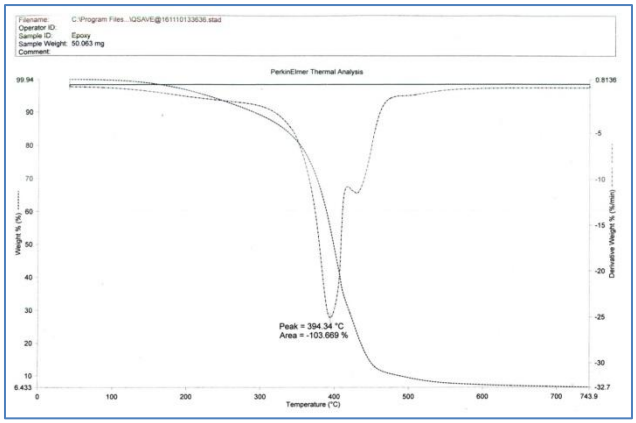

Figure 7 STA thermogram of epoxy resin

Table 8 Thermal Analysis Data of Epoxy Resin

Sample	Melting point value (°C)	Temperature range (°C)	Weight loss (%)	Nature of peak	Remarks
Epoxy resin	394.34	200-500	93.50	endo	Decomposition of cross-linked polyepoxides and graphitization

Preparation of Composites made from Jute with Epoxy Resin

Each modified waste jute fiber 120 g and various weight percentages (5, 10, 15, 20, 25 and 30 %) of epoxy resin were mixed by Henschel mixer for 2 min. The complete mixture was laid in mold. Later, this mat was carefully transferred to the hydraulic press machine for 15 min. The photographs of prepared jute fiber epoxy composites (JFE) are shown in Figure 8**.**

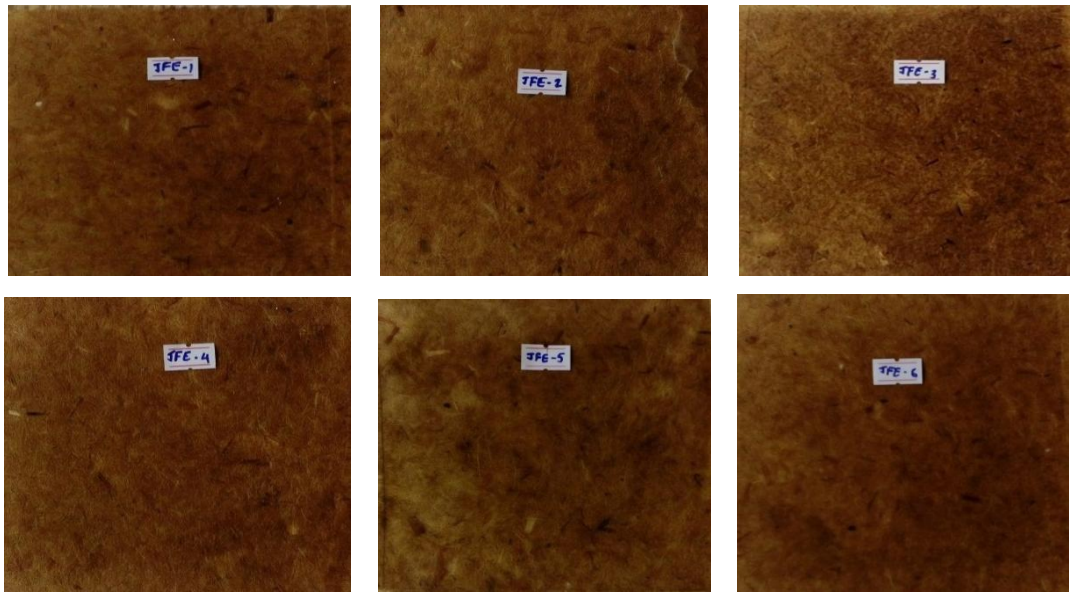

Figure 8 Photographs of jute fiber epoxy composites (JFE)

Physicochemical and Physicomechanical Properties of Composites Made From Jute and Epoxy Resin

JFE 1, JFE 2, JFE 3, JFE 4, JFE 5 and JFE 6 composites parameters such as thickness, swelling thickness, water absorption, density, modulus of rupture and hardness are presented (Table 9 and Figures 9 and 10). It can be observed that JFE 4 composite has largest modulus of rupture (MOR). The physicochemical and physicomechanical properties of composites were shown in Table 9. The quality grade composite was chosen depending on the modulus of rupture. From the results JFE 4 composite pertaining 20 % E, at applied pressure 2300 psi was higher MOR value than others. Therefore, composite JFE 4 was chosen to make the most suitable composite.

Table 9 Physicochemical and Physicomechanical Properties of Jute Fiber Epoxy Composites

Composites	E (wt %)	MOR (psi)	Thickness (cm)	Density (gcm^{-3})	Water Absorption* (%)	Swelling Thickness* (%)	Hardness Shore (D)
JFE1	5	580.34	0.72	0.7825	29.40	49.42	61
JFE2	10	785.15	0.65	0.8746	25.16	41.20	63
JFE3	15	1076.88	0.59	0.9200	22.19	33.04	64
JFE4	20	1248.20	0.60	1.2320	14.18	20.35	68
JFE5	25	1158.68	0.60	1.0962	14.99	22.08	65
JFE6	30	1099.43	0.60	0.9954	15.00	23.42	65

Applied pressure = 2300 psi
* = after 24 hour

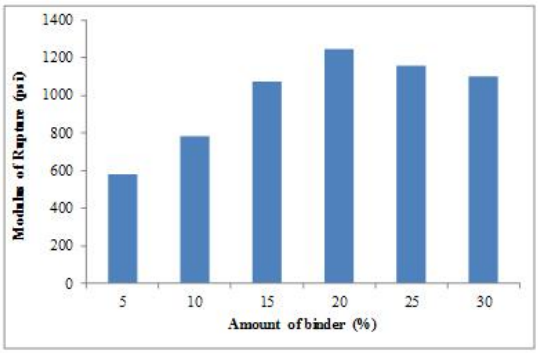

Figure 9 Modulus of rupture of JFE composites as a function of percentage of epoxy resin at 2300 psi

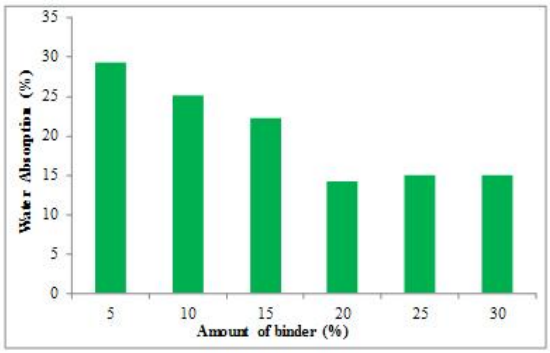

Figure 10 Water absorption of JFE composites as a function of percentage of epoxy resin at 2300 psi

Characterization of JFE 4 Composite

STA Analysis

On the basis of STA profiles, the break in temperature, corresponding dehydration, decomposition and combustion of JFE composite. The STA thermogram profiles of the thermal degradation of jute fiber epoxy composite is represented in Figure 11 and the description in Table 10. The temperature range from 50 °C to 995 °C at 20.00 °C/min. From STA curve, the

endothermic peak was observed at 361.02 °C combustion of composite. At about 500 °C the STA profiles level out, where graphitization of the residual matter may be taken place.

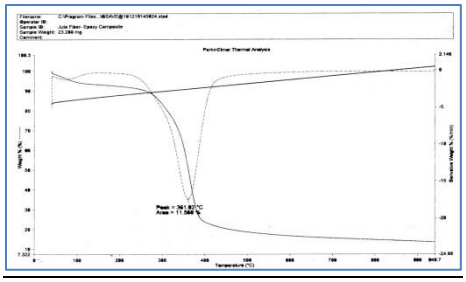

Figure 11 STA thermogram of jute fiber epoxy composite

Table 10 Thermal Analysis Data of Jute Fiber Epoxy (JFE 4) Composite

Sample	Peak Temperature (°C)	Temperature range (°C)	Weight loss (%)	Nature of peak	Remarks
	-	50-200	6.31	-	Dehydration of surface water and moisture
JFE 4	361.02	200-500	64.03	endo	Degradation and decomposition of cellulose and lignin
	-	500-800	28.06	-	Epoxy resin final residue carbon is obtained

AFM Analysis

From the AFM image of jute fiber epoxy composite, the stiffness nature of fibers can clearly observed as shown in Figure 12 and the description data in Table 11 are given. The results of epoxy surface was highlighted to build three-dimensional structure images. A roughness indicated by JFE 4 value was 900 nm which is correlated with the increasing amounts of fibrillar structure on the surface of fiber.

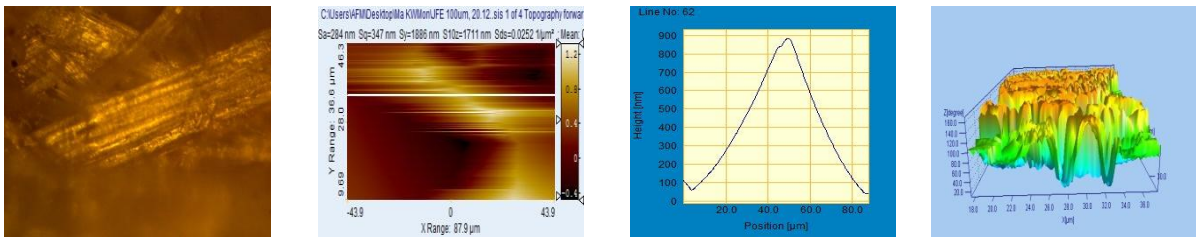

(a) (b) (c) (d)

Figure 12 AFM microphotographs of JFE 4 composite (a) morphology (b) topography (c) line profile (d) 3 Dimension

Table 11 Microscopic Analysis Data of Jute Fiber Epoxy (JFE 4) Composite

Sample	Surface roughness (nm)	Remarks
JFE 4	900	The stiffness nature of jute fiber

Conclusion

This study reveals that the use of lignin in the development new polymer composite materials. Improved composites were prepared from 5 % (w/v) NaOH used as surface modifiers of fibers to form modified waste jute fiber. The physicochemical properties of jute fiber (JF), epoxy resin (E) has carried out. Thermal nature and surface morphology of waste jute fiber and modified waste jute fiber were investigated according to STA and AFM techniques. According to STA thermograms, it was observed that alkali treated waste jute fiber has the most smooth surface. Composites namely (JFE) were prepared by mixing modified waste jute fiber with different proportions of epoxy resin (E) by using the cold pressing method at 2300 psi. The optimal condition influencing the preparation of composites based on the composition of binder (20 % of E), at pressure (2300 psi). It was found that the optimized JFE 4 composite possesses1248.20 psi modulus of rupture, 0.60 cm thickness, 1.2320 gcm^{-3} density, 14.18 % water absorption, 20.35 % swelling thickness, and 68 D hardness. The optimized JFE 4 composite was characterized by STA and AFM analysis. According to the STA thermogram profiles, the thermal decomposition of JFE 4 composite which can withstand the temperature of about 360 ˚C. The thermograms of STA confirmed the presence of lignin, an amorphous hydrophobic biopolymer with strong intermolecular, intramolecular hydrogen bond and cross linking of the molecules requiring more energy to breakdown resulting in good thermal stability of hybrid composites around 200 ˚C. The three dimensional structure images of composite were measured by Atomic Force Microscopy. From the experimental results revealed that the jute-epoxy exhibited better mechanical properties. It was found that these jute fiber reinforced epoxy composites were found to be quality grade composite

Acknowledgement

The authors would like to express their profound gratitude to the Department of Higher Education (Lower Myanmar), Ministry of Education, Yangon, Myanmar, for provision of opportunity to do this research and Myanmar Academy of Arts and Science for allowing to present this paper.

References

Abilash, N. and Sivapragash, M. (2013). "Environmental Benefit of Eco-Friendly Natural Fiber Reinforced Polymeric Composite Materials*". International Journal of Application or Innovation in Engineering and Managemen*t ,vol.2 ,pp. 395-398

Debiprasad, G., Das, K, Paul, P. and Maity, S. (2012). "Jute Composites as Wood Substitute". *International Journal of Textile Science*, vol. 1,pp. 84-93

Faruk, O., Andrzej, K., Fink, B. H. and Sain, M. (2012). "Bio-composites Reinforced with Natural Fibers". *Journal of Polymer Science,* vol.37, pp.1552-1596

Hnin Yu Wai. (2011). "Particleboards Derived from Rattan Fiber Waste". *Journal of University Research*, vol.4, pp.1-10

Myat Myat Nwe. (2008). *Preparation and Characterization of Composite (Plaster) Board Derived from Renewable Resource, Non-Wood Plant Fiber (Bagasse*). Yangon: PhD (Thesis), Department of Chemistry, University of Yangon, Myanmar

Ruxanda, B., Teaca, C. A. and Spiridon, I. (2009). "Preparation and Characterization of Composites Comprising Modified Hardwood and Wood Polymers/Poly (Vinyl Chloride)". *Journal of Bio Resources*, vol.4, pp. 1285-1304

Zin Mar Aung. (2008). *Study on Preparation and Characterization of Composite Boards Derived from Natural Fibers (Sisal Fiber) (Na-Nat-Shaw).* Yangon: PhD (Thesis), Department of Chemistry, University of Yangon, Myanmar

REMOVAL OF COLOURING MATERIALS AND IMPURITIES IN PALM OIL BY USING BENTONITE CLAY

Yi Yi Myint[1], Myat Kyaw Thu[2], Soe Soe Naing[3], Kyaw Naing[4]

Abstract

Bleaching or purification is an important step in the refining of fats and vegetable / animal oils for industrial applications. Bleaching clay primarily removes colouring pigments such as chlorophylls and carotenes but peroxide and other impurities (e.g., soaps, trace metals and phosphatides) are also important target of the bleaching process. In the research, palm oil sample was collected to carry out the adsorption of colouring materials and impurities by using raw bentonite, 4 M and 8 M HCl activated bentonite and foreign bleaching clay. In this study, raw bentonite clay was treated with 4 M HCl and 8 M HCl solutions to get better adsorption properties. Characterizations of raw bentonite clay, 4 M HCl and 8 M HCl activated bentonite clay samples were carried out by using FT IR, XRD and chemical analyses. Before bleaching processes, some properties (moisture and impurities, iodine value, peroxide value, free fatty acid content, saponification value, unsaponifiable matters, refractive index and specific gravity) were determined by AOAC and AOCS methods. After treatment with raw and acid activated bentonite clay sample, iodine value and saponification value of palm oil increased, while free fatty acids content, peroxide values, unsaponifiable matters, moisture and impurities of palm oil sample decreased. In this research, bleaching efficiencies of the bentonite clay on plam oil were determined spectrophotometrically. In this research, bleaching efficiency of the raw bentonite clay, 4 M HCl activated and 8 M HCl activated bentonite clay samples were determined at 65, 80 and 90 ºC for different contact times. The bleaching efficiencies of raw bentonite clay samples, 4 M HCl activated bentonite clay, 8 M HCl activated bentonite clay samples and foreign bleaching clay were 14.3, 42.8, 49.9 and 26.6 %, respectively, for 100 min contact time. Therefore, 8 M HCl activated bentonite clay sample give the highest bleaching efficiencies. This may concern with the structure of 8 M HCl activated bentonite clay sample. According to XRD data, 8 M HCl activated bentonite clay sample showed the amorphous nature due to the clay structure collapsing, whereas raw and 4 M HCl activated bentonite clay samples were crystalline nature. The amorphous nature of the 8 M HCl activated bentonite clay sample has more sorption ability to carotene in oil sample.

Keywords: Bentonite clay, acid activated bentonite clay, palm oil, physicochemical properties

Introduction

Palm oil originates from the fruit of *Elacis guineensis*. It is originally a tall stemmed tree belonging to the Palm family. Palm oil is a major dietary component and plays important nutritional role. Palm oil is a mixture of triglycerides of saturated and unsaturated fatty acids. Palm oil may be used in a variety of ways (Abdullah, 1994).

Bentonite is a native, colloidal, hydrated and mineral of the dioctahedral smectite group that is primarily composed of the mineral montmorillonite. The colour of bentonite is varied from white to gray, yellow, green, blue and black. Bentonites have a characteristic of waxy appearance when freshly dug and are generally soapy to touch. Hence, it is also called "mineral soap" or "soap clay". Bentonite is spread around the world including the types of locality. Bentonite occurs in France, Greece, Hungary, Poland, Romania, India, Japan and Australia. Italy is one of

[1] Dr, Assistant Lecturer, Department of Chemistry, University of Yangon
[2] Dr, Professor, Department of Chemistry, University of Yangon
[3] Dr, Associate Professor, Department of Chemistry, Meiktila University
[4] Dr, Deputy Permanent Secretary, Ministry of Education, Myanmar

the leading European bentonite producers. In Myanmar, Bentonite occurs in several places around the Kyauktaga area in Kyaukpadaung Township, Mandalay Region (Economic and Social Commission for Asia and the Pacific, 1996).

Acid activation of bentonites is one of the most important processes that have been performed to achieve desirable structural condition in edibile oil bleaching applications. Activated bentonites are removing chlorophyll, carotenoids, phospholipids, metals and oxidation products from oils (Makhoukhi *et al*., 2009).

Bleaching is an important step in the refining of vegetable oils producing light colour oil with simultaneous removal of trace metal, soaps and peroxides. This process has drawn attention to the processors of oils and technologists since it improves the appearance of oil and removes certain materials which degrades the quality of oil with time.

Among different bleaching methods, adsorptive bleaching is most commonly practiced because of its non-destructive nature and can simultaneously remove the undesired components (Bijay and Jignesh, 2009).

The removal of pigment and other trace constituents by adsorption process (bleaching) is one of the most important steps in the vegetable oil refining and this process removes the carotenes, chlorophyll and other pigments as impurities (Salawudeen *et al*., 2007).

The process makes the oil more appealing and convenient for use. Despite the health benefits derived from palm oil it must be refined to improve the purity characteristic desirable in edible oil (Barison, 1996).

The purpose of this research is to study the efficiency in removal of colouring material and impurities from crude oil by using clay mineral. Bentonite clay was used for the removal of colouring materials and impurities in palm oil sample. At first physicochemical properties (moisture and impurities, iodine value, peroxide value, free fatty acid content, saponification value, unsaponifiable matter, refractive index and specific gravity) of palm oil was determined by using appropriate methods.

Acid activation of bentonite clay samples were carried by using 4 M and 8 M HCl solution for better adsorption properties and characterized by using FT IR, TG-DTA, XRD and chemical analysis.

In this study, the bleaching efficiencies of raw and acid activated bentonite clay on palm oil sample were studied by using the various contact time and different temperatures.

Materials and Methods

All chemicals used in the research were from British Drug House Chemical Limited, Poole, England. The chemicals had been used as it was received unless otherwise stated. Apart from the glassware and other supporting equipment are balance (E Mettler, AE 160), Thermostatic shaker (Yamaha), XRD, (Regaku; D/Max 2200 Japan), FT IR (Perkin Elmer 1600) and TG-DTA (Hi-TGA 2950 Thermo Gravimetric, Shimadzu Analyzer).

Sample Collection and Characterization

The grey coloured bentonite clay sample was obtained locally from Kyaukpadaung Township, Mandalay Region. The crude palm oil used for this study was obtained from Myeik Township, Tanintharyi Region. Petroleum ether and the hydrochloric acid used were of analytical grade. The physicochemical properties of the palm oil were determined according to the AOAC and AOCS methods.

The raw bentonite clay sample was characterized by using FT IR and XRD techniques. Some chemical properties of raw bentonite clay sample were determined. The chemical properties (loss on ignition, SiO_2, Al_2O_3, CaO, MgO and $Na_2O + K_2O$ percent) were determined according to standard methods of analysis of ceramic materials (Hikichi, 1998).

Preparation of Acid Activation of Bentonite Clay

The local bentonite clay sample was ground and sieved to 200 meshes. The sample was rinsed with water several times. The washed bentonite clay was dried at 105-110 °C for four hours. Then the samples were ground and stored for further use. A 20 g of clay sample was weight into a beaker. A 200 mL of 4 M hydrochloric acid was added and stirred. Acid treatment was carried out at 90 °C for 2 h under reflux and the clay was separated by filtration. The clay residue was rinsed with water several times to remove remaining chloride ion (checked with a 1 % $AgNO_3$ solution). The washed clay material was dried at 55 °C and again crushed and passed to a 200 mesh sieve. Then, the acid activated clay was obtained. Similarly, the 8 M HCl acid activated clay was carried out using the above procedure. Acid activation was done according to the method described by Foletto *et al*. (2006).

Characterization of Bentonite Clays and Foreign Bleaching Clay

The acid activated bentonite clays and foreign bleaching clay sample were characterized by using FT IR and XRD techniques. Some chemical properties of acid activated bentonite clay samples were determined. The chemical properties (loss on ignition, SiO_2, Al_2O_3, CaO, MgO and $Na_2O + K_2O$ percent) were determined according to standard methods of analysis of ceramic materials (Hikichi, 1998).

Bleaching Process

Effect of contact time and temperature on adsorption of palm oil sample

The adsorption treatment of palm oil with bentonite clay samples (raw, 4 M, 8 M HCl acid activated bentonite and foreign bleaching clay) were carried out for different contact times (5, 15, 20, 30, 40, 50, 60, 70, 80, 90 and 100 min) at different treatment temperatures (65, 80 and 90 °C). A 5.0 g of crude palm oil was placed in a glass stopper conical flask held in a shaking water bath thermostated at a temperature that is 65 °C ± 1. When the temperature reached at 65 °C, 0.2 g of clay sample was added to the hot oil, which was then heated in the shake for different contact times (5 to 100 min) at 65 °C. After 5 min, the oil was removed from clay sample by filtration. Similarly, the oil was removed from respective conical flask for different contact times (15 to 100 min) at 65 °C. Similarly, the effect of temperature was studied at 65, 80 and 90 °C.

Bleaching efficiencies (% BE)

The absorbance of the palm oil was measured by using a UV Spectrophotometer. The bleaching efficiencies of bentonite clay samples were determined for different contact times (5, 15, 20, 30, 40, 50, 60, 70, 80, 90 and 100 min) at different treatment temperatures (65, 80 and 90 °C). A 0.1 g of palm oil sample after bleaching with bentonite clay for 5 min contact time at 65 °C was put into a conical flask and diluted by dissolving in 7.5 mL of petroleum ether (analytical grade). The mixture was poured in the cuvette and the value of the absorbance was read at 445 nm wavelength using UV-visible spectrophotometer (Kamga *et al*., 2007).

The percentage bleaching efficiency (% BE) was determined by the equation;

$$\% \text{ BE} = \frac{A_0 - A_t}{A_0} \times 100$$

Where, A_0 = absorbance of unbleached palm oil and

A_t = absorbance of bleached palm oil at time, t.

Similarly, the bleaching efficiencies of palm oils after teaching with bentonite clay samples for different contact times (5, 15, 20, 30, 40, 50, 60, 70, 80, 90 and 100 min) at treatment temperature 80 and 90 °C were determined.

Results and Discussion

In this research, raw bentonite clay sample was used as adsorbent to remove the colouring materials and impurities in crude oils. Natural occurring bentonites may show very little activity for bleaching oils and fats. For this reason, bentonite clay mineral was treated with HCl (4 M and 8 M) for two hours in order to evaluate important structural properties modifications that may affect oil bleaching. Figure 1 shows raw, 4 M and 8 M acid activated bentonite clay and foreign bleaching clay.

Characteristics of Bentonite Clay Samples

FT IR analysis

Figures 2, 3, 4 and 5 show respectively the FT IR spectra of raw, 4 M and 8 M acid activated bentonite clay samples and foreign bleaching clay sample. The data of absorption bands and possible assignments of raw, 4 M and 8 M acid activated bentonite and foreign bleaching clay are shown in Table 1. It can be observed that the hydroxyl, Si-OH, Si-H and Si-O-Si groups were presented in these spectra of bentonite clay samples.

In these spectra of the clay samples showed absorption bands between 681 and 820 cm^{-1} due to Si-O-Si stretching. The band at 800 - 950 cm^{-1} showed Si-H bending and the band at 3200 - 3700 cm^{-1} showed OH stretching vibration. The absorption bands at 1639 - 1643cm^{-1} appeared due to OH bending vibration.

XRD analysis

XRD measurement was carried on all bentonite clay samples and foreign bleaching clay sample. Figures 6, 7, 8 and 9 showed XRD measurements of raw bentonite, 4 M and 8 M acid activated bentonite clays and foreign bleaching clay, respectively. The presence of smectite (SiO_2), feldspas and quartz compounds in bentonite clay was found in the XRD diffractogram.

According to XRD data, 8 M HCl activated clay sample showed the amorphous nature, whereas the raw and 4 M HCl activated clay samples were crystalline nature.

Chemical analysis

Chemical constituents (SiO_2, Al_2O_3, Fe_2O_3, CaO, MgO, K_2O + Na_2O and loss on ignition) of the raw and acid activated bentonite clay samples were determined according to the standard method of analysis of ceramic materials. Determination of silica percent was carried out by using alkaline fusion. Table 2 shows chemical composition of clays samples.

The chemical analysis of clay samples showed a high silica content which suggests its high potential for the production of floor tiles. After treating the raw bentonite clay with acid solution was found on increase in SiO_2 concentration.

Physicochemical properties of palm oil

The physicochemical properties of crude palm oil were determined and then it was treated with various adsorbents (raw bentonite, 4 M and 8 M acid activated bentonite clays). The physicochemical properties of bleached palm oils after treating with various adsorbents were determined and shown in Table 3. The percentages of free fatty acid in palm oil sample before and after treating with various adsorbents were 10.90 % (raw), 7.24 % (4 M) and 6.61 % (8 M), respectively. Thus, it was found that free fatty acid in oil samples treated with 8 M acid activated clay was less than that treated with other two bentonite clays. The free fatty acid is among the undesirable constituent to be removed and thus its low percentage enhances the efficiency of the refining process.

It can be seen that the iodine value of palm oil after treating with 8 M activated bentonite clay was larger than that after treating with the other adsorbents. When iodine value in oil sample is greater, the unsaturated fatty acid in oil sample is greater. The saponification value increased more after treating with the 8 M activated bentonite clay. High saponification value indicates the presence of low molecular weight fatty acid. High value of saponification suggests that the palm oil can be used for soap production.

Unsaponifiable matter means hydrocarbon, alcohols and sterols. Unsaponifiable matter in palm oil samples were 0.179 % (crude), 0.177 % (raw), 0.073 % (4 M) and 0.057 % (8 M), respectively. After treating with 8 M activated bentonite clay, unsaponifiable matter in palm oil samples was found to decrease significantly.

Adsorption of carotene in palm oil

The evaluation of the amount of pigment removed was made by UV-visible spectroscopy. Adsorption of carotene in palm oil on various adsorbents (raw, 4 M and 8 M activated bentonite and foreign bleaching clay) was determined at 65, 80 and 90 °C for various contact time (5, 15, 20, 30, 40, 50, 60, 70, 80, 90 and 100 min) and the absorbance of final product read at 445 nm. Table 4 mentions the absorbance of carotene in palm oil at different temperatures and different contact times for various adsorbents. It is evident from these results that the time required to reach the adsorption equilibrium decrease as the temperature increases. The absorbance decreases as increasing the temperature and the contact time. It can be seen from the results that the absorbance value (at 445 nm) for 100 min contact time for 8 M HCl activated bentonite are 1.025 at 65 °C, 0.922 at 80 °C and 0.845 at 90 °C, respectively. The dark colour of crude oil converts to a light colour as the absorbance value decrease.

Bleaching efficiencies (% BE)

In this research, the kinetics of adsorption of palm oil carotenes at three different temperatures (65, 80 and 90 °C) and various contact times by various adsorbents (raw, 4 M HCl and 8 M HCl activated bentonite clays and foreign bleaching clay) were determined. The values of bleaching efficiencies (% BE) of various adsorbent clays samples are mentioned in Tables 5, 6, 7 and 8 for the bleaching process at contact times of 5, 15, 20, 30, 40, 50, 60, 70, 80, 90 and 100 min and three different temperatures.

As seen in these tables, the bleaching efficiency increases as the temperature and contact time increase. It was observed that the percent of bleaching efficiencies for 100 min contact time are 49.9 at 65 °C, 54.9 % at 80 °C and 58.7 at 90 °C for 8 M HCl activated clay. Figures 10, 11, 12 and 13 shows the plot of bleaching efficiencies of various adsorbents clays as a function of contact time at 65, 80 and 90 °C. Preliminary tests showed that the raw clays were effective in the adsorption of palm oil pigment, 8 M HCl activated bentonite clay had a better performance compared to other clays, this can be explained by the increase of acid concentration of the acid solution used for clay leaching.

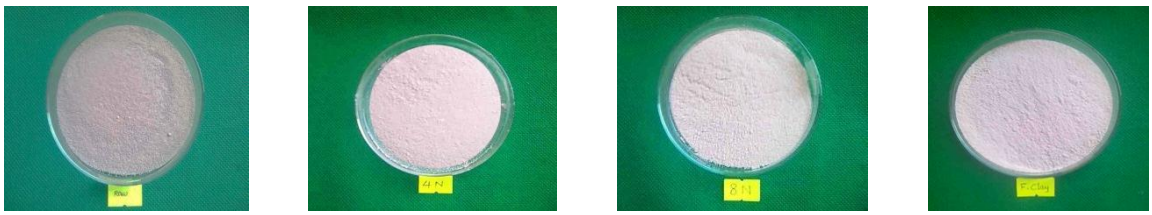

(a) (b) (c) (d)

Figure 1 Various type of bentonite clay (a) Raw bentonite (b) 4 M HCl acid activated bentonite (c) 8 M HCl acid activated bentonite (d) Foreign bleaching clay

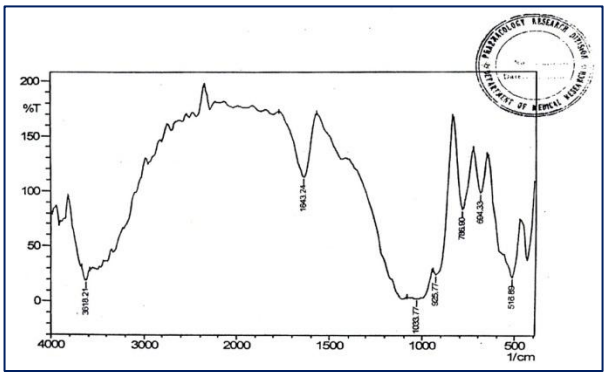

Figure 2 FT IR spectrum of raw bentonite

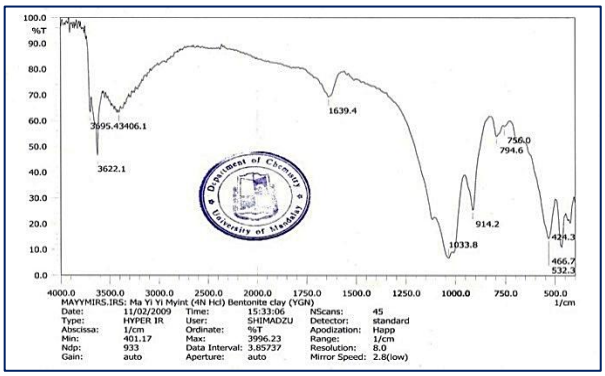

Figure 3 FT IR spectrum of 4 M HCl acid activated bentonite

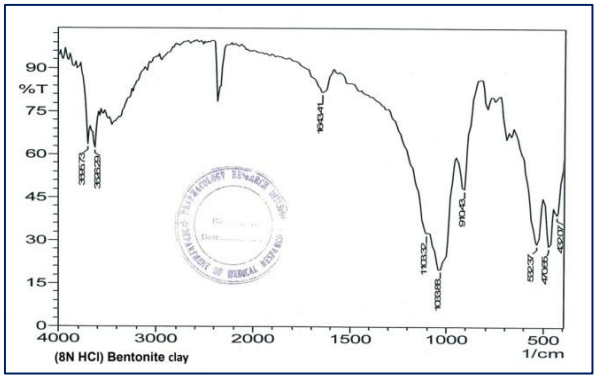

Figure 4 FT IR spectrum of 8 M HCl acid activated bentonite

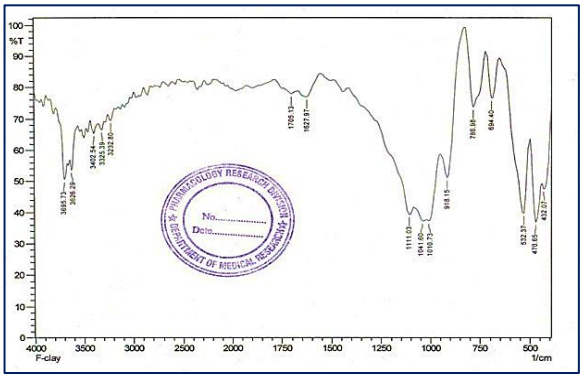

Figure 5 FT IR spectrum of foreign bleaching clay

Table 1 FT IR Data of Raw Bentonite, 4 M HCl and 8 M HCl Acid Activated Bentonite Clays and Foreign Bleaching Clay

Sr No.	Wave number (cm^{-1})					
	Raw bentonite clay	4M HCl acid activated bentonite clay	8M HCl acid activated bentonite clay	Foreign bleaching clay	Literature* Wave number	Related functional group
1	3618	3695-3406	3695- 3626	3695-3232	3700-3200	υ_{O-H}
2	1643	1639	1643	1627	1639-1643	δ_{O-H}
3	1033	1033	1033-1103	1010-111	830-1110	υ_{Si-O}
4	925	914	910	918	800-950	δ_{Si-H}
5	694-786	794,756	-	694,786	681-820	$\upsilon_{Si-O-Si}$

* Silverstein and Terence. (1991)

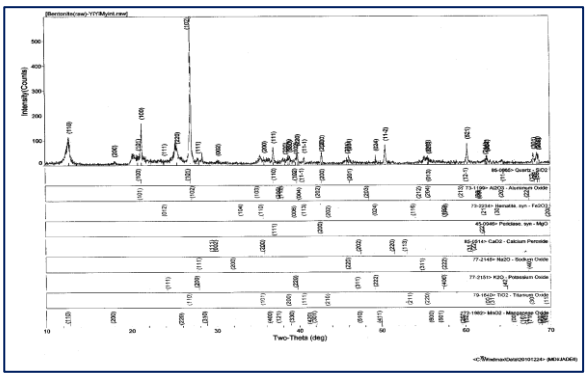

Figure 6 XRD diffractogram of raw bentonite

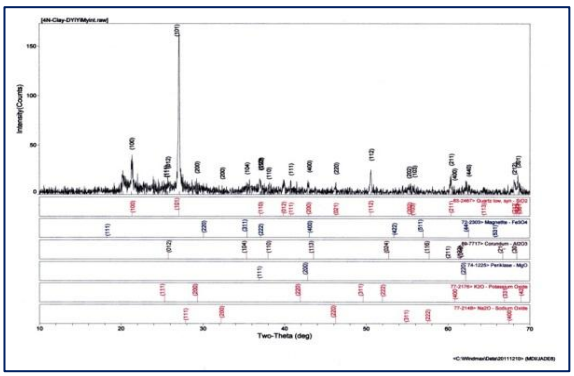

Figure 7 XRD diffractogram of 4 M HCl acid activated bentonite

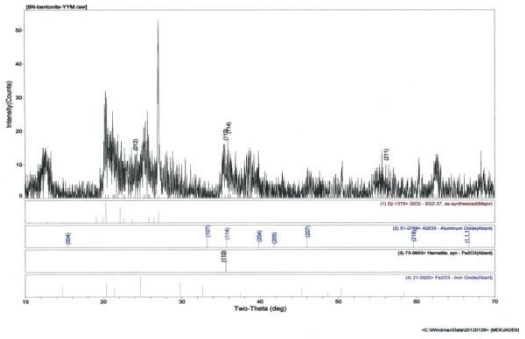

Figure 8 XRD diffractogram of 8 M HCl acid activated bentonite

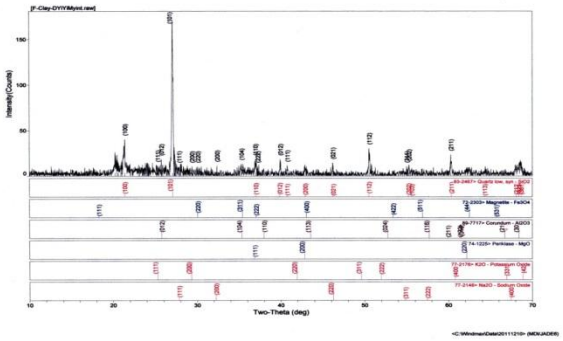

Figure 9 XRD diffractogram of foreign bleaching clay

Table 2 Chemical Composition of Bentonite Clay Samples

Sr No.	Compounds	Raw Bentonite clay (%)	4 M HCl acid activated Bentonite clay (%)	8 M HCl acid activated Bentonite clay (%)
1	SiO_2	52.54	54.68	55.94
2	Al_2O_3	30.28	29.44	29.04
3	Fe_2O_3	3.36	3.52	3.50
4	CaO	0.80	0.40	0.18
5	MgO	2.50	0.80	0.71
6	$K_2O + Na_2O$	1.55	0.30	0.21
7	Loss on ignition	10.61	10.80	10.96

Table 3 Physicochemical Properties of Raw and Acid Activated Palm Oil Samples

Sr No.	Properties	Palm oil			
		Crude oil	After bleaching with raw bentonite	After bleaching with 4 M HCl acid activated bentonite	After bleaching with 8 M HCl acid activated bentonite
1	Specific gravity (20 ° C)	0.907	0.914	0.912	0.897
2	Iodine value (%)	46.380	48.650	50.700	52.170
3	Peroxide value (meq/kg)	1.420	2.010	1.860	1.420
4	Saponification value (mg KOH/g)	201.290	192.720	193.610	195.400
5	Unsaponifiable matter (%)	0.179	0.177	0.073	0.057
6	Free fatty acid (%) (as oleic)	11.800	10.900	7.240	6.610
7	Moisture and Impurities (%)	0.129	0.102	0.078	0.034

* obtained from Myeik Township, Tanintharyi Region

Table 4 Absorbance (445 nm) of Carotene in Palm Oil at Different Temperatures and Different Contact Times on Bentonite Clay Samples

Sr No.	Contact time (min)	Absorbance (at 445 nm)											
		65 °C				80 °C				90 °C			
		Raw	4 M	8 M	F	Raw	4 M	8 M	F	Raw	4 M	8 M	F
1	5	1.929	1.833	1.598	1.699	1.913	1.679	1.432	1.552	1.752	1.514	1.403	1.389
2	15	1.875	1.719	1.462	1.681	1.848	1.620	1.362	1.506	1.747	1.490	1.293	1.373
3	20	1.871	1.630	1.427	1.662	1.786	1.525	1.270	1.466	1.695	1.379	1.230	1.354
4	30	1.869	1.551	1.390	1.647	1.767	1.425	1.214	1.418	1.643	1.328	1.146	1.306
5	40	1.864	1.519	1.381	1.613	1.702	1.377	1.189	1.386	1.557	1.292	1.113	1.248
6	50	1.854	1.349	1.226	1.598	1.656	1.336	1.106	1.288	1.530	1.231	1.071	1.200
7	60	1.839	1.357	1.149	1.575	1.647	1.259	1.071	1.254	1.507	1.202	1.010	1.186
8	70	1.934	1.309	1.180	1.562	1.635	1.229	1.034	1.214	1.480	1.160	0.963	1.166
9	80	1.814	1.190	1.082	1.540	1.626	1.154	0.978	1.168	1.452	1.125	0.921	1.148
10	90	1.801	1.185	1.055	1.512	1.553	1.118	0.929	1.144	1.442	1.085	0.859	1.136
11	100	1.753	1.170	1.025	1.501	1.516	1.104	0.922	1.134	1.435	1.068	0.845	1.118

Raw = Raw bentonite clay sample 4 M = 4 M HCl acid activated clay sample
8 M = 8 M HCl acid activated clay sample F = Foreign bleaching clay sample

Table 5 Bleaching efficiencies (% BE) of Raw Bentonite Clay Sample for Different Contact Times at 65 ºC, 80 ºC and 90 ºC

Sr No.	Contact time (min)	Bleaching Efficiencies (% BE)		
		65 °C	80 °C	90 °C
1	5	5.7	6.3	14.3
2	15	8.3	9.6	14.8
3	20	8.5	12.7	17.1
4	30	8.6	13.6	19.7
5	40	8.8	16.8	23.9
6	50	9.3	19.0	25.2
7	60	10.1	19.5	26.3
8	70	10.3	20.0	27.6
9	80	11.3	20.5	29.0
10	90	12.0	24.1	29.5
11	100	14.3	25.9	29.8

Table 6 Bleaching Efficiencies (%.BE) of 4 M HCl Activated Bentonite Clay Sample for Different Contact Times at 65 ºC, 80 ºC and 90ºC

Sr No.	Contact time (min)	Bleaching Efficiencies (% BE)		
		65 °C	80 °C	90 °C
1	5	10.4	17.9	26.0
2	15	16.0	20.8	27.1
3	20	20.3	25.5	32.6
4	30	24.2	30.4	35.1
5	40	25.2	32.7	36.9
6	50	26.3	34.7	39.3
7	60	33.7	38.5	41.3
8	70	36.7	39.9	43.4
9	80	41.8	43.6	45.0
10	90	42.1	45.4	47.0
11	100	42.8	46.0	47.8

Table 7 Bleaching Efficiencies (%.BE) of 8 M HCl Acid Activated Bentonite Clay Sample for Different Contacts Times at 65 ºC, 80 ºC and 90ºC

Sr No.	Contact time (min)	Bleaching Efficiencies (% BE)		
		65 °C	80 °C	90 °C
1	5	21.9	30.0	31.4
2	15	28.5	33.4	36.8
3	20	30.3	37.9	39.9
4	30	32.1	40.7	44.0
5	40	32.5	41.9	45.6
6	50	40.1	45.9	47.7
7	60	41.9	47.7	50.6
8	70	42.3	49.5	52.9
9	80	47.1	52.2	55.0
10	90	48.5	54.6	58.0
11	100	49.9	54.9	58.7

Table 8 Bleaching Efficiencies (% BE) of Foreign Bleaching Clay (China) for Different Contact Times at 65 ºC, 80 ºC and 90 ºC

Sr No.	Contact time (min)	Bleaching Efficiencies (% BE)		
		65°C	80°C	90°C
1	5	17.0	24.1	32.1
2	15	17.8	26.4	32.9
3	20	18.8	28.3	33.8
4	30	19.5	30.7	36.2
5	40	21.2	32.3	38.1
6	50	21.9	37.0	41.3
7	60	23.0	38.7	42.0
8	70	23.7	40.7	43.0
9	80	24.7	42.9	43.9
10	90	26.1	44.1	44.5
11	100	26.6	44.6	45.4

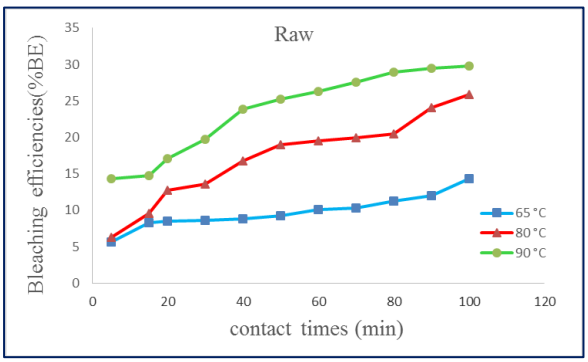

Figure 10 Plot of bleaching efficiencies of raw clay samples as a function of contact time at 65, 80 and 90 ºC

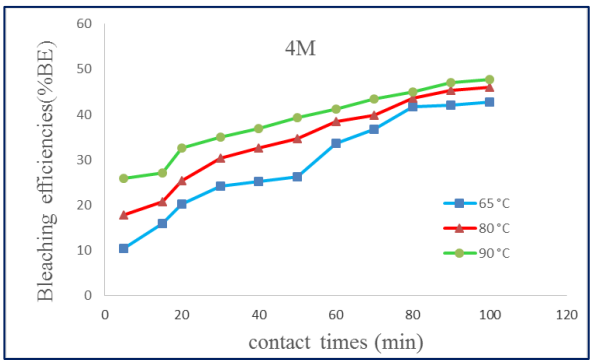

Figure 11 Plot of bleaching efficiencies of 4 M HCl activated bentonite clay samples as a function of contact time at 65, 80 and 90 °C

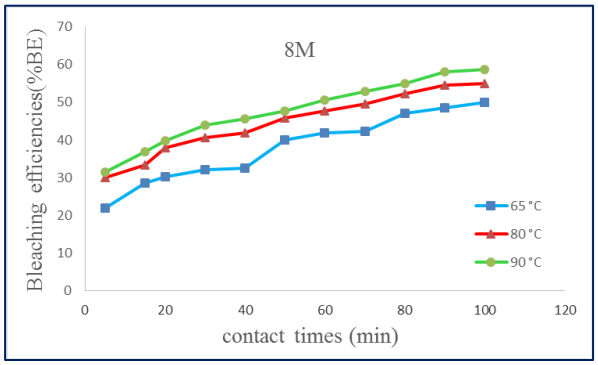

Figure 12 Plot of bleaching efficiencies of 8 M HCl activated bentonite clay samples as a function of contact time at 65, 80 and 90 °C

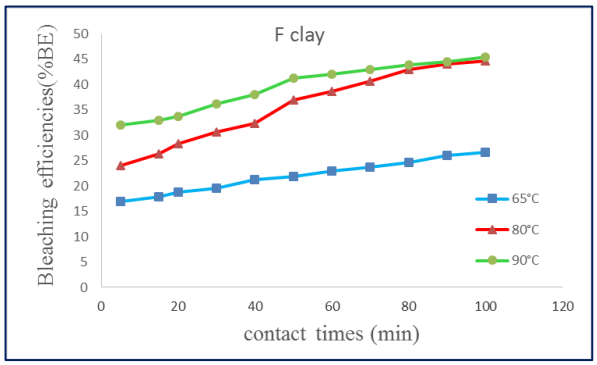

Figure 13 Plot of bleaching efficiencies of foreign bleaching clay (china) as a function of contact time at 65, 80 and 90 °C

Conclusion

In this research, palm oil sample was collected to carry out the adsorption by using raw bentonite, 4 M and 8 M HCl treated bentonite and foreign bleaching clay. In this study, raw bentonite clay was treated with 4 M HCl and 8 M HCl solutions to get better adsorption properties. After treatment with raw and acid activated bentonite clay sample, iodine value and saponification value of palm oil increased, while free fatty acids, peroxide values, unsaponifiable matters, moisture and impurities of palm oil samples decreased. The bleaching efficiencies of raw, 4 M HCl activated, 8 M HCl activated clay samples and foreign bleaching clay were 14.3, 42.8, 49.9 and 26.6 %, respectively, for 100 min contact time. Therefore 8 M HCl activated clay sample give the highest bleaching efficiencies. This may concern with the structure of 8 M HCl activated clay sample. According to XRD data, 8 M HCl activated clay sample showed the amorphous nature due to the clay structure collapsing. Whereas raw and 4 M HCl activated clay sample were crystalline nature. The amorphous nature of the 8 M HCl activated clay sample has more sorption ability to carotene in oil sample.

Acknowledgements

The authors would like to express their profound gratitude to the Department of Higher Education (Yangon Office), Ministry of Education, Yangon, Myanmar, for provision of opportunity to do this research and Myanmar Academy of Arts and Science for allowing to present this paper.

References

Abdullah, A.(1994). *Selected Reading on Palm Oil and it Uses.* Kuala Lumpur: Palm Oil Research Institute of Malaysia, Aspen Publishes Inc., pp. 151-154

Basiron, Y. (1996). *Palm Oil in Bailey's Industrial Oil and Fat Products*. New York : John Wiley & Sons, vol. 2, pp. 271-373

Bijay, K.D. and Jignesh, D. P. (2009). "Bleaching of Mustard Oil with Some Alternative Bleaching Agents and Acid Activated Clay". *J. Oleo. Sci*., vol. 58, pp. 57- 63

Economic and Social Commission for Asia and the Pacific. (1996). *Atlas of Minerals Resources of the Escape Region*, Yangon :Geology and Minerals Resources of Myanmar, pp. 113-114

Foletto, E.L., Volzone, C. and Porto, L.M. (2006). "Classification of Cottonseed Oil", *Lat. Am. Appl. Res*., vol. 36, pp. 1-7

Hikichi, Y. (1998). *Chemical and Physical Analysis of Ceramic Materials (Standard Laboratory Manuals)*. Nagoya : Minerals Research Laboratory, Nagoya Institute of Technology, Japan , pp. 3-20

Kamga, R., Nde-Aga, B. J. and Nguetnkam, J. P. (2007). "Adsorption of Palm Oil Carotene and Free Fatty Acids onto Acid Activated Camerronia Clays". *Journal of Applied Sciences*, vol. 7, pp. 2462-2467

Makhoukhi, B., Didi, M.A. and Azzouz, A. (2009). "Acid Activation of Bentonite for Use as a Vegetable Oil Bleaching Agent". *J. App. Clay, Sci.*, vol. 4, pp. 343 – 349

Salawudeen, T. O, Dada, E. O. and Alagbe, S. O. (2007). "Performance Evaluation of Acid Treated Clays for Palm Oil Bleaching". *Journal of Engineering and Applied Sciences*, vol. 2(11), pp.1677-1680

Silverstein, R. M. and C. M. Terence. (1991). *Spectrometric Identification of Organic Compounds*. New York : John Willey and Son, Inc., pp.72-126

ISOLATION AND IDENTIFICATION OF CATECHIN FROM *DIOSCOREA BULBIFERA* L. TUBERS AND SCREENING ON HYPOGLYCEMIC ACTIVITY

Kalya Cho[1], Yi Yi Win[2], Hnin Hnin Aye[3], Aye Win Oo[4]

Abstract

The key process in the development of highly effective and safe herbal medicine is isolation and identification of pharmacologically active compounds from medicinal plants and evaluation of their biological activities. In the present work, catechin, a flavanol was isolated from the ethyl acetate soluble portion of the 70 % ethanol extract from *D. bulbifera* tubers. The isolated catechin was characterized by using UV, FT IR, ^{1}H NMR, ^{13}C NMR, HSQC, COSY and HMBC spectroscopic methods. The hypoglycemic effects of pet ether, ethyl acetate and water soluble portions of the hydroalcoholic extract and isolated catechin were evaluated on alloxan induced diabetic mice. The percent reduction of blood glucose level (% R) was significant after 4 h administration of tested sample. % R of pet ether, ethyl acetate and water soluble portions, isolated catechin and antidiabetic drug, metformin were found to be 28.83 %, 41.29 %, 31.52 %, 41.62 % and 41.87 %, respectively. % R of ethyl acetate portion and isolated catechin were nearly the same as % R of metformin. The histological examination of pancreatic islet on tested mice was performed by staining with Haematoxylin and Eosin and it was found that ethyl acetate and water soluble portions as well as isolated catechin enhanced the regeneration of the alloxan damaged islet cells.

Keywords : *D. bulbifera*, catechin, alloxan, hypoglycemic effects.

Introduction

Phytopharmaceuticals play an essential role in medicine. Medicinal plants offer a great opportunity to discovered new natural therapeutic compounds. Some of these compounds may have beneficial effects on glucose homeostasis in diabetic patients without causing any undesirable effects (Mrabti *et al*., 2018). Type 2 diabetes is one of the most common metabolic diseases and characterized by hyperglycemia due to defects in insulin secretion, action or both (Zhang *et al*., 2014). The search for improved and safe natural anti diabetic agents is underway and the World Health Organization has also recommended the development of herbal medicine in this concern (Ghosh *et al*., 2012).

D. bulbifera (family Dioscoreaceae) possesses profound therapeutic potential and found throughout the tropical and sub-tropical regions of Myanmar. *D. bulbifera* tubers have been shown to contain substantial amounts of phenolic compounds and hence these tubers could be a good source of dietary antioxidant (Theerasin and Baker, 2009). Furthermore, *D. bulbifera* tubers have been used traditionally to treat diabetes due to lower glycemic index in diabetes mellitus (Williams, 2013). The current study aimed to isolate and identify one of the phenolic compounds, catechin from tubers of *D. bulbifera* and to evaluate its hypoglucemic activity on alloxan induced diabetic mice.

[1] Dr, Lecturer, Department of Chemistry, Mawlamyine University
[2] Dr, Associate Professor, Department of Chemistry, Dawei University
[3] Dr, Professor (Retd.), Department of Chemistry, Pyay University
[4] Dr, Deputy Director, Laboratory Animals Services Division, Department of Medical Research (Lower Myanmar)

Materials and Methods

Plant Material

D. bulbifera tubers were collected from Mawlamyine University Campus and scientific name of this plant was identified at Botany Department, Mawlamyine University. The collected tubers were naturally dried in the shade at room temperature and ground into coarse powder.

Preparation of crude extracts

Dried powder sample (500 g) was maceraed with 70 % ethanol (1000 mL) for one week and filtered. The filtrated was evaporated by mean of a rotatory evaporator. The hydroalcoholic extract was further separated into pet ether, ethyl acetate and water soluble fractions by successive partition method (Tiwari *et al.*, 2011).

Isolation and Identification of Phenolic Compound

The ethyl acetate soluble fraction was subjected through column chromatography over silica gel using n-hexane: ethyl acetate as gradient elution to yield five sub-fractions. From the fourth fraction (n-hexane: EtOAc, 1:2 v/v), catechin was isolated as solid material. The isolated compound was characterized by UV, IR and NMR spectroscopy using UV-Vis spectrophotometer (UV-1800, SHIMADZU, Japan), IR-Tracer (SHIMADZU, Japan) and Bruker Ultra shield Advance II 400 MHz NMR spectrometer. Correlation spectroscopy of nuclear magnetic resonance such as heteronuclear single-quantum coherence spectroscopy (HSQC) and Hetronuclear multiple-bond coherence spectroscopy (HMBC) were also used.

Experimental Animals

Albino mice of both sexes weighing 25-30 g bred at Laboratory Animal Services Division, Department of Medical Research (DMR), Yangon were used. Rearing up of animals and their upkeep in the experimental period conformed to the norms of Institutional Animals Ethics Committee (IAEC) and ethical guideline for investigations of experimental pain in conscious animals (Zimmerman, 1983).

Acute Toxicity Study

The acute toxicity study of 70 % ethanol extract was done according to the Organization for Economic Co-operation and Development (OECD, 2008) guideline No.423. Female albino mice, weighing 25-30 g, were administered with hydroalcoholic extract at 2000 mg/kg dose and 5000 mg/kg dose. Upon administration, the tested animals were closely observed individually during the first 4 h and then daily for 14 days.

Evaluation of Hypoglycemic Activity

Hypoglycemic effect of hydroalcoholic extract portions and isolated catechin was determined by alloxan induced diabetic mice and blood glucose levels were determined by DM sensor blood glucometer.

Induction of diabetes

Male albino mice were made diabetic by a single dose of intraperitoneal (IP) injection of 150 mg/kg body weight of alloxan monohydrate in sterile normal saline. The blood glucose level was checked at 72 h after alloxan injection. Blood sample was drawn from tail vein and glucose level was determined to confirm the development of diabetes (190 mg/dL and above).

Preparation of sample solutions

Firstly 1 % DMSO solution was prepared by mixing of 5 μL of DMSO and 5 mL of distilled water. Each extract and isolated compounds was separately dissolved in 1 % DMSO solution as follows.

(i) 150 mg/kg body weight dose of each extract,

(ii) 150 mg/kg body weight dose of standard drug metformin, and

(iii)15 mg/kg body weight dose of isolated catechin.

Experimental procedure

The diabetic mice were divided into six groups, each containing three mice and treated as follows;

Group I : Normal control mice,

Group II : Diabetic mice administrated with 5 mL/kg of saline water,

Group III : Diabetic mice treated with 150 mg/kg body weight dose of PE soluble fraction,

Group IV : Diabetic mice treated with 150 mg/kg body weight dose of EtOAc soluble fraction,

Group V : Diabetic mice treated with 150 mg/kg body weight dose of H_2O soluble fraction,

Group VI : Diabetic mice treated with 15 mg/kg body weight dose of isolated catechin , and

Group VII : Diabetic mice treated with 150 mg/kg body weight dose of Metformin.

Blood samples were collected from the tail vein and blood glucose levels were recorded after 1, 2, 3 and 4 h of administration using glucometer kit. The percent reduction in blood glucose level was calculated by the following equation.

$$\text{Percent reduction} = \frac{\text{FBG} - \text{blood glucose level}}{\text{FBG}} \times 100$$

where, FBG = fasting blood glucose level

Statistical Analysis

The results are expressed as mean S.E.M. The significant of various treatment was calculated (Student's t-test) using SPSS and were considered statistically significant when $p < 0.05$.

Histological Examination on Pancreas

On the seven days after experiment, each mouse from group I to VII was treated with chloroform and the pencreas were removed. Fixation was done by using 10 % formalin. After fixation, the pancreas was embedded in molten paraffin wax and the paraffin block was cut to make slides. Slides were thoroughly washed with water and stained by Haematoxylin and Eosin stain. Then pancreatic islets were examined under microscope (with the magnification 40 x). Histological examination was done by pathologist from DMR, Lower Myanmar.

Results and Discussion

Extraction of Phenolic Compounds

The solvent system, 30 : 70 % (water : ethanol) solvent ratio, was used to extract phenolic compounds from tubers of *D. bulbifera* (Demir *et al*., 2015).

Isolation and Identification of Catechin

Catechin was isolated from ethyl acetate soluble fraction of hydroalcoholic extract by using column chromatographic method and purified by recrystalization with hot water. The melting point of isolated catechin is 240-241 °C. Photographs of isolated catechin and its TLC chromatogram are shown in Figure 1.

Solvent system = $CHCl_3$:MeOH, 4:1
Spraying reagent = 10 % NaOH
R_f = 0.47

Figure 1 Photographs of the isolated catechin and its TLC chromatogram

The UV spectrum of the isolated catechin (Figure 2) shows absorption band at 280 nm ($\pi \rightarrow \pi^*$ transition) in MeOH. In the presence of NaOH, the main band 280 nm shifted to 298 nm (bathochromic shift) due to the presence of free phenolic -OH group. The FT IR spectrum of isolated catechin (Figure 3) shows a broad band around 3400-3200 cm^{-1} due to -O-H stretching in phenol. The absorption bands at 2934 cm^{-1} and 2853cm^{-1} were due to the stretching of saturated C-H group and C= C stretching of aromatic ring appeared at 1627 cm^{-1} 1251 cm^{-1}.

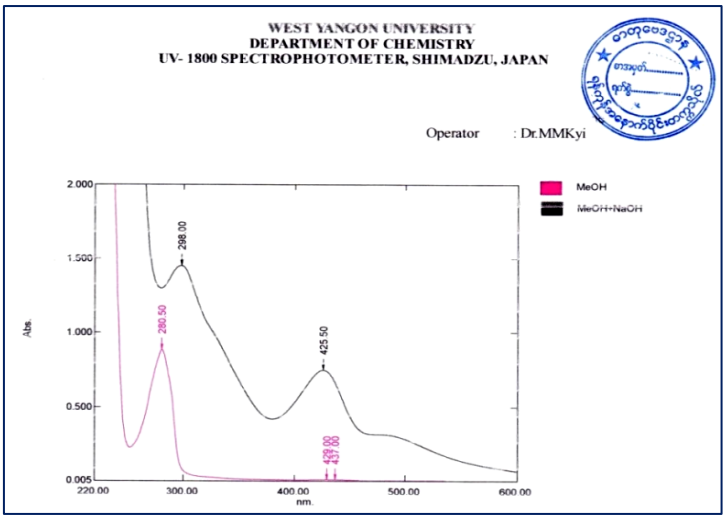

Figure 2 UV spectra of the isolated catechin from tubers of *D. bulbifera* in MeOH and MeOH + NaOH

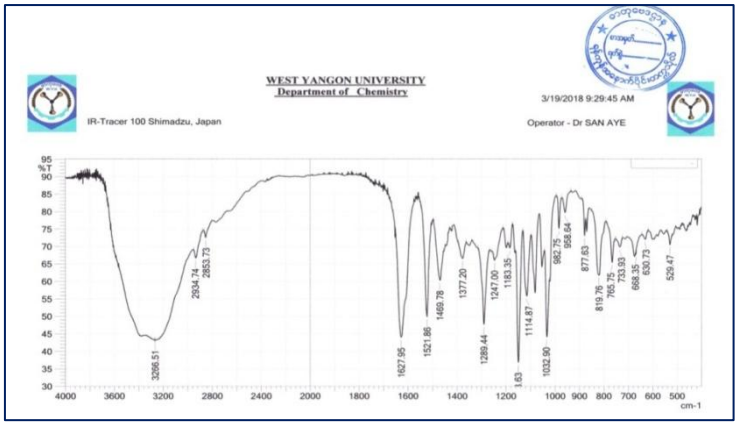

Figure 3 FT IR spectrum of the isolated catechin

The ^{13}C NMR spectrum (Figure 4) shows 15 peaks corresponding to 15 carbons, including one methylene, seven methines and seven quantanary carbons. ^{1}H NMR spectrum (Figure 5) shows nine signals. On the basis of HMQC spectrum (Figure 6), each proton correlated with corresponding carbon. The position of the H-2 chemical shift (δ_H 4.56 ppm) suggested that the flavan structure possessed the correct trans 2-3 sterochemistry. The ^{1}H-^{1}H COSY (Figure 7) shows coupling between H-3 and H-2 and also between H-3 and H-4. These positions were further confirmed by long range coupling observed in HMBC spectrum (Figure 8). The NMR data (Table 1) show signal typical of catechin and it is comparable to the reported ^{1}H and ^{13}C NMR data of catechin (Dong *et al*., 2003).

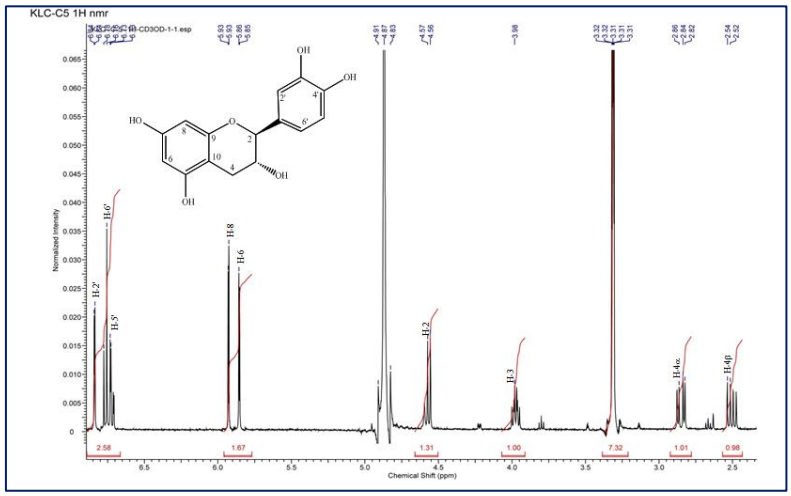

Figure 4 ^{1}H NMR spectrum of the isolated catechin (400 MHz, CD_3OD)

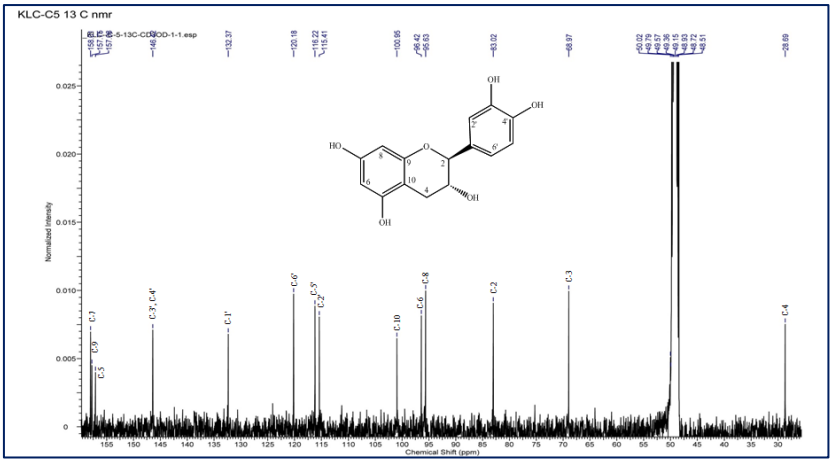

Figure 5 ^{13}C NMR spectrum of the isolated catechin (100 MHz, CD_3OD)

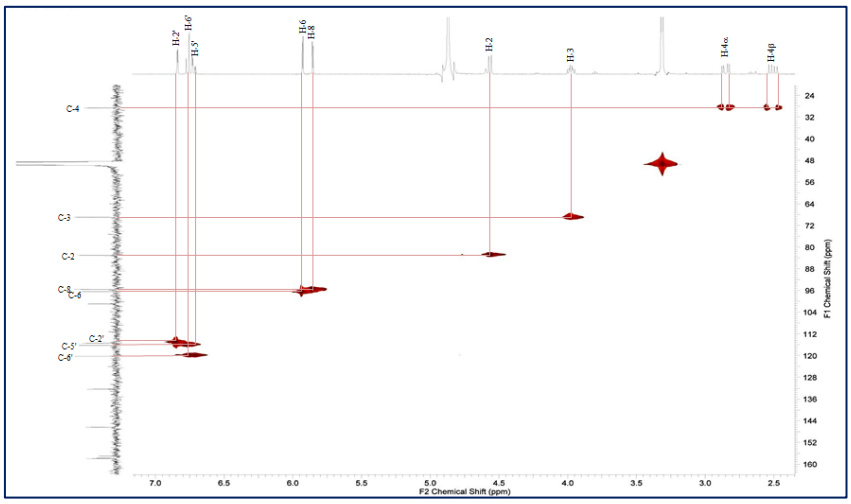

Figure 6 HSQC spectrum of the isolated catechin (400 MHz, CD_3OD)

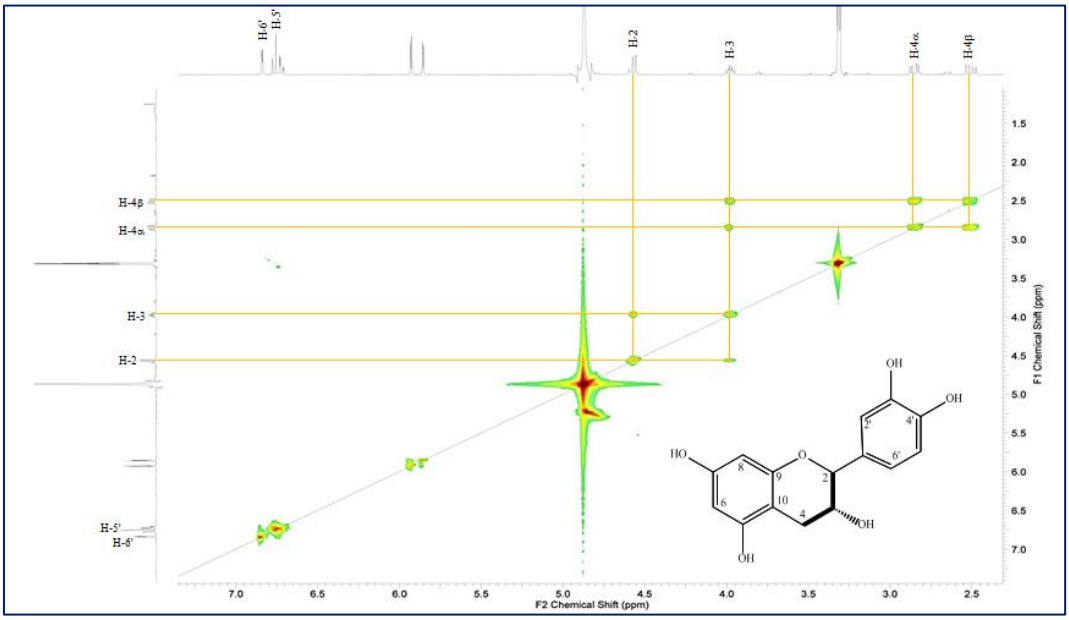

Figure 7 ^{1}H-^{1}H COSY spectrum of the isolated catechin (400 MHz, CD_3OD)

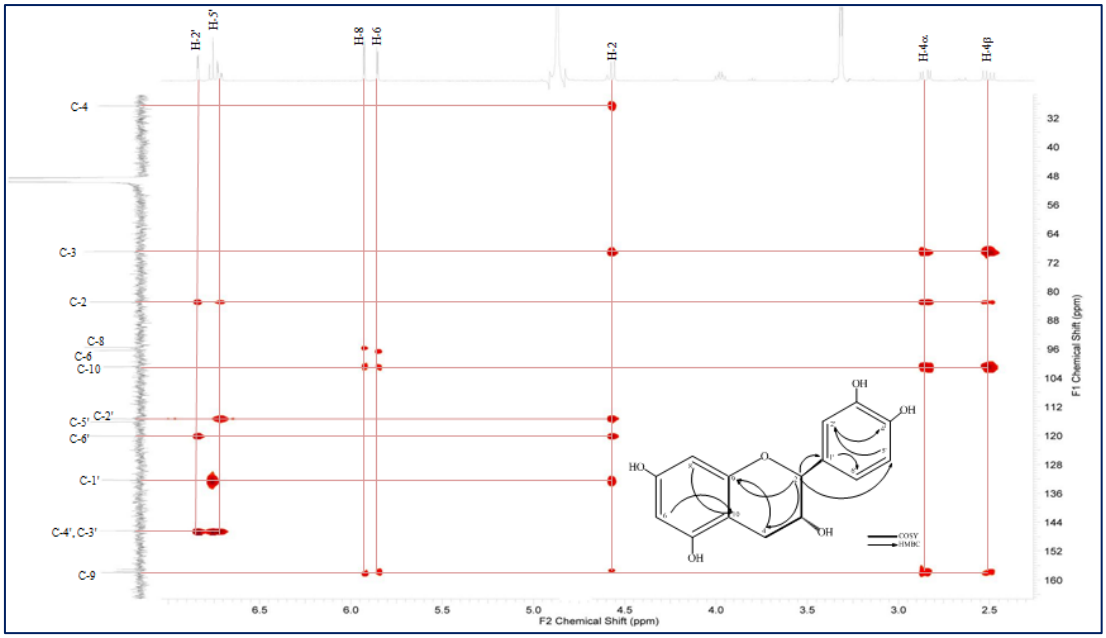

Figure 8 HMBC spectrum of the isolated catechin (400 MHz, CD_3OD)

Table 1 ^{1}H NMR, ^{13}C NMR, ^{1}H-^{1}H COSY and HMBC Data of the Isolated Catechin and Reported Data

Position	C-type	Isolated Catechin in CD_3OD		*-Catechin in CD_3OD		^{1}H-^{1}HCOSY	^{1}H-^{13}C HMBC
		$\delta_{H\ (ppm)}$	$\delta_{C\ (ppm)}$	$\delta_{H\ (ppm)}$	$\delta_{C\ (ppm)}$		
2	O–CH	4.56 (d, 1H, d, J = 8 Hz)	83.0	4.57 (d, 1H, J= 7.6 Hz)	82.3	H-2↔ H-3	H-2→C-4, C-3, C-1' C-5', C-9
3	HO–CH	3.99 (1H, m)	68.8	4.01(1H,ddd,J=5.4, 8.2, 7.6 Hz)	68.3	-	-
4	CH_2	2.85 (1H, dd, J = 6, 16 Hz)	28.7	2.88 (1H, dd, J = 5.4, 16.1 H_z)	28.2	H-4↔ H-3	H-4→ C-3,C-2, C-9, C-10
		2.51 (1H, dd, J = 8, 16 Hz)		2.52 (1H, dd, J = 8,16.1 H_z)			
5	HO–C=C	-	157.7	-	156.5	-	
6	C=CH	5.93 (1H, d, J= 2 Hz)	96.4	5.95 (1H, d, J = 1.8 H_z)	96.2	-	-
7	HO–C=C	-	158.0	-	157.0	-	H-6→ C-10
8	C=CH	5.86 (1H, d, J=2 Hz)	95.6	5.88 (1H, d, J = 1.8 H_z)	95.4	-	-
9	C=C–O	-	157.6	-	156.3	-	H-8→ C-10
10	C=C	-	100.9	-	100.7	-	-
1'	C=C	-	132.3	-	131.6	-	-
2'	C=CH	6.84 (1H, d, J=2 Hz)	115.4	6.83 (1H, d, J = 1.8H_z)	115.0	-	-
3'	HO–C=C	-	146.2	-	145.6	-	H-2'→ C-3', C-4'
4'	HO–C=C	-	146.3	-	145.7	-	-
5'	C=CH	6.78 (1H, d, J = 8 Hz)	116.2	6.77 (1H, d, J = 8 H_2)	116.0	-	-
6'	C=CH	6.73 (1H, dd, J = 2, 8 Hz)	120.1	6.72 (1H, dd, J = 1.8, 8 H_2)	119.9	-	H-5'→C-2,C-2' ,C-4'
							H-6'→ C-1'

* Dong *et al.*, 2003

Acute Toxicity Study

The female mice treated with the limit doses of 2000 mg/kg and 5000 mg/kg 70 % ethanol extract did not show any drug induced physical signs of toxicity and no drug related death occurred throughout the study period. There was no mortality after acute treatment up to 5000 mg/kg dose within 14 days, thus proving the extract being safe for use.

Hypoglycemic Activity

The hypoglycemic effect of *D. bulbifera* tubers was also studied by using alloxan induced diabetic mice. The mice developed diabetes after 72 h alloxan injection were administrated with the pet ether, ethyl acetate and water soluble fractions (150 mg/kg b.wt dose) and the isolated catechin (15 mg/kg dose). The blood glucose levels were significantly reduced after 4 h administration of each sample ($p < 0.005$). The percent reduction of blood glucose levels at 1 h, 2 h, 3 h and 4 h after treated with each fraction, the isolated catechin and metformin are shown in Table 3 and Figures 9 and 10. When compared with control group (treated with metformin), ethyl acetate soluble fraction and isolated catechin has similar hypoglycemic effect.

Table 3 Blood Glucose Levels in Alloxan Induced Diabetic Mice after Treating with PE, EtOAc and H_2O Extracts from Tubers of *D. bulbifera*, Isolated Catechin and Antidiabetic Drug Metformin [Data are represented as mean ± SEM (n = 3)]

Group No.	Treatment	Blood Glucose Concentration (mg/dL)				
		0 h	1 h	2 h	3 h	4 h
I	Normal	100.00 ± 3.39	101.00 ± 7.35	100.00 ± 5.00	100.67 ± 8.37	95.67 ± 4.03
II	Alloxan (150 mg/kg)	253.00 ± 21.25	279.00 ± 22.25	275.00 ± 29.25	275.00 ± 24.50	269.00 ± 22.50
III	PE extract (150 mg/kg)	239.33 ± 25.60	222.00 ± 24.30 (7.24 %R)	208.00 ± 27.10 (13.09 % R)	191.00 ± 26.90 (20.19 % R)	170.33 ± 27.80 *(28.83 % R)
IV	EtOAc extract (150 mg/kg)	195.33 ± 14.80	182.33 ± 16.70 (6.66 % R)	161.33 ± 16.10 (17.41 % R)	138.67 ± 18.80 (29.01 % R)	114.67 ± 20.30 *(41.29 % R)
V	H_2O extract (150 mg/kg)	239.00 ± 19.20	223.00 ± 12.60 (6.69 % R)	207.67 ± 15.80 (13.11 % R)	185.33 ± 18.00 (22.45 % R)	163.67 ± 20.80 *(31.52 % R)
VI	*Metformin (150 mg/kg) (Control)	192.67 ± 11.61	159.67 ± 11.18 (17.21 % R)	135.33 ± 16.95 (29.76 % R)	123.33 ± 15.67 (35.08 % R)	112.00 ± 14.14 *(41.87 % R)
VII	Isolated Catechin (15 mg/kg)	205.00 ± 21.60	187.67 ± 17.80 (8.45 % R)	168.00 ± 26.90 (18.05 % R)	145.33 ± 17.80 (29.11 % R)	119.67 ± 24.70 *(41.62 % R)

SEM = Standard Error Mean, R = Reduction, *P < 0.05 * = Antidiabetic drug
0 h = Before treatment 1 h – 4 h = After sample injection

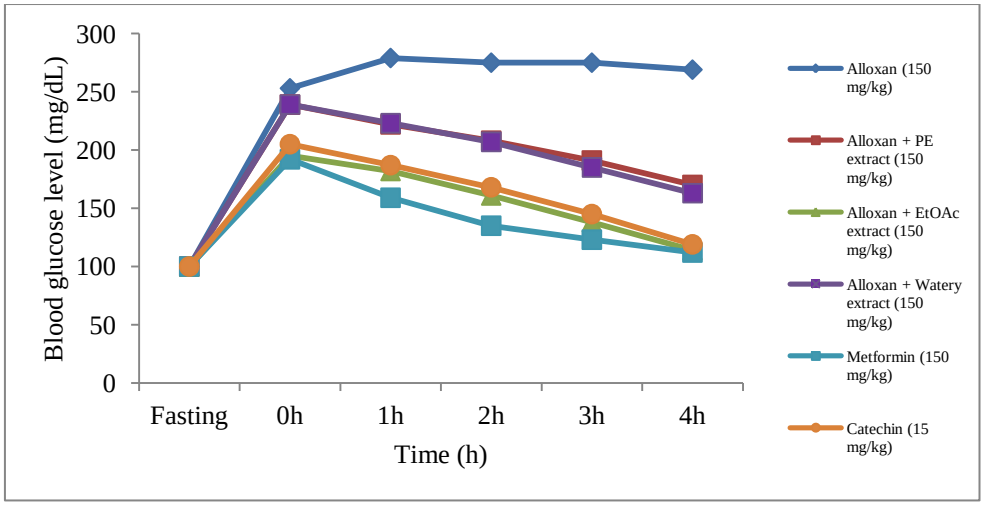

Figure 9 Effect of PE, EtOAc and H_2O extracts of tubers of *D. bulbifera*, isolated chatechin and metformin on blood glucose levels of alloxan induced diabetic mice at different times

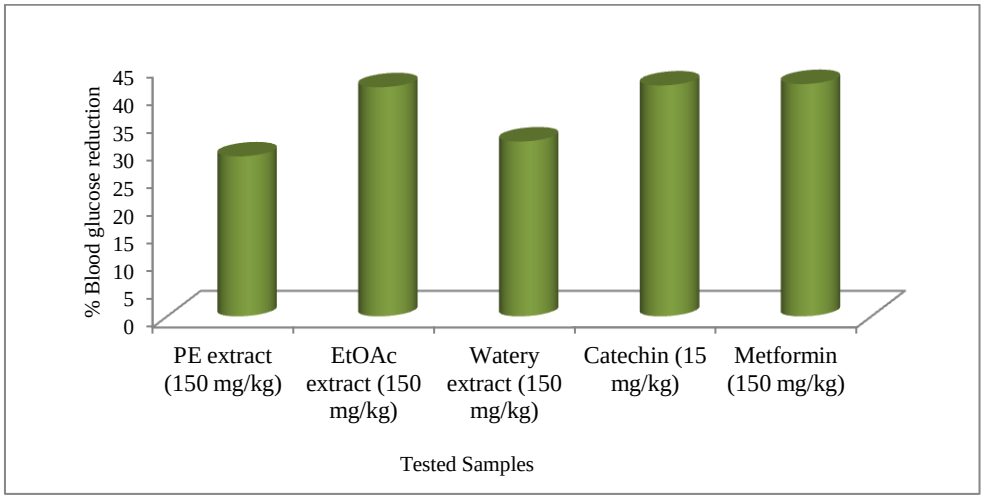

Figure 10 % Reduction of blood glucose level after administration of metformin, crude extracts and isolated catechin from tubers of *D. bulbifera*

Histological Examination of Pancreatic Cells

Histological observation of pancreatic cells was performed after 7 days administration with tested sample. The histological images obtained from mice of each group are described in Figure 11. Signs of regeneration of beta cell stimulated potentiation of insulin secretion from β cells of islets and decrease blood glucose level. The EtOAc extract and the isolated catechin induced regeneration of the islet cells. In addition these activities also showed the possible mechanism of action of *D. bulbifera* tubers for its hypoglycemic effect due to the stimulation of insulin secretion from the remnant β cells or regeneration of β cell.

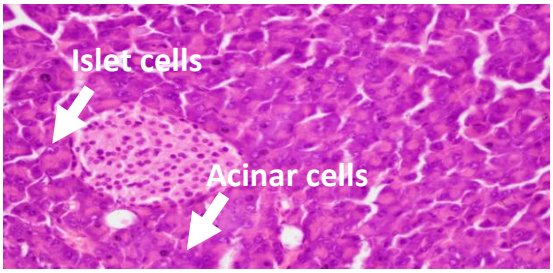

(a) Normal control mouse

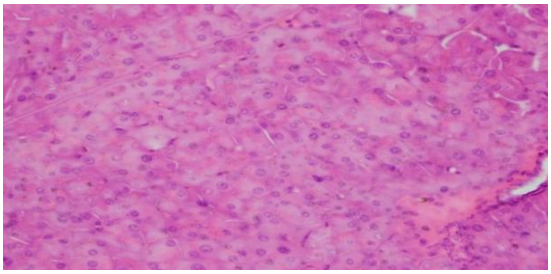

(b) Alloxan induced diabetic mouse

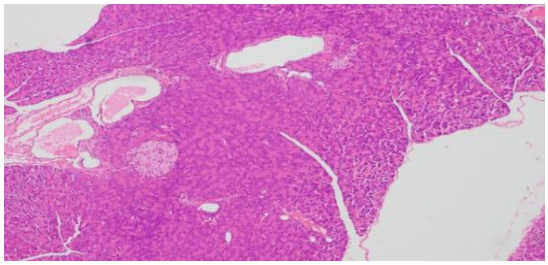

(c) Diabetic mouse treated with metformin

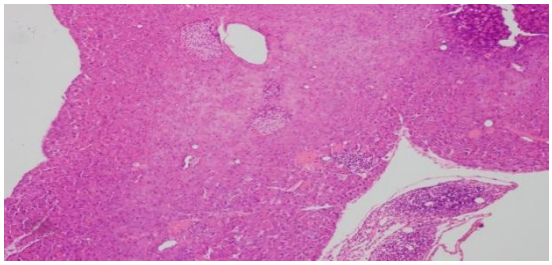

(d) Diabetic mouse treated with PE extract

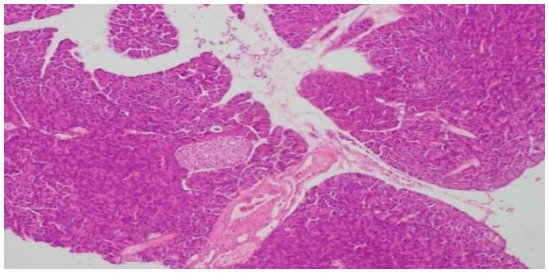

(e) Diabetic mouse treated with EtOAc extract

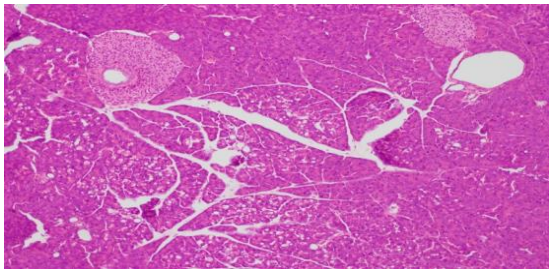

(f) Diabetic mouse treated with H_2O extract

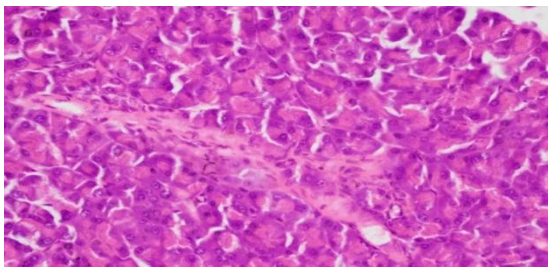

(j) Diabetic mouse treated with isolated catechin

Figure 11 Histological examination of pancreas after 7 days experiment [magnification × 40]

Conclusion

The present study deals with isolation and identification of catechin from *D. bulbifera* tubers and screening on hypoglycemic activity.

Extraction of phenolic compounds from *D. bulbifera* tubers was done by using 70 % ethanol and the resulting extract was divided into pet ether, ethyl acetate and water soluble portions. Catechin was isolated from ethyl acetate portion by column chromatography and its structure was identified by modern spectroscopic methods. The hypoglycemic effect of pet ether, ethylacetate and water soluble portions and isolated catechin was evaluated on alloxan induced diabetic mice model. The optimum hypoglycemic effect of extracts (150 mg/kg b.wt dose) and isolated catechin (15 mg/kg b.wt dose) was clear after 4 h administration where $p < 0.05$. The

percent reduction of blood glucose levels were found to be 28.83 % for pet ether fraction, 41.29 % of ethyl acetate fraction, 31.52 % for water fraction and 41.62 % for isolated catechin. So, hypoglycemic effect of ethyl acetate fraction and isolated catechin was similar to that of antidiabetic drug metformin (% reduction of blood glucose level 41.87). Histological examination of pancreatic tissue of mice from each group was done after 7 days experiment and it was found that regeneration process occurred in β islets cells and production of secretion from these cells.

Therefore, the finding from the present work will contribute the scientific validation for traditional use of *D. bulbifera* as remedy in the areas concerned with diabetes mellitus.

Acknowledgements

The authors would like to express their profound gratitude to the Department of Higher Education (Yangon Office), Ministry of Education, Yangon, Myanmar, for provision of opportunity to do this research and Myanmar Academy of Arts and Science for allowing to present this paper.

References

Demir, E., Serdar, G. and Sokmen, M. (2015). "Comparism of Some Extraction Methods for Isolation of Catechin and Caffeine from Turkish Green Tea". *International Journal of Secondary Metabolite*, vol.2(2), pp.16-25

Dong, L., Shu-Hua, Q., Da Gang and Yun-Bao, M. (2013). "A Novel Flavane from *Carapa guianensis*". *Acta Botanica* Sinica, vol.45(9), pp. 1129-1133

Ghosh, S., Ahire, M., Patil, S. and Jabgunde, A. (2012)."Antidiabetic Activity of *Gnida gluca* and *Dioscorea bulbifera* : Potent Amylase and Glucosidase Inhibitors". *PPAR Research*, vol.20, pp.1-10

Hey, M. A., Taher, M. A. M., Ali, Y. and Zaman, S. (2009). "Isolation of (+) Catechin from Acacia Catechu (Cutch Tree) by Convenient Method". *J.Sci.Res.*, vol.1(2), pp.300-305

Mrabti, H. N., Jaradat, N., Fichtali, I. and Ovedrhiri, W. (2018). "Separation, Identification and Antidiabetic Activity of Catechin Isolated from *Arbutus unedo* L.". *Plants*, vol.7(31), pp.2-9

Organization of Economic Co-operation and Development (OECD). (2008). *Acute Oral Toxicity in OECD Guideline for Testing of Chemicals.* pp.1-27

Theerasin, S. and Baker, A. T. (2019). "Analysis and Identification of Phenolic Compounds in *Discorea hispida* Dennst". *As.J.FoodAg-Lnd*, vol.2(4), pp.547-560

Tiwari, P., Kumar, B., Kaur, G. and Kaur, H. (2011). "Phytochemical Screening and Extraction: A Review". *IPS*, vol.1(1). pp.98-106

Williams, J. A., (2013) "Medicinal Plant in Australia". *Antipodean Apothecary*, Vol.4, pp. 437-444.

Zhang, J., Zhao, S., Yin, P., Han, J. and Shi, L. (2014). "α-Glucosidase Inhibitory Activity of Polyphenols from the Burs of *Castanea mollissima* Blume". *Molecules*, vol. 19, pp. 8375-8386

Zimmerman, M. (1983). "Ethical Guidelines for Investigation of Experimental Pain in Conscious Animals". *Pain*, vol.16, pp.109-110

PREPARATION AND CHARACTERIZATION OF Cu DOPED ZnO POWDER AND ITS ELECTRICAL AND OPTICAL PROPERTIES

Ei Ei Hpoo[1], Khin Than Yee[2], May Zin Oo[3]

Abstract

The main aim of the research work is to study the preparation and characterization of Cu doped ZnO powder and its electrical and optical properties. Cu doped ZnO nanocrystalline powder was prepared by using a sol-gel method. Cu doped ZnO powder ($Zn_{(1-x)}Cu_xO$) was prepared by using different dopant concentration of Cu (x = 0.03, 0.05). $Zn_{(1-x)}Cu_xO$ (x = 0.03, 0.05) was synthesized via the sol-gel technique using new organic precursors pectin and sucrose. The prepared Cu doped ZnO powder was characterized by TG - DTA , XRD, FT IR and SEM analyses.TG-DTA analysis of the synthesized Cu doped ZnO powder was carried out to determine the appropriate calcination temperature. From XRD analysis, it was observed that the crystallite size of the prepared $Zn_{(1-x)}Cu_xO$ (x= 0.03, 0.05) are 74 and 72 nm. FT IR spectra of Cu doped ZnO powder, the prominent peak of OH stretching, C-H stretching, O-C-O sym stretching and M-O stretching vibrations was observed. Morphological studies were conducted using SEM to comfirm the grain size and texture. The ac conductivities and dielectric properties of the prepared Cu doped ZnO samples was investigated in the frequency range 10 kHz – 100 kHz by LCR meter. The experimental results indicated that the ac conductivity (σ_{ac}) , dielectric loss factor (tan δ) and dielectric constant (έ) depend on the frequency. It was observed that ac conductivity is inversely proportional to the dielectric loss factor and dielectric constant. UV-Visible spectrum showed absorbance peaks in the 200-800 nm region. It was found that the absorbance does not significantly change with doping. From UV-Visible spectral data, it was found that the band gap values of $Zn_{(1-x)}Cu_xO$ (x = 0.03, 0.05) are 3.2 and 3.0 eV.

Keywords: sol-gel, dielectric loss factor, dielectric constant, ac conductivity

Introduction

Metal oxides like zinc oxide (ZnO), tin oxide (SnO_2) and indium oxide (In_2O_3) in their pure forms and also in doped forms have been extensively investigated in recent years. Among these, ZnO has gained prominence because of its abundance and non-toxicity and also because it is inexpensive compared to others. Zinc oxide (ZnO) is a II-IV semiconductor with a wide band gap of 3.37 eV and a large exciton binding energy of 60 meV at room temperature (Soitah *et al*., 2010).

Nanoparticles of ZnO are used in a variety of applications. They can be used as UV absorbent, antibacterial treatment material, catalytic agent and as an additive material in several industrial products. It is currently being used in the fabrication of solar cells, gas sensors, luminescent materials, transparent conductors, heat mirrors and coatings. (Ghosh *et al*., 2015)

Many physical properties of ZnO, such as piezoelectricity, electrical conductivity and defect structures, are greatly influenced by the presence of impurity. Several dopants (Fe, Cr, Al, Cu, Co, Mn, Mg, S, P, etc.) can lead to an increase in the surface area of the ZnO based powders. The dopants stabilize the ZnO surface, and they also promote changes in the grain size.

[1] PhD Candidate, Department of Chemistry, University of Yangon
[2] Dr, Lecturer, Department of Chemistry, University of Myeik
[3] Dr,Lecturer, Department of Chemistry, University of Yangon

The dielectric properties of pure ZnO are dependent on the presence of interstitial zinc atoms and lack of oxygen at O sites. As pure ZnO is sensitive to oxidation, absorption of O_2 results in a decrease of its dielectric properties. Therefore, different dopants have been introduced into ZnO to modify its dielectric and other properties depending on the desired applications. In many cases, when ZnO has been doped, the dielectric properties were reported to be change because of the extrinsic defects (Zhang *et al*., 2010).

Methods such as pulsed laser deposition, vapour phase transport and chemical vapour deposition have been developed for the preparation of nanostructures of ZnO. Sol-gel method is one of the most important wet chemical methods used for the preparation of metal oxide nanoparticles. ZnO nanoparticles have been obtained through the sol-gel method using both conventional and new organic precursors (sucrose and pectin).

The aim of this study is to investigate electrical and optical properties of Cu doped ZnO nanocrystalline powder by using the sol-gel method, replacing the organic compounds with commercial sucrose and pectin from banana peels. Structural and morphological characterizations of the samples were performed using powder X-ray diffraction (XRD) and scanning electron microscopy (SEM), respectively. Electrical properties were investigated using inductance capacitance resistance (LCR) measurements and optical properties by UV-Visible (UV-Vis) spectroscopy.

Materials and Methods

Sample collection

Zinc(II)sulphate heptahydrate (BDH), copper(II)sulphate pentahydrate (BDH), sucrose and pectin from banana peels. Distilled water was used as the solvent in all analyses.

Preparation of 0.03 mol and 0.05 mol Copper Doped Zinc Oxide by Sol-gel Method

The common salts $ZnSO_4.7H_2O$ and $CuSO_4.5H_2O$ (0.03 mol and 0.05 mol) were used as zinc and copper precursors. Zinc(II)sulphate was dissolved in distilled water on a warming plate at 100 °C. Next, the copper sulphate for a final composition of 0.03 mol and 0.05 mol CuO to ZnO were calculated and added to the solution. After the homogenization, a sucrose and pectin mixture with a mass ratio of 1:0.02 was added to the mixture solution under continuous stirring. The thermal treatment continues and the mixture is dried at 90-100 °C and is allowed to stand for 2 h. During this, the solution becomes highly viscous and the gel was formed. The gel was dried completely at an oven at 120 °C for 4 h. The dried gels were grounded with motar and pestle. The prepared sample was calcinated at 900 °C for 4 h. Finally, Cu doped ZnO powder was obtained.

Preparation of Copper Doped Zinc Oxide Pellets

The obtained powder (0.03 mol and 0.05 mol Cu doped ZnO) were pressed into pellets with diameter 1.5 cm and thickness 0.16 cm using MAEKAWA Testing machine.

Characterization of the Prepared Copper Doped Zinc Oxide Samples

Thermal properties of the prepared Cu doped ZnO were evaluated by TG-DTA. The powder X-ray diffraction methods are used to study the structural properties and the phase purity of the samples. The functional group of prepared Cu doped ZnO was analysed using FT IR. The morphological structure of the prepared Cu doped ZnO was characterized by SEM. The dielectric

properties and frequency dependent electrical conductivity were also determined by LCR meter in the frequency range of 10-100 kHz. The optical properties of prepared Cu doped ZnO by UV-vis spectrophotometer in the range of 200 to 800 nm was presented.

Thermogravimetric analysis of smples were performed by using TG-DTA apparatus, (Hi-TGA 2950 model). The temperature range between 0 °C and 600 °C under nitrogen gas (at a rate of 50mL/min).

X-ray diffraction (XRD) analysis was carried out using Rigaku X-ray Diffractometer, RINI 2000/PC software, Cat.No 9240 J 101, Japan. Copper tube with nickel filter was used. The diffraction pattern was recorded in terms of 2θ in the range of 10-70 °.

FT IR spectrum was recorded in the range of 4000-400 $cm^{-1}$by using 8400 SHIMADZU, Japan FT IR spectrophotometer.

The scanning electron microscopy (SEM) images were obtained by using JSM-5610 Model SEM, JEOL-Ltd., Japan.

For the electrical conductivity measurements, the obtained samples were pressed in the form of pellet using MAEKAWA Testing machine. The dielectric permittivities such as dielectric constant έ, dielectric loss factor tan δ and ac conductivity were determined using LCR-B110G meter (DC 20-10 MHz) in the frequency ranged of 10-100 kHz at ambient temperature. Frequency dependent electrical conductivity was evaluated by using dielectric equation;

$$C = \frac{\acute{\varepsilon}\,\varepsilon_0 A}{d}$$

$$\omega = 2\pi f$$

$$\sigma_{ac} = \acute{\varepsilon}\,\varepsilon_o \tan\delta\,\omega$$

where, C is capacitance (F), έ is dielectric constant, ε_0 is electrical permittivity in vacuum (8.85×10^{-14} Fcm^{-1}), d is sample thickness (cm), A is sample area ($2\pi r^2$)(cm^2), ω is circular frequency (kHz), tan δ is dielectric loss factor and σ_{ac} is electrical conductivity (μScm^{-1})

The UV-Visible spectra of powder samples are observed in the 200-800 nm range by using UV-Visible spectrophotometer. The energy band gap is determined by using the relationship;

$$\alpha = A\,(h\upsilon - E_g)^n$$

Where, hυ is photon energy, α is Absorption coeffiecient ($\alpha = 4\pi k/\lambda$), k is the absorption index or absorbance, λ is wavelength in nm, E_g is energy band gap, A is constant and n = ½ for allowed direct band gap.

Results and Discussion

0.03 mol and 0.05 mol of Cu doped ZnO powder were prepared by sol-gel method using sucrose and pectin. The resultant prepared samples were characterized by modern techniques (TG-DTA, XRD, FT IR and SEM). Moreover, their electrical and optical properties were investigated by LCR meter and UV-vis spectrophotometer.

Thermal Analysis of the Prepared Cu Doped ZnO Powder

Thermogravimetric analysis (TGA) and differential thermal analysis (DTA) thermograms of prepared $Zn_{1-x}Cu_xO$ (x = 0.03 and 0.05) are shown in Figure 1. Weight loss percent of 0.03 and 0.05 mol Cu doped ZnO are listed in Table 1. TGA curve of prepared Cu doped ZnO indicates that there are three stages of decomposition (Figure 1 (a)). Endothermic peaks observed at 72 °C and 82 °C for 0.03 and 0.05 mol of Cu doped ZnO with 5.22 and 5.36% weight loss are due to the evaporation of water presence in the Zn-Cu precursors. Endothermic peaks observed at 282 °C and 273 °C for 0.03 and 0.05 mol of Cu doped ZnO with 15.06 and 17.86% weight loss are due to the dehydroxylation of $Zn(OH)_2$. Exothermic peaks observed at 347 °C and 348 °C for 0.03 and 0.05 mol of Cu doped ZnO with the 15.34 and 17.38% weight loss are due to the decomposition of organic residues. Total weight loss of 0.03 mol and 0.05 mol Cu doped ZnO are given in Table 1.

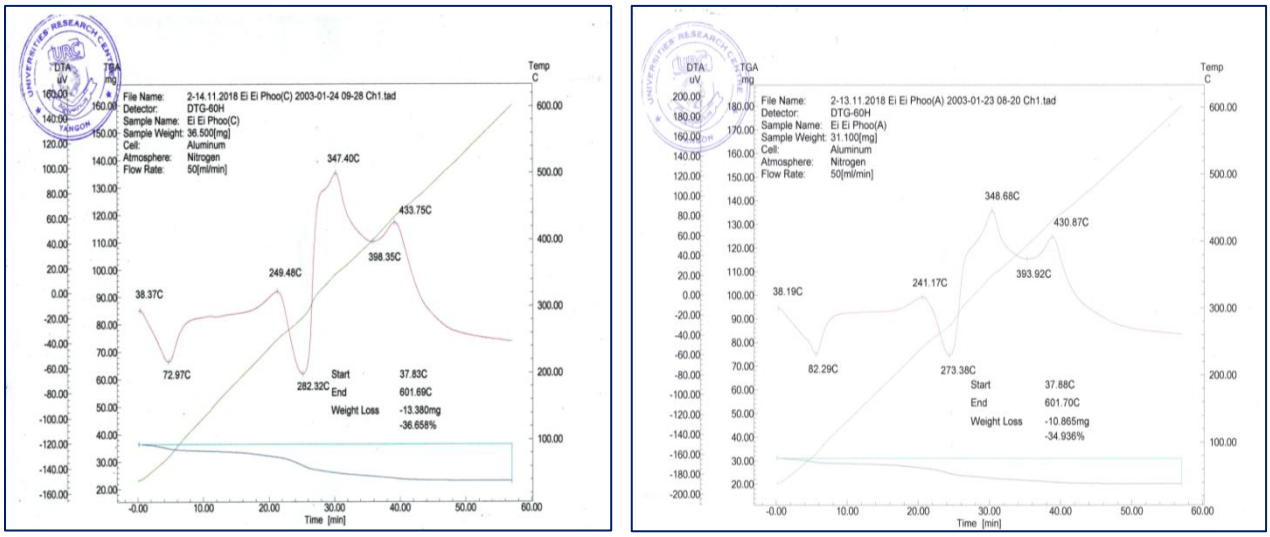

(a) (b)

Figure 1 TG-DTA thermograms of prepared (a) 0.03 mol and (b) 0.05 mol of Cu doped ZnO Powder

Table 1 Total Weight Loss Percent of Prepared 0.03 mol and 0.05 mol of Cu Doped ZnO from TG-DTA Analyses

Sample	Temperature range(°C)	Nature of peak	Weight Loss (%)	Total Weight Loss (%)
Cu doped	38-120	endo	5.22	
ZnO	120-310	endo	15.06	36.06
(0.03 mol)	310-600	exo	15.78	
Cu doped	38-120	endo	5.36	
ZnO	120-310	endo	16.14	34.94
(0.05 mol)	310-600	exo	13.44	

XRD Analysis of the Prepared Cu Doped ZnO Powder

The powder x-ray diffraction methods are used to study the structural properties and the phase purity of the samples. Figures 2 (a-b) represent the XRD pattern of prepared 0.03 mol and 0.05 mol of Cu doped ZnO. In Figure 2, the X-ray diffractions of prepared Cu doped ZnO show sharp peaks at 2θ (36.23 °) for 0.03 mol and at 2θ ~ 36.25 ° for 0.05 mol respectively. The particle size of prepared samples were determined using the Debye Scherrer equation.

$$D = k\lambda/\beta Cos\theta$$

where k is constant equal to 0.94, D and λ are the particle size in nanometers and wavelength of the radiation (1.54056 Å for Cu kα radiation), respectively.β and θ are the peak width at half-maximum intensity (FWHM) and peak position.

The particles size for 0.05 mol Cu doped ZnO was found to be 72 nm which is lower than 74 nm for 0.03 mol Cu doped ZnO. The decrease in the particle size was attributed to disorders created by the copper ions in the ZnO lattice structure. From the study it was assumed that for a smaller amount of Cu^{2+}, its ions substitute well with Zn^{2+} ions, but increasing Cu concentration causes a CuO cluster to form and isolate as an impurity phase.

The volume of unit cell and Zn-O bond length for 0.03 mol and 0.05 mol Cu doped ZnO are given in Table 2. It is observed that with the increase in Cu content, bond length increases which is attributed to the segregation of Cu. This is visible as some low-intensity peaks in XRD as the dopant concentration increases. This suggests that the crystalline quality of ZnO is improved by Cu doping.

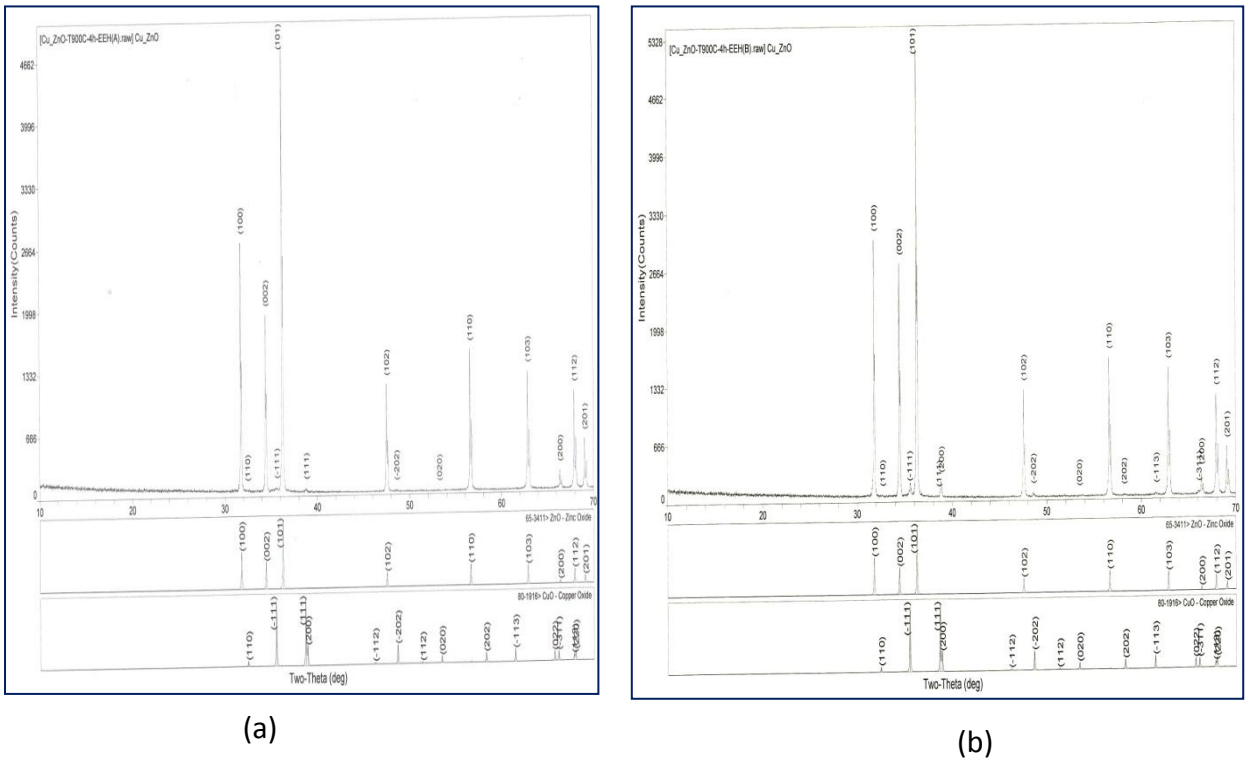

Figure 2 XRD patterns of prepared (a) 0.03 mol and (b) 0.05 mol Cu doped ZnO powder at 900 °C for 4 h

Table 2 XRD analyses of prepared 0.03 mol and 0.05 mol of Cu doped ZnO powder

Peak	(hkl)	Average Crystallite size from XRD (nm)		By using Debye Scherrer (nm)		Volume of Unit Cell (Å)^3		Zn-O bond length (Å)	
		Cu doped ZnO (0.03 mol)	Cu doped ZnO (0.05 mol)	Cu doped ZnO (0.03 mol)	Cu doped ZnO (0.05 mol)	Cu doped ZnO (0.03 mol)	Cu doped ZnO (0.05 mol)	Cu doped ZnO (0.03 mol)	Cu doped ZnO (0.05 mol)
1	100	63	100	46	83				
2	110	26.3	39.9	23	33				
3	002	100	100	76	84				
4	$\bar{1}11$	29.4	53.7	25	40				
5	101	77.7	76.1	50	50				
6	111	49.2	37.2	37	30				
7	102	100	100	73	77				
8	$\bar{2}02$	38	50.7	28	36				
9	020	56.5	100	38	62	45.81	46.06	1.95	1.96
10	110	100	100	65	67				
11	103	100	100	58	53				
12	200	90.6	77.2	46	42				
13	112	100	100	55	53				
14	201	100	100	59	54				
15	200	-	52.2	-	38				
16	202	-	37.8	-	26				
17	$\bar{1}13$	-	43.3	-	29				
18	$\bar{3}11$	-	25.7	-	17				
Average		74	72	49	48				

FT IR Analysis of the Prepared Cu Doped ZnO Powder

Figure 3 shows the FT IR spectrum of prepared Cu doped ZnO powder. The assignment data is summarized in Table 3. In the spectrum of 0.03 mol and 0.05 mol Cu doped ZnO, the peak observed at 3439 cm^{-1} corresponds to O-H stretching vibration and the peak at 1633 cm^{-1} corresponds to O-H bending vibration. Which are related to the absorbed water on the surface of nanomaterial. Another intense absorption peak at 435 cm^{-1} is related to the stretching vibrations of the Zn-O bond is described in Table 3 (Silverstein *et al*., 2003).

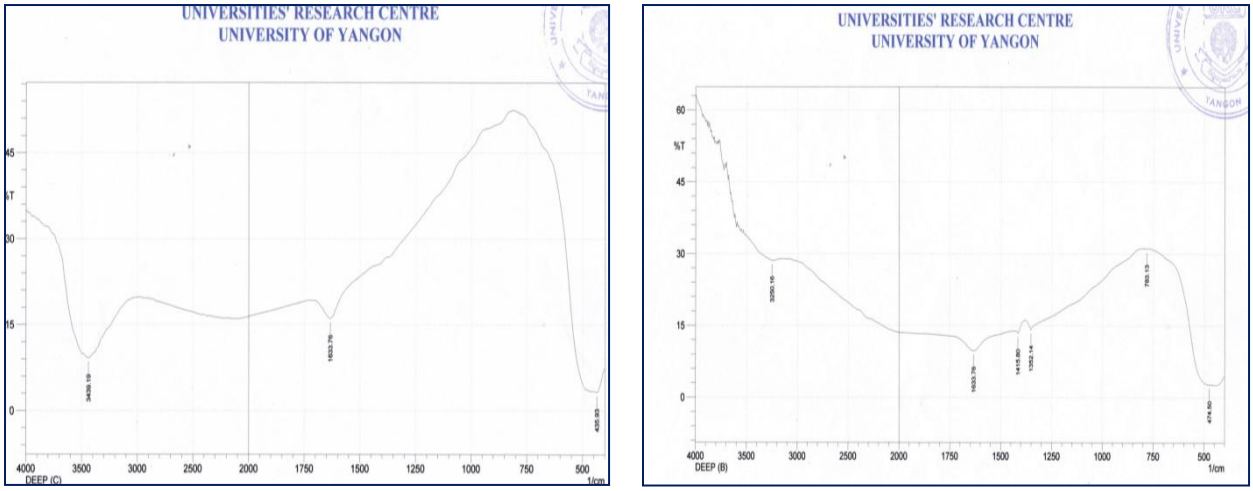

(a) (b)

Figure 3 FT IR spectra of the prepared (a) 0.03 mol and (b) 0.05 mol Cu doped ZnO powder

SEM Analysis of the Prepared Cu Doped ZnO Powder

Figures 4 (a-b) show the morphological differences between the 0.03 mol and 0.05 mol Cu doped ZnO. The SEM images reveal the formation of homogeneous and uniform distributed nanopowder. The average particle size was found to decrease with the increase in Cu doping into the ZnO matrix. The decrease in the particle size is mostly ascribed to the formation of Cu-O-Zn on the surface of the doped nanoparticles, which prevents the growth of crystal grains and assists separation of particles.

Table 3 FT IR Band Assignments of the Prepared 0.03 mol and 0.05 mol Cu doped ZnO Powder

Observed wave number (cm^{-1})		*Literature wave number (cm^{-1})	Band Assignment
0.03 mol Cu doped ZnO	**0.05 mol Cu doped ZnO**		
3439	3250	3500-3200	O-H stretching
1633	1633	1655-1630	O-H bending
-	1415 1352	1450-1350	O-C-O sym stretching
-	783	790-750	C-H bending out of plane
435	474	550-420	Zn-O stretching (or) Cu-O stretching

* Silverstein *et al*., 2003

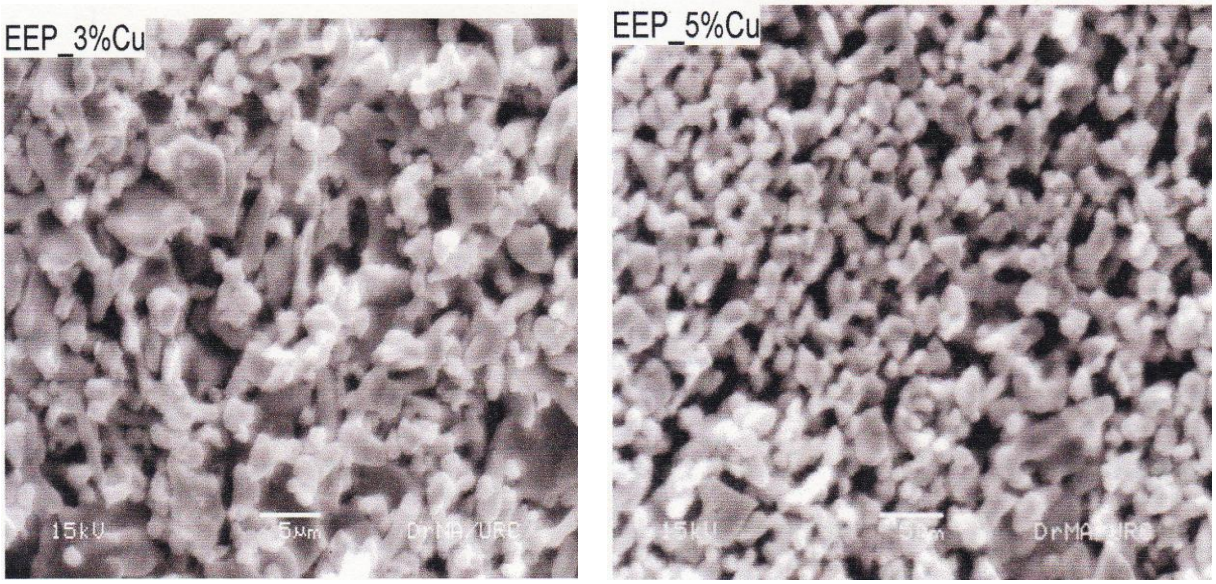

(a) (b)

Figure 4 SEM micrographs of the prepared (a) 0.03 mol and (b) 0.05 mol Cu doped ZnO powder

Dielectric Properties

The frequency dependent dielectric permittivities such as έ, tan δ and ac conductivity of prepared 0.03 mol and 0.05 mol Cu doped ZnO are presented in Figures 5 (a-c). It is seen that the ac conductivity increases slightly with frequency. This type of frequency response indicates localized conduction in the ZnO samples, where ac conductivity increases with frequency. Higher conductivity is found in 0.03 mol Cu and the level decreases with the increase in Cu doping. This may be attributed to the fact that the Cu dopant introduces defect ions (such as zinc interstitials and oxygen vacancies) in the ZnO system. Figure 5(a) presents the dielectric constant with frequency of 0.03 mol and 0.05 mol Cu doped ZnO, showing that dielectric constant decreases with increase in frequency, which can be considered as a normal dielectric behavior. The space charge polarization occurring at the interfaces at lower frequency can also be contributed to the dielectric permittivity at lower frequencies. The dielectric constant initially decreases abruptly with increase in frequency. However, it remains almost constant at higher frequencies for all samples. The reason is that beyond a particular frequency of the applied electric field, the electron exchange does not follow the alternating field. Hence, the polarization decreases causing a decrease in dielectric constant έ.

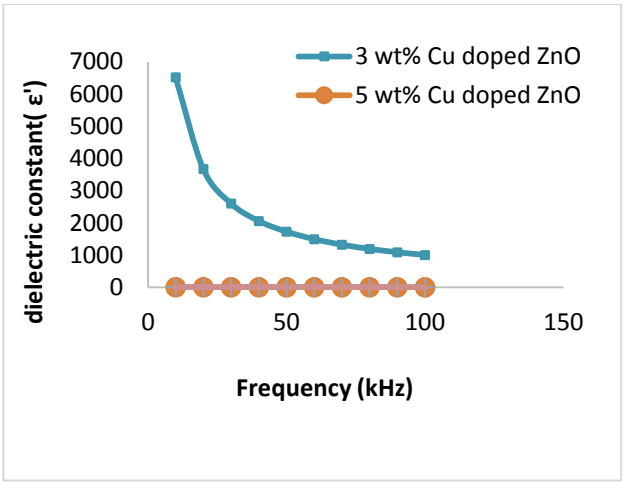

(a)

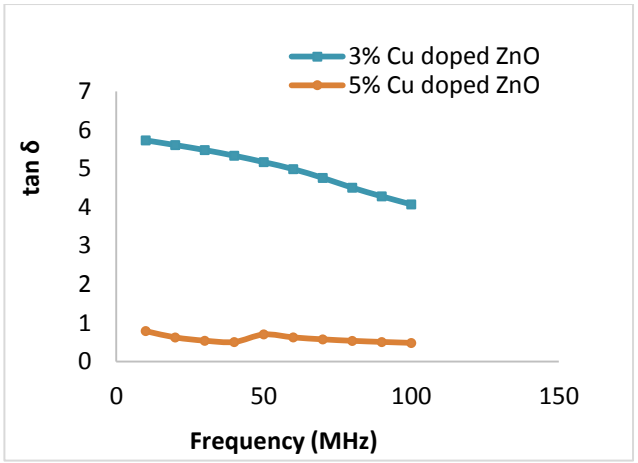

(b)

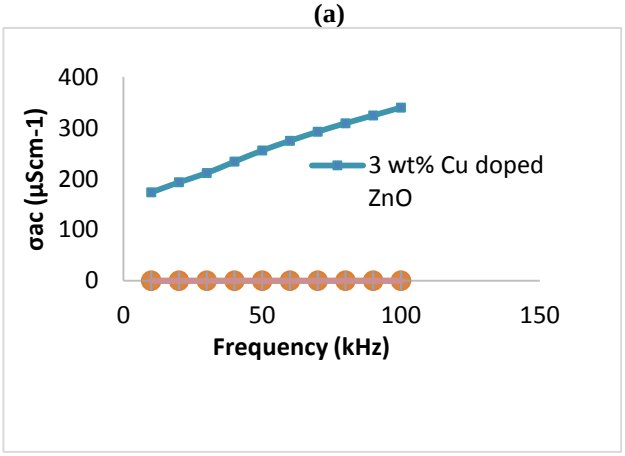

(c)

Figure 5 Plots of Relationship between (a) dielectric constant (b) dielectric loss factor and (c) electrical conductivity of prepared 0.03 mol and 0.05 mol of Cu doped ZnO powder at 4 V potential

The dielectric loss factor of 0.03 mol and 0.05 mol Cu doped ZnO as a function of frequency is shown in Figure 5(c). In nanomaterials, impurities, defects and space charge formation in the interface layers together produce an absorption current gets reduced, and hence the dielectric loss will be reduced.

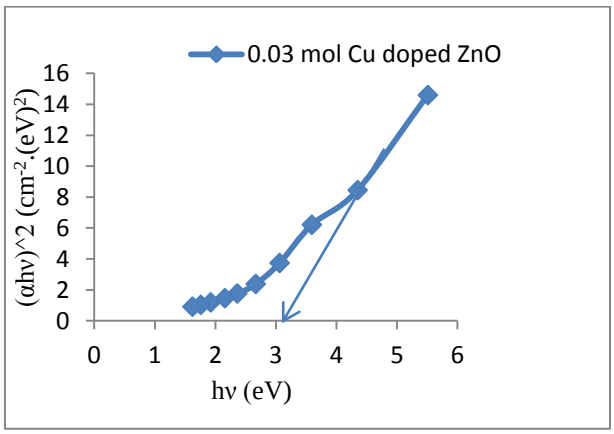

(a)

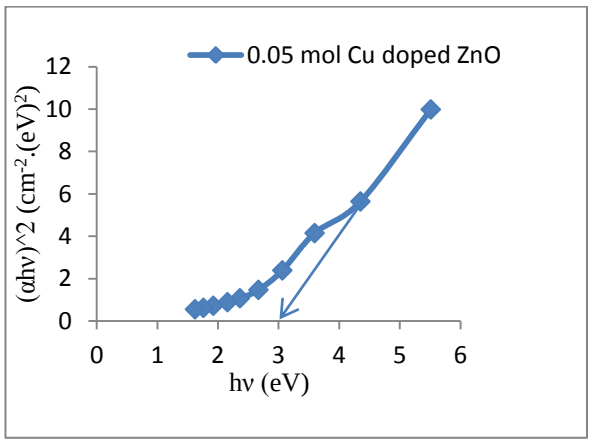

(b)

Figure 6 Variation of $(\alpha h\nu)^2$ and photon energy (hν) of prepared (a) 0.03 mol and (b) 0.05 mol Cu doped ZnO powder

Optical Properties

UV-Visible studies are conducted with an intention of measuring the optical band gap of nanocrystals. The optical band gap values were evaluated using Taucs' relation. The electronic transition is represented in Figure 6. The transition energy can be easily deduced from the zero crossing of the second derivative of the absorption spectrum. According to Fermi exclusion principle, for higher photon energies, optical transitions can only occur from the valence band up to the conduction band. Band gap gradually decreases with the doped amount of Cu. The impurity energy levels and defects always contribute to the decrease of energy gap. This implies that the addition of Cu enhances the conductance of the sample expected. However 0.05 mol of energy gap is smaller than the 0.03 mol Cu doped ZnO. By adding a trace amount of Cu, the conductivity of ZnO can be improved without altering the other properties of ZnO.

Conclusion

In this study, the structural, electrical and optical properties of 0.03 mol and 0.05 mol Cu doped ZnO powder prepared by using sol-gel method. The structural analysis confirms the formation of ZnO in both 0.03 mol and 0.05 mol Cu doped samples. Change in crystalline size is observed with the increasing doping concentration of Cu. Electrical studies confirmed that the conductivity increases slightly with frequency but decreases with doping at higher concentration whereas it increases as the concentration decrease.

Optical properties and band gap were determined by UV-Visible spectra. The energy band gap values for 0.03 mol and 0.05 mol Cu doped ZnO were found to be decreased from 3.2 to 3.0 eV. The observations of Cu doped ZnO reveal that this sample can be chosen as a semiconductor material.

Acknowledgements

The authors would like to express their profound gratitude to the Department of Higher Educaion (Lower Myanmar), Ministry of Education, Yangon, Myanmar, for provision of opportunity to do this research and Myanmar Academy of Arts and Science for allowing to present this paper.

References

Ghosh, A.,Kumari, N. and Bhattacharjee, A. (2015). "Influence of Cu Dopping on the Structural, Electrical and Optical Properties of ZnO". *Journal of Physics*, vol. 84, pp.621-635

Nakamoto, K. (1970). *Infrared Spectra of Inorganic and Coordination Compound*. New York: 2nd Edition, Wiley Interscience Publication

Soitah, T. N., Chunhui, Y. and Liang, S. (2010). "Synthesis of Fe Doping on Structural and Electrical Properties of Nanocrystalline ZnO Thin Flims Prepared by Sol-gel Dip Coating Technique". *Journal of Catalysis*, vol. 8, pp. 224-300

Silverstein, R. M., Webster,F. X.and Kiemle,D. J. (2003). *Spectrometric Identification of Organic Compounds*. New York: 7th Edition, John Wiley and Sons, Inc.

Zhang, W. H., Zhang, W. D. and Zhou, J. F. (2010). "Solvent Thermal Synthesis and Gas Sensing Properties of Fe Doped ZnO". *Journal of Material Science*, vol. 45, pp.209-220

OPTIMAL CONDITION FOR THE REMOVAL OF METHYLENE BLUE BY USING GRAPHENE OXIDE (LGO, CGO) AND THEIR PROPERTIES

Nwe Nwe Win[1], Thazin Nyo[2], Ohn Ohn Soe[3]

Abstract

Environmental pollution as a result of rapid development of technologies is one of the serious global concerns. Dyes are usually used in textile manufacturing and are one of the major contaminations in water. Thus, from an environmental point of view, the removal of dyes is of great concern, and recent applications using graphene oxides showed high adsorption ability. Graphene oxide (GO) is a highly effective absorbent of methylene blue (MB) and can be used to remove from aqueous solution. Two different graphene oxides (LGO and CGO) were synthesized from two different graphite sources by using modified Hummer method. Local graphite sample (LGP) was collected from Lin-yaung-chi mine and commercial graphite powder (CGP) was purchased from local chemical shop. The crystalline structures of different graphite varieties and prepared graphene oxides were also characterized by XRD. The optical properties of each graphite and prepared graphene oxides were characterized by UV-Vis spectrometer. The analysis of FT IR spectra was performed to investigate functional groups of graphite and the prepared GO. The surface morphologies of each graphite and prepared graphene oxides were characterized by scanning electron microscope (SEM). Graphene oxide is a material containing functional groups such as carboxyl, carbonyl, epoxy and hydroxyl, that can adsorb cationic dyes. Factors such as initial concentration of dye (MB), the dosage, temperature, contact time, rpm and pH were evaluated. The adsorption capacities of methylene blue on CGO and LGO were nearly 99% under the optimal conditions (dosage = 0.1 g, MB concentration 30 ppm, contact time = 60 min, temperature 35 ºC, rpm = 150 and pH=8). Results show that the adsorption equilibrium, the removal efficiencies were higher than 99 % and the solution can be decolorized to nearly colourless. Results show that GO is an effective adsorbent being used to treat effluents contaminated with dyes.

Keywords: Graphite, graphene oxide, modified Hummer's method, dye and adsorption capacity

Introduction

Environmental pollution is one of the main problems nowadays. The rapid development of industries and the drastic increase of population are responsible for the destruction and damaging of the environment and adversely affecting the health of the people (Atkovska *et al*, 2018). Dyes are widely used in the textile, food, cosmetics, pharmaceutical, tanneries, electroplating factories and host other industries (Sayan, 2006). The methods of colour removal from industrial effluents include biological treatment, chemical coagulation followed by sedimentation, flotation, adsorption, oxidation and photocatalytic discoloration (Ozkan and Gokcay, 2010). Among these methods sorption processes appear to be preferable techniques. Graphene oxide has proven to be a promising adsorbent for removal of pollutants from water. There are some publications which report that the synthetic GO can be used directly for water treatment and exhibit high adsorption capacities toward dyes and heavy metal ions (Long *et al.*, 2016).Graphene oxide (GO) could be used for heavy metal removal. GO can be directly used as an effective absorbent for the decoloration of methylene blue which is widely applied to dye, cotton, wood, and silk. GO has a huge absorption capacity for MB, which is competitive with other high performance absorbents. The fast absorption process of MB onto GO is one

[1] 3PhD Chem-8, Department of Chemistry, University of Yangon
[2] Dr, Lecturer, Department of Chemistry, Dagon University
[3] Dr, Associate Professor, Department of Chemistry, Loikaw University

advantage. The absorption capacity of GO is regulated by many influencing factors such as dosage, concentration, temperature, contact time, stirring speed and pH (Sheng *et al.*, 2011).

The present work is concerned with the synthesis of graphene oxide as adsorbent for removal of dye.

Materials and Methods

Materials

In this research, local graphite was collected from Lin-yaung-chi mine, Mogok Township. Commercial graphite was purchased from local chemical shop. They were used without further purification. All chemicals used were of analytical reagent grade.

Preparation of Graphene Oxides

Each graphene oxide was prepared according to the modified Hummer method (Song *et al*., 2014). 5 g of graphite and 2.5 g of $NaNO_3$ were mixed with 108 mL H_2SO_4 and 12 mL H_3PO_4, and stirred in an ice bath for 10 min. Next, 15 g of $KMnO_4$ was slowly added so that the temperature of the mixture remained below 5 °C. The suspension was then reacted for 2 h in an ice bath and stirred for 60 min before again being stirred in a 40 °C water bath for 60 min. The temperature of the mixture was adjusted to a constant 98 °C for 60 min while water was added continuously. Deionized water was further added so that the volume of the suspension was 400 mL. After 5 min, 15 mL of H_2O_2 was added to stop oxidation reaction and to reduce excess $KMnO_4$ and the colour of mixture changed to brilliant yellow.The reaction product was washed with deionized water to remove the acid and with 5% HCl solution repeatedly to remove metal ions. The GO gel-like layer starts appearing when the pH of the supernatant is neutralized, after several centrifugation rounds. All GO samples were well-dispersed as a brownish aqueous colloidal suspension of physiological pH and stable at room temperature. Finally, the product was dried at 60 ºC.

Characterization of Different Graphites and the Prepared Graphene Oxides by XRD, UV-Vis, FT IR and SEM

The different graphite varieties (LGP and CGP) and prepared graphene oxides (LGO and CGO) were characterized by XRD, UV-Vis, FT IR and SEM.

Colour Removal Efficiency of Methylene Blue Model Dye Solution by the Prepared Graphene Oxides

In this research, the prepared graphene oxides (LGO and CGO) were used for investigation of colour removal efficiency. The stock solution of methylene blue MB (1000 mg/ L) was prepared in distilled water. All working solutions were prepared by dilution of the stock solution with distilled water to get the required concentrations. Adsorption experiments were carried out in a rotary shaker at different speeds and ambient temperature, using 250 mL shaking flasks containing 50 mL different concentrations of dye solutions (5-35 mg/L). The initial pH values of the solutions were previously adjusted with 0.1 M HCl or 0.1 M NaOH using a pH meter (pH 2011).

Different doses (0.02 g-0.1 4 g) of sorbents were added to each flask. After shaking the flasks for predetermined time intervals, the samples were withdrawn from the flask and the dye solutions were separated from the sorbent by filtration. Dye concentrations in the supernatant solution were estimated by measuring absorbance at wavelength of maximum absorption of dye

with a UV-Visible (1240) spectrophotometer (Shimadzu, Japan). The removal percent was calculated by the following equation:

$$R\ \% = A_0 - A_e / A_0 \times 100$$

where, A_0 and A_e (ppm) are the liquid-phase concentrations of dye at initial and at any time t, respectively (Ahmad *et al*., 2014).

Results and Discussion

XRD Analysis

The crystalline structures of different graphite varieties and prepared graphene oxides were characterized by XRD. XRD patterns of LGP and prepared LGO are shown in Figures 1 (a) and (c). The XRD spectra of LGO shows a sharp diffraction peak at $2\theta = 10.104^{\circ}$ with an interlayer distance of 0.8747 nm. The increase in interlayer spacing from 0.3248 nm in the case of LGP to about 0.8747 nm for LGO is due to the introduction of the various functional groups that have been introduced by the oxidation of the LGP. This spacing is slightly larger than that of the d spacing of local graphite (LGP).

The XRD patterns of commercial graphite (CGP) exhibited a strong and sharp peak at 26.609º in Figure 1(b), indicating a higher ordered structure, that corresponds to a basal spacing d_{002} = 0.33473 nm. Figure 1(d) shows the pattern of prepared graphene oxide (CGO), exhibited a (001) reflection at 10.557º corresponding to a basal spacing of d_{001} = 0.8373 nm. According to Figures 1 (a, b) the crystallite sizes were found to be 56.0 nm and 40.3 nm. LGP and CGP were found to have hexagonal structure. The prepared LGO and CGO were also found to have hexagonal structure. The smallest crystallite sizes were found to be 5.13 nm and 4.05 nm (Figures 1 (c, d)).The intensity and position of the GO peak in the XRD pattern can be used as an indication of the oxidation degree. The intensities of GO peaks increase with increasing the oxidation process while the GP peak disappears in the case of the complete oxidation. The peak intensity of GO has increased by increasing the oxidation time. The interlayer distance increased clearly from GP to GO due to the presence of oxygenated functional groups and intercalated water molecules (Table 1).

UV-Visible Analysis

UV-visible spectra of GO (LGO and CGO) were measured by an UV mini-1240 Shimadzu spectrophotometer in aqueous solution. The UV-vis spectroscopic measurement was carried out in the range of (200 – 400) nm to monitor the graphite samples and the degree of oxidation for the graphene oxide samples. The maximum π -π* transition of C = C, C - C peaks of LGP and CGP were found (λ = 258.0 nm and λ = 267.3 nm).Upon oxidation of graphite, the maximum n-π* transition of C = O peaks of LGO and CGO were found (λ = 311.6 nm and λ = 307.6 nm) (Table 2 and Figure 2).

FT IR Analysis

The FT IR spectra of different graphite varieties and prepared graphene oxides were studied in the range of 400-4000 cm^{-1} using (FT IR-8400 Shimadzu, Japan) (Figure 3). FT IR spectral data showed the presence of ionizable groups such as carboxyl, carbonyl, epoxy and hydroxyl which can involve in the major absorption sites of dye removal (Sun *et al*., 2011). The peak at 3700 cm^{-1} occurs due to the infrared absorption peak of adsorbent water molecules (Table 3).

SEM Analysis

Scanning electron microscope (SEM) was used for understanding changes of morphology from graphite to graphene oxide. The scanning electron microscopy (SEM) images of the different graphites as shown in Figures 4 (a, b) are platelet like crystalline form of carbon. Figure 4 (c) showed the SEM image of LGO which resembled randomly aggregated, thin crumpled sheets. Figure 4 (d) shows that CGO image revealed the crumpled and ripple structure.

Colour removal efficiencies of LGO and CGO (Batch adsorption study)

The batch experiments were done by studying different parameters.

Effect of dosage of adsorbent

The dosage of adsorbent was varied in the range of 0.02 g to 0.14 g while keeping contact time and concentration of methylene blue at 60 min and 20 ppm, respectively. Lower amount of dosage of adsorbent removed lower percentage of colour. As the dosage of adsorbent increased the colour removal by LGO and CGO also increased. The maximum colour removal percents were observed at the dosage of 0.1 g as 95.85 % for LGO and 96.18 % for CGO (Table 4 and Figure 5).

Effect of concentration

In this study, the initial concentration of methylene blue solution was varied such as 5, 10, 15, 20, 25, 30 and 35 ppm while other factors kept constant. As the concentration increased the colour removal percent also increased (Table 5 and Figure 6). The maximum colour removal efficiency was obtained at initial concentration of 30 ppm for both LGO and CGO.

Effect of contact time

To study the effect of contact time, the contact time between the adsorbent and adsorbate was varied as 10, 20, 30, 40, 50, 60 and 70 min on rotary shaker. At 60 min contact time, the colour removal percent by LGO and CGO were found to be 98.11 % and 97.58 %. The optimal contact times of both LGO and CGO were 60 min (Table 6 and Figure 7).

Effect of temperature

To study the effect of temperature, the temperature was varied as 25, 30, 35, 40, 45, 50 and 55 °C while keeping the other parameters constant to their optimum values. The optimum temperature for colour removal efficiency was found to be 50 °C for LGO and 35 °C for CGO (Table 7 and Figure 8).

Effect of stirring speed

To study the effect of stirring speed, the stirring speeds were varied as 25, 50, 75, 100, 150, 200 and 250 rpm for each sample. The other parameters such as contact time, concentration and adsorbent dosage were set to their optimum value. The optimum stirring speeds for all samples were found to be 150 rpm (Table 8 and Figure 9).

Effect of pH

The colour removal of methylene blue solution having initial concentration of their optimal values by optimal adsorbent dosages were tested for different pH values of 2, 4, 6, 7, 8 , 10 and 12. The stirring speeds were set at 150 rpm for optimal contact time 60 min on rotary shaker. Basic condition at pH 8, LGO and CGO could remove MB (99.62 % and 99.72 %) (Table 9 and Figure 10).

The optimum parameters (dosage, concentration, contact time, stirring speed and pH) for both LGO and CGO were found to be observed the same except temperature. The optimum temperature for LGO and CGO were observed at 50 °C and 35 °C. The removal efficiencies (%) of GO from LGO and CGO were found to be observed nearly 100 %. The aqueous solution of methylene blue can be completely decolorized. Therefore GO from different sources is an excellent adsorbent which can be used to treat effluents contaminated with dye (Table 10 and Figure 11).

Table 1 Phase Identification of LGP, CGP, LGO and CGO

Samples	Miller Indies (h k l)	Bragg angle (2θ) degree	Interplannar spacing d (nm)	Phase Identification	Crystallite size (nm)
LGP	0 0 2	27.44	0.3248	Graphite	56.0
CGP	0 0 2	26.609	0.33473	Graphite	40.3
LGO	0 0 1	10.104	0.8747	Graphene oxide	5.13
CGO	0 0 1	10.557	0.8373	Graphene oxide	4.05

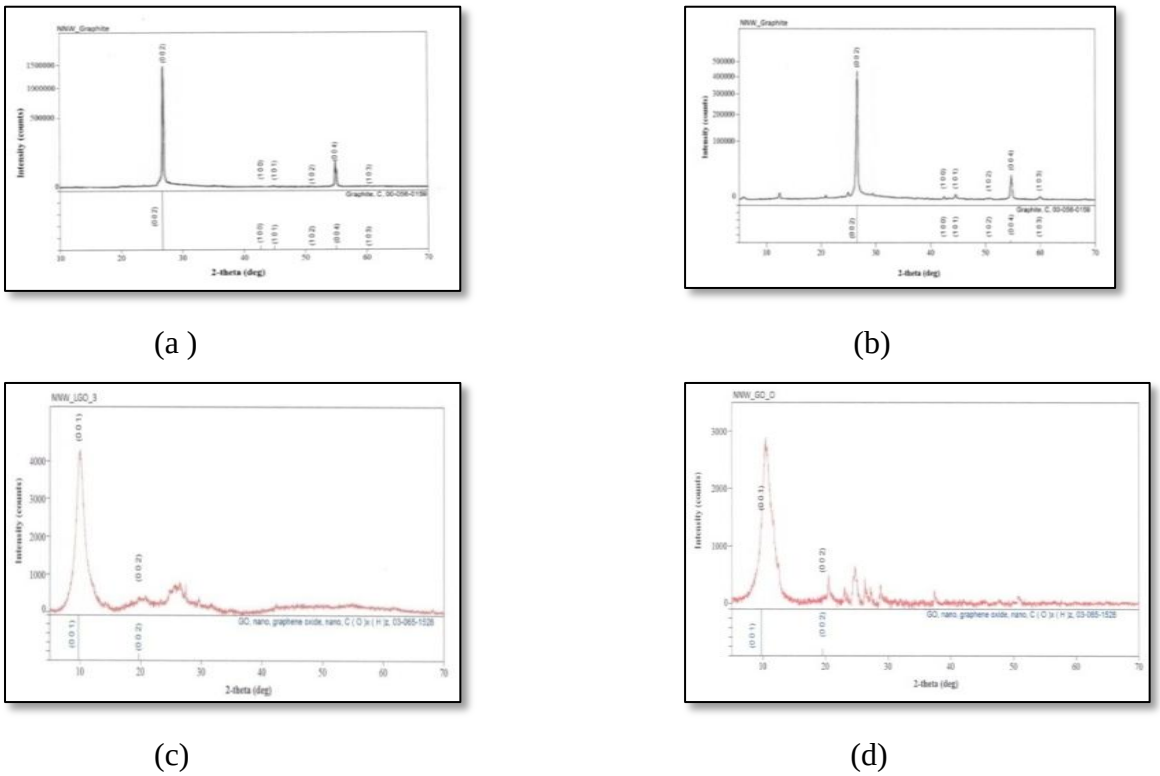

(a) (b)

(c) (d)

Figure 1 XRD diffractograms of (a) local mine graphite (LGP) (b) commercial graphite (CGP) (c) prepared graphene oxide (LGO) and (d) prepared graphene oxide (CGO)

Table 2 UV-vis Analysis of LGP, CGP, LGO and CGO

Samples	Wavelength (nm)	Band Assignment
LGP	258.0	π-π* transition of C = C , C - C
CGP	267.3	π-π* transition of C = C , C - C
LGO	311.6	n-π* transition of C = O
CGO	307.6	n-π* transition of C = O

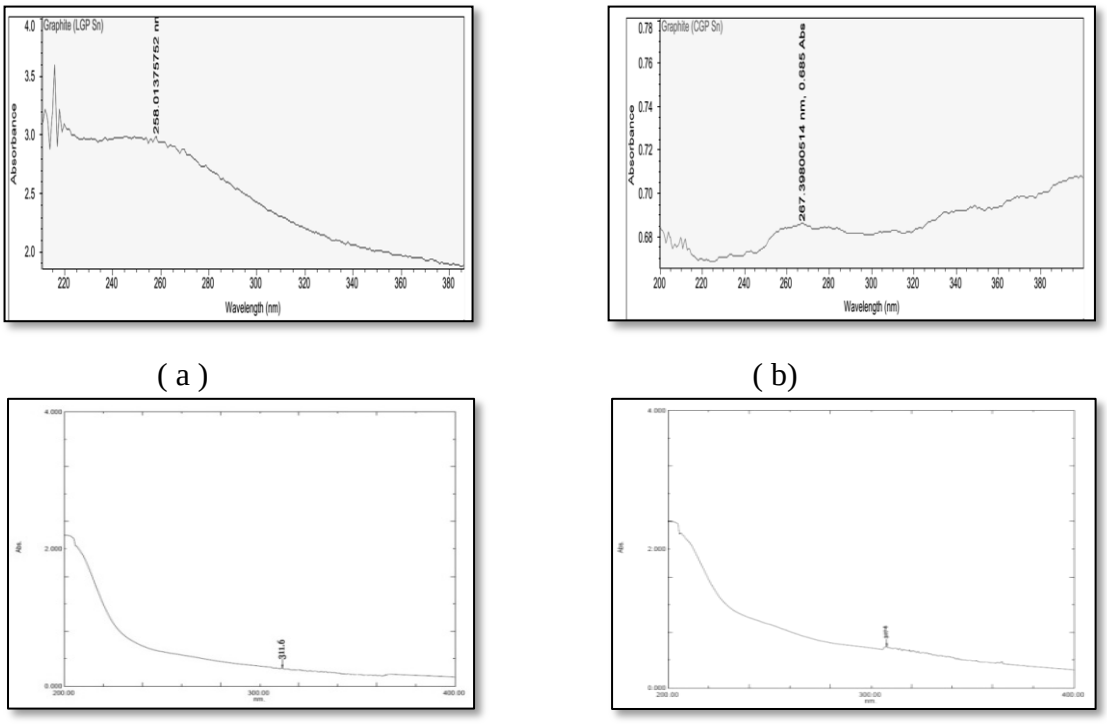

Figure 2 UV-vis spectra of (a) LGP (b) CGP (c) LGO (d) CGO

Table 3 Assignment of FT IR Spectra Data of LGP, CGP, LGO and CGO

No.	Observed value (cm^{-1})				Literature values* (cm^{-1})	Band Assignment
	LGP	CGP	LGO	CGO		
1	3624	3703	3347	3692	3200-3600	OH stretching vibration
2				3243		
3	1639	-	-	-	1600-1750	C=C stretching vibration
4	-	-	1581	1609	1540-1870	C=O stretching in carbonyl
5	-	-	-	1315	1230-1320	C-O-C stretching vibration of epoxide
6	1037	1033	1003	1030	990-1790	C-H in plane bending
7	912		912			
8	794					
9	690					C-H out of plane deformation
10	528	540	-	-	450-750	(benzene)
11	468	466				

*Sun *et al*., 2011

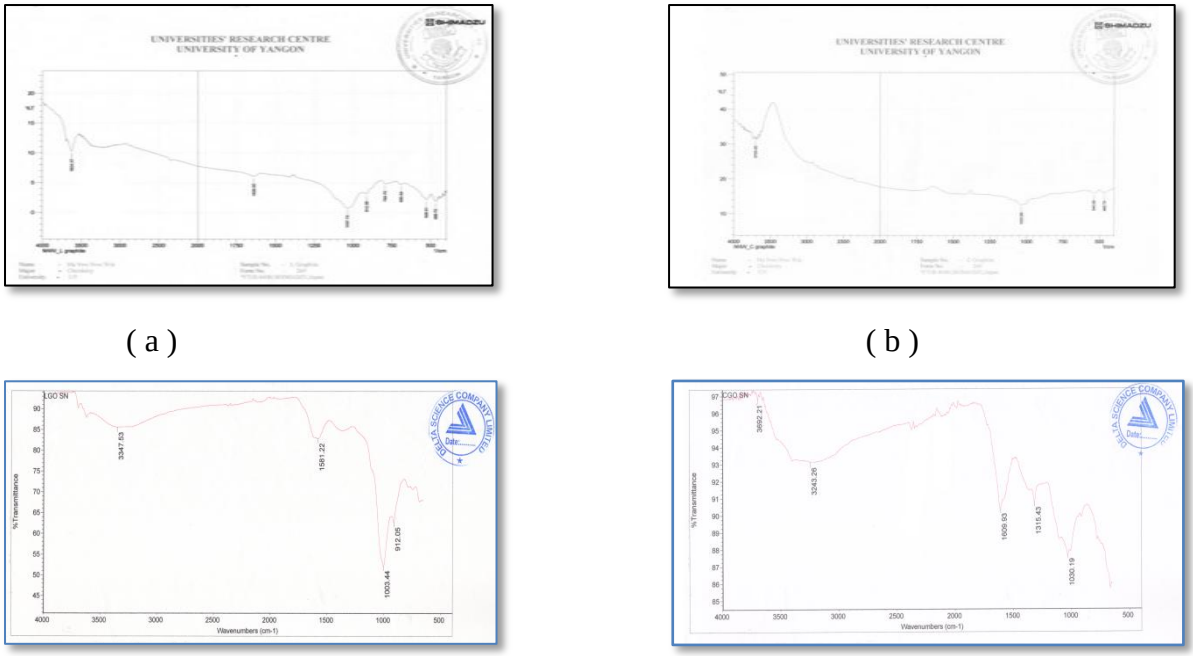

(a) (b)

(c) (d)

Figure 3 FT IR spectra of (a) LGP (b) CGP (c) LGO (d) CGO

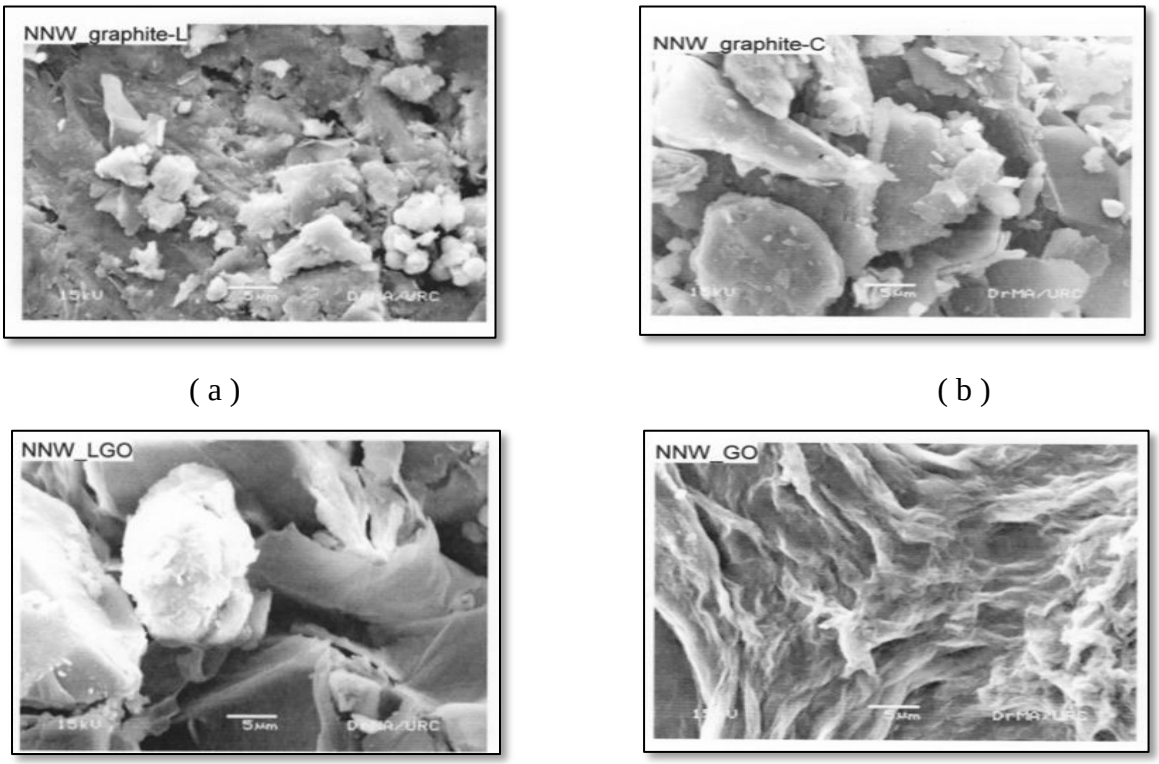

(a) (b)

(c) (d)

Figure 4 SEM micrograms of (a) LGP (b) CGP (c) LGO (d) CGO

Table 4 Removal Percent of Methylene Blue by Using Different Graphene Oxides (LGO, CGO) as a Function of Dosages

No.	Weight of Dosage (g)	Removal %	
		LGO	CGO
1	0.02	91.65 ± 0.66	88.88 ± 0.38
2	0.04	94.81 ± 0.13	94.26 ± 0.03
3	0.06	94.62 ± 0.26	95.45 ± 0.07
4	0.08	93.35 ± 0.16	96.14 ± 0.14
5	0.10	95.89 ± 0.03	96.18 ± 0.28
6	0.12	95.709 ± 0.53	94.35 ± 0.61
7	0.14	94.15 ± 0.26	95.91 ± 0.19

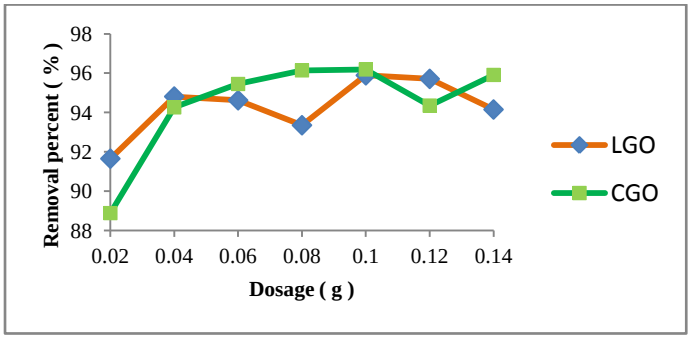

Experimental condition
Contact time = 60 min
Temperature = RT
Concentration of dye = 20 ppm
pH = 7.4
Stirring rate = 115 rpm
Volume of solution = 50 mL

Figure 5 Removal percent of methylene blue model solution by different graphene oxides as a function of dosages

Table 5 Removal Percent of Methylene Blue Model Solution by Using Different Graphene Oxides (LGO, CGO) as a Function of Concentrations

No.	Concentration of MB solution (ppm)	Removal %	
		LGO	CGO
1	5	94.93 ± 0.16	94.68 ± 0.87
2	10	96.46 ± 0.14	96.63 ± 0.34
3	15	96.78 ± 0.38	97.27 ± 0.68
4	20	96.51 ± 0.26	97.39 ± 0.08
5	25	97.09 ± 0.09	97.42 ± 0.25
6	30	97.61 ± 0.12	97.67 ± 0.46
7	35	97.00 ± 0.14	97.25 ± 0.43

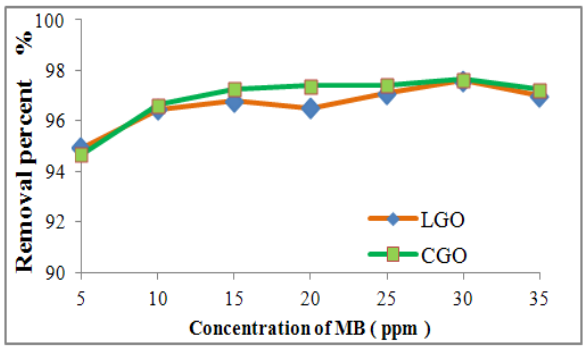

Experimental condition
Weight of dosage (LGO/CGO) = 0.1/0.1g
Contact time = 60 min
Temperature = RT
pH = 7.4
Stirring rate = 115 rpm
Volume of solution = 50 mL

Figure 6 Removal percent of methylene blue model solution by different graphene oxides as a function of concentrations of MB

Table 6 Removal Percents of Methylene Blue by Using Different Graphene Oxides (LGO, CGO) as a Function of Contact Times

No.	Contact Time (min)	Removal %	
		LGO	CGO
1	10	92.38 ± 0.06	93.27 ± 0.09
2	20	94.26 ± 0.02	97.08 ± 0.06
3	30	97.31 ± 0.09	97.71 ± 0.06
4	40	97.37 ± 0.03	98.02 ± 0.03
5	50	97.41 ± 0.04	98.03 ± 0.06
6	60	97.58 ± 0.09	98.11 ± 0.06
7	70	97.08 ± 0.02	97.67 ± 0.02

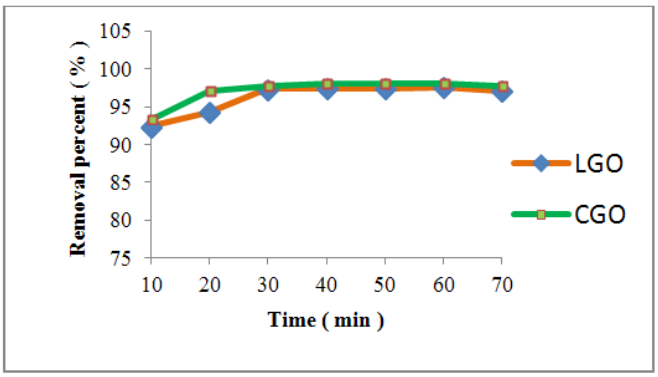

Experimental condition
Weight of dosage (LGO/CGO) = 0.1/0.1g
Concentration of dye (LGO/CGO) = 30 ppm
Temperature = RT
pH = 7.4
Stirring rate = 115 rpm
Volume of solution = 50 mL

Figure 7 Removal percent of methylene blue model solution by graphene oxides (LGO, CGO) as a function of contact times

Table 7 Removal Percents of Methylene Blue by Using Graphene Oxides (LGO, CGO) as a Function of Temperatures

No.	Temperature (ºC)	Removal %	
		LGO	CGO
1	25	98.77 ± 0.09	97.59 ± 0.06
2	30	98.86 ± 0.02	98.95 ± 0.06
3	35	98.91 ± 0.07	99.2 ± 0.04
4	40	98.95 ± 0.06	98.85 ± 0.02
5	45	99.05 ± 0.07	98.46 ± 0.12
6	50	99.50 ± 0.06	98.50 ± 0.07
7	55	99.28 ± 0.02	98.43 ± 0.06

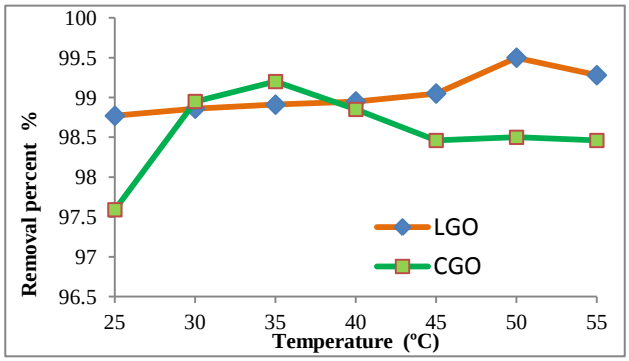

Experimental condition
Weight of dosage = 0.1 g
Stirring speed = 115 rpm
Concentration of dye = 30 ppm
Contact time = 60 min
pH = 7.4
Volume of solution = 50 mL

Figure 8 Removal percent of methylene blue model solution by graphene oxide (LGO, CGO) as a function of temperatures

Table 8 Removal Percent of Methylene Blue by Using different Graphene Oxides (LGO, CGO) as a Function of Stirring Speeds

No.	Stirring speed (rpm)	Removal %	
		LGO	CGO
1	25	82.64 ± 0.11	53.93 ± 0.29
2	50	90.64 ± 0.18	68.19 ± 0.25
3	75	91.91 ± 0.10	95.63 ± 0.05
4	100	98.69 ± 0.06	98.15 ± 0.31
5	150	99.37 ± 0.06	98.78 ± 0.06
6	200	99.19 ± 0.09	98.69 ± 0.02
7	250	98.96 ± 0.06	97.21 ± 0.19

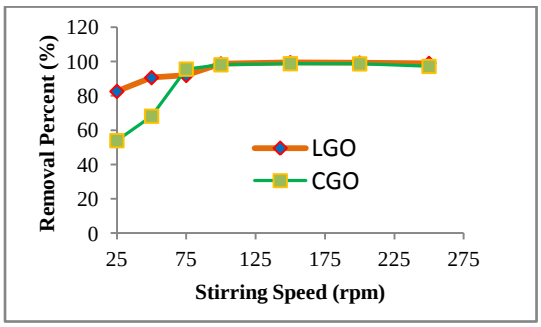

Experimental condition
Weight of dosage = 0.1 g
Concentration of dye = 30 ppm
Temperature =35ºC (CGO)/50 ºC (LGO)
pH = 7.4
Contact time = 60 min
Volume of solution = 50 mL

Figure 9 *Removal percent of methylene blue model solution by graphene oxides (LGO, CGO) as a function of stirring speeds*

Table 9 Removal Percent of Methylene Blue by Using Different Graphene Oxides (LGO, CGO) as a Function of pH

No.	pH	Removal %	
		LGO	CGO
1	2	99.13 ± 0.16	98.18 ± 0.35
2	4	98.99 ± 0.98	97.54 ± 0.02
3	6	99.57 ± 0.02	98.30 ± 0.16
4	7	99.01 ± 0.48	97.88 ± 0.71
5	8	99.62 ± 0.25	99.72 ± 0.13
6	10	98.03 ± 0.25	98.17 ± 0.32
7	12	84.96 ± 0.26	90.04 ± 0.39

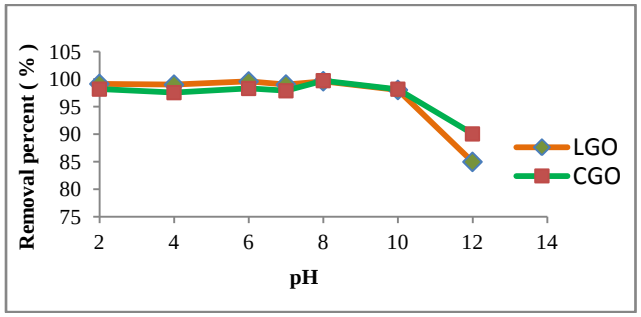

Experimental condition

Weight of dosage = 0.1 g
Concentration of dye = 30 ppm
Temperature = 35 ºC (CGO)/50 ºC (LGO)
Stirring speed = 150 rpm
Contact time = 60 min
Volume of solution = 50 mL

Figure 10 Removal percent of methylene blue model solution by prepared graphene oxides (LGO, CGO) as a function of pH

Table 10 The Optimal Parameters of Prepared Graphene Oxides (LGO, CGO) for Removal of Methylene Blue

No.	Dosage (g)	MB (ppm)	Time (min)	Temp (ºC)	rpm	pH	Removal %
LGO	0.1	30	60	50	150	8	99.67 ± 0.03
CGO	0.1	30	60	35	150	8	99.69 ± 0.03

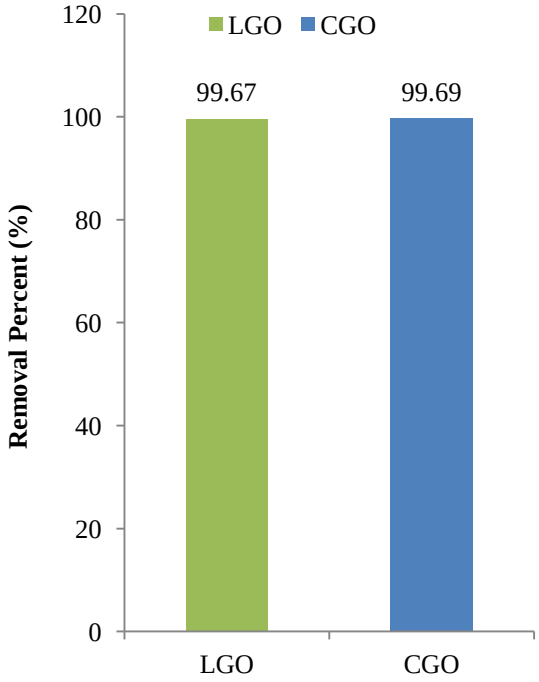

Figure 11 Comparison of removal percent of methylene blue solution under optimal condition

Conclusion

In this research, synthetic graphene oxides (LGO and CGO) were used as materials to remove the dyes from wastewaters. Removals of methylene blue by the prepared graphene oxides (LGO and CGO) were studied using model solutions of methylene blue.

In this work, the graphene oxides (LGO and CGO) produced from different graphite sources by using modified Hummer's method, were used as adsorbent to remove methylene blue (MB) from aqueous solution. Characterization of the prepared graphene oxides were carried out by XRD, UV-Vis, FT IR and SEM techniques. FT IR spectra showed the presence of ionizable groups such as carboxyl, carbonyl and hydroxyl in the graphene oxides (LGO and CGO). SEM micrographs indicated the changes of morphology from graphite to graphene oxide. Adsorption experiments were carried out at different parameters, such as dosage of GO, concentration of MB, temperature, time, stirring speed and pH. Adsorption capacity increase with increasing solution pH, MB concentration, dosage, temperature, contact time and rpm. Results show that the adsorption equilibrium, the removal efficiencies of all samples were higher than 99 % and the solution can be decolorized to almost colorless. Our results show that GO is an excellent adsorbent and can be used to treat effluents contaminated with dyes (MB concentrations).

Acknowledgements

The authors would like to thank the Myanmar Academy of Art and Science for allowing to present this paper and Professor and Head Dr Ni Ni Than , Department of Chemistry, University of Yangon, for her kind encouragement.

References

Ahmad, S., Supwatul, H. and Yuli, R. (2014). " The Effect of Contact Time and pH on Methylene Blue Removal by Volcanic Ash". *Int'l Conference on Chemical, Biological and Environmental Sciences (ICCBES)* vol. 14, pp. 11-13.

Atkovska, K., Kiril, L., Gordana, R., Aleksandar, T. D. and Anita, G. (2018). "Removal of Heavy Metal Ions from Wastewater Using Conventional and Nanosorbents : A Review". *Journal of Chemical Technology and Metallurgy,* vol. 53 (2), pp. 202-219.

Long, C., Yanhui, L., Jiankun, S., Qiuju, D., Xiaoxia, Y., Quan, J., Zonghua, W., Dechang, W. and Yanzhi, X. (2016). "Removal of Methylene Blue from Water by Cellulose/Graphene Oxide Fibers". *Journal of Experimental Nanoscience*, vol. 11(14), pp. 1156 – 1170.

Ozkan-Yucel, U.G. and Gokcayk, C.F. (2010). "Effect of Initial Azo Dye Concentration and Biomass Acclamation on Sludge Digestion and Dye Co-treatment". *Clean-Soil Air Water*, vol. 38, pp. 387–393.

Sayan, E. (2006). "Optimization and Modeling of Decolorization and COD Reduction of Reactive Dye Solutions by Ultrasound-Assisted Adsorption". *Chem. Eng. J.*, vol. 119, pp. 175–181.

Sheng, T. Y., Chen, S., Yanli, C., Aoneng, C., Yuanfang, L. and Haifang, W. (2011)." Removal of Methylene Blue from Aqueous Solution by Graphene Oxide". *Journal of Colloid and Interface Science,* vol. 359, pp. 24 – 29.

Song, J., Wang, X. and Chang, C. T. (2014). " Preparation and Characterization of Graphene Oxide". *Journal of Materials,* vol. 2014, pp. 1-6.

Sun, H., Yang, Y. and Huang, Q. (2011). " Preparation and Structural Variation of Graphite Oxide and Graphene Oxide". *Integrated Ferroelectrics an International Journal*, vol. 128, pp. 163-170.

INVESTIGATION OF CHEMICAL COMPOSITION AND SOME BIOLOGICAL PROPERTIES OF CHLOROFORM EXTRACT OF *PSEUDOMONAS AERUGINOSA*

Su Swe Su[1,2], Khine Zar Wynn Lae[3], Nwet Nwet Win[4], Daw Hla Ngwe[5]

Abstract

This research focuses on the chemical and pharmacological studies of bioactive secondary metabolites from *Pseudomonas aeruginosa* isolated by serial dilution plate method from the clinical soil sample collected in the Insein General Hospital, Yangon Region. The isolated bacteria *P.aeruginosa* identified by biochemical tests was cultured on nutrient agar medium in the large scale subsequently, the culture was centrifuged (20 min, 4 ºC, 3500 rpm). The cell-free supernatant was extracted with chloroform for 10 times to get the chloroform soluble compounds by liquid-liquid partition between chloroform and the culture solution 1:1 (v:v).This process was done according to the ultrasound-assisted extraction to give 0.03 % (w/v) of chloroform extract which was applied to investigate the chemical constituents and some biological activities. The preliminary screening of chemical constituents indicated the presence of alkaloids, α-amino acids, carbohydrates, flavonoids, phenolic compounds, polyphenols, steroids, tannins and terpenoids in the chloroform extract of *P.aeruginosa.* The total carbohydrates content (TCC), total tannins content (TTC), total phenols content (TPC), total steroids content (TSC), total flavonoids content (TFC) and total protein content of the chloroform extract determined according to the appropriate reported methods were found to be 283±2.15 mg GE/g ,177.58±5.8 mg GAE/g, 50.64±1.5 mg GAE/g, 50.43±4.01 mg CE/g , 24.70 ± 2.2mg QE/g and 4.43±0.8 mg BSAE/g respectively. The chloroform extract was found to exhibit the high antimicrobial activity against all seven tested microorganisms such as *Bacillus subtilis* (N.C.T.C-8236), *Staphylococcus auerus* (N.C.P.C-6371), *Pseudomonas aeruginosa* (6749), *Bacillus pumilus* (N.C.I.B-8982), *Candida albicans* (-), *Agrobacterium tumefacines*(N.I.T.E-09678) and *Escherichia coli* (N.C.I.B-8134) (20 mm ~40 mm) determined by agar well diffusion method. The antioxidant activity of chloroform extract was determined by DPPH radical scavenging activity assay (IC_{50} = 128.6 mg/mL).The chloroform extract was also subjected to investigate the antidiabetic activity via α-amylae and α-glucosidase inhibition activities assays. The extract was observed to possess the α-amylase inhibitory effect (IC_{50}= 3.16 μg/mL) and α-glucosidase inhibitory effect (IC_{50} = 19.5 μg/mL), however, those were weaker than the standard drug acarbose (IC_{50} = 0.02 μg/mL) and (IC_{50} = 0.04 μg/mL). The chloroform extract of *P. aeruginosa* showed significant toxicity against brine shrimp with an LD_{50} value of 1.90 mg/mL after 24 h. In antitumor activity analysis, *Agrobacterium tumerfaceins* (N.I.T.E -09678) cell was used as the tumor cell. In this study, the chloroform extract of *P. aeruginosa* was found to exhibit low value (IC_{50} =147.54 μg/mL) against *A. tumefacines* cell. *In vitro* antiproliferative activity of the chloroform extract was evaluated against A 549 (lung), Hela (cervical) and MCF-7 (breast) human cancer cell lines by using CCK-8 Assay (Cell Counting Kit-8). It was found that, the chloroform extract has the antiproliferative activity against A 549 lung cancer cell lines (IC_{50} = 12.18 μg/mL), Hela cervical cancer cell line (IC_{50} = 49.93 μg/mL) and MCF-7 breast cancer cell line (IC_{50} = 16.59 μg/mL). Furthermore, *in vitro* antiproliferative activity of the chloroform extract was also evaluated against six microorganisms such as *P.aeruginosa* (IC_{50}=98.38μg/mL), *S.auerus*(IC_{50}=155.76μg/mL),*B. pumilus* (IC_{50} = 360.23μg/mL), *B. subtilis* (IC_{50} = 411.03 μg/mL) , *C. albicans* (IC_{50} = 422.16 μg/mL), *A. tumefacines* (IC_{50} = 147.54 μg/mL) and *E. col* (IC_{50}=440.58 μg/mL).

Keywords *:* *Pseudomonas aeruginosa*, chemical constituents, antiproliferative activity, antioxidant activity, antimicrobial activity, cytotoxicity, antitumor activity, antidiabetic activity

[1] Assistant Lecturer, Department of Chemistry, University of Yangon
[2] Second Year PhD Student, Department of Chemistry, University of Yangon
[3] Dr, Lecturer, Department of Chemistry, University of Yangon
[4] Institute of Natural Medicine, University of Toyama , 2630-Sugitani,Toyama 930-0194,Japan
[5] Dr, Professor and Head (Retd.,), Department of Chemistry, University of Yangon

Introduction

Pseudomonas is a genus of gram-negative, aerobic gammaproteo-bacteria that can cause disease in animals, including humans. *Pseudomonas aeruginosa* is one of the main organisms responsible for drug-resistant nosocomial infections, and is one of the leading causes of bacteremia and pneumonia in hospitalized patients. Pseudomonads are of great interest because of their role in plant and human disease and their growing potential in biotechnological applications. The Pseudomonas common last ancestor has encountered a wide range of abiotic and biotic environments which have led to the evolution of a multitude of traits and life-styles with significant overlap among the species (Mena and Gerba, 2009). Pseudomonads are a large group of free-living bacteria that live primarily in soil, seawater, and fresh water. Especially, *P. aeruginosa* is particularly prevalent in environments, such as soil, seawater, sewage, and associated with some plants. Although commonly isolated from the marine environment, the apparent distribution has been restricted to river outfalls and shorelines (Velammal *et al.*, 1994). Contamination of recreational waters and drinking water has been associated with outbreaks of Pseudomonas. With this in mind, it should be emphasized that Pseudomonads are highly versatile and can adapt to a wide range of habitats; they can even grow in distilled water (Hardalo and Edberg, 1997). This adaptability accounts for their ubiquitous presence in the environment and accordingly they have an extensive impact on ecology, agriculture, and commerce (Mena and Gerba, 2009). *P. aeruginosa* is an opportunistic pathogen that is important in the etiology of many infectious diseases seen in humans (Silby *et al*., 2011). Infections with this bacterium are often characterized by blue pus, and the bacterium is commonly isolated from clinical specimens (wounds, burns, and urinary tract infections) (Ullstrom *et al*., 1991). For many degradation studies *Pseudomonas sp*. was selected as it is a well-known biodegrader of agrochemicals. *Pseudomonas* is a versatile genus and suggested that this genus could degrade a number of chemicals like pesticides including carbaryl, malathion, *p*-nitrophenol and parathion, bethoxazin, it is widely present in soil and can be used to clean up different xenobiotics compounds like propiconazole (Sarkar *et al.*, 2009). On the other hand, *P. aeruginosa* has been reported for use in bioremediation and use in processing polyethylene in municipal solid waste (Pathak, 2017). Given the great interest in the genus *Pseudomonas*, there are commercially available media for selective and differential growth of this genus. In this study,*P.aeruginosa* has been isolated from clinical soil samples by serial dilution plate method, followed by cultured in nutrient agar medium. In this research, chloroform extract of *P.aeruginosa* was applied to investigate the chemical constituents and some biological activities.

Materials and Methods

Sample Collection

Soil samples were collected from the Insein General Hospital, Yangon Region. Bacteriological analyses were started within 4 h after collecting the samples.

Isolation and Identification of *P. aeruginosa*

One gram of collected soil samples was weighed and added into a sterile conical flask containing 99 mL of sterile distilled water to make a dilution. The suspension was thoroughly shaken for about 30 min to disperse the individual particles. The conical flask was kept for about

30 min to settle down. Then 1 mL of soil dilution was introduced in the test tube containing 9 mL distilled water to make serial dilution of 10^{-2} to 10^{-6} using a serial pipette each time.

In addition, 100 mL of medium was boiled on a hot plate and sterilized by autoclaving for 15 min at 121 °C. The sterilized media was cooled down. The 20 mL of sterilized medium was poured into the sterilized petri-dishes containing 0.2 mL of serial dilution of each of soil sample.

The inoculate plates were shaken clockwise to make uniform distribution of the inoculums. When the agar was solidified, the inoculated plates were inverted and incubated at 37 °C for two days. The separate colonies were appeared and the different types of bacteria colonies were cultured in test tubes. The slants of media were repeatedly sub-cultured to obtain pure cultured (Atlas and Synder, 2006).

The isolated bacteria strains were sub-cultured on nutrient agar slant cultures to check its purity and incubated at 37 °C for 24 h. Then the purified culture was maintained at refrigerator. The isolates were subjected in various physiological and biochemical tests. The isolates were identified by using conventional biochemical tests such as motility test, indole test, methyl red test, gelatin test, citrate test, nitrate reduction test, catalase test, Voges-Proskauer (VP) test, urease test, starch hydrolysis test and sugar fermentation tests. (Atlas and Synder, 2006; Garcia and Isenberg, 2007) (Su Swe Su *et al.,* 2018). Moreover, the isolated bacteria *P.aeruginosa* was cultured on nutrient broth medium in the large scale subsequently, the culture was centrifuged (20 min, 4 ºC, 3500 rpm).The cell-free supernatant was extracted with chloroform for 10 times to get the chloroform soluble compounds by liquid-liquid partition between chloroform and the culture solution1:1 (v:v).This process was done according to the ultrasound-assisted extraction to give 0.03 % (w/v) of chloroform extract which was applied to investigate the chemical constituents and some biological activities.

Determination of Chemical Composition of the Chloroform Extract of *P. aeruginosa*

(a) Determination of chemical constituents present in the chloroform extract of *P. aeruginosa*

The chemical constituents such as alkaloids, α-amino acids, carbohydrates, flavonoids, phenolic compounds, polyphenols, steroids, tannins and terpenoids were determined according to the appropriate reported methods.

(b) Determination of total phenol content by Folin-Ciocalteu Reagent (FCR) method

The total phenolic content (TPC) of chloroform extract of *P. aeruginosa* was estimated by Folin-Ciocalteu (FC) method according to the procedure described by Song *et al.,* (2010). The extract solution (1000 µg/mL) was mixed with 5 mL of F-C reagent (1:10) in a test tube and incubated for about 5 min. To each test tube, 4 mL of 1 M sodium carbonate was added and the test tubes were kept at room temperature for 15 min and UV absorbance of reaction mixture was read at λ_{max} 765 nm. The blank solution was prepared as the above procedure by using distilled water instead of sample solution. Total phenol content was estimated as milligram gallic acid equivalent per gram (mg GAE/g) of extract.

(c) Determination of total flavonoid content by aluminium chloride method

The total flavonoid content (TFC) of chloroform extract of *P. aeruginosa* was estimated by Aluminium Chloride method according to the procedure described by Song *et al.* (2010). The extract solution (1000 µg/mL) was mixed with 1.5 mL of methanol, 0.2 mL of 1 % $AlCl_3$ solution

and 2.8 mL of distilled water. The absorbance of reaction mixture was at λ_{max} 415 nm. The blank solution was prepared as the above procedure by using distilled water instead of sample solution. Total flavonoid content was estimated as milligram quercetin equivalent per gram (mg QE/g) of extract.

(d) Determination of total steroid content by Zak's method

The total steroid content (TSC) of chloroform extract of *P. aeruginosa* was estimated by Zak's method according to the procedure described by Zak *et al.* (1981). The extract solution (1000 µg/mL) was prepared by ferric chloride diluting agent. The test sample solution (5 mL) was added 4.0 mL of concentrated sulphuric acid to each tube. After 30 min incubation, intensity of the colour was read at 450 nm. The blank solution was prepared as the above procedure by using ferric chloride diluting agent instead of sample solution. Total steroid content was estimated as milligram cholesterol equivalent per gram (mg CE/g) of extract.

(e) Determination of total condensed tannin by Broadhurst's method

The tannin contents of chloroform extract of *P. aeruginosa* was determined by method of Broadhurst and Jones (1978) with slight modification, using tannic acid as a reference compound. A volume of 0.4 mL of extract is added to 3 mL of a solution of vanillin and 1.5 mL of concentrated hydrochloric acid. After 15 min of incubation the absorbance was read at 500 nm. The blank solution was prepared as the above procedure by using methanol instead of sample solution. The condensed tannin was expressed as milligram of tannic acid equivalent per gram of extract.

(f) Determination of protein content by biuret method

A calibration curve of the standard protein solutions bovine serum albumin (BSA) is used to determine the total protein in the unknown. This (BSA) compound reacts with biuret reagent to give a indigo coloured product with absorption maximum at 560 nm. The sample solution (1 mL) was added with 4 mL of biuret reagent mixed and allowed to stand for 30 min at room temperature. The intensity of colour the violet to indigo developed was read at 560 nm. The blank solution was prepared as the above procedure by using distilled water instead of sample solution. The protein content was expressed as milligram of BSA equivalent per gram of sample solution.

(g) Determination of carbohydrate content by anthrone method

The total carbohydrate content was estimated by the method of anthrone (Hedge *et al.*,1962). Carbohydrate is first hydrolysed into simple sugars using dilute hydrochloric acid. In hot acidic medium glucose is dehydrated to hydroxmethyl furfural. This compound forms with anthrone a green coloured product. The extract solution (5 mL) was added with 2.5 mL of anthrone reagent and allowed to stand for 10 min. The intensity of colour the green to dark green developed was read at 630 nm. The blank solution was prepared as the above procedure by using distilled water instead of sample solution. The carbohydrate content was expressed as milligram of glucose equivalent per gram of sample.

Investigation of Some Biological Activity of Chloroform Extract of *P. aeruginosa*

(a) Investigation of antioxidant activity of chloroform extract of *P. aeruginosa*

In this experiment, DPPH (2 mg) was thoroughly dissolved in EtOH (100 mL). This solution was freshly prepared in the brown coloured reagent bottle and stored in the fridge for no longer than 24 h. The chloroform extract of *P. aeruginosa* (1.6 mg) and 10 mL of EtOH were thoroughly mixed by shaker. The mixture solution was filtered and the stock solution was obtained. By adding with EtOH, the sample solutions in different concentrations of 160, 80, 40, 20, 10 and 5 μg/mL were prepared from the stock solution. The effect on DPPH radical was determined by using the method of Marinova and Batchvarov (2011). The control solution was prepared by mixing 1.5 mL of 50 μM DPPH solution and 1.5 mL of EtOH using shaker. The test sample solution was also prepared by mixing thoroughly 1.5 mL of 50 μM DPPH solutions and 1.5 mL of each sample solution. The mixture solutions were allowed to stand at room temperature for 30 min. Then, the absorbance of each solution was measured at 517 nm by using UV-1650 spectrophotometer. Absorbance measurements were done in triplicate for each concentration and then mean values so obtained were used to calculate percent inhibition of oxidation. The capability to scavenge the DPPH radical was calculated by using the following equation: $\%\,\mathrm{RSA} = \dfrac{A_c - (A - A_b)}{A_c \times 100}$

Where, %RSA = Radical Scavenging Activity

A_c = absorbance of the control (DPPH only) solution

A_b = absorbance of the blank (EtOH + Test sample solution) solution

A = absorbance of the test sample solution

(b) Determination of antimicrobial activity of chloroform extract of *P. aeruginosa* by agar disc diffusion method

The screening of antimicrobial activity of chloroform extract of *P. aeruginosa* was carried out by agar disc diffusion method (Perez *et al*., 1990) at Fermentation Laboratory, Pharmaceutical Research Department, Ministry of Industry, Yangon, Myanmar. Six microorganisms namely *Bacillus subtilis, Staphylococcus aureus, Pseudomonas aeruginosa, Bacillus pumilus, Candida albicans* and *Escherichia coli* were used for this test.

(c) Determination of cytotoxicity

The cytotoxicity of chloroform extract of *P. aeruginosa* was investigated by using brine shrimp lethality bioassay according to the procedure described by Dockery and Tomkins, 2000. The brine shrimp (*Artemia salina*) was used in this study for cytotoxicity bioassay (Ali *et al*., 2016). Brine shrimp cysts (0.5 g) were added to the 1.5 L of artificial sea water bottle. This experiment was carried out at the Department of Chemistry, Yangon University, Myanmar. The suspension was aerated by bubbling air into the funnel and kept for 24 h at room temperature. After aeration had been removed, the suspension was kept for 1 h undisturbed, whereby the remaining unhatched eggs dropped. In order to get a higher density of larvae, one side of the separating funnel was covered with aluminium foil and the other illuminated with a lamp, whereby the phototropic larvae were gathering at the illuminated side and could be collected by pipette. The shrimp larvae were transferred to the chamber of ice cup filled with 9 mL of salt water and the dead larvae counted (number N). One mL of each solution of crude extracts (1, 10, 100, 1000 ppm) was added and the plate was then kept at room temperature in the dark. After

24 h, the dead larvae were counted in each well under the magnifier. The still living larvae (A) were killed by addition of ca. 0.5 mL methanol so that subsequently the total number of the animals (G) could be determined. The control solution was prepared as the above procedure by using distilled water instead of sample solution. The mortality (M) was calculated in %. Each test row was accompanied by a brine solution (number B). The mortality rate M was calculated by using the following formula:

$$M = \left[\frac{(A - B - N)}{(G - N)} \right] \times 100$$

M = percent of the dead larvae after 24 h
A = number of the dead larvae after 24 h
B = average number of the dead larvae in the brine solution after 24 h
N = number of the dead larvae before starting of the test.
G = total number of brine shrimps

(d) Determination of diabetic activity of chloroform extract of *P.aeruginosa*

(i) Determination of α-amylase inhibitory activity

The enzyme inhibitory activity was expressed as a decrease in units of maltose liberated *(Puls et al.1977).* A modified dinitrosalicylic acid (DNS) method was adopted to estimate the maltose equivalent 1mL of the tested samples were pre-incubated with 1 mL of phosphate buffer and 2 mL of α-amylase at 37 °C for 20 min and thereafter 0.4 mL 1% starch solution was added. The mixture was further incubated at 37 °C for 30 min. Then the reaction was stopped by adding 2 mL of DNS reagent and the contents were heated in a boiling water bath for 10 min. A blank was prepared without extract and another without the amylase enzyme, replaced by equal quantities of buffer. The absorbance was measured at 540 nm. The reducing sugar released from starch was estimated as maltose equivalent from a standard graph. Acarbose was used as standard. The anti-diabetic activity was determined through the inhibition of α-amylase which was expressed as a percentage of inhibition and calculated by the following equations:

$$\% \text{ Inhibition} = [A_{control} - (A_{Sample} - A_{Blank}) / A_{control}] \times 100$$

where, % Inhibition = % α-amylase inhibition
$A_{control}$ = absorbance without sample solution
A_{sample} = absorbance of sample
A_{Blank} = absorbance of sample + distilled water solution

The α-amylase inhibition (IC_{50}) is expressed as the test substance concentration (µg/mL) that results in a 50 % α-amylase inhibition of the sample. The IC_{50} values were calculated by linear regressive excel program. The standard deviation was also calculated by the following equation.

$$\text{Standard Deviation (SD)} = \sqrt{\frac{(\bar{x} - x_1)^2 + (\bar{x} - x_2)^2 + ...(\bar{x} - x_n)^2}{(n-1)}}$$

where, $\bar{x}$ = average % inhibition
$x_1 + x_2 + ... + x_n$ = % α-amylase inhibition of test sample solution
n = number of time

(ii) Determination of α-glucosidase inhibitory activity

The α -glucosidase inhibitory activity was measured the procedure described by (*Puls et al*. 1977). The α -glucosidase was assayed using 0.4 mL of sample extract and 1mL of 0.1 M phosphate buffer (pH 6.9) containing 2 mL of α -glucosidase solution, which was then incubated at 37 °C for 10 min. After the pre-incubation period, 0.5 mL of 0.005M *p*-nitrophenyl- α -D-glucopyranoside solution was added to each well at timed intervals. The reaction mixtures were incubated at 37 °C for 5 min. After incubation, absorbance readings of the sample was recorded at 405 nm and compared with a control that had 0.4 mL of buffer solution in place of the extract. Acarbose was used as standard. The anti-diabetic activity was determined through the inhibition of α -glucosidase which was expressed as a percentage of inhibition and calculated by the following equations:

$$\% \text{ Inhibition} = [A_{control}-(A_{Sample} - A_{Blank})/ A_{control}] \times 100$$

where,% Inhibition = % □-glucosidase inhibition

$A_{control}$ = absorbance without sample solution

A_{sample} = absorbance of sample

A_{Blank} = absorbance of sample + distilled water solution

The α - glucosidase inhibition (IC_{50}) is expressed as the test substance concentration (μg/mL) that results in a 50% α -glucosidase inhibition of the sample. The IC_{50} values were calculated by linear regressive excel program. The standard deviation was also calculated by the following equation.

$$\text{Standard Deviation (SD)} = \sqrt{\frac{(\bar{x}-x_1)^2+(\bar{x}-x_2)^2+.....(\bar{x}-x_n)^2}{(n-1)}}$$

where, $\bar{x}$ = average % inhibition

$x_1 + x_2 + \ldots + x_n$ = % α-glucosidase inhibition of test sample solution

n = number of times

(e) Determination of antiproliferative activity of chloroform extract of *P.aeruginosa* by turbidimetric assay

According to turbidimetric assay *in vitro* antiproliferative activity of chloroform extract of *P.aeruginosa* was determined against the tumor cell *A. tumerfaceins* (Elian and Herida (2015) at Department of Chemistry, University of Yangon. The diluted cell solution (9 mL) was mixed the sample solution (1 mL) was incubation in an incubator for 12 h. After incubation, absorbance readings of the samples were recorded at 600 nm and compared with a control that had the diluted cell culture and 1 mL of fresh nutrient medium was used in place of the extract as the blank. Fluorouracil (5-FU) was used as standard. The anti-proliferative activities were determined clindamycin, ciprofloxacin, ampicillin, flucloxacillin, fluconazole, aziythromycin used as a standard antibiotic through the inhibition of *Agrobacterium tumerfaceins* cell, *B. subtilis, B. pumilus, P. aeruginosa, S. aureus, C. albicans* and *E. coli*, respectively which was expressed as a percentage of inhibition and calculated by the following equations:

$$\% \text{ Inhibition} = [A_{control}-(A_{Sample} - A_{Blank})/ A_{control}] \times 100$$

where,

% Inhibition = % cell inhibition

$A_{control}$ = absorbance without sample solution

A_{sample} = absorbance of sample

A_{Blank} = absorbance of sample + fresh nutrient broth medium

The cell inhibition (IC_{50}) is expressed as the test substance concentration (µg/mL) that results in a 50% cell inhibition of the sample. The IC_{50} values were calculated by linear regressive excel program. The standard deviation was also calculated by the following equation

$$\text{Standard Deviation (SD)} = \sqrt{\frac{(\bar{x}-x_1)^2+(\bar{x}-x_2)^2+.....(\bar{x}-x_n)^2}{(n-1)}}$$

where, $\bar{x}$ = average % inhibition

$x_1 + x_2 + \ldots + x_n$ = % cell inhibition of test sample solution

n = number of times

(f) Investigation of antiproliferative activity of chloroform extract against Human Cancer Cell Lines

Antiproliferative activity of chloroform extract of *P.aeruginosa* was investigated in *in vitro* by using cancer cell lines at Division of Natural Product Chemistry, Institute of Natural Medicine, and University of Toyama, Japan. The cell lines used were Hela (human cervix cancer), A549 (lung cancer) and MCF 7 (human breast cancer). K562 µ-Minimum essential medium with L-glutamine and phenol red (α-MEM, Wako) were used for cell cultures. All media were supplemented with 10 % fetal bovine serum (FBS, sigma) and 1% antiobiotic antimycotic solution (Sigma). For MCF 7 cell, 1 % 0.1 M non-essential amino acid (NEAA, Gibco) and 1% 1mM sodium pyruvate (Gibco) were also supplemented. The *in vitro* antiproliferative activity of the crude extracts was determined by the procedure described by (Win *et al.* 2015). Briefly, each cell line was seeded in 96-well plates (2×10^3 per well) and incubated in the respective medium at 37 °C under 5 % CO_2 and 95 % air for 24 h. After the cells were washed with PBS (Nissui Pharmaceuticals), serial dilutions of the tested samples were added. After 72 h incubation, the cells were washed with PBS and 100 µL of medium containing 10 % WST-8 cell counting kit (Dojindo; Kumamoto, Japan) solution was added to the wells. After 2 h incubation, the absorbance at 450 nm was measured. The concentrations of the crude extracts were 200, 100, 10 µg/ mL and 10, 1, 0.1 mM for positive control were prepared by serial dilution. Cell viability was calculated from the mean values of the data from three wells using the equation below and antiproliferative activity was expressed as the IC_{50} (50 % inhibitory concentration) value. 5-fluorouracil (5FU) was used as positive control.

$$\text{(\%) Cell viability} = 100 \times \frac{\{Abs_{(\text{test samples})} - Abs_{(\text{blank})}\}}{\{Abs_{(\text{control})} - Abs_{(\text{blank})}\}}$$

In vitro antiproliferative activity of the chloroform extract was evaluated against A 549 (lung), Hela (cervical) and MCF-7 (breast) human cancer cell lines by using CCK-8 Assay (Cell Counting Kit-8).

Results and Discussion

In this study, *P. aeruginosa* bacterial strain, identified by the biochemical characteristics was isolated from the clinical soil sample of Insein General Hospital, Yangon Region (Su Swe Su *et al.*, 2018). The isolated bacteria *P.aeruginosa* was cultured on nutrient agar medium in the large scale subsequently, the culture was centrifuged(20min,4ºC,3500 rpm). The cell-free supernatant was extracted with chloroform for 10 times to get the chloroform soluble compounds by liquid-liquid partition between chloroform and the culture solution 1:1 (v:v). This process was done according to the ultrasound-assisted extraction to give 0.03 % (w/v) of chloroform extract which was applied to investigate the chemical constituents and some biological activities. In order to find out the types of chemical constituents present in the chloroform extract of *P.aeruginosa* was observed that various secondary metabolites such as alkaloids, α-amino acids, carbohydrates, flavonoids, phenolic compounds, polyphenols, steroids, tannins and terpenoids were observed in the chloroform extract of *P. aeruginosa* but cardiac glycosides, glycosides, organic acids, reducing sugars and starch were not found. These secondary metabolites contribute significantly towards the biological activities of chloroform extract of *P.aeruginosa* such as antidiabetic, antioxidant, antimicrobial, cytotoxicity, antiproliferative activities etc. The sample for screening was found to possess the flavonoids, phenols and tannis. Flavonoids are also present as a potent water-soluble antioxidant and free radical scavengers, which prevent from the oxidative cell damage and also have strong anticancer activity. It also helps in managing diabetes induced oxidative stress (Yadav *et al*., 2014).

Total Phenol, Total Flavonoid, Total Steroid, Total Condensed Tannin, the Protein and Total Carbohydrate Contents of the Chloroform Crude Extracts of *P.aeruginosa*

The total phenol content of the chloroform extract of *P.aeruginosa* was determined with spectrophotometric method by using Folin-Ciocalteu reagent. The total phenol content of the chloroform extract of *P.aeruginosa* was 50.64 ± 1.5 mg GAE/g. The total flavonoid content of sample was determined with spectrophotometric method by aluminium chloride reagent and was found to be 24.70 ± 2.2 mg QE/g. The total steroid content of the chloroform extract of *P.aeruginosa* was determined by Zak's method and was observed to be 50.43 ± 4.0 mg CE/g. The total tannin content in the chloroform extract of *P.aeruginosa* was estimated by Broadhurst's method and was found to be 177.58 ± 5.8 mg TAE/g. The protein content in the chloroform extract of *P.aeruginosa* was estimated by Biuret method was found to be the same content of 4.43 ± 0.8 mg BSAE/g and total carbohydrate content of the chloroform extract was determined by anthrone method was observed to be 283.0±2.15 mg GE/g. The results are shown in Table1.

Table 1 Total Phenol, Total Flavonoid, Total Steroid, Total Tannin, Total Protein and Total Carbohydrate Contents of Chloroform Extract of *P.aeruginosa*

Chemical Constituents	Contents
Total Phenol Content (mg GAE ± SD)/g of extract	50.64 ± 1.5
Total Flavonoid Content (mg QE ± SD)/g of extract	24.70 ± 2.2
Total Steroid Content (mg CE ± SD)/g of extract	50.43 ± 4.0
Total Tannin Content (mg TAE ± SD)/g of extract	177.58 ± 5.8
Total Protein Content (mg BSAE ± SD)/g of extract	4.43 ± 0.8
Total Carbohydrate Content (mg GE ± SD)/g of extract	283.0±2.15

In the experimental results, phenol, flavonoid, steroid and tannin compounds were observed in chloroform extract of *P.aeruginosa*. Tannins and carbohydrate have amazing stringent properties. They are known to hasten the healing of wounds and inflamed mucous membranes. Flavonoids are also present as a potent water-soluble antioxidant and free radical scavengers, which prevent from the oxidative cell damage and also have strong anticancer activity. It also helps in managing diabetes induced oxidative stress. The steroids are among the most widely used class of drugs and their role in the therapy of pulmonary, inflammatory, dermatological and oncological diseases has been well described (Meikle and Tyler, 1977). Protein molecule is composed of amino acids which are characterized by containing nitrogen and sometimes sulphur. There are twenty two amino acids that can be found in the human body, and about ten of these are essential, and therefore must be included in the diet. A few amino acids from protein can be converted into glucose used for fuel through a process called gluconeogenesis; this is done in quantity only during starvation (WFP, 1998).

Some Biological Activities of Chloroform Extract of *P.aeruginosa*

Antioxidant activity of the chloroform extract of *P.aeruginosa*

The antioxidant activity was measured in terms of hydrogen donating or radical scavenging ability of the chloroform extract of *P.aeruginosa* by using the stable radical DPPH. The results are shown in Table 2. The chloroform extract of *P.aeruginosa* was found to be the concentrations (IC_{50}) of 128.6 μg/mL, however, it was weaker than the standard gallic acid (IC_{50} = 0.75 μg/mL)

Table 2 Antioxidant Activity of Crude Extracts of *P.aeruginosa*

Sample	% RSA (mean ±SD) in different concentrations (μg/mL)				IC_{50} (μg/mL)
	20	40	80	160	
Chloroform Extract	16.00±2.88	17.60±2.12	40.53±3.23	56.27±2.01	128.6

Antimicrobial activity of the chloroform extract of *P.aeruginosa*

The chloroform extract of *P.aeruginosa* was subjected to screening of antimicrobial activity against six different pathogenic microbes such as *Bacillus subtilis, Staphylococcus aureus, Pseudomonas aeruginosa, Bacillus pumilus, Candida albicans and Escherichia coli* using agar well diffusion method. This method is based on zone diameter including the well diameter, in millimeter (mm). The chloroform extract of *P.aeruginosa* was found to be high in antimicrobial activity against all tested microorganisms with the inhibition zone diameter ranged between 20 ~ 40 mm. The results are shown in Table 3.

Table 3 Inhibition Zone Diameters of the Chloroform Extract of *P.aeruginosa* against Seven Microorganisms by Agar Well Diffusion Method

Organisms	Inhibition zone diameter (mm) of extract	
	$CHCl_3$	Control
Bacillus subtilis	20 (+++)	-
Staphylococcus aureus	40 (+++)	-
Pseudomonas aeruginosa	38 (+++)	-
Bacillus pumilus	40 (+++)	-
Candida albicans	40 (+++)	-
Escherichia coli	36 (+++)	-

Agar well – 10 mm, 10 mm ~ 14 mm (+), 15 mm ~ 19 mm (++), 20 mm and above (+++)

This high antimicrobial activity (20 mm ~ 40mm) against *Bacillus subtilis*(N.C.T.C-8236),*Staphylococcus aueru* (N.C.P.C6371) , *Pseudomonas aeruginosa* (6749), *Bacillus pumilus* (N.C.I.B-8982), *Candida albicans*(-) , *Escherichia coli* (N.C.I.B-8134) and *Agrobacterium tumefacines* (N.I.T.E – 09678) may be the present of the flavonoids, phenols and tannis.

Cytotoxicity of the chloroform extract of *P.aeruginosa*

The cytotoxicity of chloroform extract of *P.aeruginosa* was evaluated by brine shrimp cytotoxicity bioassay. This bioassay is general toxicity screening for bioactive phytoconstituents and their derivatives. A model animal that has been used for this purpose is the brine shrimp, *Artemia salina* (Tawaha, 2006). The cytotoxicity of the extract was expressed in term of mean ± SEM (standard error mean) and LD_{50} (50% Lethality Dose) and the results are shown in Table 4. In this experiment, standard potassium dichromate ($K_2Cr_2O_7$) and caffeine were chosen because $K_2Cr_2O_7$ is well-known toxic for this assay (Salinas and Fernendez, 2006) and caffeine is a natural product. According to the results of brine shrimp cytotoxicity bioassay, the tested sample has cytotoxic effect with the LD_{50} value of 1.90 µg/mL and it was observed to be toxic camparable to $K_2Cr_2O_7$ (LD_{50} = 1.50 µg/mL).

Table 4 Cytotoxicity of Chloroform Extract of *P.aeruginosa*

Crude extract	Dead % in different concentrations (µg/mL) of samples				LD_{50} (µg/mL)
	1	10	100	1000	
$CHCl_3$ Extract	46.66 ± 0.57	80 ±0.10	90±0.10	100±0.10	1.90
*Caffeine	0±0	0±0	9.58±0.91	12.73±0.41	>1000
*$K_2Cr_2O_7$	48.63±0.19	73.13±0.47	74.67±0.11	100±0.10	1.50

*****standard

Anti-diabetic activity of chloroform extract of *P.aeruginosa*

Based on the *in vitro* assay model, the chloroform extract of *P.aeruginosa* occurred to inhibited α-amylase and α -glucosidase enzymes. The chloroform extract of *P.aeruginosa* was demonstrated a relatively high α -amylase and α -glucosidase inhibitory activity with the values of IC_{50} values of 3.16 µg/mL (Table 5) and IC_{50} values of 19.5 µg/mL (Table 6) respectively, however, weaker than that of standard acarbose IC_{50} = 0.02 µg/mL(Table 7) and IC_{50} = 0.04 µg/mL(Table 8) . α -Amylase and α-glucosidase are key enzymes involved in starch breakdown and subsequent glucose release leading to rapid intestinal absorption. When inhibited by a high

carbohydrate diet, these enzymes are beneficial in maintaining the postprandial blood sugar level and managing hyperglycemia (Puls *et al*., 1977). A major drawback of currently used α -amylase and α -glucosidase inhibitors, such as pharmacologically beneficial acarbose, are reported to have side effects, such as abdominal distention, flatulence, tympanitis, and diarrhea. These side effects are possibly due to complete inhibition of α -amylase, leaving the carbohydrate to ferment in the colon (Bischoff, 1994). Thus, integrating natural inhibitors from dietary edible plants with strong inhibitory effects against α-amylase and α-glucosidase can be potentially targeted as a more complimentary and effective therapy for postprandial hyperglycemia control with minimal side effects.

Table 5 α-Amylase Inhibition and IC_{50} of Chloroform Extract of *P.aeruginosa*

Tested sample	% Inhibition in different concentrations (μg/mL)					IC_{50} (g/L)
	0.625	1.25	2.5	5	10	
$CHCl_3$ Extract	24.95±1.14	27.43±3.74	37.041±5.79	86.18±17.69	107.56±2.92	3.16

Table 6 α-Glucosidase Inhibition and IC_{50} of Chloroform Extract of *P.aeruginosa*

Tested sample	% Inhibition in different concentrations (mg/mL)					IC_{50} (μg/mL)
	6.25	12.5	25	50	100	
$CHCl_3$ Extract	5.62 ±1.6	24.94±0.7	69.74±0.2	84.26±0.3	98.26±1.5	19.5

Table 7 α-Amylase Inhibition and IC_{50} of Standard Acarbose

Tested sample	% Inhibition in different concentrations (μg/mL)						IC_{50} (μg/mL)
	0.009765	0.019531	0.03906	0.0781	0.156	0.31	
Acarbose	36.8±6.8	58.39±4.9	141.61±3.2	154.58±2.5	162.2±1.3	173.69±5.4	0.02

Table 8 α-Glucosidase Inhibition and IC_{50} of Standard Acarbose

Tested sample	% Inhibition in different concentrations (μg/mL)						IC_{50} (μg/mL)
	0.0390625	0.078125	0.15625	0.3125	0.625	0.31	
Acarbose	48.68±1.3	54.98±0.8	66.13±0.8	96.09±1.0	115.79±1.2	125.39±1.1	0.04

Antiproliferative Activity of Chloroform Extract of *P.aeruginosa* on *Agrobacterium tumerfaceins* cell

Antiproliferative activity of chloroform extract of *P.aeruginosa* was determined by the turbidimetric method. The turbidimetric assay technique is based on the fact that within a certain range of antibiotic concentration, the partial inhibition of the growth of the test organism occurs and there is a gradient in bacterial growth with increasing concentration of antibiotics. Peptone was used to culture for bacterial cell. Peptone is a semi-digested protein which is soluble in water and easily metabolized by the bacterial cell, provides the rich source of protein to the bacterial cell of the rapid growth. *In vitro* antiproliferative activity of the chloroform extract was evaluated against sixmicroorganisms such as *B.subtilis* (N.C.T.C8236), *S.auerus* (N.C.T.C6371),

P.aeruginosa, *B. pumilus* (N.C.I.B-8982), *C.albicans* and *E. coli* (N.C.I.B-8134). Based on the results, the chloroform extract of *P. aeruginosa* showed the highest antiproliferative activity (IC_{50} = 98.38 µg/mL), that followed by *A.tumefacines* (IC_{50} = 147.54 µg/mL),

S. auerus (IC_{50} = 155.76 µg/mL), *B. pumilus* (IC_{50} = 360.23 µg/mL2), *B.subtilis* (IC_{50} = 411.03 µg/mL) , *C.albicans* (IC_{50} = 422.16 µg/mL) , and *E. col* (IC_{50} = 440.58 µg/mL) (Table 9). However, the chloroform extract was weaker than standard antibiotics.

Table 9 Antiproliferative Activity of *P.aeriginosa* Chloroform Extract by Turbidometric Method

Tested sample	50 % Inhibition concentrations IC_{50} (µg/mL)						
	P.aeruginosa	***A.tumefacines***	***S.aureus***	***B.pumilus***	***B.subtilis***	***C.albicans***	***E.coli***
$CHCl_3$ extract	98.38	147.54	155.76	360.23	411.03	422.16	440.58
Antibiotics	70.69	0.17	143.71	212.15	98.38	118.33	196.64

Antibiotics = Clindamycin for *B.subtilis* , Flucloxacillin for *S. auerus*, Ampicillin for *P. aeruginosa*, Fluconazole for *C.albicans*, Ciprofloxacin for *B. pumilus* , Azithromycin for *E. col*, 5 FU for *A.tumefacines*

Antiproliferative Activity of the *P. aeriginosa* Chloroform Extract against Human Cancer Cell Lines

Antiproliferative activity is the activity relating to a substance used to prevent or retard the spread of cells, especially malignant cells, into surrounding tissues. Antiproliferative activity of the sample was studied in *in vitro* against human cancer cell lines. Screening of antiproliferative activities of chloroform extract of *P.aeruginosa* was done against three human cancer cell lines such as A 549 (human lung cancer), MCF7

(human breast cancer) and Hela (human cervix cancer). Antiproliferative activity was expressed as the IC_{50} (50 % inhibitory concentration) value. 5-Fluorouracil was used as positive control. The antiproliferative activity of crude extracts is summarized in Table 8. Since the lower the IC_{50} values, the higher the antiproliferative activity, in antiproliferative activity. It was observed that the chloroform extract has the antiproliferative activity against human lung cell A 549 (IC_{50} = 12.18 µg/mL) comparable to the standard 5FU (IC_{50} = 10.2 µg/mL) (Table 10) . Then, the chloroform extract has the antiproliferative activity against human breast cancer MCF7 (IC_{50} = 49.93 µg/mL) and human cervix cancer Hela (IC_{50} = 16.59 µg/mL). However, the chloroform extract was weaker than standard 5FU.

Table 10 Antiproliferative Activity of Chloroform Extract of *P. aureginosa* against Human Lung (A549), Breast (MCF7), and Cervix (HeLa) Cancer Cell Lines

Samples	50 % Inhibition (IC_{50} μg/mL) of the sample against human cancer cell lines		
	Lung A549	**Breast MCF7**	**Cervix HeLa**
ChloroformExtract	12.18	49.93	16.59
*5-Fluorouracil	10.2	11.5	6.93

A 549 = Lung cancer cell line; MCF 7 = Breast cancer cell line; Hela= Cervix cancer cell line,
*5 FU = 5 Fluorouracil

Conclusion

From the overall assessment concerning with the investigation of chemicals and biological activities on the chloroform extract 0.03 % (w/v) of *P.aeruginosa* isolated from the clinical soil sample collected in the Insein General Hospital, Yangon Region the following inferences could be deduced. Various types of secondary metabolites such as alkaloids, α-amino acids, carbohydrates, flavonoids, phenolic compounds, polyphenols, steroids, tannins and terpenoids were found to be present in chloroform extract of *P. aerugenosa.* No harmful constituent cyanogenic glycosides was observed. The chloroform extract contains significant high TCC content (283±2.15 mg GE/g),TTC content (177.58±5.8 mg GAE/g) compared to TPC content (50.64±1.5 mg GAE/g), TSC content (50.43±4.01 mg CE/g), TFC content (24.70 ± 2.2 mg QE/g) and total protein content (4.43±0.8 mg BSAE/g). It showed high antimicrobial activity (20 mm ~ 40mm) against *Bacillus subtilis* (N.C.T.C-8236), *Staphylococcus aueru*(N.C.P.C6371), *Pseudomonas aeruginosa* (6749), *Bacillus pumilus* (N.C.I.B-8982), *Candida albicans* (-) and *Escherichia coli* (N.C.I.B-8134) due to contain the flavonoids, phenols and tannis. The chloroform extract also showed DPPH free radical scavenging activity assay (IC_{50} = 128.6 mg/mL) has antioxidant activity. The chloroform extract possessed the antidiabetic activity due to its α-amylase inhibitory effect (IC_{50}= 3.16 µg/mL) and α -glucosidase inhibitory effect (IC_{50} = 19.5 µg/mL).It exhibited the cytotoxicity effect against brine shrimp (LD_{50} value of 1.91 mg/mL) indicating that it may possess the anticancer property. The chloroform extract was found to possess the antiproliferative activity against tested microorganisms in the order of *P.aeruginosa* (IC_{50} = 98.38µg/mL), *A.tumefacines* (IC_{50} =147.54 µg/mL), *B. pumilus* (IC_{50} = 155.75 µg/mL), *S.aureus* (IC_{50} = 360.23 µg/mL), *B. subtilis* (IC_{50} = 411.02 µg/mL), *E. coli* (IC_{50} = 440.58 µg/mL) and *C. albicans* (IC_{50} = 442.163 µg/mL) as well as human cancer cell lines such as A 549 lung cancer cell line (IC_{50} = 12.18 µg/mL) Hela cervical cancer cell line (IC_{50} = 49.93 µg/mL) and MCF-7 breast cancer cell line (IC_{50} = 16.59 µg/mL). It was observed that the chloroform extract has the antiproliferative activity against human lung cell A549 (IC_{50} = 12.18 µg/mL) comparable to the standard 5FU (IC_{50} = 10.2 µg/mL) among the three human cancer cell line. These data indicate that *P. aeruginosa* microorganism is the good source of bioactive compounds and this information will be beneficial for further utilization and development of anticancer compounds from soil microorganisms and as lead compounds for pharmaceutical industry in the future.

Acknowledgements

The authors would like to express their profound gratitude to the Department of Higher Education (Lower Myanmar), Ministry of Education, Yangon, Myanmar, for provision of opportunity to do this research and Myanmar Academy of Arts and Science for allowing to present this paper. Grateful thanks are also to Professor Dr Hiroyuki Morita, Institute of Natural Medicine, University of Toyama for his help and suggestions throughout course of antiproliferative activity .

References

Ali, N., Zada, A., Ali, M. and Hussain, Z. (2016). "Isolation and Identification of *Agrobacterium tumefaciens* from the Galls of Peach Tree". *Journal of Rural Development and Agriculture*, vol. 1 (1), pp. 39-48.

Aldona, B. and Raymond, S. (1994). "*Pseudomonas aeruginosa*: Infections and Treatment", *Journal of Information Health Care*, vol.4, pp. 83-84.

Atlas, R. M. and Snyder, J. W. (2006). "*Handbook of Media for Clinical Microbiology*". New York: 2nd Ed., CRC Publisher, pp. 278-339.

Bischoff, H. (1994). "Pharmacology of Glucosidase Inhibitor". *Eur. J. Clin. Invest.* vol.24, pp. 3–10.

Broadhurst, R. B. and Jones, W. T. (1978). "Analysis of Condensed Tannins using Acidified Vanillin". *J. Sci. Food Agr.*, vol. 29, pp. 788-794.

Devnath. P., Md. Kamal Uddin, F. Ahamed, Md. Towhid Hossain and M. Abul Manchur. (2011). "Extraction, Purification and Characterization of Pyocyanin Produced by *Pseudomonas aeruginosa* and Evaluation for its Antimicrobial Activity" .*International Research Journal of Biological Sciences*, **6**(5), 1-6

Dockery, M. and Tomkins, S. (2000). *Brine Shrimp Ecology*. London : 1st Ed., The British Ecology Society, pp. 92-93.

Elian, G. and Herida , R. .(2015). " Rapid Turbidimetric Assay to Determination the Potency of Daptomycin in Lyophilized Powdwer". *Journal of Pharmaceutics*, vol **7** , pp. 106-111

Garcia, L. S. and Isenberg, H. D. (2007). "*Aerobic bacteriology: Clinical Microbiology Procedures Handbook*". Washington, D.C.: 2nd Ed., vol. 3(1) , pp. 3-8.

Hardalo, C. and Edberg, S. C. (1997). "*Pseudomonas aeruginosa*: Assessment of Risk from Drinking Water". *Critical Reviews in Microbiology*, vol.23 (1), pp. 47-75.

Hedge, J. E., Hofreiter ,B.T. Whistler, R.L. and BeMiller, J.N.(1962). "*Methods in Carbohydrate Chemistry*".New York: Academic Press, vol.17, pp.420.

Marinova, G. V. and Batchvarov, V. (2011). "Evaluation of the Mehthods for Determination of the Free Radical Scavenging Activity of DPPH". *Bulgarian Journal of Agricultural Science*, vol. 17, pp. 11-24.

Meikle, A. W. and Tyler. F. H. (1977). "Potency and Duration of Action of Glucocorticoids. Effects of Hydrocortisone, Prednisolone and Dexamethasone on Human Pituitary Adrenal Function". *Am J Med*., vol. 63, pp. 200- 207.

Mena, K. D. and Gerba, C. P. (2009). "Risk Assessment of *Pseudomonas aeruginosa* in Water". *Reviews of Environmental Contamination and Toxicology*, vol.201, pp.71-115.

Pathak, V. M. (2017). "Review on the Current Status of Polymer Degradation: a Microbial Approach". *Bioresources and Bioprocessing. vol.4(15), pp.* 2197-4365

Perez, C., Paul, M. and Bazerque, P. (1990). "Antibiotic Assay by Agar Well Diffusion Method.". *Alta Bio Med Group Experiences*,vol. 15, pp. 113-115.

Puls, W., Keup, U., Krause, H. Thomas, P.G and Hoffmeister, F. (1977). "Glucosidase Inhibition: A New Approach to the Treatment of Diabetes, Obesity and Hyperlipoproteinemia". Naturwissenschaften vol, 64, pp. 536– 537.

Sarkar, S., Sreenivasan, S. and Premkumar, R. (2009) "Biodegradation of Propiconazole by *Pseudomonas putida* Isolated from Tea Rhizosphere". *Plant Soil Environ*. vol, 55,pp. 196-201.

Salinas, M. M. G. and Fernandez, S. S. (2006). "A Modified Microplate Cytotoxicity Assay with Brine Shrimp Larvae (*Artemia salina*)".*Pharmacology*, vol. 3, pp. 633–638.

Silby, M. W., Winstanley, C, Godfrey, S. A. C, Levy, S.B. and Jackson. R.W.(2011). "*Pseudomonas genomes*: Diverse and Adaptable". *FEMS Microbiol Rev*., vol , 35, pp. 652–680.

Song, F. L., Gan, R. Y., Zhang, Y., Xiao, Q., Kuang, L. and Li, H. B. (2010). "Total Phenolic Contents and Antioxidant Capacities of Selected Chinese Medicinal Plants". *Int. J. Mol. Sci.*, vol. 11, pp- 2367-2372.

Su Swe Su, Khine Zar Wynn Lae, Nwet Nwet Win and Daw Hla Ngwe. (2018). " Isolation and Identification of *Pseudomonas aeruginosa* from the Clinical Soil ". *Journal of Research University of Yangon*, vol. 8, pp.271-275.

Susan R., M. and Eduaro, C. (1960). "*Bioanalytical Chemistry"* New Jersey, 2nd Ed., vol. 3, pp. 4-7

Tawaha, K. A. (2006). "Cytotoxicity Evaluation of Jordanian Wild Plants Using Brine Shrimp Lethality Test".*J. J. Appl. Sci*., vol. 8, pp. 12–17.

Ullstrom, C. A., Siehnel, R, Woodruff, W, Steinbach, S. and Hancock, R. E. (1991). "Conservation of the Gene for Outer Membrane Protein OprF in the Family Pseudomonadaceae: Sequence of the *Pseudomonas syringae* oprF gene". *J. Bacteriol.*, vol. 173(2), pp.768-775.

Velammal, A., Aiyamperumal, B. Venugopalan,V. K. and Ajmalkhan, S. (1994). "Distribution of *Pseudomonas aeruginosa* in Pondicherry Coastal Environs". *Indian J Mar Sci*, vol. 23, pp. 239–241.

Win, N. N., Ito, T., Aimaiti, S., Imagawa, H., Ngwe, H., Abe, I. and Morita, H. (2015). "Kaempulchraols A–H, Diterpenoids from the rhizomes of *Kaempferia pulchra* collected in Myanmar". *J. Nat. Prod.*, vol. 78, pp. 1113–1118.

WFP. (1998). "*Food and Nutrition Hand Book, In; Macronutrients*", Italy, pp.1–3.

Yadav, M., Chatterji, S., Gupta, S. K. and Watal, G. (2014). "Preliminary Phytochemical Screening of Six Medicinal Plants used in Traditional Medicine". *International Journal of Pharmacy and Pharmaceutical Sciences*, vol. 6 (5), pp. 539-542.

Zak, B., Dickenman, R. C., White, E. G., Burnett, H. and Cherney, P.J. (1981). "Rapid Estimation of Free and Total Cholesterol". *Life Sciences*, vol. 24 (18), pp. 16.